INFORMATION TO USERS

This manuscript has been reproduced from the microfilm master. UMI films the text directly from the original or copy submitted. Thus, some thesis and dissertation copies are in typewriter face, while others may be from any type of computer printer.

The quality of this reproduction is dependent upon the quality of the copy submitted. Broken or indistinct print, colored or poor quality illustrations and photographs, print bleedthrough, substandard margins, and improper alignment can adversely affect reproduction.

In the unlikely event that the author did not send UMI a complete manuscript and there are missing pages, these will be noted. Also, if unauthorized copyright material had to be removed, a note will indicate the deletion.

Oversize materials (e.g., maps, drawings, charts) are reproduced by sectioning the original, beginning at the upper left-hand corner and continuing from left to right in equal sections with small overlaps.

Photographs included in the original manuscript have been reproduced xerographically in this copy. Higher quality 6" x 9" black and white photographic prints are available for any photographs or illustrations appearing in this copy for an additional charge. Contact UMI directly to order.

ProQuest Information and Learning
300 North Zeeb Road, Ann Arbor, MI 48106-1346 USA
800-521-0600

Université d'Ottawa · University of Ottawa

CRYSTAL CHEMISTRY, MÖSSBAUER SPECTROSCOPY AND PARAGENESIS OF ASTROPHYLLITE GROUP MINERALS FROM OVER- AND UNDERSATURATED ALKALINE ROCKS

by

Paula C. Piilonen, B.Sc.

A thesis submitted to the Faculty of Graduate and Post-Doctoral Studies in partial fulfillment of the requirements for the degree of Doctor of Philosophy

Ottawa-Carleton Geoscience Centre
Department of Earth Sciences, University of Ottawa
Ottawa, ON, Canada

"I would like to believe that the roads we choose depend less on economic problems or political battles or the imperfections of our external world, and more on our internal calling, which compels us to go anew into the mountains, to the heights beyond the clouds, making our way to the summits. The sparkling summits and the fathomless sky above our heads, with their grandeur and mysterious beauty, will always draw humanity, which loves all that is beautiful. This was, is and will be the magnetic strength of the mountains, independent of the worldly, trivial vanities and fusses, beyond which, at times, we cannot see the real, the beautiful, and the eternal."

Anatoli Boukreev, 1996

ABSTRACT

The crystal-chemistry and paragenesis of astrophyllite group minerals (AGM) from over- and undersaturated alkaline rocks has been documented by a combination of electron microprobe analyses, single-crystal and powder X-ray diffraction, Mössbauer spectroscopy, Fourier-transform infrared spectroscopy, nuclear reaction analysis, thermal gravitational analysis, thermal decomposition, wet-chemical methods and optical measurements. A standardized general formula for AGM has been developed, based on 31 anions, and is of the form $A_2BC_7D_2T_8O_{26}(OH)_4X_{0-1}$, where $^{[10]\text{-}[13]}A$ = K, Rb, Cs, H_3O^+, H_2O, or □; $^{[10]}B$ = Na or Ca; $^{[6]}C$ = Mn, Fe^{2+}, Fe^{3+}, Na, Mg, or Zn; D = $^{[6]}$Ti, Nb, or Zr; $^{[4]}T$ = Si or Al and $X = \phi$ = F, OH, O, or □. Results from Mössbauer spectroscopy, bond valence sums and thermodynamic calculations indicate F to order at X [ϕ(16)] whereas the monovalent anion sites in the *O*-sheet are host solely to OH^-. On this basis, eight species and two AGM polytypes are recognized, the most recent, niobokupletskite, identified from Mont Saint-Hilaire during the course of this study. The AGM heterophyllosilicate structure consists of two composite sheets stacked along [001] in a 2:1 ratio resulting in a layered *HOH* structure. Single-crystal X-ray refinements indicate the existence of two kupletskite polytypes, kupletskite-1*A* and kupletskite-*Ma2b2c*, the result of polytypic stacking of identical *HOH* layers. Mössbauer spectroscopy indicates all Fe to be present in the *O*-sheet, and Fe^{3+}/Fe_{tot} ratios in AGM to range from 0.01 to 0.21, corresponding to 0.05 to 0.56 *apfu* Fe^{3+}, confirming that Fe^{2+} is the dominant valence state for iron in the AGM structure. AGM from oversaturated alkaline intrusions are characterized by a restricted range of $Mn/Mn+Fe_{tot}$ (0.03 to 0.69) and enrichments in K, Rb, Ti (with positive values of Nb-Zr) and Si. AGM from undersaturated intrusions display a wide range in $Mn/Mn+Fe_{tot}$ (0.09 to 1.00) and have been further subdivided into a kupletskite subgroup ($Mn/Mn+Fe_{tot} \geq 0.50$) and an astrophyllite subgroup ($Mn/Mn+Fe_{tot} < 0.50$). Kupletskite subgroup samples are enriched in Na, Mn, Zn, Fe^{3+}, Nb and Zr (with positive values of Nb-Zr), whereas astrophyllite subgroup samples are enriched in K, Ca, Fe^{2+}, Ti, Zr (with negative values of Nb-Zr) and F. Crystal-chemical parameters in AGM (such as $Mn/Mn+Fe_{tot}$ and Nb/Nb+Zr) can be used as petrogenetic indicators. At Mont Saint-Hilaire (Québec), two distinct paragenetic trends are recognized in the AGM population: (1) an oxidizing magmatic to post-magmatic oxidizing trend resulting in enrichment of the AGM in Na, Mn, Fe^{3+} and Nb, and (2) a reducing trend resulting in enrichment in Ca, Fe^{2+}, Zr and F by hydrothermal or metasomatic processes. The second evolutionary trend is thought to be the result of interaction of an exsolved magmatic fluid with either meteoric waters or sediments. Both trends lend evidence for late-stage mobilization and concentration of high field-strength elements (such as Nb and Zr) in highly alkaline systems.

SOMMAIRE

Nous documentons la cristallochimie et la paragénèse des minéraux du groupe de l'astrophyllite par une combinaison de plusieurs méthodes analytiques incluant la microsonde électronique, la diffraction-X sur poudres et monocristaux, la spectroscopie de Mössbauer, la spectroscopie infra-rouge par transformée de Fourier, l'analyse par réaction nucléaire, la thermogravimétrie, la décomposition thermique, la chimie en solutions et la microscopie optique. Nous proposons une nouvelle formule chimique généralisée pour ce groupe qui est fondée sur 31 anions et dont la forme est $A_2BC_7D_2T_8O_{26}(OH)_4X_{0-1}$, où $^{[10]\text{-}[13]}A$ = K, Rb, Cs, H_3O^+, H_2O, ou □; $^{[10]}B$ = Na ou Ca; $^{[6]}C$ = Mn, Fe^{2+}, Fe^{3+}, Na, Mg, ou Zn; D = $^{[6]}$Ti, Nb, ou Zr; $^{[4]}T$ = Si ou Al et $X = \phi$ = F, OH, O, ou □. Les résultats des analyses par spectroscopie de Mössbauer, les sommes des valences ainsi que des calculs thermodynamiques indiquent tous que le fluor est préférentiellement localisé dans $X[\phi(16)]$ tandis que les sites des ions monovalents des couches-*O* sont eux occupés seulement par OH^-. Nous reconnaissons ainsi huit espèces comme membres du groupe de l'astrophyllite, la plus récente étant la niobokupletskite, découverte dans le cadre de cette étude au Mont Saint-Hilaire, et aussi deux polytypes d'empilement. La structure cristalline hétérophyllosilicatée des minéraux du groupe se caractérise par deux couches composés empilés le long de [001] dans un rapport 2 :1 et résultant en une structure *HOH* feuilletée. Des affinements-X pratiqués sur des monocristaux indiquent la présence de deux polytypes d'empilement pour la kupletskite, soit la kupletskite-1*A* et –*Ma2b2c*, tous deux les résultats de différentes séquences d'empilements des feuillets *HOH* identiques. La spectroscopie de Mössbauer nous indique que tout le fer est dans la couche-*O*, que les rapports Fe^{3+}/Fe_{tot} dans la suite d'échantillons varient de 0.01 à 0.21, correspondant à 0.05 à 0.56 atomes par unité formulaire, et confirmant ainsi la dominance du fer ferreux dans la structure de ces minéraux. Les minéraux du groupe de l'astrophyllite provenant des suites alcalines sursaturées sont caractérisés par un écart restreint de valeurs de $Mn/Mn+Fe_{tot}$ (0.03 à 0.69) et par des enrichissements en K, Rb, Ti (avec des valeurs positives de Nb-Zr) et Si. Ceux des intrusions sous-saturées possèdent un écart de valeurs $Mn/Mn+Fe_{tot}$ beaucoup plus étendu (0.09 à 1.00) et sont subdivisés en un sous-groupe de la kupletskite ($Mn/Mn+Fe_{tot} \geq 0.50$) et un sous-groupe de l'astrophyllite ($Mn/Mn+Fe_{tot} < 0.50$). Les échantillons du sous-groupe de la kupletskite sont enrichis en Na, Mn, Zn, Fe^{3+} et Zr (à des valeurs positives de Nb-Zr), tandis que ceux du sous-groupe de l'astrophyllite sont enrichis en K, Ca, Fe^{2+}, Ti, Zr (à des valeurs négatives de Nb-Zr) et F. Les paramètres cristallochimiques des minéraux du groupe de l'astrophyllite tel que $Mn/Mn+Fe_{tot}$ et Nb/Nb+Zr peuvent servir d'indicateurs pétrogénétiques. Au Mont Saint-Hilaire (Québec), la cristallisation des minéraux du groupe de l'astrophyllite a procédé selon deux lignés possibles : 1) soit sur une lignée oxidante d'origine magmatique à postmagmatique qui a mené à des enrichissements en Na, Mn, Fe^{3+} et Nb, ou soit 2) selon une lignée réduisante d'origine hydrothermale ou métasomatique qui a mené à des enrichissements en Ca, Fe^{2+}, Zr et F. Nous croyons que cette dernière lignée réduisante résulte d'une interaction entre une phase volatile exsolue du magma avec soit des eaux météoriques ou des sédiments. Les deux lignées fournissent l'évidence d'une mobilisation tardive et d'une concentration des éléments tels le Nb et le Zr dans des systèmes hautement alcalins.

ACKNOWLEDGEMENTS

First and foremost, I would like to thank my supervisors, Dr. André Lalonde and Dr. Andy McDonald. Putting into words everything I would like to thank them for is impossible, but I hope they understand and know what their endless support and encouragement means to me. So much of what I've learned from them through the years has nothing to do with mineralogy, but is just as important to the completion of this thesis. Thanks for being the best mentors, advisors, colleagues and friends I could ever have wished for. I look forward to many more years of the same.

A big thank you is extended to the guys at the Canadian Museum of Nature, Bob Gault, Scott Ercit, Joel Grice and Michel Picard, for all their help, advice, access to the collections, and use of the electron microprobe. Special thanks to Bob for his patience in probing many, many astrophyllites, discussions regarding missing elements (borium?), and for teaching me how to dig balls out of the deep corners in a squash court.

Museums and educational institutions have supplied many of the samples for this study. Thank you to the Canadian Museum of Nature (Ottawa, Canada), the Fersman Mineralogical Museum (Moscow, Russia), the Royal Ontario Museum (Toronto, Canada), the Geological Survey of Canada (Ottawa, Canada), Mineralogisk-Geologisk Museum (University of Oslo, Norway). The bulk of the samples for this study were donated by mineral collectors around the world. Along with providing sample material, these people have been instrumental in providing information regarding associated minerals, paragenesis, and in pointing me in the right direction to get samples from obscure localities and other collectors. Thanks to Peter Tarassoff, Alf Olav Larsen, Quintin Wight, Les & Elsa Horváth, Ronald Werner, Ole V. Peterson, Dmitriy Belakovskiy, Kerry Day, Marcelle Webber, Claes Christiansen, Henry DeLinde, Tyson Birkett, Steve Szilard and Abdel-Fattah Abdel-Rahman.

Thanks to Denis Rancourt for his help, supervision and use of the Mössbauer spectrometers. Thanks also to Patrick Mercier and Jim Evans for discussions regarding sheet silicates. Special thanks to Jim and his programming skills in helping to obtain octahedral flattening angles.

Thanks to Mr. Mark Cooper and Dr. Frank Hawthorne (University of Manitoba), Dr. Glen Yap (University of Ottawa), and Dr. Peter Burns (University of Notre Dame) for use of their respective single crystal X-ray diffractometers/CCDs. Andy Roberts of the Geological Survey of Canada collected X-ray diffraction patterns for two of the samples. All TGA and thermal decomposition analyses were graciously provided by Alf Olav Larsen at the Norsk Hydro Research Centre (Porsgrunn, Norway), FTIR spectra were collected by Mrs. Elizabeth Moffat at the Canadian Conservation Institute (Ottawa, Canada), and NRA analyses performed by Dr. Danielle Cherniak at the Department of Earth and Environmental Sciences at Rensselaer Polytechnic Institute (Troy, NY, USA). Thanks to Dr. Ian Swainson (NRC, Chalk River) for teaching me about neutron diffraction and the time spent collecting data at the reactor. Thanks to Mr. Ron Hartree (University of Ottawa) for whole rock XRF analyses

and powder X-ray diffraction and to Mr. George Mrazek (University of Ottawa) for thin sections and polishing of probe mounts.

Thanks to Helen DeGouffe, Sylvie Theriault and Ron Labelle for their assistance over the last four years with everything from registration to helping me befriend the fax machine and photocopier. Thanks also to all the faculty and staff in the Dept. of Earth Sciences at both the University of Ottawa and Laurentian University.

To all my friends and fellow grad students who stood by me, offered a shoulder to lean on, an ear to listen with, or just simply decided it was time to go out, have fun and be goofy rather than sitting in front of a computer, thank you. Special thanks to Laura, Joc, Jorge, Marg, Andy and André - couldn't have done it without you guys.

Last but certainly not least, thanks to my parents, brother and relatives who have always stood by me and supported me in all that I do, no matter how crazy it seemed at the time.

Financial support for this project was generously provided by the Natural Sciences and Engineering Research Council (NSERC), the University of Ottawa and Laurentian University in the form of both graduate scholarships to the author and research grants to AEL and AMM.

STATEMENT OF UNIQUE RESEARCH

Supervision of this thesis was provided by Dr. A.E. Lalonde (Dept. of Earth Sciences, University of Ottawa) and Dr. A.M. McDonald (Dept. of Earth Sciences, Laurentian University), and further advice provided by Dr. D.G. Rancourt (Dept. of Physics, University of Ottawa) and Dr. T.S. Ercit (Canadian Museum of Nature). The following is a summary of the unique research performed by the author in this study.

1. Samples for this study were provided by a number of museums and private collections, yet all analyses were performed by myself.

2. External laboratories, in which I did not personally have a hands-on role in the analyses, were used for TGA, thermal decomposition, FTIR, NRA and XRF.

3. All electron microprobe analyses were performed at the Canadian Museum of Nature and in collaboration with the supervision and guidance of Mr. R.A. Gault and Dr. T.S. Ercit.

4. Collection of single-crystal X-ray structure data was performed at the University of Ottawa, University of Notre Dame, and the University of Manitoba, with training and guidance provided by Dr. G. Yap, Dr. P. Burns and Mr. M. Cooper. Data reduction and refinement were performed by myself with guidance and advice from Dr. A.M. McDonald, Dr. J.D. Grice and Dr. T.S. Ercit.

5. Development of a standardized nomenclature and generalized formula for members of the astrophyllite group. A proposal will be submitted to the *International Mineralogical Association Commission on New Minerals and New Mineral Names* to officially redefine the astrophyllite group on a crystal-chemical basis using chemical and structural data obtained through the course of this thesis. I am the senior author and the proposal is co-authored by A.E. Lalonde and A.M. McDonald.

6. A new species of astrophyllite group mineral was discovered from the East Hill suite at Mont Saint-Hilaire, Québec. Niobokupletskite, the Nb-dominant end-member in a solid solution with kupletskite, was officially accepted by unanimous vote as a new mineral species on October 4th, 1999, by the *International Mineralogical Association Commission on New Minerals and Mineral Names* (**IMA #99-032**) and further published in *Canadian Mineralogist*, 2000, **38**, 627-639. I am the senior author on both the proposal and subsequent manuscript which are co-authored by A.E. Lalonde, A.M. McDonald and R.A. Gault.

7. The first natural example of polytypism in the astrophyllite group, as documented by single-crystal X-ray refinements, was identified from the Lovozero massif, Kola Peninsula, Russia. A comparison of the crystal structures of triclinic ($P\bar{1}$) kupletskite-1*A* and monoclinic kupletskite-*Ma2b2c* and a discussion of polytypic stacking in the astrophyllite group is the basis for a manuscript accepted for publication in *European Journal of*

Mineralogy (April 4th, 2001). I am the senior author of this manuscript which is co-authored by A.M. McDonald and A.E. Lalonde.

8. Collection of the first documented Mössbauer spectra of members of the astrophyllite group was performed under the guidance of Drs. D.G. Rancourt and A.E. Lalonde. All sample preparation, data collection and reduction was performed solely by PCP. Calculation of flattening angles was performed using a program OCTAHEDRON written by Mr. Jim Evans in collaboration with PCP.

TABLE OF CONTENTS

LIST OF FIGURES

LIST OF PLATES

CHAPTER I

LIST OF TABLES

CHAPTER II

CHAPTER III.

LIST OF ABBREVIATIONS

a	crystallographic axis
A-/A+	asymmetry parameter
Ae	aegirine
AGM	astrophyllite group mineral(s)
AOL	A.O. Larsen collection
Ast	astrophyllite
b	crystallographic axis
BVS	bond valence sum
c	speed of light
c	crystallographic axis
CCD	charge-coupled detector
CMNMC/CMNMI	Canadian Museum of Nature mineral collection
CS	center shift
E_r	recoil energy
e	electron charge
EFG	electric field gradient
EHS	East Hill suite
EMPA	electron-microprobe (analysis)
f	Mössbauer recoilless fraction
fO_2	oxygen fugacity
fS_2	sulphur fugacity
Fe-Zrt	Fe-dominant zircophyllite
FEU	Fe-dominant, undersaturated
FMM	Fersman Mineralogical Museum
FTIR	fourier transform infrared spectroscopy
GREEN	Greenland
HFSE	high field-strength element
H-sheet	heterogeneous sheet
h	Planck's constant
ICP-AES	inductively-coupled plasma atomic emission spectroscopy
IMA	International Mineralogical Association
IS	isomer shift
KHIB	Khibina massif, Kola Peninsula, Russia
Kpt	kupletskite
LANG	Langesundsfjord area, Norway
LOV	Lovozero massif, Kola Peninsula, Russia
LUKS	Luksefjell, Norway
MNU	Mn-dominant, undersaturated
MS	Mössbauer spectroscopy/spectra
MSH	Mont Saint-Hilaire
Nbkpt	niobokupletskite

NOR	Norway
NRA	nuclear reaction analysis
O-sheet	octahedral sheet
OVER	oversaturated
P(QS)	probability of the quadrupole splitting
PP	Mount Rosa, Pikes peak, Colorado, USA
PGE	platinum-group elements
POR	Point of Rocks, New Mexico, USA
Q	nuclear quadrupole moment
q	maximum electric field gradient
QS	quadrupole splitting
QSD	quadrupole splitting distribution
REE	rare-earth elements
RT	room temperature
RUS	Russia
s	seconds
SEM	scanning electron microscopy/microscope
SOD	second order Doppler shift
T-sheet	tetrahedral sheet
US	United States of America
v.u.	valence unit
W_{QSD}	width of the QSD at half maximum
Wt.%	weight percent (oxide)
Z	*c*, crystallographic axis
Zrt	zircophyllite
<CS>	average center shit
<QS>	average quadrupole splitting
Γ	Lorentzian linewidth
δ	octahedral counter-rotation
δ_0	center shift
Δ	quadrupole splitting/distortion index
$\|\Delta\|$	absolute quadrupole splitting
Ψ	octahedral flattening angle
ϕ	unidentified anion
σ	standard deviation/octahedral angle variance
τ	tetrahedral elongation
α	tetrahedral rotation angle/crystallographic angle
β	crystallographic angle
γ	crystallographic angle/gamma ray
$\langle x^2 \rangle$	mean square displacement of the probe nucleus

GENERAL INTRODUCTION

Astrophyllite group minerals (AGM) are triclinic and monoclinic, alkali titano-, niobo- and zirconosilicates that occur in peralkaline intrusive rocks ranging in composition from nepheline syenite to alkali granite, and their metamorphic equivalents. Astrophyllite, *sensu stricto*, was first discovered in a nepheline syenite pegmatite on the island of Låven, within the Larvik complex of the Oslo Rift Valley, southeast Norway, by Weibye (1844) and described in detail by Brøgger (1890). The crystal structure of astrophyllite was first determined by Peng & Ma (1963), and later refined by Woodrow (1967). To date, eight species of AGM have been described; the most recent of which from Mont Saint-Hilaire (MSH) during the course of this study.

The purpose of this study is to describe the crystal chemistry of AGM from over- and undersaturated alkaline intrusions, and to shed light on the paragenesis of these complex sheet silicate minerals using a combination of electron microprobe analysis, single-crystal X-ray diffraction and Mössbauer spectroscopy. The main objectives of this study are (1) to establish a systematic crystal-chemical nomenclature for the astrophyllite group, (2) to describe the chemical variations observed in members of the astrophyllite group, particularly with respect to Na, Mn, Fe, Zn, Mg, Ti, Zr, Nb and F, between different parageneses and localities; (3) to describe new and potentially new species and polytypes of AGM; (4) to describe, in detail, the crystal chemistry of AGM with a focus on the effects of chemical substitutions on the crystal structure; (5) to describe, for the first time, the Mössbauer spectra of members of the astrophyllite group and correlate Mössbauer spectral parameters with

crystal chemistry; and (6) to use the above findings to provide information on the paragenesis of this group of minerals.

Chapter I provides information regarding the samples used in this study, including geological setting and species descriptions.

Chapter II presents information pertaining to the chemistry and nomenclature of the astrophyllite group. A standardized general formula and cation-distribution scheme for the group has been developed with the objective to redefine the group, and this has been presented to the IMA Commission of New Minerals and Mineral Names for approval. The chemical variations of astrophyllite group minerals from over- and undersaturated intrusions are discussed and substitution schemes proposed. This chapter will be submitted for publication in the *European Journal of Mineralogy* following submission of the thesis.

Chapter III discusses the crystal chemistry of the astrophyllite group in light of 21 single-crystal X-ray structure refinements and associated electron-microprobe analyses. The details of each of the structural elements are discussed and the effects of isomorphous substitutions on the various polyhedra presented. This chapter will be submitted for publication in the *European Journal of Mineralogy* following submission of the thesis.

Chapter IV presents data obtained by Mössbauer spectroscopy on members of the astrophyllite group. The results of an oriented mosaic study are presented in order to discuss the effects of preferred orientation of crystals on the Mössbauer spectra. Details regarding the individual spectra are discussed, including Fe^{2+}/Fe^{3+} ratios and the relation between quadrupole splitting distributions and crystal-chemical parameters.

Chapter V presents the first natural example of polytypism in the astrophyllite group, kupletskite-1*A* and kupletskite-*Ma2b2c*. The crystal structures of both polytypes and their relation to each other are discussed in detail. The thermodynamic stability of triclinic and monoclinic astrophyllite group mineral polytypes is discussed. This chapter has been accepted for publication in the *European Journal of Mineralogy* (Piilonen *et al.* 2001, April 4th, 2001).

Chapter VI describes niobokupletskite, a new member of the astrophyllite group discovered at Mont Saint-Hilaire (Québec, Canada) during the course of this study. The physical and optical properties and crystal structure of niobokupletskite are presented. The paragenesis of niobokupletskite is discussed and comments made on the mobilization of Nb and Zr in hydrothermal or post-magmatic systems. This chapter was published in the *Canadian Mineralogist* (Piilonen *et al.* 2000, **38**, 627-639).

Chapter VII discusses the paragenesis of astrophyllite group minerals and comments on the role of Ti, Zr and Nb in alkaline systems. Results obtained from specimens from the Larvik complex (Norway) and Mont Saint-Hilaire (Québec, Canada) are used as a case study for this discussion.

CHAPTER I.

GEOLOGICAL SETTING AND SAMPLE DESCRIPTIONS

1.0. Sample Selection

An attempt was made to analyse members of the astrophyllite group from a number of well-documented over- and undersaturated intrusions in order to ensure the widest range of chemical and paragenetic variations as possible. In order to attain this goal, samples were obtained from various museum collections, in particular the Canadian Museum of Nature (Ottawa, Canada), the Royal Ontario Museum (Toronto, Ontario), the Fersman Mineralogical Museum (Moscow, Russia), and from a large number of generous mineral collectors. In addition, analyses of from two previous studies were included in the chemical database: Mount Gharib, Egypt (Abdel-Rahman 1992) and Greenland (Christiansen 1998).

2.0. Mont Saint-Hilaire, Québec, Canada

Mont Saint-Hilaire (MSH), located 40 km east of Montréal, Québec, is one of ten early Cretaceous alkaline intrusions collectively referred to as the Monteregian Hills (Adams 1903). The peralkaline East Hill suite (EHS) is host to a variety of rock types or microenvironments (Fig. 1) including pegmatites (PEG), altered pegmatites (APEG), natrolite pegmatites (NPEG), sodalite syenites (SS), sodalite syenite xenoliths (SSX), aplites (APLITES), and a metasomatic unit (META), all of which contain AGM. In all cases, AGM account for < 1% to 10% of the modal mineralogy of the petrological units at MSH. To date, five species of the astrophyllite group have been described: astrophyllite, kupletskite, niobokupletskite, zircophyllite and a potentially new species, Fe-dominant zircophyllite

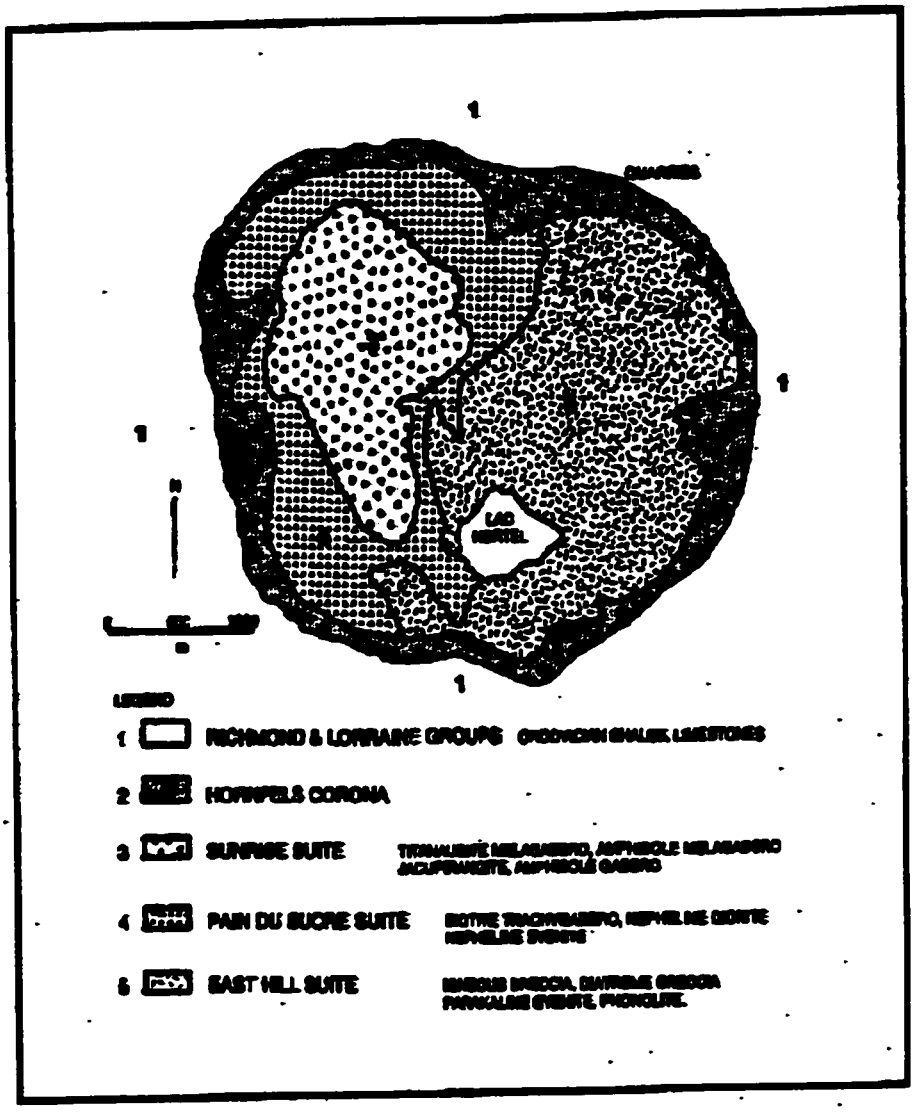

Figure 1. Mont Saint-Hilaire, Québec, Canada
(after Horváth & Gault 1990)

(Horváth & Gault 1990, Piilonen *et al.* 2000), making it the most prolific site for astrophyllite group species from either over- or undersaturated intrusions. The physical characteristics of AGM in each microenvironment are distinct and can be used to determine qualitatively the specific species in any given sample. Mont Saint-Hilaire AGM also show the widest chemical and physical diversity with respect compared to all other localities studied. Detailed sample descriptions for MSH AGM can be found in Chapter VII.

3.0. The Larvik complex, Oslo Rift Valley, Norway

During the late Carboniferous and early Permian, the southeastern region of Norway was the site of intracontinental rifting, followed by extensive plutonic and volcanic activity. The Oslo rift valley was active from approximately 305 to 240 Ma (Sundvoll *et al.* 1990, Neumann *et al.* 1992, Sundvoll *et al.* 1992), and extends approximately 400 km NNE from the Sorgenfrei-Tornquist zone to Lake Mjøsa (Fig. 2, inset). The rift is divided north-south into two grabens: (1) the Oslo graben to the north is exposed on land with an exposure level of one to three kilometers beneath the original surface, and (2) the Skagerrak graben, which is submerged and buried under younger (Mesozoic) sediments. The Oslo Region itself refers to a province of Paleozoic rocks (200 km long and 35-65 km wide) within the Oslo graben, 130 southwest of the capital city of Oslo. It is within this region that undersaturated AGM-bearing plutonic rocks of the Oslo alkaline province are found (Brøgger 1890).

Unlike most other rift valleys, which are the result of hotspot activity, the Oslo rift is the product of recurrent extensional activity along pre-existing Precambrian lineaments, driven by a weak thermal anomaly and/or decreased solidus temperatures due to increased

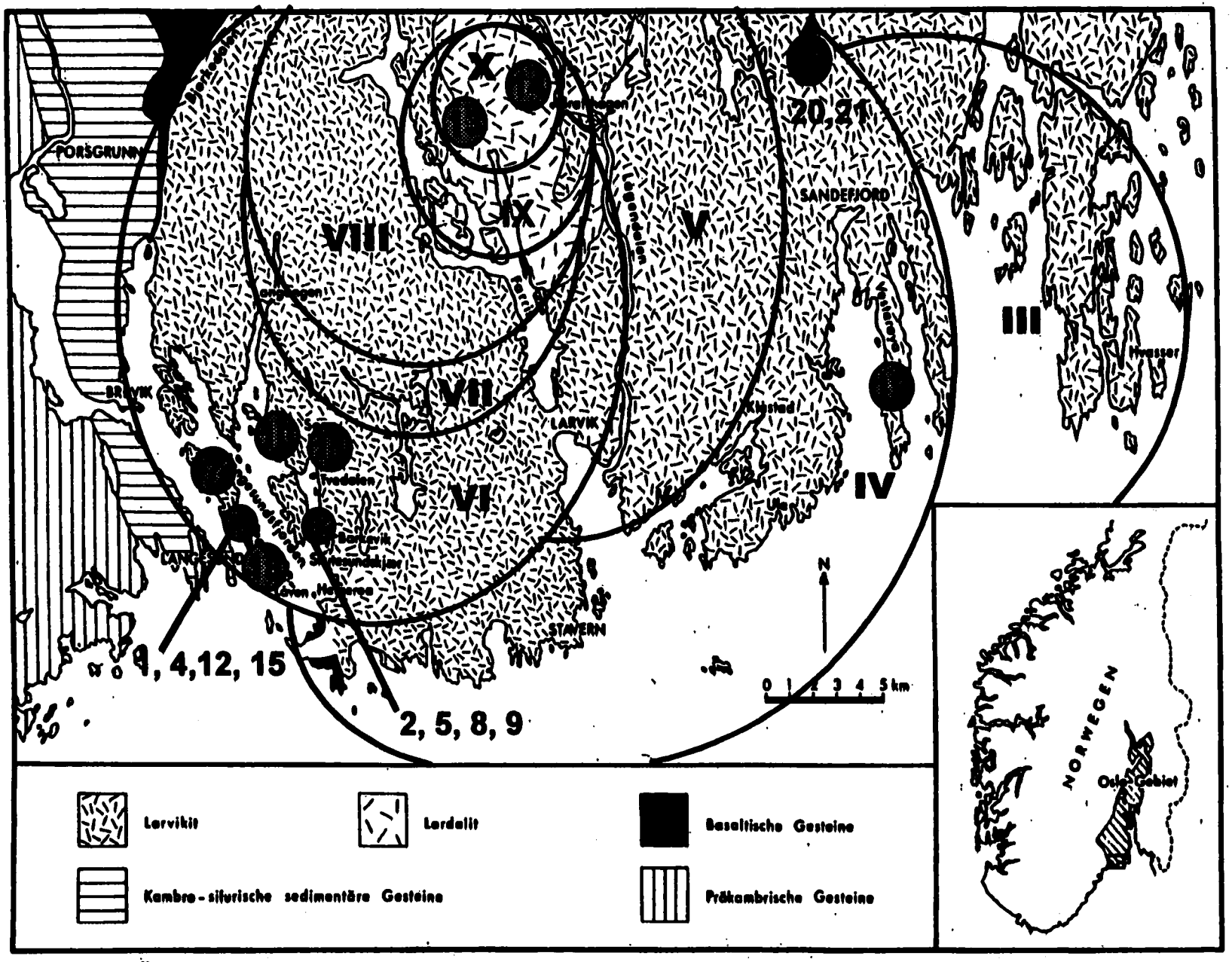

Geologische Übersichtskarte des südlichen Larvikit-Massives des Oslo-Gebietes.

Figure 2. Geological map of the Larvik complex, Langesundsfjord area, Oslo Rift, Norway. Sample localities indicated. Roman numerals indicate ring sections (RS) within the complex. (after Raade *et al.* 1980)

fluid contents in the mantle (Neumann 1994). Large-scale fractional crystallization of the parental basaltic magma at depth led to the intrusion of intermediate to felsic, over- to undersaturated plutonic rocks that extend over 5205 km^2 in the Oslo graben alone (Ramberg 1976, Neumann 1994). The tectonomagmatic evolution of the rift will be discussed briefly so that the origin of these astrophyllite group mineral-bearing plutonic rocks can be better understood.

3.1. Tectonomagmatic evolution of the Oslo Rift Valley

All geophysical and geochemical evidence compiled for the evolutionary model of the Oslo rift has been gained from studies on the Oslo graben due to the inaccessibility of the submerged Skagerrak graben. Rifting and volcanism in this area can be divided into five main periods (Neumann *et al.* 1992):

Stage 1 - Development of a shallow depression and intrusion of intermediate to felsic sills (>300 Ma).

Stage 2 - Initial rifting and basalt volcanism (300-295 Ma).

Stage 3 - Main rifting and volcanic stage (295-275 Ma).

Stage 4 - Central volcano and composite intrusion stage (275-240 Ma).

Stage 5 - Post-rift intrusion of dikes (<240 Ma).

The main magmatic stage (Stage 2) began with vertical movement and rifting along NNW-SSE to N-S-trending faults shortly after 300 Ma, reflecting ENE-WSW crustal extension, followed by extensive basaltic shield volcanism. Extrusion temperatures for the basaltic lavas have been estimated to be between 1270 and 1340 °C (Neumann 1994).

Basalts (B_1) range in composition from nephelinite, alkali basalts, olivine tholeiites, quartz tholeiites to trachybasalts, and show a northward decrease in thickness and alkalinity (Ramberg & Larsen 1978, Neumann *et al.* 1992, Neumann 1994). All basaltic rocks from Stage 1 have low Mg#'s, and are enriched in lithophile elements relative to the primordial mantle, with ratios of 50 to 100 for elements such as Th, U, Ta and La. Isotopic ratios (Rb/Sr, Sm/Nd and U-Th-Pb) indicate mixing between an undepleted mantle ($\varepsilon_{Nd} = +1$, $\varepsilon_{Sr} =$ -10 to -15), a mildly depleted mantle ($\varepsilon_{Nd} = +4$, $\varepsilon_{Sr} = -10$) and an enriched deep-crustal source (Neumann *et al.* 1988, 1990, 1994). Mixing of magmas from these heterogeneous sources occurred within deep-crustal magma chambers, at which point extensive fractionation and moderate contamination occurred, resulting in the wide range of rock compositions observed at the surface.

Stage 3, the main period of rifting, is characterized by a change from shield volcanism to more siliceous, intermediate lavas with a latitic composition, accompanied by development of extensive normal faults, fractures and dikes oriented NNW-SSE and N-S, and the development of central volcanoes on the rift floor (Neumann *et al.* 1992). Rb-Sr age dating of the flows indicates younging toward the north of the Oslo graben, with volcanism lasting from 294 ± 6 to 283 ± 8 Ma in the south, and from 290 ± 4 to 276 ± 8 Ma in the north (Sundvoll & Larsen 1990). These volcanic rocks have an areal extent of 1153 km^2 and make up 60% of the Oslo graben. Referred to as 'rhomb porphyries' due to the presence of rhomb-shaped alkali feldspar phenocrysts, these rocks grade from basalt at their base to trachyte and rhyolitic ignimbrite toward the top of the sequence. The trachyandesite flows are enriched,

relative to primordial mantle, in incompatible elements and show similar isotopic signatures as those of the stage 2 (B_1) basalts (Neumann *et al.* 1992).

Locally, sequences of basaltic lavas and trachyandesites are bounded by syenitic ring-dikes and faults, indicating that the end of the extrusive period included development of central volcanoes which, in turn, developed into calderas, marking the beginning of stage 4 (275 - 240 Ma). Following caldera collapse, large circular, post-extensional batholiths ranging in composition from intermediate to felsic (monzonites, monzosyenites and granodiorites) were intruded into the lower lava pile (Neumann *et al.* 1992). Gravity modelling has shown that these batholiths, which cover 5100 km^2 of the rift floor, reach depths of 3 to 12 km (Ramberg 1976). A number of small, gabbroic and granitic intrusions were emplaced at the same time (266 ± 6 Ma, Neumann *et al.* 1985). Following emplacement of the batholiths, late-stage intrusion of dikes, ranging in composition from basalt to syenite, continued into the Triassic period (Dons 1977).

3.2. The Larvik complex

The Larvik ring complex is located at the southern-most point of the Oslo rift in the Langesundsfjord area. It was formed during stage 4 and is the largest differentiated monzosyenitic body in the Oslo region (Neumann 1980). The complex is represented by a series of weakly over- to undersaturated intrusions, composed of both "larvikite" or monzosyenite (277 ± 3 Ma) and "lardalite" or syenite (269 ± 5 Ma, Neumann 1980) respectively, which are crosscut by quartz syenite pegmatites in the east and nepheline syenite pegmatites in the west (Brøgger 1890). The complex can be divided into 10 ring

sections (RS, Fig. 2). Ring sections 1 and 2 consist of quartz-bearing monzonite and monzosyenite (not shown on map). Moving westward in the complex (RS 3 to 8) the rocks become slightly undersaturated until RS 9 and 10 where undersaturated, nepheline-bearing monzosyenites and nepheline syenites are the dominant rock type (Neumann 1980). To account for the uniform degree of silica saturation in the intermediate rocks and the strongly divergent trends observed in the more evolved felsic rocks, Barth (1945) proposed two evolutionary trends for the rocks of the intrusion, one towards oversaturation (monzosyenite-quartz syenite-alkali granite), and one towards undersaturation (monzosyenite-syenite-nepheline syenite). The ring complex is the result of the second differentiation trend, but later alkali granite, the result of the oversaturated trend, will also be discussed. The various rock types in the complex have been described by Brøgger (1890), Neumann (1976) and Peterson (1978). The mafic mineralogy of the dikes has been studied by Neumann (1976) and Larsen & Raade (1997), and felsic minerals by Neumann (1980).

Astrophyllite group minerals have been found in RS4, 6 and 10 (Fig. 2). In RS 4, astrophyllite is rare and occurs as very coarse-grained, dark brown, platy, anhedral crystals associated with quartz and aegirine in a quartz-bearing syenite pegmatite within monzosyenite. In RS6, astrophyllite is a common species within the nepheline syenite pegmatites which are hosted by monzosyenite. The type locality for astrophyllite, the island of Låven, is also located within RS6 and was described extensively by Brøgger (1890). These pegmatites are often large, attaining dimensions of 10 to 20 m in thickness and 120 m in length (Brøgger 1890, A.O. Larsen *pers. comm.*), and occur as irregular veins or pods composed mostly of microcline, aegirine, nepheline, ferroedenite, magnetite, biotite, zircon,

and a wide range of exotic minerals that are typical of peralkaline intrusions enriched in Ti, Zr, Nb, REE, and Be (see Raade *et al.* 1980 for a complete list). Astrophyllite occurs as postmagmatic, coarse-grained (up to 3 x 3 cm), anhedral, platy to slightly tabular, dark brown to red crystals embedded in matrix (Plate 1 & 2). Crystals do not display any compositional zonation.

Syenite and nepheline syenite are the dominant rock types within RS10, the youngest and most undersaturated portion of the complex. Late-stage kupletskite occurs embedded in matrix and within vugs or fractures in nepheline syenite pegmatite. The kupletskite occurs as medium grained (average: 0.5 x 0.5 cm), anhedral, tabular to platy, brown to reddish brown crystals with a bronze luster (Plate 3). It is associated with microcline, aegirine, catapleiite, natrolite, analcime and albite. This is the first documented occurrence of kupletskite within the Larvik complex.

In addition to the pegmatites of the Larvik complex, two samples were obtained from a small alkali granite body located in the Luksefjell district, 30 to 40 north of the Langesundsfjord district (A.O. Larsen, pers. comm.). Radiometric dating of the intrusions in this northern portion of the complex indicate that they are 11 Ma younger than the host monzosyenite (A.O. Larsen & S. Dahlgren *pers. commun.*). The species of AGM described from these alkali granites is astrophyllite. It occurs as coarse-grained (ave. 0.5 x 0.75 cm), reddish-brown to orange-brown plates rimmed by quartz and embedded in a matrix of quartz, perthitic feldspar and sodic amphibole. The crystals seem to have undergone extensive oxidation and are covered by a thin unidentified black-brown coating.

Plate 1. Bladed, dark brown astrophyllite from Barkevikskjær, Larvik complex, Langesundsfjord area (Oslo rift valley, Norway; NOR8). Associated minerals include aegirine, biotite and microcline. Field of view: 8.1 cm.

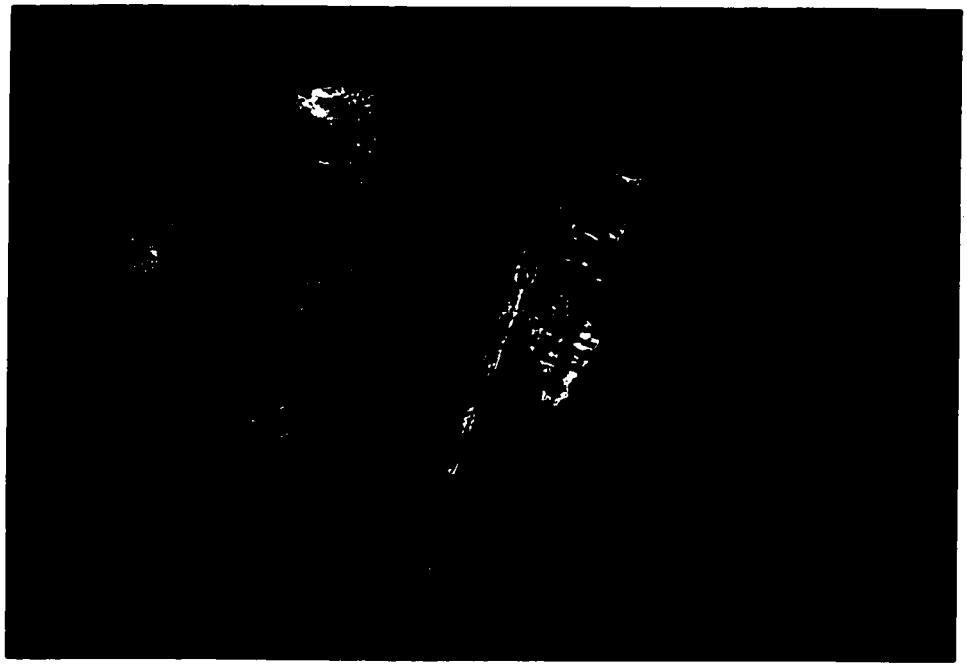

Plate 2. Platy, brown astrophyllite with microcline from Barkevikskjær, Larvik complex, Langesundsfjord area (Oslo rift valley, Norway; NOR9).
Field of view: 6.5 cm.

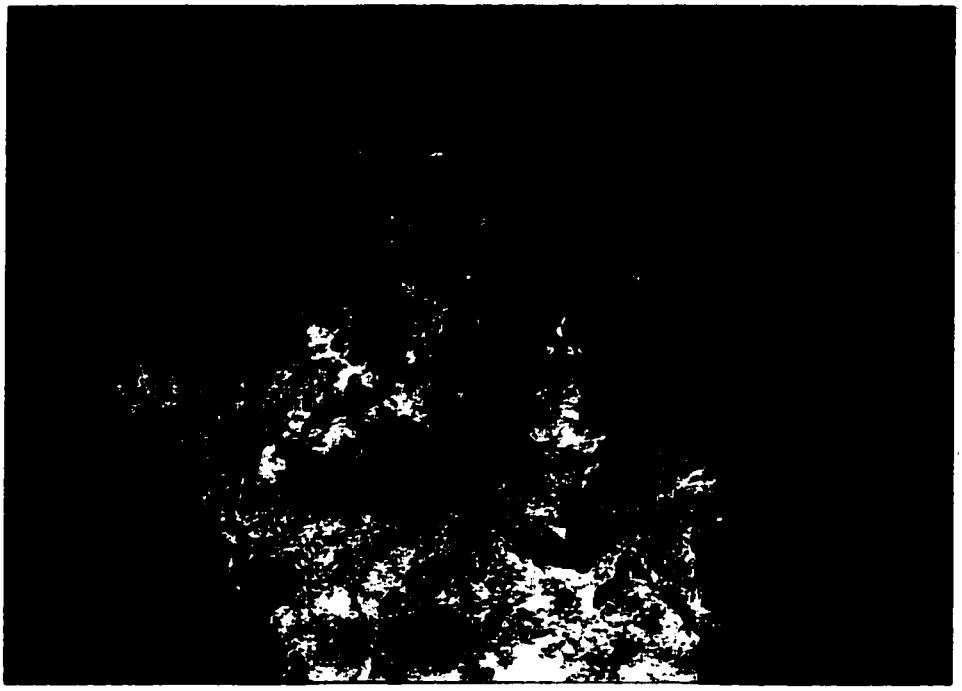

Plate 3. Orange-brown kupletskite from RS10, Lysebo, Larvik complex, Langesundsfjord area (Oslo rift valley, Norway; NOR13). Associated minerals include aegirine, albite, catapleiite, microcline and natrolite. Field of view: 4.7 cm.

4.0. GJERDINGEN, NORWAY

A number of Permian alkali granite bodies occur in the Oslo region, younger than the Larvik complex. The Gjerdingen alkali granite, often referred to as "ekerite", is a 8 km^2 pluton ESE of Lake Gjerdingen in the Nordmarka district, 30 km north of Oslo (10°42', 60°10'N). The exposure is actually composed of a number of boulders scattered along a forest trail (Raade & Haug 1982). The granite is unique as it is strongly enriched in Na, F, Mn, Ti and Zr, and is host to numerous exotic minerals (see Raade & Haug 1982 for a full list) which occur in small pegmatite lenses and miarolitic cavities. The granite is fine- to medium-grained and contains albite, microcline, aegirine and arfvedsonite. Kupletskite occurs within these miarolitic cavities as medium grained (average: 0.1 x 0.3 cm), light brown to reddish brown, subhedral, platy to tabular crystals (Plate 4).

5.0. MOUNT ROSA, PIKES PEAK, ST. PETER'S DOME, COLORADO, USA

The 1000 Ma quartz-bearing pegmatites in the Mount Rosa alkali granite (St. Peter's Dome, Pikes Peak, Colorado) have been studied extensively by Gross & Heinrich (1966). Two suites of pegmatite dikes intruded into the Pikes peak granite/fayalite granite have been described from the district; an older subalkaline Pikes Peak type, and a younger, alkaline Mount Rosa type. The Mount Rosa type pegmatites occur as tabular, irregular bodies consisting of quartz, microcline and riebeckite with accessory zircon, fluorite, thorite, pyrochlore, rutile, columbite, bertrandite and a large suite of aluminofluoride minerals. Astrophyllite, described as early as 1877, is a common secondary mineral in the exterior pegmatites. It occurs in the border zones as a late-stage replacement mineral after riebeckite,

Plate 4. Kupletskite (light brown) from the Gjerdingen alkali granite, Nordmarka, Oppland province (Norway; NOR3). Associated minerals include elpidite, nenadkevichite, narsarsukite, brookite, anatase, gearksutite ralstonite, aegirine, quartz and microcline.
Field of view: 3.5 cm.

and as late fracture-fillings in the Mount Rosa granite (Gross & Heinrich 1966). The astrophyllite is commonly very coarse grained (grains up to 2.5 x 10 x 25 cm have been discovered, ave: 3 x 2 x 2 cm), platy to slightly tabular, and dark red-brown (Plate 5). Samples are commonly strongly altered to chlorite, sericite and hematite and contain inclusions of quartz, albite, riebeckite and ilmenorutile.

6.0. THE KHIBINA-LOVOZERO COMPLEX, KOLA ALKALINE PROVINCE, RUSSIA

The Kola and Karelia alkaline province is located in northwestern Russia, north of the White Sea. Igneous rocks of the alkaline province are intruded into Archean granitic gneisses and Proterozoic metavolcanic and metasedimentary rocks of the Baltic Shield (Gerasimovsky *et al.* 1974). The Khibina and Lovozero massifs, located in the centre of the peninsula, are two of approximately 37 alkaline igneous and carbonatitic bodies in the province which range in age from the middle Proterozoic alkaline gabbros of Yelet'ozero and Gremjakha-Virmes to Hercynian, peralkaline nepheline syenites of Khibina (400 to 365 Ma, Kogarko *et al.* 1995) and Lovozero (418 to 361 Ma, Kogarko *et al.* 1995), the middle Paleozoic stages of which are related to the formation of the central Kola paleorift (Kogarko *et al.* 1995).

The Khibina-Lovozero complex (2000 km^2) is the largest alkaline complex in the world (Gerasimovsky *et al.* 1974). It comprises two layered, conical peralkaline massifs that extend to depths of greater than 8 to 10 km (Khomyakov 1995). The intrusions were emplaced into fractures in the folded Archean and Proterozoic basement, a long-lived tectonic zone with a NE strike which can be traced into Sweden and Norway (Gerasimovsky

Plate 5. Bladed astrophyllite from Mount Rosa, St. Peter's Dome, Pikes Peak (El Paso Co., Colorado; US5).
Field of view: 7.8 cm.

et al. 1974). Both intrusions have been mined extensively in the past, Khibina for apatite and nepheline, and Lovozero for apatite, eudialyte group minerals and loparite (Kogarko *et al.* 1995).

6.1. The Khibina massif

The Khibina massif (Fig. 3) covers 1327 km^2 and comprises eight main intrusive phases, decreasing in age from the periphery to the center, in which astrophyllite can be found in nepheline syenite and associated pegmatites of phases 4, 6 and 7 (Kogarko *et al.* 1995). There is no significant geochemical variation within the intrusion, and the overall composition is close to that of an average nepheline syenite.

Phase 4 consists of massive, homogeneous nepheline syenite which forms a complex, ring-like intrusive body, characterized by poikilitic textures and graphic and micropegmatitic intergrowths of alkali feldspar and nepheline thought to be of a metasomatic origin (Galakhov 1959, Tikhonenkov 1963). Additional minerals in phase 4 include aegirine, arfvedsonite, biotite, eudialyte group minerals, titanite, lamprophyllite and apatite (Kogarko *et al.* 1995). Phases 6 and 7 comprise both massive (phase 6) and trachytic (phase 7) nepheline syenites containing microcline, nepheline, aegirine, arfvedsonite, biotite and titanite. Albite-aegirine fenites and hornfels are well-developed along the outer edges of the complex, further evidence of metasomatic activity.

Astrophyllite and magnesium astrophyllite have been studied from the Khibina massif. Astrophyllite from phases 4 and 6 (specimens RUS1, 2, 4, 6, 7, & 8), in modal proportions ranging from 10 to 30%, is coarse-grained (average: 1.0 x 0.5 x 0.2 cm),

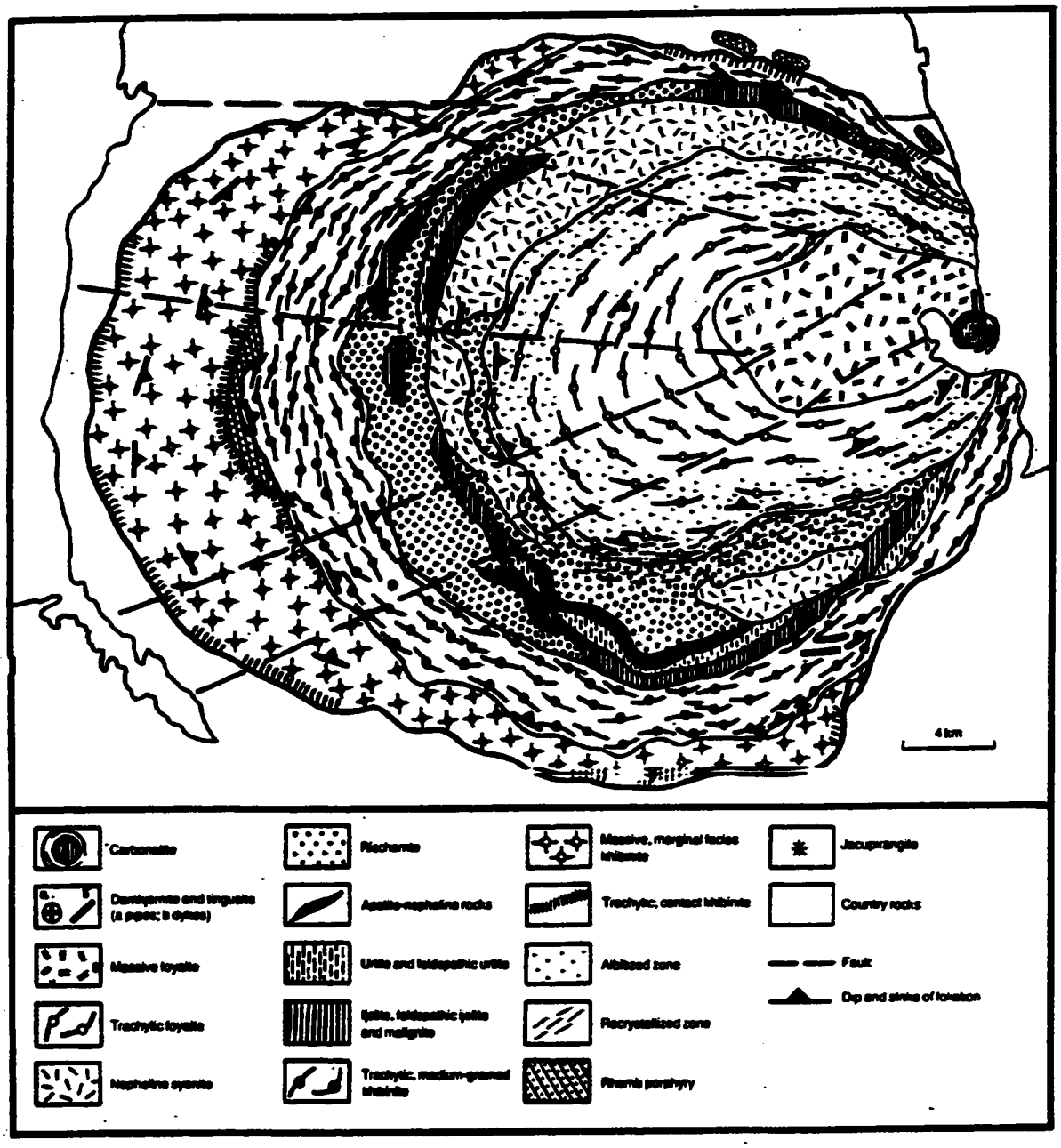

Figure 3. The Khibina massif, Kola alkaline province, Kola Peninsula, Russia (after Zak *et al.* 1972)

strongly tabular to platy, dark red-brown to orange-brown, anhedral to subhedral crystals which often occur in radiating aggregates. An intimate relation is observed between astrophyllite and aegirine, as they are often intergrown and seem to have crystallized simultaneously (Plates 6). Astrophyllite from phase 7 (RUS3) occurs as coarse-grained (average: 0.7 x 0.075 cm) tabular to lath-like, bright orange-red, subhedral crystals. The astrophyllite crystals, which account for 25 to 30% of the rock, are aligned parallel or subparallel to their *a* axis, defining the strong trachytic texture that is characteristic of Phase 7 nepheline syenites (Plate 7). The matrix consists of unaltered, granular microcline, prismatic aegirine, arfvedsonite and subhedral to euhedral nepheline. Magnesium astrophyllite from Mount Koashua occurs with villiaumite and pectolite as yellowish-green, fine-grained, extremely fibrous, matted intergrowths.

6.2. Lovozero massif

The Lovozero massif (Fig. 4), located southwest of Khibina, is a complex laccolith formed during four intrusive stages, extending to 7 km at depth with an area of 650 km^2 at surface (Kogarko *et al.* 1995). The lower part of the intrusion (phase I) consists of a concentrically zoned stock of nepheline and nosean syenites. The upper portion of the intrusion, exposed by erosion, is a rhythmically layered, differentiated sequence of urtites, foyaites and lujavrites (Phase II & III, Gerasimovsky *et al.* 1974). Coarse grained and pegmatitic nepheline syenites are often found along the outer contact of the intrusion and crosscut the earlier intrusive phases (Gerasimovsky *et al.* 1974, Kogarko *et al.* 1995).

Plate 6. Prismatic astrophyllite with aegirine, eudialyte, nepheline and microcline from the Khibina massif, Kola Peninsula (Russia; RUS2). Field of view: 8.3 cm.

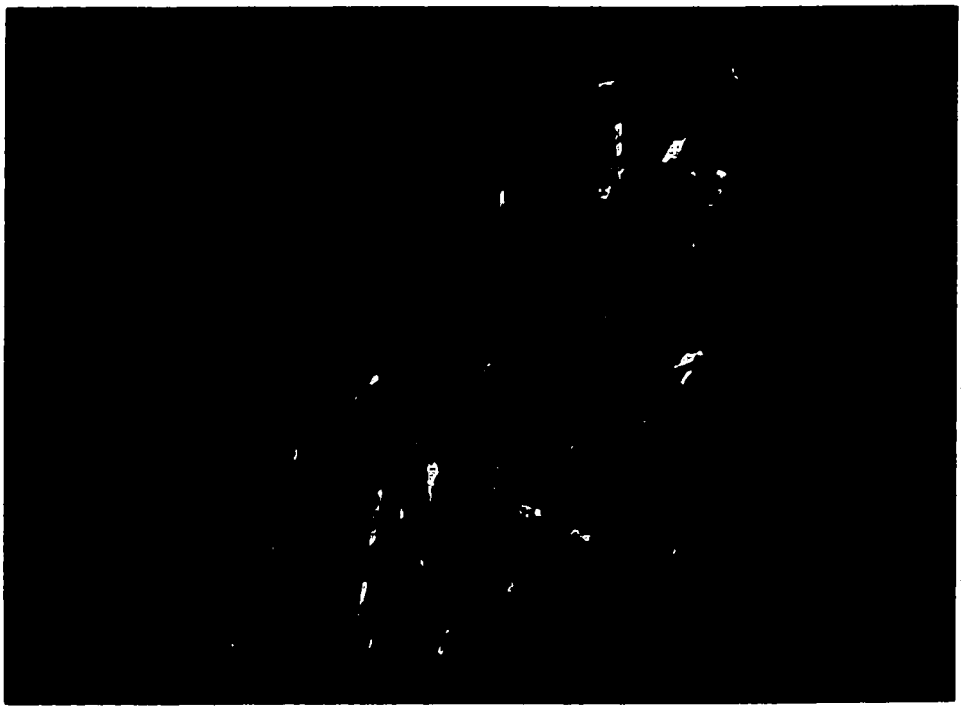

Plate 7. Prismatic astrophyllite defining a trachytic texture in nepheline syenite from the Khibina massif, Kola Peninsula (Russia; RUS3). Field of view: 7 cm.

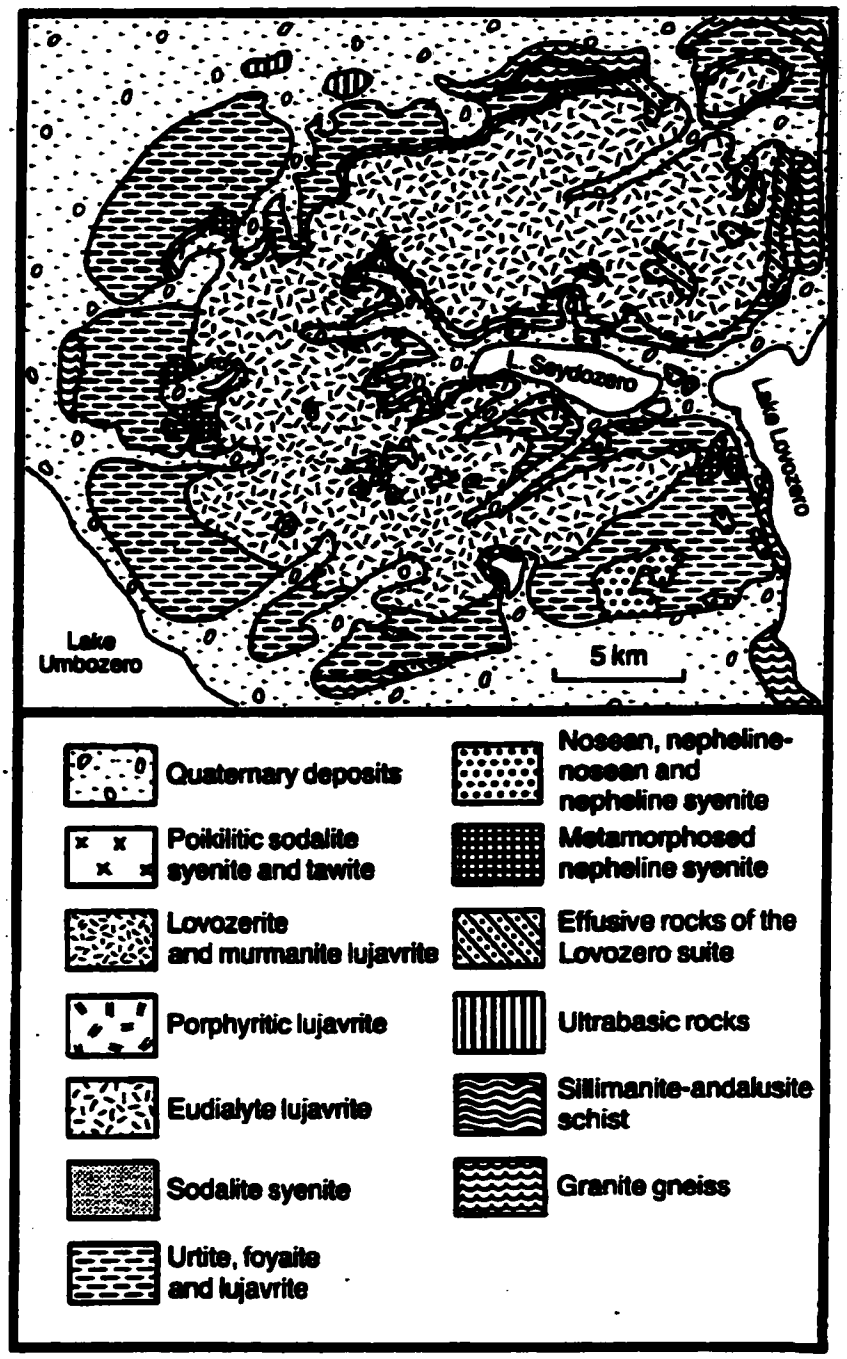

Figure 4. The Lovozero massif, Kola alkaline province, Kola Peninsula, Russia (after Gerasimovsky *et al.* 1966)

Kupletskite, a rare mineral in the Lovozero massif, was initially described by Semenov (1956) in late-stage, phase IV nepheline syenite pegmatites from the Kuivchorr (RUS12, holotype material) and Lepkhe-Nelm (RUS9) mountains of the massif. It occurs as coarse grained (average: 0.2 x 0.3 x 0.1 cm), anhedral to subhedral, dark brown, platy to acicular crystals associated with aegirine, natrolite, eudialyte group minerals, microcline, manganoan pectolite and neptunite.

7.0. Other Localities

Chemical analyses were done on AGM from two Labrador (Canada) localities: Seal Lake, the type locality for niobophyllite (LAB1), and Letitia Lake (LAB2). Only grain separates were obtained for both samples and detailed information concerning associated minerals or paragenesis is not available.

Analyses of two AGM samples from the Zomba-Malosa complex, Chilwa alkaline province (Malawi, Africa; Wooley & Platt 1988) were done. Sample AFR1 is a kupletskite from a granitic pegmatite where it occurs as coarse-grained, strongly altered and oxidized, slightly foliated grains in a pegmatite vein. It is associated with quartz, microcline and ilmenorutile. Sample AFR3 is from a nepheline syenite at Junguni Hill. It occurs as fine-grained (0.75 x 1.0 mm), acicular to lath-like, orange-brown crystals in a matrix of aegirine, sodalite, perthitic feldspar, biotite and nepheline.

Electron-microprobe data for 13 AGM from Greenland were generously provided by Mr. C.C. Christiansen (University of Copenhagen, Denmark) and have been included in the data set for the present study. Mössbauer spectroscopy was done on four of these samples

using material provided by Mr. Christiansen. Similarly, EMPA data for a suite of 18 AGM from the granitic Mount Gharib complex (Egypt, Africa) were taken from a study by Abdel-Rahman (1992) and used in this study.

CHAPTER II.

ASTROPHYLLITE GROUP MINERALS I. NOMENCLATURE AND CHEMICAL VARIATIONS

PAULA C. PIILONEN & ANDRÉ E. LALONDE
Ottawa-Carleton Geoscience Centre, Department of Earth Sciences
University of Ottawa, Ottawa, Ontario K1N 6N5

ANDREW M. McDONALD
Department of Earth Sciences, Laurentian University, Sudbury, Ontario P3E 2C6

T. SCOTT ERCIT & ROBERT A. GAULT
Mineral Sciences Division, Canadian Museum of Nature, Ottawa, ON

ALF OLAV LARSEN
Norsk Hydro ASA, Research Centre Porsgrunn, Porsgrunn, Norway

OVERVIEW

This chapter provides information concerning the nomenclature and chemical variations within AGM from both over- and undersaturated intrusions. The first part of the chapter describes the new proposed nomenclature for AGM and defines the group on a crystal-chemical basis. This section has been submitted to the *IMA Commission on New Minerals and New Mineral Names* in order to officially redefine the astrophyllite group. The second part of this chapter provides information concerning chemical variations observed in the sample suite studied. This chapter will be submitted for publication in the *European Journal of Mineralogy* following submission of the thesis.

ABSTRACT

The chemical variations of 135 samples of astrophyllite group minerals (AGM) from 15 localities have been measured by EMPA, ICP-AES, FTIR, TGA, thermal decomposition, NRA and Mössbauer spectroscopy. Data for 31 representative samples are presented. A standardized general formula for AGM has been developed and is of the form $A_2BC_7D_2T_8O_{26}(OH)_4X_{0-1}$, where $^{[10]\text{-}[13]}A$ = K, Rb, Cs, H_3O^+, H_2O, or □; $^{[10]}B$ = Na or Ca; $^{[6]}C$ = Mn, Fe^{2+}, Fe^{3+}, Na, Mg, or Zn; D = $^{[6]}$Ti, Nb, or Zr; $^{[4]}T$ = Si or Al, X = ϕ = F, OH, O, or □. Calculation of formulae for all AGM (except magnesium astrophyllite) should be based on 31 anions. If Nb_2O_5 > 5.00 wt.%, formulae should be calculated on the basis of 26 O + 4 (OH) + (F,O). If Nb_2O_5 < 5.00 wt.%, formulae should be calculated on the basis of 26 O + 5 (OH,F). Calculation of the formula for magnesium astrophyllite should be based on a total of 30 anions, with 26 O + 4 (OH,F). On this basis, the eight species of AGM have been redefined and new empirical formulae presented. Zircophyllite has been redefined as the Mn-Zr end-member in a solid solution series with Fe-zircophyllite, a potentially new species. Results from Mössbauer spectroscopy indicate Fe^{3+}/Fe_{tot} ratios in AGM to range from 0.01 to 0.21, corresponding to 0.05 to 0.56 *apfu* Fe^{3+}, confirming that Fe^{2+} is the dominant valence state for iron in the AGM structure. Both Fe^{2+} and Fe^{3+} are restricted to the *O*-sheet. Results indicate AGM from over- and undersaturated alkaline intrusions to be distinctly different in chemical composition. In oversaturated rocks the dominant member of the group is astrophyllite, *sensu stricto*. It occurs as a late-stage postmagmatic phase, enriched in Rb, Fe^{2+}, Ti, Si and F. Only samples from Gjerdingen (Norway) and Point of Rocks (New Mexico, USA) show enrichment in the kupletskite component. In contrast, undersaturated

intrusions, in particular MSH, show the greatest species diversity and range in chemical composition. Kupletskite subgroup samples are enriched in Na, Mn, Fe^{3+}, Zn, Zr and Nb, whereas astrophyllite subgroup samples are enriched in K, Ca, Fe^{2+}, Ti, Zr and Al. Enrichment of kupletskite subgroup samples in Fe^{3+}, Mn and Nb suggests crystallization under more oxidizing conditions than those of the astrophyllite subgroup. Incorporation of Nb into the astrophyllite group structure and the formation of Nb-bearing kupletskite and niobokupletskite are the result of the oxidizing substitution $M(1)^{2+} + M(2,3)^{2+} + (Zr,Ti) + F \Leftrightarrow {}^{M(1)}Na + {}^{M(2,3)}Fe^{3+} + Nb + O$. Additional substitutions include K $\Leftrightarrow$ (Cs,Rb), Si+Na $\Leftrightarrow$ Al+Ca, Ti $\Leftrightarrow$ Nb, Ti $\Leftrightarrow$ Zr, Mn $\Leftrightarrow$ Fe^{2+}, (Mg,Zn) $\Leftrightarrow$ (Mn,Fe^{2+}) and (Mn,Fe) $\Leftrightarrow$ Na. Astrophyllite group minerals from Mont Saint-Hilaire have the widest crystal-chemical diversity with five documented species (Ast, Kpt, Nbkpt, Zrt, and Fe-Zrt).

1.0. INTRODUCTION

Astrophyllite, *sensu stricto*, is a Fe-dominant alkali titanosilicate first discovered in a nepheline syenite pegmatite on the island of Låven, in the Larvik complex of the Oslo Rift Valley, southeast Norway, by Weibye in 1844 and later described in detail by Brøgger (1890). There are now eight species of astrophyllite group minerals (AGM), the most recent of which, niobokupletskite, recently described from Mont Saint-Hilaire (MSH; Piilonen *et al.* 2000). Astrophyllite group minerals have been described from many alkaline intrusions, most commonly as accessory or rock-forming minerals in quartz or nepheline syenites, alkaline granites, and their associated pegmatites, but also from metamorphic rocks such as nepheline syenite gneiss and riebeckite gneiss. Members of the astrophyllite group have been documented at the following localities: Mont Saint-Hilaire, Mont Royal and the Saint Amable sill (Québec, Canada; *e.g.* Martin 1975, Mandarino & Anderson 1989, Horváth & Gault 1990, Wight & Chao 1986), the McGerrigle plutonic complex (Gaspé, Québec; Wallace *et al.* 1990), Burpala, Dara I Pioz, the Azov region, and the Khibina and Lovozero massifs of the Kola Peninsula (Russia; Semenov 1956, Valter *et al.* 1965, Portnov & Rastsvetayeva 1966, Ganzeyev *et al.* 1969, Shi *et al.* 1998), Illimaussaq, Kangerdlugssuaq, Narssarssuk and the Werner Bjerge complex (Greenland; Brooks *et al.* 1982, Layne *et al.* 1982, Christiansen *et al.* 1998, Christiansen 1999), Zomba-Malosa (Malawi, Africa; Wooley & Platt 1988), Mount Rosa, Pikes Peak (Colorado, USA; Gross & Heinrich 1966), Hurricane Mountain (New Hampshire, USA; Dr. C. Francis, *pers. commun.*), Strange Lake, Seal Lake and Letitia Lake (Labrador, Canada; Nickel *et al.* 1964, Birkett *et al.* 1996), Mount Gharib (Egypt; Abdel-Rahman 1992), Northwest Spain (Floor 1961), the Gjerdingen intrusion

(Norway; Raade & Haug 1982), and Finland (Eskola & Sahlstein 1930).

Following Brøgger's original description in 1890, there have been relatively few detailed crystal-chemical studies of the astrophyllite group. The crystal structure of magnesium astrophyllite was first determined by Peng & Ma (1963) and the structure of triclinic astrophyllite (*sensu stricto*) was later determined by Woodrow (1967) who described it as a layered titanosilicate with strong affinities to biotite. Until recently, most analyses of AGM present in the literature were done as part of larger studies on the petrogenesis of the alkaline complexes in which they occur.

Ganzeyev *et al.* (1969) were among the first researchers to specifically investigate the isomorphous substitution of alkali cations such as Rb, Cs and Li for K in the interlayer. Similarly, Chelishchev (1972) did the only known experimental work on AGM, examining the ion exchange properties K with Na, Rb and Cs under supercritical conditions (400 to 600 °C). Results from this study indicate increasing K $\Leftrightarrow$ Na substitution with increasing temperature, with high temperatures (600 °C) favoring exchange of Rb and Cs for K.

MacDonald & Saunders (1973) produced the first extensive compilation of chemical analyses of AGM from a variety of intrusions and attempted to correlate chemical composition with paragenesis. Results from this study indicated AGM from undersaturated rocks to be characterized by higher Al, Ca, Mg, Mn, OH, F, K, Na and Zr compared to AGM from oversaturated rocks. No attempt was made to distinguish between Mn-dominant species and Fe-dominant species which display strongly contrasting chemical characteristics within a single petrogenetic environment.

Layne *et al.* (1982) did electron-microprobe analyses on astrophyllite from over- and

undersaturated pegmatite dikes at Bagnæsset and Kramers Island, Kangerdlugssuaq (East Greenland) and were the first to document a correlation between astrophyllite composition, habit and paragenesis. Tabular crystals of astrophyllite from the oversaturated dike were found to be enriched in Si, Ti, Fe, K and Na relative to prismatic, acicular astrophyllite crystals from the undersaturated dike.

Abdel-Rahman (1992) studied astrophyllite from peralkaline granites and associated metasomatized wallrocks of the Mount Gharib intrusion (Egypt, Africa) and concluded that astrophyllite is the product of a metasomatic reaction, forming at the expense of arfvedsonite.

Christiansen (1998) studied the chemical variations in a suite of AGM from various localities in Greenland and did a single crystal X-ray structure refinement on kupletskite from Kangerdlugssuaq (Christiansen *et al.* 1998).

Regardless of the number of analyses done by various authors, considerable debate still exists regarding the anionic scheme, calculation of the general formula, and AGM chemical variation trends between over- and undersaturated alkaline intrusions. This paper presents the results of an extensive study on the chemical variations observed in AGM from a large number of over- and undersaturated alkaline intrusions (Table 1), the geological setting and sample descriptions for which can be found in Chapter I. The main objectives of this study were to (1) establish a systematic crystal-chemical nomenclature for the astrophyllite group, and (2) describe the chemical variations observed in AGM, particularly with respect to Na, Mn, Fe, Zn, Mg, Ti, Zr, Nb and F, between different parageneses and localities. This is the first in a series of papers dealing with the crystal chemistry and paragenesis of AGM; details regarding crystal structure variations, Mössbauer spectroscopy, and paragenesis can

TABLE 1. LOCALITY INFORMATION FOR ASTROPHYLLITE GROUP MINERAL SAMPLES IN THIS STUDY

Sample code	Sample (Collection) #	Locality and rock type
AFR		Zomba-Malosa, Malawi, Africa
	AFR1 (OVP)	- granitic pegmatite
EGY		Mount Gharib, Egypt, Africa (analyses from Abdel-Raman, 1992)
	R1200	- peralkaline granite
	R3090	- metasomatized wallrock, peralkaline granite
GJER		Gjerdingen intrusion, Norway
	NOR3 (RW-3)	- alkali granite
GREEN		Various locations, Greenland (analyses taken from Christiansen, 1999)
	CC4	- granitic pegmatite, Astrophyllite Island, Kangerdlugssuaq
	CC7AB	- nepheline syenite pegmatite, Bagnæsset, Kangerdlugssuaq
KHIB		Khibina massif, Kola Peninsula, Russia
	RUS1	- nepheline syenite pegmatite
	RUS3 (CMNMI-44135)	- trachytic nepheline syenite
	RUS6 (CMNMI-53309)	- nepheline syenite pegmatite
LAB		Letitia Lake, Mann #1, Labrador, Canada
	LAB2 (GSC-62047)	- peralkaline nepheline gneiss
LANG		Langesundsfjord area, Oslo Rift Valley, Norway
	NOR1 (RW-1)	- nepheline syenite pegmatite (Vesle Arøya)
	NOR10 (AOL-3)	- nepheline syenite pegmatite (Saga I Quarry, Morje)
	NOR14 (AOL-7)	- nepheline syenite pegmatite (Bratthagen, Lagendalen)
LOV		Lovozero massif, Kola Peninsula, Russia
	RUS9 (HC-1048)	- nepheline syenite pegmatite (Lephke-Nelm)
LUKS		Luksefjell, Norway
	NOR21 (AOL-11)	- alkali granite pegmatite
MSH		Mont Saint-Hilaire, Québec, Canada
	MSH2 (NMNS-4)	- nepheline syenite pegmatite
	MSH3 (NMNS-5)	- nepheline syenite pegmatite
	MSH7 (NMNS-11)	- nepheline syenite pegmatite
	MSH10AB (NMNS-14)	- nepheline syenite pegmatite
	MSH18AB (NMNS-25)	- altered nepheline syenite pegmatite
	MSH19AB (NMNS-26)	- altered nepheline syenite pegmatite
	MSH20 (NMNS-27)	- nepheline syenite pegmatite
	MSH29 (CMNMC)	- metasomatic unit
	MSH31 (CMNMC-F882)	- natrolite pegmatite
	MSH42*	- nepheline syenite pegmatite
	MSH44	- sodalite syenite
	MSH45	- sodalite syenite xenolith
POR		Point of Rocks, New Mexico, USA
	US9 (HDL)	- nepheline syenite
PP		Mount Rosa, Pikes Peak, Colorado, USA
	US1 (CMNMI-44288)	- granitic pegmatite

CMNMC/CMNMI/NMNS = Canadian Museum of Nature collection, GSC = Geological Survey of Canada collection, OVP = O.V. Peterson collection, RW = R. Werner collection, CC = C. C. Christiansen collection, AOL = A.O. Larsen collection, HC = L. Horváth collection, HDL = H. DeLinde collection

* Holotype niobokupletskite

be found in Chapters II, III and VII, respectively.

2.0. Analytical Methods

2.1. Electron microprobe analysis

A total of 659 electron microprobe analyses (EMPA) were done on a JEOL 733 electron microprobe, operating in wavelength-dispersive mode, using Tracor Northern 5500 and 5600 automation software. The operating conditions were as follows: beam diameter of 20 μm, operating voltage 15 kV and a beam current of 20 nA. Data reduction was performed using a PAP routine in XMAQNT (*pers. commun.*, C. Davidson, CSIRO). A total of 24 elements were sought and the following standards were employed: Na-amphibole (Na$K\alpha$ and Si$K\alpha$), sanidine (K$K\alpha$ and Al$K\alpha$), diopside (Ca$K\alpha$ and Mg$K\alpha$), tephroite (Mn$K\alpha$), almandine (Fe$K\alpha$), rutile (Ti$K\alpha$), synthetic $MnNb_2O_6$ (Nb$L\alpha$), vlasovite (Zr$L\alpha$), zincite (Zn$L\alpha$), phlogopite (F$K\alpha$), pollucite (Cs$L\alpha$), celestite (Sr$L\alpha$), sanbornite (Ba$L\alpha$), Rb-microcline (Rb$L\alpha$), synthetic $NiTa_2O_6$ (Ta$M\alpha$), and hafnon (Hf$M\alpha$). Count times for all elements were 25 seconds or 0.5% precision, whichever was obtained first, except for Cs and Rb (100 s), and Hf (50 s). Overlap corrections for Si($K\alpha$)-Sr($L\alpha$), Zr($L\beta$)-Nb($L\alpha$) and Mn($K\beta$)-Nb($L\alpha$) were performed. Also analyzed for but not detected were Cl, La, Ce, Yb, P, Th, Pb, Ni, V, U, W, Sc, S and Mo.

Many of the AGM crystals, in particular those from MSH, show extensive chemical zoning when viewed in back-scattered electron images (BSEI). An attempt was made to analyze the composition of all the zones at a scale of > 20 μm. It was not possible to analyse smaller zones due to constraints on the beam diameter; analyses performed with beam

diameters < 20μm resulted in extensive volatilization of the sample.

2.1.1. The effects of electron-beam diameter during EMP analyses

During the course of the study it was noted that EMPA of AGM typically produced low analytical totals (≈ 96 to 98 wt.%) with a standard defocused 20 μm diameter beam. It was suspected that decomposition of the sample and migration of light elements such as Na and Si could be responsible for these low totals. Migration and volatilization (*i.e.* burn-up) of alkali elements and Si under the electron beam, the result of beam-induced heating and charging effects, have been noted by many authors in minerals, their synthetic analogues and glasses, particularly in K and/or Na-bearing silicates (Nielsen & Sigurdsson 1981, Autefage & Fontan 1985, Roberts *et al.* 1990, Spray & Rae 1995, Cooper *et al.* 1998, McDonald *pers. comm.*). A study was done to further investigate electron beam effects on the composition of AGM, the results of which are presented below.

Decomposition of AGM with respect to time at a fixed beam diameter was first investigated. Two separate samples were chosen for analysis on the basis of chemical homogeneity and lack of inclusions: NOR3, a kupletskite from the Gjerdingen intrusion, Norway, and RUS1, an astrophyllite from the Khibina massif, Kola Peninsula, Russia. The three elements most likely to undergo volatilization or migration, Si, Na, and K, were analyzed at three second intervals for a total of 105 s. Results of this study are presented in Figure 1. It can be concluded that volatilization of these elements during the specified time-period and operating conditions is insignificant at the 3σ level and can therefore be ruled out as a potential cause of low analytical totals. Previous work on AGM (T.S. Ercit *pers.*

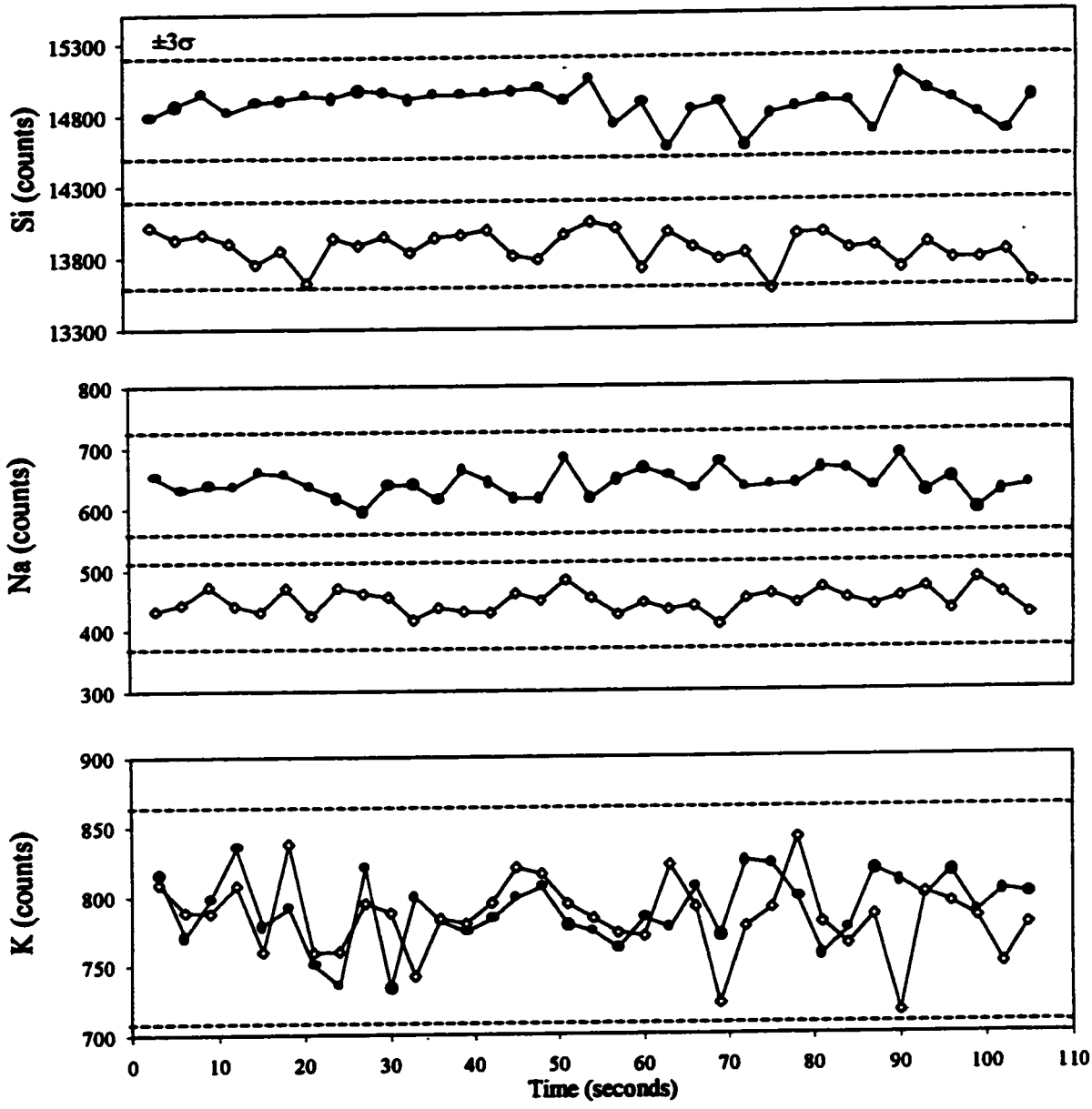

Figure 1. Decomposition curves for kupletskite (closed circles) and astrophyllite (open diamonds). Dased lines indicate ± 3σ for each sample.

commun.) using both a point-focused and a 20 μm defocused beam over a period of 360 s indicates decomposition of Si, Na and K with only the point-focused beam.

In cases where volatilization is a factor, defocusing the electron beam can help retard the amount of decay. Increasing the diameter of the electron beam results in an increased interaction volume, thus decreasing the actual beam flux (proportional to the beam-current ratio:beam-diameter ratio). To ensure that all chemical variations observed were responses to changes in analytical conditions, a single sample, NOR5 (astrophyllite, Barkevik, Langesundsfjord area, Norway), was chosen for analysis, on the basis of (1) the compositional homogeneity of the crystals, (2) lack of inclusions, and (3) large grain size, the latter allowing for multiple analyses at varying beam diameters on a single crystal. Data were obtained under identical analytical conditions through a range of beam diameters from 5 to 50 μm using 5 μm increments. Corrections (PAP) were not done on the results as this would lead to analytical error by compensating for the apparent increase or decrease of the unmobilized elements and yielding incorrect values (Spray & Rae 1995). Five points were analyzed at each beam diameter on crystals mounted both perpendicular and parallel to the (001) cleavage. Averaged counts are shown as a function of beam area in Figures 2 through 4.

Results indicate that Si is most strongly affected by the change in beam diameter. For analyses both perpendicular and parallel to the (001) cleavage, Si counts decrease as beam area increases: 3.4 % perpendicular to cleavage and 4.6 % parallel to cleavage (Figs. 2A & B). Neither Na nor K show significant variation, remaining statistically constant ($\pm 3\sigma$) throughout the range of beam diameters (Figs. 3 & 4). The most probable explanation for

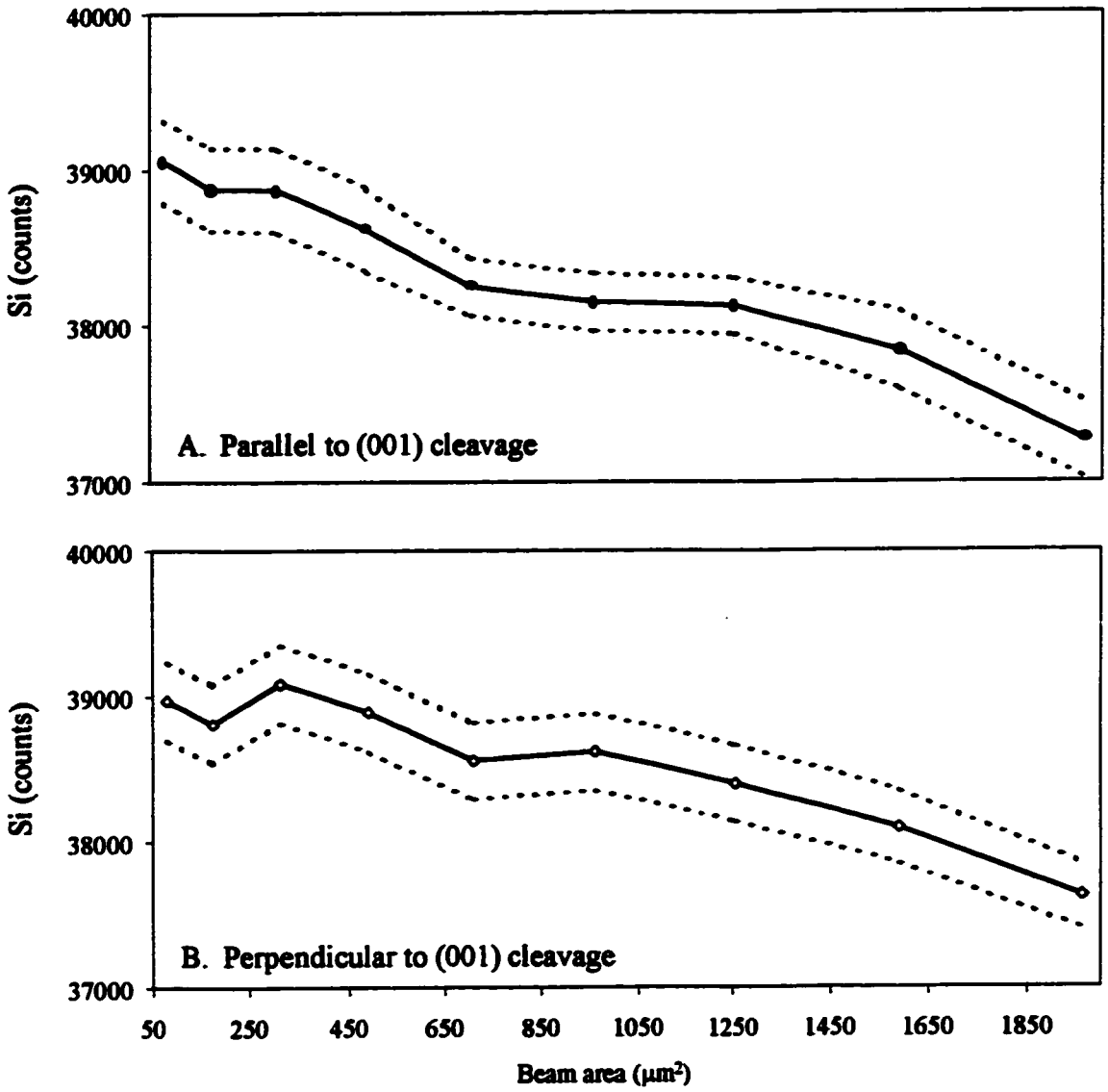

Figure 2. Decomposition of Si with respect to beam area. Dashed lines indicate ± 3σ.

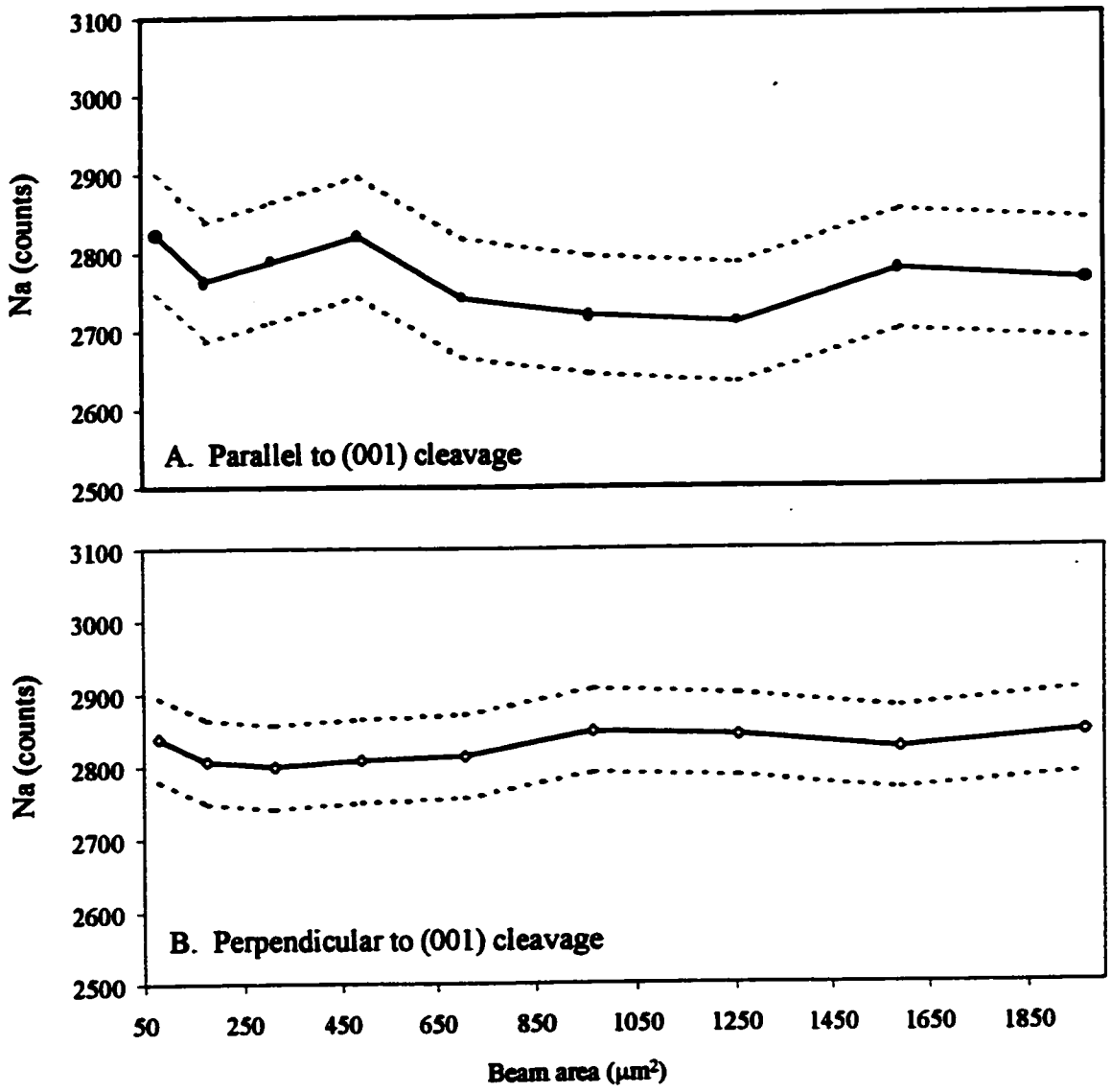

Figure 3. Decomposition of Na with respect to beam area. Dashed lines indicate ± 3σ.

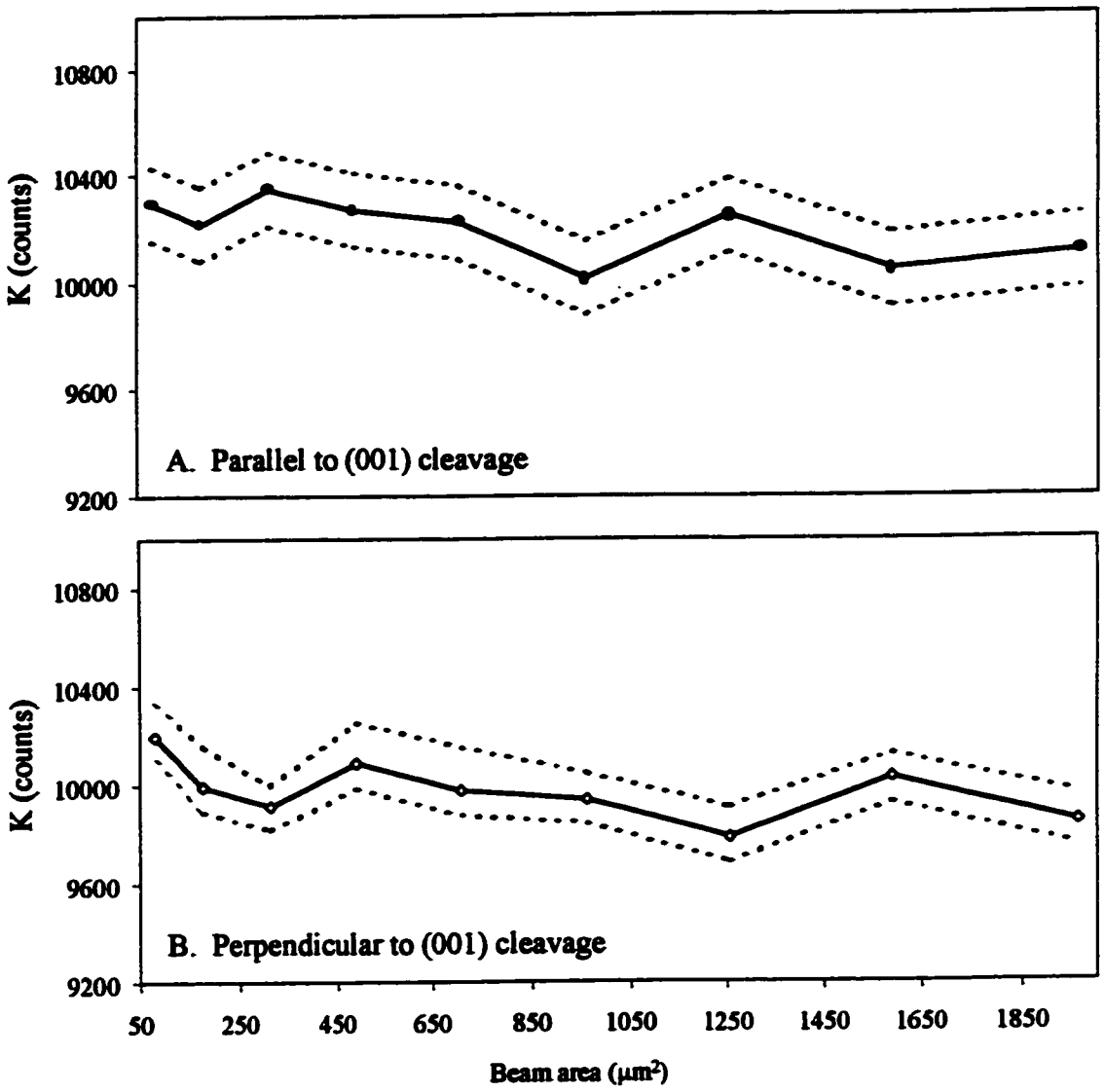

Figure 4. Decomposition of K with respect to beam area. Dashed lines indicate ± 3σ.

these results is alkali volatilization. As both Na and K occur in concentrations a magnitude lower than Si in AGM analyses; a 4 % fluctuation in counts may not be detectable due to the relatively larger standard deviations ($1\sigma = 2$ %) of the alkalis. However, a decrease in the number counts for K and Na will artificially increase the apparent counts for the other elements; as Si is the dominant element in AGM analyses, it will be most strongly affected. A 4 % reduction in counts for both K and Na accounts for a reduction of approximately 0.08 and 0.04 *apfu* for these elements, respectively. Volatilization of these elements is noted, but correction factors have not been applied to the data, as factors other than alkali volatilization may also be playing a role in the production of low analytical totals.

Although analytical totals for the majority of our AGM are < 100 % (≈ 95 to 98 %), the resultant cation sums are excellent (≈ 19.85 to 20.00 *apfu*). The fact that these sums are close to ideal suggests that the low totals are not entirely the result of errors in the experimentally determined Na_2O+K_2O contents, or that instrument calibration was inadequate, but that the counts for all the elements analyzed are depressed. The cause of the low totals is therefore likely due to a combination of factors which may or may not include: (1) standard selection, (2) differing conditions of carbon coating of samples and standards, (3) micron-sized scratching of the grains, (4) plucking of crystals out of the epoxy mount, (5) sample charging, or (6) the presence of undetected structural water or adsorbed water, either on the surface or in the interior of the crystals. The last factor is thought to be the largest contributor to the observed low oxide totals; interpretation of Fourier-transform infrared (FTIR) spectra and thermal gravitational analysis (TGA) has confirmed the presence of adsorbed water in all AGM (~ 0.2 wt. %). Analysis of such grains by EMPA will result in

analytical totals less than ideal, but as the adsorbed water is not structural, empirical formula calculations will still yield excellent cation sums.

2.2. ICP-AES analyses for Li

A suite of 15 samples from MSH were analysed for Li using ICP-AES (inductively-coupled plasma atomic emission spectroscopy). Samples were ground in a mortar and pestle, weighed (range: 6.1 to 81.0 mg depending on availability of material), and rinsed with deionized water. Digestions were done as follows: 5 mL of hydrofluoric acid was added to each sample and allowed to digest for one hour at room temperature (RT). Nitric acid (2 mL) and perchloric acid (1 mL) were then added to the solution and allowed to further digest for 24 hours (RT). An additional 5 mL of hydrofluoric acid, 2 mL nitric acid, and 1 mL perchloric acid were added to the solution and left to further digest the residual for one hour on a hot plate until all the liquid had evaporated. The final residum was mixed with 3 mL hydrochloric acid in a volumetric flask and filled to 25 mL with deionized water to be analysed by ICP-AES. Three standards were used during the analysis procedure: SY-3 (syenite rock, 92 ppm Li), MRG-1 (Mount Royal gabbro, 4.2 ppm Li) and Mica-Fe (1200 ppm Li). Lithium contents in the AGM studied range from 42.7 to 453.3 ppm.

2.3. Fourier-transform infrared spectroscopy

Fourier-transform infrared (FTIR) spectroscopy was done on selected samples in order to evaluate the presence of OH^- and to ascertain whether species such as H_2O or CO_3^{2-} are present. Samples were handpicked under the binocular microscope and then ground

under acetone in a mortar and pestle to a coarse powder (~ 20 μm). All analyses were performed on a Bomem Michelson MB-100 Fourier transform infrared spectrometer equipped with a mercury cadmium telluride (MCT) detector, at the Canadian Conservation Institute (Ottawa, Canada). A small mass of powder was mounted in a diamond-anvil microsample cell and pressure was applied to crush the sample further, thus causing it to disperse as a randomly-oriented powder. The diamond cell was then positioned in the microbeam chamber of the spectrometer. A room-temperature spectrum was collected from 4000 to 400 cm^{-1} using the spectrum of the empty diamond anvil cell collected with the same parameters as a reference.

The absorbance spectra of all AGM examined show broad peaks in the high-frequency range (4000 to 1000 cm^{-1}) attributable to O-H stretching (≈ 3600 cm^{-1} and an associated shoulder centered at ≈ 3300 cm^{-1}), adsorbed H_2O (≈ 3400 cm^{-1}), and a weak peak at ≈1650 cm^{-1} attributable to H-O-H bending of absorbed or molecular H_2O (Farmer 1974). Some of the spectra show a small peak at 1900 cm^{-1} which may be attributed to molecular H_2O. The middle- to lower-frequency end of the spectrum (1000 to 400 cm^{-1}) is characterized by symmetric Si-O stretching (≈ 1000 cm^{-1}) and bending (≈ 690 and 650 cm^{-1}) bonds. The two niobokupletskite samples (MSH10B and MSH42) show one asymmetric Si-O stretching band (≈ 965 cm^{-1}), whereas samples which are Ti-dominant have two prominent Si-O stretching bands (≈ 1050 and 960 cm^{-1}). Low-frequency bands between 400 and 450 cm^{-1} can be attributed to (Mn,Fe)-O stretching (Farmer 1974). Infrared spectra for a suite of representative AGM are shown in Figure 5.

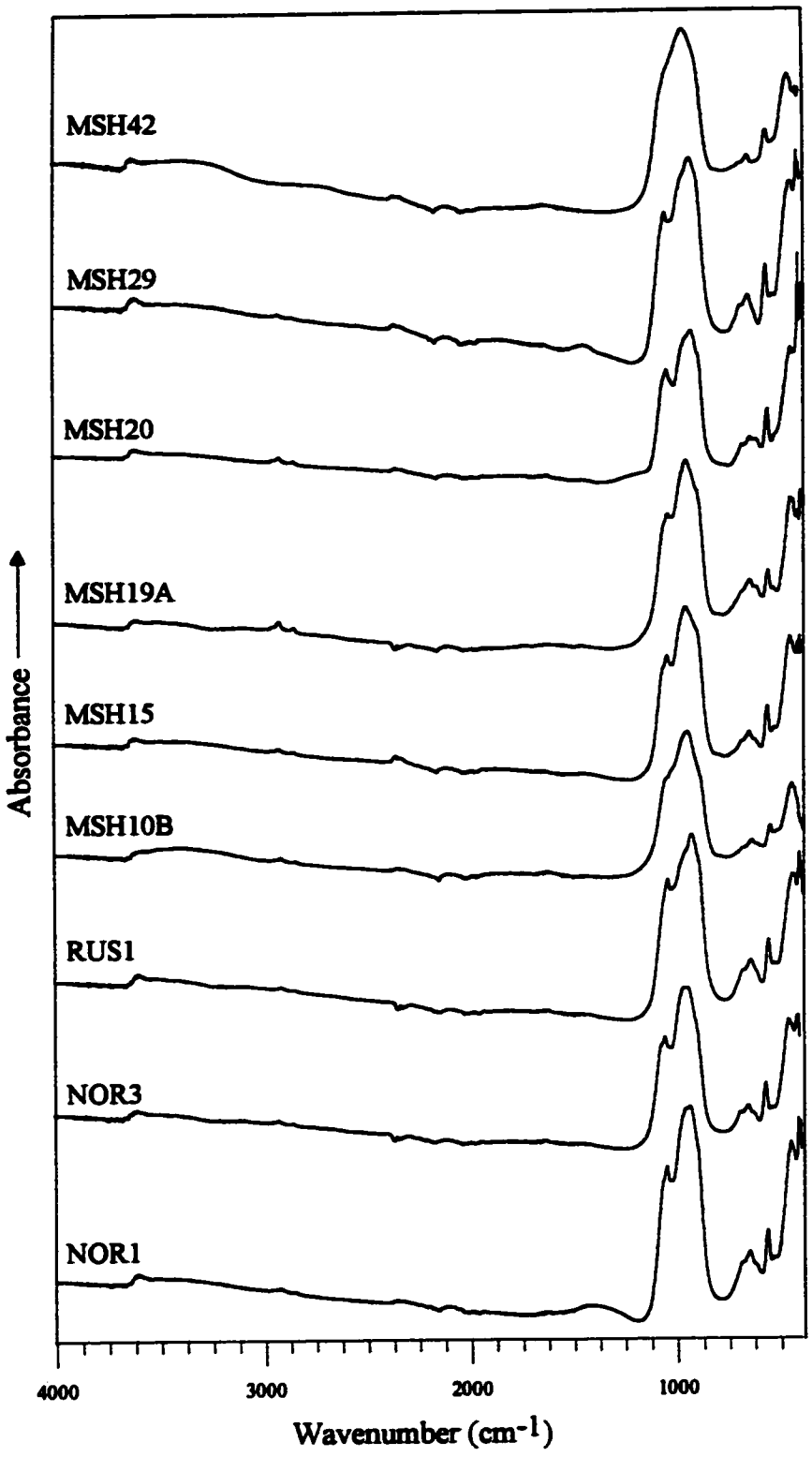

Figure. 5. FTIR absorbance spectra for representative AGM.

2.4. Nuclear reaction analysis

Nuclear reaction analysis (NRA) is a technique that has the ability, unlike most other methods, to accurately determine hydrogen contents in solids with a sensitivity on the order of 10 ppm. Nuclear reaction analysis employs MeV ion beams to induce nuclear reactions, in a solid materials (Cohen *et al.* 1972). All NRA analyses on AGM were performed by Dr. D.J. Cherniak at the Department of Earth and Environmental Sciences at Rensselaer Polytechnic Institute (Troy, NY, USA).

The most common ion beam used for hydrogen determination is ^{15}N, using the reaction:

$$^{15}N + {}^{1}H \Rightarrow {}^{4}He + \gamma\text{-ray} \quad (1).$$

A beam of ^{15}N ions is used to bombard the sample and the number of characteristic γ-rays produced (*i.e.* those that achieve resonance of 6.385 MeV) are measured. The γ-rays are detected by a scintillation detector located approximately 2 cm behind the sample. The number of γ-rays produced is directly proportional to the number of H atoms on the surface of the sample. Conversion of raw counts to H contents (H/cm^2) is given by

$$\text{H content} = KY\,\partial E/\partial x \quad (2)$$

where Y is the γ-ray yield (counts/concentration of incident ions), K is an experimental constant independent of the material being analysed, and $\partial E/\partial x$ is the energy loss of the incident ion beam (Lanford 1992). Increasing the energy of the beam allows for analysis of the sample at depth such that as the higher energy beam loses energy through surface-level collisions, resonance can only occur at increasing depth. In this way, depth profiling of H can be accomplished (Lanford 1992). For the purpose of determining H contents in AGM,

an average H content was measured assuming an average density of 3.2 g/cm^3.

Results from NRA give a range of 4.4 to 7.4x10^{21} H/cm3, corresponding to 3.1 to 5.0 H *apfu*, respectively. The range in H contents can be primarily explained by the two anion substitutions $F^- \Leftrightarrow OH^-$ and $F^- \Leftrightarrow O^{2-}$, and the chemical heterogeneity that is inherent in the samples studied.

2.5. Thermal decomposition and thermal gravitational analyses

Five samples of AGM were studied by a combination of thermal decomposition and thermal gravitational analyses (TGA). Thermal decomposition analysis (duplicate or triplicate) was done at Norsk Hydro ASA (Research Centre Porsgrunn, Norway) on a LECO RC-412 multiphase analyzer using 0.07 to 0.12 g of sample. Samples were heated in an oxygen combustion chamber to 1000 °C and the quantity of expelled water was detected using a FTIR spectrometer and calibrated using known standards. The range of measured H_2O contents given by thermal decomposition is 3.55 to 3.99 ± 0.1 wt. % H_2O, approximately 1 to 1.5 wt.% higher than calculated H_2O values. Thermal gravitational analysis of the same samples indicated that ~ 0.2 wt.% H_2O is given off below 105 °C, whereas the majority of the water was lost between 120 °C and 850 °C. The gradual loss of H_2O over a wide range of temperatures indicates that bond strengths to the H_2O groups are quite variable, suggesting that it may be adsorbed on surfaces or weakly bonded in the interlayer. The small molecular water component (1 to 1.5 wt.%) does not appear to be important on a structural level and was not detectable during single-crystal *X*-ray structure refinements.

2.6. Mössbauer spectroscopy

Until recently, Fe^{3+} was thought to be a minor component in AGM, a conclusion based primarily on wet-chemical determinations (MacDonald & Saunders 1973) and charge-balance calculations. Non-standardized anionic schemes and the presence of vacancies complicates the calculation of Fe^{2+}/Fe^{3+} ratios in AGM. Iron-bearing mineral inclusions are common in AGM (*e.g.* pyrochlore group minerals, oxides and phosphates; Plates 1 & 2), which also limit the possibility of obtaining reliable Fe^{2+}/Fe^{3+} ratios by wet-chemical methods yet yield Mössbauer spectra which are significantly different from those observed for AGM. Mössbauer spectroscopy was used in an effort to determine Fe^{2+}/Fe^{3+} ratios, while at the same time providing information on the coordination number of both Fe^{2+} and Fe^{3+} in the structure, and variations in the local electronic environment around the Fe cations. Results presented here pertain only to the Fe^{2+}/Fe^{3+} ratios as they apply to the chemical variations observed in the astrophyllite group; a detailed discussion of the ^{57}Fe Mössbauer spectroscopy of AGM is presented in Chapter IV. Details concerning the collection of Mössbauer data can also be found in Chapter IV.

Samples studied by Mössbauer spectroscopy have Mn# [$Mn/(Mn+Fe_{tot})$] which range from 0.10 to 0.81. While a wide variation in chemical composition between the samples has been noted, the Mössbauer spectra of all AGM examined are remarkably similar. The spectra display two strong absorption peaks centered at ≈ -0.1 and 2.3 mm/s and a third, weaker shoulder at ≈ 0.9 mm/s which respectively correspond to (1) the sum of the low-energy lines from $^{[6]}Fe^{2+}$ and $^{[6]}Fe^{3+}$ doublets, (2) the high-energy lines from $^{[6]}Fe^{2+}$ doublets,

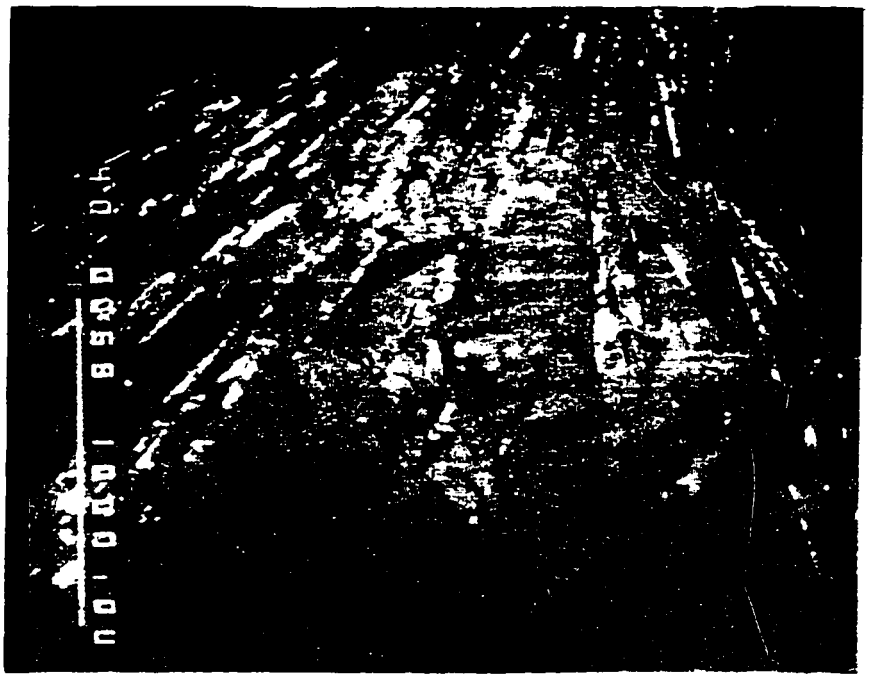

Plate 1. Back-scattered electron image of pyrochlore inclusions (white) in Nb-bearing kupletskite (grey) from MSH. Scale bar: 1000 μm

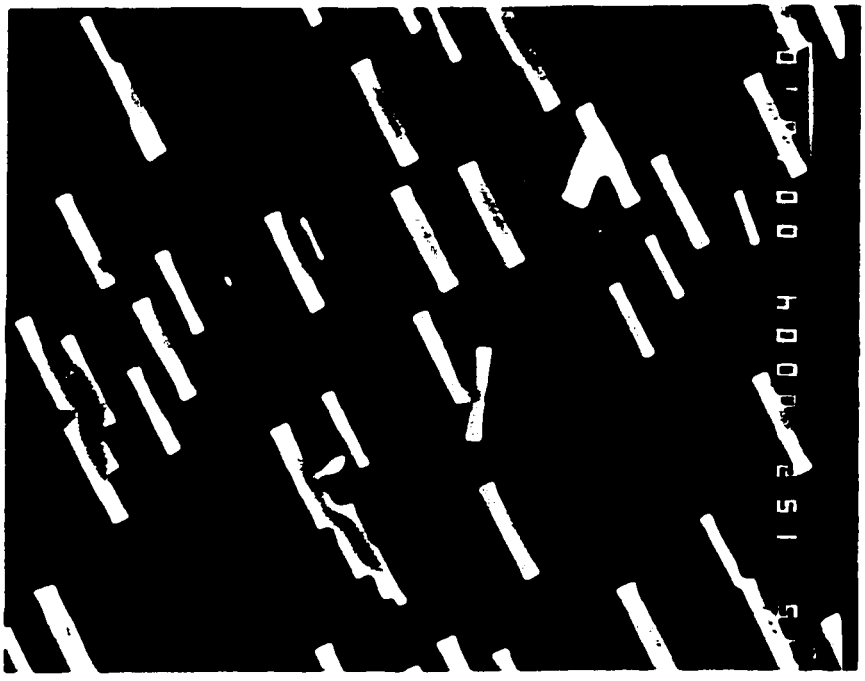

Plate 2. Back-scattered electron image of apatite inclusions (white) in kupletskite (grey) from MSH. Scale bar: 10 μm.

and (3) the high-energy lines from $^{[6]}Fe^{3+}$ doublets. Manning (1969) performed an optical spectroscopic study of an astrophyllite from St. Peter's Dome (Colorado, USA) and suggested that the observed pleochroism is the result of Ti^{3+}-Ti^{4+} intervalence electron transfer, rather than electron transfer between Fe^{2+} and Fe^{3+}. The lack of an absorption band at ~ 14,000 cm^{-1}, corresponding to an Fe^{2+}-Fe^{3+} electron transfer suggested that the two cations are not located in the same sheet and, as such, Manning (1969) proposed a $Fe^{3+} \Leftrightarrow Ti^{4+}$ substitution in *D*. Results from the Mössbauer spectroscopic study indicates that Fe^{3+} occurs only within the *O*-sheet (*C*) and does not substitute for the high field-strength elements (HFSE) in *D*. Furthermore, $^{[4]}Fe^{3+}$ does not appear to play a role in the AGM structure; the characteristic $^{[4]}Fe^{3+}$ contribution in mica spectra, occurring at ≈ 0.4 to 0.5 mm/s (Rancourt *et al.* 1992, Lalonde *et al.* 1996), is not observed in any of our spectra.

3.0. Overview of the Structure

The AGM structure (Fig. 6A and B) can be considered as two composite sheets stacked along [001] in a 2:1 ratio. The first is an *O*-sheet extending from $Z \approx 0.40$ to 0.60 in triclinic species and from $Z \approx -0.05$ to 0.05 in monoclinic kupletskite, which consists of a closest-packed sheet of MO_6 octahedra (where *M* = Mn, Fe^{2+}, Fe^{3+}, Mg or Na). There are four crystallographically distinct MO_6 *O*-sheet octahedra, designated *M*(1) through *M*(4). The *O*-sheet is sandwiched between two *H*-sheets, extending from $Z \approx -0.15$ to -0.05. The *H*-sheets consist of open-branched *zweier* [100] single chains of $[Si_4O_{12}]^{8-}$ (Liebau, 1985) which are in turn cross-linked by corner-sharing DO_6 octahedra, or DO_5 polyhedra as in magnesium astrophyllite (Shi *et al.* 1998), where *D* = Nb,Ti,Zr. The resultant Si:Ti ratio is 4:1.

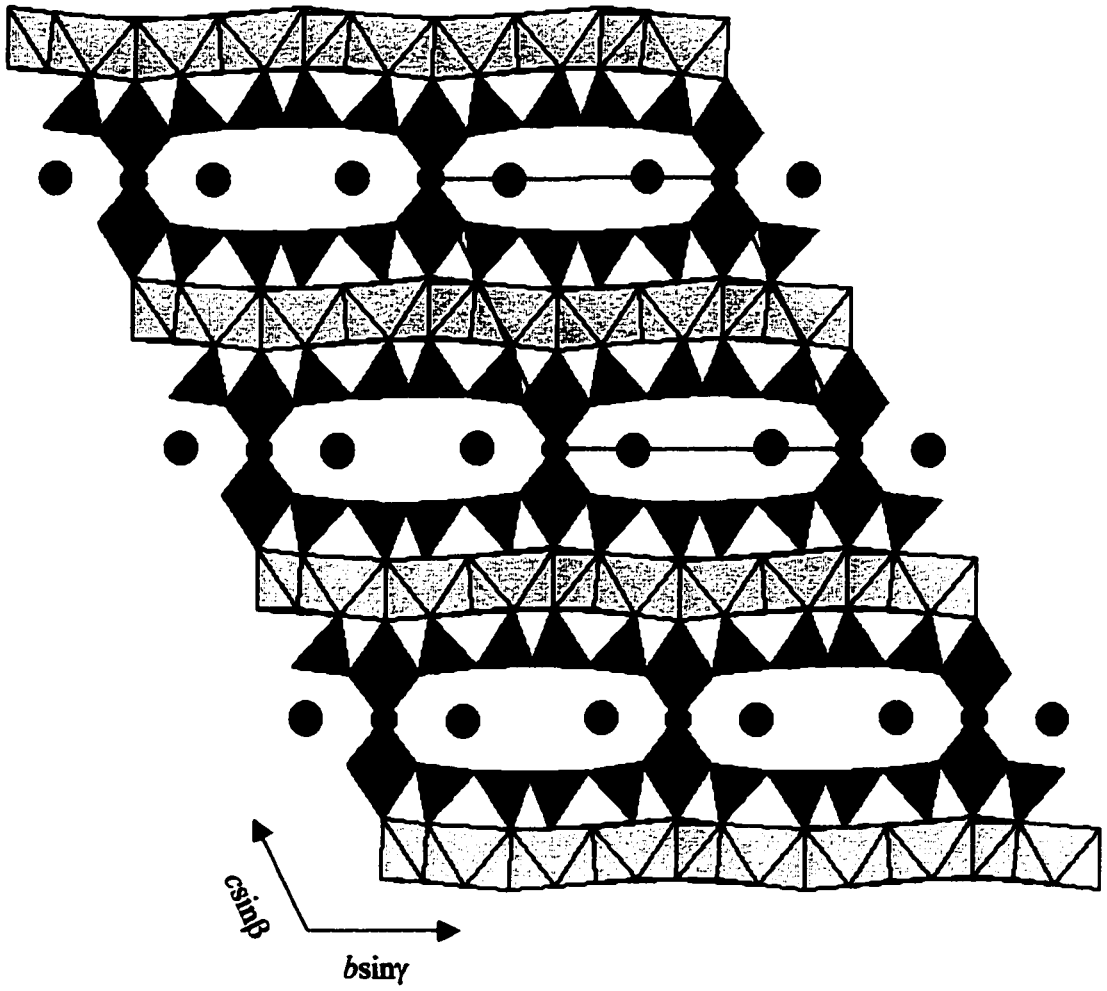

Figure 6A. Crystal structure of triclinic, $P\bar{1}$, AGM projected down [100] (unit cell outlined). *O*-sheet = yellow, *D* = blue, *T* = red, *A* = purple, *B* = green. The four *T* sites are indicated to show symmetry across the interlayer.

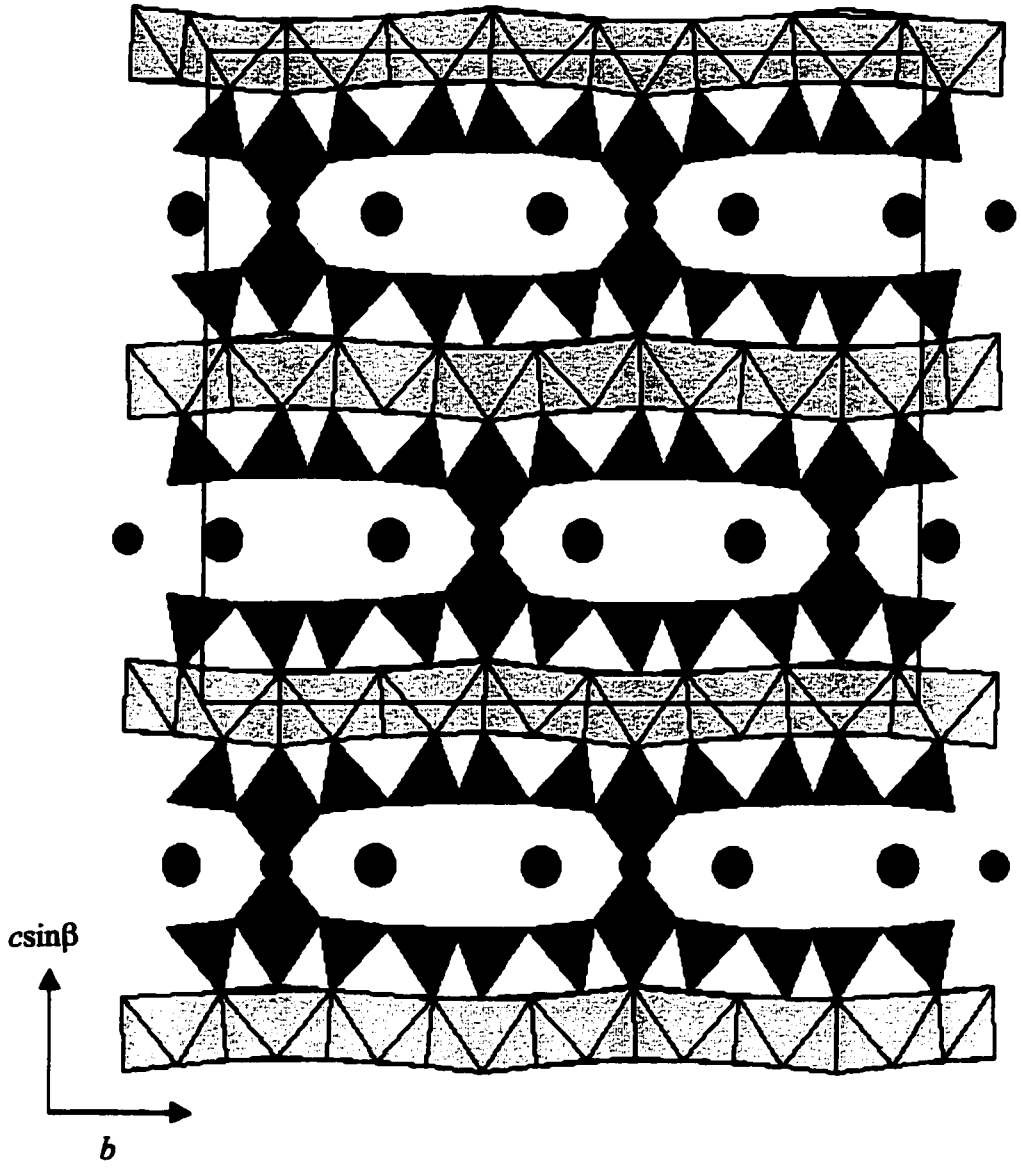

Figure 6B. Crystal structure of monoclinic, *C*2/*c*, kupletskite projected down [100] (unit cell outlined). *O*-sheet = yellow, *D* = blue, *T* = red, K = purple, Na = green. The four *T* sites are indicated to show symmetry across the interlayer.

Individual $D\phi_6$ octahedra are linked across the interlayer space *via* a common apical anion [$\phi(16)$, where ϕ = unspecified anion]. The interlayer space contains two crystallographically distinct cation sites, *A* and *B*, which are host to [11] to [13]-coordinated K and [10]-coordinated Na, respectively. Structural details of the astrophyllite group will be discussed in Chapter III.

4.0. Astrophyllite Group Nomenclature and a Standardized General Formula

4.1. Previous work

There has been little consensus among researchers regarding the correct general formula for AGM. In fact, some workers have considered AGM to be "non-stoichiometric" due to the presence of vacancies and cation sums regularly less than the ideal 20.00 *apfu*. The problem with defining a general formula for this group relates to a combination of slightly non-stoichiometric compositions exhibited by most samples (*i.e.* vacancies in the interlayer and a variable anion composition), a lack of complete and accurate chemical analyses, and a lack of in-depth single-crystal X-ray structure refinements on members of the group. The general formula currently accepted by most researchers is $A_3B_7C_2D_8X_{31}$, with formulae typically being calculated based on 31 (O+OH+F). However, a number of ideal anion compositions have been proposed including $X = 31$ (O,OH,F) (Woodrow 1967, Nickel *et al.* 1964,); 30 O (Layne *et al.* 1982); 27 O and 4 (OH,F) (Kapustin 1973); 26 O and 5 (OH,F) (MacDonald & Saunders 1973, Martin 1975, Abdel-Rahman 1992); 24 O and 7 (OH,F) (Layne *et al.* 1982); 26 O, 4 (OH) and F (Christiansen *et al.* 1998), and 26 O and 4 (OH,F) (Shi *et al.* 1998).

The most commonly accepted anion scheme used to calculate empirical formulae is 24 O and 7(OH,F). This scheme may have been used to compensate for the characteristically low analytical totals exhibited by most AGM; specifically calculation of formulae on the basis of 7 (OH,F) results in sums that are ≈ 2 wt.% higher relative to those calculated with 5(OH,F) (*i.e.* ~ 100 wt.% *versus* ~ 96-98 wt.%, respectively). However, resultant cation totals are deficient by as much as 0.50 atoms per formula unit (*apfu*; i.e. $\Sigma_{cations} < 20.00$).

The purpose of this study is to redefine the astrophyllite group on a crystal-chemical basis. This includes development of a standardized general formula and cation distribution scheme for the eight AGM described to date, and which will allow for compatibility with new species to be described in the future.

4.2. Results of the current study

4.2.1. Anionic scheme

Previously, direct measurement of the volatile contents in AGM, in particular H_2O, has been limited to TGA (Martin 1975) and wet-chemical analyses (MacDonald & Saunders 1973). In order to establish the anion composition of AGM, analyses of select samples were done by FTIR, NRA, TGA and thermal decomposition. Detailed results from these studies can be found in *Analytical Methods*. In addition, bond valence sum (BVS) calculations were done using data obtained from single-crystal X-ray structure refinements, the details for which can be found in Chapter III.

4.2.1.1. Anionic bond valence sums

Single-crystal X-ray structure refinements and bond valence calculations of 19 triclinic samples and of kupletskite-*Ma2b2c* indicate the presence of 13 sites in general positions occupied by divalent anions (BVS range: 1.842 to 2.140 *v.u.*), two sites in general positions occupied by monovalent anions [O(4) and O(5), BVS range: 0.985 to 1.177 *v.u.*], and a mixed valence site, $\phi(16)$ (where ϕ = unspecifed anion with a BVS range of 1.105 to 1.86 *v.u.*), known to contain both F and O as a result of the coupled substitution, $Ti + F \Leftrightarrow Nb + O$, proposed by Piilonen *et al.* (2000) for the incorporation of Nb into the astrophyllite group structure. The corresponding anionic scheme, based solely on results from single-crystal X-ray structure refinements, is $O_{26}(OH)_4(F,O,OH)$.

Calculations of BVS for the anions in the structure of magnesium astrophyllite (Shi *et al.* 1998) indicate 13 sites in general positions occupied by divalent anions [O(1) to O(13)], and two sites in general positions occupied by monovalent anions [O(14) and O(15)]. As F does not play a significant role in magnesium astrophyllite (F = 0.07 *apfu*, Shi *et al.* 1998), the two monovalent anions are assumed to be OH^-. The main difference between magnesium astrophyllite structure and that of other AGM is the presence of a TiO_5 tetragonal pyramid, unlike the $D\phi_6$ octahedra present in other species. The presence of such a coordination polyhedron results in the absence of one anion [*i.e.* a vacancy at $\phi(16)$] in the formula for magnesium astrophyllite relative to that of other AGM. As such, the corresponding anionic scheme for magnesium astrophyllite should be written $O_{26}(OH)_4\square$, rather than $O_{24}(OH)_4(OH,F)_2$ [as reported by Shi *et al.* (1998)] to conform to the general chemical formula proposed for AGM in this study.

4.2.2. Discussion

Given the above results, the general anionic scheme proposed for any AGM is $O_{26}(OH)_4(F,O,OH,\square)$. Given this, calculated H_2O contents should approach 3.00 wt.%, with an additional maximum F content of 1.00 wt.%. Direct determinations of volatile components by thermal decomposition indicate contents between 3.55 and 4.00 wt.%, attributable mainly to OH^-, although portions of these are known to include adsorbed, absorbed or molecular H_2O weakly bound in the interlayer. Results from TGA, which indicate $\Sigma(H_2O+F) \sim 4.00$ wt.%, and from NRA (3.9 - 5.0 *apfu* H) also support the anionic scheme 4(OH)(F,O,OH). No evidence exists in support of the currently accepted anionic scheme 7(OH,F), which would correspond to $\Sigma(H_2O+F) \sim 5.00$ wt.%..

4.2.3. Cationic composition

A total of 659 electron-microprobe analyses, 20 X-ray structure refinements, and 24 Fe^{2+}/Fe^{3+} determinations by Mössbauer spectroscopy have allowed us to examine all possible chemical variations in the astrophyllite group, and develop a standardized cation distribution scheme. The detailed crystal chemistry of each of the AGM structure components can be found in *Site Chemistry*; details given here are a summary of the site populations.

4.2.3.1. Interlayer

Results from single-crystal X-ray refinements indicate that *A* and *B* are crystallographically distinct two distinct interlayer sites are therefore recognized: $^{[10]\text{-}[13]}A$ and

$^{[10]}B$, which occur in a 2:1 ratio. Potassium is the dominant cation at *A*, with variable substitution of Cs, Rb and Sr. There is no evidence for H_3O^+, as suggested to be present in hydroastrophyllite (Hubei Geologic College 1974). The *B* site is host only to Na and Ca. Vacancies at *A* are common, with cation totals often as low as 1.71 *apfu* (ideally 2.00 *apfu*). There was no evidence for the presence of vacancies at *B*.

4.2.3.2. O-sheet (C)

The *O*-sheet in AGM contains four distinct octahedral sites, *M*(1) to *M*(4), in a 2:2:2:1 ratio (Σ_C = 7.00 *apfu*). The largest of the four octahedra, *M*(1), has been found to be occupied by Mn, Fe^{2+} and Na; *M*(2), *M*(3) and *M*(4) are occupied by Mn, Fe^{2+}, Fe^{3+}, Mg and Zn. There is no evidence for $^{[6]}$Al. Mössbauer spectroscopy indicates that all Fe occurs in the *O*-sheet, with Fe^{3+}/Fe_{tot} ratios ranging from 0.01 to 0.21, corresponding to 0.05 to 0.56 *apfu* Fe^{3+}.

4.2.3.3. H-sheet (D and T)

The *H*-sheet has the ideal composition $[(Ti,Nb,Zr)Si_4O_{12}]^{4-}$ and consists of open-branched *zweier* [100] single chains of $[Si_4O_{12}]^{8-}$ (Liebau 1985) which are in turn cross-linked by corner-sharing $D\phi_6$ octahedra in triclinic species and kupletskite-*Ma2b2c*, and by TiO_5 tetragonal pyramids in magnesium astrophyllite (Shi *et al.* 1998). There are four distinct *T* sites (Σ_T = 8.00 *apfu*) which are occupied dominantly by Si, with only minor Si ⇔ Al substitution. Mössbauer spectroscopy has indicated that Fe^{3+} is not present at the *T* sites of the AGM structure. Similarly, neither Fe^{2+} nor Fe^{3+} are found to occur at *D*, which is

occupied predominantly by Ti, Zr and Nb, with minor substitution of Hf and Ta ($\Sigma_D = 2.00$ *apfu*).

4.3. Proposed general formula for the astrophyllite group

The general formula proposed for any AGM, based on the results described above, is:

$$A_2BC_7D_2T_8O_{26}(OH)_4X_{0\text{-}1} \quad (3)$$

where $A = {}^{[10]\text{-}[13]}$K, Rb, Cs, Na, H_2O, □, and potentially H_3O^+; $B = {}^{[10]}$Na or Ca; $C = {}^{[6]}$Mn, Fe^{2+}, Fe^{3+}, Na, Mg, or Zn; $D = {}^{[6]}$Ti, Nb, or Zr; T = Si and Al, and $X = \phi$ = F, OH, O or □. Calculation of general formulae should be based on a total of 31 anions with 26 O and 5(OH,F,O,□). For magnesium astrophyllite, which has a vacant X site, the formula should be based on 30 anions with 26 O and 4(OH,F,O). To account for the variability in X in AGM resulting from the Ti + F ⇔ Nb + O substitution, two methods of formula calculation are proposed, depending on the Nb_2O_5 content of the analysis in question:

1. If $Nb_2O_5 < 5.00$ wt.% (≈ 0.5 *apfu* Nb), the formula should be calculated assuming 26 O and 5 (OH,F).

2. If $Nb_2O_5 > 5.00$ wt.%, the formula should be calculated assuming 26 O, 4 (OH) and one (F,O).

Considering results from single-crystal X-ray structure refinements and EMPA data, it is recommended that cations in the general formula be assigned to structural sites according to the following scheme:

i) Sum T to 8.00 using Si, then Al;

ii) Sum D to 2.00 using Ti, Nb, Zr, Ta and Hf;

iii) Sum *C* to 7.00 using Mn and Fe^{2+}, followed by Fe^{3+}, Mg, Zn, Ce, Y and Na;

iv) Sum *B* to 1.00 first with Ca, then with Na;

v) Sum *A* to 2.00 using excess Na from *C* and *B*, then K, Rb, Cs and Sr.

Type specimens of zircophyllite, cesium kupletskite and hydroastrophyllite could not be obtained for analysis and confirmation of their anionic scheme. Such species still have their formulae defined by 7 (OH,F) in the literature.

In the original description of zircophyllite (Kapustin 1973), the formula is given as

$$(K_{1.70}Na_{0.71}Mn_{0.35}Ca_{0.24})_{\Sigma=3.00}(Fe_{3.57}Mn_{3.43})_{\Sigma=7.00}(Zr_{1.58}Nb_{0.25}Ti_{0.17})_{\Sigma=2.00}$$

$$(Si_{7.76}Ti_{0.24})_{\Sigma=8.00}O_{24}[(OH)_{3.24}O_{2.84}F_{0.90}]_{\Sigma=6.98}\bullet 0.9H_2O. \quad (4)$$

The distribution of cations in this formula, in particular the presence of Mn in the interlayer and Ti at *T*, is inconsistent with our proposed scheme. The chemical analyses in the original description are incomplete; neither Al_2O_3 nor MgO, two important oxides in all AGM, were analysed for. This has the effect of creating an excess in cationic charge and thus higher overall cation sums at the *C*, *D* and *T* sites. As a result, Mn was assigned to the interlayer, an unconventional practice at best, and Ti to the *T* sites. Evidence in support of such site assignments has not been found in our study. Recalculation of the formula for zircophyllite, given the available chemical analyses and our proposed scheme, yields the following:

$$K_{1.67}(Na_{0.70}Ca_{0.23})_{\Sigma=0.93}(Fe_{3.52}Mn_{3.71})_{\Sigma=7.23}(Zr_{1.55}Ti_{0.40}Nb_{0.24}Hf_{0.08})_{\Sigma=2.27}$$

$$Si_{7.60}O_{26}(OH)_4(F_{0.88}OH_{0.12})_{\Sigma=1}. \quad (5)$$

It is important to note that zircophyllite has been described in the literature as the Zr-dominant end-member of a solid-solution series with astrophyllite. Calculation of the Mn# [Mn/(Mn+Fe_{tot})], using data from the analysis provided, yields a value of 0.51, indicating

that zircophyllite is Mn-dominant and therefore should be considered as the Zr-dominant end-member of a solid-solution series with kupletskite. At Mont Saint-Hilaire, zircophyllite occurs as 10 to 50 μm zones in Zr-rich kupletskite, whereas Fe-dominant zircophyllite occurs as extensively altered, acicular crystals, possibly after kupletskite or astrophyllite. The small size and poor crystallinity of these crystals made it impossible to collect single-crystal X-ray intensity data for either species. Table 2 lists the original and revised general formulae for AGM.

5.0. Site Chemistry

Table 3 lists representative EMP analyses and calculated formulae, based on the general formula proposed above, for 31 representative AGM. Due to the wide range of chemical compositions observed in the undersaturated category, samples have been further divided into two separate populations on the basis of their Mn# ($Mn/Mn+Fe_{tot}$): (1) Fe-dominant (FEU) or the *astrophyllite subgroup*, and (2) Mn-dominant (MNU) or the *kupletskite subgroup*. Figures 7 through 9 show the range in compositions observed in this study. The mean and range of compositions observed in the sample suite are presented in Figures 10A to 10C, values for which can be found in Table 4. Similar diagrams have been developed for each of the localities and are shown in Figures 11A to 11C.

5.1. Interlayer sites (A and B)

The *A* site(s) in all AGM studied are K-dominant. Potassium contents range from 1.35 to 2.07 *apfu*, with the astrophyllite subgroup samples from undersaturated localities

TABLE 2. MEMBERS OF THE ASTROPHYLLITE GROUP: ORIGINAL AND REVISED FORMULAE

Species	Original formula	Revised Formula
[1]Niobokupletskite	$K_2Na(Mn,Zn,Fe)_7(Nb,Zr,Ti)_2Si_8O_{26}(OH)_4(O,F)$	$K_2Na(Mn,Zn,Fe)_7(Nb,Zr,Ti)_2Si_8O_{26}(OH)_4(O,F)$
[2]Kupletskite	$(K,Na)_3(Mn,Fe^{2+})_7(Ti,Nb)_2Si_8O_{24}(O,OH)_7$	$K_2Na(Mn,Fe^{2+})_7(Ti,Nb)_2Si_8O_{26}(OH)_4F$
[3]Kupletskite-*Ma2b2c*	$K_2Na(Mn,Fe^{2+})_7Ti_2Si_8O_{26}(OH)_4F$	$K_2Na(Mn,Fe^{2+})_7Ti_2Si_8O_{26}(OH)_4F$
[4]Cesium kupletskite	$(Cs,K,Na)_3(Mn,Fe,Li)_7(Ti,Nb)_2Si_8O_{24}(O,OH,F)_7$	$(Cs,K)_2Na(Mn,Fe,Li)_7(Ti,Nb)_2Si_8O_{26}(OH)_4F$
[5]Astrophyllite	$(K,Na)_3(Fe^{2+},Mn)_7Ti_2Si_8O_{24}(O,OH)_7$	$K_2Na(Fe^{2+},Mn)_7Ti_2Si_8O_{26}(OH)_4F$
[6]Magnesium astrophyllite	$K_2NaNa(Fe, Mn)_4Mg_2Ti_2(Si_4O_{12})_2(OH)_4(OH,F)_2$	$K_2Na[Na(Fe, Mn)_4Mg_2]Ti_2Si_8O_{26}(OH)_4\square$
[7]Niobophyllite	$(K,Na)_3(Fe^{2+},Mn)_6(Nb,Ti)_2Si_8O_{24}(O,OH,F)_7$	$K_2Na(Fe^{2+},Mn)_7(Nb,Ti)_2Si_8O_{26}(OH)_4(F,O)$
[8]Zircophyllite	$(K,Na,Ca)_3(Fe^{2+},Mn)_7(Zr,Nb)_2Si_8O_{27}(OH,F)_4$	$K_2(Na,Ca)(Mn,Fe^{2+})_7(Zr,Nb)_2Si_8O_{26}(OH)_4F$
Fe-dominant zircophyllite		$K_2(Na,Ca)(Fe^{2+},Mn)_7(Zr,Nb)_2Si_8O_{26}(OH)_4F$
[9]Hydroastrophyllite	$(H_3O,K,Ca)_3(Fe^{2+},Mn)_{5-6}Ti_2Si_8(O,OH)_{31}$	$(H_3O,K)_2Ca(Fe^{2+},Mn)_{5-6}Ti_2Si_8O_{26}(OH)_4F$

[1]Piilonen *et al.* (2000), [2] Semenov (1956), [3]Piilonen *et al.* (2001), [4] Efimov *et al.* (1971), [5] Woodrow (1967), [6] Shi *et al.* (1998), [7] Nickel *et al.* (1964), [8] Kapustin 1973, [9] Hubei Geologic College (1974)

TABLE 3. REPRESENTATIVE ANALYSES OF ASTROPHYLLITE GROUP MINERALS*

Locality	SD (ave)	MSK	MSK	MSK	MSK	MSK	MSK	MSK	MSK	MSK	MSK	MSK	MSK	LANG	LANG	GER	LANG
Sample #	%	MSK2	MSK3	MSK7	MSK10	MSK10	MSK10	MSK10	MSK29	MSK31	MSK42	MSK44	MSK45	NOR1	NOR2	NOR3	NOR10
#**		13	10	7	5	6	6	2	5	4	3	4	6	11	12	10	4
Na_2O	1.7	3.51	3.87	2.09	2.44	2.38	2.40	2.21	2.24	1.74	2.62	1.99	2.64	2.54	1.99	3.52	1.88
K_2O	1.0	5.11	5.37	5.76	6.13	6.11	5.97	5.47	5.93	6.24	5.97	6.19	5.78	5.48	6.19	5.69	5.75
Rb_2O	2.5	0.35	0.81	0.40	0.47	0.67	0.49	0.78	0.42	0.38	0.82	0.33	0.57	0.75	0.36	0.37	0.67
Cs_2O	35.0	0.00	0.03	0.01	0.00	0.00	0.02	0.04	0.07	0.02	0.12	0.09	0.03	1.01	0.21	0.03	0.28
CaO	2.0	0.40	0.00	1.13	0.26	0.00	0.54	0.43	1.42	1.18	0.00	0.37	0.56	1.08	1.31	0.41	1.05
SrO	25.0	0.15	0.06	0.24	0.06	0.00	0.11	0.16	0.21	0.24	0.00	0.04	0.01	0.07	0.08	0.07	0.09
BaO	25.0	0.11	0.00	0.00	0.00	0.00	0.00	0.00	0.27	0.00	NA	0.00	0.00	0.00	0.00	0.00	0.00
MgO	3.0	0.46	0.51	1.21	0.53	0.16	0.41	0.44	1.49	0.59	0.15	0.18	0.68	0.81	0.76	0.36	0.85
MnO	1.5	32.38	28.11	19.34	19.95	26.98	20.06	15.51	8.50	9.83	26.37	7.12	22.70	12.48	9.15	17.63	13.12
FeO	1.0	2.00	0.71	15.15	13.94	7.05	15.09	20.49	25.45	26.02	2.64	28.94	10.65	21.23	25.90	16.01	21.43
ZnO	21.0	0.75	5.15	0.03	0.43	0.03	0.20	0.00	0.04	0.00	4.08	0.00	0.43	0.39	0.12	0.47	0.26
Al_2O_3	1.6	0.33	0.24	1.23	1.12	1.28	1.05	0.98	1.04	1.40	1.14	1.35	0.78	0.71	1.27	0.10	1.28
Y_2O_3	99.0	0.00	0.00	0.00	0.00	0.00	0.00	0.00	0.00	0.00	NA	0.00	0.00	0.00	0.00	0.00	0.00
Ce_2O_3	30.0	0.13	0.00	0.15	0.00	0.00	0.03	0.00	0.17	0.13	NA	0.30	0.00	0.11	0.11	0.23	0.28
TiO_2	0.8	11.07	6.64	6.93	5.48	0.73	6.93	6.72	10.57	7.24	1.34	5.87	7.43	9.71	7.79	9.74	7.96
SnO_2	99.0	0.00	0.00	0.00	0.00	0.00	0.00	0.00	0.00	0.00	NA	0.00	0.00	0.05	0.21	0.00	0.09
ZrO_2	2.0	0.02	0.07	5.80	1.87	4.18	0.93	4.37	1.42	4.25	3.43	4.47	0.34	1.85	4.50	1.07	3.93
HfO_2	99.0	0.02	0.00	0.22	0.00	0.00	0.00	0.13	0.00	0.13	0.00	0.00	0.00	0.01	0.11	0.00	0.11
Nb_2O_5	2.0	1.72	8.02	1.26	8.06	12.34	6.92	2.53	1.39	2.47	12.13	4.50	6.90	1.73	1.74	2.27	1.99
Ta_2O_5	31.0	0.07	0.00	0.06	0.23	0.56	0.00	0.00	0.00	0.14	0.63	0.03	0.08	0.00	0.13	0.09	0.00
SiO_2	0.5	34.66	33.66	32.00	33.14	31.75	32.82	32.66	33.77	31.89	31.85	32.81	34.35	34.96	33.87	34.92	33.41
F	10.0	1.21	0.80	1.28	0.67	0.20	0.88	1.21	1.37	1.18	0.14	0.94	0.89	1.15	1.04	1.65	1.13
H_2O	NB	2.75	2.58	2.60	2.59	2.50	2.59	2.63	2.69	2.67	2.48	2.80	2.69	2.80	2.83	2.52	2.75
O=F	NB	-0.51	-0.34	-0.54	-0.28	-0.09	-0.37	-0.51	-0.57	-0.50	-0.06	-0.40	-0.38	-0.48	-0.44	-0.69	-0.48
Total	NB	96.71	96.34	96.35	97.06	96.82	97.03	96.21	97.90	97.20	95.85	97.89	97.10	98.43	99.24	96.44	97.81

FORMULAE BASED ON 31 ANIONS

Locality	SD (ave)	MSK	MSK	MSK	MSK	MSK	MSK	MSK	MSK	MSK	MSK	MSK	MSK	LANG	LANG	GER	LANG
Sample #	%	MSK2	MSK3	MSK7	MSK10	MSK10	MSK10	MSK10	MSK29	MSK31	MSK42	MSK44	MSK45	NOR1	NOR2	NOR3	NOR10
Na	1.7	0.49	0.49	0.23	0.04	0.06	0.21	0.11	0.23	0.08	0.00	0.00	0.00	0.06	0.09	0.31	0.07
K	1.0	1.47	1.59	1.72	1.81	1.87	1.76	1.64	1.70	1.85	1.84	1.82	1.68	1.57	1.78	1.65	1.68
Rb	2.5	0.05	0.12	0.06	0.07	0.10	0.07	0.12	0.06	0.06	0.13	0.05	0.08	0.11	0.05	0.05	0.10
Cs	35.0	0.00	0.00	0.00	0.00	0.00	0.00	0.00	0.01	0.00	0.01	0.01	0.00	0.10	0.02	0.00	0.03
Sr	25.0	0.02	0.01	0.03	0.01	0.00	0.02	0.02	0.03	0.03	0.00	0.01	0.00	0.01	0.01	0.01	0.01
Ba	25.0	0.01	0.00	0.00	0.00	0.00	0.00	0.00	0.02	0.00	0.00	0.00	0.00	0.00	0.00	0.00	0.00
Sum A	NB	2.04	2.22	2.04	1.93	2.03	2.06	1.89	2.05	2.02	1.98	1.89	1.77	1.84	1.95	2.03	1.89
Na	1.7	0.90	1.00	0.72	0.94	1.00	0.87	0.89	0.66	0.71	0.95	0.89	0.86	0.74	0.68	0.90	0.74
Ca	2.0	0.10	0.00	0.28	0.06	0.00	0.13	0.11	0.34	0.29	0.00	0.09	0.14	0.26	0.32	0.10	0.26
Sum B	NB	1.00	1.00	1.00	1.00	1.00	1.00	1.00	1.00	1.00	0.95	0.98	1.00	1.00	1.00	1.00	1.00
Na	1.7	0.14	0.26	0.00	0.12	0.05	0.00	0.00	0.09	0.00	0.28	0.00	0.30	0.30	0.09	0.34	0.02
Mg	3.0	0.16	0.18	0.42	0.18	0.06	0.14	0.15	0.30	0.20	0.05	0.06	0.23	0.27	0.25	0.12	0.29
Mn	1.5	6.19	5.54	3.83	3.92	5.48	3.93	3.08	1.62	1.94	5.40	1.39	4.38	2.37	1.75	3.40	2.54
Fe^{2+}	1.0	0.38	0.14	2.96	2.70	1.41	2.92	4.01	4.78	5.07	0.53	5.59	2.02	3.98	4.88	3.05	4.09
Zn	21.0	0.12	0.89	0.00	0.07	0.01	0.03	0.00	0.01	0.00	0.73	0.00	0.07	0.06	0.02	0.08	0.04
Y	99.0	0.00	0.00	0.00	0.00	0.00	0.00	0.00	0.00	0.00	0.00	0.00	0.00	0.00	0.00	0.00	0.00
Ce	30.0	0.01	0.00	0.01	0.00	0.00	0.00	0.00	0.01	0.01	0.00	0.03	0.00	0.01	0.01	0.02	0.02
Sum C	NB	7.00	7.00	7.23	7.00	7.00	7.03	7.24	7.00	7.22	7.00	7.07	7.00	6.70	6.91	6.66	6.98
Ti	0.8	1.88	1.16	1.21	0.95	0.13	1.21	1.18	1.79	1.27	0.24	1.02	1.27	1.64	1.32	1.67	1.37
Sn	99.0	0.00	0.00	0.00	0.00	0.00	0.00	0.00	0.00	0.00	0.00	0.00	0.00	0.00	0.02	0.00	0.01
Zr	2.0	0.00	0.01	0.66	0.21	0.49	0.10	0.50	0.16	0.48	0.41	0.50	0.04	0.20	0.49	0.12	0.44
Hf	99.0	0.00	0.00	0.01	0.00	0.00	0.00	0.01	0.00	0.01	0.00	0.00	0.00	0.00	0.01	0.00	0.01
Nb	2.0	0.18	0.84	0.13	0.85	1.34	0.72	0.27	0.14	0.26	1.33	0.47	0.71	0.18	0.18	0.23	0.21
Ta	31.0	0.00	0.00	0.00	0.01	0.04	0.00	0.00	0.00	0.01	0.04	0.00	0.01	0.00	0.01	0.01	0.00
Sum D	NB	2.06	2.01	2.03	2.03	1.99	2.03	1.96	2.08	2.03	2.02	1.99	2.02	2.02	2.02	2.02	2.02
Si	0.5	7.82	7.83	7.48	7.69	7.61	7.59	7.65	7.58	7.42	7.71	7.58	7.81	7.84	7.63	7.94	7.63
Al	1.6	0.09	0.07	0.34	0.31	0.36	0.29	0.27	0.28	0.38	0.33	0.37	0.21	0.19	0.34	0.03	0.34
Sum T	NB	7.91	7.90	7.82	7.99	7.97	7.88	7.92	7.86	7.80	8.03	7.95	8.02	8.03	7.96	7.97	7.97
F	10.0	0.86	0.59	0.95	0.49	0.15	0.64	0.89	0.97	0.87	26.89	0.69	0.64	0.82	0.74	1.18	0.81
OH	NB	4.14	4.00	4.05	4.00	4.00	4.00	4.11	4.03	4.13	4.00	4.31	4.07	4.18	4.26	3.82	4.19
O	NB	30.14	30.41	30.05	30.51	30.85	30.36	30.11	30.03	30.13	30.11	30.31	30.36	30.18	30.26	29.82	30.19
Σ cation	NB	20.01	20.14	20.11	19.95	19.99	20.00	20.01	19.99	20.07	19.98	19.88	19.81	19.89	19.94	20.02	19.88
Mn#	NB	0.94	0.98	0.56	0.59	0.80	0.57	0.43	0.25	0.28	0.91	0.20	0.68	0.37	0.26	0.53	0.38

* Electron-microprobe data

** Number of analyses included in the mean

NA: Not analysed for

NB: Not determined

SD: Standard deviation

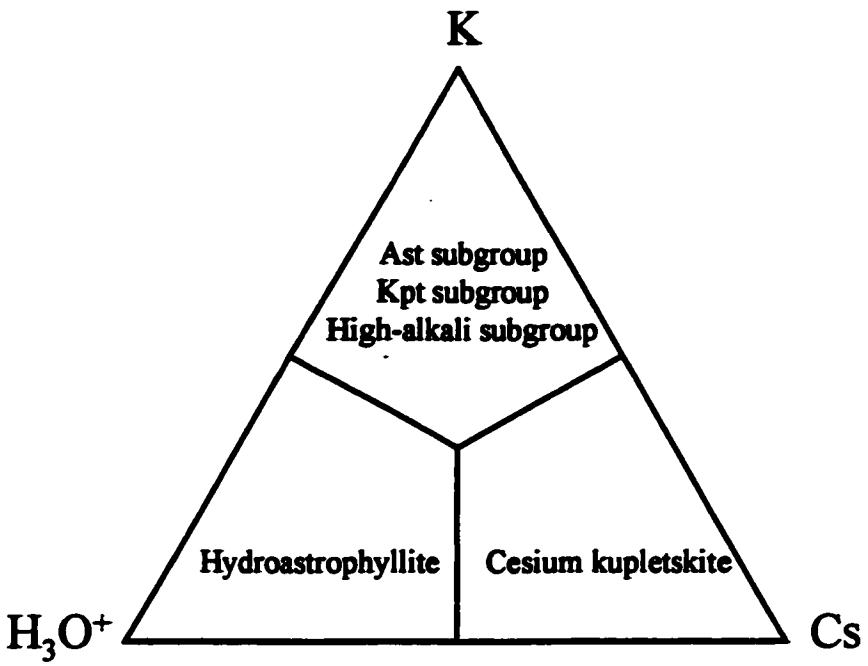

Figure 7. Ternary diagram depicting members of the astrophyllite-group based on the predominant cation at *A*. All samples in this study represent K-dominant species. Ast: astrophyllite, Kpt: kupletskite.

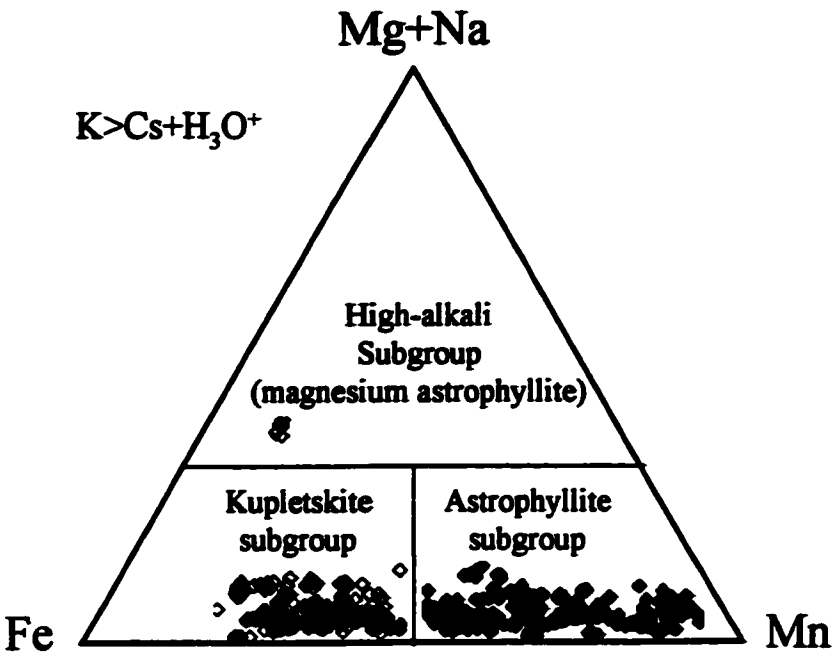

Figure 8. Ternary diagram depicting members of the astrophyllite group based on the predominant cation at *C*.

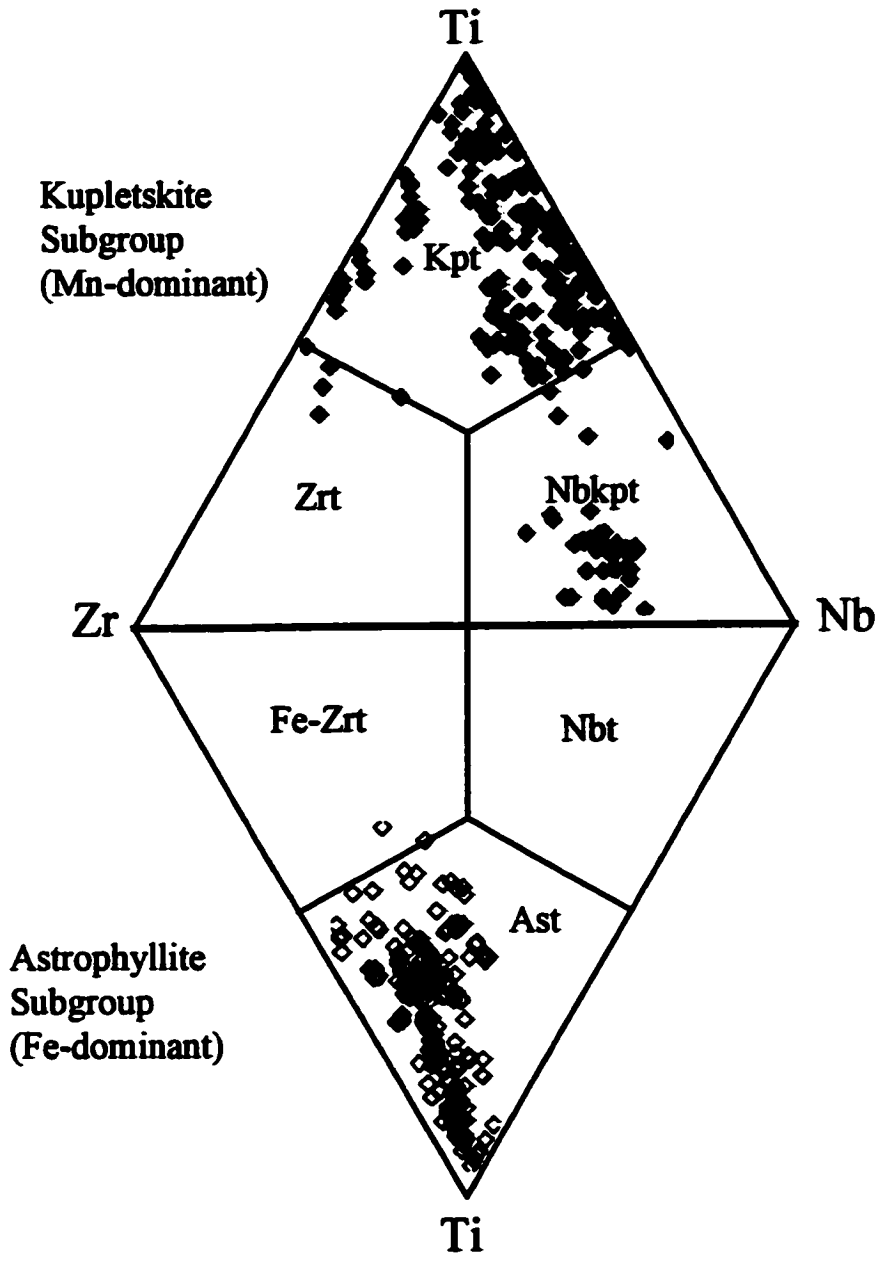

Figure 9. Ternary diagram depicting members of the astrophyllite group based on the predominant cation at *D*. Kpt: kupletskite, Zrt: zircophyllite, Nbkpt: niobokupletskite, Fe-Zrt: Fe-dominant zircophyllite, Nbt: niobophyllite, Ast: astrophyllite.

TABLE 4. MEAN AND RANGE OF CATIONS (*apfu*) IN THE ASTROPHYLLITE GROUP*

	Oversaturated			Undersaturated					
				Kupletskite Subgroup			Astrophyllite Subgroup		
Cation	Mean	Min.	Max.	Mean	Min.	Max.	Mean	Min.	Max.
Na	1.21	0.62	1.59	1.22	0.76	1.86	0.92	0.63	1.91
K	1.59	1.41	1.86	1.69	1.35	1.90	1.76	1.43	2.07
Rb	0.11	0.00	0.20	0.08	0.00	0.20	0.06	0.00	0.18
Cs	0.01	0.00	0.03	0.00	0.00	0.11	0.02	0.00	0.16
Sr	0.00	0.00	0.03	0.01	0.00	0.05	0.03	0.00	0.07
Ba	0.01	0.00	0.03	0.00	0.00	0.05	0.01	0.00	0.04
Ca	0.10	0.01	0.47	0.12	0.00	0.39	0.30	0.08	0.48
Mg	0.06	0.00	0.52	0.24	0.03	0.70	0.35	0.06	2.00
Mn	1.48	0.16	4.60	4.77	3.11	6.50	2.03	0.36	3.44
Fe^{2+}	5.04	1.99	6.71	1.79	0.00	3.37	4.53	3.07	5.67
Zn	0.16	0.00	0.82	0.12	0.00	1.73	0.02	0.00	0.11
Ti	1.52	0.51	1.97	1.19	0.10	2.04	1.50	0.82	2.08
Sn	0.04	0.00	0.24	0.00	0.00	0.04	0.00	0.00	0.03
Zr	0.14	0.00	0.35	0.21	0.00	1.02	0.33	0.00	0.81
Hf	0.00	0.00	0.02	0.00	0.00	0.03	0.01	0.00	0.04
Nb	0.31	0.04	1.68	0.61	0.06	1.51	0.19	0.04	0.49
Ta	0.01	0.00	0.13	0.01	0.00	0.05	0.01	0.00	0.04
Si	7.89	7.44	8.08	7.68	7.36	8.01	7.60	7.12	8.13
Al	0.12	0.00	0.54	0.25	0.02	0.73	0.33	0.04	0.53
F	0.89	0.00	1.32	0.63	0.00	1.07	0.81	0.54	1.17
Mn#	0.23	0.02	0.69	0.73	0.50	1.00	0.31	0.09	0.49

* Electron-microprobe analyses

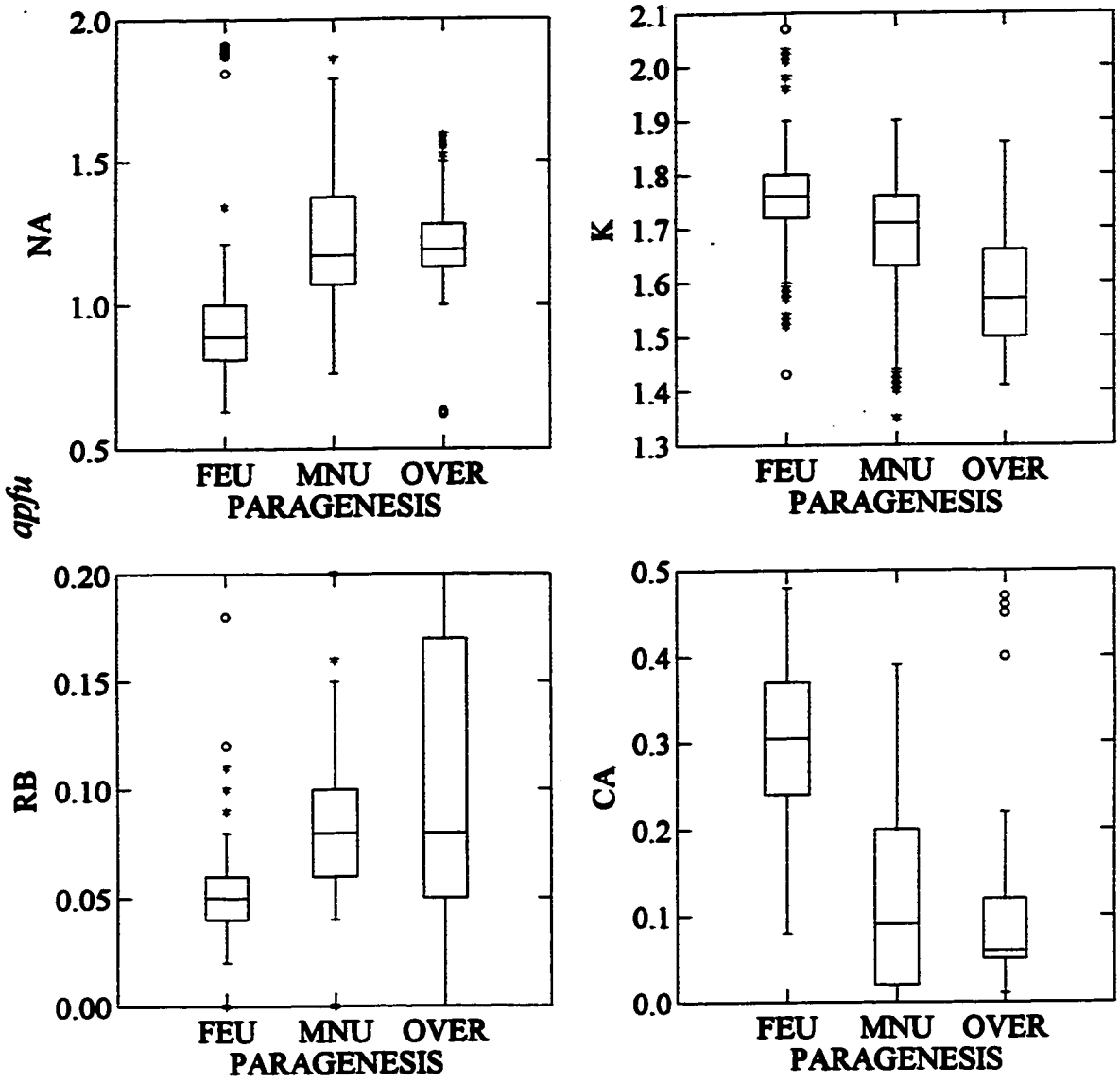

Figure 10A. Boxplots depicting the distribution of interlayer cations in AGM from SiO_2 under- and oversaturated intrusions. FEU: Fe-dominant, undersaturated; MNU: Mn-dominant, undersaturated; and OVER: oversaturated. The central horizontal line of each box represents the median of the sample. The length of each box represents the range within which the central 50% of the values fall (box edges/hinge: 1st and 3rd quartile). Lower and outer fences represent lower/upper hinge ± (1.5 • interquartile range). Whiskers represent lower/upper hinge ± (3 • interquartile range). Open circles are outliers.

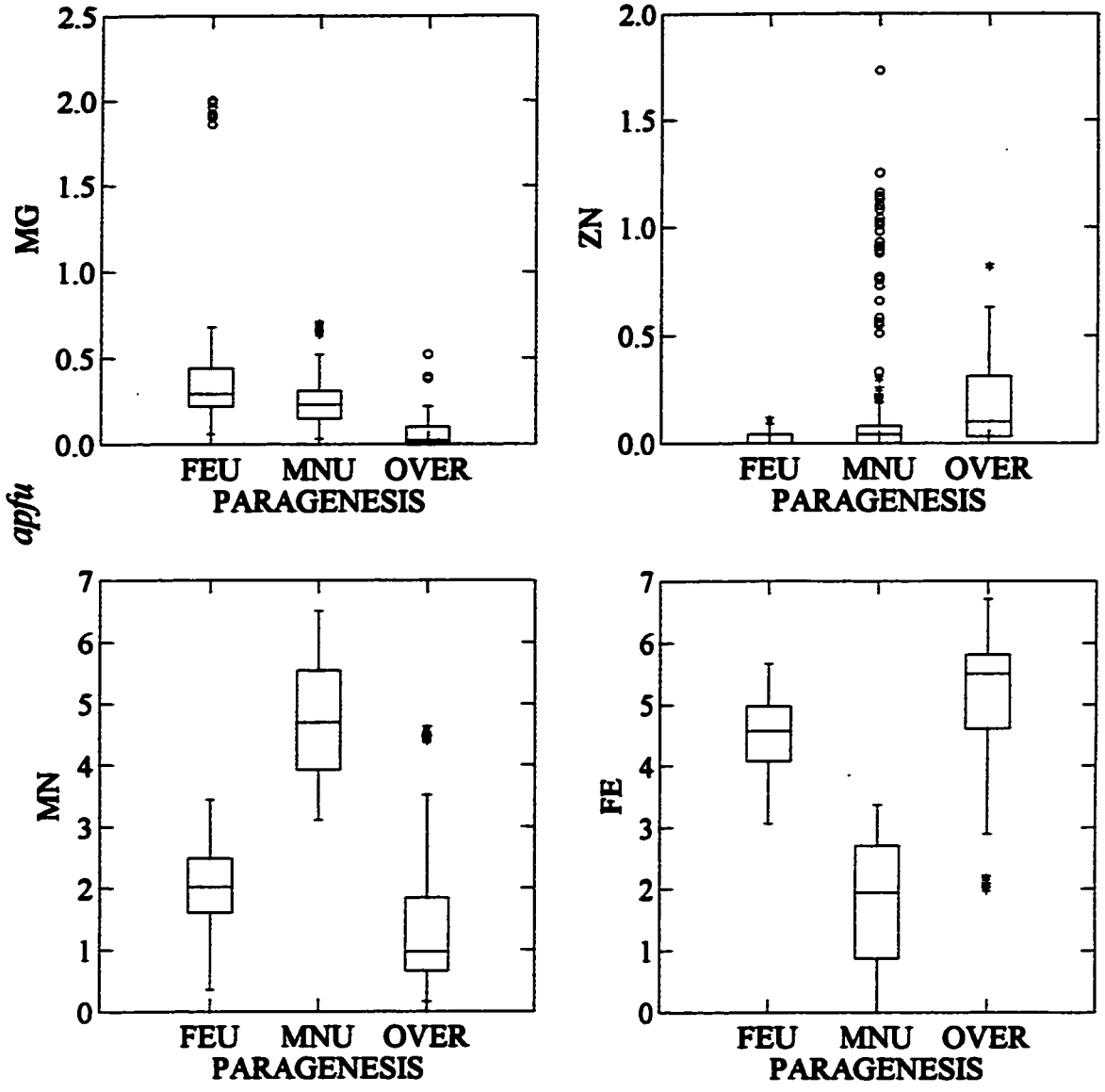

Figure 10B. Boxplots depicting the distribution of *O*-sheet cations in AGM from under- and oversaturated intrusions. Paragenesis and boxplots are defined as in Fig. 10A.

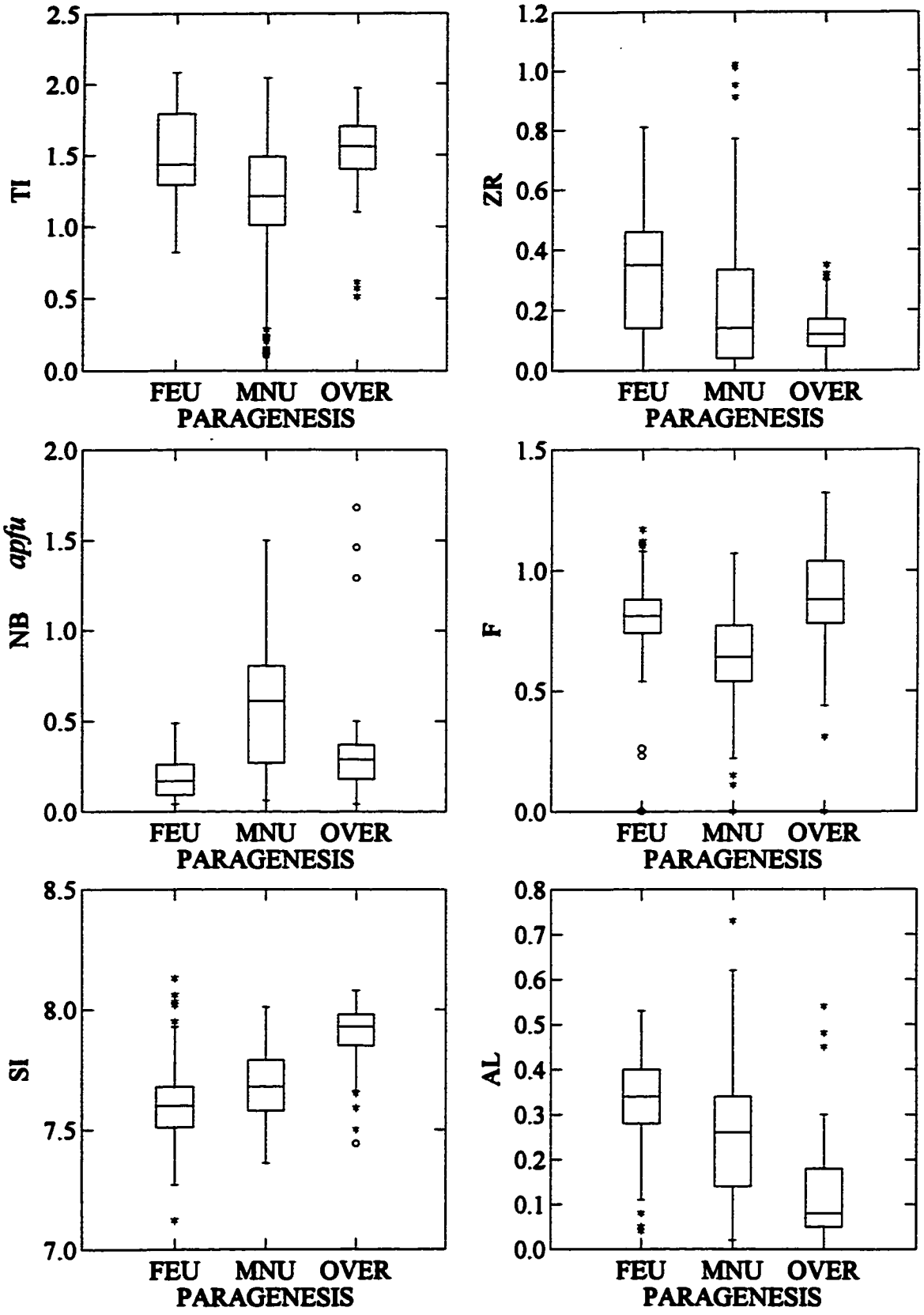

Figure 10C. Boxplots depicting the distribution of *H*-sheet cations and F in AGM from under- and oversaturated intrusions.
Paragenesis and boxplots are defined as in Fig. 10A.

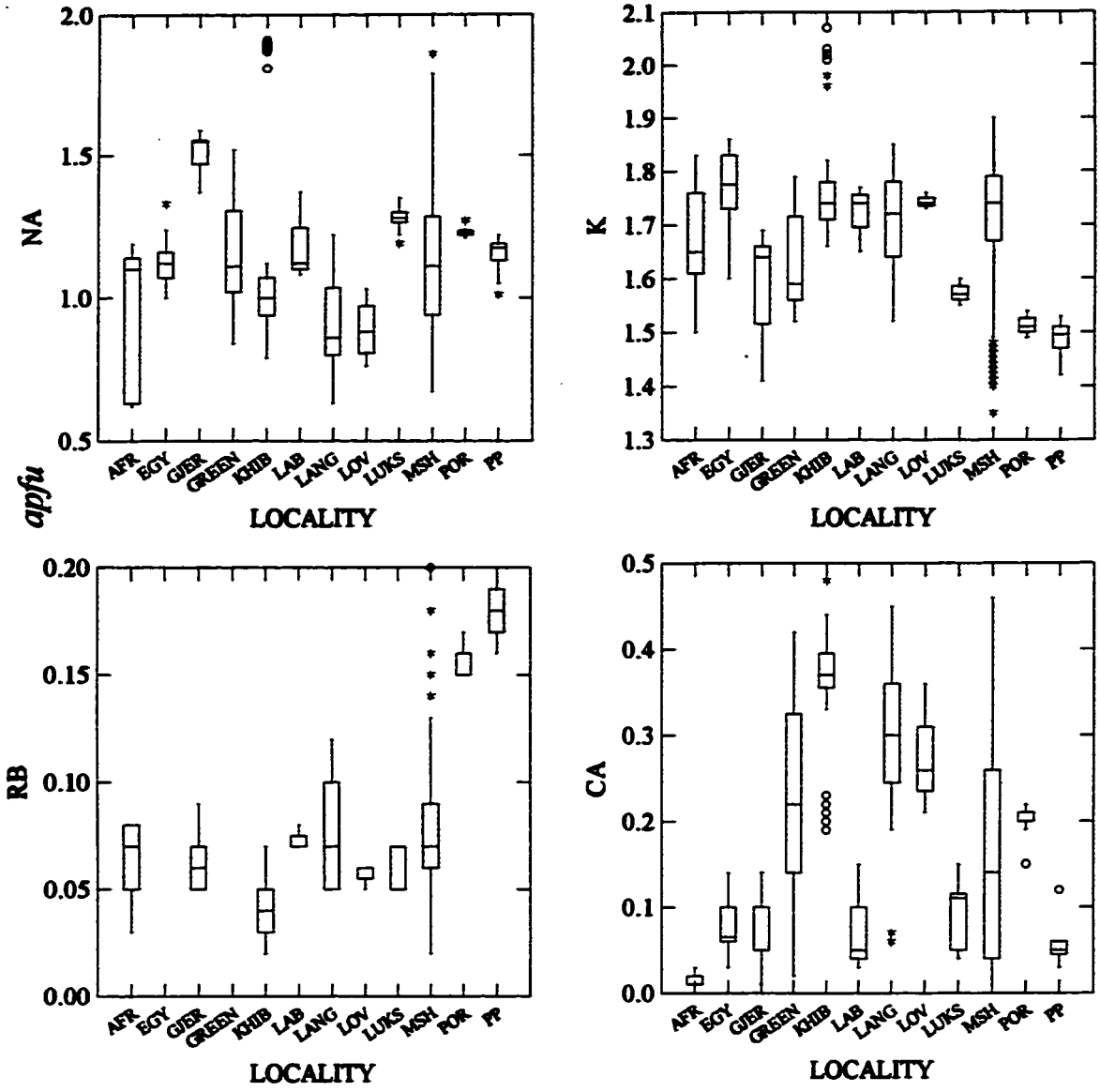

Figure 11A. Boxplots depicting the distribution of interlayer cations in AGM from under- and oversaturated intrusions. AFR: Zomba-Malosa, Malawi, Africa; EGY: Mount Gharib, Egypt; GJER: Gjerdingen, Norway; GREEN: Greenland; KHIB: Khibina massif, Kola Peninsula, Russia; LAB: Seal Lake, Labrador; LOV: Lovozero massif, Kola Peninsula, Russia; LUKS: Luksefjell, Norway; MSH: Mont Saint-Hilaire, Québec; POR: Point of Rocks, New Mexico, USA; PP: Mount Rosa, Pikes Peak, Colorado, USA
The central horizontal line of each box represents the median of the sample. The length of each box represents the range within which the central 50% of the values fall (box edges/hinge: 1st and 3rd quartile). Lower and outer fences represent lower/upper hinge ± (1.5 • interquartile range). Whiskers represent lower/upper hinge ± (3 • interquartile range). Open circles are outliers.

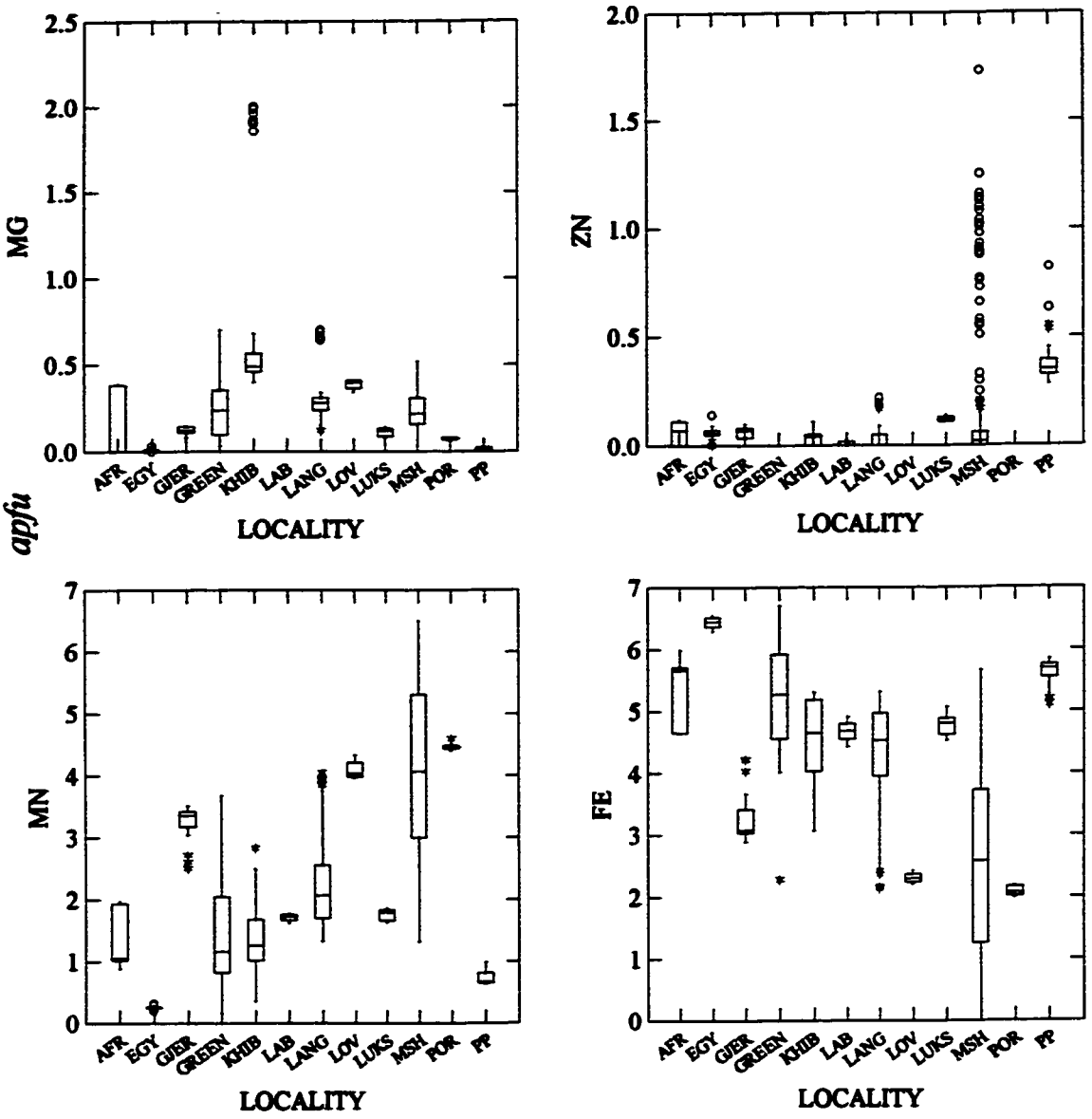

Figure 11B. Boxplots depicting the distribution of interlayer cations in AGM from under- and oversaturated intrusions.
Localities and boxplots are as defined in Fig. 11A.

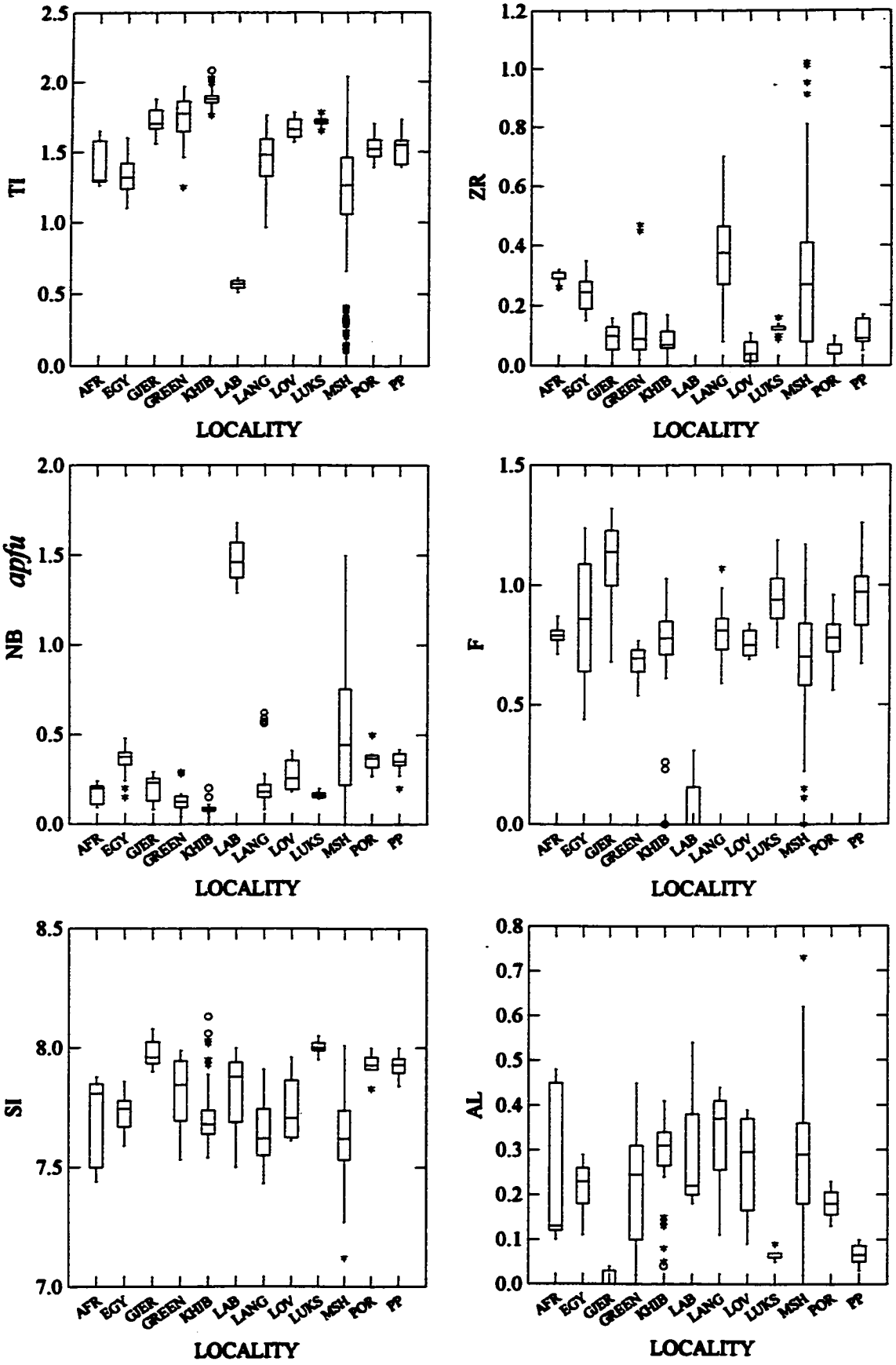

Figure 11C. Boxplots depicting the distribution of *O*-sheet cations in AGM from over- and undersaturated intrusions.
Localities and boxplots are defined as in Fig. 11A.

having the highest K contents (average: 1.76 *apfu*) and the samples from oversaturated intrusions being the most depleted in K (average: 1.59 *apfu*). Other cations substituting for K at *A* include Rb, Cs, Sr, Ba and Na. The presence of vacancies at *A* has been confirmed through single-crystal X-ray structure refinement, consistent with EMPA data which indicate cation sums at *A* as low as 1.71 *apfu* (*i.e.* 15% vacancies).

Rubidium occurs in concentrations up to 0.20 *apfu*, with samples from oversaturated intrusions displaying the highest average contents (0.11 *apfu*), whereas samples from undersaturated intrusions display slightly lower contents (0.06 and 0.08 *apfu*, respectively). As shown by Ganzeyev *et al.* (1969), the Cs ⇔ K substitution appears to be more limited than Rb ⇔ K. The highest Cs contents occur in samples from undersaturated intrusions with a maximum of 0.16 (astrophyllite subgroup) and 0.11 *apfu* (kupletskite subgroup). Cesium enrichments approaching those observed in astrophyllite from Dara I Pioz (10.08 wt. %, Ganzeyev *et al.* 1969) or in cesium kupletskite (Efimov *et al.* 1971) were not observed in any of the samples studied.

Ganzeyev *et al.* (1969) proposed that K and Na occur in crystallographically distinct sites and do not substitute isomorphously in the AGM structure. This fact is confirmed by both single-crystal X-ray structure data (which indicate that two crystallographically distinct interlayer sites, *A* and *B*, host to K and Na, respectively), and by EMPA data (which indicate that Na ⇔ K substitution is limited, occurring up to a maximum of 24.5% of available *A* sites; 0.49 *apfu* Na in kupletskite from MSH). Sodium appears to occur at *A* only if excess contents remain after *B* and *C* are filled. Lithium appears to be a trace element in the samples studied, with contents ranging from 42.7 to 453.3 ppm. However, Li contents up to

0.59 wt. % have been noted in astrophyllite from Dara I Pioz, Russia (Ganzeyev *et al.* 1969).

Ten-coordinated Na (*B*) is located in the interlayer in a cage between bridging $\phi(16)$ anions. The average Na content for all AGM in this study is 0.83 *apfu*, and Na is the dominant cation at *B* in all cases. The only other cation observed to substitute for Na is Ca, up to a maximum occupancy of 48%. The Ca content in samples from undersaturated intrusions ranges from zero to 0.48 *apfu*, with an average of 0.14 *apfu* in members of the kupletskite subgroup and 0.28 *apfu* in members of the astrophyllite subgroup. Samples from oversaturated intrusions show a range in Ca content from 0.01 to 0.40 *apfu*, the average being 0.08 *apfu*. The Ca content of all AGM correlates negatively with Na content (Fig. 12), the two being related by the coupled substitution Ca + Al $\Leftrightarrow$ Si + Na (Fig. 13).

Figure 14 shows the correlation between ($K + Na_{tot}$), the dominant interlayer cations, and the substituting cations (Rb+Cs+Sr+Ba+Ca). All points plotting above the 1:1 line represent analyses in which the sum of cations at *A* and *B* exceeds the ideal value of 3.00 *apfu*. This discrepancy is generally due to an excess of Na, which must be subsequently allocated to the [6]-coordinated *C* sites, a feature discussed in the following section.

5.2. C and Fe^{2+}/Fe^{3+} ratios

The substitution Mn $\Leftrightarrow$ Fe^{2+} at *C* results in a complete solid solution series (96% observed) between astrophyllite and kupletskite (Fig. 15). This is the dominant substitutional mechanism observed in all AGM, regardless of the bulk composition of the *O*-sheet or petrogenetic affinity. As has been noted by other authors (MacDonald & Saunders 1973; Layne *et al.* 1982), AGM from undersaturated intrusions show the strongest enrichment in

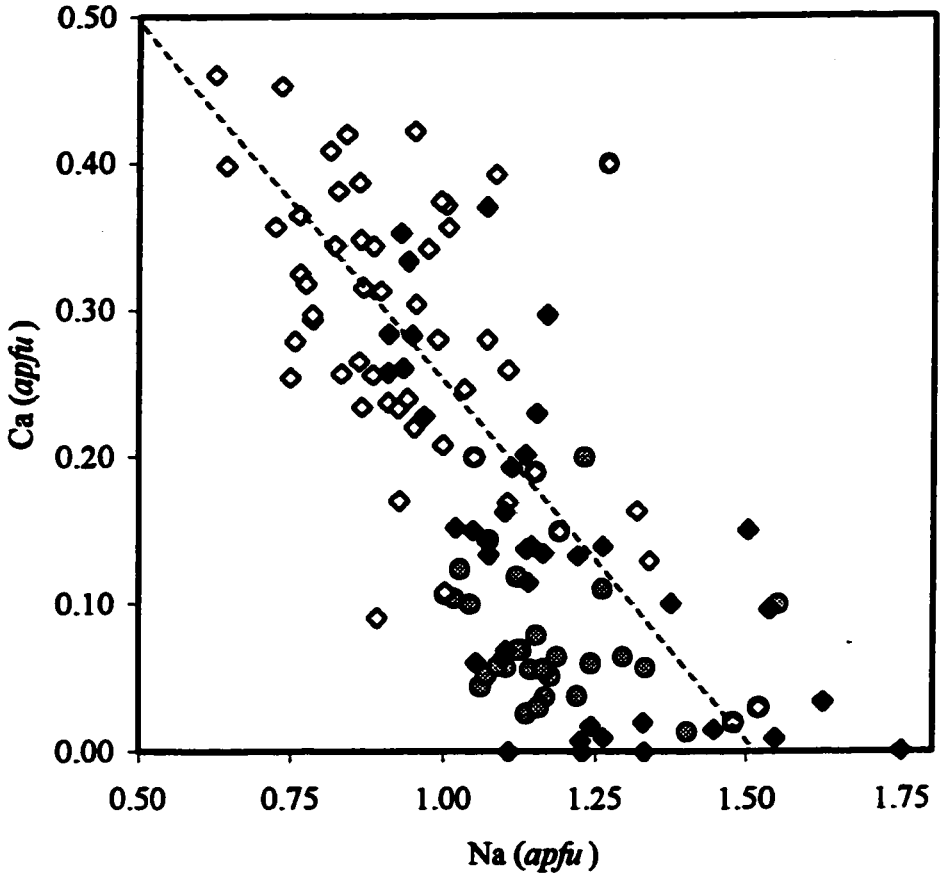

Figure 12. Content of Na *versus* that of Ca at *B* of astrophyllite group minerals. Circles: OVER, Closed diamonds: MNU; Open diamonds: FEU. 1:1 substitution line indicated.

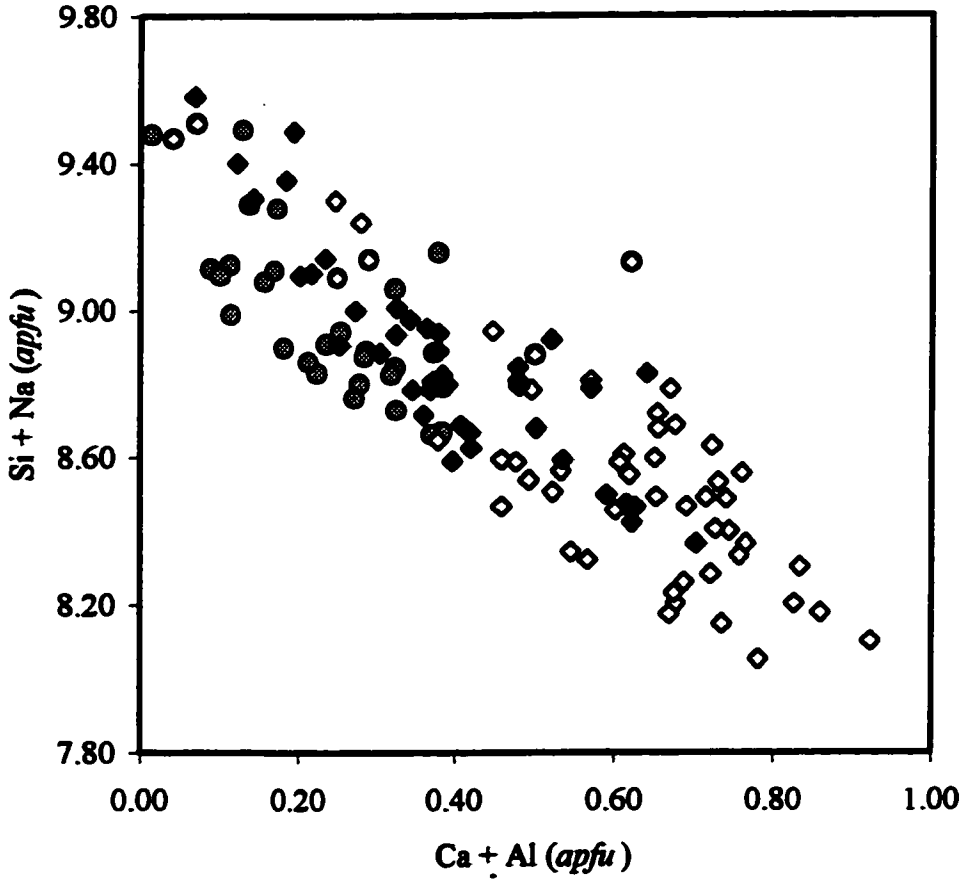

Figure 13. The coupled substitution Na + Si ⇔ Ca + Al in astrophyllite group minerals. Circles: OVER; Closed diamonds: MNU; Open diamonds: FEU.

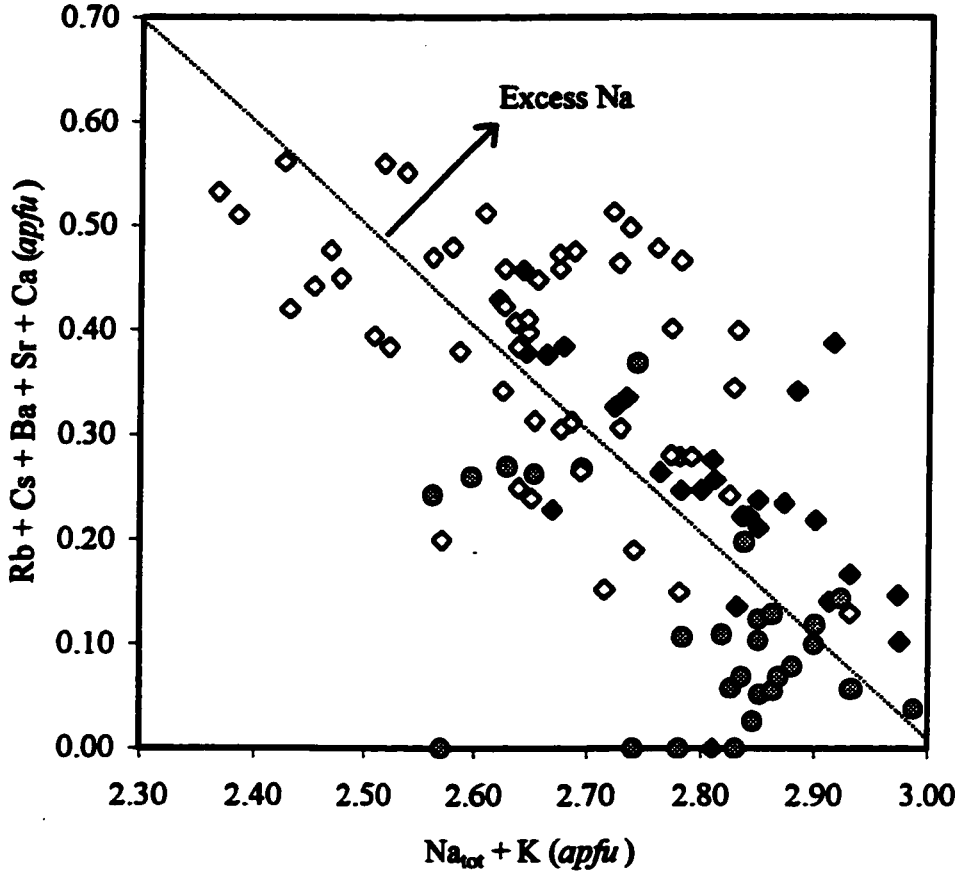

Figure 14. K+Na$_{tot}$ *versus* Rb+Cs+Sr+Ba+Ca in the interlayer of astrophyllite group minerals. The dashed line represents the 1:1 substitution line for an ideal *A+B* sum of three *apfu*. Points which plot above the line represent samples with excess Na.
Circles: OVER, Closed diamonds: MNU;
Open diamonds: FEU.

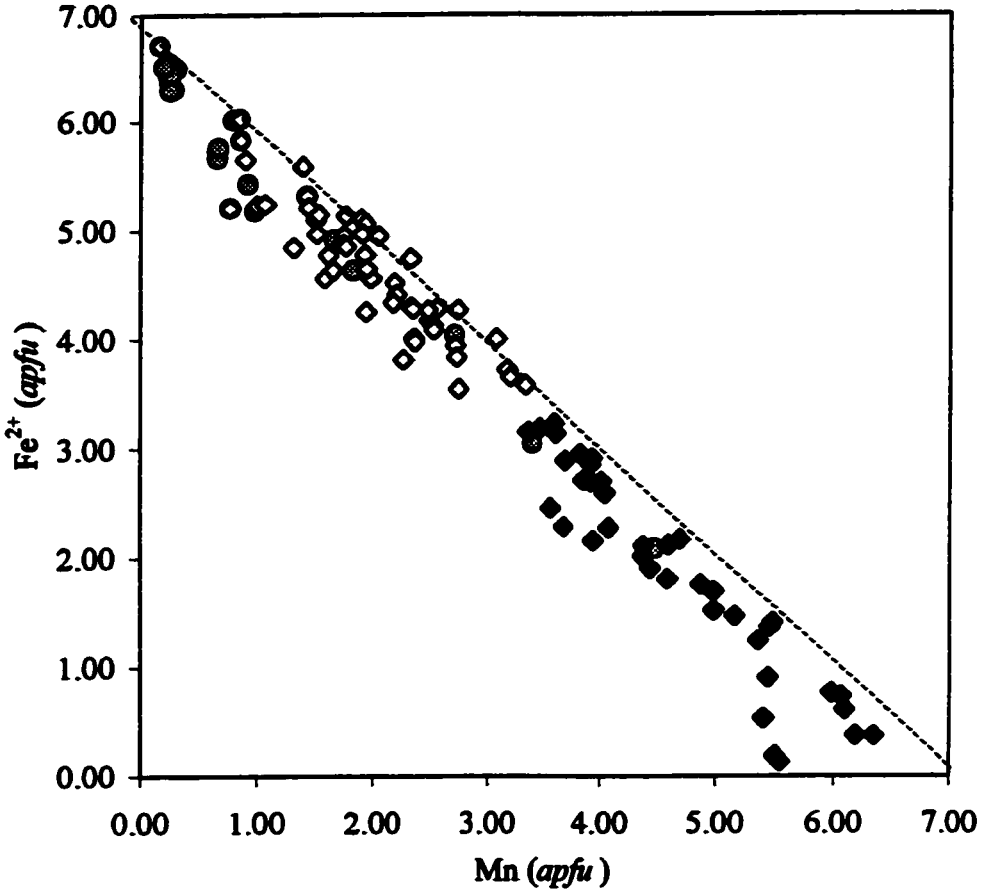

Figure 15. The content of Mn *versus* that of Fe^{2+} at *C* of astrophyllite group minerals (Linear regression, $R^2 = 0.977$). 1:1 line indicated. Circles: OVER; Closed diamonds: MNU; Open diamonds: FEU.

Mn (up to 6.34 *apfu*). However, they also show the strongest enrichments in Fe^{2+} (up to 6.71 *apfu*), leading to an extensive range of possible compositions in undersaturated environments alone (Mn# range: 0.09 to 1.00). Astrophyllite group minerals from oversaturated environments show a variable but restricted range of Mn# (0.03 to 0.69) and tend towards Fe-enrichment; only samples from the Gjerindgen (Mn#: 0.38 to 0.51) and Point of Rocks (Mn#: 0.65-0.69) intrusions show slight enrichment in the kupletskite component.

The Fe^{3+}/Fe_{tot} ratios in the AGM studied, as determined by Mössbauer spectroscopy, range from 0.01 to 0.21, corresponding to 0.05 to 0.56 *apfu* Fe^{3+} and accounting for a maximum of 8% of *C* (Table 5). Although Fe^{3+} enrichment in AGM is minor relative to Fe^{2+} and Mn, a difference in Fe^{3+}/Fe_{tot} ratios is observed between members of the kupletskite and astrophyllite subgroups. The lowest Fe^{3+}/Fe_{tot} ratios are observed in near end-member astrophyllite (ave.: 0.04, range: 0.01 to 0.08) from both over- and undersaturated rocks, whereas the highest ratios occur predominantly in members of the kupletskite subgroup (ave.: 0.10, range: 0.04 to 0.21), in particular in Nb-bearing kupletskite and niobokupletskite. The enrichment of Fe^{3+} in such samples is consistent with the oxidizing coupled substitution Ti + F $\Leftrightarrow$ Nb + O proposed for incorporation of Nb into the astrophyllite structure (Piilonen *et al.* 2000). It is well-documented in other rock-forming minerals (*e.g.* biotites, amphiboles; Czamanske & Mihálik 1972, Czamanske & Wones 1973) that an increase in oxygen fugacity (fO_2) in alkaline systems results in a decreased activity of Fe^{2+}, increased activity of Fe^{3+}, and a subsequent enrichment in Mn and Mg, concomitant with a decrease in Ti, Al and F. In particular, the dominant magmatic process controlling the distribution of Mn in silicates is oxidation (Czamanske & Mihálik 1972). It is therefore not

TABLE 5. LOCALITY INFORMATION AND Fe^{2+}/Fe^{3+} RATIOS FOR ASTROPHYLLITE GROUP MINERALS STUDIED BY ^{57}FE MÖSSBAUER SPECTROSCOPY

Sample #	Locality*	Mn#	Fe^{2+}/Fe^{3+}	Fe^{3+}/Fe_{tot}	Fe^{3+}(*apfu*)
US2	PP	0.10	11.47	0.08	0.45
US5	PP	0.15	32.33	0.03	0.16
NOR1	LANG	0.37	12.93	0.07	0.28
NOR9	LANG	0.26	17.80	0.05	0.26
RUS4	KHIB	0.37	25.39	0.04	0.14
RUS5	KHIB	0.26	15.23	0.06	0.28
RUS7	KHIB	0.26	85.96	0.01	0.05
RUS8	KHIB	0.31	17.80	0.05	0.21
CC2A	GREEN	0.13	38.06	0.03	0.17
CC7A	GREEN	0.33	46.17	0.02	0.09
MSH6	MSH	0.53	12.81	0.07	0.22
MSH7	MSH	0.56	23.81	0.04	0.12
MSH10A	MSH	0.59	3.84	0.21	0.56
MSH10B	MSH	0.80	3.85	0.21	0.29
MSH11	MSH	0.61	8.17	0.11	0.28
MSH15	MSH	0.81	15.47	0.06	0.08
MSH18A	MSH	0.57	13.16	0.07	0.21
MSH26A	MSH	0.53	11.20	0.08	0.26
MSH26B	MSH	0.41	17.38	0.05	0.20
MSH28	MSH	0.27	71.46	0.01	0.05
MSH32	MSH	0.33	30.06	0.03	0.14
MSH33	MSH	0.38	16.36	0.06	0.26
MSH34A	MSH	0.27	26.32	0.04	0.20
MSH35	MSH	0.52	17.52	0.05	0.16

* PP: Mount Rosa, St. Peter's Dome, Pike's Peak, Colorado, USA; LANG: Larvik complex, Langesundsfjord Area, Norway; KHIB: Khibina massif, Kola Peninsula, Russia; GREEN: Kangerdlugssuaq, Greenland; MSH: Mont Saint-Hilaire, Québec, Canada

surprising that in the astrophyllite group, we observe the highest Fe^{3+}/Fe_{tot} ratios in Mn-rich samples, suggesting that crystallization proceeded under oxidizing conditions. As such, by quantifying the niobokupletskite and astrophyllite components of an individual AGM, it may be possible to use this chemical information to make inferences about the prevailing fO_2 at the time of crystallization. In those intrusions that exhibit a wider species diversity and range in chemical composition of AGM (*i.e.* Mont Saint-Hilaire, Québec, Canada), we may use these components as petrogenetic indicators for determining the geochemical evolution of the magma/melt, and thus the crystallization history of the intrusion. The paragenetic implications for AGM will be discussed Chapter VII.

Assuming only typical divalent and trivalent cations (*e.g.* Mn, Fe^{2+}, Fe^{3+}, Mg, Zn, *etc.*) at *C* generally results in low cation sums ($\Sigma_C \approx 6.70$ *apfu*). Conversely, in all analyses of AGM, the total Na content is greater than the ideal sum of 1.00 *apfu* for the *B* site, indicating excess Na. Single-crystal X-ray structure refinements on 20 AGM indicate the presence of $^{[6]}$Na at the large *M*(1) site. Such refinements have shown that all Ca should be assigned to *B*, with Na added to a sum of 1.00 *apfu*. All excess Na should be assigned to *C*, up to the ideal sum of 7.00 *apfu*. The presence of $^{[6]}$Na is most likely the result of the extreme peralkalinity and Na activity of the parental alkaline melt. Astrophyllite group minerals from oversaturated rocks show the highest $^{[6]}$Na content (average: 0.26 *apfu*) with a range from 0.07 to 0.43 *apfu*, a feature which may be attributable to their elevated $^{[10]}$Ca contents. Kupletskite and astrophyllite subgroup samples from undersaturated rocks have slightly lower $^{[6]}$Na contents (average: 0.11 and 0.09 *apfu*, respectively). In magnesium astrophyllite, Na is the dominant cation at a single [6]-coordinated site within the *O*-sheet, (average: 1.10

apfu), crystallographically equivalent to *M*(1) in triclinic AGM and kupletskite-*Ma2b2c*.

Other cations assigned to *C* include Mg and Zn. Elevated Mg contents occur in AGM from undersaturated environments (up to 0.70 *apfu*), with the highest Mg content being observed in magnesium astrophyllite (2.00 *apfu*), a member of the high-alkali subgroup. The presence of a high Mg content in AGM appears to require a modification of the structure from triclinic to monoclinic in order to accommodate the smaller Mg cation, with a concomitant occupation of a single *M* site by Na. This modification is not the result of polytypic stacking (*i.e.* the structure of magnesium astrophyllite cannot be simply related to other AGM by stacking of *HOH* layers) and magnesium astrophyllite should therefore be considered as a completely different structure type. As such, the structural differences between magnesium astrophyllite and either astrophyllite or kupletskite subgroup members are significant, thus inhibiting extensive solid solution between them.

Astrophyllite group minerals from undersaturated environments, in particular members of the kupletskite subgroup, show an extensive range of Zn contents; kupletskite from syenite pegmatites at MSH contain up to 0.91 *apfu* Zn. The presence of high Zn contents supports the observation that AGM are Zn-concentrators (MacDonald & Saunders 1973). As discussed in Chapter VI, the presence of elevated Zn contents in AGM may indicate that the prevailing sulphur fugacity (fS_2) at the time of crystallization was too low to allow for the crystallization of a distinct Zn-S species (*e.g.* sphalerite, wurtzite).

5.3. D site

The *D* site is dominated by high field-strength elements (HFSE: Ti, Zr, Nb). Other

elements at *D* include Ta (maximum 0.13 *apfu*) and Hf (maximum 0.04 *apfu*). There is a strong positive correlation between Zr+Nb and Ti (Fig. 16) yet correlations between Zr and Nb are poor. This phenomenon has also been noted in eudialyte group minerals (Johnsen & Gault 1997), suggesting extensive Ti ⇔ Nb and Ti ⇔ Zr substitution, but a lack of Nb ⇔ Zr substitution. Niobium can occupy up to 75% (1.50 *apfu* Nb) of *D* in kupletskite subgroup samples, as observed in niobokupletskite from MSH, and, up to 84% (1.68 *apfu* Nb) of *D* in niobophyllite from Letitia Lake (Labrador, Canada). Niobium-bearing kupletskite and niobokupletskite samples from MSH are common hosts of pyrochlore inclusions (up to ≈ 40 μm) in fractures and along cleavage planes, suggesting late-stage enrichment of the melt or fluid in Nb.

Zirconium shows limited substitution for Ti and Nb (maximum: 1.02 *apfu* in zircophyllite from MSH), presumably due to a difference in ionic radius between the two cations ($^{[6]}Ti^{4+}$: 0.61 Å, $^{[6]}Zr^{4+}$: 0.72 Å, Shannon 1976). The dominance of Zr-rich MNU samples over Zr-rich FEU samples suggests that the presence of the large Mn^{2+} cation ($^{[6]}Mn^{2+}$: 0.83 Å *versus* $^{[6]}Fe^{2+}$: 0.78 Å, Shannon 1976) may be required to permit the expansion of the *O*-sheet imposed by the large Zr cation at *D*. The crystallographic details concerning Zr substitution and its effects on the *O*-sheet will be discussed in Chapters III and IV.

Variations in Nb and Zr between environments are best represented by Nb-Zr *versus* Ti and Nb-Zr *versus* Mn#. As shown in Figures 17 & 18, kupletskite subgroup samples (with the exception of four specimens from MSH) have strongly positive Nb-Zr values, indicating Nb>Zr. Astrophyllite subgroup samples from undersaturated environments show negative

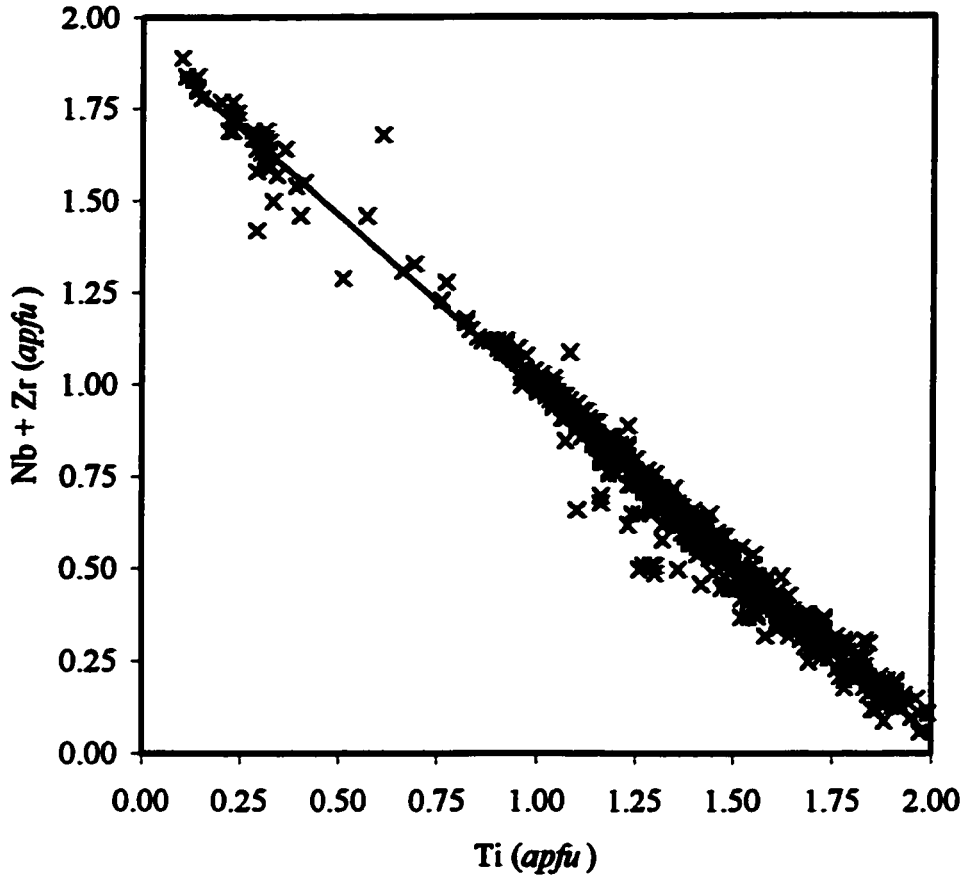

Figure 16. The content of Ti *versus* that of (Nb+Zr) in *D* of astrophyllite group minerals (Linear regression, $R^2 = 0.986$, N = 659)

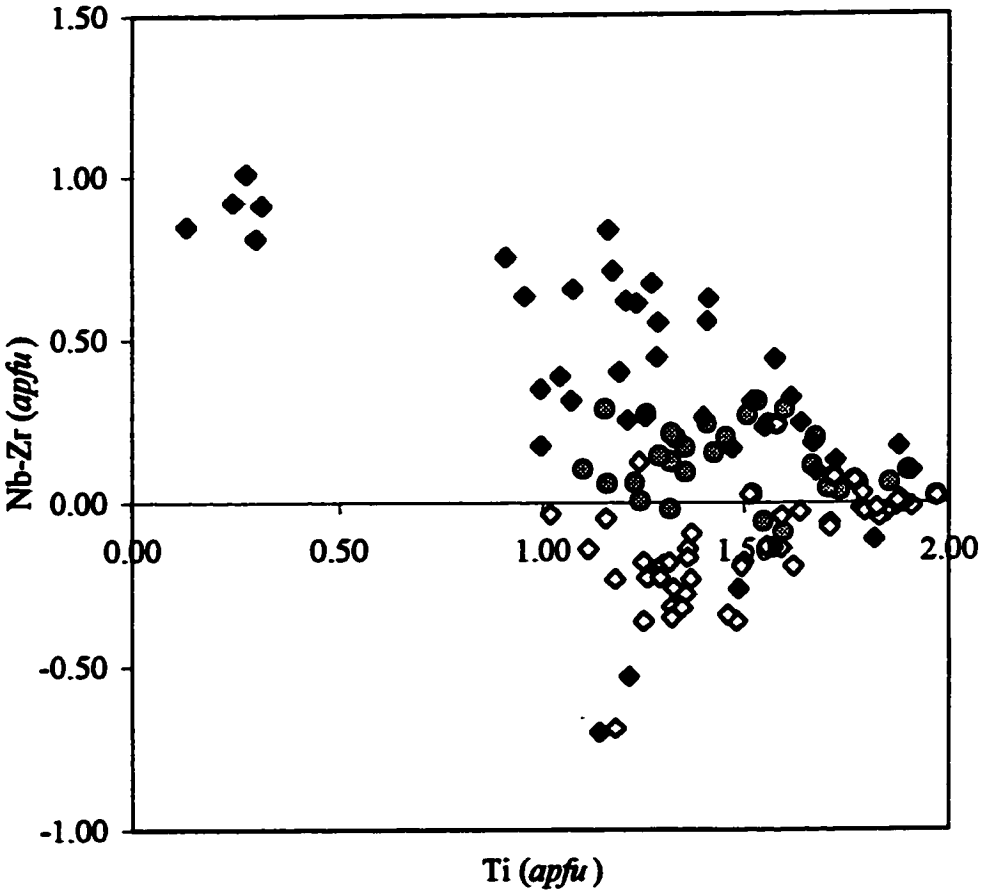

Figure 17. Ti *versus* (Nb-Zr) at *D* of astrophyllite group minerals.
Circles: OVER, Closed diamonds: MNU; Open diamonds: FEU.
In general, MNU and OVER samples have Nb>Zr whereas FEU samples have Zr>Nb.

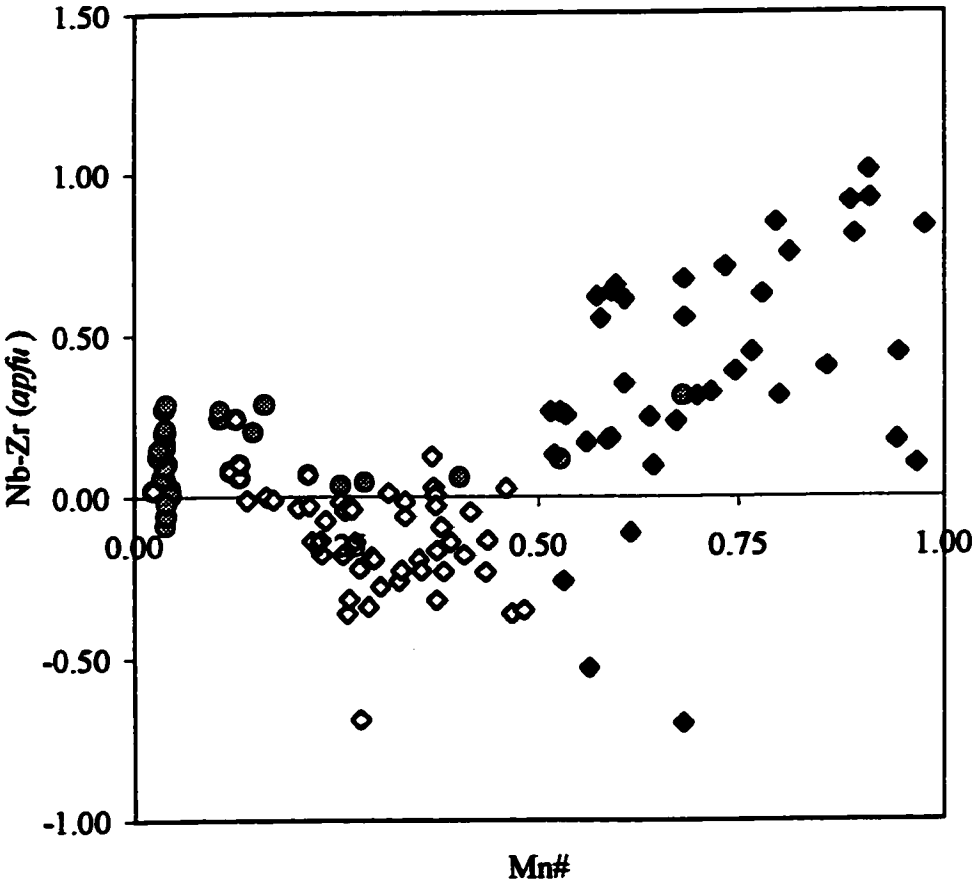

Figure 18. Mn# *versus* (Nb-Zr) at *D* of astrophyllite group minerals.
Circles: OVER, Closed diamonds: MNU; Open diamonds: FEU.
In general, MNU and OVER samples have Nb>Zr whereas FEU samples have Zr>Nb.

values of Nb-Zr, indicating enrichment in Zr. Astrophyllite group minerals from oversaturated intrusions tend to have slightly positive Nb-Zr values, indicating slight enrichments in Nb over Zr. Such samples also have the lowest Zr contents (average: 0.20 *apfu*, range: 0.03-0.35 *apfu*). The lack of Zr in AGM from such oversaturated environments is directly related to the alkalinity and degree of SiO_2 saturation of the melt from which they crystallized. At an alkalinity index [AI = (Na+K)/Al as calculated from molecular proportions] of 1.0 in saturated magmas, Zr saturation occurs early in the crystallization sequence, promoting early crystallization of zircon and inhibiting the formation of either Zr-rich alkali silicates. With increasing alkalinity and increased degree of undersaturation, alkali zirconosilicates are the dominant Zr-bearing minerals to form. Zirconium-poor astrophyllite containing inclusions of zircon have been noted from oversaturated dikes at Mount Rosa (Colorado), and on Kræmers Island (Kangerdlugssuaq, East Greenland; Layne *et al.* 1982), supporting this hypothesis.

5.4. T sites

The dominant cation occupying all four unique *T* sites in AGM is Si. Mössbauer spectroscopy of many samples shows the absence of $^{[4]}Fe^{3+}$. Similarly, site-scattering refinements of all four *T* sites during single-crystal X-ray structure refinements do not indicate significant departures from unity, implying the absence of any heavier X-ray scatterers (*e.g.* Ti, Fe^{3+}), and therefore indicating complete occupancy by Si+Al. Silicon contents range from 7.29 to 7.99 *apfu*, with Al ranging from zero to 0.47 *apfu*. As expected, a positive correlation exists between Si and Al (Fig. 19). Samples from oversaturated

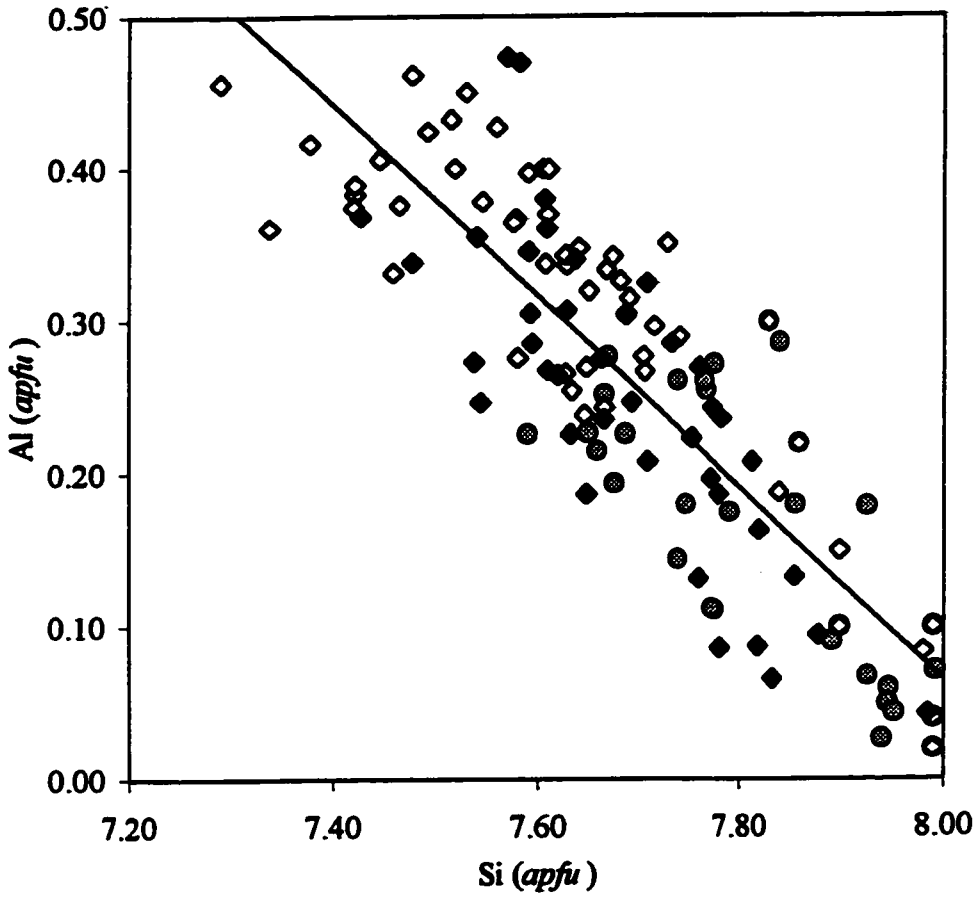

Figure 19. The content of Si *versus* that of Al in *T* in astrophyllite group minerals. Circles: OVER, Closed diamonds: MNU; Open diamonds: FEU. (Linear regression: $R^2 = 0.745$)

alkaline intrusions show the least Si ⇔ Al substitution (average: 0.21 *apfu* Al), likely reflecting crystallization under SiO_2-enriched conditions, whereas kupletskite and astrophyllite subgroup samples from undersaturated environments show the greatest Si ⇔ Al substitution (average: 0.25 and 0.32 *apfu* Al, respectively). In general, Al is a minor component in AGM from both over- and undersaturated environments, perhaps the result of depletion of the melt in Al due to early crystallization of Al-bearing minerals such as nepheline and feldspars.

5.5. Anionic scheme and the ϕ(16) site

The composition of the two monovalent anion sites in the *O*-sheet [O(4) and O(5)] and the mixed valence ϕ(16) site has been the subject of debate in past studies of AGM. In particular, we are concerned with ordering of OH and F over the three sites. It has been previously suggested that F orders preferentially at the ϕ(16) site and does not substitute for OH in the *O*-sheet (Christiansen *et al.* 1998). This basis for such an assumption is the fact that F contents in all AGM (both from this study and in the literature) exhibit a limited range between zero and one *apfu*, suggesting a single site for F. Due to their similarity in scattering powers (Mo*K*α radiation), site refinement involving F^- and O^{2-} could not be done in order to prove the validity of this ordering. Further evidence, including Mössbauer spectroscopy, thermodynamic estimates, and results from EMPA, are presented to resolve the issue of ordering of OH, F and O.

Previous Mössbauer spectroscopic work involving compositions along the annite-fluorannite join have shown F contents to exhibit a strong negative correlation with the

average quadrupole splitting (<QS>; Fig. 20, Rancourt *et al.* 1996). In these synthetic micas, the changes observed in the quadrupole splitting distributions (QSDs) are due to local distortions imposed on the $Fe\phi_6$ octahedron, the result of OH ⇔ F substitution, and the formation of local FeO_4F_2, $FeO_4(OH)F$ and $FeO_4(OH)_2$ configurations. Although not as well-developed due to more complex chemical variations, this negative trend between <QS> and F content is also observed in biotites from granites (Shabani 1999; Fig. 20). Mössbauer spectroscopy was done on a suite of AGM with F contents ranging from 0.15 to 0.97 *apfu*. If a substitution involving F and OH were occurring in the *O*-sheet of AGM [*i.e.* O(4) and O(5)], a similar trend might be expected. However, data for AGM (Figure 20) plot far from the trendline defined by the OH ⇔ F, suggesting that (1) F does not substitute for OH and (2) is not present within the *O*-sheet, but is located at an anion site which does not coordinate a Fe cation [*i.e.* $\phi(16)$].

The Fe-F avoidance principle is a well-known phenomenon in ferromagnesian minerals (Ramberg 1952, Ekström 1972, Speer 1984, Mason 1992). Iron-fluorine avoidance results in significant controls on cation ordering in minerals containing both of these species due to the greater strength of Mg-F bonds compared to Fe-F bonds. A thermodynamic approach can be used to show the preference of Mg over Fe for F (Munoz 1984):

$$FeF_2 + Mg(OH)_2 = Fe(OH)_2 + MgF_2 \quad (6).$$

The resultant ΔG_{rxn} for this exothermic reaction is –21.06 kcal, indicating that the reaction proceeds to the right and that Mg-F bonds are more likely to form. In AGM, Mn ⇔ Fe substitution predominates and Mg is generally not a major cation. We can use the same approach to evaluate the degree of Mn-F avoidance. Equilibrium values of MnF_2 were

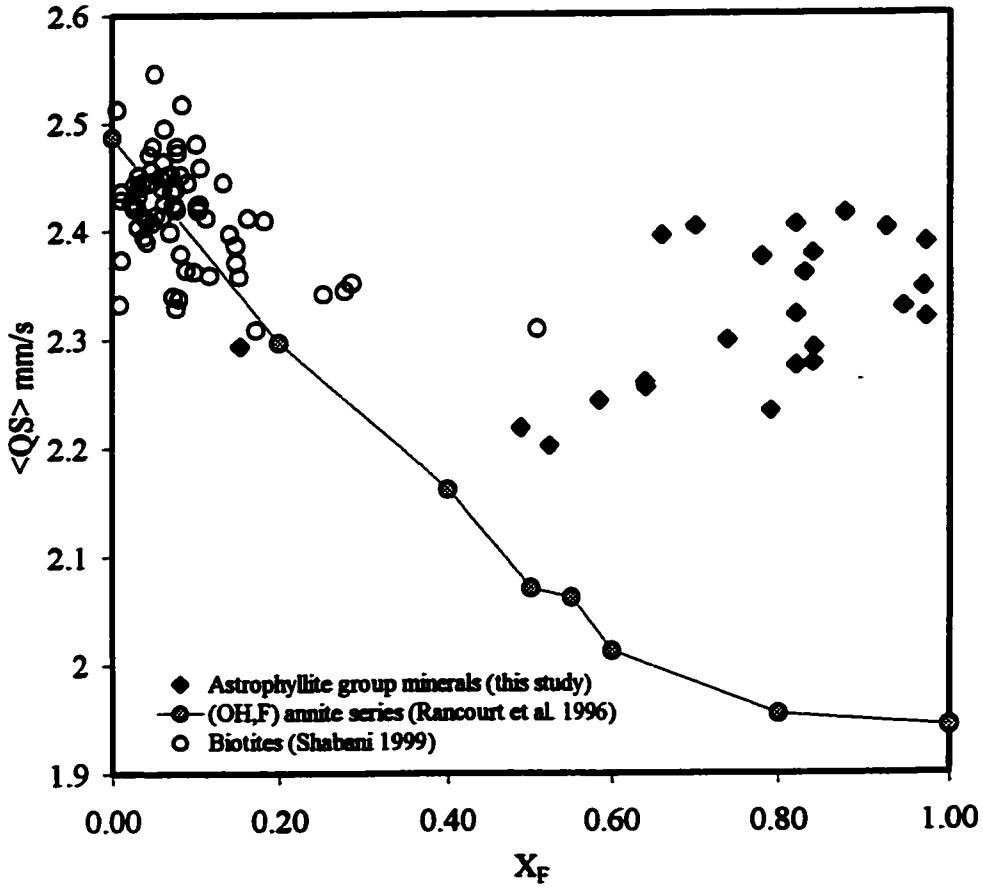

Figure 20. Average quadrupole splitting, <QS> *versus* the fraction of F (X_F) for members of the astrophyllite group and micas of the biotite series.

calculated using additive sums of free energies for Mn^{2+} and F (due to the lack of experimentally-derived values for complexes involving Mn). The preference of Mn and Fe for F can be calculated using:

$$FeF_2 + Mn(OH)_2 = Fe(OH)_2 + MnF_2 \quad (7).$$

The ΔG_{rxn} for (7) is –4 kcal (*i.e.* slightly exothermic), indicating no significant preference for Mn-F or Fe-F bonds. Experiments involving aqueous solutions with both Mn and Fe indicate that the two elements behave identically and will avoid bonding with F (Munoz & Ludington 1974, Mason 1992). This results not only in Fe-F avoidance, but Mn-F avoidance as well. The existence of Fe-F and Mn-F avoidance, coupled with the lack of a strong negative correlation between Fe-F and Mn-F (Figs. 18A & B) suggest that the monovalent anion sites O(4) and O(5), both of which are ligands to Mn and Fe cations within the *O*-sheet, are occupied solely by OH.

Similar thermodynamic experiments involving aqueous solutions of Ti, OH and F have also been done (McAulifefe & Barratt 1987, Mason 1992). Such studies indicate that Ti-F complexes are readily synthesized whereas those of Ti-OH are difficult to produce, suggesting a Ti-OH avoidance. This can be shown qualitatively using the equation

$$2FeF_2 + Ti(OH)_4 = 2Fe(OH)_2 + TiF_4 \quad (8)$$

calculated using additive sums of the free energies for Ti^{4+}, F^-, and OH^-. The ΔG_{rxn} for Eqn. 8 is –44 kcal, indicating a strong preference of Ti over Fe for F, and, by analogy, Mn. A similar situation exists for Zr. Both Zr and Ti, because of their low electronegativities, form stable complexes with F except in cases where extremely high aH^+ or aCO_2 exist (Crerar *et al.* 1985, Aja *et al.* 1995). Thermodynamic and solubility calculations for various

temperatures show that Zr preferentially complexes with OH over a wide range of pH conditions and temperatures, and will complex with F in F-rich and Ca-poor hydrothermal brines (Aja *et al.* 1995, Salvi & Williams-Jones 1995) with mixed hydroxyfluoride complexes [*e.g.* $Zr(OH)_2F_2$] as the dominant species in solution (Salvi *et al.* 2000).

Based on data acquired by Mössbauer spectroscopy, thermodynamic approximations, and given the restricted range of F contents observed in AGM, it has been shown that F orders at the $\phi(16)$ site and does not occur at the two general OH sites within the *O*-sheet. It must be emphasized that the values for free energies used in the preceding equations were derived from experiments at 25 °C and are (at best) only estimates of the processes that are at work in a magma or hydrothermal fluid. The lack of equilibrium conditions in such complex environments, coupled with the wide range of temperature, precludes the possibility of quantitatively using thermodynamic data based on standard conditions to predict complexing in melts. Nevertheless, the use of additive sums of free energies has been shown to give reasonable approximations for compounds for which thermodynamic data is not available (*i.e.* TiF_4, Krauskopf 1967) and therefore considered to be useful in this context as long as the qualitative aspect of the results is recognized.

6.0. Substitutions and Solid Solution Series in the Astrophyllite Group

In light of the chemical variations described above, solid-solution series have been confirmed, either wholly or in partial, between the following pairs of AGM:

1. astrophyllite-kupletskite (complete, $Mn \Leftrightarrow Fe^{2+}$)
2. kupletskite-niobokupletskite (complete, $Ti + F \Leftrightarrow Nb + O$)

3. astrophyllite-niobophyllite (partial, Ti + F ⇔ Nb + O)

4. kupletskite-zircophyllite (partial, Ti ⇔ Zr)

5. astrophyllite- Fe-dominant zircophyllite (partial, Ti ⇔ Zr)

The dominant substitutional mechanisms observed in the AGM studied include:

$$K \Leftrightarrow (Cs,Rb) \quad (9)$$

$$Si+Na \Leftrightarrow Al+Ca \quad (10)$$

$$Ti \Leftrightarrow Nb \text{ and } Ti \Leftrightarrow Zr \quad (11)$$

$$Mn \Leftrightarrow Fe^{2+}, (Mg,Zn) \Leftrightarrow (Mn,Fe^{2+}) \text{ and } (Mn,Fe) \Leftrightarrow Na \quad (12)$$

$$Ti + F \Leftrightarrow (Zr,Nb) + OH \text{ and } Ti + F \Leftrightarrow Nb + O \quad (13).$$

The most complex of the solid solutions involves species in which Nb is incorporated into the astrophyllite group structure. Incorporation of a pentavalent cation at *D* requires a number of considerations with respect to charge balance. Abdel-Rahman (1992) suggested that Nb enters the AGM structure *via* the substitution $Nb \Leftrightarrow Ti + \square$, and Birkett *et al.* (1996) subsequently suggested the coupled substitutions $Nb + Fe^{3+} \Leftrightarrow 2R^{4+}$ and $Nb + (Mn,Fe)^{2+} \Leftrightarrow 3Ti^{4+}$. Such mechanisms, along with not being charge-balanced, would require creation of *D*-site vacancies and/or incorporation of Fe^{2+} or Fe^{3+} at *D*, features that are not supported by the EMPA data. Similarly, single crystal X-ray structure refinements and Mössbauer spectroscopy have not indicated Fe^{2+} or Fe^{3+} to be present at *D* in any of the samples analyzed.

Incorporation of Nb^{5+} into the structure in niobokupletskite, niobophyllite and Nb-bearing kupletskite is best modeled by the coupled substitution Ti + F ⇔ Nb + O (Piilonen *et*

al. 2000). In astrophyllite subgroup samples, Zr > Nb. The dominant substitutional mechanism therefore involves Zr and not Nb, and can thus be expressed as Ti + F ⇔ Zr + OH. When calculation of the general formula was discussed in earlier sections, it was shown that Nb = 0.50 *apfu* is used as a limiting value to determine the preferred method to calculate an AGM formula. This value seems to represent a limiting value at which the two substitution mechanisms above exchange dominance in the AGM structure (Fig. 21).

The oxidation of members of the astrophyllite due to incorporation of Nb also results in $Fe^{3+} \Leftrightarrow M^{2+}$ substitution in the *O*-sheet. In order to maintain charge balance substitution of Fe^{3+} must also be accompanied by substitution of Na for M^{2+}, which has been shown by single-crystal X-ray structure refinements to occur at *M*(1). Substitution of Fe^{3+} must therefore occur either at *M*(2) or *M*(3) in order to satisfy the bond-valence requirements of the O(2) oxygen to which *M*(1), *M*(2), *M*(3) and *D* are bonded. As such, a more complex substitutional scheme has been developed for Nb-rich samples, incorporating Fe^{3+} contents derived from Mössbauer spectroscopy (Fig. 22):

$$M(1)^{2+} + M(2,3)^{2+} + (Zr,Ti) + F \Leftrightarrow {}^{M(1)}Na + {}^{M(2,3)}Fe^{3+} + Nb + O \quad (14).$$

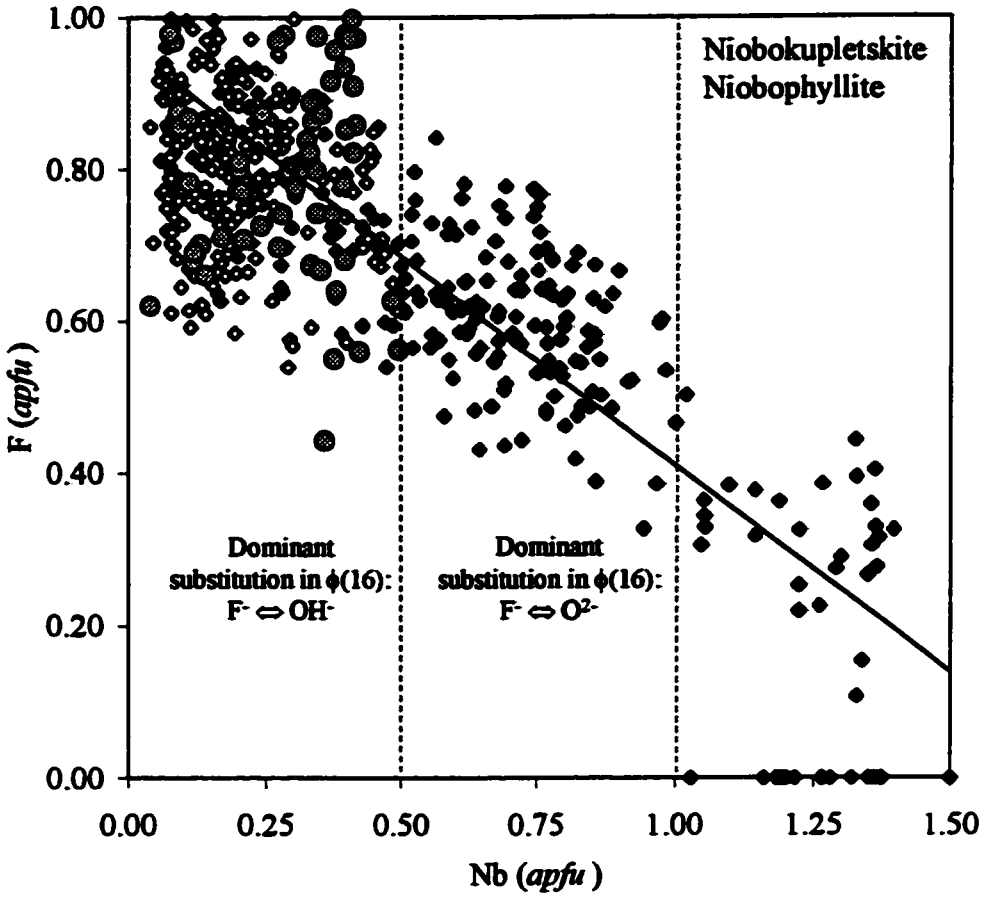

Figure 21. Content of Nb *versus* that of F. Substitution of Nb into astrophyllite group minerals occurs in niobokupletskite, niobophyllite and Nb-bearing kupletskite as the result of the substitution Ti + F ⇔ Nb + O. Samples of the astrophyllite subgroup and those from oversaturated rocks do not show significant Nb enrichment and can therefore be expressed by the substitution Ti + F ⇔ (Zr,Nb) + OH. Nb = 0.50 *apfu* represents the limiting value at which these two substitutional mechanisms exchange dominance in the AGM structure. The regression line (R^2 = 0.7601) demonstrates the strong negative correlation between Nb and F in only kupletskite subgroup samples.
Circles: OVER, Closed diamonds: MNU; Open diamonds: FEU.

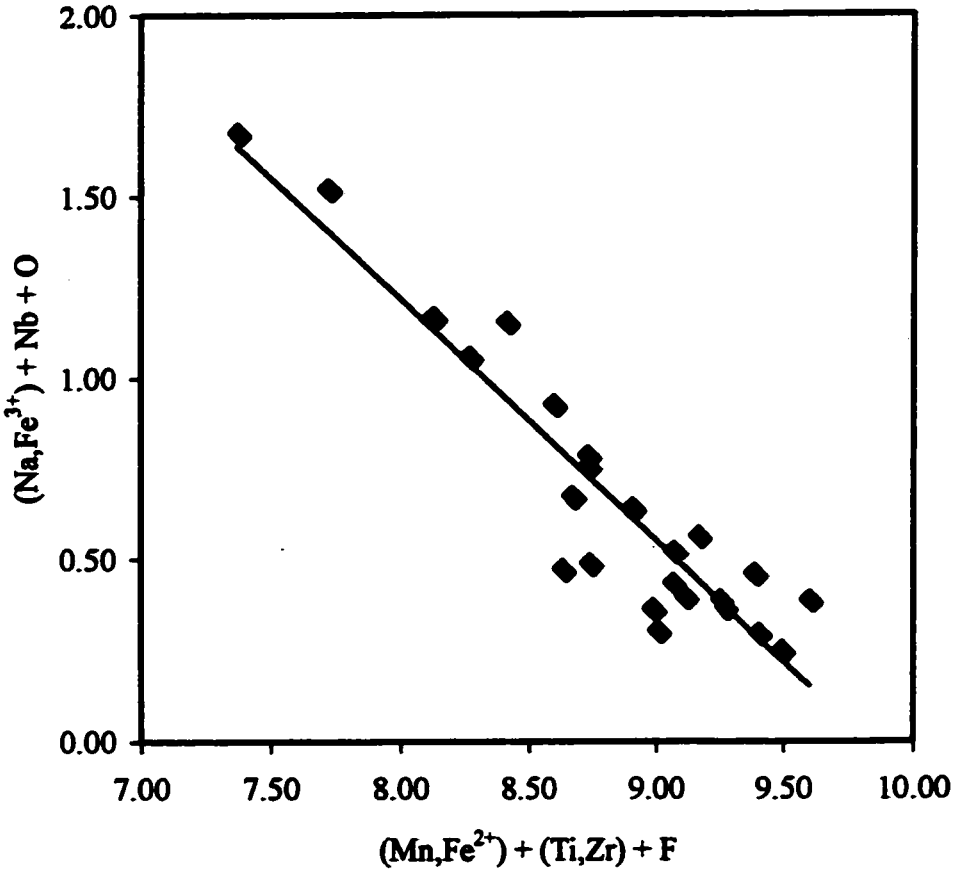

Figure 22. Substitutional mechanism for incorporation of Nb^{5+} into the AGM structure: $M^{2+} + M^{4+} + F^{-} \Leftrightarrow (Na,Fe^{3+}) + Nb^{5+} + O^{2-}$ (Linear regression, $R^2 = 0.870$)

CHAPTER III.

ASTROPHYLLITE GROUP MINERALS II: CRYSTAL STRUCTURE AND CHEMICAL VARIATIONS

PAULA C. PIILONEN
Ottawa-Carleton Geoscience Centre, Department of Earth Sciences
University of Ottawa, Ottawa, Ontario K1N 6N5

ANDREW M. McDONALD
Department of Earth Sciences, Laurentian University, Sudbury, Ontario P3E 2C6

ANDRÉ E. LALONDE
Ottawa-Carleton Geoscience Centre, Department of Earth Sciences
University of Ottawa, Ottawa, Ontario K1N 6N5

OVERVIEW

This chapter presents the first detailed study of the crystal chemistry of members of the astrophyllite group. Data from 20 single-crystal X-ray structure refinements, coupled with compositional data from EMPA and Mössbauer spectroscopy, are used to describe the structural variations present within the group and discuss the effects of isomorphous substitution (presented in Chapter II) on the structure. Following submission of this thesis, this chapter will be submitted for publication in *European Journal of Mineralogy*.

ABSTRACT

Single-crystal X-ray structure refinements, coupled with electron-microprobe analyses, were done on 20 crystals of astrophyllite group minerals (AGM) from a variety of localities and spanning a wide range of compositions including astrophyllite, *sensu stricto*, kupletskite and niobokupletskite. Members of the astrophyllite group are triclinic, $P\bar{1}$, and monoclinic, *C*2/*c* or *A*2, heterophyllosilicates and are the intermediate members of a polysomatic or homologous series that includes perraultite and mica as end-member structures. The AGM structure consists of two composite sheets stacked along [001] in a 2:1 ratio, resulting in a layered *HOH* structure reminiscent of the *TOT* structure in 2:1 phyllosilicates. The structure consists of an octahedral sheet (*O*-sheet) comprised of MO_6 octahedra (where M = Mn, Fe^{2+}, Fe^{3+}, Na, Mg or Zn) sandwiched between two heterogeneous sheets (*H*-sheets) with an ideal composition $[(Ti,Nb,Zr)Si_4O_{12}]^{4-}$. The interlayer is comprised of two crystallographically distinct cation sites, *A* and *B*, host to K and Na, respectively. The *H*-sheet consists of open-branched *zweier* [100] single $[Si_4O_{12}]^{8-}$ chains which are cross-linked by corner-sharing $D\phi_6$ octahedra in triclinic species and kupletskite-*Ma*2*b*2*c*, and DO_5 polyhedra in magnesium astrophyllite, where D = Nb,Ti,Zr. Substitution of Nb at *D* results in positional displacement of the cation toward the center of the octahedron, resulting in a more regular distribution of D-ϕ_{apical} bond lengths and a decreased distortion. Substitution of Zr at *D* results in an increase in $\langle D\text{-}\phi \rangle$ bond lengths and decreased distortion of the octahedron and seems to be limited to 50% of *D* due to crystallographic restrictions on the local *O*-sheet octahedra. Lateral fit of the *H*- and *O*-

sheets is accomplished primarily by tilting of the tetrahedra out of the (001) plane, elongation or thickening of the tetrahedra along [001], and flattening of *O*-sheet octahedra.

1.0. INTRODUCTION

Members of the astrophyllite group are alkali titano-, niobo- and zirconosilicates that characteristically occur in peralkaline nepheline syenites and their associated pegmatites, alkali granites, and their metamorphic equivalents. The crystal structure of monoclinic magnesium astrophyllite was first determined by Peng & Ma (1963) and the structure of triclinic astrophyllite subsequently determined by Woodrow (1967). Since then, structural studies of members of the astrophyllite group have been done by Christiansen *et al.* (1998; kupletskite) Shi *et al.* (1998; monoclinic magnesium astrophyllite, *A*2), Piilonen *et al.* (2000, niobokupletskite; 2001, kupletskite-1*A* and kupletskite-*Ma*2*b*2*c*), Yamnova *et al.* (2000, astrophyllite), and Zhesheng *et al.* (2000, astrophyllite).

In Chapter II we described the ranges in composition in AGM from over- and undersaturated intrusions. The extensive range in chemical compositions observed is a reflection of a crystal structure that contains numerous sites at which isomorphous substitutions may occur. In this chapter, we will describe the structural variations that result from these substitutions. In particular we are interested in (1) changes in the composition of the *O*-sheet and its effects on lateral fit of the *H*- and *O*-sheets, and (2) the effects of substitution of Zr and Nb for Ti in the $D\phi_6$ octahedron, and its influence on the local stereochemistry of both the *H*- and *O*-sheets. This study is based on single-crystal X-ray

structure refinements of 20 AGM crystals from a variety of localities, coupled with additional compositional data obtained by EMPA and Mössbauer spectroscopy.

2.0. Analytical Methods

Table 1 lists the provenance of each of the 20 samples studied. In all cases (except NOR17) chemical data were collected on the same crystal used for the single-crystal X-ray refinement (the crystal for NOR17 was lost during transfer to the probe mount). An attempt was made to cover the entire possible range in chemical variations observed in AGM. Of particular interest are variations in Na, K, Mn, Fe, Mg, Zn, Ti, Zr, Nb and F.

2.1. Electron-microprobe analyses

Electron-microprobe analyses (EMPA) were done on a JEOL 733 electron microprobe, operating in wavelength-dispersive mode, using Tracor Northern 5500 and 5600 automation software. Details concerning operating conditions and selection of standards are given in Chapter II. Table 2 contains average EMPA data for each single crystal, with chemical formulae calculated based on a total of 31 anions and 4(OH) + (F,O,OH) (as proposed in Chapter II).

2.2. X-ray crystallography

Single-crystal X-ray diffraction was done to investigate variations in the AGM structure and potential isomorphous substitutions. Intensity data were collected on three different single-crystal X-ray diffractometers. All samples analyzed were handpicked under

TABLE 1. LOCALITY INFORMATION FOR ASTROPHYLLITE GROUP MINERAL SINGLE CRYSTALS

Sample code	Sample (Collection) #	Locality and rock type
GJER		Gjerdingen intrusion, Norway
	NOR17 (LHN-5)	- alkali granite
KHIB		Khibina massif, Kola Peninsula, Russia
	RUS4 (CMNMI-53187)	- nepheline syenite pegmatite
	RUS8 (FMM-1)	- nepheline syenite pegmatite
LAB		Seal Lake, Labrador, Canada
	LAB3 (GSC-M26148-B)	- peralkaline nepheline gneiss
LANG		Langesundsfjord area, Oslo Rift Valley, Norway
	NOR1 (RW-1)	- nepheline syenite pegmatite (Vesle Arøya)
LOV		Lovozero massif, Kola Peninsula, Russia
	RUS9 (HC-1048)	- nepheline syenite pegmatite (Lephke-Nelm)
	RUS12 (FMM-56274)	- nepheline syenite pegmatite (Kuivchorr Mt.)
MSH		Mont Saint-Hilaire, Québec, Canada
	MSH2 (NMNS-4)	- nepheline syenite pegmatite
	MSH3 (NMNS-5)	- nepheline syenite pegmatite
	MSH8 (NMNS-12)	- altered nepheline syenite pegmatite
	MSH9 (NMNS-13)	- nepheline syenite pegmatite
	MSH15 (NMNS-22)	- nepheline syenite pegmatite
	MSH19A (NMNS-26)	- altered nepheline syenite pegmatite
	MSH20 (NMNS-27)	- nepheline syenite pegmatite
	MSH33A (CMNMC)	- aplite/pegmatite
	MSH34A (CMNMC)	- nepheline syenite pegmatite
	MSH38A (CMNMC)	- altered nepheline syenite pegmatite
	MSH42*	- nepheline syenite pegmatite
	MSH44	- sodalite syenite
	MSH45	- sodalite syenite xenolith
PP		Mount Rosa, Pikes Peak, Colorado, USA
	US5 (CMNMC)	- granitic pegmatite

CMNMC/CMNMI/NMNS = Canadian Museum of Nature collection, GSC = Geological Survey of Canada collection, FMM = Fersman Mineralogical Museum collection, RW = R. Werner collection, HC/LHN = L. Horváth collection,

* Holotype niobokupletskite

TABLE 2. ELECTRON-MICROPROBE DATA FOR AGM SINGLE CRYSTALS

Oxide	LAB3	NOR1	RUS4	RUS8	RUS9	RUS12	US5	MSH2	MSH3
Na_2O	2.98	2.68	2.07	2.40	2.07	2.61	2.95	2.98	3.66
K_2O	5.81	5.21	6.02	6.21	6.21	5.91	5.45	5.61	5.46
Rb_2O	0.38	1.05	0.40	0.29	0.50	0.50	1.26	0.37	0.58
Cs_2O	0.06	1.35	0.03	0.00	0.03	0.00	0.09	0.00	0.00
CaO	0.64	1.00	1.59	1.60	1.27	1.38	0.08	0.75	0.03
SrO	0.20	0.10	0.39	0.25	0.27	0.23	0.01	0.05	0.10
BaO	0.00	0.00	0.20	0.23	0.52	0.07	0.19	0.20	0.00
MgO	0.65	1.11	1.66	1.71	1.42	1.94	0.00	0.44	0.44
MnO	14.19	13.99	11.04	12.30	21.46	27.53	4.80	30.81	26.26
FeO	19.49	18.45	21.80	20.00	10.98	4.13	27.59	2.00	0.13
ZnO	0.00	0.49	0.47	0.31	0.00	0.00	2.67	0.75	6.78
Al_2O_3	0.77	1.01	1.22	1.06	1.04	0.24	0.16	0.74	0.26
Y_2O_3	0.00	0.00	0.00	0.00	0.00	0.00	0.00	0.00	0.00
Ce_2O_3	0.17	0.31	0.11	0.00	0.29	0.07	0.17	0.54	0.00
TiO_2	6.99	9.20	11.41	11.20	10.52	11.40	9.28	10.80	7.05
SnO_2	0.00	0.23	0.00	0.00	0.00	0.00	0.60	0.00	0.00
ZrO_2	6.25	1.69	0.57	0.61	0.00	0.00	0.76	0.00	0.00
HfO_2	0.00	0.00	0.00	0.00	0.00	0.00	0.00	0.00	0.00
Nb_2O_5	1.60	2.81	0.89	0.59	2.38	0.77	3.07	1.91	7.81
Ta_2O_5	0.00	0.00	0.15	0.00	0.00	0.00	0.18	0.00	0.00
SiO_2	33.63	33.98	34.85	34.55	34.64	36.35	34.45	34.29	34.60
F	1.15	1.38	1.05	0.94	1.10	1.16	1.24	1.31	0.70
H_2O	2.69	2.65	2.90	2.90	2.83	2.85	2.68	2.67	2.60
O=F	-0.48	-0.58	-0.44	-0.40	-0.46	-0.49	-0.52	-0.55	-0.29
Total	96.35	98.12	98.34	96.77	97.02	96.68	97.14	95.67	96.11

Formula based on 31 anions

Cation	LAB3	NOR1	RUS4	RUS8	RUS9	RUS12	US5	MSH2	MSH3
K	1.72	1.51	1.70	1.77	1.77	1.67	1.60	1.63	1.61
Rb	0.06	0.15	0.06	0.04	0.07	0.07	0.19	0.05	0.09
Cs	0.01	0.13	0.00	0.00	0.00	0.00	0.01	0.00	0.00
Sr	0.03	0.01	0.05	0.03	0.03	0.03	0.00	0.01	0.01
Ba	0.00	0.00	0.02	0.02	0.05	0.01	0.02	0.02	0.00
Na	0.12	0.09	0.00	0.12	0.00	0.02	0.03	0.15	0.12
ΣA	1.81	1.80	1.82	1.87	1.93	1.79	1.81	1.71	1.71
Na	0.84	0.76	0.61	0.62	0.52	0.65	0.98	0.82	0.99
Ca	0.16	0.24	0.38	0.38	0.31	0.33	0.02	0.18	0.01
ΣB	1.00	1.00	0.99	1.00	0.82	0.97	1.00	1.00	1.00
Na	0.20	0.33	0.28	0.30	0.38	0.44	0.30	0.35	0.53
Mg	0.22	0.38	0.55	0.57	0.47	0.64	0.00	0.15	0.15
Mn	2.79	2.69	2.07	2.33	4.07	5.15	0.93	5.95	5.14
Fe^{2+}	3.78	3.50	4.02	3.74	2.06	0.77	5.30	0.38	0.02
Zn	0.00	0.08	0.08	0.05	0.00	0.00	0.45	0.13	1.16
Y	0.00	0.00	0.00	0.00	0.00	0.00	0.00	0.00	0.00
Ce	0.01	0.03	0.01	0.00	0.02	0.01	0.02	0.05	0.00
ΣC	7.00	7.00	7.00	7.00	7.00	7.00	7.00	7.00	7.00
Ti	1.15	1.57	1.89	1.89	1.78	1.90	1.60	1.85	1.23
Sn	0.00	0.02	0.00	0.00	0.00	0.00	0.06	0.00	0.00
Zr	0.71	0.19	0.06	0.07	0.00	0.00	0.09	0.00	0.00
Hf	0.00	0.00	0.00	0.00	0.00	0.00	0.00	0.00	0.00
Nb	0.17	0.29	0.09	0.06	0.24	0.08	0.32	0.20	0.82
Ta	0.00	0.00	0.01	0.00	0.00	0.00	0.01	0.00	0.00
ΣD	2.02	2.06	2.05	2.01	2.02	1.97	2.07	2.05	2.04
Si	7.80	7.70	7.69	7.73	7.76	8.03	7.91	7.81	8.00
Al	0.21	0.27	0.32	0.28	0.28	0.06	0.04	0.20	0.07
ΣT	8.01	7.97	8.01	8.01	8.04	8.09	7.96	8.01	8.07
F	0.84	0.99	0.73	0.67	0.78	0.81	0.90	0.94	0.51
OH	4.16	4.01	4.27	4.33	4.23	4.20	4.10	4.06	4.00
O	30.16	30.01	30.27	30.33	26.00	26.00	30.10	30.06	30.49
Σ ost.	19.96	19.93	19.86	20.01	19.80	19.83	19.87	19.92	19.93

TABLE 2 CONTINUED

Oxide	MSH8	MSH9	MSH15	MSH15A	MSH19A	MSH20	MSH33A	MSH34	MSH38A	MSH42
Na_2O	3.04	2.62	3.12	3.38	2.65	2.82	2.37	2.33	2.44	2.62
K_2O	6.30	5.49	5.52	5.59	5.86	5.60	6.04	6.04	5.64	5.97
Rb_2O	0.51	0.46	0.58	0.58	0.38	0.74	0.40	0.35	0.44	0.82
Cs_2O	0.00	0.00	0.00	0.06	0.00	0.06	0.06	0.07	0.00	0.12
CaO	0.44	0.78	0.20	0.13	0.22	1.12	0.56	0.93	0.81	0.00
SrO	0.00	0.09	0.28	0.05	0.03	0.06	0.20	0.26	0.03	0.00
BaO	0.00	0.18	0.09	0.00	0.00	0.25	0.00	0.00	0.00	0.00
MgO	0.51	0.43	1.05	0.98	0.53	0.53	0.56	0.50	0.47	0.15
MnO	23.54	29.99	26.71	21.64	19.34	28.65	14.56	8.95	17.98	26.37
FeO	9.66	1.91	6.19	10.00	13.39	1.02	18.95	24.96	14.85	2.64
ZnO	0.64	0.67	0.00	0.26	0.28	4.45	0.00	0.00	0.22	4.08
Al_2O_3	0.96	0.86	0.40	0.63	0.43	0.70	1.29	1.32	0.58	1.14
Y_2O_3	0.00	0.00	0.00	0.00	0.00	0.00	0.00	0.00	0.00	0.00
Ce_2O_3	0.00	0.58	0.08	0.00	0.00	0.34	0.26	0.00	0.15	0.00
TiO_2	6.20	10.28	8.29	6.84	6.89	11.25	5.43	7.31	9.01	1.34
SnO_2	0.00	0.00	0.00	0.00	0.00	0.00	0.00	0.00	0.00	0.00
ZrO_2	0.38	0.00	0.10	0.50	1.92	0.00	6.30	4.36	0.49	3.43
HfO_2	0.00	0.00	0.00	0.00	0.00	0.00	0.08	0.00	0.00	0.00
Nb_2O_5	8.59	1.93	6.06	7.51	5.05	0.96	3.46	2.80	3.52	12.13
Ta_2O_5	0.00	0.00	0.00	0.00	0.00	0.00	0.00	0.16	0.00	0.63
SiO_2	34.62	35.35	35.31	34.24	34.79	34.46	32.63	33.09	35.00	31.85
F	0.87	1.09	0.91	1.00	1.01	1.19	1.08	1.20	0.91	0.14
H_2O	2.93	2.63	2.67	2.80	2.77	2.73	2.70	2.68	2.61	2.48
O=F	-0.37	-0.46	-0.38	-0.42	-0.43	-0.50	-0.45	-0.51	-0.38	-0.06
Total	98.83	94.88	97.12	95.77	95.12	96.44	96.48	96.81	94.76	95.85

Formula based on 31 anions

Cation	MSH8	MSH9	MSH15	MSH15A	MSH19A	MSH20	MSH33A	MSH34	MSH38A	MSH42
K	1.80	1.60	1.59	1.63	1.73	1.62	1.80	1.78	1.66	1.84
Rb	0.07	0.07	0.08	0.09	0.06	0.11	0.06	0.05	0.07	0.13
Cs	0.00	0.00	0.00	0.01	0.00	0.01	0.01	0.01	0.00	0.01
Sr	0.00	0.01	0.04	0.01	0.00	0.01	0.03	0.04	0.00	0.00
Ba	0.00	0.02	0.01	0.00	0.00	0.02	0.00	0.00	0.00	0.00
Na	0.01	0.00	0.03	0.03	0.00	0.18	0.02	0.00	0.00	0.00
ΣA	1.87	1.69	1.71	1.73	1.79	1.77	1.89	1.87	1.72	1.98
Na	0.87	0.62	0.95	0.97	0.78	0.73	0.86	0.77	0.66	0.95
Ca	0.11	0.19	0.05	0.03	0.05	0.27	0.14	0.23	0.20	0.00
ΣB	0.98	0.81	1.00	1.00	0.83	1.00	1.00	1.00	0.86	0.95
Na	0.45	0.54	0.38	0.51	0.41	0.34	0.20	0.27	0.43	0.28
Mg	0.17	0.15	0.35	0.34	0.18	0.18	0.20	0.17	0.16	0.05
Mn	4.47	5.79	5.10	4.20	3.78	5.51	2.88	1.75	3.50	5.40
Fe^{2+}	1.81	0.36	1.17	1.92	2.58	0.19	3.70	4.81	2.86	0.53
Zn	0.11	0.11	0.00	0.04	0.05	0.75	0.00	0.00	0.04	0.73
Y	0.00	0.00	0.00	0.00	0.00	0.00	0.00	0.00	0.00	0.00
Ce	0.00	0.05	0.01	0.00	0.00	0.03	0.02	0.00	0.01	0.00
ΣC	7.00	7.00	7.00	7.00	7.00	7.00	7.00	7.00	7.00	7.00
Ti	1.05	1.76	1.40	1.18	1.20	1.92	0.95	1.27	1.56	0.24
Sn	0.00	0.00	0.00	0.00	0.00	0.00	0.00	0.00	0.00	0.00
Zr	0.04	0.00	0.01	0.06	0.22	0.00	0.72	0.49	0.06	0.41
Hf	0.00	0.00	0.00	0.00	0.00	0.00	0.01	0.00	0.00	0.00
Nb	0.87	0.20	0.62	0.78	0.53	0.10	0.37	0.29	0.37	1.33
Ta	0.00	0.00	0.00	0.00	0.00	0.00	0.00	0.01	0.00	0.04
ΣD	1.96	1.96	2.03	2.01	1.94	2.02	2.04	2.06	1.98	2.02
Si	7.76	8.06	7.96	7.84	8.03	7.83	7.62	7.63	8.05	7.71
Al	0.25	0.23	0.10	0.17	0.12	0.19	0.36	0.36	0.16	0.33
ΣT	8.01	8.29	8.06	8.01	8.14	8.02	7.98	7.99	8.21	8.03
F	0.62	0.79	0.64	0.73	0.74	0.86	0.80	0.88	0.66	0.11
OH	4.38	4.00	4.00	4.28	4.26	4.15	4.20	4.13	4.00	4.00
O	30.38	30.21	30.36	30.28	30.26	30.15	30.20	30.13	30.34	30.89
Σ cat.	19.82	19.76	19.84	19.78	19.70	19.98	19.93	19.92	19.77	19.98

the binocular microscope to ensure that they were free of macroscopic inclusions. Grains were then observed under the polarizing microscope to ensure that they were optically homogeneous and thus single crystals. Select grains were also analyzed by the precession X-ray diffraction method to check for intergrowths and/or twinning.

Intensity data for six samples (RUS4, US5, MSH3, MSH15, MSH33A and MSH42) were collected using the Siemens SMART (Siemens Molecule Analysis Research Tool) system at the University of Ottawa consisting of a three-circle goniometer and a 1 K (diameter: 9cm, 512 x 512 pixel) CCD area-detector. Data were collected at room temperature (~25° C) using monochromatic Mo$K\alpha$ X-radiation (40 kV, 30 mA) and a fixed detector-crystal distance of 12.621 cm. A frame width (ω) of 0.3° and count exposure times of 30 seconds per frame were used as standard settings. Data collection included unit cell determination (~18 minutes) and collection of all frames data (17.5 hours). The data were reduced, filtered, integrated, and corrected for Lorentz, polarization and background effects using the Siemens software SAINT. Psi-scan absorption corrections were performed using XPREP, during which the crystals were modeled as plates on (001). A range of plate glancing angles was applied to each crystal (generally 2-9°) with the angle yielding the best transmission factors chosen for the absorption correction.

Intensity data for 11 samples (LAB3, NOR1, NOR17, RUS9, RUS12, MSH2, MSH8, MSH9, MSH15A, MSH19A, MSH34A and MSH38A) were collected using the Siemens SMART system at the University of Manitoba consisting of a four-circle goniometer and a 1 K (diameter: 9 cm, 512 x 512 pixel) CCD area-detector. Data were collected at room temperature using monochromatic Mo$K\alpha$ X-radiation (50 kV and 40 mA) and a fixed

detector-crystal distance of 4 cm. A frame width (ω) of 0.2° and count exposure times of 45 seconds were used as standard settings. Data collection consisted of 4349 frames, up to 60° 2θ, which provided 100% coverage of the diffraction sphere with a mean redundancy of 3.6. Approximately 1000 reflections with spot sizes of 2.4° (XY, in the plane) and 2.0° (Z, through the plane) were used in determination of the orientation matrix and preliminary unit cell prior to integration of all frames data. Data integration was done using the Siemens software SAINT. Absorption corrections were done using SADABS and crystals modeled as an ellipse. All reflection data were then merged using the program XPREP.

X-ray intensity data for two samples (RUS8 and MSH20) were collected on a Siemens P3 four-circle diffractometer operating at 50 kV and 40 mA, equipped with a standard serial detector. An orientation matrix was obtained by collecting intensity data for 50 random reflections within the range 12 to 35° 2θ. Following determination of the orientation matrix, half a sphere of intensity data were collected within the range 4 to 60° 2θ using scan speeds inversely proportional to peak intensity (range: 3 to 29.3° 2θ/minute) and scan range of ±1.3° 2θ with respect to peak position. In order to monitor experimental conditions over time, a check reflection ($\bar{1}\,\bar{3}\,0$) was collected every 50 reflections.

The structures for 19 triclinic samples were refined in space group $P\bar{1}$ (#2) by least-squares methods using the SHELXL-93 set of programs, whereas that of monoclinic kupletskite was solved and refined in space group $C2/c$ (#15). All atomic coordinates and temperature factors were kept as refineable parameters during the refinement process. Except for cases in which the interlayer site A was split due to positional disorder, all

displacement parameters were refined as anisotropic. Site-occupancy factors (SOF) for all anions were fixed at unity. During the initial refinement, cation assignments to the *A*, *B*, *M*(1) through *M*(4), and *D* sites were made on the basis of data obtained from EMP analyses. Scattering curves for neutral atoms were taken from Cromer and Liberman (1970). In cases where the site-scattering refinements (SREF) indicated the presence of a second scattering species, the two dominant elements were assigned to that site and the SOF constrained to be unity. Secondary isotropic-extinction corrections were applied to all data sets, but did not improve the results.

Unit-cell parameters and information pertinent to the data collection and crystal structure refinement are in Table 3. The final positional and anisotropic displacement parameters are in Appendix C. Select bond lengths are given in Table 4 and bond angles in Table 5. Information regarding individual polyhedra can be found in Table 6. Bond-valence sums (BVS) were calculated using parameters taken from Brese & O'Keeffe (1991) and are in Table 7.

The normalized bond-length variation, or distortion (Δ), for each polyhedron was calculated using the equation of Brown & Shannon (1973), subsequently modified by Shannon (1975, 1976):

$$\Delta \equiv \{ \sum_{i=1}^{n} [(l_i - l_m) l_m]^2 / n \} \bullet 10^4 \quad (1)$$

where l_i = bond length, l_m = mean bond length, and n = coordination number. The tetrahedral- and octahedral-angle variance (TAV and OAV respectively), an alternate

TABLE 3. MISCELLANEOUS DATA: ASTROPHYLLITE GROUP MINERAL STRUCTURE REFINEMENTS

Parameter	LAB3	NOR1	NOR17	RUS4	RUS8	RUS9	RUS12
Locality	Seal Lake Labrador, CAN	Larvik complex Norway	Gjerdingen Norway	Khibina massif Russia	Khibina massif Russia	Lephke-Nelm Lovozero, Russia	Mt. Kuichvorr Lovozero, Russia
Space Group	P-1	P-1	P-1	P-1	P-1	C2/c	P-1
Unit cell							
a Å	5.4049(3)	5.3857(3)	5.3784(2)	5.3776(6)	5.3754(3)	5.4022(2)	5.3925(2)
b	11.9175(6)	11.9072(7)	11.9085(5)	11.899(1)	11.8970(6)	23.226(1)	11.9283(4)
c	11.7488(6)	11.7105(7)	11.7236(4)	11.662(1)	11.6634(6)	21.1782(9)	11.7256(4)
V Å^3	666.5(1)	660.9(1)	661.09(7)	656.2(2)	655.99(6)	2646.2(3)	663.39(7)
α °	112.93(1)	113.062(1)	112.964(1)	113.114(2)	113.133(4)	90	113.044(1)
β	94.627(1)	94.614(1)	94.697(1)	94.630(2)	94.638(4)	95.246(1)	94.840(1)
γ	103.139(1)	103.098(1)	103.112(1)	103.090(2)	103.081(4)	90	103.064(1)
Crystal Size (mm)	.22 x 0.10 x 0.0	.12 x 0.09 x 0.0	.30 x 0.25 x 0.0	.28 x 0.14 x 0.0	.11 x 0.08 x 0.0	.25 x 0.25 x 0.0	.25 x 0.20 x 0.0
Mu mm^{-1}	5.29	5.60	4.76	4.86	5.32	4.94	4.30
F(000)	682.0	679.9	654.2	650.1	665.0	2662.0	638.0
$\|E^2-1\|$	1.038	1.053	1.075	1.113	1.123	1.294	1.081
CFOM	1.46	2.08	1.90	2.73	2.89	11.02	1.94
Glancing angle (°) or ellipse	ellipse	ellipse	ellipse	7	5	ellipse	ellipse
R (int) before merging (%)	4.84	4.36	5.45	5.55	4.60	5.73	6.45
R (int) after merging (%)	3.08	3.15	3.25	2.75	0.99	3.55	2.98
Tot. # of reflections used in a.c.*	5545	4172	6388	1548	764	7390	6795
Tot. # of reflections corrected during a.c	11558	11452	6388	4044	3571	23051	11309
Min./Max. transmission	0.295/0.683	0.621/0.802	0.451/0.695	0.565/0.833	0.594/0.914	0.499/0.720	0.515/0.773
$-x =< h =< x$	-7 =< h =< 7	-7 =< h =< 7	-6 =< h =< 7	-7 =< h =< 7	-7 =< h =< 7	-7 =< h =< 7	-7 =< h =< 7
$-x =< k =< x$	-16 =< k =< 16	-16 =< k =< 16	-16 =< k =< 16	-15 =< k =< 15	-0 =< k =< 16	-32 =< k =< 32	-16 =< k =< 16
$-x =< l =< x$	-16 =< l =< 16	-16 =< l =< 16	-16 =< l =< 16	-15 =< l =< 15	-16 =< l =< 15	-29 =< l =< 29	-16 =< l =< 16
Total number of reflections	6942	6883	6855	3377	3571	13834	6813
Unique reflections	3870	3836	3835	2532	3421	3865	3834
Inconsistent reflections	7	3	8	25	0	2	17
F_o>4 sigma F	2693	2334	2898	2090	2947	2217	3000
R 1 for F_o>4 sigma (%)	3.73	4.99	4.40	4.74	2.85	4.72	4.06
R 1 for all reflections (%)	6.21	9.12	6.05	6.12	3.38	8.42	5.51
wR^2 (%)	8.97	11.71	12.69	14.66	7.76	14.04	11.25
GooF = S	0.928	0.916	1.044	1.183	1.053	0.945	1.082
Max. residual e^{-1}	1.60	2.51	1.08	1.05	2.09	3.67	0.71
Diffractometer	UofM CCD	UofM CCD	UofM CCD	UofO CCD	UofM P3	UofM CCD	UofM CCD

* absorption correction

TABLE 3. CONTINUED

Parameter	US5	MSH2	MSH3	MSH8	MSH9	MSH15	MSH15A
Locality	Mount Rosa Colorado, USA	PEG MSH, CAN	PEG MSH, CAN	APEG MSH, CAN	PEG MSH, CAN	PEG MSH, CAN	PEG MSH, CAN
Space Group	P-1	P-1	P-1	P-1	P-1	P-1	P-1
Unit cell							
a Å	5.3627(8)	5.3982(2)	5.3887(8)	5.4203(2)	5.3989(3)	5.4033(6)	5.4039(2)
b	11.851(2)	11.9534(4)	11.913(2)	11.9392(4)	11.9528(7)	11.920(1)	11.9243(4)
c	11.668(2)	11.7433(4)	11.751(2)	11.7229(4)	11.7458(7)	11.741(1)	11.7394(4)
V Å^3	652.9(3)	666.79(6)	664.0(3)	667.14(7)	667.0(1)	665.7(2)	665.94(7)
α °	113.040(3)	112.9903(8)	112.961(4)	113.0010(7)	112.983(1)	112.933(3)	112.942(1)
β	94.523(2)	94.8413(7)	94.746(3)	94.7348(9)	94.854(1)	94.793(2)	94.732(1)
γ	103.093(2)	103.0664(8)	103.117(3)	103.1598(9)	103.062(1)	103.108(2)	103.135(1)
Crystal Size (mm)	.18 x 0.12 x 0.0	.40 x 0.32 x 0.0	.16 x 0.12 x 0.0	.35 x 0.32 x 0.0	.20 x 0.10 x 0.0	0.39 x 0.2 x 0.03	.40 x 0.22 x 0.0
Mu mm^{-1}	5.82	4.80	4.75	4.76	4.77	4.79	5.02
F(000)	669.6	664.8	649.7	664.0	659.2	668.4	685.6
$\|E^2-1\|$	1.138	1.081	1.028	1.027	1.076	1.031	1.015
CFOM	3.85	1.73	1.32	1.09	2.46	1.01	0.76
Glancing angle (°) or ellipse	5	ellipse	5	ellipse	ellipse	5	ellipse
R(int) before merging (%)	6.77		3.97	5.34	4.94	6.77	6.21
R(int) after merging (%)	4.12		3.67	3.02	3.12	3.01	3.00
Tot. # of reflections used in a.c.*	862		877	6642	4243	1599	7691
Tot. # of reflections corrected during a.c	4356		4613	11471	11517	4176	11415
Min./Max. transmission	0.647/0.873		0.827/0.981	0.575/0.773	0.646/0.831	0.599/0.955	0.553/0.802
$-x =< h =< x$	-7 =< h =< 6	-7 =< h =< 7	-6 =< h =< 7	-7 =< h =< 7	-7 =< h =< 6	-5 =< h =< 7	-7 =< h =< 6
$-x =< k =< x$	-15 =< k =< 15	-16 =< k =< 16	-15 =< k =< 14	-16 =< k =< 16	-16 =< k =< 16	-15 =< k =< 15	-14 =< k =< 16
$-x =< l =< x$	-14 =< l =< 15	-16 =< l =< 16	-14 =< l =< 15	-16 =< l =< 16	-16 =< l =< 16	-15 =< l =< 15	-16 =< l =< 16
Total number of reflections	3715	6877	3917	6910	6940	3641	6892
Unique reflections	2669	3853	2831	3860	3863	2669	3860
Inconsistent reflections	12	49	25	15	1	22	23
F_o>4 sigma F	1917	3241	1969	3008	2417	2178	3249
R 1 for F_o>4 sigma (%)	4.54	3.97	4.08	3.49	4.26	4.14	3.74
R 1 for all reflections (%)	7.21	4.69	7.06	4.90	8.30	5.57	4.56
w*R*^{2} (%)	15.23	11.75	11.51	9.01	9.89	16.58	10.52
GooF = S	1.056	1.084	1.107	0.974	0.916	1.091	1.07
Max. residual e^{-1}	1.38	3.75	1.92	1.87	2.55	2.20	2.37
Diffractometer	UofO CCD	UofM CCD	UofO CCD	UofM CCD	UofM CCD	UofO CCD	UofM CCD

* absorption correction

TABLE 3. CONTINUED

Parameter	MSH19A	MSH20	MSH33A	MSH34A	MSH38A	MSH42
Locality	PEG MSH, CAN	PEG MSH, CAN	APLITE MSH, CAN	PEG MSH, CAN	APEG MSH, CAN	PEG MSH, CAN
Space Group	P-1	P-1	P-1	P-1	P-1	P-1
Unit cell						
a Å	5.4206(2)	5.3879(3)	5.418(1)	5.3996(2)	5.4028(2)	5.4303(9)
b	11.9283(5)	11.9263(7)	11.933(2)	11.9152(4)	11.9178(4)	11.924(2)
c	11.7294(5)	11.7136(6)	11.742(2)	11.7077(4)	11.7000(4)	11.747(2)
V Å^3	667.46(8)	661.98(6)	668.5(4)	663.00(6)	662.73(7)	669.5(3)
α °	112.942(1)	113.049(4)	112.962(3)	113.0413(7)	113.036(1)	112.927(3)
β	94.645(1)	94.832(4)	94.620(3)	94.5707(7)	94.671(1)	94.750(3)
γ	103.246(1)	103.077(4)	103.123(4)	103.1239(8)	103.163(1)	103.175(3)
Crystal Size (mm)	.40 x 0.38 x 0.0	.42 x 0.19 x 0.0	.20 x 0.08 x 0.01	.28 x 0.25 x 0.0	.45 x 0.20 x 0.0	.21 x 0.19 x 0.0
Mu mm^{-1}	5.17	5.62	5.04	5.20	4.86	5.43
F(000)	696.6	687.0	666.4	672.0	679.0	675.5
$\|E^2-1\|$	1.066	1.112	1.062	1.086	1.061	0.985
CFOM	1.75	2.67	1.72	1.98	1.45	1.08
Glancing angle (°) or ellipse	ellipse	ellipse	4	ellipse	ellipse	ellipse
R (int) before merging (%)	5.25	4.35	6.56	5.72	7.13	0.1414
R (int) after merging (%)	3.17	1.18	5.52	3.39	3.07	0.0789
Tot. # of reflections used in a.c.*	6058	958	1099	7329	7197	724
Tot. # of reflections corrected during a.c	11491	4146	4723	11445	11363	4090
Min./Max. transmission	0.591/0.831	0.604/0.914	0.771/0.982	0.348/0.695	0.466/0.746	0.343/0.664
$-x =< h =< x$	-7 =< h =< 7	-7 =< h =< 7	-6 =< h =< 7	-7 =< h =< 7	-7 =< h =< 7	-7 =< h =< 7
$-x =< k =< x$	-16 =< k =< 16	0 =< k =< 16	-15 =< k =< 13	-16 =< k =< 16	-15 =< k =< 16	-11 =< k =< 16
$-x =< l =< x$	-16 =< l =< 16	-16 =< l =< 15	-15 =< l =< 15	-16 =< l =< 16	-16 =< l =< 16	-15 =< l =< 15
Total number of reflections	6949	3584	3945	6895	6854	5219
Unique reflections	3869	3443	2871	3842	3828	3023
Inconsistent reflections	21	0	26	28	27	77
F_o>4 sigma F	2865	2850	2183	3142	3115	1779
R 1 for F_o>4 sigma (%)	4.16	3.14	4.16	3.66	3.45	0.0597
R 1 for all reflections (%)	5.93	3.97	6.25	4.59	4.43	0.1023
wR^2 (%)	10.71	8.34	13.61	10.10	9.61	0.1912
GooF = S	0.998	1.078	1.130	1.025	1.054	1.085
Max. residual e^{-1}	2.54	2.70	1.05	1.73	2.60	1.34
Diffractometer	UofM CCD	UofM P3	UofO CCD	UofM CCD	UofM CCD	UofO CCD

* absorption correction

TABLE 4. SELECT BOND LENGTHS (Å) FOR ASTROPHYLLITE GROUP MINERALS

SAMPLE	LAB3	NOR1	NOR17	RUS4	RUS8	RUS9	RUS12	US5	MSH2	MSH3
***M*(1)O_4(OH) octahedron**										
M(1)-O(2)	2.146(3)	2.170(3)	2.172(3)	2.163(5)	2.168(2)	2.178(3)	2.189(2)	2.137(5)	2.188(2)	2.187(4)
M(1)-O(5)	2.177(3)	2.174(4)	2.185(3)	2.175(5)	2.179(2)	2.187(4)	2.198(3)	2.156(5)	2.193(2)	2.212(5)
M(1)-O(6)	2.154(3)	2.162(3)	2.182(3)	2.158(5)	2.158(2)	2.172(3)	2.191(2)	2.147(5)	2.181(2)	2.192(4)
M(1)-O(3)	2.190(2)	2.190(4)	2.202(3)	2.185(5)	2.190(2)	2.199(4)	2.216(2)	2.172(5)	2.206(2)	2.218(4)
M(1)-O(7)	2.208(2)	2.204(4)	2.195(3)	2.206(5)	2.199(2)	2.213(4)	2.214(2)	2.174(5)	2.207(2)	2.221(4)
M(1)-O(1)	2.232(3)	2.231(4)	2.225(3)	2.223(4)	2.221(2)	2.234(4)	2.244(2)	2.205(5)	2.230(2)	2.244(4)
<*M*(1)-O>	2.185	2.189	2.194	2.185	2.186	2.197	2.209	2.165	2.201	2.212
***M*(2)O_4(OH)$_2$ octahedron**										
M(2)-O(7)	2.111(3)	2.105(3)	2.113(3)	2.085(5)	2.095(2)	2.118(3)	2.128(2)	2.087(5)	2.129(2)	2.121(4)
M(2)-O(5)	2.111(3)	2.106(4)	2.111(3)	2.093(5)	2.097(2)	2.112(3)	2.130(2)	2.079(5)	2.132(2)	2.131(4)
M(2)-O(5)	2.132(3)	2.135(4)	2.141(3)	2.128(5)	2.131(2)	2.149(4)	2.144(2)	2.116(5)	2.150(2)	2.139(4)
M(2)-O(6)	2.205(3)	2.195(4)	2.211(3)	2.192(5)	2.192(2)	2.207(4)	2.222(2)	2.199(5)	2.217(2)	2.214(4)
M(2)-O(7)	2.216(3)	2.216(3)	2.219(3)	2.210(5)	2.210(2)	2.224(4)	2.231(2)	2.208(5)	2.240(2)	2.226(4)
M(2)-O(2)	2.230(3)	2.248(4)	2.253(3)	2.247(5)	2.247(2)	2.252(4)	2.254(3)	2.233(5)	2.267(2)	2.262(4)
<*M*(2)-O>	2.168	2.168	2.175	2.159	2.162	2.177	2.185	2.154	2.189	2.182
***M*(3)O_4(OH)$_2$ octahedron**										
M(3)-O(1)	2.128(2)	2.112(3)	2.126(3)	2.112(5)	2.108(2)	2.127(3)	2.135(2)	2.098(5)	2.138(2)	2.127(4)
M(3)-O(4)	2.117(3)	2.129(4)	2.125(3)	2.110(5)	2.113(2)	2.124(4)	2.137(3)	2.107(5)	2.143(2)	2.134(4)
M(3)-O(3)	2.138(3)	2.133(3)	2.137(3)	2.109(5)	2.120(2)	2.140(3)	2.153(2)	2.115(5)	2.156(2)	2.148(4)
M(3)-O(6)	2.152(3)	2.149(4)	2.157(3)	2.141(4)	2.137(2)	2.158(4)	2.170(2)	2.137(5)	2.179(2)	2.163(4)
M(3)-O(4)	2.184(3)	2.186(4)	2.199(3)	2.168(6)	2.180(2)	2.198(4)	2.204(2)	2.175(5)	2.206(2)	2.201(4)
M(3)-O(2)	2.209(3)	2.225(4)	2.225(3)	2.232(5)	2.232(2)	2.238(4)	2.237(2)	2.210(5)	2.245(2)	2.244(4)
<*M*(3)-O>	2.155	2.156	2.162	2.145	2.148	2.164	2.173	2.140	2.178	2.170
***M*(4)O_4(OH)$_2$ octahedron**										
M(4)-O(4)	2.088(3)	2.080(4)	2.092(3)	2.077(5)	2.083(2)	2.093(3)	2.087(2)	2.074(5)	2.112(2)	2.081(4)
M(4)-O(4)	2.088(3)	2.080(4)	2.092(3)	2.077(5)	2.083(2)	2.093(3)	2.087(2)	2.074(5)	2.112(2)	2.081(4)
M(4)-O(1)	2.151(2)	2.142(3)	2.146(3)	2.148(5)	2.137(2)	2.146(4)	2.135(2)	2.145(5)	2.163(2)	2.132(4)
M(4)-O(1)	2.151(2)	2.142(3)	2.146(3)	2.148(5)	2.137(2)	2.146(4)	2.135(2)	2.145(5)	2.163(2)	2.132(4)
M(4)-O(3)	2.171(3)	2.165(3)	2.171(3)	2.157(5)	2.159(2)	2.170(4)	2.156(2)	2.163(5)	2.183(2)	2.163(4)
M(4)-O(3)	2.171(3)	2.165(3)	2.171(3)	2.157(5)	2.159(2)	2.170(4)	2.156(2)	2.163(5)	2.183(2)	2.163(4)
<*M*(4)-O>	2.137	2.129	2.136	2.127	2.126	2.136	2.126	2.127	2.153	2.125
***D*ϕ_6 octahedron**										
D-O(2)	1.877(3)	1.835(4)	1.811(3)	1.808(5)	1.797(2)	1.823(3)	1.807(3)	1.844(5)	1.808(2)	1.863(4)
D-O(12)	1.979(3)	1.958(4)	1.950(3)	1.956(5)	1.957(2)	1.957(3)	1.959(3)	1.936(6)	1.962(2)	1.950(4)
D-O(11)	1.986(3)	1.962(4)	1.956(3)	1.965(5)	1.958(2)	1.967(3)	1.960(3)	1.945(6)	1.965(2)	1.950(5)
D-O(9)	1.981(3)	1.956(4)	1.953(3)	1.947(6)	1.958(2)	1.951(3)	1.956(2)	1.945(5)	1.961(2)	1.949(4)
D-O(15)	1.989(3)	1.966(4)	1.950(3)	1.957(5)	1.962(2)	1.969(3)	1.959(3)	1.950(5)	1.968(2)	1.963(4)
D-ϕ(16)	2.104(0)	2.086(1)	2.095(1)	2.094(1)	2.097(0)	2.068(1)	2.084(1)	2.090(1)	2.081(0)	2.037(1)
<*D*-ϕ>	1.986	1.961	1.953	1.955	1.955	1.956	1.954	1.952	1.958	1.952

TABLE 4. CONTINUED

SAMPLE	LAB3	NOR1	NOR17	RUS4	RUS8	RUS9	RUS12	US5	MSH2	MSH3
T(1) tetrahedron										
T(1)-O(15)	1.588(3)	1.601(4)	1.605(3)	1.610(6)	1.604(2)	1.602(3)	1.612(3)	1.590(6)	1.611(2)	1.601(5)
T(1)-O(11)	1.595(3)	1.602(4)	1.601(3)	1.596(5)	1.601(2)	1.603(3)	1.611(3)	1.598(6)	1.610(2)	1.605(5)
T(1)-O(1)	1.630(3)	1.624(4)	1.623(3)	1.612(5)	1.626(2)	1.630(3)	1.622(3)	1.626(5)	1.626(2)	1.624(5)
T(1)-O(13)	1.639(3)	1.636(4)	1.644(3)	1.648(5)	1.632(2)	1.648(3)	1.649(3)	1.632(5)	1.645(2)	1.644(5)
<*T*(1)-O>	1.613(3)	1.616	1.618	1.617	1.616	1.621	1.624	1.612	1.623	1.619
T(2) tetrahedron										
T(2)-O(13)	1.605(3)	1.617(4)	1.613(3)	1.607(5)	1.616(2)	1.614(3)	1.613(2)	1.605(5)	1.618(2)	1.617(5)
T(2)-O(3)	1.617(3)	1.613(4)	1.609(3)	1.627(6)	1.616(2)	1.623(3)	1.614(3)	1.609(5)	1.615(2)	1.607(5)
T(2)-O(8)	1.633(3)	1.642(4)	1.635(3)	1.634(5)	1.633(2)	1.639(4)	1.642(3)	1.638(5)	1.641(2)	1.634(4)
T(2)-O(10)	1.635(3)	1.637(4)	1.637(3)	1.633(5)	1.635(2)	1.639(4)	1.642(3)	1.635(5)	1.642(2)	1.642(4)
<*T*(2)-O>	1.622	1.627	1.624	1.625	1.625	1.629	1.628	1.622	1.629	1.625
T(3) tetrahedron										
T(3)-O(14)	1.613(3)	1.620(4)	1.605(3)	1.616(5)	1.614(2)	1.613(3)	1.611(3)	1.598(5)	1.615(2)	1.608(5)
T(3)-O(6)	1.628(3)	1.624(4)	1.612(3)	1.620(5)	1.628(2)	1.633(3)	1.614(3)	1.603(5)	1.625(2)	1.615(5)
T(3)-O(10)	1.642(3)	1.639(4)	1.637(3)	1.640(5)	1.642(2)	1.652(4)	1.639(3)	1.629(5)	1.642(2)	1.647(4)
T(3)-O(8)	1.643(3)	1.639(4)	1.640(3)	1.644(6)	1.641(2)	1.651(3)	1.642(2)	1.633(5)	1.644(2)	1.643(4)
<*T*(3)-O>	1.6315(3)	1.631	1.624	1.630	1.631	1.637	1.627	1.616	1.632	1.628
T(4) tetrahedron										
T(4)-O(9)	1.594(3)	1.598(4)	1.598(3)	1.604(6)	1.601(2)	1.608(3)	1.610(3)	1.585(5)	1.607(2)	1.607(4)
T(4)-O(12)	1.595(3)	1.601(4)	1.603(3)	1.606(5)	1.601(2)	1.610(3)	1.613(3)	1.597(6)	1.608(2)	1.614(5)
T(4)-O(7)	1.634(3)	1.625(4)	1.628(3)	1.628(6)	1.628(2)	1.634(3)	1.626(3)	1.623(5)	1.627(2)	1.619(5)
T(4)-O(14)	1.632(3)	1.629(4)	1.643(3)	1.632(6)	1.632(2)	1.632(3)	1.640(3)	1.641(6)	1.642(2)	1.640(4)
<*T*(4)-O>	1.614(3)	1.613	1.618	1.618	1.616	1.621	1.622	1.612	1.621	1.620
B-O(12)x2	2.624(4)	2.607(5)	2.620(4)	2.589(7)	2.592(3)	2.596(4)	2.599(3)	2.618(7)	2.613(3)	2.628(6)
B-O(9)x2	2.627(4)	2.612(5)	2.602(4)	2.592(7)	2.592(3)	2.606(4)	2.596(3)	2.626(7)	2.593(3)	2.629(6)
B-O(11)x2	2.648(4)	2.630(5)	2.634(4)	2.609(7)	2.613(3)	2.600(4)	2.604(3)	2.642(8)	2.614(3)	2.640(6)
B-O(15)x2	2.618(4)	2.612(5)	2.609(4)	2.589(7)	2.586(3)	2.590(4)	2.610(3)	2.626(8)	2.614(3)	2.634(6)
B-ϕ(16)x2	2.702(0)	2.693(0)	2.689(0)	2.689(0)	2.688(0)	2.701(0)	2.696(0)	2.681(0)	2.699(0)	2.694(1)
<*B*-ϕ>	2.644	2.631	2.631	2.614	2.614	2.619	2.621	2.639	2.627	2.645
K(1a)-O(12)	2.874(4)	2.913(5)	2.826(4)	2.850(7)	2.842(3)		2.836(3)	2.842(7)	2.837(3)	2.868(6)
K(1a)-O(15)	2.876(4)	2.900(5)	2.834(4)	2.857(7)	2.845(3)		2.839(3)	2.849(7)	2.834(3)	2.873(6)
K(1a)-O(11)	2.867(4)	2.904(4)	2.837(4)	2.869(7)	2.851(3)		2.847(3)	2.834(7)	2.842(3)	2.889(6)
K(1a)-O(9)	2.889(4)	2.934(5)	2.845(4)	2.880(7)	2.856(3)		2.852(3)	2.852(7)	2.850(3)	2.883(6)
K(1a)-ϕ(16)	3.115(1)	3.184(2)	3.058(2)	3.199(2)	3.100(1)		3.093(1)	3.067(3)	3.092(1)	3.136(5)
K(1a)-O(14)	3.420(4)	3.393(4)	3.389(3)	3.392(6)	3.375(3)		3.399(3)	3.412(7)	3.398(3)	3.390(5)
K(1a)-O(13)	3.469(4)	3.426(4)	3.444(4)	3.425(7)	3.429(3)		3.429(3)	3.447(6)	3.459(3)	3.424(5)
K(1a)-O(14)	3.453(4)	3.430(5)	3.443(4)	3.406(7)	3.423(3)		3.429(3)	3.429(7)	3.429(3)	3.431(6)
K(1a)-O(13)	3.476(3)	3.438(5)	3.470(3)	3.428(7)	3.437(3)		3.442(3)	3.453(6)	3.466(3)	3.448(6)
K(1a)-O(8)	3.621(3)	3.562(4)	3.648(3)	3.594(6)	3.602(2)		3.606(3)	3.625(6)	3.604(3)	3.596(6)
K(1a)-O(10)	3.682(3)	3.617(4)		3.637(6)	3.649(3)		3.699(3)	3.669(6)	3.713(3)	3.650(6)
K(1a)-O(10)	3.718(3)	3.637(4)		3.684(6)	3.690(3)		3.705(3)		3.721(3)	3.671(6)
<K(1a)-ϕ>	3.288	3.278	3.179	3.268	3.258		3.265	3.225	3.270	3.272
K(1a)-K(1b)			0.851(23)				0.917(18)			0.621(18)
K(1b)-ϕ(16)			2.206(23)				2.176(18)			2.515(18)
K(1b)-O(15)			2.417(20)				2.392(18)			2.526(17)
K(1b)-O(11)			2.427(19)				2.397(18)			2.547(16)
K(1b)-O(12)			2.419(21)				2.392(17)			2.551(16)
K(1b)-O(9)			2.430(20)				2.407(17)			2.559(16)
K(1b)-O(13)										
K(1b)-O(14)										
<K(1b)-ϕ>			2.380				2.353			2.540

TABLE 4. CONTINUED

SAMPLE	MSH8	MSH9	MSH15	MSH15A	MSH19A	MSH20	MSH33A	MSH34	MSH38A	MSH42
***M*(1)O_5(OH) octahedron**										
M(1)-O(2)	2.183(2)	2.188(3)	2.186(5)	2.180(2)	2.169(3)	2.187(2)	2.139(5)	2.142(2)	2.169(2)	2.179(8)
M(1)-O(5)	2.190(2)	2.192(3)	2.197(4)	2.192(2)	2.185(3)	2.191(2)	2.188(4)	2.166(2)	2.184(2)	2.194(8)
M(1)-O(6)	2.182(2)	2.185(3)	2.189(4)	2.190(2)	2.175(3)	2.180(2)	2.142(4)	2.143(2)	2.172(2)	2.190(7)
M(1)-O(3)	2.207(2)	2.204(3)	2.207(5)	2.208(2)	2.197(2)	2.206(2)	2.189(4)	2.177(2)	2.199(2)	2.209(7)
M(1)-O(7)	2.223(2)	2.209(3)	2.226(5)	2.215(2)	2.216(3)	2.209(2)	2.225(4)	2.202(2)	2.207(2)	2.221(7)
M(1)-O(1)	2.240(2)	2.230(3)	2.233(4)	2.239(2)	2.200(3)	2.231(2)	2.236(4)	2.226(2)	2.229(2)	2.247(7)
<*M*(1)-O>	2.204	2.201	2.206	2.204	2.190	2.201	2.187	2.176	2.193	2.207
***M*(2)O_4(OH)$_2$ octahedron**										
M(2)-O(7)	2.124(2)	2.130(3)	2.113(4)	2.122(2)	2.119(3)	2.123(2)	2.121(4)	2.103(2)	2.110(2)	2.133(8)
M(2)-O(5)	2.115(2)	2.139(3)	2.118(5)	2.119(2)	2.112(3)	2.131(2)	2.107(5)	2.096(2)	2.111(2)	2.124(7)
M(2)-O(5)	2.146(2)	2.149(3)	2.157(5)	2.146(2)	2.140(3)	2.142(2)	2.149(5)	2.130(2)	2.142(2)	2.152(8)
M(2)-O(6)	2.217(2)	2.223(3)	2.217(5)	2.213(2)	2.218(2)	2.216(2)	2.210(4)	2.192(2)	2.212(2)	2.211(7)
M(2)-O(7)	2.232(2)	2.236(3)	2.228(4)	2.224(2)	2.231(3)	2.229(2)	2.220(4)	2.213(2)	2.222(2)	2.254(7)
M(2)-O(2)	2.253(2)	2.261(3)	2.258(4)	2.255(2)	2.244(3)	2.263(2)	2.230(4)	2.238(2)	2.246(2)	2.252(8)
<*M*(2)-O>	2.181	2.190	2.182	2.180	2.177	2.184	2.173	2.162	2.174	2.188
***M*(3)O_4(OH)$_2$ octahedron**										
M(3)-O(1)	2.138(2)	2.139(3)	2.130(4)	2.136(2)	2.135(3)	2.135(2)	2.129(4)	2.119(2)	2.125(2)	2.143(7)
M(3)-O(4)	2.133(2)	2.146(3)	2.132(4)	2.130(2)	2.122(3)	2.137(2)	2.117(5)	2.112(2)	2.122(2)	2.145(7)
M(3)-O(3)	2.149(2)	2.158(3)	2.159(4)	2.147(2)	2.149(3)	2.152(2)	2.133(4)	2.125(2)	2.140(2)	2.151(7)
M(3)-O(6)	2.164(2)	2.174(3)	2.176(4)	2.166(2)	2.172(2)	2.171(2)	2.143(4)	2.144(2)	2.163(2)	2.169(7)
M(3)-O(4)	2.206(2)	2.211(3)	2.196(5)	2.202(2)	2.200(3)	2.198(2)	2.174(4)	2.181(2)	2.195(2)	2.210(8)
M(3)-O(2)	2.237(2)	2.246(3)	2.232(5)	2.232(2)	2.218(3)	2.242(2)	2.217(4)	2.214(2)	2.227(2)	2.232(8)
<*M*(3)-O>	2.171	2.179	2.171	2.169	2.166	2.173	2.152	2.149	2.162	2.175
***M*(4)O_4(OH)$_2$ octahedron**										
M(4)-O(4)	2.095(2)	2.118(3)	2.086(5)	2.089(2)	2.094(3)	2.085(2)	2.088(5)	2.085(2)	2.091(2)	2.097(7)
M(4)-O(4)	2.095(2)	2.118(3)	2.086(5)	2.089(2)	2.094(3)	2.085(2)	2.088(5)	2.085(2)	2.091(2)	2.097(7)
M(4)-O(1)	2.149(2)	2.165(3)	2.146(4)	2.141(2)	2.155(2)	2.145(2)	2.158(4)	2.154(2)	2.154(2)	2.149(8)
M(4)-O(1)	2.149(2)	2.165(3)	2.146(4)	2.141(2)	2.155(2)	2.145(2)	2.158(4)	2.154(2)	2.154(2)	2.149(8)
M(4)-O(3)	2.184(2)	2.182(3)	2.169(4)	2.170(2)	2.182(2)	2.171(2)	2.170(4)	2.171(2)	2.181(2)	2.181(7)
M(4)-O(3)	2.184(2)	2.182(3)	2.169(4)	2.170(2)	2.182(2)	2.171(2)	2.170(4)	2.171(2)	2.181(2)	2.181(7)
<*M*(4)-O>	2.143	2.155	2.134	2.133	2.144	2.134	2.139	2.137	2.142	2.142
***D*ϕ_6 octahedron**										
D-O(2)	1.887(2)	1.809(3)	1.866(4)	1.876(2)	1.885(3)	1.794(2)	1.894(5)	1.866(2)	1.854(2)	1.929(8)
D-O(12)	1.968(2)	1.958(3)	1.960(5)	1.956(2)	1.967(3)	1.956(2)	1.984(6)	1.970(3)	1.960(2)	1.998(9)
D-O(11)	1.974(3)	1.964(3)	1.966(5)	1.967(3)	1.978(3)	1.959(2)	1.998(5)	1.983(3)	1.967(2)	2.001(9)
D-O(9)	1.965(2)	1.956(3)	1.965(5)	1.957(2)	1.970(3)	1.956(2)	1.990(5)	1.970(2)	1.964(2)	1.987(8)
D-O(15)	1.973(2)	1.963(3)	1.966(5)	1.964(2)	1.973(3)	1.966(2)	1.996(5)	1.980(2)	1.969(2)	1.994(8)
D-ϕ(16)	2.014(0)	2.082(1)	2.034(1)	2.033(0)	2.047(1)	2.086(1)	2.095(1)	2.096(0)	2.056(0)	1.981(1)
<*D*-ϕ>	1.964	1.955	1.960	1.959	1.970	1.953	1.993	1.978	1.962	1.982

TABLE 4. CONTINUED

SAMPLE	MSH8	MSH9	MSH15	MSH15A	MSH19A	MSH20	MSH33A	MSH34	MSH38A	MSH42
T(1) tetrahedron										
T(1)-O(15)	1.604(2)	1.611(3)	1.603(6)	1.602(2)	1.603(3)	1.603(2)	1.597(5)	1.595(2)	1.600(2)	1.595(9)
T(1)-O(11)	1.606(3)	1.612(3)	1.603(5)	1.603(3)	1.603(3)	1.607(2)	1.592(6)	1.594(3)	1.605(2)	1.585(9)
T(1)-O(1)	1.627(2)	1.625(3)	1.628(5)	1.622(2)	1.627(3)	1.621(2)	1.626(4)	1.625(2)	1.625(2)	1.628(8)
T(1)-O(13)	1.636(2)	1.640(3)	1.646(5)	1.638(2)	1.641(3)	1.641(2)	1.632(5)	1.628(2)	1.641(2)	1.631(9)
<*T*(1)-O>	1.618	1.622	1.620	1.616	1.619	1.618	1.612	1.611	1.618	1.610
T(2) tetrahedron										
T(2)-O(13)	1.617(2)	1.619(3)	1.609(5)	1.615(2)	1.613(3)	1.617(2)	1.614(5)	1.618(3)	1.613(2)	1.614(9)
T(2)-O(3)	1.618(2)	1.620(3)	1.612(5)	1.616(2)	1.621(3)	1.612(2)	1.626(5)	1.620(2)	1.614(2)	1.620(7)
T(2)-O(8)	1.638(3)	1.637(3)	1.630(5)	1.644(2)	1.645(3)	1.642(2)	1.628(5)	1.636(2)	1.642(2)	1.638(8)
T(2)-O(10)	1.635(3)	1.638(3)	1.643(5)	1.636(2)	1.642(3)	1.637(2)	1.637(5)	1.636(2)	1.643(2)	1.654(8)
<*T*(2)-O>	1.627	1.629	1.624	1.628	1.630	1.627	1.626	1.628	1.628	1.632
T(3) tetrahedron										
T(3)-O(14)	1.621(3)	1.618(3)	1.615(5)	1.619(2)	1.614(3)	1.617(2)	1.618(5)	1.619(2)	1.616(2)	1.630(9)
T(3)-O(6)	1.631(2)	1.622(3)	1.611(5)	1.618(2)	1.624(3)	1.617(2)	1.644(5)	1.631(2)	1.621(2)	1.629(7)
T(3)-O(10)	1.652(3)	1.648(3)	1.647(5)	1.648(2)	1.645(3)	1.646(2)	1.643(5)	1.645(2)	1.642(2)	1.630(9)
T(3)-O(8)	1.650(2)	1.653(3)	1.650(5)	1.643(2)	1.640(3)	1.643(2)	1.653(5)	1.645(2)	1.643(2)	1.645(8)
<*T*(3)-O>	1.639	1.635	1.631	1.632	1.631	1.631	1.640	1.635	1.631	1.634
T(4) tetrahedron										
T(4)-O(9)	1.606(3)	1.613(3)	1.598(5)	1.606(3)	1.607(3)	1.608(2)	1.595(5)	1.601(3)	1.601(2)	1.591(9)
T(4)-O(12)	1.606(2)	1.615(3)	1.607(5)	1.604(3)	1.604(3)	1.609(2)	1.595(5)	1.602(3)	1.601(2)	1.591(9)
T(4)-O(7)	1.625(2)	1.629(3)	1.625(5)	1.626(2)	1.628(3)	1.626(2)	1.625(5)	1.630(2)	1.632(2)	1.613(8)
T(4)-O(14)	1.629(2)	1.637(3)	1.639(5)	1.633(2)	1.634(3)	1.637(2)	1.624(5)	1.624(3)	1.635(2)	1.607(9)
<*T*(4)-O>	1.617	1.624	1.617	1.617	1.618	1.620	1.610	1.614	1.617	1.601
B-O(12)x2	2.632(3)	2.620(3)	2.645(7)	2.627(3)	2.645(4)	2.610(3)	2.626(7)	2.613(4)	2.612(3)	2.642(15)
B-O(9)x2	2.614(3)	2.600(4)	2.627(6)	2.626(3)	2.605(4)	2.585(3)	2.617(7)	2.615(3)	2.595(3)	2.641(13)
B-O(11)x2	2.640(3)	2.611(3)	2.636(6)	2.651(3)	2.667(4)	2.614(3)	2.638(7)	2.639(4)	2.637(3)	2.662(13)
B-O(15)x2	2.622(3)	2.615(3)	2.635(6)	2.630(3)	2.604(4)	2.601(3)	2.623(7)	2.618(4)	2.601(3)	2.665(14)
B-◊(16)x2	2.710(0)	2.699(0)	2.702(0)	2.702(0)	2.710(0)	2.694(0)	2.709(0)	2.700(0)	2.701(0)	2.715(0)
<*B*-◊>	2.644	2.629	2.649	2.647	2.646	2.621	2.643	2.637	2.629	2.665
K(1a)-O(12)	2.897(3)	2.825(4)	2.850(7)	2.880(3)	2.885(4)	2.834(3)	2.910(7)	2.890(3)	2.871(3)	2.831(25)
K(1a)-O(15)	2.896(3)	2.839(4)	2.866(6)	2.877(3)	2.890(4)	2.840(3)	2.891(7)	2.888(3)	2.868(3)	3.046(28)
K(1a)-O(11)	2.894(3)	2.836(4)	2.865(6)	2.873(3)	2.871(4)	2.846(3)	2.897(7)	2.882(3)	2.862(3)	2.843(23)
K(1a)-O(9)	2.912(3)	2.852(4)	2.876(6)	2.888(3)	2.905(4)	2.852(3)	2.916(7)	2.901(4)	2.888(3)	3.073(30)
K(1a)-◊(16)	3.178(1)	3.086(2)	3.117(2)	3.131(1)	3.151(1)	3.098(1)	3.164(3)	3.148(1)	3.130(1)	3.256(16)
K(1a)-O(14)	3.381(3)	3.398(3)	3.395(6)	3.391(3)	3.381(4)	3.378(3)	3.412(6)	3.404(3)	3.376(3)	3.245(34)
K(1a)-O(13)	3.447(3)	3.456(3)	3.447(6)	3.451(3)	3.443(4)	3.437(3)	3.465(6)	3.456(3)	3.436(3)	3.266(33)
K(1a)-O(14)	3.438(3)	3.438(4)	3.435(6)	3.440(3)	3.462(4)	3.432(3)	3.449(7)	3.434(3)	3.439(3)	
K(1a)-O(13)	3.450(3)	3.475(4)	3.462(6)	3.453(3)	3.481(4)	3.441(3)	3.477(6)	3.459(3)	3.455(3)	
K(1a)-O(8)	3.544(3)	3.601(4)	3.597(5)	3.590(3)	3.577(4)	3.588(3)	3.582(6)	3.587(3)	3.581(3)	3.409(23)
K(1a)-O(10)	3.621(3)	3.710(4)	3.659(6)	3.655(3)	3.633(4)	3.684(3)	3.653(6)	3.628(3)	3.639(3)	
K(1a)-O(10)	3.643(3)		3.701(6)	3.690(3)	3.670(4)	3.689(3)	3.678(6)	3.691(3)	3.672(3)	
<K(1a)-◊>	3.275	3.229	3.272	3.277	3.279	3.260	3.291	3.281	3.268	3.121
K(1a)-K(1b)										0.36
K(1b)-◊(16)										3.225(8)
K(1b)-O(15)										2.843(17)
K(1b)-O(11)										2.996(16)
K(1b)-O(12)										2.994(17)
K(1b)-O(9)										2.879(19)
K(1b)-O(13)										3.347(19)
K(1b)-O(14)										3.289(19)
<K(1b)-◊>										3.082

TABLE 5A. O-*M*-O BOND ANGLES (°) FOR MEMBERS OF THE ASTROPHYLLITE GROUP

SAMPLE	LAB3	NOR1	NOR17	RUS4	RUS8	RUS9	RUS12	US5	MSH2	MSH3
M(1)										
O5-*M*1-O2	86.7	87.2	87.7	86.8	87.1	87.3	87.9	86.7	88.1	88.3
O3-*M*1-O2	86.3	87.0	87.3	86.4	86.9	87.2	87.8	86.4	87.9	88.0
O7-*M*1-O2	97.0	96.4	96.3	96.6	96.4	95.9	95.6	97.0	95.4	95.7
O1-*M*1-O2	95.4	95.2	94.7	95.1	95.2	94.7	94.5	95.4	94.1	94.7
O5-*M*1-O6	93.8	93.7	93.0	94.3	94.0	93.7	92.7	94.2	92.7	92.4
O3-*M*1-O6	91.4	91.5	90.7	92.2	91.8	91.6	90.8	91.3	90.9	90.8
O1-*M*1-O6	83.9	83.8	84.4	83.8	83.6	84.1	84.8	83.5	85.0	84.5
O3-*M*1-O5	93.9	93.8	92.7	94.2	94.0	93.5	93.3	93.9	92.8	92.9
O7-*M*1-O5	79.5	79.7	80.0	79.4	79.4	80.1	79.8	79.8	80.1	80.0
O1-*M*1-O3	80.0	79.8	70.9	79.8	79.7	80.0	79.5	80.0	80.4	79.8
O1-*M*1-O7	106.4	106.5	107.2	106.4	106.8	106.3	107.2	106.1	106.6	107.1
O7-*M*1-O6	85.3	85.2	85.9	84.9	85.0	85.4	86.0	85.4	86.0	85.7
M(2)										
O5-*M*2-O5	83.0	83.4	84.0	82.9	83.1	83.7	84.2	82.8	84.0	84.5
O6-*M*2-O5	94.5	93.6	92.5	93.7	93.7	93.1	92.2	94.1	92.4	92.3
O2-*M*2-O5	86.2	86.8	87.4	86.6	87.0	87.3	87.9	86.1	87.6	88.4
O7-*M*2-O5	93.6	93.4	92.6	94.0	93.5	92.8	91.9	94.2	91.9	91.9
O5-*M*2-O7	95.9	96.2	96.3	96.3	96.3	96.2	96.0	96.8	96.4	95.5
O6-*M*2-O7	86.4	86.8	87.1	87.0	86.8	86.8	87.3	86.2	87.0	87.6
O7-*M*2-O7	84.4	84.8	85.1	84.3	84.4	84.9	85.4	84.5	85.8	85.2
O2-*M*2-O5	103.1	102.9	102.9	102.7	102.7	102.5	102.9	103.0	102.7	102.1
O7-*M*2-O5	80.3	80.2	80.4	80.3	80.2	80.7	80.6	79.9	80.3	81.5
O2-*M*2-O6	81.2	81.4	81.7	81.2	81.2	81.8	81.9	81.3	82.3	82.0
O7-*M*2-O6	95.4	95.5	95.0	95.8	96.0	95.1	94.6	95.8	94.6	94.4
O2-*M*2-O7	95.9	94.9	94.9	95.2	95.0	95.1	94.8	95.2	94.8	94.5
M(3)										
O4-*M*3-O1	96.2	95.9	95.9	96.1	95.9	96.0	95.9	96.3	95.8	95.8
O6-*M*3-O1	86.5	87.1	87.4	87.0	86.9	87.1	88.0	86.4	87.3	88.1
O4-*M*3-O1	83.4	83.3	83.9	83.6	83.5	83.5	83.3	83.6	84.5	83.2
O2-*M*3-O1	96.0	95.2	95.1	95.0	95.1	95.3	95.3	95.6	95.0	95.1
O3-*M*3-O4	84.0	84.1	84.5	83.9	84.2	84.2	84.0	84.3	85.0	84.0
O4-*M*3-O4	79.7	80.4	80.3	79.8	80.2	80.5	81.3	79.8	80.7	81.3
O2-*M*3-O4	102.3	101.6	101.7	101.7	101.4	101.3	101.6	101.8	101.7	101.1
O6-*M*3-O3	93.1	92.8	91.9	92.9	92.8	92.5	91.8	92.9	91.6	91.8
O4-*M*3-O3	94.5	94.5	93.4	94.9	94.4	94.0	93.3	94.8	92.8	93.4
O2-*M*3-O3	86.0	87.0	87.6	86.6	87.0	87.2	88.1	86.0	87.7	88.3
O4-*M*3-O6	95.2	95.2	94.4	95.9	95.8	95.1	93.7	95.3	94.0	94.2
O2-*M*3-O6	82.9	82.9	83.6	82.7	82.8	83.2	83.4	83.2	83.7	83.6
M(4)										
O1-*M*4-O4	94.8	94.9	94.0	95.1	94.8	94.4	93.9	95.1	93.8	94.0
O1-*M*4-O4	85.2	85.2	86.0	84.9	85.2	85.6	86.2	84.9	86.2	86.0
O3-*M*4-O4	83.9	84.5	84.5	83.5	84.0	84.2	85.2	83.9	85.1	84.9
O3-*M*4-O4	96.1	95.5	95.5	96.5	96.1	95.8	94.8	96.1	94.9	95.1
O3-*M*4-O1	82.2	82.4	82.4	82.2	82.3	82.6	83.3	81.6	82.4	83.6
O3-*M*4-O1	97.8	97.6	97.6	97.8	97.7	97.4	96.7	98.5	97.6	96.4
D										
O9-*D*-O2	97.6	97.9	98.1	98.6	98.8	98.1	98.5	97.6	98.1	96.2
O15-*D*-O2	98.8	98.4	98.8	99.6	99.7	98.7	98.9	98.3	99.1	96.8
O12-*D*-O2	98.0	98.0	98.2	99.2	99.0	98.7	98.7	97.9	98.2	96.4
O11-*D*-O2	98.6	98.6	98.7	99.1	99.4	98.6	99.2	98.2	99.0	96.7
O9-*D*-O16	81.8	81.9	81.5	81.1	80.8	81.8	81.2	82.1	81.4	83.5
O15-*D*-O16	81.8	81.7	81.6	80.8	80.7	81.4	81.3	82.0	81.4	83.6
O12-*D*-O16	81.6	81.6	81.5	80.6	80.7	81.3	81.0	81.9	81.4	83.2
O11-*D*-O16	81.8	81.8	81.7	81.1	80.8	81.4	81.2	82.0	81.5	83.7
O12-*D*-O9	89.7	90.1	89.6	89.8	89.6	90.1	89.6	89.4	89.6	89.3
O11-*D*-O9	88.1	87.8	87.8	87.2	87.5	87.7	87.6	88.8	87.8	89.0
O12-*D*-O15	88.1	88.4	88.5	87.9	87.9	87.9	88.3	88.6	88.6	89.7
O11-*D*-O15	89.4	89.1	89.1	89.4	89.2	89.3	89.2	88.8	88.8	89.1

TABLE 5A CONTINUED

SAMPLE	MSH8	MSH9	MSH15	MSH15A	MSH19A	MSH20	MSH33A	MSH34	MSH38A	MSH42
M(1)										
O5-*M*1-O2	87.4	88.1	87.8	87.8	87.1	88.1	86.3	86.4	87.3	87.9
O3-*M*1-O2	87.4	88.0	87.8	87.5	86.9	87.9	86.0	86.1	87.1	87.4
O7-*M*1-O2	96.1	95.3	96.3	96.1	96.7	95.4	96.7	96.9	96.5	96.1
O1-*M*1-O2	94.6	94.3	94.6	94.6	95.0	94.2	95.4	95.3	95.0	94.5
O5-*M*1-O6	93.7	92.5	92.8	93.1	93.6	92.6	94.5	94.5	93.5	93.3
O3-*M*1-O6	91.2	90.7	90.6	90.9	91.1	90.9	91.8	92.1	91.2	91.2
O1-*M*1-O6	84.1	84.9	84.5	84.4	84.1	85.0	83.5	83.7	84.0	84.1
O3-*M*1-O5	93.1	92.7	92.6	93.0	93.1	93.1	93.9	94.4	93.1	92.9
O7-*M*1-O5	79.9	79.9	80.3	79.8	80.0	79.7	80.0	79.3	80.0	80.5
O1-*M*1-O3	80.3	80.4	80.0	79.9	80.4	80.1	80.0	80.1	80.4	80.3
O1-*M*1-O7	106.5	106.8	106.8	107.0	106.3	106.9	106.0	106.1	106.4	106.0
O7-*M*1-O6	85.5	86.2	85.3	85.5	85.4	85.9	85.5	85.0	85.4	85.4
M(2)										
O5-*M*2-O5	83.3	84.2	84.1	83.8	83.3	84.1	83.1	82.6	83.5	83.4
O6-*M*2-O5	93.2	92.4	92.3	92.7	93.5	92.4	94.6	94.8	93.3	93.3
O2-*M*2-O5	87.5	87.6	88.0	87.7	86.9	87.6	86.0	85.7	87.1	87.8
O7-*M*2-O5	92.6	91.8	92.4	92.4	93.1	92.1	93.3	94.2	93.1	92.0
O5-*M*2-O7	96.2	96.1	95.9	96.0	96.3	96.1	95.8	96.3	96.2	96.0
O6-*M*2-O7	87.0	87.1	87.4	87.2	86.7	87.1	86.4	86.2	86.7	87.0
O7-*M*2-O7	84.4	85.6	84.5	84.6	84.3	85.5	84.5	84.2	84.4	84.7
O2-*M*2-O5	102.7	102.8	102.6	102.7	103.1	102.8	102.6	103.1	102.7	102.5
O7-*M*2-O5	80.7	80.2	81.2	80.6	80.6	80.3	80.9	79.8	80.5	80.7
O2-*M*2-O6	82.3	82.3	82.4	82.2	81.9	82.1	81.0	81.1	81.9	82.9
O7-*M*2-O6	94.4	94.6	93.9	94.5	94.3	94.7	95.5	96.0	94.8	93.9
O2-*M*2-O7	95.5	94.9	95.1	95.3	95.7	94.8	96.3	95.9	95.4	92.5
M(3)										
O4-*M*3-O1	96.1	95.6	96.4	96.0	96.6	96.1	96.2	96.1	96.3	95.9
O6-*M*3-O1	87.1	87.4	87.4	87.5	86.7	87.6	86.1	86.3	86.8	87.1
O4-*M*3-O1	83.2	84.6	83.3	83.2	83.5	83.6	83.3	83.5	83.6	82.9
O2-*M*3-O1	95.5	95.0	95.3	95.5	95.7	95.1	96.3	95.9	95.3	95.8
O3-*M*3-O4	84.3	85.1	84.0	84.1	84.1	84.3	83.7	84.1	84.4	84.2
O4-*M*3-O4	80.5	80.9	80.5	80.5	80.2	81.0	79.3	79.5	80.2	80.7
O2-*M*3-O4	101.4	101.7	101.7	101.5	102.0	101.4	102.4	101.8	101.7	101.2
O6-*M*3-O3	92.2	91.5	91.9	92.1	92.4	91.7	93.8	93.5	92.2	92.3
O4-*M*3-O3	93.8	92.8	93.6	93.7	93.9	93.4	95.0	95.1	93.9	93.7
O2-*M*3-O3	87.5	87.6	87.8	87.7	86.9	87.8	85.5	85.6	87.1	87.6
O4-*M*3-O6	94.3	93.7	94.0	94.3	94.3	94.1	95.6	96.0	94.7	93.8
O2-*M*3-O6	83.9	83.8	83.9	83.7	83.6	83.6	82.8	82.7	83.5	84.3
M(4)										
O1-*M*4-O4	94.4	93.7	94.5	94.2	94.4	93.8	95.3	95.1	94.6	94.5
O1-*M*4-O4	85.6	86.3	85.5	85.8	85.6	86.2	84.7	84.9	85.5	85.5
O3-*M*4-O4	84.4	85.3	84.9	84.5	84.0	85.1	83.5	96.5	95.9	84.6
O3-*M*4-O4	95.6	94.8	95.1	95.5	96.0	94.9	96.5	83.6	84.1	95.4
O3-*M*4-O1	82.9	82.3	82.8	82.9	82.6	82.9	82.2	81.9	82.5	83.1
O3-*M*4-O1	97.1	97.7	97.2	97.1	97.4	97.1	97.8	98.2	97.5	96.9
D										
O9-*D*-O2	95.7	97.8	96.2	96.1	96.8	98.6	97.4	97.8	97.3	94.0
O15-*D*-O2	96.6	99.1	96.5	96.6	97.5	99.3	99.0	98.8	98.1	95.1
O12-*D*-O2	95.8	98.1	96.3	96.3	96.5	98.7	97.8	98.4	97.4	94.7
O11-*D*-O2	96.5	99.2	96.8	96.5	97.1	99.0	98.4	98.5	97.9	94.5
O9-*D*-O16	83.8	81.5	83.6	83.6	82.9	81.0	81.8	81.6	82.3	85.5
O15-*D*-O16	83.9	81.6	83.7	83.8	82.9	81.1	81.8	81.8	82.3	85.4
O12-*D*-O16	83.8	81.3	83.5	83.5	83.1	81.0	81.9	81.4	82.3	85.1
O11-*D*-O16	83.9	81.4	83.4	83.8	83.3	81.2	81.9	81.8	82.4	85.7
O12-*D*-O9	89.9	89.2	89.1	89.9	89.9	89.4	90.1	89.9	90.3	89.9
O11-*D*-O9	88.7	87.9	88.9	89.0	88.8	87.7	87.7	88.1	88.1	89.6
O12-*D*-O15	89.2	88.8	89.9	89.1	88.7	88.5	88.2	88.1	88.3	90.5
O11-*D*-O15	89.5	89.1	89.2	89.2	89.2	88.9	89.4	89.2	89.2	88.6

TABLE 5B. SELECTED BOND ANGLES (°) FOR MEMBERS OF THE ASTROPHYLLITE GROUP

SAMPLE	LAB3	NOR1	NOR17	RUS4	RUS8	RUS9	RUS12	US5	MSH2	MSH3
(M,D,T)-O-*T*										
*M*3-O1-*T*1	120.7	121.1	120.7	121.3	121.0	120.8	120.8	120.6	120.7	121.1
*M*4-O1-*T*1	117.9	118.2	118.8	117.8	118.0	118.6	119.6	117.4	118.6	119.2
*M*1-O1-*T*1	124.0	123.0	123.2	123.6	123.0	123.3	122.9	123.6	124.1	122.7
*M*3-O3-*T*2	122.1	122.1	123.0	122.2	122.3	122.5	119.7	122.0	123.1	123.4
*M*4-O3-*T*2	118.5	118.7	118.3	118.1	118.6	118.9	123.0	117.9	118.7	119.8
*M*1-O3-*T*2	122.1	122.2	122.6	121.2	121.7	121.9	121.7	122.3	122.8	121.8
*M*3-O6-*T*3	120.0	120.1	121.3	120.3	120.4	120.7	121.5	120.6	121.0	121.2
*M*1-O6-*T*3	122.7	122.2	122.9	121.9	121.9	122.0	122.6	122.7	122.8	122.7
*M*2-O6-*T*3	120.0	120.5	120.6	120.2	120.0	120.6	121.0	119.9	121.2	120.9
*M*2-O7-*T*4	120.9	120.9	120.6	121.4	120.8	120.9	120.7	120.8	120.6	121.2
*M*1-O7-*T*4	122.5	122.5	122.1	121.8	122.1	122.7	122.5	122.3	122.9	122.2
*M*2-O7-*T*4	118.9	119.2	120.1	118.9	119.0	119.3	120.2	118.6	120.1	120.1
*T*3-O8-*T*2	139.7	139.3	139.8	139.3	139.7	139.3	139.5	138.9	139.7	139.8
*T*3-O10-*T*2	139.8	139.0	139.2	139.2	138.9	138.9	139.4	139.2	139.7	138.1
*T*1-O13-*T*2	143.0	142.4	142.4	141.8	142.6	142.6	141.4	143.6	143.1	140.8
*T*4-O14-*T*3	143.8	143.5	143.2	143.3	143.5	143.2	143.3	144.4	143.5	142.4
D-O9-*T*4	143.0	143.4	143.2	142.8	142.1	143.3	142.3	142.7	142.4	144.3
D-O11-*T*1	141.5	141.7	141.8	141.4	141.1	141.7	141.6	141.8	141.2	143.9
D-O12-*T*4	141.5	141.5	141.4	140.3	140.5	141.7	141.2	141.7	141.8	142.9
D-O15-*T*1	141.3	141.1	141.6	140.5	140.3	141.5	141.4	141.8	141.0	143.0
O-*T*-O										
O11-*T*1-O15	110.1	110.5	110.8	109.6	109.9	110.7	110.1	111.7	110.5	111.0
O1-*T*1-O15	111.5	111.4	111.1	111.4	111.6	111.2	111.2	110.9	111.1	111.0
O13-*T*1-O15	106.2	105.8	106.2	105.8	106.1	106.2	106.3	106.0	106.4	106.0
O1-*T*1-O11	111.2	111.7	111.1	111.6	111.7	111.5	111.8	110.8	111.5	111.3
O13-*T*1-O11	105.9	105.5	106.2	105.8	105.7	105.6	105.9	105.7	105.9	105.5
O13-*T*1-O1	111.7	111.6	111.3	112.3	111.7	111.4	111.3	111.5	111.3	111.9
O3-*T*2-O13	111.7	111.6	112.3	111.8	111.4	111.4	111.7	111.6	111.7	111.9
O8-*T*2-O13	106.5	106.3	106.7	106.4	106.7	106.6	106.3	106.9	106.7	105.6
O10-*T*2-O13	106.4	106.7	106.4	106.7	106.8	106.4	106.4	106.6	107.0	106.3
O8-*T*2-O3	110.2	110.3	110.4	110.8	110.5	110.7	110.7	110.4	110.2	110.9
O10-*T*2-O3	110.5	110.9	110.5	110.5	110.8	110.9	110.8	110.5	110.3	111.2
O10-*T*2-O8	111.4	110.9	110.4	110.5	110.4	110.7	110.7	110.8	110.7	110.8
O6-*T*3-O14	111.2	111.1	112.1	111.5	111.5	111.5	111.9	111.3	111.5	112.2
O10-*T*3-O14	106.0	106.2	105.9	106.4	106.1	106.4	106.0	106.5	106.2	105.5
O8-*T*3-O14	106.4	106.2	106.4	105.9	106.6	106.3	106.3	106.2	106.4	106.2
O10-*T*3-O6	110.9	111.1	110.8	110.7	110.9	110.7	110.6	111.1	110.7	111.3
O8-*T*3-O6	111.1	111.8	111.2	111.8	111.5	111.7	111.6	111.6	111.4	111.4
O8-*T*3-O10	110.9	110.1	110.3	110.2	110.2	110.1	110.4	109.9	111.5	110.0
O12-*T*4-O9	110.0	109.8	110.4	109.6	109.7	110.1	109.6	111.7	110.0	110.7
O14-*T*4-O9	105.7	105.9	106.0	106.4	105.4	106.0	105.9	105.4	105.9	105.4
O7-*T*4-O9	111.7	111.5	111.5	112.0	112.0	111.3	111.9	111.7	111.8	111.7
O14-*T*4-O12	106.2	106.1	106.1	105.4	106.1	106.2	106.3	105.6	106.2	105.9
O7-*T*4-O12	111.6	111.7	111.5	111.7	111.8	111.2	111.5	111.3	111.3	111.1
O7-*T*4-O14	111.5	111.6	111.1	111.5	111.6	111.9	111.3	111.0	111.4	111.8

TABLE 5B. CONTINUED

SAMPLE	MSH8	MSH9	MSH15	MSH15A	MSH19A	MSH20	MSH33	MSH34	MSH38	MSH42
(M,D,T)-O-*T*										
*M*3-O1-*T*1	120.6	120.8	120.7	120.6	120.6	120.8	120.9	121.0	120.8	120.5
*M*4-O1-*T*1	118.3	118.6	118.5	118.9	118.2	119.2	117.6	117.4	118.0	118.1
*M*1-O1-*T*1	123.8	124.1	123.4	123.3	123.8	123.5	124.3	124.1	123.7	124.2
*M*3-O3-*T*2	123.2	122.9	123.0	123.0	122.8	123.0	121.8	121.7	123.0	123.2
*M*4-O3-*T*2	119.0	118.7	119.3	119.0	118.6	119.2	118.5	118.1	118.5	119.2
*M*1-O3-*T*2	122.1	122.9	122.3	122.2	122.3	122.4	121.6	121.9	122.4	122.0
*M*3-O6-*T*3	120.7	121.3	120.8	120.9	120.5	121.2	122.4	122.2	120.6	120.5
*M*1-O6-*T*3	122.5	122.9	123.2	122.7	122.8	122.7	119.8	119.6	122.7	122.5
*M*2-O6-*T*3	121.0	121.0	121.3	121.2	120.8	121.0	119.4	119.8	120.7	121.6
*M*2-O7-*T*4	120.7	120.4	121.3	120.5	120.4	120.6	121.1	120.8	120.6	121.0
*M*1-O7-*T*4	122.4	122.6	121.7	122.2	122.6	122.5	119.0	122.7	122.4	123.4
*M*2-O7-*T*4	119.7	120.4	120.1	119.9	119.5	120.2	123.0	118.3	119.3	118.9
*T*3-O8-*T*2	139.4	139.2	139.7	139.4	139.3	139.2	139.6	139.2	139.3	139.4
*T*3-O10-*T*2	139.2	139.2	138.6	139.1	139.4	139.1	139.8	139.3	139.0	139.9
*T*1-O13-*T*2	142.6	143.6	142.1	142.1	143.1	142.5	143.2	143.1	142.8	142.0
*T*4-O14-*T*3	143.0	143.7	142.4	142.6	143.1	143.3	143.9	143.8	143.0	143.1
D-O9-*T*4	145.0	142.7	144.4	144.6	144.4	142.1	143.1	142.7	143.9	145.9
D-O11-*T*1	143.2	141.1	143.1	143.2	142.1	141.3	141.3	141.1	141.9	144.5
D-O12-*T*4	143.6	141.5	142.8	143.5	142.8	141.0	142.4	141.4	142.3	144.3
D-O15-*T*1	143.6	141.5	143.4	143.3	142.9	141.1	141.0	141.2	142.0	143.7
O-*T*-O										
O11-*T*1-O15	110.9	110.3	111.1	111.2	111.3	110.5	109.7	110.4	110.8	112.3
O1-*T*1-O15	110.8	110.8	110.5	111.0	111.0	111.3	111.5	111.2	111.1	110.8
O13-*T*1-O15	106.2	106.9	106.3	106.1	106.3	106.4	106.2	106.0	106.0	105.2
O1-*T*1-O11	111.2	111.6	111.4	111.2	111.0	111.5	111.7	111.5	111.3	110.8
O13-*T*1-O11	105.4	106.0	105.6	105.4	105.5	105.7	105.4	105.4	105.5	104.8
O13-*T*1-O1	112.1	111.2	111.8	111.7	111.6	111.3	112.0	112.1	111.9	112.7
O3-*T*2-O13	111.2	111.4	111.7	111.6	111.4	111.5	111.1	111.4	111.6	111.4
O8-*T*2-O13	106.4	106.7	106.3	106.4	106.6	106.6	106.3	106.5	106.7	106.2
O10-*T*2-O13	106.5	106.8	106.6	106.7	106.5	106.9	106.6	106.8	106.6	106.2
O8-*T*2-O3	110.8	110.4	110.6	110.6	111.4	110.5	110.5	110.5	110.6	110.8
O10-*T*2-O3	110.7	110.6	111.0	110.7	110.6	110.8	110.7	110.7	110.5	110.1
O10-*T*2-O8	111.2	110.9	110.5	110.7	111.3	110.4	111.6	110.8	110.8	112.0
O6-*T*3-O14	111.2	111.5	111.8	111.6	111.3	111.6	111.1	110.9	111.4	110.5
O10-*T*3-O14	105.7	106.2	104.9	105.6	105.4	105.8	106.3	106.2	105.6	105.9
O8-*T*3-O14	106.2	106.6	106.0	106.0	106.1	106.5	106.4	106.3	106.2	106.3
O10-*T*3-O6	110.9	110.7	111.7	111.0	111.2	110.8	110.9	111.0	111.3	110.9
O8-*T*3-O6	111.5	111.5	111.2	111.6	111.6	111.7	110.9	111.5	111.5	111.8
O8-*T*3-O10	111.0	110.1	110.9	110.8	111.1	110.2	111.1	110.7	110.6	111.2
O12-*T*4-O9	110.6	110.5	111.5	110.6	110.6	110.1	109.5	109.7	109.8	110.7
O14-*T*4-O9	105.4	105.7	105.1	105.1	105.3	105.5	105.9	105.7	105.5	105.1
O7-*T*4-O9	111.6	111.5	112.1	111.4	111.4	111.9	111.7	111.7	111.6	111.4
O14-*T*4-O12	106.0	106.4	105.5	106.2	106.2	106.2	106.5	105.9	106.3	105.4
O7-*T*4-O12	111.0	111.4	110.8	111.3	111.2	111.5	111.2	111.7	111.4	110.9
O7-*T*4-O14	112.0	111.1	111.6	111.9	111.9	111.3	111.8	111.9	111.9	113.1

TABLE 5C . O-*T*-O BOND ANGLES (°) FOR MEMBERS OF THE ASTROPHYLLITE GROUP

SAMPLE	LAB3	NOR1	NOR17	RUS4	RUS8	RUS9	RUS12	US5	MSH2	MSH3
O11-*T*1-O15	110.14	110.47	110.75	109.58	109.93	110.73	110.1	111.69	110.45	111.04
O1-*T*1-O15	111.49	111.4	111.07	111.38	111.57	111.18	111.21	110.9	111.11	110.95
O13-*T*1-O15	106.19	105.81	106.19	105.83	106.08	106.19	106.26	106.01	106.4	105.95
O1-*T*1-O11	111.2	111.73	111.14	111.62	111.65	111.5	111.81	110.83	111.46	111.29
O13-*T*1-O11	105.9	105.49	106.22	105.84	105.65	105.6	105.9	105.73	105.93	105.46
O13-*T*1-O1	111.67	111.62	111.26	112.28	111.66	111.38	111.3	111.48	111.26	111.92
O3-*T*2-O13	111.69	111.59	112.27	111.82	111.39	111.36	111.73	111.59	111.73	111.85
O8-*T*2-O13	106.48	106.33	106.71	106.42	106.72	106.55	106.32	106.92	106.74	105.58
O10-*T*2-O13	106.39	106.66	106.42	106.65	106.84	106.42	106.43	106.61	106.99	106.26
O8-*T*2-O3	110.22	110.33	110.41	110.83	110.52	110.67	110.74	110.38	110.21	110.92
O10-*T*2-O3	110.54	110.92	110.49	110.45	110.82	110.94	110.79	110.46	110.34	111.24
O10-*T*2-O8	111.4	110.88	110.42	110.53	110.42	110.74	110.66	110.78	110.74	110.76
O6-*T*3-O14	111.22	111.13	112.06	111.53	111.5	111.52	111.85	111.3	111.45	112.2
O10-*T*3-O14	106.01	106.23	105.9	106.4	106.06	106.37	106.02	106.52	106.17	105.49
O8-*T*3-O14	106.42	106.24	106.41	105.91	106.56	106.25	106.25	106.17	106.39	106.16
O10-*T*3-O6	110.92	111.1	110.75	110.7	110.85	110.74	110.55	111.11	110.69	111.34
O8-*T*3-O6	111.13	111.78	111.16	111.82	111.45	111.66	111.6	111.64	111.4	111.4
O8-*T*3-O10	110.94	110.11	110.34	110.24	110.21	110.09	110.36	109.88	111.54	109.98
O12-*T*4-O9	109.98	109.79	110.38	109.56	109.65	110.07	109.63	111.65	110	110.72
O14-*T*4-O9	105.67	105.88	105.96	106.35	105.39	106.02	105.86	105.35	105.85	105.36
O7-*T*4-O9	111.65	111.46	111.47	111.95	111.98	111.29	111.9	111.7	111.84	111.7
O14-*T*4-O12	106.17	106.09	106.13	105.43	106.09	106.15	106.28	105.57	106.21	105.89
O7-*T*4-O12	111.6	111.71	111.5	111.7	111.8	111.21	111.54	111.27	111.28	111.14
O7-*T*4-O14	111.47	111.63	111.13	111.52	111.58	111.87	111.33	110.96	111.38	111.75

TABLE 5C . CONTINUED

SAMPLE	MSH8	MSH9	MSH15	MSH15	MSH19	MSH20	MSH33	MSH34	MSH38	MSH42
O11-*T*1-O15	110.87	110.31	111.06	111.2	111.3	110.53	109.73	110.38	110.84	112.29
O1-*T*1-O15	110.84	110.81	110.5	111.04	110.99	111.28	111.54	111.22	111.08	110.79
O13-*T*1-O15	106.21	106.85	106.28	106.09	106.28	106.37	106.2	106.01	105.95	105.18
O1-*T*1-O11	111.2	111.55	111.41	111.15	111.01	111.45	111.68	111.48	111.34	110.78
O13-*T*1-O11	105.38	105.96	105.58	105.37	105.46	105.66	105.4	105.39	105.52	104.84
O13-*T*1-O1	112.11	111.15	111.79	111.74	111.58	111.28	111.98	112.08	111.85	112.74
O3-*T*2-O13	111.19	111.39	111.71	111.61	111.39	111.53	111.11	111.43	111.6	111.35
O8-*T*2-O13	106.43	106.65	106.3	106.43	106.58	106.55	106.27	106.49	106.66	106.21
O10-*T*2-O13	106.48	106.75	106.6	106.65	106.46	106.89	106.55	106.83	106.58	106.24
O8-*T*2-O3	110.76	110.37	110.57	110.62	111.39	110.51	110.51	110.45	110.57	110.81
O10-*T*2-O3	110.66	110.63	111.02	110.74	110.61	110.83	110.65	110.72	110.51	110.12
O10-*T*2-O8	111.17	110.93	110.48	110.65	111.28	110.39	111.62	110.79	110.8	111.96
O6-*T*3-O14	111.21	111.48	111.78	111.58	111.3	111.61	111.13	110.91	111.42	110.54
O10-*T*3-O14	105.71	106.23	104.94	105.55	105.37	105.77	106.29	106.15	105.59	105.87
O8-*T*3-O14	106.18	106.6	106	106.02	106.06	106.48	106.43	106.33	106.18	106.26
O10-*T*3-O6	110.92	110.74	111.69	111.03	111.18	110.8	110.88	111.02	111.25	110.94
O8-*T*3-O6	111.54	111.52	111.21	111.63	111.58	111.69	110.88	111.52	111.54	111.8
O8-*T*3-O10	111.04	110.06	110.92	110.76	111.07	110.24	111.06	110.68	110.58	111.17
O12-*T*4-O9	110.64	110.47	111.54	110.56	110.59	110.1	109.52	109.65	109.84	110.7
O14-*T*4-O9	105.35	105.65	105.05	105.14	105.32	105.45	105.86	105.7	105.53	105.11
O7-*T*4-O9	111.56	111.53	112.07	111.41	111.42	111.93	111.68	111.65	111.58	111.36
O14-*T*4-O12	105.95	106.42	105.5	106.22	106.18	106.2	106.54	105.94	106.33	105.37
O7-*T*4-O12	111.03	111.39	110.77	111.31	111.17	111.5	111.2	111.65	111.42	110.91
O7-*T*4-O14	112.03	111.12	111.6	111.92	111.89	111.34	111.79	111.94	111.85	113.1

TABLE 6. MISCELLANEOUS PARAMETERS FOR AGM POLYHEDRA

Sample	LAB3	NOR1	NOR17	RUS4	RUS8	RUS9	RUS12	US5	MSH2	MSH3
Polyhedral volume (Å^3)										
VM(1)	13.521	13.721	13.721	13.526	13.535	13.795	14.003	13.158	13.896	14.084
VM(2)	13.253	13.432	13.432	13.107	13.157	13.467	13.631	12.990	13.718	13.613
VM(3)	13.041	13.223	13.223	12.884	12.954	13.252	13.440	12.801	13.548	13.337
VM(4)	12.748	12.783	12.783	12.551	12.568	12.764	12.642	12.543	13.099	12.623
VD	10.226	9.711	9.711	9.705	9.707	9.760	9.714	9.722	9.766	9.791
VT(1)	2.148	2.169	2.169	2.162	2.159	2.177	2.190	2.141	2.188	2.169
VT(2)	2.187	2.193	2.193	2.200	2.197	2.214	2.208	2.184	2.215	2.196
VT(3)	2.223	2.190	2.190	2.216	2.223	2.245	2.203	2.159	2.215	2.207
VT(4)	2.148	2.168	2.168	2.167	2.156	2.180	2.185	2.141	2.184	2.175
Distortions (quadratic elongation, Δ)										
DM(1)	1.854	1.15	0.600	1.116	0.895	0.937	0.732	1.038	0.528	0.737
DM(2)	5.431	6.504	6.489	7.946	7.168	6.057	5.657	8.171	6.204	6.136
DM(3)	2.236	3.193	3.086	4.245	4.265	3.634	2.897	3.497	3.016	3.581
DM(4)	2.74	2.843	2.381	2.829	2.255	2.268	1.845	3.262	1.928	2.530
DD	10.939	13.685	17.642	17.931	19.713	13.130	16.846	13.593	16.442	6.685
DT(1)	1.839	0.847	1.106	1.411	0.694	1.423	0.893	1.227	0.765	1.116
DT(2)	0.573	0.586	0.602	0.447	0.309	0.434	0.767	0.839	0.594	0.718
DT(3)	0.561	0.279	0.881	0.557	0.487	0.945	0.749	0.910	0.546	1.089
DT(4)	1.425	0.738	1.289	0.607	0.813	0.552	0.536	1.844	0.801	0.577
Octahedral Flattening (Ψ, °)										
$\Psi_{M(1)}$	59.392	59.311	58.976	59.488	59.430	59.136	58.919	59.392	58.712	58.865
$\Psi_{M(2)}$	59.400	59.189	58.866	59.321	59.277	58.957	58.686	59.518	58.729	58.463
$\Psi_{M(3)}$	59.296	59.011	58.673	59.174	59.040	58.889	58.578	59.200	58.465	58.558
$\Psi_{M(4)}$	59.292	59.102	58.882	59.445	59.243	58.993	58.430	59.514	58.677	58.472
$\Psi_{average}$	59.345	59.153	58.849	59.357	59.248	58.993	58.653	59.406	58.646	58.590
Octahedral Counter-rotation (δ, °)										
$\delta_{M(1)}$	0.252	0.178	0.177	0.193	0.198	0.108	0.100	0.238	0.167	0.135
$\delta_{M(2)}$	0.548	0.569	0.555	0.718	0.668	0.571	0.578	0.429	0.357	0.762
$\delta_{M(3)}$	0.252	0.562	0.456	0.435	0.482	0.520	0.897	0.131	0.335	0.913
$\delta_{M(4)}$	0.000	0.002	0.004	0.000	0.006	0.000	0.002	0.005	0.000	0.007
$\delta_{average}$	0.263	0.328	0.298	0.337	0.339	0.300	0.394	0.201	0.215	0.454

TABLE 6. CONTINUED

Sample	LAB3	NOR1	NOR17	RUS4	RUS8	RUS9	RUS12	US5	MSH2	MSH3
Octahedral angle variance (σ)										
$\sigma_{M(1)}$	61.09	60.06	57.81	61.97	62.60	56.47	57.43	60.46	52.50	56.54
$\sigma_{M(2)}$	52.77	49.59	45.53	51.47	50.79	45.48	43.37	54.52	43.52	38.53
$\sigma_{M(3)}$	49.91	44.56	40.81	47.49	44.88	42.34	39.30	47.47	37.81	38.27
$\sigma_{M(4)}$	48.56	44.85	42.02	51.61	47.80	43.03	33.04	53.75	38.51	33.10
Tetrahedral tilting [°, with respect to (001)]										
$TT(1)$	7.19	6.85	6.75	6.62	6.94	6.64	6.49	6.91	7.27	6.00
$TT(2)$	2.12	2.00	2.32	2.17	1.95	1.82	2.60	1.57	2.15	2.65
$TT(3)$	0.93	0.78	1.17	0.81	0.78	0.80	1.02	0.39	0.83	1.18
$TT(4)$	7.34	7.14	7.04	7.24	7.25	6.92	7.35	7.23	7.53	6.82
Tetrahedral rotation (α, °)										
$\alpha_{T(ave)}$	1.07	1.06	1.11	0.86	1.03	1.37	1.42	0.93	1.56	1.26
Tetrahedral thickening angles (τ, °)										
$\tau_{T(1)}$	111.45	111.58	111.16	111.76	111.63	111.35	111.44	111.07	111.28	111.39
$\tau_{T(2)}$	110.82	110.95	111.06	111.03	110.91	110.99	111.09	110.81	110.76	111.34
$\tau_{T(3)}$	111.09	111.34	111.32	111.35	111.27	111.31	111.33	111.35	111.18	111.65
$\tau_{T(4)}$	111.57	111.60	111.37	111.72	111.79	111.46	111.59	111.31	111.50	111.53
Tetrahedral angle variance (σ)										
$\sigma_{T(1)}$	7.17	8.74	6.30	8.52	8.05	7.60	7.06	7.76	6.55	8.49
$\sigma_{T(2)}$	5.76	5.42	5.52	5.34	4.40	5.32	5.81	4.54	4.33	7.60
$\sigma_{T(3)}$	6.27	6.42	6.81	6.79	6.12	6.19	6.89	6.10	6.76	8.35
$\sigma_{T(4)}$	7.78	7.61	7.04	8.28	8.86	7.08	7.38	9.47	7.31	8.85

TABLE 6. CONTINUED

Sample	MSH8	MSH9	MSH15	MSH15	MSH19	MSH20	MSH33	MSH34	MSH38	MSH42
Polyhedral volume ($Å^3$)										
VM(1)	13.941	13.873	13.967	13.916	13.770	13.869	13.560	13.356	13.720	13.990
VM(2)	13.559	13.702	13.582	13.535	13.456	13.615	13.365	13.123	13.400	13.687
VM(3)	13.400	13.551	13.386	13.350	13.276	13.440	12.967	12.928	13.213	13.468
VM(4)	12.898	13.111	12.750	12.743	12.900	12.769	12.750	12.715	12.863	12.902
VD	9.970	9.727	9.903	9.899	10.043	9.695	10.340	10.096	9.886	10.304
VT(1)	2.169	2.181	2.174	2.159	2.169	2.167	2.140	2.136	2.167	2.129
VT(2)	2.207	2.209	2.192	2.209	2.218	2.208	2.204	2.220	2.210	2.223
VT(3)	2.252	2.235	2.218	2.223	2.217	2.220	2.256	2.226	2.218	2.230
VT(4)	2.161	2.186	2.162	2.164	2.169	2.176	2.135	2.151	2.163	2.095
Distortions (quadratic elongation, Δ)										
DM(1)	0.956	0.488	0.650	0.782	0.526	0.594	2.851	1.944	0.910	1.041
DM(2)	6.275	5.606	6.512	5.925	6.343	6.144	5.106	6.467	6.356	6.059
DM(3)	3.057	3.043	2.729	2.892	2.516	3.026	2.485	2.930	3.126	2.470
DM(4)	2.919	1.578	2.689	2.467	2.948	2.849	2.859	3.029	3.099	2.611
DD	3.729	16.390	6.254	5.415	5.684	18.877	8.531	11.347	8.914	1.526
DT(1)	0.711	0.526	1.256	0.847	1.011	0.844	1.175	0.992	1.023	1.558
DT(2)	0.346	0.306	0.726	0.597	0.695	0.614	0.254	0.275	0.794	0.961
DT(3)	0.630	0.889	1.196	0.696	0.578	0.715	0.630	0.441	0.554	0.166
DT(4)	0.430	0.375	0.964	0.599	0.642	0.562	0.840	0.642	1.014	0.370
Octahedral Flattening (Ψ, °)										
$\Psi_{M(1)}$	59.058	58.690	58.902	59.015	59.140	58.797	59.438	59.567	59.111	58.913
$\Psi_{M(2)}$	58.937	58.685	58.659	58.831	59.123	58.750	59.358	59.678	59.070	58.788
$\Psi_{M(3)}$	58.779	58.396	58.736	58.760	58.982	58.599	59.523	59.402	58.892	58.726
$\Psi_{M(4)}$	58.891	58.614	58.799	58.799	59.076	58.566	59.510	59.520	59.077	58.786
$\Psi_{average}$	58.916	58.596	58.774	58.851	59.080	58.678	59.457	59.542	59.037	58.803
Octahedral Counter-rotation (δ, °)										
$\delta_{M(1)}$	0.182	0.209	0.037	0.142	0.194	0.162	0.264	0.274	0.214	0.160
$\delta_{M(2)}$	0.680	0.369	0.739	0.654	0.598	0.426	0.595	0.486	0.589	0.573
$\delta_{M(3)}$	0.495	0.322	0.595	0.632	0.343	0.644	0.145	0.162	0.352	0.528
$\delta_{M(4)}$	0.004	0.007	0.002	0.001	0.005	0.001	0.000	0.001	0.002	0.003
$\delta_{average}$	0.340	0.227	0.343	0.357	0.285	0.308	0.251	0.231	0.289	0.316

TABLE 6. CONTINUED

Sample	MSH8	MSH9	MSH15	MSH15	MSH19	MSH20	MSH33	MSH34	MSH38	MSH42
Octahedral angle variance (σ)										
$\sigma_{M(1)}$	56.35	53.19	55.88	57.90	56.82	54.77	60.09	62.31	56.73	53.24
$\sigma_{M(2)}$	45.70	43.32	41.69	44.53	48.46	43.65	51.24	57.14	47.36	41.00
$\sigma_{M(3)}$	41.34	36.73	41.72	41.57	44.93	39.02	53.50	50.73	43.34	40.41
$\sigma_{M(4)}$	40.56	37.97	39.21	39.30	44.49	35.91	52.49	53.49	44.70	38.70
Tetrahedral tilting [°, with respect to (001)]										
$TT(1)$	6.64	7.40	6.52	6.47	6.95	6.79	7.44	7.14	6.81	6.31
$TT(2)$	1.92	1.81	2.24	2.14	1.88	2.10	1.83	1.72	1.85	2.28
$TT(3)$	0.81	0.80	1.20	1.06	0.88	0.86	0.82	0.58	0.80	0.87
$TT(4)$	6.74	7.33	6.65	6.69	6.90	7.25	7.25	7.33	6.90	6.87
Tetrahedral rotation (α, °)										
$\alpha_{T(ave)}$	1.39	1.81	1.27	1.25	1.33	1.58	1.18	0.93	1.21	1.49
Tetrahedral thickening angles (τ, °)										
$\tau_{T(1)}$	111.38	111.17	111.23	111.31	111.19	111.34	111.73	111.59	111.42	111.44
$\tau_{T(2)}$	110.87	110.80	111.10	110.99	111.13	110.96	110.76	110.87	110.89	110.76
$\tau_{T(3)}$	111.22	111.25	111.56	111.41	111.35	111.37	110.96	111.15	111.40	111.09
$\tau_{T(4)}$	111.54	111.35	111.48	111.55	111.49	111.59	111.56	111.75	111.62	111.79
Tetrahedral angle variance (σ)										
$\sigma_{T(1)}$	8.23	5.77	7.61	8.33	7.75	7.14	8.56	8.67	8.32	12.39
$\sigma_{T(2)}$	5.42	4.66	5.59	5.22	5.87	4.64	5.71	4.79	4.97	6.60
$\sigma_{T(3)}$	7.37	5.79	9.59	8.10	8.34	6.90	5.72	6.20	7.67	6.98
$\sigma_{T(4)}$	8.82	7.11	10.51	8.73	8.37	8.18	6.98	8.46	7.89	11.23

TABLE 7. BOND VALENCE SUMS (*v.u.*)* FOR ASTROPHYLLITE GROUP MINERALS

LAB3	*A*	*B*	*M*(1)	*M*(2)	*M*(3)	*M*(4)	*D*	*T*(1)	*T*(2)	*T*(3)	*T*(4)	Σ
O(1)			0.267		0.345	0.320 ↓x2		0.984				1.916
O(2)			0.336	0.262	0.277		0.986					1.861
O(3)			0.299		0.336	0.304 ↓x2			1.019			1.958
OH(4)					0.651	0.378 ↓x2						1.029
OH(5)			0.310	0.702								1.012
O(6)			0.329	0.280	0.323					0.989		1.921
O(7)			0.285	0.663							0.973	1.921
O(8)	0.017								0.976	0.950		1.943
O(9)	0.122	0.122 ↓x2					0.744				1.084	2.072
O(10)	0.027								0.971	0.953		1.951
O(11)	0.129	0.115 ↓x2					0.734	1.082				2.060
O(12)	0.127	0.123 ↓x2					0.749				1.082	2.081
O(13)	0.051							0.960	1.053			2.064
O(14)	0.056									1.030	0.979	2.065
O(15)	0.126	0.125 ↓x2					0.728	1.102				2.081
ϕ(16)	0.066 →x2	0.072 ↓x2 →					0.498 →x2					1.272
Σ	0.721	1.114	1.826	1.877	1.932	2.004	4.439	4.128	4.019	3.922	4.118	

NOR1	*A*	*B*	*M*(1)	*M*(2)	*M*(3)	*M*(4)	*D*	*T*(1)	*T*(2)	*T*(3)	*T*(4)	Σ
O(1)			0.305		0.337	0.327 ↓x2		1.000				1.969
O(2)			0.359	0.238	0.248		0.997					1.842
O(3)			0.340		0.318	0.307 ↓x2			1.030			1.995
OH(4)					0.598	0.387 ↓x2						0.985
OH(5)			0.355	0.719								1.074
O(6)			0.367	0.275	0.305					1.000		1.947
O(7)			0.328	0.610							0.997	1.935
O(8)	0.019								0.953	0.960		1.932
O(9)	0.118	0.135 ↓x2					0.719				1.073	2.045
O(10)	0.032								0.965	0.953		1.950
O(11)	0.127	0.128 ↓x2					0.707	1.061				2.023
O(12)	0.125	0.136 ↓x2					0.715				1.064	2.040
O(13)	0.053							0.968	1.019			2.040
O(14)	0.057									1.011	0.987	2.055
O(15)	0.129	0.135 ↓x2					0.700	1.064				2.028
ϕ(16)	0.054 →x2	0.072 ↓x2 →					0.452 →x2					1.166
Σ	0.714	1.222	2.054	1.842	1.802	2.004	4.290	4.093	3.967	3.931	4.121	

NOR17	*A*(1a)	*A*(1b)	*B*	*M*(1)	*M*(2)	*M*(3)	*M*(4)	*D*	*T*(1)	*T*(2)	*T*(3)	*T*(4)	Σ
O(1)				0.309		0.403	0.382 ↓x2		1.003				2.097
O(2)				0.357	0.282	0.309		1.041					1.989
O(3)				0.329		0.391	0.357 ↓x2			1.041			2.118
OH(4)						0.735	0.442 ↓x2						1.177
OH(5)				0.345	0.795								1.140
O(6)				0.348	0.316	0.371					1.033		2.068
O(7)				0.336	0.721							0.989	2.046
O(8)	0.015									0.971	0.958		1.944
O(9)	0.126	0.023	0.122 ↓x2					0.709				1.073	2.053
O(10)										0.965	0.965		1.930
O(11)	0.129	0.024	0.112 ↓x2					0.703	1.064				2.032
O(12)	0.132	0.024	0.116 ↓x2					0.715				1.058	2.045
O(13)	0.049								0.947	1.030			2.026
O(14)	0.054										1.053	0.950	2.057
O(15)	0.130	0.024	0.120 ↓x2					0.715	1.053				2.042
ϕ(16)	0.071 →x2	0.043 →x2	0.068 ↓x2 →					0.425 →x2					1.216
Σ	0.706	0.138	1.078	2.024	2.114	2.209	2.362	4.308	4.067	4.007	4.009	4.070	

* constants taken from Brese & O'Keeffe (1991)

TABLE 7. CONTINUED

RUS4	*A*	*B*	*M*(1)	*M*(2)	*M*(3)	*M*(4)	*D*	*T*(1)	*T*(2)	*T*(3)	*T*(4)	Σ
O(1)			0.311		0.355	0.319		1.033				2.018
O(2)			0.366	0.239	0.257		1.029					1.891
O(3)			0.345		0.357	0.312			0.992			2.006
OH(4)					0.661	0.386						1.047
OH(5)			0.354	0.711								1.065
O(6)			0.371	0.278	0.328					1.011		1.988
O(7)			0.326	0.635							0.989	1.950
O(8)	0.017								0.973	0.947		1.937
O(9)	0.125	0.147					0.707				1.056	2.035
O(10)	0.030								0.976	0.958		1.964
O(11)	0.129	0.140					0.674	1.079				2.022
O(12)	0.137	0.149					0.690				1.050	2.026
O(13)	0.058							0.937	1.047			2.042
O(14)	0.061									1.022	0.979	2.062
O(15)	0.134	0.149					0.688	1.039				2.010
ϕ(16)	0.065	0.080					0.412					1.114
Σ	0.756	1.330	2.073	1.863	1.958	2.034	4.200	4.088	3.988	3.938	4.074	

RUS8	*A*	*B*	*M*(1)	*M*(2)	*M*(3)	*M*(4)	*D*	*T*(1)	*T*(2)	*T*(3)	*T*(4)	Σ
O(1)			0.313		0.375	0.328		0.995				2.011
O(2)			0.361	0.237	0.268		1.067					1.933
O(3)			0.340		0.362	0.309			1.022			2.033
OH(4)					0.679	0.380						1.059
OH(5)			0.350	0.679								1.029
O(6)			0.371	0.275	0.347					0.989		1.982
O(7)			0.332	0.618							0.989	1.939
O(8)	0.018								0.976	0.955		1.949
O(9)	0.133	0.146					0.690				1.064	2.033
O(10)	0.029								0.971	0.953		1.953
O(11)	0.134	0.138					0.690	1.064				2.026
O(12)	0.137	0.146					0.692				1.064	2.039
O(13)	0.055							0.979	1.022			2.061
O(14)	0.060									1.027	0.979	2.066
O(15)	0.136	0.149					0.683	1.056				2.024
ϕ(16)	0.069	0.081					0.412					1.124
Σ	0.771	1.320	2.067	1.809	2.031	2.034	4.234	4.094	3.991	3.924	4.096	

RUS9	*A1*	*A2*	*B*	*M*(1)	*M*(2)	*M*(3)	*M*(4)	*D*	*T*(1)	*T*(2)	*T*(3)	*T*(4)	Σ
O(1)				0.302		0.388	0.370		0.984				2.044
O(2)				0.351	0.284	0.288		1.013					1.936
O(3)				0.332		0.375	0.347			1.003			2.057
OH(4)						0.712	0.427						1.139
OH(5)				0.343	0.790								1.133
O(6)				0.357	0.321	0.357					0.976		2.011
O(7)				0.320	0.714							0.973	2.007
O(8)										0.960	0.930		1.890
O(9)		0.130	0.139					0.717				1.044	2.030
O(10)										0.960	0.927		1.887
O(11)	0.139		0.141					0.686	1.058				2.024
O(12)		0.137	0.143					0.705				1.039	2.024
O(13)	0.064								0.937	1.027			2.028
O(14)		0.031									1.030	0.979	2.040
O(15)	0.138		0.145					0.683	1.061				2.027
ϕ(16)	0.061	0.071	0.072					0.461					1.340
Σ	0.743	0.667	1.320	2.005	2.109	2.031	2.288	4.265	4.040	3.950	3.863	4.035	

TABLE 7. CONTINUED

RUS12	A(1a)	A(1b)	B	M(1)	M(2)	M(3)	M(4)	D	T(1)	T(2)	T(3)	T(4)	Σ
O(1)				0.294		0.383	0.358↕		1.005				2.090
O(2)				0.342	0.278	0.290		1.038					1.948
O(3)				0.318		0.364	0.337↕			1.027			2.046
OH(4)						0.698	0.407↕						1.105
OH(5)				0.334	0.763								1.097
O(6)				0.339	0.303	0.348					1.027		2.017
O(7)				0.319	0.687							0.995	2.001
O(8)	0.017									0.953	0.953		1.923
O(9)	0.126	0.022	0.140↕					0.693				1.039	2.020
O(10)	0.024									0.953	0.960		1.937
O(11)	0.127	0.023	0.137↕					0.687	1.036				2.010
O(12)	0.131	0.023	0.138↕					0.689				1.030	2.011
O(13)	0.053								0.935	1.030			2.018
O(14)	0.055										1.036	0.958	2.049
O(15)	0.130	0.022	0.135↕					0.689	1.033				2.009
ϕ(16)	0.065↕→	0.030↕→	0.076↕→					0.428↕→					1.198
Σ	0.728	0.120	1.252	1.946	2.031	2.083	2.204	4.224	4.009	3.963	3.976	4.022	

US5	A	B	M(1)	M(2)	M(3)	M(4)	D	T(1)	T(2)	T(3)	T(4)	Σ
O(1)			0.286		0.374	0.329↕		0.995				1.984
O(2)			0.343	0.260	0.276		0.988					1.867
O(3)			0.313		0.357	0.314↕			1.041			2.025
OH(4)					0.669	0.399↕						1.068
OH(5)			0.327	0.750								1.077
O(6)			0.335	0.285	0.336					1.058		2.014
O(7)			0.311	0.663							1.003	1.977
O(8)	0.019								0.963	0.976		1.958
O(9)	0.146	0.103↕					0.752				1.111	2.112
O(10)	0.017								0.971	0.987		1.975
O(11)	0.153	0.099↕					0.752	1.073				2.077
O(12)	0.151	0.143↕					0.770				1.076	2.140
O(13)	0.058							0.979	1.053			2.090
O(14)	0.063									1.073	0.955	2.091
O(15)	0.147	0.105↕					0.742	1.096				2.090
ϕ(16)	0.081↕→	0.063↕→					0.457↕→					1.202
Σ	0.835	0.950	1.915	1.958	2.012	2.084	4.461	4.143	4.028	4.094	4.145	

MSH2	A	B	M(1)	M(2)	M(3)	M(4)	D	T(1)	T(2)	T(3)	T(4)	Σ
O(1)			0.305		0.384	0.361↕		0.995				2.045
O(2)			0.342	0.273	0.288		1.046					1.949
O(3)			0.326		0.366	0.342↕			1.025			2.059
OH(4)					0.699	0.415↕						1.114
OH(5)			0.337	0.771								1.108
O(6)			0.349	0.313	0.344					0.997		2.003
O(7)			0.325	0.692							0.992	2.009
O(8)	0.017								0.955	0.947		1.919
O(9)	0.129	0.142↕					0.692				1.047	2.010
O(10)	0.026								0.953	0.953		1.932
O(11)	0.133	0.135↕					0.685	1.039				1.992
O(12)	0.134	0.135↕					0.690				1.044	2.003
O(13)	0.051							0.945	1.016			2.012
O(14)	0.056									1.025	0.953	2.034
O(15)	0.135	0.135↕					0.676	1.036				1.982
ϕ(16)	0.067↕→	0.077↕→					0.437↕→					1.162
Σ	0.748	1.248	1.984	2.049	2.081	2.236	4.226	4.015	3.949	3.922	4.036	

TABLE 7. CONTINUED

MSH3	A(1a)	A(1b)	B	M(1)	M(2)	M(3)	M(4)	D	T(1)	T(2)	T(3)	T(4)	Σ
O(1)				0.295		0.400	0.312		1.000				2.007
O(2)				0.344	0.282	0.292		0.976					1.894
O(3)				0.317		0.378	0.287			1.047			2.029
OH(4)						0.721	0.360						1.081
OH(5)				0.322	0.795								1.117
O(6)				0.340	0.321	0.364					1.025		2.050
O(7)				0.314	0.724							1.014	2.052
O(8)	0.016									0.973	0.950		1.939
O(9)	0.110	0.052	0.102					0.773				1.047	2.084
O(10)	0.026									0.953	0.940		1.919
O(11)	0.109	0.054	0.099					0.771	1.053				2.086
O(12)	0.113	0.054	0.103					0.771				1.027	2.068
O(13)	0.048	0.004							0.947	1.019			2.018
O(14)	0.052	0.004									1.044	0.958	2.058
O(15)	0.112	0.059	0.101					0.745	1.064				2.081
ϕ(16)	0.055	0.059	0.062					0.585					1.522
Σ	0.641	0.286	0.934	1.932	2.122	2.155	1.918	4.621	4.064	3.992	3.959	4.046	

MSH8	A	B	M(1)	M(2)	M(3)	M(4)	D	T(1)	T(2)	T(3)	T(4)	Σ
O(1)			0.297		0.380	0.365		0.992				2.034
O(2)			0.348	0.282	0.291		0.932					1.853
O(3)			0.326		0.369	0.333			1.016			2.044
OH(4)					0.703	0.423						1.126
OH(5)			0.341	0.785								1.126
O(6)			0.348	0.310	0.355					0.981		1.994
O(7)			0.312	0.697							0.997	2.006
O(8)	0.022								0.963	0.932		1.917
O(9)	0.121	0.118					0.755				1.050	2.044
O(10)	0.035								0.971	0.927		1.933
O(11)	0.127	0.109					0.737	1.050				2.023
O(12)	0.126	0.112					0.749				1.050	2.037
O(13)	0.056							0.968	1.019			2.043
O(14)	0.063									1.008	0.987	2.058
O(15)	0.126	0.114					0.739	1.056				2.035
ϕ(16)	0.059	0.068					0.616					1.480
Σ	0.735	1.036	1.972	2.074	2.098	2.242	4.528	4.066	3.969	3.848	4.084	

MSH9	A	B	M(1)	M(2)	M(3)	M(4)	D	T(1)	T(2)	T(3)	T(4)	Σ
O(1)			0.305		0.378	0.344		0.997				2.024
O(2)			0.342	0.274	0.284		1.038					1.938
O(3)			0.328		0.360	0.329			1.011			2.028
OH(4)					0.629	0.391						1.020
OH(5)			0.339	0.752								1.091
O(6)			0.345	0.304	0.344					1.005		1.998
O(7)			0.323	0.685							0.965	1.973
O(8)	0.018								0.965	0.925		1.908
O(9)	0.134	0.154					0.698				1.030	2.016
O(10)	0.014								0.963	0.937		1.914
O(11)	0.139	0.149					0.684	1.033				2.005
O(12)	0.144	0.146					0.694				1.025	2.009
O(13)	0.050							0.958	1.014			2.022
O(14)	0.057									1.016	0.965	2.038
O(15)	0.138	0.149					0.684	1.036				2.007
ϕ(16)	0.069	0.084					0.434					1.105
Σ	0.763	1.364	1.982	2.015	1.995	2.128	4.232	4.024	3.953	3.883	4.007	

TABLE 7. CONTINUED

MSH15	A	B	M(1)	M(2)	M(3)	M(4)	D	T(1)	T(2)	T(3)	T(4)	Σ
O(1)			0.303		0.388	0.367		0.989				2.047
O(2)			0.344	0.286	0.295		0.969					1.894
O(3)			0.325		0.359	0.345			1.033			2.062
OH(4)					0.711	0.432						1.143
OH(5)			0.334	0.794								1.128
O(6)			0.341	0.319	0.342					1.036		2.038
O(7)			0.309	0.734							0.997	2.040
O(8)	0.017								0.984	0.932		1.933
O(9)	0.122	0.114					0.745				1.073	2.054
O(10)	0.028								0.950	0.940		1.918
O(11)	0.126	0.112					0.739	1.058				2.035
O(12)	0.131	0.109					0.751				1.047	2.038
O(13)	0.051							0.942	1.041			2.034
O(14)	0.057									1.025	0.960	2.042
O(15)	0.126	0.112					0.739	1.058				2.035
ϕ(16)	0.062	0.062					0.568					1.394
Σ	0.720	1.028	1.956	2.133	2.095	2.288	4.511	4.047	4.008	3.933	4.077	

MSH15A	A	B	M(1)	M(2)	M(3)	M(4)	D	T(1)	T(2)	T(3)	T(4)	Σ
O(1)			0.298		0.381	0.375		1.005				2.059
O(2)			0.351	0.284	0.294		0.950					1.879
O(3)			0.324		0.370	0.347			1.025			2.066
OH(4)					0.705	0.432						1.137
OH(5)			0.338	0.789								1.127
O(6)			0.340	0.318	0.351					1.016		2.025
O(7)			0.318	0.714							0.995	2.027
O(8)	0.019								0.947	0.950		1.916
O(9)	0.126	0.106					0.763				1.050	2.045
O(10)	0.031								0.968	0.937		1.936
O(11)	0.131	0.099					0.743	1.058				2.031
O(12)	0.129	0.106					0.765				1.056	2.056
O(13)	0.054							0.963	1.025			2.042
O(14)	0.060									1.014	0.976	2.050
O(15)	0.130	0.105					0.749	1.061				2.045
ϕ(16)	0.065	0.062					0.576					1.406
Σ	0.745	1.028	1.969	2.105	2.101	2.308	4.546	4.087	3.962	3.917	4.077	

MSH19A	A	B	M(1)	M(2)	M(3)	M(4)	D	T(1)	T(2)	T(3)	T(4)	Σ
O(1)			0.331		0.384	0.316		0.992				2.023
O(2)			0.359	0.289	0.307		0.915					1.870
O(3)			0.334		0.369	0.293			1.008			2.004
OH(4)					0.718	0.372						1.090
OH(5)			0.345	0.796								1.141
O(6)			0.354	0.311	0.347					1.000		2.012
O(7)			0.317	0.705							0.989	2.011
O(8)	0.020								0.945	0.958		1.923
O(9)	0.120	0.125					0.727				1.047	2.019
O(10)	0.033								0.953	0.945		1.931
O(11)	0.132	0.105					0.711	1.058				2.006
O(12)	0.127	0.112					0.732				1.056	2.027
O(13)	0.053							0.955	1.030			2.038
O(14)	0.059									1.027	0.973	2.059
O(15)	0.125	0.125					0.720	1.058				2.028
ϕ(16)	0.061	0.062					0.542					1.340
Σ	0.745	1.068	2.040	2.101	2.118	1.962	4.347	4.063	3.936	3.930	4.065	

TABLE 7. CONTINUED

MSH20	A	B	M(1)	M(2)	M(3)	M(4)	D	T(1)	T(2)	T(3)	T(4)	Σ
O(1)			0.305		0.391	0.302		1.008				2.006
O(2)			0.344	0.278	0.293		1.058					1.973
O(3)			0.326		0.373	0.281			1.033			2.013
OH(4)					0.717	0.353						1.070
OH(5)			0.339	0.784								1.123
O(6)			0.350	0.316	0.354					1.019		2.039
O(7)			0.323	0.712							0.995	2.030
O(8)	0.018								0.953	0.950		1.921
O(9)	0.134	0.148					0.683				1.044	2.009
O(10)	0.030								0.965	0.942		1.937
O(11)	0.136	0.136					0.678	1.047				1.997
O(12)	0.141	0.138					0.683				1.041	2.003
O(13)	0.054							0.955	1.019			2.028
O(14)	0.060									1.019	0.965	2.044
O(15)	0.139	0.142					0.665	1.058				2.004
ϕ(16)	0.068	0.078					0.414					1.122
Σ	0.780	1.268	1.987	2.090	2.128	1.872	4.181	4.068	3.970	3.930	4.045	

MSH33A	A	B	M(1)	M(2)	M(3)	M(4)	D	T(1)	T(2)	T(3)	T(4)	Σ
O(1)			0.300		0.328	0.314		0.995				1.937
O(2)			0.389	0.252	0.259		0.977					1.877
O(3)			0.340		0.324	0.304			0.995			1.963
OH(4)					0.629	0.379						1.008
OH(5)			0.341	0.663								1.004
O(6)			0.386	0.265	0.316					0.947		1.914
O(7)			0.309	0.595							0.997	1.901
O(8)	0.028								0.989	0.925		1.942
O(9)	0.110	0.127					0.754				1.082	2.073
O(10)	0.029								0.965	0.950		1.944
O(11)	0.117	0.121					0.738	1.090				2.066
O(12)	0.112	0.124					0.766				1.082	2.084
O(13)	0.048							0.979	1.027			2.054
O(14)	0.055									1.016	1.000	2.071
O(15)	0.118	0.127					0.742	1.076				2.063
ϕ(16)	0.055	0.071					0.538					1.328
Σ	0.672	1.140	2.065	1.775	1.856	1.994	4.515	4.140	3.976	3.838	4.161	

MSH34A	A	B	M(1)	M(2)	M(3)	M(4)	D	T(1)	T(2)	T(3)	T(4)	Σ
O(1)			0.307		0.340	0.318		0.997				1.962
O(2)			0.385	0.248	0.263		1.000					1.896
O(3)			0.350		0.335	0.304			1.011			2.000
OH(4)					0.634	0.384						1.018
OH(5)			0.361	0.698								1.059
O(6)			0.384	0.281	0.317					0.981		1.963
O(7)			0.327	0.624							0.984	1.935
O(8)	0.030								0.968	0.945		1.943
O(9)	0.116	0.127					0.756				1.064	2.063
O(10)	0.030								0.968	0.945		1.943
O(11)	0.123	0.119					0.729	1.084				2.055
O(12)	0.120	0.127					0.756				1.061	2.064
O(13)	0.052							0.989	1.016			2.057
O(14)	0.056									1.014	1.000	2.070
O(15)	0.121	0.125					0.734	1.082				2.062
ϕ(16)	0.059	0.072					0.497					1.256
Σ	0.707	1.140	2.114	1.851	1.889	2.012	4.472	4.152	3.963	3.885	4.109	

TABLE 7. CONTINUED

MSH38A	*A*	*B*	*M*(1)	*M*(2)	*M*(3)	*M*(4)	*D*	*T*(1)	*T*(2)	*T*(3)	*T*(4)	Σ
O(1)			0.306		0.398	0.366↓		0.997				2.067
O(2)			0.360	0.291	0.302		0.957					1.910
O(3)			0.332		0.382	0.340↓			1.027			2.081
OH(4)					0.732	0.433↓						1.165
OH(5)			0.345	0.802								1.147
O(6)			0.357	0.318	0.360					1.008		2.043
O(7)			0.325	0.728							0.979	2.032
O(8)	0.019								0.953	0.950		1.922
O(9)	0.122	0.132↓					0.712				1.064	2.030
O(10)	0.031								0.950	0.953		1.934
O(11)	0.131	0.117↓					0.705	1.053				2.006
O(12)	0.128	0.126↓					0.719				1.064	2.037
O(13)	0.053							0.955	1.030			2.038
O(14)	0.059									1.022	0.971	2.052
O(15)	0.129	0.130↓					0.701	1.067				2.027
ϕ(16)	0.063→	0.071→					0.497→					1.262
Σ	0.707	1.152	2.025	2.139	2.174	2.278	4.291	4.072	3.960	3.933	4.078	

MSH42	*A*(1a)	*A*(1b)	*B*	*M*(1)	*M*(2)	*M*(3)	*M*(4)	*D*	*T*(1)	*T*(2)	*T*(3)	*T*(4)	Σ
O(1)				0.29		0.36	0.35↓		0.99				1.99
O(2)				0.35	0.28	0.28		0.95					1.86
O(3)				0.32		0.36	0.32↓			1.01			2.01
OH(4)						0.67	0.41↓						1.08
OH(5)				0.34	0.76								1.10
O(6)				0.34	0.31	0.35					0.99		1.99
O(7)				0.31	0.66							1.03	2.00
O(8)	0.01	0.01								0.96	0.94		1.92
O(9)	0.03	0.07	0.10↓					0.79				1.09	2.08
O(10)		0.02								0.92	0.98		1.92
O(11)	0.06	0.06	0.10↓					0.76	1.11				2.09
O(12)	0.06	0.05	0.10↓					0.71				1.09	2.01
O(13)	0.02	0.03							0.98	1.03			2.06
O(14)	0.02	0.04									0.98	1.05	2.09
O(15)	0.03	0.08	0.10↓					0.78	1.08				2.07
ϕ(16)	0.02→	0.02→	0.06→					0.81→					1.86
Σ	0.25	0.38	0.96	1.95	2.01	2.02	2.16	4.80	4.16	3.92	3.89	4.26	

measure of the distortion of a polyhedra, was calculated using the equations developed by Robinson *et al.* (1971) for tetrahedra and octahedra:

$$\mathrm{TAV} = \sigma_T^2 = \sum_{i=1}^{6} [(\mathrm{O}\text{-}T\text{-}\mathrm{O}) - 109.47)^2/5 \quad (2)$$

$$\mathrm{OAV} = \sigma_M^2 = \sum_{i=1}^{12} [(\mathrm{O}\text{-}M\text{-}\mathrm{O}) - 90)^2/11 \quad (3).$$

The octahedral flattening angle (Ψ) is defined as the angle between the perpendicular to the trigonal upper or lower faces and the average diagonal length. Values of Ψ were calculated using the program OCTAHEDRON (Evans 2000). Given the coordinates of the points of an MO_6 octahedron $\{\mathbf{x}_i, i = 1 \text{ to } 6\}$, the M-O bond length, flattening angle, ψ, and the counter-rotation angle, δ, can easily be found. The geometric center of the octahedron is:

$$\mathbf{c} = \frac{1}{6}\sum_{i=1}^{6} \mathbf{x}_i \quad (4)$$

Assuming that the cation is at the center of the octahedron, the mean M-O bond length is

$$d = \frac{1}{6}\sum_{i=1}^{6} |\mathbf{x}_i - \mathbf{c}| \quad (5).$$

In order to find the flattening and counter-rotation angles, the coordinate system has to be shifted so that the origin is at **c** and reoriented such that the Z-axis is parallel to the average normal vector of the top and bottom faces. In spherical coordinates the new positions of the anions are $\mathbf{r}_i = \{r_i, \theta_i, \phi_i\}$. A least-squares method is used to fit the coordinates to an octahedron where flattening and counter-rotation are the only distortions from octahedral symmetry. If $\{\mathbf{r}_1, \mathbf{r}_2, \mathbf{r}_3\}$ form the top face and $\{\mathbf{r}_4, \mathbf{r}_5, \mathbf{r}_6\}$ form the bottom face, this procedure gives:

$$\psi = \frac{1}{6}\sum_{i=1}^{3}\phi_i - \frac{1}{6}\sum_{i=4}^{6}\phi_i + \frac{\pi}{2} \text{ and } \delta = -\frac{1}{6}\sum_{i=1}^{3}\theta_i + \frac{1}{6}\sum_{i=4}^{6}\theta_i + \frac{\pi}{6} \quad (6).$$

The tetrahedral thickening angle (τ), ideally 109.47° for an undistorted tetrahedron, was calculated as:

$$\tau_T = \sum_{i=1}^{3} (O_{basal}\text{-}T\text{-}O_{apical})/3 \quad (7).$$

Polyhedral volumes and tetrahedral tilt angles [with respect to the (001) plane] were calculated using the program IVTON (Balić-Žunić & Vicković 1996). The tetrahedral rotation angle (α) was calculated using the following formula assuming an ideal O_{br}-O_{br}-O_{br} angle of 120°:

$$\alpha = 1/2\,|120 - \langle O_{br}\text{-}O_{br}\text{-}O_{br}\rangle| \quad (8).$$

3.0. Site-assignment Procedure

In all the members of the astrophyllite group that were included in this study, K is the dominant interlayer cation at *A*. In a number of the triclinic structures, refinement of *A* with K alone resulted in exceptionally large U_{11} anisotropic displacement factors, coupled with a large positive residual in the difference Fourier map (>2.5 e^{-1}). In samples where refinement of the SOF indicated the presence of a lighter X-ray scatterer, Na was assigned to *A*. Similarly, when refinement of the SOF indicated the presence of a heavier X-ray scatterer, Rb was assigned to *A* at a fixed occupancy, as indicated by the EMPA data. In samples where the shape of the anisotropic displacement ellipsoid of the site to which K was assigned suggested that it was positionally disordered, refinement of the site occupancies failed to

improve the displacement factors. The site was therefore modeled as two split sites, K(1a) and K(1b). In these cases, displacement factors for K(1a) and K(1b) were constrained to be equal and refined isotropically.

Sodium was assigned to *B* in all samples. Calcium was later included in the refinement when the SOF for *B* indicated the presence of a heavier X-ray scatterer. Refined occupancies of Ca in AGM correlate well with values obtained from EMPA data (Fig. 1).

Manganese and Fe were initially assigned to *M*(1) through *M*(4), depending on which cation was indicated to be dominant at *C* by the single-crystal EMPA data. Site-scattering refinement (SREF) of *M*(1) consistently yields occupancies less than unity (by 10 to 15%), indicating the presence of a weaker *X*-ray scatterer. Electron-microprobe data indicate an excess of Na in the majority of samples when compared to results obtained from SREF of *A* and *B*. The occupancy of *M*(1) was therefore refined with (Mn,Fe) and Na. A plot of the total SREF content of Na *versus* total Na as analyzed by EMPA indicates good agreement between the two methods (Fig. 2). The presence of Na at *M*(1) site is not uncommon in AGM. For example, magnesium astrophyllite (Shi *et al.* 1998) exhibits a dominance of Na within a single octahedrally coordinated site equivalent to *M*(1) in triclinic samples and kupletskite-*Ma2b2c*. Substitution of Na for Mn in octahedral coordination, although not common, has also been noted in other minerals, including samuelsonite (Moore & Araki 1977), barytolamprophyllite (Rastsvetaeva & Dorfman 1995), vuonnemite (Ercit *et al.* 1998), alkali clinoamphiboles from MSH (Taylor 1999), and eudialyte group minerals from MSH (Johnsen & Grice 1999).

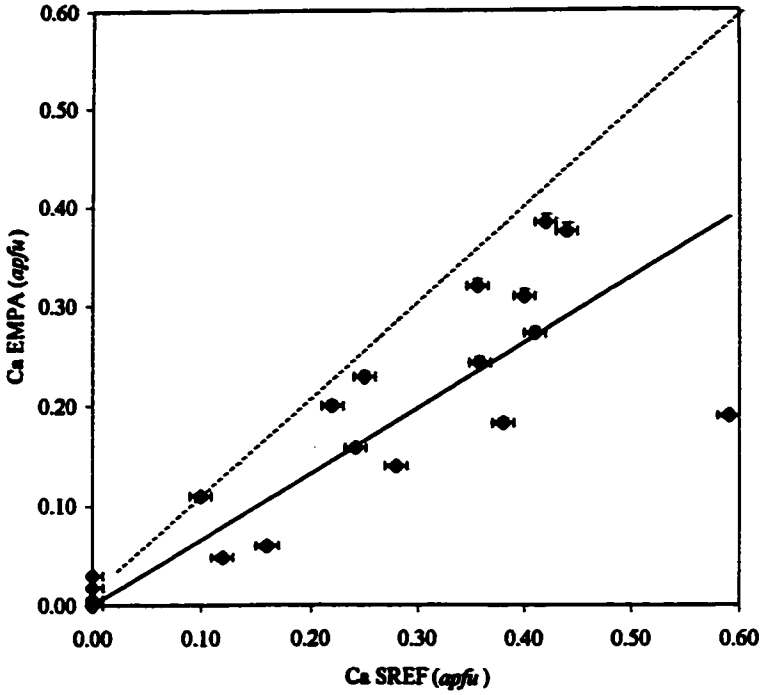

Figure 1. Comparison of site refinement and electron-microprobe data: Ca SREF *versus* Ca EMPA (*apfu*). The 1:1 substitution line is indicated (dashed). Linear regression: $y = 0.6596x$, $R^2 = 0.688$. Analytical errors indicated.

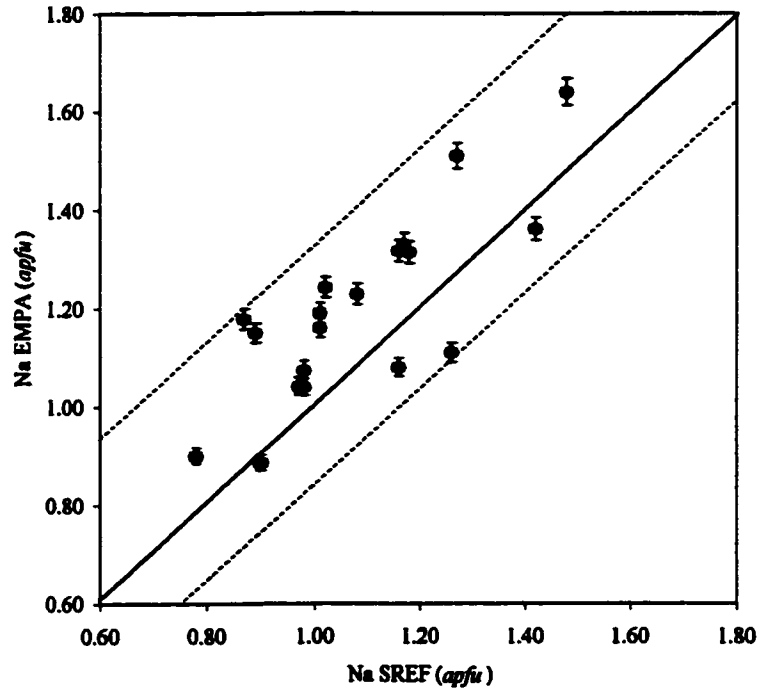

Figure 2. Comparison of site refinement and electron-microprobe data: Na_{tot} SREF *versus* Na_{tot} EMPA (*apfu*). The 1:1 substitution line is indicated as a solid line. Dashed lines outline the range in data points observed. Analytical errors indicated.

Site scattering refinements for *M*(2), *M*(3) and *M*(4) generally yield site occupancies close to unity. Slight departures from unity at these three sites are due to substitution of Mn for Fe. Refinement of both Mn and Fe within a single site is not possible as the two cations have almost identical scattering powers (Mo*K*α radiation). In samples where site-scattering refinements indicated significant departures from the ideal (Fe,Mn) occupancies (*i.e.* >10%) and the presence of a lighter or heavier *X*-ray scatterer, Mg or Zn, the third most abundant octahedrally coordinated *C* cations indicated by EMPA, were assigned to the site in question, with the total site occupancy constrained to be unity.

With the exception of niobokupletskite, in which Nb is the dominant cation, Ti was assigned to *D* in all structure refinements. In all but one case, site-scattering refinement of *D* indicated varying departures from unity and the presence of a heavier X-ray scatterer. Either Nb or Zr was subsequently refined at *D*, depending on which element was indicated to be the second most abundant in *D* by EMPA, with the total site occupancy constrained to be unity.

As EMPA results indicate only minor Al, present only within the *T* sites, and Mössbauer spectroscopy did not indicate $^{[4]}Fe^{3+}$ (Chapter IV), all four *T* sites were modeled as Si. Site-scattering refinements of the four *T* sites in all samples did not indicate significant departures from unity, and thus the presence of other tetrahedrally coordinated cations (*e.g.* Ti) can be dismissed.

Bond-valence sums indicate the presence of 13 general positions occupied by divalent anions, two general positions for monovalent anions in the *O*-sheet [O(4) and O(5)], and a mixed-valence site, ϕ(16). Bond valence sums for all anions [except O(4), O(5) and ϕ(16)] are close to the ideal value of 2.00 *v.u.* (range: 1.842 to 2.140 *v.u.*), confirming their identity

as O^{2-}. The O(2) anion, bonded to *M*(1), *M*(2), *M*(3) and *D*, has BVS which are consistently low (1.842 to 1.973 *v.u.*, ave.: 1.903 *v.u.*) due to the presence of Na in *M*(1) and HFSE at *D* which contribute less than the required 1 *v.u.* (Ti^{4+}: 4/6 *v.u.*, Nb^{5+}: 5/6 *v.u.*); all other divalent anions in the *O*-sheet are coordinated by three *M* cations (3 x 2/6 = 1.00 *v.u.*) and one *T* cation (1 x 4/4 = 1.00 *v.u.*), resulting in values close to the ideal 2.00 *v.u.* Consequently, the *M*(1)-O(2) bond is shortened to account for this bond-valence deficiency. Bond-valence sums to O(4) and O(5) range from 0.985 to 1.177 *v.u.* (ave.: 1.089 *v.u.*), close to the ideal sum of 1.00 *v.u.* for a monovalent anion and confirming their identity as either OH or F. Ordering of OH and F at the O(4), O(5) and ϕ(16) sites was discussed in Chapter II where it was concluded that, on the basis of results from Mössbauer spectroscopy and thermodynamic calculations, the sites present in the *O*-sheet [O(4) and O(5)] are occupied solely by OH, whereas ϕ(16) hosts both F and O. Bond valence sums to ϕ(16) are variable, ranging from 1.105 to 1.86 *v.u.* (ave.: 1.293 *v.u.*), consistent with the proposed $F^- \Leftrightarrow O^{2-}$ substitution at this site. An attempt was made to refine the site occupancy of ϕ(16) with both F and O but results did not prove to be valid due to low total F contents (<1.00 *apfu*) and the similarity in scattering powers (Mo*K*α radiation) between F and O. Bond-valence sums confirm the anionic scheme proposed in Chapter II as being $O_{26}(OH)_4(F,O,\square)$.

4.0. Overview of the Structure

The nomenclature and procedure for calculation of AGM chemical formulae is outlined in Chapter II. The general formula for AGM can be written as

$$A_2BC_7D_2T_8O_{26}(OH)_4X_{0\text{-}1} \quad (9)$$

where $A = {}^{[10]}$-$^{[13]}$K, Rb, Cs, Na, H_3O^+, H_2O, or □; $B = {}^{[10]}$Na or Ca; $C = {}^{[6]}$Mn, Fe^{2+}, Fe^{3+}, Na, Mg, or Zn; $D = {}^{[6]}$Ti, Nb, or Zr; T = Si and Al, and $X = \phi$ = F, OH, O, or □.

Ferraris *et al.* (1996), Ferraris (1997) and Christiansen *et al.* (1999) have described AGM and other modular titanosilicates such as bafertisite (Pen & Sheng 1963), perraultite (Yamnova *et al.* 1998), nafertisite (Ferraris *et al.*, 1996), lamprophyllite (Saf'yanov *et al.*, 1983; Johnsen, 1996) and yoshimuraite (McDonald *et al.*, 2000) as heterophyllosilicates. Such minerals have an *HOH* structure, reminiscent of the *TOT* structure in 2:1 phyllosilicates, where TiO_5 or TiO_6 polyhedra in the heterogeneous sheet (*H*-sheet) proxy for the usual $(Si,Al)O_4$ tetrahedra in phyllosilicate *T*-sheets. Members of the astrophyllite group can be considered to be an intermediate member of a polysomatic (Ferraris *et al.*, 1996) or homologous (Christiansen *et al.*, 1999) series which also includes perraultite and mica as the end-member structures. A comparison of these minerals shows that they all have (1) an *HOH* structure, (2) an *a* axial length of approximately 5.4 Å, corresponding to the *a* value in micas, and (3) $d_{001} \approx 10.9$ Å. The homologous series can be expressed by indicating the number of diorthosilicate groups separating rows of *D* octahedra: $n = 1$ in perraultite and bafertisite, $n = 2$ in AGM, $n = 3$ in nafertisite, and $n = \infty$ in micas (modified from Ferraris *et al.*, 1996 and Christiansen *et al.* 1999).

In bafertisite, lamprophyllite and yoshimuraite, the *H*-sheet is comprised of dimers of $[Si_2O_7]^{6-}$ which are linked *via* corner-sharing to TiO_6 octahedra or TiO_5 tetragonal pyramids, resulting in a Si:Ti ratio of 2:1 The offset between successive *HOH* layers is such that the Ti are not linked across the interlayer as observed in AGM and nafertisite. In nafertisite, the *H*-layer consists of open branched *zweier* [100] double chains of $[Si_{12}O_{34}]^{20-}$ (Liebau 1985)

which are crosslinked by TiO_6 octahedra which are linked across the interlayer, resulting in a Si:Ti ratio of 6:1 (Ferraris *et al.* 1996). Members of the astrophyllite group are the intermediate member in the polysomatic series ($n = 2$).

The AGM structure can be subdivided into two main composite sheets stacked along [001] in a 2:1 ratio. The first is an *O*-sheet extending from $Z \approx 0.40$ to 0.60 in triclinic species and from $Z \approx -0.05$ to 0.05 in kupletskite-*Ma2b2c*, consisting of a closest-packed sheet of MnO_6, FeO_6, MgO_6, or NaO_6 octahedra (Fig. 3). The *O*-sheet is sandwiched between two *H*-sheets related by an inversion center in triclinic species and a two-fold axis parallel to *b* in kupletskite-*Ma2b2c*, extending from $Z \approx -0.15$ to -0.05. The *H*-sheet has the ideal composition $[(Ti,Nb,Zr)Si_4O_{12}]^{4-}$ and consists of open-branched *zweier* [100] single chains of $[Si_4O_{12}]^{8-}$ (Liebau 1985) which are cross-linked by corner-sharing $D\phi_6$ octahedra in triclinic species and kupletskite-*Ma2b2c*, and DO_5 polyhedra in magnesium astrophyllite (Shi *et al.* 1998) where D = Nb,Ti,Zr (Fig. 4). The resultant Si:(Ti,Nb,Zr) ratio is 4:1. Individual $D\phi_6$ octahedra are linked across the interlayer *via* a common apical anion [$\phi(16)$, where ϕ = unspecified anion]. This $\phi(16)$ anion is at the inversion center in triclinic species, at special position 4*e* (-0.5,y,-0.25) in kupletskite-*Ma2b2c*, and is absent in magnesium astrophyllite (Shi *et al.* 1998). There is a misfit between the *O*- and *H*-sheets, similar to that in micas, resulting in tilting and rotation of SiO_4 tetrahedra and distortion or corrugation of the *O*-sheet. The degree to which this misfit occurs is dependent on the composition of the *O*-sheet, decreasing with increasing size of the *O*-sheet cations (Woodrow 1967, Christiansen *et al.* 1998, Shi *et al.* 1998). The steric details of this misfit will be discussed further in subsequent sections.

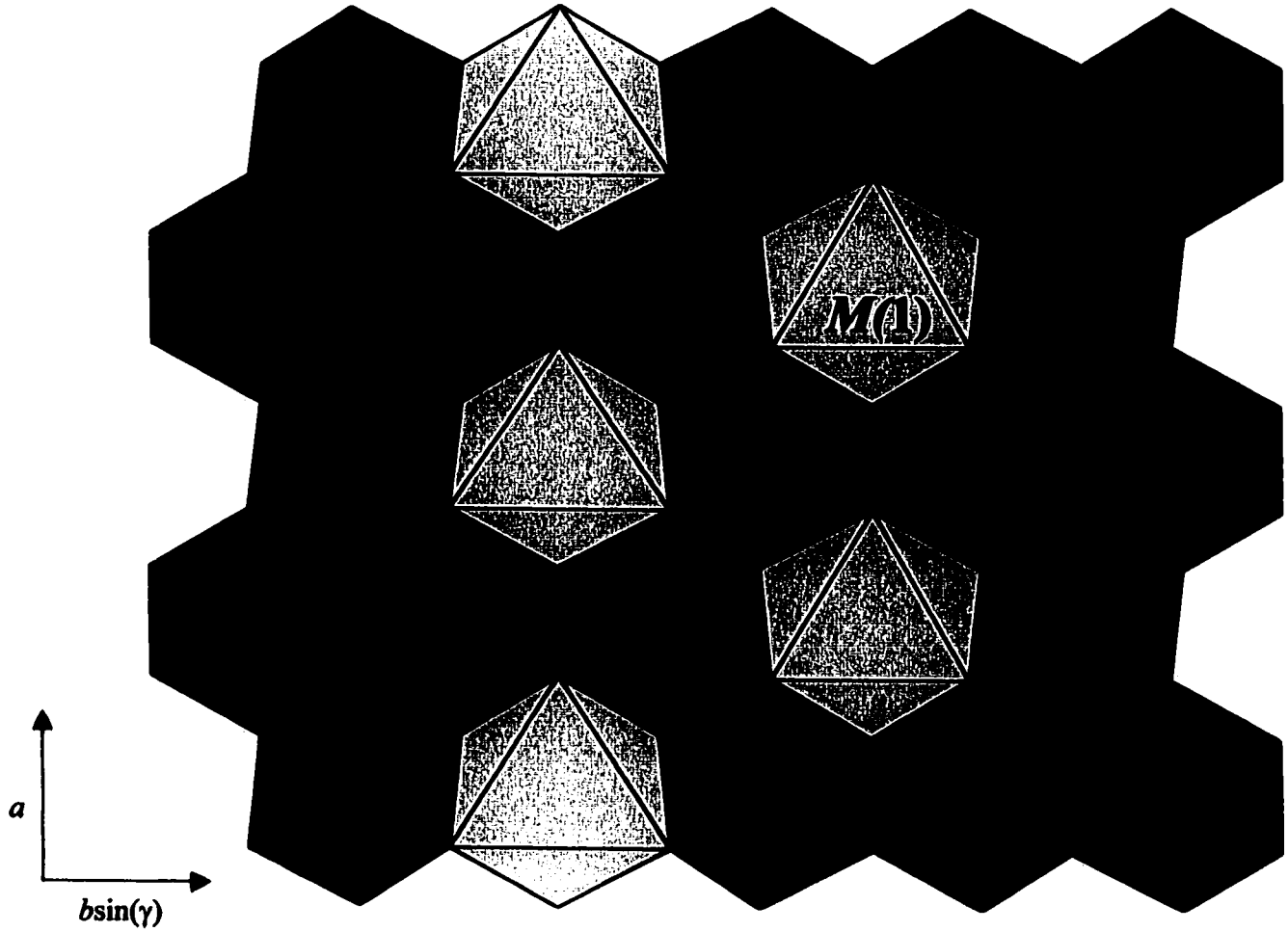

Figure 3. The *O*-sheet in AGM projected down [001].

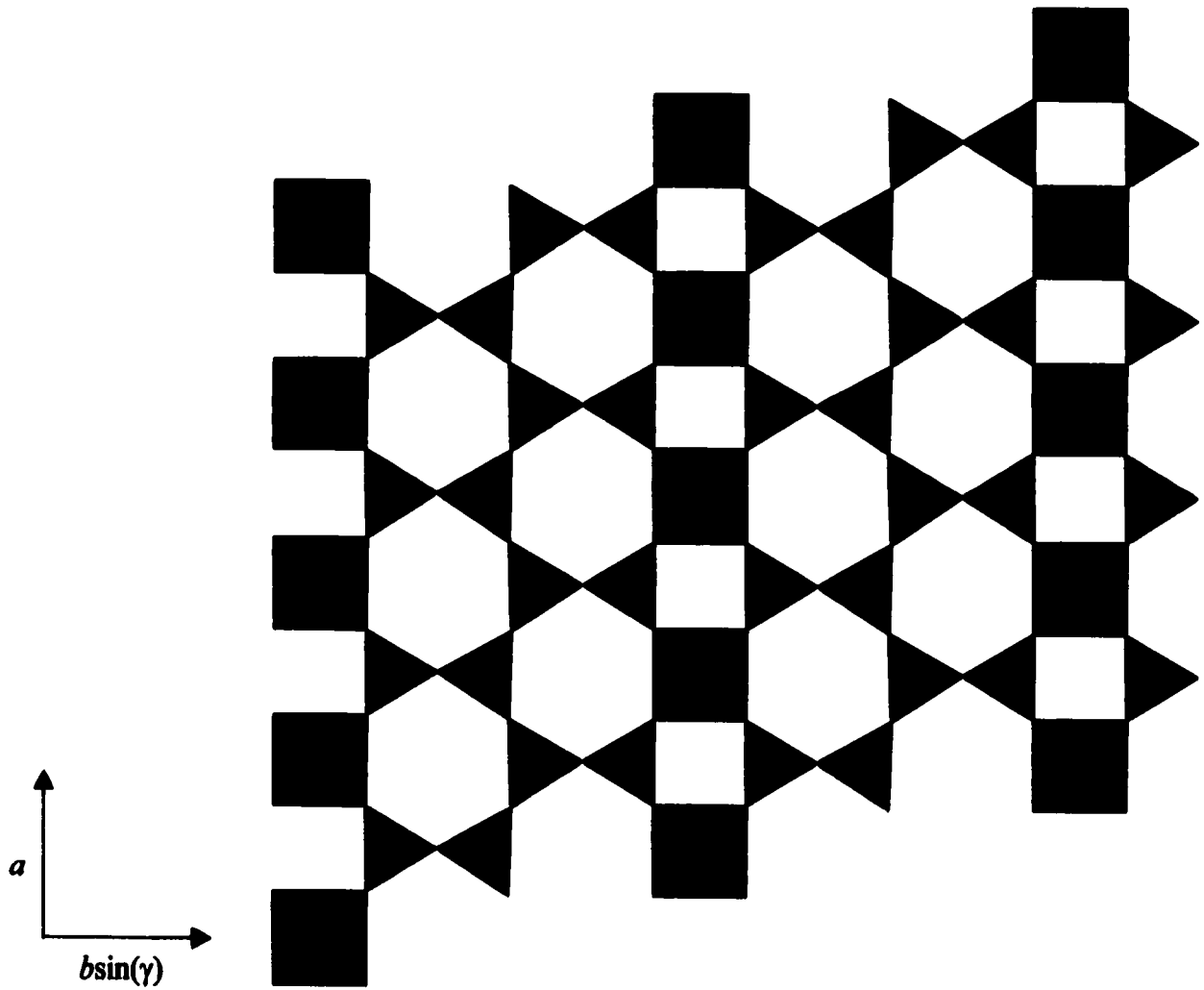

Figure 4. The *H*-sheet in AGM projected down [001] showing open branched *zweier* single chains of $[Si_4O_{12}]^{8-}$ parallel to [100]. $^{[4]}T$ = red, $^{[6]}D$ = blue.

The interlayer of triclinic samples contains two crystallographically distinct, strongly ordered sites: a 10-coordinated site (*B*) host to Na and Ca, and a larger [11]- to [13]-coordinated site (*A*) dominated by K but which often contains Rb, Cs, Na, vacancies, and/or H_2O. In monoclinic kupletskite-*Ma2b2c*, there are three distinct interlayer sites, *A*(1), *A*(2) and *B*. The stacking of *HOH* layers along [001] results in an excellent (001) cleavage that is slightly more brittle than observed in other phyllosilicates due to the existence of the bridging ϕ(16) anion within the interlayer. The crystal structures of triclinic, $P\bar{1}$, AGM and monoclinic, *C2/c*, kupletskite are shown in Figures 6A and 6B in Chapter II.

5.0. Site Descriptions

5.1. Interlayer

The *A* cations are located in a large, [13]-coordinated cavity located between adjacent *H*-sheet chains (Fig. 5 & 6) and is host to predominantly K and to a lesser extent Cs, Rb, Na and □. Large anisotropic-displacement factors along U_{11}, coupled with a large positive residual in the difference-Fourier map (>2.5 e^-) in the majority of triclinic samples suggest that this site is positionally disordered within the (001) plane (Fig. 7). Difference-Fourier maps indicate the electron density to be spread out in the (001) plane. In such cases, the position was refined as two non-equivalent cation sites with coordinates taken from the difference-Fourier map. The two split positions are located between 0.36 to 0.851 Å from each other in the (001) plane. A decrease in displacement factors is observed when the site is modeled as positionally disordered. This is similar to what is observed in amphiboles with high *A* site occupancies (Hawthorne 1981). However, unlike in amphiboles where the degree

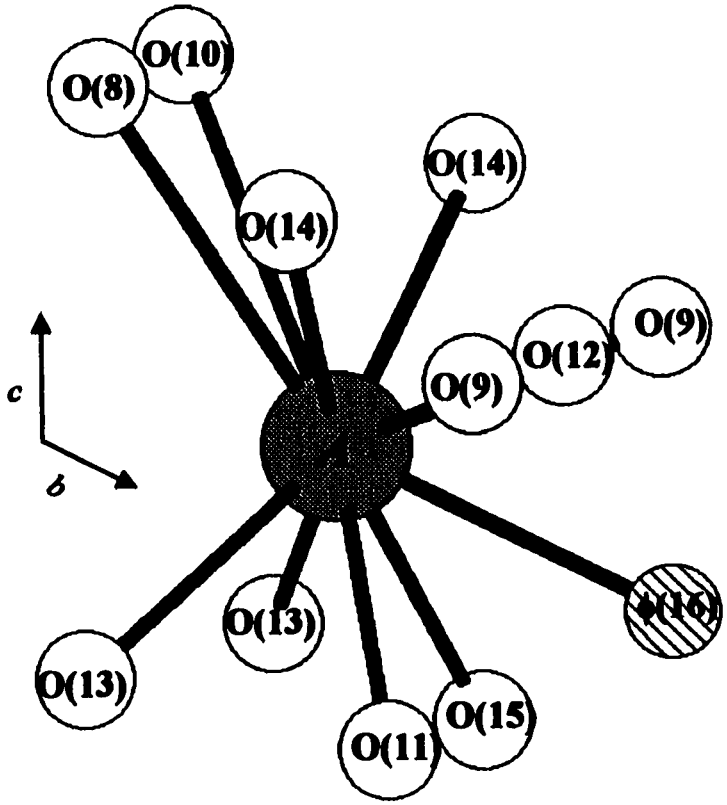

Figure 5. The $A\phi_{12}$ polyhedron. Distances range from 2.825 to 3.746 Å.

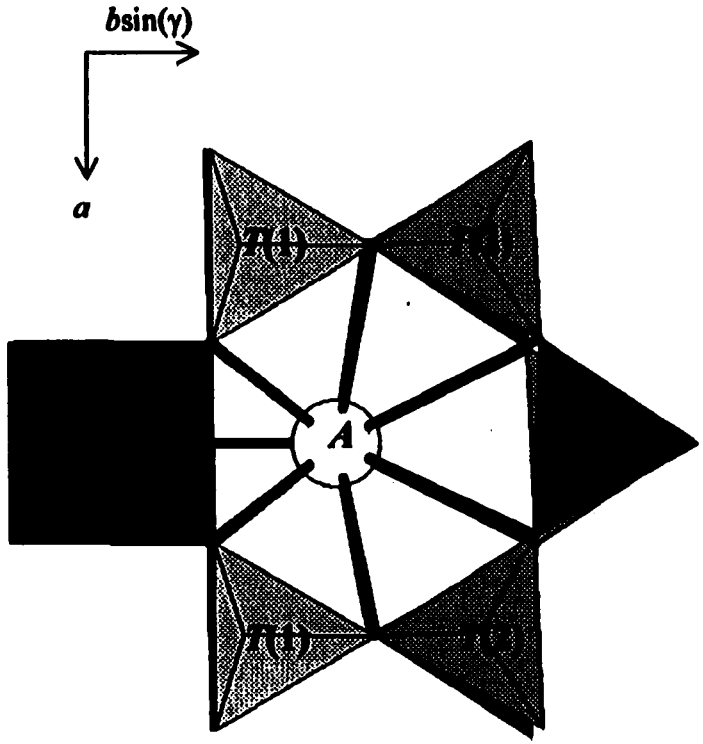

Figure 6. The configuration of the *H*-sheet chains around the *A site* in the (001) plane. Upper chain shown. Lower chain (clockwise): *T*(4), *T*(3), *T*(2), *T*(3) and *T*(4). Splitting of the *A* site results in displacement of *A* along *b*sin(γ) of 0.3 to 0.9 Å.

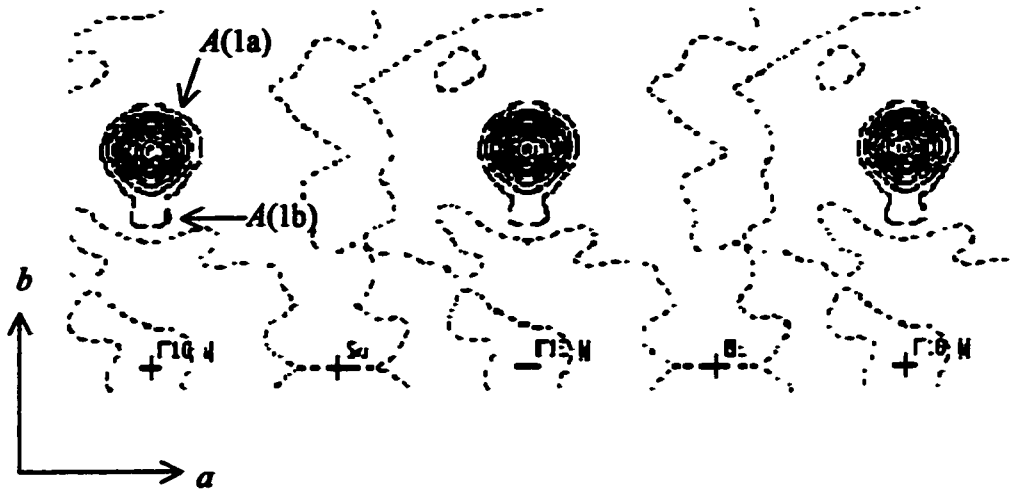

Figure 7. Difference-Fourier map through the *A* site in astrophyllite group minerals, showing splitting of *A* into *A*(1a) and *A*(1b). Interlayer shown projected on the (001) plane.

of disorder of *A* can be attributed to the site occupancy, there does not seem to be any correlation between site occupancy and/or site chemistry and the degree of disorder in AGM.

One of the main differences between the structures of monoclinic and triclinic kupletskite, aside from the *HOH* stacking sequence, is the degree of disorder at the *A* site (Chapter V). In triclinic kupletskite from the Lovozero massif (Russia), the *A* site shows positional disorder comparable to that observed in other triclinic samples [*A*(1a)-*A*(1b) = 0.917 Å]. However, in kupletskite-*Ma2b2c*, the *A* cation lies on two special positions, both of which have well-constrained anisotropic displacement factors which do not indicate disorder (U_{eq} = 0.0451 Å).

Bond lengths to *A* range from 2.826 to 3.721 Å. The *A*(1a) site in disordered triclinic samples is generally [11]-coordinated, with longer average bond lengths (range: 3.179 to 3.291 Å) than those observed at the [5] to [7] coordinated *A*(1b) satellite position (range: 2.353 to 3.082 Å). The overall coordination of the *A* site in both triclinic and monoclinic samples is [13].

The *B* site is located at a special position in [10]-coordinated cages along *a* between $D\phi_6$ pairs. The $BO_8\phi_2$ polyhedra (Fig. 8) is bonded to 2 x O(9), O(11), O(12), O(15) and ϕ(16) and is occupied predominantly by Na and, to a lesser extent, Ca (up to 0.40 *apfu*). There is no evidence for other cations or vacancies at *B*. The *B*-ϕ distances range from 2.589 to 2.715 Å with an average of 2.635 Å. The <*B*-ϕ> bond length is negatively correlated with Ca contents as determined by both EMPA and SREF (Fig. 9).

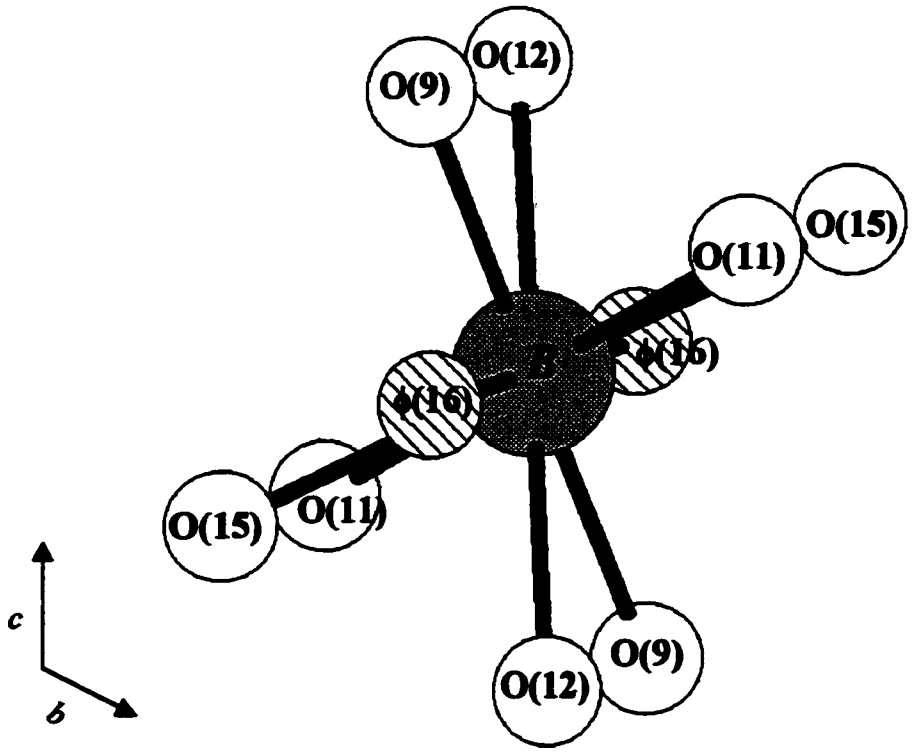

Figure 8. The $BO_8\phi_2$ polyhedron. Distances range from 2.589 to 2.715 Å

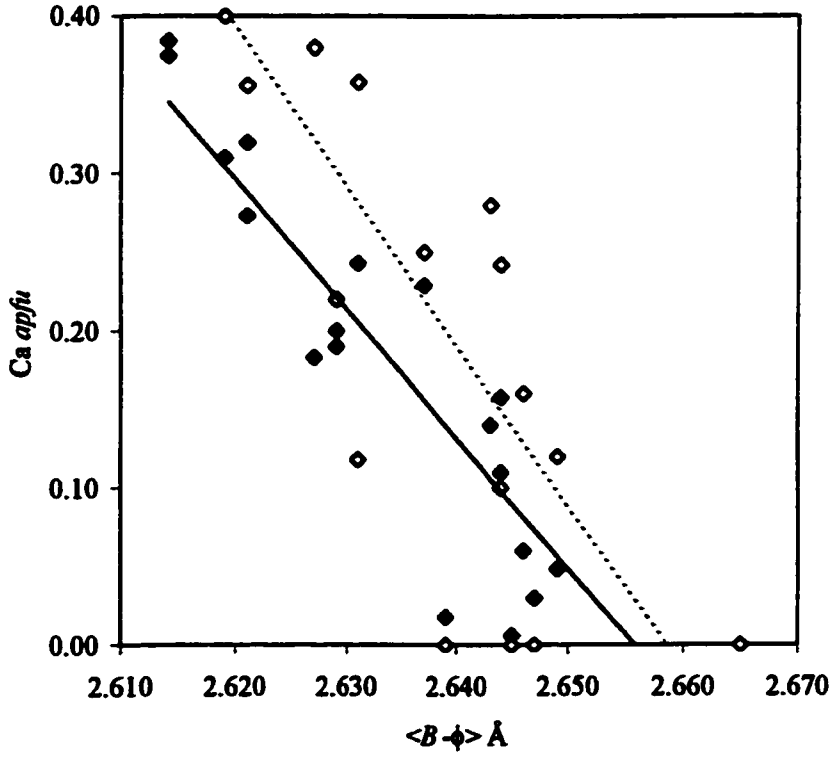

Figure 9. Average B-ϕ bond length *versus* the content of Ca.
Closed diamonds indicate Ca contents from EMPA ($R^2 = 0.823$). Open diamonds indicate Ca contents derived from SREF ($R^2 = 0.599$).

5.2. O-sheet

There are four crystallographically distinct *O*-sheet octahedra, designated *M*(1) through *M*(4), which occur in a 2:2:2:1 ratio. The *O*-sheet can be divided into three main units: (1) a strip of *M*(2) octahedra, linked *via* common edges, which form continuous zigzag single chains parallel to [100]; (2) a composite chain parallel to [100] comprised of alternating *M*(3) and *M*(4) octahedra in a 2:1 ratio; and (3) isolated *M*(1) octahedra which cross-link the two octahedral chains (Fig. 10). The combination of chain-like structural elements within the *O*-sheet and open-branched *zweier* single [100] chains in the *H*-sheet has a pronounced effect on the morphology of AGM: a preferential elongation of crystals in the [100] direction, the development of a secondary, moderate parting along {010}, and the formation of acicular to tabular crystals. Attachment of the *O*-sheet to the *H*-sheet occurs *via* apical oxygens from the *H*-sheet tetrahedra [O(1), O(3), O(6) and O(7)] and *via* the $D\phi_6$ apical oxygen, O(2) (Fig. 11). The wide range in chemistry observed in AGM is predominantly due to the multiple octahedral local environments within the *O*-sheet into which cations may substitute. The steric details of the *O*-sheet must be understood in order to understand its effect on cation ordering and its effect on the adjacent *H*-sheets.

The variation in grand mean bond length, <<*M*-O>>, as a function of grand mean ionic radius, <<r*M*>>, is shown in Figure 12 (ionic radii from Shannon 1976). The positive correlation (R^2 = 0.938) is described by the linear-regression equation <<*M*-O>> = 1.752+1.183r*M*. The Mn# [Mn/(Mn+Fe_{tot})] of the samples studied ranges from 0.15 to 1.00. Not surprising then is the finite range observed on Figure 12 between <<r*M*>> 0.78 and 0.83 Å, corresponding to pure Fe- and Mn-dominant species respectively ($r^{[6]}Fe^{2+}$: 0.78 Å,

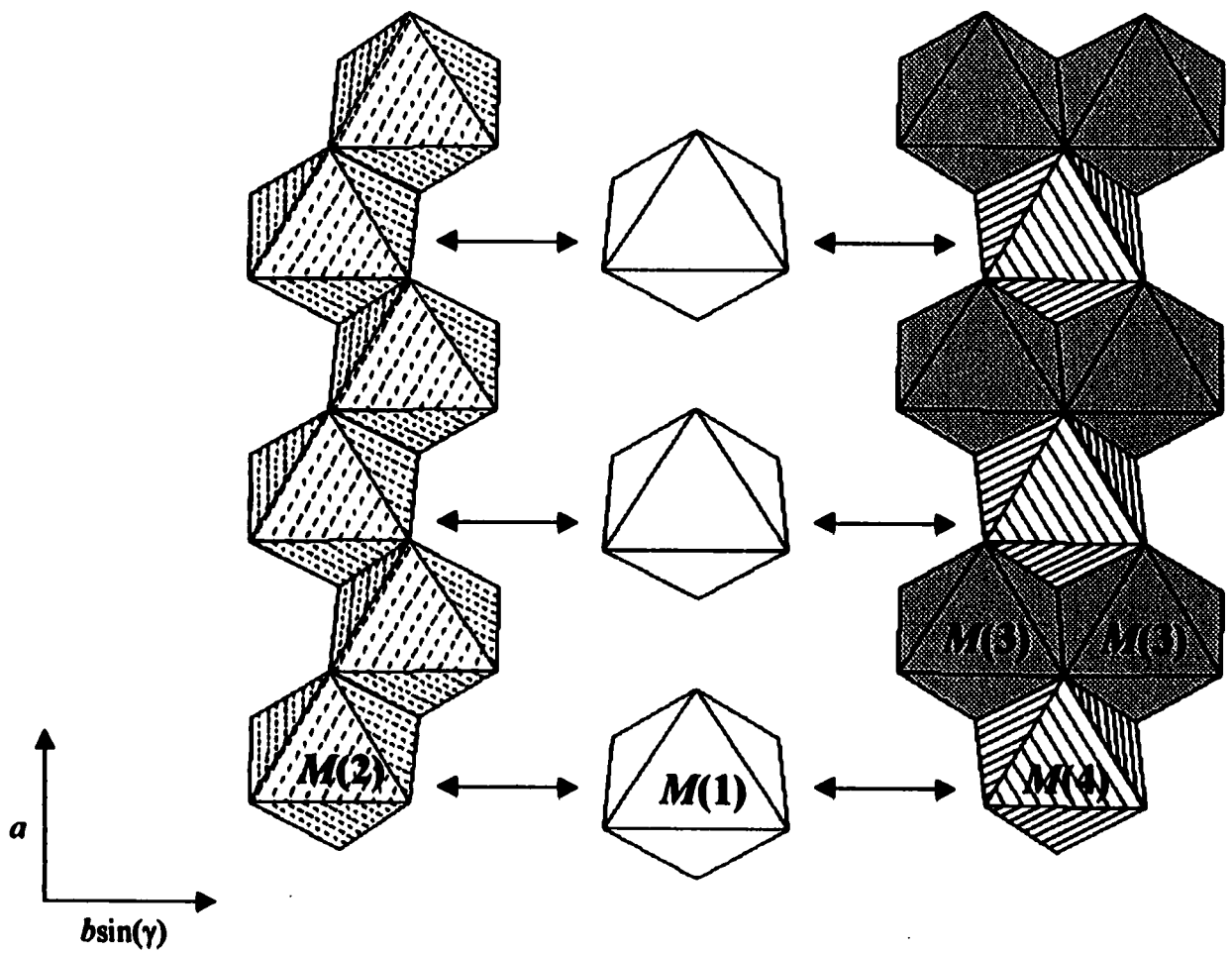

Figure 10. The three strips of octahedra of the AGM *O*-sheet. The *M*(2) octahedra form chains parallel to [100]. *M*(3) and *M*(4) alternate along [100] in a 2:1 ratio. *M*(1), the largest and least distorted of the octahedra, links the two composite strips together to form infinite sheets in the (001) plane.

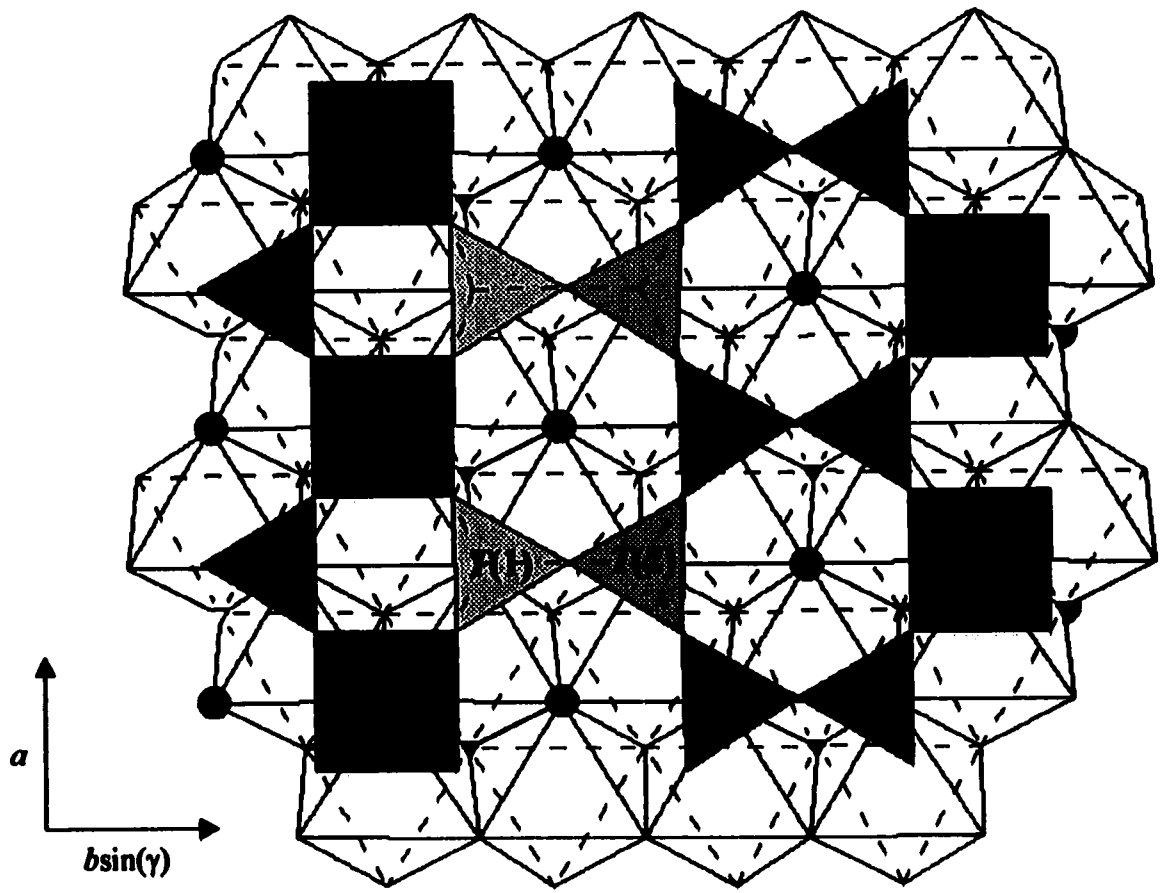

Figure 11. The attachment of the *H*-sheet to the *O*-sheet. *T* sites; grey shades as indicated, *D* = black, *M* sites shown outlined. The OH groups are indicated as solid circles.

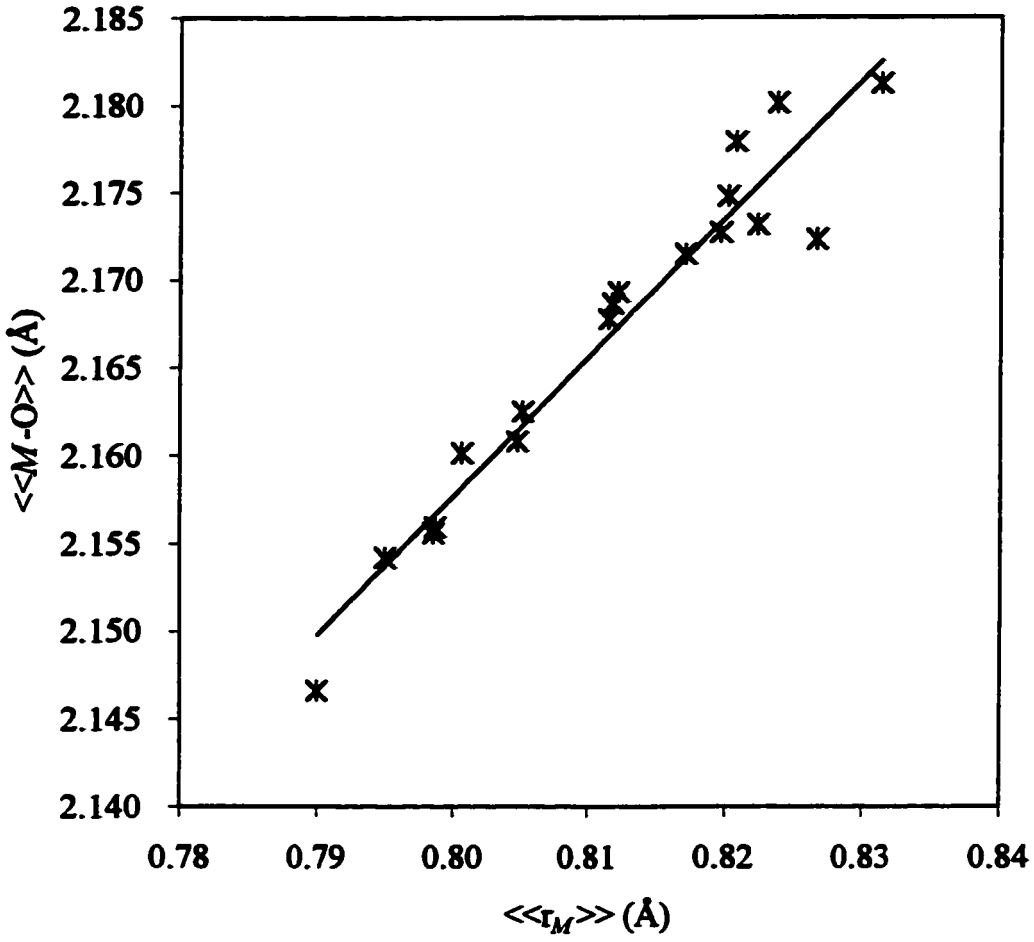

Figure 12. Variation in grand mean *M*-O bond length, <<*M*-O>>, with mean ionic radius, <<r*M*>>, of the *O*-sheet. Linear regression, $R^2 = 0.938$.

$r^{[6]}Mn^{2+}$: 0.83 Å, Shannon 1976). The scatter observed in the trend may be due to the slight differences between refined site occupancies and EMPA data. While it is important to examine the relation between <<*M*-O>> and <<*rM*>> in the *O*-sheet, the ligancy and local environment of each of the four individual octahedra varies from sample to sample. Unfortunately, due to the presence of more than two cations at each of the four *M* sites, coupled with the inability to refine the SOF for sites with both Mn and Fe, two cations with very similar scattering curves (Mo*K*α radiation), poor correlations are observed between the calculated average ionic radii of each *M* site with <*M*-O>.

The distortion index, calculated for each individual octahedron, is a direct reflection of the local environment of the cation due to variations in site chemistry, bond lengths and bond angles. Table 6 lists values for two distortion parameters, Δ, the bond length distortion, and σ, the octahedral angle variance (OAV), for each octahedron. Calculation of Δ takes into consideration average cation radius by normalizing the parameter to the average bond length, and also corrects for the coordination number. Consequently, it is a measure of distortions within the polyhedra resulting from stretching or compression of *M*-O bonds which break the ideal trigonal symmetry of the octahedron, often referred to as rectangular distortions. Conversely, the OAV takes into consideration only the angular variance within the octahedra. Robinson *et al.* (1971) found σ to be a convenient and realistic measure of the distortion of a polyhedron that shows variation in both bond lengths and bond angles. In AGM, a discrepancy is noted between the two parameters such that Δ indicates the relative degree of distortion to be represented by the sequence $M(2) > M(3,4) > M(1)$, whereas the OAV indicates $M(1) > M(2) > M(3) > M(4)$, which also corresponds to the order of decreasing size

of each of the *M* octahedra. Figure 13 shows the positive correlation between the OAV and the <<r*M*>>. In the *O*-sheet of AGM, the OAV is not an adequate measure of the total distortion of each octahedron as it does not take into account rectangular distortions (*i.e.* stretching or compression of bond lengths within the octahedron); the OAV is only a direct reflection of trigonal distortions (*i.e.* compression or extension of the octahedron resulting in a trigonal antiprism whose *M*-O distances remain equal in length; Robinson *et al.* 1971). In particular, the OAV is strongly positively correlated with the octahedral flattening angle, Ψ (Fig. 14, $R^2 = 0.983$), and the two terms may be used interchangeably. Figure 15 shows the relation between OAV and Ψ for each of the four *M* octahedra. The less than ideal correlation for the *M*(1) octahedron will be discussed in further sections. Ideally, in AGM which contain octahedra that have undergone both rectangular and isometric or trigonal distortions, both the Δ and OAV/Ψ distortion parameters should be taken into account when describing the geometry of a given octahedron.

The *M*(1) site occurs as isolated octahedra, bridging strips of *M*(2) and *M*(3,4) octahedra. The largest of the four *O*-sheet octahedra, *M*(1) is coordinated by five O^{2-} and one OH^- [OH(5); Fig. 16). Figure 17A shows the regular distribution of bond lengths in *M*(1), which range from 2.137 to 2.247 Å with an average of 2.195 Å, close to the ideal for a $^{[6]}Mn^{2+}$-O bond (2.21 Å; Ondik & Smith 1962). This regular distribution of bond lengths is consistent with *M*(1) being the least distorted of the four octahedra; Δ values range from 0.488 to 2.851.

In an ideal, holosymmetric octahedron, the flattening angle, Ψ, measured at the point between the *M*-O bond and a line perpendicular to the upper and lower trigonal faces through

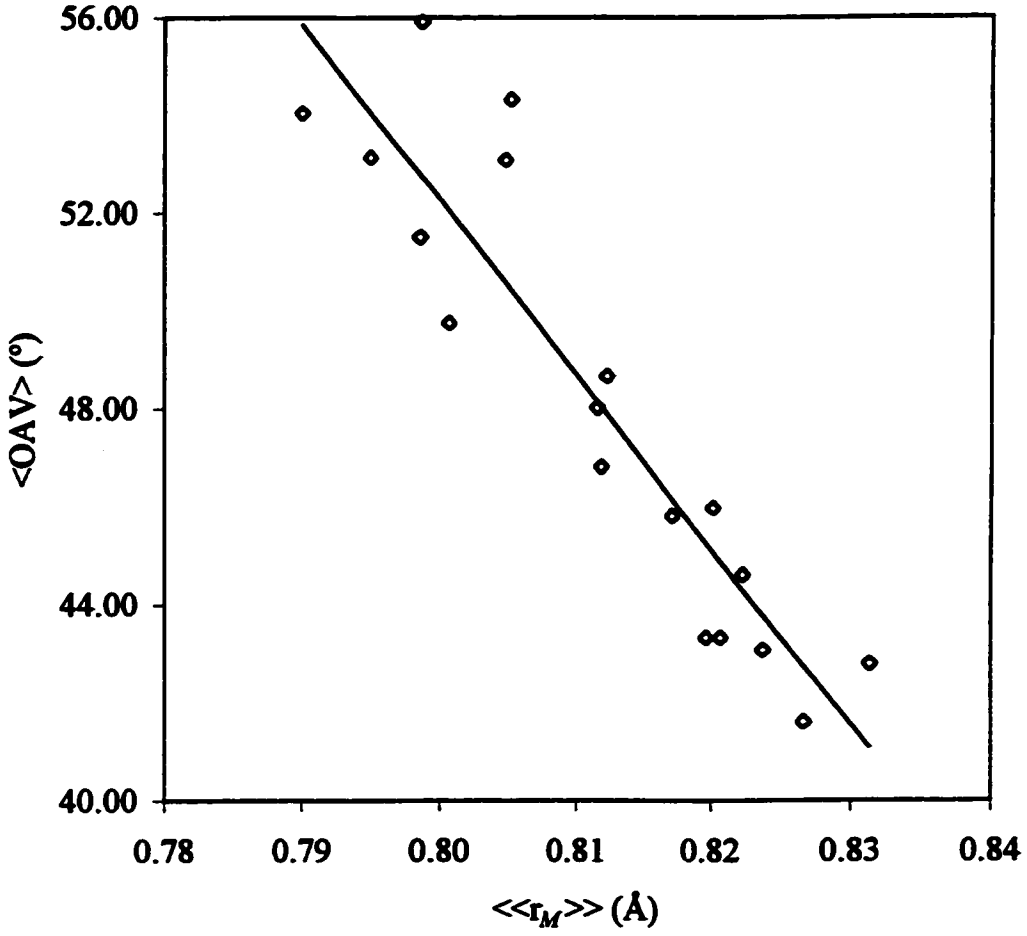

Figure 13. Average ionic radius, <<r*M*>>, *versus* the average octahedral angle variance, <OAV>, for the *O*-sheet octahedra. Linear regression, $R^2 = 0.846$.

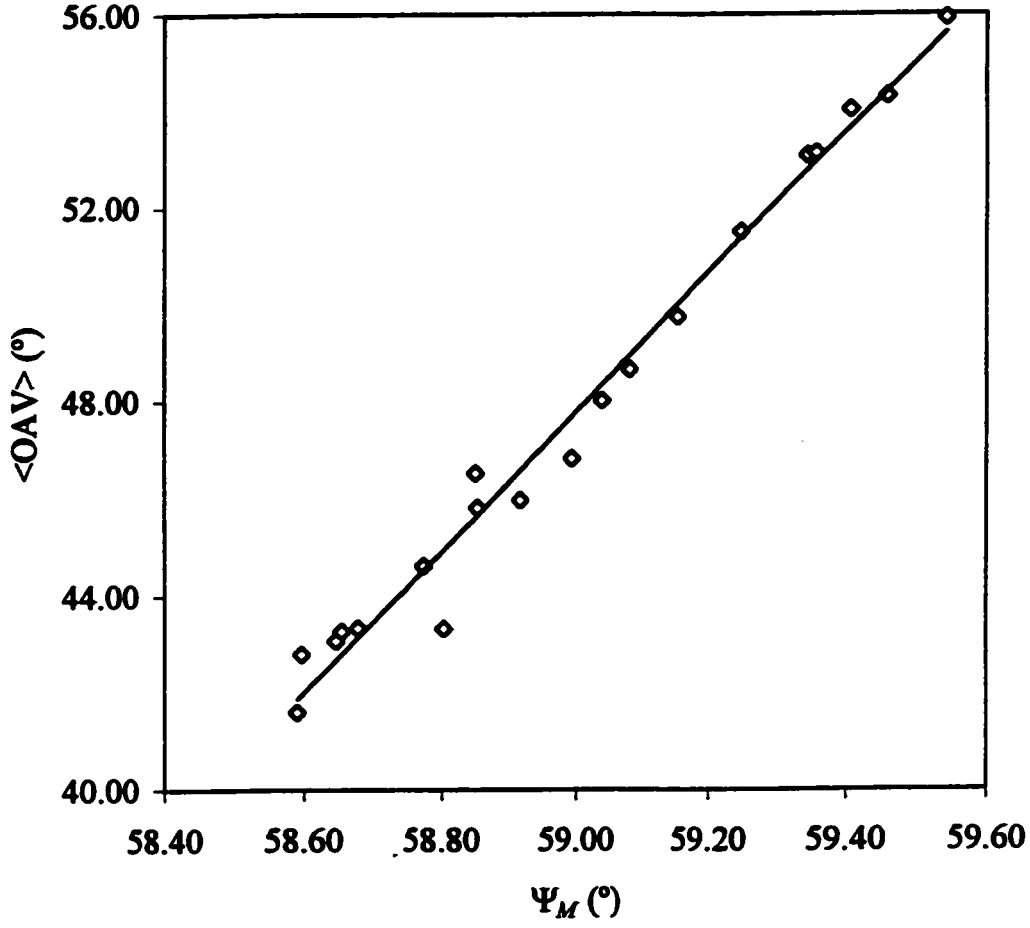

Figure 14. Average octahedral flattening (Ψ) *versus* the average octahedral angle variance, <OAV>, for the *O*-sheet octahedra. Linear regression, $R^2 = 0.983$.

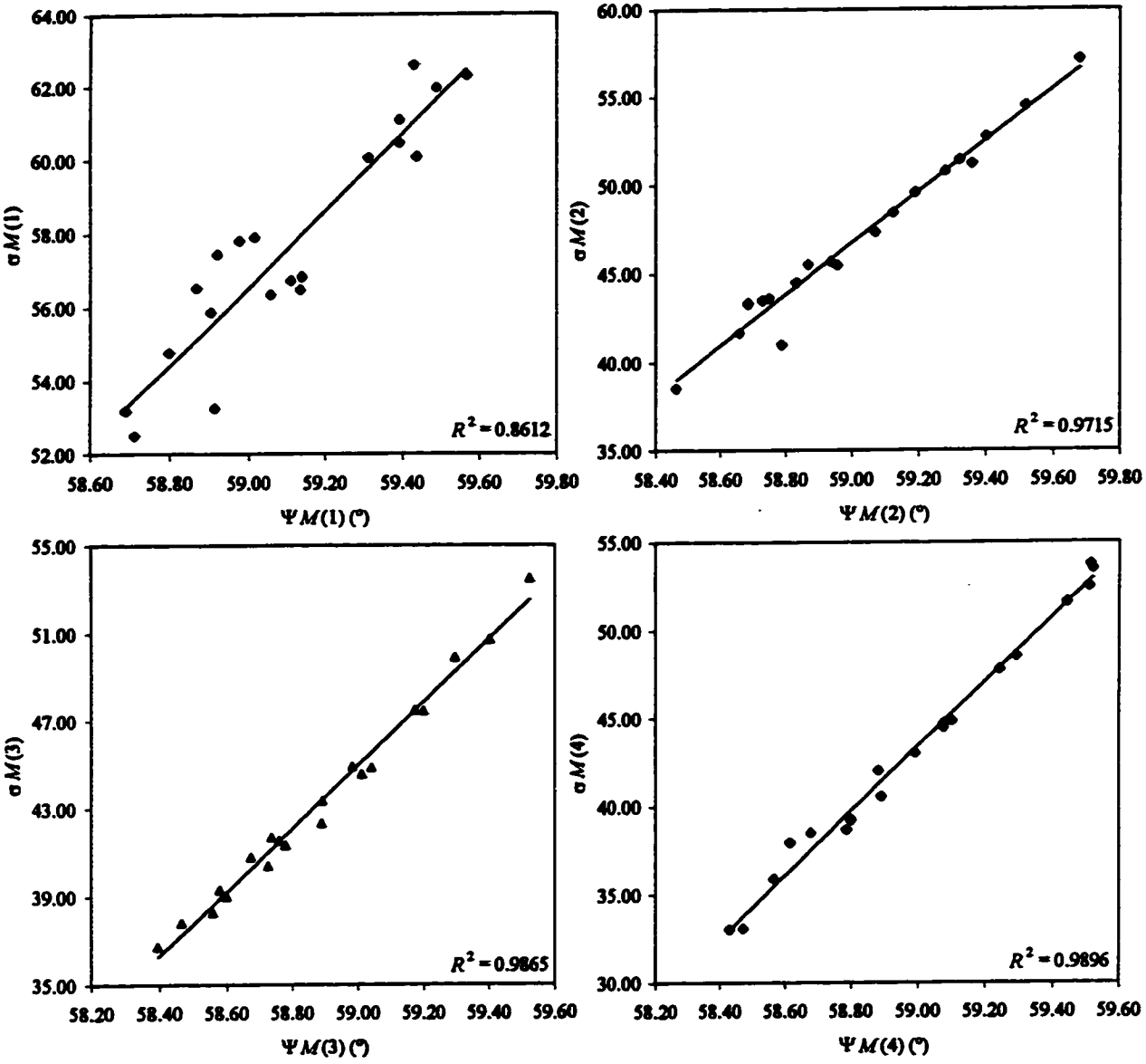

Figure 15. Octahedral flattening (Ψ) versus the octahedral angle variance (OAV) for each of the *M* sites in the *O*-sheet.

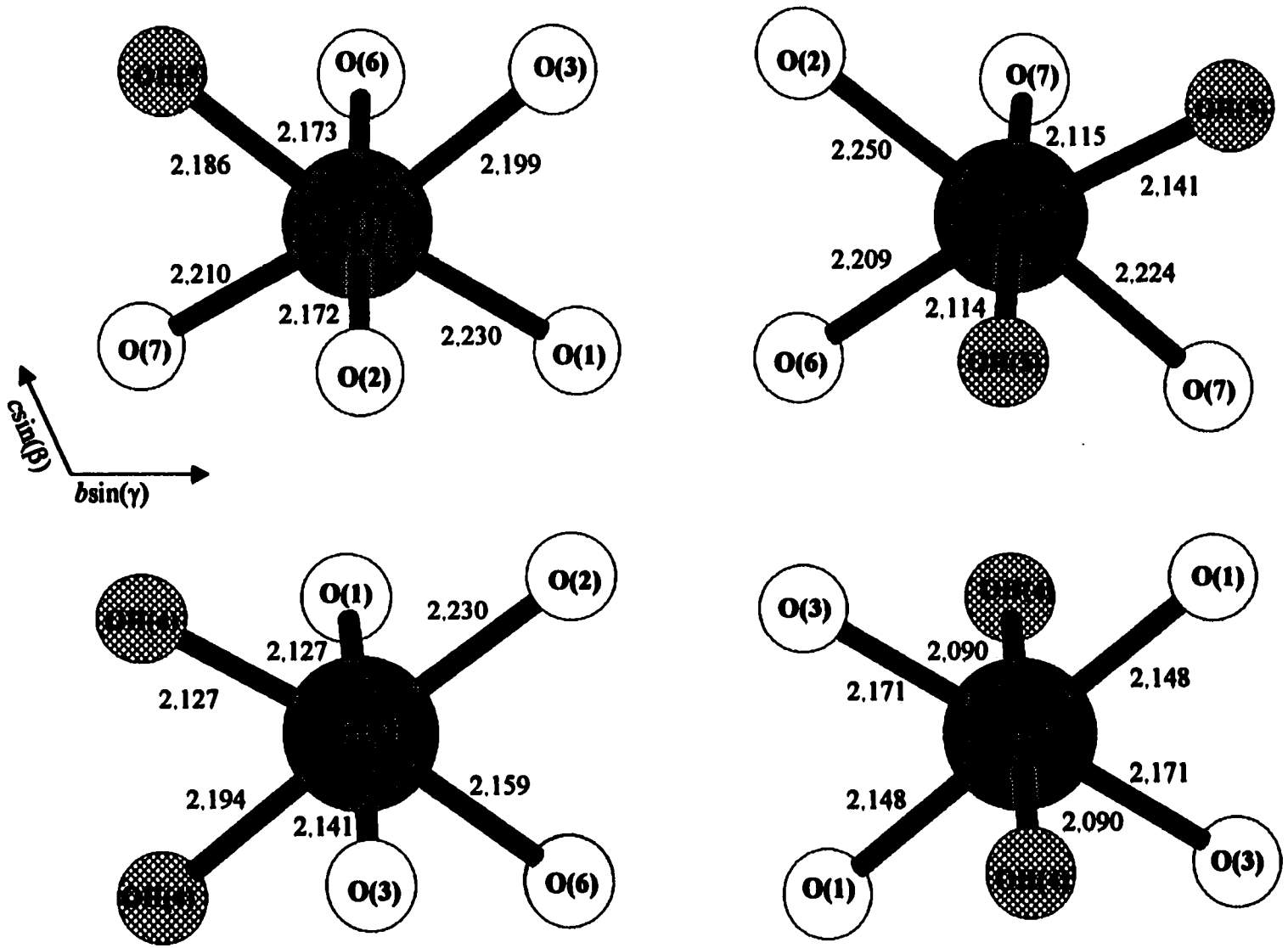

Figure 16. The $M(1)O_5(OH)$, $M(2)O_4(OH)_2$, $M(3)O_4(OH)_2$ and $M(4)O_4(OH)_2$ octahedra in AGM. Average distances are given in Å.

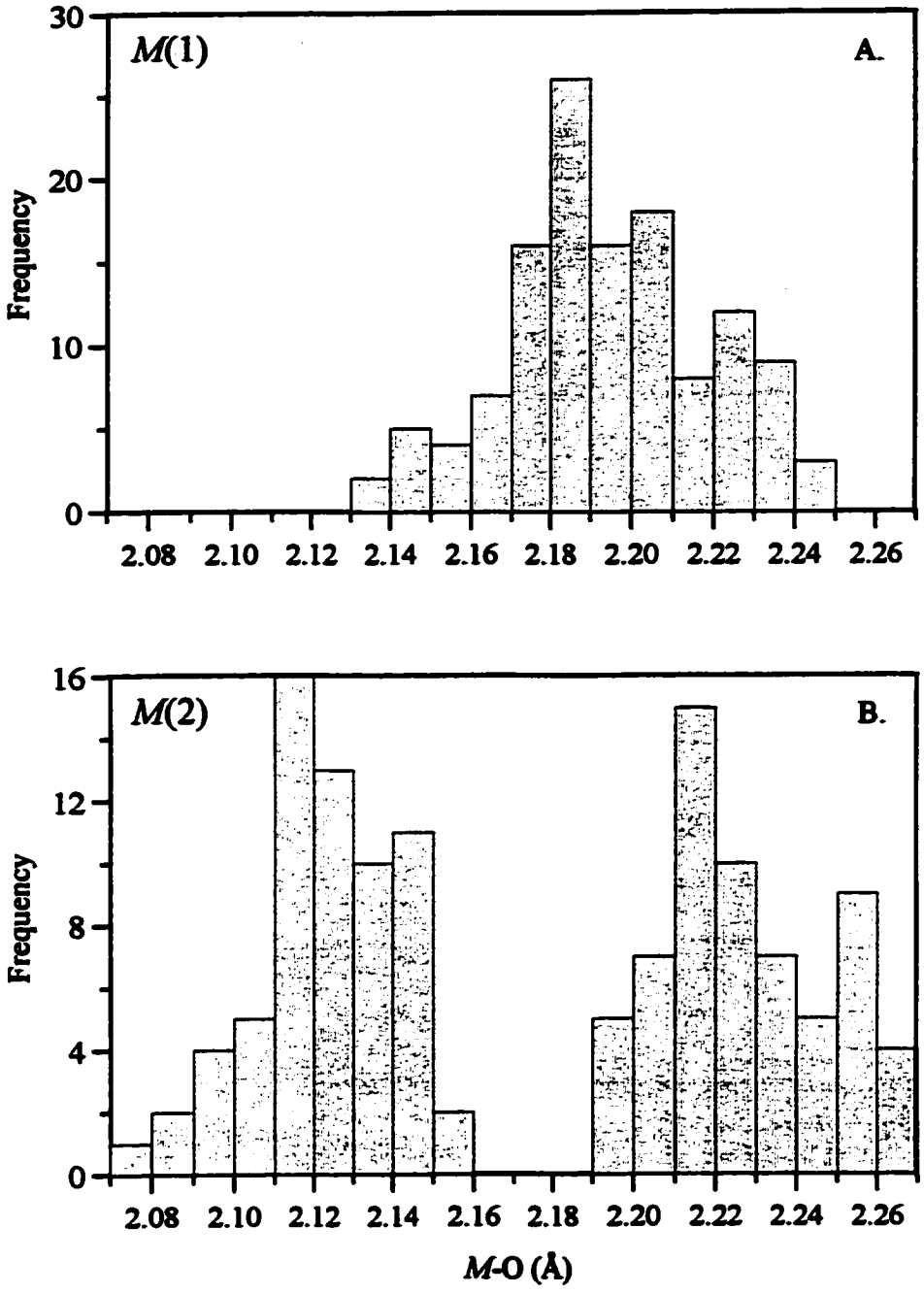

Figure 17. Distribution of *M*-O bond distances in the *O*-sheet of AGM

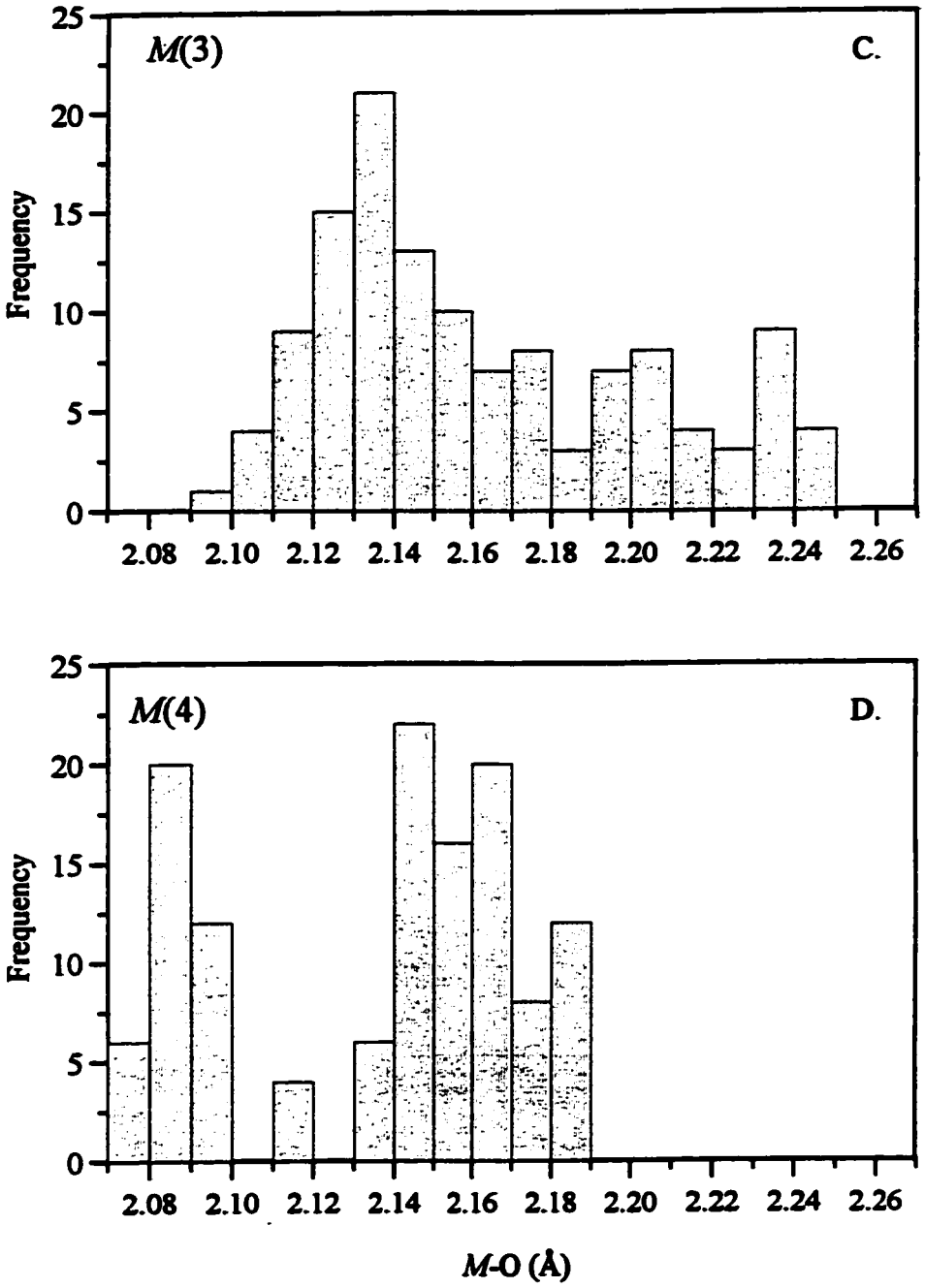

Figure 17. continued

the central cation, is 54.74°. Flattening of the octahedron in the (001) plane in order to facilitate lateral fit with the larger *H*-sheets results in values of Ψ higher than the ideal. Typical values for Ψ in sheet silicates range from 58 to 60° (Bailey 1984). In general, average Ψ angles are negatively correlated with the average ionic radius, r*M*, or the size of the octahedra (Fig. 18). Although *M*(1) is the largest of the four *O*-sheet octahedra, it displays the greatest degree of flattening, with Ψ values ranging from 58.690 to 59.567° (average: 59.113°). This is the inverse of what is expected and may be due to the fact that it must flatten within the (001) plane to bridge the adjacent chains of *M*(2) and *M*(3,4) octahedra, as shown in Figure 9.

As noted earlier, the *M*(1) site is host to typical divalent cations such as Mn and Fe, as well as Na (max.: 0.52 *apfu*). However, attempts to refine the SOF of *M*(1) with Fe results in characteristically low BVS (≈ 1.91 *v.u.*) whereas refinement of the SOF with Mn in all cases resulted in BVS close to the ideal 2.00 *v.u.*. Although it is not possible to refine both Mn and Fe within the same site, the longer average bond lengths, coupled with the closer to ideal BVS in *M*(1) when refined with the larger Mn cation suggest that Mn orders preferentially over Fe at this site.

The *M*(2) and M(3) sites are both coordinated by four O and 2 OH, with a *cis* configuration of the OH^- groups [*M*(2): OH(5) X 2, *M*(3): OH(4) X 2], and are host to Mn, Fe, Mg and Zn. The *M*(2) site is unique in the AGM structure as it forms continuous, zigzag chains of edge-sharing octahedra parallel to [100]; all other *M* sites share, at most, one common edge with crystallographically equivalent octahedra. Bond lengths in *M*(2) range from 2.079 to 2.267 Å. The *M*(2) octahedra is elongate across the O(2)-*M*(2)-O(7) linkage,

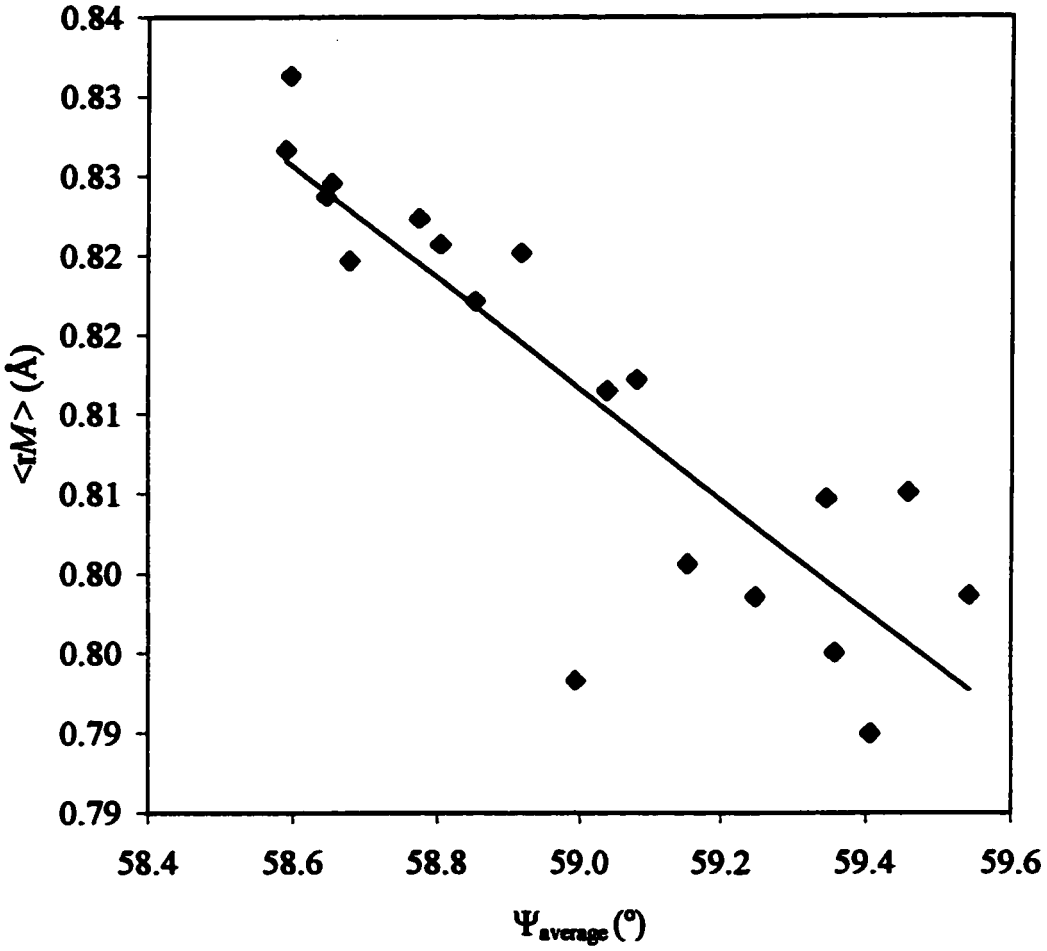

Figure 18. Average octahedral flattening, Ψ, *versus* the average ionic radius, <r*M*> in the *O*-sheet. Linear regression, $R^2 = 0.753$.

and shortened along *M*-OH(5) bonds along the shared edges, resulting in a bimodal distribution of bond lengths (Fig. 17B). This irregular distribution in bond lengths results in a strong rectangular distortion of *M*(2); Δ values range from 5.106 to 8.171 (average: 6.319) with flattening angles which are similar to those observed for *M*(1), ranging from 58.463 to 59.678° (average: 59.014°).

The *M*(3) octahedron is part of a composite chain parallel to *X*, and consisting of alternating *M*(3) and *M*(4) octahedra in a 2:1 ratio. Both octahedra are only slightly distorted relative to *M*(2) ($\Delta_{ave.}$: 3.104 and 2.600 for *M*(3) and *M*(4), respectively). Bond lengths to *M*(3) range from 2.098 to 2.246 Å with an average of 2.163 Å. Unlike *M*(2), *M*(3)-O bond lengths show a regular distribution with only a slight skew towards bond lengths approximating 2.135 Å, close to the ideal Fe^{2+}-O bond length of 2.14 Å (Ondik & Smith 1962), consistent with the suggestion that Fe^{2+} preferentially orders at *M*(2), *M*(3) and *M*(4) over *M*(1).

The *M*(4) site occupies special position 1*g* (0,½,½) in the triclinic structures and special position 4*c* (¼,¼,0) in kupletskite-*Ma2b2c*. The *M*(4) octahedron, the smallest in the AGM *O*-sheet (volume range: 12.551 to 13.111 $Å^3$), is coordinated by four O^{2-} and two OH^-, with a *trans* configuration of the OH- groups [2 x OH(4)]. Bond lengths to *M*(4) range from 2.074 to 2.184 Å (ave.: 2.136 Å). A bimodal distribution of bond lengths is observed (Fig. 17D) as distances to the two OH(4) anions are short (range: 2.098 to 2.127 Å) and those to the four O^{2-} are longer (range: 2.132 to 2.184 Å). Site-occupancy refinement indicates ordering of small divalent cations (such as Mg and Zn) extensively at both *M*(3) and *M*(4) relative to *M*(2).

5.3. H-sheet

5.3.1. $D\phi_6$ octahedron

The *D* site in triclinic AGM and kupletskite-*Ma2b2c* is coordinated by five O and ϕ(16), a mixed-anion site containing F and O, a result of the coupled substitution (Ti,Zr) + F $\Leftrightarrow$ Nb + O. Apical anions include O(2), which is also bonded to *M*(1), *M*(2) and *M*(3) in the *O*-sheet, and ϕ(16). Basal anions include O(9) and O(12), which are also bonded to *T*(4), and O(11) and O(15), also bonded to *T*(1). In monoclinic magnesium astrophyllite, the ϕ(16) site is vacant, resulting in a tetragonal pyramidal geometry for the DO_5 polyhedron (Shi *et al.* 1998). All structures in this study were found to contain octahedrally-coordinated *D* cations. Titanium contents in the samples studied range from 0.24 to 1.92 *apfu*, Nb contents from 0.06 to 1.33 *apfu*, and Zr contents from zero to 0.72 *apfu* (Table 2). Titanium contents as measured by EMPA are in excellent agreement with those calculated from SOF refinement at the *D* site (Fig. 19). Refinement of the SOF for the *D* site was only possible with two elements, Ti and either Zr or Nb. As both Nb and Zr are heavier X-ray scatterers than Ti, the difference between unity and the refined Ti content is equivalent to the sum of Nb+Zr. Bond-valence sums to *D* range from 4.064 *v.u.* in Zr- and Nb-free astrophyllite to 4.800 *v.u.* in niobokupletskite.

There is a wide range in bond lengths is observed in the $D\phi_6$ octahedron, ranging from 1.794 to 2.097 Å. The $D\phi_6$ octahedron is elongated along the [001] tetrad axis. The average distance to the four basal oxygens is 1.966 Å, close to the ideal length of 1.98 Å for a Ti-O bond (Ondik & Smith 1962) and slightly less than observed in other alkali

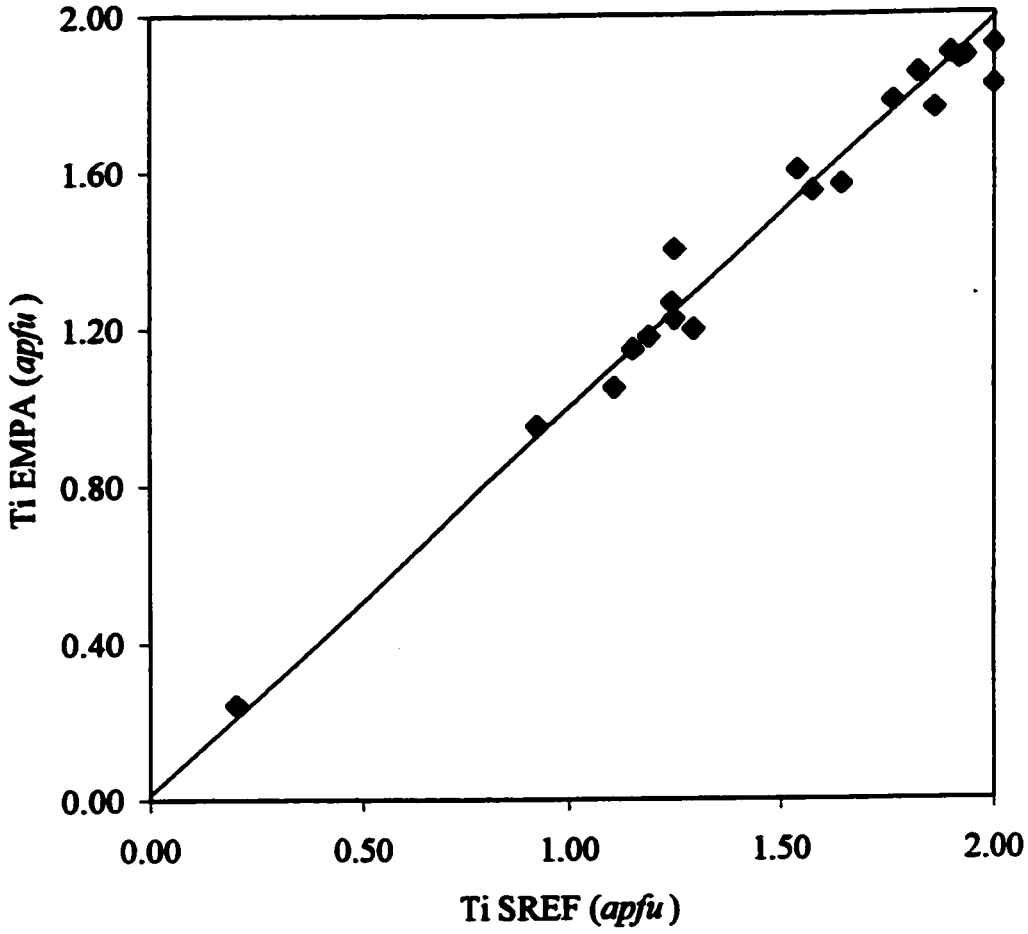

Figure 19. Comparison of Ti contents derived from site occupancy refinement (SREF) and electron-microprobe analyses (EMPA). The 1:1 line is indicated.

titanosilicates with octahedrally-coordinated Ti (*e.g.* seidozerite, Simonov & Belov 1960; lomonosovite, Khalilov 1990; tienshanite, Cooper *et al.* 1998; vuonnemite, Ercit *et al.* 1998). Bond lengths to O(9) and O(12) are, on average, slightly shorter than bond lengths to the opposite O(11) and O(15) oxygens (ave.: 1.962 and 1.969 Å, respectively). Angles between basal oxygens range from 87.2 to 90.5° (ave.: 88.9°), close to the ideal 90° (Fig. 20).

The average D-ϕ bond length, $\langle D\text{-}\phi \rangle$, is a function of the average ionic radius of the cations at the D site, as shown in Fig. 21. As Ti and Nb have almost identical ionic radii ($r^{[6]}Ti^{4+}$: 0.61 Å, $r^{[6]}Nb^{5+}$: 0.64 Å, Shannon 1976), the average cationic radius, and thus the size of the $D\phi_6$ octahedra, is primarily a function of the presence of the larger Zr cation ($r^{[6]}Zr^{4+}$: 0.72 Å, Shannon 1976). Figure 22 shows the relationship between $\langle D\text{-}\phi \rangle$ and Zr content in AGM. Although substitution of Nb for Ti does not affect the overall size of the $D\phi_6$ octahedron, it does have a pronounced control on the bond length variations observed in the octahedra, in particular the distribution of apical bond lengths. Unlike in AGM, isomorphous substitution of both Zr and Nb for Ti in other titanosilicates is limited. In AGM, the presence of Ti, Nb and Zr in varying ratios imposes a strong influence on the local geometry of the $D\phi_6$ octahedron and distinction must be made as to which substitutional mechanism, Zr $\Leftrightarrow$ Ti or Nb $\Leftrightarrow$ Ti, the structural change can be attributed.

Apical bond-lengths display the greatest range in values, ranging from 1.794 to 2.104 Å and have a strong bimodal distribution (Fig. 23). In general, D-O(2) bonds are the shortest (ave.: 1.845 Å), ranging from 1.794 Å in Nb- and Zr-free kupletskite, to 1.929 Å in niobokupletskite. However, D-O(2) bond lengths are long (ave.: 2.069 Å), ranging from 1.981 Å in MSH42, niobokupletskite from MSH, to 2.104 Å in LAB3, a Zr-rich astrophyllite

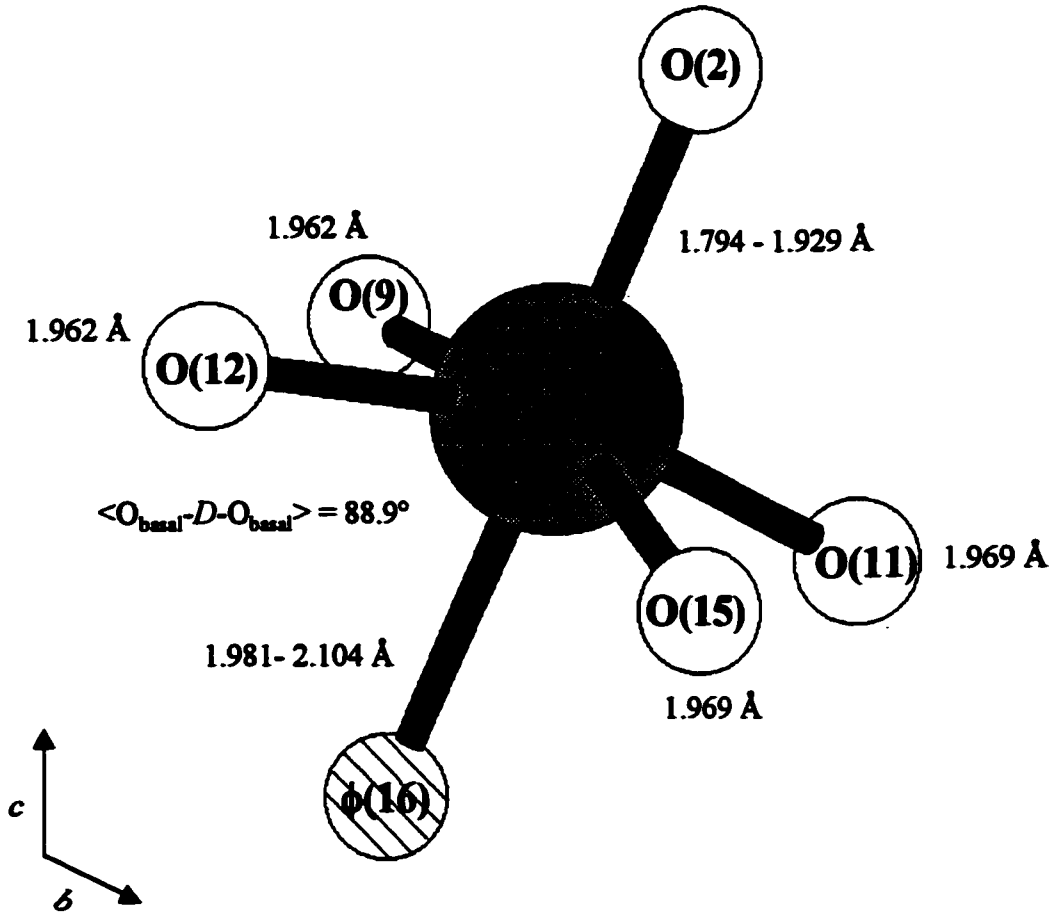

Figure 20. The $D\phi_6$ octahedra in AGM. Average distances (Å) and bond angles (°) shown.

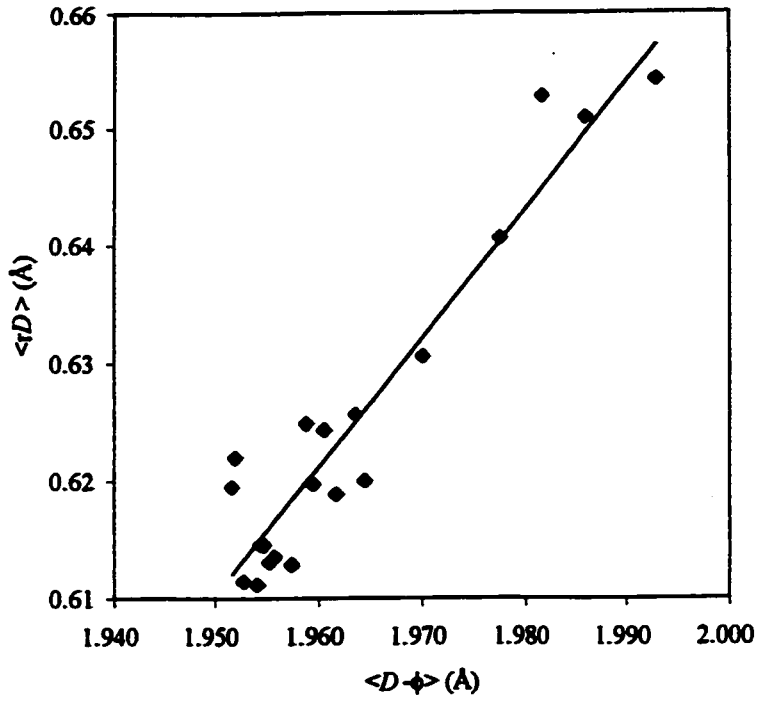

Figure 21. The variation in mean D-ϕ bond length with average ionic radius of the D cations. Linear regression, $R^2 = 0.899$.

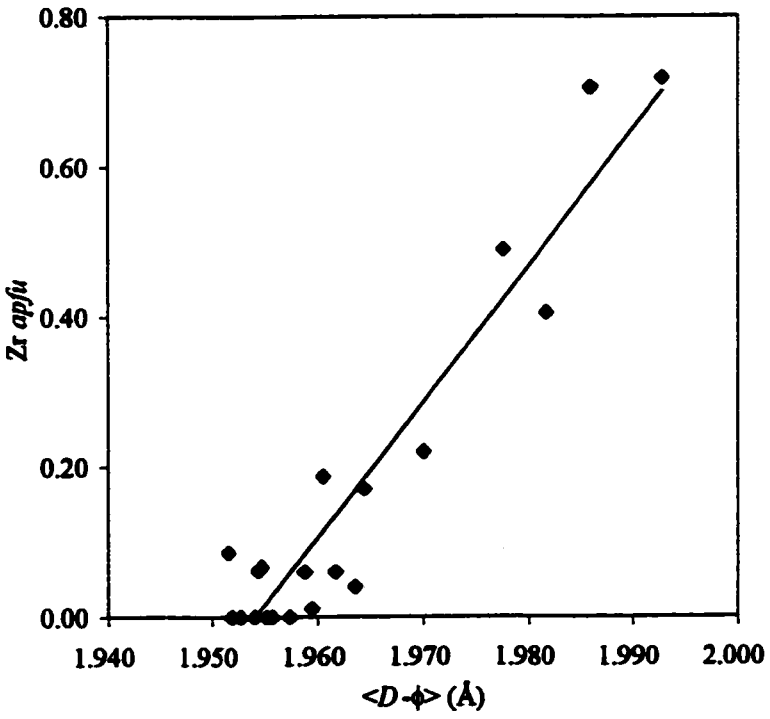

Figure 22. The variation in mean D-ϕ bond length with Zr content (*apfu*). Linear regression, $R^2 = 0.901$.

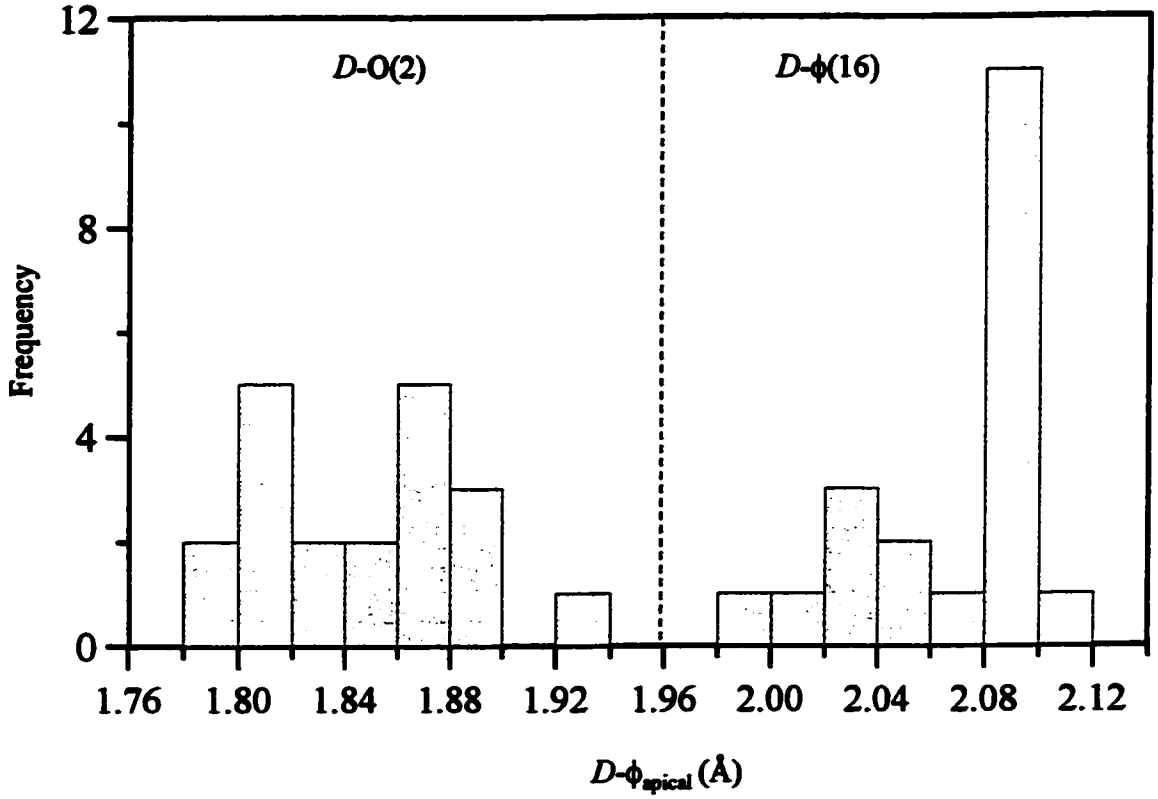

Figure 23. Bimodal distribution of D-ϕ_{apical} bond lengths observed in the $D\phi_6$ octahedra in AGM.

from Seal Lake (Labrador, Canada). A bimodal distribution of apical bond lengths in TiO_6 octahedra is a common feature in other titanosilicates (Table 8) including bafertisite (Pen & Sheng 1963), innelite (Chernov *et al.* 1971), tienshanite (Cooper *et al.* 1998), vuonnemite (Ercit *et al.* 1998) and normandite (Perchiazzi *et al.* 2000). Removal of one of the apical anions [*i.e.* $\phi(16)$ in triclinic AGM] results in a further shortening of the remaining $Ti\text{-}O_{apical}$ bond as observed not only in monoclinic magnesium astrophyllite [$Ti\text{-}O_{apical}$ = 1.755 Å, Shi *et al.* 1998), but in other titanosilicates with [5]-coordinated Ti such as lamprophyllite ($Ti\text{-}O_{apical}$ = 1.68 Å, Saf'yanov *et al.* 1983) and yoshimuraite ($Ti\text{-}O_{apical}$ = 1.773 Å, McDonald *et al.* 2000).

It has been discussed by Megaw (1968a,b) that off-center displacement of a cation in an octahedron occurs when the effective radius of the cation is such that the unstressed *M*-O bond length is $< 1/\sqrt{2}$ times the oxygen diameter. This is particularly apparent for small cations with high charge (*e.g.* Ti and Nb). In these cases, the mutual attraction and repulsion effects within the octahedron result in 'stressed' bonds to the point where the anion-anion repulsion has caused the cation-anion bond to be extended beyond its unstressed value (Megaw 1968ab). The resultant tension in the O-*M*-O bond length is relaxed by off-center displacement of the cation and relaxation of the O-O edges (Megaw 1968ab). The presence of larger cations (e.g. Zr) cation leads to smaller displacements and longer overall bond lengths with a more regular distribution. In titanosilicates with TiO_5 tetragonal pyramids (*e.g.* lamprophyllite, innelite, yoshimuraite, *etc.*), this effect is most prominent with the Ti cation displaced away from the square plane towards the apex. In TiO_5 polyhedra, Ti-O distances to the four basal oxygens range from 1.9 to 2.0 Å, whereas bond lengths to the

TABLE 8. COMPARISON OF Ti-ϕ APICAL BOND LENGTHS IN ASTROPHYLLITE GROUP MINERALS AND OTHER TITANO- AND NIOBOSILICATES

Mineral	$^{[CN]}D$	D-O_{apical} (Å)	D-ϕ_{apical} (Å)	Ti SOF
Astrophyllite group minerals				
[1]Niobokupletskite	[6](Nb,Ti)	1.929	1.981	0.11
Nb-bearing kupletskite	[6](Ti,Nb)	1.887	2.014	0.553
Nb-bearing kupletskite	[6](Ti,Nb)	1.866	2.034	0.624
Kupletskite	[6]Ti	1.794	2.086	1.00
[2]Magnesium astrophyllite	[5]Ti	1.755	–	1.00
Other titano- and niobosilicates				
[3]Bafertisite	[6]Ti	1.823	2.062	1.00
[4]Innelite	[6]Ti	1.90	2.09	1.00
[5]Janhaugite	[6](Ti,Zr)	1.849	2.221	0.67
	[6](Ti,Zr)	1.830	2.268	0.73
[6]Normandite (AF)	[6](Ti,Zr)	1.863	2.064	0.612
[6]Normandite (MSH)	[6](Ti,Nb)	1.781	2.303	0.876
[7]Tienshanite	[6]Ti	1.763	2.200	1.00
	[6](Ti,Nb)	1.824	2.138	0.64
[8]Vuonnemite (K)	[6]Ti	1.734	2.129	1.00
	[6](Nb,Ti)	1.758	2.238	0.165
[9]Ba-lamprophyllite	[5]Ti	1.660	–	0.70
[4]Innelite	[5]Ti	1.62	–	1.00
	[5]Ti	1.71	–	1.00
[10]Lamprophyllite	[5]Ti	1.68	–	1.00
[11]Yoshimuraite	[5]Ti	1.773	–	0.69

CN: coordination number, *D*: [5] or [6]Ti, Zr or Nb, SOF: Site occupancy factor
[1]Piilonen *et al.* (2000), [2]Shi *et al.* (1998), [3]Pen & Sheng (1963), [4]Chernov *et al.* (1971), [5]Annehed *et al.* (1985), [6]Perchizzi *et al.* (2000, AF: Amdrup Fjord, MSH: Mont Saint-Hilaire), [7]Cooper *et al.* (1998), [8]Ercit *et al.* (1998, K: Kola Peninsula), [9]Rastsvetaeva & Dorfman (1995), [10]Saf'yanov *et al.* (1983), [11]McDonald *et al.* (2000).

apical oxygens are short, ranging from 1.68 to 1.78 Å.

In AGM, the highly asymmetric nature of the bonding in the $D\phi_6$ octahedra can be shown to be dependent on the composition of both *D* and the $\phi(16)$ site. Assuming electronegativities for Ti, Nb and Zr of 1.5, 1.6 and 1.4, respectively, the covalent character of the *D*-O(2) and *D*-$\phi(16)$ bonds in AGM can be calculated knowing the composition of the $\phi(16)$ site for each composition (Table 9). Calculated bond characters show that the Ti-O(2) bond is 8% more covalent than the Ti-$\phi(16)$ bond, resulting in stronger bonding of the Ti to the O(2) apical oxygen and thus shorter *D*-O(2) bond lengths relative to *D*-$\phi(16)$. Substitution of Nb for Ti and O for F results in a symmetrical O(2)-Nb-O(16) bond which is more covalent overall than the asymmetric O(2)-Ti-F(16) bond observed in Ti-dominant samples. Substitution of Nb for Ti results in a shortening of the *D*-$\phi(16)$ bond and a subsequent lengthening of the *D*-O(2) bond. As such, Nb becomes more centrally located in the octahedron, rather than being displaced along *Z* toward the *O*-sheet as is the case in Ti-dominant AGM. This is evident when examining the variation in $<\phi(16)$-*D*-$O_{basal}>$ and $<$O(2)-*D*-$O_{basal}>$ bond angles (Fig. 24). Incorporation of Nb at *D* results in an increase of the $<\phi(16)$-*D*-$O_{basal}>$ angles (range: 80.7 to 85.4°) and a concomitant decrease of the $<$O(2)-*D*-$O_{basal}>$ bond angles (range: 94.6 to 99.2°; Fig. 25). This displacement can also be measured by the difference in lengths between the *D*-O(2) and *D*-$\phi(16)$ bonds. In Ti-dominant samples, this difference is at a maximum (0.292 Å in MSH20), whereas in Nb-dominant samples, the bond lengths are closer to being equal and the difference is small (0.052 Å in MSH42, niobokupletskite). The net result of these modifications is a significant decrease in

TABLE 9. CALCULATED IONIC CHARACTER* OF THE APICAL BOND LENGTHS IN THE $D\phi_6$ OCTAHEDRA

D cation	O(2)	φ(16) anion	Ionic character	
			D-O(2)	*D*-φ(16)
Ti	O^{2-}	F^-	0.393	0.465
Nb	O^{2-}	O^{2-}	0.378	0.378
Zr	O^{2-}	F^-	0.408	0.478

* Ionic character = $1\text{-}e^{-1/4(XA-XB)}$ where XA is the electronegativity of the anion and XB is the electronegativity of the cation. $X(F^-) = 4.0$, $X(O^{2-}) = 3.5$, $X(Ti^{4+}) = 1.5$, $X(Nb^{5+}) = 1.6$, $X(Zr^{4+}) = 1.4$.

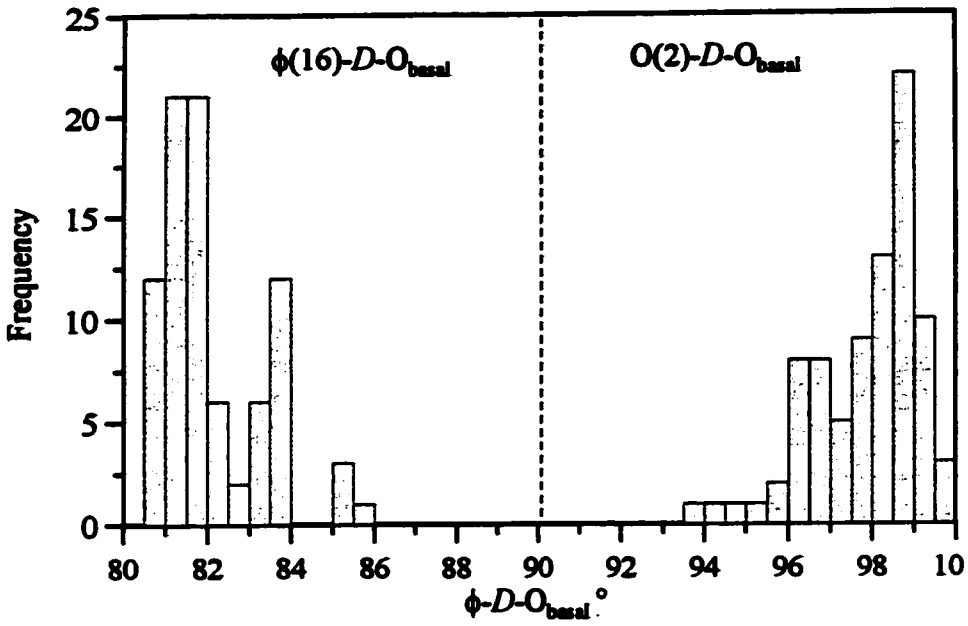

Figure 24. Distribution of O(2)-*D*-O_{basal} and φ(16)-*D*-O_{basal} bond angles in the $D\phi_6$ octahedra.

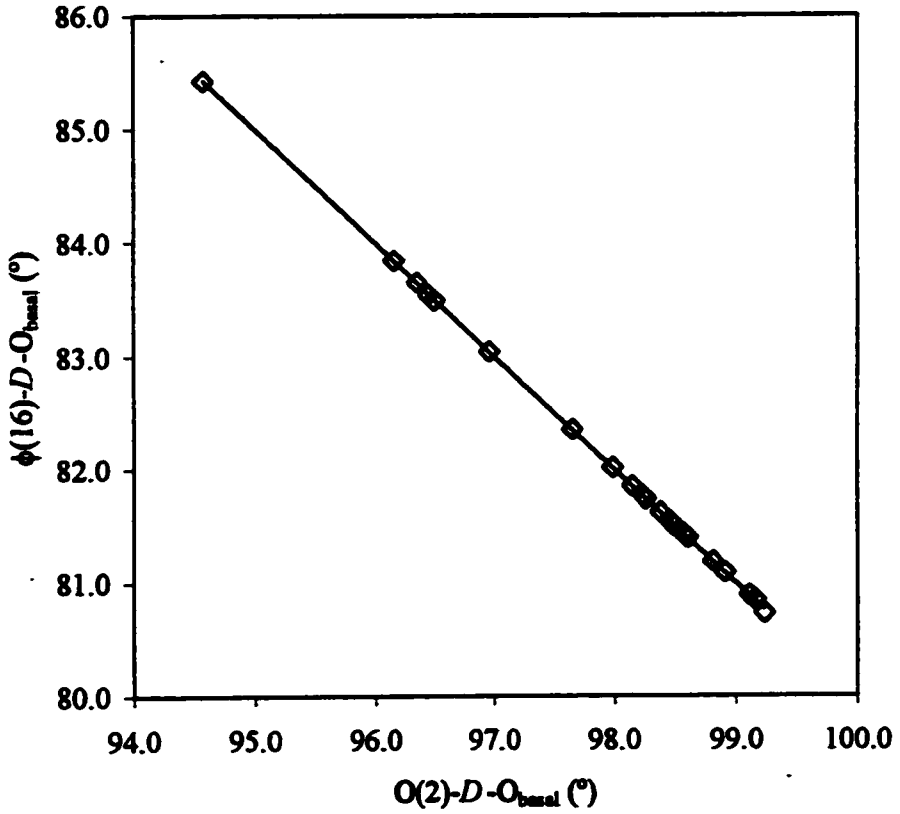

Figure 25. Correlation between O(2)-*D*-O_{basal} and φ(16)-*D*-O_{basal} bond angles in the $D\phi_6$ octahedra. (Linear regression, $R^2 = 1.00$)

the distortion of the *D* octahedron with increasing Nb ⇔ Ti substitution. Figure 26 shows the correlation between the O_{apical}-*D*-O_{basal} bond angles and the distortion index, Δ.

A plot of *D*-O(2) versus *D*-ϕ(16) reveals two distinct trends: (1) increasing *D*-O(2) with decreasing *D*-ϕ(16), and (2) increasing *D*-O(2) at constant *D*-ϕ(16) (Fig. 27). Plotting the contents of Zr and Nb on this graph shows the first trend to be the result of increasing Nb ⇔ Ti substitution and the second the result of Ti ⇔ Zr substitution. This confirms the observation that substitution of Nb decreases the *D*-ϕ(16) bond length, whereas lengthening of the *D*-O(2) bond length is due to displacement of the cation within the octahedron. Although the two bonds change in length relative to each another, the total O(2)-*D*-ϕ(16) bond length along the [001] axis remains unchanged (Fig. 28A). Samples in which Ti ⇔ Zr substitution is dominant (indicated by the open diamonds on Figure 27) have a constant *D*-ϕ(16) bond length which is similar to the maximum observed in Nb-free structures. The increase in *D*-O(2) is due to substitution of the larger Zr cation and expansion of all the bonds in the octahedron (Fig. 23). Figure 28B shows the associated expansion of the O(2)-*D*-ϕ(16) bond length due to Zr substitution.

Substitution of Zr for Ti centers the cation within the octahedron and results in a more regular distribution of bond lengths, a feature also observed in other zirconosilicates with minimal (Ti,Nb) ⇔ Zr substitution such as låvenite (Mellini 1981), sabinaite (McDonald 1996) and eudialyte group minerals (Johnsen & Grice 1999).

The maximum observed Zr content in AGM is 1.02 *apfu*, suggesting that the maximum Ti ⇔ Zr substitution is ≈ 50%. This limited substitution does not seem to be a

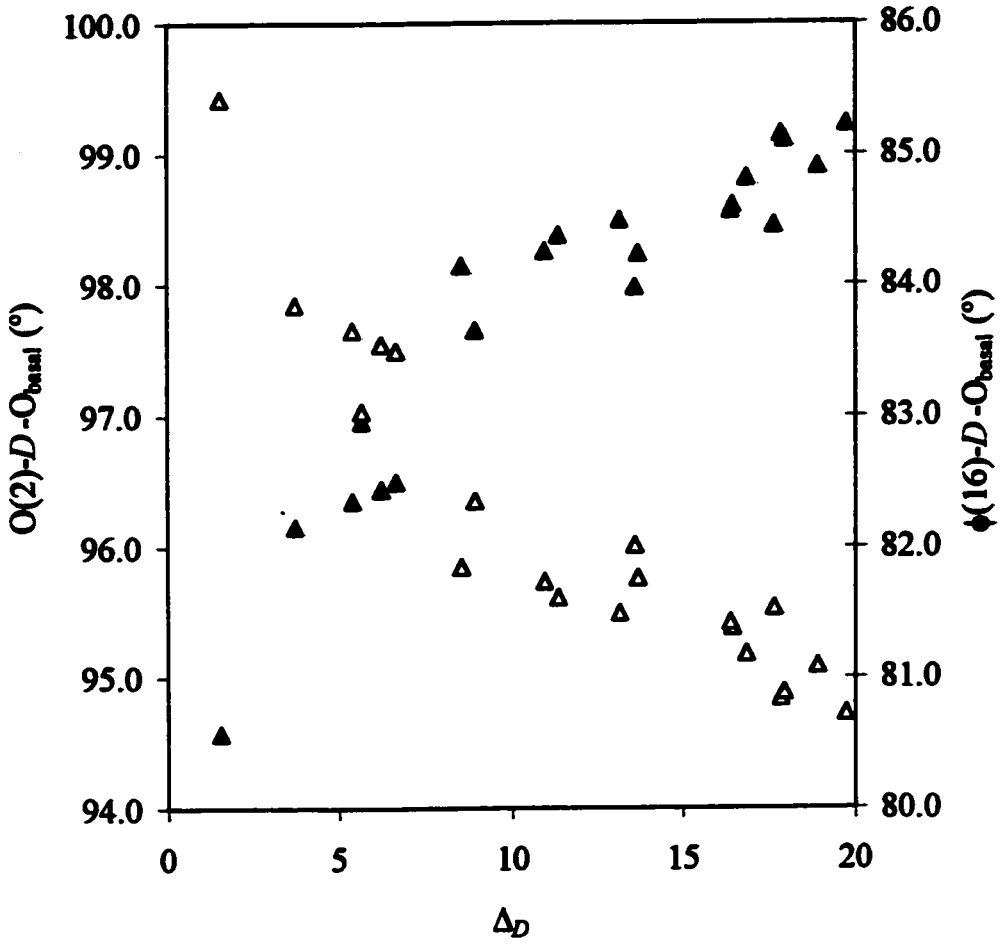

Figure 26. Distortion of the $D\phi_6$ octahedra *versus* the ϕ_{apical}-*D*-O_{basal} bond angles.
Closed triangles: O(2)-*D*-O_{basal}
Open triangles: ϕ(16)-*D*-O_{basal}

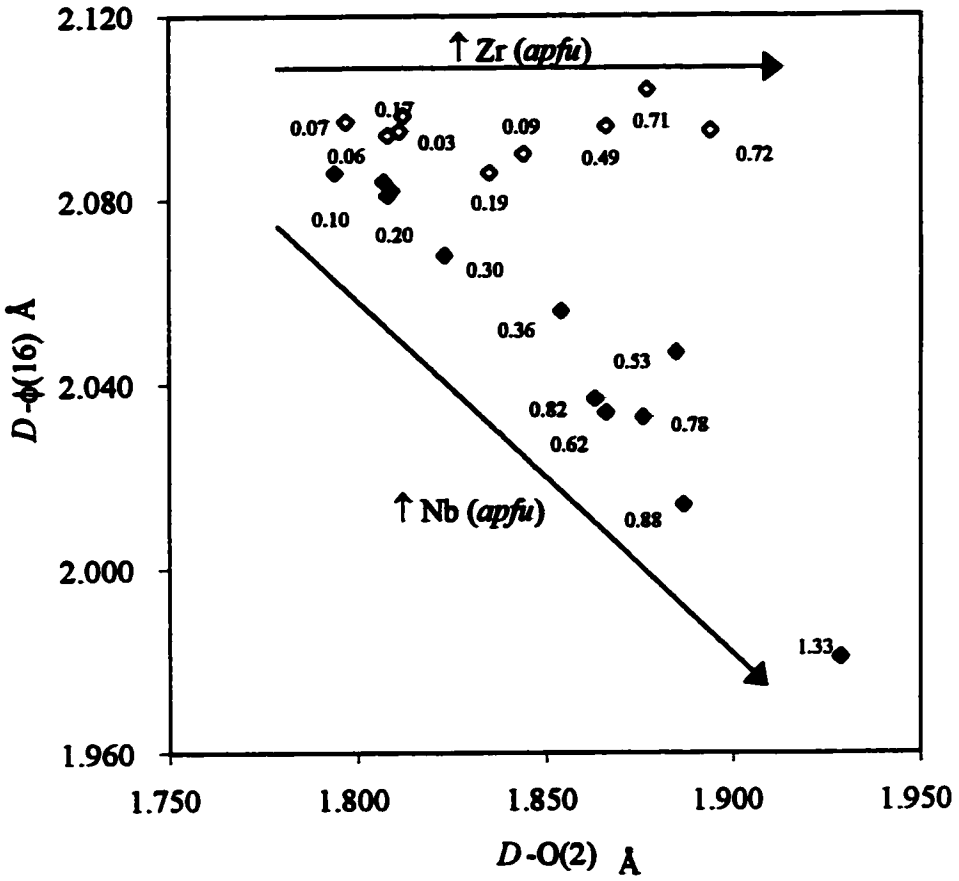

Figure 27. Control by HFSE contents on apical bond lengths in the $D\phi_6$ octahedra.

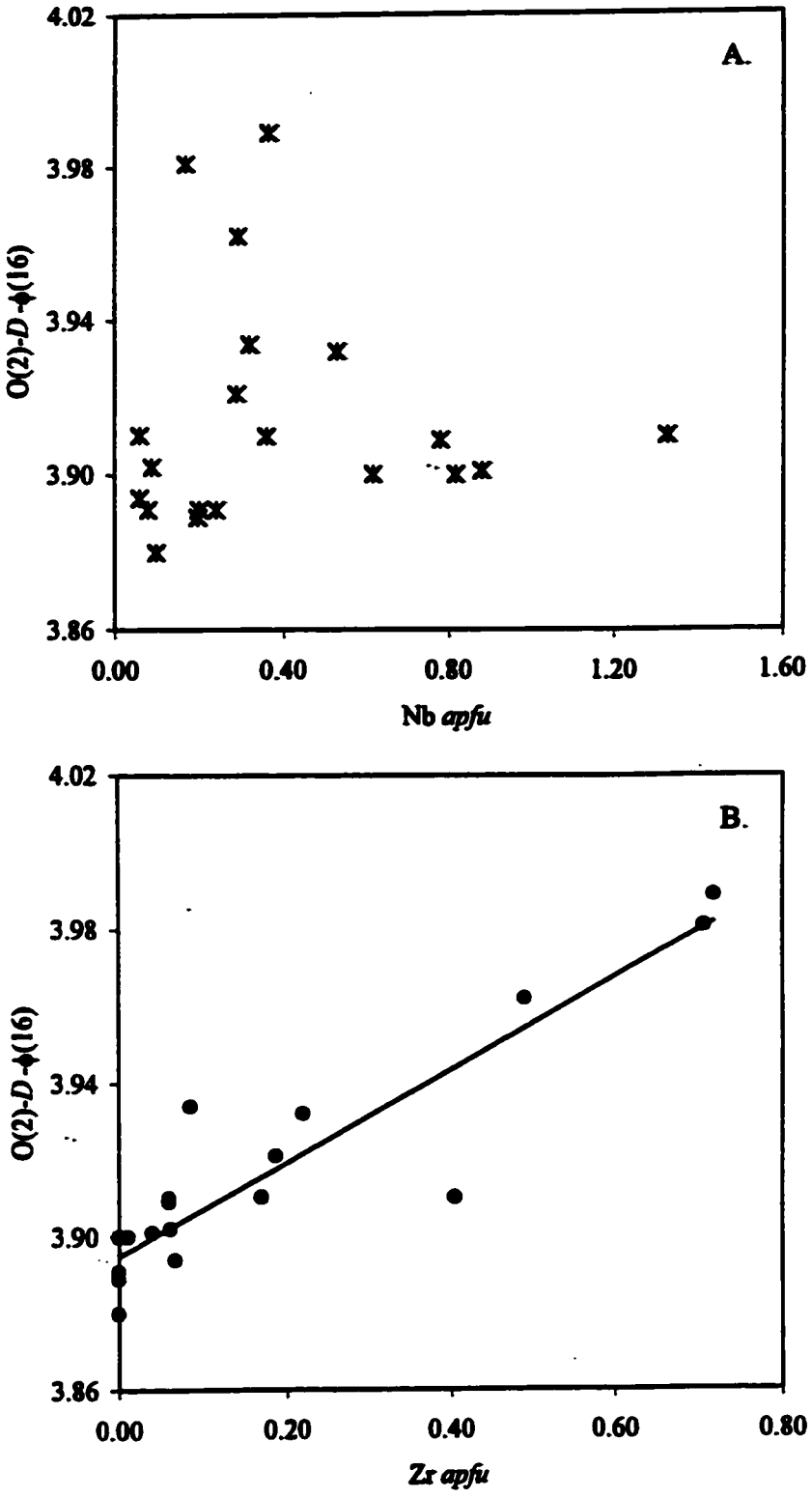

Figure 28. Variation in O(2)-*D*-ϕ(16) bond length with composition in *D*
A. Effect of Nb ⇔ Ti substitution: no correlation
B. Effect of Zr ⇔ Ti substitution: $R^2 = 0.844$

function of geochemistry or a lack of Zr in the system; Zr-bearing AGM are commonly associated with other zirconosilicates, indicating no lack of Zr during crystallization. It is suggested that the limited substitution of Zr for Ti is due to crystal-chemical rather than geochemical constraints. As is discussed in detail in Chapter IV, substitution of Zr into *D* results in a lengthening of the *D*-O(2) bond and shortening of *M*(1,2,3)-O(2) bonds in the *O*-sheet. This shortening results in increased flattening of the *M* octahedra and an increase in the *O*-sheet dimensions which cannot be accounted for by structural change in the *H*-sheet.

In most zirconosilicates, Zr resides at either [6]- or [8]-coordinated sites and substitution of Nb or Ti for Zr is minimal (*e.g.* vlasovite, Voronkov & Pyatenko 1962; wadeite, Tikhonenkov 1964; låvenite, Mellini 1981; minerals of the eudialyte group, Johnsen & Grice 1999). The lack of (Ti,Nb) ⇔ Zr substitution in such minerals is not the result of geochemical controls on the crystallizing magma; in alkaline systems Zr and Ti are commonly occur together in exceptionally high concentrations and there is no reason to think that there was a lack of either element present when the zirconosilicates crystallized.

With the exception of seidozerite, Zr in zirconosilicates occurs in isolated polyhedra, forming a 3D-network with SiO_4 tetrahedra, displaying a negative tendency towards polymerization (Pyatenko & Voronkov 1978). On the other hand, Ti polyhedra in titanosilicates tend to polymerize, most commonly *via* apices and even *via* common edges. In fact, natural examples of crystal structures with discrete, isolated Ti octahedra are rare, which may suggest that these structures are metastable (Pyatenko & Voronkov 1978). In cases where there is substantial Ti and Zr in a mineral, the two cations tend to partially or completely order (Pyatenko & Voronkov 1978; *e.g.* rosenbuchite, Shibaeva *et al.* 1964,

sabinaite, McDonald 1996). Complete solid-solution series between minerals with Ti and Zr end-members have not been found. In AGM, due to the presence of substantial concentrations of Nb, it was not possible to evaluate the degree of ordering of Ti and Zr.

5.3.2. T sites

There are four crystallographically unique tetrahedral sites in the AGM structure, labeled *T*(1) through *T*(4). The *T*(1) and *T*(4) sites are each coordinated by one bridging (*br*) [O(13) and O(14), respectively] and three non-bridging (*nb*) oxygens [*T*(1): O(1), O(11) and O(15), *T*(4): O(7), O(9) and O(12)]. The *T*(1) and *T*(4) tetrahedra share corners with the $D\phi_6$ octahedra *via* non-bridging O, forming *T*(1,4)-O_{nb}-*D* linkages perpendicular to [100]. *T*(2) and *T*(3) tetrahedra are each coordinated by three bridging and one non-bridging oxygens [*T*(2): bridging O(8), O(10) and O(13), non-bridging: O(3); *T*(3): bridging: O(8), O(10), and O(14), non-bridging: O(6)]. The *T*(2) and *T*(3) tetrahedra alternate along the length of the chain, forming O(8)-*T*(2)-O(10)-*T*(3) linkages parallel to [100]. *T*(1) and *T*(4), the branches of the chain, are linked *via* bridging oxygens to the main chain by O(13) and O(14). Bond-valence sums to the four *T* sites range from 3.838 to 4.260 *v.u.*

Bond lengths in all four tetrahedra range from 1.590 to 1.654 Å, consistent with values expected for essentially Al-free tetrahedra. The distribution of *T*-O bond lengths in AGM is shown in Figure 29. In general, *T*-O_{br} > *T*-O_{nb} (ave.: 1.598 and 1.585 Å respectively), a feature which is observed in all silicates because of the presence of a second Si atom linked to the O^{2-} of the Si-O bond results in repulsion of the two Si^{4+} cations, weakening, and therefore elongating, the Si-O_{br} bond (Cruickshank 1961, Brown & Gibbs

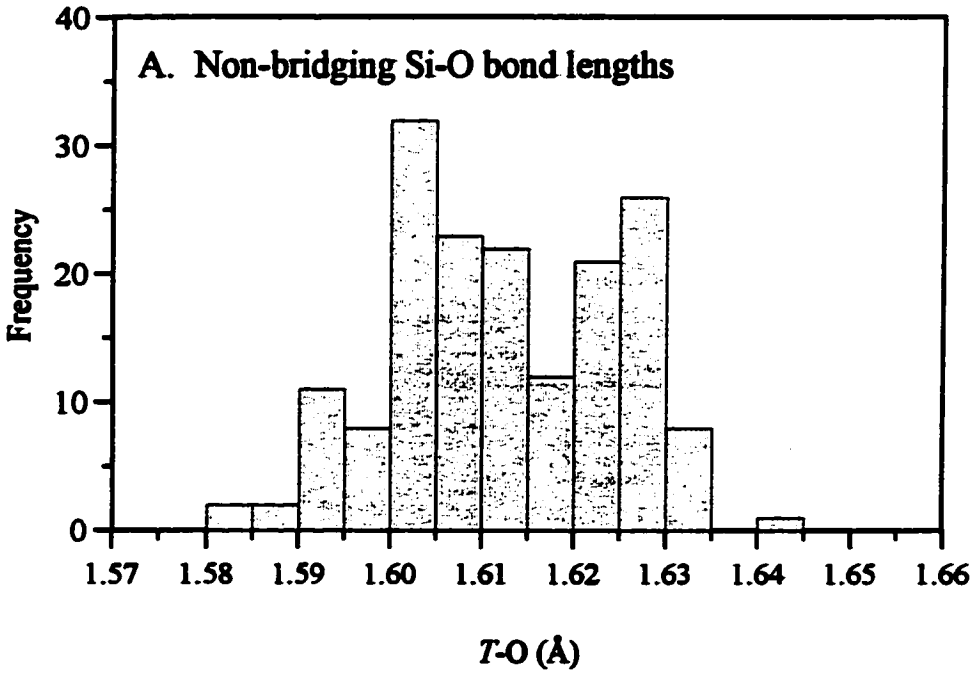

Figure 29. Distribution of *T*-O bond distances in the *H*-sheet of AGM.
A: Non-bridging Si-O bonds (Å)

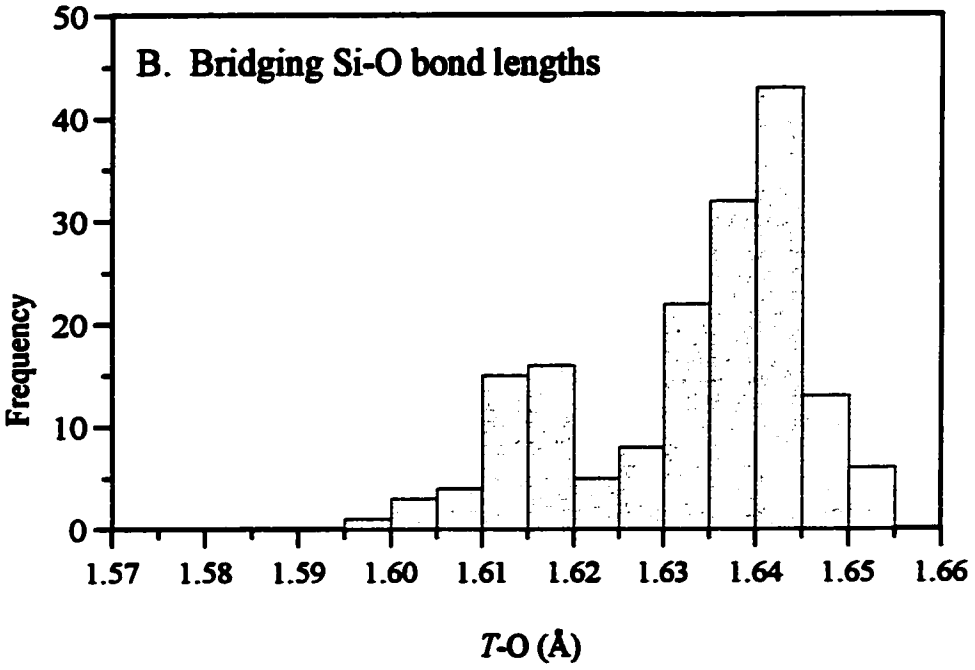

Figure 29. Continued.
B: Bridging Si-O bonds (Å)

1969, Liebau 1985). Similarly, O-Si-O bond angles should decrease in magnitude such that O_{nb}-Si-O_{nb} > O_{br}-Si-O_{nb} (Liebau 1985). In AGM, O-Si-O bond angles range from 104.8 to 112.3°, yet the trend deviates slightly from that expected because the $D\phi_6$ octahedron has characteristics more similar to that of a SiO_4 tetrahedron (*i.e.* part of the anionic framework) compared to the octahedra of the *O*-sheet; O_{nb}-Si-O_{br} bond angles which include anions of the $D\phi_6$ octahedron are similar in magnitude to O_{br}-Si-O_{br} bonds angles. Five distinct populations of O-Si-O bond angles are observed, decreasing magnitude in the order I > II > III > IV > VI (Fig. 30,Table 5B and 5C):

I. O_{nb}-Si-O_{nb}, where O_{nb} are from the *O*-sheet and $D\phi_6$ only [*e.g.* O(1)-Si(1)-O(15)],

II. O_{nb}-Si-O_{br}, where O_{nb} is from the *O*-sheet only [*e.g.* O(1)-Si(1)-O(13)],

III. O_{nb}-Si-O_{nb}, where O_{nb} are from the $D\phi_6$ octahedron [*e.g.* O(11)-Si(1)-O(15)],

IV. O_{br}-Si-O_{br} [*e.g.* O(8)-Si(3)-O(10)],

V. O_{br}-Si-O_{nb}, where O_{nb} is from the $D\phi_6$ octahedron [*e.g.* O(13)-Si(1)-O(11)].

A similar trend is observed with *T*-O-(*T*,*D*,*M*) bond angles. *T*-O-*M* angles (where *M* = *O*-sheet cation) are characteristically smaller than Si-O-Si angles, a result once again of the greater repulsion of Si atoms compared to that of larger, lower valence *M* cations such as Mn^{2+} or Fe^{2+} (Liebau 1985). *T*-O-*M* angles in AGM range from 117.4 to 124.3° (ave.: 121.1°), significantly smaller than the *T*-O-*T* angles which range from 138.1 to 144.4°, with an average, 141.1°, close to the ideal angle of 139° for a strain-free Si-O-Si bond (Liebau 1985; Fig. 31). Two populations of *T*-O-*T* bond angles are observed: (1) those of the main tetrahedral chain, *T*(2)-O-*T*(3), with an average value of ≈ 139°, and (2) those of tetrahedra on the branches of the chain, *T*(1)-O-*T*(2) and *T*(3)-O-*T*(4), with a slightly higher average

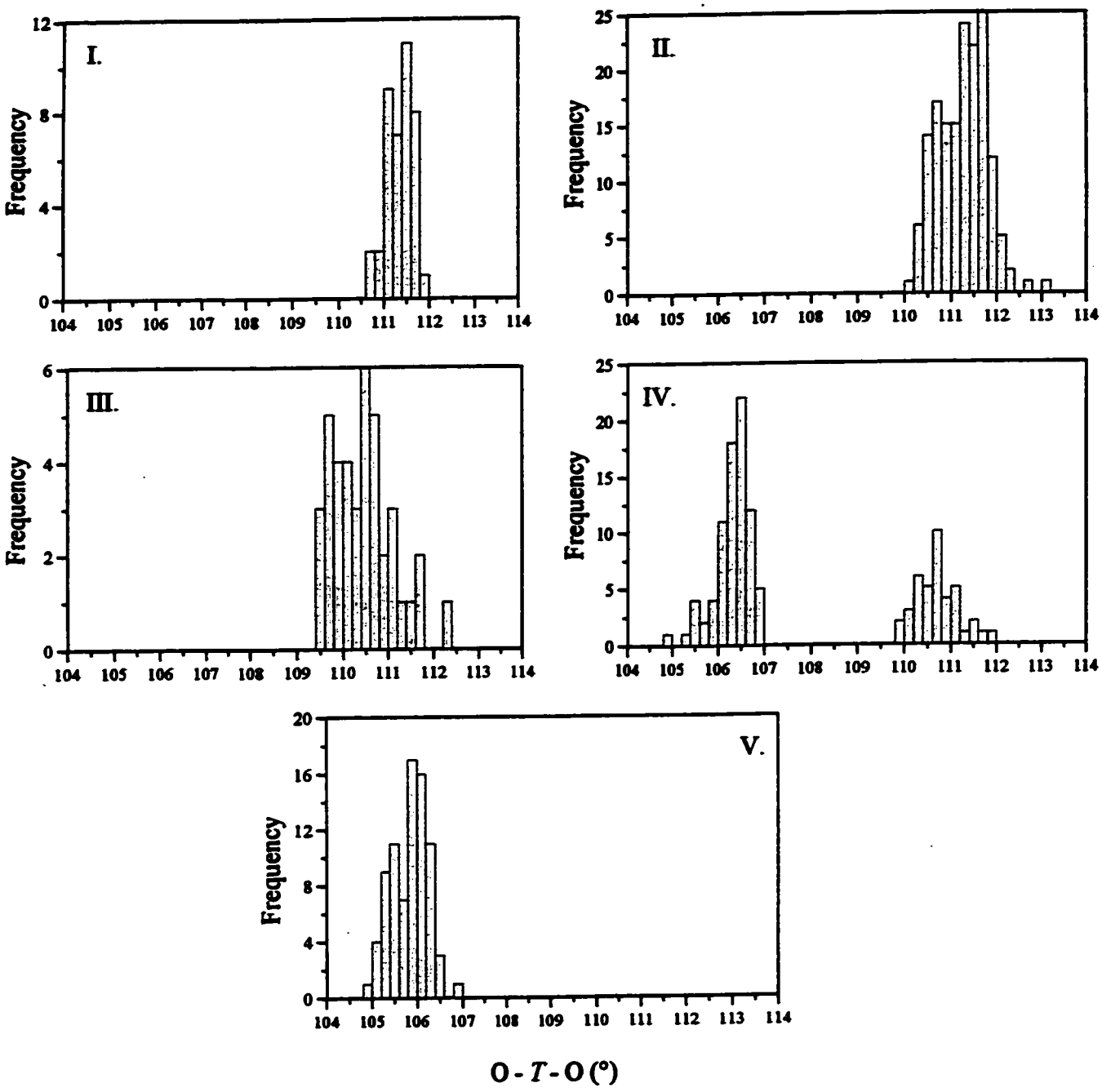

Figure 30. Distribution of O-*T*-O bond angles. Five subgroups of bond angles exist in AGM:

I. O_{nb}-Si-O_{nb}: O_{nb} from the *O*-sheet and *D*
II. O_{nb}-Si-Obr: O_{nb} from *O*-sheet, O_{br}
III. O_{nb}-Si-O_{nb}: O_{nb} from *D* only
IV. O_{br}-Si-Obr: O_{br} only
V. O_{nb}-Si-O_{br}: O_{nb} from *D*, O_{br}

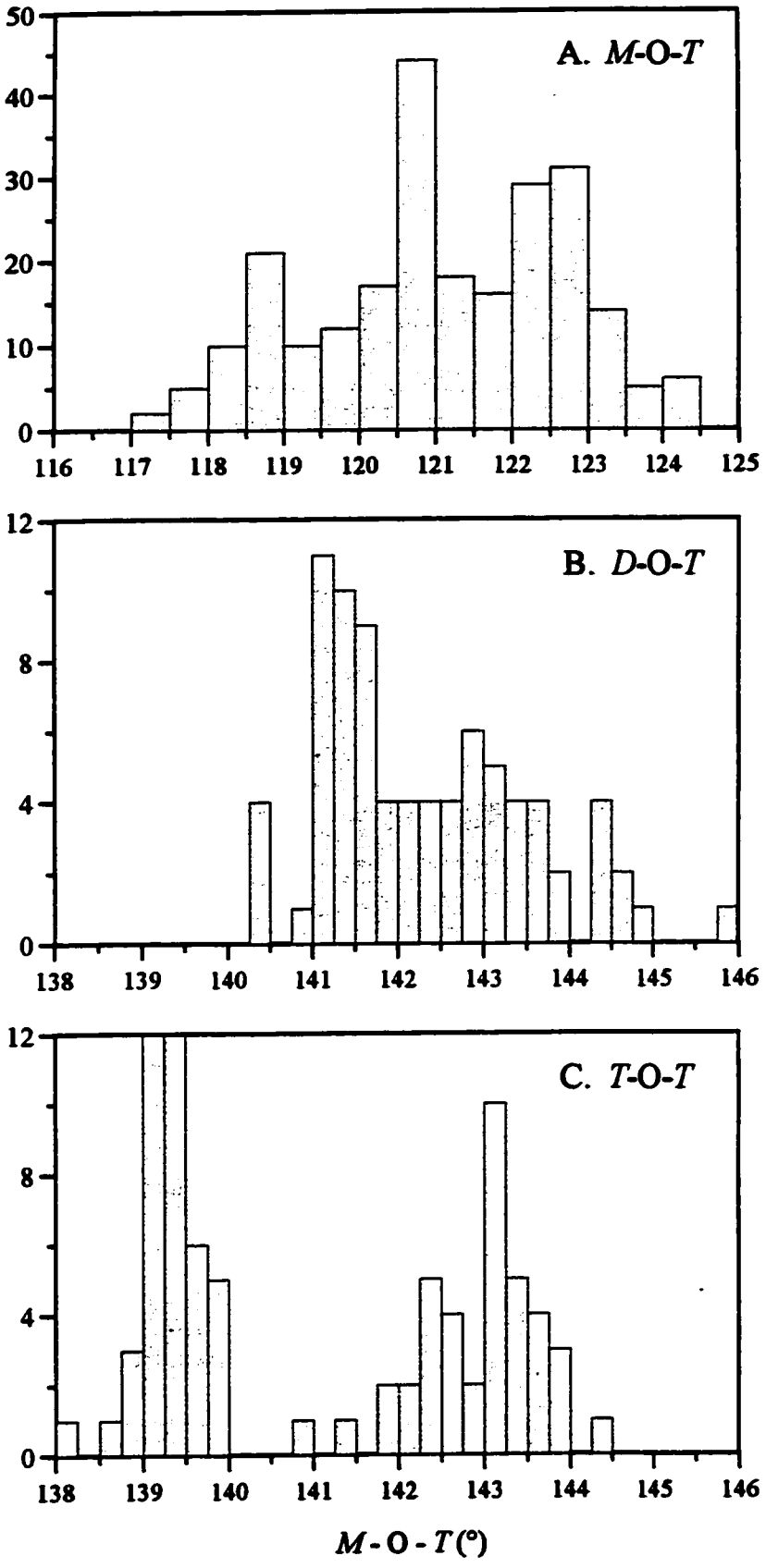

Figure 31. Distribution of *M*-O-Si bond angles:
A: *M*-O-*T*, B: *D*-O-*T*, *C*: *T*-O-*T*

value of 143° (Fig. 31), suggesting slightly increased strain on the *T*(1) and *T*(4) tetrahedra. *T*-O-*D* linkages show a range of bond angles between 140.3 and 145.9° (ave.: 142.3°), comparable to *T*-O-*T* linkages between tetrahedra of the main chain [*T*(2) & T(3)] and the outer branches [*T*(1) & *T*(4)]. Again, it is shown that the $D\phi_6$ octahedron shares close affinities with SiO_4 tetrahedra and not with octahedra normally considered to be part of the cationic structure (*i.e.* the *O*-sheet).

Large differences in basal bond lengths are observed in the *T*(1) and *T*(4) tetrahedra due to (1) displacement of the *T* cation toward the $D\phi_6$ octahedron, and (2) tilting of the tetrahedra out of the (001) plane. As a result, *T*(1)-O(13) and *T*(4)-O(14) are the longest *T*-O bonds observed in the structure (range: 1.607 to 1.649 Å, average: 1.640 and 1.633 Å, respectively). In order to maintain a mean bond order of ≈ 1.5 in the tetrahedron and a BVS for the Si of ≈ 4.00 *v.u*, an increase in a particular bond length in the tetrahedron must be accompanied by a decrease in length of the remaining bonds (Robinson 1963). Subsequently, *T*(1)-O(11,15) and *T*(4)-O(9,12) are extremely short, ranging from 1.585 to 1.615 with an average of 1.603 Å, 0.017 Å shorter than the ideal Si-O bond length of 1.62 Å (Liebau 1985). *T*(1) and *T*(4) are, on average, the most distorted tetrahedra in the AGM structure ($\Delta T(1)_{ave}$: 1.045, $\Delta T(4)_{ave}$: 0.773). Shortening of these bonds may also be the result of a displacement of the Si cation due to tilting of the *T*(1) and *T*(4) tetrahedra toward the $D\phi_6$ octahedron. Similarly, *T*(2)-O(13) and *T*(3)-O(14) bonds are also short (average: 1.614 and 1.615 Å, respectively) to maintain a BVS of 2.00 *v.u.* at the bridging oxygens O(13) and O(14).

6.0. Lateral Fit of the *H*-and *O*-Sheets

There is a mismatch in size between the *O*- and *H*-sheets, similar to that observed between the tetrahedral (*T*) sheets and *O*-sheets in other 2:1 phyllosilicates (Bailey 1984). In true micas, the lateral dimensions of the *T*-sheet are larger than those of the adjacent *O*-sheets. The mismatch between the *T*- and *O*-sheets is compensated by the rotation, tilting and elongation of the tetrahedra, along with flattening and rotation of the octahedra. In AGM, a similar response is observed. However, the composition of the *O*-sheet in AGM is quite different than that of a mica; specifically, it is dominated by larger Mn^{2+} cations ($r^{[6]}Mn^{2+}$: 0.83 Å) rather than smaller cations such as Fe^{2+} (0.78 Å), Mg (0.72 Å) and Al (0.54 Å; ionic radii from Shannon 1976). Similarly, the presence of the $D\phi_6$ octahedron in the *H*-sheet results in a larger *H*-sheet than in mica *T*-sheets. As a result, the methods by which the AGM structure adapts to the mismatch are slightly different than observed in 2:1 phyllosilicates. The dominant mechanisms by which *H*-*O*-sheet lateral fit occurs are: (1) trigonal distortion of the *O*-sheet octahedra, namely isometric flattening and counter-rotation and (2) rotation, tilting and elongation of tetrahedra in the *H*- and *T*-sheets.

Isometric flattening of the octahedra is one of the primary ways by which the lateral dimensions of *O*-sheet increase. Flattening angles in the *O*-sheet octahedra range from 58.4 to 59.7°, similar to other 2:1 phyllosilicates which commonly have Ψ values which range from 58 to 61° (Bailey 1984). Flattening angles in AGM are most similar to those in Fe^{2+}-bearing samples of the biotite series (58 to 59°), a result of their similarity in *O*-sheet chemistry, rather than Al- and Mg-bearing species such as muscovite and phlogopite ($\Psi = 60$

to 61°; Bailey 1984). Flattening of octahedra in the AGM *O*-sheet is dependent on the size of the *M* cation such that increased r*M* results in decreased octahedral flattening (Fig. 32). In AGM, the increase in r*M* is due to increased Mn $\Leftrightarrow$ Fe^{2+} substitution (closed diamonds, Fig. 32) whereas in members of the biotite series, the dominant substitution is Fe^{2+} $\Leftrightarrow$ Mg (open circles, Fig. 32; Shabani 1999). The larger Ψ angles in AGM compared to those of the biotite series, which have substantially smaller values for r*M*, are due to the larger dimensions of the *H*-sheet to which the *O*-sheet must attach. As will be discussed in detail in Chapter IV, octahedral flattening in AGM is further complicated by the presence of the $D\phi_6$ octahedron within the *H*-sheet. The apical O(2) oxygen of the $D\phi_6$ octahedron is bonded to three octahedra within the *O*-sheet, *M*(1), *M*(2) and *M*(3). Bond lengths to O(2) from *M*(2) and *M*(3) are the longest observed in the *O*-sheet due to elongation of the *M*-O(2) bonds, a response to the presence of Nb or Zr at *D* in order to satisfy bond-valence requirements at the O(2) oxygen [*M*(2)-O(2): 2.230 to 2.267 Å, *M*(3)-O(2): 2.209 to 2.246 Å). Conversely, *M*(1)-O(2) bond lengths are short (range: 2.137 to 2.189 Å). This lengthening and shortening of *M*-O(2) bonds results in a corrugated appearance of the *O*-sheet around O(2) and the $D\phi_6$ octahedron.

Reduction in the lateral dimensions of the *H*-sheet occurs by rotation of adjacent tetrahedra in opposite directions in the (001) plane. In an ideal six-membered SiO_4 tetrahedral ring, the angle O_{br}-O_{br}-O_{br} of the basal oxygens is 120°; deviation from this value is the result of tetrahedral rotation (α). Rotational angles in true micas range from 1.4 to 11.0° in trioctahedral species, and from 6.0 to 19.1° in dioctahedral species (Bailey 1984). In AGM, O_{br}-O_{br}-O_{br} angles range from 114.76 to 125.64°, with an average of 119.6°, close to

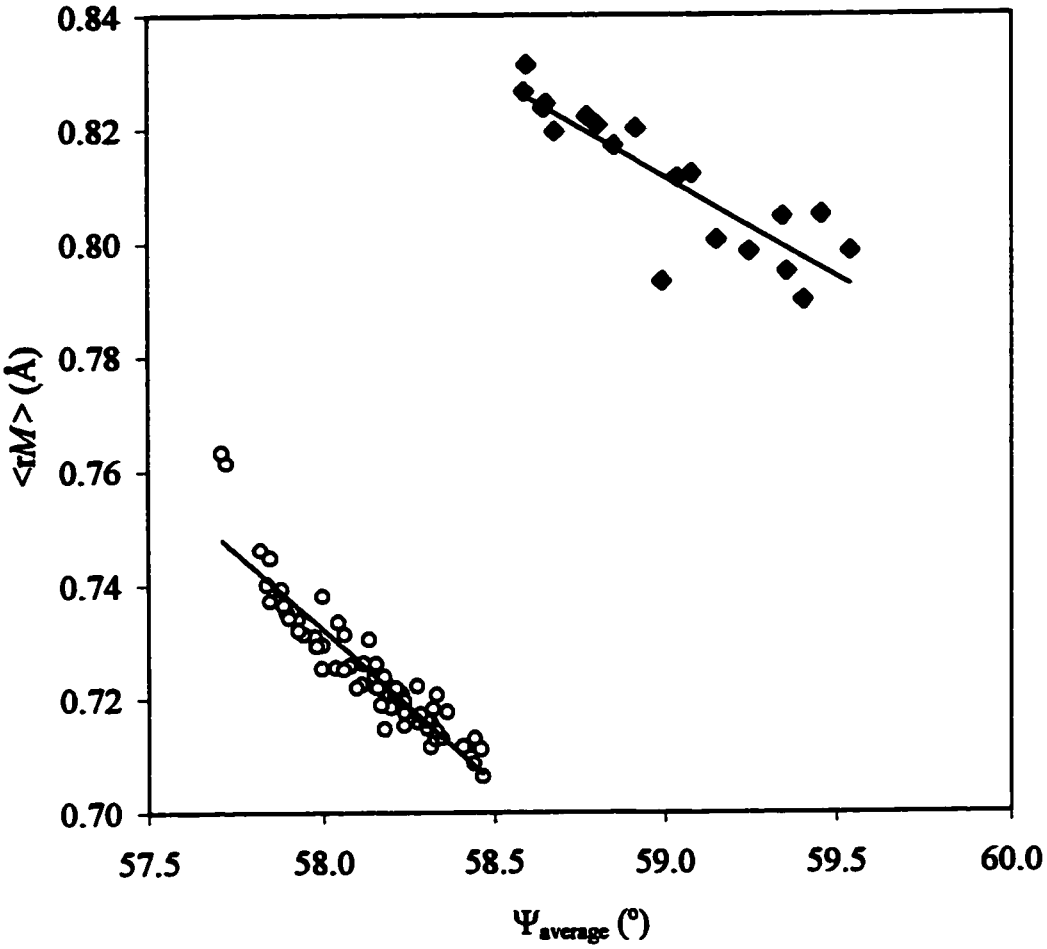

Figure 32. Average octahedral flattening ($\Psi_{average}$) of the *O*-sheet *versus* the average ionic radius (r*M*) in AGM (closed diamonds) and members of the biotite series (open circles; Shabani 1999).
AGM. Linear regression: $R^2 = 0.753$
Biotite. Linear regression: $R^2 = 0.869$

the ideal 120°, and tetrahedral rotation angles (α) range from 0 to 2.82° (average: 1.24°). Figure 33 shows the relative rotation of the tetrahedra in the *H*-sheet. As with micas, rotation of adjacent tetrahedra in AGM is in opposite directions. The α values in AGM are insignificant in terms of altering the lateral dimensions of the *H*-sheet in order to compensate for the misfit with the *O*-sheet. As such, another mechanism must compensate for ideal sheet mismatch.

Isometric flattening and counter-rotation of the *O*-sheet octahedra results in elongation of the octahedral edges in an attempt to compensate for the mismatch between the *O*- and *H*-sheets. In order for the lateral dimensions of the *H*-sheet to match these elongated edges, the tetrahedra are thickened along [001] by elongation of Si-O_{apical} bond lengths and widening of O_{apical}-Si-O_{basal} bond angles, and are tilted out of the (001) plane. The ideal tetrahedral angle, τ = O_{apical}-Si-O_{basal}, is 109.47° which can be increased by elongation and decreased by shortening of Si-O_{apical} bonds (Bailey 1984). In AGM, τ angles range from 110.8 to 111.8°, indicating $\approx$ 2% thickening of the tetrahedra in the [001] direction, comparable to that observed in true micas (which have τ angles ranging from 108 to 114°, Bailey 1984). The *T*(1) and *T*(4) tetrahedra show increased thickening (average: 111.76 and 111.79°, respectively) compared to *T*(2) and *T*(3) (average: 111.34 and 111.65°, respectively), the result of increased tilting out of the (001) plane of the *T*(1) and *T*(4) tetrahedra (discussed below).

The main mechanism by which lateral misfit of the sheets in AGM is reduced is by tilting of the tetrahedra out of the (001) plane. Tilting of the *T*(1) and *T*(4) tetrahedra brings the apices of the tetrahedra towards the O(2) apex of the $D\phi_6$ octahedron whereas *T*(2) and

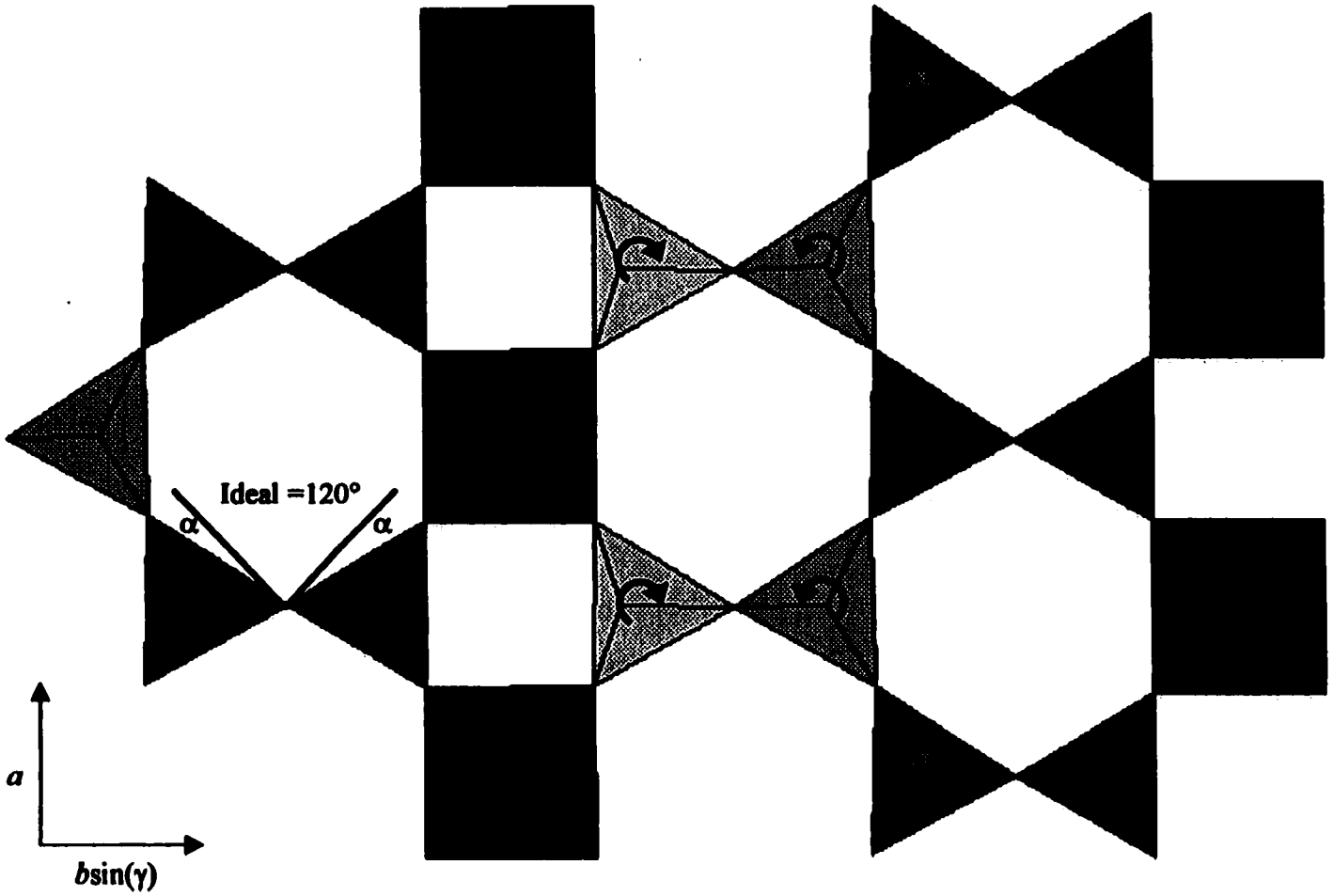

Figure 33. Tetrahedral rotation (arrows) in the *H*-sheet. The ideal O_{br}-O_{br}-O_{br} angle is 120 ° (exaggerated in order to show α angles). Tetrahedral rotation angles (α) range from 0 to 2.82 ° (average: 1.24 °). Dark grey: *D*. Tetrahedra are shaded from dark grey [*T*(1)] to light grey [*T*(4)].

T(3) are tilted in opposite directions, towards each other and the main SiO_4 chain of the *H*-sheet. The presence of the larger $D\phi_6$ octahedra results in increased thickening of the *T*(1) and *T*(4) tetrahedra (as discussed above) and increased tilting; *T*(1) and *T*(4) are tilted a substantial amount more out of the (001) plane (average: 6.80 and 7.09°, respectively) than *T*(2) and *T*(3) (average: 2.06 and 0.87°, respectively), adding to the strongly corrugated appearance of the *HOH* layers.

7.0. Conclusions

The complex chemical compositions exhibited by members of the astrophyllite group results in a wide range of structural variations. The relations between composition and crystal structure are summarized here:

1. Members of the astrophyllite group are heterophyllosilicates and are the intermediate members of a polysomatic (or homologous) series with perraultite and mica as the end-member structures. The AGM structure consists of two composite sheets stacked along [001] in a 2:1 ratio resulting in a layered *HOH* structure.

2. The interlayer in triclinic AGM consists of two crystallographically distinct cation sites, *A* and *B*, whereas three distinct sites occur in kupletskite-*Ma2b2c*, *A*(1), *A*(2) and *B*. The $^{[13]}A$ site(s) contains predominantly K, with minor substitution of Rb, Cs and Na and up to 15% vacancies. In many cases, the *A* site is positionally disordered and there is smearing of electron density in the (001) plane. In such cases, *A* was modeled as a split site and refined isotropically. The $^{[10]}B$ site is host to predominantly Na with up to 40% occupancy by Ca.

3. The *O*-sheet (octahedral sheet) consists of four crystallographically distinct MO_6 octahedra, designated *M*(1) through *M*(4), in a 2:2:2:1 ratio, respectively, and contain Mn, Fe^{2+}, Fe^{3+}, Na, Mg and Zn as the principal cations. The *M*(1) octahedron is the largest, least distorted within the *O*-sheet and contains significant $^{[6]}$Na. Manganese is thought to order at *M*(1). The *M*(2) octahedra are highly distorted and form zig-zag chains parallel to *X*. The *M*(2) and *M*(3) sites form a composite chain parallel to *X* and are occupied by Mn, Fe^{2+}, Fe^{3+}, Mg and Zn.

4. The *H*-sheet (heterogeneous sheet) has the ideal composition $[(Ti,Nb,Zr)Si_4O_{12}]^{4-}$ and consists of open-branched *zweier* [100] single chains of $[Si_4O_{12}]^{8-}$ which are cross-linked by corner-sharing $D\phi_6$ octahedra in triclinic species and kupletskite-*Ma2b2c*, and DO_5 polyhedra in magnesium astrophyllite where *D* = Nb,Ti,Zr. Substitution of Nb for Ti at *D* results in lengthening of the *D*-O(2) bond, shortening of the *D*-ϕ(16) bond, and positional displacement of the *D* cation towards the center of the octahedron, with an overall decrease in the distortion index, Δ. Substitution of Zr for Ti at *D* results in an increase in all *D*-ϕ bond lengths and a simultaneous decrease in Δ. Crystallographic restrictions limit the maximum Zr content in AGM to approximately one *apfu* (50% occupancy of *D*).

5. There are four tetrahedrally-coordinated sites in the AGM structure, designated *T*(1) through *T*(4). All four sites contain dominantly Si with only minor substitution of Al. *T*(1) and *T*(4) are located on the branches of the *zweier* single chains and share oxygens with the $D\phi_6$ octahedron whereas *T*(2) and *T*(3) are located in the central portion of the chain and share only apical oxygens with the *O*-sheet.

6. There is a lateral misfit between the *H*- and *O*-sheets, similar to that observed in 2:1 phyllosilicates. Lateral misfit increases with increasing Mn ⇔ Fe and Zr ⇔ (Ti,Nb) substitution. *H-O*-sheet lateral fit in the AGM structure occurs predominantly by tilting of the tetrahedra out of the (001) plane, thickening or elongation of the tetrahedra along [001], and flattening of the *O*-sheet octahedra.

CHAPTER IV.

ASTROPHYLLITE GROUP MINERALS III. ^{57}Fe MÖSSBAUER SPECTROSCOPY

1.0. INTRODUCTION TO MÖSSBAUER SPECTROSCOPY

Mössbauer spectroscopy is a nuclear absorption spectroscopy that allows for precise measurement of the hyperfine structure of nuclear levels of a probe nucleus. This structure is the result of hyperfine interactions (interactions between the nucleus and its electronic environment) produced by transitions between the ground and excited states of a specific probe isotope. The most commonly used probe isotope, and that which is used in this study, is ^{57}Fe with a transition energy of 14.4 keV.

In materials with strong bonds between atoms such as liquids and solids, Mössbauer spectroscopy is made possible by a phenomenon known as the Mössbauer effect (Mössbauer 1958). When a sample is bombarded by incident gamma (γ)-ray radiation, nuclear transitions will take place at resonant energies. A certain fraction of the energy emission and absorption events are recoilless and the associated kinetic energy is therefore negligible. This fraction, f, is known as the Mössbauer recoilless fraction (Rancourt 1998) and can be defined as

$$f = \exp[-E_r\langle x^2\rangle/\hbar c] \quad (1)$$

where E_r is the recoil energy of the free nucleus and $\langle x^2\rangle$ is the mean square displacement of the Mössbauer probe nucleus. Only recoilless events will contribute to the Mössbauer spectrum and will thus be measured.

The ^{57}Fe probe isotope has a ground state, I = 1/2, and a first excited state, I = 3/2. There are three hyperfine interactions which will cause splitting of these nuclear energy

levels: the electric monopole interaction, the electric quadrupole or electric field gradient (EFG) interaction, and the magnetic dipole or hyperfine field interaction (Rancourt 1998).

The isomer shift (IS) is the result of an electric monopole interaction and is an extremely sensitive measure of the local electronic density; it is therefore a measure of the valence state of the probe nucleus. Mössbauer spectroscopy allows for the determination of the actual measured resonance position, the center shift (CS or δ) which is a linear combination of the IS and a second order Doppler shift (SOD, Rancourt 1998):

$$CS = IS + SOD \quad (2).$$

The interaction between the electric quadrupole moment of the nucleus and the local EFG results in symmetrical splitting of the first excited state into two sublevels, $I = \pm 3/2$ and $I = \pm 1/2$. In the Mössbauer spectrum, two absorption peaks are now evident, the splitting between which is called the quadrupole splitting (QS or Δ), equal to the energy splitting between the two sublevels. The QS (Rancourt 1998) is given by:

$$\Delta = (e^2qQ/2)[1+\eta^2/3]^{1/2} \quad (3)$$

where e is the electron charge, q, or V_{zz}, is the maximum electric field gradient, Q is the nuclear quadrupole moment, and Δ is given in mm/s. The local EFG has a strong relation to the symmetry of the cation site and local structure. The QS is a sensitive indicator of the coordination of the Fe and of local crystal-chemical variations around the site in question (Rancourt 1998). Within a given structure, changes in the local environment around the Fe atom result in a range in QS values, and thus a quadrupole splitting distribution (QSD).

2.0. PURPOSE OF THE STUDY

Until recently, Fe^{3+} was thought a minor component in AGM, a conclusion based primarily on wet-chemical determinations (MacDonald & Saunders 1973) or by calculation of Fe^{2+}/Fe^{3+} ratios from electron microprobe data. Varying anionic schemes and the presence of vacancies complicates the calculation of Fe^{2+}/Fe^{3+} ratios in AGM. Iron-bearing mineral inclusions are common in AGM (*e.g.* pyrochlore group minerals, oxides and phosphates) which also limit the possibility of obtaining reliable Fe^{2+}/Fe^{3+} ratios by wet-chemical methods yet yield Mössbauer spectra which are significantly different from those observed for AGM. Mössbauer spectroscopy has been used extensively to obtain accurate and precise site populations for Fe^{2+} and Fe^{3+} in a variety of silicate minerals including members of the mica group (*e.g.* Dyar & Burns 1986, Rancourt *et al.* 1992, Rancourt *et al.* 1994, Redhammer *et al.* 1995, Lalonde *et al.* 1996, Rancourt *et al.* 1996, Shabani 1999), clinopyroxenes (*e.g.* Annersten & Nyambok 1980, Piilonen *et al.* 1998), and amphiboles (*e.g.* Bancroft & Burns 1969, Bancroft & Brown 1975). This study represents the first of its kind for AGM. The Fe^{2+}/Fe^{3+} ratio, a direct measure of the prevailing oxygen fugacity at the time of crystallization of the sample, will be used to elucidate the paragenesis of AGM of varying chemical compositions and from different rock types. The measured Fe^{3+} contents will also be used to develop substitutional schemes (discussed in Chapter II).

The Mössbauer spectra and associated parameters for AGM are described in detail. Given the correct method for extraction of the complex set of hyperfine parameters that are contained in a Mössbauer spectrum, Mössbauer spectroscopy is also a powerful tool for

probing the local environments around Fe atoms. Not only can information regarding coordination number be gained, but spectral information may be helpful in evaluating crystallographic distortions, local chemical disorder, spin structure and magnetic moment magnitudes. New methods developed for extraction of quadrupole splitting distributions (QSDs, *e.g.* Rancourt 1989, Rancourt & Ping 1991, Rancourt 1994a, Rancourt 1994b, Rancourt *et al.* 1994) have allowed true intrinsic QSDs to be extracted from Mössbauer spectra. This allows for detailed comparisons of local distortion and chemical environments that cannot be obtained by other methods. To date, such detailed studies have been done on a synthetic annite-oxyannite series (Christie *et al.* 1993), synthetic and natural members of the phlogopite-annite series (Rancourt *et al.* 1994, Redhammer *et al.* 1995), synthetic members of the (OH,F)-annite series (Rancourt *et al.* 1996), and a large suite of biotites (Shabani 1999). Recent advances in the theoretical derivation of EFG and QS distributions and their relations to crystal chemical parameters such as octahedral flattening and counter rotation (Evans 2001), coupled with extensive data from single-crystal X-ray refinements, will allow us in the future to attempt to correlate crystal chemical and Mössbauer spectral parameters for AGM.

3.0. Experimental Methods

3.1. Sample selection

The samples studied by Mössbauer spectroscopy were chosen from both over- and undersaturated alkaline complexes, and span a wide a range of chemical composition. The sample suite in this study includes astrophyllite, kupletskite and niobokupletskite from Mont

Saint-Hilaire (Québec), the Khibina massif (Kola peninsula, Russia), Mount Rosa (Pikes Peak batholith, Colorado), the Oslo rift valley, Langesundsfjord area (Norway), and Kræmer Island and Bagnæsset, Kangerdlugssuaq intrusion (Greenland). Table 1 lists the sample provenance and species. An attempt was made to choose compositionally homogeneous samples. However, kupletskite samples from Mont Saint-Hilaire (MSH) commonly display complex diffuse and concentric chemical zoning (< 20 μm) that could not be avoided. Results therefore represent an average of these zones. All were separated by hand under a binocular microscope to ensure a sample purity of >98%. Samples were cleaved to very thin flakes and examined under intense light to ensure that no other minerals were present as inclusions. Special care was taken to avoid portions of samples that displayed alteration or oxidation which could adversely affect the resultant Fe^{2+}/Fe^{3+} ratios.

3.2. Preparation of Mössbauer absorbers and data collection

Absorbers for Mössbauer spectroscopy were prepared with an ideal mass of sample ($\approx$ 50 mg), calculated for our 0.5 inch diameter holders using the technique developed by Rancourt *et al.* (1993) to ensure the maximum signal-to-noise ratio. The sample was crushed in acetone to minimize oxidation by atmospheric oxygen and the powdered material suspended in petroleum jelly and stirred to ensure a random orientation of crystals within a circular aluminum mount (aperture: 0.5 inch, thickness: 0.6 cm). Detailed information pertaining to sample preparation and data collection can be found in Appendix D. The spectra were obtained using a ^{57}Co (in a rhodium matrix) single-line thin source at room temperature (RT = 21 to 22 °C). The transducer was employed in constant-acceleration mode

TABLE 1. LOCALITY INFORMATION FOR ASTROPHYLLITE GROUP MINERALS STUDIED BY ^{57}FE MÖSSBAUER SPECTROSCOPY

Sample code	Sample (Collection) #	Locality and rock type
GREEN		Greenland
	CC2A	- syenite pegmatite (Kræmer Island, Kangerdlugssuaq)
	CC7A	- nepheline syenite pegmatite (Bagnæsset, Kangerdlugssuaq)
KHIB		Khibina massif, Kola Peninsula, Russia
	RUS4 (CMNMI-53187)	- nepheline syenite pegmatite
	RUS5 (CMNMI-44295)	- nepheline syenite pegmatite
	RUS7 (CMNMC)	- nepheline syenite pegmatite
	RUS8 (FMM-1)	- nepheline syenite pegmatite
LANG		Langesundsfjord area, Oslo Rift Valley, Norway
	NOR1 (RW-1)	- nepheline syenite pegmatite (Vesle Arøya)
	NOR9 (AOL2b)	- nepheline syenite pegmatite (Barkevikskjær)
MSH		Mont Saint-Hilaire, Québec, Canada
	MSH6 (NMNS-8)	- nepheline syenite pegmatite
	MSH7 (NMNS-11)	- nepheline syenite pegmatite
	MSH10AB (NMNS-14)	- nepheline syenite pegmatite
	MSH11 (NMNS-15)	- nepheline syenite pegmatite
	MSH15 (NMNS-22)	- nepheline syenite pegmatite
	MSH18A (NMNS-25)	- altered nepheline syenite pegmatite
	MSH26AB (CMNMC)	- sodalite syenite
	MSH28 (CMNMC)	- metasomatic unit
	MSH32 (CMNMC)	- natrolite pegmatite
	MSH33 (CMNMC)	- aplite/pegmatite
	MSH34A (CMNMC)	- nepheline syenite pegmatite
	MSH35 (CMNMC)	- aplite/pegmatite
PP		Mount Rosa, Pikes Peak, Colorado, USA
	US2 (CMNMI-29977)	- granitic pegmatite
	US5 (CMNMC)	- granitic pegmatite

CMNMC/CMNMI/NMNS = Canadian Museum of Nature collection, FMM = Fersman Mineralogical Museum collection, AOL = A.O. Larsen collection, CC = C.C. Christiansen collection, RW = R. Werner collection.

over a Doppler velocity range of ±4.0 mm/s. Spectra were calibrated with an ^{57}Fe-enriched iron foil at RT. Data were collected in 1024 channels and folded to obtain a flat background and a zero velocity position corresponding to the CS (δ) of metallic α-Fe at RT in the resultant 512-channel calibrated spectra. All spectra were corrected for thickness effects, assuming an absorber Mössbauer recoilless fraction of 0.7. By applying full thickness corrections to the spectra by the method outlined by Rancourt (1989), as implemented in the program Recoil (Lagarec & Rancourt 1998), it is possible to obtain the intrinsic absorber resonance cross-section and further, to generate a thin-limit spectrum. This thin-limit spectrum is representative of what would be observed with an ideally thin absorber. Spectra were fitted using the Voigt-based quadrupole splitting distribution (QSD) method of Rancourt & Ping (1991) as implemented in the program Recoil (Lagarec & Rancourt 1998). This method assumes that the QSD for each generalized site within the spectrum is composed of a number (N) of Gaussian components. The corresponding lineshape in the fit is therefore neither Gaussian nor Lorentzian but a sum of Voigt lines. The Lorentzian linewidth (Γ) is assumed to be the same for each of the spectral contributions and has been fixed at the natural width of 0.097 mm/s (Rancourt 1994). This allows for QSDs from different samples to be compared directly. All broadening of the spectral lines is therefore assumed to be due to the additional physical process known as inhomogeneous broadening. The continuous valence-state specific QSDs obtained are the result of variations in the local environment around the probe nucleus caused by local distortions or atomic disorder. It should be noted that the number of Gaussian components chosen is based on statistics and the individual components do not have particular physical or crystal-chemical meaning. They are

mathematical entities used to ensure that the true QSD of the spectral contribution is well represented by the sum of Gaussians.

During initial collection of the spectra, it was evident that a strong textural problem was present in the majority of the absorbers. This is due to the fact that AGM have not only an excellent {001} cleavage, but also a parting along {010} which enhances the formation of acicular to tabular crystals, thus significantly increasing the possibility of texture effects. The spectral area ratio is given by the parameter A-/A+, where A- and A+ are the spectral areas of the low- and high-energy peaks of the doublet, respectively. In an ideal, randomly oriented absorber, the spectral areas of the low and high energy peaks of each doublet are equal, A-/A+ = 1 and is subsequently not refined. Non-randomness or texture in the absorber results in an asymmetry in spectral area between the two peaks of the doublet which can also result in errors in measured Fe^{2+}/Fe^{3+} ratios and extracted QSDs. It is therefore necessary to model these texture effects by allowing the individual Lorentzian doublets to have refineable site-specific asymmetries (Fig. 1). As there is trade-off between the A-/A+ parameters for Fe^{2+} and Fe^{3+}, only that for Fe^{2+} was allowed to be variable, whereas for the minor Fe^{3+} component, A-/A+ was fixed at unity. Ferrous iron A-/A+ values for AGM range from 1.0 (not refined) to 1.294 (highly acicular crystals), indicating up to 30% greater spectral area in the low energy peak of the doublet as compared to that of the high energy peak.

In an attempt to reduce the effects of texture, select absorbers were restirred and data collected once again under identical conditions. In most cases (*i.e.* > 95%), preferred orientation effects could not be eliminated simply by restirring the absorber. Results presented in this study therefore include refinement of the A-/A+ parameter. The concern in

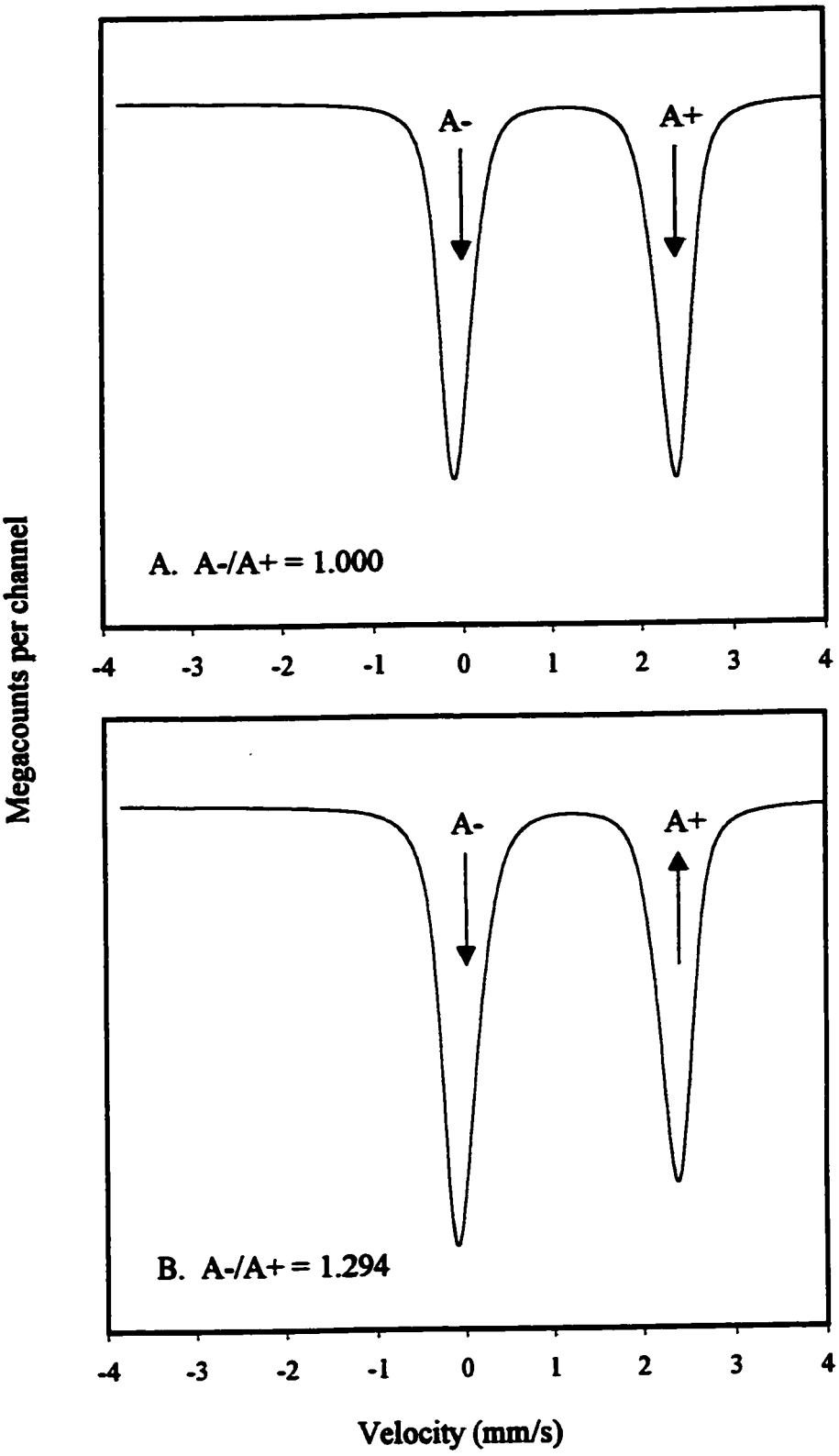

Figure 1. Effects of non-randomness in the absorber on astrophyllite group mineral Mössbauer spectra (MSH10B)

A. Random absorber: A-/A+ = 1.000

B. Textured absorber: A-/A+ = 1.294

refinement of this parameter is its effect on the resultant spectral parameters and the Fe^{2+}/Fe^{3+} ratios. For only one sample (MSH10B) did this procedure result in a reduction of the A-/A+ parameter from 1.214 to an ideal 1.000 (Fig. 2). Comparison of the Fe^{3+}/Fe_{tot} ratios between these two spectra indicate values which are statistically identical: 0.19(1) and 0.21(1) for textured and random absorbers, respectively. Similarly, Rancourt *et al.* (1994b) have shown that allowing the asymmetry parameter to be fitted in spectra with minor, often unavoidable texture (~5 - 10%) results in QSDs which are indistinguishable from those obtained with non-textured absorbers. In order to further evaluate the effects of preferred orientation (with respect to the γ-ray flux) on the spectrum and to justify the decision to refine A-/A+, an oriented mosaic was prepared and a detailed study undertaken.

4.0. The Oriented Mosaic

In order to evaluate the effects of preferred orientation on the Mössbauer spectrum of AGM, an oriented mosaic of cleaved grains was prepared. The sample chosen was a well-characterized Nb-rich kupletskite from a pegmatite dike at Mont Saint-Hilaire, Québec (MSH10A).

4.1. Experimental methods

The mosaic was prepared using an ideal mass for a one inch square absorber (107.5 mg). The inclusion-free sample was cleaved on {001}, affixed to tape, and centered on a goniometer head capable of 360° rotation perpendicular (θ angle) and parallel (ϕ angle) to the γ-ray flux (Fig. 3). The goniometer apparatus was set in front of the detector at a fixed

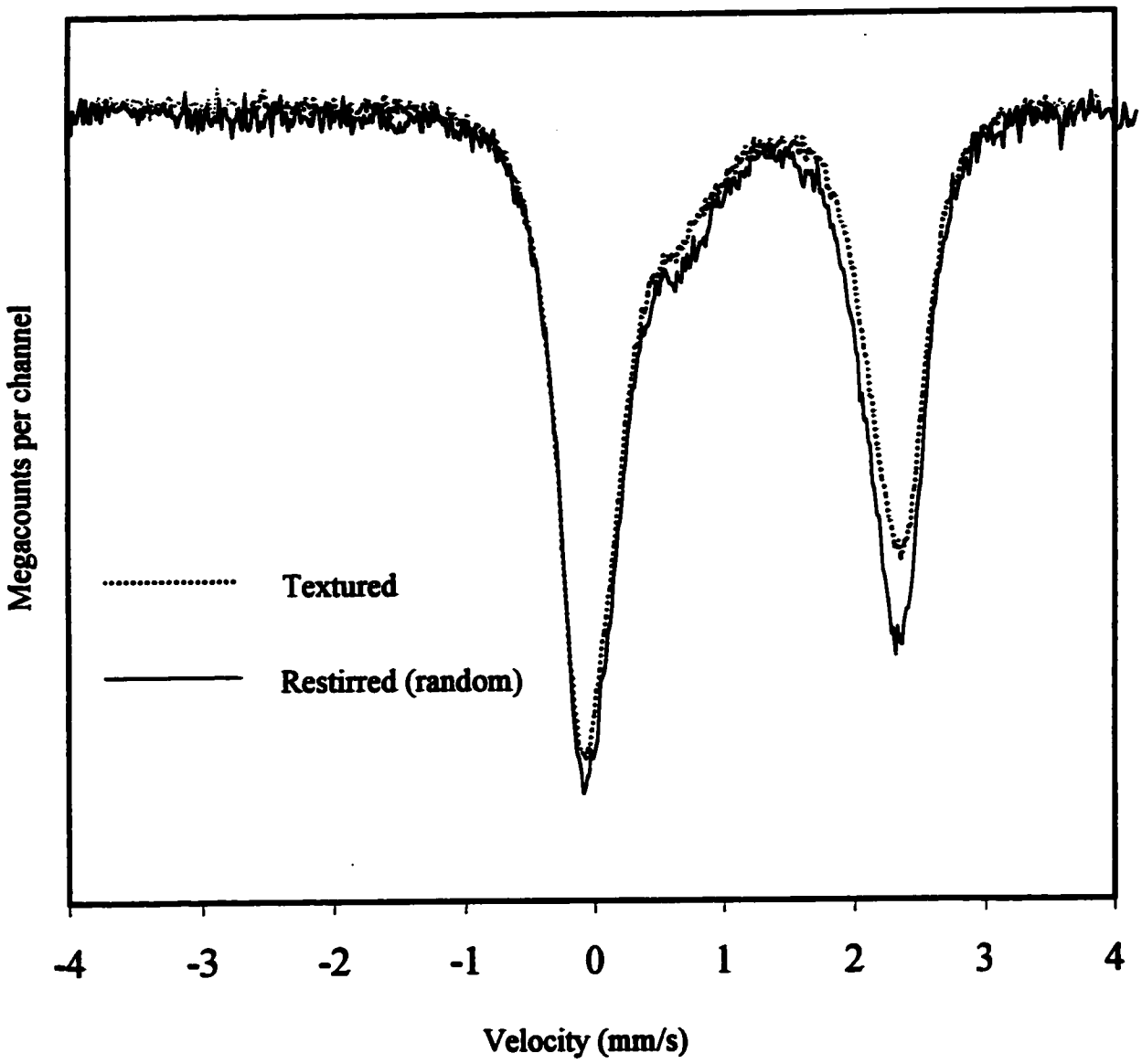

Figure 2. Effects of preferred orientation on the spectrum from astrophyllite group mineral absorbers.
Dashed line: A-/A+: 1.214, Fe^{3+}/Fe_{tot}: 0.19
Solid line: A-/A+: 1.000, Fe^{3+}/Fe_{tot}: 0.21
$\Delta Fe^{3+}/Fe_{tot} = 0.02$ (0.03 *apfu* Fe^{3+})

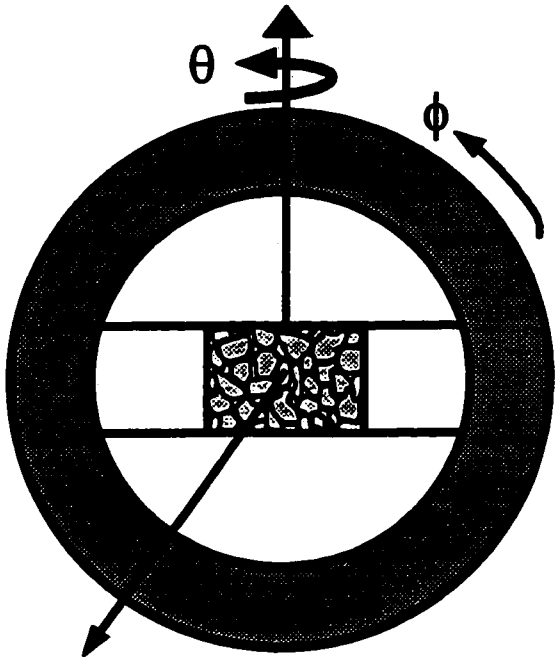

Figure 3. Oriented mosaic experimental setup.
At $\theta = 0°$, the incident γ-ray beam is perpendicular to the (001).cleavage plane on which all crystals are lying.

distance of 12.5 cm, with the sample-to-source distance fixed at 9.5 cm. As with the regular, randomly oriented absorbers, data were obtained at room temperature using a ^{57}Co source in a rhodium matrix and the same experimental conditions as described in the previous section. The initial spectrum was obtained with both rotational angles, θ and ϕ, set at zero degrees. Subsequent spectra were collected every 15° θ (θ = 0, 15, 30, 45 and 60°), and near the magic angle, $\theta = 55°$. Spectra were also collected at $\phi = 30$ and 60° to ensure that the mosaic was randomly oriented within the (001) plane. Following collection of all mosaic data, the crystals were removed and an ideal mass of sample was separated in order to produce a randomly oriented absorber. Spectra were fitted with the Voigt-based quadrupole splitting distribution method of Rancourt & Ping (1991) as implemented in the program RECOIL (Lagarec & Rancourt 1998). Both the randomly oriented absorber and the mosaic spectra can be described by 1-3 fits, with the Fe^{3+} generalized site modeled using a single Gaussian QSD component and the Fe^{2+} generalized site modeled using three Gaussian QSD components. All spectra were corrected for thickness effects, assuming an ideal Mössbauer recoilless fraction of 0.7. Thickness corrections for the mosaic spectra were done by calculating the apparent thickness at each θ angle assuming a density of 3.34 g/cm^3 and 10% pore space. Such corrections are not exactly correct for the mosaic absorber because they ignore polarization effects due to the preferred orientation, but in order to be consistent with the randomly oriented absorber and to minimize effects due to absorber thickness, corrections were done. The Fe^{2+} and Fe^{3+} A-/A+ parameters for the randomly oriented absorber was not refined and fixed at unity. All parameters obtained during the fitting of the randomly oriented absorber data, except the A-/A+ parameter, were taken as constants and applied to

the mosaic spectra during the fitting process of the mosaic spectra (Table 2). The Fe^{3+}/Fe_{tot} ratio obtained from the randomly oriented absorber (Fe^{3+}/Fe_{tot} = 0.19) was applied to all mosaic spectra. In order to do this, six Voigt lines were fitted to each of the mosaic spectrum to obtain the total spectral area. The Fe^{3+}/Fe_{tot} ratio was then applied to each component of each generalized site. By fixing all spectral parameters, including the Fe^{3+}/Fe_{tot} ratio, variations in spectral peak areas observed at the various angles (Table 3) are known to be the result of changes in the orientation of the EFG of Fe with respect to the incident γ-ray beam.

4.2. Results

The raw folded spectra for the oriented mosaic at each θ angle are shown in Figure 4. Figure 5 shows the thickness-corrected spectrum for the randomly oriented absorber. The solid line running through the data points is the resultant 1-3 fit. The additional solid lines represent the separate contributions for both the Fe^{2+} and Fe^{3+} doublets. Figures 6A to 6F show the thickness-corrected oriented mosaic spectra that have been fitted with parameters obtained from the randomly oriented absorber. As will be discussed and elaborated on in further sections, the Mössbauer spectra of all AGM display two strong absorption peaks centered at ≈ -0.1 and 2.3 mm/s and a third, weaker shoulder at ≈ 0.9 mm/s. These three absorption peaks correspond to (1) the sum of the low-energy lines from $^{[6]}Fe^{2+}$ and $^{[6]}Fe^{3+}$ doublets, (2) the high-energy lines from $^{[6]}Fe^{2+}$ doublets, and (3) the high-energy lines from $^{[6]}Fe^{3+}$ doublets, respectively. As Fe^{2+} is the dominant valence state for Fe in the astrophyllite group structure, variations observed in spectral area between the two generalized sites, Fe^{2+} and Fe^{3+}, are more evident in the Fe^{2+} doublet.

TABLE 2. MÖSSBAUER SITE DISTRIBUTION PARAMETERS FOR THE RANDOMLY ORIENTED MOSAIC SAMPLE

	δ0 (mm/s)	δ1	A (counts·mm/s)	A- /A+
Fe^{2+}	1.029(8)	0.043(3)	145100(1300)	1*
Fe^{3+}	0.28(2)	0*	33750(840)	1*

		p (%)	⟨Δ⟩ (mm/s)	σΔ (mm/s)
Fe^{2+}	comp. 1	14	2.06(17)	0.59(22)
	comp. 2	68(16)	2.412(57)	0.252(30)
	comp. 3	18(19)	1.94(15)	0.222(91)
Fe^{3+}	comp. 1	100*	0.742(32)	0.573(31)

	<CS> (mm/s)	<|Δ|> (mm/s)	stdev (|Δ|)	skew (|Δ|)
Fe^{2+}	1.13	2.28	0.37	-0.56
Fe^{3+}	0.29	0.80	0.50	0.52

reduced $\chi^2 = 1.274$

Site populations (%): Fe^{2+} 81.13(40) Fe^{3+} 18.87(40)

* fixed value

TABLE 3. A-/A+ PARAMETERS FOR ORIENTED MOSAIC SPECTRA

θ (°)	A-/A+ Fe^{2+}	A-/A+ Fe^{3+}
0	2.183	0.733
15	2.007	0.782
30	1.647	0.711
45	1.207	0.613
55	1.003	0.937
60	0.932	0.774

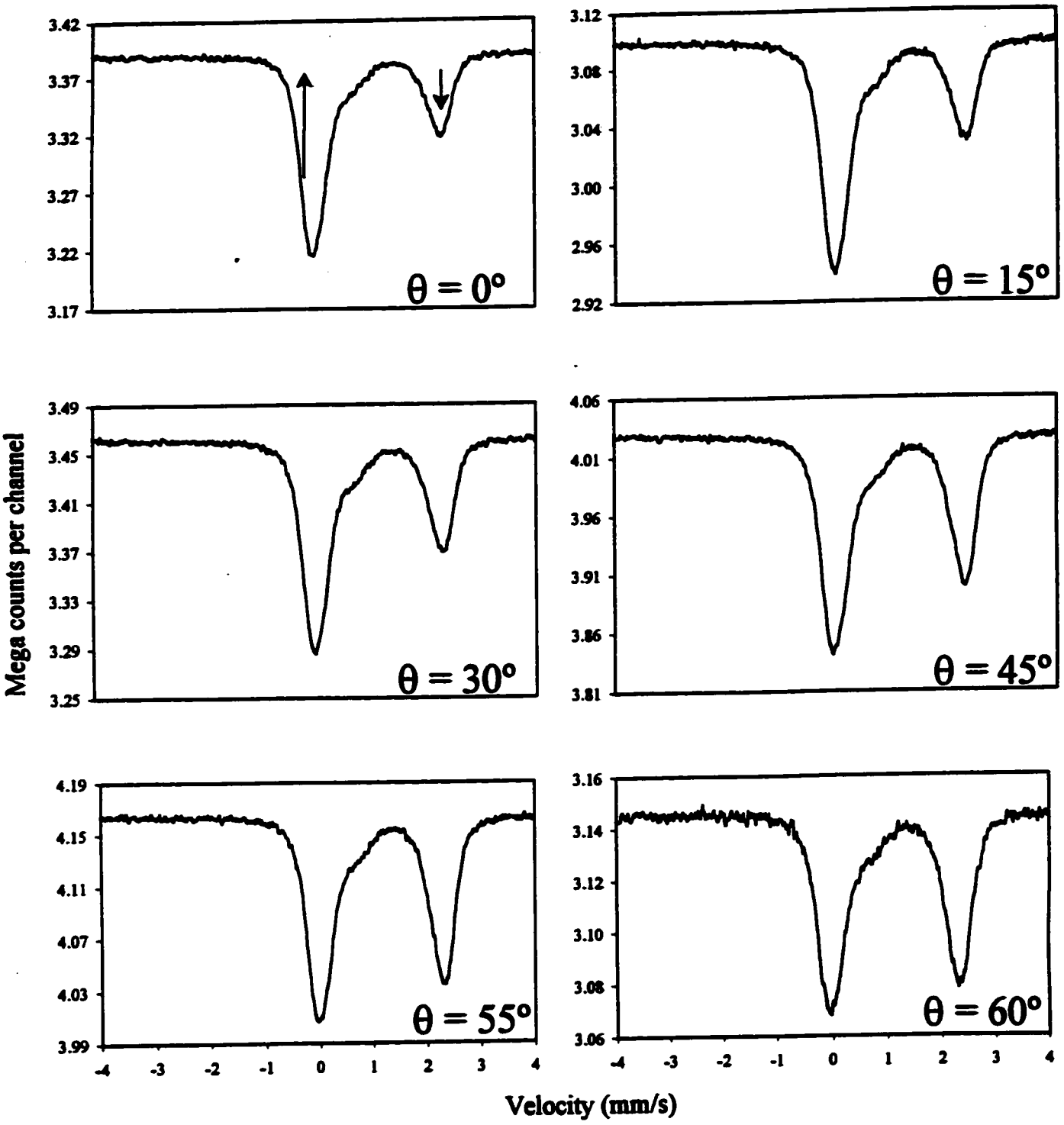

Figure. 4. Folded, raw Mössbauer spectra collected at various θ angles. Note the deepening of the high-energy contribution with increasing angle (indicated by arrows). At θ = 0°, the γ-ray beam is aligned parallel to [001], and represents the most extreme case of texture.

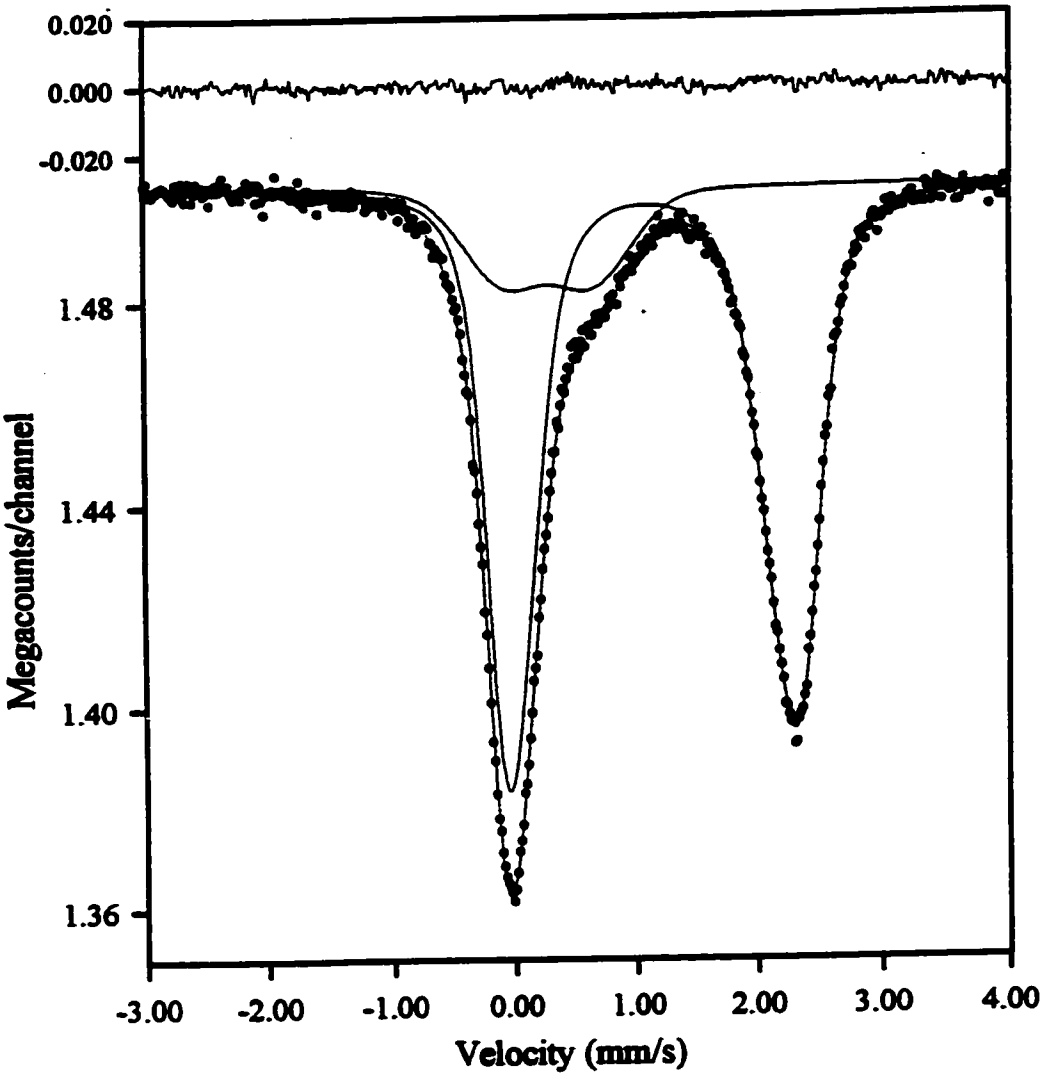

Figure 5. Thickness corrected, folded room temperature ^{57}Fe Mössbauer spectrum of the randomly oriented sample used for the oriented mosaic. The solid line running through the data points is the fit result. The fit for the Fe^{2+} and Fe^{3+} contributions are also shown as a solid line. A-/A+ = 1.000.

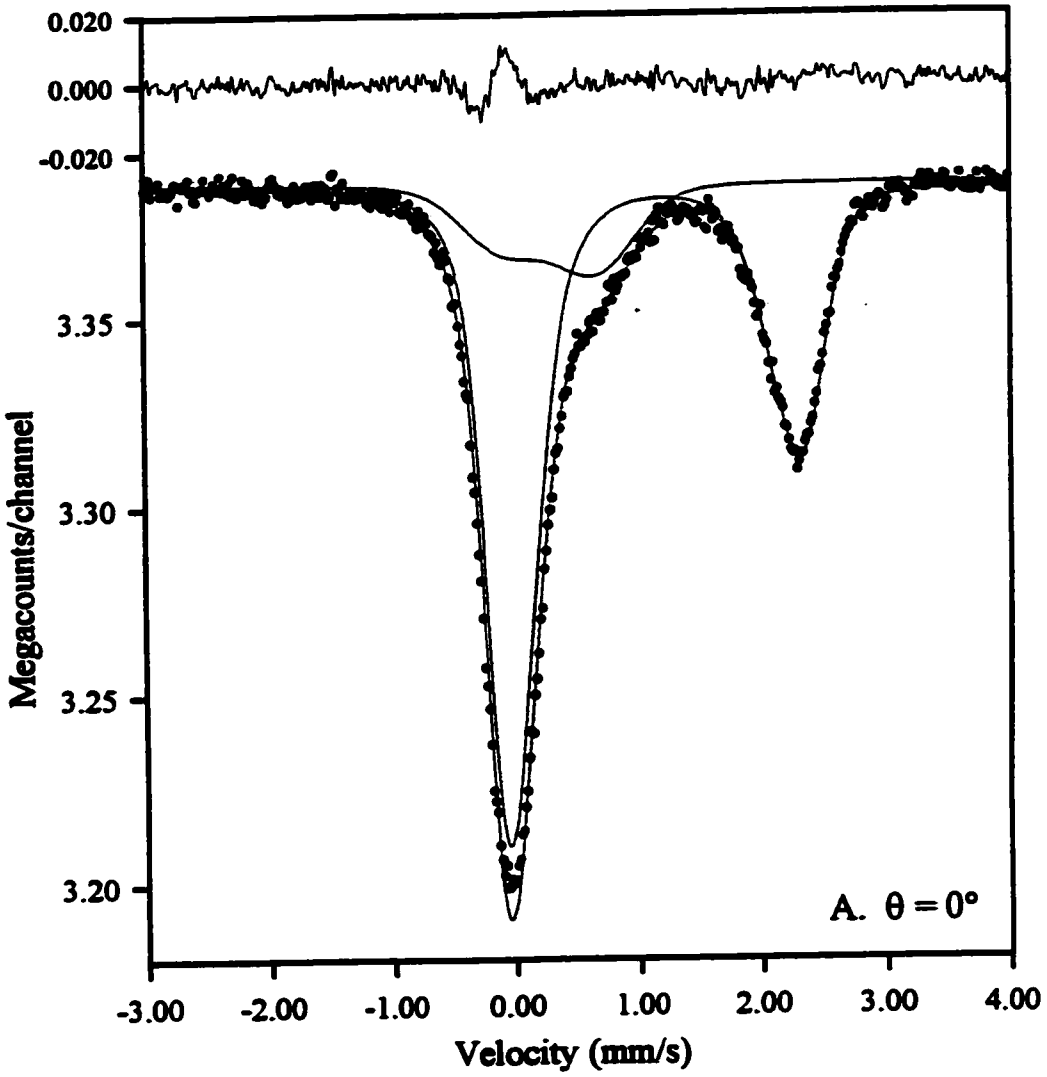

Figure 6 (A-F). Thickness corrected, folded room temperature ^{57}Fe Mössbauer spectra of the oriented mosaic. The solid line running through the data points is the fit result. The fit for the Fe^{2+} and Fe^{3+} contributions are also shown as a solid line.

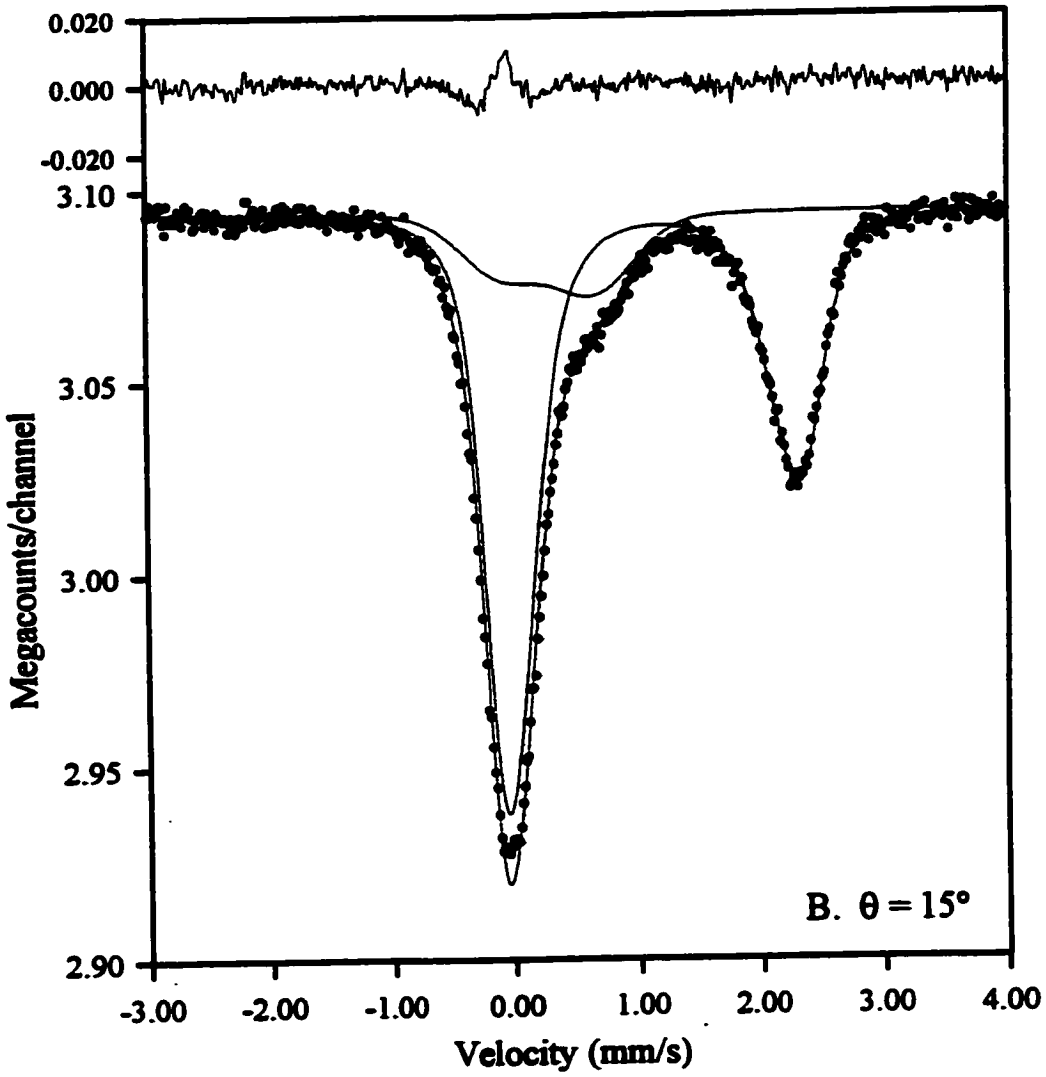
0.020
0.000
-0.020
3.10
3.05
3.00
2.95
2.90
Megacounts/channel
B. θ = 15°
-3.00
-2.00
-1.00
0.00
1.00
2.00
3.00
4.00
Velocity (mm/s)

Figure 6B.

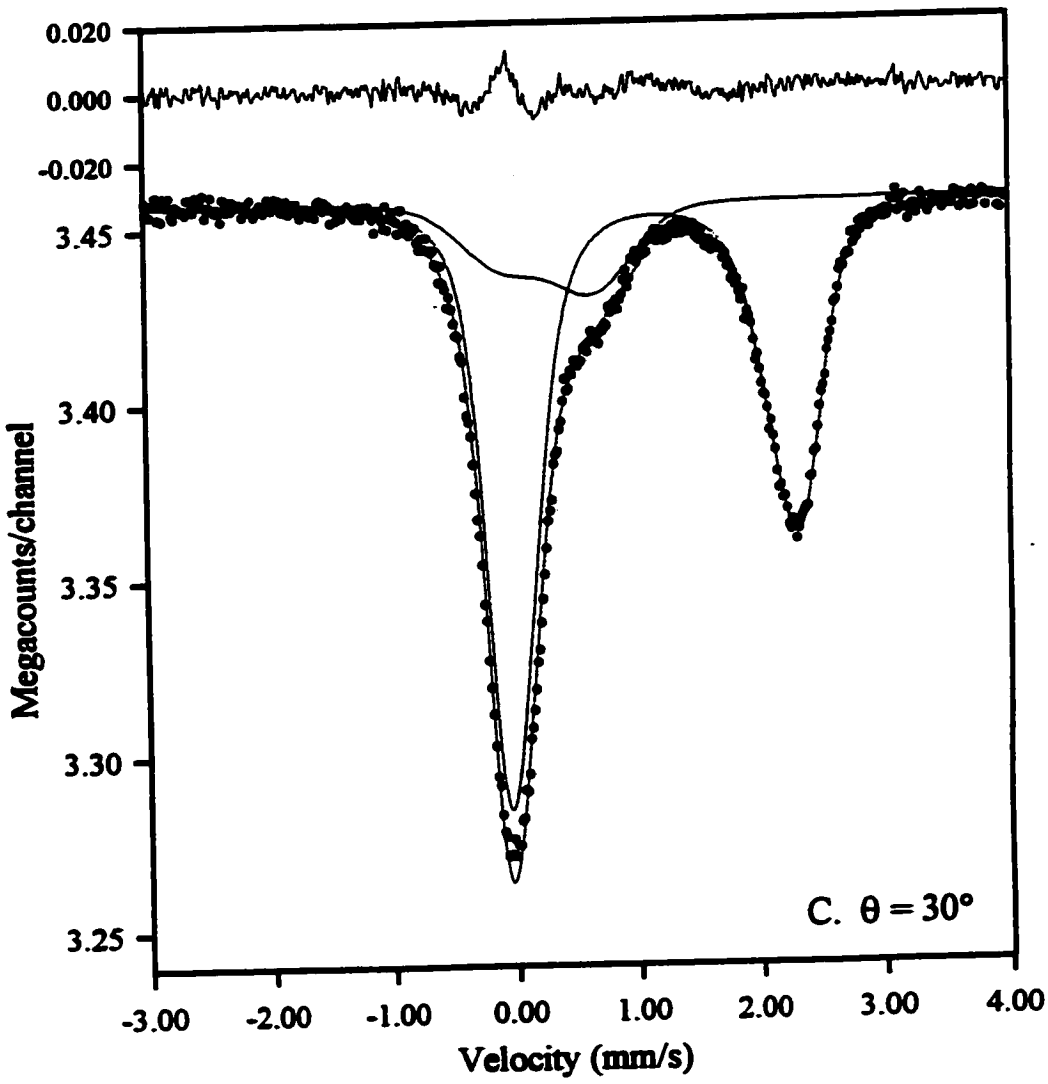
0.020
0.000
-0.020
3.45
3.40
3.35
3.30
3.25
Megacounts/channel
C. θ = 30°
-3.00
-2.00
-1.00
0.00
1.00
2.00
3.00
4.00
Velocity (mm/s)

Figure 6C.

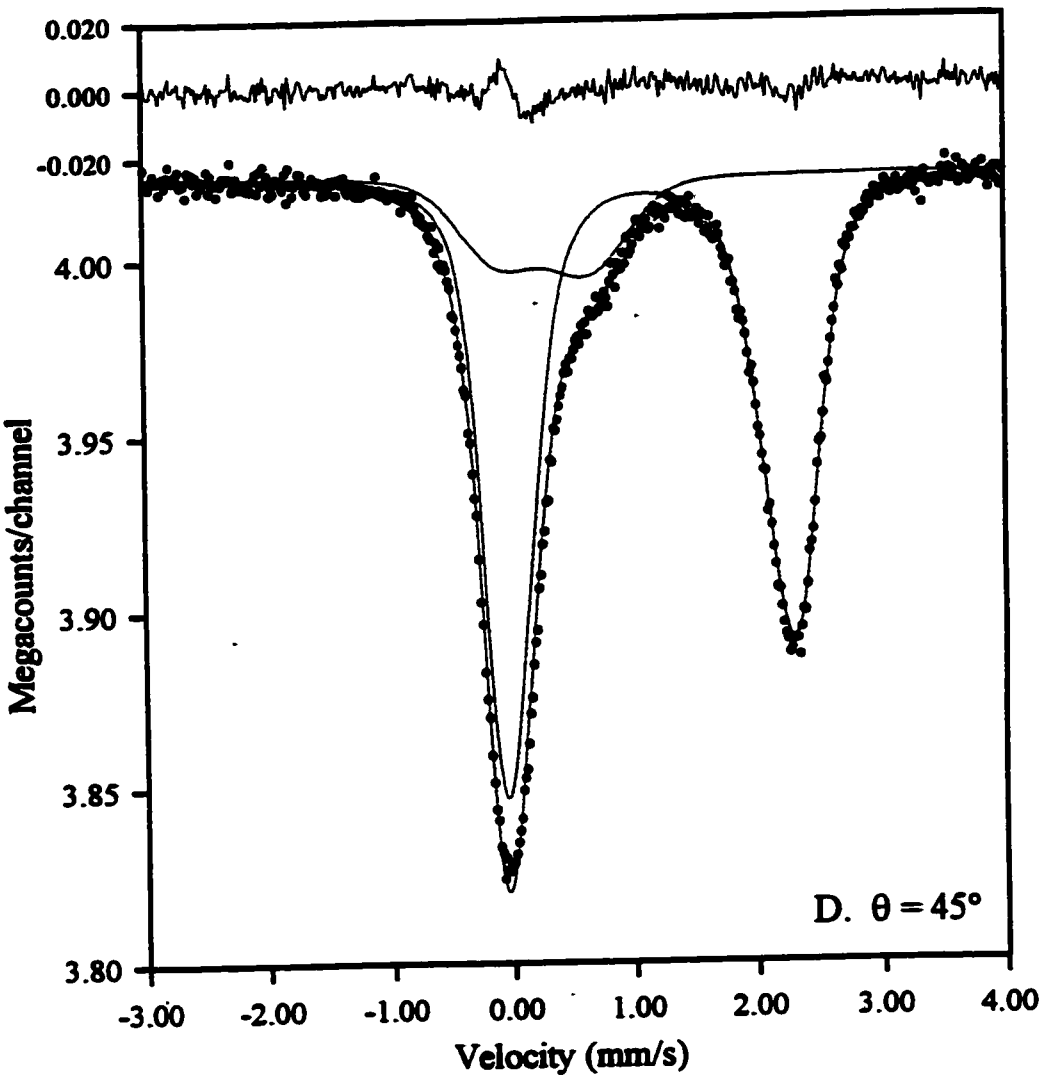
0.020
0.000
-0.020
4.00
3.95
3.90
3.85
3.80
Megacounts/channel
D. θ = 45°
-3.00
-2.00
-1.00
0.00
1.00
2.00
3.00
4.00
Velocity (mm/s)

Figure 6D.

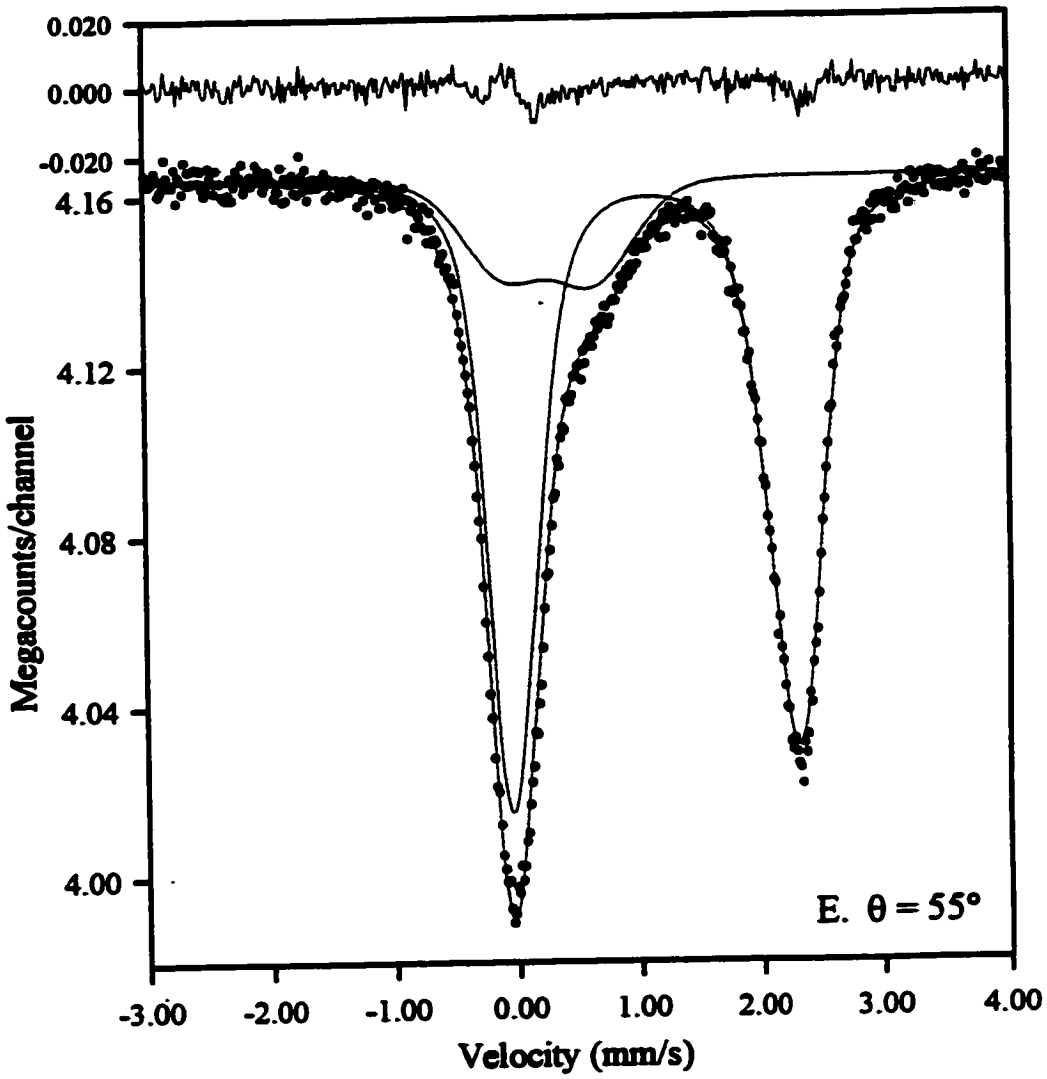
0.020
0.000
-0.020
4.16
4.12
4.08
4.04
4.00
Megacounts/channel
E. θ = 55°
-3.00
-2.00
-1.00
0.00
1.00
2.00
3.00
4.00
Velocity (mm/s)

Figure 6E.

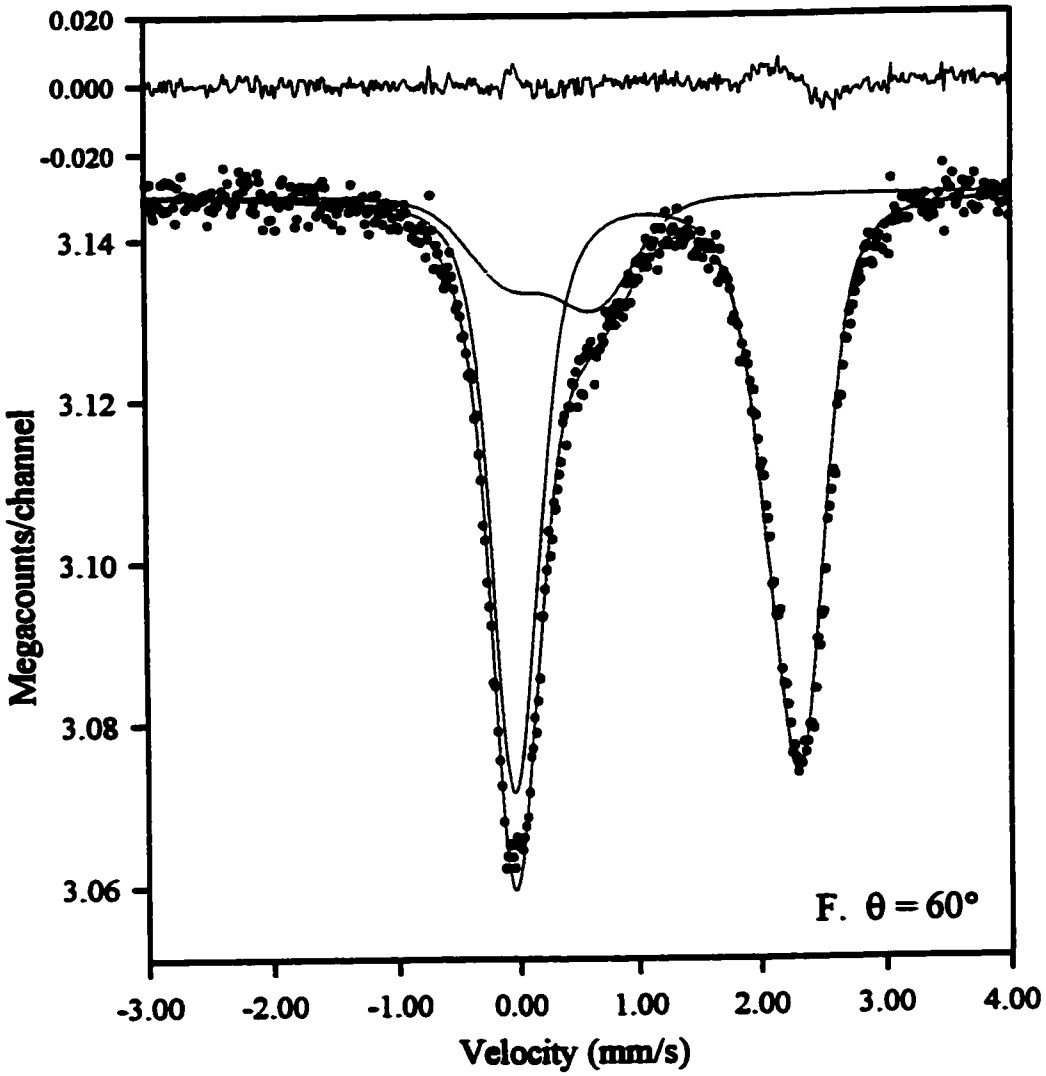
0.020
0.000
-0.020
3.14
3.12
3.10
3.08
3.06
Megacounts/channel
F. θ = 60°
-3.00
-2.00
-1.00
0.00
1.00
2.00
3.00
4.00
Velocity (mm/s)

Figure 6F.

At $\theta = 0°$, the effect on the Mössbauer spectrum of preferred orientation is at a maximum; all grains are lying flat on (001) with the incident γ-ray direction perpendicular to this plane. The resultant spectrum (Figs. 4 and 6A) shows noticeable, strong asymmetry in the two dominant peaks such that the low-energy contribution contains more spectral area than the corresponding high-energy peak. This asymmetry cannot simply be due to hidden Fe^{3+} components in the low-energy region of the spectra; Fe^{3+} accounts for only 19% of the total spectral area. Refinement of the A-/A+ parameter for this spectrum gives 2.187 and 0.733 for the Fe^{2+} and Fe^{3+} generalized sites, respectively.

Increasing the angular value between the incident γ-ray beam and the (001) plane of the oriented mosaic from $\theta = 0°$ to $\theta = 45°$ results in a visible deepening of the high energy peak of the Fe^{2+} doublet, and a subsequent decrease in relative spectral area of the low energy peak, known to contain both low energy lines from octahedrally-coordinated Fe^{2+} and Fe^{3+}. Refined A-/A+ values for Fe^{2+} decrease from 2.007 to 1.207, whereas those for Fe^{3+} increase slightly to 0.782, and then decrease to 0.613. At $\theta = 55°$, the magic angle, neither generalized site should display asymmetry and the A-/A+ parameters should be equal (*i.e.* A-/A+ = 1.000). The A-/A+ values for Fe^{2+} and Fe^{3+} at $\theta = 55°$ for the oriented mosaic data are 1.003 and 0.937, respectively, indicating negligible asymmetry in the Fe^{2+} generalized site and minor asymmetry in the Fe^{3+} generalized site.. In general, as A-/A+ for the Fe^{2+} generalized site decreases, an increase is observed in the Fe^{3+} A-/A+ value which suggests that the two asymmetry parameters are inversely correlated; an increase in spectral area of the low-energy peak of the Fe^{2+} doublet is concomitant with a decrease in spectral area of the low-energy peak of the Fe^{3+} doublet.

Figure 7 shows that the Fe^{2+} A-/A+ value varies widely (ΔA-/A+ = 1.251), but regularly, with change in angular position relative to the incident γ-ray beam, whereas the Fe^{3+} A-/A+ shows only minimal variation (ΔA-/A+ = 0.324) with angular position. The importance of the Fe^{2+} doublet in all the spectra allows us to determine with great reliability the Fe^{2+} spectral parameters. It is therefore not surprising that Fe^{2+} A-/A+ values seem to be considerably more robust than those of Fe^{3+}. The slightly erratic variations of the Fe^{3+} A-/A+ values at high angles may result from the increased difficulty in fitting this parameter when the low energy peak of the Fe^{3+} doublet is hidden in the low energy Fe^{2+} peak and significant trade-off between the Fe^{2+} and Fe^{3+} parameters occurs. In order to avoid this problem, Hargraves *et al.* (1990) ignored the Fe^{3+} contribution by removing the data in the relevant channels, thus fitting only the remaining Fe^{2+} doublet. In this study, since we are interested in knowing the effects of preferred orientation on both the Fe^{2+} and Fe^{3+} A-/A+ values, we have chosen not to take this approach. In doing so, we have shown that the variation in Fe^{3+} A-/A+ values is minor compared to that of the dominant Fe^{2+} doublet. To eliminate trade-off between parameters and to ensure accurate and precise Fe^{3+}/Fe_{tot} ratios in cases where preferred orientation effects cannot be overcome by restirring the absorber it is suggested that only the Fe^{2+} A-/A+ parameter be refined and the Fe^{3+} A-/A+ value fixed at unity.

The theoretical A-/A+ curves with respect to the angle of incidence between the incident γ-ray direction and the principal EFG direction, $\theta_{\gamma q}$, were calculated using the following equations for the relative intensities of the two lines of the doublet (Rancourt 1998):

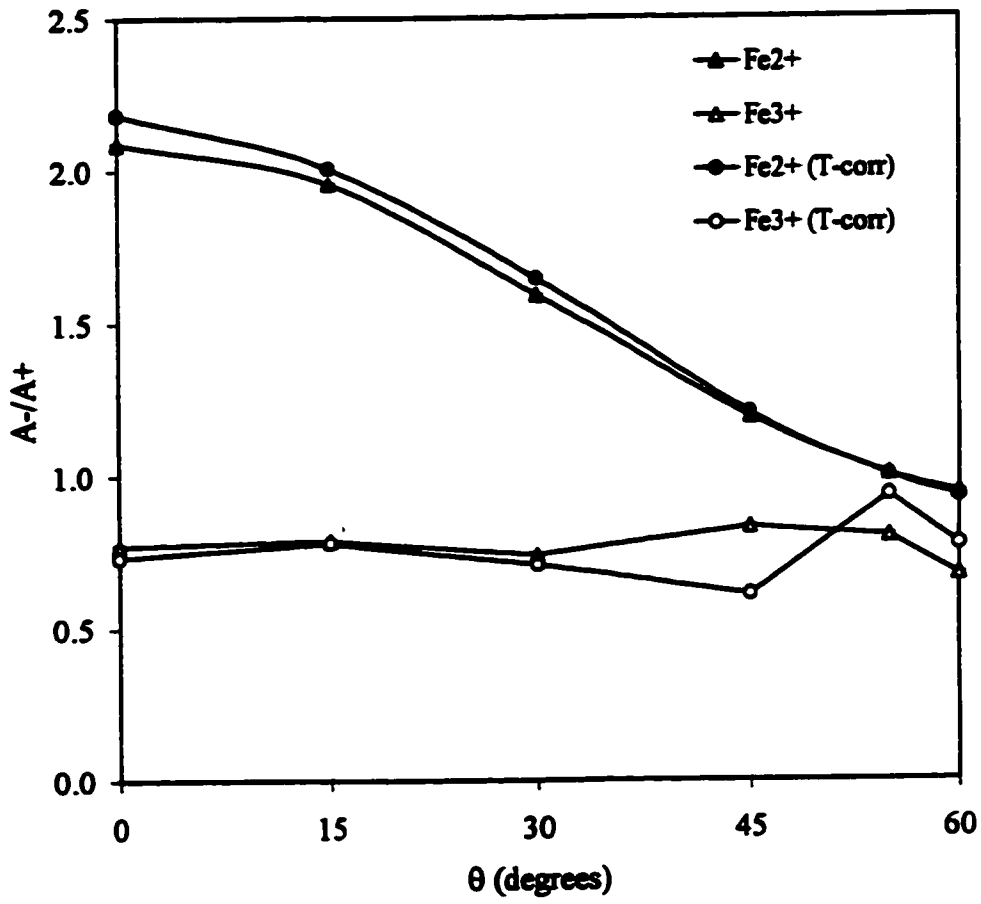

Figure 7. Observed variations in A-/A+ at each value of θ for uncorrected and thickness corrected (T-corr) oriented mosaic data.

$$A_1 = 2 + 3\sin^2\theta_{\gamma q} \quad (4)$$

$$A_2 = 3 + 3\cos^2\theta_{\gamma q} \quad (5)$$

where $\theta_{\gamma q}$ is the angle between the incident γ-ray direction and the EFG. In this way, the measured data may be compared to expected values, and the sign of the quadrupole splitting, e^2qQ, and the principal EFG direction can be obtained. The theoretical curves in Fig. 8 indicate EFG directions for Fe^{2+} to be close to perpendicular to (001) and that for Fe^{3+} to be within the (001) plane. Comparison of the calculated A-/A+ curve for a near-normal EFG direction with the observed trend indicates that the EFG principal direction for Fe^{2+} in the oriented mosaic is not exactly perpendicular to the (001) plane (Fig. 8) and therefore lies at some angle to the incident γ-ray direction. The fact that the sample in question is randomly oriented in the (001) plane precludes the possibility of exactly determining the relations between EFG and crystallographic directions; the EFG will be described by a distribution of directions. However, it can be shown that e^2qQ is negative, similar to other phyllosilicates (Hargraves *et al.* 1990, Rancourt & Lalonde 1995).

5.0. Description of the Mössbauer spectra

The Mössbauer spectra of all AGM analyzed are remarkably similar, with two strong absorption peaks centered at ≈ -0.1 and 2.3 mm/s and a third, weaker shoulder at ≈ 0.9 mm/s. These three absorption peaks correspond to (1) the sum of the low-energy lines from $^{[6]}Fe^{2+}$ and $^{[6]}Fe^{3+}$ doublets, (2) the high-energy lines from $^{[6]}Fe^{2+}$ doublets, and (3) the high-energy lines from $^{[6]}Fe^{3+}$ doublets, respectively. Fitting parameters and associated errors for select spectra can be found in Table 4. Typical examples of Mössbauer spectra are shown in Figs.

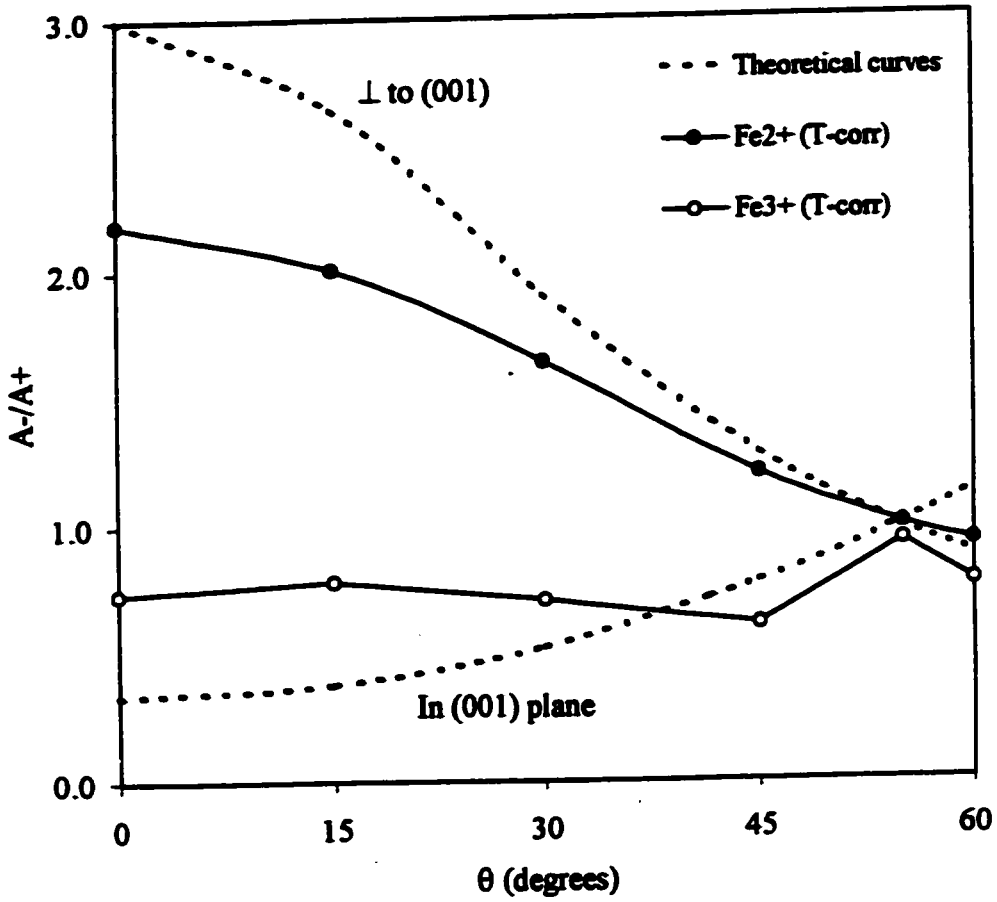

Figure 8. Theoretical and observed variations in A-/A+ at each value of θ. The dashed line represents the theoretical curve for single, near-normal EFG direction ($e^2qQ < 0$).

TABLE 4. MOSSBAUER DATA FOR ASTROPHYLLITE GROUP MINERALS

Sample	File	x^2	BG	δ_0[2+]	δ_1[2+]	<CS> [2+]	Δ_1[2+]	σ_1[2+]	A_1[2+] %	Δ_2[2+]
MSH32	PCP008	1.420	2954.8	1.15696	-0.0061	1.145	2.525	0.177	50.4	2.317
MSH18A	PCP009	1.324	3227.5	1.177	-0.0151	1.143	2.398	0.243	54.9	2.129
RUS5	PCP014	1.400	3338.1	1.1582	-0.0073	1.141	2.414	0.193	54.3	2.23
MSH10A	PCP015	1.252	3111.2	1.170	-0.0091	1.150	2.49	0.22	32	2.16
MSH10B	PCP016	0.961	2553.7	1.076	0.0251	1.133	2.453	0.228	64.4	2.06
MSH11	PCP020	1.302	2441.4	1.169	-0.0109	1.144	2.375	0.244	54.4	2.128
MSH28	PCP021	1.170	474.3	1.1493	-0.0035	1.141	2.408	0.222	66	2.232
MSH15	PCP022	1.273	4622.4	1.1753	-0.0122	1.149	2.361	0.248	46	2.159
RUS4	PCP023	1.018	1089.0	1.1310	0.0039	1.140	2.475	0.176	34.1	2.285
MSH7	PCP025	0.994	1561.5	1.119	0.0067	1.134	2.452	0.204	61.8	2.221
US5	PCP028	1.153	1160.7	1.1252	0.0060	1.139	2.448	0.182	56	2.314
NOR9	PCP029	1.455	1299.4	1.1212	0.0079	1.140	2.517	0.203	69.1	2.285
US2	PCP030	1.250	108.0	1.1090	0.0114	1.136	2.502	0.187	57	2.370
MSH33	PCP031	1.153	465.9	1.110	0.0099	1.134	2.527	0.183	51	2.329
NOR1	PCP032	1.180	1570.0	1.1538	-0.0046	1.143	2.493	0.208	36	2.200
MSH6	PCP033	1.204	1109.4	1.156	-0.0025	1.150	2.559	0.168	35	2.290
MSH34A	PCP034	0.976	223.3	1.135	0.0039	1.144	2.547	0.143	24	2.43
RUS8	PCP036	1.040	303.2	1.111	0.0140	1.143	2.458	0.196	51	2.36
CC2A	PCP037	1.149	284.7	1.114	0.0135	1.146	2.70	0.50	7	2.521
CC7A	PCP038	1.136	1348.1	1.1729	-0.0081	1.154	2.509	0.206	62.3	2.251
MSH26A	PCP039	1.104	669.6	1.142	0.0002	1.142	2.462	0.200	41	2.147
MSH26B	PCP040	1.042	380.5	1.155	-0.0050	1.143	2.530	0.187	48	2.273
RUS7	PCP041	1.213	447.3	1.133	-0.0039	1.124	2.415	0.174	46	2.248
MSH35	PCP042	1.259	960.1	1.154	-0.0090	1.134	2.40	0.249	47	2.15

NOTE: [2+]: $^{[6]}Fe^{2+}$; [3+]: $^{[6]}Fe^{3+}$; * = fixed value; BG: background in kilocounts;
Lorentzian HWHM: 0.097; A-/A+ [3+]: 1*

TABLE 4. CONTINUED

Sample	σ_2[2+]	A_2[2+] %	Δ_3[2+]	σ_3[2+]	A_3[2+] %	A-/A+ [2+]	<QS> [2+]	SD [2+]	QS_{peak} [2+]	$P(QS_{peak})$
MSH32	0.392	40.5	2.114	0.153	9.0	1.2063	2.403	0.314	2.509	1.504
MSH18A	0.535	33.7	1.946	0.173	11.4	1.2943	2.256	0.4	2.374	1.135
RUS5	0.476	29.5	1.995	0.159	16.2	1.1869	2.292	0.339	2.397	1.365
MSH10A	0.30	50	1.91	0.75	18.7	1.156	2.219	0.453	2.361	1.102
MSH10B	0.71	19.2	1.940	0.186	16.4	1	2.294	0.427	2.443	1.227
MSH11	0.551	37	1.918	0.152	8.7	1.1975	2.244	0.413	2.358	1.135
MSH28	0.494	24.4	1.921	0.121	9.2	1.1529	2.32	0.339	2.402	1.38
MSH15	0.542	35	1.90	0.219	19	1.1705	2.202	0.413	2.305	1.028
RUS4	0.484	29.9	2.14	0.243	36	1.0921	2.299	0.348	2.407	1.284
MSH7	0.490	24.9	1.965	0.159	13.3	1.0330	2.33	0.344	2.444	1.394
US5	0.429	24.3	2.10	0.194	19.5	1.1287	2.348	0.297	2.42	1.597
NOR9	0.532	18.3	2.052	0.168	12.5	1.1036	2.416	0.333	2.51	1.49
US2	0.551	12	2.19	0.230	31	1.1219	2.389	0.305	2.461	1.543
MSH33	0.56	15	2.17	0.258	34	1.1272	2.376	0.336	2.489	1.433
NOR1	0.71	15	2.14	0.284	49	1.1622	2.276	0.394	2.39	1.161
MSH6	0.320	57	2.24	0.73	8	1.1461	2.379	0.358	2.515	1.396
MSH34A	0.28	44	2.26	0.38	32	1.1523	2.406	0.312	2.513	1.516
RUS8	0.51	19	2.08	0.229	31	1.0422	2.323	0.334	2.411	1.33
CC2A	0.153	25	2.329	0.287	68	1.0701	2.404	0.304	2.47	1.511
CC7A	0.439	30.0	2.039	0.113	7.6	1.1192	2.396	0.331	2.499	1.436
MSH26A	0.502	40	2.06	0.20	19	1.104	2.261	0.392	2.411	1.157
MSH26B	0.52	23	2.16	0.23	29	1.1851	2.361	0.351	2.486	1.337
RUS7	0.482	30	2.05	0.192	24	1.2429	2.278	0.336	2.382	1.391
MSH35	0.85	12	2.06	0.31	41	1.177	2.234	0.422	2.318	1.145

TABLE 4. CONTINUED

Sample	$QS_{H\text{-}edge}$	$QS_{L\text{-}edge}$	W_{QS}	S_k	<CS> [3+]	<QS> [3+]	SD [3+]	Fe^{2+}/Fe^{3+}	Fe_{3+}/Fe_{tot}
MSH32	2.745	2.168	0.577	0.106	0.297	0.854	0.492	30.06(45)	0.03
MSH18A	2.698	1.879	0.819	0.118	0.316	0.912	0.379	13.16(69)	0.07
RUS5	2.654	1.964	0.69	0.105	0.282	0.907	0.415	15.23(47)	0.06
MSH10A	2.699	1.891	0.808	0.142	0.31	0.902	0.399	3.84(97)	0.21
MSH10B	2.728	2.019	0.709	0.149	0.304	0.826	0.481	3.85(65)	0.21
MSH11	2.681	1.876	0.805	0.114	0.347	0.853	0.443	8.17(85)	0.11
MSH28	2.678	2.059	0.619	0.082	0.296	0.925	0.503	71.46(66)	0.01
MSH15	2.668	1.756	0.912	0.103	0.294	0.979	0.356	15.47(63)	0.06
RUS4	2.674	1.956	0.718	0.108	0.278	0.878	0.417	25.39(56)	0.04
MSH7	2.701	2.097	0.604	0.114	0.311	0.822	0.526	23.81(65)	0.04
US5	2.659	2.102	0.557	0.072	0.256	1.037	0.392	32.33(30)	0.03
NOR9	2.764	2.201	0.563	0.094	0.281	0.938	0.456	17.80(35)	0.05
US2	2.712	2.135	0.577	0.072	0.282	0.943	0.405	11.47(36)	0.08
MSH33	2.734	2.123	0.611	0.113	0.289	0.855	0.462	16.36(81)	0.06
NOR1	2.769	2.035	0.734	0.114	0.319	1.04	0.408	12.93(58)	0.07
MSH6	2.755	2.126	0.629	0.136	0.3*	0.873	0.442	12.81(91)	0.07
MSH34A	2.742	2.174	0.568	0.107	0.263	1.082	0.443	26.32(78)	0.04
RUS8	2.681	1.989	0.692	0.088	0.27	0.95	0.546	17.80(98)	0.05
CC2A	2.709	2.112	0.597	0.066	0.3*	0.822	0.393	38.06(73)	0.03
CC7A	2.76	2.17	0.59	0.103	0.305*	0.925	0.424	46.17(56)	0.02
MSH26A	2.701	1.907	0.794	0.15	0.311	0.964	0.417	11.20(11)	0.08
MSH26B	2.742	2.063	0.679	0.125	0.299	0.893	0.383	17.38(92)	0.05
RUS7	2.626	1.963	0.663	0.104	0.276	0.762	0.342	85.96(88)	0.01
MSH35	2.662	1.879	0.783	0.084	0.281	0.846	0.404	17.52(12)	0.05

9A through F. The solid line through the data points is the resultant fit. The additional solid lines represent the separate contributions for the Fe^{2+} and Fe^{3+} doublets. All spectra were fitted using a 1-3 model: the Fe^{3+} doublet was modeled using a single Gaussian QSD component whereas the Fe^{2+} doublet was modeled using the sum of three Gaussian QSD components.

Each spectral contribution (or generalized site) in the spectrum is modeled as having its own QSD which corresponds to a specific valence state and coordination number and that is characterized by a number of parameters. In the Voigt-based QSD method, given that the QS is much more sensitive to local environment than the center shift (δ), it is assumed that δ and Δ are linearly coupled such that

$$\delta = \delta_0 + \delta_1 \bullet \Delta \quad (6)$$

where δ_0 and δ_1 are coupling parameters characteristic of a particular cation species or anion coordination (Rancourt *et al.* 1994a). In this way, QSDs and an associated distribution of δ are obtained. In all fits of AGM spectra, δ_1 for the Fe^{2+} site was allowed to refine, whereas it was fixed at zero for Fe^{3+}.

The QSD can be characterized by: (1) the average QS, <QS>; (2) the QS value at which the probability density is the highest, QS_{peak},; (3) the value of the probability density at QS_{peak}, $P(QS_{peak})$ which is an inverse measure of the width or standard deviation of the QSD; (4) the high and low energy edges of the QSD at half maximum of $P(QS_{peak})$, $QS_{H\text{-}edge}$ and $QS_{L\text{-}edge}$; (5) the width of the QSD at half maximum of $P(QS_{peak})$, W_{QSD}; (6) the skewness of the QSD, S_k, defined by QS_{peak}-<QS>; and (7) the standard deviation of the QSD, σ_{QSD}. We will examine correlations between individual Mössbauer spectral parameters and further

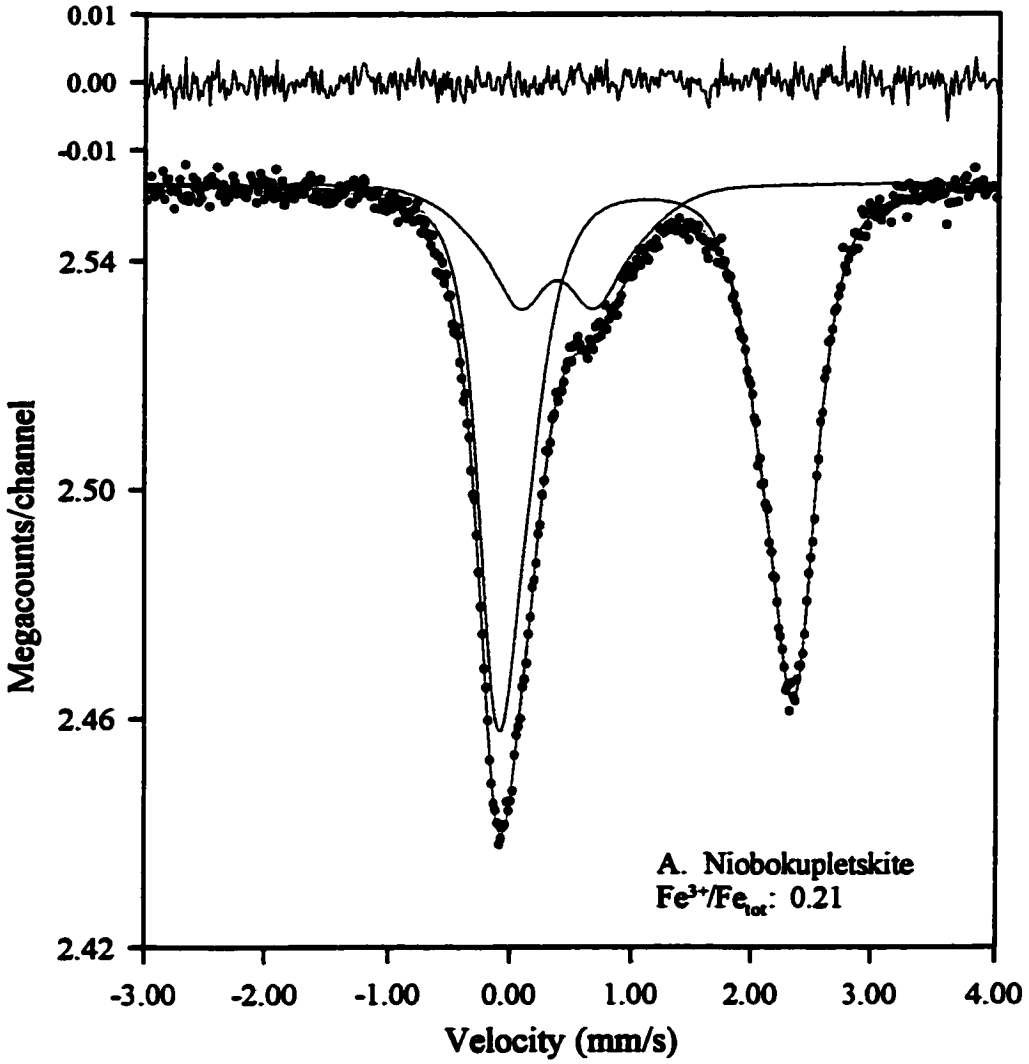

Figure 9A-F. Select Mössbauer spectra of astrophyllite group minerals.
The solid line through the spectral data represents the best fit. The subspectral contributions corresponding to $^{[6]}Fe^{2+}$ and $^{[6]}Fe^{3+}$ are shown superimposed on the data. The difference between the observed and calculated spectra is shown on an exaggerated vertical scale at the top of the figure.
A. Niobokupletskite from Mont Saint-Hilaire (MSH10B).
Mn# = 0.80, $Fe^{3+}/Fe_{tot} = 0.21$.

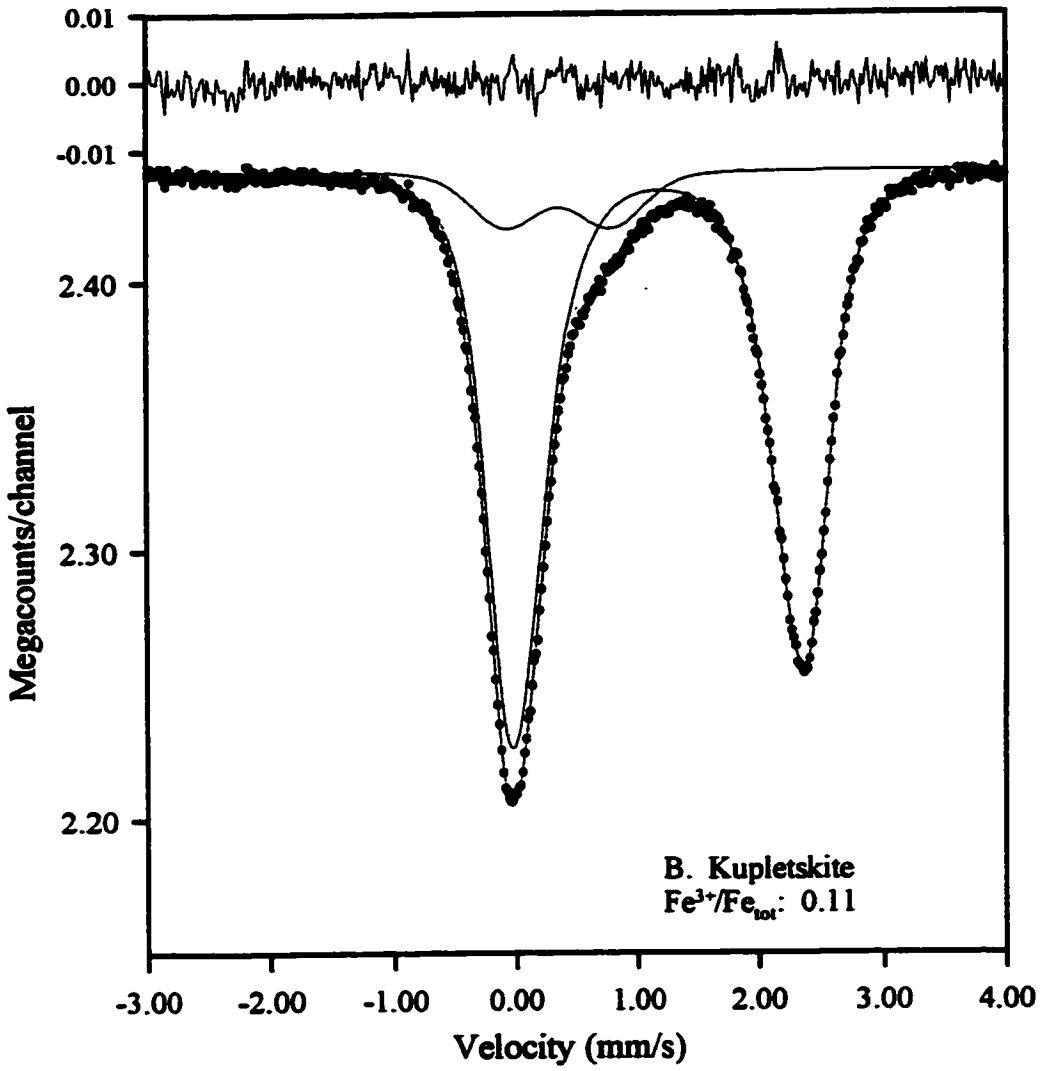

Figure 9B. Kupletskite from Mont Saint-Hilaire (MSH11).
Mn# = 0.61, Fe^{3+}/Fe_{tot} = 0.11.

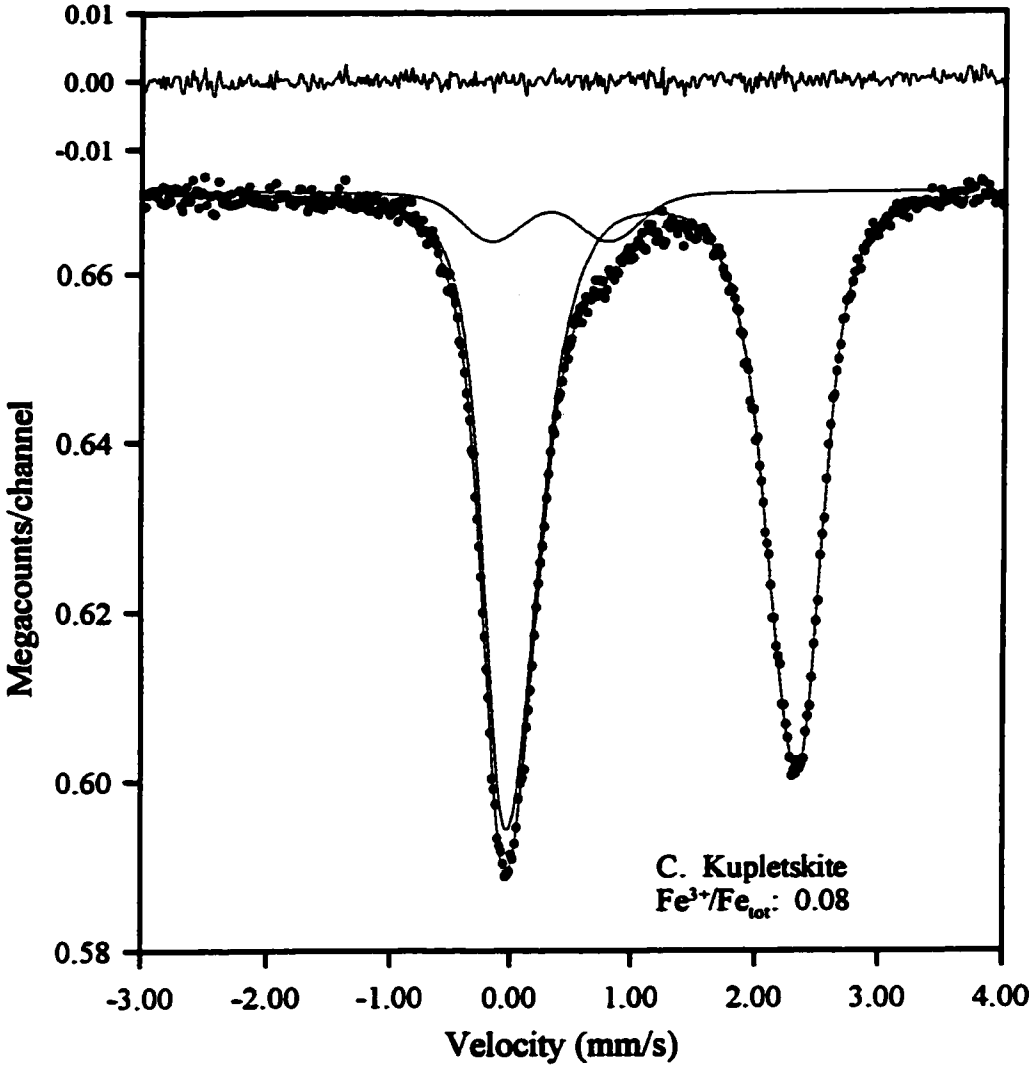

Figure 9C. Kupletskite from Mont Saint-Hilaire (MSH26A).
Mn# = 0.53, Fe^{3+}/Fe_{tot} = 0.08.

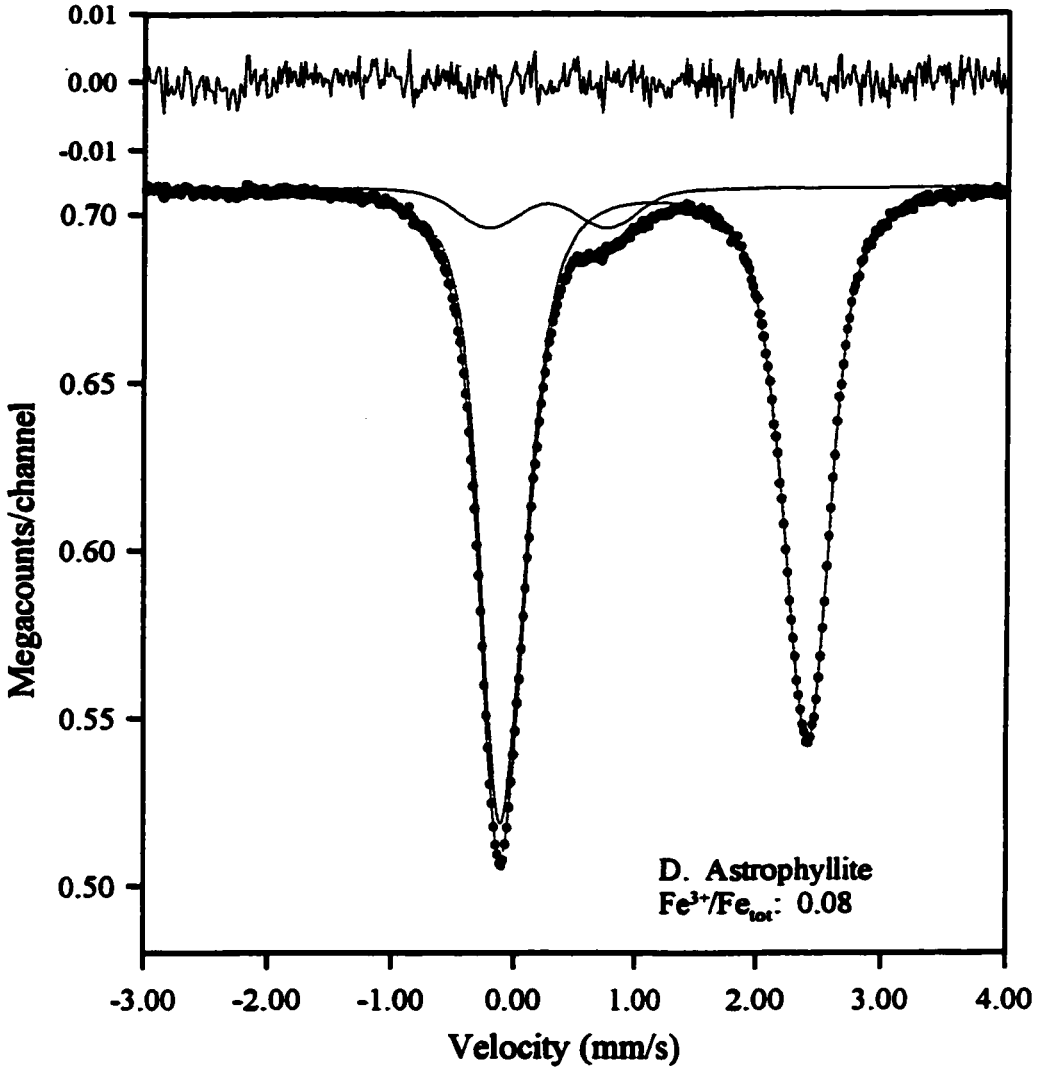

Figure 9D. Astrophyllite from Mount Rosa (US2).
Mn# = 0.10, Fe^{3+}/Fe_{tot} = 0.08.

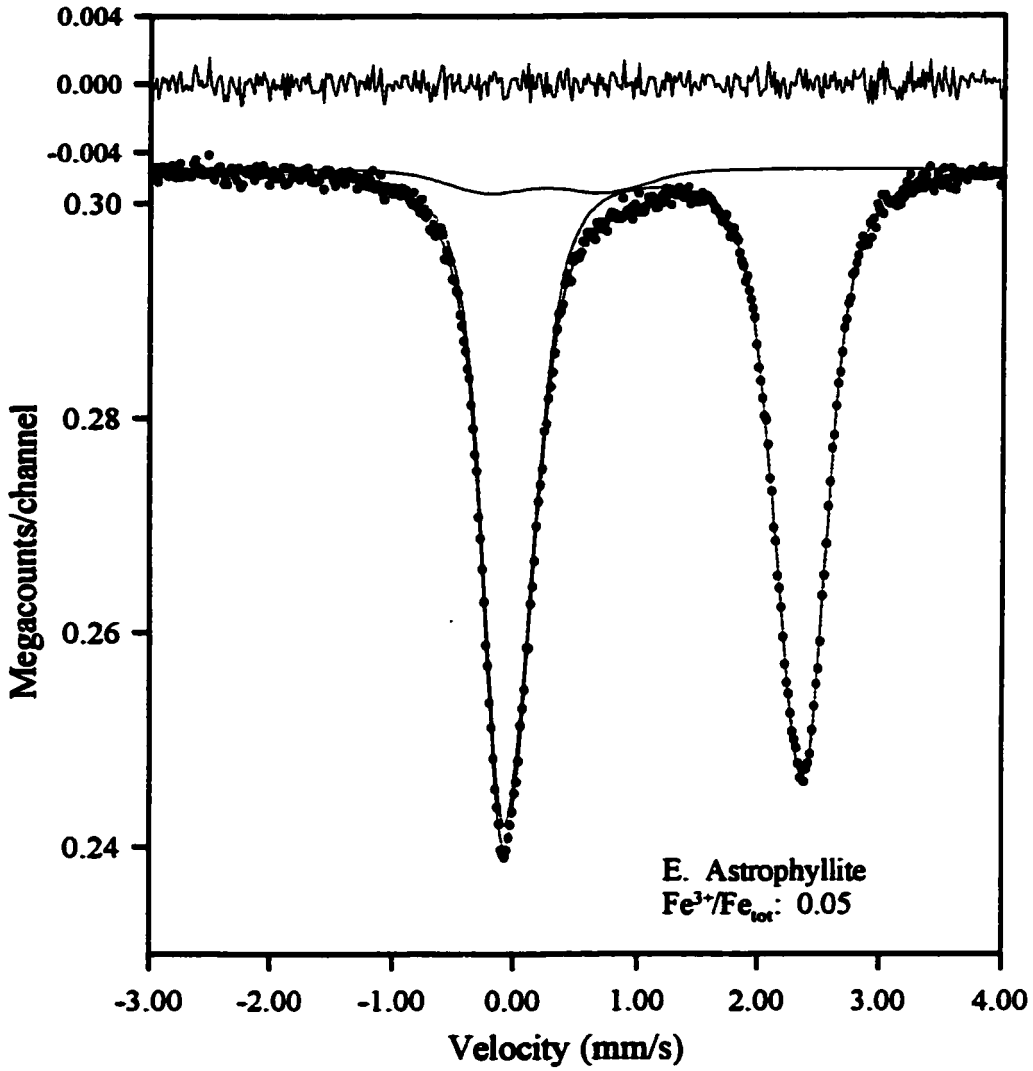

Figure 9E. Astrophyllite from the Khibina Massif, Kola Peninsula (RUS8). Mn# = 0.31, Fe^{3+}/Fe_{tot} = 0.05.

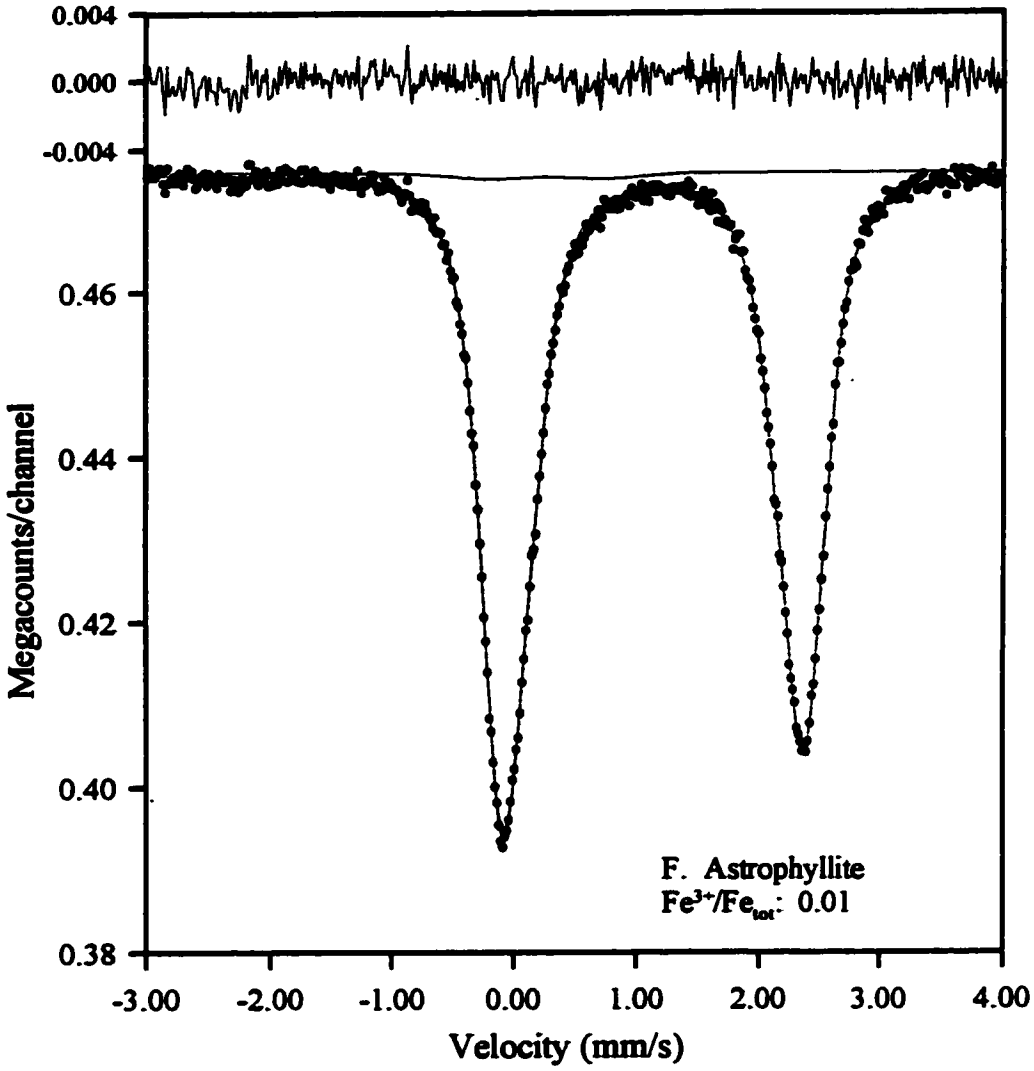

Figure 9F. Astrophyllite from Mont Saint-Hilaire (MSH28)
Mn# = 0.27, Fe^{3+}/Fe_{tot} = 0.01.

examine correlations between Mössbauer spectral and key AGM crystal-chemical parameters.

5.1. Fe^{3+} contribution

All Fe^{3+} contributions were modeled using a single Gaussian QSD component; attempts to add a second Gaussian component resulted in no decrease in the final reduced χ^2. Centre shifts, with respect to a-Fe CS for Fe^{3+}, range from 0.256 to 0.347 mm/s, lower than that observed for most biotite-series micas (average: 0.4 to 0.5 mm/s; Dyar & Burns 1986, Lalonde *et al.* 1996, Rancourt *et al.* 1996, Shabani 1999). Average QS values for Fe^{3+} in AGM range from 0.762 to 1.082 mm/s, corresponding to values observed for Fe^{3+} in octahedral coordination in structurally similar minerals such as those of the mica group (*e.g.* Rancourt *et al.* 1994a, Lalonde *et al.* 1996, Shabani 1999). Extraction of the exact average CS (<CS>) and <QS> is difficult due to (1) the minor spectral contribution from Fe^{3+}, and (2) the hidden low energy line of the $^{[6]}Fe^{3+}$ doublet within the low energy line of the Fe^{2+} doublet which results in overlap and trade-off between the two lines. Tetrahedrally-coordinated Fe^{3+} does not seem to play a role in the AGM structure; the characteristic $^{[4]}Fe^{3+}$ contribution of mica with <CS> of ≈ 0.15 to 0.25 mm/s and <QS> of ≈ 0.4 to 0.5 mm/s (Rancourt *et al.* 1992, Rancourt *et al.* 1994a, Lalonde *et al.* 1996) is not observed in any of our spectra.

Figure 10 shows typical Fe^{3+} QSDs for AGM. The Fe^{3+} QSDs for all samples are characterized by a relatively wide distribution with a peak at ≈ 0.75 to 1.00 mm/s and a long tail at high QS values, extending past 2.00 mm/s.

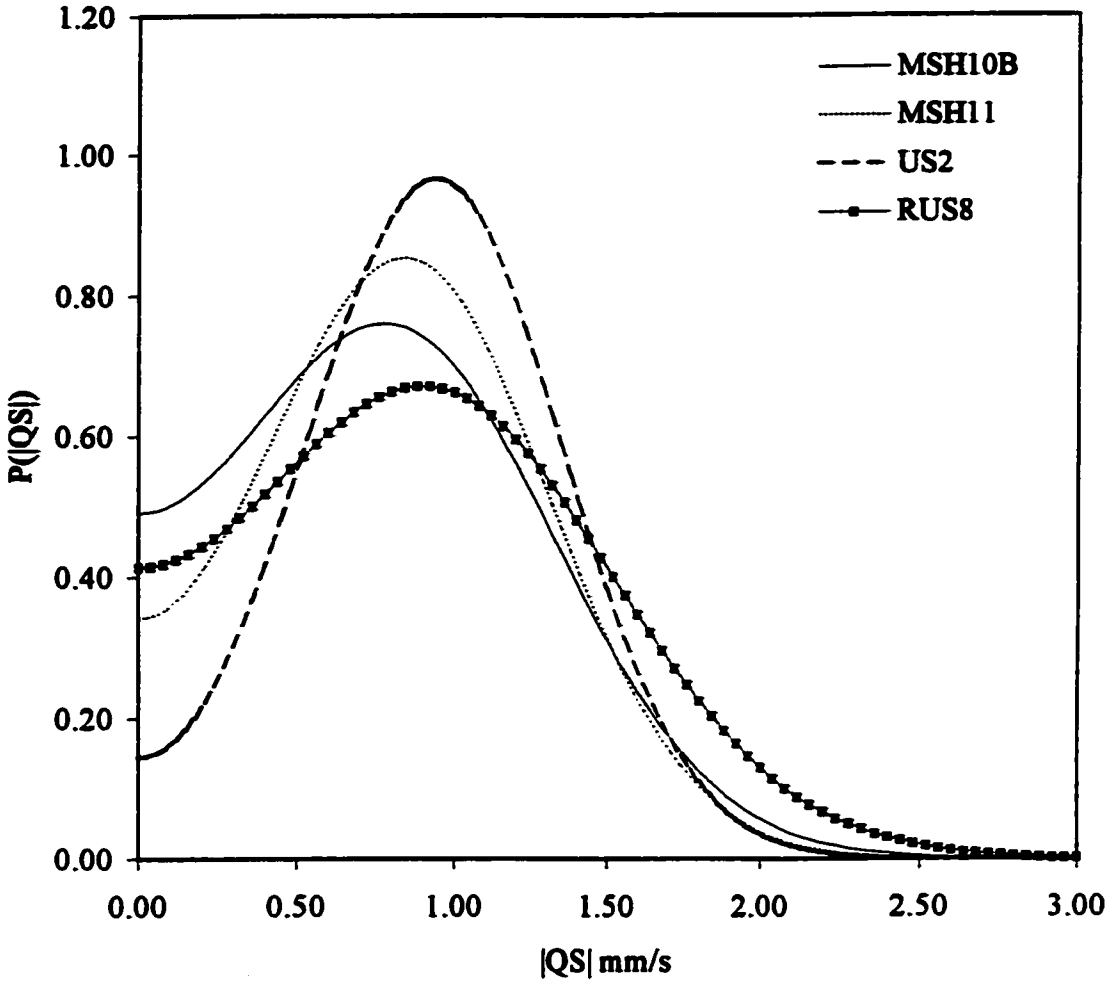

Figure 10. Representative quadrupole splitting distributions for the Fe^{3+} generalized site.

The Fe^{3+}/Fe_{tot} ratio, obtained from measured subspectral areas assuming equal recoilless fractions of Fe^{2+} and Fe^{3+}, is a robust parameter as it is constrained by the Fe^{2+} spectral contribution. The Fe^{3+}/Fe_{tot} ratios obtained by Mössbauer spectroscopy indicate Fe^{3+} to be a minor component in AGM. Fe^{3+}/Fe_{tot} ratios range from 0.01 to 0.21 with an average of 0.06, corresponding to 0.05 to 0.56 *apfu*, or from 0.01 to 0.08% of available *O*-sheet sites. Although the Fe^{3+} content in AGM is minimal relative to Fe^{2+} and Mn contents, a difference in Fe^{3+}/Fe_{tot} ratios is observed between members of the kupletskite and astrophyllite subgroups. The lowest Fe^{3+}/Fe_{tot} ratios occur in almost end-member astrophyllite (ave.: 0.04, range: 0.01 to 0.08) from both over- and undersaturated rocks, whereas the highest ratios occur predominantly in members of the kupletskite subgroup (ave.: 0.10, range: 0.04 to 0.21), in particular Nb-bearing kupletskite and niobokupletskite, consistent with the oxidizing substitution

$$M(1)^{2+} + M(2,3)^{2+} + (Zr,Ti) + F \Leftrightarrow {}^{M(1)}Na + {}^{M(2,3)}Fe^{3+} + Nb + O \quad (7)$$

proposed for incorporation of Nb into the astrophyllite structure. The isomorphous substitution of Fe^{3+} into the astrophyllite group structure will be discussed in detail in further sections.

5.2. Fe^{2+} contribution

Astrophyllite group minerals are characterized by a dominant Fe^{2+} doublet centered at approximately 1.14 mm/s, with a range of <CS> of 1.124 to 1.154 mm/s, slightly higher than those obtained for micas (average: 1.11 to 1.13; Lalonde *et al.* 1996, Shabani 1999), indicative of Fe^{2+} in octahedral coordination. Average QS values range from 2.202 to 2.416

mm/s, lower than those observed for members of the biotite series, which commonly have values ranging from 2.3 to 2.5 mm/s (*e.g.* Rancourt *et al.* 1994a, Lalonde *et al.* 1996, Shabani 1999).

A general trend in QSDs is observed from broad distributions (W_{QSD}: 0.912 mm/s) with small <QS> (2.202 mm/s) and QS_{peak} (2.305 mm/s) values, to narrow distributions (W_{QSD}: 0.563 mm/s) with large <QS> (2.416 mm/s) and QS_{peak} (2.510 mm/s) values (Fig. 11). As a result, there is a negative correlation between <QS> and W_{QSD} and a positive correlation between <QS> and QS_{peak}. This is identical to what is observed in biotites from granitic rocks, as is shown in Figures 12 & 13 (Shabani 1999). In general, AGM show lower <QS> than biotites, but linear regression of the two data sets indicates that they can be combined and expressed by the equation: $W_{QSD} = 4.390 - 1.603\langle QS\rangle$ ($R^2 = 0.833$).

Figure 14 shows the relation between the $QS_{H\text{-}edge}$ and $QS_{L\text{-}edge}$ of the QSD. The $QS_{H\text{-}edge}$ shows only minor variation within the sample suite, a characteristic that will be further discussed when examining crystal-chemical controls on QSDs. The $QS_{L\text{-}edge}$ shows much wider variation within the sample suite and is strongly correlated with both the <QS> and QS_{peak}, (Fig. 15) such that an increase in $QS_{L\text{-}edge}$ is concomitant with an increase in <QS> and QS_{peak}.

The QSDs in the sample suite studied are a direct reflection of the distribution of local distortion environments (LDEs) around Fe in the structure, resulting from cationic or anionic substitutions at neighbouring sites, and thus reflect changes in the local stereochemistry and geometry of the Fe site. In order to fully understand the observed QSDs, detailed electronic structure calculations on known atomic structures are required. Such

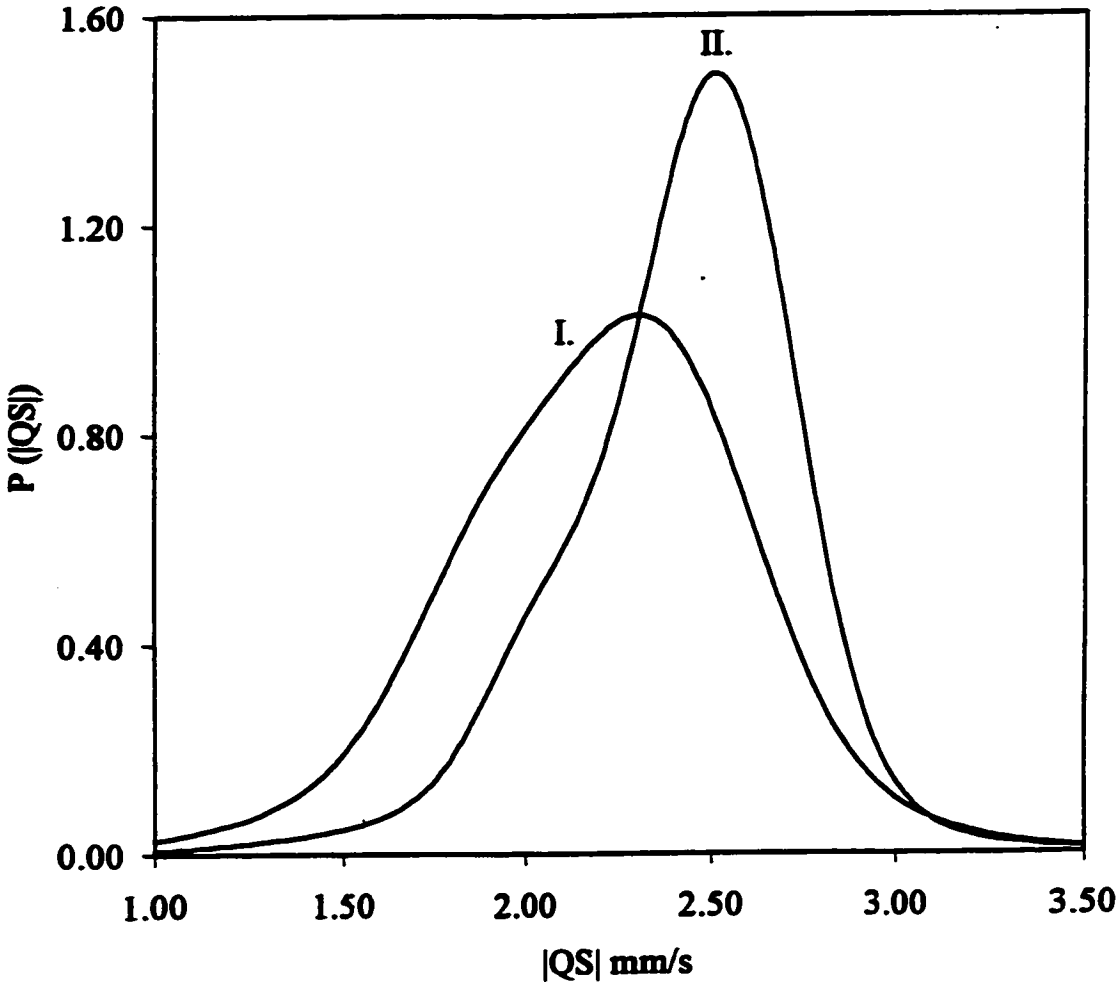

Figure 11. End-member quadrupole splitting distributions for the Fe^{2+} generalized site.
I. W_{QSD}: 0.912 mm/s, <QS>: 2.202 mm/s, QS_{peak}: 2.305 mm/s
II. W_{QSD}: 0.563 mm/s, <QS>: 2.416 mm/s, QS_{peak}: 2.510 mm/s
(Note: average values presented)

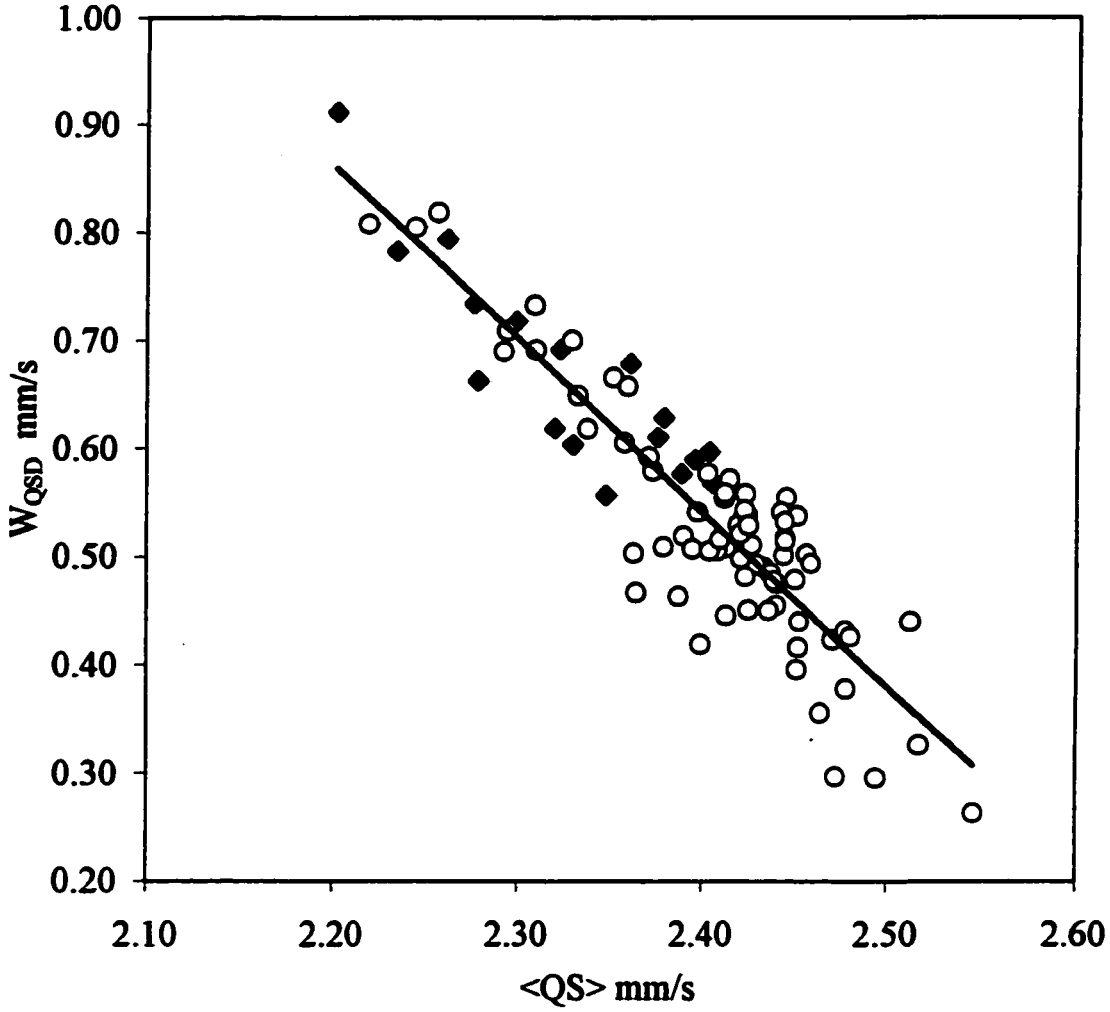

Figure 12. Average QS *versus* the width (W) of the QSD for astrophyllite group minerals (closed diamonds) and biotites (open circles).
Linear regression: $W_{QSD} = 4.390 - 1.603\langle QS\rangle$ ($R^2 = 0.833$)
Biotite data from Shabani (1999)

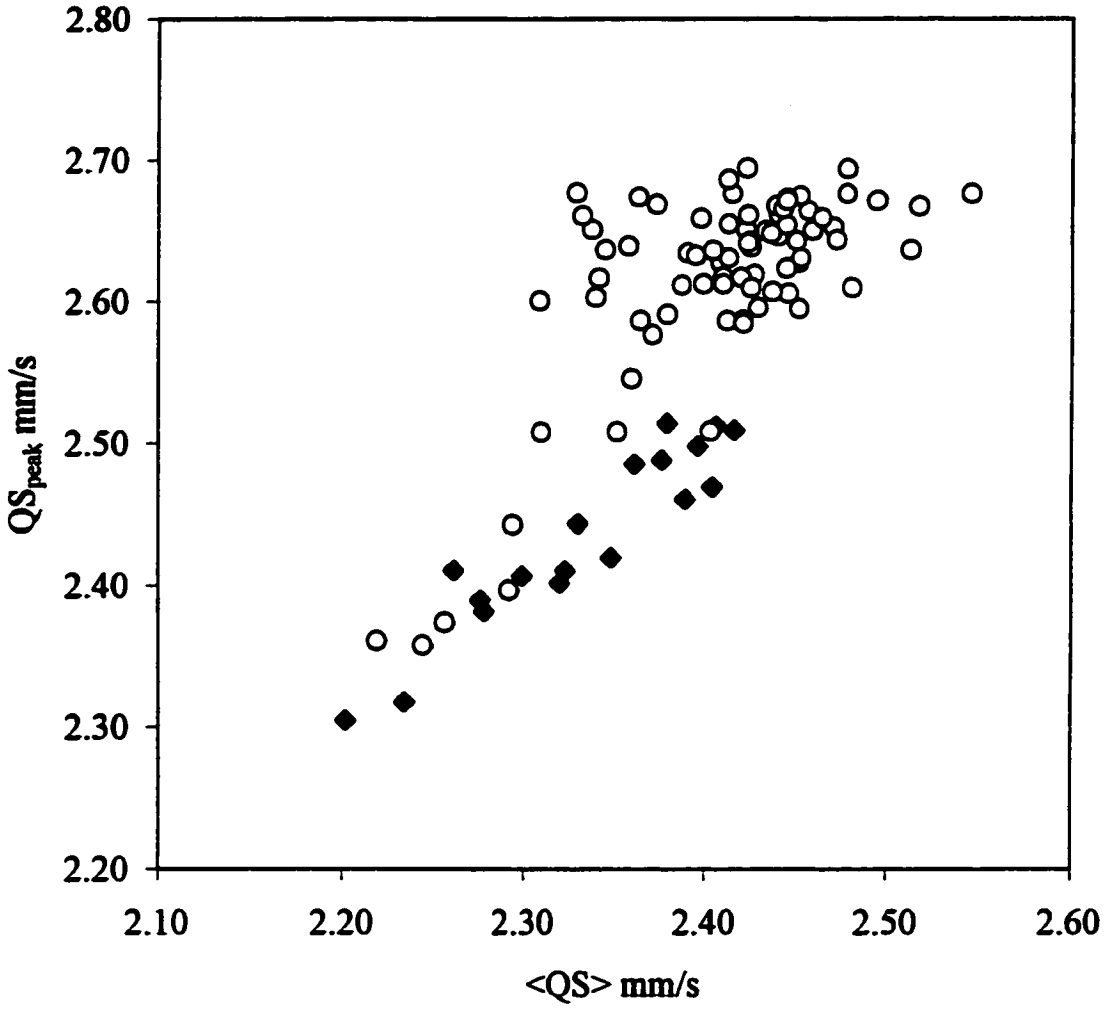

Figure 13. Average QS *versus* the QS_{peak} of the QSD for astrophyllite group minerals (closed diamonds) and biotites (open circles). Biotite data from Shabani (1999)

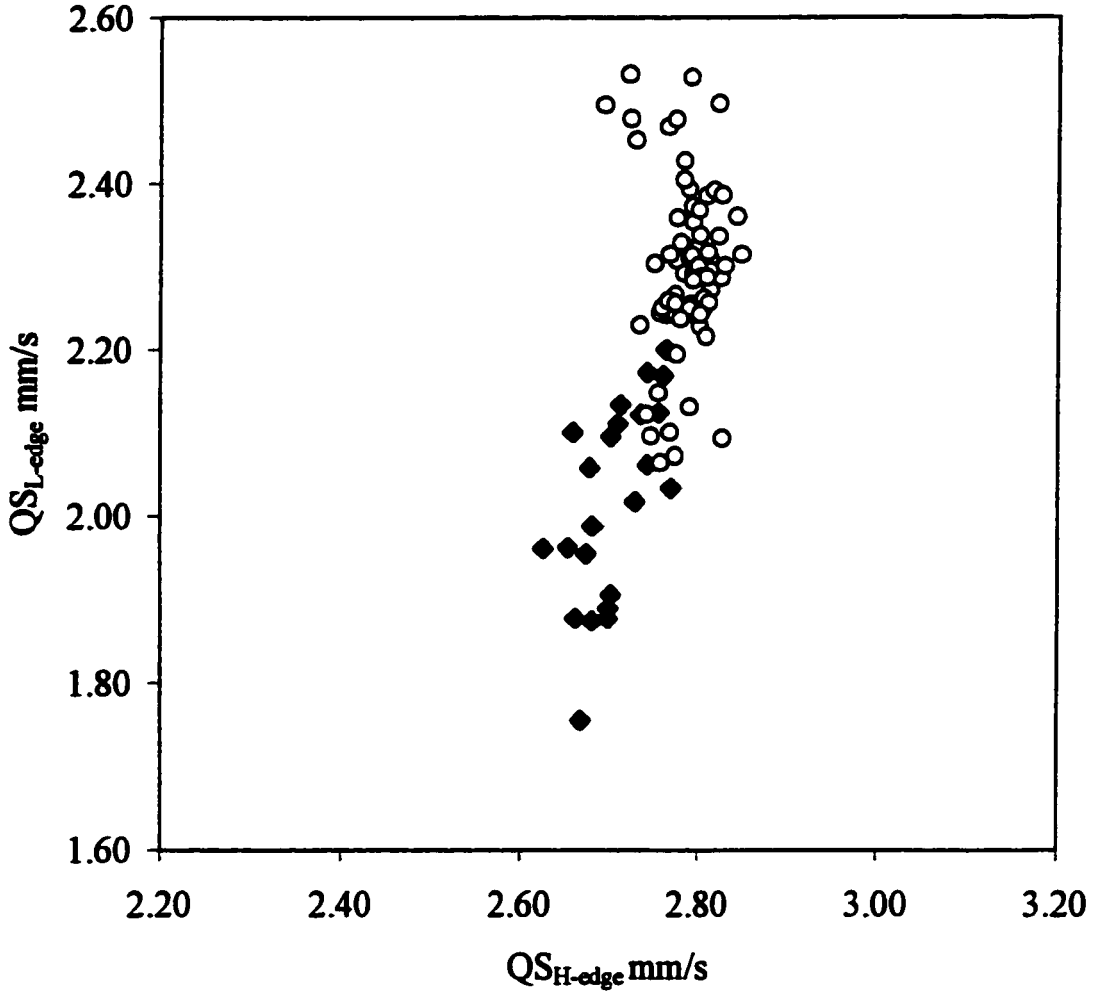

Figure 14. The relationship between the QS high energy edge (H-edge) and low energy edge (L-edge) of the QSD in astrophyllite group minerals (closed diamonds) and biotites (open circles). Biotite data from Shabani (1999)

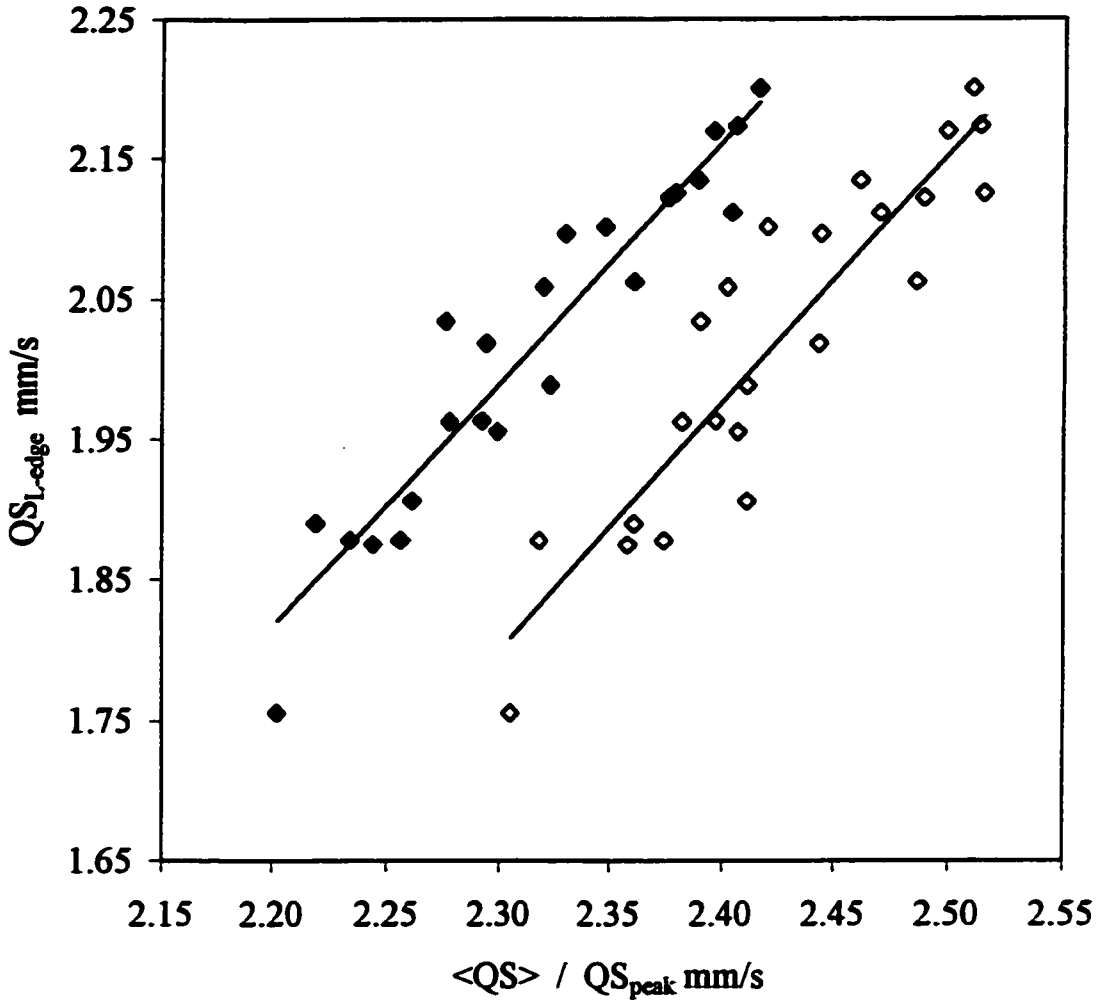

Figure 15. The relation between the <QS>/QS_{peak} and the low energy edge (L-edge) of the QSD in astrophyllite group minerals.
Closed diamonds: <QS> ($R^2 = 0.905$)
Open diamonds: QS_{peak} ($R^2 = 0.831$)

calculations are currently underway (Evans 2001) and preliminary results will be referred to in this chapter. Although a conclusive chapter on the origin and meaning of QSDs in the astrophyllite group is premature, an attempt is made here to present the data and to show that, in the astrophyllite group, there are significant correlations between known crystallographic parameters and QSDs.

6.0. DISCUSSION

Previous authors (*e.g.* Redhammer 1998; Shabani 1999) have shown <QS> to be a function of the average radius (r*M*) of the octahedrally-coordinated cations in the *O*-sheet of phyllosilicates. Figure 16 shows the negative correlation between r*M* and <QS> for AGM and, for comparison purposes, a suite of true micas from the annite-phlogopite series. In the annite-phlogopite series, increased substitution of Fe^{2+} (rFe^{2+}: 0.78 Å) in annite for Mg^{2+} (rMg^{2+}: 0.72 Å) in phlogopite results in smaller <QS> and thus a negative correlation between <QS> and Fe# [Fe/(Fe+Mg)] (Rancourt *et al.* 1994, Redhammer *et al.* 1995). Given that the dominant substitution in the astrophyllite group *O*-sheet is Mn ⇔ Fe, the Mn# [Mn/(Mn+Fe_{tot})] is used to describe its composition. Figure 17 shows the negative correlation between <QS> and increasing Mn#. The substitution of Mn^{2+} (rMn^{2+}: 0.83 Å) for Fe^{2+} results in an increased grand mean *M*-O bond length, <<*M*-O>>, and decreased octahedral flattening (Ψ) required for lateral fit of the adjacent *H*- and *O*-sheets. This flattening has a strong influence on the local distortion environment of the octahedra and is an important crystallographic parameter to which the <QS> may be associated. Unfortunately, crystallographic data could not be obtained for all samples for which

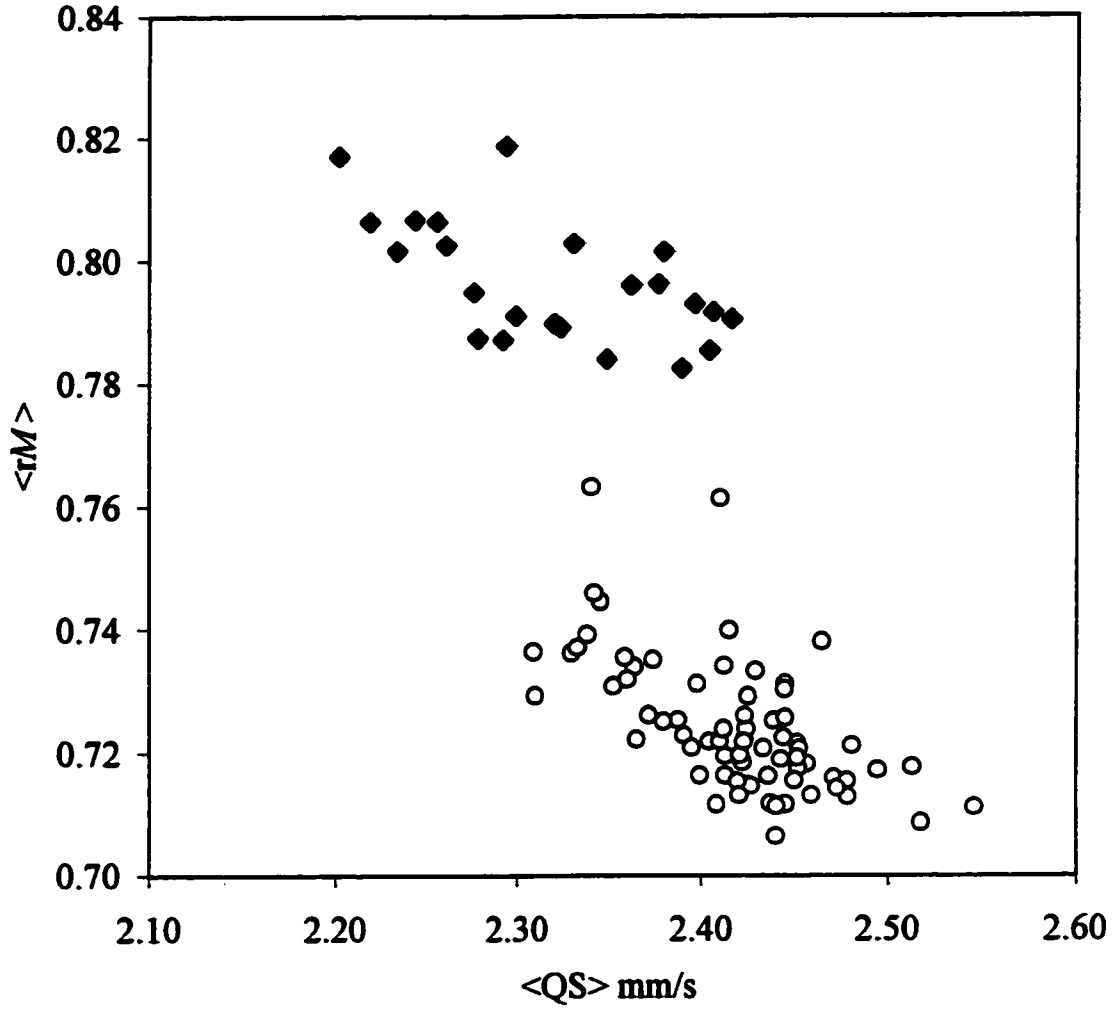

Figure 16. <QS> *versus* the average octahedral radius, <r*M*> in astrophyllite group minerals (closed diamonds) and in members of the annite-phlogopite series (open circles; data taken from Shabani 1999).

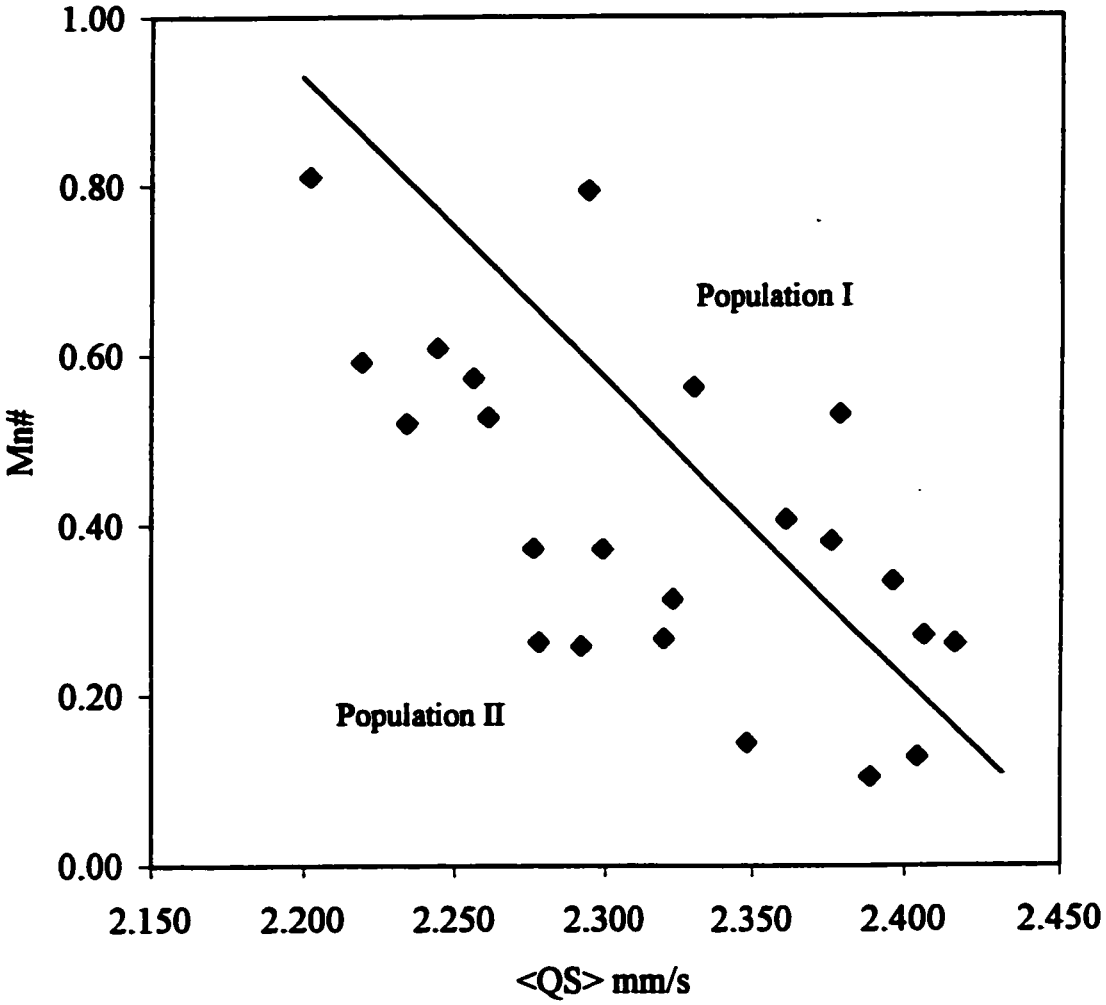

Figure 17. <QS> *versus* Mn# in astrophyllite group minerals. Note the presence of two populations within the sample suite.

Mössbauer spectra were obtained, but using the data available, it can be shown that a strong positive correlation exists between the average Ψ angle and <QS> (Fig. 18). The main trend observed between <QS> and Mn# is therefore due to decreased octahedral flattening as a result of increased Mn ⇔ Fe substitution. Theoretical electronic structure calculations by Evans (2001) based on FeO_6^{10-} and $Fe(OH)_6^{4-}$ clusters in an ideal dioctahedral mica *O*-sheet have also indicate octahedral flattening to be the dominant crystallographic parameter responsible for variations in QSDs.

A plot of <QS> *versus* Mn# shows a negative correlation between the two parameters and the existence of two distinct populations of AGM samples: one Zr-rich (> 0.40 *apfu* Zr) and one Zr-deficient (< 0.40 *apfu* Zr). The two populations have parallel linear-regression lines, suggesting that, in all cases, the dominant cause of variations in <QS> is the Mn# (Fig. 19). The presence of a high Zr content (>0.40 *apfu*) causes a shift in the observed range of <QS> such that at any given value of Mn#, Zr-deficient samples will have lower <QS> than Zr-rich samples. The range of <QS> observed in both populations is comparable (Zr-deficient: 0.185 mm/s, Zr-rich: 0.122 mm/s). Within the two populations, Zr-rich samples have QSDs that are shifted to higher energies, relative to the Zr-deficient suite, and thus show larger values of QS_{peak}, $QS_{H\text{-}edge}$ and $QS_{L\text{-}edge}$. Zr-deficient samples have QS_{peak} values ranging from 2.305 to 2.470 mm/s (average: 2.398 mm/s), $QS_{H\text{-}edge}$ values ranging from 2.626 to 2.769 mm/s (average: 2.689 mm/s), and $QS_{L\text{-}edge}$ values ranging from 1.756 to 2.135 mm/s (average: 1.980 mm/s). Zr-rich AGM have QS_{peak} values ranging from 2.443 to 2.513 mm/s (average: 2.489 mm/s), $QS_{H\text{-}edge}$ values ranging from 2.701 to 2.764 mm/s (average:

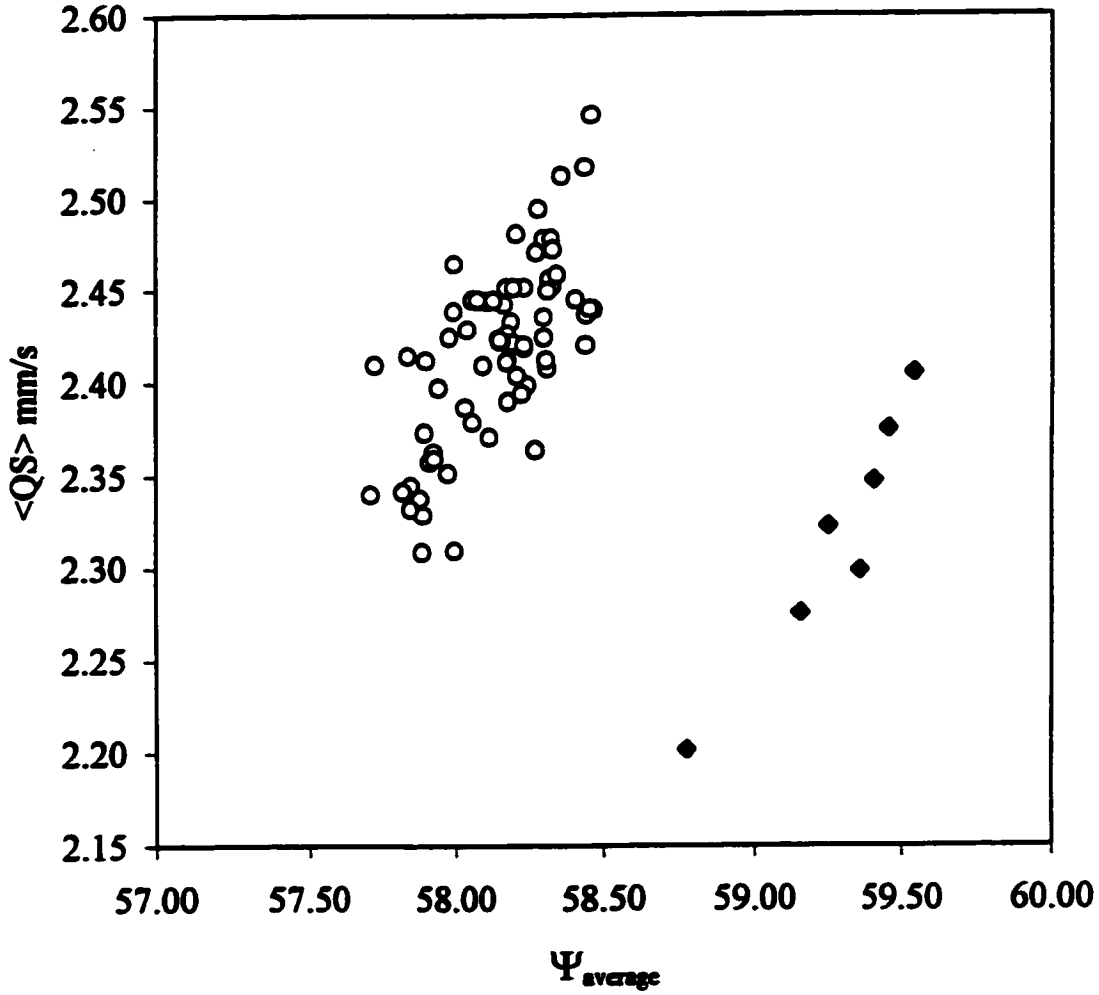

Figure 18. Average flattening angle, Ψ, *versus* <QS> in astrophyllite group minerals (closed diamonds) and members of the annite-phlogopite series (open circles; data from Shabani 1999).

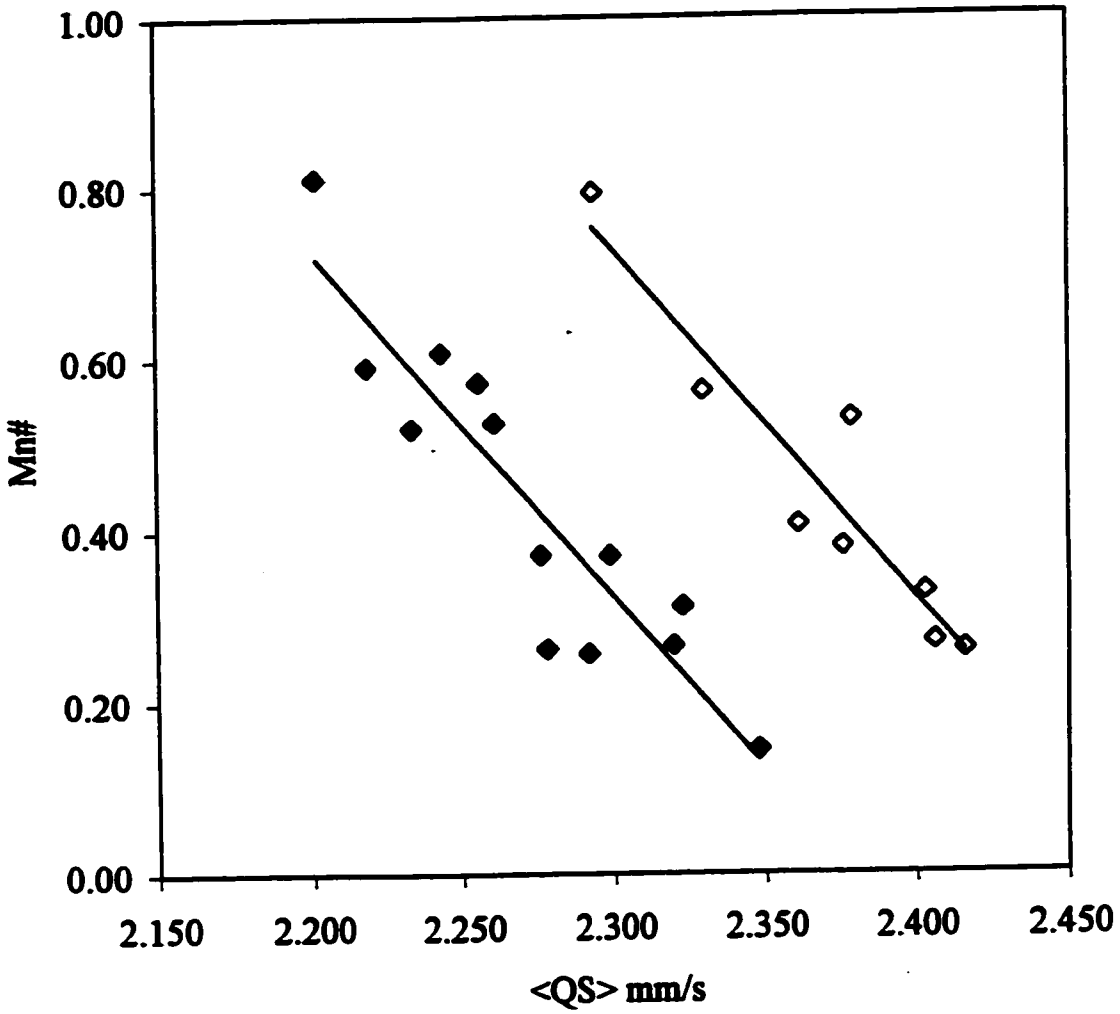

Figure 19. <QS> *versus* Mn# in astrophyllite group minerals showing the two populations.
Closed diamonds: Zr-deficient (< 0.40 *apfu* Zr)
Open diamonds: Zr-rich (> 0.40 *apfu* Zr)

2.739 mm/s) and $QS_{L\text{-}edge}$ values ranging from 2.019 to 1.274 mm/s (average: 2.121 mm/s). Figures 20A and B show the QSDs for both populations of AGM.

The monotonic and regular variation from low to high Mn# observed in QSDs within each AGM population suggest that the changes in the LDEs are progressive and gradual and do not represent a structural discontinuity. In contrast, the discontinuity between Zr-deficient and Zr-rich populations, most evident in the position of the $QS_{H\text{-}edge}$, suggests a mechanism other than simple octahedral flattening for the observed changes in the LDE. In particular, the higher $QS_{H\text{-}edge}$ in the Zr-rich population suggests a maximum LDE with a higher degree of distortion than that of the Zr-deficient population. The reasons for this difference lie in the local geometry of the $D\phi_6$ octahedra and its influence on the *O*-sheet octahedra. In particular, we are interested in the O(2)-*D*-ϕ(16) distance along which the $D\phi_6$ octahedron is elongated. The apical O(2) oxygen of the $D\phi_6$ octahedron is also bonded to three octahedra in the *O*-sheet, *M*(1), *M*(2) and *M*(3). Increased substitution of Zr, a significantly larger cation than either Nb or Ti, results in increased overall *D*-ϕ bond lengths and a lengthening of the O(2)-*D*-ϕ(16) distance, which causes a concomitant shortening of the *M*-O(2) bond lengths (Fig. 21). The distortion due to shortening of the *M*-O(2) bond in each of the three individual octahedra is a local effect and is responsible for the shift in QSDs to higher overall values. As Zr is not the only element to substitute for Ti at *D*, this effect will be more apparent when Zr contents are elevated (*i.e.* > 0.40 *apfu*). In general, samples which contain > 0.40 *apfu* Zr contain little Nb and therefore the resultant structural affects are attributable only to Zr.

Each QS value in the distribution corresponds to a set of particular LDEs that are defined by the positions of the coordinating anions around the Fe ions. Each LDE has its

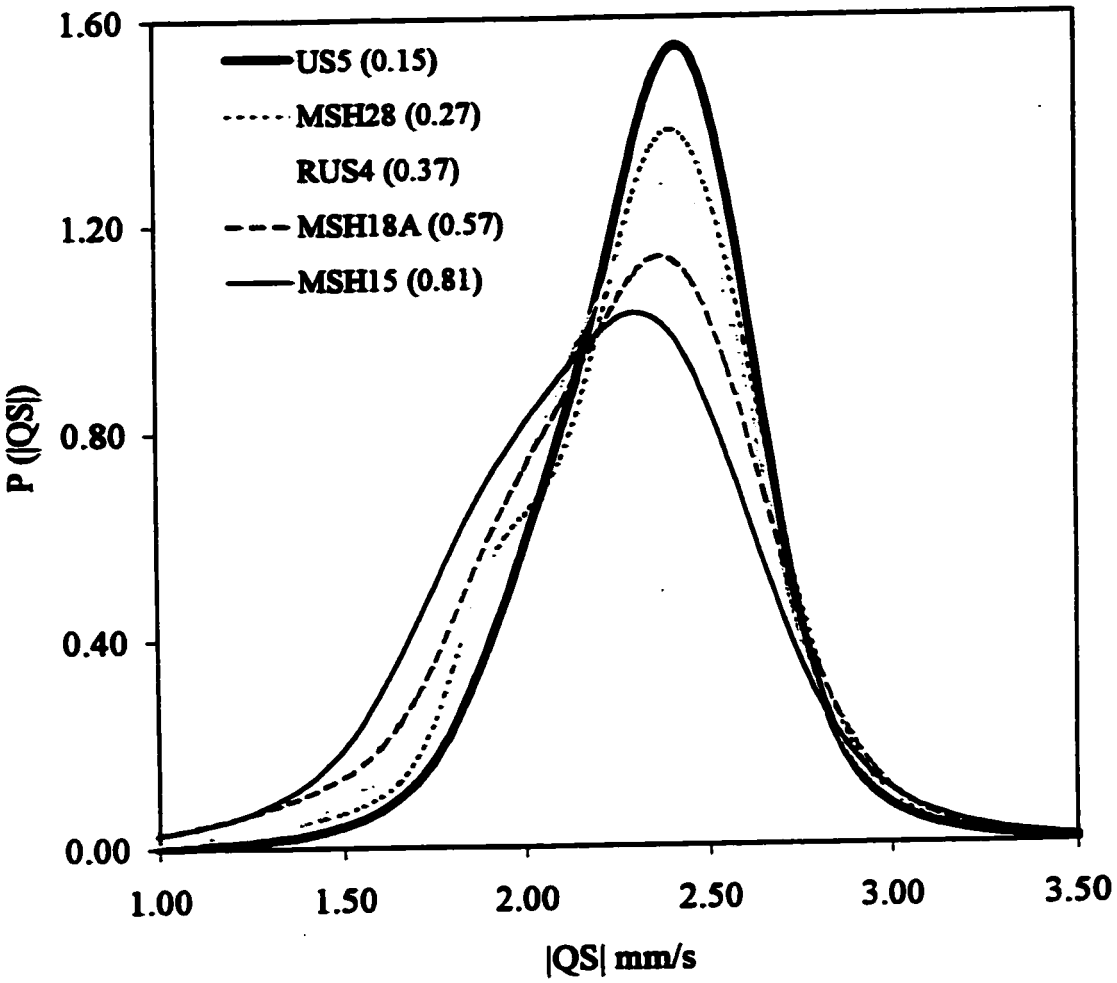

Figure 20A. Representative quadrupole splitting distributions for the Fe^{2+} generalized site in Zr-poor astrophyllite group minerals (Mn# in brackets).

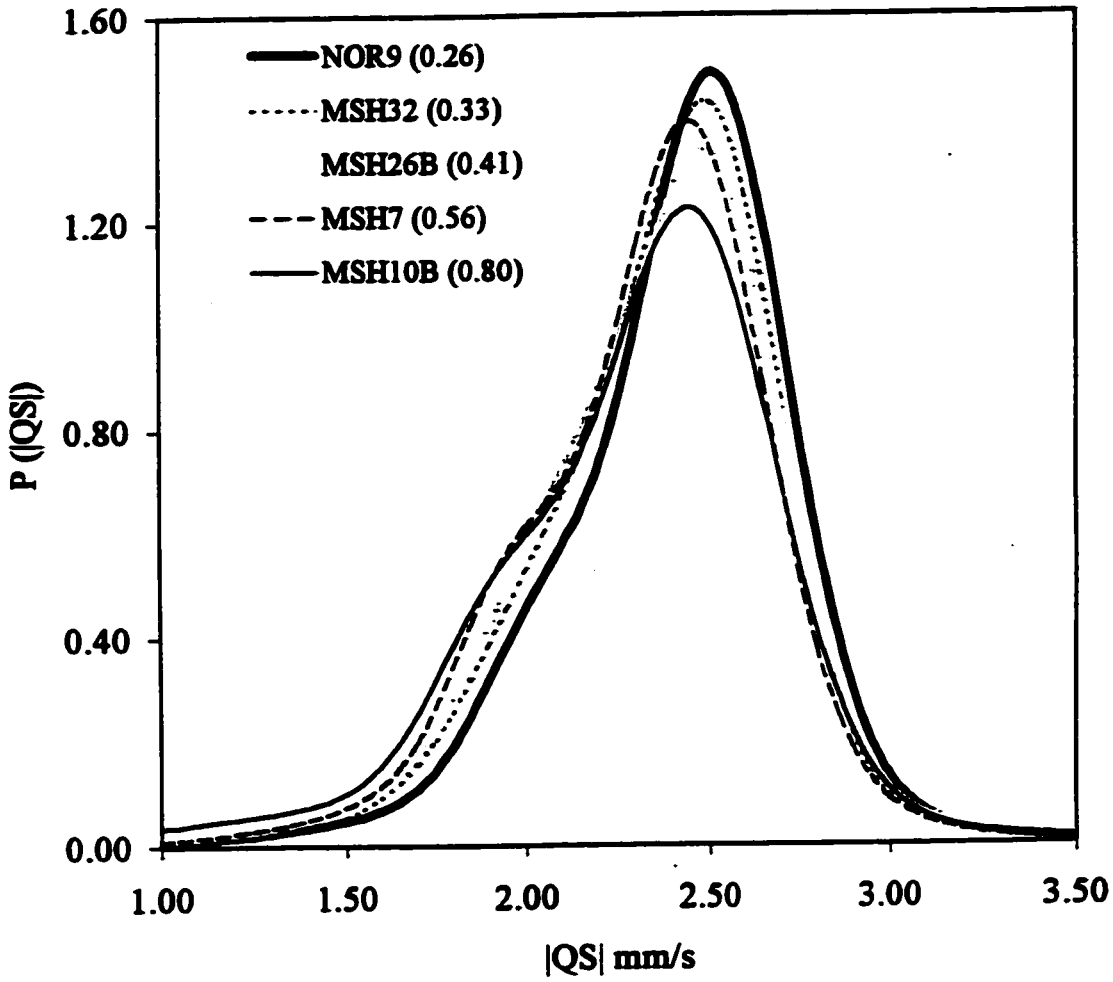

Figure 20B. Representative quadrupole splitting distributions for the Fe^{2+} generalized site in Zr-rich astrophyllite group minerals (Mn# in brackets).

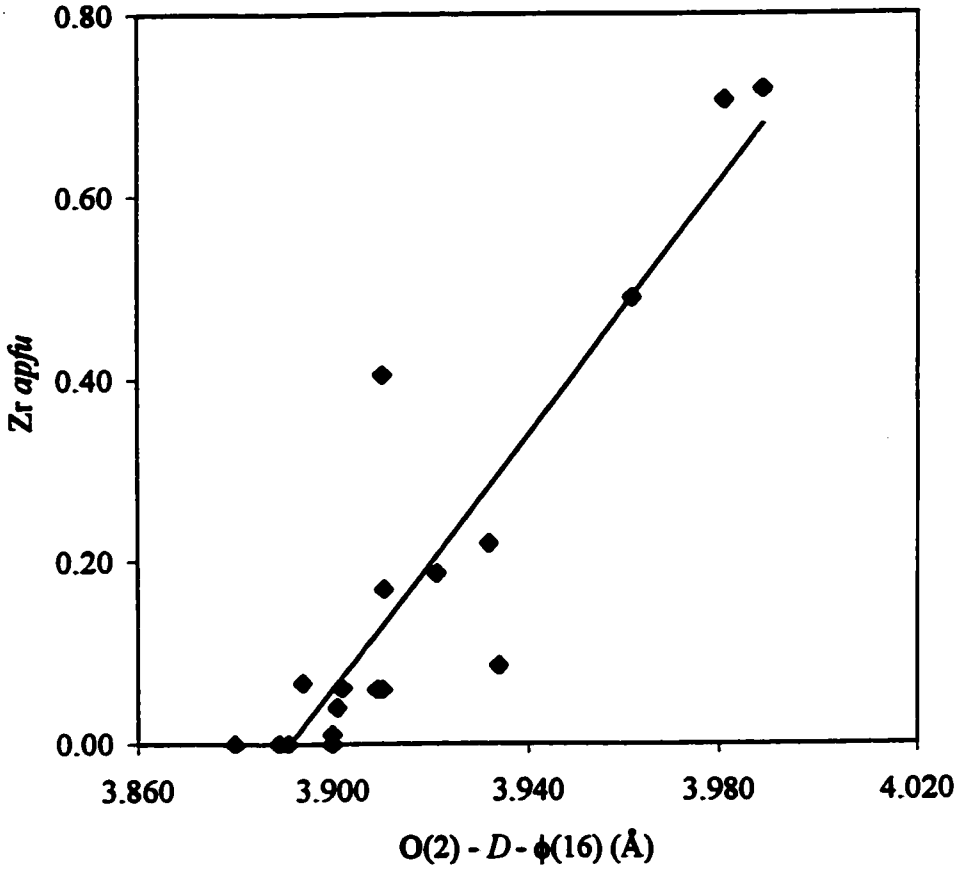

Figure 21A. The Zr content *versus* the O(2)-*D*-ϕ(16) distance in the $D\phi_6$ octahedron. Linear regression, $R^2 = 0.844$

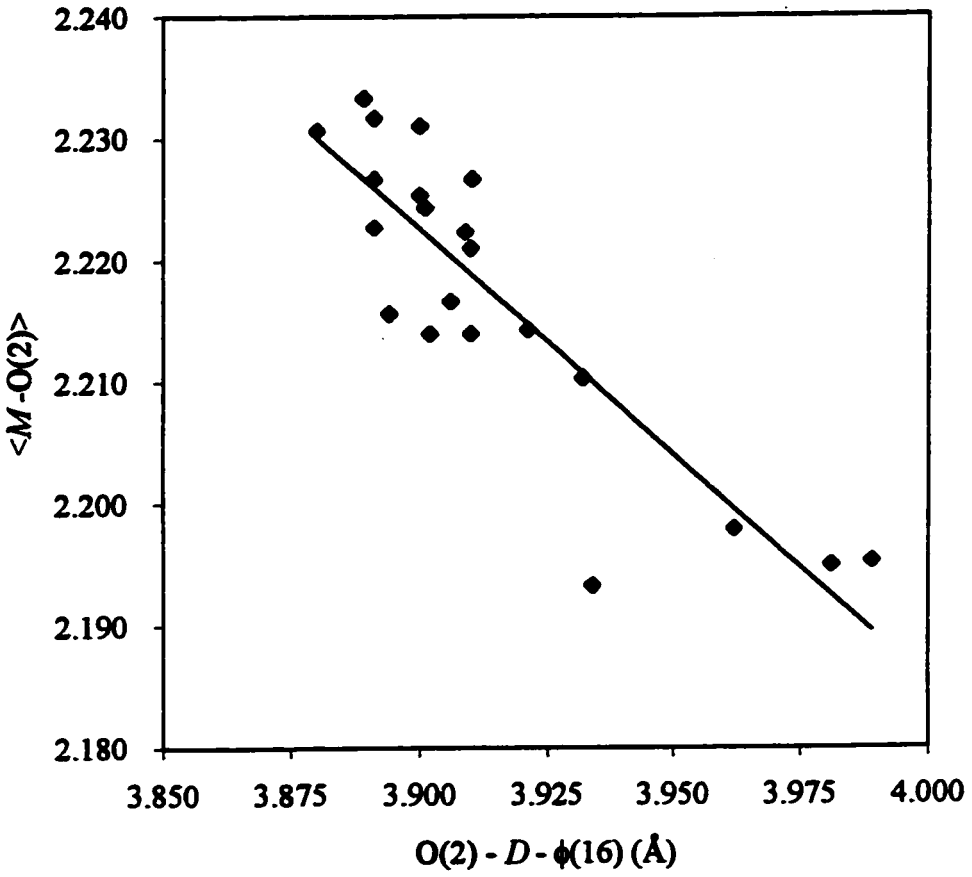

Figure 21B. The O(2)-*D*-ϕ(16) distance *versus* <*M*-O(2)>
Linear regression, $R^2 = 0.765$

own Fe^{2+} population, the sum of which is proportional to $P(QS_{peak})$. In both suites, as the Mn content increases, the bimodal character of the QSD becomes less evident. With increasing Mn#, the QSD peak centered at ≈ 1.9 and 2.0 mm/s in Zr-deficient and Zr-rich samples, respectively, grows with a concomitant depopulation and decrease in the $P(QS_{peak})$ (QS_{peak} ≈ 2.4 and 2.5 mm/s for Zr-deficient and Zr-rich samples, respectively).

The presence of a bimodal distribution of QSDs is common in phyllosilicates such as muscovite and members of the biotite series. In muscovites, the dominant QSD peaks at 3.0 and 2.1 mm/s have been attributed to Fe^{2+} in *cis* and *trans* sites, respectively (Shabani *et al.* 1998, Shabani 1999). Similarly, electronic-structure calculations (Evans 2001) indicate the short, broad peak at low QS values to correspond to Fe^{2+} at the *trans* sites and the high, narrow peak at higher QS values to correspond to Fe^{2+} at the smaller *cis* sites. In AGM, both *cis* [*M*(2) and *M*(3)] and *trans* [*M*(4)] sites are present, as well as a site coordinated by five O^{2-} and one OH^- group [*M*(1)]. Unlike in micas, the *trans M*(4) site in the astrophyllite group structure is the smallest of the four *O*-sheet sites. It is not possible at this time to unequivocally attribute the peaks in the astrophyllite group QSDs to any of these four sites due to a lack of electronic structure calculations. We can, however, suggest potential reasons for the bimodal character of the QSDs based on known crystallographic features and comparison with results from trioctahedral micas.

The P(QS) distributions can be interpreted as LDE population distributions with the value of $P(QS_{peak})$ inversely proportional to σ_{QSD}. Astrophyllite group samples with the highest σ_{QSD}, and thus the largest variation in LDE populations, are those which have high Mn# (*i.e.* kupletskite, niobokupletskite and Mn-rich astrophyllite). This may be due to

increased substitution of Mn, Na, Fe^{3+} at *M* sites surrounding the Fe^{2+} cation, and increased substitution of HFSE such as Zr and Nb at *D*, consistent with results from EMP data, all of which would result in an increased variety of local environments around Fe.

Low QS values have been attributed to highly distorted or "defect" sites in micas such as annite and fluorannite (Rancourt *et al.* 1994, 1996, Redhammer 1998). Given this inverse correlation between octahedral distortion and QS (Hawthorne 1988), the peak at 1.9 mm/s may be assigned to the most highly distorted octahedron in the AGM structure, *M*(2). The depopulation of this peak at high Mn# may suggest preferential ordering of Fe at *M*(2) at low Fe activities. The bulk of the QSD centered at 2.4 to 2.5 mm/s is attributed to Fe^{2+} at the *M*(1), *M*(3) and *M*(4) octahedra.

Future work involving electronic-structure calculations similar to those performed by Evans (2001) is planned. These calculations should be helpful in understanding the effects of isometric distortion (such as flattening) on the QSDs, and rectangular distortions (such as bond length shortening due to substitution of Zr in the *H*-sheet).

7.0. Conclusions

1. AGM have room temperature ^{57}Fe Mössbauer spectra which are characterized by two strong absorption peaks centered at ≈ -0.1 and 2.3 mm/s and a third, weaker shoulder at ≈ 0.9 mm/s, corresponding to (1) the sum of the low-energy lines from $^{[6]}Fe^{2+}$ and $^{[6]}Fe^{3+}$ doublets, (2) the high-energy lines from $^{[6]}Fe^{2+}$ doublets, and (3) the high-energy lines from $^{[6]}Fe^{3+}$ doublets, respectively. No evidence for $^{[4]}Fe^{3+}$ was found in the samples studied.

2. Fe^{3+}/Fe_{tot} ratios in AGM range from 0.01 to 0.21, corresponding to 0.05 to 0.56 *apfu* Fe^{3+}. Manganese-rich samples of the kupletskite subgroup show the highest enrichment in Fe^{3+}. The highest observed ratios occur in niobian kupletskite and niobokupletskite, consistent with the oxidizing substitution $M(1)^{2+} + M(2,3)^{2+} + (Zr,Ti) + F \Leftrightarrow {}^{M(1)}Na + {}^{M(2,3)}Fe^{3+} + Nb + O$ proposed for incorporation of Nb into the astrophyllite group structure.

3. Centre shift values for $^{[6]}Fe^{3+}$ range from 0.256 to 0.347 mm/s and <QS> values range from 0.762 to 1.082 mm/s. Centre shift values for $^{[6]}Fe^{2+}$ range from 1.124 to 1.154 mm/s, with <QS> values from 2.202 to 2.416 mm/s.

4. A general trend in QSDs is observed from broad distributions with small <QS> and QS_{peak} values, to narrow distributions with large <QS> and QS_{peak} values. Variations in <QS> are dominantly the result of octahedral flattening (Ψ) within the *O*-sheet octahedra. Increased Mn# due to the Mn $\Leftrightarrow$ Fe substitution results in decreased Ψ required to achieve lateral fit between the *H*- and *O*-sheets. The <QS> has been shown to be negatively correlated with Mn# and positively correlated with Ψ.

5. Two distinct populations of QSDs can be recognized on the basis of the Zr content of the sample. Zr-rich samples (Zr > 0.40 *apfu*) have larger values of QS_{peak}, $QS_{H\text{-}edge}$ and $QS_{L\text{-}edge}$ compared to Zr-deficient samples (Zr < 0.40 *apfu*). This shift in QSDs of Zr-rich samples to higher average values is attributable to additional distortion of the *M*(1), *M*(2) and *M*(3) octahedra in the form of shortening of *M*-O(2) bonds due to increase of the O(2)-*D*-ϕ(16) distance in the $D\phi_6$ octahedron.

CHAPTER V.

KUPLETSKITE POLYTYPES FROM THE LOVOZERO MASSIF, KOLA PENINSULA, RUSSIA: KUPLETSKITE-1*A* AND KUPLETSKITE-*Ma2b2c*

PAULA C. PIILONEN
Ottawa-Carleton Geoscience Centre, Department of Earth Sciences
University of Ottawa, Ottawa, Ontario K1N 6N5

ANDREW M. McDONALD
Department of Earth Sciences, Laurentian University, Sudbury, Ontario P3E 2C6

ANDRÉ E. LALONDE
Ottawa-Carleton Geoscience Centre, Department of Earth Sciences
University of Ottawa, Ottawa, Ontario K1N 6N5

Accepted for publication in *European Journal of Mineralogy* (April 4th, 2001)

OVERVIEW

Derivations of theoretical AGM polytypes have been performed by a number of authors (*e.g.* Vrublevskaya & Zvyagin 1976, Zvyagin & Vrublevskaya 1976, Dornberger-Schiff *et al.* 1985), yet until recently only two of these structural modifications had been recognized in nature. This chapter provides the results obtained from single-crystal X-ray structure determinations of two holotype kupletskite samples from the Lovozero massif (Kola Peninsula, Russia). Kupletskite, originally described by Semenov (1956), is found to occur in both triclinic, $P\bar{1}$, and monoclinic, *C*2/*c*, structural modifications. The two structures differ only in the stacking sequence of an identical *HOH* layer. The results from this study represent the first natural example of polytypism in the astrophyllite group, as determined by single-crystal X-ray structure determinations, and suggests the possibility for further research into stacking disorders in AGM.

ABSTRACT

The crystal structures of two kupletskite [$K_2NaMn_7Ti_2Si_8O_{26}(OH)_4F$] polytypes, (1) triclinic, space group $P\bar{1}$, and (2) monoclinic, space group $C2/c$, from nepheline syenite pegmatites of the Lovozero massif, Russia, have been determined. The two structures differ in the stacking sequence of an identical *HOH* layer (where *H* = heterophyllosilicate and *O* = octahedral): in the triclinic structure, individual *HOH* layers are related by a centre of symmetry, resulting in a *+HOH/+HOH/+HOH* stacking sequence with a one-layer period; in monoclinic kupletskite, adjacent *HOH* layers are related by a two-fold axis parallel to *b*, resulting in a *+HOH/-HOH/+HOH* stacking sequence with a two-layer period. The resultant relationship between the unit cell parameters of monoclinic kupletskite-*Ma2b2c* and triclinic kupletskite-1*A* are as follows: $a_{monoclinic} = a_{triclinic}$, $b_{monoclinic} = 2(b\sin\gamma)_{triclinic}$, and $c_{monoclinic}$ spans two *HOH* layers. These results represent the first single-crystal X-ray structure determination of polytypes in the astrophyllite group.

Key words: astrophyllite group, kupletskite, polytype, Lovozero, *HOH* layer

SOMMAIRE

Nous avons déterminé la structure cristalline de deux polytypes de kupletskite, un premier triclinique de symétrie spatiale $P\bar{1}$, et l'autre monoclinique, de symétrie spatiale $C2/c$, tous deux provenant des pegmatites de syénite à néphéline du massif Lovozero en Russie. Les deux structures se distinguent par leurs séquences d'empilements de couches *HOH* (où *H* = couche hétérophyllosilicatée et *O* = couche octaédrique): dans l'échantillon triclinique, les couches *HOH* individuelles sont reliées les unes aux autres par un centre de

symétrie, produisant ainsi une séquence d'empilement du type *+HOH/+HOH/+HOH* ayant une périodicité d'une couche alors que dans l'exemple monoclinique, les couches *HOH* adjacentes sont reliées les unes aux autres par une rotation d'ordre 2 parallèle à *b*, ce qui mène à une séquence d'empilement du type *+HOH/-HOH/+HOH* avec une périodicité de deux couches. La correspondance entre les paramètres réticulaires du polytype monoclinique (kupletskite-*Ma2b2c*) et celui triclinique (kupletskite-1*A*) est la suivante : $a_{monoclinique} = a_{triclinique}$, $b_{monoclinique} = 2(b\sin\gamma)_{triclinique}$, et le paramètre $c_{monoclinique}$ s'étend sur deux couches *HOH*. Cette étude documente pour la première fois l'existence du polytypisme dans le groupe de l'astrophyllite par des méthodes de diffraction-X sur monocristaux.

Mots-clés: groupe de l'astrophyllite, kupletskite, polytype, Lovozero, couche *HOH*

1.0. INTRODUCTION

Astrophyllite group minerals (AGM) are alkali titano-, niobo- and zirconosilicates which have the general formula $A_2BC_7D_2T_8O_{26}(OH)_4X_{0-1}$ where $A = {}^{[10-13]}$K, Rb, Cs, Na, H_3O, H_2O, or □; $B = {}^{[10]}$Na or Ca; $C = {}^{[6]}$Mn, Fe^{2+}, Fe^{3+}, Na, Mg, or Zn; $D = {}^{[6]}$Ti, Nb, or Zr; T = Si and Al, X = F, OH, O, or □ (Piilonen *et al.* 2000). Kupletskite, ideally $K_2NaMn_7Ti_2Si_8O_{26}(OH)_4F$, one of eight known AGM, is found in SiO_2-oversaturated alkaline rocks such as Point of Rocks, New Mexico, USA (DeMark 1984), Gjerdingen, Norway (Raade & Haug 1982), and the Junguni intrusion, Chilwa, Malawi (Woolley & Platt 1988), and SiO_2-undersaturated intrusions such as the Lovozero massif, Kola Peninsula (Semenov 1956) and the Azov region, Russia (Valter *et al.* 1965), the Larvik complex, Langesundsfjord area, Norway (Piilonen unpublished data), the Werner Bjerge complex and

Kangerdlugssuaq, East Greenland (Brooks *et al.* 1982, Christiansen *et al.* 1998), and Mont Saint-Hilaire, Québec, Canada (Horváth & Gault 1990; Piilonen *et al.* 2000).

Kupletskite was initially described by Semenov (1956) from nepheline syenite pegmatites in the Lepkhe-Nelm and Kuivchorr mountains of the Lovozero massif, Kola Peninsula, Russia. It occurs as coarse-grained (up to 0.5 cm), anhedral to subhedral, dark brown, platy to acicular crystals associated with aegirine, natrolite, eudialyte group minerals, microcline, mangano-pectolite, and neptunite. In the original description, no data pertaining to the space group or cell parameters were provided, and only monoclinic or triclinic (pseudomonoclinic) symmetry was proposed. Peng & Ma (1963) described a Mn-dominant astrophyllite from Russia with triclinic symmetry ($P\bar{1}$) but did not elaborate on its relationship with kupletskite. Christiansen *et al.* (1998) refined the structure of a kupletskite from Kangerdlugssuaq, east Greenland, and confirmed it to be triclinic, space group $P\bar{1}$. Structure analyses on holotype kupletskite from Mount Kuivchorr (Lovozero) and a sample from Lephke-Nelm were performed as part of a larger study on the crystal chemistry and paragenesis of members of the astrophyllite group. During data collection, the possibility of a monoclinic polytype was recognized and further analyses were performed.

Crystal structure analyses confirm kupletskite from Mount Kuivchorr to be triclinic, space group $P\bar{1}$, whereas that from Lephke-Nelm was found to be monoclinic, space group *C*2/*c*. The existence of two structural states for kupletskite is the result of polytypism in the astrophyllite group. The objectives of the following study are to: (1) describe and compare the crystal structures of triclinic and monoclinic kupletskite, (2) discuss the mechanism for polytype formation in AGM, and (3) to introduce polytype nomenclature into the

astrophyllite group in accordance with the guidelines proposed by the IMA Commission on New Minerals and Mineral Names (Bailey *et al.* 1978, Nickel & Grice 1998).

2.0. CHEMICAL COMPOSITION

Two kupletskite samples were analysed: RUS9 (Lephke-Nelm) and RUS12 (holotype material, Mount Kuivchorr). Chemical analyses were performed on a JEOL 733 electron microprobe in wavelength-dispersive mode using Tracor Northern 5500 and 5600 automation software. Details regarding operating conditions and standard selection can be found in Chapter II. Complete electron microprobe data can be found in Table 1. Chemical formulae were calculated on the basis of 31 anions and 5(OH,F,O) as determined from the crystal structure analysis.

3.0. X-RAY CRYSTALLOGRAPHY

X-ray powder diffraction data for RUS9 and RUS12 were collected with a 114.6 Debye-Scherrer camera employing Cu$K\alpha$ radiation (Ni-filtered) operating at 45 kV and 20 mA (24 hour exposure) and 40 kV and 30 mA (6 hour exposure), respectively. Observed and calculated (PowderCell 1999) *X*-ray powder diffraction patterns for both polytypes are presented in Table 2. Monoclinic and triclinic kupletskite polytypes can be distinguished on the basis of their *X*-ray powder diffraction patterns in two main regions. The most evident difference between the two patterns is the presence of a moderately strong (I_{obs} = 30) peak at ~ 9.8 Å in triclinic modifications that is absent in monoclinic kupletskite. Secondly, in triclinic kupletskite, a broad band is observed between 30 and 40° 2θ (Cu$K\alpha$ radiation),

Table 1. Chemical composition of triclinic (RUS12) and monoclinic (RUS9) kupletskite*

	RUS12			RUS9		
Oxide	1	2	Ave.	1	2	Ave.
Na_2O	2.60	2.61	2.61	2.14	2.00	2.07
K_2O	5.90	5.92	5.91	6.16	6.25	6.21
Rb_2O	0.51	0.49	0.50	0.50	0.50	0.50
Cs_2O	0.00	0.00	0.00	0.00	0.05	0.03
CaO	1.37	1.38	1.38	1.24	1.30	1.27
SrO	0.25	0.20	0.23	0.29	0.24	0.27
BaO	0.00	0.13	0.07	0.55	0.48	0.52
MgO	1.96	1.92	1.94	1.38	1.45	1.42
MnO	27.55	27.50	27.53	21.47	21.44	21.46
FeO	4.11	4.15	4.13	10.91	11.05	10.98
Al_2O_3	0.23	0.25	0.24	1.00	1.08	1.04
Ce_2O_3	0.00	0.14	0.07	0.32	0.25	0.29
ZrO_2	0.00	0.00	0.00	0.00	0.00	0.00
TiO_2	11.45	11.35	11.40	10.31	10.72	10.52
Nb_2O_5	0.79	0.75	0.77	2.37	2.38	2.38
SiO_2	36.67	36.02	36.35	34.47	34.81	34.64
F	1.25	1.06	1.16	1.05	1.14	1.10
H_2O	2.82	2.87	2.85	2.83	2.83	2.83
O=F	-0.53	-0.45	-0.49	-0.44	-0.48	-0.46
Total	96.93	96.43	96.68	96.55	97.49	97.02
Formula based on 31 anions						
K	1.65	1.68	1.67	1.77	1.78	1.77
Rb	0.07	0.07	0.07	0.07	0.07	0.07
Cs	0.00	0.00	0.00	0.00	0.01	0.00
Sr	0.03	0.03	0.03	0.04	0.03	0.03
Ba	0.00	0.01	0.01	0.05	0.04	0.05
Na	0.00	0.04	0.02	0.00	0.00	0.00
Sum *A*	1.76	1.82	1.79	1.93	1.93	1.93
Na	0.63	0.67	0.65	0.58	0.46	0.52
Ca	0.32	0.33	0.33	0.30	0.31	0.31
Sum *B*	0.95	1.00	0.97	0.88	0.77	0.82
Na	0.48	0.41	0.44	0.36	0.40	0.38
Mg	0.64	0.64	0.64	0.46	0.48	0.47
Mn	5.13	5.17	5.15	4.10	4.04	4.07
Fe^{2+}	0.76	0.77	0.77	2.06	2.06	2.06
Ce	0.00	0.01	0.01	0.03	0.02	0.02
Sum *C*	7.01	7.00	7.00	7.00	7.00	7.00
Ti	1.89	1.90	1.90	1.75	1.80	1.78
Nb	0.08	0.08	0.08	0.24	0.24	0.24
Zr	0.00	0.00	0.00	0.00	0.00	0.00
Sum *D*	1.97	1.98	1.97	1.99	2.04	2.02
Si	8.05	8.00	8.03	7.77	7.75	7.76
Al	0.06	0.06	0.06	0.27	0.28	0.28
Sum *T*	8.11	8.06	8.09	8.04	8.03	8.04
F	0.87	0.74	0.81	0.75	0.80	0.78
OH	4.13	4.26	4.20	4.25	4.21	4.23
O	26.00	26.00	26.00	26.00	26.00	26.00
Σcat.	19.79	19.86	19.83	19.83	19.77	19.80

* Electron-microprobe data

Table 2. X-ray powder diffraction data for triclinic and monoclinic kupletskite

Triclinic, kupletskite-1A*					Monoclinic, kupletskite-Ma 2b 2c**				
d_{meas}	d_{calc}	I_{obs}	I_{calc}	*hkl*	d_{meas}	d_{calc}	I_{obs}	I_{calc}	*hkl*
10.589	10.587	100	100	001	10.589	10.545	100	100	002
	10.529		30	010					
						10.173		45	021
9.853	9.828	30	23	$0\bar{1}1$					
5.757	5.790	20	7	$0\bar{2}1$	5.795	5.806	<5	8	040
					5.107	5.086	<5	<5	042
4.436	4.413	10	5	$\bar{1}\bar{1}1$	4.399	4.391	<5	5	$\bar{1}31$
4.338	4.348	7	<5	$1\bar{2}0$		4.260		<5	131
4.111	4.110	<5	<5	$\bar{1}02$		3.903		5	044
3.763	3.757	<5	<5	$0\bar{2}3$	3.897	3.894	<5	<5	$\bar{1}14$
3.713	3.717	10	5	$1\bar{2}2$					
						3.620		14	133
3.528	3.529	40	27	003	3.522	3.515	40	30	006
	3.276		<5	$0\bar{3}3$					
3.276		20			3.255	3.268	<5	<5	134
	3.272		9	$\bar{1}\bar{1}3$					
					3.170	3.172	<5	16	$\bar{1}35$
3.095	3.089	12	7	$\bar{1}22$	3.096	3.120	<5	<5	063
3.035	3.031	12	7	$1\bar{2}3$	2.931	2.942	<5	8	135
2.861	2.862	5	<5	$1\bar{3}3$	2.855	2.852	<5	<5	065
						2.847		6	154
2.820	2.820	<5	<5	121					
2.782	2.783	20	16	$\bar{1}\bar{3}1$	2.783	2.782	20	38	171
2.659	2.662	15	18	$\bar{2}11$	2.661	2.665	10	18	$\bar{2}02$
2.648	2.647	12	12	004					
					2.634	2.636	15	12	008
2.582	2.582	35	20	130	2.580	2.578	30	37	173
2.491	2.490	15	13	$\bar{2}12$	2.494	2.490	8	14	$\bar{2}04$
2.405	2.408	12	5	$\bar{1}41$	2.400	2.400	5	9	$\bar{1}75$
2.299	2.301	15	6	131	2.293	2.296	10	13	175
2.240	2.239	10	10	$\bar{2}13$	2.240	2.237	5	9	$\bar{2}06$
	2.120		<5	$\bar{1}42$					
	2.117		<5	005	2.110	2.112	15	7	$\bar{1}77$
2.114		15				2.109		<5	0.0.10
	2.113		<5	$\bar{1}\bar{3}5$					
2.045	2.047	5	6	$2\bar{1}3$	2.046	2.048	5	6	206
2.015	2.012	5	<5	$1\bar{4}5$	2.010	2.013	<5	5	177
1.766	1.768	<5	5	133	1.761	1.762	12	12	179
1.743	1.743	<5	7	$\bar{2}15$	1.738	1.739	<5	7	$\bar{2}.0.10$
1.661	1.660	5	9	$0\bar{7}3$	1.661	1.661	<5	<5	333
						1.659		9	0.14.0
1.629	1.630	<5	<5	$\bar{1}44$	1.624	1.623	<5	5	$\bar{1}.7.11$
1.582	1.581	<5	6	$\bar{3}\bar{2}2$	1.584	1.583	<5	13	$\bar{3}71$
	1.581		6	$3\bar{5}1$					
					1.508	1.506	<5	<5	0.0.14
1.443	1.444	<5	<5	$\bar{1}45$	1.439	1.437	<5	<5	$\bar{1}.7.13$
1.412	1.415	<5	<5	$2\bar{1}6$	1.411	1.413	<5	<5	2.0.12

* 6 hour exposure. ** 24 hour exposure.

CuKα radiation, Ni filtered, Debye-Scherrer camera 114.6 mm in radius, with intensities visually estimated. The values of *d* are expressed in Å.

corresponding to approximately ~ 2.656 Å. Close examination of this band reveals two separate peaks, spaced closely together at 2.659 and 2.648 Å. In monoclinic kupletskite, the splitting of these peaks is more pronounced and the two peaks easily resolved (2.661 and 2.634 Å).

Intensity data for both crystals were collected using the Siemens SMART system consisting of a four-circle goniometer and a 1 K (diameter: 9 cm, 512 x 512 pixel) charge-coupled device (CCD) area detector. Data were collected at room temperature using monochromatic Mo$K\alpha$ *X*-radiation, with the *X*-ray tube operating at 50 kV and 40 mA, and a fixed detector-crystal distance of 4 cm. A frame width (ω) of 0.2° and count exposure times of 45 s were used. Data collection consisted of 4349 frames, out to $2\theta = 60°$, which provided 100% coverage of the diffraction sphere with a mean redundancy of 3.6 times. Approximately 1000 reflections with spot sizes of 2.4 ° (*XY*, in the plane) and 2.0° (*Z*, through the plane) were used in determination of the orientation matrix and preliminary unit cell prior to integration of all frames data. The data were reduced, filtered, integrated, and corrected for Lorentz, polarization and background effects using the Siemens software SAINT. Absorption corrections were performed using SADABS and crystals were modeled as an ellipse. All reflection data were then merged using the program XPREP (Bruker Analytical X-ray Systems, 1997). Information pertinent to the data collection and crystal structure can be found in Table 3.

The structure of RUS12 was refined using starting parameters taken from niobokupletskite (Piilonen *et al.* 2000), an isostructural AGM. Phasing of a set of normalized structure factors gave a mean $|E^2-1|$ of 1.071, suggesting $P\bar{1}$ as the most probable

TABLE 3. MISCELLANEOUS DATA FOR KUPLETSKITE-1*A* AND KUPLETSKITE-*Ma2b2c*

Parameter	Kupletskite-1*A*	Kupletskite-*Ma2b2c*
Space Group	$P\bar{1}$	*C2/c*
a (Å)	5.3925(2)	5.4022(2)
b	11.9283(4)	23.226(1)
c	11.7256(4)	21.1782(9)
α (°)	113.044(1)	90
β	94.840(1)	95.246(1)
γ	103.064	90
V (Å^3)	663.39(7)	2646.2(3)
Z	1	4
Crystal morpholgy	plate flattened on {001}	
Crystal Size (mm^3)	0.25x0.20x0.03	0.25x0.25x0.03
μ (Mo*K*α) cm^{-1}	4.30	4.94
Reflections collected	6813	13834
Unique reflections	3834	3865
R_{int} (%)	2.98	3.55
Min/Max Trans.	0.515/0.773	0.499/0.720
$\|E^2-1\|$	1.081	1.294
Min/Max Indices	$-7 \le h \le 7$	$-7 \le h \le 7$
	$-16 \le k \le 16$	$-32 \le k \le 32$
	$-16 \le l \le 16$	$-29 \le l \le 29$
Criterion for Observed Reflections	$F_o > 4\sigma(F_o)$	
Final *R* (%)	4.06	4.72
wR^2 (%)	11.25	14.04
Diffractometer parameters (for both data collections)		
Diffractometer	SIEMENS 4-circle CCD	
Radiation	Mo*K*α (40 kV, 30 mA)	
2θ Range (°)	$4.82 \le 2\theta \le 57.26$	

$R = \Sigma(|F_o|-|F_c|)/\Sigma|F_o|$

$wR^2 = [\Sigma(w)F_o^2 - F_c^2)^2/\Sigma[w(F_o^2)^2]^{1/2}$, $w = 1/\sigma^2(F_o)$

space group, consistent with data obtained for other triclinic astrophyllite group minerals (Peng & Ma 1963, Woodrow 1967, Christiansen *et al.* 1998, Piilonen *et al.* 2000). The structure refined to $R = 5.26\%$ and $wR^2 = 14.58\%$ with isotropic displacement factors and reduced to $R = 4.06\%$ and $wR^2 = 11.25\%$ with anisotropic displacement factors. An isotropic extinction correction was applied but did not improve the final residual. Initial site assignments were as follows: Mn to all four crystallographically distinct *M* sites [*M*(1) to *M*(4)], Ti to *D*, and Na to *B*. Refinement of the site occupancy factors included assigning Na to *M*(1), Mg to *M*(4), Nb to *D*, Si to *T*, and Ca to *B* and K to *A*, in accordance with the need for either a heavier or lighter *X*-ray scatterer at the given site, and in keeping with the electron microprobe data for the crystal. The shape of the anisotropic displacement ellipsoid of the K site suggested that the K cation was positionally disordered and it was therefore modeled as two split sites, *K*(1a) and *K*(1b), displaced 0.917 Å from each other in the (001) plane. Displacement factors for *K*(1a) and *K*(1b) were constrained to be equal and refined isotropically. The final positional and isotropic displacement parameters are given in Table 4. Bond valence sums were calculated using parameters taken from Brese & O'Keeffe (1991) and can be found in Table 5.

During unit cell and orientation matrix determination, it was noted that sample RUS9 gave a metrically monoclinic cell with *b* and *c* parameters approximately double with respect to those of the triclinic species ($b_{monoclinic}$ 23.226 Å *versus* $b_{triclinic}$ 11.9283 Å, $c_{monoclinic}$ 21.1782 Å *versus* $c_{triclinic}$ 11.7256 Å). Possible space groups included *Cc* and *C2/c*, with combined figures of merit of 32.58 and 11.92, respectively. Phasing of a set of normalized structure factors gave a mean $|E^2-1|$ of 1.294 suggesting the centrosymmetric space group

Table 4. Positional and displacement parameters and site occupancies for triclinic kupletskite

Atom	*x*	*y*	*z*	*sof*	$^{*}U_{11}$	U_{22}	U_{33}	U_{23}	U_{13}	U_{12}	U_{eq}
Mn(1)	0.8500(1)	0.20620(5)	0.47875(6)	0.809(5)	89(3)	96(3)	107(3)	46(2)	17(2)	21(2)	97(2)
Na(1)	0.8500(1)	0.20620(5)	0.47875(6)	0.191(5)	89(3)	96(3)	107(3)	46(2)	17(2)	21(2)	97(2)
Mn(2)	0.27901(9)	0.06668(5)	0.48702(5)	0.974(3)	103(3)	113(3)	125(3)	57(2)	30(2)	30(2)	111(2)
Mn(3)	0.4223(1)	0.35220(5)	0.48391(5)	0.881(5)	103(3)	112(3)	133(3)	65(2)	34(2)	36(2)	110(2)
Mg(3)	0.4223(1)	0.35220(5)	0.48391(5)	0.119(5)	103(3)	112(3)	133(3)	65(2)	34(2)	36(2)	110(2)
Mn(4)	0	0.5	0.5	0.299(3)	90(5)	88(4)	105(5)	38(3)	10(3)	17(3)	97(3)
Mn(4)	0	0.5	0.5	0.201(3)	90(5)	88(4)	105(5)	38(3)	10(3)	17(3)	97(3)
Ti	0.0795(1)	0.08598(5)	0.19683(5)	0.948(4)	69(3)	94(3)	93(3)	41(2)	12(2)	21(2)	85(2)
Nb	0.0795(1)	0.08598(5)	0.19683(5)	0.052(4)	69(3)	94(3)	93(3)	41(2)	12(2)	21(2)	85(2)
Si(1)	0.6785(2)	0.27194(8)	0.23032(9)	1.00	89(4)	73(4)	86(4)	30(3)	9(3)	16(3)	86(2)
Si(2)	0.8128(2)	0.54570(8)	0.25292(9)	1.00	119(4)	85(4)	93(4)	40(3)	11(3)	15(3)	101(2)
Si(3)	0.3781(2)	0.67477(8)	0.25541(9)	1.00	119(4)	89(4)	104(4)	49(3)	12(3)	21(3)	104(2)
Si(4)	0.5081(2)	0.93072(8)	0.23432(9)	1.00	91(4)	92(4)	86(4)	48(3)	12(3)	21(3)	88(2)
K(1a)	0.1321(2)	0.2645(1)	0.9961(1)	0.885(4)							365(4)
K(1b)	0.093(3)	0.186(2)	0.998(2)	0.115(4)							365(4)
Na	0.5	0	0	0.322(6)	192(9)	122(8)	83(8)	35(5)	6(5)	25(5)	140(6)
Ca	0.5	0	0	0.178(6)	192(9)	122(8)	83(8)	35(5)	6(5)	25(5)	140(6)
O(1)	0.7290(4)	0.3203(2)	0.3824(2)	1.00	121(11)	135(11)	89(11)	37(9)	31(9)	35(9)	118(5)
O(2)	0.1483(4)	0.1593(2)	0.3675(2)	1.00	135(11)	136(11)	104(12)	35(9)	18(9)	31(9)	131(5)
O(3)	0.1292(4)	0.3949(2)	0.5948(2)	1.00	104(11)	135(11)	95(11)	38(9)	3(9)	15(8)	119(5)
OH(4)	0.2935(5)	0.4627(2)	0.3980(2)	1.00	132(11)	146(11)	147(12)	62(10)	31(9)	36(9)	142(5)
OH(5)	0.9921(4)	0.1189(2)	0.5951(2)	1.00	126(11)	155(11)	158(13)	58(10)	28(10)	32(9)	150(5)
O(6)	0.5572(4)	0.2586(2)	0.5921(2)	1.00	113(11)	124(11)	113(12)	57(9)	16(9)	23(9)	116(5)
O(7)	0.5749(4)	0.0133(2)	0.3866(2)	1.00	116(11)	150(11)	85(11)	45(9)	12(9)	42(9)	118(5)
O(8)	0.0724(4)	0.5917(2)	0.2007(2)	1.00	143(12)	223(13)	137(13)	72(10)	20(10)	-19(10)	182(6)
O(9)	0.2460(5)	0.0417(3)	0.8296(3)	1.00	215(13)	246(14)	158(14)	25(11)	62(11)	-78(11)	250(6)
O(10)	0.4319(5)	0.4153(2)	0.7994(2)	1.00	196(12)	202(12)	141(13)	60(10)	15(10)	118(10)	174(5)
O(11)	0.1297(6)	0.8100(3)	0.8330(3)	1.00	352(15)	295(14)	184(14)	115(12)	100(12)	253(12)	240(6)
O(12)	0.2646(5)	0.9567(3)	0.1693(3)	1.00	294(14)	228(13)	157(13)	23(11)	-72(11)	170(11)	236(6)
O(13)	0.2665(5)	0.6074(2)	0.8089(2)	1.00	292(14)	102(11)	136(12)	50(9)	14(11)	16(10)	186(6)
O(14)	0.5721(5)	0.2222(2)	0.8031(3)	1.00	314(14)	109(11)	175(13)	84(10)	48(11)	41(10)	195(6)
O(15)	0.3807(5)	0.1906(3)	0.1672(3)	1.00	159(12)	310(15)	167(14)	119(12)	-37(10)	-106(11	241(6)
F(16)	0	0	0	0.50	37(13)	67(13)	52(14)	27(11)	3(11)	31(10)	49(6)

$^{*}U$ij x 10^{4} Å

TABLE 5. EMPIRICAL BOND-VALENCES (*v.u.*) FOR TRICLINIC KUPLETSKITE

	A(1a)	*A*(1b)	*B*	*M*(1)	*M*(2)	*M*(3)	*M*(4)	*D*	*T*(1)	*T*(2)	*T*(3)	*T*(4)	Σ
O(1)				0.294		0.383	0.358 ↓X2		1.005				2.090
O(2)				0.342	0.278	0.290		1.038					1.948
O(3)				0.318		0.364	0.337 ↓X2			1.027			2.046
OH(4)						0.698	0.407 ↓X2						1.105
OH(5)				0.334	0.763								1.097
O(6)				0.339	0.303	0.348					1.027		2.017
O(7)				0.319	0.687							0.995	2.001
O(8)	0.017									0.953	0.953		1.923
O(9)	0.126	0.022	0.140 ↓X2					0.693				1.039	2.020
O(10)	0.024									0.953	0.960		1.937
O(11)	0.127	0.023	0.137 ↓X2					0.687	1.036				2.010
O(12)	0.131	0.023	0.138 ↓X2					0.689				1.030	2.011
O(13)	0.053								0.935	1.030			2.018
O(14)	0.055										1.036	0.958	2.049
O(15)	0.130	0.022	0.135 ↓X2					0.689	1.033				2.009
(16)	0.065 →X2	0.030 →X2	0.076 ↓X2 →					0.428 ↓X2					1.198
Σ	0.728	0.120	1.252	1.946	2.031	2.083	2.204	4.224	4.009	3.963	3.976	4.022	

* constants from Brese & O'Keeffe (1991)

C2/c as the most probable choice. The structure of monoclinic RUS9 was solved using direct methods in space group *C2/c* and further refined using the SHELXL-93 set of programs (Sheldrick 1993). The positions of all major cations and 12 O^{2-} atoms were located on the *E*-map. The remaining cation and anion positions were located using difference Fourier maps during the refinement. The structure refined to $R = 7.20\%$ and $wR^2 = 19.99\%$ with isotropic displacement factors and reduced to $R = 4.72\%$ and $wR^2 = 14.04\%$ with anisotropic displacement factors. An isotropic extinction correction was applied but did not improve the final residual. The final positional and isotropic displacement parameters are given in Table 6. Bond valence sums were calculated using parameters taken from Brese & O'Keeffe (1991) and can be found in Table 7. Select bond lengths for both samples can be found in Table 8.

4.0. POLYTYPISM IN THE ASTROPHYLLITE GROUP

By definition, a mineral is polytypic if it occurs in several structural modifications which are related to each other by stacking of layers identical in structure and composition such that differences in the structural states are due only to differences in stacking sequences (Bailey *et al.* 1978, Guinier *et al.* 1984, Nickel & Grice 1998). Polytypism in the astrophyllite group has been proposed by a number of workers and recognized in electron diffraction studies (Vrublevskaya & Zvyagin 1976, Zvyagin & Vrublevskaya 1976, Dornberger-Schiff *et al.* 1985, Christiansen *et al.* 1999). The basis for the theoretical derivation of 14 modular polytypic AGM structures by Zvyagin & Vrublevskaya (1976), and later by Dornberger-Schiff *et al.* (1985), was that of "building layers" or "modules", each

Table 6. Positional and displacement parameters and site occupancies for monoclinic kupletskite

Atom	x	y	z	sof	*U_{11}	U_{22}	U_{33}	U_{23}	U_{13}	U_{12}	U_{eq}
Mn(1)	0.2527(1)	0.39265(3)	0.00989(3)	0.913(7)	94(4)	88(4)	134(4)	-2(4)	17(2)	0(5)	105(2)
Na(1)	0.2527(1)	0.39265(3)	0.00989(3)	0.087(7)	94(4)	88(4)	134(4)	-2(4)	17(2)	0(5)	105(2)
Mn(2)	0.7461(1)	0.03613(3)	-0.00589(3)	0.990(3)	92(4)	86(4)	158(4)	13(3)	28(3)	-3(4)	111(2)
Mn(3)	0.7468(1)	0.17930(3)	-0.00728(3)	0.966(4)	95(4)	92(4)	150(4)	6(4)	35(3)	9(5)	111(2)
Mn(4)	0.25	0.25	0	0.431(4)	95(6)	91(5)	140(5)	-18(5)	6(4)	2(5)	109(3)
Mg(4)	0.25	0.25	0	0.069(4)	95(6)	91(5)	140(5)	-18(5)	6(4)	2(5)	109(3)
Ti	-0.4641(1)	0.10716(3)	-0.15196(3)	0.881(4)	77(3)	130(3)	145(4)	-17(3)	12(2)	-5(3)	117(2)
Nb	-0.4641(1)	0.10716(3)	-0.15196(3)	0.119(4)	77(3)	130(3)	145(4)	-17(3)	12(2)	-5(3)	117(2)
Si(1)	0.0417(2)	0.19281(5)	-0.13490(6)	1.00	85(6)	101(6)	113(6)	27(4)	6(4)	4(4)	100(3)
Si(2)	0.0391(2)	0.32547(5)	-0.12427(6)	1.00	167(6)	107(6)	112(6)	1(5)	11(4)	-3(5)	129(3)
Si(3)	0.9601(2)	0.11053(5)	0.12310(6)	1.00	154(6)	101(5)	113(5)	6(5)	13(4)	-7(5)	123(2)
Si(4)	1.0417(2)	0.02169(5)	-0.13312(6)	1.00	114(6)	75(6)	105(6)	2(4)	11(4)	1(4)	98(3)
K(1)	-0.5	0.24270(9)	-0.25	0.50	568(13)	495(12)	285(10)	0	20(9)	0	451(5)
K(2)	0.5	-0.02746(9)	-0.25	0.50	579(13)	416(11)	280(10)	0	31(9)	0	425(5)
Na	-1.0	0.10683(8)	-0.25	0.301(7)	266(11)	142(10)	75(9)	0	5(6)	0	162(6)
Ca	-1.0	0.10683(8)	-0.25	0.199(7)	266(11)	142(10)	75(9)	0	5(6)	0	162(6)
O(1)	0.0676(5)	0.1842(2)	-0.0582(1)	1.00	109(15)	121(17)	88(14)	-8(13)	-5(12)	-4(15)	107(7)
O(2)	0.5672(5)	0.1077(2)	-0.0655(1)	1.00	117(14)	119(14)	113(14)	-1(15)	1(11)	-8(15)	117(6)
O(3)	0.0672(5)	0.3234(2)	-0.0474(1)	1.00	86(15)	140(16)	100(14)	-19(15)	14(11)	-12(16)	108(6)
OH(4)	-0.0652(6)	0.2477(2)	0.0505(1)	1.00	117(16)	152(16)	163(16)	-36(15)	42(13)	3(16)	142(7)
OH(5)	0.4343(6)	0.0391(2)	0.0474(1)	1.00	139(17)	123(17)	188(17)	-11(16)	23(13)	-7(16)	150(7)
O(6)	0.9289(5)	0.1094(2)	0.0457(1)	1.00	129(14)	109(14)	109(14)	-14(16)	17(11)	-14(16)	115(6)
O(7)	1.0664(5)	0.0309(2)	-0.0563(1)	1.00	126(16)	127(17)	104(15)	-10(13)	17(12)	-7(15)	119(7)
O(8)	0.2753(7)	0.3593(1)	-0.1507(2)	1.00	337(21)	335(20)	154(18)	12(15)	4(15)	-174(17	277(9)
O(9)	-0.7252(6)	0.0491(2)	-0.1645(2)	1.00	315(20)	385(22)	179(18)	-58(16)	95(16)	-208(17	289(9)
O(10)	-0.2240(7)	0.3557(2)	-0.1510(2)	1.00	339(21)	360(21)	174(19)	41(15)	27(16)	207(17)	291(9)
O(11)	0.2749(6)	0.1660(2)	-0.1663(2)	1.00	313(20)	380(22)	175(18)	28(16)	81(15)	200(17)	286(9)
O(12)	0.7863(6)	0.0486(2)	-0.1655(2)	1.00	296(20)	353(21)	203(18)	-59(16)	-66(15)	207(16)	289(9)
O(13)	0.0367(7)	0.2615(1)	-0.1542(2)	1.00	431(22)	107(15)	164(16)	-10(13)	8(15)	-7(15)	235(8)
O(14)	0.9628(7)	0.0464(1)	0.1523(2)	1.00	486(23)	115(16)	172(17)	32(13)	27(16)	1(15)	258(8)
O(15)	-0.2133(6)	0.1660(2)	-0.1666(2)	1.00	279(19)	382(22)	178(18)	68(16)	-75(15)	-195(17	285(9)
F(16)	-0.5	0.1064(2)	-0.25	0.50	222(19)	264(20)	172(19)	0	2(15)	0	220(8)

*Uij x 10^4 Å

TABLE 7. EMPIRICAL BOND-VALENCES ($v.u.$) FOR MONOCLINIC KUPLETSKITE

	A(1)	*A*(2)	*B*	*M*(1)	*M*(2)	*M*(3)	*M*(4)	*D*	*T*(1)	*T*(2)	*T*(3)	*T*(4)	Σ
O(1)				0.302		0.388	0.370 ↓×2		0.984				2.044
O(2)				0.351	0.284	0.288		1.013					1.936
O(3)				0.332		0.375	0.347 ↓×2			1.003			2.057
OH(4)						0.712	0.427 ↓×2						1.139
OH(5)				0.343	0.790								1.133
O(6)				0.357	0.321	0.357					0.976		2.011
O(7)				0.320	0.714							0.973	2.007
O(8)										0.960	0.930		1.890
O(9)		0.130 ↓×2	0.139 ↓×2					0.717				1.044	2.030
O(10)										0.960	0.927		1.887
O(11)	0.139 ↓×2		0.141 ↓×2					0.686	1.058				2.024
O(12)		0.137 ↓×2	0.143 ↓×2					0.705				1.039	2.024
O(13)	0.064 ↓×2								0.937	1.027			2.028
O(14)		0.031 ↓×2									1.030	0.979	2.040
O(15)	0.138 ↓×2		0.145 ↓×2					0.683	1.061				2.027
OH(16)	0.061 →×2	0.071 →×2	0.077 →×2					0.461 →×2					1.340
Σ	0.743	0.667	1.320	2.005	2.109	2.031	2.288	4.265	4.040	3.950	3.863	4.035	

* constants from Brese & O'Keeffe (1991)

TABLE 8. SELECT BOND LENGTHS (Å) FOR TRICLINIC AND MONOCLINIC KUPLETSKITE

$P\bar{1}$		$C2/c$	
A		***A*(1)**	
K(1a)-O(12)	2.836(3)	K(1)-O(11)	2.861(4)
K(1a)-O(15)	2.839(3)	K(1)-O(11)	2.861(4)
K(1a)-O(11)	2.847(3)	K(1)-O(15)	2.863(4)
K(1a)-O(9)	2.852(3)	K(1)-O(15)	2.863(4)
K(1a)-ϕ(16)	3.093(1)	K(1)-ϕ(16)	3.167(4)
K(1a)-O(14)	3.399(3)	K(1)-O(13)	3.391(4)
K(1a)-O(13)	3.429(3)	K(1)-O(13)	3.391(4)
K(1a)-O(14)	3.429(3)	K(1)-O(13)	3.411(4)
K(1a)-O(13)	3.442(3)	K(1)-O(13)	3.411(4)
K(1a)-O(8)	3.606(3)	<K(1)-ϕ>	3.135
K(1a)-O(10)	3.699(3)		
K(1a)-O(10)	3.705(3)	***A*(2)**	
<K(1a)-ϕ>	3.265	K(2)-O(12)	2.866(4)
		K(2)-O(12)	2.866(4)
K(1b)-ϕ(16)	2.176(18)	K(2)-O(9)	2.866(4)
K(1b)-O(15)	2.392(18)	K(2)-O(9)	2.886(4)
K(1b)-O(11)	2.397(18)	K(2)-ϕ(16)	3.108(4)
K(1b)-O(12)	2.392(17)	K(2)-O(14)	3.417(4)
K(1b)-O(9)	2.407(17)	K(2)-O(14)	3.417(4)
<K(1b)-ϕ>	2.353	<K(2)-ϕ>	3.064
***B*ϕ_{10} polyhedra**			
B-O(12)x2	2.599(3)	2.596(4)	
B-O(9)x2	2.596(3)	2.606(4)	
B-O(11)x2	2.604(3)	2.600(4)	
B-O(15)x2	2.610(3)	2.590(4)	
B-ϕ(16)x2	2.696(0)	2.701(0)	
<*B*-ϕ>	2.621	2.619	

	$P\bar{1}$	$C2/c$
***M*(1)O_5(OH) octahedron**		
M(1)-O(2)	2.189(2)	2.178(3)
M(1)-O(5)	2.198(3)	2.187(4)
M(1)-O(6)	2.191(2)	2.172(3)
M(1)-O(3)	2.216(2)	2.199(4)
M(1)-O(7)	2.214(2)	2.213(4)
M(1)-O(1)	2.244(2)	2.234(4)
<*M*(1)-O>	2.209	2.197
***M*(2)O_4(OH)$_2$ octahedron**		
M(2)-O(7)	2.128(2)	2.118(3)
M(2)-O(5)	2.130(2)	2.112(3)
M(2)-O(5)	2.144(2)	2.149(4)
M(2)-O(6)	2.222(2)	2.207(4)
M(2)-O(7)	2.231(2)	2.224(4)
M(2)-O(2)	2.254(3)	2.252(4)
<*M*(2)-O>	2.185	2.177
***M*(3)O_4(OH)$_2$ octahedron**		
M(3)-O(1)	2.135(2)	2.127(3)
M(3)-O(4)	2.137(3)	2.124(4)
M(3)-O(3)	2.153(2)	2.140(3)
M(3)-O(6)	2.170(2)	2.158(4)
M(3)-O(4)	2.204(2)	2.198(4)
M(3)-O(2)	2.237(2)	2.238(4)
<*M*(3)-O>	2.173	2.164
***M*(3)O_4(OH)$_2$ octahedron**		
M(4)-O(4)x2	2.087(2)	2.093(3)
M(4)-O(1)x2	2.135(2)	2.146(4)
M(4)-O(3)x2	2.156(2)	2.170(4)
<*M*(4)-O>	2.126	2.136

	$P\bar{1}$	$C2/c$
***D*ϕ_6 octahedron**		
D-O(2)	1.807(3)	1.823(3)
D-O(12)	1.959(3)	1.957(3)
D-O(11)	1.960(3)	1.967(3)
D-O(9)	1.956(2)	1.951(3)
D-O(15)	1.959(3)	1.969(3)
D-ϕ(16)	2.084(1)	2.068(1)
<*D*-ϕ>	1.954	1.956
***T*(1) tetrahedron**		
T(1)-O(15)	1.612(3)	1.602(3)
T(1)-O(11)	1.611(3)	1.603(3)
T(1)-O(1)	1.622(3)	1.630(3)
T(1)-O(13)	1.649(3)	1.648(3)
<*T*(1)-O>	1.624	1.621
***T*(2) tetrahedron**		
T(2)-O(13)	1.613(2)	1.614(3)
T(2)-O(3)	1.614(3)	1.623(3)
T(2)-O(8)	1.642(3)	1.639(4)
T(2)-O(10)	1.642(3)	1.639(4)
<*T*(2)-O>	1.628	1.629
***T*(3) tetrahedron**		
T(3)-O(14)	1.611(3)	1.613(3)
T(3)-O(6)	1.614(3)	1.633(3)
T(3)-O(10)	1.639(3)	1.652(4)
T(3)-O(8)	1.642(2)	1.651(3)
<*T*(3)-O>	1.627	1.637
***T*(4) tetrahedron**		
T(4)-O(9)	1.610(3)	1.608(3)
T(4)-O(12)	1.613(3)	1.610(3)
T(4)-O(7)	1.626(3)	1.634(3)
T(4)-O(14)	1.640(3)	1.632(3)
<*T*(4)-O>	1.622	1.621

consisting of a combination of two neighboring *H*-sheets linked *via* a common apical anion, and an independent *O*-sheet. In such an approach, a centered orthogonal cell defined by two octahedra wide (*a*) and seven octahedra long (*b*) is used. The base of each of seven *O*-sheet octahedra is regarded as a regular triangular network of anions, resulting in seven possible attachment points for the adjacent *H-H* layer. The mutual disposition of the *H-H* units over apical positions (*HHO* units) results in four geometrically different *HHOHH* units and 14 possible polytypes with either triclinic, monoclinic or orthorhombic symmetry (Zvyagin & Vrublevskaya 1976). Four of these 14 derived structures are based on the same triclinic subcell as the present polytype pair. Only three of these arrangements have been found in nature: monoclinic magnesium astrophyllite (#1; Peng & Ma 1963, Shi *et al.* 1998), triclinic AGM (#3; Woodrow 1967, Christiansen *et al.* 1998, Piilonen *et al.* 2000), and kupletskite-*Ma2b2c* (#6). It should be noted that monoclinic magnesium astrophyllite and the other triclinic members of the astrophyllite group should not be considered to be polytypic derivatives of each other – structurally and chemically, magnesium astrophyllite is distinctly different in that the *H*-sheet contains [5]-coordinated TiO_5 polyhedra and the *O*-sheet hosts significant amounts of Na and Mg.

Possible crystallographic mechanisms for the formation of astrophyllite group polytypes include cation ordering, changes in packing of coordinating anions, variations in orientation of the *O*-sheet octahedra with respect to the adjacent *H*-sheets, as is observed in lamprophyllite-2*M* and lamprophyllite-2*O* (Johnsen 1996), or by complete translation of the *HOH* layer by combinations of symmetry elements not evidenced in the triclinic structure. Since the minerals of the astrophyllite group are defined as layered silicates composed of

HOH layers that are similar to the *TOT* layers in mica, the present polytype pair can similarly be described as variations in the stacking of *HOH* layers. As such, the "building layer" chosen for this study is the *HOH* layer.

The structural make-up of the *HOH* layers in triclinic and monoclinic kupletskite differs only in the designation of the single, albeit split, *A* site in triclinic species as *A*(1) and *A*(2) in the monoclinic species. In all other aspects, individual *HOH* layers are structurally identical. Chemically, the two samples differ only slightly in Mn/(Mn+Fe): 0.87 (triclinic), and 0.66 (monoclinic). Triclinic kupletskite (RUS12) also shows a slight enrichment in Na, Mg and depletion in Nb and Al with respect to monoclinic kupletskite (RUS9).

In the triclinic structure (Fig. 1), adjacent *HOH* layers are related to each other by a center of symmetry. Stacking can thus be described as either *+HOH/+HOH/+HOH*, or simply +++, with a layer-stacking period of one. This polytypic form is equivalent to #3 derived by Zvyagin & Vrublevskaya (1976). A displacement of $\approx$ 5 Å along *b* exists between adjacent layers, resulting in an offset of the adjacent layers such that the apices of the $D\phi_6$ octahedra do not define an orthogonal arrangement.

In monoclinic kupletskite (Fig. 2), adjacent *HOH* layers are related by a two-fold axis parallel to *b*, resulting in a stacking period along *c* of two differently oriented *HOH* layers herein defined as *+HOH* and *–HOH*. In this way, neither attachment points of the *H*-sheet nor first neighbor coordination spheres are compromised, and the *HOH* layer is geometrically to that observed in triclinic species. The resulting stacking sequence with a two-layer period can be described as *+HOH/-HOH/+HOH*, or simply +-+-. This polytypic form is equivalent to #6 derived by Zvyagin & Vrublevskaya (1976). A more orthogonal configuration is

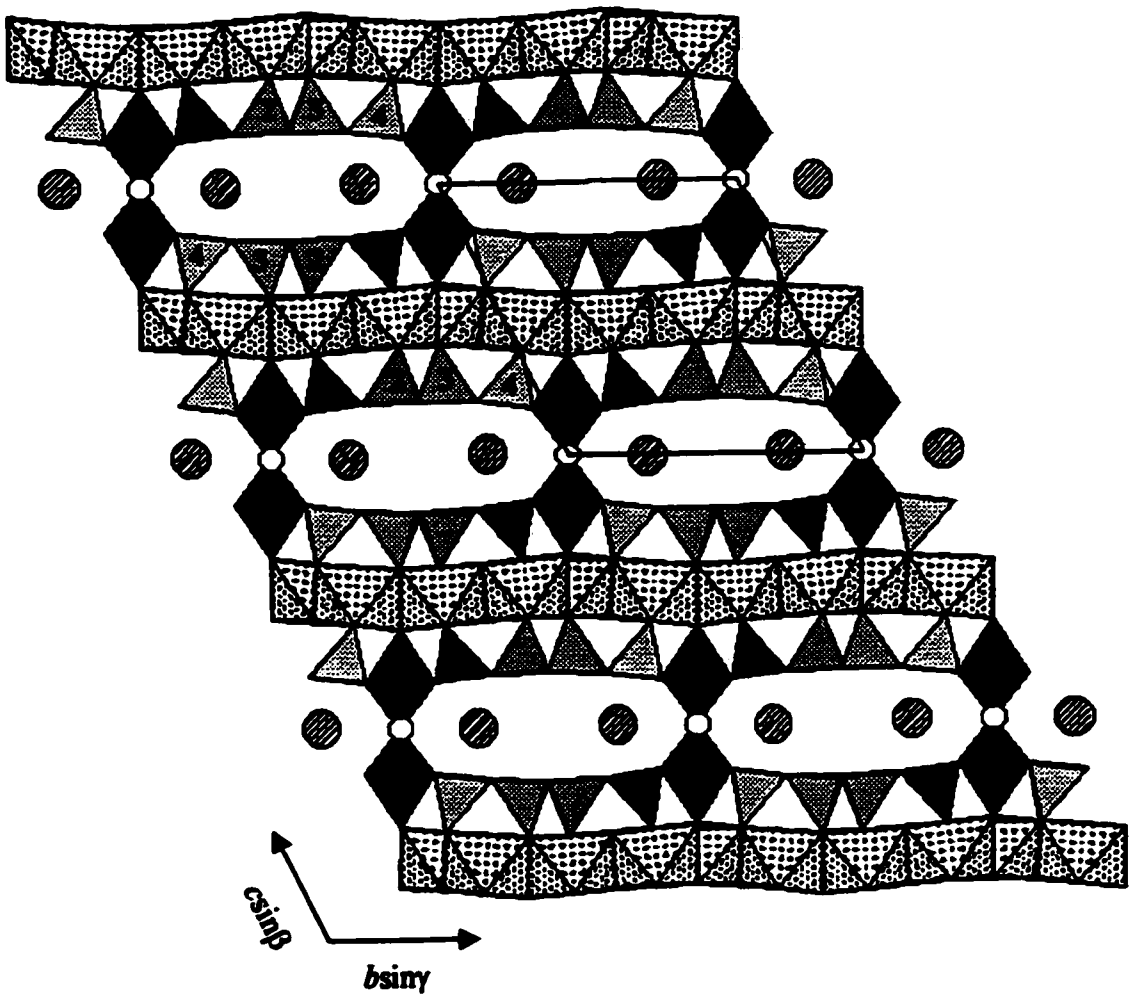

Figure 1. Crystal structure of triclinic, $P\bar{1}$, kupletskite, projected down [100] (unit cell outlined). *A* = hatched, *B* = white, *O*-sheet = stippled, *D* = dark grey, *T*(1) to *T*(4) = medium grey to light grey. The four *T* sites are numbered to illustrate the symmetry across the interlayer.

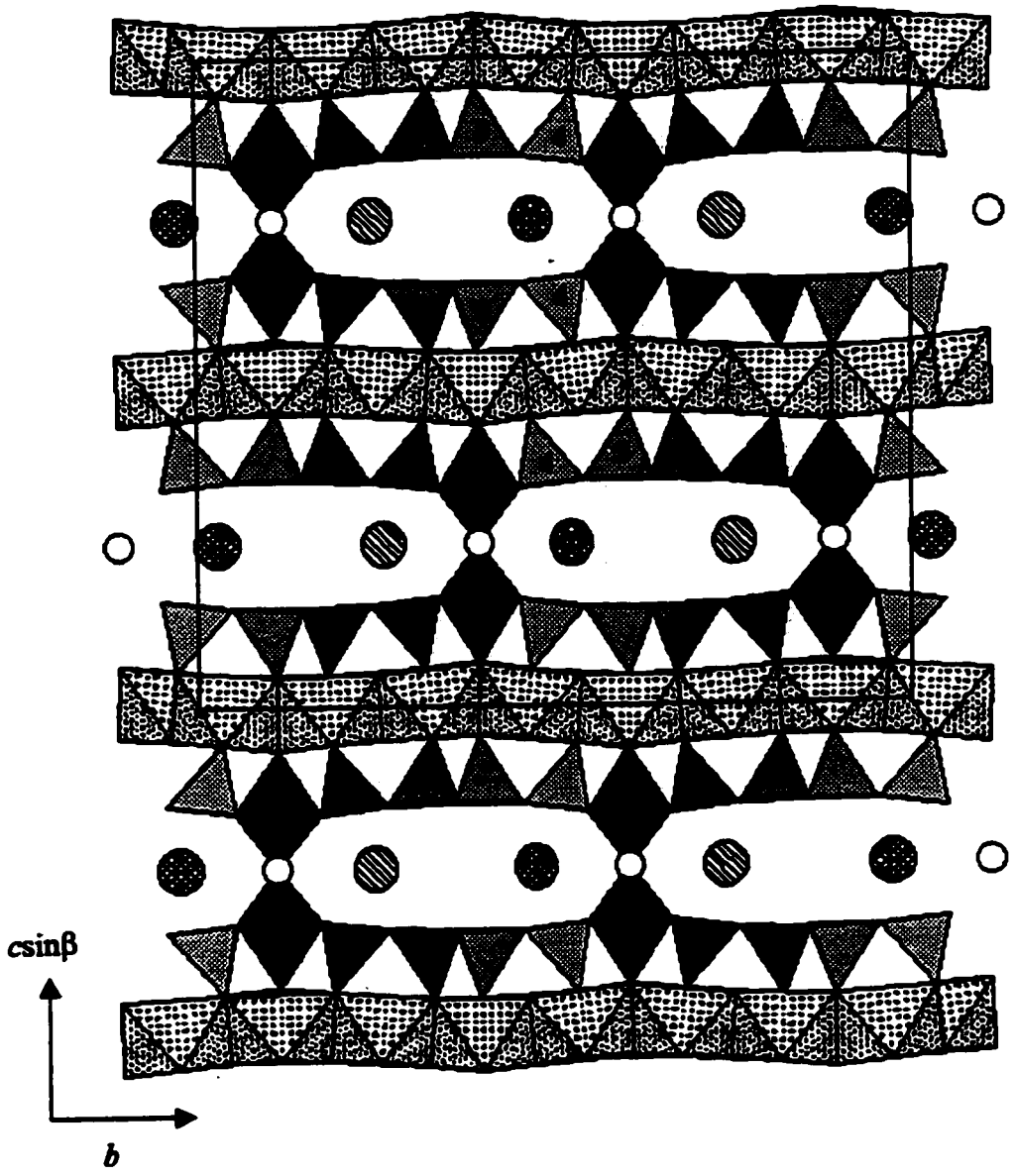

Figure 2. Crystal structure of monoclinic, *C*2/*c*, kupletskite projected down [100] (unit cell outlined). *A*(1) = hatched, *A*(2) = diagonal lines, *B* = white, *O*-sheet = stippled, *D* = dark grey, *T*(1) to *T*(4) = medium grey to light grey. The four *T* sites are numbered to illustrate the symmetry across the interlayer.

achieved such that *D*-ϕ(16)-*D* polyhedral pairs lie in planes perpendicular to (001). The resultant relationship between the unit cell parameters of monoclinic and triclinic kupletskite are as follows: $a_{monoclinic} = a_{triclinic}$, $b_{monoclinic} = 2(b\sin\gamma)_{triclinic}$, and $c_{monoclinic}$ spans two *HOH* layers. Figure 3 depicts the stacking sequence differences between the two polytypes.

In accordance with IMA guidelines for the nomenclature of polytypes, triclinic varieties of kupletskite should be referred to as kupletskite-1*A*. Monoclinic species, in which both the *b* and *c* parameters extend over two periods respect to the triclinic primitive subcell, should be referred to as kupletskite-*Ma*2*b*2*c* (Bailey *et al.* 1978, Nickel & Grice 1998).

5.0. Discussion

As with other 1:1 and 2:1 phyllosilicates, the physical and/or crystal chemical mechanisms responsible for polytype formation in AGM are unknown. A study of 20 AGM from both over- and undersaturated intrusions revealed only one monoclinic modification (kukpletskite-*Ma*2*b*2*c*), suggesting that triclinic AGM are energetically more favorable under a wide range of crystallization conditions. The presence of a split *A* site in the kupletskite-1*A*, a feature common to other triclinic AGM, and the lack of such disorder in kupletskite-*Ma*2*b*2*c* may also suggest that kupletskite-1*A* is more stable than that of the monoclinic polytype.

It has been suggested (Zvyagin & Vrublevskaya 1976) that the degree of uniformity in the distribution of DO_6 or DO_5 polyhedra may be responsible for the formation of AGM polytypes. Attachment of Ti cations to the *O*-sheet results in an imbalance in charge distribution and bond valence associated with the O(2) apical oxygen and the three

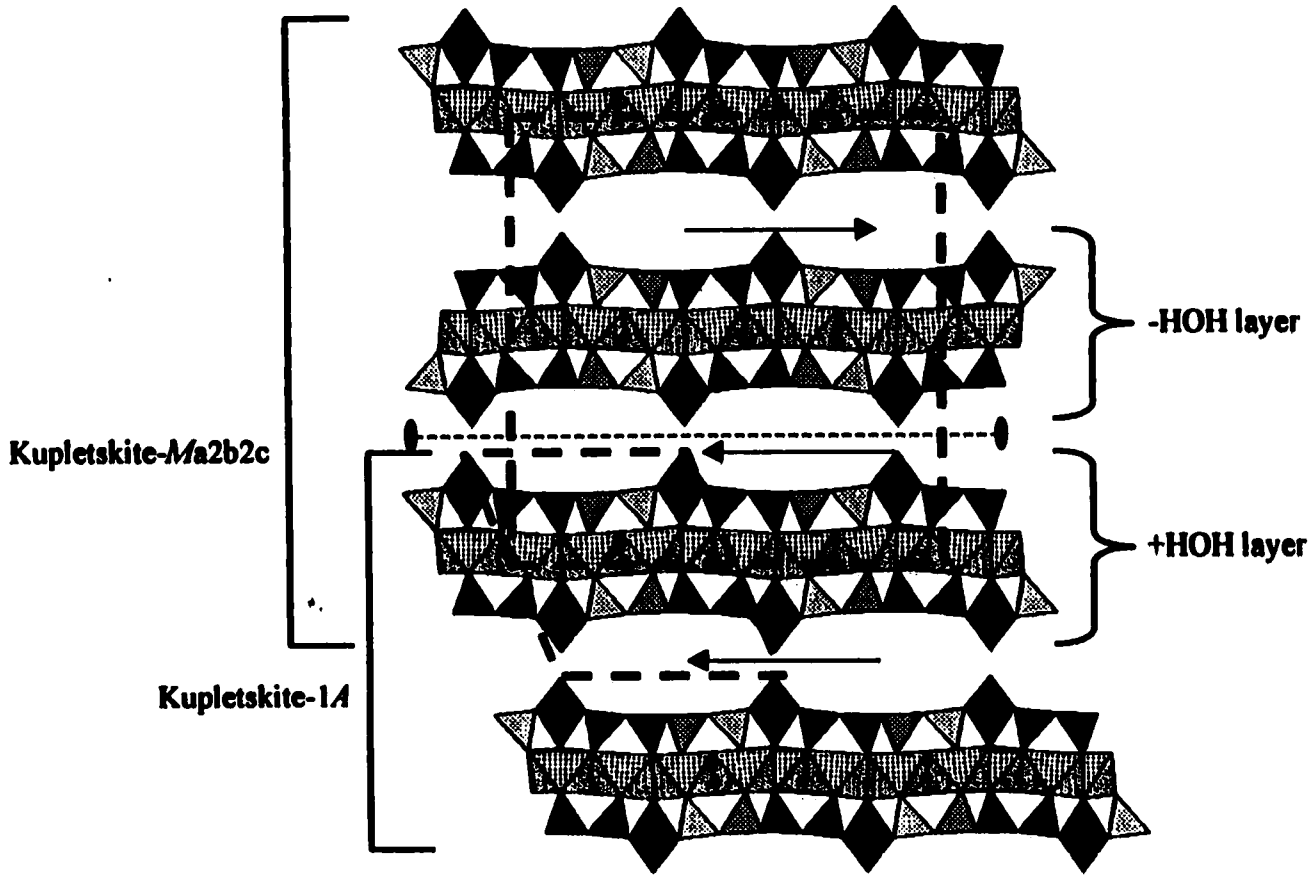

Figure 3. Monoclinic and triclinic kupletskite polytypes projected down [100]. Unit cells for both structures are outlined. In kupletskite-*Ma*2*b*2*c*, *+HOH* and *-HOH* layers are related to each other by the two-fold rotation around *b*. Arrows depict stacking sequence.

octahedral sites to which it is bonded, *M*(1), *M*(2) and *M*(3); the most favorable arrangement of Ti cations is such that this imbalance is distributed uniformly over the entire structure so as to avoid charge overloading. In monoclinic magnesium astrophyllite, DO_5 polyhedra are related by a two-fold axis and are located on either side of the *M*(1) octahedron in planes parallel to [001]. As a result, two of the oxygens coordinating the *M*(1) octahedron are underbonded. This charge imbalance is accounted for by the dominance of Na, a large monovalent cation, in *M*(1). In triclinic modifications of AGM, the DO_6 polyhedra are uniformly distributed such that charge imbalance is minimized and does not occur repeatedly in any given part of the structure. In kupletskite-*Ma2b2c*, the distribution of DO_6 octahedra is closer to that observed in triclinic species: pairs of octahedra in alternate layers are located in planes perpendicular to (001), resulting in only partial uniformity and therefore long-range overloading of electrical charge on the *O*-sheet octahedra. Unlike magnesium astrophyllite, kupletskite-*Ma2b2c* does not have a dominance of Na in *M*(1) to overcome this charge imbalance.

The high *R* values (> 4.0 %) observed in many of the structure refinements, coupled with extensive streaking observed in precession photographs, suggest the possibility of additional polytypic intergrowths or stacking disorder in the astrophyllite group, in agreement with electron diffraction studies performed by Zvyagin & Vrubleskaya (1976). Further work by high resolution TEM may be required to elucidate these problems.

CHAPTER VI

NIOBOKUPLETSKITE, A NEW ASTROPHYLLITE GROUP MINERAL FROM MONT SAINT-HILAIRE, QUÉBEC, CANADA: DESCRIPTION AND CRYSTAL STRUCTURE

PAULA C. PIILONEN and ANDRÉ E. LALONDE
Ottawa-Carleton Geoscience Centre, Department of Earth Sciences
University of Ottawa, Ottawa, Ontario K1N 6N5

ANDREW M. McDONALD
Department of Earth Sciences, Laurentian University, Sudbury, Ontario P3E 2C6

ROBERT A. GAULT
Research Division, Canadian Museum of Nature, Ottawa, Ontario K1P 6P4

OVERVIEW

During the course of this study, a new member of the astrophyllite group was discovered from Mont Saint-Hilaire (Québec, Canada). Niobokupletskite, the Nb-dominant end-member in a solid solution with kupletskite, was officially accepted by unanimous vote as a new mineral species on October 4th, 1999, by the *International Mineralogical Association Commission on New Minerals and Mineral Names* (IMA #99-032). Information concerning the crystal structure, physical properties, mineral associations and paragenesis of niobokupletskite were published in *Canadian Mineralogist*, 2000, **38**, 627-639.

ABSTRACT

Niobokupletskite is a new member of the astrophyllite group found in nepheline syenite pegmatites at Mont Saint-Hilaire, Quebec, in association with aegirine, albite, analcime, calcio-ancylite-(Ce), calcite, catapleiite, epididymite, fluorite, genthelvite, microcline, natrolite, pyrochlore, rhodochrosite and wurtzite. It is transparent, with a vitreous lustre, brittle with a perfect {001} cleavage and has uneven to splintery fracture. Niobokupletskite is biaxial positive, α 1.718(1), β 1.733(1), $\gamma_{calc.}$ 1.750(1), $2V_{meas.} = 87(2)^\circ$. It is triclinic, $P\bar{1}$, a 5.4303(9), b 11.924(2), c 11.747(2) Å, α 112. 927(3), β 94.750(3), γ 103.175(3)°, V 669.5(3) Å^3. The average result of three electron microprobe analyses is: Na_2O 2.62, K_2O 5.97, Rb_2O 0.82, Cs_2O 0.12, MgO 0.15, MnO 26.37, FeO 2.64, ZnO 4.08, Al_2O_3 1.14, TiO_2 1.34, ZrO_2 3.43, Nb_2O_5 12.13, Ta_2O_5 0.63, SiO_2 31.85, F 0.14, H_2O(*calc.*) 2.48, total 95.85 wt. %, corresponding to $(K_{1.84}Rb_{0.13}Cs_{0.01})_{\Sigma 1.98}Na_{0.95}(Mn_{5.40}Zn_{0.73}Fe_{0.53}Na_{0.28}Mg_{0.05})_{\Sigma 6.99}(Nb_{1.33}Zr_{0.40}Ti_{0.24}Ta_{0.04})_{\Sigma 2.01}(Si_{7.71}Al_{0.32})_{\Sigma 8.03}O_{26}(OH)_{4.00}(O_{0.89}F_{0.11})_{\Sigma 1.00}$ on the basis of 31 anions, or, ideally, $K_2Na(Mn,Zn,Fe)_7(Nb,Zr,Ti)_2Si_8O_{26}(OH)_4(O,F)$. Niobokupletskite is a heterophyllosilicate with a *HOH*-structure consisting of a sheet of close-packed octahedra (*O*-sheet) sandwiched between two heterogeneous sheets (*H*-sheets) with a Si:Nb ratio of 4:1. It forms a solid solution series with kupletskite *via* the coupled substitution $Ti^{4+} + F^-/OH^- \Leftrightarrow Nb^{5+} + O^{2-}$. Niobokupletskite is a post-magmatic phase and possibly the result of late-stage remobilization of Nb *via* oxidized residual fluids.

Keywords: niobokupletskite, astrophyllite group mineral, Mont Saint-Hilaire, Québec, new mineral species, crystal structure, heterophyllosilicate, solid solution series, kupletskite

SOMMAIRE

La niobokupletskite est une nouvelle espèce, membre du groupe de l'astrophyllite, que l'on retrouve dans les pegmatites à néphéline du Mont Saint-Hilaire, Québec, en association avec l'aegyrine, l'analcime, la calcite, la catapléite, l'épididymite, la fluorine, la genthelvite, le microcline, la natrolite, le pyrochlore, la rhodocrosite et la wurtzite. C'est un minéral transparent, avec éclat vitreux, cassant avec un clivage {001} parfait et une fracture irrégulière à fibreuse. La niobokupletskite est biaxe positive avec α 1.718(1), β 1.733(1), γ_{calc} 1.750(1), $2V_{observé}$ = 87(2)°. Le minéral est triclinique, groupe spatial $P\bar{1}$, avec paramètres réticulaires a 5.4303(9), b 11.924(2), c 11.747(2) Å, α 112. 927(3), β 94.750(3), γ 103.175(3)°, V 669.5(3) Å^3. La moyenne de trois déterminations par microsonde à électrons donne: Na_2O 2.62, K_2O 5.97, Rb_2O 0.82, Cs_2O 0.12, MgO 0.15, MnO 26.37, FeO 2.64, ZnO 4.08, Al_2O_3 1.14, TiO_2 1.34, ZrO_2 3.43, Nb_2O_5 12.13, Ta_2O_5 0.63, SiO_2 31.85, F 0.14, H_2O(*calc.*) 2.48, somme 95.85 wt. %, ce qui correspond à la formule structurale suivante: $(K_{1.84}Rb_{0.13}Cs_{0.01})_{\Sigma 1.98}Na_{0.95}(Mn_{5.40}Zn_{0.73}Fe_{0.53}Na_{0.28}Mg_{0.05})_{\Sigma 6.99}(Nb_{1.33}Zr_{0.40}Ti_{0.24}Ta_{0.04})_{\Sigma 2.01}(Si_{7.71}Al_{0.32})_{\Sigma 8.03}O_{26}(OH)_{4.00}(O_{0.89}F_{0.11})_{\Sigma 1.00}$ basée sur 31 anions ou idéalement, $K_2Na(Mn,Zn,Fe)_7(Nb,Zr,Ti)_2Si_8O_{26}(OH)_4(O,F)$. La niobokupletskite est un hétérophyllosilicate avec une struture *HOH* composée de couches d'octaèdres avec entassement maximal qui se retrouvent emprisonnées entre deux couches hétérogènes (couches *H*) ayant un rapport Si:Nb de 4:1. Elle constitute une solution solide avec la kupletskite par la substitution $Ti^{4+} + F^-/OH^- \Leftrightarrow Nb^{5+} + O^{2-}$. La niobokupletskite est d'origine

postmagmatique et provient possiblement d'une remobilisation tardive du Nb par un fluide résiduels oxydés.

Mots-clés: niobokupletskite, minéral du groupe de l'astrophyllite, Mont Saint-Hilaire, Québec, nouvelle espèce minérale, structure cristalline, hétérophyllosilicate, solution solide, kupletskite.

1.0. INTRODUCTION

Niobokupletskite, ideally $K_2Na(Mn,Zn,Fe)_7(Nb,Zr,Ti)_2Si_8O_{26}(OH)_4(O,F)$, is a new astrophyllite group mineral (AGM) discovered in the nepheline syenite pegmatites in the Poudrette Quarry at Mont Saint-Hilaire, Québec. With the addition of niobokupletskite, the Nb-analogue of kupletskite, eight species of AGM are now recognized (Table 1). Niobokupletskite is the third member of the astrophyllite group, along with astrophyllite and kupletskite, to be described from this locality (Horváth & Gault 1990). The name niobokupletskite comes from the fact that it is the Nb-analogue of kupletskite (Semenov 1956). The mineral species and the name have been approved by the IMA Commission on New Minerals and New Mineral Names. Holotype material has been deposited at the Canadian Museum of Nature, Ottawa (catalogue no. CMNMC 82924). The purpose of this paper is to describe niobokupletskite, discuss its structure in relation to kupletskite, and to comment on its paragenesis. Extensive information concerning the structure and chemical variations of a large suite of AGM, including niobokupletskite, will be presented in further papers.

2.0. Occurrence and Description

Mont Saint-Hilaire (MSH), located 40 km east of Montreal, Quebec, is one of ten early Cretaceous alkaline intrusions collectively referred to as the Monteregian Hills (Adams 1903). The peralkaline East Hill Suite is host to a variety of petrological microenvironments (Piilonen *et al.* 1998), all of which contain AGM except for the so-called marble xenoliths. Niobokupletskite occurs in nepheline syenite pegmatites as a late-stage mineral.

Three distinct types of niobokupletskite have been discovered, each with their own specific occurrence and associated mineral assemblage. Type-I niobokupletskite (holotype material) occurs as anhedral to subhedral, platy to tabular, light beige to yellow epitaxic overgrowths on primary, dark brown kupletskite associated with aegirine, albite, microcline and pyrochlore. The primary kupletskite is zoned, possessing a relatively Nb-rich core and a Ti-enriched rim; this zonation is indicated by an arrow in Figure 1B (BSEI) with dark zones corresponding to Ti-enrichment, and light zones indication of Nb-enrichment. Type-II niobokupletskite occurs as dense, fibrous, light yellow-brown overgrowths on coarse grained, primary kupletskite associated with primary and secondary aegirine, albite, calcio-ancylite-(Ce), catapleiite, microcline, natrolite, pyrochlore and rhodochrosite. Type-III niobokupletskite occurs as overgrowths on primary kupletskite as very fine grained bronze to silvery brown, acicular crystals in sheaf-like aggregates, originally described as "witch's broom astrophyllite" (Wight & Chao 1986). Type-III niobokupletskite is associated with primary and secondary aegirine, albite, analcime, calcio-ancylite-(Ce), calcite, catapleiite, epididymite, fluorite, genthelvite, microcline, natrolite, pyrochlore, rhodochrosite, and wurtzite.

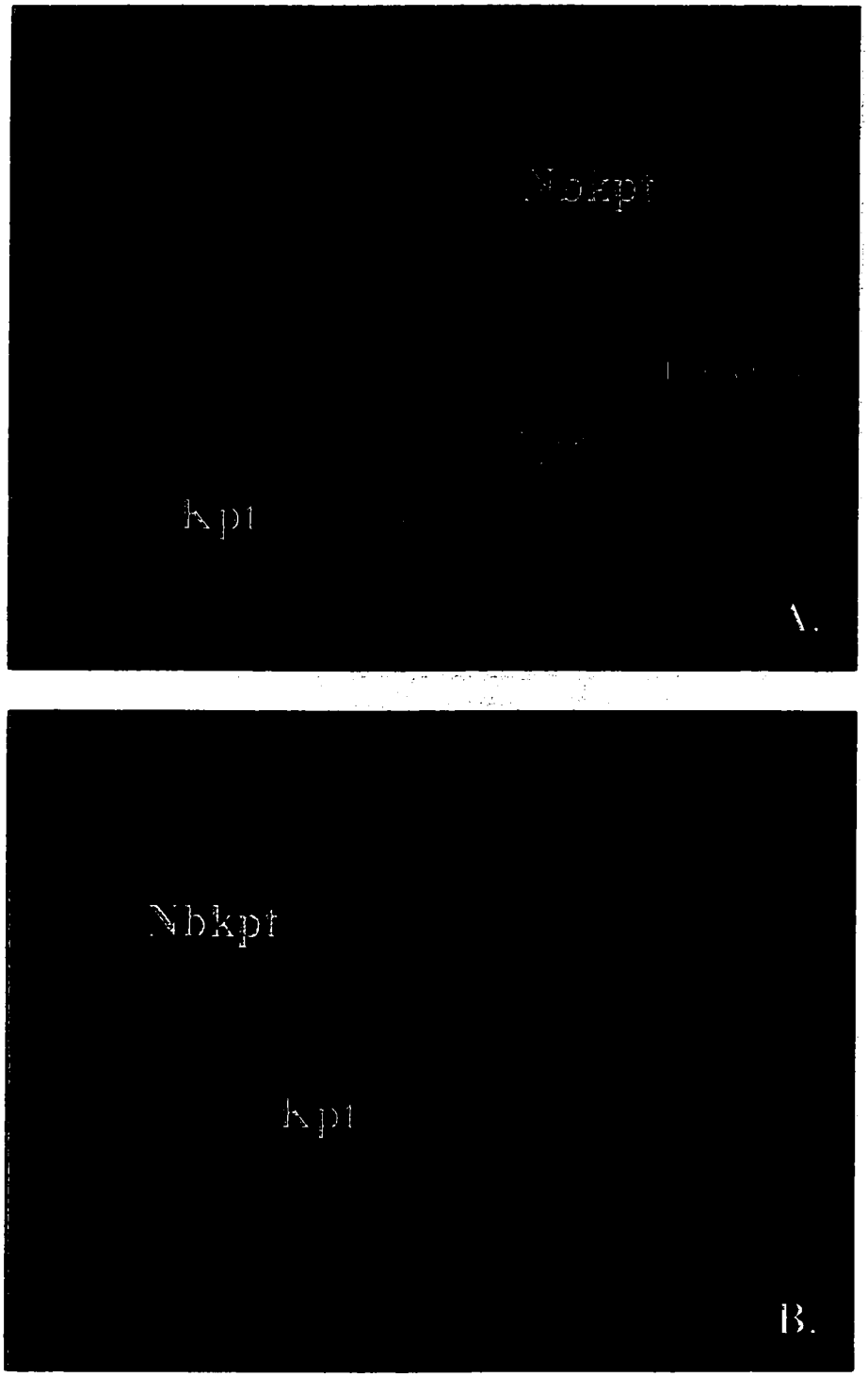

Figure 1. Back-scattered electron images of Type-I niobokupletskite. A. Nb-rich kupletskite (Kpt, dark grey) with irregular zonation and a sharp contact with niobokupletskite (Nkpt, light grey). Note the pyrochlore inclusions (white) along fractures in the kupletskite. B. Niobokupletskite (Nkpt) rimming kupletskite (Kpt). The zoning in the kupletskite is from Nb-poor to Nb-rich in the direction of the arrow (dark to medium grey). Scale bar: 100 μm.

Niobokupletskite has a perfect {001} cleavage, is vitreous, brittle, and has an uneven to splintery fracture. It does not fluoresce under either short- or long-wave ultraviolet light. It has a Mohs hardness of 3 to 4. Niobokupletskite sinks in methylene iodide (density of 3.325 g/cm^3) and has a calculated density of 3.46 g/cm^3.

Niobokupletskite is biaxial positive, with indices of refraction of α = 1.718(1), β = 1.733(1), and γ_{calc} = 1.750 (for λ = 598 nm); $2V_{meas}$ = 87(2)° (Kamb's method). A measured value for γcould not be obtained owing to the orientation of the selected grain on the spindle. The optical orientation is $Z = c$ with X and Y in the (001) plane. It is pleochroic with $X \approx Y$ light orange-yellow, and Z red-brown. A Gladstone-Dale calculation gives a compatibility index of 0.005, which is regarded as superior (Mandarino 1981).

3.0. Chemical Composition

Chemical analyses of Type-I, II and III niobokupletskite were performed on a JEOL 733 electron microprobe at the Canadian Museum of Nature using Tracor Northern 5500 and 5600 automation in wavelength dispersive mode. Details regarding data collection can be found in Chapter II. Complete EMPA data for niobokupletskite can be found in Table 2. Chemical formulae were calculated on the basis of 31 anions as determined during crystal structure analysis. The average of three EMPA of Type-I niobokupletskite gives the empirical formula $(K_{1.84}Rb_{0.13}Cs_{0.01})_{\Sigma 1.98}Na_{0.95}(Mn_{5.40}Zn_{0.73}Fe_{0.53}Na_{0.28}Mg_{0.05})_{\Sigma 6.99}(Nb_{1.33}Zr_{0.40}Ti_{0.24}Ta_{0.04})_{\Sigma 2.01}(Si_{7.71}Al_{0.32})_{\Sigma 8.03}O_{26}(OH)_{4.00}(O_{0.89}F_{0.11})_{\Sigma 1.00}$ or, ideally, $K_2Na(Mn,Zn,Fe)_7(Nb,Zr,Ti)_2Si_8O_{26}(OH)_4(O,F)$. Chemically, Type-II and Type-III

TABLE 2. EMPA ANALYSES OF NIOBOKUPLETSKITE

	TYPE I				TYPE II	TYPE III
Oxide	1	2	3	Ave.		
Na_2O	2.69	2.49	2.67	2.62	2.37	2.66
K_2O	6.03	5.92	5.95	5.97	6.04	5.76
Rb_2O	0.82	0.81	0.84	0.82	0.66	0.91
Cs_2O	0.12	0.13	0.10	0.12	0.00	0.00
CaO	0.00	0.00	0.00	0.00	0.10	0.03
SrO	0.00	0.00	0.00	0.00	0.04	0.00
MgO	0.13	0.15	0.18	0.15	0.18	0.43
MnO	26.11	26.40	26.61	26.37	26.60	30.13
FeO	2.63	2.73	2.55	2.64	7.44	3.71
ZnO	4.31	4.29	3.65	4.08	0.25	0.00
Al_2O_3	1.21	1.02	1.20	1.14	1.18	1.69
TiO_2	1.12	1.26	1.65	1.34	1.63	1.67
ZrO_2	3.23	4.23	2.84	3.43	4.80	3.56
HfO_2	0.00	0.00	0.00	0.00	0.04	0.00
Nb_2O_5	12.84	11.54	12.00	12.13	10.64	11.40
Ta_2O_5	0.44	0.74	0.71	0.63	0.48	0.25
SiO_2	31.93	31.80	31.82	31.85	32.06	31.86
F	0.43	0.00	0.00	0.14	0.34	0.29
H_2O	2.50	2.47	2.47	2.48	2.52	2.52
O=F	-0.18	0.00	0.00	-0.06	-0.14	-0.12
Total	96.36	95.98	95.24	95.85	97.23	96.75
Formula based on 31 anions						
K	1.85	1.83	1.84	1.84	1.83	1.75
Rb	0.13	0.13	0.13	0.13	0.10	0.14
Cs	0.01	0.01	0.01	0.01	0.00	0.00
Sr	0.00	0.00	0.00	0.00	0.01	0.00
Na	0.00	0.00	0.00	0.00	0.07	0.19
Sum *A*	1.99	1.97	1.99	1.98	2.01	2.08
Na	0.90	0.98	0.97	0.95	1.04	1.18
Ca	0.00	0.00	0.00	0.00	0.03	0.01
Sum *B*	0.90	0.98	0.97	0.95	1.00	1.00
Na	0.35	0.20	0.29	0.28	0.05	0.05
Mg	0.05	0.05	0.07	0.05	0.06	0.15
Mn	5.31	5.43	5.48	5.40	5.36	6.06
Fe^{2+}	0.53	0.55	0.52	0.53	1.48	0.74
Zn	0.76	0.77	0.66	0.73	0.04	0.00
Sum *C*	7.00	7.00	7.00	7.00	7.00	7.00
Ti	0.20	0.23	0.30	0.24	0.29	0.30
Zr	0.38	0.50	0.34	0.41	0.56	0.41
Hf	0.00	0.00	0.00	0.00	0.00	0.00
Nb	1.39	1.27	1.32	1.33	1.14	1.23
Ta	0.03	0.05	0.05	0.04	0.03	0.02
Sum *D*	2.00	2.05	2.00	2.02	2.03	1.95
Si	7.67	7.72	7.73	7.71	7.62	7.57
Al	0.34	0.29	0.34	0.33	0.33	0.47
Sum *T*	8.01	8.01	8.08	8.03	7.96	8.04
O	26.67	27.00	27.00	26.89	26.74	26.78
OH	4.00	4.00	4.00	4.00	4.00	4.00
F	0.33	0.00	0.00	0.11	0.26	0.22
Σ anions	31.00	31.00	31.00	31.00	31.00	31.00
Σ cations	19.90	20.01	20.03	19.98	19.98	20.07

niobokupletskite differ from the type material only by being deficient in Zn (<0.04 *apfu*, Table 2).

4.0. Infrared Analysis

The infrared spectrum of niobokupletskite was obtained using a Bomem Michelson MB-100 Fourier transform infrared spectrometer equipped with a mercury cadmium telluride (MCT) detector. A single crystal of the type material was initially dried in an oven at 50 °C for 30 minutes, mounted in a diamond-anvil microsample cell, and the spectrum collected over the range of 4000 to 400 cm^{-1}. The absorbance spectrum (Fig. 2) shows broad peaks in the high-frequency range (4000 to 1000 cm^{-1}) attributable to O-H stretching (3626 cm^{-1} and associated shoulder centered at 3396 cm^{-1}), and a weak peak at 1647 cm^{-1} attributable to H-O-H bending of absorbed or molecular H_2O (Farmer 1974). The lack of recognizable H_2O in the structure refinement suggests that this contribution is likely due to adsorbed water not driven off during the drying process. The middle- to lower-frequency end of the spectrum (1000 to 400 cm^{-1}) is characterized by symmetric Si-O stretching (964 and 812 cm^{-1}) and bending (696 and 654 cm^{-1}). Low-frequency bands at 457, 418 and 405 cm^{-1} can be attributed to Mn-O stretching (Farmer 1974).

5.0. Mössbauer Spectroscopy

The wide range of chemical compositions and the presence of structural vacancies preclude the possibility of using stoichiometry to calculate Fe^{2+}/Fe^{3+} values in AGM. Mössbauer spectroscopy was therefore employed to determine the proportions and

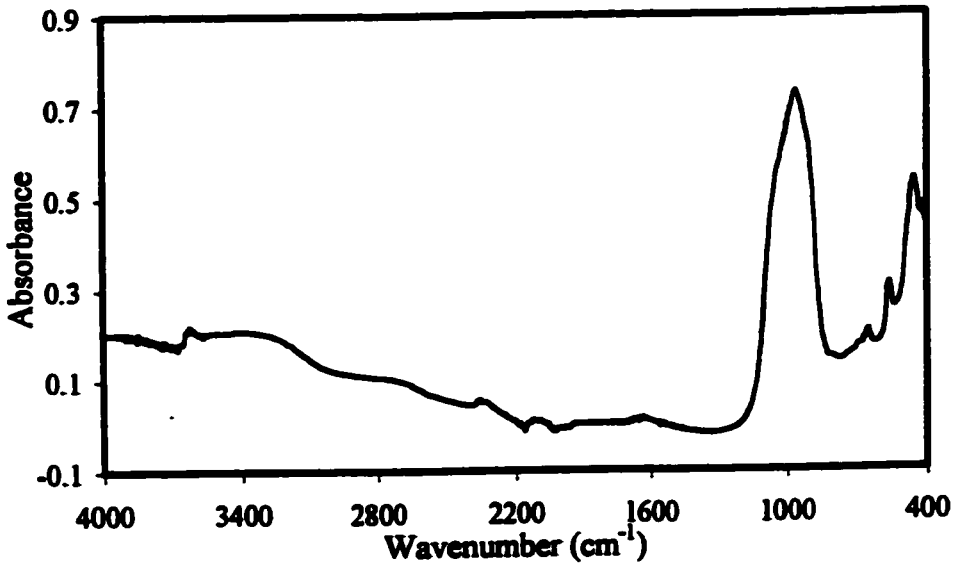

Figure 2. Infrared transmittance spectrum of niobokupletskite.

distributions of Fe^{2+} and Fe^{3+} in niobokupletskite and to shed light on the oxidation conditions at the time of crystallization. Insufficient quantities of holotype (Type-I) niobokupletskite precluded the possibility of obtaining a Mössbauer spectrum; an absorber for a sample of fibrous Type-II niobokupletskite was therefore prepared by crushing an ideal mass of sample [55.1 mg; calculated using the technique of Rancourt *et al.* (1993)]. Crushing was done in acetone to minimize oxidation in the presence of atmospheric oxygen. The powdered niobokupletskite was suspended in petroleum jelly to ensure a random orientation of crystals within the circular aluminum mount (aperture: 1.0 cm, thickness: 0.6 cm). Details regarding collection of Mössbauer data can be found in Chapter IV.

The Mössbauer spectrum of niobokupletskite is shown in Figure 3, and the site distribution parameters and associated errors in Table 3. The spectrum is characterized by three main absorption peaks at ≈ -0.07, 0.81 and 2.33 mm/s, corresponding to: (1) the sum of the low-energy lines from $^{[6]}Fe^{2+}$ and $^{[6]}Fe^{3+}$ doublets, (2) the high-energy lines from $^{[6]}Fe^{3+}$ doublets, and (3) the high-energy lines from $^{[6]}Fe^{2+}$ doublets, respectively. All Fe is found to be located in the *O*-sheet. The dominant feature in the spectrum is a wide doublet, attributable to $^{[6]}Fe^{2+}$ (modeled as having three Gaussian components), which has an average center shift (CS) of 1.13 mm/s (with respect to α-Fe at room temperature) and an average quadrupole splitting distribution (QSD) of 2.33 mm/s. The low energy side of this doublet displays a pronounced shoulder as a result of the presence of a second doublet (modeled as two Gaussian components) with an average CS of 0.38 mm/s and an average QSD of 0.81 mm/s, corresponding $^{[6]}Fe^{3+}$. There is no evidence for $^{[4]}Fe^{3+}$. The resultant Fe^{3+}/Fe_{tot} ratio obtained from analysis of the spectral areas is 0.215(7), corresponding to 0.33 *apfu* Fe^{3+}, a

TABLE 3. MÖSSBAUER SITE DISTRIBUTION PARAMETERS FOR TYPE-II NIOBOKUPLETSKITE

	δ0 (mm/s)	δ1	A (counts·mm/s)	A- /A+
Fe^{2+}	1.07(3)	0.03(1)	118600(1600)	1*
Fe^{3+}	0.38(3)	0*	32500(1300)	1*

		p (%)	⟨Δ⟩ (mm/s)	σΔ (mm/s)
Fe^{2+}	comp. 1	46	2.24(5)	0.5(1)
	comp. 2	7(15)	1.98(2)	0.2(2)
	comp. 3	46(2)	2.47(4)	0.20(4)
Fe^{3+}	comp. 1	27	0.6(1)	0.2(2)
	comp. 2	73(3)	0.8(3)	0.7(1)

	<CS> (mm/s)	<|Δ|> (mm/s)	stdev (|Δ|)	skew (|Δ|)
Fe^{2+}	1.13	2.33	0.39	-0.41
Fe^{3+}	0.38	0.81	0.52	0.89

reduced $\chi^2 = 0.96$

Site populations (%): Fe^{2+} 78.5(7) Fe^{3+} 21.5(7)

* fixed value

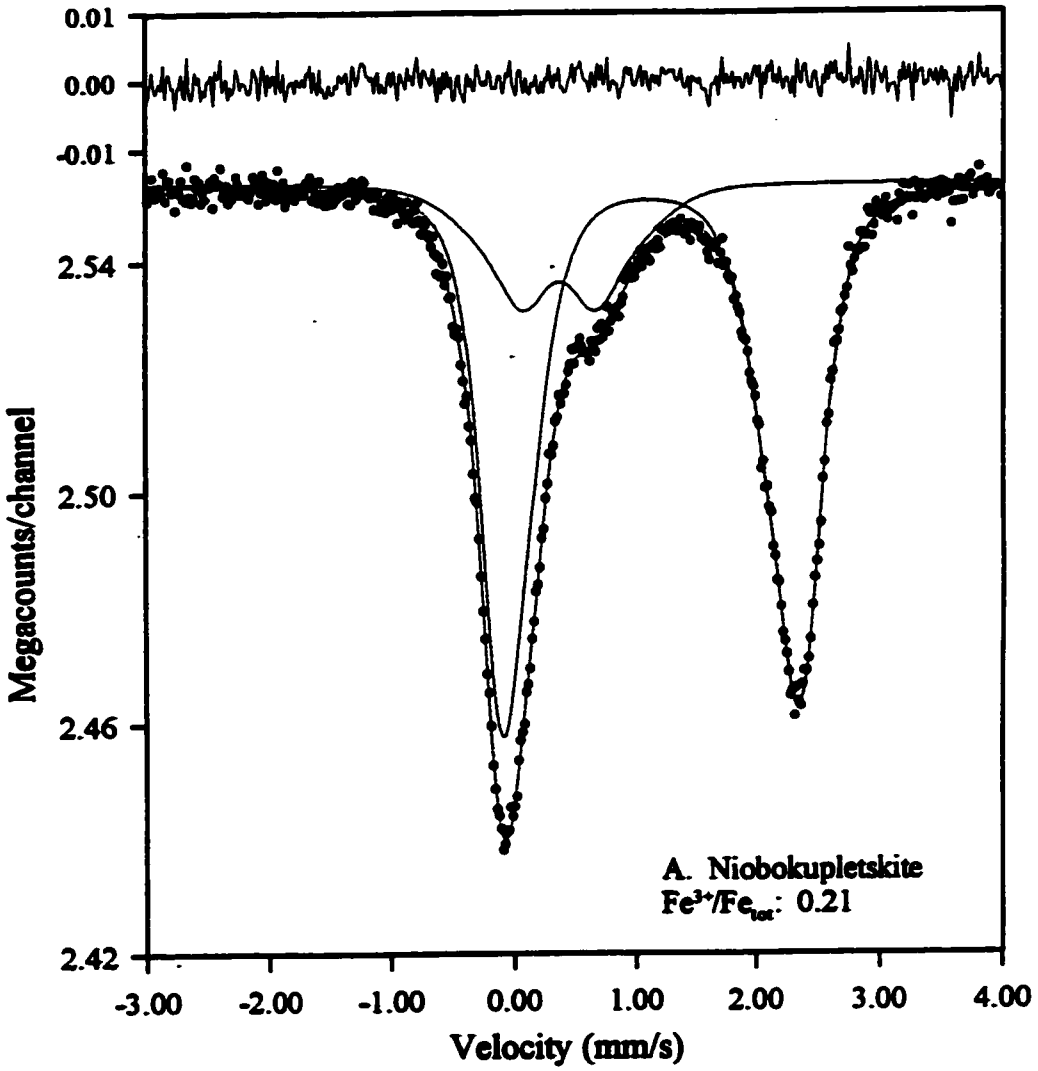

Figure 3. Mössbauer spectrum of Type-II niobokupletskite. The solid line through the spectral data represents the best fit. The subspectral contributions corresponding to $^{[6]}Fe^{2+}$ and $^{[6]}Fe^{3+}$ are shown superimposed on the data. The difference between the observed and calculated spectrum is shown on an exaggerated vertical scale at the top of the figure.

high value compared to those obtained for other samples of AGM from a variety of intrusions (average $Fe^{3+}/Fe_{tot} \approx 0.07$, Chapter II).

6.0. X-Ray Crystallography

A chemically homogeneous grain of Type-I niobokupletskite (0.21 x 0.19 x 0.02 mm) was selected from those within the electron-microprobe epoxy mount for a single-crystal X-ray diffraction study. *X*-ray powder diffraction data were collected with a 114.6 mm Debye-Scherrer camera with Cu$K\alpha$ radiation (Ni-filtered), operating at 45 kV and 20 mA, and are presented in Table 4. *X*-ray intensity data were collected using the Siemens SMART (Siemens Molecule Analysis Research Tool) system at the University of Ottawa which consists of a PLATFORM three-circle goniometer and a 1 K (diameter: 9 cm, 512 x 512 pixel) charge-coupled device (CCD) area detector. Data were collected at room temperature using monochromatic Mo$K\alpha$ *X*-radiation (40 kV, 30 mA) and a fixed detector-crystal distance of 12.621 cm. A frame width (ω) of 0.3° and count exposure times of 30 seconds per frame were the standard setting. A hemisphere of data was collected for $4.82 \leq 2\theta \leq 57.26$ with minimum and maximum indices of $-7 \leq h \leq 7$, $-11 \leq k \leq 16$, and $-15 \leq l \leq 15$. The data were reduced, filtered, integrated, and corrected for Lorentz, polarization and background effects using the Siemens program SAINT. A Ψ-scan data set of 724 reflections was used during absorption corrections where the crystal was modeled as an ellipsoid using the program XPREP. The merging *R* decreased from 14.14% before the absorption correction to 7.89% after the absorption correction, giving minimum and maximum transmission factors of 0.343

TABLE 4. X-RAY POWDER DIFFRACTION DATA FOR NIOBOKUPLETSKITE

d_{meas}	d_{calc}	I_{obs}	I_{calc}	hkl	d_{meas}	d_{calc}	I_{obs}	I_{calc}	hkl
10.707	10.619	100	100	001		2.403		6	$1\bar{3}4$
	10:532		38	010	2.322	2.325	10	4	$2\bar{1}2$
9.883	9.826	<5	17	$0\bar{1}1$	2.308	2.308	10	5	131
	5.829		<1	$0\bar{1}2$		2.299		5	$1\bar{4}4$
5.840	5.785	5	12	$0\bar{2}1$	2.254	2.255	<5	<1	$0\bar{5}1$
4.405	4.432	20	10	$\bar{1}\bar{1}1$		2.250		7	$\bar{2}13$
	4.367		5	$1\bar{2}0$	2.222	2.223	<5	3	$2\bar{4}1$
	4.346		3	101		2.216		2	$\bar{2}\bar{2}2$
	4.335		7	$1\bar{2}1$		2.203		2	$\bar{2}\bar{2}1$
4.100	4.098	<5	<1	012	2.130	2.124	5	3	$\bar{1}42$
	4.083		6	021		2.124		3	005
3.816	3.795	5	3	$\bar{1}21$	2.118	2.118	5	1	140
	3.778		2	$1\bar{1}2$		2.115		3	$\bar{1}\bar{3}5$
	3.761		6	$0\bar{2}3$	2.056	2.060	<5	4	$2\bar{1}3$
3.536	3.540	50	40	003	2.023	2.025	<5	3	132
	3.539		10	111		2.017		3	$1\bar{4}5$
3.294	3.281	20	13	$\bar{1}\bar{1}3$	1.995	1.999	<5	2	$\bar{1}51$
	3.275		2	$0\bar{3}3$		1.987		2	$\bar{2}14$
3.147	3.137	<5	5	022		1.983		2	$\bar{2}\bar{3}2$
3.108	3.099	<5	11	$\bar{1}22$	1.933	1.930	<5	1	015
	3.046		<1	$\bar{1}\bar{2}3$		1.928		2	$0\bar{6}3$
3.047	3.044	<5	10	$1\bar{2}3$		1.774		7	133
	2.996		5	013	1.769	1.767	5	7	$1\bar{4}6$
	2.993		2	$\bar{1}31$		1.764		2	$2\bar{6}2$
2.988	2.980	<5	<1	031		1.762		1	$3\bar{3}0$
2.887	2.886	5	5	$1\bar{3}3$	1.751	1.750	<5	7	$\bar{2}15$
	2.877		4	$0\bar{1}4$	1.660	1.659	5	11	$0\bar{7}3$
	2.876		6	112	1.633	1.634	<5	4	$\bar{1}44$
	2.831		4	121		1.634		2	$\bar{1}\bar{2}7$
2.824	2.822	<5	1	$1\bar{4}1$		1.631		2	240
	2.819		2	$\bar{1}\bar{3}2$		1.628		4	$\bar{1}\bar{3}7$
2.793	2.787	40	22	$\bar{1}\bar{3}1$		1.628		2	$\bar{2}\bar{4}5$
	2.784		23	$1\bar{4}2$	1.589	1.589	5	9	$3\bar{5}1$
2.677	2.679	30	19	$\bar{2}11$		1.589		9	$\bar{3}\bar{2}2$
	2.668		3	$\bar{1}\bar{1}4$	1.575	1.575	<5	<1	$\bar{2}\bar{5}3$
	2.655		10	004		1.575		<1	$2\bar{7}2$
2.587	2.587	40	19	130		1.573		2	$3\bar{5}0$
	2.580		18	$1\bar{4}3$		1.572		1	$\bar{3}\bar{2}3$
2.503	2.504	20	16	$\bar{2}12$					
2.409	2.412	10	6	$\bar{1}41$					

CuKa radiation, Ni filtered, 45 kV, 20 mA, 24 hour exposure, 114.6 mm Debye-Scherrer camera.
I's visually estimated.

and 0.664 respectively. Phasing of a set of normalized structure factors gave a mean value $|E^2-1|$ of 0.985 suggesting the centrosymmetric space group $P\bar{1}$, a feature consistent with other studies of triclinic AGM (Peng & Ma 1963, Woodrow 1967, Christiansen *et al.* 1998). Information pertinent to the data collection and crystal structure can be found in Table 5. The structure of niobokupletskite was refined by least-squares methods using the SHELXL-93 set of programs (Sheldrick 1993), with starting parameters taken from Christiansen *et al.* (1998) for a kupletskite from Kangerdlugssuaq, Greenland. During the initial refinement, Mn, the dominant octahedrally coordinated cation indicated by EMPA, was assigned $M(1)$ to $M(4)$, whereas Nb was assigned to D on the basis of data obtained by EMPA. Refinement of the site occupancy factors resulted in values less than unity for $M(1)$ and D and values greater than unity for $M(2)$, $M(3)$, and $M(4)$. Sodium was assigned to $M(1)$ and Ti assigned to D. Zinc, a heavier X-ray scatterer than Mn and the second most abundant element observed in the EMPA data, was assigned to $M(2)$, $M(3)$ and $M(4)$; ordering of Zn over these four sites is discussed below. The shape of the anisotropic displacement ellipsoid of the site assigned to K suggested that it was positionally disordered and it was therefore modeled as two split sites, $^{[9]}K(1a)$ and $^{[10]}K(1b)$, displaced 0.36Å from each other along X. Displacement factors for $K(1a)$ and $K(1b)$ were constrained to be equal and refined isotropically. The structure refined to $R = 9.40\%$ and $wR^2 = 26.11\%$ with isotropic displacement factors and to $R = 5.97\%$ and $wR^2 = 19.22\%$ with anisotropic displacement factors. An isotropic extinction correction was applied but did not improve the results. The high final R value is attributable to slippage along the {001} cleavage, imposed during extraction of the crystal from the epoxy mount, and also to microfractures observed in the crystal in BSE images (Fig. 1A). The final positional and

TABLE 5. MISCELLANEOUS DATA: NIOBOKUPLETSKITE

Space Group	$P\bar{1}$	Diffractometer	SIEMENS CCD
a (Å)	5.4303(9)	Radiation	MoKα (40 kV, 30 mA)
b	11.924(2)	Crystal Shape	plate
c	11.747(2)	Crystal Size	0.21 x 0.19 x 0.02 mm
α (°)	112.927(3)	μ (MoKα)	5.33 cm^{-1}
β	94.750(3)	Min/Max Trans.	0.343/0.664
γ	103.175(3)	$\|E^2-1\|$	0.985
V ($Å^3$)	669.5(3)	CFOM	1.08
Z	1		

Chemical Formula	$K_2Na(Mn,Zn,Fe)_7(Nb,Zr,Ti)_2Si_8O_{26}(OH)_4(O,F)$
2θ Range	$4.82 \le 2\theta \le 57.26$
Min/Max Indices	$-7 \le h \le 7$, $-11 \le k \le 16$, $-15 \le l \le 15$
No. of Unique Reflections	3023
No. of Observed Reflections	1779
Criterion for Observed Reflections	$F_o > 4\sigma(F_o)$
Final R (%)	5.97
wR^2 (%)	19.12

$R = \Sigma(|F_o|-|F_c|)/\Sigma|F_o|$

$wR^2 = [\Sigma(w)F_o^2 - F_c^2)^2/\Sigma[w(F_o^2)^2]^{1/2}$, $w = 1/\sigma^2(F_o)$

isotropic displacement parameters are given in Table 6 and selected bond lengths are given in Table 7. Bond valence sums were calculated using parameters taken from Brese & O'Keefe (1991) and can be found in Table 8. The observed and calculated structure-factors are available from the Depository of Unpublished Data, CISTI, National Research Council of Canada, Ottawa, Ontario K1A 0S2, Canada.

7.0. Description Of The Crystal Structure

Niobokupletskite is isostructural with other triclinic AGM. Details regarding the crystal structure can be found in Chapter III.

7.1. Interlayer

The interlayer of niobokupletskite contains both Na and K in two distinct sites. Sodium is [10]-coordinated and located between bridging apices of the NbO_6 octahedra. Bond lengths range from 2.64(1) to 2.715(0) Å. Refinement of the site occupancy factor gives 0.90, suggesting the presence of vacancies or a lighter scatterer (*e.g.* H_2O, H_3O^+). Electron microprobe data indicate 1.23 *apfu* of Na in niobokupletskite, suggesting an "excess" of Na if compared with results obtained from the structure refinement. This excess Na has been accounted for in the *M*(1) octahedral site. Substitution of Ca for Na within the interlayer is common in more Fe-rich AGM (*e.g.* Christiansen *et al.* 1998), but was not detected in Type-I niobokupletskite. Bond lengths to the two split sites assigned to K are as follows: $^{[9]}K$(1a) 2.83(2) to 3.41(2)Å, $^{[10]}K$(1b) 2.84(2) to 3.57(2)Å. A high site occupancy factor for

TABLE 6. POSITIONAL AND DISPLACEMENT PARAMETERS AND SITE OCCUPANCIES FOR NIOBOKUPLETSKITE

Atom	x	y	z	sof	$^{*}U_{11}$	U_{22}	U_{33}	U_{23}	U_{13}	U_{12}	U_{eq}
Mn(1)	0.8511(3)	0.2057(2)	0.4794(2)	0.91(1)	26(9)	138(11)	163(11)	67(8)	27(7)	31(7)	106(6)
Na	0.8511(3)	0.2057(2)	0.4794(2)	0.09(1)	26(9)	138(11)	163(11)	67(8)	27(7)	31(7)	106(6)
Mn(2)	0.2790(3)	0.0680(2)	0.4871(1)	0.90(3)	38(8)	164(11)	174(10)	91(8)	44(6)	39(7)	115(6)
Zn(2)	0.2790(3)	0.0680(2)	0.4871(1)	0.10(3)	38(8)	164(11)	174(10)	91(8)	44(6)	39(7)	115(6)
Mn(3)	0.4211(3)	0.3512(2)	0.4844(1)	0.85(3)	43(8)	154(11)	185(10)	88(8)	43(6)	35(7)	119(6)
Zn(3)	0.4211(3)	0.3512(2)	0.4844(1)	0.15(3)	43(8)	154(11)	185(10)	88(8)	43(6)	35(7)	119(6)
Mn(4)	0	0.5	0.5	0.33(2)	13(10)	131(14)	166(13)	55(10)	20(8)	-4(9)	110(8)
Zn(4)	0	0.5	0.5	0.17(2)	13(10)	131(14)	166(13)	55(10)	20(8)	-4(9)	110(8)
Nb	0.0749(2)	0.0818(1)	0.1865(1)	0.90(1)	4(5)	133(6)	178(6)	77(5)	37(4)	26(4)	100(4)
Ti	0.0749(2)	0.0818(1)	0.1865(1)	0.10(1)	4(5)	133(6)	178(6)	77(5)	37(4)	26(4)	100(4)
Si(1)	0.6786(6)	0.2745(3)	0.2314(3)	1.00	68(14)	186(18)	154(16)	103(14)	45(11)	60(12)	120(7)
Si(2)	0.8133(6)	0.5470(3)	0.2526(3)	1.00	95(14)	136(17)	146(16)	76(14)	23(12)	24(13)	122(7)
Si(3)	0.3765(6)	0.6737(3)	0.2552(3)	1.00	89(15)	167(18)	149(16)	84(14)	9(11)	18(13)	133(7)
Si(4)	0.5070(5)	0.9296(3)	0.2362(3)	1.00	49(14)	108(16)	139(15)	47(14)	21(11)	18(12)	103(7)
K(1a)	0.097(6)	0.278(1)	0.995(1)	0.41(6)							433(17)
K(1b)	0.164(4)	0.2754(8)	0.9956(8)	0.48(6)							433(17)
Rb(1b)	0.164(4)	0.2754(8)	0.9956(8)	0.065							433(17)
Na	0.5	0	0	0.45	148(39)	200(46)	147(39)	46(33)	-11(28)	33(29)	179(24)
O(1)	0.728(1)	0.3194(7)	0.3832(7)	1.00	28(33)	226(45)	165(39)	102(37)	33(29)	73(32)	126(16)
O(2)	0.146(1)	0.1600(8)	0.3682(7)	1.00	134(40)	167(45)	176(41)	74(37)	21(32)	45(35)	158(17)
O(3)	0.130(1)	0.3931(7)	0.5949(6)	1.00							88(15)
OH(4)	0.295(1)	0.4631(8)	0.3991(7)	1.00	102(36)	210(44)	146(38)	84(36)	74(30)	114(34)	134(16)
OH(5)	0.993(1)	0.1179(7)	0.5944(7)	1.00	104(37)	133(42)	142(38)	23(35)	67(30)	13(32)	139(16)
O(6)	0.559(1)	0.2576(7)	0.5915(6)	1.00	24(32)	161(42)	107(36)	60(34)	24(28)	19(30)	96(16)
O(7)	0.573(1)	0.0134(7)	0.3865(7)	1.00	37(33)	74(39)	184(40)	61(34)	0(29)	-11(29)	102(16)
O(8)	0.072(2)	0.5915(8)	0.2004(7)	1.00	184(43)	284(52)	222(47)	91(43)	131(37)	36(39)	235(20)
O(9)	0.250(2)	0.043(1)	0.8260(9)	1.00	268(53)	597(76)	210(49)	30(51)	51(42)	-337(52)	486(33)
O(10)	0.433(2)	0.4144(8)	0.7988(7)	1.00	215(46)	359(57)	186(46)	98(44)	22(37)	116(42)	254(21)
O(11)	0.129(2)	0.803(1)	0.8297(9)	1.00	683(78)	595(75)	238(52)	182(55)	22(51)	534(67)	431(29)
O(12)	0.267(2)	0.954(1)	0.1723(9)	1.00	709(79)	516(72)	185(49)	-78(45)	-189(50)	526(65)	498(35)
O(13)	0.266(2)	0.6062(8)	0.8075(8)	1.00	508(63)	106(45)	140(41)	18(37)	35(39)	77(45)	266(22)
O(14)	0.571(2)	0.2206(8)	0.8024(8)	1.00	568(66)	88(45)	206(46)	58(40)	29(44)	-14(45)	311(24)
O(15)	0.385(2)	0.197(1)	0.1693(8)	1.00	308(55)	559(74)	240(50)	202(53)	-56(43)	-247(52)	431(30)
O(16)	0	0	0	0.50	76(52)	277(72)	213(62)	121(54)	65(42)	96(47)	172(35)

$^{*}U$ij x 10^{4}

TABLE 7. SELECTED INTERATOMIC DISTANCES (Å) FOR NIOBOKUPLETSKITE

M(1)-O(2)	2.179(8)	*T*(1)-O(11)	1.585(9)	*D*-O(2)	1.929(8)
M(1)-O(6)	2.190(7)	*T*(1)-O(15)	1.595(9)	*D*-O(16)	1.981(1)
M(1)-OH(5)	2.194(8)	*T*(1)-O(1)	1.628(8)	*D*-O(9)	1.987(8)
M(1)-O(3)	2.209(7)	*T*(1)-O(13)	1.631(9)	*D*-O(15)	1.994(8)
M(1)-O(7)	2.221(7)	<*T*(1)-O>	1.604	*D*-O(12)	1.998(9
M(1)-O(1)	2.247(7)			*D*-O(11)	2.001(9)
<*M*(1)-O>	2.207	*T*(2)-O(13)	1.614(9)	<*D*-O>	1.982
		T(2)-O(3)	1.620(7)		
M(2)-OH(5)	2.124(7)	*T*(2)-O(8)	1.638(8)	*K*(1a)-O(12)	2.83(2)
M(2)-O(7)	2.133(8)	*T*(2)-O(10)	1.654(8)	*K*(1a)-O(11)	2.85(2)
M(2)-OH(5)	2.152(8)	<*T*(2)-O>	1.629	*K*(1a)-O(15)	3.04(2)
M(2)-O(6)	2.211(7)			*K*(1a)-O(9)	3.07(2)
M(2)-O(2)	2.252(8)	*T*(3)-O(6)	1.629(7)	*K*(1a)-O(14)	3.25(3)
M(2)-O(7)	2.254(7)	*T*(3)-O(14)	1.630(9)	*K*(1a)-O(16)	3.26(1)
<M2-O>	2.188	*T*(3)-O(10)	1.630(9)	*K*(1a)-O(13)	3.27(3)
		T(3)-O(8)	1.645(8)	*K*(1a)-O(8)	3.41(2)
				<*K*(1a)-O>	3.12
M(3)-O(1)	2.143(7)	<*T*(3)-O>	1.634		
M(3)-OH(4)	2.145(7)	*K*(1b)-O(12)	2.99(2)	*K*(1b)-O(15)	2.84(2)
M(3)-O(3)	2.151(7)	*T*(4)-O(9)	1.591(9)	*K*(1b)-O(9)	2.88(2)
M(3)-O(6)	2.169(7)	*T*(4)-O(12)	1.591(9)	*K*(1b)-O(11)	3.00(2)
				K(1b)-O(16)	3.224(9)
M(3)-OH(4)	2.210(8)	*T*(4)-O(14)	1.607(9)	*K*(1b)-O(14)	3.29(2)
M(3)-O(2)	2.232(8)	*T*(4)-O(7)	1.613(8)	*K*(1b)-O(13)	3.35(2)
<M(3)-O>	2.175	<*T*(4)-O>	1.601	*K*(1b)-O(10)	3.56(1)
				K(1b)-O(8)	3.57(2)
M(4)-OH(4)	2.097(7) x 2	Na-O(12)	2.64(1) x 2	<*K*(1b)-O>	3.19
M(4)-O(1)	2.149(8) x 2	Na-O(9)	2.64(1) x 2		
M(4)-O(3)	2.181(7) x 2	Na-O(11)	2.66(1) x 2		
<*M*(4)-O>	2.142	Na-O(15)	2.66(1) x 2		
		Na-O(16)	2.715(0) x 2		
		<Na-O>	2.66		

TABLE 8. EMPIRICAL BOND-VALENCES (*vu*) FOR NIOBOKUPLETSKITE*

	Na	*K*(1a)	*K*(1b)	*M*(1)	*M*(2)	*M*(3)	*M*(4)	*D*	*T*(1)	*T*(2)	*T*(3)	*T*(4)	Σ
O(1)				0.29		0.36	0.35 ↓×2		0.99				1.99
O(2)				0.35	0.28	0.28		0.95					1.86
O(3)				0.32		0.36	0.32 ↓×2			1.01			2.01
OH(4)						0.67	0.41 ↓×2						1.08
OH(5)				0.34	0.76								1.10
O(6)				0.34	0.31	0.35					0.99		1.99
O(7)				0.31	0.66							1.03	2.00
O(8)		0.01	0.01							0.96	0.94		1.92
O(9)	0.10 ↓×2	0.03	0.07					0.79				1.09	2.08
O(10)			0.02							0.92	0.98		1.92
O(11)	0.10 ↓×2	0.06	0.06					0.76	1.11				2.09
O(12)	0.10 ↓×2	0.06	0.05					0.71				1.09	2.01
O(13)		0.02	0.03						0.98	1.03			2.06
O(14)		0.02	0.04								0.98	1.05	2.09
O(15)	0.10 ↓×2	0.03	0.08					0.78	1.08				2.07
O(16)	0.08 ↓×2 →	0.02 →×3	0.02 →×3					0.81 →×3					1.86
Σ	0.96	0.25	0.38	1.95	2.01	2.02	2.16	4.80	4.16	3.92	3.89	4.26	

* constants from Brese & O'Keefe (1991)

Note: Valences for *M* and *D* sites were calculated using the following weighted averages: M(1): (Mn0.91Na0.09), *M*(2): ($Mn_{0.9}Zn_{0.1}$), *M*(3): ($Mn_{0.85}Zn_{0.15}$), *M*(4): ($Mn_{0.33}Zn_{0.17}$), *D*: ($Nb_{0.90}Ti_{0.10}$), K(1b): ($K_{0.48}Rb_{0.06}$)

K(1b) (0.62) indicates the presence of a heavier scatterer. Rubidium, fixed at the EMPA value of 0.13 *apfu*, was therefore assigned to this site.

7.2. O-sheet

The *O*-sheet of niobokupletskite is identical to that of kupletskite with additional Zn, Fe, Na and Mg. The largest, and least distorted, of the four octahedra, *M*(1), is coordinated by five O^{2-} and one OH^- [OH(5)], with a <*M*(1)-O> distance of 2.207 Å [volume: 13.990 $Å^3$, calculated in IVTON (Balić-Žunić & Vicković 1996); distortion (Δ): 1.041, calculated using the equation for quadratic elongation (Brown & Shannon 1973)]. The *M*(1) site in niobokupletskite is slightly larger than that of kupletskite (<*M*(1)-O>: 2.203 Å, volume: 13.858 $Å^3$; Christiansen *et al.* 1998) owing to the presence of Na. Site-scattering refinements (SREF) of *M*(1) consistently yielded occupancies less than unity, indicating the presence of a weaker scatterer or vacancies. Electron-microprobe data, and a low site occupancy factor for the site assigned to Na, indicate an "excess" of Na. The occupancy of *M*(1) was therefore refined with both Mn and Na, resulting in site populations consistent with EMPA data (SREF: 0.18 *apfu*, EMPA: 0.28 *apfu*) and a bond-valence sum of 1.95 *vu*. The presence of Na within the *M*(1) site is not an uncommon feature in AGM. For example, monoclinic magnesium astrophyllite (Shi *et al.* 1998), exhibits dominance of Na within a single octahedral site which is the equivalent to *M*(1) in triclinic species, and has also been noted in other AGM from MSH. Substitution of Na for Mn in octahedral coordination, although not common, has also been noted in other minerals including samuelsonite (Moore & Araki 1977), barytolamprophyllite (Rastsvetaeva & Dorfman 1995), vuonnemite (Ercit *et al.* 1998), and in

alkali clinoamphiboles from MSH (Taylor 1999). It may be attributable to high activities of Na within the crystallizing magma.

The *M*(2), *M*(3) and *M*(4) sites are larger and less distorted than those observed in kupletskite, probably owing to the increased extent of substitution of Mn for Fe in niobokupletskite. The *M*(2) and *M*(3) sites have a *cis* configuration [*M*(2): OH(5) x 2, *M*(3): OH(4) x 2] with average <*M*-O> distances of 2.188 and 2.175 Å respectively, whereas *M*(4) is a *trans*-site [OH(4) x 2] with an average <*M*(4)-O> distance of 2.142 Å. The *M*(2) octahedra, the most distorted in the AGM *O*-sheet (Δ: 6.059), are unique as they form continuous zigzag chains parallel to the *X* axis; all other *M* sites share at most one common edge with crystallographically equivalent octahedra. The combination of continuous chains of *M*(2) octahedra and open-branched *zweier* single chains parallel to *X* has a pronounced effect on the morphology of astrophyllite-group minerals: a preferential elongation of crystals in the *X* direction, the development of a secondary, moderate cleavage along {010}, and the formation of acicular to tabular crystals.

Site-scattering refinements indicate departures from ideal Mn occupancies and the presence of a stronger *X*-ray scatterer in all of *M*(2), *M*(3) and *M*(4). Zinc, the second most abundant cation in the EMPA data, was refined in all three of these sites, with the total site occupancy constrained to be unity. Zinc populations for each of these three sites are as follows: *M*(2) 0.10, *M*(3) 0.15, *M*(4) 0.34, resulting in total Zn contents in agreement with those obtained by electron microprobe (SREF: 0.84, EMPA: 0.73 *apfu*). Bond valence sums indicate these site occupancy factors to be reasonable [*M*(2): 2.01 *vu*, *M*(3): 2.02 *vu*, *M*(4): 2.16 *vu*]. Results of this refinement suggest that Zn, a cation much smaller than Mn ($^{[6]}Zn^{2+}$:

0.74 Å, $^{[6]}Mn^{2+}$: 0.83 Å; Shannon 1976) preferentially orders at *M*(4), the smallest of the four *M* sites [volumes: *M*(2) 13.687, *M*(3) 13.460, *M*(4) 12.902 Å^3].

7.3. H-sheet

There are four distinct tetrahedrally coordinated sites (*T*) in the niobokupletskite structure. As EMPA reveal only minor Al^{3+} (average: 0.34 *apfu*), and Mössbauer spectroscopy did not indicate $^{[4]}Fe^{3+}$, all four *T* sites were modeled with only Si^{4+} during the structure refinement. Bond lengths within the four tetrahedral sites range from 1.585(9) to 1.654(8) Å. In niobokupletskite, *T*(1) and *T*(4) each share two basal, non-bridging (nb) oxygen atoms with the basal plane of the NbO_6 octahedra [*T*(1): O(15), O(11) and *T*(4): O(9), O(12)]. Shorter bond lengths to these basal oxygen atoms (<*T*(1)-O_{nb}> 1.590 Å, <*T*(4)-O_{nb}> 1.591 Å) result in a tilting of *T*(1) and *T*(4) 6.31° and 6.87° out of the (001) plane, respectively, toward the NbO_6 octahedra. However, *T*(2) and *T*(3), tetrahedra within the open-branched *zweier* single chains which do not share common oxygen atoms with the NbO_6 octahedra, are tilted only 2.28° and 0.87° out of the (001) plane respectively, and display slightly longer basal <*T*-O> bond lengths than *T*(1) and *T*(4) (<*T*(2)-O_{basal}> 1.629 Å, <*T*(3)-O_{basal}> 1.635 Å).

In niobokupletskite, bond valence sums (Table 8) indicate the presence of a divalent anion in the O(16) position (1.86 *vu*), unlike Ti-dominant AGM, for which bond valence calculations indicate a monovalent anion (OH or F, Christiansen *et al.* 1998). The substitution of O^{2-} at the O(16) position is required in order to balance the excess positive charge

attributable to Nb^{5+} resulting from the $Nb^{5+} \Leftrightarrow Ti^{4+}$ substitution. The following coupled substitution is therefore suggested for the incorporation of Nb^{5+} into the AGM structure:

$$Ti^{4+} + F^-/OH^- \Leftrightarrow Nb^{5+} + O^{2-} \quad (1)$$

The same mechanism for substitution has been suggested for the incorporation of Ti and F into the wöhlerite structure (Mellini & Merlino 1979). The presence of O^{2-} at the O(16) position results in an local increase in symmetry along *Z* within the DO_6 octahedra due to the presence of a strong O(2)-Nb-O(16) bond rather than the weaker, asymmetric O(2)-Ti-F bond observed in other Ti-dominant astrophyllite-group minerals. The subsequent shortening of *D*-O(16) and lengthening of *D*-O(2) are direct results of Nb being positionally more central within the polyhedra, rather than being displaced along *Z* towards the *O*-layer as is the case with Ti polyhedra (Chapter III). The <O(16)-D-O_{basal}> bond angles are increased [85.4°, niobokupletskite; 80.8°, kupletskite (Christiansen *et al.* 1998)] and <O(2)-D-O_{basal}> are decreased [niobokupletskite: 94.6°; kupletskite: 99.2° (Christiansen *et al.* 1998)] as a result of this displacement. The net result of all these modifications is the significant decrease in distortion of the *D* polyhedra [Δ(niobokupletskite): 1.526 *versus* Δ(kupletskite): 17.840].

8.0. Discussion

The proposed coupled substitution scheme between kupletskite and niobokupletskite appears to be extensive. In samples of Mn-dominant AGM from a variety of SiO_2-undersaturated localities, including MSH, Lovozero (Kola Peninsula, Russia) and the Oslo rift (Langesundsfjord area, Norway), a strong negative correlation exists between Nb and Ti (Fig.

4) and between Nb and F (Fig.5). The average Nb content of Mn-dominant AGM from these localities ranges from 0.06 to 1.33 *apfu* (67% Nb-Ti substitution) with an average F content of 0.11 to 0.95 *apfu* (89% O-F substitution).

The incorporation of Zn into the niobokupletskite structure, and into AGM in general, may offer an indication of the sulfur fugacity (fS_2) at the time of crystallization. Electron-microprobe analyses indicate a bimodal distribution of Zn in niobokupletskite (Table 1); Type-I niobokupletskite contains 0.73 *apfu* Zn whereas Type-II and Type-III do not contain essential Zn (Table 2). Type III niobokupletskite is associated with wurtzite and genthelvite [$Zn_4Be_3(SiO_4)_3S$], two of only six Zn-bearing species to be described from Mont Saint-Hilaire (Horváth & Gault 1990). The presence of a (Zn,S)-bearing species in association with Zn-free niobokupletskite (Type-III) and of Zn-bearing niobokupletskite in the absence of associated Zn-S species (Type-I), suggests that Zn readily enters into the AGM structure in conditions where the fS_2 is too low to allow for the crystallization of a separate Zn-S species. The presence of wurtzite (the S-deficient hexagonal polymorph of ZnS) rather than sphalerite is of interest in this respect. Hydrothermal synthesis studies of the univariant wurtzite-sphalerite boundary have shown wurtzite to be stable at low fS_2 ($< 10^{-10}$ atm), and in a wide range of temperatures, as low as 100 °C in diagenetic environments, contradictory to the previously established inversion temperature of 1020 °C (Scott & Barnes 1972). At higher fS_2 ($> 10^{-10}$ atm) and lower temperatures (<465 °C), sphalerite is the dominant ZnS polymorph. Sphalerite is ubiquitous at MSH as a late-stage phase in all the microenvironments, most commonly associated with other S-bearing species (*i.e.* pyrite,

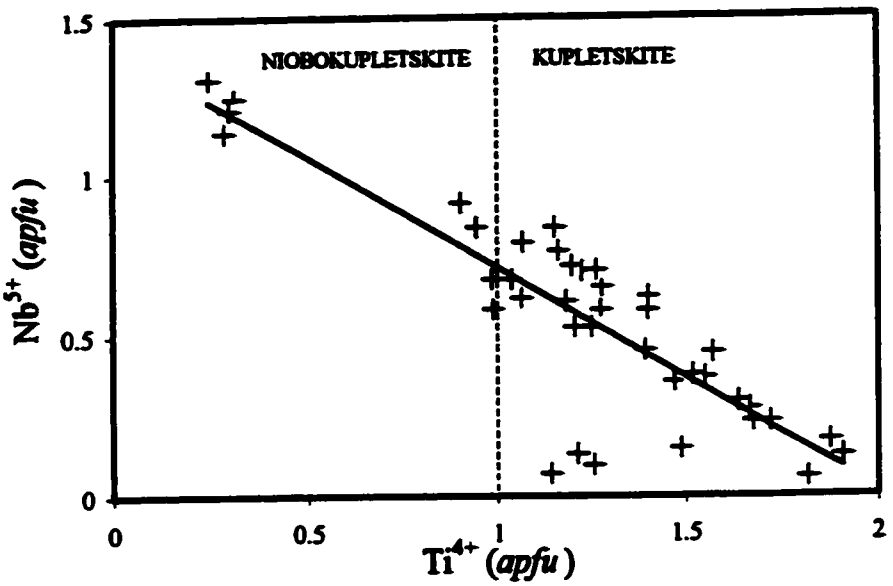

Figure 4. Content of Ti^{4+} versus that of Nb^{5+} in the kupletskite-niobokupletskite solid-solution series. (Linear fit, R^2: 0.742)

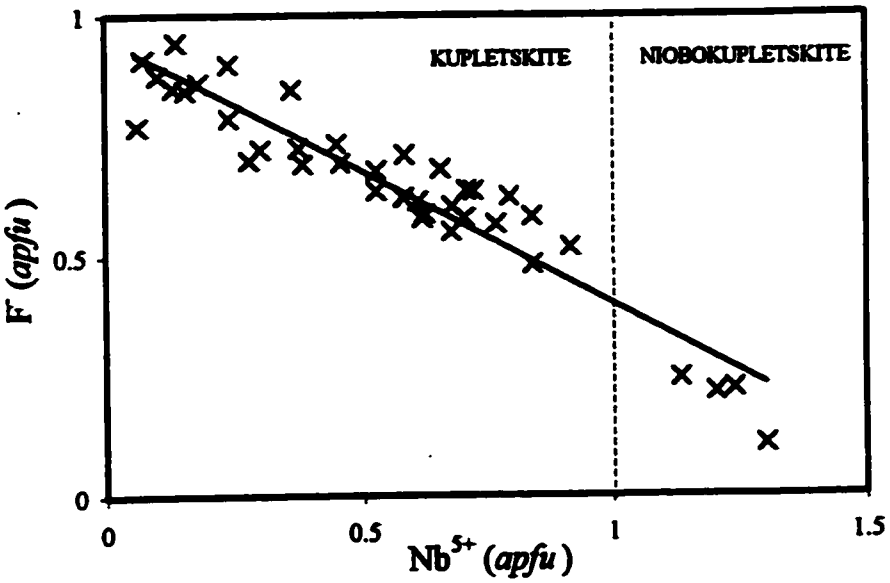

Figure 5. Content of Nb^{5+} versus that of F in the kupletskite-niobokupletskite solid-solution series. (Linear fit, R^2: 0.893)

pyrrhotite; Horváth & Gault 1990). The absence of sphalerite in samples containing niobokupletskite suggests that the fS_2 was too low to permit sphalerite formation, resulting in the formation of either S-deficient wurtzite or of zincian niobokupletskite.

The controls on the distribution of high-field strength elements in the magma, and subsequently into alkali titano-, zircono- and niobosilicates such as those of the astrophyllite group, may contribute to an understanding of the parageneses of these minerals. For example, in peralkaline systems, zirconium shows a high solubility and a highly incompatible nature until the final stages of crystallization (Bowden 1966, Larsen 1973, Watson 1979, Dunn & McCallum 1982, Linthout 1984, Rubin *et al.* 1993). The high solubility of Zr in alkali-rich magmas can be attributed to the fact that Zr acts as network-modifier (Linthout 1984). An increase in the alkali content in the melt (Na+K) results in an increase in the proportion of non-bridging oxygen atoms to which Zr will preferentially bond, inhibition of $^{[7]}Zr$ and $^{[8]}Zr$, and promotion of $^{[6]}Zr$, leading to the incorporation of minor Zr into silicates such as pyroxenes and amphiboles which have [6]-coordinated sites similar to those occupied by Zr in the melt polymers (*e.g.* aegirine; Piilonen *et al.* 1998). Decreasing temperature, increased Ca, and increased fO_2 results in melt polymerization, decreased solubility of Zr, increased bonding between ZrO_6 and SiO_4 groups, and the formation of charge-balanced $^{[6]}Zr$-O-(Si,Na) bonds within the melt (Linthout 1984, Farges *et al.* 1994). In all samples of niobokupletskite, the Zr:Ti ratio is greater than one (Zr/Ti: 1.38 to 1.91), suggesting that conditions were such to allow for decreased Zr solubility and preferential incorporation of Zr rather than Ti into the niobokupletskite structure. The high Fe^{3+}/Fe_{tot} ratio obtained by Mössbauer spectroscopy and the coupled substitution of Nb^{5+} and O^{2-} in the niobokupletskite series are both suggestive of a

highly oxidizing environment for niobokupletskite. As such, it appears that Zr and Nb may behave similarly in a peralkaline melt, unlike Zr and Ti which behave independently and either partition into discrete Zr or Ti phases or else are strongly ordered into separate sites in a given mineral structure (Pyatenko & Voronkov 1978). The late-stage development of (Ca+Si+Nb)-bearing pyrochlore-group minerals in fractures within both niobokupletskite and primary kupletskite, and the presence of abundant late-stage catapleiite in association with niobokupletskite, suggest an increase in the (Ca+Zr+Nb) concentration during the final stages of crystallization from a residual melt, followed by the formation of niobo- and zirconosilicates. Zirconium-rich niobokupletskite may represent an intermediate phase between early Zr-rich pyroxene and late-stage Zr-Nb minerals (*e.g.* catapleiite, franconite). The source of Nb in niobokupletskite may be attributed to the local dissolution of primary Nb-rich kupletskite (on which fibres of the former have nucleated on) or Nb-bearing minerals such as those of eudialyte group. More information regarding the distribution of Nb at MSH is required before either scenario can be clearly demonstrated.

CHAPTER VII.

THE PARAGENESIS OF ASTROPHYLLITE GROUP MINERALS AT MONT SAINT-HILAIRE, QUÉBEC: EVIDENCE FOR Nb AND Zr ENRICHMENT BY LATE-STAGE POST-MAGMATIC AND HYDROTHERMAL PROCESSES

1.0. INTRODUCTION

Previous studies of AGM have focused primarily on the documentation of chemical variations, as well as limited crystal structure analyses, with little attention being paid to understanding the paragenesis of these complex minerals. Abdel-Rahman (1992), in a study involving the metasomatized wallrocks in a 2 to 3 km aureole surrounding the Mount Gharib A-type granite (Egypt) suggested that the common association astrophyllite+arfvedsonite+albite+fluorite is the result of alkali metasomatism by exsolved F-rich fluids. Abdel-Rahman (1992) further proposed that fibrous overgrowths of astrophyllite+albite at arfvedsonite-perthite grain margins are the result of albitization and metasomatic replacement of arfvedsonite by astrophyllite. A similar occurrence has been noted at Mount Rosa (Pikes Peak, Colorado, USA) where astrophyllite replaces riebeckite in the border zones of the exterior granitic pegmatites (Gross & Heinrich 1966).

In some intrusions, such as at MSH, not only are AGM observed as overgrowths on primary magmatic phases such as amphibole and eudialyte group minerals, but there is also evidence for multiple periods of AGM crystallization within individual environments, clearly indicating significant changes in chemistry of the melt or fluid during crystallization. Such changes in AGM composition permit comments to be made on the petrogenetic evolution of AGM, as well as offering insights into the geochemical evolution of the melt from which

these minerals crystallized. The purpose of this chapter is to discuss the paragenesis of AGM from the peralkaline East Hill suite at Mont Saint-Hilaire (Québec, Canada). In addition, the use of crystal-chemical parameters, such as Mn# and the high field-strength element (HFSE) content in minerals such as AGM, will be discussed.

2.0. East Hill Suite, Mont Saint-Hilaire (Québec, Canada)

Members of the astrophyllite group occur in seven distinct microenvironments in the peralkaline East Hill suite (EHS) at MSH: syenite pegmatites (PEG), altered syenite pegmatites (APEG), aplites (APLITE), sodalite syenites (SS), sodalite syenite xenoliths (SSX), natrolite pegmatites (NPEG), and in a metasomatic unit associated with the hornfels (META). Five species of AGM occur at MSH: astrophyllite, *sensu stricto*, kupletskite, niobokupletskite, zircophyllite, and a potentially new species Fe-zircophyllite (Table 1). In general, all AGM from MSH are late-stage minerals that crystallized from post-magmatic, hydrothermal or metasomatic melts or fluids. The presence of AGM throughout the differentiated EHS allows us to trace the compositional evolution of AGM throughout the crystallizational history of the individual microenvironments. Figures 1 and 2 show the distribution of AGM species in the EHS at MSH and Figures 3A to 3C shows the compositional ranges in AGM from each of the microenvironments. Average EMPA data for MSH AGM are in Appendix B.

TABLE 1. DISTRIBUTION OF ASTROPHYLLITE GROUP MINERAL SPECIES IN THE MICROENVIRONMENTS OF THE EAST HILL SUITE, MONT SAINT-HILAIRE, QUÉBEC

Microenvironment	AGM Species	Alkalinity Index (AI*)
Syenite pegmatites (PEG)	kupletskite niobokupletskite zircophyllite	> 1.3**
Altered syenite pegmatites (APEG)	kupletskite astrophyllite niobokupletskite Fe-zircophyllite	> 1.3
Natrolite pegmatites (NPEG)	astrophyllite	0.99 - 1.02 (ave.: 1.00)
Aplites (APLITE)	kupletskite astrophyllite	> 1.2
Sodalite syenite (SS)	kupletskite niobokupletskite astrophyllite	1.33✧
Sodalite syenite xenoliths (SSX)	kupletskite astrophyllite	1.21 - 1.77 (ave.: 1.35)
Metasomatic unit (META)	astrophyllite kupletskite	1.28

*Alkalinity index (AI): whole rock (K+Na)/Al in molecular proportions
** extrapolated from other microenvironments
✧ data from Rajasekaran (1967)

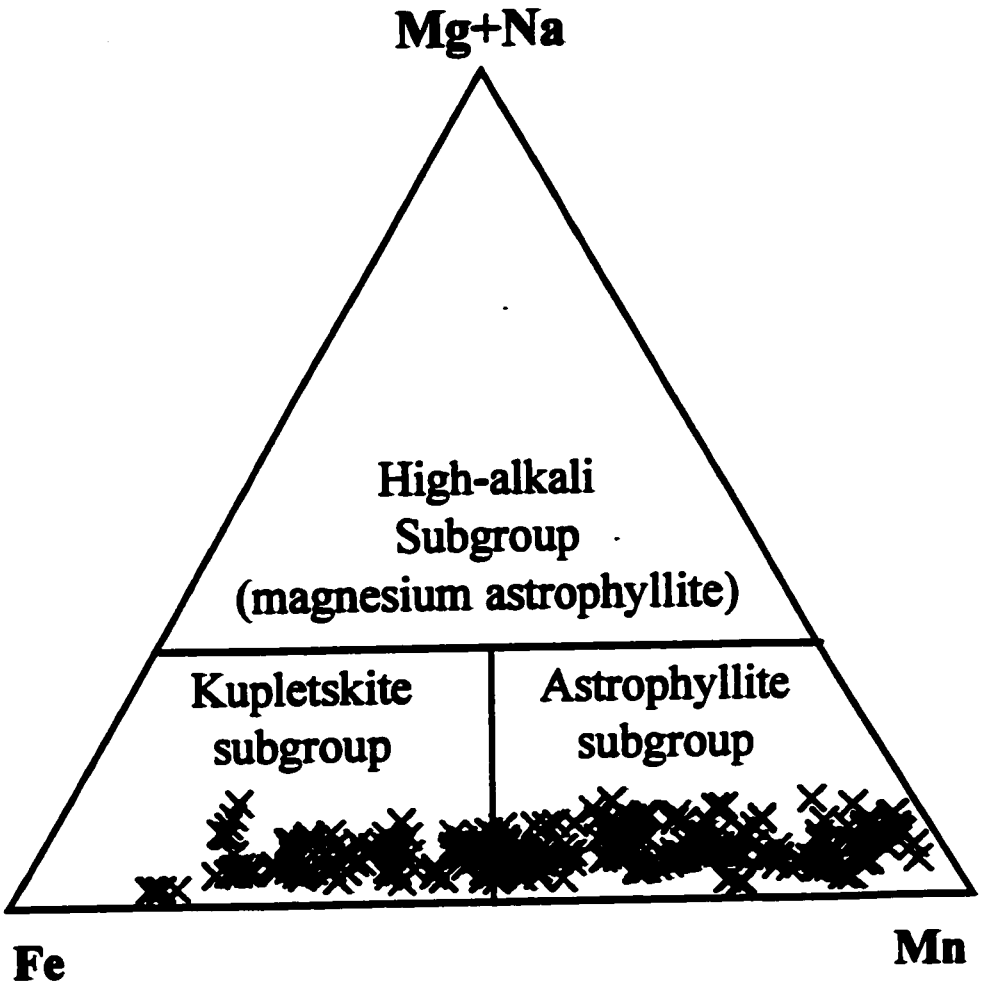

Figure 1. Classification of MSH AGM based on the composition of the *O*-sheet.

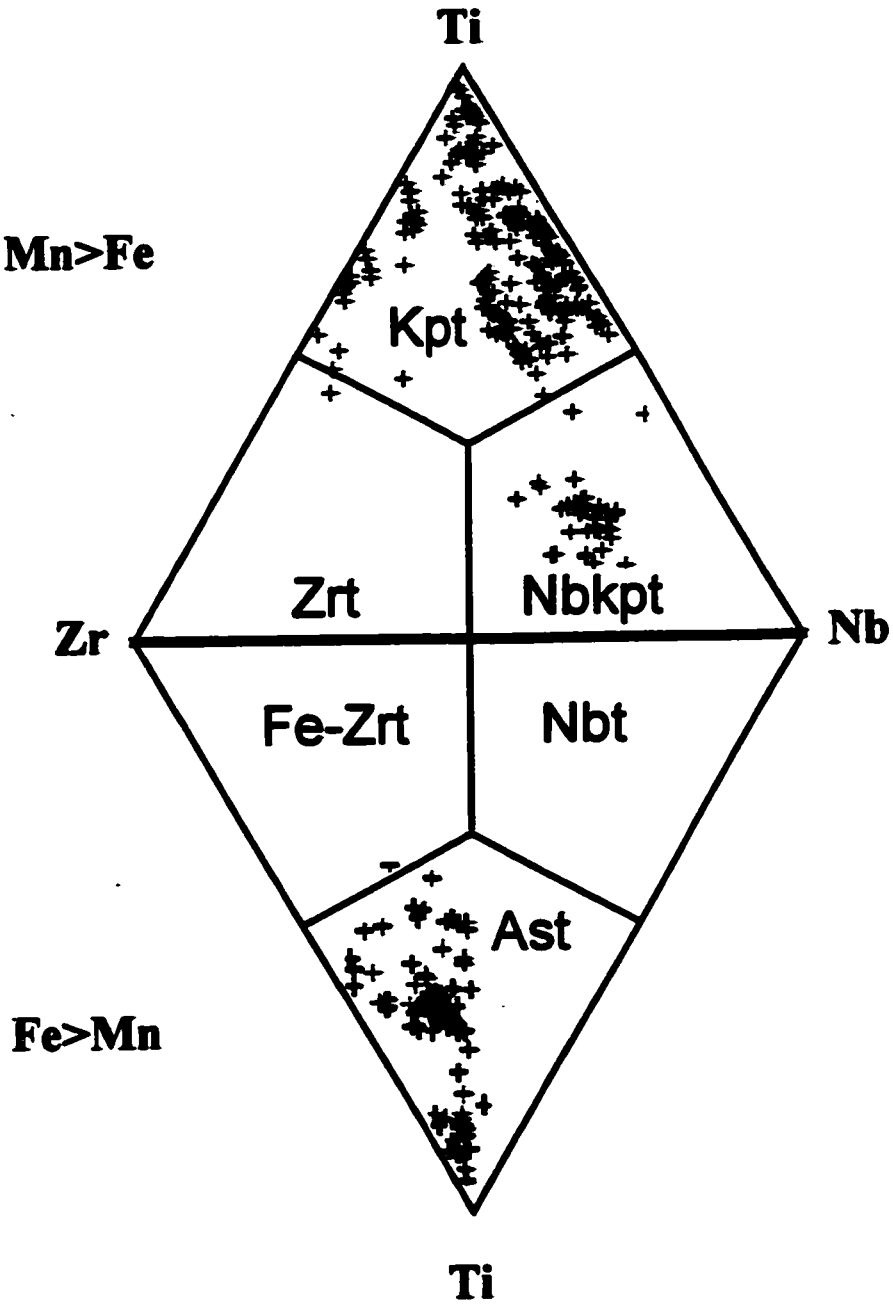

Figure 2. Classification of MSH AGM based on the composition of the *H*-sheet. Kpt: kupletskite, Nbkpt: niobokupletskite, Zrt: zircophyllite, Nbt: niobophyllite, Fe-Zrt: Fe-dominant zircophyllite, Ast: astrophyllite.

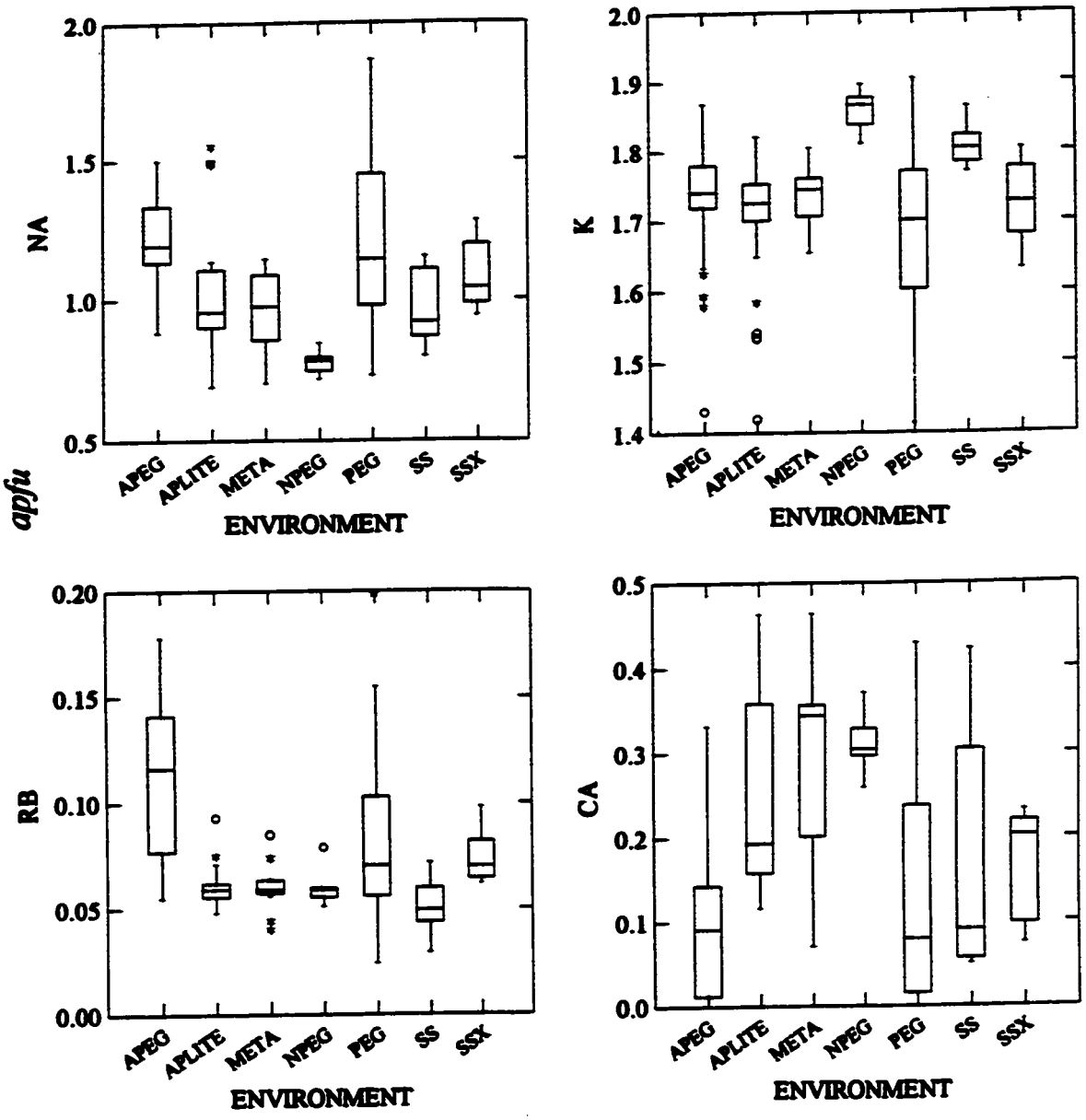

Figure 3A. Boxplots depicting the distribution of interlayer cations in AGM from MSH. APEG: altered pegmatites, APLITE, META: metasomatic unit, NPEG: natrolite pegmatites, PEG: unaltered pegmatites, SS: sodalite syenite, SSX: sodalite syenite xenoliths. The central horizontal line of each box represents the median of the population. The length of each box represents the range within which the central 50% of the values fall (box edges/hinge: 1st and 3rd quartile). Lower and outer fences represent lower/upper hinge ± (1.5 • interquartile range). Whiskers represent lower/upper hinge ± (3 • interquartile range). Open circles are outliers.

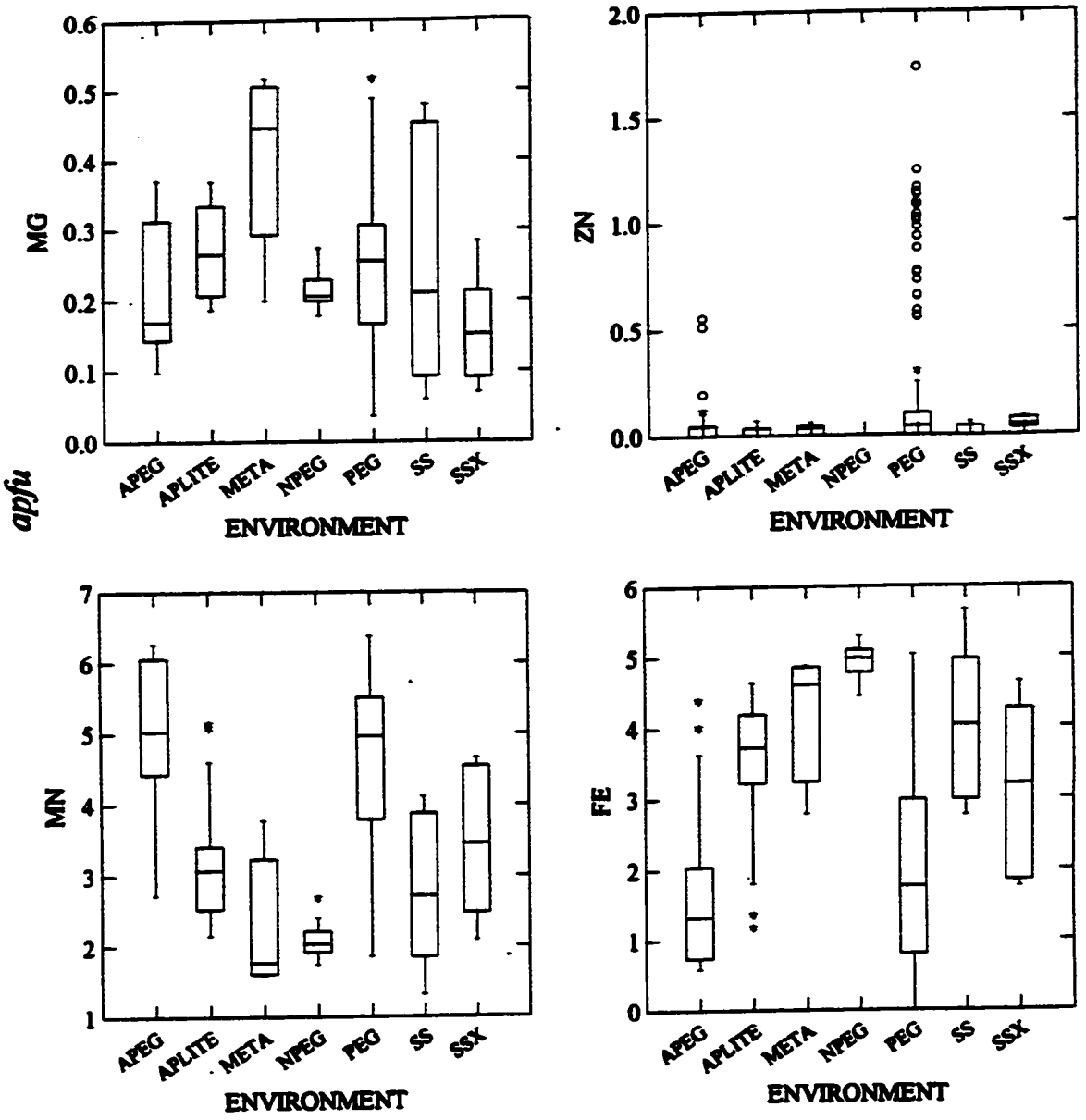

Figure 3B. Boxplots depicting the distribution of *H*-sheet cations in AGM from MSH. Environments and boxplots are defined as in Figure 3A.

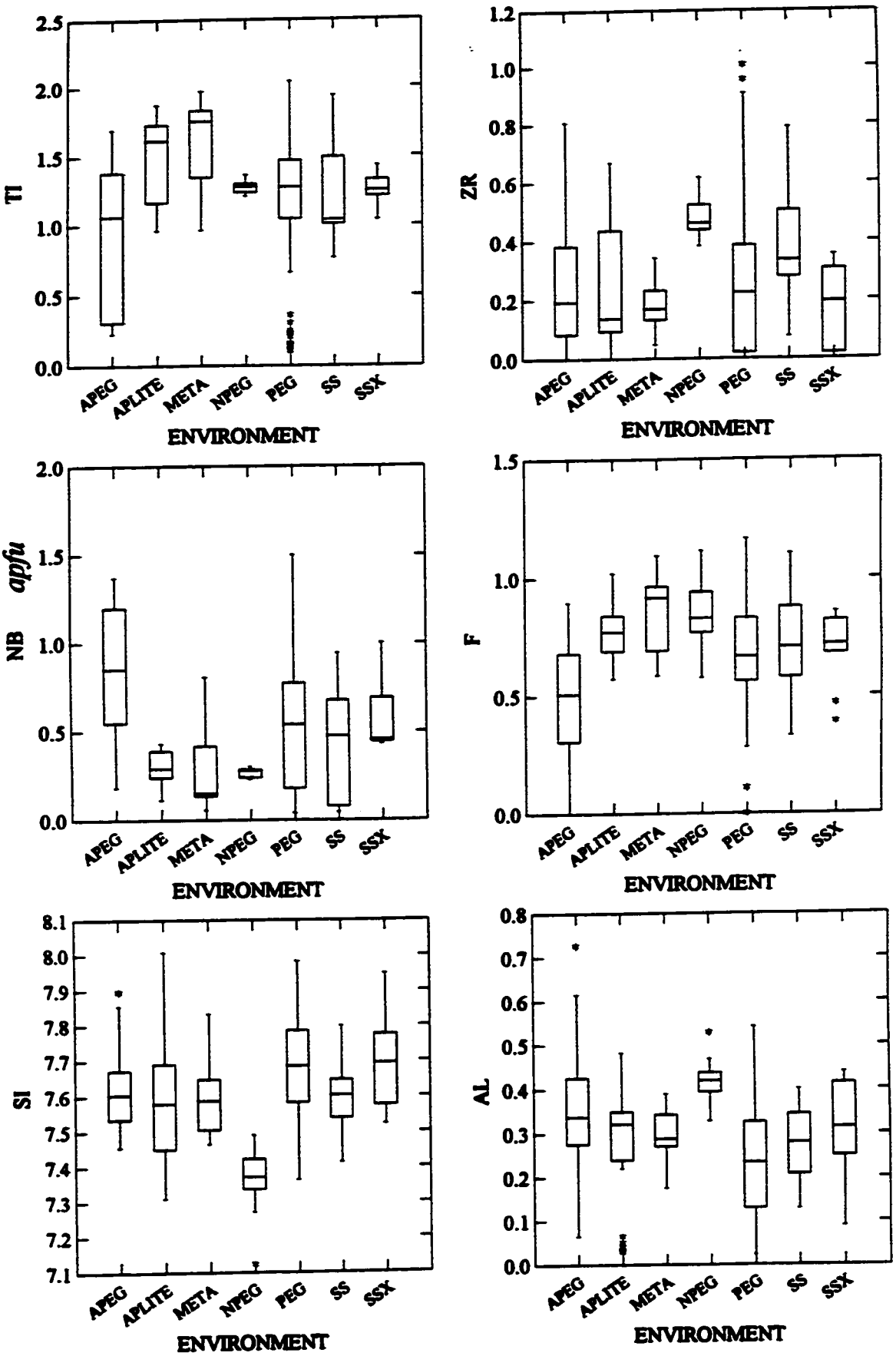

Figure 3C. Boxplots depicting distribution of interlayer cations and F in AGM from MSH. Environments and boxplots are defined as in Figure 3A.

2.1. Syenitic pegmatites (PEG and APEG)

Pegmatite dikes, which range from a few centimeters to a meter or more in width, cross-cut all other rock types within the EHS (Horváth & Gault 1990). Minerals of the astrophyllite group occur in three types of pegmatites: (1) unaltered syenitic pegmatites (APEG), (2) altered syenitic pegmatites (APEG), and (3) natrolite pegmatites (NPEG).

In the PEG and APEG, kupletskite occurs as coarse grained (up to 3 x 2 x 1 cm) tabular to platy, subhedral to anhedral, dark red-brown, orange-yellow or pale lavender polycrystalline aggregates embedded in the matrix or within vugs (Plate 1). It is commonly associated with primary aegirine, albite, catapleiite, microcline and rhodochrosite. Primary kupletskite in both the PEG and APEG is commonly overgrown by a second generation of fibrous matted AGM. In the PEG, this secondary overgrowth is dominantly Nb-bearing kupletskite or niobokupletskite. Fibrous zircophyllite, although rare, has been observed nucleating on kupletskite, indicating a late-stage enrichment in Zr, with Zr > Nb. Zoning within individual primary crystals is complex and ranges from regular and concentric to diffuse and random.

Many of the pegmatites have undergone varying degrees of hydrothermal alteration. Such pegmatites are characterized by a wide range of secondary minerals including fibrous aegirine, ancylite-(Ce), calcite, genthelvite, chlorite group minerals, oxides such as hematite and birnessite, and sulphides including wurtzite. Secondary fibrous overgrowths on primary kupletskite in the APEG are niobokupletskite, Zr-bearing astrophyllite and a potential new species, Fe-zircophyllite (Plates 2 & 3). Figures 4 & 5 show the compositional range of AGM from PEG and APEG.

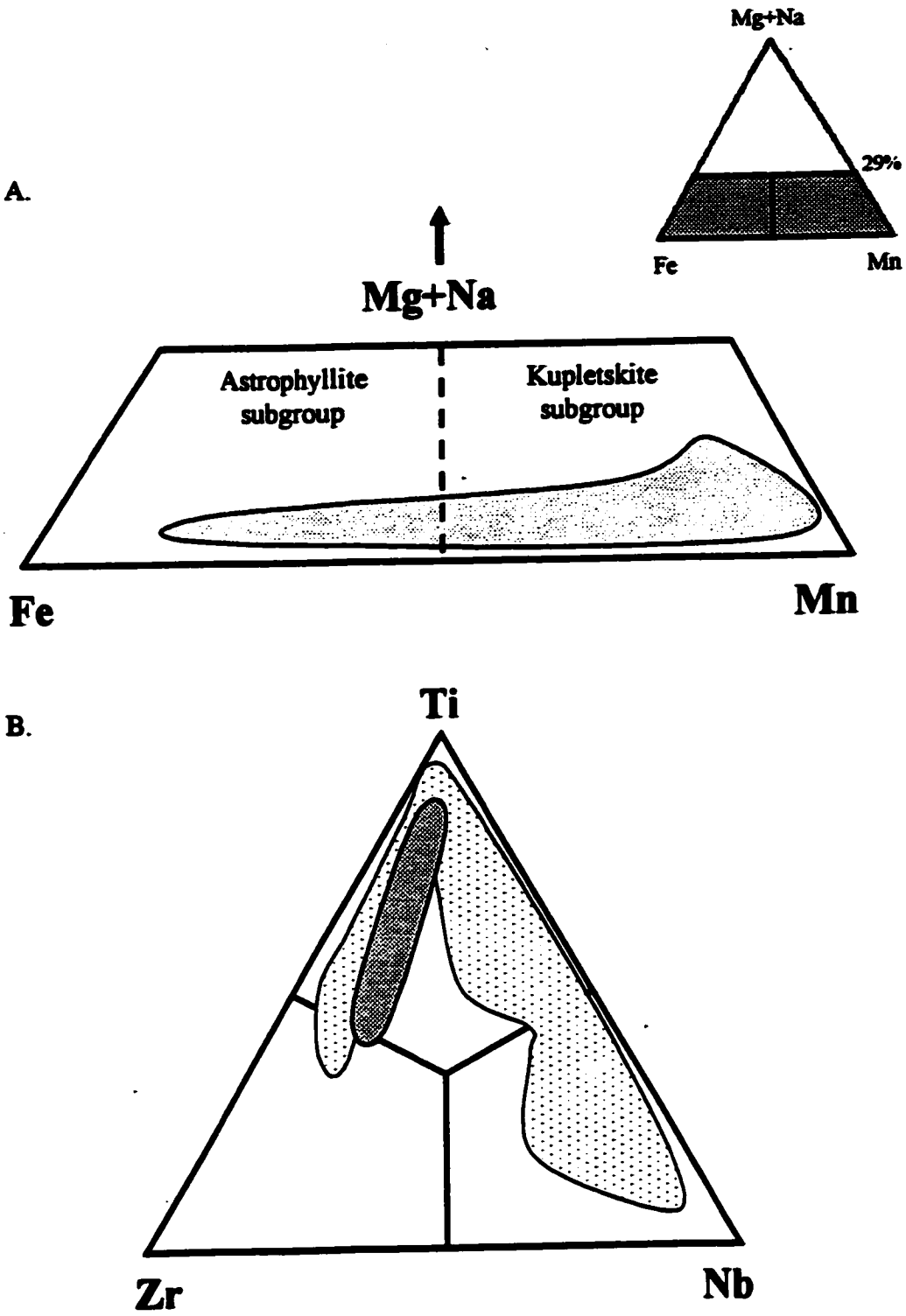

Figure 4. Composition of AGM from the syenitic pegmatites at MSH
A. Fe-Mn-(Mg+Na) compositional space.
B. Speckled fill = Kupletskite subgroup: kupletskite, niobokupletskite and zircophyllite
Solid fill: Astrophyllite subgroup: astrophyllite and Fe-zircophyllite

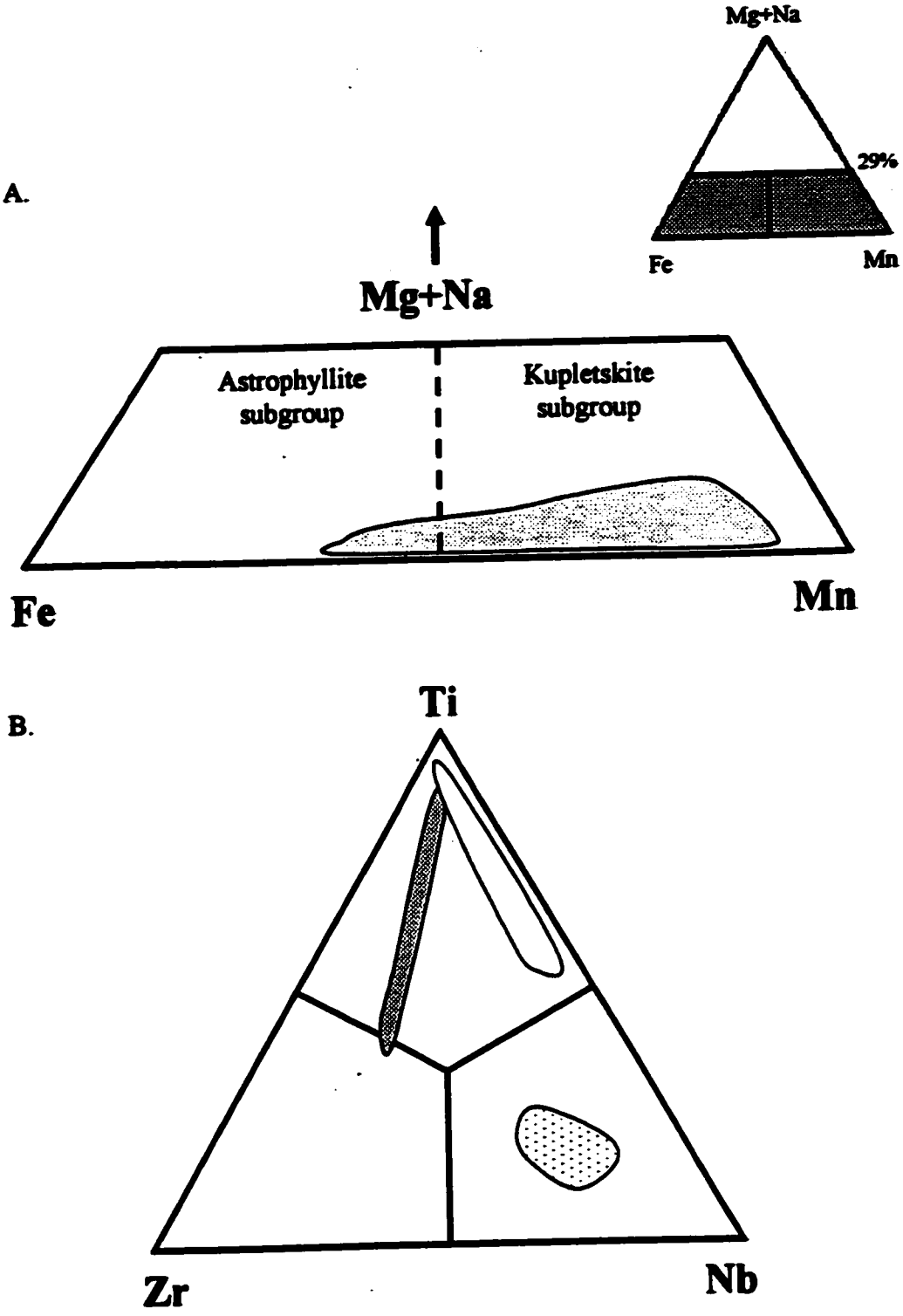

Figure 5. Composition of AGM from the altered syenitic pegmatites at MSH.
A. Fe-Mn-(Mg+Na) compositional space.
B. Speckled fill = Kupletskite subgroup: kupletskite and niobokupletskite
Solid fill: Astrophyllite subgroup: astrophyllite and Fe-zircophyllite

Plate 1. Primary kupletskite (dark brown) and fibrous niobokupletskite (light brown) with rhodochrosite and microcline in a syenitic pegmatite from Mont Saint-Hilaire (MSH10AB). Field of view: 4.1 cm.

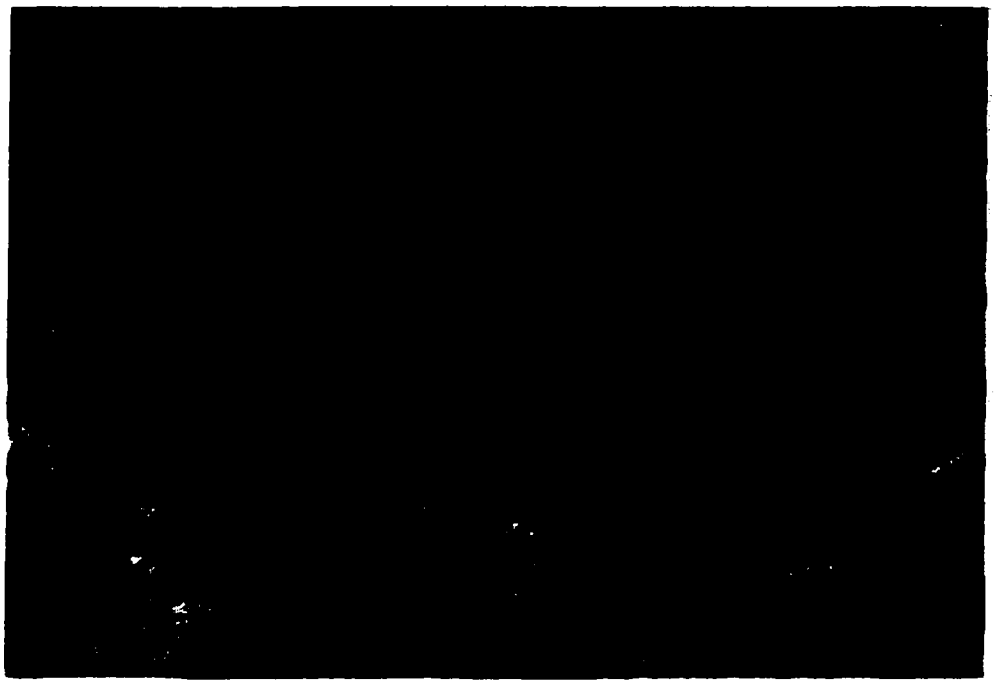

Plate 2. Primary kupletskite (dark brown) with a fibrous overgrowth of Zr-bearing astrophyllite (orange-brown) in an altered syenitic pegmatite from Mont Saint-Hilaire, Québec (MSH23AB).
Field of view: 5.5 cm.

Plate 3. Primary kupletskite with a fibrous overgrowth of Zr-bearing astrophyllite and secondary dogtooth spar calcite in an altered syenitic pegmatite from Mont Saint-Hilaire, Québec (MSH26AB).
Field of view: 4.2 cm.

Examination of the compositional variation present in the pegmatite AGM reveals three distinct populations: (1) primary kupletskite, (2) secondary kupletskite subgroup AGM, and (3) secondary astrophyllite subgroup AGM. In general, primary kupletskite is enriched in Na, Mn, Nb and F, yet extensive compositional zoning is observed in BSEI. In Plates 4A and 4B, zoning within the kupletskite results in an increase in Mn and Nb towards the rims until niobokupletskite develops. In Plates 5A and 5B, this zoning is reversed, and enrichment in Ca, Fe^{2+}, Zr and F is observed from core to rim. Secondary overgrowths of AGM on primary kupletskite also follow these compositional trends, resulting in late-stage development of niobokupletskite, zircophyllite and Fe-zircophyllite. Figures 6 and 7 show the composition of primary kupletskite and secondary overgrowths with respect to the two most important substitutional mechanisms responsible for the zoning, Mn $\Leftrightarrow$ Fe and Nb $\Leftrightarrow$ Zr. Secondary kupletskite subgroup AGM (Population I) show increased enrichment in both Mn and Nb, whereas secondary astrophyllite subgroup AGM (Population II) show increased enrichment in both Fe^{2+} and Zr. Figure 8 shows primary and secondary PEG and APEG AGM compositions with respect to two important crystal chemical and geochemical parameters, Mn# and Nb/(Nb+Zr). Trend A-A′ is the result of increased enrichment in Mn and Nb. However, examination of the chemical characteristics for these samples also indicates enrichment from A-A′ in Fe^{3+}, O^{2-} (due to the coupled substitution Ti + F $\Leftrightarrow$ Nb + O), decreased Ti, and decreased Nb/(Nb+Zr) but with Nb>Zr, resulting in Nb-bearing kupletskite and niobokupletskite. Trend B-B′ is characterized by enrichment in Fe^{2+} and Zr, with increased Ca, Ti and F, decreased Nb/(Nb+Zr) but with Zr>Nb, resulting in Fe-zircophyllite and Zr-bearing astrophyllite. The divergent nature of evolutionary trends within

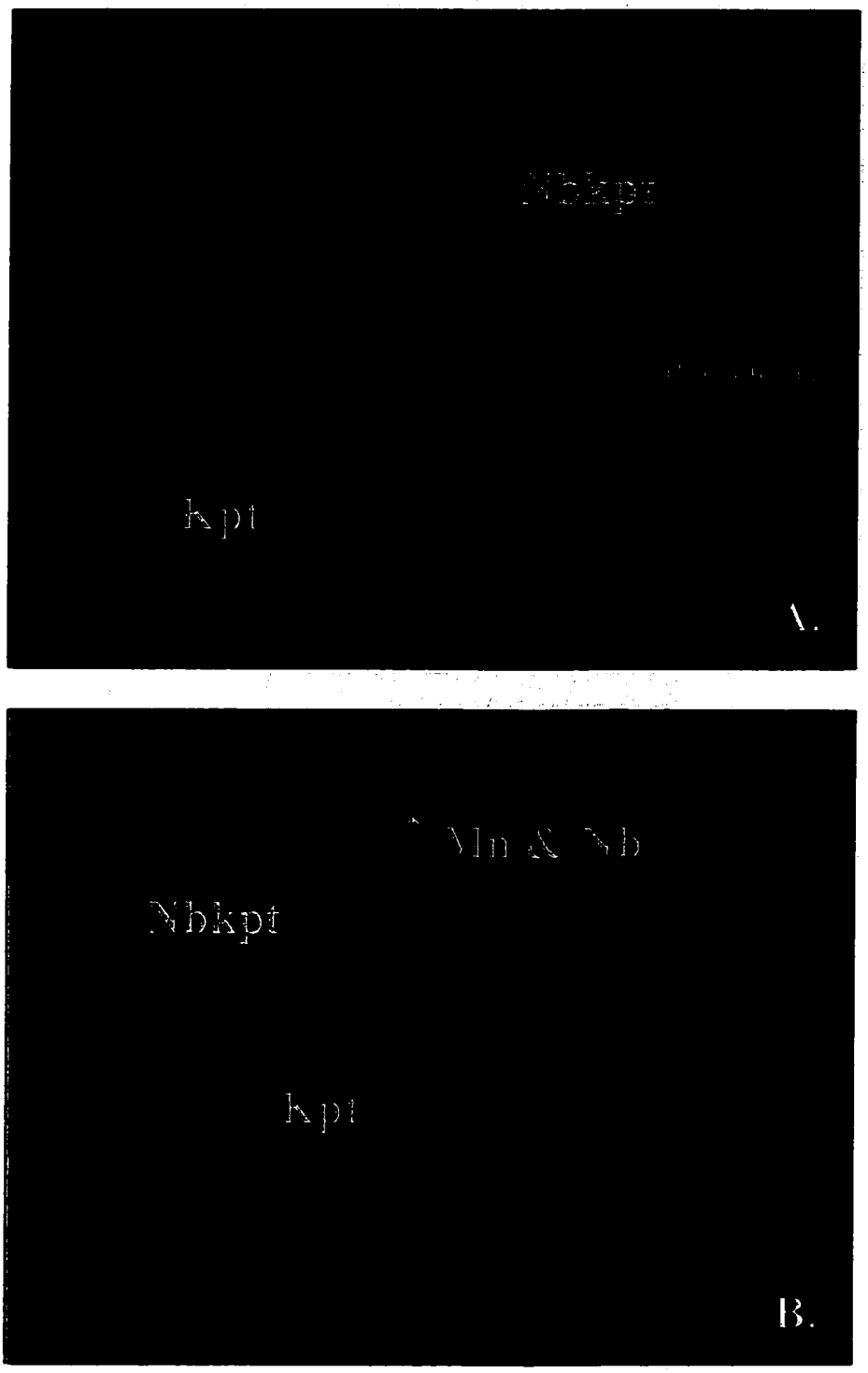

Plate 4. Back-scattered electron images of compositional zoning in AGM from syenitic pegmatites at Mont Saint-Hilaire (Québec, Canada). Trend A-A′: Increasing Mn and Nb with decreasing Fe^{2+} and Ti. Kpt: kupletskite, Nbkpt: niobokupletskite.

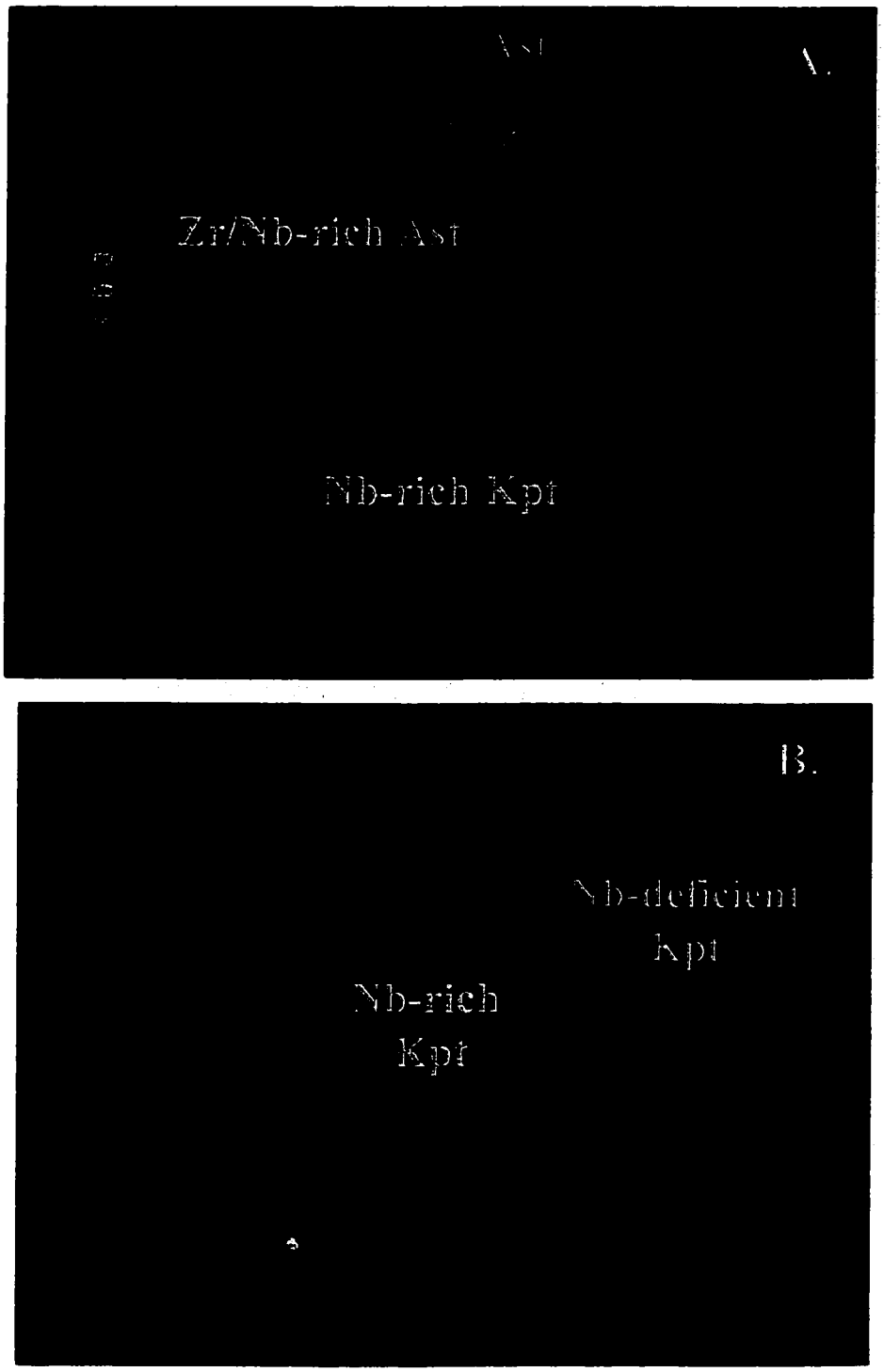

Plate 5. Back-scattered electron images of compositional zoning in AGM from syenitic pegmatites at Mont Saint-Hilaire (Québec, Canada). Trend B-B′: Decreased Mn and Nb with increasing Ca, Fe, Ti, Zr and F. Kpt: kupletskite, Ast: astrophyllite.

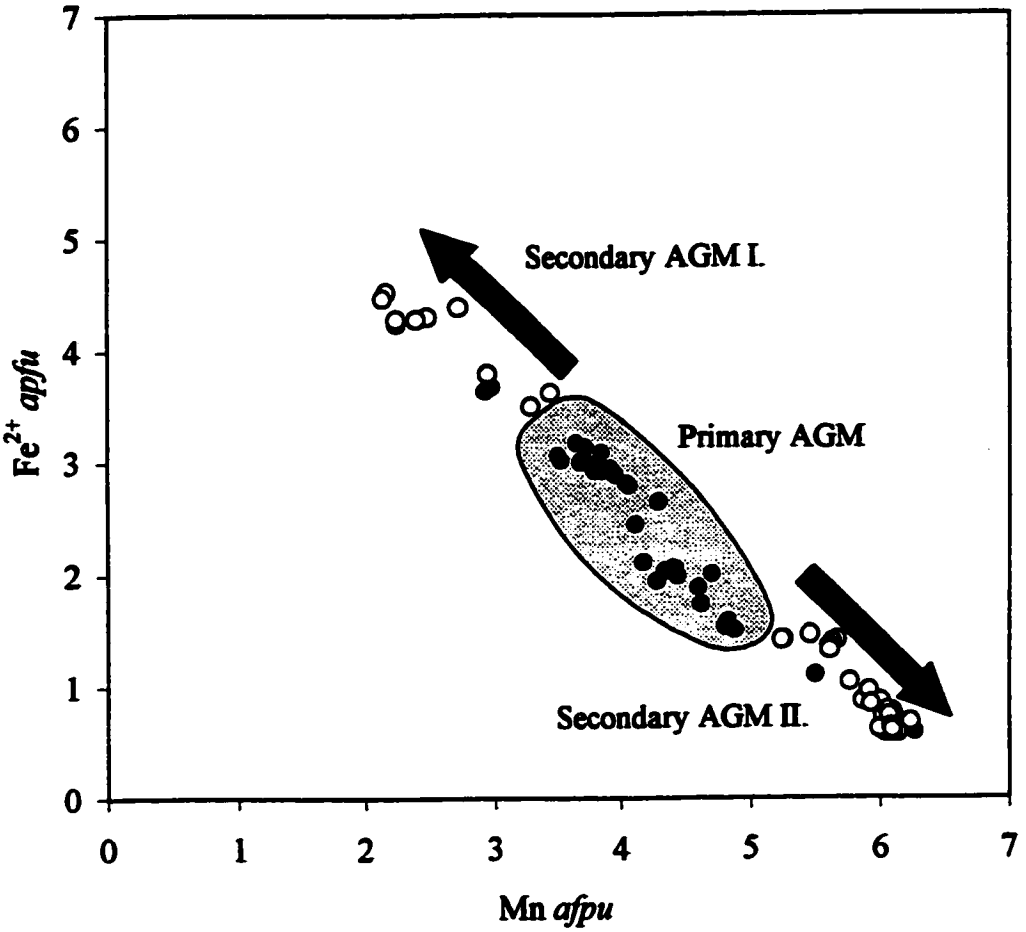

Figure 6. Compositional zoning in AGM from the syenitic pegmatites. Primary kupletskite shows compositional zoning toward both Fe^{2+} and Mn enrichment in secondary overgrowths.

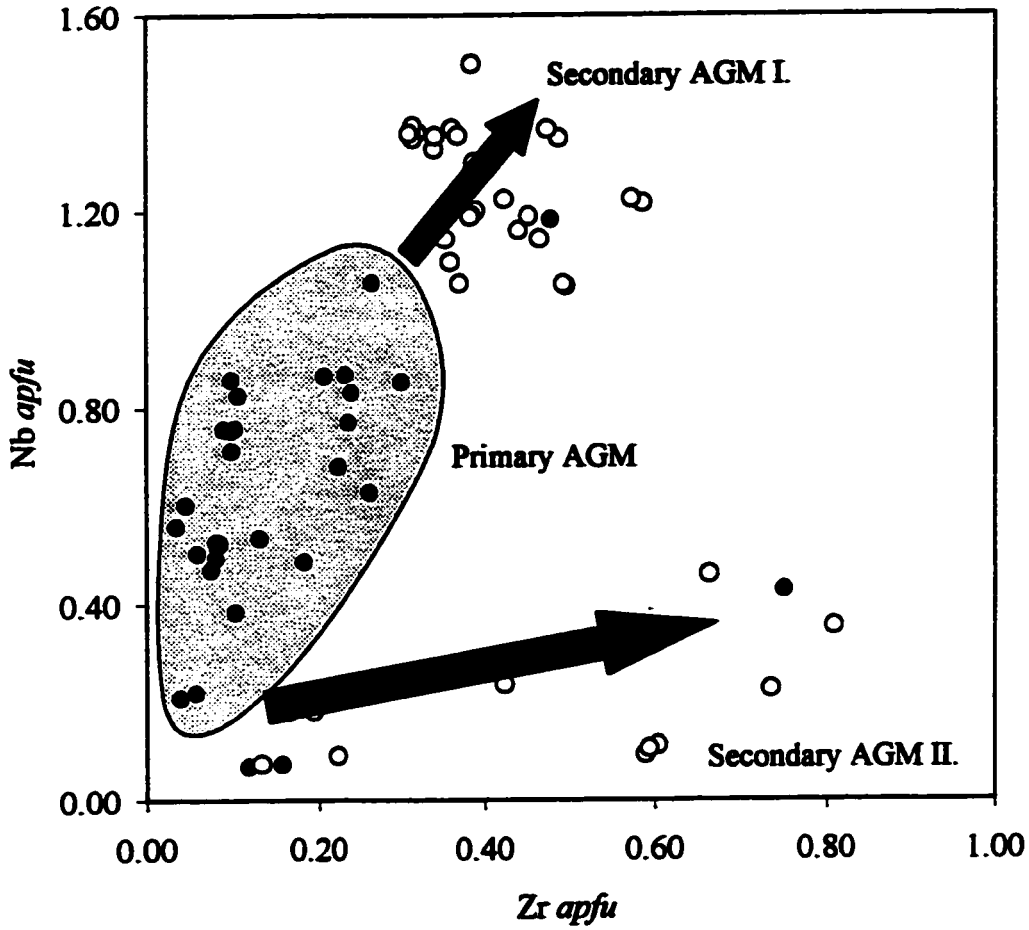

Figure 7. Compositional zoning in AGM from the syenitic pegmatites. Primary kupletskite shows compositional zoning toward both Nb (I) and Zr (II) enrichment.

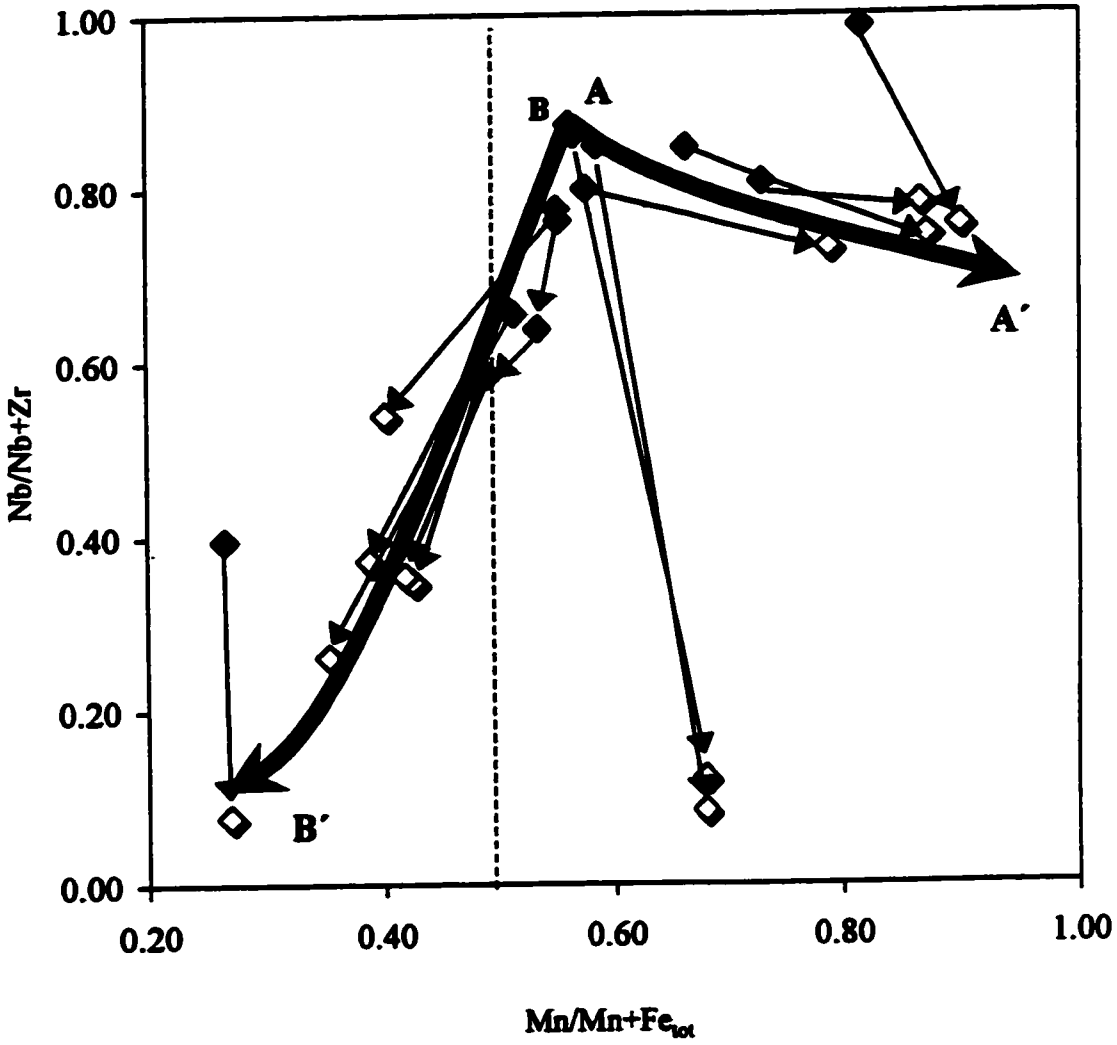

Figure 8. Evolution of MSH AGM from the syenitic pegmatites.
A-A′. Increased Mn#, decreased Nb/Zr with Nb>Zr,
decreased Ti+F, and increased Fe^{3+}/Fe_{tot}
B-B′. Decreased Mn#, decreased Nb/Zr with Zr>Nb,
increased Ca+Ti+F and decreased Fe^{3+}/Fe_{tot}

the syenitic pegmatites, coupled with sharp contrast in chemistry and habits between the coarse-grained primary kupletskite and the fibrous overgrowths, suggests drastically different conditions of crystallization and two distinct melt or fluid compositions.

2.2. Natrolite pegmatites (NPEG)

The natrolite pegmatites (NPEG) are mineralogically distinct from the PEG and APEG. These pegmatite bodies or pods are dominated by the presence of very coarse grained (> 5 cm) corroded sodic amphibole, microcline and natrolite with trace rhodochrosite and calcite (Plate 6 & 7). The NPEG are thought to represent the pegmatitic equivalent of the miarolitic cavities that occur in the nepheline syenite which have a similar mineralogical assemblage including aegirine, analcime, astrophyllite, ilmenite, microcline and natrolite (Horváth & Gault 1990).

Astrophyllite, *sensu stricto*, is the only AGM in the NPEG. Chemically, this astrophyllite is almost pure end-member, being strongly enriched in K, Fe^{2+}, Ti and F (Fig. 9). It occurs as golden to medium brown, strongly acicular, radiating crystals up to 2 cm long with a length:width ratio of up to 200. Astrophyllite is found within vugs, and, less commonly, embedded in the matrix. In certain samples, the astrophyllite is found within corroded cores of early amphibole, suggesting late-stage development of the AGM and replacement of the primary mafic phase. The most probable source of hydrothermal fluids for post-magmatic crystallization of the astrophyllite is exsolved H_2O-saturated fluids from the relatively anhydrous nepheline syenite.

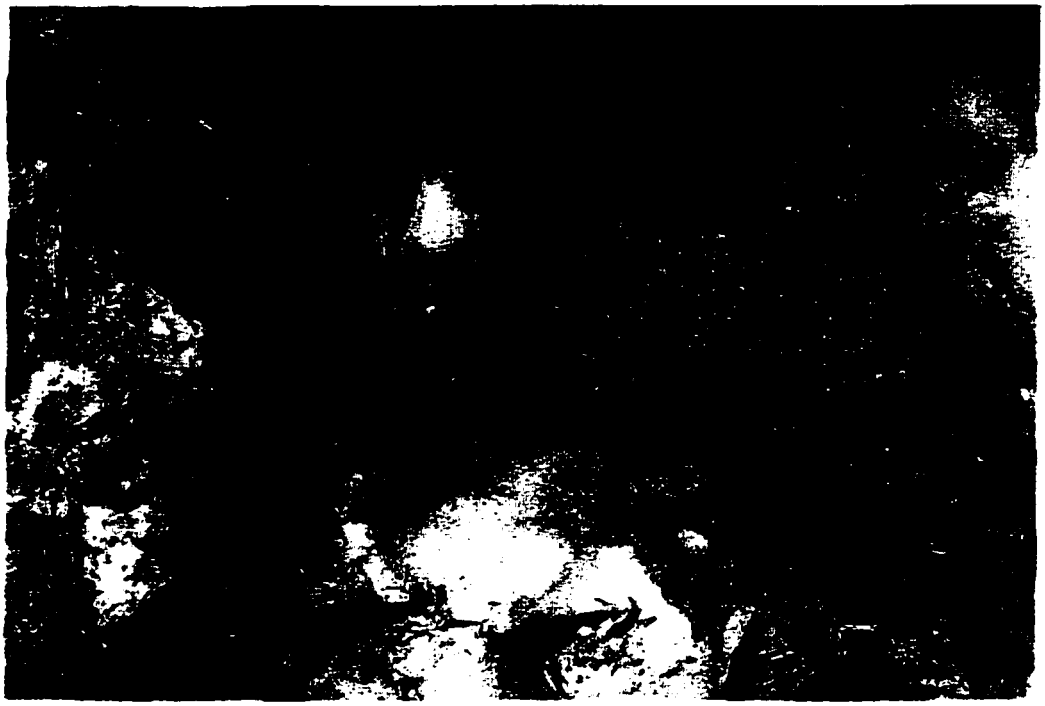

Plate 6. Astrophyllite in the natrolite pegmatites at Mont Saint-Hilaire (Québec, Canada). Associated minerals include microcline, natrolite and analcime (MSH31). Field of view: 9 cm.

Plate 7. Astrophyllite in the natrolite pegmatites at Mont Saint-Hilaire (Québec, Canada). Associated minerals include calcite, rhodochrosite, microcline, natrolite and analcime (MSH32). Field of view: 5.8 cm.

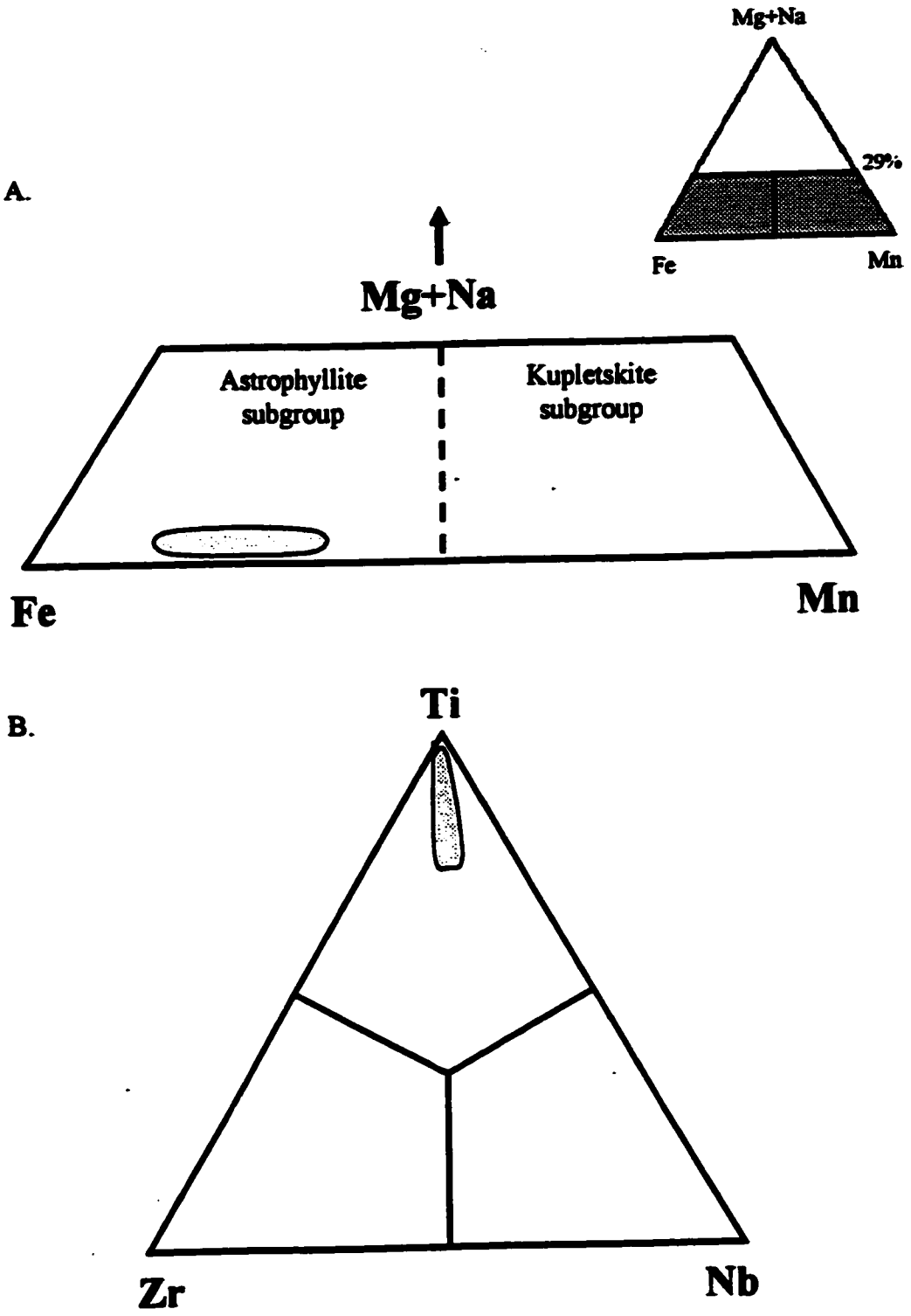

Figure 9. Composition of AGM from the natrolite pegmatites at MSH.
A. Fe-Mn-(Mg+Na) compositional space.
B. Solid fill: Astrophyllite subgroup: astrophyllite

2.3. Aplites (APLITE)

The aplites are considered to represent the outermost portions or chilled margins of the syenitic pegmatite dikes. The aplites consist predominantly of fine- to medium-grained microcline, analcime, aegirine and albite. Both astrophyllite and kupletskite occur in the aplites as fine- to medium-grained, red-brown, acicular to tabular crystals embedded in matrix (Plate 8). Compositionally, AGM in the aplites define a range from Mn# 0.33 to 0.81 (ave.: 0.48), similar to that in the PEG and APEG (Fig. 10). Kupletskite subgroup samples are slightly enriched in Na_{tot} ($Na_{tot} = {}^{[6]}Na + {}^{[10]}Na$; max: 1.55 *apfu*) and Mg (max: 0.37 *apfu*) and depleted in both Nb and Zr. Astrophyllite subgroup samples show enrichment in Ca (max: 0.46 *apfu*) and Zr (max: 0.67 *apfu*).

2.4. Sodalite syenite (SS)

Massive sodalite syenite is host primarily to members of the biotite series, sodalite, microcline and eudialyte group minerals (Horváth & Gault 1990). Astrophyllite is the only AGM described from the SS where it occurs as prismatic to acicular, medium-grained crystals (< 1 cm long) embedded in the sodalite matrix (Plate 9). Of note is that astrophyllite and eudialyte group minerals, two mineral groups which possess similar crystal-chemistries, do not seem to crystallize contemporaneously; in all cases, astrophyllite overgrows the eudialyte. This feature has also been noted from other localities such as at the Khibina massif (Kola Peninsula, Russia), where eudialyte group minerals are abundant in the nepheline syenites. In all cases, late-stage astrophyllite overgrows altered eudialyte group minerals. Experimental studies by Christophe-Michel-Lévy (1961) indicate eudialyte, *sensu*

Plate 8. Radiating astrophyllite in aplite with analcime and microcline (MSH33). Field of view: 5.1 cm.

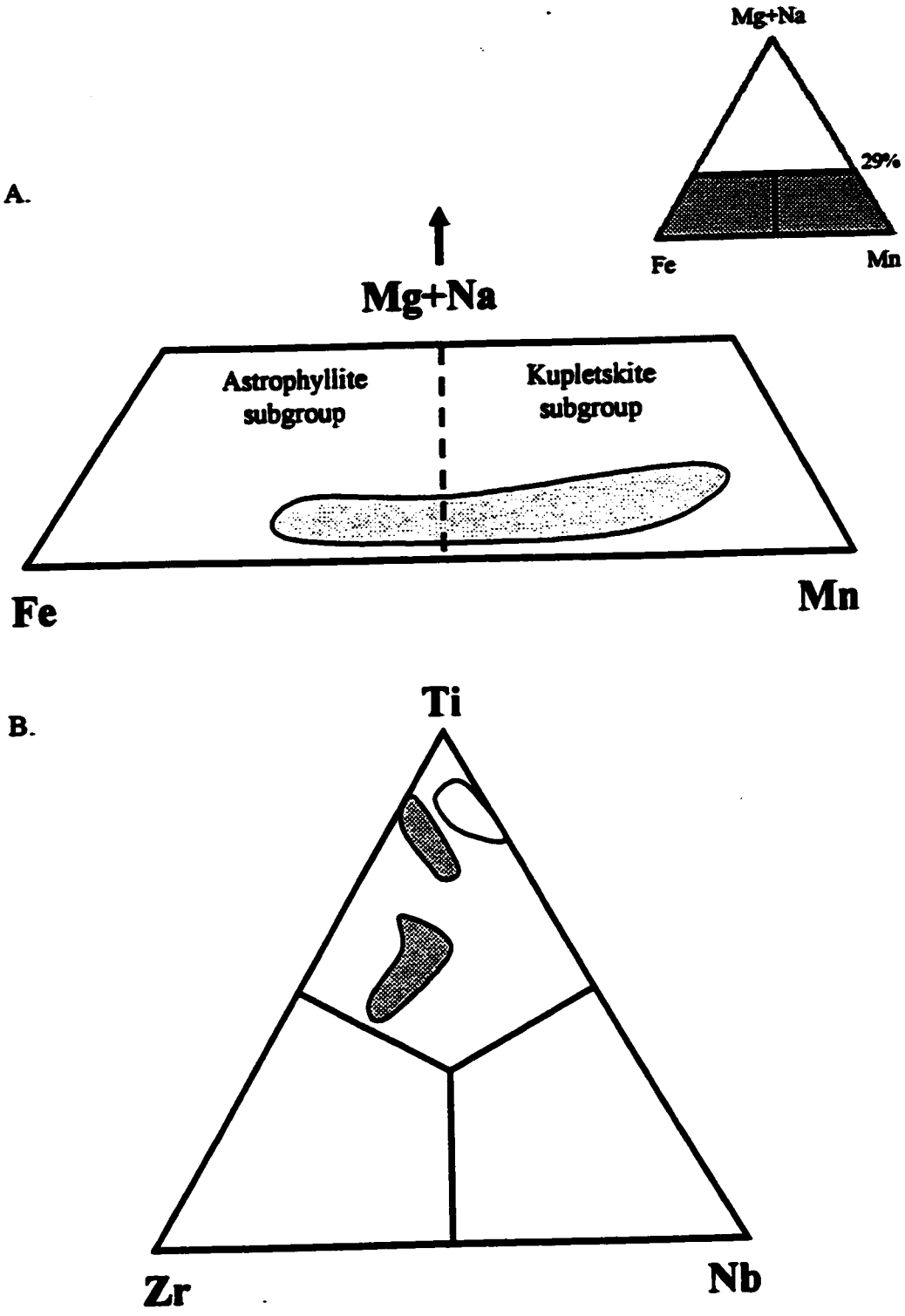

Figure 10. Composition of AGM from the aplites at MSH.
A. Fe-Mn-(Mg+Na) compositional space.
B. Speckled fill = Kupletskite subgroup: kupletskite
Solid fill: Astrophyllite subgroup: astrophyllite

Plate 9. Astrophyllite (Ast) with annite, microcline and sodalite in sodalite syenite from Mont Saint-Hilaire (Québec, Canada; MSH44). Field of view: 3.7 cm.

stricto, to be stable above 440 °C, where it commonly crystallizes with both sodalite and aegirine in the experimental system Na-Ca-Fe-Zr-Si-CO_2-H_2O. Crystallization of sodalite syenite at MSH may have resulted in exsolution of F- and H_2O-rich fluids, allowing late-stage crystallization (at lower temperatures) of astrophyllite, a mineral enriched in OH and F relative to eudialyte [ideal Σ(OH+F+Cl): eudialyte: 2.0 *apfu*, AGM: 5.0 *apfu*]. The lower limit for the crystallization of eudialyte (440 °C) may represent an upper limit for crystallization of AGM.

Both kupletskite and astrophyllite occur in the SS at MSH (Fig. 11). Compositionally, although kupletskite exists, it is enriched in the astrophyllite component with Mn# ranging from 0.19 to 0.59 (ave.: 0.41). Kupletskite samples are slightly enriched in Nb (up to 0.95 *apfu*), whereas astrophyllite samples are enriched in K, Fe^{2+}, Ti, and contain up to 0.79 *apfu* Zr.

2.5. Sodalite syenite xenoliths (SSX)

Dark-grey, massive nepheline syenite (containing essential nepheline, plagioclase, kaersutite and annite) contains angular to rounded xenoliths of sodalite syenite ranging in size from a few centimeters to a few meters (Horváth & Gault 1990). The sodalite syenite xenoliths (SSX) are comprised predominantly of > 90% sodalite, microcline and analcime, but are also host to a wide array of rare and unusual minerals, many of which have not been found in other microenvironments. The mineralogy of these xenoliths is characterized by an abundance of Na-, REE-, P- and F-bearing phases including aegirine, eudialyte group minerals, and rare minerals, occurring in vugs and interstices, including members of the

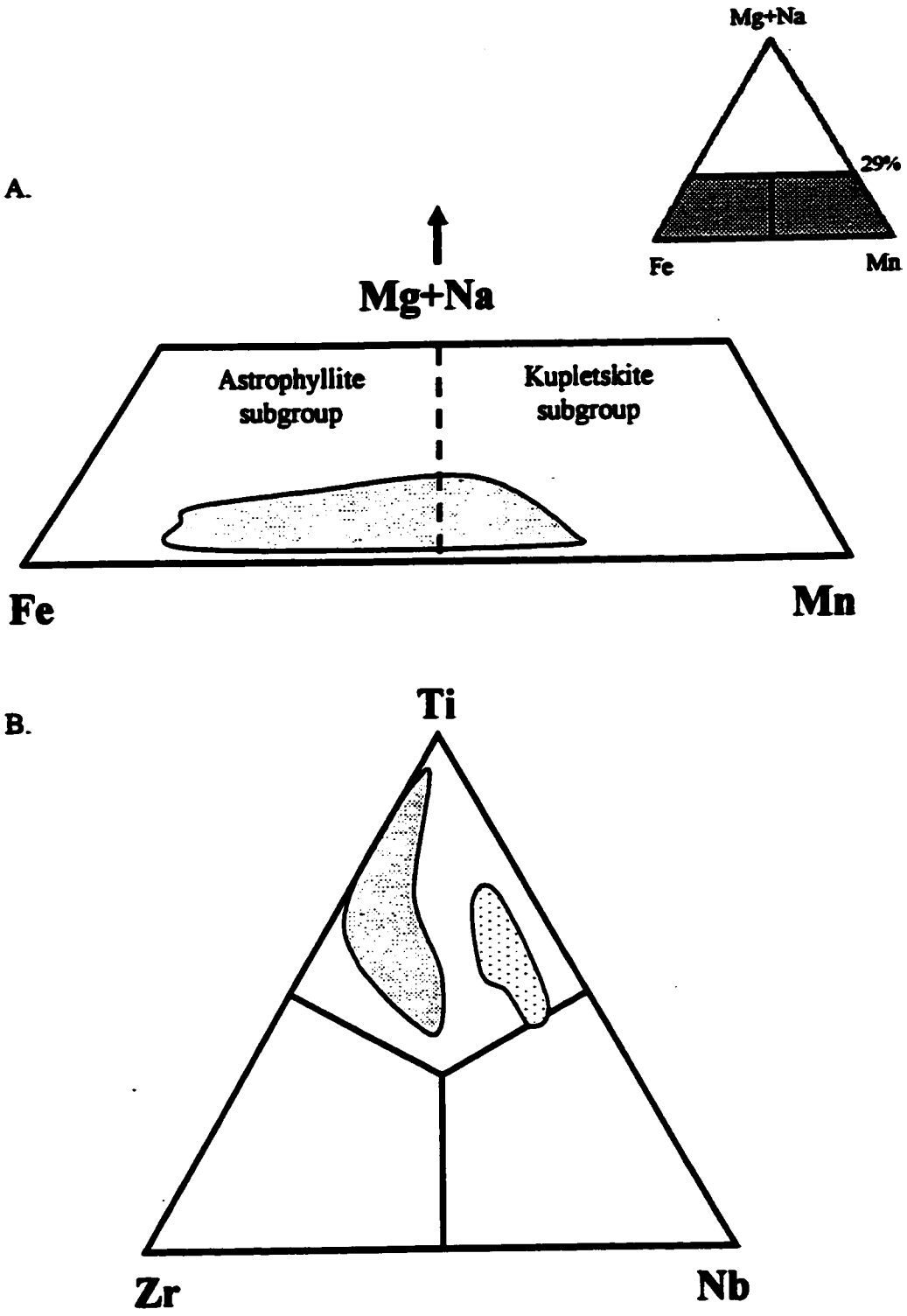

Figure 11. Composition of AGM from the sodalite syenites at MSH.
A. Fe-Mn-(Mg+Na) compositional space.
B. Speckled fill = Kupletskite subgroup: kupletskite and niobokupletskite
Solid fill: Astrophyllite subgroup: astrophyllite

lovozerite group, abenakiite-(Ce), phosinaite-(Ce), vuonnemite, thermonatrite and villiaumite (Horváth & Gault 1990). The late-stage crystallization of such minerals may due to exsolution of Na-F-rare-element-rich fluids exsolved from the sodalite syenite during crystallization.

Kupletskite and astrophyllite (Mn#: 0.31 to 0.72, ave.: 0.53, Fig. 12) in the SSX occur as tabular to slightly elongate, fine grained (0.75 x 0.20 mm), reddish brown plates in vugs and embedded in matrix. They display a compositional range slightly more enriched in Na, Rb, Mn and Nb than the associated AGM in the SS. The enrichments in Na and rare elements such as Rb and Nb is consistent with the overall geochemistry of the SSX.

2.6. Metasomatic unit (META)

The Ordovician host-rocks of the Lorraine and Richmond groups (fossiliferous limestones, shales and siltstones) were metamorphosed during the emplacement of the intrusion, resulting in a hornfels unit 10 to several hundred meters in thickness surrounding the MSH complex. Large blocks of hornfels also occur within the intrusion itself, presumably the result of slumping and calving of sediments from the roof of the chamber into the magma during intrusion. Primary sedimentary structures, including bedding and fossils are preserved within these hornfels blocks and can be used to trace the direction of slumping of the sediments. The hornfels unit very fine-grained, ranging in colour from dark grey to brown-green. This dense rock is often criss-crossed by very thin, mineralized veins, ranging in width from two to five centimeters, which are host to a wide array of minerals not

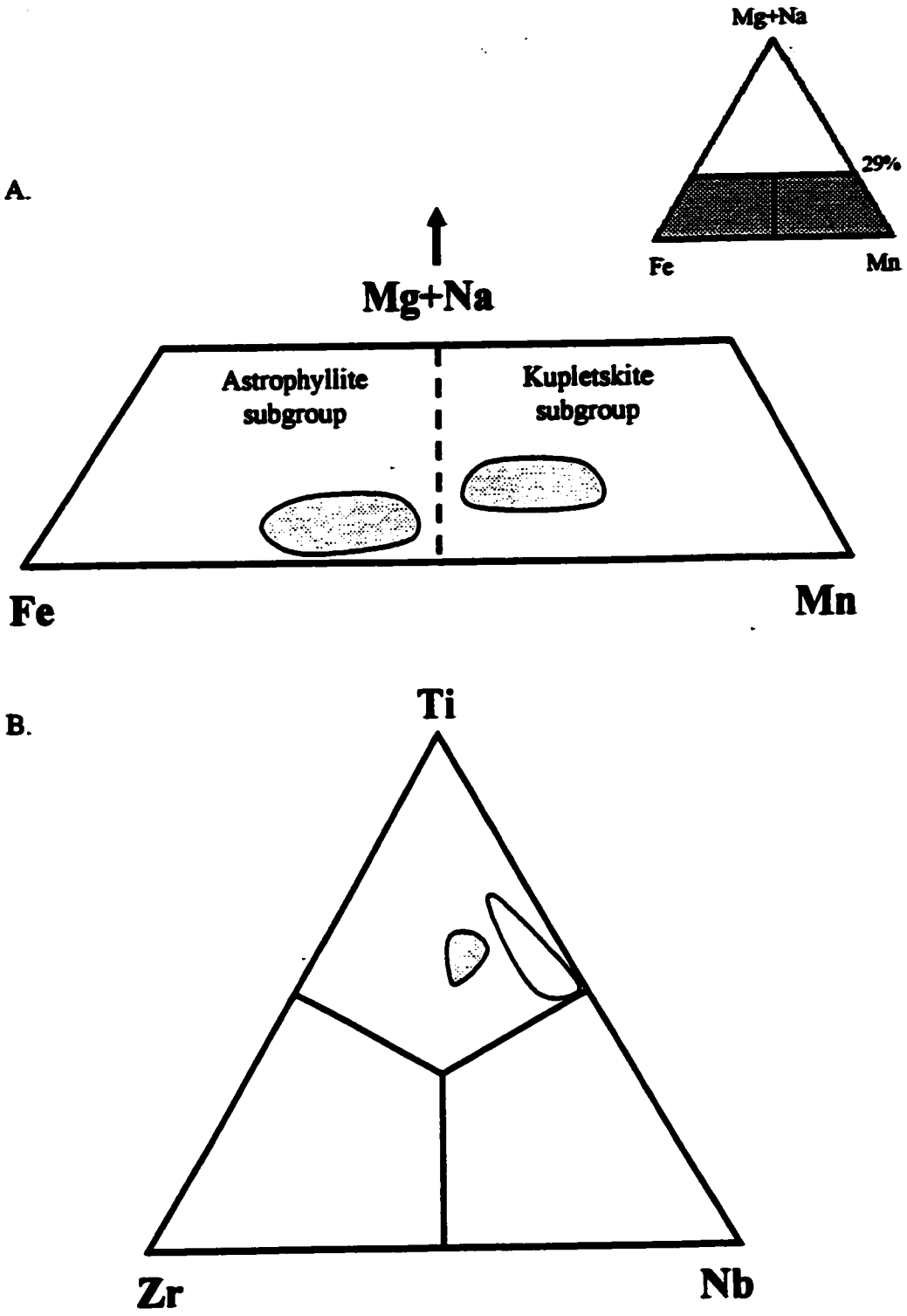

Figure 12. Composition of AGM from the sodalite syenite xenoliths at MSH.
A. Fe-Mn-(Mg+Na) compositional space.
B. Speckled fill = Kupletskite subgroup: kupletskite
Solid fill: Astrophyllite subgroup: astrophyllite

commonly found in other microenvironments including euhedral smokey quartz, dolomite, siderite, calcite, pyrite, riebeckite, aegirine and all three TiO_2 polymorphs.

Associated with the hornfels is a fine grained unit which displays varying degrees of metasomatism by exsolved fluids from the crystallizing intrusion. Chemically, the metasomatic unit is very similar to the nepheline syenite in the main part of the intrusion, but shows slight enrichments in SiO_2 and rare elements (REE, Nb, Zr, Sr, Ba, *etc.*), along with a depletion in Al_2O_3 (Table 2). The ground mass of this metasomatic unit is host to a mineral assemblage characteristic of a fenite: aegirine, albite and natrolite with lesser modal volumes of carbonate and sodalite. Unlike a regular fenite, the metasomatized rock at MSH contains AGM.

In samples MSH28 and MSH29, AGM occur as coarse-grained (0.7 x 0.3 cm average), orange to orange-red, platy to prismatic porphyroblasts embedded in a dense, fine grained metasomatized matrix consisting predominantly of albite, aegirine and minor sodalite. The cores of these astrophyllite porphyroblasts are strongly corroded or poikiolitic, with euhedral, fine-grained inclusions of albite. The intermediate zones of the crystals are well-crystallized and partially terminated. A sharp contact separates these intermediate zones from a corroded or poikiolitic rim, similar to that observed in the cores (Plates 10 & 11). All crystals are optically continuous and do not display chemical zoning. The discontinuity in texture across individual grains may reflect the kinetics of the system during crystallization such that equilibrium with the metasomatizing fluids was reached only at certain periods during growth of the crystal.

TABLE 2. WHOLE ROCK GEOCHEMISTRY* FOR SELECTED MICROENVIRONMENTS AT MONT SAINT-HILAIRE, QUÉBEC

Oxide (wt.%)	Sodalite Syenite	Nepheline Syenite	Metasomatic Unit
SiO_2	48.20	51.87	59.32
Al_2O_3	24.23	19.47	13.60
Fe_2O_3	4.32	6.76	6.22
MnO	0.24	0.28	1.39
MgO	0.02	1.26	0.64
CaO	0.41	4.45	1.13
Na_2O	17.84	9.72	8.48
K_2O	1.99	3.34	3.18
TiO_2	0.08	1.33	0.81
P_2O_5	0.06	0.54	0.16
Trace elements (ppm)			
Ba	14	1443	526
Rb	126	82	360
Sr	21	2760	431
Y	36	49	400
Zr	1210	619	4041
Nb	184	177	1743
La	88	139	793
Ce	149	249	1132
Nd	43	96	339
Pb	1	6	35
Th	29	19	62

* X-ray fluorescence data

Plate 10. Astrophyllite porphyroblasts in the metasomatic unit at Mont Saint-Hilaire (Québec, Canada; MSH29). The fine grained groundmass consists of albite, aegirine, sodalite and carbonate. Field of view: 10 cm.

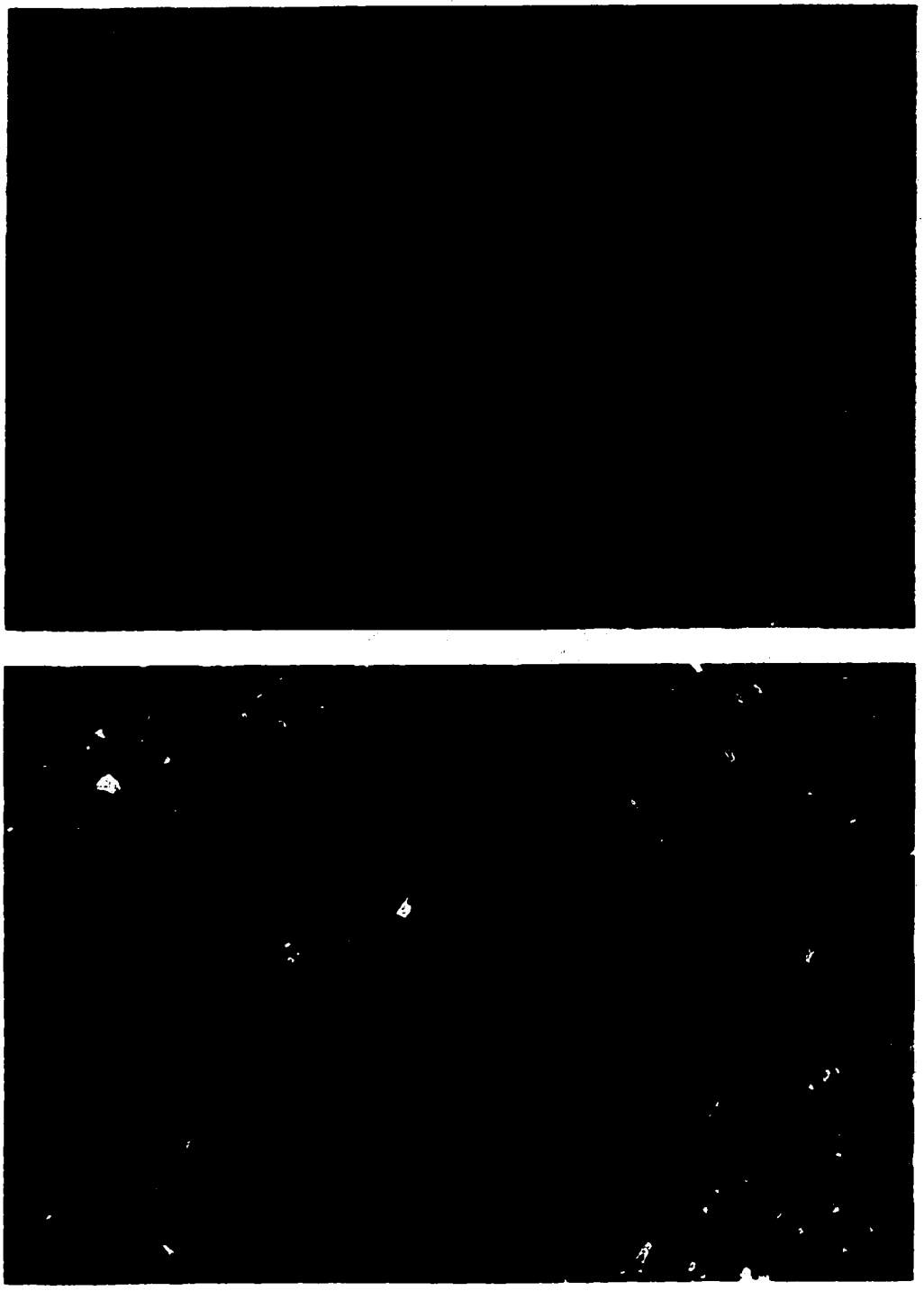

Plate 11. Photomicrograph of astrophyllite porphyroblast in plane polarized (top) and cross polarized light (bottom; MSH28) from the metasomatic unit. Note the optical continuity throughout the grain. Field of view: 2 mm.

Compositionally, these porphyroblasts are astrophyllite and characterized by enrichment in Ca, Mg, Fe^{2+} and Ti (Fig. 13), possibly a reflection of the chemistry of the sedimentary rocks, in particular the shales and limestones with which the metasomatizing fluids reacted.

In sample MSH41, the astrophyllite occurs as medium-grained (0.5 cm), radiating sprays of acicular crystals randomly distributed in a fine-grained matrix of albite, sodalite, natrolite and aegirine. The astrophyllite has undergone metasomatic replacement, with cores comprised of sodalite, natrolite, aegirine, pyrochlore and two unidentified minerals, a Na-Mn-silicate and a Na-Zr-silicate (Plates 12 & 13). Sample MSH49 displays the most intensive interaction between metasomatized sediments and an exsolved magmatic or fenitizing fluid. Bleaching of the matrix is evident within a distinct zone in the rock which contains prismatic, polycrystalline aggregates of astrophyllite up to one centimeter wide, along with prismatic albite and minor aegirine. The elongated astrophyllite crystals have grown perpendicular to the edges of the bleached zone, similar to aegirine in the syenitic pegmatites. Texturally, the astrophyllite crystals are similar to those in MSH28/29, although the cores are less poikiolitic, presumably due to more favorable conditions for crystallization in equilibrium with metasomatizing fluids (Plate 14). The contact between the bleached zone and the less metasomatized hornfels is gradual and characterized by an increase in the modal percentage of aegirine. This bleaching, along with a dominant matrix of Na-, Fe^{3+}- and F-bearing minerals such albite, aegirine and astrophyllite, strongly suggests the presence of exsolved, oxidized magmatic fluids, reminiscent of the effects of Na-Fe^{3+}-F-rich fluids which result in fenites surrounding carbonatite-syenite complexes.

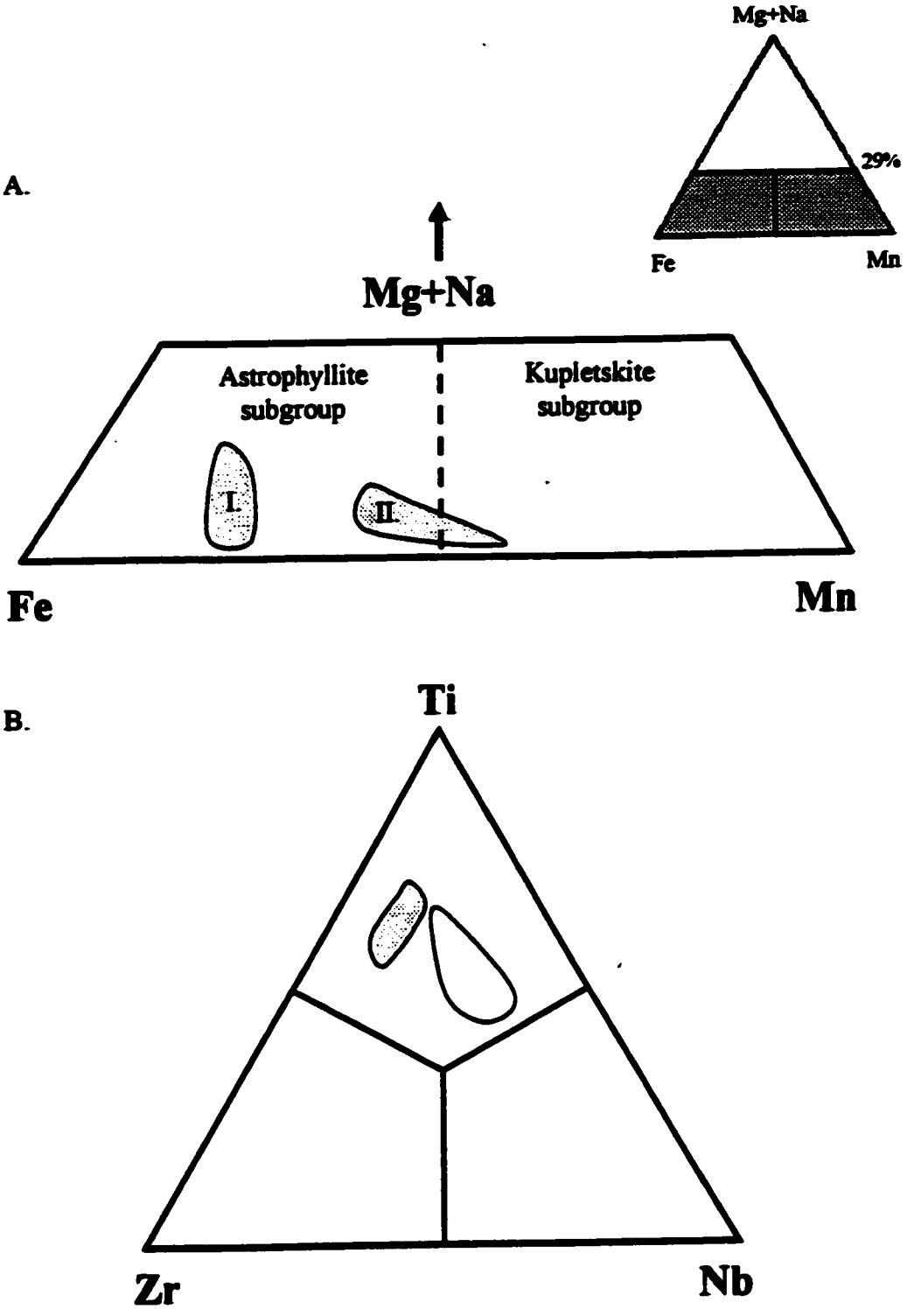

Figure 13. Composition of AGM from the metasomatic unit at MSH.
A. Fe-Mn-(Mg+Na) compositional space showing the two populations of AGM porphyroblasts.
B. Speckled fill = Kupletskite subgroup: kupletskite
Solid fill: Astrophyllite subgroup: astrophyllite

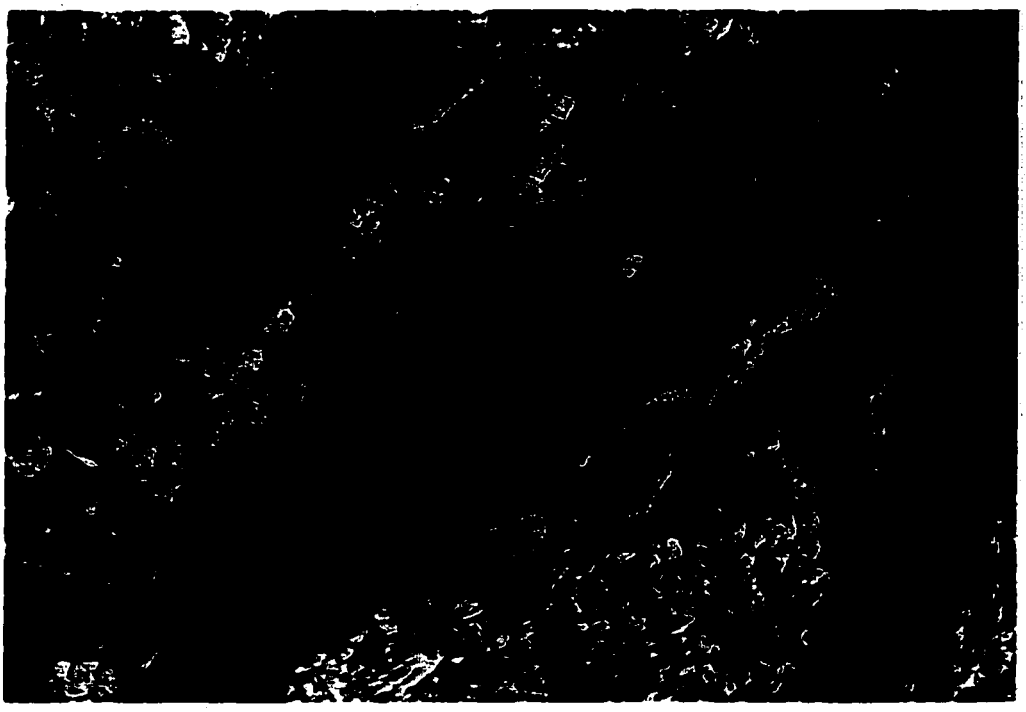

Plate 12. Photomicrograph of astrophyllite in plane polarized light (MSH41). The fine grained groundmass consists predominantly of aegirine and albite. Field of view: 2 mm.

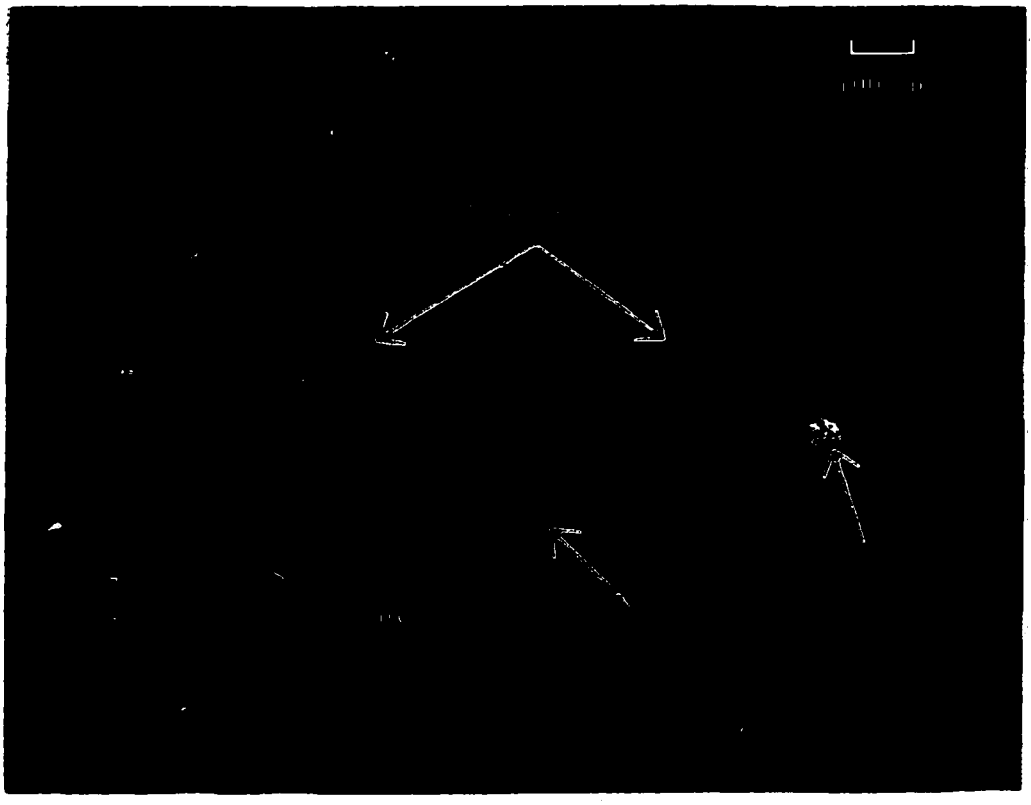

Plate 13. Backscattered electron image of astrophyllite (MSH41, medium grey) altering to aegirine (dark grey), sodalite, natrolite (black), pyrochlore (white) and unidentified Na-Mn and Na-Zr silicates. Scale bar: 100 μm.

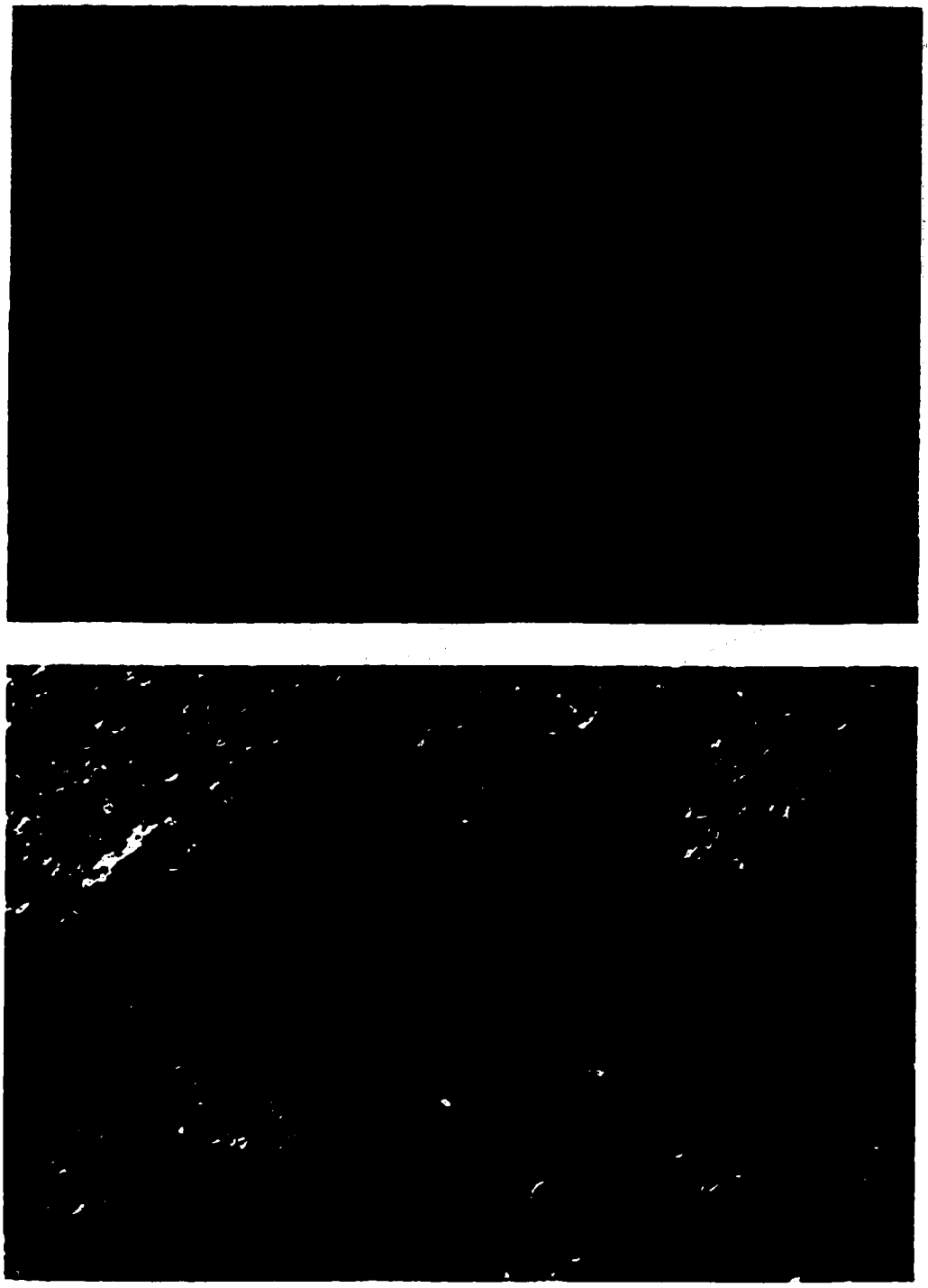

Plate 14. Photomicrograph of astrophyllite porphyroblasts in plane polarized (top) and cross polarized light (bottom; MSH49) from the metasomatic unit. The fine grained groundmass consists predominantly of albite and aegirine. Field of view: 2 mm.

3.0. THE RELATIONSHIP BETWEEN COMPOSITION AND CRYSTAL HABIT

One of the interesting features of MSH AGM, and not noted from any of the other intrusions studied, is the correlation between chemical composition, in particular Mn#, and crystal habit. Ignoring the fibrous overgrowths of niobokupletskite, zircophyllite and Fe-zircophyllite on the primary PEG/APEG kupletskite (which are chemically distinct from the bulk of AGM in the EHS), it can be shown that the length:width ratio of the AGM crystals increases with decreasing Mn#. This is of particular importance to both professionals and collectors who have an interest in MSH minerals. Species identification at MSH is often difficult and often requires chemical analysis to attach a species name to a member of a mineral group (*e.g.* the eudialyte group, REE carbonates, *etc.*). With AGM, it is possible to attach a species name, although qualitative, to the sample in question by examination of the physical properties and knowledge of the microenvironment from which the sample came, without need for costly chemical analysis.

Crystals which are blocky or slightly tabular (length:width ratio: 1:1 or 2:1; *e.g.* Plate 1), such as those from the PEG, APEG and SSX, all have Mn#>0.50 and are members of the kupletskite subgroup. These crystals are primary magmatic phases as they are often subhedral with moderately developed terminations and display extensive, complex compositional zoning due to growth in conditions of chemical disequilibrium. As the Fe^{2+} content increases, the AGM crystals become increasing elongate along [100] and do not display compositional zoning. In the APLITE and SSX, the crystals have compositions where Mn#<0.50 (*i.e.* astrophyllite subgroup) but the sample still contains significant Mn. The astrophyllite crystals are more strongly elongate and slightly prismatic (length:width

ratio: 5:1; Plate 8) compared to those of the PEG and APEG. A further increase in Fe^{2+} correlates with development of prismatic to acicular crystals, similar to textures observed in the SS (length:width ratio: 10:1; Plate 9). At the extreme end of the spectrum are AGM from the NPEG which contain almost end-member astrophyllite (Mn# = 0.25 to 0.38). These crystals are strongly acicular and occur in radiating sprays with a length: width ratio approaching 200 (Plate 6 & 7).

4.0. Paragenesis of MSH AGM and late-stage enrichment of HFSE

The wide diversity in chemical composition displayed by AGM at MSH is a direct reflection of the heterogeneous conditions under which these minerals crystallized. All AGM at MSH are late-stage and seem to be an intermediate phase in the evolutionary history of the intrusion, crystallizing temporally between common rock-forming minerals (*e.g.* pyroxenes, amphiboles and micas) and the late-stage exotic mineral assemblage for which MSH is so famous (*i.e.* alkali titano- and zirconosilicates, REE carbonates, silicophosphates, *etc.*). The disequilibrium in such a complex system makes it difficult to relate AGM chemistry to earlier-formed phases, but on the basis of composition, habit and associated minerals, AGM can be used to help define the evolutionary history of the magmatic and post-magmatic conditions under which they crystallized. Using this information, two distinct sets of igneous processes are proposed for AGM crystallization at MSH: (1) primary and post-magmatic (PEG, APEG, SS, SSX and NPEG), and (2) hydrothermal and metasomatic (APEG and META). Both the magmatic oxidizing and hydrothermal trends offer evidence for mobilization and late-stage enrichment in HFSE such as Nb and Zr.

4.1. Primary magmatic - post-magmatic oxidizing trend

Oxidation trends in magmatic systems, although not common, have been noted in a number of syenitic and granitic igneous complexes, including the plutonic rocks of the Oslo rift valley (Norway; Czamanske & Mihálik 1972, Czamanske & Wones 1973, Neumann 1976), and the Baie-des-Mouton syenite complex (Québec; Lalonde & Martin 1983). The principle oxidizing agent in all cases is H_2O, whether it is exsolved from the crystallizing intrusion or the surrounding host rocks, or has infiltrated the open system from external sources. In order for H_2O to act as an oxidizing agent in a magma, it must first reach saturation and exsolve from the melt. Disassociation of H_2O into H_2 and O_2 and loss of H_2 must also occur, at which time oxidation is initiated. At MSH, the presence of igneous breccias, pegmatite dikes, metasomatized or fenitized wallrocks, and miarolitic cavities, coupled with the abundance of volatile-bearing minerals such as villiaumite, fluorite and sodalite, suggests that the initial magma was enriched in volatiles and H_2O, and that saturation of the melt in these components occurred early in the crystallizational history of the intrusion. Furthermore, the presence of abundant carbonate minerals, in particular rhodochrosite, calcite and siderite in such microenvironments suggests that CO_2 was an important part of this volatile phase. Crystallization of the relatively anhydrous nepheline syenite, regarded to be the earliest formed microenvironment in the intrusion (Piilonen *et al.* 1998), would have lead to early H_2O-saturation and rapid exsolution of a volatile- CO_2- and H_2O-rich phase into which incompatible and rare elements such as REE, Zr and Nb would have been concentrated. Crystallization of astrophyllite and replacement amphibole from residual fluids within miarolitic cavities in the nepheline syenite (NPEG) would be the first

indication of H_2O-saturation and an increase in alkalinity. The further explosive formation of igneous breccias and emplacement of pegmatite dikes by the H_2O-rich melt may have allowed for interaction with oxidizing atmospheric oxygen and/or meteoric fluids, resulting in further oxidation and contamination of the system.

The fibrous nature of many of the pegmatite and cavity minerals (such as AGM and metasomatic aegirine; Piilonen *et al.* 1998) suggests rapid crystallization due to a sharp change in conditions (*i.e. P, T,* etc.). Such drastic changes in *P* and *T* conditions also support the hypothesis of an open system and an increase in the opportunity for interaction with the surrounding atmosphere. As a result, many of the late-stage microenvironments and associated mineral assemblages may have fO_2 that were externally buffered by the fluctuating conditions in the exsolved volatile phase, rather than being internally buffered by the crystallizing parental magma.

Oxidation of a magma leads to decreased activity of FeO and increased activity of Fe_2O_3, resulting in oxide and silicate minerals enriched in Fe^{3+}. Studies of mafic minerals from plutonic complexes exhibiting magmatic oxidation trends show that fractionation in such systems is characterized by increasing Na, Fe^{3+}, Mn and Mg, with decreasing Fe^{2+}, Ti and Al in the crystallizing silicates and oxides (Czamanske & Mihálik 1972, Czamanske & Wones 1973, Lalonde & Martin 1983). Piilonen *et al.* (1998) showed EHS pyroxene compositions to be depleted in the Hd component and restricted to the Di-Ae tieline due to high Fe^{3+}/Fe^{2+} ratios and elevated oxygen fugacities (fO_2). Furthermore, studies on Fe-bearing trioctahedral micas from MSH (Lalonde *et al.* 1996) indicate annite and siderophyllite from the EHS syenites to be characterized by a range of Fe^{3+}/Fe_{tot} from 0.079

to 0.282, enrichment in Mn, depletion in Ti relative to earlier formed biotites, and Si+Al abundances that are insufficient to fill the tetrahedral sites, thus requiring incorporation of $^{[4]}Fe^{3+}$. Lalonde *et al.* (1996) further suggested that the high Fe^{3+}/Fe_{tot} values of MSH micas are primary in origin. Similarly, amphiboles from the late syenitic pegmatites at MSH display enrichments in $^{[6]}Na$ (0.65 *apfu*), Fe^{3+} (0.61 *apfu*) and Mn (0.77 *apfu*).

Enrichment in Na, Mn and Fe^{3+} with increasing fractionation and fO_2 are the common links with these minerals, the AGM at MSH being no exceptions. In primary kupletskite from MSH, trend A-A′ results in an increase in Mn#, Nb and Fe^{3+} with increasing fractionation (Fig. 8). During igneous differentiation or fractionation, Mn^{2+} follows Fe^{2+} such that the concentrations of both cations in the rock steadily decrease with a decrease in the modal percentage of mafic minerals into which they may be incorporated (Černý *et al.* 1985). During late stages of differentiation, the larger size of the Mn^{2+} cation ($r^{[6]}Mn^{2+}$: 0.83 Å, Shannon 1976) relative to Fe^{2+} ($r^{[6]}Fe^{2+}$: 0.78 Å, Shannon 1976) increases its tendency toward behaviour as an incompatible element, becoming fractionated into late-stage melts (Černý *et al.* 1985). However, the lower electronegativity and ionization potential of Mn^{2+} compared to Fe^{2+} further complicate the fractionation of Mn in magmas. An increase in fO_2 in the magma results in oxidation of the Fe^{2+} to Fe^{3+}, with a further separation of Mn^{2+} and Fe^{3+} on the basis of their crystal-chemical and geochemical tendencies. As stated earlier, exsolution of a volatile-CO_2-H_2O-rich phase from a crystallizing intrusion can lead to magmatic oxidation. This exsolved fluid may also be responsible for transportation and extreme fractionation of Mn in late-stage features such as the syenitic pegmatites at MSH. Shaw (1974) and Hildreth (1979, 1981) have suggested that the enrichment of Mn^{2+} can only

be explained by an affinity to the exsolved volatile and H_2O components of a silicic magma. Furthermore, Shawe (1968) and Bailey (1977) proposed complexing of Mn^{2+} with F, further supporting the affinity of Mn^{2+} to the oxidized, volatile phase of the magma. The Mn-enrichment trends coupled with the enrichments in Fe^{3+} in PEG/APEG and SSX AGM at MSH are thought to be a response to extreme fractionation under oxidizing conditions.

The extreme enrichment of Nb, and often Zr, in kupletskite subgroup AGM in the PEG, APEG and SSX may be due to the presence of a volatile-CO_2-H_2O-rich phase in this strongly peralkaline, oxidized melt. Both Nb and Zr are incompatible elements in peralkaline systems and show high solubility until the final stages of crystallization, at which time they form alkali zircono- and niobosilicates, Nb carbonates and Nb oxides (Bowden 1966, Watson 1979, Dunn & McCallum 1982, Linnen & Keppler 1997, Horng *et al.* 1999). Furthermore, Zr and Nb are also highly mobile in F-rich alkaline systems and can be leached from earlier formed minerals by hydrothermal fluids, becoming concentrated and subsequently precipitated in veins and fractures (Möller 1986, Aja *et al.* 1995, Salvi *et al.* 2000). In particular, Nb is known to be highly mobile in fenitizing fluids enriched in Na, F and Fe^{3+} (Möller 1986).

The behaviour of Nb and Zr in peralkaline systems is in striking contrast to their behaviour in SiO_2-saturated systems with calcalkaline or subalkaline affinities. In peraluminous and subaluminous melts, Nb is concentrated into Ti phases such as rutile, ilmenite and titanite (Linnen & Keppler 1997, Horng *et al.* 1999) and does not form discrete Nb minerals except in the case of extreme enrichment of Nb in late-stage granitic pegmatites (*e.g.* columbite, manganocolumbite; Černý *et al.* 1985). Although columbite and

manganocolumbite are common in granitic pegmatites, they are rare in peralkaline syenite pegmatites due to their high solubility in alkaline melts, even at low temperature (Linnen & Keppler 1997). Zirconium mineralization in calcalkaline to subalkaline plutonic rocks is similarly simple, being limited to early crystallization of zircon.

Niobium and Zr solubility in alkaline melts greatly increases with the alkalinity index (AI: K+Na/Al) of the melt (Watson 1979, Linnen & Keppler 1997). In order to stabilize HFSE, an excess of non-bridging oxygens (NBO) must be present in the melt. In peraluminous and metaluminous melts, there are no free NBO and thus Nb and Zr saturate early in the crystallizational history of the melt. In peralkaline systems, Na and K act as network modifiers and generate NBO; for every mole of excess Na_2O or K_2O, two NBO are generated to which Nb and Zr can bond. Studies by Horng *et al.* (1999) on the solubility of rutile and the interactions of M^{5+} cations in anhydrous haplogranite melts have shown that the solubility of Nb in the melt is increased *via* the following equilibrium equation:

$$2\text{Ti-O-K} + \text{Nb-O-Nb} = 2\text{K-O-Nb} + \text{Ti-O-Ti} \quad (1).$$

Increased alkalinity results in formation of alkali-Nb complexes and promotes crystallization of pure rutile rather than Nb-bearing rutile as is observed in peraluminous melts. Of further interest is the fact that Mn^{2+}, concentrated in late-stage oxidized peralkaline melts, is also a network modifier and will further generate two NBO to which Nb and Zr may bond, increasing their stability, and thus solubility, in the melt. The presence of (Na,K)-Nb-Mn complexes in the melt may further promote crystallization of Nb-bearing kupletskite and niobokupletskite.

The common association of rhodochrosite and other carbonates with niobokupletskite and Nb-bearing kupletskite is further evidence of a volatile-rich melt enriched in CO_2. As an example of a CO_2-rich melt, we can compare the behaviour of Nb in carbonate-rich syenitic pegmatites with carbonatites in which the Ta/Nb ratio is generally much less than unity, and often 1/100 only (Möller 1986). During separation of an immiscible carbonate- and alkaline silicate liquid, Ta is strongly enriched in the silicate phase and Nb into the resulting carbonate liquid, depressing the Ta/Nb ratio in the carbonatite (Hamilton *et al.* 1989). The fractionation of Nb is due to its increased solubility in carbonate-, fluoride- and phosphate-rich fluids due to the stability Nb-F and Nb-CO_3 complexes within the melt at temperatures between 50 and 450 °C (Aleksandrov 1967, Möller 1986). Precipitation of CO_3^{2-} as carbonate minerals in the PEG and APEG at MSH would result in decreased solubility of Nb and crystallization of Nb-bearing minerals. As stated above, in highly peralkaline systems, Nb is highly soluble and mobile, forming complexes with alkalis such as Na and K. As a result, decreased solubility of Nb in the melt due to carbonate crystallization may also promote crystallization of alkali niobosilicates such as niobokupletskite. Local Nb-enrichment in pegmatites in the form of fibrous overgrowths of niobokupletskite is likely the result of post-magmatic leaching of Nb from earlier formed minerals and mobilization of Nb in the late-stage Na-Mn-Nb-rich pegmatite fluids.

4.2. Hydrothermal and metasomatic alteration

In direct contrast to the Na-Mn-Nb-Fe^{3+}-enrichment observed in the PEG, APEG, APLITE and SSX AGM under oxidizing magmatic and post-magmatic conditions, the compositional evolution observed in AGM from the PEG and APEG toward enrichment in Ca, Fe^{2+}, Ti, Zr and F (Trend B-B′) is suggestive of crystallization from a more reduced, F-rich alkaline melt or hydrothermal fluid. The fibrous, slightly altered nature of the Fe-zircophyllite and Zr-bearing astrophyllite in the PEG and APEG is also suggestive of crystallization from deuteric or hydrothermal fluids.

Like Nb, Zr behaves as an incompatible element until the final stages of crystallization. The solubility of Zr in alkaline systems is also proportional to the alkalinity index, fO_2 and the volatile content (in particular F) of the melt (Watson 1979). An increased alkali content in the melt would inhibit polymerization and increase the percentage of NBO which are required for stabilization of ZrO_6 complexes. In contrast, in highly polymerized melts, Zr is present in either [7]- or [8]-coordinated sites considered to be precursor complexes required for zircon crystallization in calcalkaline rocks (Farges *et al.* 1991). Decreasing the solubility of Zr in a peralkaline melt can be accomplished by increasing the polymerization, decreasing temperature, increasing fO_2 or by the introduction of network formers such as Ca and Al (Watson 1979). As a result, stable charge-balanced $^{[6]}$Zr-O-Si-Na complexes are formed, the precursors to alkali zirconosilicate crystallization.

In most geological systems, HFSE, in particular Zr, Ti and REE's, are considered to be immobile during fluid-rock interactions. However, there is evidence that under highly alkaline F-rich conditions, Zr can be transported by hydrothermal fluids as Zr-OH-F

complexes. Zirconium mobilization in strongly alkaline, F-rich hydrothermal fluids has been documented in a number of intrusions, including Strange Lake (Québec-Labrador, Canada; Birkett *et al.* 1992, Salvi & Williams-Jones 1990, 1995, 1996), the Trans-Pecos Magmatic Province (Texas, USA; Rubin *et al.* 1993), and the Tamazeght alkalic complex (Morocco; Salvi *et al.* 2000). Evidence for Zr mobilization is provided by the presence of secondary Zr minerals in hydrothermally altered or metasomatized rocks, and the presence of Zr-bearing daughter minerals, in particular baddeleyite (Philippot & Selverstone 1991, Belkin 1992) and weloganite (Vard & Williams-Jones 1993) in fluid inclusions.

The formation of fibrous ($Ca+Fe^{2+}+Zr$-F)-bearing astrophyllite and Fe-zircophyllite after primary Nb-bearing kupletskite in PEG and APEG at MSH can be modeled by a cation exchange reaction:

$$K_2Na(Mn,Fe^{3+})_7(Nb,Ti)_2Si_8O_{26}(OH)_4O + 0.5Ca^{2+} + 7Fe^{2+} + F^- + Zr^{4+} \Leftrightarrow$$

$$K_2(Na,Ca)Fe^{2+}{}_7(Zr,Ti)_2Si_8O_{26}(OH)_4F + 0.5Na^+ + 7(Mn^{2+}Fe^{3+}) + O^{2-} + Nb^{5+} \quad (2)$$

or

$$\text{niobokupletskite} + 0.5Ca^{2+} + 7Fe^{2+} + F^- + Zr^{4+} \Leftrightarrow$$

$$\text{Fe-zircophyllite} + 0.5Na^+ + 7(Mn^{2+}Fe^{3+}) + O^{2-} + Nb^{5+} \quad (3).$$

Similar cation-exchange reactions have been proposed for the formation of secondary Ca-bearing zirconosilicates such as armstrongite, calcium catapleiite and gittinsite at Strange Lake (Québec-Labrador border, Canada; Salvi & Williams-Jones 1990, 1995, 1996) and the Tamazeght alkalic complex (Morocco; Salvi *et al.* 2000). In all cases, Ca-metasomatism seems to have played a role in concentrating Zr and the formation of zirconosilicates. The

main question that arises is whether or not the HFSE were transported in the metasomatizing Ca-bearing fluid, or introduced by another source.

Transportation of HFSE, in particular Zr, in hydrothermal or metasomatizing fluids requires elevated concentrations of F and OH. In aqueous solutions, Zr forms stable complexes with small anionic species such as F^- and OH^- due to its low electronegativity (Aja *et al.* 1995, Salvi *et al.* 2000). Except at high activities of H^+ and/or low F^- (*e.g.* CO_2-rich systems), Zr will tend to form mixed hydroxy-fluoride complexes, with $Zr(OH)_4F_2$ as the predominant species in solution over a wide pH range (Aja *et al.* 1995, Salvi *et al.* 2000). At MSH, it is likely that Zr was carried as hydroxy-fluoride complexes by a late-stage F-rich fluid, similar to that suggested for formation of Nb-bearing kupletskite and niobokupletskite in the PEG, APEG and SSX. The elevated Zr contents in such AGM support this hypothesis, suggesting that Zr and Nb were transported together until conditions forced them to separate on the basis of their crystal-chemical and geochemical tendencies. The enrichment of the Zr-bearing astrophyllite at MSH in Ca further suggests late-stage Ca metasomatism, similar to what is observed at Strange Lake and the Tamazeght complex. However, it is not tenable that the fluid responsible for Ca enrichment was also responsible for Zr transportation; a fluid saturated in both Ca and F would have resulted in early crystallization of fluorite and a decrease in the solubility of Zr, promoting crystallization of zircon. Secondly, peralkaline fluids exsolved from the crystallizing intrusion would contain little to no Ca (Ca having been fractionated out into earlier phases such as plagioclase and amphibole), yet would be strongly enriched in F. At Strange Lake and the Tamazeght complex, recognizing that the Ca-metasomatizing fluid could not have kept HFSE in solution, Salvi & Williams-Jones (1996)

and Salvi *et al.* (2000) proposed that they were carried by an exsolved magmatic fluid. Late-stage interaction between this fluid, enriched in Zr and F, with either a Ca-enriched meteoric fluid or by interaction with the surrounding limestones would result in precipitation of fluorite, decreasing the activity of F and promoting the crystallization of zirconosilicates.

An identical process can be invoked to explain the formation of Fe-zircophyllite and other zirconosilicates at MSH. Exsolution of a highly alkaline, oxidized, F-bearing solution from the cooling intrusion would have leached HFSE such as Nb and Zr from earlier formed minerals (Rubin *et al.* 1993, Piilonen *et al.* 1998), thus promoting late-stage magmatic and post-magmatic crystallization of AGM. In the majority of the pegmatites, this exsolved fluid evolved to more oxidized compositions, thus promoting crystallization of Na-enriched kupletskite, Nb-bearing kupletskite and niobokupletskite. Early interaction of these fluids with the hornfels unit seems to have resulted in varying degrees of fenitization and albitization of the hornfels and crystallization of AGM as porphyroblasts or phenocrysts.

Further migration of the hydrothermal fluid, depleted in Mn and Nb, would have resulted in alteration and leaching of Zr from of primary minerals (sodium zirconosilicates, Zr-bearing AGM, and Zr-bearing inosilicates such as aegirine and arfvedsonite; Farges *et al* 1994, Piilonen *et al.* 1998) and further concentration of Zr into the aqueous phase. If pegmatite formation occurred in close proximity to the hornfels or a marble xenolith, or mixed with Ca-bearing meteoric waters, interaction of the oxidized Na-F-(Zr,Nb)-rich fluid with a reduced, Ca-CO_2-rich fluid would have caused precipitation of fluorite, carbonate and an astrophyllite enriched in Ca, Fe^{2+}, Zr and F.

5.0. SUMMARY

Using a combination of whole-rock geochemistry for each of the microenvironments host to AGM and the evolutionary scheme proposed for the East Hill suite by Piilonen *et al.* (1998), it is possible to correlate AGM composition (in particular Mn# and Nb+Zr content) with progressive evolution of the suite. In particular, at MSH, we are able to classify the paragenesis of AGM, based on their chemical composition, as either magmatic or hydrothermal (Fig. 14). Similarly, we can correlate these crystal-chemical parameters with the geochemistry of the host rocks in which the AGM occur. Figure 15 shows the correlation between Mn# and the alkalinity index [AI = (Na+K)/Al, calculated using molecular proportions], obtained from whole rock X-ray fluorescence (XRF) data. As whole rock alkalinity increases with increasing fractionation, AGM become progressively more enriched in Mn, Nb and Zr, the result of crystallization from exsolved peralkaline fluids. For comparison, results obtained for AGM from the alkaline Larvik complex (Langesundsfjord area, Oslo rift, Norway) are also presented on Figure 15 (AI data from Neumann 1980). A similar trend is observed, with increasing Mn# during progressive fractionation of the ring sections in the complex. The overall alkalinity of the Larvik complex is lower relative to MSH, and this is reflected in the lower overall Mn# and (Nb+Zr) content of the AGM.

The systematic variations observed in AGM composition, coupled with the alkalinity of the microenvironment, allow us to further develop the evolutionary scheme proposed for the EHS at MSH, shown in Figure 16. The crystal-chemical characteristics of the AGM at MSH correlate well with the evolutionary scheme developed on the basis of aegirine compositional trends by Piilonen *et al.* (1998), suggesting that the crystal chemistry of AGM,

as with other rock-forming minerals, may be used as petrogenetic indicators in alkaline igneous rocks.

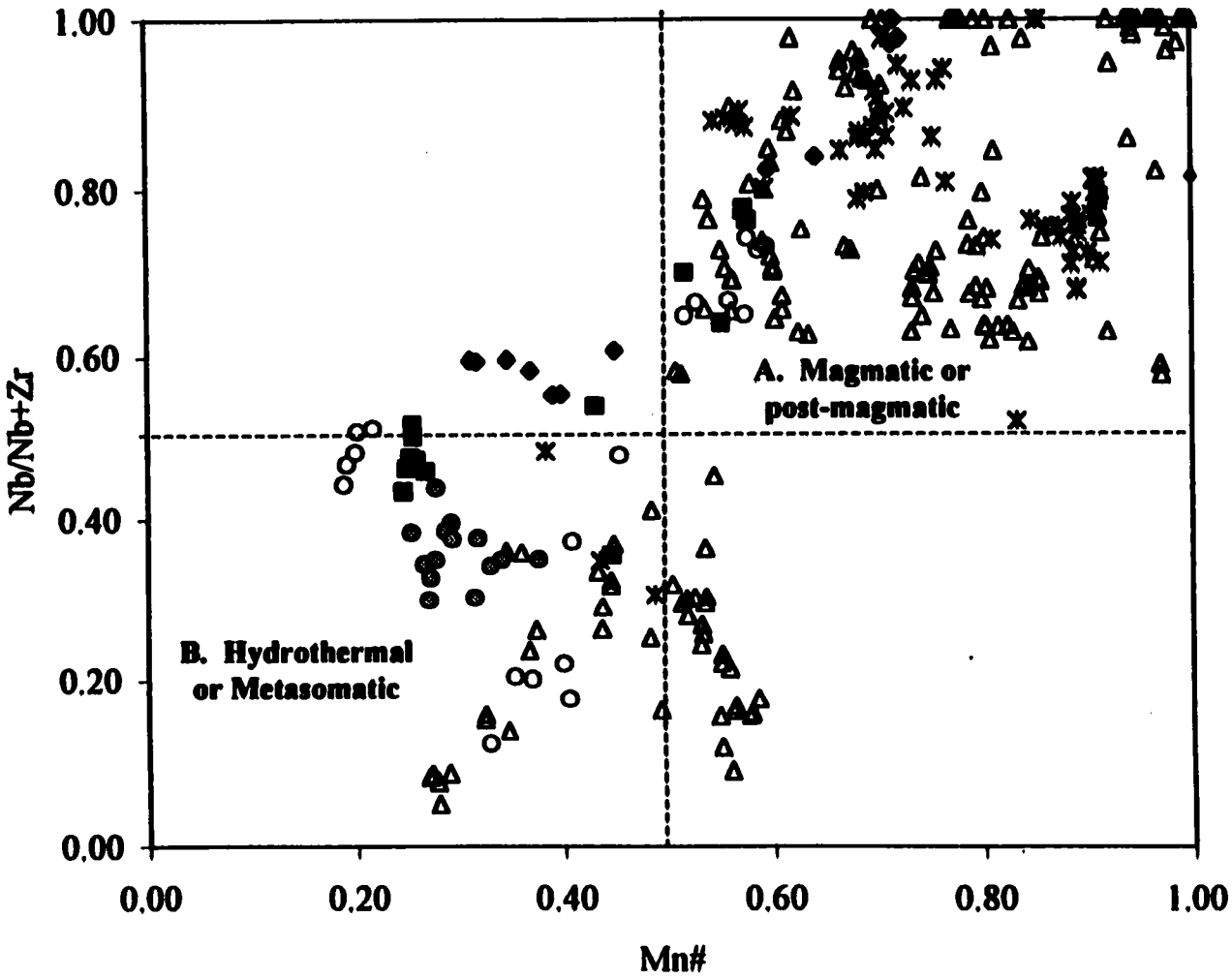

Figure 14. Paragenesis discrimination plot for astrophyllite group minerals in the East Hill suite at Mont Saint-Hilaire. A. Magmatic or post-magmatic. B. Hydrothermal or metasomatic. Open triangles: syenite pegmatites (PEG); Crosses: altered syenite pegmatites (APEG); Filled circles: natrolite pegmatites (NPEG); Open circles: sodalite syenite (SS); Closed diamonds: sodalite syenite xenoliths (SSX); Closed squares: metasomatic unit (META).

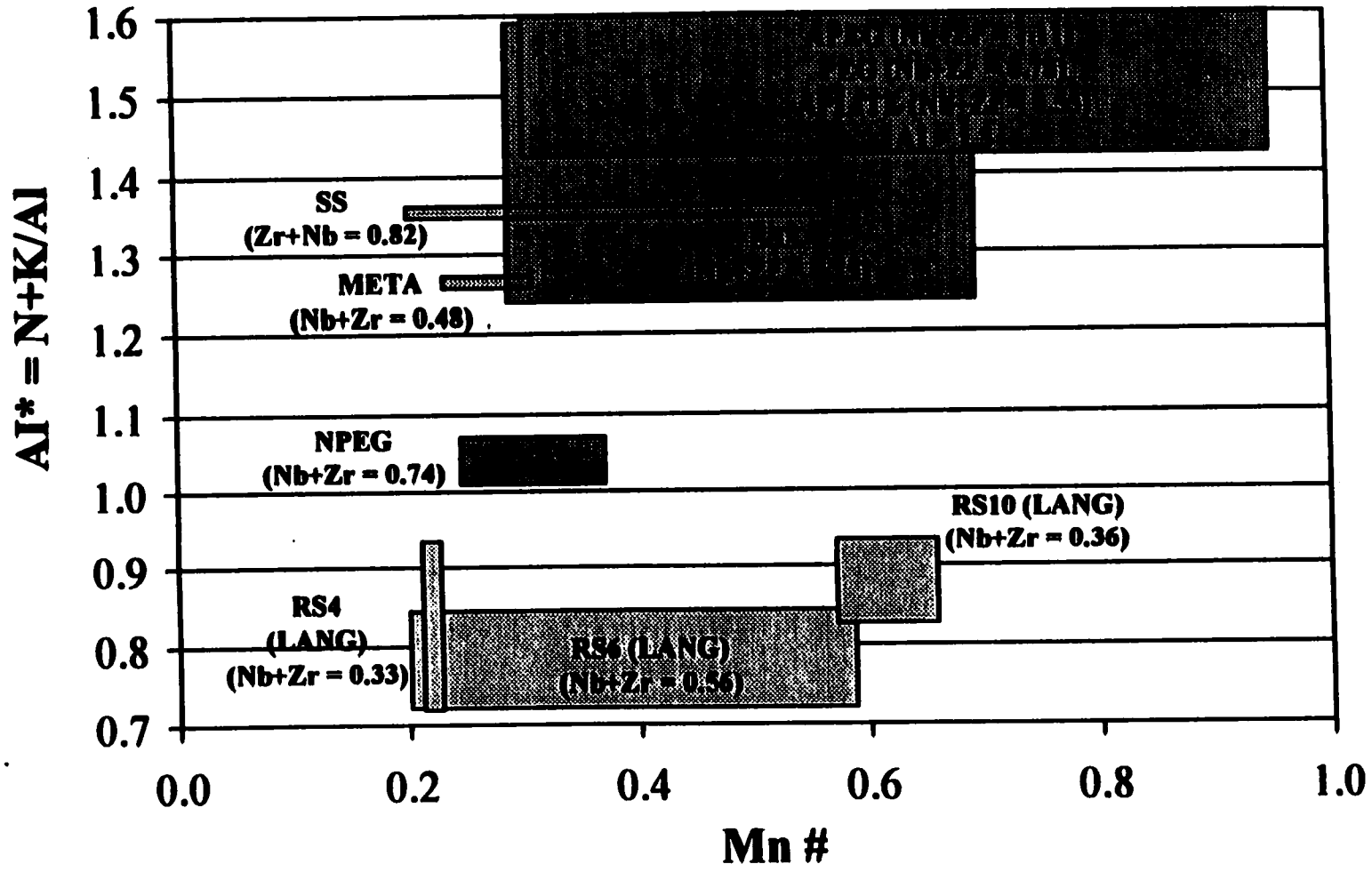

Figure 15. Mn# in astrophyllite group minerals *versus* the whole rock alkalinity index (AI) for Mont Saint-Hilaire (Québec, Canada, dark grey) and the Larvik complex (Langesundsfjord area, Norway, LANG). Nb+Zr values are averages in *apfu*.
NPEG: natrolite pegmatite, META: metasomatic unit, SSX: sodalite syenite xenolith, SS: sodalite syenite, APLITE: aplite, PEG: syenite pegmatite, APEG: altered syenite pegmatite.

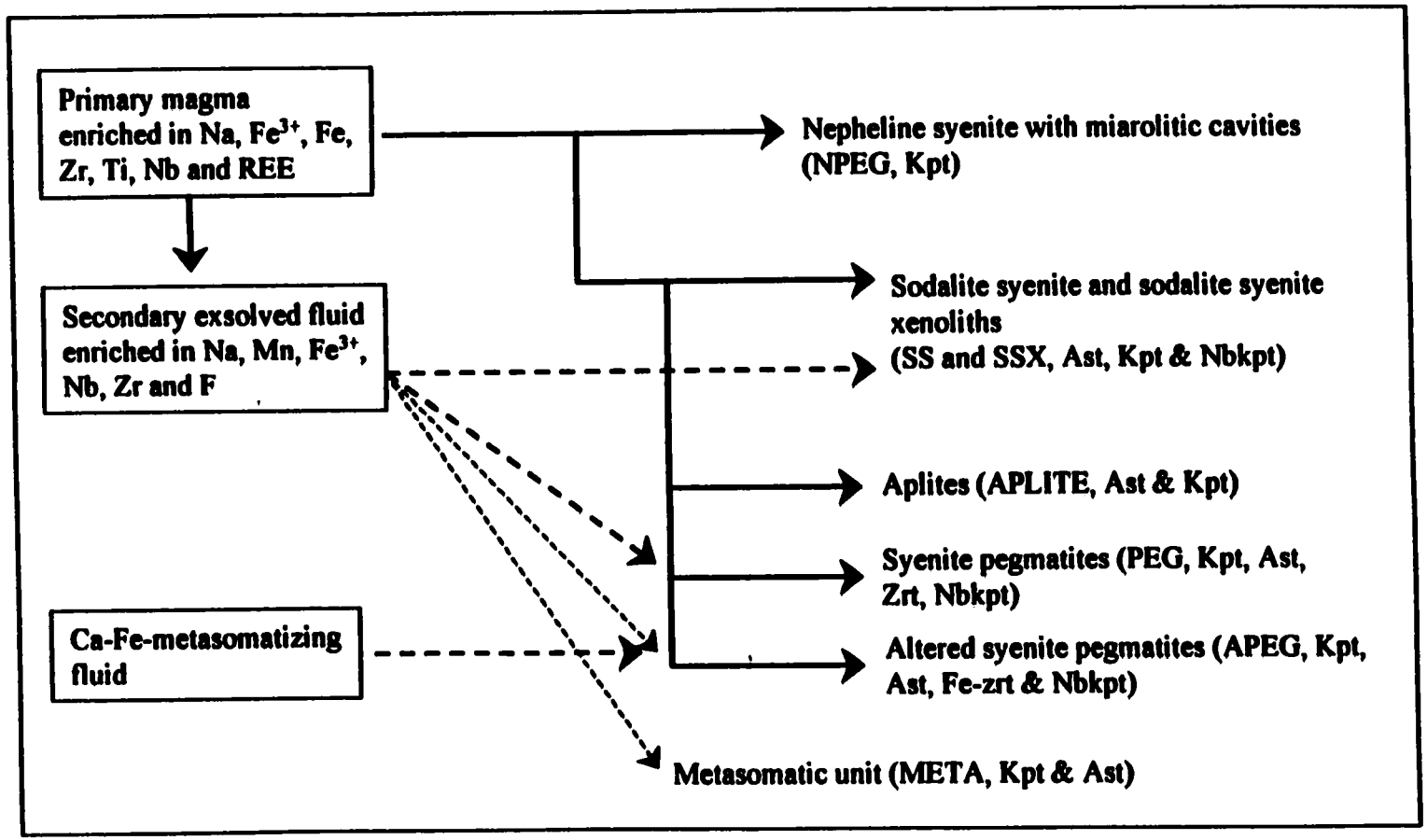

Figure 16. Schematic representation of the paragenetic sequence of the East Hill suite at Mont Saint-Hilaire. Modified from Piilonen *et al.* (1998) to include the paragenesis of astrophyllite group minerals. Solid lines indicate magmatic trends. Dashed lines indicate the influence of a fluid phase. Kpt: kupletskite, Ast: astrophyllite, Zrt: zircophyllite, Fe-zrt: Fe-zircophyllite, Nbkpt: niobokupletskite.

REFERENCES

ABDEL-RAHMAN, A.F.M. (1992): Mineral chemistry and paragenesis of astrophyllite from Egypt. *Mineral. Mag.* **56**, 17-26.

ADAMS, F.D. (1903): The Monteregian Hills - A Canadian petrological province. *J. Geol.* **11**, 239-282.

AJA, S.U., WOOD, S.A. & WILLIAMS-JONES, A.E. (1995): The aqueous geochemistry of Zr and the solubility of some Zr-bearing minerals. *Appl. Geochem.* **10**, 603-620.

ALEKSANDROV, I.V. (1967): Niobium in carbon dioxide solutions and considerations concerning migration of rare elements under hydrothermal conditions. *Geokhimiya* 684-693.

ANNEHED, H., FÄLTH, L. & RAADE, G. (1985): The crystal structure of janhaugite, a sorosilicate of the cuspidine family. *Neues. Jahrb. Mineral. Monatsh* **1**, 7-18.

ANNERSTEN, H. & NYAMBOK, I.O. (1980): The Mössbauer effect study of iron distribution in clinopyroxenes. *Kenya J. Sci. Tech.* **1**, 117-124.

AUTEFAGE, F. & FONTAN, F. (1985): Comportement de minéraux hydratés au cours de leur analyse à la microsonde électronique. *Bull. Minéral.* **108**, 293-304.

BAILEY, J.C. (1977): Fluorine in granitic rocks and melts: a review. *Chem. Geol.* **13**, 13-60.

BAILEY, S.W., FRANK-KAMENETSKII, V.A., GOLDSZTAUB, S., KATO, A., PABST, A., SCHULTZ, H., TAYLOR, H.F.W., FLEISCHER, M. AND WILSON, A.J.C. (1978): Report of the International Mineralogical Association (IMA)-International Union of Crystallography (IUCr) Joint Committee on nomenclature. *Can. Mineral.* **16**, 113-117.

_____ (1984): Crystal chemistry of the true micas. *In* Micas (S.W. Bailey, ed.). *Rev. Mineral.* **13**, 13-60.

BALIĆ-ŽUNIĆ, T. & VICKOVIĆ, K. (1996): IVTON. A program for the calculation of geometrical aspects of crystal structures and some crystal chemical applications. *J. Appl. Crystallogr.* **29**, 305-306.

BANCROFT, G.M. & BURNS, R.G. (1969): Mössbauer and absorption spectral study of alkali amphiboles. *Mineral. Soc. Am. Spec. Pap.* **2**, 137-148.

_____ & BROWN, J.R. (1975): A Mössbauer study of coexisting hornblendes and biotites: Quantitative Fe^{3+}/Fe^{2+} ratios. *Am. Mineral.* **60**, 265-272.

BARTH, T.F.W. (1945): Studies on the igneous rock complex of the Oslo Region. II. Systematic petrography of the plutonic rocks. *Skr. Nor. Vidensk. - Akad. Oslo I* **9**, 104.

BELKIN, H.E. (1992): Baddeleyite (ZrO_2), a hydrothermal mineral in Mesozoic mafic intrusive rocks, eastern North America: Implications for aqueous transport and solubility of zirconium. *2nd Ann. Goldschmidt Conference. Abstr.* A-7.

BIRKETT, T.C., TRZCIENSKI, W.E. & STIRLING, J.A.R. (1996): Occurrence and compositions of some Ti-bearing minerals in the Strange Lake intrusive complex, Québec-Labrador boundary. *Can. Mineral.* **34**, 779-801.

BOWDEN, P. (1966): Zirconium in younger granites of northern Nigeria. *Geochim. Cosmochim. Acta* **30**, 985-993.

BRESE, N.E. & O'KEEFE, M. (1991): Bond-valence parameters for solids. *Acta Crystallogr.* **B47**, 192-197.

BRØGGER, W.C. (1890): *Die mineralien syenitpegmatitgänge der Südnorwegischen augit- und nephelinsyenite*. Verlag Von Milhelm Engelmann.

BROOKS, C.K., ENGELL, J., LARSEN, L.M. AND PEDERSEN, A.K. (1982): Mineralogy of Werner Bjerge alkaline complex, East Greenland. *Meddelelser om Grønland, Geoscience* **7**, 38 pp.

BROWN, I.D. & SHANNON, R.D. (1973): Empirical bond length - bond strength curves for oxides. *Acta Crystallogr.* **A29**, 266-282.

BROWN, G.E. & GIBBS, G.V. (1969): Oxygen coordination and the Si-O bond. *Am. Mineral.* **54**, 1528-1539.

BRUKER ANALYTICAL X-RAY SYSTEMS (1997): XPREP - Data preparation and Reciprocal Space Exploration.

ČERNÝ, P., MEINTZER, R. & ANDERSON, A.J. (1985): Extreme fractionation in rare-element granitic pegmatites: Selected examples of data and mechanisms. *Can. Mineral.* **23**, 381-421.

CHAO, G.Y. (1991): Perraultite, a new hydrous Na-K-Ba-Mn-Ti-Nb silicate species from Mont Saint-Hilaire, Québec. *Can. Mineral.* **29**, 355-358.

CHELISHCHEV, N.F. (1972): Ion exchange properties of astrophyllites under supercritical Conditions. *Geokhimiya* **7**, 856-860.

CHERNOV, A.N., ILYUKHIN, V.V., MAKSIMOV, B.A. & BELOV, N.V. (1971): Crystal structure of innelite, $Na_2Ba_3(Ba,K,Mn)(Ca,Na)Ti(TiO_2)_2[Si_2O_7]_2(SO_4)_2$. *Sov. Phys. Crystallogr.* **16**, 65-69.

CHRISTIANSEN, C.C. (1998): *Mineralogisk, krystalkemisk og krystallografisk undersogelse af astrophylitgruppens medlemmer fra mineralforekomster i Grønland.* M.Sc. Thesis, Univ. Copenhagen. Copenhagen, Denmark (in Danish).

_____, JOHNSEN, O. & STÅHL, K. (1998): Crystal structure of kupletskite from the Kangerdlugssuaq intrusion, East Greenland. *Neues. Jahrb. Mineral. Monatsh.* **6**, 253-264.

_____, MAKOVICKY, E. AND JOHNSEN, O. (1999): Homology and typism in heterophyllosilicates: An alternative approach. *Neues. Jahrb. Mineral. Abh.* **2**, 153-189.

CHRISTIE, I.A.D., RANCOURT, D.G., KODAMA, H., MURAD, E. & ROBERT, J.L. (1993): Oxidation of synthetic annite mica characterized by ^{57}FeMossbauer spectroscopy: Hydrogen de-intercalation and host layer valence state populations. *In* Chemical Physics of Intercalation II. (eds. J.E. Fisher, P. Bernier, S. Roth & S.A. Solin). Plenum, New York, 387-391.

CHRISTOPHE-MICHEL-LEVY, M. (1961): Reproduction artificielle de quelques minéraux riches en zirconium (zircon, eudialyte, catapléite, elpidite); comparison avec leurs conditions naturelles de formation. *Bull. Soc. Franc. Minéral. Cristallogr.* **84**, 165-169.

COHEN, B.L., FINK, C.L. & DEGNAN, J.H. (1972): Nondestructive analysis for trace amounts of hydrogen. *J. Appl. Phys.* **43** 19-25.

COOPER, M.A., HAWTHORNE, F.C., ROBERTS, A.C., GRICE, J.D., STIRLING, J.A. & MOFFATT, E.A. (1998): Georgeericksenite, $Na_6CaMg(IO_3)_6(CrO_4)_2(H_2O)_{12}$, a new mineral from Ofician, Chacabuco, Chile: Description and crystal structure. *Am. Mineral.* **83**, 390-399.

_____, _____, & GREW, E.S. (1998): Refinement of the crystal structure of tienshanite: Short-range-order constraints on chemical composition. *Can. Mineral.* **36**, 1305-1310.

CRERAR, D. WOOD, S. & BRANTLEY, S. (1985): Chemical controls on solubility of ore-forming minerals in hydrothermal systems. *Can. Mineral.* **23**, 333-352.

CROMER, D.T. & LIBERMAN, D. (1970): Relativistic calculation of anomalous scattering

Factors for X-rays. *J. Chem. Phys.* **53**, 1891-1898.

CRUICKSHANK, D.W.J. (1961): The role of 3*d*-orbitals in π-bonds between (a) silicon, phosphorous, sulphur and chlorine and (b) oxygen or nitrogen. *J. Chem. Soc.* 5486-5504.

CURRIE, K.L. (1970): An hypothesis on the origin of alkaline rocks suggested by the tectonic setting on the Monteregian Hills. *Can. Mineral.* **10**, 411-420.

_____ (1983): An interim report on the geology and petrology of the Mont Saint Hilaire pluton, Quebec. *Geol. Sur. Can. Pap.* **83-1B**, 39-46.

_____, Eby, G.N. & Gittins, J. (1986): The petrology of the Mont Saint-Hilaire complex, southern Québec: an alkaline gabbro-peralkaline syenite association. *Lithos* **19**, 65-81.

CZAMANSKE, G.K. & MIHÁLIK, P. (1972): Oxidation during magmatic differentiation, Finnmarka Complex, Oslo area, Norway: Part 1, The opaque oxides. *J. Petrol.* **13**, 493-509.

_____ & WONES, D.R. (1973): Oxidation during magmatic differentiation, Finnmarka Complex, Oslo area, Norway: Part 2, The mafic silicates. *J. Petrol.* **14**, 349-380.

DEMARK, R.S. (1984): Minerals of Point of Rocks, New Mexico. *Mineral. Rec.* **15**, 149-156.

DONS, J.A. (1977): Diabase from Stig, 209 m.y. *Nytt Oslofeltgruppen* **4**, 29-31.

DORNBERGER-SCHIFF, K., DRITS, V.A., DUROVIC, S. AND ZVYAGIN, V.V. (1985): Special form of polytypism potentially occurring in astrophyllite structures. *Sov. Phys. Crystallogr.* **30**, 292-294.

DUNN, T. & MCCALLUM, I.S. (1982): The partitioning of Zr and Nb between diopside and melts in the system diopside-albite-anorthite. *Geochim. Cosmochim. Acta* **46**, 623-629.

DYAR, M.D. & BURNS, R.G. (1986): Mössbauer spectral study of ferruginous one-layer trioctahedral micas. *Am. Mineral.* **72**, 102-112.

EFIMOV, A.F., DUSMATOV, V.D., GANZEEV, A.A. & KATAEVA, Z.T. (1971): Cesium kupletskite, a new mineral. *Dokl. Akad. Nauk SSSR* **197**, 1394-1397.

EKSTROM, T.K. (1972): The distribution of fluorine among some coexisting minerals. *Contrib. Mineral. Petrol.* **34**, 192-200.

ERCIT, T.S., COOPER, M.A., & HAWTHORNE, F.C. (1998): The crystal structure of vuonnemite, $Na_{11}Ti^{4+}Nb_2(Si_2O_7)_2(PO_4)_2O_3(F,OH)$, a phosphate-bearing sorosilicate of the lomonosovite group. *Can. Mineral.* **36**, 1311-1320.

ESKOLA, P. & SAHLSTEIN, TH.G. (1930): On astrophyllite-bearing nepheline syenite gneiss. *Bull. Comm. Geol. Finland* **15**, 77-88.

EVANS, R.J. (2000): OCTAHEDRON. A program for calculation of octahedral flattening angles and counter rotations. Univ. Ottawa, Ottawa, Canada.

_____ (2001): *The electric field gradient of octahedral Fe^{2+} in layer silicates: Theory with applications to Mössbauer spectroscopy*. M.Sc. Thesis, Univ. Ottawa, Ottawa, Canada.

FAIRBAIRN, H.W., FAURE, G., PINSON, W.H., HURLEY, P.M. & POWELL, J.L. (1963): Whole rock age and discordant biotite in the Monteregian igneous province, Québec. *J. Geophys. Res.* **68**, 6515-6522.

FARGES, F., PONADER, C.W. & BROWN, G.E. (1991): Structural environment of incompatible elements in silicate glass/melt systems: I. Zirconium at trace levels. *Geochim. Cosmochim. Acta* **55**, 1563-1574.

_____, BROWN, G.E. & VELDE, D. (1994): Structural environment of Zr in two inosilicates from Cameroon: mineralogical and geochemical implications. *Am. Mineral.* **79**, 838-847.

FARMER, V.C. (1974): Infrared Spectra of Minerals. *Mineral. Soc. (London), Monogr.* **4**.

FERRARIS, G., IVALDI, G., KHOMYAKOV, A.P., SOBOLEVA, S.V., BELLUSO, E. & PAVESE, A. (1996): Nafertisite, a layer titanosilicate member of a polysomatic series including mica. *Eur. J. Mineral.* **8**, 241-249.

_____ (1997): Polysomatism as a tool for correlating properties and structure. *In* EMU Notes in Mineralogy: Modular aspects of minerals. **1**, 275-295

FLOOR, P. (1961): Astrofilita, un mineral nuevo en Espana, notas y communicaciones. *Inst. Geol. Mineral Espana.* **62**, 59-69.

GALAKHOV, A.V. (1959): *The rischorrites of the Khibina alkaline massif.* Izd-vo. *Akad. Nauk. SSSR.* Moscow. 169 p.

GANZEYEV, A.A., YEFIMOV, A.F.& SEMENOVA, N.G. (1969): Isomorphism of the alkali metals in minerals of the astrophyllite group. *Geochem. Int.* **6**, 295-300.

GERASIMOVSKY, V.I., VOLKOV, V.P., KOGARKO, L.N. & POLYAKOV, A.I. (1974): Kola Peninsula. In *The Alkaline Rocks* (ed. H. Sørensen). John Wiley & Sons, NY. 206-220.

_____, _____, _____, A.I., SAPRYKINA, T.V. & BALASHOV, Y.A. (1966): *Geochemistry of the Lovozero alkaline massif*. Nauka., Moscow.

GILBERT, L.A. & FOLAND, K.A. (1986): The Mont Saint Hilaire plutonic complex: occurrence of excess ^{40}Ar and short intrusion history. *Can. J. Earth Sci.* **23**, 948-958.

GREEN, T.H. (1994): Experimental studies of trace-element partitioning applicable to Igneous petrogenesis. *Chem. Geol.* **117**, 1-36.

GROSS, E.B. & HEINRICH, E.WM. (1966): Petrology and mineralogy of the Mount Rosa area, El Paso and Teller counties, Colorado. II. Pegmatites. *Am. Mineral.* **51**, 299-323.

GUINIER, A., BOKIJ, G.B., BOLL--DORNBERGER, K., COWLEY, J.M., ĎUROVIČ, S., JAGODZINSKI, H., KRISHNA, P., DEWOLFF, P.M., ZVYAGIN, B.B., COX, D.E., GOODMAN, P., HAHN, T., KUCHITSU, K., AND ABRAHAMS, S.C. (1984): Nomenclature of polytype structures - Report of the International Union of Crystallography Ad-Hoc Committee on the nomenclature of disordered, modulated and polytype structures. *Acta Crystallogr.* **A40**, 399-404.

HAMILTON, D.L., BEDSON, P. & ESSEN, J. (1989): The behaviour of trace elements in the Evolution of carbonatites. *In* Carbonatites: Genesis and evolution (ed. K. Bell). Unwin Hyman.

HAWTHORNE, F.C. (1981): Crystal chemistry of the amphiboles. *In* Amphiboles and Other Hydrous Pyriboles - Mineralogy (ed. D. R. Veblen). *Rev. Mineral.* **9A**, 1-102.

_____ (1988): Mössbauer spectroscopy. *In* Spectroscopic methods in mineralogy and geology (ed. F.C. Hawthorne). *Rev. Mineral.* **18**, 255-340.

HARGRAVES, P., RANCOURT, D.G. & LALONDE, A.E. (1990): Single-crystal Mössbauer study of phlogopite mica. *Can. J. Phys.* **68**, 128-144.

HILDRETH, W. (1979): The Bishop Tuff: evidence for the origin of compositional zoning in silicic magma chambers. *Geol. Soc. Amer., Spec. Pap.* **180**, 43-75.

_____ (1981): Gradients in silicic magma chambers: implications for lithospheric magmatism. *J. Geophys. Res.* **86**, 10153-10192.

HORNG, W-S., HESS, P.C. & GAN, H. (1999): The interactions of M^{+5} cations (Nb^{+5}, Ta^{+5}, or P^{+5}) and anhydrous haplogranite melts. *Geochim. Cosmochim. Acta* **63**, 2419-2428.

HORVÁTH, L. & GAULT, R.A. (1990): The Mineralogy of Mont Saint-Hilaire Quebec. *Mineral Rec.* **21**, 284-359.

HUBEI GEOLOGIC COLLEGE, X-RAY LABORATORY (1974): The crystal chemistry of astrophyllite group minerals. *Sci. Geol. Sin.* **1**, 18-33 (in Chinese).

JOHNSEN, O. (1996): TEM observations and *X*-ray powder data on lamprophyllite polytypes from Gardiner Complex, East Greenland. *Neues. Jahrb. Mineral. Monatsh.*, **9**, 407-417.

_____ & GAULT, R.A. (1997): Chemical variation in eudialyte. *Neues. Jahrb. Mineral. Abh.* **171**, 215-237.

_____ & GRICE, J.D. (1999): The crystal chemistry of the eudialyte group. *Can. Mineral.* **37**, 865-890.

KHALILOV, A.D. (1990): Refinement of the crystal structure of β-lomonosovite from the Lovozero alkaline massif. *Miner. Zhurn.* **12**, 10-18. (in Russ.).

KAPUSTIN, Y.L. (1973): Zircophyllite, the zirconium analogue of astrophyllite. *Int. Geol. Rev.* **15**, 621-625.

KHOMYAKOV, A.P. (1995): *Mineralogy of Hyperagpaitic Alkaline Rocks*. Clarendon Press, Oxford. 223.

KOENIG, G.A. (1877): Über das vorkommen von astrophyllit, arfvedsonit und zirkon in El Paso Co., Colorado. *Zeit. Kryst. Mineral.* **1**, 423-433.

KOGARKO, L.N., KONONOVA, V.A., ORLOVA, M.P. & WOOLLEY, A.R. (1995): *Alkaline Rocks And Carbonatites of the World, Part Two: Former USSR*. Chapman & Hall. London.

KRAUSKOPF, K.B. (1967): *Introduction to Geochemistry*. McGraw-Hill, New York.

LAGAREC, K & RANCOURT, D.G. (1998): Recoil. Mössbauer spectral analysis software. Univ. Ottawa, Canada.

LALONDE, A.E. & MARTIN, R.F. (1983): The Baie-des-Moutons syenitic complex, la Tabatière, Québec II. The ferromagnesian minerals. *Can. Mineral.* **21**, 81-91.

_____, RANCOURT, D.G. & CHAO, G.Y. (1996): Fe-bearing trioctahedral micas from Mont Saint-Hilaire, Québec, Canada. *Mineral. Mag.* **60**, 447-460.

LANFORD, W.A. (1992): Analysis for hydrogen by nuclear reaction and energy recoil detection. *Nuc. Inst. Meth. Phys. Res.* **B66**, 65-82.

LARSEN, L. (1973): Measurement of solubility of zircon ($ZrSiO_4$) in synthetic granitic melts. *Eos* **54**, 479.

LARSEN, A.O. & RAADE, G. (1997): Pyroksener fra Oslofeltets syenittpegmatitter. *Norsk. Bergv. Skrif.* **12**, 16-21.

LAYNE, G.D., RUCKLIDGE, J.C.& BROOKS, C.K. (1982): Astrophyllite from Kangerdlugssuaq, East Greenland. *Mineral. Mag.* **45**, 149-156.

LIEBAU, F. (1985): *Structural Chemistry of Silicates: Structure, Bonding and Classification.* Springer-Verlag, Berlin.

LINNEN, R.L. & KEPPLER, H. (1997): Columbite solubility in granitic melts: consequences for the enrichment and fractionation of Nb and Ta in the Earth's crust. *Contrib. Mineral. Petrol.* **128**, 213-227.

LINTHOUT, K. (1984): Alkali-zirconosilicates in peralkaline rocks. *Contrib. Mineral. Petrol.* **86**, 155-158.

LONDON, D. (1992): The application of experimental petrology to the genesis and crystallization of granitic pegmatites. *Can. Mineral.* **30**, 499-540.

MACDONALD, R. & SAUNDERS, M.J. (1973): Chemical variation in minerals of the astrophyllite group. *Mineral. Mag.* **39**, 97-111.

MANDARINO, J.A. (1981): The Gladstone-Dale relationship. IV. The compatibility concept and its application. *Can. Mineral.* **19**, 441-450.

_____ & ANDERSON, V. (1989): *Monteregian Treasures.* Cambridge Univ. Press, New York.

MANNING, P.G. (1969): On the origin of colour and pleochroism of astrophyllite and brown clintonite. *Can. Mineral.* **9**, 663-677.

MARTIN, D. (1975): *Studies of astrophyllite from Mont Saint-Hilaire.* B.Sc. thesis, Carleton Univ. Ottawa, Canada.

MASON, R.A. (1992): Models of order and iron-fluorine avoidance in biotite. *Can. Mineral.* **30**, 343-354.

MCAULIFFE, C.A. & BARRATT, D.S. (1987): Titanium. *In* Comprehensive Coordination

Chemistry. 3. Main Group and Early Transition Elements (eds. G. Wilkinson, R.D. Gillard & J.A. McCleverty), Pergamon, Oxford, 323-362.

MCDONALD, A.M. (1996): The crystal structure of sabinaite, $Na_4Zr_2TiO_4(CO_3)_4$. *Can. Mineral.* **34**, 811-815.

_____, GRICE, J.D. & CHAO, G.Y. (2000): The crystal structure of yoshimuraite, a layered Ba-Mn-Ti silicophosphate, with comments on five-coordinated Ti^{4+}. *Can. Mineral.* **38**, 649-656.

MEGAW, H.D. (1968a): A simple theory of the off centre displacement of cations in octahedral environments. *Acta Crystallogr.* **B24**, 149-153.

_____ (1968b): The thermal expansion of interatomic bonds, illustrated by experimental evidence from certain niobates. *Acta Crystallogr.* **A24**, 589-604.

MELLINI, M. & MERLINO, S. (1979): Refinement of the crystal structure of wöhlerite. *Tschermaks Mineral. Petrogr. Mitt.* **26**, 109-123.

_____ (1981): Refinement of the crystal structure of låvenite. *Tschermaks Mineral. Petrogr. Mitt.* **28**, 99-112.

MÖLLER, P. (1986): REE(Y), Nb, and Ta enrichment in pegmatites and carbonatite-alkalic rock complexes. *In* Lanthanides, Tantalum and Niobium: Mineralogy, geochemistry, characteristics of primary ore deposits, prospecting, processing and applications (eds. P. Möller, P. Černý & F. Saupe). Springer-Verlag, 103-144.

MOORE, P.B. & ARAKI, T. (1977): Samuelsonite: its crystal structure and relation to apatite and octacalcium phosphate. *Am. Mineral.* **62**, 229-245.

MÖSSBAUER, R.L. (1958): Kernresonanzfluoresent von gammastrahlung in Ir^{191}. *Z. Phys.* **151**, 124-143.

MUNOZ, J.L. (1984): F-OH and Cl-OH exchange in micas with applications to hydrothermal ore deposits. *In* Micas (S.W. Bailey, ed.). *Rev. Mineral.* **13**, 469-493.

_____ & Ludington, S.D. (1974): Fluoride-hydroxyl exchange in biotite. *Am. J. Sci.* **274**, 2212-2221.

NEUMANN, E.-R. (1976): Compositional relations among pyroxenes, amphiboles and other mafic phases in the Oslo Region plutonic rocks. *Lithos* **9**, 85-109.

_____ (1980): Petrogenesis of the Oslo Region larvikites and associated rocks. *J. Petrol.* **21**, 499-531.

_____, LARSEN, B.T. & SUNDVOLL, B. (1985): Compositional variations among gabbroic intrusions in the Oslo rift. *Lithos* **18**, 35-59.

_____, TILTON, G.R. & TUEN, E. (1988): Sr, Nd and Pb isotope geochemistry of the Oslo Rift igneous province, southeast Norway. *Geochim. Cosmochim. Acta* **52**, 1997-2007.

_____, SUNDVOLL, B., & ØVERLI, P.E. (1990): A mildly depleted upper mantle beneath southeast Norway: evidence from basalts in the Permo-Carboniferous Oslo Rift. *Tectonophys.* **178**, 89-107.

_____, OLSEN, K.H., BALDRIDGE, W.S. & SUNDVOLL, B. (1992): The Oslo Rift: A review. *Tectonophys.* **208**, 1-18.

_____ (1994): The Oslo Rift: P-T relations and lithospheric structure. *Tectonophys.* **240**, 159-172.

NICKEL, E.H., ROWLAND, J.F. & CHARETTE, D.J. (1964): Niobophyllite - The niobium analogue of astrophyllite; a new mineral from Seal Lake, Labrador. *Can. Mineral.* **8**, 40-52.

_____ & GRICE, J.D. (1998): The IMA Commission on New Minerals and Mineral Names: Procedures and guidelines on mineral nomenclature. *Can. Mineral.* **36**, 913-926.

NIELSEN, C.H. & SIGURDSSON, H. (1981): Quantitative methods for electron microprobe analysis of sodium in natural and synthetic glasses. *Am. Mineral.* **66**, 547-552.

ONDIK, H. & SMITH, D. (1962): Interatomic distances in inorganic compounds. In *International Tables for X-ray Crystallography III: Interatomic and Interionic Distances* (eds. C.H. MacGillavry & G.D. Rieck). Kynoch Press, Birmingham, England, 257-274.

PENG, C.C. & MA, C.S. (1963): Crystal structure of astrophyllite and a new type of band silicate radical. *Sci. Sin.* **12**, 272-276 (in Russian).

PEN, Z.Z. & SHENG, T.C. (1963): Crystal structure of bafertisite, a new mineral from China. *Sci. Sin.* **12**, 278-280 (in Russian).

PERCHIAZZI, N., MCDONALD, A.M., GAULT, R.A., JOHNSEN, O. & MERLINO, S. (2000): The Crystal structure of normandite and its crystal-chemical relationships with låvenite. *Can. Mineral.* **38**, 641-648.

PETERSEN, J.S. (1978): Structure of the Larvikite-Lardalite Complex, Oslo Region, Norway, and its evolution. *Geol. Rundsch.* **67**, 330-342.

PHILIPPOT, P. & SELVERSTONE, J. (1991): Trace-element-rich brines in eclogitic veins: Implications for fluid composition and transport during subduction. *Contrib. Mineral. Petrol.* **106**, 417-430.

PIILONEN, P.C., MCDONALD, A.M. & LALONDE, A.E. (1998): The crystal chemistry of aegirine from Mont Saint-Hilaire, Québec. *Can. Mineral.* **36**, 779-792.

_____, LALONDE, A.E., MCDONALD, A.M. & GAULT, R.A. (2000): Niobokupletskite, a new astrophyllite group mineral from Mont Saint-Hilaire, Québec: Description and crystal structure. *Can. Mineral.* **38**, 627-639.

_____, MCDONALD, A.M. & LALONDE, A.E. (2001): Kupletskite polytypes from the Lovozero massif, Kola Peninsula, Russia: Kupletskite-1*A* and kupletskite-*Ma2b2c*. *Eur. J. Mineral.* (in press).

PORTNOV, A.M. & RASTSVETAYEVA, R.K. (1966): Vlasovit I margantsevyy astrofillit v shchelochnykh siyenit-pegmatitakh Severnogo Pribaykal'ya. *Dokl. Akad. Nauk. SSSR* **4**, 941-943.

PYATENKO, Y.A. & VORONKOV, A.A. (1978): Comparative crystal-chemical functions of titanium and zirconium in mineral structures. *Int. Geol. Rev.* **20**, 1050-1058.

RAADE, G., HAUG, J., KRISTIANSEN, R. & LARSEN, A.O. (1980): Langesundsfjord. *Lapis* **5**, 22-28.

_____ & _____(1982): Gjerdingen - Fundstelle seltener Mineralien in Norwegen. *Lapis* **7**, 9-15.

RAJASEKARAN, K.C. (1967): *Mineralogy and petrology of nepheline syenite in Mont Saint-Hilaire, Québec*. Ph.D. Thesis, McGill Univ. Montréal, Canada.

RAMBERG, H. (1952): Chemical bonds and the distribution of cations in silicates. *J. Geol.* **60**, 331-355.

RAMBERG, I.B. (1976): Gravimetry interpretation of the Oslo Graben and associated igneous rocks. *Norg. Geol. Unders.* **337**, 55-73.

_____ & LARSEN, B.T. (1978): Tectonomagmatic evolution. In *The Oslo Paleorift. A Review and Guide to Excursions* (eds. Dons, J.A. & Larsen, B.T.). *Norg. Geol. Unders.* **337**, 55-73.

RANCOURT, D.G. (1989): Accurate site populations from Mössbauer spectroscopy. *Nucl. Instrum. Methods Phys. Res.* **B44**, 199-210.

_____ & PING, J.Y. (1991): Voigt-based methods for arbitrary-shape static hyperfine parameter distributions in Mössbauer spectroscopy. *Nucl. Instrum. Methods Phys. Res.* **B58**, 85-97.

_____, Dang, M.-Z. & Lalonde, A.E. (1992): Mössbauer spectroscopy of tetrahedral Fe^{3+} in trioctahedral micas. *Am. Mineral.* **77**, 34-43.

_____, MCDONALD, A.M., LALONDE, A.E. & PING, J.Y. (1993): Mössbauer absorber thickness for accurate site populations in Fe-bearing minerals. *Am. Mineral.* **78**, 1-7.

_____ (1994a): Mössbauer spectroscopy of minerals I. Inadequacy of Lorentzian-line doublets in fitting spectra arising from quadrupole splitting distributions. *Phys. Chem. Mineral.* **21**, 244-249.

_____ (1994b): Mössbauer spectroscopy of minerals II. Problem of resolving cis and trans octahedral Fe^{2+} sites. *Phys. Chem. Mineral.* **21**, 250-257.

_____, Ping, J.Y. & Berman, R.G. (1994): Mössbauer spectroscopy of minerals III. Octahedral-site Fe^{2+} quadrupole splitting distributions in the phlogopite-annite series. *Phys. Chem. Mineral.* **21**, 258-267.

_____ & Lalonde, A.E. (1995): Method for getting site-specific EFG information from sheet silicates: Application to micas. *Int. Conf. App. Mössbauer Effect*, Greece (abstr.)

_____, PING, J.Y., BOUKILI & ROBERT, J.-L. (1996): Octahedral-site Fe^{2+} quadrupole spliiting distributions from Mössbauer spectroscopy along the (OH,F)-annite join. *Phys. Chem. Mineral.* **23**, 63-71.

_____ (1998): Mössbauer spectroscopy in clay science. *Hyperfine Interact.* **117**, 3-38.

RASTSVETAEVA, R.K. & DORFMAN, M.D. (1995): Crystal structure of Ba-lamprophyllite in the isomorphous lamprophyllite-barytolamprophyllite series. *Kristallografiya* **40**, 1026-1029 (in Russ.).

REDHAMMER, G.J., DACHS, E. & AMTHAUER, G. (1995): Mössbauer spectroscopic and X-ray powder diffraction studies of synthetic micas on the join annite $KFe_3AlSi_3O_{10}(OH)_2$-phlogopite $KMg_3AlSi_3O_{10}(OH)_2$. *Phys. Chem. Mineral.* **22**, 282-294.

_____ (1998): Characterization of synthetic trioctahedral micas by Mössbauer spectroscopy. *In* Mössbauer spectroscopy in Clay Science (ed. D.G. Rancourt). *Hyperfine Interact.* **117**, 85-115.

ROBERTS, A.C., SABINA, A.P., ERCIT, T.S., GRICE, J.D., SZYMAŃSKI, & RAMIK, R.A. (1990): Voggite, a new hydrated Na-Zr hydroxide-phosphate-carbonate from the Francon Quarry, Montreal, Québec. *Can. Mineral.* **28**, 155-159.

ROBINSON, E.A. (1963): Characteristic vibrational frequencies of oxygen compounds of silicon, phosphorous and chlorine: correlation of stretching frequencies and force constants with bond lengths and bond orders. *Can. J. Chem.* **41**, 3021-3033.

ROBINSON, K., GIBBS, G.V. & RIBBE, P.H. (1971): Quadratic elongation: A quantitative measure of distortion in coordination polyhedra. *Science* **172**, 567-570.

RUBIN, J.N., HENRY, C.D., & PRICE, J.G. (1993): The mobility of zirconium and other "immobile" elements during hydrothermal alteration. *Chem. Geol.* **110**, 29-47.

SAF'YANOV, Y.N., VASIL'EVA, N.O., GOLOVACHEV, V.P., KUZ'MIN, É.A., & BELOV, N.V. (1983): Crystal structure of lamprophyllite. *Sov. Phys. Crystallogr.*, **28**, 207-209.

SALVI, S. & WILLAIMS-JONES, A.E. (1990): The role of hydrothermal processes in the granite hosted Zr, Y, REE deposit at Strange Lake, Québec/Labrador: Evidence from fluid inclusions. *Geochim. Cosmochim. Acta* **54**, 2403-2418.

_____ & _____ (1995): Zirconosilicate phase relations in the Strange Lake (Lac Brisson) pluton, Québec-Labrador, Canada. *Am. Mineral.* **80**, 1031-1040.

_____ & _____ (1996): The role of hydrothermal processes in concentrating the HFSE in the Strange Lake peralkaline complex, northeastern Canada. *Geochim. Cosmochim. Acta* **60**, 1917-1932.

_____, FONTAN, F., MONCHOUX, P., WILLIAMS-JONES, A.E. & MOINE, B. (2000): Hydrothermal mobilization of high field strength elements in alkaline igneous systems: Evidence from the Tamazeght complex (Morocco). *Econ. Geol.* **95**, 559-576.

SCHMAHL, W.W. & TILLMANNS (1987): Isomorphic substitutions, straight Si-O-Si geometry and disorder of tetrahedral tilting in batisite, $(Ba,K)(K,Na)Na(Ti,Fe,Nb,Zr)Si_4O_{14}$. *Neues. Jahrb. Mineral. Monatsh* **3**, 107-118.

SCOTT, S.D. & BARNES, H.L. (1972): Sphalerite-wurtzite equilibria and stoichiometry. *Geochim. Cosmochim. Acta* **36**, 1275-1295.

SEMENOV, E.I. (1956): Kupletskite - a new mineral of the astrophyllite group. *Dokl. Akad. Nauk. SSSR.* **108**, 933-936.

SHABANI, A.A.T., RANCOURT, D.G. & LALONDE, A.E. (1998): Determination of cis and trans Fe^{2+} populations in $2M_1$ muscovite by Mössbauer spectroscopy. *Hyperfine Interact.* **117**, 117-129.

_____ (1999): *Mineral chemistry and Mössbauer spectroscopy of micas from granitic rocks of the Canadian Appalachians.* Ph.D. Thesis, Univ. Ottawa. Ottawa, Canada.

SHANNON, R.D. (1975): Systematic studies of interatomic distances in oxides. *In* Petrophysics (ed. R.G.J. Strens). John Wiley & Sons, New York.

_____ (1976): Revised effective ionic radii and systematic studies of interatomic distances in halides and chalcogenides. *Acta Crystallogr.* **A32**, 751-767.

SHAW, H.R. (1974): Diffusion of H2O in granitic liquids. *In* Geochemical Transport and Kinetics (eds. A.W. Hoffman, B.J. Giletti, H.S. Yoder, Jr. & R.A. Yund). *Carnegie Inst. Washington Publ.* **634**, 139-170.

SHAWE, D.R. (1968): Geology of the Spor Mountain beryllium district, Utah. *In* Ore Deposits of the United States, 1933-1967, **2** (ed. J.D. Ridge). *Amer. Inst. Mining Metall. Petrol. Eng.*, New York, 1148-1161.

SHELDRICK, G.M. (1993): SHELXL-93. Program for the refinement of crystal structures. University of Göttingen, Germany.

SHI, NICHENG., MA, ZHESHENG., LI, Guowu., YAMNOVA, N.A. & PUSHCHAROVSKY, D.YU (1998): Structure refinement of monoclinic astrophyllite. *Acta Crystallogr.* **B54**, 109-114.

SHIBAEVA, R.P., SIMONOV, V.I. & BELOV, N.V. (1964): Crystal structure of the Ca, Na, Zr, Ti silicate rosenbuschite, $Ca_{3.5}Na_{2.5}Zr(Ti,Mn,Nb)[Si_2O_7]_2F_2O(F,O)$. *Sov. Phys. Crystallogr.* **8**, 406-413.

SIMONOV, V.I. & BELOV, N.V. (1960): The determination of the structure of seidozerite. *Sov. Phys. Crystallogr.* **4**, 146-157.

SPEER, J.A. (1984): Micas in igneous rocks. *In* Micas (S.W. Bailey, ed.). *Rev. Mineral.* **13**, 299-356.

SPRAY, J.G. & RAE, D.A. (1995): Quantitative electron-microprobe analysis of alkali silicate

glasses: A review and user guide. *Can. Mineral.* **33**, 323-332.

SUNDVOLL, B., LARSEN, B.T. & WANDAAS, B. (1992): Early magmatic phase in the Oslo Rift and its related stress regime. *Tectonophys.* **240**, 173-189.

_____ & _____ (1990): Rb-Sr isotope systematics in the magmatic rocks of the Oslo Rift. *Norg. Geol. Unders.* **418**, 27-48.

TAYLOR, R. (1999): *The crystal chemistry of amphiboles from Mont Saint-Hilaire, Québec.* B.Sc. thesis, Laurentian University, Canada.

TIKHONENKOV, I.P. (1963): *Nepheline syenites and pegmatites of the northern part of the Khibina massif and the role of postmagmatic occurrences in their formation.* Editorial House of the USSR, Moscow. 247.

_____ (1964): Zirconium minerals. *In* Geochemistry, mineralogy and genetic types of deposits of rare elements. Vol. II: Mineralogy of rare elements. Izd-vo Nauka, Russia.

VALTER, A.A., ERYOMENKO, G.K. AND LEESENKO, T.A. (1965): Kupletskite from the alkaline rocks of the Azov Region. *Min. Sborn.* **19**, 248-252.

VARD, E. & WILLIAMS-JONES, A.E. (1993): A fluid inclusion study of vug minerals in dawsonite-altered phonolite sills, Montréal, Québec: Implications for HFSE mobility. *Contrib. Mineral. Petrol.* **113**, 410-423.

VORONKOV, A.A. & PYATENKO, A. (1962): The crystal structure of vlasovite. *Sov. Phys. Crystallogr.* **6**, 755-760.

VRUBLEVSKAYA, Z.V. AND ZVYAGIN, B.B. (1976): Diffraction characteristics of polytypic forms of astrophyllite. *Sov. Phys. Crystallogr.* 21, 546-549.

WALLACE, G.M., WHALEN, J.B. & MARTIN, R.F. (1990): Agpaitic and miaskitic nepheline syenites of the McGerrigle plutonic complex, Gaspe, Québec: An unusual petrological association. *Can. Mineral.* **28**, 251-266.

WATSON, B.E. (1979): Zircon saturation in felsic liquids: experimental results and applications to trace element geochemistry. *Contrib. Mineral. Petrol.* **70**, 407-419.

WIGHT, Q. & CHAO, G.Y. (1986): Mont Saint-Hilaire Revisited. *Rocks and Minerals* **61**, 182-197.

WOODROW, P.J. (1967): The crystal structure of astrophyllite. *Acta Crystallogr.* **22**, 673-678.

WOOLEY, A.R. AND PLATT, G.R. (1988): The peralkaline nepheline syenites of the Junguni intrusion, Chilwa province, Malawi. *Mineral. Mag.*, **52**, 425-433.

YAMNOVA, N.A., EGOROV-TISMENKO, YU.K. AND PEKOV, I.V. (1998): Crystal structure of perraultite from the Coastal Region of the Sea of Azov. *Crystallogr. Rep.* **43**, 401-410.

_____ & _____ (2000): Refined crystal structure of iron rich triclinic astrophyllite. *Kritallographia* **N4-45**, 642-647 (in Russian).

ZAK, S.I., KAMENEV, E.A. & MINAKOV, F.V. (1972): *The Khibina Alkaline Massif.* Nedra, Moscow, 175 p.

ZHESHENG, M., GUOWU, L., NICHENG, S., HUYUN, Z., DANIAN, Y. & PUSHCHAROVSKY, D.Y. (2000): Structure refinement of astrophyllite. *Sci. China.* **30D**, 399-406 (in Chinese).

ZVYAGIN, B.B. AND VRUBLEVSKAYA, Z.V. (1976): Polytypic forms of astrophyllite. *Sov. Phys. Crystallogr.* **21**, 542-545.

APPENDIX A.

SAMPLE DESCRIPTIONS

SAMPLE DESCRIPTIONS OF AGM FROM NORWAY					
Sample	Collection #	Location	Rock Type	Description	Associated Minerals
NOR1	RW1	Vesle Aroya, Langesundsfjorden, Larvik, Vestfold, Norway	nepheline syenite pegmatite in larvikite	coarse grained (3.0 x 2.5 cm ave.), dark brown to bronze, tabular to platy books embedded in microcline and intergrown with aegirine needles (commonly perpen. to astrophyllite cleavage)	aegirine microcline
NOR2	RW2	Barkevikskjaer, Langesundsfjorden, Larvik, Vestfold, Norway	nepheline syenite pegmatite in larvikite	coarse grained (1.5 x 0.8 cm ave.) dark brown to golden brown, tabular crystals embedded in microcline and albite SEM work shows small zircon inclusions	aegirine microcline albite zircon
NOR3	RW3	Gjerdingen, Nordmarka, Oppland Province, Norway	ekerite - alkali granite	light brown to orange-brown, medium grained (0.3 x 0.1 cm ave.) subhedral, tabular to platy crystals embedded in matrix and in vugs	elpidite (red), nenadkevichite narsarsukite, brookite anatase, gearksutite ralstonite, aegirine, quartz microcline
NOR4	LHN1	Vesle Aroya, Langesundsfjorden, Norway	nepheline syenite pegmatite in larvikite	grain separate - dark brown to red brown, tabular crystals	microcline, albite, aegirine SEM indicates sphalerite and biotite inclusions
NOR5	LHN2	Barkevik, Langesundsfjorden, Norway	nepheline syenite pegmatite larvikite	grain separate - very coarse, dark brown crystals up to 2 cm in length	SEM indicates albite inclusions
NOR6	CMNMI 44294	Brevik, Telemark Co. Norway	nepheline syenite pegmatite in larvikite	grain separate - very coarse grained, dark brown to reddish-brown, platy crystals	SEM indicates zircon, albite and titanite inclusions
NOR7	AOL1	Bronnebukta, Siktesoya, Langesundsfjorden, Norway	nepheline syenite pegmatite in larvikite	coarse grained, dark brown, tabular to platy, anhedral grains embedded in matrix	microcline, muscovite nepheline, natrolite
NOR8	AOL2a	Barkevikskjaer, Langesundsfjorden, Norway	nepheline syenite pegmatite in larvikite	tabular to prismatic, yellow-brown, coarse grained crystals (1.1 x 0.1 cm ave.) slightly radiating pattern embedded in matrix	aegirine, microcline biotite
NOR9	AOL2b	Barkevikskjaer,	nepheline syenite pegmatite	coarse grained (up to 3.5 x 1.5 cm),	albite, microcline

		Langesundsfjorden, Norway	in larvikite	dark brown, tabular, subhedral crystals	
				embedded in a very coarse grained	
				albite matrix	
NOR10	AOL3	Saga I Quarry, Morje,	nepheline syenite pegmatite	pegmatitic, monomineralic specimen	microcline, albite
		Porsgrunn, Norway	in larvikite	dark brown to orange brown, blocky	aegirine
				crystals	
NOR11	AOL4	Tuften Quarry, Tvedalen,	nepheline syenite pegmatite	pegmatitic, dark brown, tabular to	small inclusions of aegirine
		Larvik, Norway	in larvikite	blocky crystal in microcline	microcline
NOR12	AOL5	Vesle Aroya	nepheline syenite pegmatite	coarse grained, dark brown, blocky	aegirine, annite
		Langesundsfjorden, Norway	in larvikite	crystals (2.9 x 2.1 cm ave.)	albite, leifite
NOR13	AOL6	Lysebo, Larvik, Norway	nepheline syenite pegmatite	reddish brown, platy crystals (0.9 x 0.5 ave.)	microcline, aegirine
		(east of Langesundsfjord)	in lardalite	embedded in microcline	catapleiite, natrolite, albite
NOR14	AOL7	Bratthagen, Lagendalen	nepheline syenite pegmatite	medium grained (0.5 x 0.3 cm ave.), brown	aegirine
		Larvik, Norway	in lardalite	to reddish-brown, anhedral, tabular	analcime
				crystals with a bronze luster	microcline
				embedded in matrix but concentrated	
				along fractures and small vugs	
				overgrowing aegirine	
NOR15	LHN3	Vesle Aroya	nepheline syenite pegmatite	coarse grained grain separate	none
	HC#726	Langesundsfjord, Norway	in larvikite	orange-brown, platy crystals	
NOR16	LHN4	Teinaholmen	unknown	grain separate	none
	HC#837	Langesundsfjord, Norway	pegmatite	dark red-brown, coarse grained, platy	
				(up to 0.5 cm)	
NOR17	LHN5	Gjerdingen, Nordmarka,	alkali granite	grain separate	none
		Oppland Province, Norway		light brown, platy (same as NOR3)	
NOR18	AOL8	Vora, Vesteroya	pegmatite in Langesundsfjord	very coarse grained, dark red-brown	aegirine
		Sandefjord	complex	anhedral masses of platy crystals	
NOR19	#28647				
	Oslo Geol.	Island of Laven	nepheline syenite	grain separate	none
	Museum	Langesundsfjord, Norway	pegmatite	dark red-brown, up to 1.5 cm wide and	
				0.3 cm thick	
				platy crystals	

NOR20	AOL10	Luksefjell district	alkali granite	reddish-brown, coarse-grained plates	quartz
		(30-40 km N of Langesundsfjord)	pegmatite hosted in	ave. 1.5 x 1.0 cm	perthitic feldspar
			larvikite	highly altered/oxidized to a black/brown	sodic amphibole and a
				coating	hornblende
				pegmatite grains rimmed by quartz and	minor plagioclase
				embedded in matrix	
				anhedral grains within granite host	
NOR21	AOL11	Luksefjell district	alkali grainite	red-orange, anhedral, platy grains	quartz, perthitic feldspar
		(30-40 km N of Langesundsfjord)	pegmatite hosted in	up to 0.2 x 0.2 cm	2 amphiboles
			larvikite		

SAMPLE DESCRIPTIONS OF AGM FROM USA					
Sample	Collection #	Location	Rock Type	Description	Associated Minerals
US1	CMNMI	Mount Rosa	quartz pegmatite	grain separate	inclusions of ilmenorutile
	44288	St. Peter's Dome, Pike's Peak	in alkali granite	dark yellow-brown, very coarse grained	
		El Paso Co., Colorado		platy, up to 2 cm long	
				slightly altered/oxidized with a	
				white coating	
US2	CMNMI	Mount Rosa	quartz pegmatite	same as US1	none
	49977	St. Peter's Dome, Pike's Peak	in alkali granite		
		El Paso Co., Colorado			
US3	KGD11	Mount Rosa	quartz pegmatite	very coarse grained, blocky to tabular	quartz
		St. Peter's Dome, Pike's Peak	in alkali granite	crystals interleaved with quartz	
		El Paso Co., Colorado		ave. 4.4 x 2.9 cm	
				brown-bronze colour with extensive	
				oxidation staining	
US4	CMNMC	Mount Rosa	quartz-riebeckite pegmatite	elongate, coarse grained laths of golden-	quartz, riebeckite, hematite
		St. Peter's Dome, Pike's Peak	in alkali granite	brown astrophyllite	
		El Paso Co., Colorado		ave. 2.8 x 0.7 cm	
				embedded in matrix	
US5	CMNMC	Mount Rosa	quartz pegmatite	orange-brown, coarse grained laths	quartz, albite, hematite
		St. Peter's Dome, Pike's Peak	in alkali granite	embedded in matrix	medium granular to
		El Paso Co., Colorado		ave. 2.0 x 0.3 cm	pegmatitic host
				range: 0.6 x 0.1 to 3.3 x 0.5 cm	
US6	HdL	3M Quarry, Pulaski Co.	quartz-microcline	very fine grained, acicular, radiating sprays	microcline, aegirine,
US7		Arkansas	pegmatite	of pinkish-beige AGM in vugs	biotite, fluorite, amphibole,
US8				silky lustre	quartz
US9		Point of Rocks, Cofax Co.	nepheline syenite	very fine grained, acicular sprays in a vug	nepheline, cancrinite, aegirine
		New Mexico		light brown to beige	microcline

SAMPLE DESCRIPTIONS OF AGM FROM RUSSIA					
Sample	Collection #	Location	Rock Type	Description	Associated Minerals
RUS1	PCP	Khibina massif	nepheline syenite	radiating, dark orange-brown laths	perthitic feldspar, plagioclase
		Kola Peninsula	pegmatite	ave. 3..0 x 0.15 cm	nepheline, sodic amphibole,
				unaltered, pristine crystals as a primary	hornblende
				phase in the matrix	
RUS2	PCP	Khibina massif	nepheline syenite	radiating, dark red-brown laths embedded	eudialyte, aegirine, nepheline
		Kola Peninsula	pegmatite	in matrix	(alkali feldspar)
				individual crystals: 2.3 x 0.1 cm	
				intergrown with fibrous aegirine	
				subhedral	
				radiation halos common	
RUS3	CMNMI	Khibina massif	trachytic nepheline	tabular to lath-like, bright orange,	microcline
	44135	Kola Peninsula	syenite	subhedral crystals	subhedral/euhedral nepheline
				trachytic texture defined by astrophyllite	aegirine, amphibole
				also large clots of astrophyllite	matrix is coarse grained,
				individual crystals: 0.7 x 0.075 cm	granular, unaltered
RUS4	CMNMI	Khibina massif	nepheline syenite	grain separate	eudialyte, aegirine, microcline
	53187	Kola Peninsula	pegmatite	dark red-brown, platy, coarse grained	
RUS5	CMNMI	Khibina massif	nepheline syenite	grain separate	aegirine
	44295	Kola Peninsula	pegmatite	dark red-brown, platy, coarse grained	
RUS6	CMNMI	Khibina massif	?	grain separate	none
	53309	Kola Peninsula		fibrous to acicular, yellow-green	
				matted grains	
RUS7	CMNMC	Eveslogchorr Mt.	nepheline syenite	platy, dark red-brown, pegmatitic grains	eudialyte, microcline, albite
		Khibina massif	pegmatite	up to 0.9 x 0.9 cm	amphibole
		Kola Peninsula		anhedral masses	
				intergrown with acicular, bent, amphibole	
RUS8	FMMI	Eveslogchorr Mt.	nepheline syenite	coarse grained, tabular to bladed,	aegirine, microcline, amphibole
		Khibina massif	pegmatite	parallel aggregates (slightly radiating)	
		Kola Peninsula		dark red-brown, highly vitreous	
				average: 1.3 x 0.15 cm	
RUS9	HC#1048	Lephke-Nelm	nepheline syenite	coarse grained, dark brown-black	microcline, natrolite,

		Lovozero massif	pegmatite	blocky crystals	eudialyte, aegirine
		Kola Peninsula		grain separate	
RUS10	HC	Mt. Koashua	?	very fine grained, yellow powdery material	villiaumite, pectolite
		Khibina massif			
		Kola Peninsula			
RUS11	PT	Mount Yukspor	?	brownish green-yellow	none
		Khibina massif		fibrous, matted, very fine grained	
		Kola Peninsula		<0.01 mm	
RUS12	#56274	Mount Kuivchorr	nepheline syenite	coarse grained, anhedral, dark brown	none
	Fersmann	Lovozero massif	pegmatite	crystals (grain separate)	
	Museum	Kola Peninsula		holotype kupletskite originally described	
				by Semenov (1956)	

SAMPLE DESCRIPTIONS FOR AGM FROM GREENLAND					
Sample	Collection #	Location	Rock Type	Description	Associated Minerals
CC1	NAN-A-CC1	Nanna pegmatite	nepheline syenite	platy, subhedral, up to 5 cm	feldspar, aegirine, natrolite
		Narssarssuk, Gardar Province	pegmatite	brown	nafertisite, analcime
					catapleiite
CC2	KR-A-CC2	Kraemer Island	syenite pegmatite	platy and fibrous, orange-brown	quartz, orthoclase, plagioclase
		Kangerdlugssuaq		1.0 to 3.0 cm	arfvedsonite, zircon, ilmenite
CC3	KV-A-CC3	Kvanefjeld, Illimaussaq	alkaline syenite	elongate	perthitic feldspar, nepheline
		Gardar Province		1.0 x 0.05 cm, red-brown	arfvedsonite, aegirine, quartz,
					kataphorite
CC4	AS-A-CC4	Astrophyllite Island	quartz pegmatite	platy	plagioclase, microcline
		Kangerdlugssuaq		0.5 to 1.5 cm, subhedral, brown	quartz, aegirine, arfvedsonite
					ilmenite, eudialyte
CC5	BA-A-CC5	Bagnaesset	schistose nepheline	elongate	nepheline, plagioclase
		Kangerdlugssuaq	syenite	0.5 to 1.5 cm long x 0.05 to 0.2 cm wide	aegirine, microcline, zircon
				red-brown	biotite
CC6	KR-A-CC6	Kraemer Island	peralkaline	fine grained (<2mm)	quartz, perthitic K-feldspar
		Kangerdlugssuaq	granite	brown	aegirine, arfvedsonite
CC7	BA-A-CC7	Bagnaesset	nepheline syenite	tabular and elongate	perthitic K-feldspar, nepheline
		Kangerdlugssuaq	pegmatite	Primary: 3.0 x 0.3 x 0.05 cm, brown,	aegirine, eudialyite, kataphorite
				subhedral to euhedral	
				Secondary: aggregates of tabular xtals	
				<0.2 cm, brown	
CC8	AM-K-CC8	Amdrup Fjord	alkaline syenite	platy, anhedral to sudbhedral	potassium feldspar, aegirine
		Kangerdlugssuaq	pegmatite	0.1 to 0.5 cm, brown	perthitic feldspar, lavenite,
					catapleiite, hjordahlite
					eudialyte, kentbrooksite
CC10	NAR-A-CC10	Narssarssuk	quartz pegmatite	euhedral laths up to 10 cm long	quartz, feldspar, aegirine
		Gardar Province		brown	calcite, rhodochrosite
					apatite
CC11	SI-A-CC11	Sioarssuite	alkaline syenite	elongate, 0.1 to 0.3 cm	potassium feldspar, aegirine
		Illimaussaq		brown	nepheline, titanite

CC12	NAN-A-CC1	Nanna pegmatite	nepheline syenite	acicular, fibrous, brown	feldspar, aegirine, natrolite
		Narssarssuk, Gardar Province	pegmatite		nafertisite, analcime
					catapleiite
CC13	NAN-A-CC1	Nanna pegmatite	nepheline syenite	platy to bladed, brown	feldspar, aegirine, natrolite
		Narssarssuk, Gardar Province	pegmatite	5.0 x 0.5 cm	nafertisite, analcime
					catapleiite
Sample data taken from Christiansen (1998)					

SAMPLE DESCRIPTIONS FOR AGM FROM MISCELLANEOUS LOCALITIES					
Sample	Collection #	Location	Rock Type	Description	Associated Minerals
AFR1	OVP	Zomba-Malosa	quartz pegmatite	coarse grained, thick (0.6 cm) vein of	quartz, microcline
		Chilwa alkaline province		AGM crosscutting matrix of quartz and	ilmenorutile, corroded
		Malawi, Africa		microcline	amphibole
				AGM is highly altered/oxidized and	
				exhibits strong zonation under BSEI	
				vein is weakly foliated	
				dark brown, platy	
AFR3	HC	Junguni Hill, Zomba	nepheline syenite	fine grained, interstitial, acicular to lath-like	nepheline, perthitic feldspar,
		Chilwa alkaline province		orange-brown, 0.75 x 0.1 mm	aegirine, sodalite, biotite
		Malawi, Africa			
LAB1	M26148	Ten Mile Lake, Seal Lake	peralkaline gneiss	brown-orange, very fine grained (<0.5 mm)	quartz, barylite, aegirine
	ROM	Labrador, Canada		acicular, foliated	REE phosphates
LAB2	GSC62047	Letitia Lake, Mann #1	peralkaline gneiss	very fine grained (0.2 x 0.025mm), acicular	quartz, barylite, microcline,
		Labrador, Canada		dark orange-brown	calcic amphibole and a
				granoblastic felsic matrix with foliation	potassic-iron amphibole
				defined by amphibole and Nbt	REE phosphates

SAMPLE DESCRIPTIONS OF AGM FROM MONT SAINT-HILAIRE					
Sample	Collection #	Location	Rock Type	Description	Associated Minerals
MSH1	NMNS-1	East Hill Suite, Mont Saint-Hilaire, Quebec	nepheline syenite pegmatite	very fine grained (<1.0 mm), purple to brown, subhedral, tabular crystals transparent to translucent intergrown with rhodochrosite coated by a white unknown powder	euhedral rhodochrosite polylithionite catapleiite, aegirine albite, ancylite
MSH2	NMNS-4	East Hill Suite, Mont Saint-Hilaire Quebec	nepheline syenite pegmatite	very fine grained (<1.0 mm), platy, transparent brown-grey crystals micron-scale black inclusions intergrown with albite and rhodochrosite	rhodochrosite calcite, polylithionite ancylite, genthelvite primary and secondary aegirine
MSH3	NMNS-5	East Hill Suite, Mont Saint-Hilaire	nepheline syenite pegmatite	coarse grained, tabular to platy crystals (0.9 cm long x 0.35 cm wide average) light to dark brown colour lighter brown on cleavage surfaces intimately associated with aegirine - appear to be coexisting overgrown by tetranatrolite	aegirine natrolite, tetranatrolite albite catapleiite (SEM shows pyrochlore inclusions within grains)
MSH4	NMNS-6ab	East Hill Suite, Mont Saint-Hilaire Quebec	nepheline syenite pegmatite	dark red-brown, tabular to platy crystals (1.6 x 1.5 cm in largest book) penetrated by prismatic aegirine overgrowing primary, corroded aegirine and in a reaction with serandite	primary and secondary aegirine serandite white mica analcime, rhodochrosite microcline, albite, natrolite (SEM shows zircon inclusions mantled by pyrochlore)
MSH5AB	NMNS-7ab	East Hill Suite, Mont Saint-Hilaire Quebec	nepheline syenite pegmatite	5A - coarse grained (0.75 cm), tabular, dark brown, slightly radiating crystals 5B - same as 5a but with light grey-purple rims replaced by fibrous aegirine, analcime in one vug	aegirine, albite, natrolite, analcime, microcline
MSH6	NMNS-8	East Hill Suite, Mont Saint-Hilare Quebec	nepheline syenite pegmatite	very coarse grained (2.1 x 0.3 cm), prismatic to tabular, light brown to gold crystals penetrated by aegirine	aegirine natrolite, tetranatrolite albite, catapleiite
MSH7	NMNS-11	East Hill Suite, Mont Saint-Hilaire Quebec	nepheline syenite pegmatite	very coarse grained (up to 3.5 cm long, 0.1 to 0.2 cm wide), prismatic to tabular,	natrolite, aegirine albite, microcline

				yellow to golden brown crystals	
				intergrown with aegirine and natrolite	
MSH8	NMNS-12	East Hill Suite, Mont Saint-Hilaire	altered nepheline	dark, red-brown, platy crystals (0.5 x 0.8 cm)	primary and secondary aegirine
		Quebec	syenite pegmatite	subhedral to euhedral	(primary aegirine appears to
					be breaking down)
					natrolite, albite,
					leucophanite, microcline
					genthelvite, epididymite
					white mica
MSH9	NMNS-13	East Hill Suite, Mont Saint-Hilaire	nepheline syenite pegmatite	purplish-brown/black, fine grained,	coarse grained rhodochrosite
		Quebec		blocky, subhedral crystals up to 1 mm wide	aegirine
				also occurs as fibrous sprays in vugs	albite, calcite,
MSH10AB	NMNS-14	East Hill Suite, Mont Saint-Hilaire	nepheline syenite pegmatite	10A - dark brown, platy, coarse grained	microcline, aegirine
		Quebec		10B - lighter brown, slightly fibrous,	rhodochrosite
				crystals which occur as rims on 10a	
MSH11	NMNS-15	East Hill Suite, Mont Saint-Hilaire	nepheline syenite pegmatite	grain separate - dark brown, tabular to	rhodochrosite
		Quebec		platy, coarse grained (2.2x2.1x0.5 cm)	trace aegirine, analcime, albite
				crystals	
MSH12	NMNS-16	East Hill Suite, Mont Saint-Hilaire	nepheline syenite pegmatite	coarse grained (1.0x0.2 cm), tabular,	microcline, albite
		Quebec		slightly radiating crystals	aegirine, analcime
				dark red-brown	rhodochrosite, natrolite
				locally pale brown and fibrous	ancylite, fluorite, calcite
					altered amphibole
MSH13	NMNS-17	East Hill Suite, Mont Saint-Hilaire	nepheline syenite pegmatite	fine grained, radiating, dark red-brown	euhedral rhodochrosite,
		Quebec		crystals (0.2 x 0.1 cm) in vugs	albite, microcline, natrolite
					green fluorite, aegirine
					ancylite
MSH14	NMNS-20ab	East Hill Suite, Mont Saint-Hilaire	nepheline syenite pegmatite	coarse grained (0.9 x 0.1 cm ave.), randomly-	aegirine, microcline
		Quebec		oriented to slightly radiating, tabular to	serandite, rhodochrosite
				prismatic, dark brown crystals	tetranatrolite, albite
				embedded in microcline	polylithionite
MSH15	NMNS-22	East Hill Suite, Mont Saint-Hilaire	nepheline syenite pegmatite	grain separate - dark brown, coarse grained,	aegirine, euhedral natrolite
		Quebec		random mosaic of grains	tetranatrolite
				lighter brown bands on edges	

				crystal growth orientation appears to	
				have changed continuously	
MSH16	NMNS-23	East Hill Suite, Mont Saint-Hilaire	nepheline syenite pegmatite	small (0.1 x 0.075 cm), blocky clusters of	microcline, rhodochrosite
		Quebec		reddish-brown crystals overgrowing	natrolite, tetranatrolite
				aegirine	sphalerite, ancylite, fluorite
MSH17	NMNS-24	East Hill Suite, Mont Saint-Hilaire	nepheline-amphibole	coarse grained (2.6 x 2.2 cm), platy, dark	strongly corroded amphibole
		Quebec	syenite pegmatite	red-brown, anhedral crystals	microcline, aegirine, natrolite
				commonly zoned with both dark and	albite, analcime, eudialyte,
				light bands - varying growth directions	catapleiite, tetranatrolite
					helvite
MSh18AB	NMNS-25	East Hill Suite, Mont Saint-Hilaire	altered nepheline	18A - coarse grained, platy, dark brown	microcline, aegirine, calcite
		Quebec	syenite pegmatite	grains which do not appear altered	ancylite, catapleiite
				18B - fibrous, light brown, altered grains	siderite
				AGM growing in aegirine cavity	
MSH19AB	NMNS-26	East Hill Suite, Mont Saint-Hilaire	nepheline syenite pegmatite	19A - fresh, platy, dark brown crystals	aegirine, calcite
		Quebec		(0.9 x 0.4 cm ave.)	albite
				19B - light brown-yellow, fibrous coating	
				on 19A	
MSH20	NMNS-27	East Hill Suite, Mont Saint-Hilaire	nepheline syenite pegmatite	brown-black with a purplish tint (more	primary and secondary aegirine
		Quebec		visible in thin section)	serandite, catapleiite
				medium grained (0.3 x 0.2 cm) and tabular	purple fluorite, natrolite
MSH21	NMNS-29	East Hill Suite, Mont Saint-Hilaire	sodalite xenolith (?)	prismatic to tabular, slightly radiating,	sodalite, rhodochrosite, calcite
		Quebec	pegmatitic metasomatic	(0.7 x 0.15cm ave.) predominantly in vugs	pyrite, chalcopyrite, fluorite
			unit	golden brown to dark brown in colour	aegirine, albite, microcline
MSH22	NMNS-31	East Hill Suite, Mont Saint-Hilaire	pegmatite	coarse grained (1.1 x 1.1 cm ave.), dark	natrolite, tetranatrolite
		Quebec		brown, random aggregates of crystals	primary and secondary aegirine
				penetrated by primary aegirine	catapleiite
MSH23AB	NMNS-32ab	East Hill Suite, Mont Saint-Hilaire	altered nepheline	23A - coarse grained, platy (1.9 x 1.2 cm),	aegirine, catapleiite
		Quebec	syenite pegmatite	dark brown, anhedral crystals	birnessite, natrolite
				rimmed by 23B	tetranatrolite, rhodochrosite
				23B - a fibrous, light brown-orange rim	calcite, ancylite, chamosite
				(0.3 cm wide) around 23A	
MSH24	CMNMC	East Hill Suite, Mont Saint-Hilaire	aplite/nepheline syenite	light golden brown, slightly radiating,	coarse grained elpidite

	Exchange	Quebec	pegmatite	fibrous crystals (up to 0.3 cm long)	microcline, sphalerite
				more commonly as a very fine grained,	serandite, aegirine
				powdery coating	galena, pyrochlore
					albite
MSH25	CMNMC	East Hill Suite, Mont Saint-Hilaire	altered nepheline	very pale golden brown, fibrous to	birnessite, tetranatrolite
	Exchange	Quebec	syenite pegmatite	prismatic 'haystack' sprays	calcite, aegirine
				commonly coated with birnessite	microcline
MSH26AB	CMNMC	East Hill Suite, Mont Saint-Hilaire	sodalite syenite	26A - dark brown, platy grains (0.4 x 0.4 cm)	aegirine, calcite
	Exchange	Quebec		26B - golden brown, fibrous grains at	microcline, rhodochrosite
				the rims of 26A	
MSH27	CMNMC	East Hill Suite, Mont Saint-Hilaire	nepheline syenite	fine grained (0.4 x 0.1 cm), reddish-brown,	aegirine, microcline
	Exchange	Quebec	pegmatite with aplite	tabular to prismatic, radiating sprays	hackmanite, eudialyte
				embedded in matrix	annite, sulphides
					nepheline, rhodochrosite
MSH28	CMNMC	East Hill Suite, Mont Saint-Hilaire	metasomatic unit	medium grained (0.7 x 0.3 cm ave.), tabular	aegirine, sodalite
	Exchange	Quebec		to platy porphyroblasts in very fine grained	nepheline porphyroblasts
				hornfels	carbonate
				bright orange-brown colour	
MSH29	CMNMC	East Hill Suite, Mont Saint-Hilaire	metasomatic unit	identical to MSH28	identical to MSH28
	Exchange	Quebec			
MSH30	CMNMC	East Hill Suite, Mont Saint-Hilaire	natrolite	acicular, radiating sprays of light brown-	microcline, albite
	Exchange	Quebec	pegmatite	bronze crystals (0.5 x 0.02 cm ave.)	natrolite, analcime
				in vugs and embedded in microcline	aegirine
MSH31	CMNMC	East Hill Suite, Mont Saint-Hilaire	natrolite	dark brown, acicular, radiating sprays	pegmatitic analcime
	F88-2	Quebec	pegmatite	up to 2 cm long (xtals 0.01-0.02 cm wide)	microcline
				in vugs and embedded in microcline,	aegirine, rhodochrosite
				analcime and altered amphibole	altered amphibole
MSH32	CMNMC	East Hill Suite, Mont Saint-Hilaire	natrolite	light brown/bronze, acicular, radiating	pegmatitic natrolite
	Exchange	Quebec	pegmatite	sprays (crystals 0.9 x 0.02 cm ave.)	microcline, aegirine
				in vugs and after amphibole	altered amphibole
					rhodochrosite, albite
MSH33	CMNMC	East Hill Suite, Mont Saint-Hilaire	aplite/pegmatite	prismatic to tabular, dark brown to	aegirine, microcline
	Exchange	Quebec		golden brown, coarse grained	sodalite

				(1.7 x 0.15 cm ave.)	
				radiating sprays with curved or	
				bent crystals embedded in matrix	
MSH34AB	CMNMC	East Hill Suite, Mont Saint-Hilaire	nepheline syenite pegmatite	34A - tabular, medium brown (0.9 x 0.4 cm)	microcline, albite
	Exchange	Quebec		34B - yellow-brown, fibrous, acicular	nepheline, aegirine
				grains extending outwards from 34A	
				coarser grains coexisting with aegirine	
MSH35	CMNMC	East Hill Suite, Mont Saint-Hilaire	aplite/pegmatite	coarse grained, dark red-brown	microcline, aegirine, sodalite
	Exchange	Quebec		ave. 1.2 x 1.3 cm, anhedral, platy	very fine aplitic zone on end
				embedded in matrix	of sample
MSH36AB	PT96B	East Hill Suite, Mont Saint-Hilaire	altered nepheline	36A - coarse grained, tabular to platy,	microcline, aegirine
		Quebec, collected July 12, 1970	syenite pegmatite	dark reddish-brown crystals overgrown	catapleiite, ancylite
				by 36B	fluorite, wurtzite, genthelvite
				36B - silver-bronze, acicular "feathery"	
				radiating sprays overgrowing 36A	
				very fine grained (0.1 x 0.005 cm ave.)	
				"witch's broom astrophyllite"	
MSH37	KGD9	East Hill Suite, Mont Saint-Hilaire	nepheline syenite pegmatite	yellow-brown, fibrous grain separate	not known
		Quebec			
MSH38AB	CMNMC	East Hill Suite, Mont Saint-Hilaire	altered nepheline	38A - dark brown, platy, coarse-grained	aegirine, albite, microcline
	Exchange		syenite pegmatite	crystals (2.0 x 1.2 cm ave.) rimmed by 38B	birnessite, ancylite
				38B - red-brown, fibrous, almost powdery	
				rims around 38A	
MSH39AB	PT293	East Hill Suite, Mont Saint-Hilaire	nepheline syenite pegmatite	39A - coarse grained, tabular to platy,	microcline
		Quebec		dark brown crystals (0.5 x 0.5 cm ave.)	aegirine
		collected July 4th, 1994		surrounded by 39B	analcime
				39B - silky pink-beige, fibrous sprays,	
				very fine grained, surrounding 39A	
				and altered aegirine grain	
MSH40AB	PT	East Hill Suite, Mont Saint-Hilaire	altered nepheline	identical to MSH36	microcline
		Quebec	syenite pegmatite	40A - coarse grained, dark brown crystals	aegirine
				40B - fibrous, feathery, silver-bronze,	catapleiite
				radiating aggregates overgrowing 40A	
MSH41	PCP	East Hill Suit, Mont Saint-Hilaire	metasomatic unit	tabular to slightly platy crystals	matrix consists of sodalite,

		Quebec		ave. 0.56 x 0.3 mm	natrolite, clumps of aegirine,
				bright orange-red colour	Na-Mn and Na-Zr silicates
				cores are completely corroded	are alteration products of
					AGM
					pyrochlore
MSH42	PCP/AMM	East Hill Suite, Mont Saint-Hilaire	nepheline syenite	fine to medium grained, strongly zoned	aegirine, sodic amphibole
		Quebec	pegmatite	dark brown to light beige, platy	microcline
				subhedral	
				Nbkpt type specimen	
MSH43	PCP/AMM	East Hill Suite, Mont Saint-Hilaire	nepheline syenite	coarse grained, dark brown, platy crystals	arfvedsonite, albite,
		Quebec	pegmatite	ave. 0.9 x 0.8 x 0.2 cm	rhodochrosite, aegirine
				subhedral to euhedral	natrolite
MSH44	PCP/AMM	East Hill Suite, Mont Saint-Hilaire	sodalite syenite	acicular to tabular, red-orange crystals	sodalite, biotite, amphibole
		Quebec		1.2 cm long, 0.025 cm wide	
				crystals are directly adjacent to a large	
				biotite crystal	
MSH45	PCP/AMM	East Hill Suite, Mont Saint-Hilaire	sodalite syenite	fine to medium grained	aegirine, sodalite, villiaumite
		Quebec	xenolith	ave. 1.0 x 0.2 mm	nepheline, biotite
				interstitial and intergrown with aegirine	
				tabular to acicular, orange-red	
MSH46	KGD	East Hill Suite, Mont Saint-Hilaire	sodalite syenite	coarse grained (ave. 8 mm x 0.5 mm)	aegirine, biotite, sodalite
		Quebec	xenolith	acicular, radiating crystals	
				orange-red, embedded in matrix	
MSH47	JVV	East Hill Suite, Mont Saint-Hilaire	aplite	very fine grained, acicular to slightly	microcline, aegirine
		Quebec		tabular crystals in a vug	
				(ave. < 0.5 mm long)	
				beige to light brown aggregates and as	
				a coating on the aplite surface	
MSH48	PCP	East Hill Suite, Mont Saint-Hilaire	contact rock/aplite	red-brown, rosettes of tabular crystals	microcline, aegirine, biotite
		Quebec		ave. 2 mm x 0.5 mm	nepheline, sodalite
MSH49	PCP	East Hill Suite, Mont Saint-Hilaire	metasomatic unit	pegmatitic vein cross-cutting a very	matrix of vein: sodalite
		Quebec		fine grained metasomatic unit	natrolite, aegirine
				vein contains tabular to acicular AGM	

				0.4 x 0.1 cm (ave)	
				AGM are all aligned perpendicular to the	
				contacts of the vein	

APPENDIX B.

ELECTRON MICROPROBE ANALYSES

AVERAGE EMPA FOR AGM

	Malawi, Africa (AFR)									Mount Gharib, Egypt, Africa (Ref: Abdel-Rahman 1988)								
Sample	AFR1	AFR3	LAR2	UR1	UR2	UR3	UR4	UR5	UR9	R1180	R1200	R1201	R1202	R3000	R1730	R1731	R1732	R2180
#	6	3	3	8	9	4	3	3	7									
Na_2O	2.53	1.43	2.67	2.66	2.66	2.39	2.65	2.58	2.80	2.86	2.73	2.93	2.68	3.14	2.59	2.39	2.33	2.62
K_2O	5.49	6.24	5.84	5.07	5.13	5.13	4.93	5.10	5.21	6.29	6.23	6.31	6.12	5.72	6.26	6.45	6.28	6.60
Rb_2O	0.46	0.31	0.49	1.28	1.16	1.12	1.32	1.27	1.06									
Cs_2O	0.10	0.00	0.31	0.14	0.14	0.16	0.10	0.10	0.09									
CaO	0.52	1.90	0.31	0.21	0.26	0.18	0.15	0.23	0.82	0.16	0.35	0.26	0.11	0.24	0.50	0.52	0.45	0.25
SrO	0.07	0.21	0.00	0.00	0.01	0.00	0.01	0.01	0.03									
BaO	0.15	0.32	0.00	0.11	0.20	0.20	0.20	0.18	0.00									
MgO	0.00	1.15	0.00	0.04	0.06	0.05	0.00	0.05	0.21	0.03	0.02	0.08	0.01	0.02	0.04	0.04	0.03	0.02
MnO	5.17	10.18	8.76	3.44	3.40	3.46	5.09	4.78	23.25	1.46	1.37	1.36	1.32	1.55	1.35	1.23	1.63	1.39
FeO	30.03	24.63	24.20	30.06	29.40	30.07	27.28	28.45	11.00	35.26	34.54	34.79	35.82	34.42	34.91	34.85	34.98	35.07
ZnO	0.50	0.00	0.06	1.85	2.05	2.05	3.77	2.52	0.00	0.31	0.39	0.33	0.52	0.89	0.31	0.57	0.53	0.20
Al_2O_3	0.44	1.73	1.16	0.22	0.33	0.25	0.19	0.16	0.67	1.10	0.69	0.88	0.98	0.43	0.97	1.00	1.06	0.84
Y_2O_3	0.00	0.00	0.00	0.00	0.00	0.00	0.00	0.00	0.00									
Cr_2O_3	0.06	0.06	0.07	0.06	0.06	0.04	0.00	0.00	0.00									
TiO_2	7.48	9.55	3.23	9.89	8.12	8.76	9.37	9.77	8.97	6.65	9.74	8.22	8.07	9.23	6.92	7.38	7.44	8.91
SnO_2	1.80	0.00	0.00	0.75	0.91	1.02	0.55	0.42	0.00	0.20	0.16	0.18	0.21	0.44	0.19	0.08	0.09	0.12
ZrO_2	2.59	2.71	0.00	0.00	1.44	0.82	0.51	0.63	0.49	2.57	2.24	2.13	2.11	1.61	2.92	2.62	2.99	1.64
HfO_2	0.18	0.05	0.00	0.04	0.16	0.21	0.06	0.05	0.00									
Nb_2O_5	2.03	1.02	14.15	3.21	3.87	3.46	3.34	2.62	3.56	3.82	1.50	4.00	4.28	2.01	3.73	3.44	3.29	3.82
Ta_2O_5	1.18	0.86	0.10	0.00	0.00	0.00	0.00	0.00	0.00									
SiO_2	33.98	33.13	34.00	34.83	34.26	34.60	34.97	34.86	34.90	35.61	35.74	34.98	35.03	35.50	34.82	35.06	34.53	35.26
F	1.05	1.17	0.14	1.12	1.33	1.39	1.45	1.34	1.08	0.92	1.46	1.35	0.81	1.77	0.78	1.06	1.17	1.46
H_2O	2.76	2.77	2.80	2.75	2.62	2.61	2.61	2.65	2.79	2.93	2.69	2.74	3.01	2.52	2.96	2.84	2.78	2.70
O=F	-0.44	-0.49	-0.06	-0.47	-0.56	-0.58	-0.61	-0.57	-0.45									
Total	98.09	98.14	98.03	97.63	97.31	97.35	97.94	97.21	96.47	100.16	99.85	100.54	101.08	99.49	99.25	99.53	99.58	100.90
Chemical formulae calculated based on 31 cations																		
Na_{tot}	1.13	0.63	1.19	1.18	1.19	1.06	1.17	1.14	1.23	1.22	1.15	1.24	1.14	1.33	1.12	1.03	1.00	1.10
Na	0.13	0.07	0.00	0.00	0.00	0.00	0.00	0.00	0.07	0.08	0.00	0.00	0.05	0.13	0.07	0.00	0.01	0.00
K	1.61	1.80	1.72	1.48	1.51	1.50	1.43	1.69	1.51	1.77	1.73	1.76	1.71	1.60	1.78	1.82	1.78	1.83
Rb	0.07	0.05	0.07	0.19	0.17	0.16	0.19	0.19	0.16									
Cs	0.01	0.00	0.03	0.01	0.01	0.02	0.01	0.01	0.01									
Sr	0.01	0.03	0.00	0.00	0.00	0.00	0.00	0.00	0.00									
Ba	0.01	0.03	0.00	0.01	0.02	0.02	0.02	0.02	0.00									
Sum A	1.84	1.97		1.69	1.71	1.70	1.65	1.70	1.75	1.85	1.73	1.76	1.76	1.73	1.85	1.82	1.79	1.83
Na	0.87	0.54	0.92	0.95	0.94	0.96	0.96	0.94	0.78	0.96	0.92	0.94	0.97	0.94	0.88	0.88	0.89	0.94
Ca	0.13	0.46	0.08	0.05	0.06	0.04	0.04	0.06	0.20	0.04	0.08	0.06	0.03	0.06	0.12	0.12	0.11	0.06
Sum B	1.00	1.00		1.00	1.00	1.00	1.00	1.00	0.98	1.00	1.00	1.00	1.00	1.00	1.00	1.00	1.00	1.00
Na	0.13	0.02	0.00	0.27	0.30	0.20	0.20	0.21	0.37	0.18	0.38	0.31	0.11	0.26	0.17	0.21	0.10	0.34
Mg	0.00	0.39	0.00	0.01	0.02	0.02	0.00	0.02	0.07	0.01	0.01	0.03	0.00	0.01	0.01	0.01	0.01	0.01
Mn	1.01	1.95	1.71	0.67	0.66	0.67	0.98	0.92	4.47	0.27	0.25	0.25	0.25	0.29	0.26	0.23	0.31	0.26
Fe^{2+}	5.78	4.65	4.67	5.74	5.66	5.76	5.18	5.43	2.00	6.49	6.30	6.36	6.55	6.30	6.51	6.45	6.50	6.37
Zn	0.09	0.00	0.01	0.31	0.35	0.35	0.63	0.42	0.00	0.05	0.07	0.05	0.08	0.14	0.05	0.09	0.09	0.03
Y	0.00	0.00	0.00	0.00	0.00	0.00	0.00	0.00	0.00									
Ca	0.00	0.01	0.01	0.01	0.00	0.00	0.00	0.00	0.00									
Sum C	7.01	7.00	6.40	7.00	7.00	7.00	7.00	7.00	7.00	7.00	7.00	7.00	7.00	7.00	7.00	7.00	7.00	7.00
Ti	1.29	1.62	0.56	1.56	1.41	1.51	1.60	1.68	1.53	1.10	1.60	1.35	1.33	1.52	1.16	1.23	1.24	1.46
Sn	0.17	0.00	0.00	0.07	0.08	0.09	0.05	0.04	0.00	0.02	0.01	0.02	0.02	0.04	0.02	0.01	0.01	0.01
Zr	0.29	0.30	0.00	0.00	0.16	0.00	0.06	0.07	0.05	0.28	0.24	0.23	0.23	0.17	0.32	0.28	0.32	0.17
Hf	0.01	0.00	0.00	0.00	0.01	0.01	0.00	0.00	0.00									
Nb	0.21	0.10	1.48	0.33	0.40	0.36	0.34	0.27	0.37	0.38	0.15	0.40	0.42	0.20	0.38	0.34	0.33	0.38
Ta	0.07	0.00	0.01	0.00	0.00	0.00	0.00	0.00	0.00									
Sum D	2.05	2.03	2.04	2.05	2.07	2.07	2.05	2.06	1.95	1.78	1.99	1.99	1.99	1.93	1.87	1.86	1.90	2.01
Si	7.82	7.48	7.83	7.95	7.89	7.93	7.95	7.95	7.93	7.84	7.79	7.65	7.67	7.78	7.77	7.77	7.67	7.66
Al	0.12	0.46	0.31	0.06	0.09	0.07	0.05	0.04	0.18	0.29	0.18	0.23	0.25	0.11	0.26	0.26	0.28	0.22
Sum T	7.94	7.94	8.15	8.01	7.98	8.00	8.00	8.00	8.11	8.13	7.97	7.88	7.92	7.89	8.02	8.03	7.95	7.87
F	0.77	0.84	0.10	0.81	0.97	1.01	1.04	0.97	0.77	0.64	1.00	0.93	0.56	1.23	0.55	0.74	0.82	1.00
OH	4.23	4.17	4.00	4.19	4.03	3.99	3.96	4.03	4.23	4.31	3.90	3.99	4.39	3.67	4.40	4.20	4.11	3.92
O	30.23	30.17	30.90	30.19	30.03	29.99	29.96	30.03	30.23	26.00	26.00	26.00	26.00	26.00	26.00	26.00	26.00	26.00
Cations	19.83	19.94	19.67	19.73	19.73	19.66	19.70	19.74	19.80	19.75	19.69	19.62	19.67	19.54	19.74	19.71	19.64	19.72

number of analyses in mean

AVERAGE EMPA FOR AGM

										Greenland (CC: Christiansen 1998)								
Sample #	R2181	R2340	R2341	R2342	R1440	R1441	R1442	R1443	R1444	CC1	CC2A	CC2B	CC3	CC4	CC5	CC6	CC7A	CC7B
Na_2O	2.72	2.51	2.56	2.79	2.57	2.68	2.66	2.51	2.42	2.60	2.64	2.39	2.97	2.78	2.28	3.53	2.69	3.15
K_2O	6.60	6.34	6.21	6.19	6.47	6.16	6.28	6.57	6.53	5.84	5.54	5.26	5.53	5.62	6.26	5.51	6.07	5.66
Rb_2O																		
Cs_2O																		
CaO	0.13	0.22	0.25	0.24	0.44	0.30	0.30	0.61	0.42	1.18	0.78	0.82	1.67	0.65	1.18	0.14	1.18	0.56
SrO																		
BaO																		
MgO	0.03	0.02	0.02	0.02	0.03	0.01	0.02	0.02	0.01	1.32	0.26	0.31	1.58	0.68	0.78	0.08	0.96	1.15
MnO	1.31	1.42	1.40	1.36	1.32	1.39	1.43	1.04	1.08	15.81	4.50	4.41	4.10	7.62	10.13	4.24	11.60	12.08
FeO	34.99	35.53	35.61	35.79	34.47	34.63	35.41	35.30	35.00	17.65	31.01	31.83	28.09	28.76	25.44	32.33	23.43	21.82
ZnO	0.34	0.28	0.34	0.38	0.01	0.25	0.11	0.35	0.28									
Al_2O_3	0.75	1.05	1.01	0.71	0.69	0.44	0.56	0.87	0.86	1.66	0.40	1.13	0.85	0.40	1.39	0.14	1.12	0.56
Y_2O_3																		
Ce_2O_3																		
TiO_2	7.63	6.98	7.99	8.80	8.11	9.48	8.03	7.93	7.69	9.45	10.52	9.25	11.40	10.63	8.65	10.28	10.24	10.84
SnO_2	0.17	0.00	0.00	0.00	0.00	0.00	0.00	0.00	0.00									
ZrO_2	1.77	1.85	1.72	1.46	2.44	2.84	3.30	2.30	2.34	1.79	0.69	0.37	0.20	0.69	4.12	0.83	1.69	1.02
HfO_2																		
Nb_2O_5	4.64	4.87	4.80	3.16	3.57	2.49	3.37	3.74	3.96	1.15	1.25	2.67	1.16	1.38	1.05	1.67	1.17	1.42
Ta_2O_5																		
SiO_2	35.02	35.33	35.28	35.99	35.41	35.77	35.53	34.40	34.51	32.98	35.58	34.58	35.47	35.70	33.90	35.87	34.90	35.94
F	1.67	0.90	0.98	1.82	0.63	1.27	1.29	1.70	1.21	0.80	0.99	1.03	0.99	0.94	1.08	1.00	0.93	0.88
H_2O	2.57	2.95	2.92	2.55	3.06	2.80	2.78	2.53	2.75	3.26	2.87	2.82	2.92	2.94	2.83	2.89	2.94	3.00
O=F										0.80	0.41	0.43	0.42	0.40	0.45	0.42	0.39	0.37
Total	100.34	100.25	100.29	101.26	99.02	100.51	101.07	99.87	99.06	94.69	96.61	96.44	96.52	98.39	98.64	98.09	98.32	98.30
Chemical formulae calculated based on 31 cations																		
Na_{tot}	1.16	1.07	1.09	1.16	1.02	1.13	1.12	1.07	1.04	1.16	1.15	1.05	1.27	1.19	0.99	1.52	1.07	1.34
Na	0.00	0.00	0.00	0.00	0.00	0.00	0.00	0.00	0.00	0.37	0.12	0.23	0.17	0.31	0.24	0.40	0.19	0.22
K	1.85	1.78	1.74	1.70	1.83	1.71	1.75	1.85	1.86	1.71	1.59	1.52	1.56	1.59	1.79	1.56	1.72	1.59
Rb																		
Cs																		
Sr																		
Ba																		
Sum A	1.85	1.78	1.74	1.70	1.83	1.71	1.75	1.85	1.86	2.08	1.71	1.75	1.73	1.90	2.03	1.96	1.91	1.81
Na	0.97	0.95	0.94	0.94	0.90	0.93	0.93	0.86	0.90	0.71	0.81	0.80	0.60	0.85	0.72	0.97	0.72	0.87
Ca	0.03	0.05	0.06	0.06	0.10	0.07	0.07	0.14	0.10	0.29	0.19	0.20	0.40	0.15	0.28	0.03	0.28	0.13
Sum B	1.00	1.00	1.00	1.00	1.00	1.00	1.00	1.00	1.00	1.00	1.00	1.00	1.00	1.00	1.00	1.00	1.00	1.00
Na	0.28	0.15	0.15	0.24	0.35	0.41	0.26	0.23	0.23	0.08	0.22	0.02	0.50	0.03	0.03	0.15	0.16	0.25
Mg	0.01	0.01	0.01	0.01	0.01	0.00	0.01	0.01	0.00	0.45	0.09	0.10	0.52	0.22	0.26	0.03	0.32	0.38
Mn	0.24	0.26	0.26	0.25	0.25	0.26	0.26	0.20	0.20	3.08	0.86	0.85	0.77	1.43	1.93	0.80	2.18	2.36
Fe^{2+}	6.41	6.54	6.53	6.44	6.40	6.29	6.45	6.51	6.52	3.39	5.83	6.03	5.21	5.32	4.78	6.02	4.34	4.01
Zn	0.06	0.05	0.06	0.06	0.00	0.04	0.02	0.06	0.05									
Y																		
Ce																		
Sum C	7.00	7.00	7.00	7.00	7.00	7.00	7.00	7.00	7.00	7.00	7.00	7.00	7.00	7.00	7.00	7.00	7.00	7.00
Ti	1.26	1.16	1.32	1.42	1.35	1.55	1.32	1.32	1.29	1.63	1.78	1.58	1.90	1.77	1.46	1.72	1.71	1.79
Sn	0.02	0.00	0.00	0.00	0.00	0.00	0.00	0.00	0.00									
Zr	0.19	0.20	0.18	0.15	0.26	0.30	0.35	0.25	0.25	0.20	0.07	0.04	0.02	0.07	0.45	0.09	0.18	0.11
Hf																		
Nb	0.46	0.48	0.49	0.31	0.36	0.24	0.33	0.37	0.40	0.12	0.13	0.28	0.12	0.14	0.11	0.17	0.12	0.14
Ta																		
Sum D	1.92	1.84	1.90	1.88	1.98	2.09	2.00	1.94	1.94	1.95	1.98	1.90	2.04	1.98	2.02	1.98	2.01	2.04
Si	7.68	7.78	7.74	7.75	7.86	7.77	7.74	7.59	7.69	7.58	7.99	7.83	7.86	7.90	7.61	7.99	7.74	7.90
Al	0.19	0.27	0.26	0.18	0.18	0.11	0.14	0.23	0.23	0.45	0.10	0.30	0.22	0.10	0.37	0.04	0.29	0.15
Sum T	7.87	8.05	8.00	7.93	8.04	7.88	7.88	7.82	7.91	8.03	8.09	8.13	8.08	8.00	7.98	8.03	8.03	8.05
F	1.16	0.63	0.68	1.24	0.44	0.87	0.89	1.19	0.85	0.80	0.70	0.74	0.69	0.66	0.76	0.71	0.66	0.61
OH	3.76	4.33	4.27	3.66	4.52	4.06	4.04	3.72	4.08	5.00	4.30	4.26	4.31	4.34	4.24	4.29	4.34	4.39
O	26.00	26.00	26.00	26.00	26.00	26.00	26.00	26.00	26.00	26.00	26.00	26.00	26.00	26.00	26.00	26.00	26.00	26.00
Cations	19.64	19.66	19.63	19.51	19.84	19.69	19.63	19.60	19.71	20.06	19.78	19.78	19.85	19.88	20.03	19.97	19.95	19.90

n number of analyses in mean

AVERAGE EMPA FOR AGM

Mont Saint-Hilaire, Québec, Canada (MSH)

Sample	CC8	CC10	CC11	CC13	MSH2	MSH3	MSH4	MSH5	MSH6	MSH7	MSH8	MSH9	MSH10A	MSH10B	MSH11	MSH12	MSH13	MSH14
#					13	10	15	9	11	7	9	8	5	6	5	6	8	6
Na_2O	2.53	3.46	1.96	2.12	3.51	3.87	3.44	3.17	2.11	2.89	3.05	3.65	2.44	2.38	2.57	2.12	2.10	2.75
K_2O	6.22	5.42	5.62	5.89	5.11	5.37	5.30	5.34	5.73	5.76	5.58	4.95	6.13	6.11	5.86	5.84	6.15	5.68
Rb_2O					0.35	0.81	0.83	0.69	0.36	0.40	0.52	0.60	0.47	0.67	0.56	0.36	0.41	0.71
Cs_2O					0.00	0.03	0.09	0.10	0.08	0.01	0.01	0.10	0.00	0.00	0.00	0.01	0.02	0.18
CaO	1.57	0.07	1.76	0.99	0.40	0.00	0.04	0.06	1.36	1.13	0.40	0.14	0.26	0.00	0.07	0.09	1.06	0.07
SrO					0.15	0.06	0.16	0.17	0.24	0.24	0.10	0.09	0.06	0.00	0.11	0.23	0.10	0.19
BaO					0.11	0.00	0.00	0.00	0.04	0.00	0.00	0.03	0.00	0.00	0.00	0.00	0.00	0.00
MgO	2.15	0.10	1.80	0.35	0.46	0.51	0.74	0.76	1.21	1.21	0.61	0.46	0.53	0.16	0.69	0.45	0.87	0.75
MnO	19.78	0.84	4.80	9.18	32.38	28.11	27.68	27.35	18.44	19.34	24.71	32.61	19.95	26.98	20.88	17.01	23.65	25.26
FeO	12.49	36.35	30.41	26.97	2.00	0.71	4.09	6.95	16.47	15.15	9.03	1.94	13.94	7.05	13.57	18.53	11.06	8.72
ZnO					0.75	5.15	1.91	0.44	0.03	0.03	1.19	0.51	0.43	0.03	0.29	0.00	0.03	0.32
Al_2O_3	1.02	0.07	1.21	1.68	0.33	0.24	0.48	0.67	1.36	1.23	0.82	0.32	1.12	1.28	1.02	0.87	1.31	0.86
Y_2O_3					0.00	0.00	0.00	0.00	0.00	0.00	0.00	0.00	0.00	0.00	0.00	0.00	0.00	0.00
Ce_2O_3					0.13	0.00	0.01	0.04	0.19	0.15	0.00	0.00	0.00	0.00	0.03	0.00	0.02	0.05
TiO_2	11.05	11.85	11.43	7.32	11.07	6.64	6.82	6.05	8.61	6.93	6.70	9.14	5.48	0.73	7.18	7.58	8.15	5.97
SnO_2					0.00	0.00	0.00	0.00	0.00	0.00	0.00	0.00	0.00	0.00	0.00	0.00	0.00	0.00
ZrO_2	1.58	0.17	0.82	4.26	0.02	0.07	1.88	2.69	3.68	5.80	0.51	0.07	1.87	4.18	0.85	4.70	0.25	2.57
HfO_2					0.02	0.00	0.02	0.00	0.00	0.22	0.00	0.00	0.00	0.00	0.00	0.12	0.00	0.00
Nb_2O_5	0.60	0.41	0.75	2.82	1.72	0.02	5.83	5.84	1.45	1.26	7.31	4.32	0.86	12.34	6.82	1.71	5.63	6.43
Ta_2O_5					0.07	0.00	0.00	0.00	0.10	0.06	0.01	0.02	0.23	0.56	0.00	0.00	0.02	0.00
SiO_2	35.37	36.19	34.43	33.83	34.66	33.66	33.45	32.47	32.34	32.80	32.77	33.89	33.14	31.75	33.52	33.04	32.85	32.91
F	1.10	0.89	1.03	0.75	1.21	0.00	0.04	0.78	1.16	1.28	0.78	1.02	0.67	0.20	0.81	1.01	0.86	0.82
H_2O	2.89	2.98	2.88	2.93	2.75	2.98	2.64	2.57	2.71	2.60	2.98	2.88	2.99	2.90	2.65	2.76	2.67	2.67
O=F	0.47	0.37	0.43	0.32	-0.51	-0.34	-0.36	-0.33	-0.49	-0.54	-0.33	-0.43	-0.28	-0.09	-0.34	-0.43	-0.36	-0.35
Total	97.88	98.41	97.66	97.99	96.71	96.34	96.61	95.82	97.17	96.35	96.36	96.11	97.06	96.82	97.55	96.80	96.84	96.57
Chemical formulae calculated based on 31 cations																		
Na_{tot}	1.07	1.48	0.84	0.94	1.54	1.75	1.55	1.45	0.94	0.95	1.38	1.62	1.10	1.11	1.14	0.95	0.93	1.24
Na	0.11	0.40	0.14	0.18	0.49	0.49	0.49	0.46	0.28	0.23	0.48	0.61	0.04	0.06	0.18	0.17	0.19	0.26
K	1.74	1.53	1.59	1.71	1.47	1.59	1.57	1.61	1.68	1.72	1.66	1.45	1.81	1.87	1.71	1.73	1.80	1.69
Rb					0.05	0.12	0.12	0.10	0.05	0.06	0.08	0.09	0.07	0.10	0.08	0.05	0.06	0.11
Cs					0.00	0.00	0.01	0.01	0.01	0.00	0.00	0.01	0.00	0.00	0.00	0.00	0.00	0.02
Sr					0.02	0.01	0.02	0.02	0.03	0.03	0.01	0.01	0.01	0.00	0.01	0.03	0.01	0.03
Ba					0.01	0.00	0.00	0.00	0.00	0.00	0.00	0.00	0.00	0.00	0.00	0.00	0.00	0.00
Sum A	1.85	1.93	1.73	1.89	2.04	2.22	2.21	2.21	2.05	2.04	2.23	2.18	1.93	2.03	1.99	1.98	2.07	2.10
Na	0.63	0.98	0.58	0.76	0.90	1.00	0.99	0.98	0.67	0.72	0.90	0.97	0.94	1.00	0.88	0.78	0.74	0.98
Ca	0.37	0.02	0.42	0.24	0.10	0.00	0.01	0.02	0.33	0.28	0.10	0.03	0.06	0.00	0.12	0.22	0.26	0.02
Sum B	1.00	1.00	1.00	1.00	1.00	1.00	1.00	1.00	1.00	1.00	1.00	1.00	1.00	1.00	1.00	1.00	1.00	1.00
Na	0.33	0.10	0.12	0.00	0.14	0.26	0.07	0.00	0.00	0.00	0.00	0.04	0.12	0.05	0.07	0.00	0.00	0.00
Mg	0.70	0.03	0.33	0.12	0.16	0.18	0.26	0.27	0.41	0.42	0.21	0.16	0.18	0.06	0.24	0.15	0.30	0.26
Mn	3.68	0.16	0.90	1.77	6.19	5.54	5.44	5.45	3.59	3.83	4.87	6.34	3.92	5.48	4.04	3.33	4.60	4.98
Fe^{2+}	2.29	6.71	5.65	5.14	0.38	0.14	0.91	1.37	3.16	2.96	1.77	0.37	2.70	1.41	2.60	3.59	2.12	1.70
Zn					0.12	0.09	0.33	0.08	0.01	0.00	0.20	0.09	0.07	0.01	0.05	0.00	0.01	0.06
Y					0.00	0.00	0.00	0.00	0.00	0.00	0.00	0.00	0.00	0.00	0.00	0.00	0.00	0.00
Ce					0.01	0.00	0.00	0.00	0.02	0.01	0.00	0.00	0.00	0.00	0.00	0.00	0.00	0.00
Sum C	7.00	7.00	7.00	7.03	7.00	7.00	7.00	7.17	7.19	7.23	7.85	7.00	7.00	7.00	7.00	7.07	7.02	7.00
Ti	1.82	1.97	1.91	1.25	1.88	1.16	1.19	1.07	1.49	1.21	1.17	1.38	0.95	0.13	1.23	1.32	1.41	1.04
Sn					0.00	0.00	0.00	0.00	0.00	0.00	0.00	0.00	0.00	0.00	0.00	0.00	0.00	0.00
Zr	0.17	0.02	0.09	0.47	0.00	0.01	0.21	0.31	0.41	0.66	0.06	0.01	0.21	0.49	0.10	0.53	0.03	0.29
Hf					0.00	0.00	0.00	0.00	0.00	0.01	0.00	0.00	0.00	0.00	0.00	0.01	0.00	0.00
Nb	0.06	0.04	0.08	0.29	0.18	0.04	0.61	0.62	0.15	0.13	0.77	0.45	0.85	1.34	0.71	0.18	0.58	0.68
Ta					0.00	0.00	0.00	0.00	0.01	0.00	0.00	0.00	0.01	0.04	0.00	0.00	0.00	0.00
Sum D	2.05	2.03	2.08	2.01	2.06	2.01	2.02	2.00	2.06	2.03	2.00	2.04	2.03	1.99	2.03	2.04	2.02	2.01
Si	7.76	7.99	7.65	7.53	7.82	7.83	7.76	7.65	7.43	7.68	7.63	7.78	7.69	7.61	7.66	7.65	7.54	7.66
Al	0.27	0.02	0.32	0.45	0.09	0.07	0.13	0.19	0.37	0.34	0.23	0.09	0.31	0.36	0.28	0.24	0.36	0.24
Sum T	8.03	8.01	7.97	7.98	7.91	7.90	7.89	7.83	7.80	7.82	7.86	7.87	7.99	7.97	7.94	7.88	7.90	7.90
F	0.77	0.62	0.72	0.54	0.86	0.99	0.62	0.58	0.84	0.95	0.57	0.74	0.49	0.15	0.58	0.74	0.63	0.61
OH	4.24	4.38	4.28	4.46	4.14	4.00	4.00	4.04	4.16	4.05	4.00	4.11	4.00	4.00	4.05	4.26	4.09	4.14
O	26.00	26.00	26.00	26.00	30.14	30.41	30.38	30.42	30.16	30.05	30.43	30.26	30.51	30.85	30.42	30.26	30.37	30.39
Cations	19.93	19.97	19.78	19.91	20.01	20.14	20.12	20.21	20.09	20.11	20.14	20.08	19.95	19.99	19.96	19.98	20.01	20.01

number of analyses in mean

AVERAGE EMPA FOR AGM

Sample	MBH15	MBH16	MBH17	MBH18A	MBH18B	MBH19A	MBH19B	MBH20	MBH21	MBH22	MBH23A	MBH24a	MBH24A	MBH24B	MBH27	MBH28	MBH29	MBH30
n	10	9	6	6	2	9	8	6	5	3	4	1	7	5	4	1	5	4
Na_2O	2.97	2.56	2.51	2.40	2.21	2.28	2.03	2.87	2.16	2.06	2.41	1.99	2.32	2.08	1.66	1.86	2.24	1.89
K_2O	5.74	5.94	5.89	5.97	5.47	6.00	6.06	5.34	5.98	6.08	6.02	5.91	6.06	6.17	6.11	6.21	5.93	6.24
Rb_2O	0.68	0.53	0.38	0.49	0.78	0.40	0.30	0.61	0.40	0.45	0.47	0.48	0.37	0.30	0.35	0.44	0.42	0.42
Cs_2O	0.00	0.05	0.03	0.02	0.04	0.05	0.00	0.08	0.00	0.03	0.00	0.00	0.04	0.00	0.16	0.00	0.07	0.03
CaO	0.08	0.56	0.08	0.54	0.43	0.63	0.97	0.57	0.94	1.16	0.58	1.26	0.61	0.96	1.85	1.41	1.42	1.30
SrO	0.10	0.12	0.20	0.11	0.16	0.17	0.20	0.16	0.10	0.16	0.08	0.19	0.15	0.18	0.22	0.23	0.21	0.25
BaO	0.01	0.00	0.00	0.00	0.00	0.10	0.06	0.23	0.17	0.12	0.00	0.00	0.00	0.07	0.13	0.14	0.27	0.00
MgO	0.63	0.83	0.87	0.41	0.44	0.81	1.16	0.46	0.93	0.95	0.41	0.92	0.81	1.06	0.99	0.94	1.49	0.63
MnO	27.27	26.57	19.29	20.06	15.51	18.51	12.77	20.64	17.17	22.68	20.15	16.14	18.20	13.97	11.43	9.18	8.50	10.32
FeO	6.47	7.66	15.34	15.09	20.49	16.38	21.72	9.99	16.42	11.10	14.90	19.22	16.63	20.65	23.10	25.51	25.45	25.30
ZnO	0.06	0.00	0.20	0.20	0.00	0.13	0.00	5.39	0.28	0.19	0.26	0.20	0.19	0.04	0.00	0.00	0.04	0.00
Al_2O_3	0.71	0.91	0.78	1.05	0.98	0.99	0.94	0.35	1.14	1.14	0.98	1.32	0.90	0.90	1.51	1.40	1.04	1.66
Y_2O_3	0.00	0.00	0.00	0.00	0.00	0.00	0.00	0.00	0.00	0.00	0.00	0.00	0.00	0.00	0.00	0.00	0.00	0.00
Cr_2O_3	0.00	0.02	0.00	0.03	0.00	0.04	0.00	0.20	0.07	0.06	0.05	0.18	0.03	0.04	0.20	0.26	0.17	0.19
TiO_2	5.25	8.18	8.66	6.93	6.72	7.03	7.79	11.18	8.12	9.05	7.45	8.68	7.19	7.67	10.63	9.30	10.57	7.37
SnO_2	0.00	0.00	0.00	0.00	0.00	0.00	0.00	0.00	0.00	0.00	0.00	0.00	0.00	0.00	0.00	0.00	0.00	0.00
ZrO_2	1.46	0.00	1.72	0.93	4.37	2.46	4.41	0.26	1.72	1.25	0.94	2.37	2.34	3.98	1.21	2.36	1.42	4.15
HfO_2	0.00	0.00	0.00	0.00	0.13	0.00	0.15	0.00	0.00	0.00	0.00	0.00	0.03	0.00	0.00	0.23	0.00	0.07
Nb_2O_5	0.79	6.05	3.51	6.92	2.53	5.05	1.68	1.26	4.35	3.61	6.33	2.89	4.99	2.51	1.17	2.16	1.39	2.70
Ta_2O_5	0.07	0.00	0.11	0.00	0.00	0.15	0.08	0.00	0.19	0.00	0.00	0.00	0.02	0.06	0.03	0.00	0.00	0.19
SiO_2	33.98	33.56	34.13	32.82	32.66	33.09	33.19	34.73	33.13	33.31	33.19	31.61	32.58	33.48	32.59	32.79	33.77	31.17
F	0.72	0.82	1.19	0.88	1.21	0.94	1.25	1.18	0.96	1.01	0.94	1.17	0.87	1.15	1.06	1.35	1.37	1.06
H_2O	2.50	2.64	2.76	2.59	2.63	2.68	2.67	2.74	2.65	2.81	2.65	2.67	2.66	2.64	2.78	2.65	2.69	2.70
O=F	-0.30	-0.34	-0.50	-0.37	-0.51	-0.40	-0.53	-0.50	-0.41	-0.42	-0.40	-0.49	-0.37	-0.48	-0.45	-0.57	-0.57	-0.45
Total	96.88	96.64	97.82	97.03	96.21	97.40	96.90	96.72	96.94	96.81	97.38	96.62	96.52	97.42	96.73	97.94	97.90	96.95
Chemical formulae calculated based on 31 cations																		
Na_m	1.33	1.13	1.10	1.07	1.00	1.02	0.91	1.26	0.97	0.91	1.07	0.90	1.05	0.92	0.73	0.82	0.97	0.76
Na	0.18	0.19	0.18	0.21	0.11	0.17	0.15	0.17	0.08	0.05	0.18	0.21	0.20	0.16	0.17	0.13	0.23	0.09
K	1.78	1.74	1.70	1.76	1.64	1.76	1.78	1.55	1.75	1.77	1.76	1.73	1.80	1.80	1.78	1.88	1.70	1.86
Rb	0.10	0.08	0.06	0.07	0.12	0.06	0.04	0.09	0.06	0.07	0.07	0.07	0.06	0.04	0.05	0.06	0.06	0.06
Cs	0.00	0.00	0.00	0.00	0.00	0.00	0.00	0.01	0.00	0.00	0.00	0.00	0.00	0.00	0.02	0.01	0.01	0.00
Sr	0.01	0.02	0.03	0.02	0.02	0.02	0.03	0.02	0.02	0.02	0.01	0.03	0.02	0.02	0.03	0.03	0.03	0.03
Ba	0.00	0.00	0.00	0.00	0.00	0.01	0.01	0.02	0.02	0.01	0.00	0.00	0.01	0.01	0.01	0.01	0.02	0.00
Sum A	1.99	2.02	1.97	2.06	1.89	2.03	2.00	1.85	1.93	1.92	2.03	2.06	2.09	2.03	2.05	2.05	2.05	2.05
Na	0.98	0.86	0.84	0.87	0.89	0.85	0.76	0.86	0.77	0.72	0.86	0.69	0.85	0.77	0.55	0.66	0.66	0.68
Ca	0.02	0.14	0.16	0.13	0.11	0.15	0.24	0.14	0.23	0.28	0.14	0.31	0.15	0.23	0.45	0.34	0.34	0.32
Sum B	1.00	1.00	1.00	1.00	1.00	1.00	1.00	1.00	1.00	1.00	1.00	1.00	1.00	1.00	1.00	1.00	1.00	1.00
Na	0.17	0.00	0.00	0.00	0.00	0.00	0.00	0.23	0.12	0.14	0.03	0.00	0.00	0.00	0.02	0.03	0.00	0.00
Mg	0.22	0.28	0.29	0.14	0.15	0.28	0.40	0.16	0.32	0.32	0.14	0.32	0.28	0.36	0.34	0.32	0.50	0.22
Mn	5.36	5.16	3.69	3.93	3.08	3.61	2.49	5.58	3.36	4.38	3.92	3.17	3.60	2.72	2.21	1.77	1.62	2.05
Fe^{2+}	1.25	1.47	2.90	2.92	4.01	3.14	4.18	0.19	3.15	2.12	2.86	3.73	3.23	3.95	4.41	4.86	4.78	4.95
Zn	0.01	0.00	0.03	0.03	0.00	0.02	0.00	0.91	0.05	0.03	0.04	0.03	0.03	0.01	0.00	0.00	0.01	0.00
Y	0.00	0.00	0.00	0.00	0.00	0.00	0.00	0.00	0.00	0.00	0.00	0.00	0.00	0.00	0.00	0.00	0.00	0.00
Cr	0.00	0.00	0.01	0.00	0.00	0.00	0.00	0.02	0.01	0.01	0.00	0.02	0.00	0.00	0.02	0.02	0.01	0.02
Sum C	7.00	7.00	7.00	7.03	7.24	7.06	7.06	7.00	7.00	7.00	7.00	7.27	7.15	7.03	7.00	7.00	7.00	7.23
Ti	0.91	1.41	1.47	1.21	1.18	1.21	1.34	1.91	1.40	1.55	1.28	1.52	1.25	1.31	1.83	1.59	1.79	1.30
Sn	0.00	0.00	0.00	0.00	0.00	0.00	0.00	0.00	0.00	0.00	0.00	0.00	0.00	0.00	0.00	0.00	0.00	0.00
Zr	0.17	0.00	0.19	0.10	0.50	0.28	0.50	0.03	0.20	0.14	0.11	0.27	0.27	0.45	0.14	0.26	0.16	0.47
Hf	0.00	0.00	0.00	0.00	0.01	0.00	0.01	0.00	0.00	0.00	0.00	0.00	0.00	0.00	0.00	0.02	0.00	0.00
Nb	0.92	0.63	0.36	0.72	0.27	0.53	0.18	0.13	0.46	0.37	0.66	0.29	0.53	0.27	0.12	0.22	0.14	0.29
Ta	0.00	0.00	0.01	0.00	0.00	0.01	0.00	0.00	0.01	0.00	0.00	0.00	0.00	0.00	0.00	0.00	0.00	0.01
Sum D	2.00	2.04	2.02	2.03	1.96	2.03	2.03	2.06	2.06	2.06	2.05	2.08	2.05	2.03	2.08	2.09	2.08	2.07
Si	7.77	7.69	7.71	7.79	7.65	7.61	7.63	7.88	7.63	7.59	7.62	7.34	7.54	7.66	7.45	7.47	7.58	7.29
Al	0.20	0.25	0.21	0.20	0.27	0.27	0.25	0.09	0.31	0.31	0.26	0.36	0.25	0.24	0.41	0.38	0.28	0.46
Sum T	7.97	7.94	7.92	7.88	7.92	7.88	7.89	7.97	7.93	7.90	7.88	7.70	7.79	7.91	7.85	7.84	7.86	7.75
F	0.52	0.59	0.85	0.64	0.89	0.68	0.91	0.85	0.70	0.73	0.68	0.86	0.64	0.83	0.77	0.97	0.97	0.79
OH	4.00	4.03	4.15	4.00	4.11	4.11	4.09	4.15	4.07	4.27	4.05	4.14	4.13	4.04	4.23	4.03	4.03	4.21
O	30.48	30.41	30.15	30.36	30.11	30.32	30.09	30.15	30.30	30.27	30.32	30.14	30.36	30.17	30.23	30.03	30.03	30.21
Cations	19.97	20.00	19.91	20.00	20.01	19.99	19.98	19.89	19.93	19.88	19.96	20.11	20.08	20.00	19.99	19.98	19.99	20.10

n number of analyses in mean

AVERAGE EMPA FOR AGM

Sample:	MH01	MH02	MH03A	MH03B	MH04A	MH04B	MH05	MH06A	MH06B	MH08A	MH08B	MH09A	MH40A	MH40B	MH42	MH43	MH44	MH45
#	4	3	7	8	8	4	9	7	11	7	7	8	6	13	3	4	4	6
Na_2O	1.74	1.70	2.05	1.69	1.93	1.94	2.11	2.56	2.76	2.68	2.53	2.30	2.66	2.66	2.62	2.68	1.99	2.64
K_2O	6.24	6.21	5.94	6.20	5.96	5.91	5.91	5.84	5.93	6.01	5.91	6.05	6.03	5.76	5.97	5.90	6.19	5.78
Rb_2O	0.38	0.39	0.37	0.27	0.32	0.18	0.42	0.64	0.91	0.47	0.37	0.33	0.52	0.91	0.82	0.44	0.33	0.57
Cs_2O	0.02	0.00	0.03	0.02	0.13	0.00	0.04	0.06	0.00	0.02	0.00	0.07	0.02	0.00	0.12	0.01	0.00	0.03
CaO	1.18	1.26	0.68	1.13	0.95	1.02	1.45	0.93	0.04	0.53	0.56	0.99	1.22	0.03	0.00	0.28	0.37	0.56
SrO	0.24	0.23	0.27	0.40	0.36	0.23	0.19	0.06	0.00	0.03	0.17	0.32	0.09	0.00	0.00	0.01	0.04	0.01
BaO	0.00	0.00	0.00	0.06	0.00	0.00	0.18	0.02	0.00	0.00	0.00	0.00	0.02	0.00		0.00	0.00	0.00
MgO	0.59	0.65	0.57	0.50	0.59	0.69	0.98	0.89	0.44	0.37	0.11	0.65	1.02	0.43	0.15	0.68	0.18	0.68
MnO	9.83	11.72	13.06	13.09	9.71	9.61	10.01	25.30	29.91	20.10	23.89	12.06	23.09	20.13	26.37	20.76	7.12	22.70
FeO	26.02	24.18	21.99	22.17	26.43	25.32	16.81	7.06	3.88	13.77	11.18	21.24	10.06	3.71	2.64	13.52	28.94	10.65
ZnO	0.00	0.00	0.00	0.00	0.00	0.00	0.11	0.14	0.02	0.16	0.14	0.08	0.22	0.00	4.08	0.29	0.00	0.43
Al_2O_3	1.40	1.50	1.36	1.43	1.22	0.96	1.02	1.24	1.69	1.25	0.48	1.33	0.83	1.69	1.14	0.87	1.35	0.78
Y_2O_3	0.00	0.00	0.00	0.00	0.00	0.00	0.00	0.00	0.00	0.00	0.00	0.00	0.00	0.00		0.00	0.00	0.00
Ce_2O_3	0.13	0.11	0.30	0.25	0.05	0.00	0.07	0.07	0.00	0.02	0.02	0.18	0.00	0.00		0.00	0.30	0.00
TiO_2	7.24	7.13	6.35	7.02	7.02	6.69	10.09	7.36	1.76	6.10	6.52	7.04	8.91	1.67	1.34	5.76	5.87	7.43
SnO_2	0.00	0.00	0.00	0.00	0.00	0.00	0.00	0.00	0.00	0.00	0.00	0.00	0.00	0.00		0.00	0.00	0.00
ZrO_2	4.25	4.16	4.53	3.68	3.58	6.56	0.96	1.21	3.01	1.25	6.79	3.14	0.62	3.56	3.43	2.96	4.47	0.34
HfO_2	0.13	0.08	0.16	0.24	0.26	0.42	0.02	0.00	0.00	0.00	0.01	0.01	0.00	0.00	0.00	0.00	0.00	0.00
Nb_2O_5	2.47	2.34	3.55	2.38	2.53	0.59	2.20	5.54	11.01	7.51	0.67	2.50	3.69	11.40	12.13	6.55	4.50	6.50
Ta_2O_5	0.14	0.00	0.28	0.20	0.34	0.12	0.00	0.03	0.26	0.00	0.00	0.28	0.00	0.25	0.63	0.08	0.03	0.08
SiO_2	31.89	31.42	31.80	32.11	32.27	32.47	33.20	32.07	32.13	32.34	33.72	32.61	34.16	31.86	31.85	33.08	32.81	34.35
F	1.18	1.25	1.07	1.06	1.13	1.27	1.10	0.86	0.30	0.85	1.24	1.07	0.97	0.29	0.14	0.77	0.94	0.89
H_2O	2.67	2.69	2.70	2.74	2.71	2.59	2.78	2.69	2.54	2.55	2.63	2.72	2.84	2.52	2.48	2.61	2.89	2.69
O=F	-0.50	-0.53	-0.45	-0.45	-0.47	-0.53	-0.46	-0.36	-0.13	-0.36	-0.52	-0.45	-0.41	-0.12	-0.06	-0.32	-0.40	-0.38
Total	97.20	96.40	97.31	97.36	97.71	96.02	97.28	95.71	97.26	95.72	96.34	96.10	96.54	95.77	95.85	97.51	97.89	97.10
Chemical formulae calculated based on 31 cations																		
Na_m	0.79	0.77	0.93	0.76	0.87	0.88	0.93	1.15	1.26	1.22	1.14	1.03	1.17	1.23		1.10	0.89	1.16
Na	0.00	0.00	0.10	0.04	0.10	0.14	0.28	0.23	0.18	0.23	0.22	0.19	0.20	0.18	0.00	0.09	0.00	0.00
K	1.85	1.86	1.77	1.83	1.76	1.77	1.71	1.73	1.79	1.80	1.76	1.79	1.74	1.75	1.84	1.73	1.82	1.68
Rb	0.06	0.06	0.06	0.04	0.05	0.03	0.06	0.10	0.14	0.07	0.06	0.05	0.08	0.14	0.13	0.07	0.05	0.08
Cs	0.00	0.00	0.00	0.00	0.01	0.00	0.00	0.01	0.00	0.00	0.00	0.01	0.00	0.00	0.00	0.00	0.01	0.00
Sr	0.03	0.03	0.04	0.05	0.05	0.03	0.03	0.01	0.00	0.00	0.02	0.04	0.01	0.00	0.00	0.00	0.01	0.00
Ba	0.00	0.00	0.00	0.01	0.00	0.00	0.02	0.00	0.00	0.00	0.00	0.00	0.00	0.00	0.00	0.00	0.00	0.00
Sum A	2.02	2.04	1.96	1.97	1.97	1.97	2.10	2.07	2.10	2.11	2.06	2.08	2.03	2.07	1.98	1.89	1.89	1.77
Na	0.71	0.68	0.83	0.72	0.77	0.74	0.65	0.77	0.90	0.87	0.86	0.75	0.70	0.90	0.95	0.93	0.89	0.86
Ca	0.29	0.32	0.17	0.28	0.23	0.26	0.35	0.23	0.01	0.13	0.14	0.25	0.30	0.01	0.00	0.07	0.09	0.14
Sum B	1.00	1.00	1.00	1.00	1.00	1.00	1.00	1.00	1.00	1.00	1.00	1.00	1.00	1.00	0.95	1.00	0.98	1.00
Na	0.00	0.00	0.00	0.00	0.00	0.00	0.00	0.15	0.10	0.13	0.06	0.00	0.27	0.05	0.28	0.00	0.00	0.30
Mg	0.29	0.33	0.29	0.31	0.17	0.34	0.33	0.31	0.16	0.13	0.04	0.33	0.34	0.15	0.05	0.23	0.06	0.23
Mn	1.34	2.33	2.74	2.56	1.90	1.91	3.46	4.99	5.98	4.01	4.70	2.53	4.44	6.06	5.40	4.04	1.39	4.38
Fe^{2+}	5.07	4.75	4.27	4.29	5.11	4.97	3.19	1.52	0.77	2.78	2.18	4.13	1.91	0.74	0.53	2.60	5.59	2.02
Zn	0.00	0.00	0.00	0.00	0.00	0.00	0.02	0.02	0.00	0.05	0.02	0.01	0.04	0.00	0.73	0.05	0.00	0.07
Y	0.00	0.00	0.00	0.00	0.00	0.00	0.00	0.00	0.00	0.00	0.00	0.00	0.00	0.00	0.00	0.00	0.00	0.00
Ce	0.01	0.01	0.03	0.02	0.00	0.00	0.01	0.01	0.00	0.00	0.00	0.02	0.00	0.00	0.00	0.00	0.03	0.00
Sum C	7.22	7.32	7.24	7.18	7.18	7.13	7.01	7.00	7.00	7.00	7.00	7.00	7.00	7.00	7.00	7.00	7.07	7.00
Ti	1.27	1.26	1.11	1.36	1.36	1.18	1.72	1.28	0.31	1.08	1.14	1.37	1.52	0.30	0.24	0.99	1.02	1.27
Sn	0.00	0.00	0.00	0.00	0.00	0.00	0.00	0.00	0.00	0.00	0.00	0.00	0.00	0.00	0.00	0.00	0.00	0.00
Zr	0.48	0.48	0.52	0.42	0.40	0.75	0.11	0.14	0.35	0.14	0.77	0.36	0.07	0.41	0.41	0.33	0.50	0.04
Hf	0.01	0.01	0.01	0.02	0.02	0.03	0.00	0.00	0.00	0.00	0.00	0.00	0.00	0.00	0.00	0.00	0.00	0.00
Nb	0.26	0.25	0.38	0.25	0.26	0.06	0.24	0.59	1.26	0.80	0.07	0.26	0.38	1.22	1.33	0.68	0.47	0.71
Ta	0.01	0.00	0.02	0.01	0.02	0.01	0.00	0.00	0.02	0.00	0.00	0.02	0.00	0.02	0.04	0.01	0.00	0.01
Sum D	2.03	1.99	2.03	2.05	2.07	2.03	2.07	2.01	1.94	2.01	1.99	2.01	1.97	1.95	2.02	2.01	1.99	2.02
Si	7.42	7.38	7.42	7.42	7.46	7.43	7.54	7.64	7.58	7.59	7.86	7.58	7.75	7.57	7.71	7.78	7.58	7.81
Al	0.38	0.42	0.37	0.39	0.33	0.27	0.27	0.36	0.47	0.35	0.13	0.36	0.22	0.47	0.33	0.24	0.37	0.21
Sum T	7.80	7.79	7.80	7.81	7.79	7.80	7.81	7.98	8.05	7.94	7.99	7.94	7.98	8.04	8.03	8.02	7.95	8.02
F	0.87	0.93	0.79	0.77	0.82	0.94	0.79	0.63	0.23	0.63	0.91	0.79	0.69	0.22	26.89	0.56	0.69	0.64
OH	4.13	4.07	4.21	4.23	4.18	4.06	4.21	4.37	4.77	4.37	4.09	4.21	4.31	4.78	4.11	4.44	4.31	4.36
O	30.13	30.07	30.21	30.23	30.18	30.06	30.21	30.37	30.77	30.37	30.09	30.21	30.31	30.78	30.11	30.44	30.31	30.36
Cations	20.07	20.14	20.03	20.01	20.01	20.01	19.99	20.06	20.09	20.06	20.03	20.03	19.98	20.07	19.98	19.92	19.88	19.81

number of analyses in mean

AVERAGE EMPA FOR AGM

				Langesundsfjord Area, Norway (NOR)													
Sample	MSH46	MSH47	MSH48	NOR1	NOR2	NOR3	NOR4	NOR5	NOR6	NOR7	NOR8	NOR9	NOR10	NOR11	NOR12	NOR13	NOR14	NOR15
n	6	5	6	11	12	10	8	7	6	4	4	4	4	3	4	3	4	4
Na_2O	2.21	3.45	2.45	2.54	1.99	3.52	1.97	1.91	1.82	2.34	1.78	1.46	1.88	1.65	1.95	2.59	2.64	1.74
K_2O	5.95	5.31	5.78	5.48	6.19	5.89	6.10	6.01	6.11	5.45	5.99	5.91	5.75	5.46	5.55	5.83	5.93	5.90
Rb_2O	0.44	0.49	0.41	0.75	0.36	0.37	0.50	0.44	0.42	0.69	0.36	0.39	0.67	0.63	0.65	0.33	0.35	0.50
Cs_2O	0.04	0.05	0.09	1.01	0.21	0.03	0.22	0.18	0.23	0.57	0.18	0.56	0.28	1.53	0.78	0.02	0.01	0.18
CaO	0.83	0.63	0.68	1.08	1.31	0.41	1.38	1.39	1.46	0.34	1.22	1.63	1.05	1.01	1.09	0.81	0.85	1.50
SrO	0.03	0.01	0.02	0.07	0.08	0.07	0.24	0.11	0.14	0.07	0.10	0.14	0.09	0.05	0.10	0.05	0.04	0.15
BaO	0.00	0.00	0.00	0.00	0.00	0.00	0.04	0.02	0.00	0.00	0.04	0.05	0.00	0.00	0.00	0.19	0.00	0.03
MgO	0.26	0.03	0.59	0.01	0.76	0.36	0.07	0.77	0.08	0.42	0.93	0.67	0.85	0.50	0.68	2.10	1.95	0.89
MnO	12.57	24.12	13.86	12.48	9.15	17.63	7.79	11.06	7.39	19.50	10.29	9.06	13.12	16.13	12.07	20.98	18.98	7.87
FeO	21.85	9.64	19.70	21.23	25.90	16.01	26.55	23.13	27.08	13.97	23.98	25.93	21.43	18.66	22.52	11.65	13.29	26.95
ZnO	0.17	0.00	0.36	0.39	0.12	0.47	0.00	0.00	0.34	1.14	0.00	0.00	0.26	0.00	0.27	0.00	0.51	0.00
Al_2O_3	1.44	0.16	1.19	0.71	1.27	0.10	1.46	1.37	1.56	1.04	1.18	1.59	1.28	1.56	0.99	0.71	0.63	1.50
Y_2O_3	0.00	0.00	0.00	0.00	0.00	0.00	0.00	0.00	0.00	0.00	0.00	0.00	0.00	0.00	0.00	0.00	0.00	0.00
Ce_2O_3	0.00	0.00	0.00	0.11	0.11	0.23	0.13	0.15	0.13	0.08	0.21	0.31	0.28	0.26	0.23	0.11	0.00	0.21
TiO_2	7.86	9.56	6.61	9.71	7.79	9.74	8.60	7.56	9.19	5.78	7.91	8.63	7.96	7.00	8.70	10.05	10.02	9.24
SnO_2	0.00	0.00	0.00	0.05	0.21	0.00	0.00	0.07	0.00	0.35	0.19	0.04	0.09	0.12	0.04	0.00	0.00	0.00
ZrO_2	2.78	0.09	3.90	1.85	4.90	1.07	3.02	4.02	2.43	3.62	4.19	4.04	3.93	4.87	3.24	1.27	0.85	2.57
HfO_2	0.00	0.00	0.00	0.01	0.11	0.00	0.07	0.21	0.04	0.08	0.12	0.11	0.11	0.28	0.09	0.00	0.00	0.07
Nb_2O_5	4.18	3.27	3.77	1.73	1.74	2.27	1.56	1.88	1.31	5.58	1.81	0.86	1.99	1.85	1.63	2.34	2.74	1.45
Ta_2O_5	0.00	0.00	0.00	0.00	0.13	0.00	0.00	0.03	0.00	0.00	0.00	0.00	0.00	0.00	0.00	0.09	0.12	0.00
SiO_2	32.50	35.53	32.97	34.96	33.87	34.92	32.64	32.28	32.54	33.29	33.89	33.10	33.41	32.84	33.75	35.08	35.29	33.60
F	1.84	0.88	1.87	1.15	1.84	1.45	1.84	1.88	1.19	0.97	1.14	1.22	1.13	1.27	1.11	1.28	1.80	1.14
H_2O	2.72	2.92	2.71	2.88	2.83	2.92	2.74	2.73	2.89	2.98	2.75	2.71	2.75	2.59	2.76	2.77	2.91	2.77
O=F	-0.44	-0.37	-0.45	-0.48	-0.44	-0.49	-0.44	-0.42	-0.50	-0.41	-0.48	-0.51	-0.48	-0.53	-0.47	-0.54	-0.42	-0.48
Total	95.00	96.57	95.09	98.43	99.26	96.44	96.26	95.88	96.64	97.36	97.68	97.87	97.81	97.83	97.73	97.73	97.67	97.76
Chemical formulae calculated based on 31 anions																		
Na_M	1.00	1.00	1.11	1.11	0.87	1.55	0.88	0.86	0.81	1.05	0.78	0.65	0.83	0.75	0.86	1.11	1.13	0.76
Mn	0.07	0.33	0.11	0.06	0.00	0.31	0.21	0.20	0.22	0.03	0.02	0.00	0.07	0.00	0.05	0.11	0.09	0.05
K	1.77	1.52	1.72	1.57	1.78	1.65	1.80	1.79	1.79	1.62	1.74	1.72	1.68	1.64	1.62	1.65	1.68	1.70
Rb	0.07	0.07	0.06	0.11	0.05	0.05	0.07	0.07	0.06	0.10	0.05	0.06	0.10	0.10	0.10	0.05	0.05	0.07
Cs	0.00	0.01	0.01	0.10	0.02	0.00	0.02	0.02	0.02	0.06	0.02	0.05	0.03	0.15	0.08	0.00	0.00	0.02
Sr	0.00	0.00	0.00	0.01	0.01	0.01	0.03	0.02	0.02	0.01	0.01	0.02	0.01	0.01	0.01	0.01	0.00	0.02
Ba	0.00	0.00	0.00	0.00	0.00	0.00	0.00	0.00	0.00	0.00	0.00	0.00	0.00	0.00	0.00	0.02	0.00	0.00
Sum A	1.92	1.93	1.90	1.84	1.95	2.03	2.15	2.10	2.12	1.81	1.85	1.86	1.89	1.89	1.85	1.83	1.82	1.87
Na	0.79	0.86	0.83	0.74	0.68	0.98	0.66	0.65	0.59	0.94	0.64	0.60	0.74	0.75	0.73	0.81	0.80	0.64
Ca	0.21	0.15	0.17	0.26	0.32	0.10	0.34	0.35	0.41	0.06	0.30	0.40	0.26	0.25	0.27	0.19	0.20	0.36
Sum B	1.00	1.01	1.00	1.00	1.00	1.00	1.00	1.00	1.00	1.00	0.94	1.00	1.00	1.00	1.00	1.00	1.00	1.00
Na	0.13	0.32	0.16	0.30	0.00	0.34	0.01	0.01	0.00	0.00	0.12	0.04	0.02	0.00	0.07	0.19	0.25	0.08
Mg	0.09	0.28	0.20	0.27	0.25	0.12	0.30	0.27	0.30	0.15	0.32	0.23	0.29	0.18	0.23	0.09	0.65	0.30
Mn	2.49	4.50	2.73	2.37	1.75	3.40	1.53	2.19	1.44	3.85	1.98	1.75	2.54	3.21	2.33	3.94	3.56	1.51
Fe^{2+}	4.27	1.81	3.84	3.98	4.88	3.05	5.15	4.52	5.21	2.71	4.56	4.95	4.09	3.66	4.30	2.16	2.46	5.10
Zn	0.03	0.00	0.06	0.06	0.02	0.00	0.00	0.00	0.06	0.19	0.00	0.00	0.04	0.00	0.04	0.00	0.08	0.00
Y	0.00	0.00	0.00	0.00	0.00	0.00	0.00	0.00	0.00	0.00	0.00	0.00	0.00	0.00	0.00	0.00	0.00	0.00
Ce	0.00	0.00	0.00	0.01	0.01	0.02	0.01	0.01	0.01	0.01	0.02	0.03	0.02	0.02	0.02	0.01	0.00	0.02
Sum C	7.01	7.00	7.00	6.79	6.91	6.66	6.99	6.99	7.02	6.91	6.88	6.96	6.98	7.06	6.93	6.81	6.75	6.93
Ti	1.24	1.62	1.16	1.64	1.32	1.67	1.50	1.32	1.59	1.00	1.35	1.48	1.37	1.25	1.69	1.68	1.67	1.57
Sn	0.00	0.00	0.00	0.00	0.02	0.00	0.00	0.01	0.00	0.03	0.02	0.00	0.01	0.01	0.00	0.00	0.00	0.00
Zr	0.32	0.01	0.44	0.28	0.49	0.12	0.34	0.46	0.27	0.41	0.47	0.45	0.44	0.36	0.36	0.14	0.09	0.28
Hf	0.00	0.00	0.00	0.00	0.01	0.00	0.00	0.01	0.00	0.01	0.01	0.01	0.01	0.02	0.01	0.00	0.00	0.00
Nb	0.44	0.33	0.40	0.18	0.18	0.23	0.16	0.20	0.14	0.59	0.19	0.09	0.21	0.20	0.17	0.24	0.27	0.15
Ta	0.00	0.00	0.00	0.00	0.01	0.01	0.00	0.00	0.00	0.00	0.00	0.00	0.00	0.00	0.00	0.01	0.01	0.00
Sum D	2.00	1.96	2.00	2.02	2.02	2.02	2.01	2.00	2.00	2.03	2.03	2.03	2.02	2.03	2.03	2.05	2.04	2.01
Si	7.39	7.99	7.88	7.84	7.63	7.94	7.52	7.55	7.49	7.73	7.89	7.56	7.63	7.52	7.70	7.78	7.82	7.61
Al	0.40	0.01	0.33	0.19	0.34	0.03	0.40	0.38	0.42	0.29	0.32	0.43	0.34	0.43	0.27	0.19	0.16	0.40
Sum T	7.99	8.03	8.01	8.03	7.96	7.97	7.92	7.92	7.92	8.02	8.00	7.99	7.97	7.95	7.97	7.97	7.98	8.01
F	0.77	0.62	0.78	0.82	0.74	1.18	0.76	0.74	0.86	0.71	0.82	0.88	0.81	0.94	0.80	0.90	0.70	0.82
OH	4.23	4.38	4.22	4.18	4.26	3.82	4.24	4.26	4.14	4.29	4.18	4.12	4.19	4.06	4.20	4.10	4.30	4.18
O	30.23	30.38	30.22	30.18	30.26	29.82	30.24	30.26	30.14	30.29	30.18	30.12	30.19	30.06	30.20	30.10	30.30	30.18
Cations	19.91	19.92	19.91	19.89	19.94	20.02	20.08	20.02	20.06	19.86	19.92	19.88	19.88	19.94	19.86	19.85	19.85	19.88

n number of analyses in mean

AVERAGE EMPA FOR AGM

Khibina and Lovozero massifs, Kola Peninsula, Russia (RUS)

Sample #	NOR16 3	NOR17 3	NOR18 7	NOR19 7	NOR20 7	NOR21 8	RUS1 7	RUS2 5	RUS3 7	RUS4 6	RUS5 6	RUS6 7	RUS7 3	RUS8 3	RUS9 4
Na_2O	1.64	3.24	2.96	2.12	2.95	2.88	2.21	2.34	2.54	2.32	2.34	4.68	1.90	2.00	2.09
K_2O	5.92	4.95	4.95	5.35	5.42	5.46	6.25	6.28	5.95	6.17	6.08	7.58	6.07	6.05	6.08
Rb_2O	0.45	0.56	1.24	0.58	0.37	0.47	0.26	0.32	0.24	0.44	0.38	0.17	0.25	0.23	0.40
Cs_2O	0.13	0.14	0.50	1.32	0.09	0.12	0.01	0.04	0.03	0.05	0.05	0.00	0.00	0.00	0.00
CaO	1.46	0.06	0.66	1.22	0.27	0.46	1.77	1.56	1.66	1.58	1.50	0.94	1.59	1.62	1.08
SrO	0.04	0.02	0.04	0.23	0.02	0.04	0.30	0.25	0.27	0.25	0.23	0.07	0.25	0.29	0.20
BaO	0.00	0.00	0.00	0.00	0.00	0.02	0.16	0.15	0.18	0.28	0.24	0.17	0.23	0.27	0.43
MgO	0.85	0.37	0.32	0.99	0.25	0.38	1.38	1.48	1.40	1.75	1.46	6.27	1.47	1.61	1.23
MnO	12.16	14.34	7.80	13.99	8.68	9.55	5.69	7.81	5.39	12.10	8.46	2.19	8.75	10.30	21.47
FeO	22.40	21.59	25.82	18.30	25.95	24.50	28.25	26.14	28.37	20.66	24.59	20.66	24.75	22.88	12.18
ZnO	0.00	0.00	0.00	0.76	0.75	0.68	0.00	0.25	0.00	0.48	0.31	0.00	0.31	0.35	0.00
Al_2O_3	1.48	0.00	0.31	1.28	0.27	0.23	1.29	1.16	1.07	1.34	1.14	0.37	1.26	1.31	0.92
Y_2O_3	0.00	0.00	0.00	0.00	0.00	0.00	0.00	0.00	0.00	0.00	0.00	0.00	0.00	0.00	0.00
Ce_2O_3	0.16	0.00	0.00	0.00	0.00	0.00	0.09	0.04	0.05	0.13	0.08	0.02	0.05	0.18	0.22
TiO_2	7.51	11.03	9.88	8.93	10.18	10.02	11.22	11.09	11.40	11.27	10.99	12.78	10.65	11.24	9.74
SnO_2	0.00	0.00	0.00	0.00	0.00	0.00	0.00	0.00	0.00	0.00	0.00	0.00	0.00	0.00	0.00
ZrO_2	4.07	0.28	1.80	2.46	1.07	1.13	0.82	1.04	0.68	0.71	1.19	0.00	1.11	0.58	0.47
HfO_2	0.19	0.00	0.00	0.06	0.01	0.01	0.00	0.00	0.00	0.00	0.00	0.00	0.00	0.00	0.00
Nb_2O_5	2.19	0.90	1.24	1.37	1.49	1.66	0.79	0.85	0.74	0.83	0.86	1.18	0.95	0.75	2.94
Ta_2O_5	0.17	0.00	0.00	0.00	0.00	0.00	0.16	0.07	0.16	0.00	0.02	0.15	0.10	0.04	0.00
SiO_2	33.30	36.09	34.70	33.31	35.27	35.42	34.27	34.68	34.95	34.54	34.80	38.64	34.22	34.51	34.72
F	1.06	1.24	1.18	1.12	1.19	1.43	1.13	1.08	1.22	1.06	1.20	0.11	1.18	1.16	1.02
H_2O	2.78	2.76	2.70	2.70	2.74	2.63	2.84	2.87	2.82	2.89	2.81	3.57	2.78	2.82	2.87
O=F	-0.45	-0.52	-0.50	-0.47	-0.50	-0.60	-0.48	-0.46	-0.51	-0.44	-0.51	-0.05	-0.50	-0.49	-0.43
Total	97.53	97.84	95.61	95.62	96.45	96.48	98.41	98.24	98.60	98.39	98.21	99.50	97.38	97.68	97.62
Chemical formulae calculated based on 31 cations															
Na_{tot}	0.73	1.40	1.32	0.95	1.30	1.26	0.95	1.00	1.08	0.99	1.01	1.88	0.83	0.86	0.91
Na	0.02	0.30	0.08	0.03	0.15	0.08	0.15	0.07	0.18	0.12	0.05	0.00	0.05	0.05	0.00
K	1.73	1.41	1.45	1.58	1.57	1.58	1.77	1.78	1.67	1.74	1.72	2.00	1.73	1.72	1.74
Rb	0.07	0.08	0.18	0.09	0.05	0.07	0.04	0.05	0.03	0.06	0.05	0.02	0.04	0.03	0.06
Cs	0.01	0.01	0.05	0.13	0.01	0.01	0.00	0.00	0.00	0.00	0.01	0.00	0.00	0.00	0.00
Sr	0.01	0.00	0.01	0.03	0.00	0.00	0.04	0.03	0.03	0.03	0.03	0.01	0.03	0.04	0.03
Ba	0.00	0.00	0.00	0.00	0.00	0.00	0.01	0.01	0.02	0.02	0.02	0.01	0.02	0.02	0.04
Sum A	1.83	1.81	1.77	1.86	1.78	1.75	2.01	1.94	1.94	1.99	1.88	2.05	1.87	1.86	1.86
Na	0.64	0.99	0.84	0.70	0.94	0.89	0.58	0.63	0.61	0.63	0.64	0.78	0.62	0.61	0.69
Ca	0.36	0.01	0.16	0.30	0.06	0.11	0.42	0.37	0.39	0.37	0.36	0.21	0.38	0.39	0.26
Sum B	1.00	1.00	1.00	1.00	1.00	1.00	1.00	1.00	1.00	1.00	1.00	0.99	1.00	1.00	0.95
Na	0.06	0.12	0.40	0.23	0.21	0.29	0.22	0.30	0.30	0.25	0.31	1.10	0.16	0.20	0.22
Mg	0.29	0.12	0.11	0.34	0.08	0.13	0.46	0.49	0.46	0.58	0.48	1.93	0.49	0.53	0.41
Mn	2.35	2.72	1.52	2.75	1.67	1.83	1.07	1.32	1.01	2.27	1.59	0.38	1.66	1.94	4.07
Fe^{2+}	4.28	4.04	4.97	3.55	4.92	4.64	5.24	4.85	5.23	3.82	4.56	3.58	4.64	4.25	2.28
Zn	0.00	0.00	0.00	0.13	0.13	0.11	0.00	0.04	0.00	0.08	0.05	0.00	0.05	0.06	0.00
Y	0.00	0.00	0.00	0.00	0.00	0.00	0.00	0.00	0.00	0.00	0.00	0.00	0.00	0.00	0.00
Ce	0.01	0.00	0.00	0.00	0.00	0.00	0.01	0.00	0.00	0.01	0.01	0.00	0.00	0.01	0.02
Sum C	6.94	6.88	7.00	7.00	7.00	7.00	7.00	7.00	7.00	7.00	7.00	7.00	7.00	7.00	7.00
Ti	1.29	1.86	1.71	1.56	1.73	1.71	1.87	1.85	1.89	1.88	1.83	1.99	1.79	1.88	1.64
Sn	0.00	0.00	0.00	0.00	0.00	0.00	0.00	0.00	0.00	0.00	0.00	0.00	0.00	0.00	0.00
Zr	0.45	0.03	0.20	0.28	0.12	0.12	0.09	0.11	0.07	0.08	0.13	0.00	0.12	0.06	0.05
Hf	0.01	0.00	0.00	0.00	0.00	0.00	0.00	0.00	0.00	0.00	0.00	0.00	0.00	0.00	0.00
Nb	0.23	0.09	0.13	0.14	0.15	0.17	0.08	0.08	0.07	0.08	0.09	0.11	0.10	0.08	0.30
Ta	0.01	0.00	0.00	0.00	0.00	0.00	0.01	0.00	0.01	0.00	0.00	0.01	0.01	0.00	0.00
Sum D	1.99	1.98	2.04	1.98	2.01	2.00	2.05	2.05	2.05	2.03	2.05	2.11	2.02	2.02	1.99
Si	7.61	8.07	7.98	7.73	7.99	8.02	7.61	7.69	7.70	7.64	7.71	8.00	7.67	7.67	7.77
Al	0.40	0.00	0.08	0.35	0.07	0.06	0.34	0.30	0.28	0.35	0.30	0.00	0.33	0.34	0.24
Sum T	8.01	8.07	8.06	8.08	8.06	8.08	7.95	7.99	7.98	7.99	8.01	8.00	8.00	8.02	8.02
F	0.77	0.88	0.86	0.82	0.85	1.03	0.80	0.76	0.85	0.74	0.84	0.07	0.84	0.82	0.72
OH	4.23	4.13	4.14	4.18	4.15	3.97	4.20	4.24	4.15	4.26	4.16	4.93	4.16	4.18	4.28
O	30.23	30.13	30.14	30.18	30.15	29.97	30.20	30.24	30.15	30.26	30.16	30.93	30.16	30.18	30.28
Cations	19.84	19.86	19.87	19.92	19.85	19.83	20.01	19.98	19.97	20.01	19.94	20.24	19.89	19.90	19.81

0 number of analyses in mean

ELECTRON MICROPROBE ANALYSES OF MONT SAINT-HILAIRE AGM

OXIDE	MSH2a PT 1	PT 2	PT 3	PT 4	MSH2b PT 5	PT 6	PT 7	PT 8	MSH2c PT 9	PT 10	PT 11	PT 12	PT 13	MSH2 Average	MSH3a PT 14
Na_2O	3.47	3.52	3.33	3.52	3.44	3.51	3.48	3.41	3.59	3.81	3.80	3.74	3.05	3.51	3.76
K_2O	5.08	4.94	5.17	4.95	5.24	5.21	5.22	5.22	5.08	4.97	4.97	4.94	5.50	5.11	5.36
Rb_2O	0.28	0.29	0.31	0.40	0.33	0.29	0.32	0.33	0.43	0.41	0.36	0.38	0.44	0.35	0.76
Cs_2O	0.00	0.00	0.00	0.00	0.00	0.00	0.00	0.00	0.00	0.00	0.00	0.00	0.00	0.00	0.00
CaO	0.31	0.36	0.46	0.46	0.41	0.39	0.36	0.33	0.28	0.33	0.30	0.28	0.74	0.40	0.00
SrO	0.12	0.15	0.15	0.17	0.19	0.17	0.15	0.18	0.10	0.15	0.15	0.16	0.17	0.15	0.00
BaO	0.00	0.27	0.22	0.00	0.00	0.00	0.00	0.18	0.16	0.00	0.19	0.22	0.19	0.11	0.00
MgO	0.39	0.49	0.55	0.38	0.47	0.46	0.44	0.44	0.43	0.52	0.51	0.52	0.43	0.46	0.35
MnO	32.68	31.71	31.47	32.66	32.94	32.52	32.99	32.66	32.35	32.08	32.50	32.27	32.07	32.38	27.73
FeO	1.76	2.01	1.89	2.11	2.02	1.91	1.93	2.03	1.97	2.05	2.20	2.05	2.13	2.00	0.00
ZnO	0.76	0.82	0.93	1.03	0.82	0.79	0.70	0.68	0.55	0.66	0.64	0.62	0.69	0.75	6.50
Al_2O_3	0.20	0.33	0.47	0.24	0.23	0.27	0.24	0.26	0.31	0.30	0.33	0.29	0.79	0.33	0.17
Y_2O_3	0.00	0.00	0.00	0.00	0.00	0.00	0.00	0.00	0.00	0.00	0.00	0.00	0.00	0.00	0.00
Ce_2O_3	0.00	0.17	0.35	0.00	0.16	0.00	0.00	0.00	0.17	0.19	0.00	0.19	0.52	0.13	0.00
TiO_2	11.23	11.30	11.31	10.90	10.99	11.04	11.09	10.84	10.64	11.17	11.16	11.18	11.04	11.07	6.64
SnO_2	0.00	0.00	0.00	0.00	0.00	0.00	0.00	0.00	0.00	0.00	0.00	0.00	0.00	0.00	0.00
ZrO_2	0.00	0.00	0.00	0.23	0.00	0.00	0.00	0.00	0.00	0.00	0.00	0.00	0.00	0.02	0.00
HfO_2	0.00	0.00	0.00	0.00	0.00	0.30	0.00	0.00	0.00	0.00	0.00	0.00	0.00	0.02	0.00
Nb_2O_5	1.57	1.56	1.83	1.51	1.66	1.75	1.71	1.94	2.00	1.71	1.61	1.49	2.05	1.72	7.46
Ta_2O_5	0.14	0.10	0.09	0.07	0.10	0.12	0.08	0.11	0.00	0.00	0.00	0.07	0.00	0.07	0.00
SiO_2	35.69	34.44	34.83	35.27	35.22	35.18	34.65	34.74	34.00	34.63	33.92	33.72	34.27	34.66	33.03
F	1.39	0.93	1.25	1.22	1.30	1.03	1.12	0.96	1.17	1.41	1.25	1.34	1.31	1.21	0.79
H_2O	2.70	2.86	2.75	2.77	2.74	2.86	2.79	2.87	2.71	2.65	2.70	2.63	2.71	2.75	2.53
O=F	-0.59	-0.39	-0.53	-0.51	-0.55	-0.43	-0.47	-0.40	-0.49	-0.59	-0.53	-0.56	-0.55	-0.51	-0.33
Total	97.19	95.92	97.03	97.38	97.71	97.37	96.80	96.77	95.45	96.45	96.06	95.53	97.55	96.71	94.74
Chemical formulae calculated based on 31 anions															
Na_{tot}	1.50	1.55	1.45	1.53	1.49	1.52	1.52	1.49	1.60	1.67	1.68	1.66	1.33	1.54	1.73
Na	0.33	0.43	0.31	0.52	0.50	0.42	0.54	0.46	0.58	0.57	0.72	0.69	0.31	0.49	0.57
K	1.44	1.43	1.48	1.41	1.49	1.49	1.50	1.50	1.49	1.43	1.45	1.45	1.58	1.47	1.62
Rb	0.04	0.04	0.05	0.06	0.05	0.04	0.05	0.05	0.06	0.06	0.05	0.06	0.06	0.05	0.12
Cs	0.00	0.00	0.00	0.00	0.00	0.00	0.00	0.00	0.00	0.00	0.00	0.00	0.00	0.00	0.00
Sr	0.02	0.02	0.02	0.02	0.03	0.02	0.02	0.02	0.01	0.02	0.02	0.02	0.02	0.02	0.00
Ba	0.00	0.02	0.02	0.00	0.00	0.00	0.00	0.02	0.01	0.00	0.02	0.02	0.02	0.01	0.00
Sum A	1.83	1.95	1.87	2.01	2.06	1.97	2.11	2.05	2.16	2.08	2.26	2.24	1.99	2.04	2.31
Na	0.93	0.91	0.84	0.89	0.90	0.91	0.91	0.92	0.93	0.92	0.93	0.93	0.82	0.90	1.00
Ca	0.07	0.09	0.16	0.11	0.10	0.09	0.09	0.08	0.07	0.08	0.07	0.07	0.18	0.10	0.00
Sum B	1.00	1.00	1.00	1.00	1.00	1.00	1.00	1.00	1.00	1.00	1.00	1.00	1.00	1.00	1.00
Na	0.25	0.20	0.30	0.12	0.09	0.20	0.07	0.11	0.08	0.18	0.03	0.04	0.19	0.14	0.16
Mg	0.13	0.17	0.18	0.13	0.16	0.15	0.15	0.15	0.15	0.18	0.17	0.18	0.14	0.16	0.12
Mn	6.17	6.10	5.98	6.19	6.23	6.16	6.30	6.24	6.28	6.14	6.27	6.27	6.11	6.19	5.58
Fe^{2+}	0.33	0.38	0.36	0.40	0.38	0.36	0.36	0.38	0.38	0.39	0.42	0.39	0.40	0.38	0.00
Zn	0.13	0.14	0.15	0.17	0.14	0.13	0.12	0.11	0.09	0.11	0.11	0.11	0.11	0.12	1.14
Y	0.00	0.00	0.00	0.00	0.00	0.00	0.00	0.00	0.00	0.00	0.00	0.00	0.00	0.00	0.00
Ce	0.00	0.01	0.03	0.00	0.01	0.00	0.00	0.00	0.01	0.02	0.00	0.02	0.04	0.01	0.00
Sum C	7.00	7.00	7.00	7.00	7.00	7.00	7.00	7.00	7.00	7.00	7.00	7.00	7.00	7.00	7.00
Ti	1.88	1.93	1.91	1.83	1.85	1.86	1.88	1.84	1.84	1.90	1.91	1.93	1.87	1.88	1.19
Sn	0.00	0.00	0.00	0.00	0.00	0.00	0.00	0.00	0.00	0.00	0.00	0.00	0.00	0.00	0.00
Zr	0.00	0.00	0.00	0.03	0.00	0.00	0.00	0.00	0.00	0.00	0.00	0.00	0.00	0.00	0.00
Hf	0.00	0.00	0.00	0.00	0.00	0.02	0.00	0.00	0.00	0.00	0.00	0.00	0.00	0.00	0.00
Nb	0.16	0.16	0.19	0.15	0.17	0.18	0.17	0.20	0.21	0.18	0.17	0.15	0.21	0.18	0.80
Ta	0.01	0.01	0.01	0.00	0.01	0.01	0.01	0.01	0.00	0.00	0.00	0.00	0.00	0.00	0.00
Sum D	2.05	2.10	2.10	2.02	2.02	2.06	2.06	2.04	2.04	2.07	2.08	2.09	2.07	2.06	1.99
Si	7.95	7.82	7.81	7.89	7.86	7.87	7.81	7.84	7.80	7.82	7.73	7.73	7.70	7.82	7.84
Al	0.05	0.09	0.12	0.06	0.06	0.07	0.06	0.07	0.08	0.08	0.09	0.08	0.21	0.09	0.05
Sum T	8.01	7.91	7.94	7.95	7.93	7.94	7.88	7.91	7.88	7.90	7.82	7.81	7.91	7.91	7.89
F	0.98	0.67	0.89	0.86	0.92	0.73	0.80	0.69	0.85	1.01	0.90	0.97	0.93	0.86	0.59
OH	4.02	4.33	4.11	4.14	4.08	4.27	4.20	4.32	4.15	3.99	4.10	4.03	4.07	4.14	4.00
O	30.02	30.33	30.11	30.14	30.08	30.27	30.20	30.32	30.15	29.99	30.10	30.03	30.07	30.14	30.41
Cations	19.88	19.96	19.90	19.98	20.01	19.97	20.04	20.00	20.08	20.05	20.15	20.14	19.98	20.01	20.19

ELECTRON MICROPROBE ANALYSES OF MONT SAINT-HILAIRE AGM

OXIDE	MSH3b PT 16	PT 17	PT 18	PT 19	PT 20	MSH3c PT 21	PT 22	PT 23	PT 24	MSH3 Average	MSH4a PT 25	PT 26	PT 27	PT 28	PT 29
Na_2O	3.85	4.07	3.93	3.89	3.92	3.67	3.70	3.98	3.97	3.87	3.23	3.19	3.45	3.44	3.61
K_2O	5.71	5.29	5.38	5.33	5.42	5.44	5.28	5.16	5.31	5.37	5.59	5.44	5.41	5.43	5.00
Rb_2O	1.31	0.57	0.79	0.86	0.99	0.75	0.76	0.79	0.53	0.81	0.69	0.72	0.75	0.63	1.02
Cs_2O	0.00	0.00	0.00	0.00	0.17	0.09	0.00	0.00	0.00	0.03	0.11	0.14	0.12	0.00	0.17
CaO	0.00	0.00	0.00	0.04	0.00	0.00	0.00	0.00	0.00	0.00	0.06	0.05	0.06	0.10	0.00
SrO	0.00	0.00	0.00	0.19	0.12	0.10	0.13	0.00	0.10	0.06	0.19	0.17	0.21	0.27	0.16
BaO	0.00	0.00	0.00	0.00	0.00	0.00	0.00	0.00	0.00	0.00	0.00	0.00	0.00	0.00	0.00
MgO	0.14	0.32	0.37	1.18	0.55	1.07	0.40	0.35	0.39	0.51	0.82	0.81	0.83	0.94	0.56
MnO	28.00	28.53	28.36	28.37	28.18	29.33	27.60	27.39	27.60	28.11	27.21	26.99	27.47	26.47	28.26
FeO	0.36	0.12	0.13	2.50	1.12	2.53	0.15	0.00	0.14	0.71	6.80	6.54	6.31	6.92	0.27
ZnO	5.85	6.19	6.07	1.77	3.86	1.47	6.36	6.63	6.79	5.15	0.44	0.67	1.21	0.57	5.04
Al_2O_3	0.48	0.08	0.18	0.20	0.24	0.32	0.44	0.18	0.12	0.24	0.59	0.65	0.58	0.36	0.30
Y_2O_3	0.00	0.00	0.00	0.00	0.00	0.00	0.00	0.00	0.00	0.00	0.00	0.00	0.00	0.00	0.00
Ce_2O_3	0.00	0.00	0.00	0.00	0.00	0.00	0.00	0.00	0.00	0.00	0.00	0.00	0.00	0.15	0.00
TiO_2	3.74	7.89	6.32	7.47	6.16	6.30	6.98	6.83	8.06	6.64	6.31	6.35	6.74	8.44	6.84
SnO_2	0.00	0.00	0.00	0.00	0.00	0.00	0.00	0.00	0.00	0.00	0.00	0.00	0.00	0.00	0.00
ZrO_2	0.31	0.00	0.00	0.00	0.00	0.41	0.00	0.00	0.00	0.07	2.93	3.12	2.55	1.51	0.00
HfO_2	0.00	0.00	0.00	0.00	0.00	0.00	0.00	0.00	0.00	0.00	0.00	0.00	0.00	0.00	0.00
Nb_2O_5	11.89	5.99	8.60	6.97	9.33	8.22	7.88	7.80	6.10	8.02	5.54	5.46	4.79	3.53	7.33
Ta_2O_5	0.00	0.00	0.00	0.00	0.00	0.00	0.00	0.00	0.00	0.00	0.00	0.00	0.00	0.00	0.00
SiO_2	32.87	32.96	33.83	34.38	34.02	33.89	33.37	34.25	33.96	33.66	33.55	33.48	33.22	33.43	33.20
F	0.52	0.81	0.91	0.91	0.82	0.80	0.74	0.92	0.76	0.80	0.65	0.87	0.92	0.97	0.85
H_2O	2.55	2.54	2.59	2.61	2.60	2.60	2.57	2.59	2.58	2.58	2.59	2.59	2.81	2.78	2.54
O=F	-0.22	-0.34	-0.38	-0.38	-0.35	-0.34	-0.31	-0.39	-0.32	-0.34	-0.27	-0.37	-0.39	-0.41	-0.36
Total	97.36	95.02	97.08	96.29	97.15	96.65	96.56	96.49	96.09	96.34	97.02	96.87	97.04	95.53	95.86
Chemical formulae calculated based on 31 anions:															
Na_{tot}	1.76	1.86	1.76	1.73	1.75	1.64	1.67	1.79	1.79	1.75	1.45	1.43	1.55	1.55	1.65
Na	0.48	0.79	0.51	0.43	0.32	0.48	0.39	0.40	0.54	0.49	0.47	0.44	0.56	0.54	0.42
K	1.72	1.59	1.59	1.56	1.60	1.60	1.57	1.52	1.57	1.59	1.65	1.61	1.59	1.61	1.50
Rb	0.20	0.09	0.12	0.13	0.15	0.11	0.11	0.12	0.08	0.12	0.10	0.11	0.11	0.09	0.16
Cs	0.00	0.00	0.00	0.00	0.02	0.01	0.00	0.00	0.00	0.00	0.01	0.01	0.01	0.00	0.02
Sr	0.00	0.00	0.00	0.03	0.02	0.01	0.02	0.00	0.01	0.01	0.03	0.02	0.03	0.04	0.02
Ba	0.00	0.00	0.00	0.00	0.00	0.00	0.00	0.00	0.00	0.00	0.00	0.00	0.00	0.00	0.00
Sum A	2.40	2.47	2.22	2.14	2.10	2.21	2.10	2.04	2.21	2.22	2.26	2.20	2.31	2.28	2.12
Na	1.00	1.00	1.00	0.99	1.00	1.00	1.00	1.00	1.00	1.00	0.99	0.99	0.99	0.98	1.00
Ca	0.00	0.00	0.00	0.01	0.00	0.00	0.00	0.00	0.00	0.00	0.02	0.01	0.02	0.03	0.00
Sum B	1.00	1.00	1.00	1.00	1.00	1.00	1.00	1.00	1.00	1.00	1.00	1.00	1.00	1.00	1.00
Na	0.28	0.08	0.25	0.31	0.43	0.16	0.28	0.38	0.25	0.26	0.00	0.00	0.00	0.03	0.23
Mg	0.05	0.11	0.13	0.40	0.19	0.37	0.14	0.12	0.14	0.18	0.28	0.28	0.29	0.33	0.20
Mn	5.59	5.71	5.56	5.51	5.51	5.73	5.45	5.37	5.43	5.54	5.34	5.29	5.37	5.19	5.64
Fe^{2+}	0.07	0.02	0.03	0.48	0.22	0.49	0.03	0.00	0.03	0.14	1.32	1.27	1.22	1.34	0.05
Zn	1.02	1.08	1.04	0.30	0.66	0.25	1.10	1.13	1.16	0.89	0.08	0.12	0.21	0.10	0.88
Y	0.00	0.00	0.00	0.00	0.00	0.00	0.00	0.00	0.00	0.00	0.00	0.00	0.00	0.00	0.00
Ce	0.00	0.00	0.00	0.00	0.00	0.00	0.00	0.00	0.00	0.00	0.00	0.00	0.00	0.01	0.00
Sum C	7.00	7.00	7.00	7.00	7.00	7.00	7.00	7.00	7.00	7.00	7.01	6.95	7.08	7.00	7.00
Ti	0.66	1.40	1.10	1.29	1.07	1.09	1.23	1.19	1.41	1.16	1.10	1.11	1.17	1.47	1.21
Sn	0.00	0.00	0.00	0.00	0.00	0.00	0.00	0.00	0.00	0.00	0.00	0.00	0.00	0.00	0.00
Zr	0.04	0.00	0.00	0.00	0.00	0.05	0.00	0.00	0.00	0.01	0.33	0.35	0.29	0.17	0.00
Hf	0.00	0.00	0.00	0.00	0.00	0.00	0.00	0.00	0.00	0.00	0.00	0.00	0.00	0.00	0.00
Nb	1.27	0.64	0.90	0.72	0.97	0.86	0.83	0.82	0.64	0.84	0.58	0.57	0.50	0.37	0.78
Ta	0.00	0.00	0.00	0.00	0.00	0.00	0.00	0.00	0.00	0.00	0.00	0.00	0.00	0.00	0.00
Sum D	1.96	2.04	2.00	2.01	2.04	2.00	2.06	2.00	2.05	2.01	2.01	2.03	1.96	2.01	1.99
Si	7.74	7.78	7.83	7.89	7.85	7.82	7.79	7.92	7.89	7.83	7.77	7.75	7.67	7.74	7.83
Al	0.13	0.02	0.05	0.05	0.07	0.09	0.12	0.05	0.03	0.07	0.16	0.18	0.16	0.10	0.08
Sum T	7.88	7.81	7.88	7.94	7.91	7.90	7.91	7.97	7.92	7.90	7.93	7.93	7.83	7.84	7.91
F	0.39	0.61	0.67	0.66	0.60	0.58	0.55	0.67	0.56	0.59	0.48	0.64	0.67	0.71	0.63
OH	4.00	4.00	4.00	4.00	4.00	4.00	4.00	4.00	4.00	4.00	4.00	4.00	4.33	4.29	4.00
O	30.61	30.40	30.33	30.34	30.40	30.42	30.45	30.33	30.44	30.41	30.52	30.36	30.33	30.29	30.37
Cations	20.24	20.31	20.10	20.09	20.05	20.11	20.09	20.02	20.17	20.14	20.22	20.11	20.17	20.13	20.09

ELECTRON MICROPROBE ANALYSES OF MONT SAINT-HILAIRE AGM

OXIDE	MSH4b PT 30	PT 31	PT 32	PT 33	MSH4c PT 34	PT 35	PT 36	MSH4d PT 37	PT 38	PT 39	MSH4 Average	MSH5a PT 41	PT 42	MSH5b PT 43	PT 44
Na_2O	3.59	3.85	3.41	3.87	3.32	3.83	3.21	3.22	3.23	3.11	3.44	3.33	3.23	3.04	3.10
K_2O	5.28	5.20	5.29	5.12	5.27	5.03	5.42	5.41	5.39	5.25	5.30	5.33	5.34	5.31	5.42
Rb_2O	0.82	0.89	0.85	1.03	0.89	0.98	0.63	0.87	0.80	0.83	0.83	0.66	0.68	0.67	0.72
Cs_2O	0.08	0.10	0.00	0.14	0.13	0.18	0.13	0.00	0.00	0.00	0.09	0.00	0.00	0.21	0.24
CaO	0.10	0.00	0.07	0.00	0.00	0.00	0.07	0.00	0.07	0.00	0.04	0.07	0.10	0.09	0.06
SrO	0.20	0.00	0.21	0.12	0.18	0.09	0.17	0.15	0.14	0.13	0.16	0.18	0.20	0.17	0.19
BaO	0.00	0.00	0.00	0.00	0.00	0.00	0.00	0.00	0.00	0.00	0.00	0.00	0.00	0.00	0.00
MgO	0.89	0.49	0.84	0.51	0.83	0.39	0.85	0.79	0.78	0.76	0.74	0.84	0.79	0.79	0.71
MnO	27.93	27.95	27.64	28.09	27.11	28.27	26.22	28.18	28.34	29.00	27.68	29.03	28.43	25.39	25.15
FeO	5.83	0.12	5.97	0.65	6.74	0.18	7.92	5.43	5.29	5.40	4.69	5.45	5.71	9.38	9.25
ZnO	0.68	5.91	0.54	5.42	0.46	5.70	0.40	0.63	0.47	0.51	1.91	0.53	0.57	0.31	0.40
Al_2O_3	0.34	0.19	0.37	0.29	0.53	0.28	0.55	0.75	0.63	0.79	0.48	0.51	0.55	0.64	0.79
Y_2O_3	0.00	0.00	0.00	0.00	0.00	0.00	0.00	0.00	0.00	0.00	0.00	0.00	0.00	0.00	0.00
Ce_2O_3	0.00	0.00	0.00	0.00	0.00	0.00	0.00	0.00	0.00	0.00	0.01	0.00	0.00	0.00	0.15
TiO_2	8.12	7.00	8.00	7.00	6.60	6.79	6.93	5.68	5.83	5.66	6.82	6.74	6.45	6.34	5.98
SnO_2	0.00	0.00	0.00	0.00	0.00	0.00	0.00	0.00	0.00	0.00	0.00	0.00	0.00	0.00	0.00
ZrO_2	2.14	0.00	2.21	0.26	2.92	0.00	2.72	2.69	2.59	2.54	1.88	2.74	2.46	2.86	2.70
HfO_2	0.00	0.00	0.00	0.00	0.00	0.00	0.30	0.00	0.00	0.00	0.02	0.00	0.00	0.00	0.00
Nb_2O_5	3.90	7.87	4.17	7.44	5.48	8.15	5.03	6.30	5.99	6.92	5.83	4.75	5.31	5.24	5.92
Ta_2O_5	0.00	0.00	0.00	0.00	0.00	0.00	0.00	0.00	0.00	0.00	0.00	0.00	0.00	0.00	0.00
SiO_2	34.51	34.21	34.45	33.51	33.79	33.54	33.94	32.06	32.46	32.39	33.45	32.23	32.39	32.44	32.14
F	1.03	0.75	0.83	0.68	0.79	0.78	0.78	0.94	0.81	0.99	0.84	0.83	0.84	0.98	0.97
H_2O	2.83	2.60	2.91	2.57	2.60	2.58	2.61	2.53	2.53	2.55	2.64	2.80	2.54	2.55	2.54
O=F	-0.43	-0.32	-0.35	-0.29	-0.33	-0.33	-0.33	-0.40	-0.34	-0.42	-0.36	-0.35	-0.35	-0.41	-0.41
Total	97.83	96.81	97.41	96.41	97.31	97.19	97.55	95.23	95.01	96.01	96.61	95.67	95.23	96.00	96.02
Chemical formulae calculated based on 31 anions															
Na_{tot}	1.57	1.72	1.50	1.75	1.48	1.73	1.43	1.48	1.49	1.42	1.55	1.52	1.48	1.39	1.42
Na	0.46	0.39	0.33	0.54	0.43	0.45	0.42	0.48	0.50	0.42	0.49	0.53	0.51	0.41	0.43
K	1.52	1.53	1.53	1.52	1.55	1.49	1.59	1.64	1.63	1.57	1.57	1.60	1.61	1.59	1.63
Rb	0.12	0.13	0.12	0.15	0.13	0.15	0.09	0.13	0.12	0.13	0.12	0.10	0.10	0.10	0.11
Cs	0.01	0.01	0.00	0.01	0.01	0.02	0.01	0.00	0.00	0.00	0.01	0.00	0.00	0.02	0.02
Sr	0.03	0.00	0.03	0.02	0.02	0.01	0.02	0.02	0.02	0.02	0.02	0.03	0.03	0.02	0.03
Ba	0.00	0.00	0.00	0.00	0.00	0.00	0.00	0.00	0.00	0.00	0.00	0.00	0.00	0.00	0.00
Sum A	2.14	2.07	2.02	2.24	2.15	2.12	2.14	2.27	2.28	2.13	2.21	2.26	2.25	2.15	2.22
Na	0.98	1.00	0.98	1.00	1.00	1.00	0.98	1.00	0.98	1.00	0.99	0.98	0.98	0.98	0.99
Ca	0.02	0.00	0.02	0.00	0.00	0.00	0.02	0.00	0.02	0.00	0.01	0.02	0.03	0.02	0.02
Sum B	1.00	1.00	1.00	1.00	1.00	1.00	1.00	1.00	1.00	1.00	1.00	1.00	1.00	1.00	1.00
Na	0.14	0.33	0.18	0.21	0.05	0.28	0.03	0.00	0.00	0.00	0.07	0.00	0.00	0.00	0.00
Mg	0.30	0.17	0.28	0.18	0.29	0.14	0.29	0.28	0.28	0.27	0.26	0.29	0.28	0.28	0.25
Mn	5.35	5.47	5.31	5.55	5.29	5.57	5.10	5.66	5.69	5.77	5.44	5.78	5.70	5.06	5.03
Fe^{2+}	1.10	0.02	1.13	0.13	1.30	0.04	1.52	1.08	1.05	1.06	0.91	1.07	1.13	1.84	1.83
Zn	0.11	1.01	0.09	0.93	0.08	0.98	0.07	0.11	0.08	0.09	0.33	0.09	0.10	0.05	0.07
Y	0.00	0.00	0.00	0.00	0.00	0.00	0.00	0.00	0.00	0.00	0.00	0.00	0.00	0.00	0.00
Ce	0.00	0.00	0.00	0.00	0.00	0.00	0.00	0.00	0.00	0.00	0.00	0.00	0.00	0.00	0.01
Sum C	7.00	7.00	7.00	7.00	7.00	7.00	7.00	7.13	7.10	7.19	7.00	7.23	7.20	7.23	7.18
Ti	1.38	1.22	1.36	1.23	1.14	1.19	1.20	1.01	1.04	1.00	1.19	1.19	1.15	1.12	1.06
Sn	0.00	0.00	0.00	0.00	0.00	0.00	0.00	0.00	0.00	0.00	0.00	0.00	0.00	0.00	0.00
Zr	0.24	0.00	0.24	0.03	0.33	0.00	0.30	0.31	0.30	0.29	0.21	0.31	0.28	0.33	0.31
Hf	0.00	0.00	0.00	0.00	0.00	0.00	0.02	0.00	0.00	0.00	0.00	0.00	0.00	0.00	0.00
Nb	0.40	0.82	0.43	0.78	0.57	0.86	0.52	0.68	0.64	0.69	0.61	0.50	0.57	0.56	0.63
Ta	0.00	0.00	0.00	0.00	0.00	0.00	0.00	0.00	0.00	0.00	0.00	0.00	0.00	0.00	0.00
Sum D	2.02	2.04	2.04	2.04	2.04	2.05	2.04	2.00	1.98	1.98	2.02	2.01	2.00	2.01	2.00
Si	7.80	7.90	7.81	7.82	7.78	7.80	7.79	7.61	7.70	7.61	7.76	7.57	7.66	7.63	7.58
Al	0.09	0.05	0.10	0.08	0.14	0.08	0.15	0.21	0.18	0.22	0.13	0.14	0.15	0.18	0.22
Sum T	7.89	7.95	7.91	7.90	7.93	7.88	7.94	7.82	7.87	7.83	7.89	7.71	7.81	7.80	7.80
F	0.74	0.55	0.60	0.50	0.58	0.57	0.57	0.71	0.61	0.74	0.62	0.62	0.63	0.73	0.72
OH	4.26	4.00	4.41	4.00	4.00	4.00	4.00	4.00	4.00	4.00	4.09	4.38	4.00	4.00	4.00
O	30.26	30.45	30.41	30.50	30.43	30.43	30.43	30.30	30.39	30.26	30.38	30.38	30.37	30.27	30.28
Cations	20.05	20.05	19.96	20.18	20.12	20.09	20.11	20.22	20.23	20.14	20.12	20.21	20.26	20.19	20.21

ELECTRON MICROPROBE ANALYSES OF MONT SAINT-HILAIRE AGM

OXIDE	PT 61	PT 62	MSH6 Average	MSH7a PT 63	PT 64	PT 65	PT 66	PT 67	MSH7b PT 70	PT 71	MSH7 Average	MSH8a PT 72	PT 73	MSH8b PT 74	PT 75
Na_2O	2.20	2.07	2.11	2.16	2.18	2.06	2.06	2.13	2.08	1.97	2.09	3.08	3.30	3.38	3.08
K_2O	5.68	5.71	5.73	5.68	5.80	5.74	5.83	5.65	5.73	5.87	5.76	5.78	5.64	5.46	5.56
Rb_2O	0.33	0.33	0.36	0.41	0.41	0.45	0.43	0.45	0.33	0.34	0.40	0.58	0.57	0.55	0.50
Cs_2O	0.08	0.09	0.08	0.00	0.00	0.10	0.00	0.00	0.00	0.00	0.01	0.00	0.00	0.00	0.00
CaO	1.27	1.46	1.36	1.09	1.17	0.94	0.92	0.84	1.45	1.52	1.13	0.39	0.40	0.42	0.34
SrO	0.25	0.19	0.24	0.23	0.23	0.27	0.26	0.26	0.20	0.24	0.24	0.00	0.15	0.17	0.08
BaO	0.14	0.14	0.04	0.00	0.00	0.00	0.00	0.00	0.00	0.00	0.00	0.00	0.00	0.00	0.00
MgO	1.18	1.22	1.21	1.31	1.41	1.08	1.03	0.95	1.19	1.50	1.21	0.47	1.00	0.94	0.55
MnO	18.15	19.40	18.44	19.23	19.02	19.72	20.05	20.05	18.85	18.44	19.34	24.29	26.32	26.00	24.49
FeO	17.12	15.56	16.47	15.31	15.71	14.62	14.76	14.37	15.61	15.69	15.15	10.64	4.63	4.53	9.60
ZnO	0.00	0.00	0.03	0.00	0.00	0.00	0.00	0.00	0.10	0.09	0.03	0.60	3.06	3.28	1.11
Al_2O_3	1.33	1.32	1.36	1.23	1.21	1.19	1.24	1.13	1.35	1.25	1.23	1.01	0.24	0.31	1.06
Y_2O_3	0.00	0.00	0.00	0.00	0.00	0.00	0.00	0.00	0.00	0.00	0.00	0.00	0.00	0.00	0.00
Ce_2O_3	0.20	0.00	0.19	0.23	0.24	0.20	0.15	0.00	0.00	0.21	0.15	0.00	0.00	0.00	0.00
TiO_2	8.43	8.94	8.61	7.54	7.27	5.33	4.82	4.26	9.02	10.25	6.93	6.17	8.51	8.14	6.03
SnO_2	0.00	0.00	0.00	0.00	0.00	0.00	0.00	0.00	0.00	0.00	0.00	0.00	0.00	0.00	0.00
ZrO_2	3.70	3.27	3.68	5.54	5.55	7.99	8.31	8.67	3.24	1.28	5.80	0.65	0.00	0.00	0.42
HfO_2	0.00	0.00	0.00	0.00	0.34	0.34	0.35	0.48	0.00	0.00	0.22	0.00	0.00	0.00	0.00
Nb_2O_5	1.55	0.96	1.45	0.99	0.80	1.60	1.70	2.01	0.99	1.14	1.26	7.76	5.79	5.99	8.10
Ta_2O_5	0.09	0.06	0.10	0.00	0.00	0.10	0.12	0.00	0.00	0.20	0.06	0.00	0.00	0.07	0.00
SiO_2	31.85	32.03	32.34	32.13	32.15	32.38	31.71	31.56	31.83	32.25	32.00	31.97	34.52	34.33	32.23
F	0.87	1.14	1.16	1.45	1.21	1.17	1.24	1.37	1.35	1.16	1.28	0.64	0.85	0.90	0.91
H_2O	2.83	2.69	2.71	2.53	2.65	2.66	2.60	2.50	2.57	2.70	2.60	2.55	2.64	2.62	2.56
O=F	-0.37	-0.48	-0.49	-0.61	-0.51	-0.49	-0.52	-0.58	-0.57	-0.49	-0.54	-0.27	-0.36	-0.38	-0.38
Total	96.88	96.10	97.17	96.04	96.84	97.45	97.06	96.10	95.33	95.61	96.35	96.31	97.06	96.71	96.24
Chemical formulae calculated based on 31 anions:															
Na_{tot}	0.99	0.93	0.94	0.98	0.98	0.93	0.94	0.98	0.94	0.88	0.95	1.40	1.46	1.50	1.40
Na	0.30	0.29	0.28	0.25	0.27	0.17	0.17	0.20	0.30	0.26	0.23	0.50	0.36	0.38	0.48
K	1.68	1.69	1.68	1.69	1.72	1.71	1.75	1.72	1.71	1.73	1.72	1.73	1.58	1.59	1.66
Rb	0.05	0.05	0.05	0.06	0.06	0.07	0.07	0.07	0.05	0.05	0.06	0.09	0.08	0.08	0.08
Cs	0.01	0.01	0.01	0.00	0.00	0.01	0.00	0.00	0.00	0.00	0.00	0.00	0.00	0.00	0.00
Sr	0.03	0.03	0.03	0.03	0.03	0.04	0.04	0.04	0.03	0.03	0.03	0.00	0.02	0.02	0.01
Ba	0.01	0.01	0.00	0.00	0.00	0.00	0.00	0.00	0.00	0.00	0.00	0.00	0.00	0.00	0.00
Sum A	2.08	2.08	2.05	2.03	2.08	1.98	2.02	2.02	2.08	2.07	2.04	2.32	2.04	2.08	2.23
Na	0.69	0.64	0.67	0.73	0.71	0.77	0.77	0.79	0.64	0.62	0.72	0.90	0.90	0.90	0.92
Ca	0.32	0.36	0.33	0.27	0.29	0.24	0.23	0.21	0.36	0.38	0.28	0.10	0.10	0.10	0.09
Sum B	1.00	1.00	1.00	1.00	1.00	1.00	1.00	1.00	1.00	1.00	1.00	1.00	1.00	1.00	1.00
Na	0.00	0.00	0.00	0.00	0.00	0.00	0.00	0.00	0.00	0.00	0.00	0.00	0.19	0.22	0.00
Mg	0.41	0.42	0.41	0.46	0.49	0.38	0.36	0.34	0.41	0.52	0.42	0.17	0.34	0.32	0.19
Mn	3.56	3.81	3.59	3.80	3.74	3.89	4.00	4.04	3.72	3.61	3.83	4.84	5.07	5.04	4.85
Fe^{2+}	3.31	3.02	3.16	2.99	3.05	2.85	2.91	2.86	3.04	3.03	2.96	2.09	0.88	0.87	1.88
Zn	0.00	0.00	0.01	0.00	0.00	0.00	0.00	0.00	0.02	0.02	0.00	0.10	0.51	0.55	0.19
Y	0.00	0.00	0.00	0.00	0.00	0.00	0.00	0.00	0.00	0.00	0.00	0.00	0.00	0.00	0.00
Ce	0.02	0.00	0.02	0.02	0.02	0.02	0.01	0.00	0.00	0.02	0.01	0.00	0.00	0.00	0.00
Sum C	7.30	7.25	7.19	7.26	7.30	7.13	7.28	7.24	7.20	7.18	7.23	7.20	7.00	7.00	7.12
Ti	1.47	1.56	1.49	1.32	1.27	0.93	0.85	0.76	1.58	1.78	1.21	1.09	1.46	1.40	1.06
Sn	0.00	0.00	0.00	0.00	0.00	0.00	0.00	0.00	0.00	0.00	0.00	0.00	0.00	0.00	0.00
Zr	0.42	0.37	0.41	0.63	0.63	0.91	0.95	1.01	0.37	0.14	0.66	0.08	0.00	0.00	0.05
Hf	0.00	0.00	0.00	0.00	0.02	0.02	0.02	0.03	0.00	0.00	0.01	0.00	0.00	0.00	0.00
Nb	0.16	0.10	0.15	0.06	0.08	0.17	0.18	0.22	0.10	0.12	0.13	0.83	0.60	0.62	0.86
Ta	0.01	0.00	0.01	0.00	0.00	0.01	0.01	0.00	0.00	0.01	0.00	0.00	0.00	0.00	0.00
Sum D	2.05	2.03	2.06	2.02	2.01	2.04	2.02	2.02	2.05	2.06	2.03	1.99	2.05	2.02	1.97
Si	7.37	7.43	7.43	7.50	7.47	7.54	7.46	7.51	7.42	7.44	7.48	7.52	7.86	7.85	7.54
Al	0.36	0.36	0.37	0.34	0.33	0.33	0.34	0.32	0.37	0.34	0.34	0.28	0.06	0.08	0.29
Sum T	7.73	7.79	7.80	7.83	7.80	7.87	7.81	7.83	7.79	7.78	7.82	7.80	7.92	7.94	7.83
F	0.64	0.84	0.84	1.07	0.89	0.86	0.92	1.03	1.00	0.85	0.95	0.48	0.61	0.65	0.67
OH	4.36	4.16	4.16	3.93	4.11	4.14	4.08	3.97	4.00	4.15	4.05	4.00	4.00	4.00	4.00
O	30.36	30.16	30.16	29.93	30.11	30.14	30.08	29.97	30.00	30.15	30.05	30.52	30.39	30.35	30.33
Cations	20.16	20.15	20.09	20.14	20.19	20.02	20.12	20.09	20.13	20.09	20.11	20.31	20.02	20.03	20.15

ELECTRON MICROPROBE ANALYSES OF MONT SAINT-HILAIRE AGM

OXIDE	PT 45	PT 46	MSH5c PT 48	PT 49	PT 50	MSH5 Average	MSH6a PT 51	PT 52	PT 53	MSH6b PT 54	PT 55	PT 56	PT 57	PT 58	MSH6c PT 59
Na_2O	3.04	3.13	3.17	3.21	3.28	3.17	1.94	2.07	2.08	2.08	2.13	2.21	2.17	2.11	2.19
K_2O	5.38	5.45	5.29	5.18	5.39	5.34	5.77	5.70	5.75	5.74	5.65	5.78	5.73	5.72	5.78
Rb_2O	0.71	0.69	0.64	0.68	0.79	0.69	0.32	0.33	0.36	0.38	0.36	0.35	0.39	0.41	0.39
Cs_2O	0.19	0.23	0.00	0.00	0.00	0.10	0.09	0.09	0.00	0.00	0.09	0.11	0.09	0.11	0.12
CaO	0.07	0.06	0.05	0.04	0.00	0.06	1.61	1.54	1.57	1.31	1.31	1.21	1.17	1.18	1.28
SrO	0.15	0.18	0.15	0.19	0.15	0.17	0.25	0.22	0.28	0.23	0.21	0.24	0.27	0.25	0.25
BaO	0.00	0.00	0.00	0.00	0.00	0.00	0.00	0.00	0.00	0.14	0.00	0.00	0.00	0.00	0.00
MgO	0.71	0.75	0.77	0.76	0.76	0.76	1.22	1.18	1.42	1.11	1.19	1.19	1.22	1.19	1.15
MnO	25.04	25.54	29.15	29.03	29.36	27.35	19.65	18.96	18.38	18.56	18.36	18.07	18.20	17.76	17.33
FeO	9.22	8.42	5.06	5.00	5.02	6.95	15.54	15.66	16.33	16.61	16.11	17.09	16.69	17.14	17.31
ZnO	0.31	0.35	0.48	0.49	0.49	0.44	0.00	0.00	0.00	0.11	0.11	0.11	0.00	0.00	0.00
Al_2O_3	0.95	0.77	0.60	0.60	0.65	0.67	1.48	1.34	1.66	1.35	1.28	1.31	1.25	1.27	1.38
Y_2O_3	0.00	0.00	0.00	0.00	0.00	0.00	0.00	0.00	0.00	0.00	0.00	0.00	0.00	0.00	0.00
Ce_2O_3	0.18	0.00	0.00	0.00	0.00	0.04	0.16	0.17	0.26	0.20	0.17	0.19	0.30	0.19	0.21
TiO_2	5.42	5.95	5.94	5.84	5.78	6.05	9.37	8.84	8.52	8.46	8.63	8.35	8.44	8.41	8.30
SnO_2	0.00	0.00	0.00	0.00	0.00	0.00	0.00	0.00	0.00	0.00	0.00	0.00	0.00	0.00	0.00
ZrO_2	2.79	2.70	2.58	2.68	2.72	2.69	3.33	3.49	4.41	4.00	3.44	3.96	3.66	3.63	3.64
HfO_2	0.00	0.00	0.00	0.00	0.00	0.00	0.00	0.00	0.00	0.00	0.00	0.00	0.00	0.00	0.00
Nb_2O_5	6.45	6.07	6.31	6.01	6.54	5.84	0.70	1.13	1.64	1.39	1.60	1.83	1.70	1.63	1.83
Ta_2O_5	0.00	0.00	0.00	0.00	0.00	0.00	0.10	0.10	0.12	0.10	0.08	0.11	0.11	0.10	0.13
SiO_2	31.90	32.70	32.89	32.73	32.83	32.47	32.39	32.90	32.70	32.72	32.52	32.61	31.96	32.42	31.59
F	0.69	0.58	0.66	0.81	0.69	0.78	1.47	1.13	0.88	1.31	1.13	1.30	1.18	1.12	1.25
H_2O	2.52	2.55	2.56	2.54	2.57	2.57	2.58	2.75	2.91	2.66	2.72	2.67	2.68	2.72	2.62
O=F	-0.29	-0.24	-0.28	-0.34	-0.29	-0.33	-0.62	-0.48	-0.37	-0.55	-0.48	-0.55	-0.50	-0.47	-0.53
Total	95.43	95.87	96.02	95.45	96.73	95.82	97.35	97.12	98.90	97.91	96.61	98.15	96.71	96.89	96.23
Chemical formulae calculated based on 31 anions															
Na_{tot}	1.40	1.43	1.44	1.47	1.49	1.45	0.86	0.92	0.91	0.92	0.95	0.98	0.97	0.94	0.99
Na	0.42	0.44	0.45	0.48	0.49	0.46	0.25	0.29	0.29	0.24	0.27	0.27	0.26	0.23	0.31
K	1.63	1.64	1.58	1.56	1.61	1.61	1.68	1.66	1.65	1.67	1.66	1.68	1.69	1.68	1.72
Rb	0.11	0.10	0.10	0.10	0.12	0.10	0.05	0.05	0.05	0.06	0.05	0.05	0.06	0.06	0.06
Cs	0.02	0.02	0.00	0.00	0.00	0.01	0.01	0.01	0.00	0.00	0.01	0.01	0.01	0.01	0.01
Sr	0.02	0.03	0.02	0.03	0.02	0.02	0.03	0.03	0.04	0.03	0.03	0.03	0.04	0.03	0.03
Ba	0.00	0.00	0.00	0.00	0.00	0.00	0.00	0.00	0.00	0.01	0.00	0.00	0.00	0.00	0.00
Sum A	2.20	2.23	2.15	2.16	2.23	2.21	2.03	2.04	2.03	2.01	2.02	2.05	2.06	2.02	2.13
Na	0.98	0.99	0.99	0.99	1.00	0.98	0.61	0.62	0.62	0.68	0.68	0.71	0.71	0.71	0.68
Ca	0.02	0.02	0.01	0.01	0.00	0.02	0.39	0.38	0.38	0.32	0.32	0.30	0.29	0.29	0.32
Sum B	1.00	1.00	1.00	1.00	1.00	1.00	1.00	1.00	1.00	1.00	1.00	1.00	1.00	1.00	1.00
Na	0.00	0.00	0.00	0.00	0.00	0.00	0.00	0.00	0.00	0.00	0.00	0.00	0.00	0.00	0.00
Mg	0.25	0.26	0.27	0.27	0.27	0.27	0.42	0.40	0.48	0.38	0.41	0.40	0.42	0.41	0.40
Mn	5.05	5.10	5.79	5.80	5.81	5.45	3.80	3.67	3.51	3.59	3.58	3.49	3.57	3.47	3.42
Fe^{2+}	1.84	1.66	0.99	0.99	0.98	1.37	2.97	2.99	3.08	3.17	3.10	3.26	3.23	3.30	3.37
Zn	0.05	0.06	0.08	0.09	0.09	0.08	0.00	0.00	0.00	0.02	0.02	0.02	0.00	0.00	0.00
Y	0.00	0.00	0.00	0.00	0.00	0.00	0.00	0.00	0.00	0.00	0.00	0.00	0.00	0.00	0.00
Ce	0.02	0.00	0.00	0.00	0.00	0.00	0.01	0.01	0.02	0.02	0.01	0.02	0.03	0.02	0.02
Sum C	7.21	7.08	7.13	7.13	7.14	7.17	7.20	7.08	7.08	7.17	7.12	7.18	7.25	7.19	7.21
Ti	0.97	1.05	1.05	1.04	1.02	1.07	1.61	1.52	1.44	1.45	1.49	1.43	1.47	1.46	1.46
Sn	0.00	0.00	0.00	0.00	0.00	0.00	0.00	0.00	0.00	0.00	0.00	0.00	0.00	0.00	0.00
Zr	0.32	0.31	0.30	0.31	0.31	0.31	0.37	0.39	0.48	0.45	0.39	0.44	0.41	0.41	0.41
Hf	0.00	0.00	0.00	0.00	0.00	0.00	0.00	0.00	0.00	0.00	0.00	0.00	0.00	0.00	0.00
Nb	0.69	0.65	0.67	0.64	0.69	0.62	0.07	0.12	0.17	0.14	0.17	0.19	0.18	0.17	0.19
Ta	0.00	0.00	0.00	0.00	0.00	0.00	0.01	0.01	0.01	0.01	0.01	0.01	0.01	0.01	0.01
Sum D	1.99	2.01	2.01	1.98	2.02	2.00	2.06	2.03	2.10	2.05	2.05	2.07	2.07	2.04	2.07
Si	7.59	7.70	7.71	7.71	7.67	7.65	7.40	7.52	7.37	7.46	7.49	7.43	7.40	7.47	7.36
Al	0.27	0.21	0.17	0.17	0.18	0.19	0.40	0.36	0.44	0.36	0.35	0.35	0.34	0.35	0.38
Sum T	7.86	7.92	7.88	7.88	7.85	7.83	7.80	7.88	7.81	7.83	7.83	7.78	7.74	7.82	7.74
F	0.52	0.43	0.49	0.60	0.51	0.58	1.06	0.82	0.63	0.95	0.82	0.94	0.86	0.82	0.92
OH	4.00	4.00	4.00	4.00	4.00	4.04	3.94	4.18	4.37	4.06	4.18	4.06	4.14	4.18	4.08
O	30.48	30.57	30.51	30.40	30.49	30.42	29.94	30.18	30.37	30.06	30.18	30.06	30.14	30.18	30.08
Cations	20.25	20.24	20.18	20.16	20.23	20.21	20.09	20.02	20.02	20.05	20.03	20.08	20.12	20.07	20.16

ELECTRON MICROPROBE ANALYSES OF MONT SAINT-HILAIRE AGM

OXIDE	PT 76	MH8c PT 79	PT 80	PT 81	PT 82	MH8 Average	MH8c PT 89	PT 92	PT 93	MH84 PT 94	PT 95	PT 96	PT 97	PT 98	MH89 Average
Na_2O	2.97	2.91	2.88	2.85	3.00	3.05	3.65	3.59	3.55	3.67	3.78	3.51	3.75	3.66	3.65
K_2O	5.76	5.52	5.69	5.50	5.54	5.58	4.75	4.91	4.99	5.15	5.00	4.96	4.68	5.18	4.95
Rb_2O	0.50	0.52	0.52	0.47	0.51	0.52	0.50	0.34	0.33	0.94	0.83	0.51	0.37	1.01	0.60
Cs_2O	0.00	0.10	0.00	0.00	0.00	0.01	0.10	0.00	0.00	0.20	0.19	0.00	0.00	0.27	0.10
CaO	0.36	0.54	0.39	0.42	0.37	0.40	0.25	0.12	0.24	0.05	0.00	0.21	0.23	0.00	0.14
SrO	0.10	0.12	0.11	0.08	0.10	0.10	0.18	0.13	0.12	0.00	0.00	0.14	0.13	0.00	0.09
BaO	0.00	0.00	0.00	0.00	0.00	0.00	0.00	0.00	0.26	0.00	0.00	0.00	0.00	0.00	0.03
MgO	0.50	0.50	0.50	0.49	0.51	0.61	0.41	0.34	0.45	0.53	0.47	0.50	0.40	0.59	0.46
MnO	24.14	24.30	24.40	24.47	24.01	24.71	33.25	33.34	32.81	31.26	32.19	32.68	33.70	31.68	32.61
FeO	10.22	10.70	10.46	10.17	10.35	9.03	2.04	1.86	1.99	1.93	1.72	2.10	1.98	1.88	1.94
ZnO	0.65	0.51	0.44	0.42	0.61	1.19	0.42	0.52	0.75	0.44	0.44	0.50	0.53	0.49	0.51
Al_2O_3	0.97	0.85	1.05	0.85	1.04	0.82	0.08	0.11	0.28	0.64	0.41	0.32	0.16	0.54	0.32
Y_2O_3	0.00	0.00	0.00	0.00	0.00	0.00	0.00	0.00	0.00	0.00	0.00	0.00	0.00	0.00	0.00
Ce_2O_3	0.00	0.00	0.00	0.00	0.00	0.00	0.00	0.00	0.00	0.00	0.00	0.00	0.00	0.00	0.00
TiO_2	6.01	7.17	5.89	6.28	6.11	6.70	11.09	10.75	10.92	5.55	7.59	10.06	11.17	5.99	9.14
SnO_2	0.00	0.00	0.00	0.00	0.00	0.00	0.00	0.00	0.00	0.00	0.00	0.00	0.00	0.00	0.00
ZrO_2	0.17	0.84	0.97	0.82	0.74	0.51	0.00	0.00	0.00	0.00	0.00	0.42	0.17	0.00	0.07
HfO_2	0.00	0.00	0.00	0.00	0.00	0.00	0.00	0.00	0.00	0.00	0.00	0.00	0.00	0.00	0.00
Nb_2O_5	8.60	6.30	8.10	7.21	7.91	7.31	1.31	1.72	1.49	9.63	6.97	2.68	1.35	9.41	4.32
Ta_2O_5	0.00	0.00	0.00	0.00	0.00	0.01	0.00	0.07	0.09	0.00	0.00	0.00	0.00	0.00	0.02
SiO_2	32.00	32.81	32.61	32.51	31.96	32.77	33.68	34.02	34.12	32.88	34.17	33.93	34.64	33.71	33.89
F	0.70	0.89	0.69	0.65	0.76	0.78	1.19	1.18	1.38	0.68	0.89	0.89	1.08	0.83	1.02
H_2O	2.55	2.59	2.58	2.55	2.54	2.58	2.69	2.70	2.63	2.56	2.62	2.85	2.81	2.61	2.68
O=F	-0.29	-0.37	-0.29	-0.27	-0.32	-0.33	-0.50	-0.50	-0.58	-0.29	-0.37	-0.37	-0.45	-0.35	-0.43
Total	95.90	96.79	96.99	95.46	95.74	96.36	95.08	95.21	95.82	95.82	96.89	95.89	96.70	97.50	96.11
Chemical formulae calculated based on 31 cations															
Na_{tot}	1.36	1.31	1.30	1.30	1.37	1.38	1.63	1.60	1.57	1.67	1.68	1.56	1.64	1.63	1.62
Na	0.45	0.44	0.40	0.41	0.46	0.48	0.69	0.63	0.63	0.53	0.48	0.60	0.70	0.44	0.61
K	1.73	1.63	1.69	1.65	1.67	1.66	1.40	1.44	1.45	1.54	1.46	1.45	1.35	1.52	1.45
Rb	0.08	0.08	0.08	0.07	0.08	0.08	0.07	0.05	0.05	0.14	0.12	0.08	0.05	0.15	0.09
Cs	0.00	0.01	0.00	0.00	0.00	0.00	0.01	0.00	0.00	0.02	0.02	0.00	0.00	0.03	0.01
Sr	0.01	0.02	0.02	0.01	0.01	0.01	0.02	0.02	0.02	0.00	0.00	0.02	0.02	0.00	0.01
Ba	0.00	0.00	0.00	0.00	0.00	0.00	0.00	0.00	0.02	0.00	0.00	0.00	0.00	0.00	0.00
Sum A	2.27	2.18	2.18	2.14	2.22	2.23	2.20	2.14	2.17	2.24	2.09	2.14	2.12	2.14	2.18
Na	0.91	0.87	0.90	0.89	0.91	0.90	0.94	0.97	0.94	0.99	1.00	0.95	0.94	1.00	0.97
Ca	0.09	0.13	0.10	0.11	0.09	0.10	0.06	0.03	0.06	0.01	0.00	0.05	0.06	0.00	0.03
Sum B	1.00	1.00	1.00	1.00	1.00	1.00	1.00	1.00	1.00	1.00	1.00	1.00	1.00	1.00	1.00
Na	0.00	0.00	0.00	0.00	0.00	0.00	0.00	0.00	0.00	0.15	0.19	0.01	0.00	0.19	0.04
Mg	0.18	0.17	0.17	0.17	0.18	0.21	0.14	0.12	0.15	0.19	0.16	0.17	0.14	0.20	0.16
Mn	4.82	4.77	4.81	4.88	4.79	4.87	6.50	6.49	6.35	6.21	6.24	6.33	6.44	6.17	6.34
Fe^{2+}	2.01	2.08	2.04	2.00	2.04	1.77	0.39	0.36	0.38	0.38	0.33	0.40	0.37	0.36	0.37
Zn	0.11	0.09	0.08	0.07	0.11	0.20	0.07	0.09	0.13	0.08	0.07	0.08	0.09	0.08	0.09
Y	0.00	0.00	0.00	0.00	0.00	0.00	0.00	0.00	0.00	0.00	0.00	0.00	0.00	0.00	0.00
Ce	0.00	0.00	0.00	0.00	0.00	0.00	0.00	0.00	0.00	0.00	0.00	0.00	0.00	0.00	0.00
Sum C	7.12	7.11	7.09	7.13	7.12	7.05	7.10	7.05	7.01	7.00	7.00	7.00	7.04	7.00	7.00
Ti	1.07	1.25	1.03	1.11	1.08	1.17	1.92	1.86	1.88	0.98	1.31	1.73	1.90	1.04	1.58
Sn	0.00	0.00	0.00	0.00	0.00	0.00	0.00	0.00	0.00	0.00	0.00	0.00	0.00	0.00	0.00
Zr	0.02	0.10	0.11	0.09	0.09	0.06	0.00	0.00	0.00	0.00	0.00	0.05	0.02	0.00	0.01
Hf	0.00	0.00	0.00	0.00	0.00	0.00	0.00	0.00	0.00	0.00	0.00	0.00	0.00	0.00	0.00
Nb	0.92	0.66	0.85	0.77	0.84	0.77	0.14	0.18	0.15	1.02	0.72	0.28	0.14	0.98	0.45
Ta	0.00	0.00	0.00	0.00	0.00	0.00	0.00	0.00	0.01	0.00	0.00	0.00	0.00	0.00	0.00
Sum D	2.00	2.01	1.99	1.97	2.01	2.00	2.06	2.04	2.04	2.00	2.03	2.06	2.05	2.01	2.04
Si	7.54	7.61	7.59	7.66	7.53	7.63	7.77	7.82	7.80	7.71	7.82	7.76	7.82	7.75	7.78
Al	0.27	0.23	0.29	0.24	0.29	0.23	0.02	0.03	0.08	0.18	0.11	0.09	0.04	0.15	0.09
Sum T	7.81	7.84	7.87	7.89	7.82	7.86	7.79	7.85	7.87	7.89	7.94	7.85	7.86	7.89	7.87
F	0.52	0.65	0.51	0.48	0.57	0.57	0.87	0.86	1.00	0.50	0.64	0.64	0.77	0.60	0.74
OH	4.00	4.00	4.00	4.00	4.00	4.00	4.13	4.14	4.00	4.00	4.00	4.36	4.23	4.00	4.11
O	30.48	30.35	30.49	30.52	30.43	30.43	30.13	30.14	30.00	30.50	30.36	30.36	30.23	30.40	30.26
Cations	20.19	20.13	20.13	20.14	20.17	20.14	20.15	20.08	20.09	20.12	20.05	20.04	20.06	20.04	20.08

ELECTRON MICROPROBE ANALYSES OF MONT SAINT-HILAIRE AGM

OXIDE	MSH10Aa PT 1	PT 2	MSH10Ab PT 3	PT 4	MSH10Ac PT 5	MSH10A Average	MSH10Ba PT 8	PT 9	PT 10	MSH10Bb PT 11	MSH10Bc PT 14	PT 15	MSH10B Average	MSH11a PT 16	PT 17
Na_2O	2.31	2.56	2.42	2.50	2.43	2.44	2.13	2.54	2.33	2.19	2.64	2.47	2.38	2.48	2.57
K_2O	6.32	6.05	6.20	5.94	6.12	6.13	6.18	6.12	6.02	6.15	6.11	6.05	6.11	5.94	5.83
Rb_2O	0.50	0.42	0.46	0.50	0.46	0.47	0.63	0.71	0.72	0.60	0.75	0.60	0.67	0.55	0.56
Cs_2O	0.00	0.00	0.00	0.00	0.00	0.00	0.00	0.00	0.00	0.00	0.00	0.00	0.00	0.00	0.00
CaO	0.37	0.26	0.25	0.27	0.14	0.26	0.00	0.00	0.00	0.00	0.00	0.00	0.00	0.41	0.42
SrO	0.08	0.00	0.12	0.00	0.08	0.06	0.00	0.00	0.00	0.00	0.00	0.00	0.00	0.11	0.09
BaO	0.00	0.00	0.00	0.00	0.00	0.00	0.00	0.00	0.00	0.00	0.00	0.00	0.00	0.00	0.00
MgO	0.64	0.51	0.67	0.69	0.12	0.53	0.13	0.20	0.18	0.10	0.20	0.15	0.16	0.68	0.69
MnO	19.16	21.18	17.91	18.12	23.37	19.95	27.69	25.82	26.82	27.89	26.03	27.63	26.98	20.51	20.60
FeO	15.32	12.73	15.85	15.73	10.09	13.94	7.01	7.09	7.28	6.98	7.13	6.79	7.05	14.07	14.01
ZnO	0.36	0.78	0.26	0.22	0.53	0.43	0.00	0.19	0.00	0.00	0.00	0.00	0.03	0.23	0.22
Al_2O_3	1.41	0.76	1.24	1.00	1.17	1.12	1.90	0.98	1.04	1.69	0.99	1.06	1.28	1.11	1.03
Y_2O_3	0.00	0.00	0.00	0.00	0.00	0.00	0.00	0.00	0.00	0.00	0.00	0.00	0.00	0.00	0.00
Ce_2O_3	0.00	0.00	0.00	0.00	0.00	0.00	0.00	0.00	0.00	0.00	0.00	0.00	0.00	0.00	0.15
TiO_2	6.18	6.40	5.20	5.73	3.87	5.48	0.56	0.79	0.77	0.59	0.86	0.78	0.73	6.28	6.41
SnO_2	0.00	0.00	0.00	0.00	0.00	0.00	0.00	0.00	0.00	0.00	0.00	0.00	0.00	0.00	0.00
ZrO_2	0.86	2.00	2.07	2.12	2.29	1.87	3.27	4.17	5.00	4.08	3.65	4.90	4.18	1.26	1.39
HfO_2	0.00	0.00	0.00	0.00	0.00	0.00	0.00	0.00	0.00	0.00	0.00	0.00	0.00	0.00	0.00
Nb_2O_5	8.16	6.56	8.32	7.43	9.83	8.06	13.74	12.41	11.20	12.68	12.69	11.30	12.34	7.63	7.40
Ta_2O_5	0.19	0.17	0.38	0.41	0.00	0.23	0.35	0.49	0.62	0.70	0.41	0.80	0.56	0.00	0.00
SiO_2	32.38	33.92	33.26	33.75	32.39	33.14	30.59	32.28	32.14	31.21	32.56	31.69	31.75	33.09	32.83
F	0.53	0.79	0.69	0.88	0.44	0.67	0.00	0.00	0.00	0.42	0.37	0.43	0.20	0.79	0.75
H_2O	2.58	2.61	2.60	2.61	2.53	2.59	2.48	2.50	2.49	2.51	2.52	2.50	2.50	2.60	2.59
O=F	-0.22	-0.33	-0.29	-0.37	-0.19	-0.28	0.00	0.00	0.00	-0.18	-0.16	-0.18	-0.09	-0.33	-0.32
Total	97.13	97.37	97.61	97.53	95.67	97.06	96.66	96.29	96.61	97.62	96.76	96.97	96.82	97.41	97.23
Chemical formulae calculated based on 31 cations															
Na_{tot}	1.04	1.14	1.08	1.11	1.12	1.10	1.00	1.18	1.09	1.01	1.22	1.15	1.11	1.11	1.15
Na	0.13	0.08	0.00	0.00	0.00	0.04	0.00	0.00	0.08	0.01	-0.05	0.15	0.06	0.19	0.26
K	1.88	1.77	1.83	1.74	1.85	1.81	1.90	1.88	1.85	1.87	1.85	1.85	1.87	1.75	1.72
Rb	0.08	0.06	0.07	0.07	0.07	0.07	0.10	0.11	0.11	0.09	0.12	0.09	0.10	0.08	0.08
Cs	0.00	0.00	0.00	0.00	0.00	0.00	0.00	0.00	0.00	0.00	0.00	0.00	0.00	0.00	0.00
Sr	0.01	0.00	0.02	0.00	0.01	0.01	0.00	0.00	0.00	0.00	0.00	0.00	0.00	0.02	0.01
Ba	0.00	0.00	0.00	0.00	0.00	0.00	0.00	0.00	0.00	0.00	0.00	0.00	0.00	0.00	0.00
Sum A	2.09	1.91	1.89	1.81	1.93	1.93	2.00	1.95	2.03	1.98	1.92	2.09	2.03	2.04	2.07
Na	0.91	0.94	0.91	0.92	0.96	0.94	1.00	0.97	1.00	1.00	1.00	1.00	1.00	0.90	0.90
Ca	0.09	0.06	0.06	0.07	0.04	0.06	0.00	0.00	0.00	0.00	0.00	0.00	0.00	0.10	0.10
Sum B	1.00	1.00	0.97	0.99	1.00	1.00	1.00	0.97	1.00	1.00	1.00	1.00	1.00	1.00	1.00
Na	0.00	0.13	0.17	0.19	0.16	0.12	0.00	0.22	0.01	0.00	0.27	0.00	0.05	0.01	0.00
Mg	0.22	0.18	0.23	0.24	0.04	0.18	0.05	0.07	0.07	0.04	0.07	0.05	0.06	0.23	0.24
Mn	3.77	4.12	3.50	3.52	4.70	3.92	5.67	5.25	5.46	5.63	5.24	5.61	5.48	4.00	4.04
Fe^{2+}	2.98	2.45	3.06	3.02	2.00	2.70	1.42	1.42	1.46	1.39	1.42	1.36	1.41	2.71	2.71
Zn	0.06	0.13	0.04	0.04	0.09	0.07	0.00	0.03	0.00	0.00	0.00	0.00	0.01	0.04	0.04
Y	0.00	0.00	0.00	0.00	0.00	0.00	0.00	0.00	0.00	0.00	0.00	0.00	0.00	0.00	0.00
Ce	0.00	0.00	0.00	0.00	0.00	0.00	0.00	0.00	0.00	0.00	0.00	0.00	0.00	0.00	0.01
Sum C	7.04	7.00	7.00	7.00	7.00	7.00	7.13	7.00	7.00	7.06	7.00	7.03	7.00	7.00	7.04
Ti	1.08	1.11	0.90	0.99	0.69	0.95	0.10	0.14	0.14	0.11	0.15	0.14	0.13	1.09	1.12
Sn	0.00	0.00	0.00	0.00	0.00	0.00	0.00	0.00	0.00	0.00	0.00	0.00	0.00	0.00	0.00
Zr	0.10	0.22	0.23	0.24	0.27	0.21	0.39	0.49	0.59	0.47	0.42	0.57	0.49	0.14	0.16
Hf	0.00	0.00	0.00	0.00	0.00	0.00	0.00	0.00	0.00	0.00	0.00	0.00	0.00	0.00	0.00
Nb	0.86	0.68	0.87	0.77	1.06	0.85	1.50	1.35	1.22	1.37	1.36	1.23	1.34	0.80	0.77
Ta	0.01	0.01	0.02	0.03	0.00	0.01	0.02	0.03	0.04	0.05	0.03	0.05	0.04	0.00	0.00
Sum D	2.05	2.02	2.03	2.02	2.01	2.03	2.01	2.01	1.98	1.99	1.97	1.99	1.99	2.03	2.05
Si	7.53	7.79	7.67	7.75	7.69	7.69	7.39	7.75	7.73	7.44	7.74	7.60	7.61	7.62	7.60
Al	0.39	0.21	0.34	0.27	0.33	0.31	0.54	0.28	0.30	0.48	0.28	0.30	0.36	0.30	0.28
Sum T	7.92	8.00	8.01	8.02	8.02	7.99	7.93	8.03	8.02	7.92	8.02	7.90	7.97	7.92	7.88
F	0.39	0.57	0.50	0.64	0.33	0.49	0.00	0.00	0.00	0.32	0.28	0.33	0.15	0.58	0.55
OH	4.00	4.00	4.00	4.00	4.00	4.00	4.00	4.00	4.00	4.00	4.00	4.00	4.00	4.00	4.00
O	30.61	30.43	30.50	30.36	30.67	30.51	31.00	31.00	31.00	30.68	30.72	30.67	30.85	30.42	30.45
Cations	20.10	19.94	19.92	19.84	19.96	19.95	20.07	19.99	20.04	19.95	19.91	20.01	19.99	19.99	20.03

ELECTRON MICROPROBE ANALYSES OF MONT SAINT-HILAIRE AGM

OXIDE	MSH11b PT 18	PT 19	PT 20	MSH11 Average	MSH12a PT 21	PT 22	MSH12b PT 23	PT 24	MSH12c PT 25	PT 26	MSH12 Average	MSH13a PT 27	PT 28	PT 29	MSH13b PT 30
Na_2O	2.54	2.45	2.81	2.57	2.13	2.06	2.06	2.06	2.18	2.23	2.12	2.24	2.11	2.01	1.97
K_2O	5.81	5.90	5.84	5.86	6.00	5.84	5.86	5.83	5.80	5.73	5.84	6.10	6.28	6.29	6.13
Rb_2O	0.59	0.55	0.54	0.56	0.33	0.39	0.39	0.37	0.35	0.34	0.36	0.41	0.43	0.43	0.43
Cs_2O	0.00	0.00	0.00	0.00	0.08	0.00	0.00	0.00	0.00	0.00	0.01	0.00	0.00	0.00	0.00
CaO	0.40	0.55	0.58	0.47	0.94	0.87	1.00	0.99	0.81	0.72	0.89	1.10	1.13	0.99	1.10
SrO	0.11	0.10	0.14	0.11	0.19	0.23	0.22	0.23	0.23	0.25	0.23	0.09	0.12	0.00	0.12
BaO	0.00	0.00	0.00	0.00	0.00	0.00	0.00	0.00	0.00	0.00	0.00	0.00	0.00	0.00	0.00
MgO	0.63	0.64	0.83	0.69	0.62	0.34	0.57	0.52	0.35	0.28	0.45	0.85	0.79	0.80	0.89
MnO	20.98	21.16	21.13	20.88	15.73	19.26	14.85	15.37	17.38	19.47	17.01	23.22	23.35	23.57	23.78
FeO	13.37	13.30	13.10	13.57	20.60	17.00	19.72	19.46	18.15	16.25	18.53	11.56	11.93	11.22	10.50
ZnO	0.29	0.34	0.38	0.29	0.00	0.00	0.00	0.00	0.00	0.00	0.00	0.24	0.00	0.00	0.00
Al_2O_3	1.18	1.28	0.49	1.02	0.80	0.99	1.06	1.10	0.65	0.64	0.87	1.03	1.51	1.65	1.48
Y_2O_3	0.00	0.00	0.00	0.00	0.00	0.00	0.00	0.00	0.00	0.00	0.00	0.00	0.00	0.00	0.00
Ce_2O_3	0.00	0.00	0.00	0.00	0.00	0.00	0.00	0.00	0.00	0.00	0.00	0.00	0.00	0.00	0.00
TiO_2	6.42	7.46	9.33	7.18	8.21	7.32	7.69	7.57	7.55	7.16	7.58	8.68	7.79	7.41	8.21
SnO_2	0.00	0.00	0.00	0.00	0.00	0.00	0.00	0.00	0.00	0.00	0.00	0.00	0.00	0.00	0.00
ZrO_2	1.09	0.14	0.37	0.85	4.13	4.72	3.96	4.19	5.42	5.75	4.70	0.40	0.29	0.41	0.00
HfO_2	0.00	0.00	0.00	0.00	0.21	0.00	0.25	0.00	0.00	0.23	0.12	0.00	0.00	0.00	0.00
Nb_2O_5	7.74	6.95	4.38	6.82	1.59	2.13	2.15	2.09	1.14	1.14	1.71	4.94	6.23	6.64	5.92
Ta_2O_5	0.00	0.00	0.00	0.00	0.00	0.00	0.00	0.00	0.00	0.00	0.00	0.00	0.00	0.00	0.00
SiO_2	33.02	33.14	35.53	33.52	33.93	32.67	32.55	32.58	33.42	33.09	33.04	32.99	33.04	32.59	32.44
F	0.83	0.61	1.07	0.81	1.05	0.96	1.04	1.05	0.91	1.06	1.01	0.91	0.87	0.60	1.07
H_2O	2.60	2.60	2.88	2.65	2.82	2.78	2.71	2.71	2.81	2.72	2.76	2.86	2.64	2.60	2.60
O=F	-0.35	-0.26	-0.45	-0.34	-0.44	-0.40	-0.44	-0.44	-0.38	-0.45	-0.43	-0.38	-0.37	-0.25	-0.45
Total	97.25	96.92	98.95	97.55	98.92	97.16	95.65	95.68	96.77	96.61	96.80	97.23	98.14	96.96	96.19
Chemical formulae calculated based on 31 anions															
Na_{tot}	1.14	1.09	1.20	1.14	0.93	0.93	0.93	0.93	0.98	1.01	0.95	0.99	0.93	0.90	0.88
Na	0.17	0.20	0.05	0.18	0.16	0.14	0.18	0.18	0.18	0.19	0.17	0.26	0.21	0.14	0.13
K	1.71	1.73	1.65	1.71	1.73	1.73	1.75	1.74	1.71	1.70	1.73	1.77	1.82	1.85	1.80
Rb	0.09	0.08	0.08	0.08	0.05	0.06	0.06	0.06	0.05	0.05	0.05	0.06	0.06	0.06	0.06
Cs	0.00	0.00	0.00	0.00	0.01	0.00	0.00	0.00	0.00	0.00	0.00	0.00	0.00	0.00	0.00
Sr	0.02	0.01	0.02	0.01	0.03	0.03	0.03	0.03	0.03	0.03	0.03	0.01	0.02	0.00	0.02
Ba	0.00	0.00	0.00	0.00	0.00	0.00	0.00	0.00	0.00	0.00	0.00	0.00	0.00	0.00	0.00
Sum A	1.98	2.02	1.79	1.99	1.97	1.96	2.01	2.01	1.97	1.97	1.98	2.11	2.11	2.06	2.02
Na	0.90	0.86	0.86	0.88	0.77	0.78	0.75	0.75	0.80	0.82	0.78	0.73	0.73	0.76	0.73
Ca	0.10	0.14	0.14	0.12	0.23	0.22	0.25	0.25	0.20	0.18	0.22	0.27	0.28	0.25	0.27
Sum B	1.00	1.00	1.00	1.00	1.00	1.00	1.00	1.00	1.00	1.00	1.00	1.00	1.00	1.00	1.00
Na	0.06	0.03	0.29	0.07	0.00	0.00	0.01	0.00	0.00	0.00	0.00	0.00	0.00	0.00	0.02
Mg	0.22	0.22	0.27	0.24	0.21	0.12	0.20	0.18	0.12	0.10	0.15	0.29	0.27	0.28	0.31
Mn	4.10	4.13	3.96	4.04	3.01	3.78	2.94	3.04	3.40	3.84	3.33	4.48	4.50	4.60	4.65
Fe^{2+}	2.58	2.56	2.42	2.60	3.89	3.29	3.85	3.80	3.51	3.16	3.59	2.20	2.27	2.16	2.03
Zn	0.05	0.06	0.06	0.05	0.00	0.00	0.00	0.00	0.00	0.00	0.00	0.04	0.00	0.00	0.00
Y	0.00	0.00	0.00	0.00	0.00	0.00	0.00	0.00	0.00	0.00	0.00	0.00	0.00	0.00	0.00
Ce	0.00	0.00	0.00	0.00	0.00	0.00	0.00	0.00	0.00	0.00	0.00	0.00	0.00	0.00	0.00
Sum C	7.00	7.00	7.00	7.00	7.11	7.19	7.00	7.02	7.03	7.10	7.07	7.02	7.03	7.04	7.00
Ti	1.11	1.29	1.55	1.23	1.40	1.28	1.35	1.33	1.31	1.25	1.32	1.49	1.33	1.29	1.43
Sn	0.00	0.00	0.00	0.00	0.00	0.00	0.00	0.00	0.00	0.00	0.00	0.00	0.00	0.00	0.00
Zr	0.12	0.02	0.04	0.10	0.46	0.53	0.45	0.48	0.61	0.65	0.53	0.04	0.03	0.05	0.00
Hf	0.00	0.00	0.00	0.00	0.01	0.00	0.02	0.00	0.00	0.02	0.01	0.00	0.00	0.00	0.00
Nb	0.81	0.72	0.44	0.71	0.16	0.22	0.23	0.22	0.12	0.12	0.18	0.51	0.64	0.69	0.62
Ta	0.00	0.00	0.00	0.00	0.00	0.00	0.00	0.00	0.00	0.00	0.00	0.00	0.00	0.00	0.00
Sum D	2.04	2.03	2.03	2.03	2.03	2.03	2.05	2.03	2.04	2.04	2.04	2.04	2.00	2.02	2.04
Si	7.61	7.63	7.85	7.66	7.66	7.57	7.61	7.61	7.73	7.70	7.65	7.52	7.51	7.51	7.49
Al	0.32	0.35	0.13	0.28	0.21	0.27	0.29	0.30	0.18	0.18	0.24	0.28	0.41	0.45	0.40
Sum T	7.93	7.98	7.98	7.94	7.88	7.84	7.90	7.91	7.90	7.88	7.88	7.80	7.92	7.96	7.89
F	0.61	0.44	0.75	0.58	0.75	0.70	0.77	0.78	0.67	0.78	0.74	0.66	0.63	0.44	0.78
OH	4.00	4.00	4.25	4.05	4.25	4.30	4.23	4.22	4.34	4.22	4.26	4.34	4.00	4.00	4.00
O	30.40	30.56	30.25	30.42	30.25	30.30	30.23	30.22	30.34	30.22	30.26	30.34	30.37	30.56	30.22
Cations	19.95	20.03	19.80	19.96	19.98	20.01	19.96	19.97	19.95	19.99	19.98	19.96	20.06	20.08	19.95

ELECTRON MICROPROBE ANALYSES OF MONT SAINT-HILAIRE AGM

OXIDE	PT 31	MSH13c PT 32	PT 33	PT 34	MSH13 Average	MSH14a PT 35	PT 36	MSH14b PT 37	PT 38	MSH14c PT 39	PT 40	MSH14 Average	MSH15a PT 41	PT 42	MSH15b PT 43
Na_2O	2.21	1.96	2.09	2.19	2.10	2.62	2.83	2.65	2.67	2.73	3.02	2.75	3.07	3.07	2.88
K_2O	6.00	6.17	6.09	6.11	6.15	5.79	5.54	5.72	5.67	5.80	5.54	5.68	5.71	5.70	5.74
Rb_2O	0.38	0.41	0.39	0.38	0.41	0.74	0.66	0.77	0.72	0.73	0.65	0.71	0.57	0.57	0.57
Cs_2O	0.09	0.00	0.09	0.00	0.02	0.22	0.15	0.22	0.22	0.18	0.11	0.18	0.00	0.00	0.00
CaO	1.03	1.06	0.99	1.08	1.06	0.06	0.09	0.07	0.06	0.00	0.14	0.07	0.14	0.12	0.16
SrO	0.12	0.12	0.08	0.11	0.10	0.17	0.18	0.19	0.17	0.18	0.23	0.19	0.17	0.16	0.14
BaO	0.00	0.00	0.00	0.00	0.00	0.00	0.00	0.00	0.00	0.00	0.00	0.00	0.00	0.00	0.00
MgO	0.90	0.85	0.92	0.92	0.87	0.68	0.80	0.73	0.69	0.71	0.87	0.75	0.91	0.92	0.89
MnO	23.80	24.46	23.29	23.75	23.65	25.12	25.22	25.80	24.73	25.06	25.65	25.26	23.75	23.61	22.26
FeO	10.77	10.29	11.21	11.02	11.06	8.94	8.84	8.78	9.01	8.42	8.34	8.72	10.12	10.18	11.41
ZnO	0.00	0.00	0.00	0.00	0.03	0.28	0.32	0.32	0.38	0.30	0.34	0.32	0.22	0.20	0.21
Al_2O_3	1.01	1.55	1.21	1.06	1.31	1.03	0.51	0.98	0.98	1.14	0.49	0.86	0.48	0.42	0.80
Y_2O_3	0.00	0.00	0.00	0.00	0.00	0.00	0.00	0.00	0.00	0.00	0.00	0.00	0.00	0.00	0.00
Ce_2O_3	0.00	0.15	0.00	0.00	0.02	0.16	0.00	0.15	0.00	0.00	0.00	0.05	0.00	0.00	0.00
TiO_2	8.44	8.14	8.07	8.45	8.15	5.21	6.92	5.43	5.24	5.22	7.80	5.97	7.00	7.08	6.99
SnO_2	0.00	0.00	0.00	0.00	0.00	0.00	0.00	0.00	0.00	0.00	0.00	0.00	0.00	0.00	0.00
ZrO_2	0.33	0.00	0.21	0.34	0.25	2.82	2.46	2.83	2.87	2.81	1.60	2.57	0.57	0.78	0.44
HfO_2	0.00	0.00	0.00	0.00	0.00	0.00	0.00	0.00	0.00	0.00	0.00	0.00	0.00	0.00	0.00
Nb_2O_5	4.73	5.71	5.86	5.01	5.63	7.48	4.88	7.07	7.31	7.28	4.58	6.43	7.55	6.74	7.51
Ta_2O_5	0.00	0.00	0.00	0.16	0.02	0.00	0.00	0.00	0.00	0.00	0.00	0.00	0.00	0.00	0.00
SiO_2	33.54	32.53	32.72	32.97	32.85	32.15	33.76	32.31	32.72	32.39	34.15	32.91	33.80	34.41	33.54
F	0.86	0.72	0.84	1.02	0.86	0.71	0.84	1.05	0.72	0.87	0.75	0.82	0.94	1.08	0.94
H_2O	2.88	2.59	2.60	2.61	2.67	2.54	2.85	2.57	2.56	2.55	2.93	2.67	2.62	2.63	2.61
O=F	-0.36	-0.30	-0.35	-0.43	-0.36	-0.30	-0.35	-0.44	-0.30	-0.37	-0.32	-0.35	-0.40	-0.45	-0.40
Total	96.73	96.41	96.30	96.75	96.84	96.42	96.50	97.20	96.41	96.00	96.87	96.57	97.22	97.22	96.69
Chemical formulae calculated based on 31 anions															
Na_{tot}	0.98	0.88	0.94	0.98	0.93	1.20	1.27	1.20	1.21	1.25	1.34	1.24	1.36	1.36	1.28
Na	0.18	0.14	0.18	0.24	0.19	0.21	0.24	0.22	0.21	0.20	0.28	0.26	0.29	0.22	0.19
K	1.75	1.82	1.80	1.79	1.80	1.74	1.63	1.70	1.70	1.74	1.61	1.69	1.67	1.66	1.68
Rb	0.06	0.06	0.06	0.06	0.06	0.11	0.10	0.12	0.11	0.11	0.10	0.11	0.08	0.08	0.08
Cs	0.01	0.00	0.01	0.00	0.00	0.02	0.02	0.02	0.02	0.02	0.01	0.02	0.00	0.00	0.00
Sr	0.02	0.02	0.01	0.02	0.01	0.02	0.02	0.03	0.02	0.03	0.03	0.03	0.02	0.02	0.02
Ba	0.00	0.00	0.00	0.00	0.00	0.00	0.00	0.00	0.00	0.00	0.00	0.00	0.00	0.00	0.00
Sum A	2.01	2.04	2.05	2.10	2.07	2.11	2.01	2.08	2.06	2.09	2.02	2.10	2.06	1.98	1.98
Na	0.75	0.74	0.76	0.73	0.74	0.99	0.98	0.98	0.99	1.00	0.97	0.98	0.97	0.97	0.96
Ca	0.25	0.26	0.25	0.27	0.26	0.02	0.02	0.02	0.02	0.00	0.03	0.02	0.03	0.03	0.04
Sum B	1.00	1.00	1.00	1.00	1.00	1.00	1.00	1.00	1.00	1.00	1.00	1.00	1.00	1.00	1.00
Na	0.04	0.00	0.00	0.00	0.00	0.00	0.04	0.00	0.02	0.05	0.10	0.00	0.11	0.16	0.13
Mg	0.31	0.29	0.32	0.32	0.30	0.24	0.28	0.25	0.24	0.25	0.30	0.26	0.31	0.31	0.31
Mn	4.60	4.79	4.56	4.62	4.60	5.02	4.92	5.10	4.91	4.99	4.96	4.98	4.60	4.55	4.33
Fe^{2+}	2.05	1.99	2.17	2.12	2.12	1.76	1.70	1.71	1.77	1.66	1.59	1.70	1.94	1.94	2.19
Zn	0.00	0.00	0.00	0.00	0.01	0.05	0.05	0.06	0.07	0.05	0.06	0.06	0.04	0.03	0.04
Y	0.00	0.00	0.00	0.00	0.00	0.00	0.00	0.00	0.00	0.00	0.00	0.00	0.00	0.00	0.00
Ce	0.00	0.01	0.00	0.00	0.00	0.01	0.00	0.01	0.00	0.00	0.00	0.00	0.00	0.00	0.00
Sum C	7.00	7.08	7.04	7.05	7.02	7.08	7.00	7.14	7.00	7.00	7.00	7.00	7.00	7.00	7.00
Ti	1.45	1.42	1.40	1.46	1.41	0.92	1.20	0.95	0.92	0.92	1.34	1.04	1.21	1.21	1.21
Sn	0.00	0.00	0.00	0.00	0.00	0.00	0.00	0.00	0.00	0.00	0.00	0.00	0.00	0.00	0.00
Zr	0.04	0.00	0.02	0.04	0.03	0.32	0.28	0.32	0.33	0.32	0.18	0.29	0.06	0.09	0.05
Hf	0.00	0.00	0.00	0.00	0.00	0.00	0.00	0.00	0.00	0.00	0.00	0.00	0.00	0.00	0.00
Nb	0.49	0.60	0.61	0.52	0.58	0.80	0.51	0.75	0.78	0.77	0.47	0.68	0.78	0.69	0.78
Ta	0.00	0.00	0.00	0.01	0.00	0.00	0.00	0.00	0.00	0.00	0.00	0.00	0.00	0.00	0.00
Sum D	1.97	2.01	2.04	2.03	2.02	2.05	1.98	2.02	2.03	2.02	1.99	2.01	2.05	1.99	2.04
Si	7.65	7.52	7.56	7.57	7.54	7.58	7.78	7.54	7.67	7.62	7.80	7.66	7.74	7.84	7.71
Al	0.27	0.42	0.33	0.29	0.36	0.29	0.14	0.27	0.27	0.32	0.13	0.24	0.13	0.11	0.22
Sum T	7.92	7.94	7.89	7.86	7.90	7.86	7.92	7.81	7.94	7.94	7.93	7.90	7.87	7.95	7.93
F	0.62	0.53	0.61	0.74	0.63	0.53	0.61	0.78	0.53	0.65	0.54	0.61	0.68	0.78	0.68
OH	4.38	4.00	4.00	4.00	4.09	4.00	4.39	4.00	4.00	4.00	4.46	4.14	4.00	4.00	4.00
O	30.38	30.47	30.39	30.26	30.37	30.47	30.39	30.23	30.47	30.35	30.46	30.39	30.32	30.22	30.32
Cations	19.90	20.07	20.02	20.04	20.01	20.10	19.91	20.05	20.03	20.05	19.94	20.01	19.98	19.93	19.94

ELECTRON MICROPROBE ANALYSES OF MONT SAINT-HILAIRE AGM

				MSH15c				MSH15	MSH16a		MSH16b		MSH16c		MSH16d
OXIDE	PT 44	PT 45	PT 46	PT 47	PT 48	PT 49	PT 50	Average	PT 51	PT 52	PT 53	PT 54	PT 55	PT 56	PT 57
Na_2O	3.22	3.45	2.37	3.28	3.32	2.49	2.54	2.97	2.13	2.70	2.21	2.91	2.36	2.87	2.24
K_2O	5.66	5.59	6.00	5.50	5.55	6.05	5.93	5.74	6.09	5.87	6.08	5.89	5.94	5.81	6.01
Rb_2O	0.61	0.68	0.75	0.72	0.63	0.82	0.83	0.68	0.59	0.62	0.53	0.44	0.57	0.47	0.53
Cs_2O	0.00	0.00	0.00	0.00	0.00	0.00	0.00	0.00	0.09	0.00	0.09	0.00	0.10	0.00	0.09
CaO	0.16	0.09	0.00	0.06	0.09	0.00	0.00	0.08	0.85	0.54	0.69	0.29	0.68	0.38	0.82
SrO	0.24	0.16	0.08	0.00	0.00	0.00	0.00	0.10	0.13	0.15	0.08	0.09	0.12	0.10	0.12
BaO	0.14	0.00	0.00	0.00	0.00	0.00	0.00	0.01	0.00	0.00	0.00	0.00	0.00	0.00	0.00
MgO	1.07	0.98	0.25	0.38	0.40	0.27	0.27	0.63	0.85	0.97	0.84	0.80	0.81	0.87	0.79
MnO	26.47	26.63	31.77	27.67	27.71	31.44	31.36	27.27	26.97	26.62	26.49	26.39	26.63	26.32	26.31
FeO	6.53	6.31	2.80	5.36	5.88	3.03	3.11	6.47	7.77	7.90	7.99	7.52	7.62	7.66	7.76
ZnO	0.00	0.00	0.00	0.00	0.00	0.00	0.00	0.06	0.00	0.00	0.00	0.00	0.00	0.00	0.00
Al_2O_3	0.27	0.37	1.22	0.42	0.21	1.49	1.46	0.71	1.31	0.58	1.34	0.39	1.33	0.49	1.51
Y_2O_3	0.00	0.00	0.00	0.00	0.00	0.00	0.00	0.00	0.00	0.00	0.00	0.00	0.00	0.00	0.00
Ce_2O_3	0.00	0.00	0.00	0.00	0.00	0.00	0.00	0.00	0.16	0.00	0.00	0.00	0.00	0.00	0.00
TiO_2	7.46	6.28	2.01	5.90	7.29	1.24	1.26	5.25	8.54	9.06	7.75	8.22	7.62	8.41	7.84
SnO_2	0.00	0.00	0.00	0.00	0.00	0.00	0.00	0.00	0.00	0.00	0.00	0.00	0.00	0.00	0.00
ZrO_2	0.00	0.26	5.26	0.20	0.00	3.67	3.43	1.46	0.00	0.00	0.00	0.00	0.00	0.00	0.00
HfO_2	0.00	0.00	0.00	0.00	0.00	0.00	0.00	0.00	0.00	0.00	0.00	0.00	0.00	0.00	0.00
Nb_2O_5	7.28	8.51	9.62	9.38	7.23	11.74	12.33	8.79	5.67	4.60	6.92	6.17	6.88	5.69	6.19
Ta_2O_5	0.00	0.00	0.00	0.00	0.00	0.33	0.35	0.07	0.00	0.00	0.00	0.00	0.00	0.00	0.00
SiO_2	34.81	34.76	32.63	33.94	34.32	32.06	31.49	33.58	32.95	34.49	32.54	34.52	33.06	34.24	32.32
F	1.03	0.86	0.00	0.73	1.03	0.00	0.59	0.72	0.89	1.03	0.78	0.67	0.79	0.76	0.84
H_2O	2.65	2.64	2.53	2.58	2.60	2.52	2.52	2.59	2.62	2.84	2.60	2.63	2.61	2.62	2.57
O=F	-0.43	-0.36	0.00	-0.31	-0.43	0.00	-0.25	-0.30	-0.37	-0.43	-0.33	-0.28	-0.33	-0.32	-0.35
Total	97.16	97.20	97.29	95.82	95.83	97.15	97.22	96.88	97.24	97.54	96.60	96.64	96.79	96.37	95.59
Chemical formulae calculated based on 31 anions															
Na_{tot}	1.42	1.52	1.09	1.48	1.48	1.15	1.17	1.33	0.95	1.18	0.99	1.29	1.05	1.27	1.01
Na	0.14	0.21	0.09	0.10	0.19	0.15	0.17	0.18	0.15	0.19	0.16	0.17	0.15	0.23	0.19
K	1.64	1.62	1.81	1.63	1.63	1.84	1.80	1.70	1.78	1.69	1.79	1.72	1.74	1.70	1.79
Rb	0.09	0.10	0.11	0.11	0.09	0.13	0.13	0.10	0.09	0.09	0.08	0.07	0.08	0.07	0.08
Cs	0.00	0.00	0.00	0.00	0.00	0.00	0.00	0.00	0.01	0.00	0.01	0.00	0.01	0.00	0.01
Sr	0.03	0.02	0.01	0.00	0.00	0.00	0.00	0.01	0.02	0.02	0.01	0.01	0.02	0.01	0.02
Ba	0.01	0.00	0.00	0.00	0.00	0.00	0.00	0.00	0.00	0.00	0.00	0.00	0.00	0.00	0.00
Sum A	1.91	1.95	2.03	1.84	1.91	2.11	2.10	1.99	2.04	1.99	2.05	1.96	2.00	2.01	2.08
Na	0.96	0.98	1.00	0.99	0.98	1.00	1.00	0.98	0.79	0.87	0.83	0.93	0.83	0.91	0.80
Ca	0.04	0.02	0.00	0.02	0.02	0.00	0.00	0.02	0.21	0.13	0.17	0.07	0.17	0.09	0.21
Sum B	1.00	1.00	1.00	1.00	1.00	1.00	1.00	1.00	1.00	1.00	1.00	1.00	1.00	1.00	1.00
Na	0.32	0.34	0.00	0.39	0.32	0.00	0.00	0.17	0.00	0.11	0.00	0.19	0.07	0.14	0.02
Mg	0.36	0.33	0.09	0.13	0.14	0.10	0.10	0.22	0.29	0.33	0.29	0.27	0.28	0.30	0.27
Mn	5.08	5.13	6.37	5.44	5.41	6.34	6.32	5.36	5.23	5.07	5.18	5.10	5.18	5.10	5.19
Fe^{3+}	1.24	1.20	0.55	1.04	1.13	0.60	0.62	1.25	1.49	1.49	1.54	1.44	1.47	1.47	1.51
Zn	0.00	0.00	0.00	0.00	0.00	0.00	0.00	0.01	0.00	0.00	0.00	0.00	0.00	0.00	0.00
Y	0.00	0.00	0.00	0.00	0.00	0.00	0.00	0.00	0.00	0.00	0.00	0.00	0.00	0.00	0.00
Ce	0.00	0.00	0.00	0.00	0.00	0.00	0.00	0.00	0.01	0.00	0.00	0.00	0.00	0.00	0.00
Sum C	7.00	7.00	7.01	7.00	7.00	7.04	7.03	7.00	7.02	7.00	7.02	7.00	7.00	7.00	7.00
Ti	1.27	1.07	0.36	1.03	1.26	0.22	0.23	0.91	1.47	1.53	1.35	1.41	1.32	1.45	1.37
Sn	0.00	0.00	0.00	0.00	0.00	0.00	0.00	0.00	0.00	0.00	0.00	0.00	0.00	0.00	0.00
Zr	0.00	0.03	0.61	0.02	0.00	0.43	0.40	0.17	0.00	0.00	0.00	0.00	0.00	0.00	0.00
Hf	0.00	0.00	0.00	0.00	0.00	0.00	0.00	0.00	0.00	0.00	0.00	0.00	0.00	0.00	0.00
Nb	0.75	0.88	1.03	0.98	0.75	1.26	1.33	0.92	0.59	0.47	0.72	0.64	0.72	0.59	0.65
Ta	0.00	0.00	0.00	0.00	0.00	0.02	0.02	0.00	0.00	0.00	0.00	0.00	0.00	0.00	0.00
Sum D	2.02	1.98	2.00	2.04	2.02	1.93	1.97	2.00	2.06	2.00	2.07	2.05	2.03	2.04	2.03
Si	7.89	7.91	7.73	7.88	7.91	7.63	7.49	7.77	7.54	7.76	7.52	7.88	7.60	7.84	7.53
Al	0.07	0.10	0.34	0.12	0.06	0.42	0.41	0.20	0.35	0.15	0.37	0.11	0.36	0.13	0.41
Sum T	7.96	8.01	8.07	7.99	7.97	8.05	7.90	7.97	7.89	7.92	7.88	7.99	7.96	7.97	7.94
F	0.74	0.62	0.00	0.54	0.75	0.00	0.44	0.52	0.64	0.73	0.57	0.48	0.57	0.55	0.62
OH	4.00	4.00	4.00	4.00	4.00	4.00	4.00	4.00	4.00	4.27	4.00	4.00	4.00	4.00	4.00
O	30.26	30.38	31.00	30.46	30.25	31.00	30.56	30.48	30.36	30.27	30.43	30.52	30.43	30.45	30.38
Cations	19.88	19.94	20.10	19.87	19.90	20.14	19.99	19.97	20.01	19.90	20.02	19.99	19.99	20.01	20.05

ELECTRON MICROPROBE ANALYSES OF MONT SAINT-HILAIRE AGM

OXIDE	PT 58	MSH16 Average	MSH17a PT 59	PT 60	MSH17b PT 61	PT 62	MSH17c PT 63	PT 64	MSH17 Average	MSH18Aa PT 65	PT 66	MSH18Ab PT 67	PT 68	MSH18Ac PT 69	PT 70
Na_2O	3.02	2.56	2.58	2.56	2.33	2.46	2.51	2.64	2.51	2.57	2.53	2.28	2.31	2.36	2.32
K_2O	5.83	5.94	5.83	5.95	5.94	5.97	5.98	5.89	5.89	5.85	6.01	5.92	5.94	6.02	6.05
Rb_2O	0.45	0.53	0.37	0.39	0.40	0.40	0.36	0.37	0.38	0.47	0.51	0.49	0.48	0.49	0.47
Cs_2O	0.00	0.05	0.10	0.00	0.09	0.00	0.00	0.00	0.03	0.00	0.00	0.09	0.00	0.00	0.00
CaO	0.24	0.56	0.73	0.68	0.76	0.76	0.60	0.52	0.68	0.63	0.45	0.53	0.60	0.52	0.51
SrO	0.13	0.12	0.21	0.20	0.18	0.21	0.19	0.20	0.20	0.15	0.11	0.11	0.10	0.10	0.11
BaO	0.00	0.00	0.00	0.00	0.00	0.00	0.00	0.00	0.00	0.00	0.00	0.00	0.00	0.00	0.00
MgO	0.74	0.83	0.84	0.83	0.85	0.92	0.88	0.89	0.87	0.39	0.32	0.44	0.42	0.42	0.44
MnO	26.79	26.57	17.69	17.85	19.06	19.22	20.56	21.35	19.29	20.79	21.84	18.98	19.62	19.70	19.40
FeO	7.09	7.66	17.08	17.59	15.15	15.19	14.01	13.00	15.34	14.49	13.65	16.17	15.94	15.14	15.17
ZnO	0.00	0.00	0.22	0.00	0.24	0.21	0.24	0.26	0.20	0.00	0.22	0.25	0.19	0.25	0.30
Al_2O_3	0.34	0.91	0.76	0.66	1.00	0.91	0.84	0.52	0.78	0.63	1.18	1.24	1.14	1.13	0.96
Y_2O_3	0.00	0.00	0.00	0.00	0.00	0.00	0.00	0.00	0.00	0.00	0.00	0.00	0.00	0.00	0.00
Ce_2O_3	0.00	0.02	0.00	0.16	0.21	0.17	0.00	0.00	0.09	0.00	0.00	0.15	0.00	0.00	0.00
TiO_2	8.02	8.18	8.80	9.06	8.50	8.68	8.17	8.74	8.66	7.86	6.22	6.82	6.74	6.86	7.07
SnO_2	0.00	0.00	0.00	0.00	0.00	0.00	0.00	0.00	0.00	0.00	0.00	0.00	0.00	0.00	0.00
ZrO_2	0.00	0.00	1.99	1.80	1.60	1.62	1.57	1.76	1.72	1.17	0.94	0.90	0.88	0.80	0.88
HfO_2	0.00	0.00	0.00	0.00	0.00	0.00	0.00	0.00	0.00	0.00	0.00	0.00	0.00	0.00	0.00
Nb_2O_5	6.25	6.05	2.94	2.71	3.88	3.92	4.37	3.21	3.51	5.12	7.87	7.25	7.20	7.24	6.83
Ta_2O_5	0.00	0.00	0.23	0.26	0.15	0.00	0.00	0.00	0.11	0.00	0.00	0.00	0.00	0.00	0.00
SiO_2	34.35	33.56	34.17	34.53	33.97	34.17	33.75	34.17	34.13	33.45	32.34	32.59	32.49	32.78	33.28
F	0.78	0.82	1.26	1.34	1.11	1.09	1.14	1.17	1.19	0.86	0.94	0.73	0.91	0.98	0.83
H_2O	2.62	2.64	2.72	2.71	2.79	2.82	2.76	2.74	2.76	2.60	2.58	2.59	2.59	2.59	2.60
O=F	-0.33	-0.34	-0.53	-0.56	-0.47	-0.46	-0.48	-0.49	-0.50	-0.36	-0.40	-0.31	-0.38	-0.41	-0.35
Total	96.32	96.64	97.99	98.72	97.74	98.26	97.45	96.74	97.82	96.66	97.32	97.22	97.16	96.97	96.87
Chemical formulae calculated based on 31 cations															
Na_{tot}	1.34	1.13	1.13	1.11	1.02	1.07	1.11	1.17	1.10	1.15	1.14	1.02	1.04	1.06	1.04
Na	0.22	0.19	0.23	0.25	0.07	0.12	0.21	0.23	0.18	0.31	0.25	0.16	0.19	0.16	0.09
K	1.71	1.74	1.68	1.70	1.71	1.71	1.73	1.65	1.70	1.72	1.78	1.75	1.76	1.78	1.78
Rb	0.07	0.08	0.05	0.06	0.06	0.06	0.05	0.05	0.06	0.07	0.08	0.07	0.07	0.07	0.07
Cs	0.00	0.00	0.01	0.00	0.01	0.00	0.00	0.00	0.00	0.00	0.00	0.01	0.00	0.00	0.00
Sr	0.02	0.02	0.03	0.03	0.02	0.03	0.03	0.03	0.03	0.02	0.02	0.02	0.01	0.01	0.02
Ba	0.00	0.00	0.00	0.00	0.00	0.00	0.00	0.00	0.00	0.00	0.00	0.00	0.00	0.00	0.00
Sum A	2.00	2.02	2.00	2.03	1.87	1.92	2.02	1.96	1.97	2.12	2.12	2.00	2.03	2.02	1.95
Na	0.94	0.86	0.82	0.84	0.82	0.82	0.85	0.87	0.84	0.84	0.89	0.87	0.85	0.87	0.87
Ca	0.06	0.14	0.18	0.16	0.18	0.18	0.15	0.13	0.16	0.16	0.11	0.13	0.15	0.13	0.13
Sum B	1.00	1.00	1.00	1.00	1.00	1.00	1.00	1.00	1.00	1.00	1.00	1.00	1.00	1.00	1.00
Na	0.19	0.09	0.08	0.03	0.14	0.13	0.05	0.06	0.08	0.00	0.00	0.00	0.00	0.03	0.08
Mg	0.25	0.28	0.28	0.28	0.29	0.31	0.30	0.30	0.29	0.13	0.11	0.15	0.15	0.15	0.15
Mn	5.20	5.16	3.38	3.39	3.65	3.66	3.96	4.12	3.69	4.07	4.29	3.73	3.85	3.86	3.79
Fe^{2+}	1.36	1.47	3.22	3.30	2.87	2.85	2.66	2.48	2.90	2.80	2.65	3.13	3.09	2.93	2.93
Zn	0.00	0.00	0.04	0.00	0.04	0.04	0.04	0.04	0.03	0.00	0.04	0.04	0.03	0.04	0.05
Y	0.00	0.00	0.00	0.00	0.00	0.00	0.00	0.00	0.00	0.00	0.00	0.00	0.00	0.00	0.00
Ce	0.00	0.00	0.00	0.01	0.02	0.01	0.00	0.00	0.01	0.00	0.00	0.01	0.00	0.00	0.00
Sum C	7.00	7.00	7.00	7.00	7.00	7.00	7.00	7.00	7.00	7.00	7.09	7.07	7.12	7.00	7.00
Ti	1.38	1.41	1.49	1.53	1.45	1.47	1.40	1.50	1.47	1.37	1.09	1.19	1.17	1.19	1.23
Sn	0.00	0.00	0.00	0.00	0.00	0.00	0.00	0.00	0.00	0.00	0.00	0.00	0.00	0.00	0.00
Zr	0.00	0.00	0.22	0.20	0.18	0.18	0.17	0.20	0.19	0.13	0.11	0.10	0.10	0.09	0.10
Hf	0.00	0.00	0.00	0.00	0.00	0.00	0.00	0.00	0.00	0.00	0.00	0.00	0.00	0.00	0.00
Nb	0.65	0.63	0.30	0.27	0.40	0.40	0.45	0.33	0.36	0.54	0.83	0.76	0.75	0.76	0.71
Ta	0.00	0.00	0.01	0.02	0.01	0.00	0.00	0.00	0.01	0.00	0.00	0.00	0.00	0.00	0.00
Sum D	2.03	2.04	2.03	2.01	2.03	2.04	2.02	2.02	2.02	2.03	2.02	2.05	2.03	2.04	2.04
Si	7.87	7.69	7.71	7.73	7.68	7.68	7.67	7.78	7.71	7.73	7.51	7.55	7.53	7.58	7.68
Al	0.09	0.25	0.20	0.17	0.27	0.24	0.23	0.14	0.21	0.17	0.32	0.34	0.31	0.31	0.26
Sum T	7.97	7.94	7.91	7.91	7.95	7.92	7.89	7.92	7.92	7.90	7.83	7.89	7.84	7.89	7.94
F	0.57	0.59	0.90	0.95	0.79	0.77	0.82	0.84	0.85	0.63	0.69	0.54	0.67	0.72	0.61
OH	4.00	4.03	4.10	4.05	4.21	4.23	4.18	4.16	4.15	4.00	4.00	4.00	4.00	4.00	4.00
O	30.44	30.41	30.10	30.05	30.21	30.23	30.18	30.16	30.15	30.37	30.31	30.47	30.33	30.28	30.39
Cations	20.00	20.00	19.94	19.95	19.85	19.88	19.93	19.90	19.91	20.05	20.06	20.01	20.01	19.95	19.94

ELECTRON MICROPROBE ANALYSES OF MONT SAINT-HILAIRE AGM

	MSH18A	MSH18Ba	MSH18Bb	MSH18B	MSH19Aa		MSH19Ab		MSH19Ac				MSH19A	MSH19Ba	
OXIDE	Average	PT 72	PT 73	Average	PT 80	PT 82	PT 83	PT 84	PT 85	PT 86	PT 87	PT 88	Average	PT 89	PT 90
Na_2O	2.40	2.49	1.93	2.21	2.38	1.68	2.52	2.41	2.29	2.62	2.53	1.82	2.28	2.01	1.93
K_2O	5.97	4.83	6.11	5.47	6.02	6.11	5.93	6.04	6.10	5.79	5.95	6.08	6.00	5.97	6.15
Rb_2O	0.49	1.19	0.36	0.78	0.47	0.29	0.45	0.48	0.39	0.45	0.39	0.29	0.40	0.22	0.20
Cs_2O	0.02	0.08	0.00	0.04	0.00	0.00	0.00	0.10	0.09	0.10	0.10	0.00	0.05	0.00	0.00
CaO	0.54	0.32	0.54	0.43	0.27	1.78	0.14	0.24	0.37	0.41	0.28	1.54	0.63	1.10	1.08
SrO	0.11	0.14	0.17	0.16	0.08	0.27	0.12	0.11	0.19	0.14	0.15	0.25	0.17	0.25	0.20
BaO	0.00	0.00	0.00	0.00	0.00	0.49	0.00	0.00	0.00	0.00	0.00	0.30	0.10	0.00	0.00
MgO	0.41	0.37	0.51	0.44	0.69	1.21	0.55	0.73	0.42	0.83	0.77	1.26	0.81	1.34	1.42
MnO	20.06	13.85	17.17	15.51	19.81	15.62	20.64	19.90	18.54	18.91	19.12	15.51	18.51	11.21	11.62
FeO	15.09	22.63	18.34	20.49	15.10	19.56	14.51	14.72	16.32	15.67	15.56	19.57	16.38	23.67	22.18
ZnO	0.20	0.00	0.00	0.00	0.27	0.00	0.27	0.00	0.00	0.27	0.25	0.00	0.13	0.00	0.00
Al_2O_3	1.05	0.76	1.19	0.98	1.22	1.40	1.09	1.18	0.60	0.55	0.78	1.10	0.99	0.96	1.04
Y_2O_3	0.00	0.00	0.00	0.00	0.00	0.00	0.00	0.00	0.00	0.00	0.00	0.00	0.00	0.00	0.00
Ce_2O_3	0.03	0.00	0.00	0.00	0.00	0.18	0.00	0.00	0.00	0.00	0.00	0.17	0.04	0.00	0.00
TiO_2	6.93	8.84	4.59	6.72	5.39	10.96	4.76	5.49	4.68	7.87	6.35	10.76	7.03	7.51	7.67
SnO_2	0.00	0.00	0.00	0.00	0.00	0.00	0.00	0.00	0.00	0.00	0.00	0.00	0.00	0.00	0.00
ZrO_2	0.93	1.71	7.02	4.37	2.11	1.08	2.67	1.81	6.62	1.63	2.33	1.45	2.46	5.42	5.28
HfO_2	0.00	0.00	0.26	0.13	0.00	0.00	0.00	0.00	0.00	0.00	0.00	0.00	0.00	0.24	0.29
Nb_2O_5	6.92	1.73	3.32	2.53	7.88	0.68	8.15	8.14	4.08	4.68	6.01	0.75	5.05	1.09	0.91
Ta_2O_5	0.00	0.00	0.00	0.00	0.23	0.00	0.00	0.28	0.00	0.27	0.38	0.00	0.15	0.15	0.15
SiO_2	32.82	33.50	31.81	32.66	32.23	33.31	32.84	31.89	33.35	33.42	33.39	34.29	33.09	33.23	33.53
F	0.88	1.22	1.19	1.21	0.66	1.31	0.86	0.74	0.96	0.82	0.85	1.31	0.94	1.46	1.27
H_2O	2.59	2.65	2.61	2.63	2.57	2.71	2.59	2.55	2.77	2.88	2.60	2.75	2.68	2.59	2.67
O=F	-0.37	-0.51	-0.50	-0.51	-0.28	-0.55	-0.36	-0.31	-0.40	-0.35	-0.36	-0.55	-0.40	-0.61	-0.53
Total	97.03	95.80	96.62	96.21	97.11	98.09	97.73	96.50	97.37	96.96	97.43	98.65	97.48	97.80	97.06
Chemical formulae calculated based on 31 anions															
Na_{tot}	1.07	1.12	0.88	1.00	1.08	0.73	1.13	1.10	1.03	1.17	1.13	0.79	1.02	0.89	0.86
Na	0.21	0.20	0.02	0.11	0.15	0.16	0.17	0.16	0.09	0.27	0.20	0.15	0.17	0.16	0.11
K	1.76	1.43	1.84	1.64	1.79	1.75	1.75	1.81	1.81	1.70	1.75	1.73	1.76	1.74	1.80
Rb	0.07	0.18	0.06	0.12	0.07	0.04	0.07	0.07	0.06	0.07	0.06	0.04	0.06	0.03	0.03
Cs	0.00	0.01	0.00	0.00	0.00	0.00	0.00	0.01	0.01	0.01	0.01	0.00	0.00	0.00	0.00
Sr	0.02	0.02	0.02	0.02	0.01	0.04	0.02	0.02	0.03	0.02	0.02	0.03	0.02	0.03	0.03
Ba	0.00	0.00	0.00	0.00	0.00	0.04	0.00	0.00	0.00	0.00	0.00	0.03	0.01	0.00	0.00
Sum A	2.06	1.84	1.94	1.89	2.02	2.03	2.00	2.07	2.00	2.06	2.04	1.97	2.03	1.97	1.96
Na	0.87	0.92	0.86	0.89	0.93	0.57	0.97	0.94	0.91	0.90	0.93	0.63	0.85	0.73	0.74
Ca	0.13	0.08	0.14	0.11	0.07	0.43	0.04	0.06	0.09	0.10	0.07	0.37	0.15	0.27	0.27
Sum B	1.00	1.00	1.00	1.00	1.00	1.00	1.00	1.00	1.00	1.00	1.00	1.00	1.00	1.00	1.00
Na	0.00	0.00	0.00	0.00	0.00	0.00	0.00	0.00	0.03	0.00	0.00	0.00	0.00	0.00	0.02
Mg	0.14	0.13	0.18	0.15	0.24	0.41	0.19	0.26	0.15	0.28	0.27	0.42	0.28	0.46	0.49
Mn	3.93	2.72	3.44	3.08	3.92	2.97	4.05	3.96	3.65	3.68	3.74	2.92	3.61	2.17	2.25
Fe^{2+}	2.92	4.39	3.63	4.01	2.95	3.68	2.81	2.89	3.17	3.01	3.00	3.64	3.14	4.53	4.25
Zn	0.03	0.00	0.00	0.00	0.05	0.00	0.05	0.00	0.00	0.05	0.04	0.00	0.02	0.00	0.00
Y	0.00	0.00	0.00	0.00	0.00	0.00	0.00	0.00	0.00	0.00	0.00	0.00	0.00	0.00	0.00
Ce	0.00	0.00	0.00	0.00	0.00	0.02	0.00	0.00	0.00	0.00	0.00	0.01	0.00	0.00	0.00
Sum C	7.03	7.24	7.24	7.24	7.16	7.07	7.10	7.11	7.00	7.01	7.05	7.00	7.06	7.15	7.00
Ti	1.21	1.54	0.82	1.18	0.95	1.85	0.83	0.97	0.82	1.36	1.10	1.80	1.21	1.29	1.32
Sn	0.00	0.00	0.00	0.00	0.00	0.00	0.00	0.00	0.00	0.00	0.00	0.00	0.00	0.00	0.00
Zr	0.10	0.19	0.81	0.50	0.24	0.12	0.30	0.21	0.75	0.18	0.26	0.16	0.28	0.60	0.59
Hf	0.00	0.00	0.02	0.01	0.00	0.00	0.00	0.00	0.00	0.00	0.00	0.00	0.00	0.02	0.02
Nb	0.72	0.18	0.36	0.27	0.83	0.07	0.85	0.87	0.43	0.49	0.63	0.08	0.53	0.11	0.09
Ta	0.00	0.00	0.00	0.00	0.02	0.00	0.00	0.02	0.00	0.02	0.02	0.00	0.01	0.01	0.01
Sum D	2.03	1.92	2.00	1.96	2.03	2.04	1.99	2.06	2.00	2.04	2.02	2.03	2.03	2.03	2.03
Si	7.59	7.78	7.52	7.65	7.53	7.49	7.61	7.50	7.75	7.67	7.70	7.63	7.61	7.60	7.67
Al	0.29	0.21	0.33	0.27	0.34	0.37	0.30	0.33	0.16	0.15	0.21	0.29	0.27	0.26	0.28
Sum T	7.88	7.98	7.85	7.92	7.86	7.86	7.91	7.82	7.92	7.82	7.92	7.92	7.88	7.86	7.96
F	0.64	0.90	0.89	0.89	0.49	0.93	0.63	0.55	0.71	0.60	0.62	0.92	0.68	1.06	0.92
OH	4.00	4.10	4.11	4.11	4.00	4.07	4.00	4.00	4.29	4.41	4.00	4.08	4.11	3.94	4.08
O	30.36	30.10	30.11	30.11	30.51	30.07	30.37	30.45	30.29	30.41	30.38	30.08	30.32	29.94	30.08
Cations	20.00	19.98	20.03	20.01	20.08	20.01	19.99	20.06	19.91	19.93	20.02	19.93	19.99	20.01	19.94

ELECTRON MICROPROBE ANALYSES OF MONT SAINT-HILAIRE AGM

OXIDE	MSH19Bb PT 91	PT 92	PT 93	PT 94	PT 95	PT 96	MSH19B Average	MSH20a PT 1	PT 2	MSH20b PT 3	PT 4	MSH20c PT 5	PT 6	MSH20 Average	MSH21a PT 7
Na_2O	2.21	1.95	2.16	2.24	1.90	1.87	2.03	3.16	3.11	3.16	2.99	2.35	2.46	2.87	2.55
K_2O	6.00	6.03	5.94	6.06	6.10	6.23	6.06	5.08	5.40	5.16	5.39	5.44	5.58	5.34	5.99
Rb_2O	0.53	0.36	0.30	0.26	0.26	0.23	0.30	0.51	0.51	0.68	0.51	0.76	0.67	0.61	0.57
Cs_2O	0.00	0.00	0.00	0.00	0.00	0.00	0.00	0.08	0.09	0.14	0.00	0.15	0.00	0.08	0.00
CaO	0.40	1.21	0.51	0.77	1.52	1.15	0.97	0.21	0.31	0.20	0.39	0.97	1.16	0.57	0.30
SrO	0.15	0.20	0.17	0.19	0.23	0.19	0.20	0.14	0.13	0.10	0.20	0.18	0.18	0.16	0.12
BaO	0.00	0.22	0.00	0.00	0.26	0.00	0.06	0.15	0.00	0.26	0.36	0.29	0.29	0.23	0.00
MgO	0.64	0.93	1.02	1.17	1.38	1.35	1.16	0.46	0.50	0.22	0.49	0.51	0.57	0.46	0.72
MnO	16.58	15.16	12.52	12.28	11.64	11.17	12.77	31.54	31.38	24.18	30.08	26.14	28.52	28.64	19.25
FeO	17.93	19.81	21.92	22.19	22.44	23.63	21.72	0.95	0.98	0.72	1.07	1.10	1.11	0.99	14.58
ZnO	0.00	0.00	0.00	0.00	0.00	0.00	0.00	3.39	3.38	10.24	3.51	7.31	4.52	5.39	0.34
Al_2O_3	1.19	1.06	0.55	0.65	1.03	1.04	0.94	0.09	0.11	0.10	0.29	0.77	0.75	0.35	1.14
Y_2O_3	0.00	0.00	0.00	0.00	0.00	0.00	0.00	0.00	0.00	0.00	0.00	0.00	0.00	0.00	0.00
Ce_2O_3	0.00	0.00	0.00	0.00	0.00	0.00	0.00	0.00	0.00	0.14	0.21	0.53	0.31	0.20	0.14
TiO_2	4.92	10.06	5.86	7.72	10.69	7.87	7.79	10.96	10.83	10.21	11.50	11.75	11.85	11.18	5.56
SnO_2	0.00	0.00	0.00	0.00	0.00	0.00	0.00	0.00	0.00	0.00	0.00	0.00	0.00	0.00	0.00
ZrO_2	5.82	2.00	6.42	3.76	1.20	5.38	4.41	0.72	0.81	0.00	0.00	0.00	0.00	0.26	2.05
HfO_2	0.00	0.21	0.00	0.22	0.00	0.25	0.15	0.00	0.00	0.00	0.00	0.00	0.00	0.00	0.00
Nb_2O_5	4.38	0.88	2.15	2.27	0.73	1.04	1.68	1.05	1.25	2.87	0.99	0.73	0.57	1.24	7.73
Ta_2O_5	0.00	0.00	0.00	0.00	0.14	0.17	0.08	0.00	0.00	0.00	0.00	0.00	0.00	0.00	0.34
SiO_2	32.65	33.09	32.90	33.26	33.30	33.53	33.19	35.73	35.50	34.81	35.15	33.47	33.73	34.73	32.99
F	0.91	1.24	1.44	1.08	1.36	1.25	1.25	1.21	0.97	1.23	1.20	1.37	1.12	1.18	0.87
H_2O	2.78	2.68	2.51	2.73	2.64	2.72	2.67	2.78	2.89	2.69	2.76	2.60	2.74	2.74	2.59
O=F	-0.38	-0.52	-0.61	-0.45	-0.57	-0.53	-0.53	-0.51	-0.41	-0.52	-0.51	-0.58	-0.47	-0.50	-0.37
Total	96.71	96.57	95.76	96.40	96.25	98.66	96.90	97.70	97.74	96.59	96.78	95.84	95.66	96.72	97.47
Chemical formulae calculated based on 31 anions															
Na_{tot}	1.00	0.87	0.98	1.00	0.84	0.82	0.91	1.37	1.35	1.40	1.31	1.05	1.09	1.26	1.14
Na	0.10	0.16	0.11	0.19	0.21	0.10	0.15	0.28	0.28	0.10	0.16	0.07	0.12	0.17	0.12
K	1.79	1.76	1.78	1.79	1.78	1.80	1.78	1.45	1.54	1.51	1.55	1.60	1.63	1.55	1.77
Rb	0.08	0.05	0.05	0.04	0.04	0.03	0.04	0.07	0.07	0.10	0.07	0.11	0.10	0.09	0.09
Cs	0.00	0.00	0.00	0.00	0.00	0.00	0.00	0.01	0.01	0.01	0.00	0.02	0.00	0.01	0.00
Sr	0.02	0.03	0.02	0.03	0.03	0.03	0.03	0.02	0.02	0.01	0.03	0.02	0.02	0.02	0.02
Ba	0.00	0.02	0.00	0.00	0.02	0.00	0.01	0.01	0.00	0.02	0.03	0.03	0.03	0.02	0.00
Sum A	1.99	2.03	1.96	2.04	2.08	1.96	2.00	1.84	1.92	1.76	1.84	1.85	1.90	1.85	1.99
Na	0.90	0.70	0.87	0.81	0.63	0.72	0.76	0.95	0.93	0.95	0.86	0.76	0.72	0.86	0.93
Ca	0.10	0.30	0.13	0.19	0.37	0.28	0.24	0.05	0.07	0.05	0.14	0.24	0.29	0.14	0.07
Sum B	1.00	1.00	1.00	1.00	1.00	1.00	1.00	1.00	1.00	1.00	1.00	1.00	1.00	1.00	1.00
Na	0.00	0.00	0.00	0.00	0.00	0.00	0.00	0.14	0.15	0.35	0.29	0.22	0.26	0.23	0.09
Mg	0.22	0.32	0.36	0.40	0.47	0.46	0.40	0.15	0.17	0.08	0.17	0.18	0.20	0.16	0.25
Mn	3.28	2.94	2.49	2.40	2.25	2.14	2.49	5.97	5.95	4.69	5.74	5.11	5.54	5.50	3.77
Fe^{3+}	3.50	3.80	4.31	4.29	4.28	4.47	4.18	0.18	0.18	0.14	0.20	0.21	0.21	0.19	2.82
Zn	0.00	0.00	0.00	0.00	0.00	0.00	0.00	0.56	0.56	1.73	0.58	1.25	0.77	0.91	0.06
Y	0.00	0.00	0.00	0.00	0.00	0.00	0.00	0.00	0.00	0.00	0.00	0.00	0.00	0.00	0.00
Ce	0.00	0.00	0.00	0.00	0.00	0.00	0.00	0.00	0.00	0.01	0.02	0.05	0.03	0.02	0.01
Sum C	7.00	7.06	7.15	7.09	7.00	7.07	7.06	7.00	7.00	7.00	7.00	7.00	7.00	7.00	7.00
Ti	0.86	1.73	1.04	1.34	1.83	1.34	1.34	1.84	1.82	1.76	1.95	2.04	2.04	1.91	0.97
Sn	0.00	0.00	0.00	0.00	0.00	0.00	0.00	0.00	0.00	0.00	0.00	0.00	0.00	0.00	0.00
Zr	0.66	0.22	0.74	0.42	0.13	0.59	0.50	0.08	0.09	0.00	0.00	0.00	0.00	0.03	0.23
Hf	0.00	0.01	0.00	0.02	0.00	0.02	0.01	0.00	0.00	0.00	0.00	0.00	0.00	0.00	0.00
Nb	0.46	0.09	0.23	0.24	0.08	0.11	0.18	0.11	0.13	0.30	0.10	0.08	0.06	0.13	0.81
Ta	0.00	0.00	0.00	0.00	0.01	0.01	0.00	0.00	0.00	0.00	0.00	0.00	0.00	0.00	0.02
Sum D	1.99	2.06	2.00	2.02	2.05	2.07	2.03	2.03	2.04	2.06	2.05	2.11	2.10	2.06	2.03
Si	7.62	7.58	7.73	7.68	7.60	7.59	7.63	7.98	7.94	7.97	7.92	7.72	7.73	7.88	7.63
Al	0.33	0.29	0.15	0.18	0.28	0.28	0.25	0.02	0.03	0.03	0.08	0.21	0.20	0.09	0.31
Sum T	7.95	7.87	7.88	7.86	7.87	7.86	7.89	8.01	7.97	8.00	8.00	7.93	7.94	7.97	7.94
F	0.67	0.90	1.07	0.79	0.98	0.90	0.91	0.86	0.69	0.89	0.86	1.00	0.81	0.85	0.64
OH	4.33	4.10	3.93	4.21	4.02	4.11	4.09	4.15	4.31	4.11	4.14	4.00	4.19	4.15	4.00
O	30.33	30.10	29.93	30.21	30.02	30.11	30.09	30.15	30.31	30.11	30.14	30.00	30.19	30.15	30.36
Cations	19.93	20.01	19.99	20.01	20.00	19.96	19.98	19.87	19.93	19.82	19.89	19.89	19.93	19.89	19.95

ELECTRON MICROPROBE ANALYSES OF MONT SAINT-HILAIRE AGM

OXIDE	MSH21b PT 8	MSH21b PT 9	MSH21b Pt 10	MSH21b PT 11	MSH21b PT 12	MSH21 Average
Na_2O	1.63	1.66	2.37	2.49	2.47	2.20
K_2O	6.24	6.02	5.96	5.78	5.85	5.97
Rb_2O	0.31	0.27	0.33	0.37	0.49	0.39
Cs_2O	0.00	0.00	0.10	0.00	0.00	0.02
CaO	1.94	1.85	0.10	0.28	0.32	0.80
SrO	0.27	0.28	0.11	0.12	0.12	0.17
BaO	0.45	0.40	0.00	0.00	0.00	0.14
MgO	1.38	1.22	0.38	0.57	0.76	0.84
MnO	14.69	14.70	16.52	18.25	18.95	17.06
FeO	19.73	18.53	16.66	15.09	14.17	16.46
ZnO	0.27	0.28	0.20	0.25	0.26	0.27
Al_2O_3	1.42	1.45	0.88	0.63	1.04	1.09
Y_2O_3	0.00	0.00	0.00	0.00	0.00	0.00
Ce_2O_3	0.19	0.00	0.00	0.00	0.00	0.06
TiO_2	11.73	11.13	4.11	6.24	5.93	7.45
SnO_2	0.00	0.00	0.00	0.00	0.00	0.00
ZrO_2	0.43	1.13	4.55	3.00	2.01	2.20
HfO_2	0.00	0.00	0.00	0.00	0.00	0.00
Nb_2O_5	0.55	0.67	6.89	5.75	7.03	4.77
Ta_2O_5	0.13	0.13	0.32	0.00	0.35	0.21
SiO_2	33.55	33.07	32.08	33.41	32.61	32.95
F	1.30	1.04	0.76	0.79	0.80	0.93
H_2O	2.74	2.80	2.49	2.56	2.55	2.62
O=F	-0.55	-0.44	-0.32	-0.33	-0.34	-0.39
Total	98.41	96.19	94.49	95.25	95.37	96.20
Chemical formulae calculated based on 31 anions						
Na_{tot}	0.71	0.73	1.11	1.13	1.13	0.99
Na	0.15	0.01		0.03	0.08	0.08
K	1.78	1.75	1.83	1.73	1.76	1.77
Rb	0.04	0.04	0.05	0.06	0.07	0.06
Cs	0.00	0.00	0.01	0.00	0.00	0.00
Sr	0.04	0.04	0.00	0.02	0.02	0.02
Ba	0.04	0.04	0.00	0.00	0.00	0.01
Sum A	2.04	1.87		1.83	1.93	1.93
Na	0.54	0.55		0.93	0.92	0.77
Ca	0.46	0.45	0.03	0.07	0.08	0.20
Sum B	1.00	1.00		1.00	1.00	1.00
Na	0.02	0.18		0.18	0.13	0.12
Mg	0.46	0.41	0.14	0.20	0.27	0.29
Mn	2.78	2.83	3.37	3.62	3.78	3.36
Fe^{2+}	3.68	3.53	3.35	2.96	2.79	3.19
Zn	0.04	0.05	0.04	0.04	0.05	0.05
Y	0.00	0.00	0.00	0.00	0.00	0.00
Ce	0.02	0.00	0.00	0.00	0.00	0.00
Sum C	7.00	7.00		7.00	7.00	7.00
Ti	1.97	1.91	0.74	1.10	1.05	1.29
Sn	0.00	0.00	0.00	0.00	0.00	0.00
Zr	0.05	0.13	0.53	0.34	0.23	0.25
Hf	0.00	0.00	0.00	0.00	0.00	0.00
Nb	0.06	0.07	0.75	0.61	0.75	0.51
Ta	0.01	0.01	0.02	0.00	0.02	0.01
Sum D	2.08	2.11	2.04	2.05	2.05	2.06
Si	7.48	7.53	7.72	7.83	7.67	7.64
Al	0.37	0.39	0.25	0.17	0.29	0.30
Sum T	7.86	7.92	7.97	8.01	7.96	7.94
F	0.92	0.75	0.58	0.59	0.60	0.68
OH	4.08	4.25	4.00	4.00	4.00	4.06
O	30.08	30.25	30.42	30.41	30.41	30.32
Cations	19.97	19.89	19.94	19.89	19.93	19.93

ELECTRON MICROPROBE ANALYSES OF MONT SAINT-HILAIRE AGM

Sample:	MSH22a	MSH22b	MSH22c	MSH22	MSH23Aa	MSH23Ab			MSH23A	MSH23B	MSH34a	MSH36Aa	MSH36Ab		MSH36Ac
OXIDE	PT 13	PT 15	PT 16	Average	PT 17	PT 19	PT 20	PT 21	Average	Average	PT 30	PT 35	PT 36	PT 37	PT 38
Na_2O	2.09	2.03	2.05	2.06	2.54	2.37	2.45	2.27	2.41	2.33	1.99	2.05	2.55	2.49	2.40
K_2O	6.11	6.11	6.03	6.08	5.97	6.08	6.00	6.03	6.02	5.97	5.91	6.14	6.05	6.11	5.95
Rb_2O	0.45	0.47	0.43	0.45	0.49	0.48	0.42	0.49	0.47	0.30	0.48	0.28	0.41	0.34	0.43
Cs_2O	0.00	0.10	0.00	0.03	0.00	0.00	0.00	0.00	0.00	0.00	0.00	0.00	0.10	0.00	0.09
CaO	1.22	1.06	1.21	1.16	0.49	0.56	0.71	0.57	0.58	0.54	1.26	1.41	0.20	0.30	0.23
SrO	0.16	0.16	0.17	0.16	0.10	0.00	0.11	0.09	0.08	0.25	0.19	0.24	0.12	0.13	0.09
BaO	0.21	0.15	0.00	0.12	0.00	0.00	0.00	0.00	0.00	0.00	0.00	0.30	0.00	0.00	0.00
MgO	0.76	0.98	1.11	0.95	0.33	0.39	0.49	0.42	0.41	0.10	0.92	1.32	0.52	0.64	0.55
MnO	25.59	20.23	22.22	22.68	21.63	19.52	19.82	19.64	20.15	24.48	16.14	14.00	19.28	18.02	20.29
FeO	8.97	13.18	11.16	11.10	13.86	15.43	15.16	15.16	14.90	11.45	19.22	21.28	15.47	17.13	14.52
ZnO	0.22	0.00	0.36	0.19	0.24	0.22	0.26	0.31	0.26	0.00	0.20	0.00	0.25	0.00	0.26
Al_2O_3	1.12	1.16	1.13	1.14	0.86	1.28	0.52	1.25	0.98	0.50	1.32	0.85	0.68	0.66	1.25
Y_2O_3	0.00	0.00	0.00	0.00	0.00	0.00	0.00	0.00	0.00	0.00	0.00	0.00	0.00	0.00	0.00
Ce_2O_3	0.18	0.00	0.00	0.06	0.00	0.00	0.18	0.00	0.05	0.00	0.18	0.00	0.00	0.00	0.00
TiO_2	9.03	8.60	9.52	9.05	7.13	6.63	9.16	6.86	7.45	6.88	8.68	10.93	5.91	5.76	5.28
SnO_2	0.00	0.00	0.00	0.00	0.00	0.00	0.00	0.00	0.00	0.00	0.00	0.00	0.00	0.00	0.00
ZrO_2	0.77	1.81	1.17	1.25	1.20	1.12	0.41	1.02	0.94	6.28	2.37	1.44	2.98	3.19	2.57
HfO_2	0.00	0.00	0.00	0.00	0.00	0.00	0.00	0.00	0.00	0.26	0.00	0.00	0.00	0.00	0.00
Nb_2O_5	3.65	3.72	3.46	3.61	6.86	7.35	3.86	7.23	6.33	0.91	2.80	0.44	6.46	6.37	7.41
Ta_2O_5	0.00	0.00	0.00	0.00	0.00	0.00	0.00	0.00	0.00	0.00	0.00	0.00	0.00	0.00	0.00
SiO_2	32.89	33.28	33.77	33.31	33.15	32.76	33.93	32.91	33.19	33.31	31.61	33.12	32.75	32.68	31.02
F	0.87	1.07	1.08	1.01	0.80	0.81	1.10	1.06	0.94	1.55	1.17	0.98	0.83	0.74	0.61
H_2O	2.86	2.77	2.81	2.81	2.61	2.60	2.77	2.61	2.65	2.48	2.67	2.84	2.57	2.56	2.50
O=F	-0.37	-0.45	-0.45	-0.42	-0.34	-0.34	-0.46	-0.45	-0.40	-0.65	-0.49	-0.41	-0.35	-0.31	-0.26
Total	96.78	96.43	97.23	96.81	97.93	97.25	96.88	97.47	97.38	96.63	96.62	97.33	96.78	96.81	95.19
Chemical formulae calculated based on 31 cations															
Na_{tot}	0.93	0.90	0.90	0.91	1.13	1.06	1.08	1.01	1.07	1.01	0.90	0.90	1.16	1.13	1.12
Na	0.23	0.00	0.00	0.05	0.25	0.17	0.20	0.08	0.18	0.15	0.21	0.25	0.21	0.20	0.18
K	1.79	1.79	1.74	1.77	1.75	1.79	1.75	1.77	1.76	1.78	1.75	1.78	1.80	1.82	1.82
Rb	0.07	0.07	0.06	0.07	0.07	0.07	0.06	0.07	0.07	0.05	0.07	0.04	0.06	0.05	0.07
Cs	0.00	0.01	0.00	0.00	0.00	0.00	0.00	0.00	0.00	0.00	0.00	0.00	0.01	0.00	0.01
Sr	0.02	0.02	0.02	0.02	0.01	0.00	0.02	0.01	0.01	0.03	0.03	0.03	0.02	0.02	0.01
Ba	0.02	0.01	0.00	0.01	0.00	0.00	0.00	0.00	0.00	0.00	0.00	0.03	0.00	0.00	0.00
Sum A	2.12	1.90	1.82	1.92	2.09	2.04	2.03	1.93	2.03	2.01	2.06	2.12	2.10	2.10	2.08
Na	0.70	0.68	0.68	0.72	0.88	0.86	0.83	0.86	0.86	0.86	0.69	0.66	0.95	0.93	0.94
Ca	0.30	0.26	0.29	0.28	0.12	0.14	0.17	0.14	0.14	0.14	0.31	0.34	0.05	0.08	0.06
Sum B	1.00	0.94	0.97	1.00	1.00	1.00	1.00	1.00	1.00	1.00	1.00	1.00	1.00	1.00	1.00
Na	0.00	0.22	0.22	0.14	0.00	0.03	0.05	0.07	0.03	0.00	0.00	0.00	0.00	0.00	0.00
Mg	0.26	0.34	0.37	0.32	0.11	0.13	0.17	0.14	0.14	0.04	0.32	0.45	0.18	0.22	0.20
Mn	4.97	3.92	4.25	4.38	4.21	3.82	3.83	3.82	3.92	4.84	3.17	2.69	3.82	3.57	4.12
Fe^{2+}	1.72	2.52	2.11	2.12	2.66	2.98	2.89	2.91	2.86	2.24	3.73	4.04	3.02	3.35	2.91
Zn	0.04	0.00	0.06	0.03	0.04	0.04	0.04	0.05	0.04	0.00	0.03	0.00	0.04	0.00	0.05
Y	0.00	0.00	0.00	0.00	0.00	0.00	0.00	0.00	0.00	0.00	0.00	0.00	0.00	0.00	0.00
Ce	0.02	0.00	0.00	0.01	0.00	0.00	0.02	0.00	0.00	0.00	0.02	0.00	0.00	0.00	0.00
Sum C	7.00	7.00	7.00	7.00	7.02	7.00	7.00	7.00	7.00	7.12	7.27	7.18	7.06	7.14	7.27
Ti	1.56	1.48	1.62	1.55	1.23	1.15	1.57	1.19	1.28	1.17	1.52	1.87	1.04	1.01	0.95
Sn	0.00	0.00	0.00	0.00	0.00	0.00	0.00	0.00	0.00	0.00	0.00	0.00	0.00	0.00	0.00
Zr	0.09	0.20	0.13	0.14	0.13	0.13	0.05	0.11	0.11	0.72	0.27	0.16	0.34	0.36	0.30
Hf	0.00	0.00	0.00	0.00	0.00	0.00	0.00	0.00	0.00	0.02	0.00	0.00	0.00	0.00	0.00
Nb	0.38	0.39	0.35	0.37	0.71	0.77	0.40	0.75	0.66	0.10	0.29	0.05	0.68	0.67	0.80
Ta	0.00	0.00	0.00	0.00	0.00	0.00	0.00	0.00	0.00	0.00	0.00	0.00	0.00	0.00	0.00
Sum D	2.02	2.07	2.10	2.06	2.08	2.05	2.02	2.05	2.05	2.01	2.08	2.07	2.06	2.05	2.06
Si	7.54	7.62	7.62	7.59	7.61	7.57	7.74	7.56	7.62	7.78	7.34	7.52	7.65	7.64	7.44
Al	0.30	0.31	0.30	0.31	0.23	0.35	0.14	0.34	0.26	0.14	0.36	0.23	0.19	0.18	0.35
Sum T	7.84	7.93	7.92	7.90	7.84	7.92	7.88	7.90	7.88	7.92	7.70	7.74	7.84	7.82	7.79
F	0.63	0.78	0.77	0.73	0.58	0.59	0.79	0.77	0.68	1.14	0.86	0.70	0.61	0.55	0.46
OH	4.37	4.23	4.23	4.27	4.00	4.00	4.21	4.00	4.05	3.86	4.14	4.30	4.00	4.00	4.00
O	30.37	30.23	30.23	30.27	30.42	30.41	30.21	30.23	30.32	29.86	30.14	30.30	30.39	30.45	30.54
Cations	19.98	19.84	19.81	19.88	20.03	20.00	19.92	19.88	19.96	20.02	20.11	20.13	20.06	20.11	20.20

ELECTRON MICROPROBE ANALYSES OF MONT SAINT-HILAIRE AGM

Sample	MSH26A4			MSH26A	MSH26Ba		MSH26Bb			MSH26B	MSH27a		MSH27b		MSH27
OXIDE	PT 39	PT 40	PT 41	Average	PT 42	PT 43	PT 44	PT 45	PT 46	Average	PT 47	PT 48	PT 49	PT 50	Average
Na_2O	1.79	2.51	2.44	2.32	1.94	2.14	1.90	2.34	2.08	2.08	1.57	1.63	1.73	1.70	1.66
K_2O	6.14	5.94	6.07	6.05	6.19	6.15	6.20	6.19	6.12	6.17	6.28	6.26	5.99	5.92	6.11
Rb_2O	0.32	0.33	0.48	0.37	0.24	0.40	0.27	0.40	0.20	0.30	0.37	0.37	0.32	0.34	0.35
Cs_2O	0.00	0.00	0.10	0.04	0.00	0.00	0.00	0.00	0.00	0.00	0.13	0.18	0.14	0.19	0.16
CaO	1.71	0.21	0.21	0.61	1.43	0.47	1.62	0.20	1.08	0.96	1.90	1.89	1.80	1.81	1.85
SrO	0.30	0.15	0.00	0.15	0.23	0.21	0.25	0.00	0.19	0.18	0.23	0.23	0.19	0.22	0.22
BaO	0.34	0.00	0.00	0.09	0.17	0.00	0.16	0.00	0.00	0.07	0.17	0.18	0.16	0.00	0.13
MgO	1.40	0.70	0.52	0.81	1.41	0.79	1.38	0.35	1.35	1.06	0.99	1.04	0.96	0.97	0.99
MnO	15.38	19.87	20.53	18.20	12.60	14.01	12.17	19.81	11.25	13.97	11.75	11.50	11.37	11.11	11.43
FeO	18.78	15.01	14.22	16.63	21.78	20.80	22.60	14.80	23.25	20.65	23.57	23.49	22.23	23.10	23.10
ZnO	0.21	0.35	0.28	0.19	0.00	0.00	0.00	0.22	0.00	0.04	0.00	0.00	0.00	0.00	0.00
Al_2O_3	1.20	0.64	1.01	0.90	0.92	0.47	1.06	1.20	0.86	0.90	1.66	1.59	1.35	1.43	1.51
Y_2O_3	0.00	0.00	0.00	0.00	0.00	0.00	0.00	0.00	0.00	0.00	0.00	0.00	0.00	0.00	0.00
Ce_2O_3	0.18	0.00	0.00	0.03	0.19	0.00	0.00	0.00	0.00	0.04	0.21	0.24	0.16	0.18	0.20
TiO_2	11.19	6.10	5.13	7.19	10.45	6.06	9.95	4.32	7.55	7.67	10.75	11.04	10.45	10.27	10.63
SnO_2	0.00	0.00	0.00	0.00	0.00	0.00	0.00	0.00	0.00	0.00	0.00	0.00	0.00	0.00	0.00
ZrO_2	0.66	2.89	2.64	2.34	2.10	7.01	2.34	2.85	5.59	3.98	0.82	0.92	1.56	1.54	1.21
HfO_2	0.23	0.00	0.00	0.03	0.00	0.00	0.00	0.00	0.00	0.00	0.00	0.00	0.00	0.00	0.00
Nb_2O_5	0.65	5.79	7.81	4.99	0.57	1.63	0.65	8.86	0.84	2.51	1.13	1.08	1.20	1.28	1.17
Ta_2O_5	0.00	0.17	0.00	0.02	0.15	0.00	0.00	0.00	0.17	0.06	0.00	0.00	0.00	0.13	0.03
SiO_2	32.21	32.58	32.32	32.38	34.13	33.73	33.86	32.20	33.48	33.48	32.51	32.89	32.12	32.85	32.59
F	1.32	1.03	0.57	0.87	1.56	1.26	1.32	0.44	1.15	1.15	1.37	0.86	1.16	0.86	1.06
H_2O	2.63	2.56	2.95	2.66	2.60	2.64	2.71	2.54	2.73	2.64	2.65	2.92	2.68	2.87	2.78
O=F	-0.56	-0.43	-0.24	-0.37	-0.66	-0.53	-0.56	-0.19	-0.48	-0.48	-0.58	-0.36	-0.49	-0.36	-0.45
Total	96.09	96.40	97.04	96.52	98.01	97.24	97.88	96.54	97.41	97.42	97.48	97.94	95.08	96.41	96.73
Chemical formulae calculated based on 31 anions															
Na_{tot}	0.80	1.14	1.10	1.05	0.84	0.96	0.83	1.07	0.92	0.92	0.69	0.71	0.78	0.75	0.73
Na	0.22	0.19	0.15	0.20	0.15	0.08	0.22	0.12	0.19	0.16	0.16	0.17	0.13	0.11	0.17
K	1.80	1.77	1.80	1.80	1.77	1.81	1.78	1.86	1.79	1.80	1.82	1.80	1.78	1.73	1.78
Rb	0.05	0.05	0.07	0.06	0.04	0.06	0.04	0.06	0.03	0.04	0.05	0.05	0.05	0.05	0.05
Cs	0.00	0.00	0.01	0.00	0.00	0.00	0.00	0.00	0.00	0.00	0.01	0.02	0.01	0.02	0.02
Sr	0.04	0.02	0.00	0.02	0.03	0.03	0.03	0.00	0.03	0.02	0.03	0.03	0.03	0.03	0.03
Ba	0.03	0.00	0.00	0.01	0.02	0.00	0.01	0.00	0.00	0.01	0.02	0.02	0.02	0.00	0.01
Sum A	2.14	2.04	2.04	2.09	2.00	1.98	2.09	2.05	2.03	2.03	2.09	2.09	2.01	1.94	2.05
Na	0.58	0.95	0.95	0.85	0.66	0.88	0.61	0.95	0.74	0.77	0.54	0.54	0.55	0.56	0.55
Ca	0.42	0.05	0.05	0.15	0.34	0.12	0.39	0.05	0.27	0.23	0.46	0.46	0.45	0.44	0.45
Sum B	1.00	1.00	1.00	1.00	1.00	1.00	1.00	1.00	1.00	1.00	1.00	1.00	1.00	1.00	1.00
Na	0.00	0.00	0.00	0.00	0.04	0.00	0.00	0.00	0.00	0.00	0.00	0.00	0.10	0.08	0.02
Mg	0.48	0.24	0.18	0.28	0.47	0.27	0.46	0.12	0.46	0.36	0.34	0.35	0.33	0.33	0.34
Mn	3.00	3.94	4.05	3.60	2.39	2.74	2.32	3.96	2.18	2.72	2.26	2.20	2.24	2.15	2.21
Fe^{2+}	3.61	2.94	2.77	3.23	4.08	4.02	4.25	2.92	4.45	3.95	4.48	4.43	4.32	4.42	4.41
Zn	0.04	0.06	0.05	0.03	0.00	0.00	0.00	0.04	0.00	0.01	0.00	0.00	0.00	0.00	0.00
Y	0.00	0.00	0.00	0.00	0.00	0.00	0.00	0.00	0.00	0.00	0.00	0.00	0.00	0.00	0.00
Ce	0.02	0.00	0.00	0.00	0.02	0.00	0.00	0.00	0.00	0.00	0.02	0.02	0.01	0.02	0.02
Sum C	7.14	7.18	7.04	7.15	7.00	7.04	7.04	7.04	7.09	7.03	7.10	7.00	7.00	7.00	7.00
Ti	1.94	1.07	0.90	1.25	1.76	1.05	1.68	0.77	1.30	1.31	1.84	1.87	1.83	1.77	1.83
Sn	0.00	0.00	0.00	0.00	0.00	0.00	0.00	0.00	0.00	0.00	0.00	0.00	0.00	0.00	0.00
Zr	0.07	0.33	0.30	0.27	0.23	0.79	0.26	0.33	0.62	0.45	0.09	0.10	0.18	0.17	0.14
Hf	0.02	0.00	0.00	0.00	0.00	0.00	0.00	0.00	0.00	0.00	0.00	0.00	0.00	0.00	0.00
Nb	0.07	0.61	0.82	0.53	0.06	0.17	0.07	0.95	0.09	0.27	0.12	0.11	0.13	0.13	0.12
Ta	0.00	0.01	0.00	0.00	0.01	0.00	0.00	0.00	0.01	0.00	0.00	0.00	0.00	0.01	0.00
Sum D	2.09	2.03	2.02	2.05	2.06	2.01	2.01	2.04	2.02	2.03	2.05	2.08	2.13	2.08	2.08
Si	7.41	7.63	7.52	7.54	7.65	7.80	7.62	7.60	7.66	7.66	7.39	7.42	7.46	7.51	7.45
Al	0.33	0.18	0.28	0.25	0.24	0.13	0.28	0.33	0.23	0.24	0.45	0.42	0.37	0.39	0.41
Sum T	7.74	7.80	7.80	7.79	7.89	7.93	7.90	7.93	7.89	7.91	7.84	7.84	7.83	7.90	7.85
F	0.96	0.76	0.42	0.64	1.11	0.92	0.94	0.33	0.83	0.83	0.99	0.61	0.85	0.62	0.77
OH	4.04	4.00	4.58	4.13	3.89	4.08	4.06	4.00	4.17	4.04	4.02	4.39	4.15	4.38	4.23
O	30.04	30.24	30.58	30.36	29.89	30.08	30.06	30.67	30.17	30.17	30.02	30.39	30.15	30.38	30.23
Cations	20.12	20.05	19.90	20.08	19.95	19.96	20.03	20.06	20.03	20.00	20.07	20.01	19.96	19.91	19.99

ELECTRON MICROPROBE ANALYSES OF MONT SAINT-HILAIRE AGM

Sample	MSH28	MSH29a	MSH29b		MSH29c		MSH29	MSH30a		MSH30b		MSH30	MSH31a		MSH31c
OXIDE	PT 53	PT 58	PT 59	PT 60	PT 61	PT 62	Average	PT 65	PT 66	PT 67	PT 68	Average	PT 72	PT 73	PT 76
Na_2O	1.86	2.06	2.30	2.16	2.25	2.42	2.24	1.67	1.60	1.73	1.74	1.69	1.91	1.61	1.72
K_2O	6.21	5.98	5.89	5.87	6.12	5.81	5.93	6.17	6.39	6.15	6.23	6.24	6.22	6.26	6.22
Rb_2O	0.44	0.41	0.40	0.42	0.44	0.41	0.42	0.38	0.40	0.36	0.53	0.42	0.35	0.37	0.40
Cs_2O	0.09	0.14	0.00	0.12	0.11	0.00	0.07	0.10	0.00	0.00	0.00	0.03	0.00	0.08	0.00
CaO	1.41	1.44	1.45	1.33	1.50	1.38	1.42	1.13	1.37	1.19	1.49	1.30	1.06	1.30	1.19
SrO	0.23	0.21	0.22	0.19	0.22	0.19	0.21	0.20	0.23	0.24	0.31	0.25	0.22	0.23	0.24
BaO	0.14	0.23	0.30	0.29	0.24	0.29	0.27	0.00	0.00	0.00	0.00	0.00	0.00	0.00	0.00
MgO	0.94	1.34	1.52	1.54	1.50	1.54	1.49	0.98	0.55	0.98	0.79	0.83	0.68	0.52	0.56
MnO	9.18	8.54	8.22	8.75	8.49	8.49	8.50	10.28	9.72	10.11	11.18	10.32	11.46	8.90	9.47
FeO	25.51	26.04	25.52	25.90	25.06	24.71	25.45	25.28	25.68	25.54	24.71	25.30	24.99	26.59	25.88
ZnO	0.00	0.00	0.00	0.00	0.20	0.00	0.04	0.00	0.00	0.00	0.00	0.00	0.00	0.00	0.00
Al_2O_3	1.40	1.17	1.05	0.97	1.09	0.94	1.04	1.58	1.71	1.40	1.93	1.66	1.22	1.62	1.34
Y_2O_3	0.00	0.00	0.00	0.00	0.00	0.00	0.00	0.00	0.00	0.00	0.00	0.00	0.00	0.00	0.00
Ce_2O_3	0.26	0.18	0.21	0.00	0.26	0.19	0.17	0.16	0.18	0.16	0.25	0.19	0.00	0.22	0.15
TiO_2	9.30	10.30	10.71	10.76	10.64	10.46	10.57	7.31	7.81	7.28	7.07	7.37	7.87	7.33	7.00
SnO_2	0.00	0.00	0.00	0.00	0.00	0.00	0.00	0.00	0.00	0.00	0.00	0.00	0.00	0.00	0.00
ZrO_2	2.36	1.65	1.51	1.15	1.27	1.53	1.42	3.93	3.39	3.83	5.45	4.15	3.59	4.11	4.71
HfO_2	0.23	0.00	0.00	0.00	0.00	0.00	0.00	0.28	0.00	0.00	0.00	0.07	0.23	0.00	0.00
Nb_2O_5	2.16	1.53	1.25	1.33	1.38	1.48	1.39	2.78	2.87	2.60	2.54	2.70	2.35	2.77	2.16
Ta_2O_5	0.00	0.00	0.00	0.00	0.00	0.00	0.00	0.20	0.17	0.21	0.19	0.19	0.28	0.28	0.00
SiO_2	32.79	34.02	32.82	33.51	33.96	34.52	33.77	31.55	31.71	30.72	30.68	31.17	32.84	32.44	31.75
F	1.35	1.36	1.52	1.52	1.10	1.33	1.37	0.78	1.36	1.10	1.01	1.06	1.10	1.11	1.30
H_2O	2.65	2.72	2.57	2.61	2.83	2.73	2.69	2.84	2.59	2.63	2.75	2.70	2.77	2.73	2.48
O=F	-0.57	-0.57	-0.64	-0.64	-0.46	-0.56	-0.57	-0.33	-0.57	-0.46	-0.43	-0.45	-0.46	-0.47	-0.63
Total	97.94	98.74	96.82	97.78	98.31	97.86	97.90	96.87	97.15	95.36	98.42	96.95	98.67	98.01	96.13
Chemical formulae calculated based on 31 anions															
Na_{tot}	0.82	0.89	1.02	0.94	0.98	1.05	0.97	0.76	0.72	0.80	0.78	0.76	0.85	0.72	0.78
Na	0.13	0.17	0.35	0.26	0.18	0.12	0.23	0.04	0.06	0.10	0.15	0.09	0.10	0.04	0.08
K	1.80	1.70	1.71	1.69	1.75	1.65	1.70	1.84	1.89	1.87	1.85	1.86	1.81	1.84	1.87
Rb	0.06	0.06	0.06	0.06	0.06	0.06	0.06	0.06	0.06	0.06	0.08	0.06	0.05	0.06	0.06
Cs	0.01	0.01	0.00	0.01	0.01	0.00	0.01	0.01	0.00	0.00	0.00	0.00	0.00	0.01	0.00
Sr	0.03	0.03	0.03	0.03	0.03	0.03	0.03	0.03	0.03	0.03	0.04	0.03	0.03	0.03	0.03
Ba	0.01	0.02	0.03	0.03	0.02	0.03	0.02	0.00	0.00	0.00	0.00	0.00	0.00	0.00	0.00
Sum A	2.05	1.99	2.18	2.07	2.05	1.88	2.05	1.97	2.04	2.06	2.12	2.05	1.99	1.97	2.04
Na	0.66	0.66	0.65	0.68	0.64	0.67	0.66	0.72	0.66	0.70	0.63	0.68	0.74	0.68	0.70
Ca	0.34	0.34	0.35	0.32	0.36	0.33	0.34	0.28	0.34	0.30	0.37	0.32	0.26	0.32	0.30
Sum B	1.00	1.00	1.00	1.00	1.00	1.00	1.00	1.00	1.00	1.00	1.00	1.00	1.00	1.00	1.00
Na	0.03	0.07	0.02	0.00	0.16	0.26	0.09	0.00	0.00	0.00	0.00	0.00	0.00	0.00	0.00
Mg	0.32	0.45	0.52	0.52	0.50	0.51	0.50	0.20	0.19	0.21	0.27	0.22	0.23	0.18	0.20
Mn	1.77	1.61	1.59	1.67	1.61	1.60	1.62	2.03	1.91	2.04	2.20	2.05	2.21	1.73	1.89
Fe^{2+}	4.86	4.86	4.86	4.88	4.68	4.61	4.78	4.94	4.98	5.09	4.80	4.95	4.77	5.11	5.09
Zn	0.00	0.00	0.00	0.00	0.03	0.00	0.01	0.00	0.00	0.00	0.00	0.00	0.00	0.00	0.00
Y	0.00	0.00	0.00	0.00	0.00	0.00	0.00	0.00	0.00	0.00	0.00	0.00	0.00	0.00	0.00
Ce	0.02	0.02	0.02	0.00	0.02	0.02	0.01	0.01	0.02	0.01	0.02	0.02	0.00	0.02	0.01
Sum C	7.00	7.00	7.00	7.06	7.00	7.00	7.00	7.19	7.10	7.35	7.29	7.23	7.21	7.04	7.19
Ti	1.59	1.73	1.84	1.82	1.79	1.76	1.79	1.28	1.36	1.30	1.23	1.30	1.35	1.27	1.24
Sn	0.00	0.00	0.00	0.00	0.00	0.00	0.00	0.00	0.00	0.00	0.00	0.00	0.00	0.00	0.00
Zr	0.26	0.18	0.17	0.13	0.14	0.17	0.16	0.45	0.38	0.45	0.62	0.47	0.40	0.46	0.54
Hf	0.02	0.00	0.00	0.00	0.00	0.00	0.00	0.02	0.00	0.00	0.00	0.00	0.02	0.00	0.00
Nb	0.22	0.15	0.13	0.14	0.14	0.15	0.14	0.29	0.30	0.28	0.27	0.29	0.24	0.29	0.23
Ta	0.00	0.00	0.00	0.00	0.00	0.00	0.00	0.01	0.01	0.01	0.01	0.01	0.02	0.02	0.00
Sum D	2.09	2.06	2.13	2.08	2.07	2.07	2.08	2.06	2.06	2.04	2.13	2.07	2.02	2.03	2.01
Si	7.47	7.59	7.48	7.55	7.59	7.70	7.58	7.37	7.36	7.32	7.12	7.29	7.49	7.46	7.47
Al	0.38	0.31	0.28	0.26	0.29	0.25	0.28	0.44	0.47	0.39	0.53	0.46	0.33	0.44	0.37
Sum T	7.84	7.90	7.76	7.80	7.88	7.95	7.86	7.81	7.83	7.71	7.65	7.75	7.82	7.90	7.84
F	0.97	0.96	1.10	1.08	0.78	0.94	0.97	0.58	1.00	0.83	0.74	0.79	0.79	0.81	1.12
OH	4.03	4.04	3.91	3.92	4.22	4.06	4.03	4.42	4.00	4.17	4.26	4.21	4.21	4.19	3.88
O	30.03	30.04	29.91	29.92	30.22	30.06	30.03	30.42	30.00	30.17	30.26	30.21	30.21	30.19	29.88
Cations	19.98	19.94	20.07	20.02	20.01	19.90	19.99	20.03	20.02	20.15	20.19	20.10	20.05	19.94	20.07

ELECTRON MICROPROBE ANALYSES OF MONT SAINT-HILAIRE AGM

Sample		MSH31	MSH32a	MSH32b		MSH32	MSH33Aa		MSH33Ab		MSH33Ac	MSH33Ad		MSH33A	MSH33Ba
OXIDE	PT 77	Average	PT 79	PT 80	PT 81	Average	PT 1	PT 2	PT 3	PT 4	PT 5	PT 7	PT 8	Average	PT 9
Na_2O	1.72	1.74	1.78	1.69	1.63	1.70	2.02	2.18	2.09	1.91	2.12	2.08	1.93	2.05	1.70
K_2O	6.24	6.24	6.28	6.22	6.13	6.21	6.00	5.87	5.74	5.93	5.96	6.09	5.96	5.94	6.23
Rb_2O	0.39	0.38	0.37	0.39	0.40	0.39	0.39	0.37	0.36	0.39	0.36	0.39	0.36	0.37	0.27
Cs_2O	0.00	0.02	0.00	0.00	0.00	0.00	0.00	0.00	0.00	0.10	0.00	0.08	0.00	0.03	0.13
CaO	1.16	1.18	1.18	1.27	1.34	1.26	0.77	0.78	0.74	0.88	0.46	0.60	0.55	0.68	0.99
SrO	0.26	0.24	0.20	0.24	0.25	0.23	0.26	0.25	0.26	0.22	0.27	0.31	0.30	0.27	0.38
BaO	0.00	0.00	0.00	0.00	0.00	0.00	0.00	0.00	0.00	0.00	0.00	0.00	0.00	0.00	0.13
MgO	0.58	0.59	0.67	0.65	0.64	0.65	0.55	0.60	0.57	0.54	0.59	0.60	0.56	0.57	0.59
MnO	9.50	9.83	12.04	13.45	9.67	11.72	12.40	12.71	12.48	12.10	16.18	15.78	15.40	13.86	11.13
FeO	26.61	26.02	23.70	22.60	26.23	24.18	23.54	23.24	23.54	23.91	19.11	20.13	19.84	21.90	24.72
ZnO	0.00	0.00	0.00	0.00	0.00	0.00	0.00	0.00	0.00	0.00	0.00	0.00	0.00	0.00	0.00
Al_2O_3	1.40	1.40	1.46	1.53	1.52	1.50	1.44	1.14	1.50	1.76	1.16	1.29	1.24	1.36	1.50
Y_2O_3	0.00	0.00	0.00	0.00	0.00	0.00	0.00	0.00	0.00	0.00	0.00	0.00	0.00	0.00	0.00
Ce_2O_3	0.15	0.13	0.00	0.16	0.17	0.11	0.25	0.25	0.23	0.47	0.32	0.29	0.28	0.30	0.18
TiO_2	6.76	7.24	6.84	7.30	7.26	7.13	6.71	7.30	6.55	7.19	5.49	5.79	5.42	6.35	7.47
SnO_2	0.00	0.00	0.00	0.00	0.00	0.00	0.00	0.00	0.00	0.00	0.00	0.00	0.00	0.00	0.00
ZrO_2	4.57	4.25	4.50	3.76	4.21	4.16	3.74	4.05	3.75	3.10	5.52	5.71	5.81	4.53	3.47
HfO_2	0.29	0.13	0.00	0.00	0.23	0.08	0.00	0.00	0.32	0.00	0.27	0.22	0.30	0.16	0.30
Nb_2O_5	2.59	2.47	2.62	2.19	2.20	2.34	4.04	2.71	4.09	3.80	3.58	3.37	3.29	3.55	2.82
Ta_2O_5	0.00	0.14	0.00	0.00	0.00	0.00	0.43	0.28	0.68	0.54	0.00	0.00	0.00	0.28	0.37
SiO_2	30.53	31.89	31.38	31.27	31.60	31.42	31.24	32.24	31.73	31.47	31.97	32.00	31.92	31.80	31.74
F	0.99	1.18	1.14	1.40	1.20	1.25	1.08	1.16	0.95	0.78	1.11	1.07	1.37	1.07	1.06
H_2O	2.68	2.67	2.65	2.52	2.64	2.60	2.69	2.68	2.78	2.86	2.66	2.72	2.53	2.70	2.72
O=F	-0.42	-0.50	-0.48	-0.59	-0.51	-0.53	-0.45	-0.49	-0.40	-0.33	-0.47	-0.45	-0.58	-0.45	-0.45
Total	96.00	97.20	96.33	96.05	96.81	96.40	97.09	97.32	97.96	97.62	96.66	98.07	96.48	97.31	97.45
Chemical formulae calculated based on 31 cations															
$Na_{tot.}$	0.79	0.79	0.81	0.77	0.74	0.77	0.92	0.98	0.94	0.86	0.97	0.94	0.88	0.93	0.77
Na	0.09	0.08	0.11	0.09	0.08	0.09	0.11	0.17	0.12	0.08	0.08	0.09	0.02	0.10	0.01
K	1.90	1.85	1.88	1.87	1.83	1.86	1.79	1.74	1.70	1.76	1.79	1.81	1.79	1.77	1.85
Rb	0.06	0.06	0.06	0.06	0.06	0.06	0.06	0.06	0.05	0.06	0.05	0.06	0.06	0.06	0.04
Cs	0.00	0.00	0.00	0.00	0.00	0.00	0.00	0.00	0.00	0.01	0.00	0.01	0.00	0.00	0.01
Sr	0.04	0.03	0.03	0.03	0.03	0.03	0.04	0.03	0.04	0.03	0.04	0.04	0.04	0.04	0.05
Ba	0.00	0.00	0.00	0.00	0.00	0.00	0.00	0.00	0.00	0.00	0.00	0.00	0.00	0.00	0.01
Sum A	2.08	2.02	2.08	2.06	2.00	2.04	2.00	2.00	1.91	1.93	1.96	2.00	1.91	1.96	1.98
Na	0.70	0.71	0.70	0.68	0.66	0.68	0.81	0.81	0.82	0.78	0.88	0.85	0.86	0.83	0.75
Ca	0.30	0.29	0.30	0.32	0.34	0.32	0.19	0.19	0.18	0.22	0.12	0.15	0.14	0.17	0.25
Sum B	1.00	1.00	1.00	1.00	1.00	1.00	1.00	1.00	1.00	1.00	1.00	1.00	1.00	1.00	1.00
Na	0.00	0.00	0.00	0.00	0.00	0.00	0.00	0.00	0.00	0.00	0.00	0.00	0.00	0.00	0.00
Mg	0.21	0.20	0.24	0.23	0.22	0.23	0.19	0.21	0.20	0.19	0.21	0.21	0.20	0.20	0.21
Mn	1.92	1.94	2.40	2.68	1.92	2.33	2.46	2.50	2.45	2.38	3.22	3.11	3.07	2.74	2.19
Fe^{2+}	5.30	5.07	4.66	4.45	5.13	4.75	4.61	4.51	4.57	4.64	3.76	3.91	3.91	4.27	4.81
Zn	0.00	0.00	0.00	0.00	0.00	0.00	0.00	0.00	0.00	0.00	0.00	0.00	0.00	0.00	0.00
Y	0.00	0.00	0.00	0.00	0.00	0.00	0.00	0.00	0.00	0.00	0.00	0.00	0.00	0.00	0.00
Ce	0.01	0.01	0.00	0.01	0.02	0.01	0.02	0.02	0.02	0.04	0.03	0.03	0.02	0.03	0.02
Sum C	7.44	7.22	7.29	7.38	7.28	7.32	7.29	7.23	7.24	7.25	7.22	7.25	7.21	7.24	7.22
Ti	1.21	1.27	1.21	1.29	1.28	1.26	1.18	1.27	1.14	1.26	0.97	1.01	0.96	1.11	1.31
Sn	0.00	0.00	0.00	0.00	0.00	0.00	0.00	0.00	0.00	0.00	0.00	0.00	0.00	0.00	0.00
Zr	0.53	0.48	0.52	0.43	0.48	0.48	0.43	0.46	0.42	0.35	0.63	0.65	0.67	0.52	0.39
Hf	0.02	0.01	0.00	0.00	0.02	0.01	0.00	0.00	0.02	0.00	0.02	0.02	0.02	0.01	0.02
Nb	0.28	0.26	0.28	0.23	0.23	0.25	0.43	0.28	0.43	0.40	0.38	0.35	0.35	0.38	0.30
Ta	0.00	0.01	0.00	0.00	0.00	0.00	0.03	0.02	0.04	0.03	0.00	0.00	0.00	0.02	0.02
Sum D	2.04	2.03	2.00	1.96	2.00	1.99	2.06	2.03	2.06	2.04	2.00	2.03	2.00	2.03	2.04
Si	7.27	7.42	7.38	7.37	7.39	7.38	7.32	7.48	7.36	7.31	7.52	7.44	7.52	7.42	7.38
Al	0.39	0.38	0.41	0.43	0.42	0.42	0.40	0.31	0.41	0.48	0.32	0.35	0.34	0.37	0.41
Sum T	7.66	7.80	7.78	7.79	7.81	7.79	7.72	7.79	7.77	7.79	7.84	7.79	7.87	7.80	7.80
F	0.75	0.87	0.85	1.04	0.89	0.93	0.80	0.85	0.70	0.57	0.83	0.79	1.02	0.79	0.78
OH	4.25	4.13	4.15	3.96	4.11	4.07	4.20	4.15	4.30	4.43	4.17	4.21	3.98	4.21	4.22
O	30.25	30.13	30.15	29.96	30.11	30.07	30.20	30.15	30.30	30.43	30.17	30.21	29.98	30.21	30.22
Cations	20.22	20.07	20.15	20.19	20.09	20.14	20.06	20.06	19.98	20.02	20.02	20.07	19.98	20.03	20.04

ELECTRON MICROPROBE ANALYSES OF MONT SAINT-HILAIRE AGM

Sample	MSH33Bb		MSH33Bc		MSH33B4			MSH33B	MSH34Aa	MSH34Ab		MSH34Ac		MSH34A
OXIDE	PT 10	PT 11	PT 12	PT 13	PT 14	PT 15	PT 16	Average	PT 17	PT 18	PT 19	PT 20	PT 21	PT 22	PT 23
Na_2O	1.71	1.73	1.86	1.88	1.51	1.59	1.53	1.69	1.79	1.89	1.91	1.91	2.02	2.24	1.86
K_2O	6.24	6.32	6.18	6.23	6.22	6.07	6.12	6.20	6.12	6.06	6.03	6.02	5.87	5.81	5.87
Rb_2O	0.29	0.24	0.26	0.26	0.29	0.29	0.27	0.27	0.36	0.35	0.35	0.30	0.25	0.31	0.31
Cs_2O	0.00	0.00	0.00	0.00	0.00	0.00	0.00	0.02	0.14	0.15	0.15	0.15	0.11	0.10	0.13
CaO	1.09	1.10	0.99	0.88	1.39	1.38	1.19	1.13	0.98	0.91	1.02	1.03	0.78	0.80	1.08
SrO	0.38	0.42	0.45	0.50	0.35	0.38	0.36	0.40	0.42	0.42	0.38	0.33	0.28	0.37	0.34
BaO	0.00	0.00	0.00	0.14	0.00	0.00	0.18	0.06	0.00	0.00	0.00	0.00	0.00	0.00	0.00
MgO	0.85	0.97	1.10	0.85	1.06	0.91	0.87	0.90	0.46	0.49	0.51	0.48	0.54	0.55	0.47
MnO	12.99	13.32	13.30	13.19	13.16	14.59	13.04	13.09	9.50	9.19	9.56	9.74	11.45	9.69	8.53
FeO	22.56	21.63	22.34	22.38	21.49	20.66	21.57	22.17	26.47	26.43	26.94	27.25	24.75	26.24	27.51
ZnO	0.00	0.00	0.00	0.00	0.00	0.00	0.00	0.00	0.00	0.00	0.00	0.00	0.00	0.00	0.00
Al_2O_3	1.42	1.32	1.16	1.23	1.77	1.31	1.71	1.43	1.34	1.24	1.35	1.41	0.86	0.73	1.43
Y_2O_3	0.00	0.00	0.00	0.00	0.00	0.00	0.00	0.00	0.00	0.00	0.00	0.00	0.00	0.00	0.00
Ce_2O_3	0.22	0.33	0.29	0.26	0.24	0.00	0.30	0.23	0.23	0.00	0.00	0.00	0.00	0.00	0.00
TiO_2	8.16	8.12	8.24	7.89	8.10	6.73	7.85	7.82	7.68	7.52	7.87	7.71	7.58	8.14	7.99
SnO_2	0.00	0.00	0.00	0.00	0.00	0.00	0.00	0.00	0.00	0.00	0.00	0.00	0.00	0.00	0.00
ZrO_2	3.31	3.30	3.73	3.67	3.10	5.98	2.91	3.68	3.64	3.56	3.32	3.35	4.37	4.35	2.85
HfO_2	0.26	0.25	0.36	0.00	0.00	0.46	0.30	0.24	0.25	0.25	0.22	0.24	0.26	0.27	0.29
Nb_2O_5	2.53	2.49	1.96	2.51	2.76	1.13	2.83	2.38	2.64	2.74	2.77	3.16	2.18	1.46	2.68
Ta_2O_5	0.19	0.16	0.00	0.00	0.39	0.15	0.33	0.20	0.23	0.19	0.44	0.52	0.13	0.00	0.66
SiO_2	31.98	32.16	32.33	32.92	31.99	32.08	31.64	32.11	32.14	31.65	32.27	32.11	32.60	33.01	32.18
F	1.03	1.41	0.87	1.16	1.15	1.02	0.77	1.06	1.08	1.19	0.96	0.99	1.20	1.19	1.16
H_2O	2.76	2.58	2.85	2.73	2.71	2.73	2.85	2.74	2.73	2.63	2.81	2.81	2.67	2.69	2.69
O=F	-0.43	-0.59	-0.37	-0.49	-0.48	-0.43	-0.32	-0.45	-0.45	-0.50	-0.40	-0.42	-0.51	-0.50	-0.49
Total	97.54	97.25	97.90	98.19	97.20	97.03	96.29	97.36	97.74	96.36	98.45	99.09	97.39	97.45	97.54
Chemical formulae calculated based on 31 anions															
Na_{tot}	0.77	0.78	0.83	0.83	0.67	0.72	0.69	0.76	0.80	0.86	0.85	0.85	0.91	1.00	0.83
Na	0.04	0.05	0.07	0.05	0.02	0.06	0.00	0.04	0.05	0.09	0.10	0.10	0.10	0.20	0.10
K	1.84	1.86	1.81	1.82	1.83	1.81	1.82	1.83	1.81	1.82	1.77	1.76	1.73	1.71	1.73
Rb	0.04	0.04	0.04	0.04	0.04	0.04	0.04	0.04	0.05	0.05	0.05	0.04	0.04	0.05	0.05
Cs	0.00	0.00	0.00	0.00	0.00	0.00	0.00	0.00	0.01	0.02	0.02	0.02	0.01	0.01	0.01
Sr	0.05	0.06	0.06	0.07	0.05	0.05	0.05	0.05	0.06	0.06	0.05	0.04	0.04	0.05	0.05
Ba	0.00	0.00	0.00	0.01	0.00	0.00	0.02	0.01	0.00	0.00	0.00	0.00	0.00	0.00	0.00
Sum A	1.97	2.00	1.98	1.98	1.94	1.96	1.93	1.97	1.98	2.03	1.99	1.96	1.92	2.01	1.94
Na	0.73	0.73	0.76	0.79	0.66	0.66	0.69	0.72	0.76	0.77	0.75	0.75	0.81	0.80	0.73
Ca	0.27	0.27	0.24	0.22	0.34	0.35	0.30	0.28	0.24	0.23	0.25	0.25	0.19	0.20	0.27
Sum B	1.00	1.00	1.00	1.00	1.00	1.00	0.99	1.00	1.00	1.00	1.00	1.00	1.00	1.00	1.00
Na	0.00	0.00	0.00	0.00	0.00	0.00	0.00	0.00	0.00	0.00	0.00	0.00	0.00	0.00	0.00
Mg	0.29	0.33	0.38	0.29	0.36	0.32	0.30	0.31	0.16	0.17	0.18	0.16	0.19	0.19	0.16
Mn	2.54	2.61	2.59	2.55	2.57	2.88	2.58	2.56	1.86	1.83	1.86	1.89	2.25	1.89	1.67
Fe^{2+}	4.35	4.18	4.29	4.28	4.14	4.03	4.21	4.29	5.13	5.19	5.17	5.22	4.79	5.06	5.32
Zn	0.00	0.00	0.00	0.00	0.00	0.00	0.00	0.00	0.00	0.00	0.00	0.00	0.00	0.00	0.00
Y	0.00	0.00	0.00	0.00	0.00	0.00	0.00	0.00	0.00	0.00	0.00	0.00	0.00	0.00	0.00
Ce	0.02	0.03	0.02	0.02	0.02	0.00	0.03	0.02	0.02	0.00	0.00	0.00	0.00	0.00	0.00
Sum C	7.20	7.15	7.28	7.14	7.09	7.22	7.12	7.18	7.17	7.19	7.21	7.27	7.22	7.14	7.15
Ti	1.42	1.41	1.42	1.36	1.40	1.18	1.38	1.36	1.34	1.33	1.36	1.33	1.32	1.41	1.39
Sn	0.00	0.00	0.00	0.00	0.00	0.00	0.00	0.00	0.00	0.00	0.00	0.00	0.00	0.00	0.00
Zr	0.37	0.37	0.42	0.41	0.35	0.68	0.33	0.42	0.41	0.41	0.37	0.37	0.49	0.49	0.32
Hf	0.02	0.02	0.02	0.00	0.00	0.03	0.02	0.02	0.02	0.02	0.01	0.02	0.02	0.02	0.02
Nb	0.26	0.26	0.20	0.26	0.29	0.12	0.30	0.25	0.28	0.29	0.29	0.33	0.23	0.15	0.28
Ta	0.01	0.01	0.00	0.00	0.02	0.01	0.02	0.01	0.01	0.01	0.03	0.03	0.01	0.00	0.04
Sum D	2.08	2.07	2.07	2.02	2.06	2.02	2.05	2.05	2.06	2.06	2.06	2.08	2.07	2.07	2.05
Si	7.38	7.43	7.43	7.52	7.37	7.48	7.38	7.42	7.44	7.44	7.41	7.35	7.55	7.61	7.44
Al	0.39	0.36	0.31	0.33	0.48	0.36	0.47	0.39	0.37	0.34	0.37	0.38	0.24	0.20	0.39
Sum T	7.77	7.79	7.74	7.85	7.85	7.84	7.85	7.81	7.81	7.78	7.78	7.73	7.78	7.81	7.83
F	0.75	1.03	0.63	0.84	0.84	0.75	0.57	0.77	0.79	0.88	0.70	0.72	0.88	0.87	0.85
OH	4.25	3.97	4.37	4.16	4.16	4.25	4.43	4.23	4.21	4.12	4.30	4.28	4.12	4.13	4.15
O	30.25	29.97	30.37	30.16	30.16	30.25	30.43	30.23	30.21	30.12	30.30	30.28	30.12	30.13	30.15
Cations	20.02	20.01	20.07	19.99	19.94	20.04	19.94	20.01	20.01	20.06	20.03	20.04	19.99	20.03	19.97

ELECTRON MICROPROBE ANALYSES OF MONT SAINT-HILAIRE AGM

Sample	MSH34A	MSH34Ba			MSH34Bb	MSH34B	MSH35a		MSH35b		MSH35c		MSH35d	
OXIDE	PT 24	Average	PT 25	PT 26	PT 27	PT 28	Average	PT 30	PT 31	PT 32	PT 33	PT 34	PT 35	PT 36	PT 37
Na_2O	1.83	1.93	1.90	1.95	1.95	1.95	1.94	2.06	1.98	2.18	2.23	2.22	2.17	2.07	2.00
K_2O	5.93	5.96	5.90	5.94	5.85	5.94	5.91	5.99	5.89	5.90	5.80	5.93	5.87	5.88	5.92
Rb_2O	0.29	0.32	0.19	0.16	0.16	0.19	0.18	0.44	0.42	0.40	0.41	0.45	0.42	0.41	0.40
Cs_2O	0.11	0.13	0.00	0.00	0.00	0.00	0.00	0.00	0.13	0.00	0.00	0.00	0.00	0.00	0.10
CaO	0.97	0.95	1.00	1.00	1.00	1.07	1.02	1.42	1.50	1.46	1.48	1.27	1.34	1.49	1.51
SrO	0.34	0.36	0.23	0.25	0.22	0.22	0.23	0.18	0.23	0.20	0.22	0.16	0.15	0.22	0.21
BaO	0.00	0.00	0.00	0.00	0.00	0.00	0.00	0.17	0.25	0.13	0.19	0.00	0.14	0.23	0.25
MgO	0.48	0.50	0.70	0.66	0.68	0.72	0.69	1.04	0.98	1.05	1.08	0.82	0.71	1.04	0.96
MnO	10.01	9.71	10.10	9.36	9.40	9.57	9.61	15.59	15.78	17.53	17.94	20.89	22.14	17.34	17.48
FeO	25.81	26.43	25.15	25.63	25.43	25.05	25.32	19.57	18.99	17.62	17.29	13.64	13.13	16.99	16.79
ZnO	0.00	0.00	0.00	0.00	0.00	0.00	0.00	0.00	0.21	0.18	0.19	0.00	0.00	0.19	0.21
Al_2O_3	1.39	1.22	1.04	0.95	0.98	0.87	0.96	1.23	1.19	0.92	0.89	0.87	0.82	0.98	1.13
Y_2O_3	0.00	0.00	0.00	0.00	0.00	0.00	0.00	0.00	0.00	0.00	0.00	0.00	0.00	0.00	0.00
Ce_2O_3	0.16	0.05	0.00	0.00	0.00	0.00	0.00	0.15	0.00	0.15	0.00	0.00	0.16	0.00	0.16
TiO_2	8.07	7.82	6.59	6.72	6.47	6.96	6.69	9.79	9.97	10.14	10.44	9.80	10.13	10.40	9.93
SnO_2	0.00	0.00	0.00	0.00	0.00	0.00	0.00	0.00	0.00	0.00	0.00	0.00	0.00	0.00	0.00
ZrO_2	3.22	3.58	6.45	6.65	6.86	6.29	6.56	1.08	1.05	1.25	1.12	0.86	0.88	0.74	0.76
HfO_2	0.26	0.26	0.53	0.41	0.40	0.32	0.42	0.00	0.00	0.00	0.00	0.00	0.00	0.00	0.21
Nb_2O_5	2.62	2.53	0.66	0.65	0.69	0.37	0.59	2.33	2.38	1.88	1.92	2.67	2.31	2.21	2.54
Ta_2O_5	0.58	0.34	0.16	0.13	0.20	0.00	0.12	0.00	0.00	0.00	0.00	0.00	0.00	0.00	0.00
SiO_2	32.20	32.27	32.29	32.38	32.60	32.62	32.47	32.88	32.26	33.86	34.02	33.20	33.37	33.13	32.08
F	1.24	1.13	1.13	1.57	1.21	1.15	1.27	1.18	1.00	0.98	1.10	1.18	1.15	1.20	1.01
H_2O	2.66	2.71	2.65	2.45	2.62	2.64	2.59	2.73	2.78	2.88	2.84	2.71	2.75	2.72	2.76
O=F	-0.52	-0.47	-0.48	-0.66	-0.51	-0.48	-0.53	-0.50	-0.42	-0.41	-0.46	-0.50	-0.48	-0.51	-0.43
Total	97.65	97.71	96.20	96.20	96.22	95.45	96.02	97.34	96.57	98.29	98.83	96.18	97.16	96.74	95.98
Chemical formulae calculated based on 31 cations															
Na_{tot}	0.82	0.87	0.87	0.89	0.89	0.89	0.88	0.91	0.88	0.95	0.96	0.99	0.96	0.91	0.90
Na	0.06	0.10	0.12	0.14	0.14	0.16	0.14	0.26	0.25	0.30	0.31	0.25	0.28	0.24	0.27
K	1.75	1.76	1.77	1.78	1.75	1.78	1.77	1.74	1.73	1.69	1.65	1.73	1.70	1.71	1.75
Rb	0.04	0.05	0.03	0.02	0.02	0.03	0.03	0.06	0.06	0.06	0.06	0.07	0.06	0.06	0.06
Cs	0.01	0.01	0.00	0.00	0.00	0.00	0.00	0.00	0.01	0.00	0.00	0.00	0.00	0.00	0.01
Sr	0.05	0.05	0.03	0.03	0.03	0.03	0.03	0.02	0.03	0.03	0.03	0.02	0.02	0.03	0.03
Ba	0.00	0.00	0.00	0.00	0.00	0.00	0.00	0.02	0.02	0.01	0.02	0.00	0.01	0.02	0.02
Sum A	1.91	1.97	1.95	1.98	1.94	2.00	1.97	2.10	2.11	2.08	2.07	2.07	2.08	2.06	2.14
Na	0.76	0.77	0.75	0.75	0.75	0.73	0.74	0.65	0.63	0.65	0.65	0.69	0.67	0.64	0.63
Ca	0.24	0.23	0.25	0.25	0.25	0.27	0.26	0.35	0.37	0.35	0.35	0.31	0.33	0.36	0.38
Sum B	1.00	1.00	1.00	1.00	1.00	1.00	1.00	1.00	1.00	1.00	1.00	1.00	1.00	1.00	1.00
Na	0.00	0.00	0.00	0.00	0.00	0.00	0.00	0.00	0.00	0.00	0.00	0.05	0.00	0.03	0.00
Mg	0.17	0.17	0.25	0.23	0.24	0.25	0.24	0.35	0.34	0.35	0.36	0.28	0.24	0.35	0.33
Mn	1.96	1.90	2.01	1.86	1.87	1.91	1.91	3.01	3.08	3.33	3.39	4.05	4.26	3.35	3.43
Fe^{2+}	4.99	5.11	4.94	5.03	4.98	4.93	4.97	3.73	3.65	3.31	3.22	2.61	2.50	3.24	3.25
Zn	0.00	0.00	0.00	0.00	0.00	0.00	0.00	0.00	0.04	0.03	0.03	0.00	0.00	0.03	0.04
Y	0.00	0.00	0.00	0.00	0.00	0.00	0.00	0.00	0.00	0.00	0.00	0.00	0.00	0.00	0.00
Ce	0.01	0.00	0.00	0.00	0.00	0.00	0.00	0.01	0.00	0.01	0.00	0.00	0.01	0.00	0.01
Sum C	7.12	7.18	7.20	7.13	7.09	7.09	7.13	7.10	7.10	7.03	7.00	7.00	7.02	7.00	7.06
Ti	1.40	1.36	1.17	1.19	1.14	1.23	1.18	1.68	1.73	1.71	1.75	1.69	1.73	1.78	1.73
Sn	0.00	0.00	0.00	0.00	0.00	0.00	0.00	0.00	0.00	0.00	0.00	0.00	0.00	0.00	0.00
Zr	0.36	0.40	0.74	0.76	0.78	0.72	0.75	0.12	0.12	0.14	0.12	0.10	0.10	0.08	0.09
Hf	0.02	0.02	0.04	0.03	0.03	0.02	0.03	0.00	0.00	0.00	0.00	0.00	0.00	0.00	0.01
Nb	0.27	0.26	0.07	0.07	0.07	0.04	0.06	0.24	0.25	0.19	0.19	0.28	0.24	0.23	0.27
Ta	0.04	0.02	0.01	0.01	0.01	0.00	0.01	0.00	0.00	0.00	0.00	0.00	0.00	0.00	0.00
Sum D	2.09	2.07	2.02	2.05	2.04	2.01	2.03	2.04	2.09	2.04	2.06	2.06	2.07	2.09	2.10
Si	7.44	7.46	7.59	7.60	7.64	7.68	7.63	7.49	7.42	7.60	7.58	7.61	7.59	7.55	7.43
Al	0.38	0.33	0.29	0.26	0.27	0.24	0.27	0.33	0.32	0.24	0.23	0.24	0.22	0.26	0.31
Sum T	7.81	7.79	7.88	7.87	7.91	7.92	7.89	7.82	7.75	7.84	7.81	7.84	7.81	7.81	7.74
F	0.91	0.82	0.84	1.17	0.90	0.86	0.94	0.85	0.73	0.70	0.78	0.86	0.83	0.86	0.74
OH	4.09	4.18	4.16	3.83	4.10	4.14	4.06	4.15	4.27	4.31	4.23	4.15	4.17	4.14	4.26
O	30.09	30.18	30.16	29.83	30.10	30.14	30.06	30.15	30.27	30.31	30.23	30.15	30.17	30.14	30.26
Cations	19.93	20.01	20.04	20.02	19.98	20.02	20.01	20.05	20.05	19.99	19.97	19.97	19.97	19.96	20.04

ELECTRON MICROPROBE ANALYSES OF MONT SAINT-HILAIRE AGM

Sample		MSH35	MSH36Aa			MSH36Ab				MSH36A	MSH36Ba				
OXIDE	PT 38	Average	PT 39	PT 40	PT 41	PT 42	PT 44	PT 45	PT 46	Average	PT 62	PT 63	PT 64	PT 65	PT 66
Na_2O	2.09	2.11	2.51	2.52	2.55	2.80	2.20	2.61	2.71	2.56	2.29	2.51	2.55	2.60	2.48
K_2O	6.02	5.91	5.93	5.91	5.89	5.83	5.68	5.72	5.90	5.84	5.37	5.72	5.88	5.89	5.96
Rb_2O	0.40	0.42	0.54	0.55	0.53	0.58	0.83	0.92	0.56	0.64	0.81	0.91	0.94	0.87	0.85
Cs_2O	0.09	0.04	0.07	0.09	0.08	0.00	0.08	0.00	0.08	0.06	0.00	0.00	0.00	0.00	0.00
CaO	1.56	1.45	1.20	1.23	1.17	0.90	1.13	0.00	0.87	0.93	0.10	0.11	0.07	0.06	0.08
SrO	0.18	0.19	0.04	0.08	0.05	0.07	0.09	0.03	0.08	0.06	0.00	0.00	0.00	0.00	0.00
BaO	0.24	0.18	0.00	0.00	0.14	0.00	0.00	0.00	0.00	0.02	0.00	0.00	0.00	0.00	0.00
MgO	1.11	0.98	0.93	0.93	0.90	1.03	1.04	0.42	1.01	0.89	0.90	0.61	0.48	0.59	0.50
MnO	17.36	18.01	22.63	22.59	23.60	24.69	28.09	30.88	24.60	25.30	27.92	29.60	29.34	29.81	30.28
FeO	17.28	16.81	10.26	10.60	9.82	7.71	5.71	2.99	7.96	7.86	6.67	4.44	4.82	4.36	3.73
ZnO	0.00	0.11	0.29	0.23	0.00	0.21	0.00	0.00	0.28	0.14	0.00	0.22	0.00	0.00	0.00
Al_2O_3	1.16	1.02	1.24	1.22	1.19	0.99	1.38	1.61	1.06	1.24	2.60	2.01	1.90	2.07	1.95
Y_2O_3	0.00	0.00	0.00	0.00	0.00	0.00	0.00	0.00	0.00	0.00	0.00	0.00	0.00	0.00	0.00
Ce_2O_3	0.00	0.07	0.00	0.00	0.00	0.19	0.30	0.00	0.00	0.07	0.00	0.00	0.00	0.00	0.00
TiO_2	10.22	10.09	8.00	8.20	8.28	8.13	9.23	1.76	7.92	7.36	1.64	2.27	1.79	1.64	1.93
SnO_2	0.00	0.00	0.00	0.00	0.00	0.00	0.00	0.00	0.00	0.00	0.00	0.00	0.00	0.00	0.00
ZrO_2	0.88	0.96	0.75	0.71	0.73	0.30	1.47	4.09	0.40	1.21	3.21	3.15	3.36	3.32	3.34
HfO_2	0.00	0.02	0.00	0.00	0.00	0.00	0.00	0.00	0.00	0.00	0.00	0.00	0.00	0.00	0.00
Nb_2O_5	2.41	2.29	5.02	5.04	5.00	5.29	1.72	10.93	5.78	5.54	9.83	10.38	11.17	11.09	11.19
Ta_2O_5	0.00	0.00	0.00	0.00	0.00	0.00	0.00	0.19	0.00	0.03	0.67	0.52	0.64	0.52	0.49
SiO_2	33.99	33.20	33.00	32.82	33.19	33.03	32.97	31.63	33.44	32.87	31.59	32.30	31.64	31.64	31.99
F	1.07	1.10	1.09	1.04	0.97	0.79	1.12	0.00	0.98	0.86	0.46	0.52	0.00	0.00	0.49
H_2O	2.85	2.78	2.99	2.99	2.61	2.57	2.71	2.50	2.60	2.60	2.53	2.56	2.52	2.52	2.55
O=F	-0.45	-0.46	-0.46	-0.44	-0.41	-0.33	-0.47	0.00	-0.41	-0.36	-0.19	-0.22	0.00	0.00	-0.21
Total	98.46	97.28	95.63	95.92	96.29	94.78	95.28	96.28	95.82	95.71	96.39	97.61	97.10	96.98	97.61
Chemical formulae calculated based on 31 anions															
Na_{tot}	0.91	0.93	1.13	1.13	1.14	1.27	0.99	1.21	1.21	1.15	1.05	1.14	1.18	1.20	1.13
Na	0.16	0.28	0.21	0.26	0.22	0.28	0.26	0.21	0.15	0.23	0.08	0.16	0.20	0.21	0.08
K	1.71	1.71	1.75	1.74	1.73	1.74	1.68	1.75	1.73	1.73	1.63	1.71	1.79	1.79	1.79
Rb	0.06	0.06	0.08	0.08	0.08	0.09	0.12	0.14	0.08	0.10	0.12	0.14	0.14	0.13	0.13
Cs	0.01	0.00	0.01	0.01	0.01	0.00	0.01	0.00	0.01	0.01	0.00	0.00	0.00	0.00	0.00
Sr	0.02	0.03	0.01	0.01	0.01	0.01	0.01	0.00	0.01	0.01	0.00	0.00	0.00	0.00	0.00
Ba	0.02	0.02	0.00	0.00	0.01	0.00	0.00	0.00	0.00	0.00	0.00	0.00	0.00	0.00	0.00
Sum A	1.98	2.10	2.05	2.11	2.05	2.11	2.08	2.11	1.99	2.07	1.83	2.00	2.12	2.13	2.00
Na	0.63	0.65	0.70	0.70	0.71	0.78	0.72	1.00	0.79	0.77	0.98	0.97	0.98	0.99	0.98
Ca	0.37	0.35	0.30	0.31	0.29	0.23	0.28	0.00	0.22	0.23	0.03	0.03	0.02	0.02	0.02
Sum B	1.00	1.00	1.00	1.00	1.00	1.00	1.00	1.00	1.00	1.00	1.00	1.00	1.00	1.00	1.00
Na	0.12	0.00	0.21	0.17	0.21	0.21	0.01	0.00	0.27	0.15	0.00	0.01	0.00	0.00	0.07
Mg	0.37	0.33	0.32	0.32	0.31	0.36	0.36	0.15	0.35	0.31	0.32	0.21	0.17	0.21	0.18
Mn	3.28	3.46	4.43	4.42	4.60	4.88	5.50	6.27	4.80	4.99	5.61	5.87	5.91	6.01	6.03
Fe^{2+}	3.23	3.19	1.98	2.05	1.89	1.50	1.10	0.60	1.53	1.52	1.32	0.87	0.96	0.87	0.73
Zn	0.00	0.02	0.05	0.04	0.00	0.04	0.00	0.00	0.05	0.02	0.00	0.04	0.00	0.00	0.00
Y	0.00	0.00	0.00	0.00	0.00	0.00	0.00	0.00	0.00	0.00	0.00	0.00	0.00	0.00	0.00
Ce	0.00	0.01	0.00	0.00	0.00	0.02	0.03	0.00	0.00	0.01	0.00	0.00	0.00	0.00	0.00
Sum C	7.00	7.01	7.00	7.00	7.00	7.00	7.00	7.02	7.00	7.00	7.25	7.00	7.04	7.08	7.00
Ti	1.72	1.72	1.39	1.43	1.43	1.43	1.61	0.32	1.37	1.28	0.29	0.40	0.32	0.29	0.34
Sn	0.00	0.00	0.00	0.00	0.00	0.00	0.00	0.00	0.00	0.00	0.00	0.00	0.00	0.00	0.00
Zr	0.10	0.11	0.09	0.08	0.08	0.03	0.17	0.48	0.05	0.14	0.37	0.36	0.39	0.39	0.38
Hf	0.00	0.00	0.00	0.00	0.00	0.00	0.00	0.00	0.00	0.00	0.00	0.00	0.00	0.00	0.00
Nb	0.24	0.24	0.53	0.53	0.52	0.56	0.18	1.18	0.60	0.59	1.05	1.10	1.20	1.19	1.19
Ta	0.00	0.00	0.00	0.00	0.00	0.00	0.00	0.01	0.00	0.00	0.04	0.03	0.04	0.03	0.03
Sum D	2.06	2.07	2.00	2.03	2.03	2.02	1.95	1.99	2.02	2.01	1.76	1.89	1.95	1.90	1.94
Si	7.59	7.54	7.63	7.58	7.63	7.70	7.63	7.58	7.70	7.64	7.49	7.56	7.53	7.53	7.52
Al	0.31	0.27	0.34	0.33	0.32	0.27	0.38	0.46	0.29	0.34	0.73	0.55	0.53	0.58	0.54
Sum T	7.89	7.81	7.97	7.92	7.95	7.98	8.00	8.04	7.99	7.98	8.22	8.11	8.06	8.11	8.06
F	0.76	0.79	0.80	0.76	0.71	0.58	0.82	0.00	0.71	0.63	0.35	0.39	0.00	0.00	0.36
OH	4.25	4.21	4.00	4.00	4.00	4.00	4.18	4.00	4.00	4.03	4.00	4.00	4.00	4.00	4.00
O	30.25	30.21	30.20	30.24	30.30	30.42	30.18	31.00	30.29	30.37	30.66	30.62	31.00	31.00	30.64
Cations	19.93	19.99	20.02	20.06	20.04	20.11	20.03	20.15	20.00	20.06	20.06	20.01	20.18	20.23	20.00

ELECTRON MICROPROBE ANALYSES OF MONT SAINT-HILAIRE AGM

Sample:	MSH36Bb						MSH36B	MSH38Aa		MSH38Ab		MSH38Ac			MSH38A
OXIDE	PT 67	PT 68	PT 69	PT 70	PT 71	PT 72	Average	PT 47	PT 48	PT 49	PT 50	PT 51	PT 52	PT 53	Average
Na_2O	2.98	2.97	2.96	3.04	2.98	3.03	2.76	2.69	2.60	2.74	2.79	2.72	2.72	2.51	2.68
K_2O	6.09	6.08	5.94	6.03	6.16	6.15	5.93	6.00	6.17	5.98	5.91	6.04	5.96	6.04	6.01
Rb_2O	0.94	0.94	0.94	0.95	0.90	0.94	0.91	0.46	0.47	0.51	0.46	0.49	0.47	0.46	0.47
Cs_2O	0.00	0.00	0.00	0.00	0.00	0.00	0.00	0.06	0.00	0.00	0.00	0.00	0.00	0.07	0.02
CaO	0.00	0.00	0.00	0.00	0.00	0.00	0.04	0.39	0.43	0.59	0.56	0.62	0.56	0.57	0.53
SrO	0.00	0.00	0.00	0.00	0.00	0.00	0.00	0.00	0.00	0.06	0.03	0.03	0.04	0.04	0.03
BaO	0.00	0.00	0.00	0.00	0.00	0.00	0.00	0.00	0.00	0.00	0.00	0.00	0.00	0.00	0.00
MgO	0.32	0.31	0.29	0.28	0.29	0.29	0.44	0.27	0.29	0.42	0.40	0.37	0.41	0.43	0.37
MnO	30.64	30.32	30.36	30.02	30.44	30.29	29.91	22.04	21.78	19.55	19.36	19.13	19.84	19.53	20.18
FeO	3.02	3.13	3.10	3.16	3.13	3.09	3.88	11.86	12.36	14.49	14.61	14.63	14.47	13.97	13.77
ZnO	0.00	0.00	0.00	0.00	0.00	0.00	0.02	0.20	0.00	0.23	0.20	0.21	0.30	0.00	0.16
Al_2O_3	1.37	1.32	1.29	1.36	1.37	1.32	1.69	1.26	1.23	1.26	1.26	1.24	1.24	1.25	1.25
Y_2O_3	0.00	0.00	0.00	0.00	0.00	0.00	0.00	0.00	0.00	0.00	0.00	0.00	0.00	0.00	0.00
Ce_2O_3	0.00	0.00	0.00	0.00	0.00	0.00	0.00	0.00	0.14	0.00	0.00	0.00	0.00	0.00	0.02
TiO_2	1.66	1.63	1.69	1.73	1.68	1.71	1.76	5.54	5.58	6.29	6.27	6.33	6.31	6.35	6.10
SnO_2	0.00	0.00	0.00	0.00	0.00	0.00	0.00	0.00	0.00	0.00	0.00	0.00	0.00	0.00	0.00
ZrO_2	2.83	2.77	2.71	2.75	2.96	2.68	3.01	1.29	1.31	1.13	1.22	1.18	1.24	1.25	1.23
HfO_2	0.00	0.00	0.00	0.00	0.00	0.00	0.00	0.00	0.00	0.00	0.00	0.00	0.00	0.00	0.00
Nb_2O_5	12.92	12.73	12.71	12.88	12.42	12.62	11.81	8.31	8.30	7.20	7.27	7.18	7.15	7.18	7.51
Ta_2O_5	0.00	0.00	0.00	0.00	0.00	0.00	0.26	0.00	0.00	0.00	0.00	0.00	0.00	0.00	0.00
SiO_2	32.67	32.80	32.10	32.59	32.01	32.09	32.13	31.90	32.02	32.56	32.40	32.62	32.64	32.26	32.34
F	0.55	0.36	0.44	0.00	0.53	0.00	0.30	0.85	0.65	0.87	0.94	1.04	0.94	0.64	0.85
H_2O	2.57	2.56	2.53	2.54	2.54	2.52	2.54	2.53	2.54	2.57	2.56	2.57	2.58	2.53	2.55
O=F	-0.23	-0.15	-0.19	0.00	-0.22	0.00	-0.13	-0.36	-0.27	-0.37	-0.40	-0.44	-0.40	-0.27	-0.36
Total	98.33	97.77	96.88	97.33	97.18	96.73	97.26	95.30	95.59	96.08	95.85	95.96	96.47	94.82	95.72
Chemical formulae calculated based on 31 anions															
Na_{tot}	1.35	1.35	1.36	1.39	1.37	1.40	1.26	1.24	1.19	1.24	1.27	1.23	1.23	1.15	1.22
Na	0.09	0.08	0.17	0.11	0.18	0.23	0.18	0.23	0.22	0.27	0.28	0.18	0.28	0.13	0.23
K	1.81	1.82	1.80	1.81	1.86	1.87	1.79	1.81	1.86	1.78	1.76	1.80	1.77	1.82	1.80
Rb	0.14	0.14	0.14	0.14	0.14	0.14	0.14	0.07	0.07	0.08	0.07	0.07	0.07	0.07	0.07
Cs	0.00	0.00	0.00	0.00	0.00	0.00	0.00	0.01	0.00	0.00	0.00	0.00	0.00	0.01	0.00
Sr	0.00	0.00	0.00	0.00	0.00	0.00	0.00	0.00	0.00	0.01	0.00	0.00	0.01	0.01	0.00
Ba	0.00	0.00	0.00	0.00	0.00	0.00	0.00	0.00	0.00	0.00	0.00	0.00	0.00	0.00	0.00
Sum A	2.04	2.04	2.10	2.06	2.18	2.24	2.10	2.12	2.15	2.14	2.11	2.06	2.13	2.03	2.11
Na	1.00	1.00	1.00	1.00	1.00	1.00	0.99	0.90	0.89	0.85	0.86	0.85	0.86	0.86	0.87
Ca	0.00	0.00	0.00	0.00	0.00	0.00	0.01	0.10	0.11	0.15	0.14	0.16	0.14	0.14	0.13
Sum B	1.00	1.00	1.00	1.00	1.00	1.00	1.00	1.00	1.00	1.00	1.00	1.00	1.00	1.00	1.00
Na	0.26	0.27	0.19	0.29	0.18	0.17	0.10	0.10	0.08	0.12	0.13	0.20	0.08	0.17	0.13
Mg	0.11	0.11	0.10	0.10	0.10	0.10	0.16	0.10	0.10	0.15	0.14	0.13	0.14	0.15	0.13
Mn	6.04	6.01	6.09	5.99	6.10	6.11	5.98	4.42	4.36	3.87	3.84	3.78	3.91	3.91	4.01
Fe^{2+}	0.59	0.61	0.61	0.62	0.62	0.62	0.77	2.35	2.44	2.83	2.86	2.85	2.81	2.76	2.70
Zn	0.00	0.00	0.00	0.00	0.00	0.00	0.00	0.04	0.00	0.04	0.04	0.04	0.05	0.00	0.03
Y	0.00	0.00	0.00	0.00	0.00	0.00	0.00	0.00	0.00	0.00	0.00	0.00	0.00	0.00	0.00
Ce	0.00	0.00	0.00	0.00	0.00	0.00	0.00	0.00	0.01	0.00	0.00	0.00	0.00	0.00	0.00
Sum C	7.00	7.00	7.00	7.00	7.00	7.00	7.00	7.00	7.00	7.00	7.00	7.00	7.00	7.00	7.00
Ti	0.29	0.29	0.30	0.31	0.30	0.31	0.31	0.99	0.99	1.10	1.10	1.11	1.10	1.13	1.08
Sn	0.00	0.00	0.00	0.00	0.00	0.00	0.00	0.00	0.00	0.00	0.00	0.00	0.00	0.00	0.00
Zr	0.32	0.32	0.31	0.32	0.34	0.31	0.35	0.15	0.15	0.13	0.14	0.13	0.14	0.14	0.14
Hf	0.00	0.00	0.00	0.00	0.00	0.00	0.00	0.00	0.00	0.00	0.00	0.00	0.00	0.00	0.00
Nb	1.36	1.35	1.36	1.37	1.33	1.36	1.26	0.89	0.89	0.76	0.77	0.76	0.75	0.77	0.80
Ta	0.00	0.00	0.00	0.00	0.00	0.00	0.02	0.00	0.00	0.00	0.00	0.00	0.00	0.00	0.00
Sum D	1.97	1.95	1.98	2.00	1.97	1.98	1.94	2.02	2.03	1.99	2.01	2.00	2.00	2.04	2.01
Si	7.61	7.68	7.60	7.68	7.57	7.64	7.58	7.55	7.57	7.60	7.58	7.61	7.59	7.63	7.59
Al	0.38	0.36	0.36	0.38	0.38	0.37	0.47	0.35	0.34	0.35	0.35	0.34	0.34	0.35	0.35
Sum T	7.99	8.04	7.96	8.06	7.95	8.01	8.05	7.90	7.91	7.95	7.93	7.95	7.93	7.98	7.94
F	0.41	0.27	0.33	0.00	0.40	0.00	0.23	0.64	0.49	0.64	0.70	0.77	0.69	0.48	0.63
OH	4.00	4.00	4.00	4.00	4.00	4.00	4.00	4.00	4.00	4.00	4.00	4.00	4.00	4.00	4.00
O	30.60	30.73	30.67	31.00	30.60	31.00	30.77	30.36	30.51	30.36	30.30	30.23	30.31	30.52	30.37
Cations	20.00	20.03	20.04	20.12	20.09	20.23	20.09	20.05	20.10	20.08	20.05	20.01	20.05	20.05	20.06

ELECTRON MICROPROBE ANALYSES OF MONT SAINT-HILAIRE AGM

Sample	MSH38a		MSH38b					MSH38B	MSH39Aa			MSH39Ab		MSH39Ac	
OXIDE	PT 73	PT 75	PT 76	PT 77	PT 78	PT 79	PT 80	Average	PT 54	PT 55	PT 56	PT 57	PT 58	PT 59	PT 60
Na_2O	2.45	2.53	2.51	2.58	2.49	2.54	2.63	2.53	2.04	2.10	1.93	2.36	2.37	2.58	2.79
K_2O	5.97	6.00	5.94	5.90	5.80	5.90	5.83	5.91	6.18	6.01	6.10	6.09	5.99	5.96	5.92
Rb_2O	0.46	0.31	0.37	0.37	0.37	0.36	0.35	0.37	0.33	0.33	0.32	0.35	0.36	0.32	0.34
Cs_2O	0.00	0.00	0.00	0.00	0.00	0.00	0.00	0.00	0.08	0.00	0.07	0.08	0.08	0.08	0.09
CaO	0.67	0.65	0.52	0.53	0.54	0.52	0.51	0.56	1.23	1.21	1.23	0.87	0.95	0.75	0.61
SrO	0.22	0.18	0.19	0.15	0.14	0.13	0.20	0.17	0.29	0.28	0.28	0.34	0.35	0.34	0.39
BaO	0.00	0.00	0.00	0.00	0.00	0.00	0.00	0.00	0.00	0.00	0.00	0.00	0.00	0.00	0.00
MgO	0.12	0.12	0.12	0.11	0.09	0.10	0.09	0.11	0.55	0.54	0.54	0.69	0.61	0.72	0.98
MnO	23.62	23.07	23.97	23.83	23.72	24.16	24.26	23.80	11.03	10.94	10.80	13.91	13.47	14.35	17.71
FeO	10.83	11.95	11.38	11.20	11.35	10.80	10.72	11.18	23.69	23.80	23.79	20.05	20.33	19.13	15.27
ZnO	0.26	0.00	0.23	0.00	0.00	0.21	0.27	0.14	0.00	0.00	0.00	0.00	0.00	0.25	0.39
Al_2O_3	0.56	0.58	0.43	0.43	0.48	0.45	0.46	0.48	1.73	1.72	1.77	1.20	1.25	0.80	0.68
Y_2O_3	0.00	0.00	0.00	0.00	0.00	0.00	0.00	0.00	0.00	0.00	0.00	0.00	0.00	0.00	0.00
Ce_2O_3	0.00	0.00	0.00	0.00	0.00	0.16	0.00	0.02	0.23	0.24	0.30	0.24	0.20	0.00	0.24
TiO_2	6.23	6.17	6.67	6.68	6.59	6.61	6.68	6.52	7.86	8.00	7.92	7.51	7.40	7.72	9.30
SnO_2	0.00	0.00	0.00	0.00	0.00	0.00	0.00	0.00	0.00	0.00	0.00	0.00	0.00	0.00	0.00
ZrO_2	9.11	6.73	6.44	6.41	6.26	6.51	6.10	6.79	2.68	2.66	2.66	3.73	3.70	4.06	2.07
HfO_2	0.00	0.00	0.00	0.08	0.00	0.00	0.00	0.01	0.00	0.00	0.00	0.07	0.00	0.00	0.00
Nb_2O_5	0.71	0.84	0.62	0.63	0.69	0.65	0.57	0.67	2.84	2.90	2.88	2.37	2.58	1.53	1.74
Ta_2O_5	0.00	0.00	0.00	0.00	0.00	0.00	0.00	0.00	0.27	0.39	0.30	0.27	0.27	0.14	0.00
SiO_2	33.53	34.30	34.09	33.80	33.30	33.66	33.33	33.72	32.09	32.00	32.03	33.21	32.61	33.17	33.80
F	1.34	1.15	1.43	1.21	1.08	1.24	1.20	1.24	1.10	1.05	1.04	1.19	1.29	0.96	1.14
H_2O	2.62	2.70	2.56	2.64	2.67	2.62	2.61	2.63	2.71	2.73	2.73	2.68	2.60	2.75	2.72
O=F	-0.56	-0.48	-0.60	-0.51	-0.45	-0.52	-0.51	-0.52	-0.46	-0.44	-0.44	-0.50	-0.54	-0.40	-0.48
Total	98.13	96.79	96.87	96.04	95.11	96.10	95.31	96.34	96.46	96.46	96.25	96.71	95.87	95.21	95.70
Chemical formulae calculated based on 31 anions															
Na_{tot}	1.09	1.13	1.13	1.17	1.14	1.15	1.20	1.14	0.92	0.95	0.87	1.06	1.07	1.17	1.24
Na	0.04	0.16	0.24	0.23	0.27	0.26	0.33	0.22	0.21	0.22	0.15	0.12	0.17	0.23	0.20
K	1.75	1.77	1.75	1.76	1.75	1.76	1.75	1.76	1.83	1.78	1.81	1.79	1.78	1.78	1.74
Rb	0.07	0.05	0.06	0.06	0.06	0.05	0.05	0.06	0.05	0.05	0.05	0.05	0.05	0.05	0.05
Cs	0.00	0.00	0.00	0.00	0.00	0.00	0.00	0.00	0.01	0.00	0.01	0.01	0.01	0.01	0.01
Sr	0.03	0.02	0.03	0.02	0.02	0.02	0.03	0.02	0.04	0.04	0.04	0.05	0.05	0.05	0.05
Ba	0.00	0.00	0.00	0.00	0.00	0.00	0.00	0.00	0.00	0.00	0.00	0.00	0.00	0.00	0.00
Sum A	1.89	2.00	2.07	2.06	2.09	2.09	2.16	2.06	2.13	2.09	2.05	2.01	2.06	2.11	2.05
Na	0.84	0.84	0.87	0.87	0.86	0.87	0.87	0.86	0.69	0.70	0.69	0.79	0.76	0.81	0.85
Ca	0.17	0.16	0.13	0.13	0.14	0.13	0.13	0.14	0.31	0.30	0.31	0.22	0.24	0.19	0.15
Sum B	1.00	1.00	1.00	1.00	1.00	1.00	1.00	1.00	1.00	1.00	1.00	1.00	1.00	1.00	1.00
Na	0.22	0.13	0.02	0.07	0.00	0.02	0.00	0.06	0.02	0.02	0.03	0.16	0.14	0.13	0.19
Mg	0.04	0.04	0.04	0.04	0.03	0.04	0.03	0.04	0.19	0.19	0.19	0.24	0.21	0.25	0.34
Mn	4.61	4.52	4.70	4.71	4.74	4.78	4.84	4.70	2.17	2.15	2.13	2.72	2.66	2.84	3.45
Fe^{2+}	2.09	2.31	2.20	2.19	2.24	2.11	2.11	2.18	4.60	4.62	4.63	3.87	3.97	3.74	2.94
Zn	0.04	0.00	0.04	0.00	0.00	0.04	0.05	0.02	0.00	0.00	0.00	0.00	0.00	0.04	0.07
Y	0.00	0.00	0.00	0.00	0.00	0.00	0.00	0.00	0.00	0.00	0.00	0.00	0.00	0.00	0.00
Ce	0.00	0.00	0.00	0.00	0.00	0.01	0.00	0.00	0.02	0.02	0.03	0.02	0.02	0.00	0.02
Sum C	7.00	7.00	7.00	7.00	7.01	7.00	7.03	7.00	7.00	7.00	7.00	7.00	7.00	7.00	7.00
Ti	1.08	1.07	1.16	1.17	1.17	1.16	1.18	1.14	1.37	1.40	1.39	1.30	1.30	1.36	1.61
Sn	0.00	0.00	0.00	0.00	0.00	0.00	0.00	0.00	0.00	0.00	0.00	0.00	0.00	0.00	0.00
Zr	1.02	0.76	0.73	0.73	0.72	0.74	0.70	0.77	0.30	0.30	0.30	0.42	0.42	0.46	0.23
Hf	0.00	0.00	0.00	0.01	0.00	0.00	0.00	0.00	0.00	0.00	0.00	0.01	0.00	0.00	0.00
Nb	0.07	0.09	0.07	0.07	0.07	0.07	0.06	0.07	0.30	0.30	0.30	0.25	0.27	0.16	0.18
Ta	0.00	0.00	0.00	0.00	0.00	0.00	0.00	0.00	0.02	0.03	0.02	0.02	0.02	0.01	0.00
Sum D	2.18	1.92	1.95	1.97	1.96	1.97	1.95	1.99	1.99	2.03	2.01	1.99	2.01	1.99	2.02
Si	7.72	7.93	7.89	7.89	7.85	7.86	7.85	7.86	7.45	7.43	7.45	7.66	7.61	7.75	7.77
Al	0.15	0.16	0.12	0.12	0.13	0.12	0.13	0.13	0.47	0.47	0.49	0.33	0.34	0.22	0.18
Sum T	7.88	8.09	8.01	8.00	7.99	7.99	7.98	7.99	7.93	7.90	7.94	7.99	7.95	7.97	7.96
F	0.98	0.84	1.05	0.89	0.81	0.92	0.89	0.91	0.81	0.77	0.77	0.87	0.95	0.71	0.83
OH	4.02	4.16	3.95	4.11	4.20	4.08	4.11	4.09	4.19	4.23	4.24	4.13	4.05	4.29	4.17
O	30.02	30.16	29.95	30.11	30.20	30.08	30.11	30.09	30.19	30.23	30.24	30.13	30.05	30.29	30.17
Cations	19.95	20.01	20.03	20.04	20.05	20.04	20.11	20.03	20.05	20.02	19.99	19.99	20.02	20.07	20.03

ELECTRON MICROPROBE ANALYSES OF MONT SAINT-HILAIRE AGM

Sample:	MSH39A	MSH39A	MSH40Aa	MSH40Ab			MSH40Ac		MSH40A	MSH40Ba					
OXIDE	PT 61	Average	PT 81	PT 82	PT 83	PT 84	PT 85	PT 86	Average	PT 87	PT 88	PT 89	PT 90	PT 91	PT 92
Na_2O	2.20	2.30	2.70	2.69	2.52	2.71	2.69	2.64	2.66	2.64	2.61	2.50	2.46	2.50	2.60
K_2O	6.14	6.05	6.05	6.05	6.17	6.01	5.92	5.95	6.03	5.46	5.87	5.71	5.84	5.69	5.75
Rb_2O	0.28	0.33	0.50	0.48	0.52	0.52	0.55	0.53	0.52	0.86	0.89	0.88	0.88	0.97	0.86
Cs_2O	0.09	0.07	0.00	0.00	0.07	0.06	0.00	0.00	0.02	0.00	0.00	0.00	0.00	0.00	0.00
CaO	1.07	0.99	1.38	1.36	1.24	1.19	0.98	1.18	1.22	0.07	0.00	0.04	0.05	0.05	0.05
SrO	0.27	0.32	0.09	0.08	0.07	0.10	0.10	0.08	0.09	0.00	0.00	0.00	0.00	0.00	0.00
BaO	0.00	0.00	0.00	0.00	0.00	0.00	0.13	0.00	0.02	0.00	0.00	0.00	0.00	0.00	0.00
MgO	0.58	0.65	1.11	1.09	0.95	1.03	1.00	0.93	1.02	0.56	0.44	0.46	0.41	0.47	0.46
MnO	10.63	12.86	21.99	22.53	22.72	22.55	24.95	23.78	23.09	29.03	30.04	30.72	30.57	29.61	29.84
FeO	23.83	21.24	11.25	10.33	10.75	10.68	8.28	9.06	10.06	5.33	3.95	3.42	3.74	4.26	3.84
ZnO	0.00	0.08	0.24	0.21	0.18	0.31	0.17	0.21	0.22	0.00	0.00	0.00	0.00	0.00	0.00
Al_2O_3	1.50	1.33	0.50	0.54	1.20	0.84	0.83	1.09	0.83	2.23	1.94	1.70	1.99	2.19	1.66
Y_2O_3	0.00	0.00	0.00	0.00	0.00	0.00	0.00	0.00	0.00	0.00	0.00	0.00	0.00	0.00	0.00
Ce_2O_3	0.00	0.18	0.00	0.00	0.00	0.00	0.00	0.00	0.00	0.00	0.00	0.00	0.00	0.00	0.00
TiO_2	6.97	7.84	10.03	10.04	8.15	8.63	8.27	8.31	8.91	1.86	1.57	1.75	1.28	1.63	1.77
SnO_2	0.00	0.00	0.00	0.00	0.00	0.00	0.00	0.00	0.00	0.00	0.00	0.00	0.00	0.00	0.00
ZrO_2	3.53	3.14	0.35	0.51	0.72	0.93	0.67	0.52	0.62	3.10	3.33	3.87	3.48	3.67	3.74
HfO_2	0.00	0.01	0.00	0.00	0.00	0.00	0.00	0.00	0.00	0.00	0.00	0.00	0.00	0.00	0.00
Nb_2O_5	3.16	2.50	2.06	2.16	4.78	3.74	4.56	4.86	3.69	10.81	11.90	10.98	12.11	11.45	10.65
Ta_2O_5	0.61	0.28	0.00	0.00	0.00	0.00	0.00	0.00	0.00	0.60	0.37	0.53	0.56	0.63	0.34
SiO_2	32.00	32.61	35.22	35.18	33.16	34.00	33.90	33.48	34.16	32.13	31.58	31.42	31.75	31.53	31.52
F	0.80	1.07	1.06	1.05	0.97	1.00	0.83	0.88	0.97	0.51	0.00	0.00	0.37	0.34	0.00
H_2O	2.82	2.72	2.84	2.84	2.81	2.82	2.89	2.86	2.84	2.56	2.52	2.50	2.54	2.54	2.49
O=F	-0.34	-0.45	-0.45	-0.44	-0.41	-0.42	-0.35	-0.37	-0.41	-0.21	0.00	0.00	-0.16	-0.14	0.00
Total	96.15	96.10	96.92	96.70	96.58	96.70	96.37	95.99	96.54	97.53	97.01	96.48	97.88	97.38	95.57
Chemical formulae calculated based on 31 anions															
Na_{tot}	1.00	1.03	1.17	1.17	1.12	1.19	1.19	1.17	1.17	1.20	1.20	1.16	1.12	1.15	1.22
Na	0.24	0.19	0.20	0.12	0.24	0.26	0.20	0.16	0.20	0.22	0.20	0.17	0.12	0.10	0.23
K	1.83	1.79	1.73	1.73	1.80	1.74	1.72	1.74	1.74	1.63	1.78	1.75	1.76	1.72	1.77
Rb	0.04	0.05	0.07	0.07	0.08	0.08	0.08	0.08	0.08	0.13	0.14	0.14	0.13	0.15	0.13
Cs	0.01	0.01	0.00	0.00	0.01	0.01	0.00	0.00	0.00	0.00	0.00	0.00	0.00	0.00	0.00
Sr	0.04	0.04	0.01	0.01	0.01	0.01	0.01	0.01	0.01	0.00	0.00	0.00	0.00	0.00	0.00
Ba	0.00	0.00	0.00	0.00	0.00	0.00	0.01	0.00	0.00	0.00	0.00	0.00	0.00	0.00	0.00
Sum A	2.16	2.08	2.02	1.93	2.13	2.10	2.03	1.99	2.03	1.99	2.12	2.05	2.01	1.96	2.13
Na	0.73	0.75	0.67	0.67	0.70	0.71	0.76	0.71	0.70	0.98	1.00	0.99	0.99	0.99	0.99
Ca	0.27	0.25	0.33	0.33	0.30	0.29	0.24	0.29	0.30	0.02	0.00	0.01	0.01	0.01	0.01
Sum B	1.00	1.00	1.00	1.00	1.00	1.00	1.00	1.00	1.00	1.00	1.00	1.00	1.00	1.00	1.00
Na	0.03	0.09	0.30	0.38	0.18	0.23	0.23	0.30	0.27	0.00	0.00	0.00	0.02	0.06	0.00
Mg	0.20	0.23	0.37	0.37	0.32	0.35	0.34	0.32	0.34	0.20	0.16	0.16	0.14	0.17	0.17
Mn	2.11	2.53	4.18	4.28	4.41	4.34	4.82	4.61	4.44	5.76	6.06	6.24	6.10	5.93	6.10
Fe^{2+}	4.66	4.13	2.11	1.94	2.06	2.03	1.58	1.74	1.91	1.05	0.79	0.69	0.74	0.84	0.78
Zn	0.00	0.01	0.04	0.04	0.03	0.05	0.03	0.04	0.04	0.00	0.00	0.00	0.00	0.00	0.00
Y	0.00	0.00	0.00	0.00	0.00	0.00	0.00	0.00	0.00	0.00	0.00	0.00	0.00	0.00	0.00
Ce	0.00	0.02	0.00	0.00	0.00	0.00	0.00	0.00	0.00	0.00	0.00	0.00	0.00	0.00	0.00
Sum C	7.00	7.00	7.00	7.00	7.00	7.00	7.00	7.00	7.00	7.00	7.00	7.09	7.00	7.00	7.04
Ti	1.23	1.37	1.69	1.70	1.40	1.48	1.42	1.43	1.52	0.33	0.28	0.32	0.23	0.29	0.32
Sn	0.00	0.00	0.00	0.00	0.00	0.00	0.00	0.00	0.00	0.00	0.00	0.00	0.00	0.00	0.00
Zr	0.40	0.36	0.04	0.06	0.08	0.10	0.08	0.06	0.07	0.35	0.39	0.45	0.40	0.42	0.44
Hf	0.00	0.00	0.00	0.00	0.00	0.00	0.00	0.00	0.00	0.00	0.00	0.00	0.00	0.00	0.00
Nb	0.33	0.26	0.21	0.22	0.50	0.38	0.47	0.50	0.38	1.15	1.28	1.19	1.29	1.22	1.16
Ta	0.04	0.02	0.00	0.00	0.00	0.00	0.00	0.00	0.00	0.04	0.02	0.04	0.04	0.04	0.02
Sum D	2.00	2.01	1.94	1.97	1.98	1.96	1.96	1.99	1.97	1.87	1.97	1.99	1.95	1.98	1.94
Si	7.49	7.58	7.90	7.90	7.59	7.73	7.74	7.67	7.75	7.53	7.52	7.53	7.48	7.46	7.60
Al	0.41	0.36	0.13	0.14	0.32	0.23	0.22	0.29	0.22	0.62	0.54	0.48	0.55	0.61	0.47
Sum T	7.90	7.94	8.03	8.04	7.91	7.95	7.96	7.96	7.98	8.15	8.06	8.01	8.04	8.07	8.07
F	0.59	0.79	0.75	0.75	0.70	0.72	0.60	0.64	0.69	0.38	0.00	0.00	0.28	0.25	0.00
OH	4.41	4.21	4.25	4.26	4.30	4.28	4.40	4.36	4.31	4.00	4.00	4.00	4.00	4.00	4.00
O	30.41	30.21	30.25	30.26	30.30	30.28	30.40	30.36	30.31	30.62	31.00	31.00	30.72	30.75	31.00
Cations	20.06	20.03	19.98	19.94	20.03	20.01	19.95	19.94	19.98	20.00	20.15	20.15	20.00	20.01	20.19

ELECTRON MICROPROBE ANALYSES OF MONT SAINT-HILAIRE AGM

Sample				MSH40B				MSH40B	MSH42					MSH42	MSH43	
OXIDE	PT 93	PT 94	PT 95	PT 96	PT 97	PT 98	PT 99	Average						Average	PT 51	PT 52
Na_2O	2.52	2.59	2.58	2.90	2.94	2.86	2.90	2.66	2.69	2.49	2.67	2.62	2.62	2.62	2.40	2.50
K_2O	5.87	5.82	5.75	5.74	5.78	5.86	5.76	5.76	6.03	5.92	5.95	5.97	5.97	5.97	5.90	5.87
Rb_2O	0.92	0.95	0.94	0.92	0.93	0.90	0.94	0.91	0.82	0.81	0.84	0.82	0.82	0.82	0.45	0.46
Cs_2O	0.00	0.00	0.06	0.00	0.00	0.00	0.00	0.00	0.12	0.13	0.10	0.12	0.12	0.12	0.00	0.05
CaO	0.00	0.06	0.05	0.00	0.00	0.00	0.00	0.03	0.00	0.00	0.00	0.00	0.00	0.00	0.33	0.32
SrO	0.00	0.02	0.00	0.00	0.00	0.00	0.00	0.00	0.00	0.00	0.00	0.00	0.00	0.00	0.03	0.00
BaO	0.00	0.00	0.00	0.00	0.00	0.00	0.00	0.00	0.00	0.00	0.00	0.00			0.00	0.00
MgO	0.46	0.50	0.47	0.35	0.33	0.33	0.29	0.43	0.13	0.15	0.18	0.15	0.15	0.15	0.66	0.69
MnO	29.83	30.43	29.85	30.49	30.53	30.43	30.36	30.13	26.11	26.40	26.61	26.37	26.37	26.37	20.51	21.66
FeO	3.91	3.78	3.70	2.96	2.98	3.24	3.09	3.71	2.63	2.73	2.55	2.64	2.64	2.64	13.86	12.68
ZnO	0.00	0.00	0.00	0.00	0.00	0.00	0.00	0.00	4.31	4.29	3.65	4.08	4.08	4.08	0.30	0.36
Al_2O_3	1.71	1.51	1.52	1.35	1.35	1.47	1.36	1.69	1.21	1.02	1.20	1.14	1.14	1.14	1.09	0.71
Y_2O_3	0.00	0.00	0.00	0.00	0.00	0.00	0.00	0.00	0.00	0.00	0.00	0.00			0.00	0.00
Ce_2O_3	0.00	0.00	0.00	0.00	0.00	0.00	0.00	0.00	0.00	0.00	0.00	0.00			0.00	0.00
TiO_2	1.69	2.31	2.16	1.30	1.35	1.55	1.54	1.67	1.12	1.26	1.65	1.34	1.34	1.34	5.40	5.85
SnO_2	0.00	0.00	0.00	0.00	0.00	0.00	0.00	0.00	0.00	0.00	0.00	0.00			0.00	0.00
ZrO_2	3.98	4.30	4.21	3.12	3.21	3.37	2.96	3.56	3.23	4.23	2.84	3.43	3.43	3.43	2.82	3.34
HfO_2	0.00	0.00	0.00	0.00	0.00	0.00	0.00	0.00	0.00	0.00	0.00	0.00	0.00	0.00	0.00	0.00
Nb_2O_5	10.56	9.79	9.70	12.73	12.70	12.17	12.62	11.40	12.84	11.54	12.00	12.13	12.13	12.13	7.21	6.03
Ta_2O_5	0.23	0.00	0.00	0.00	0.00	0.00	0.00	0.25	0.44	0.74	0.71	0.63	0.63	0.63	0.15	0.00
SiO_2	31.51	32.08	31.69	32.34	32.36	32.22	32.09	31.86	31.93	31.80	31.82	31.85	31.85	31.85	33.44	34.22
F	0.42	0.41	0.48	0.00	0.41	0.39	0.48	0.29	0.43	0.00	0.00	0.14	0.14	0.14	0.73	0.81
H_2O	2.50	2.53	2.50	2.52	2.54	2.54	2.53	2.52	2.50	2.47	2.47	2.48	2.48	2.48	2.60	2.62
O=F	-0.18	-0.17	-0.20	0.00	-0.17	-0.16	-0.20	-0.12	-0.18	0.00	0.00	-0.06	-0.06	-0.06	-0.31	-0.34
Total	95.93	96.91	95.45	96.72	97.24	97.17	96.72	96.77	96.36	95.98	95.24	95.85	95.85	95.85	97.58	97.83
Chemical formulae calculated based on 31 cations																
Na_{tot}	1.17	1.19	1.20	1.34	1.35	1.31	1.33	1.23	1.25	1.17	1.26	1.23			1.07	1.11
Na	0.17	0.20	0.20	0.18	0.15	0.15	0.14	0.18	0.00	0.00	0.00	0.00	0.00	0.00	0.11	0.11
K	1.80	1.76	1.76	1.74	1.74	1.77	1.74	1.75	1.85	1.83	1.84	1.84	1.84	1.84	1.73	1.71
Rb	0.14	0.15	0.15	0.14	0.14	0.14	0.14	0.14	0.13	0.13	0.13	0.13	0.13	0.13	0.07	0.07
Cs	0.00	0.00	0.01	0.00	0.00	0.00	0.00	0.00	0.01	0.01	0.01	0.01	0.01	0.01	0.00	0.01
Sr	0.00	0.00	0.00	0.00	0.00	0.00	0.00	0.00	0.00	0.00	0.00	0.00	0.00	0.00	0.00	0.00
Ba	0.00	0.00	0.00	0.00	0.00	0.00	0.00	0.00	0.00	0.00	0.00	0.00	0.00	0.00	0.00	0.00
Sum A	2.11	2.11	2.11	2.07	2.03	2.05	2.03	2.07	1.99	1.97	1.99	1.98	1.98	1.98	1.91	1.89
Na	1.00	0.99	0.99	1.00	1.00	1.00	1.00	0.99	0.90	0.98	0.97	0.95	0.95	0.95	0.92	0.92
Ca	0.00	0.02	0.01	0.00	0.00	0.00	0.00	0.01	0.00	0.00	0.00	0.00	0.00	0.00	0.08	0.08
Sum B	1.00	1.00	1.00	1.00	1.00	1.00	1.00	1.00	0.90	0.98	0.97	0.95	0.95	0.95	1.00	1.00
Na	0.00	0.00	0.02	0.15	0.20	0.16	0.19	0.05	0.35	0.20	0.29	0.28	0.28	0.28	0.05	0.08
Mg	0.16	0.18	0.17	0.12	0.12	0.12	0.10	0.15	0.05	0.05	0.07	0.05	0.05	0.05	0.23	0.24
Mn	6.06	6.10	6.07	6.14	6.10	6.09	6.10	6.06	5.31	5.43	5.48	5.40	5.40	5.40	4.00	4.20
Fe^{2+}	0.78	0.75	0.74	0.59	0.59	0.64	0.61	0.74	0.53	0.55	0.52	0.53	0.53	0.53	2.67	2.43
Zn	0.00	0.00	0.00	0.00	0.00	0.00	0.00	0.00	0.76	0.77	0.66	0.73	0.73	0.73	0.05	0.06
Y	0.00	0.00	0.00	0.00	0.00	0.00	0.00	0.00	0.00	0.00	0.00	0.00	0.00	0.00	0.00	0.00
Ce	0.00	0.00	0.00	0.00	0.00	0.00	0.00	0.00	0.00	0.00	0.00	0.00	0.00	0.00	0.00	0.00
Sum C	7.01	7.03	7.00	7.00	7.00	7.00	7.00	7.00	7.00	7.00	7.00	7.00	7.00	7.00	7.00	7.00
Ti	0.31	0.41	0.39	0.23	0.24	0.28	0.28	0.30	0.20	0.23	0.30	0.24	0.24	0.24	0.94	1.01
Sn	0.00	0.00	0.00	0.00	0.00	0.00	0.00	0.00	0.00	0.00	0.00	0.00	0.00	0.00	0.00	0.00
Zr	0.47	0.50	0.49	0.36	0.37	0.39	0.34	0.41	0.38	0.50	0.34	0.41	0.41	0.41	0.32	0.37
Hf	0.00	0.00	0.00	0.00	0.00	0.00	0.00	0.00	0.00	0.00	0.00	0.00	0.00	0.00	0.00	0.00
Nb	1.15	1.05	1.05	1.37	1.35	1.30	1.35	1.22	1.39	1.27	1.32	1.33	1.33	1.33	0.75	0.62
Ta	0.02	0.00	0.00	0.00	0.00	0.00	0.00	0.02	0.03	0.05	0.05	0.04	0.04	0.04	0.01	0.00
Sum D	1.93	1.96	1.94	1.96	1.96	1.96	1.97	1.95	2.00	2.05	2.00	2.02	2.02	2.02	2.01	2.00
Si	7.56	7.60	7.61	7.69	7.63	7.61	7.61	7.57	7.67	7.72	7.73	7.71	7.71	7.71	7.83	
Al	0.48	0.42	0.43	0.38	0.38	0.41	0.38	0.47	0.34	0.29	0.34	0.33	0.33	0.33	0.30	0.19
Sum T	8.04	8.02	8.04	8.06	8.01	8.02	7.99	8.04	8.01	8.01	8.08	8.03	8.03	8.03	8.00	8.02
F	0.32	0.31	0.37	0.00	0.31	0.29	0.36	0.22	0.33	0.00	0.00	0.11	26.89	0.53	0.59	
OH	4.00	4.00	4.00	4.00	4.00	4.00	4.00	4.00	4.00	4.00	4.00	4.00	4.00	4.00	4.00	
O	30.68	30.69	30.64	31.00	30.69	30.71	30.64	30.78	26.67	27.00	27.00	26.89	30.11	30.47	30.41	
Cations	20.09	20.11	20.09	20.09	20.00	20.04	19.99	20.07	19.90	20.01	20.03	19.98	19.98	19.92	19.92	

ELECTRON MICROPROBE ANALYSES OF MONT SAINT-HILAIRE AGM

Sample			MSH43	MSH44				MSH44	MSH45						MSH45
OXIDE	PT 53	PT 54	Average	PT 65	PT 66	PT 67	PT 68	Ave	PT 69	PT 70	PT 71	PT 72	PT 73	PT 74	Ave
Na_2O	2.48	2.53	2.48	1.89	1.99	2.05	2.02	1.99	2.93	2.92	2.72	2.62	2.27	2.36	2.64
K_2O	6.00	5.81	5.90	6.18	6.24	6.26	6.08	6.19	5.73	5.65	5.79	5.84	5.83	5.84	5.78
Rb_2O	0.46	0.39	0.44	0.33	0.31	0.32	0.34	0.33	0.57	0.56	0.65	0.66	0.50	0.47	0.57
Cs_2O	0.00	0.00	0.01	0.09	0.08	0.09	0.08	0.09	0.00	0.00	0.06	0.00	0.08	0.06	0.03
CaO	0.23	0.24	0.28	0.43	0.37	0.31	0.36	0.37	0.39	0.42	0.35	0.30	0.96	0.92	0.56
SrO	0.00	0.00	0.01	0.02	0.04	0.04	0.05	0.04	0.00	0.00	0.00	0.00	0.03	0.04	0.01
BaO	0.00	0.00	0.00	0.00	0.00	0.00	0.00	0.00	0.00	0.00	0.00	0.00	0.00	0.00	0.00
MgO	0.64	0.73	0.68	0.18	0.18	0.17	0.18	0.18	0.65	0.61	0.58	0.56	0.84	0.82	0.68
MnO	20.49	20.37	20.76	7.76	7.16	6.71	6.83	7.12	23.71	23.72	23.81	23.70	19.91	21.32	22.70
FeO	13.86	13.66	13.52	28.45	28.75	29.31	29.25	28.94	9.63	9.28	9.55	9.59	13.72	12.11	10.65
ZnO	0.26	0.25	0.29	0.00	0.00	0.00	0.00	0.00	0.47	0.44	0.46	0.40	0.31	0.50	0.43
Al_2O_3	1.08	0.61	0.87	1.42	1.47	1.20	1.31	1.35	0.37	0.33	1.01	1.07	1.00	0.87	0.78
Y_2O_3	0.00	0.00	0.00	0.00	0.00	0.00	0.00	0.00	0.00	0.00	0.00	0.00	0.00	0.00	0.00
Ce_2O_3	0.00	0.00	0.00	0.34	0.36	0.25	0.24	0.30	0.00	0.00	0.00	0.00	0.00	0.00	0.00
TiO_2	5.10	6.68	5.76	5.97	5.85	5.87	5.80	5.87	7.75	7.86	6.10	5.98	8.43	8.44	7.43
SnO_2	0.00	0.00	0.00	0.00	0.00	0.00	0.00	0.00	0.00	0.00	0.00	0.00	0.00	0.00	0.00
ZrO_2	2.92	2.74	2.96	4.09	4.22	4.85	4.70	4.47	0.18	0.14	0.00	0.00	0.89	0.80	0.34
HfO_2	0.00	0.00	0.00	0.00	0.00	0.00	0.00	0.00	0.00	0.00	0.00	0.00	0.00	0.00	0.00
Nb_2O_5	7.62	5.35	6.55	4.64	4.72	4.16	4.46	4.50	6.84	6.67	9.27	9.60	4.50	4.49	6.90
Ta_2O_5	0.17	0.00	0.08	0.13	0.00	0.00	0.00	0.03	0.00	0.00	0.00	0.00	0.19	0.30	0.08
SiO_2	33.42	34.43	33.88	32.73	32.71	32.89	32.89	32.81	35.13	35.11	33.49	33.44	34.36	34.54	34.35
F	0.74	0.78	0.77	0.89	0.84	1.07	0.97	0.94	0.95	1.05	0.53	0.64	0.99	1.20	0.89
H_2O	2.60	2.61	2.61	2.83	2.84	2.73	2.79	2.80	2.66	2.65	2.60	2.60	2.85	2.75	2.69
O=F	-0.31	-0.33	-0.32	-0.37	-0.35	-0.45	-0.41	-0.40	-0.40	-0.44	-0.22	-0.27	-0.42	-0.51	-0.38
Total	97.76	96.86	97.51	97.99	97.78	97.83	97.94	97.89	97.56	96.97	96.74	96.73	97.24	97.33	97.10
Chemical formulae calculated based on 31 anions															
Na_{tot}	1.11	1.13	1.10	0.85	0.89	0.92	0.90	0.89	1.28	1.28	1.22	1.17	0.99	1.03	1.16
Na	0.10	0.05	0.09	0.01	0.00	0.00	0.00	0.00	0.02	0.00	0.09	0.00	0.00	0.00	0.00
K	1.76	1.70	1.73	1.82	1.84	1.85	1.79	1.82	1.65	1.63	1.71	1.72	1.68	1.68	1.68
Rb	0.07	0.06	0.07	0.05	0.05	0.05	0.05	0.05	0.08	0.08	0.10	0.10	0.07	0.07	0.08
Cs	0.00	0.00	0.00	0.01	0.01	0.01	0.01	0.01	0.00	0.00	0.01	0.00	0.01	0.01	0.00
Sr	0.00	0.00	0.00	0.00	0.01	0.01	0.01	0.01	0.00	0.00	0.00	0.00	0.00	0.01	0.00
Ba	0.00	0.00	0.00	0.00	0.00	0.00	0.00	0.00	0.00	0.00	0.00	0.00	0.00	0.00	0.00
Sum A	1.93	1.81	1.89	1.89	1.90	1.91	1.86	1.89	1.75	1.71	1.90	1.82	1.76	1.76	1.77
Na	0.94	0.94	0.93	0.84	0.89	0.92	0.90	0.89	0.91	0.87	0.91	0.92	0.73	0.75	0.86
Ca	0.06	0.06	0.07	0.11	0.09	0.08	0.09	0.09	0.09	0.10	0.09	0.07	0.23	0.22	0.14
Sum B	1.00	1.00	1.00	0.95	0.98	1.00	0.99	0.98	1.00	0.97	1.00	0.99	0.96	0.97	1.00
Na	0.07	0.13	0.08	0.00	0.00	0.00	0.00	0.00	0.36	0.42	0.22	0.26	0.27	0.28	0.30
Mg	0.22	0.25	0.23	0.06	0.06	0.06	0.06	0.06	0.22	0.21	0.20	0.19	0.28	0.28	0.23
Mn	4.00	3.96	4.04	1.52	1.40	1.32	1.34	1.39	4.53	4.55	4.66	4.63	3.81	4.07	4.38
Fe^{2+}	2.67	2.62	2.60	5.49	5.56	5.67	5.65	5.59	1.82	1.76	1.85	1.85	2.59	2.29	2.02
Zn	0.04	0.04	0.05	0.00	0.00	0.00	0.00	0.00	0.08	0.07	0.08	0.07	0.05	0.08	0.07
Y	0.00	0.00	0.00	0.00	0.00	0.00	0.00	0.00	0.00	0.00	0.00	0.00	0.00	0.00	0.00
Ce	0.00	0.00	0.00	0.03	0.03	0.02	0.02	0.03	0.00	0.00	0.00	0.00	0.00	0.00	0.00
Sum C	7.00	7.00	7.00	7.10	7.05	7.07	7.06	7.07	7.00	7.00	7.00	7.00	7.00	7.00	7.00
Ti	0.88	1.15	0.99	1.04	1.02	1.02	1.01	1.02	1.32	1.34	1.06	1.04	1.43	1.43	1.27
Sn	0.00	0.00	0.00	0.00	0.00	0.00	0.00	0.00	0.00	0.00	0.00	0.00	0.00	0.00	0.00
Zr	0.33	0.31	0.33	0.46	0.48	0.55	0.53	0.50	0.02	0.02	0.00	0.00	0.10	0.09	0.04
Hf	0.00	0.00	0.00	0.00	0.00	0.00	0.00	0.00	0.00	0.00	0.00	0.00	0.00	0.00	0.00
Nb	0.79	0.56	0.68	0.48	0.49	0.44	0.47	0.47	0.70	0.68	0.97	1.00	0.46	0.46	0.71
Ta	0.01	0.00	0.01	0.01	0.00	0.00	0.00	0.00	0.00	0.00	0.00	0.00	0.01	0.02	0.01
Sum D	2.02	2.01	2.01	1.99	1.99	2.00	2.00	1.99	2.03	2.04	2.03	2.04	2.00	2.00	2.02
Si	7.70	7.90	7.78	7.56	7.56	7.61	7.59	7.58	7.93	7.95	7.74	7.72	7.76	7.79	7.81
Al	0.29	0.17	0.24	0.39	0.40	0.33	0.36	0.37	0.10	0.09	0.28	0.29	0.27	0.23	0.21
Sum T	7.99	8.06	8.02	7.94	7.96	7.94	7.95	7.95	8.02	8.04	8.01	8.01	8.03	8.02	8.02
F	0.54	0.57	0.56	0.65	0.61	0.78	0.71	0.69	0.68	0.75	0.39	0.47	0.71	0.86	0.64
OH	4.00	4.00	4.00	4.35	4.39	4.22	4.29	4.31	4.00	4.00	4.00	4.00	4.29	4.14	4.07
O	30.46	30.43	30.44	30.35	30.39	30.22	30.29	30.31	30.32	30.25	30.61	30.53	30.29	30.14	30.36
Cations	19.94	19.89	19.92	19.86	19.88	19.91	19.86	19.88	19.81	19.75	19.93	19.86	19.75	19.75	19.81

ELECTRON MICROPROBE ANALYSES OF MONT SAINT-HILAIRE AGM

Sample:	MSH46						MSH46						MSH47		
OXIDE	PT 1	PT 2	PT 3	PT 4	PT 5	PT 7	Average	PT 15	PT 17	PT 18	PT 19	PT 20	Average	PT 8	PT 9
Na_2O	2.33	2.32	2.22	2.12	2.16	2.08	2.21	3.40	3.43	3.43	3.42	3.56	3.45	2.51	2.38
K_2O	5.82	5.91	6.01	6.02	6.05	5.89	5.95	4.93	5.53	5.41	5.33	5.35	5.31	5.73	5.83
Rb_2O	0.42	0.41	0.42	0.44	0.44	0.48	0.44	0.64	0.39	0.52	0.41	0.49	0.49	0.41	0.40
Cs_2O	0.00	0.05	0.05	0.07	0.06	0.00	0.04	0.07	0.06	0.07	0.00	0.07	0.05	0.10	0.09
CaO	0.80	0.79	0.81	0.87	0.83	0.90	0.83	0.78	0.53	0.70	0.63	0.50	0.63	0.62	0.65
SrO	0.04	0.04	0.00	0.05	0.02	0.01	0.03	0.03	0.00	0.00	0.03	0.00	0.01	0.04	0.01
BaO	0.00	0.00	0.00	0.00	0.00	0.00	0.00	0.00	0.00	0.00	0.00	0.00	0.00	0.00	0.00
MgO	0.32	0.29	0.23	0.21	0.20	0.29	0.26	0.95	0.71	0.88	0.81	0.79	0.83	0.60	0.61
MnO	13.09	13.47	11.82	10.55	10.83	15.65	12.57	26.87	18.97	26.89	23.69	24.18	24.12	14.43	14.26
FeO	20.76	20.64	22.69	23.81	23.71	19.47	21.85	6.24	15.14	7.27	9.93	9.61	9.64	18.94	19.21
ZnO	0.18	0.24	0.18	0.23	0.19	0.00	0.17	0.00	0.00	0.00	0.00	0.00	0.00	0.40	0.40
Al_2O_3	1.32	1.22	1.51	1.50	1.51	1.59	1.44	0.24	0.15	0.19	0.12	0.11	0.16	1.16	1.18
Y_2O_3	0.00	0.00	0.00	0.00	0.00	0.00	0.00	0.00	0.00	0.00	0.00	0.00	0.00	0.00	0.00
Ce_2O_3	0.00	0.00	0.00	0.00	0.00	0.00	0.00	0.00	0.00	0.00	0.00	0.00	0.00	0.00	0.00
TiO_2	6.85	6.91	7.08	7.29	7.12	7.09	7.06	9.69	9.55	9.56	9.88	9.13	9.56	6.61	6.60
SnO_2	0.00	0.00	0.00	0.00	0.00	0.00	0.00	0.00	0.00	0.00	0.00	0.00	0.00	0.00	0.00
ZrO_2	3.11	3.04	2.61	2.65	2.71	2.55	2.78	0.43	0.00	0.00	0.00	0.00	0.09	3.78	3.76
HfO_2	0.00	0.00	0.00	0.00	0.00	0.00	0.00	0.00	0.00	0.00	0.00	0.00	0.00	0.00	0.00
Nb_2O_5	4.15	4.06	4.16	4.21	4.28	4.24	4.18	2.66	3.38	3.48	2.83	4.01	3.27	3.75	3.93
Ta_2O_5	0.00	0.00	0.00	0.00	0.00	0.00	0.00	0.00	0.00	0.00	0.00	0.00	0.00	0.00	0.00
SiO_2	32.85	32.81	32.08	32.49	32.54	32.21	32.50	35.50	35.55	35.57	35.46	35.57	35.53	33.05	33.22
F	0.96	0.98	1.11	1.10	0.92	1.15	1.04	0.83	1.01	0.82	0.88	0.85	0.88	1.00	1.05
H_2O	2.76	2.74	2.66	2.69	2.78	2.66	2.72	2.93	2.86	2.97	2.90	2.93	2.92	2.74	2.73
O=F	-0.40	-0.41	-0.47	-0.46	-0.39	-0.48	-0.44	-0.35	-0.43	-0.35	-0.37	-0.36	-0.37	-0.42	-0.44
Total	95.35	95.51	95.17	95.84	95.97	95.78	95.60	95.84	96.83	97.41	95.95	96.80	96.57	95.45	95.87
Chemical formulae calculated based on 31 anions															
Na_{tot}	1.05	1.05	1.01	0.96	0.98	0.94	1.00	1.49	1.49	1.49	1.50	1.55	1.50	1.14	1.07
Na	0.04	0.09	0.14	0.01	0.04	0.17	0.07	0.31	0.31	0.39	0.32	0.34	0.33	0.11	0.05
K	1.73	1.76	1.80	1.79	1.80	1.76	1.77	1.42	1.58	1.54	1.53	1.53	1.52	1.71	1.73
Rb	0.06	0.06	0.06	0.07	0.07	0.07	0.07	0.09	0.06	0.08	0.06	0.07	0.07	0.06	0.06
Cs	0.00	0.01	0.01	0.01	0.01	0.00	0.00	0.01	0.01	0.01	0.00	0.01	0.01	0.01	0.01
Sr	0.01	0.01	0.00	0.01	0.00	0.00	0.00	0.00	0.00	0.00	0.00	0.00	0.00	0.01	0.00
Ba	0.00	0.00	0.00	0.00	0.00	0.00	0.00	0.00	0.00	0.00	0.00	0.00	0.00	0.00	0.00
Sum A	1.84	1.92	2.02	1.88	1.91	1.99	1.92	1.83	1.96	2.01	1.92	1.95	1.93	1.89	1.84
Na	0.80	0.80	0.80	0.78	0.79	0.78	0.79	0.81	0.87	0.83	0.85	0.88	0.86	0.85	0.84
Ca	0.20	0.20	0.20	0.22	0.21	0.23	0.21	0.19	0.13	0.17	0.15	0.12	0.15	0.16	0.16
Sum B	1.00	1.00	1.00	1.00	1.00	1.00	1.00	1.00	1.00	1.00	1.00	1.00	1.01	1.00	1.00
Na	0.22	0.16	0.07	0.16	0.15	0.00	0.13	0.37	0.31	0.27	0.33	0.33	0.32	0.18	0.19
Mg	0.11	0.10	0.08	0.07	0.07	0.10	0.09	0.32	0.24	0.29	0.27	0.27	0.28	0.21	0.21
Mn	2.59	2.67	2.35	2.08	2.14	3.10	2.49	5.13	3.61	5.09	4.53	4.60	4.59	2.85	2.80
Fe^{2+}	4.05	4.03	4.46	4.64	4.62	3.80	4.27	1.18	2.84	1.36	1.87	1.81	1.81	3.69	3.73
Zn	0.03	0.04	0.03	0.04	0.03	0.00	0.03	0.00	0.00	0.00	0.00	0.00	0.00	0.07	0.07
Y	0.00	0.00	0.00	0.00	0.00	0.00	0.00	0.00	0.00	0.00	0.00	0.00	0.00	0.00	0.00
Ce	0.00	0.00	0.00	0.00	0.00	0.00	0.00	0.00	0.00	0.00	0.00	0.00	0.00	0.00	0.00
Sum C	7.00	7.00	7.00	7.00	7.00	7.00	7.01	7.00	7.00	7.00	7.00	7.00	7.00	7.00	7.00
Ti	1.20	1.21	1.25	1.28	1.25	1.25	1.24	1.64	1.61	1.61	1.68	1.54	1.62	1.16	1.15
Sn	0.00	0.00	0.00	0.00	0.00	0.00	0.00	0.00	0.00	0.00	0.00	0.00	0.00	0.00	0.00
Zr	0.35	0.35	0.30	0.30	0.31	0.29	0.32	0.05	0.00	0.00	0.00	0.00	0.01	0.43	0.43
Hf	0.00	0.00	0.00	0.00	0.00	0.00	0.00	0.00	0.00	0.00	0.00	0.00	0.00	0.00	0.00
Nb	0.44	0.43	0.44	0.44	0.45	0.45	0.44	0.27	0.34	0.35	0.29	0.41	0.33	0.40	0.41
Ta	0.00	0.00	0.00	0.00	0.00	0.00	0.00	0.00	0.00	0.00	0.00	0.00	0.00	0.00	0.00
Sum D	1.99	1.99	1.99	2.02	2.01	1.98	2.00	1.96	1.96	1.96	1.97	1.95	1.96	1.98	1.99
Si	7.67	7.66	7.54	7.57	7.58	7.52	7.59	8.01	7.98	7.94	8.00	7.99	7.99	7.71	7.71
Al	0.36	0.34	0.42	0.41	0.41	0.44	0.40	0.06	0.04	0.05	0.03	0.03	0.04	0.32	0.32
Sum T	8.03	8.00	7.96	7.98	7.99	7.96	7.99	8.07	8.02	7.99	8.03	8.02	8.03	8.03	8.03
F	0.71	0.72	0.83	0.81	0.68	0.85	0.77	0.59	0.72	0.58	0.63	0.60	0.62	0.74	0.77
OH	4.29	4.28	4.17	4.19	4.32	4.15	4.23	4.41	4.28	4.42	4.37	4.40	4.38	4.26	4.23
O	30.29	30.28	30.17	30.19	30.32	30.15	30.23	30.41	30.28	30.42	30.37	30.40	30.38	30.26	30.23
Cations	19.86	19.91	19.97	19.89	19.91	19.94	19.91	19.86	19.94	19.96	19.92	19.92	19.92	19.91	19.87

ELECTRON MICROPROBE ANALYSES OF MONT SAINT-HILAIRE AGM

Sample OXIDE	PT 10	PT 11	PT 13	PT 14	MSH48 Average
Na_2O	2.44	2.46	2.45	2.44	2.45
K_2O	5.77	5.77	5.77	5.83	5.78
Rb_2O	0.41	0.42	0.41	0.41	0.41
Cs_2O	0.07	0.10	0.09	0.08	0.09
CaO	0.70	0.62	0.74	0.74	0.68
SrO	0.00	0.05	0.01	0.03	0.02
BaO	0.00	0.00	0.00	0.00	0.00
MgO	0.59	0.60	0.57	0.56	0.59
MnO	13.73	14.63	12.93	13.15	13.86
FeO	19.54	18.90	20.92	20.70	19.70
ZnO	0.34	0.40	0.30	0.29	0.36
Al_2O_3	1.19	1.15	1.22	1.23	1.19
Y_2O_3	0.00	0.00	0.00	0.00	0.00
Ce_2O_3	0.00	0.00	0.00	0.00	0.00
TiO_2	6.49	6.55	6.68	6.71	6.61
SnO_2	0.00	0.00	0.00	0.00	0.00
ZrO_2	3.90	3.92	4.06	4.00	3.90
HfO_2	0.00	0.00	0.00	0.00	0.00
Nb_2O_5	3.77	4.02	3.61	3.51	3.77
Ta_2O_5	0.00	0.00	0.00	0.00	0.00
SiO_2	32.90	33.05	32.96	32.63	32.97
F	1.08	0.93	1.13	1.20	1.07
H_2O	2.69	2.78	2.69	2.64	2.71
O=F	-0.45	-0.39	-0.48	-0.51	-0.45
Total	95.16	95.96	96.07	95.64	95.69
Chemical formulae calculated based on 31 anions					
$Na_{tot.}$	1.11	1.11	1.10	1.11	1.11
Na	0.10	0.09	0.14	0.19	0.11
K	1.72	1.71	1.71	1.74	1.72
Rb	0.06	0.06	0.06	0.06	0.06
Cs	0.01	0.01	0.01	0.01	0.01
Sr	0.00	0.01	0.00	0.00	0.00
Ba	0.00	0.00	0.00	0.00	0.00
Sum A	1.89	1.88	1.92	2.00	1.90
Na	0.82	0.85	0.82	0.82	0.83
Ca	0.18	0.15	0.18	0.19	0.17
Sum B	1.00	1.00	1.00	1.00	1.00
Na	0.19	0.17	0.14	0.11	0.16
Mg	0.21	0.21	0.20	0.20	0.20
Mn	2.72	2.88	2.54	2.60	2.73
Fe^{2+}	3.83	3.67	4.06	4.05	3.84
Zn	0.06	0.07	0.05	0.05	0.06
Y	0.00	0.00	0.00	0.00	0.00
Ce	0.00	0.00	0.00	0.00	0.00
Sum C	7.00	7.00	7.00	7.00	7.00
Ti	1.14	1.15	1.17	1.18	1.16
Sn	0.00	0.00	0.00	0.00	0.00
Zr	0.45	0.44	0.46	0.46	0.44
Hf	0.00	0.00	0.00	0.00	0.00
Nb	0.40	0.42	0.38	0.37	0.40
Ta	0.00	0.00	0.00	0.00	0.00
Sum D	1.99	2.01	2.01	2.01	2.00
Si	7.70	7.68	7.66	7.63	7.68
Al	0.33	0.32	0.33	0.34	0.33
Sum T	8.03	8.00	7.99	7.97	8.01
F	0.80	0.68	0.83	0.89	0.78
OH	4.20	4.32	4.17	4.11	4.22
O	30.20	30.32	30.17	30.11	30.22
Cations	19.90	19.89	19.92	19.97	19.91

APPENDIX C.

ATOMIC POSITIONS, SITE OCCUPANCY FACTORS AND ANISOTROPIC DISPLACEMENT PARAMETERS FOR AGM SINGLE-CRYSTAL X-RAY STRUCTURE REFINEMENTS

POSITIONAL AND DISPLACEMENT PARAMETERS AND SITE OCCUPANCIES FOR NOR1

Atom	x	y	z	sof	*U_{11}	U_{22}	U_{33}	U_{23}	U_{13}	U_{12}	U_{eq}
Mn(1)	0.8499(1)	0.20611(8)	0.47983(8)	0.887(7)	80(5)	86(5)	116(5)	47(3)	21(3)	20(3)	93(3)
Na(1)	0.8499(1)	0.20611(8)	0.47983(8)	0.113(7)	80(5)	86(5)	116(5)	47(3)	21(3)	20(3)	93(3)
Fe(2)	0.2806(1)	0.06742(7)	0.48877(7)	0.955(4)	90(4)	99(4)	141(4)	63(3)	35(3)	31(3)	104(2)
Fe(3)	0.4228(1)	0.35251(8)	0.48585(8)	0.936(4)	88(4)	102(4)	144(4)	64(3)	32(3)	28(3)	106(3)
Fe(4)	0	0.5	0.5	0.425(4)	77(6)	75(6)	116(6)	38(5)	12(4)	14(4)	92(4)
Mg(4)	0	0.5	0.5	0.075(4)	77(6)	75(6)	116(6)	38(5)	12(4)	14(4)	92(4)
Ti	0.0791(1)	0.08609(7)	0.19716(7)	0.822(5)	50(4)	69(4)	112(4)	44(3)	18(3)	16(3)	75(2)
Nb	0.0791(1)	0.08609(7)	0.19716(7)	0.178(5)	50(4)	69(4)	112(4)	44(3)	18(3)	16(3)	75(2)
Si(1)	0.6782(3)	0.2724(13)	0.2324(1)	1.00	101(7)	80(7)	101(7)	43(6)	12(5)	16(5)	94(3)
Si(2)	0.8140(3)	0.5464(1)	0.2539(1)	1.00	115(7)	71(7)	118(7)	43(6)	15(6)	22(6)	102(3)
Si(3)	0.3797(3)	0.6749(1)	0.2565(1)	1.00	113(7)	86(7)	112(7)	52(6)	17(6)	23(6)	102(7)
Si(4)	0.5069(3)	0.9317(1)	0.2361(1)	1.00	98(7)	69(7)	85(6)	36(5)	10(5)	17(5)	84(3)
K	0.1373(3)	0.2731(2)	0.9966(1)	0.914(6)	612(13)	727(15)	249(9)	128(9)	54(8)	174(10)	559(8)
Rb	0.1373(3)	0.2731(2)	0.9966(1)	0.086(6)	612(13)	727(15)	249(9)	128(9)	54(8)	174(10)	559(8)
Na	0.5	0	0	0.321(8)	264(16)	154(14)	108(12)	39(9)	15(10)	29(10)	187(9)
Ca	0.5	0	0	0.179(8)	264(16)	154(14)	108(12)	39(9)	15(10)	29(10)	187(9)
O(1)	0.7260(6)	0.3195(3)	0.3847(3)	1.00	92(18)	103(18)	90(17)	17(15)	31(14)	28(15)	102(7)
O(2)	0.1491(7)	0.1607(3)	0.3706(3)	1.00	94(18)	112(18)	101(17)	25(15)	12(14)	25(15)	110(7)
O(3)	0.1273(7)	0.3925(3)	0.5936(3)	1.00	105(18)	127(19)	100(17)	42(15)	4(14)	9(15)	117(8)
OH(4)	0.2961(7)	0.4628(3)	0.3999(3)	1.00	134(19)	93(18)	144(19)	47(16)	19(15)	40(15)	124(8)
OH(5)	0.9904(7)	0.1174(3)	0.5927(3)	1.00	174(20)	128(20)	133(19)	58(16)	31(16)	19(16)	148(8)
O(6)	0.5569(7)	0.2571(3)	0.5901(3)	1.00	121(18)	100(18)	86(17)	26(15)	5(14)	20(15)	110(7)
O(7)	0.5732(7)	0.0146(3)	0.3884(3)	1.00	91(18)	131(19)	104(17)	57(15)	16(14)	36(15)	105(7)
O(8)	0.0756(7)	0.5906(4)	0.2014(4)	1.00	132(20)	224(22)	160(20)	59(17)	39(16)	-13(17)	190(9)
O(9)	0.2472(8)	0.4033(4)	0.8266(4)	1.00	245(24)	346(27)	152(21)	-9(19)	72(19)	-181(20)	330(12)
O(10)	0.4282(8)	0.4143(4)	0.7989(4)	1.00	267(23)	191(21)	136(19)	46(17)	12(17)	98(18)	201(9)
O(11)	0.1280(9)	0.8077(5)	0.8305(4)	1.00	554(32)	471(30)	170(22)	155(22)	135(22)	430(27)	337(12)
O(12)	0.2653(9)	0.9572(4)	0.1713(4)	1.00	425(28)	323(26)	139(21)	-23(19)	-96(20)	293(23)	311(11)
O(13)	0.2669(8)	0.6073(3)	0.8061(4)	1.00	465(28)	57(19)	129(19)	30(16)	9(19)	15(19)	234(10)
O(14)	0.5725(8)	0.2205(4)	0.8016(4)	1.00	403(27)	134(21)	171(21)	86(17)	27(19)	29(19)	239(10)
O(15)	0.3830(8)	0.1918(4)	0.1683(4)	1.00	206(23)	475(30)	168(21)	-176(22)	-55(18)	-215(21)	331(12)
F(16)	0	0	0	0.50	231(25)	170(24)	118(22)	65(19)	15(19)	53(20)	173(10)
H(1)	0.33(1)	0.379(3)	0.359(6)	1.00							0.04
H(2)	1.01(1)	0.152(6)	0.6851(7)	1.00							0.04

*Uij x 10^4 Å

POSITIONAL AND DISPLACEMENT PARAMETERS AND SITE OCCUPANCIES FOR NOR17

Atom	x	y	z	sof	*U_{11}	U_{22}	U_{33}	U_{23}	U_{13}	U_{12}	U_{eq}
Mn(1)	0.8494(1)	0.20507(6)	0.47814(6)	0.898(6)	82(3)	85(3)	117(3)	42(2)	20(2)	16(2)	96(2)
Na(1)	0.8494(1)	0.20507(6)	0.47814(6)	0.102(6)	82(3)	85(3)	117(3)	42(2)	20(2)	16(2)	96(2)
Mn(2)	0.2797(1)	0.06681(6)	0.48767(6)	0.985(3)	94(3)	99(3)	139(3)	59(2)	37(2)	25(2)	107(2)
Mn(3)	0.4222(1)	0.35156(6)	0.48427(6)	1.000(3)	94(3)	99(3)	140(3)	61(2)	35(2)	28(2)	107(2)
Mn(4)	0	0.5	0.5	0.500(2)	81(4)	73(4)	128(4)	40(3)	17(3)	9(3)	97(2)
Ti	0.0801(1)	0.08649(6)	0.19765(6)	0.900(4)	61(3)	81(3)	110(3)	42(2)	16(2)	15(2)	85(2)
Nb	0.0801(1)	0.08649(6)	0.19765(6)	0.100(4)	61(3)	81(3)	110(3)	42(2)	16(2)	15(2)	85(2)
Si(1)	0.6788(2)	0.2719(1)	0.2313(1)	1.00	95(5)	70(5)	108(5)	33(4)	17(4)	9(4)	95(2)
Si(2)	0.8141(2)	0.5467(1)	0.2546(1)	1.00	102(5)	78(5)	117(5)	40(4)	18(4)	14(4)	102(2)
Si(3)	0.3798(2)	0.6758(1)	0.2566(1)	1.00	99(5)	77(5)	128(5)	49(4)	23(4)	13(4)	102(2)
Si(4)	0.5074(2)	0.9318(1)	0.2353(1)	1.00	94(5)	82(5)	102(5)	46(4)	15(4)	12(4)	93(2)
K(1a)	0.1332(3)	0.2616(2)	0.9954(2)	0.871(5)							451(5)
Na(1b)	0.097(4)	0.189(2)	0.997(2)	0.129(5)							451(5)
Na	0.5	0	0	0.441(7)	207(12)	111(11)	76(10)	29(8)	18(8)	33(8)	137(7)
Ca	0.5	0	0	0.059(7)	207(12)	111(11)	76(10)	29(8)	18(8)	33(8)	137(7)
O(1)	0.7283(5)	0.3187(3)	0.3832(2)	1.00	128(13)	106(13)	112(13)	36(11)	24(10)	21(11)	120(5)
O(2)	0.1484(5)	0.1599(3)	0.3686(3)	1.00	130(13)	107(13)	104(13)	12(11)	5(10)	16(11)	129(5)
O(3)	0.1286(5)	0.3922(3)	0.5936(2)	1.00	102(13)	116(13)	112(13)	41(11)	7(10)	16(10)	116(5)
OH(4)	0.2972(5)	0.4624(3)	0.3990(3)	1.00	95(13)	134(14)	163(14)	65(12)	22(10)	28(11)	130(6)
OH(5)	0.9927(5)	0.1185(3)	0.5938(3)	1.00	118(13)	135(14)	144(14)	42(11)	26(11)	41(11)	137(6)
O(6)	0.5572(5)	0.2579(3)	0.5913(3)	1.00	110(13)	118(13)	124(13)	45(11)	17(10)	20(11)	122(5)
O(7)	0.5747(5)	0.0140(3)	0.3878(2)	1.00	132(13)	128(14)	101(12)	44(11)	30(10)	25(11)	123(5)
O(8)	0.0744(5)	0.5919(3)	0.2027(3)	1.00	96(13)	184(15)	154(14)	57(12)	18(11)	2(11)	156(6)
O(9)	0.2467(6)	0.0399(3)	0.8273(3)	1.00	266(17)	289(19)	189(16)	-19(14)	110(14)	-175(14)	328(9)
O(10)	0.4284(5)	0.4134(3)	0.7983(3)	1.00	119(13)	202(15)	160(14)	76(12)	21(11)	80(12)	154(6)
O(11)	0.1262(7)	0.8077(4)	0.8305(3)	1.00	530(23)	459(23)	197(16)	160(17)	141(16)	429(20)	332(9)
O(12)	0.2631(7)	0.9572(3)	0.1717(3)	1.00	433(20)	309(20)	160(16)	-25(14)	-81(14)	283(17)	318(8)
O(13)	0.2682(6)	0.6066(3)	0.8063(3)	1.00	376(18)	92(14)	167(15)	57(12)	16(13)	24(13)	220(7)
O(14)	0.5720(6)	0.2215(3)	0.8020(3)	1.00	368(18)	112(14)	174(15)	77(12)	45(13)	38(13)	218(7)
O(15)	0.3822(6)	0.1905(4)	0.1683(3)	1.00	201(16)	446(22)	168(16)	143(16)	-55(12)	-186(15)	323(9)
F(16)	0	0	0	0.50	163(16)	156(17)	182(17)	74(14)	48(13)	59(13)	163(7)

*Uij x 10^4 Å

POSITIONAL AND DISPLACEMENT PARAMETERS AND SITE OCCUPANCIES FOR RUS4

Atom	*x*	*y*	*z*	*sof*	$^{*}U_{11}$	U_{22}	U_{33}	U_{23}	U_{13}	U_{12}	U_{eq}
Mn(1)	0.8492(2)	0.2063(1)	0.4801(1)	0.91(1)	92(6)	108(6)	166(7)	68(5)	34(4)	38(4)	116(4)
Na(1)	0.8492(2)	0.2063(1)	0.4801(1)	0.09(1)	92(6)	108(6)	166(7)	68(5)	34(4)	38(4)	116(4)
Fe(2)	0.2806(2)	0.06751(9)	0.4890(1)	0.958(6)	96(6)	126(6)	167(6)	79(5)	49(4)	46(4)	120(4)
Fe(3)	0.4233(2)	0.3531(1)	0.4863(1)	0.86(1)	102(6)	114(6)	192(7)	87(5)	48(4)	48(4)	124(4)
Mg(3)	0.4233(2)	0.3531(1)	0.4863(1)	0.14(1)	102(6)	114(6)	192(7)	87(5)	48(4)	48(4)	124(4)
Fe(4)	0	0.5	0.5	0.392(7)	84(9)	101(8)	143(9)	56(7)	23(6)	36(6)	106(5)
Mg(4)	0	0.5	0.5	0.108(7)	84(9)	101(8)	143(9)	56(7)	23(6)	36(6)	106(5)
Ti	0.0796(2)	0.0868(1)	0.1989(1)	0.965(8)	54(6)	95(6)	137(7)	64(5)	30(4)	38(4)	87(4)
Nb	0.0796(2)	0.0868(1)	0.1989(1)	0.035(8)	54(6)	95(6)	137(7)	64(5)	30(4)	38(4)	87(4)
Si(1)	0.6778(3)	0.2723(2)	0.2322(2)	1.00	119(9)	74(8)	121(9)	42(7)	31(7)	31(7)	104(4)
Si(2)	0.8140(4)	0.5459(2)	0.2531(2)	1.00	112(9)	90(8)	168(10)	58(8)	20(7)	37(7)	121(4)
Si(3)	0.3797(4)	0.6749(2)	0.2559(2)	1.00	126(9)	110(9)	144(10)	70(8)	32(7)	46(7)	118(4)
Si(4)	0.5066(3)	0.9317(2)	0.2356(2)	1.00	125(9)	102(8)	113(9)	65(7)	34(7)	45(7)	104(4)
K	0.1345(5)	0.2674(2)	0.9961(2)	0.92(3)	654(19)	409(15)	287(14)	125(11)	68(12)	124(12)	463(10)
Na	0.1345(5)	0.2674(2)	0.9961(2)	0.08(3)	654(19)	409(15)	287(14)	125(11)	68(12)	124(12)	463(10)
Na	0.5	0	0	0.28(1)	234(19)	181(17)	122(17)	81(13)	27(12)	67(12)	172(11)
Ca	0.5	0	0	0.22(1)	234(19)	181(17)	122(17)	81(13)	27(12)	67(12)	172(11)
O(1)	0.7252(9)	0.3185(4)	0.3840(4)	1.00	181(25)	60(21)	85(23)	7(19)	-13(19)	2(18)	124(10)
O(2)	0.1472(9)	0.1605(4)	0.3705(5)	1.00	172(25)	108(22)	133(25)	47(20)	5(20)	32(19)	141(10)
O(3)	0.1291(9)	0.3924(5)	0.5924(5)	1.00	127(25)	171(24)	162(26)	75(22)	57(20)	53(19)	148(10)
OH(4)	0.2980(10)	0.4628(5)	0.4012(5)	1.00	211(27)	167(25)	144(26)	85(22)	39(21)	58(21)	167(10)
OH(5)	0.9910(10)	0.1167(5)	0.5922(5)	1.00	169(26)	115(23)	95(24)	0(20)	16(20)	24(19)	145(10)
O(6)	0.5560(9)	0.2576(4)	0.5903(5)	1.00	134(24)	115(22)	113(24)	64(20)	32(19)	25(19)	117(10)
O(7)	0.5706(9)	0.0147(5)	0.3890(5)	1.00	143(25)	184(25)	169(27)	95(22)	48(21)	69(20)	153(10)
O(8)	0.0744(10)	0.5897(5)	0.2004(5)	1.00	215(29)	255(29)	113(26)	22(23)	17(22)	-45(22)	234(12)
O(9)	0.2465(12)	0.0399(6)	0.8278(5)	1.00	289(33)	317(32)	116(27)	-29(25)	32(24)	-154(25)	323(14)
O(10)	0.4265(11)	0.4137(5)	0.7996(5)	1.00	280(31)	247(28)	147(27)	47(24)	-11(23)	130(24)	230(12)
O(11)	0.1306(13)	0.8087(6)	0.8311(6)	1.00	533(40)	382(35)	176(30)	111(28)	82(28)	377(32)	321(15)
O(12)	0.2637(12)	0.9566(6)	0.1695(6)	1.00	415(36)	311(32)	216(31)	50(27)	-59(27)	284(29)	309(15)
O(13)	0.2686(11)	0.6071(5)	0.8076(5)	1.00	429(35)	94(24)	231(30)	116(23)	69(26)	22(23)	244(13)
O(14)	0.5757(12)	0.2210(5)	0.8026(6)	1.00	475(38)	190(27)	253(32)	146(26)	98(28)	91(26)	288(14)
O(15)	0.3813(11)	0.1899(6)	0.1670(6)	1.00	209(30)	434(37)	305(35)	196(31)	9(27)	-166(26)	352(15)
F(16)	0	0	0	0.50	196(31)	230(31)	89(28)	72(25)	22(24)	62(25)	170(12)
H(1)	0.25(2)	0.44(1)	0.309(2)	1.00							840(463)
H(2)	1.08(2)	0.16(1)	0.681(3)	1.00							658(388)

$^{*}U$ij x 10^{4} Å

POSITIONAL AND DISPLACEMENT PARAMETERS AND SITE OCCUPANCIES FOR RUS8

Atom	x	y	z	sof	*U_{11}	U_{22}	U_{33}	U_{23}	U_{13}	U_{12}	U_{eq}
Mn(1)	0.84960(7)	0.20628(4)	0.47984(4)	0.900(5)	76(2)	92(2)	122(2)	51(2)	27(1)	28(1)	93(1)
Na(1)	0.84960(7)	0.20628(4)	0.47984(4)	0.100(5)	76(2)	92(2)	122(2)	51(2)	27(1)	28(1)	93(1)
Fe(2)	0.28050(7)	0.06758(4)	0.48885(4)	0.946(2)	77(2)	101(2)	128(2)	59(2)	35(1)	32(1)	97(1)
Fe(3)	0.42326(7)	0.35296(4)	0.48618(4)	0.847(4)	79(2)	97(2)	134(2)	59(2)	36(1)	36(1)	97(1)
Mg(3)	0.42326(7)	0.35296(4)	0.48618(4)	0.153(4)	79(2)	97(2)	134(2)	59(2)	36(1)	36(1)	97(1)
Fe(4)	0	0.5	0.5	0.385(3)	68(3)	78(3)	115(3)	41(2)	17(2)	23(2)	87(2)
Mg(4)	0	0.5	0.5	0.115(3)	68(3)	78(3)	115(3)	41(2)	17(2)	23(2)	87(2)
Ti	0.8010(8)	0.08710(4)	0.19911(4)	0.958(4)	54(2)	86(2)	86(2)	37(2)	14(1)	22(1)	75(1)
Zr	0.8010(8)	0.08710(4)	0.19911(4)	0.042(4)	54(2)	86(2)	86(2)	37(2)	14(1)	22(1)	75(1)
Si(1)	0.6780(1)	0.27199(6)	0.23169(7)	1.00	81(3)	73(3)	92(3)	34(3)	13(2)	17(2)	83(1)
Si(2)	0.8139(1)	0.54579(7)	0.25301(7)	1.00	84(3)	81(3)	114(3)	45(3)	20(2)	22(2)	92(1)
Si(3)	0.3798(1)	0.67496(7)	0.25557(7)	1.00	89(3)	88(3)	108(3)	48(3)	19(2)	25(2)	93(1)
Si(4)	0.5068(1)	0.93187(7)	0.23565(7)	1.00	88(3)	82(3)	83(3)	40(3)	17(2)	25(2)	82(1)
K	0.1338(2)	0.2657(1)	0.99575(9)	0.90(1)	633(7)	378(6)	251(5)	105(4)	43(4)	94(5)	442(4)
Na	0.1338(2)	0.2657(1)	0.99575(9)	0.10(1)	633(7)	378(6)	251(5)	105(4)	43(4)	94(5)	442(4)
Na	0.5	0	0	0.291(6)	183(6)	126(6)	75(6)	34(4)	19(4)	42(4)	132(4)
Ca	0.5	0	0	0.209(6)	183(6)	126(6)	75(6)	34(4)	19(4)	42(4)	132(4)
O(1)	0.7264(3)	0.3194(2)	0.3849(2)	1.00	105(8)	121(8)	95(9)	40(7)	21(7)	27(7)	110(3)
O(2)	0.1480(3)	0.1603(2)	0.3698(2)	1.00	124(8)	129(9)	100(9)	45(7)	15(7)	33(7)	120(4)
O(3)	0.1286(3)	0.3929(2)	0.5936(2)	1.00	105(8)	123(8)	117(9)	59(7)	17(7)	31(7)	113(3)
OH(4)	0.2974(3)	0.4619(2)	0.3998(2)	1.00	110(8)	126(9)	153(10)	60(8)	27(7)	39(7)	128(4)
OH(5)	0.9910(4)	0.1170(2)	0.5929(2)	1.00	124(8)	127(9)	148(9)	52(8)	31(7)	33(7)	135(4)
O(6)	0.5561(3)	0.2576(2)	0.5899(2)	1.00	110(8)	106(8)	113(9)	48(7)	17(7)	29(7)	110(3)
O(7)	0.5728(3)	0.01493(2)	0.3890(2)	1.00	119(8)	123(8)	85(8)	41(7)	21(7)	39(7)	109(3)
O(8)	0.0743(4)	0.5904(2)	0.2008(2)	1.00	154(9)	270(11)	149(10)	67(9)	41(8)	-25(8)	212(4)
O(9)	0.2474(4)	0.0410(2)	0.8284(2)	1.00	218(10)	309(12)	161(11)	-15(10)	92(9)	-141(9)	302(6)
O(10)	0.4275(4)	0.4146(2)	0.8003(2)	1.00	235(10)	267(11)	158(11)	64(9)	29(8)	173(9)	211(4)
O(11)	0.1283(5)	0.8085(2)	0.8314(2)	1.00	469(14)	426(14)	166(110	139(11)	132(10)	391(13)	297(6)
O(12)	0.2644(5)	0.9569(2)	0.1702(2)	1.00	369(13)	296(12)	169(11)	-7(9)	-70(9)	264(11)	290(6)
O(13)	0.2673(5)	0.6080(2)	0.8069(2)	1.00	418(13)	90(9)	140(10)	55(8)	37(9)	28(9)	223(5)
O(14)	0.5718(5)	0.2208(2)	0.8025(2)	1.00	437(13)	104(9)	160(10)	81(8)	55(10)	44(9)	231(5)
O(15)	0.3824(4)	0.1901(3)	0.1667(2)	1.00	164(10)	435(15)	165(11)	145(11)	-43(8)	-164(10)	298(6)
F(16)	0	0	0	0.50	166(10)	142(10)	93(10)	41(9)	19(8)	43(9)	137(4)

*Uij x 10^4 Å

POSITIONAL AND DISPLACEMENT PARAMETERS AND SITE OCCUPANCIES FOR RUS9

Atom	x	y	z	sof	*U_{11}	U_{22}	U_{33}	U_{23}	U_{13}	U_{12}	U_{eq}
Mn(1)	0.2527(1)	0.39265(3)	0.00989(3)	0.913(7)	94(4)	88(4)	134(4)	-2(4)	17(2)	0(5)	105(2)
Na(1)	0.2527(1)	0.39265(3)	0.00989(3)	0.087(7)	94(4)	88(4)	134(4)	-2(4)	17(2)	0(5)	105(2)
Mn(2)	0.7461(1)	0.03613(3)	-0.00589(3	0.990(3)	92(4)	86(4)	158(4)	13(3)	28(3)	-3(4)	111(2)
Mn(3)	0.7468(1)	0.17930(3)	-0.00728(3	0.966(4)	95(4)	92(4)	150(4)	6(4)	35(3)	9(5)	111(2)
Mn(4)	0.25	0.25	0	0.431(4)	95(6)	91(5)	140(5)	-18(5)	6(4)	2(5)	109(3)
Mg(4)	0.25	0.25	0	0.069(4)	95(6)	91(5)	140(5)	-18(5)	6(4)	2(5)	109(3)
Ti	-0.4641(1)	0.10716(3)	-0.15196(3	0.881(4)	77(3)	130(3)	145(4)	-17(3)	12(2)	-5(3)	117(2)
Nb	-0.4641(1)	0.10716(3)	-0.15196(3	0.119(4)	77(3)	130(3)	145(4)	-17(3)	12(2)	-5(3)	117(2)
Si(1)	0.0417(2)	0.19281(5)	-0.13490(6	1.00	85(6)	101(6)	113(6)	27(4)	6(4)	4(4)	100(3)
Si(2)	0.0391(2)	0.32547(5)	-0.12427(6	1.00	167(6)	107(6)	112(6)	1(5)	11(4)	-3(5)	129(3)
Si(3)	0.9601(2)	0.11053(5)	0.12310(6)	1.00	154(6)	101(5)	113(5)	6(5)	13(4)	-7(5)	123(2)
Si(4)	1.0417(2)	0.02169(5)	-0.13312(6	1.00	114(6)	75(6)	105(6)	2(4)	11(4)	1(4)	98(3)
K1	-0.5	0.24270(9)	-0.25	0.50	568(13)	495(12)	285(10)	0	20(9)	0	451(5)
K2	0.5	-0.02746(9	-0.25	0.50	579(13)	416(11)	280(10)	0	31(9)	0	425(5)
Na	-1.0	0.10683(8)	-0.25	0.301(7)	266(11)	142(10)	75(9)	0	5(6)	0	162(6)
Ca	-1.0	0.10683(8)	-0.25	0.199(7)	266(11)	142(10)	75(9)	0	5(6)	0	162(6)
O(1)	0.0676(5)	0.1842(2)	-0.0582(1)	1.00	109(15)	121(17)	88(14)	-8(13)	-5(12)	-4(15)	107(7)
O(2)	0.5672(5)	0.1077(2)	-0.0655(1)	1.00	117(14)	119(14)	113(14)	-1(15)	1(11)	-8(15)	117(6)
O(3)	0.0672(5)	0.3234(2)	-0.0474(1)	1.00	86(15)	140(16)	100(14)	-19(15)	14(11)	-12(16)	108(6)
OH(4)	-0.0652(6)	0.2477(2)	0.0505(1)	1.00	117(16)	152(16)	163(16)	-36(15)	42(13)	3(16)	142(7)
OH(5)	0.4343(6)	0.0391(2)	0.0474(1)	1.00	139(17)	123(17)	188(17)	-11(16)	23(13)	-7(16)	150(7)
O(6)	0.9289(5)	0.1094(2)	0.0457(1)	1.00	129(14)	109(14)	109(14)	-14(16)	17(11)	-14(16)	115(6)
O(7)	1.0664(5)	0.0309(2)	-0.0563(1)	1.00	126(16)	127(17)	104(15)	-10(13)	17(12)	-7(15)	119(7)
O(8)	0.2753(7)	0.3593(1)	-0.1507(2)	1.00	337(21)	335(20)	154(18)	12(15)	4(15)	-174(17)	277(9)
O(9)	-0.7252(6)	0.0491(2)	-0.1645(2)	1.00	315(20)	385(22)	179(18)	-58(16)	95(16)	-208(17)	289(9)
O(10)	-0.2240(7)	0.3557(2)	-0.1510(2)	1.00	339(21)	360(21)	174(19)	41(15)	27(16)	207(17)	291(9)
O(11)	0.2749(6)	0.1660(2)	-0.1663(2)	1.00	313(20)	380(22)	175(18)	28(16)	81(15)	200(17)	286(9)
O(12)	0.7863(6)	0.0486(2)	-0.1655(2)	1.00	296(20)	353(21)	203(18)	-59(16)	-66(15)	207(16)	289(9)
O(13)	0.0367(7)	0.2615(1)	-0.1542(2)	1.00	431(22)	107(15)	164(16)	-10(13)	8(15)	-7(15)	235(8)
O(14)	0.9628(7)	0.0464(1)	0.1523(2)	1.00	486(23)	115(16)	172(17)	32(13)	27(16)	1(15)	258(8)
O(15)	-0.2133(6)	0.1660(2)	-0.1666(2)	1.00	279(19)	382(22)	178(18)	68(16)	-75(15)	-195(17)	285(9)
F(16)	-0.5	0.1064(2)	-0.25	0.50	222(19)	264(20)	172(19)	0	2(15)	0	220(8)

*Uij x 10^4 Å

POSITIONAL AND DISPLACEMENT PARAMETERS AND SITE OCCUPANCIES FOR RUS12

Atom	x	y	z	sof	*U_{11}	U_{22}	U_{33}	U_{23}	U_{13}	U_{12}	U_{eq}
Mn(1)	0.8500(1)	0.20620(5)	0.47875(6)	0.809(5)	89(3)	96(3)	107(3)	46(2)	17(2)	21(2)	97(2)
Na(1)	0.8500(1)	0.20620(5)	0.47875(6)	0.191(5)	89(3)	96(3)	107(3)	46(2)	17(2)	21(2)	97(2)
Mn(2)	0.27901(9)	0.06668(5)	0.48702(5)	0.974(3)	103(3)	113(3)	125(3)	57(2)	30(2)	30(2)	111(2)
Mn(3)	0.4223(1)	0.35220(5)	0.48391(5)	0.881(5)	103(3)	112(3)	133(3)	65(2)	34(2)	36(2)	110(2)
Mg(3)	0.4223(1)	0.35220(5)	0.48391(5)	0.119(5)	103(3)	112(3)	133(3)	65(2)	34(2)	36(2)	110(2)
Mn(4)	0	0.5	0.5	0.299(3)	90(5)	88(4)	105(5)	38(3)	10(3)	17(3)	97(3)
Mg(4)	0	0.5	0.5	0.201(3)	90(5)	88(4)	105(5)	38(3)	10(3)	17(3)	97(3)
Ti	0.0795(1)	0.08598(5)	0.19683(5)	0.948(4)	69(3)	94(3)	93(3)	41(2)	12(2)	21(2)	85(2)
Nb	0.0795(1)	0.08598(5)	0.19683(5)	0.052(4)	69(3)	94(3)	93(3)	41(2)	12(2)	21(2)	85(2)
Si(1)	0.6785(2)	0.27194(8)	0.23032(9)	1.00	89(4)	73(4)	86(4)	30(3)	9(3)	16(3)	86(2)
Si(2)	0.8128(2)	0.54570(8)	0.25292(9)	1.00	119(4)	85(4)	93(4)	40(3)	11(3)	15(3)	101(2)
Si(3)	0.3781(2)	0.67477(8)	0.25541(9)	1.00	119(4)	89(4)	104(4)	49(3)	12(3)	21(3)	104(2)
Si(4)	0.5081(2)	0.93072(8)	0.23432(9)	1.00	91(4)	92(4)	86(4)	48(3)	12(3)	21(3)	88(2)
K	0.1321(2)	0.2645(1)	0.9961(1)	0.885(4)							365(4)
Na	0.093(3)	0.186(2)	0.998(2)	0.115(4)							365(4)
Na	0.5	0	0	0.322(6)	192(9)	122(8)	83(8)	35(5)	6(5)	25(5)	140(6)
Ca	0.5	0	0	0.178(6)	192(9)	122(8)	83(8)	35(5)	6(5)	25(5)	140(6)
O(1)	0.7290(4)	0.3203(2)	0.3824(2)	1.00	121(11)	135(11)	89(11)	37(9)	31(9)	35(9)	118(5)
O(2)	0.1483(4)	0.1593(2)	0.3675(2)	1.00	135(11)	136(11)	104(12)	35(9)	18(9)	31(9)	131(5)
O(3)	0.1292(4)	0.3949(2)	0.5948(2)	1.00	104(11)	135(11)	95(11)	38(9)	3(9)	15(8)	119(5)
OH(4)	0.2935(5)	0.4627(2)	0.3980(2)	1.00	132(11)	146(11)	147(12)	62(10)	31(9)	36(9)	142(5)
OH(5)	0.9921(4)	0.1189(2)	0.5951(2)	1.00	126(11)	155(11)	158(13)	58(10)	28(10)	32(9)	150(5)
O(6)	0.5572(4)	0.2586(2)	0.5921(2)	1.00	113(11)	124(11)	113(12)	57(9)	16(9)	23(9)	116(5)
O(7)	0.5749(4)	0.0133(2)	0.3866(2)	1.00	116(11)	150(11)	85(11)	45(9)	12(9)	42(9)	118(5)
O(8)	0.0724(4)	0.5917(2)	0.2007(2)	1.00	143(12)	223(13)	137(13)	72(10)	20(10)	-19(10)	182(6)
O(9)	0.2460(5)	0.0417(3)	0.8296(3)	1.00	215(13)	246(14)	158(14)	25(11)	62(11)	-78(11)	250(6)
O(10)	0.4319(5)	0.4153(2)	0.7994(2)	1.00	196(12)	202(12)	141(13)	60(10)	15(10)	118(10)	174(5)
O(11)	0.1297(6)	0.8100(3)	0.8330(3)	1.00	352(15)	295(14)	184(14)	115(12)	100(12)	253(12)	240(6)
O(12)	0.2646(5)	0.9567(3)	0.1693(3)	1.00	294(14)	228(13)	157(13)	23(11)	-72(11)	170(11)	236(6)
O(13)	0.2665(5)	0.6074(2)	0.8089(2)	1.00	292(14)	102(11)	136(12)	50(9)	14(11)	16(10)	186(6)
O(14)	0.5721(5)	0.2222(2)	0.8031(3)	1.00	314(14)	109(11)	175(13)	84(10)	48(11)	41(10)	195(6)
O(15)	0.3807(5)	0.1906(3)	0.1672(3)	1.00	159(12)	310(15)	167(14)	119(12)	-37(10)	-106(11)	241(6)
F(16)	0	0	0	0.50	37(13)	67(13)	52(14)	27(11)	3(11)	31(10)	49(6)

*Uij x 10^4 Å

POSITIONAL AND DISPLACEMENT PARAMETERS AND SITE OCCUPANCIES FOR US5

Atom	x	y	z	sof	*U_{11}	U_{22}	U_{33}	U_{23}	U_{13}	U_{12}	U_{eq}
Fe(1)	0.8493(2)	0.2055(1)	0.4801(1)	0.891(8)	95(6)	89(6)	130(6)	53(5)	29(4)	18(4)	103(4)
Na(1)	0.8493(2)	0.2055(1)	0.4801(1)	0.109(8)	95(6)	89(6)	130(6)	53(5)	29(4)	18(4)	103(4)
Fe(2)	0.2801(2)	0.06747(9)	0.4893(1)	1.00	104(5)	111(5)	152(6)	69(4)	40(4)	23(4)	118(3)
Fe(3)	0.4226(2)	0.35234(9)	0.4862(1)	1.00	86(5)	96(5)	146(6)	57(4)	43(4)	29(4)	105(3)
Fe(4)	0	0.5	0.5	0.50	67(6)	75(7)	126(7)	27(6)	29(5)	17(5)	94(3)
Ti	0.0786(2)	0.08633(9)	0.1981(1)	0.769(7)	67(5)	74(5)	148(6)	54(4)	28(4)	10(3)	95(4)
Nb	0.0786(2)	0.08633(9)	0.1981(1)	0.231(7)	67(5)	74(5)	148(6)	54(4)	28(4)	10(3)	95(4)
Si(1)	0.6771(3)	0.2719(2)	0.2330(2)	1.00	130(9)	122(10)	125(10)	54(8)	28(7)	38(7)	125(4)
Si(2)	0.8154(3)	0.5468(2)	0.2546(2)	1.00	110(9)	93(9)	137(10)	34(8)	29(7)	25(7)	118(4)
Si(3)	0.3807(3)	0.6757(2)	0.2573(2)	1.00	128(9)	111(10)	123(10)	63(8)	19(7)	28(7)	118(4)
Si(4)	0.5081(3)	0.9337(2)	0.2371(2)	1.00	119(9)	102(10)	122(10)	59(8)	20(7)	22(7)	113(4)
K	0.1315(5)	0.2640(3)	0.9962(2)	0.929(9)	878(21)	652(19)	266(14)	117(12)	44(12)	145(14)	640(11)
Rb	0.1315(5)	0.2640(3)	0.9962(2)	0.071(9)	878(21)	652(19)	266(14)	117(12)	44(12)	145(14)	640(11)
Na	0.5	0	0	0.479(8)	351(28)	135(25)	126(25)	59(20)	23(19)	37(19)	209(15)
O(1)	0.7254(8)	0.3180(4)	0.3857(5)	1.00	120(22)	74(24)	138(26)	77(21)	9(19)	-4(18)	107(10)
O(2)	0.1471(8)	0.1615(4)	0.3730(5)	1.00	114(22)	90(24)	155(27)	74(22)	7(19)	-3(18)	119(10)
O(3)	0.1265(8)	0.3910(4)	0.5928(5)	1.00	84(21)	102(24)	158(26)	67(22)	35(19)	34(18)	108(10)
OH(4)	0.2982(9)	0.4625(4)	0.4010(5)	1.00	157(23)	71(24)	140(27)	65(22)	22(20)	35(19)	115(10)
OH(5)	0.9901(9)	0.1162(5)	0.5911(5)	1.00	143(23)	141(26)	127(27)	49(23)	23(20)	53(20)	137(10)
O(6)	0.5599(8)	0.2581(4)	0.5908(4)	1.00	85(21)	113(24)	104(25)	38(21)	-9(21)	5(18)	109(10)
O(7)	0.5733(8)	0.0165(4)	0.3898(5)	1.00	110(21)	115(25)	95(25)	35(21)	-13(18)	1(18)	117(10)
O(8)	0.0774(9)	0.5903(5)	0.2016(5)	1.00	161(24)	226(29)	174(29)	35(25)	25(21)	-5(21)	214(12)
O(9)	0.2452(11)	0.0410(6)	0.8252(5)	1.00	345(33)	445(40)	139(32)	-103(29)	126(27)	-272(29)	447(20)
O(10)	0.4263(9)	0.4128(5)	0.7979(5)	1.00	197(26)	258(31)	198(30)	86(26)	-21(22)	54(22)	226(12)
O(11)	0.1250(14)	0.8066(7)	0.8287(6)	1.00	771(48)	711(51)	232(36)	196(37)	226(35)	670(44)	482(20)
O(12)	0.2634(13)	0.9584(6)	0.1735(6)	1.00	686(45)	402(40)	163(33)	-36(31)	-205(31)	371(35)	446(19)
O(13)	0.2687(11)	0.6064(5)	0.8039(5)	1.00	556(38)	81(27)	163(30)	62(24)	29(27)	11(26)	279(14)
O(14)	0.5736(12)	0.2201(5)	0.7995(6)	1.00	595(39)	108(28)	269(34)	143(27)	49(29)	1(27)	323(15)
O(15)	0.3823(11)	0.1921(7)	0.1705(6)	1.00	277(30)	694(49)	177(33)	209(35)	-60(25)	-321(31)	462(20)
F(16)	0	0	0	0.50	187(29)	191(32)	158(33)	79(28)	6(24)	45(24)	180(13)
H(1)	0.27(2)	0.416(8)	0.309(1)	1.00							406(270)
H(1)	1.03(2)	0.143(8)	0.683(2)	1.00							343(272)

*Uij x 10^4 Å

POSITIONAL AND DISPLACEMENT PARAMETERS AND SITE OCCUPANCIES FOR MSH2

Atom	x	y	z	sof	*U_{11}	U_{22}	U_{33}	U_{23}	U_{13}	U_{12}	U_{eq}
Mn(1)	0.84974(9)	0.20565(4)	0.47864(5)	0.891(6)	98(3)	99(3)	123(3)	51(2)	26(2)	26(2)	105(2)
Na(1)	0.84974(9)	0.20565(4)	0.47864(5)	0.109(6)	98(3)	99(3)	123(3)	51(2)	26(2)	26(2)	105(2)
Mn(2)	0.27981(9)	0.06664(4)	0.48689(5)	0.994(3)	109(3)	113(3)	141(3)	62(2)	38(2)	33(2)	117(2)
Mn(3)	0.42217(9)	0.35146(4)	0.48358(5)	0.985(3)	110(3)	112(3)	148(3)	64(2)	41(2)	38(2)	118(2)
Mn(4)	0	0.5	0.5	0.477(4)	102(4)	90(3)	121(4)	39(2)	17(2)	23(2)	107(2)
Mg(4)	0	0.5	0.5	0.023(4)	102(4)	90(3)	121(4)	39(2)	17(2)	23(2)	107(2)
Ti	0.07888(9)	0.08599(5)	0.19615(5)	0.910(4)	80(3)	91(2)	106(3)	42(2)	20(2)	22(2)	93(2)
Nb	0.07888(9)	0.08599(5)	0.19615(5)	0.090(4)	80(3)	91(2)	106(3)	42(2)	20(2)	22(2)	93(2)
Si(1)	0.6782(2)	0.27155(7)	0.22990(8)	1.00	96(4)	78(3)	86(4)	28(3)	12(3)	15(3)	91(2)
Si(2)	0.8119(2)	0.54638(8)	0.25308(8)	1.00	110(4)	83(3)	113(3)	43(3)	19(3)	19(3)	103(2)
Si(3)	0.3770(2)	0.67531(8)	0.25548(8)	1.00	111(4)	93(3)	114(4)	53(3)	25(3)	23(3)	103(2)
Si(4)	0.5080(2)	0.93132(7)	0.23431(8)	1.00	97(4)	86(3)	85(4)	37(3)	15(3)	18(3)	90(2)
K	0.1320(2)	0.2634(1)	0.9950(1)	0.84(1)	564(8)	429(7)	279(6)	115(5)	49(5)	102(5)	444(4)
Na	0.1320(2)	0.2634(1)	0.9950(1)	0.16(1)	564(8)	429(7)	279(6)	115(5)	49(5)	102(5)	444(4)
Na	0.5	0	0	0.309(6)	190(8)	112(7)	80(7)	37(5)	13(5)	26(5)	132(5)
Ca	0.5	0	0	0.191(6)	190(8)	112(7)	80(7)	37(5)	13(5)	26(5)	132(5)
O(1)	0.7280(4)	0.3176(2)	0.3818(2)	1.00	130(10)	126(10)	90(10)	43(8)	15(8)	29(8)	118(4)
O(2)	0.1461(4)	0.1589(2)	0.3666(2)	1.00	135(10)	121(10)	92(10)	39(8)	10(8)	25(8)	121(4)
O(3)	0.1289(4)	0.3924(2)	0.5947(2)	1.00	117(10)	115(10)	114(10)	41(8)	16(8)	24(8)	119(4)
OH(4)	0.2977(4)	0.4629(2)	0.3974(2)	1.00	149(11)	136(11)	138(11)	57(9)	17(8)	38(9)	142(4)
OH(5)	0.9924(4)	0.1188(2)	0.5944(2)	1.00	132(11)	136(10)	134(11)	49(9)	17(8)	28(9)	139(4)
O(6)	0.5586(4)	0.2572(2)	0.5914(2)	1.00	140(10)	105(9)	98(10)	43(8)	20(8)	32(8)	115(4)
O(7)	0.5757(4)	0.0140(2)	0.3864(2)	1.00	134(10)	119(10)	77(9)	44(8)	14(8)	30(8)	111(4)
O(8)	0.0709(4)	0.5928(2)	0.2012(2)	1.00	152(11)	214(11)	151(11)	63(9)	43(9)	-9(9)	187(5)
O(9)	0.2472(5)	0.0414(2)	0.8297(2)	1.00	174(12)	240(12)	139(11)	28(9)	66(9)	-59(10)	220(5)
O(10)	0.4330(5)	0.4149(2)	0.7989(2)	1.00	218(12)	209(11)	156(11)	71(9)	26(9)	116(10)	187(5)
O(11)	0.1288(5)	0.8091(2)	0.8335(2)	1.00	333(14)	281(13)	143(11)	91(10)	82(10)	230(11)	224(5)
O(12)	0.2642(5)	0.9571(2)	0.1705(2)	1.00	274(13)	242(12)	144(11)	39(10)	-32(10)	162(11)	223(5)
O(13)	0.2658(5)	0.6068(2)	0.8068(2)	1.00	300(13)	109(10)	136(11)	54(9)	26(9)	22(9)	188(5)
O(14)	0.5721(5)	0.2214(2)	0.8019(2)	1.00	293(13)	104(9)	149(11)	64(9)	40(10)	24(9)	185(5)
O(15)	0.3811(5)	0.1910(2)	0.1664(2)	1.00	131(11)	283(13)	166(12)	101(10)	-23(9)	-78(9)	219(5)
F(16)	0	0	0	0.50	180(13)	137(11)	95(12)	38(10)	15(10)	36(10)	143(5)

*Uij x 10^4 Å

POSITIONAL AND DISPLACEMENT PARAMETERS AND SITE OCCUPANCIES FOR LAB3

Atom	*x*	*y*	*z*	*sof*	$^{*}U_{11}$	U_{22}	U_{33}	U_{23}	U_{13}	U_{12}	U_{eq}
Fe(1)	0.8501(1)	0.20583(5)	0.47990(5)	0.876(5)	130(3)	125(3)	175(3)	69(2)	39(2)	40(2)	140(2)
Na(1)	0.8501(1)	0.20583(5)	0.47990(5)	0.124(5)	130(3)	125(3)	175(3)	69(2)	39(2)	40(2)	140(2)
Fe(2)	0.2806(1)	0.06789(5)	0.48911(5)	0.956(2)	138(3)	143(3)	189(3)	82(2)	46(2)	50(2)	150(2)
Fe(3)	0.4227(1)	0.35217(5)	0.48551(5)	0.944(3)	134(3)	137(3)	196(3)	81(2)	47(2)	49(2)	149(2)
Fe(4)	0	0.5	0.5	0.436(3)	122(5)	118(4)	171(4)	61(3)	29(3)	31(3)	137(3)
Mg(4)	0	0.5	0.5	0.064(3)	122(5)	118(4)	171(4)	61(3)	29(3)	31(3)	137(3)
Ti	0.07953(9)	0.08683(4)	0.19795(5)	0.575(5)	107(3)	132(2)	180(3)	73(2)	31(2)	39(2)	136(2)
Zr	0.07953(9)	0.08683(4)	0.19795(5)	0.425(5)	107(3)	132(2)	180(3)	73(2)	31(2)	39(2)	136(2)
Si(1)	0.6785(2)	0.27350(9)	0.2323(1)	1.00	171(5)	115(4)	151(5)	48(4)	24(4)	35(4)	150(2)
Si(2)	0.8143(2)	0.54736(9)	0.2549(1)	1.00	164(5)	128(4)	174(5)	69(4)	25(4)	39(4)	154(2)
Si(3)	0.3785(2)	0.67503(9)	0.25728(9)	1.00	155(5)	132(4)	173(5)	73(4)	25(4)	43(4)	150(2)
Si(4)	0.5065(2)	0.93127(9)	0.2366(1)	1.00	164(5)	133(4)	143(5)	66(4)	27(4)	40(4)	154(2)
K	0.1338(3)	0.2666(1)	0.9958(1)	0.949(5)	925(14)	504(8)	341(7)	147(6)	71(7)	129(8)	616(6)
Na	0.5	0	0	0.379(6)	307(13)	196(10)	176(10)	66(7)	43(8)	57(8)	233(7)
Ca	0.5	0	0	0.121(6)	307(13)	196(10)	176(10)	66(7)	43(8)	57(8)	233(7)
O(1)	0.7272(5)	0.3188(2)	0.3842(2)	1.00	157(14)	164(12)	151(12)	69(10)	35(10)	46(10)	156(5)
O(2)	0.1486(5)	0.1623(2)	0.3746(2)	1.00	155(14)	196(12)	212(14)	79(11)	16(11)	49(10)	191(6)
O(3)	0.1272(5)	0.3917(2)	0.5930(2)	1.00	149(14)	175(12)	163(12)	72(10)	30(10)	49(10)	161(5)
OH(4)	0.2986(5)	0.4631(2)	0.4016(2)	1.00	158(14)	162(12)	213(14)	74(10)	36(11)	37(10)	180(5)
OH(5)	0.9892(5)	0.1164(2)	0.5922(2)	1.00	189(14)	168(12)	203(13)	88(10)	45(11)	51(10)	183(5)
O(6)	0.5602(5)	0.2574(2)	0.5896(2)	1.00	153(13)	187(12)	169(13)	70(10)	27(10)	51(10)	170(5)
O(7)	0.5728(5)	0.0145(2)	0.3890(2)	1.00	143(13)	146(11)	167(13)	64(10)	23(10)	28(10)	155(5)
O(8)	0.0740(5)	0.5912(3)	0.2030(3)	1.00	222(16)	289(14)	225(15)	87(12)	50(12)	3(12)	264(6)
O(9)	0.2493(7)	0.0416(3)	0.8262(3)	1.00	391(21)	497(20)	245(17)	-29(15)	168(15)	-242(16)	497(11)
O(10)	0.4276(6)	0.4132(3)	0.7968(3)	1.00	272(17)	342(15)	229(15)	112(13)	37(12)	163(13)	271(7)
O(11)	0.1287(8)	0.8057(3)	0.8302(3)	1.00	819(29)	678(23)	257(17)	217(17)	212(18)	634(23)	495(10)
O(12)	0.2664(7)	0.9566(3)	0.1723(3)	1.00	646(25)	460(19)	2683(18	-8(15)	-116(17)	429(19)	480(10)
O(13)	0.26754(7)	0.6050(2)	0.8046(3)	1.00	638(24)	141(13)	215(15)	100(11)	39(15)	56(14)	336(8)
O(14)	0.5727(7)	0.2208(2)	0.8003(3)	1.00	646(24)	145(13)	225(15)	86(12)	45(15)	30(14)	353(8)
O(15)	0.3873(6)	0.1927(3)	0.1686(3)	1.00	289(19)	636(23)	244(16)	178(16)	-70(14)	-274(16)	472(10)
F(16)	0	0	0	0.50	227(18)	213(15)	211(16)	95(13)	40(13)	69(13)	214(7)

$^{*}U$ij x 10^{4} Å

POSITIONAL AND DISPLACEMENT PARAMETERS AND SITE OCCUPANCIES FOR MSH3

Atom	*x*	*y*	*z*	*sof*	$^{*}U_{11}$	U_{22}	U_{33}	U_{23}	U_{13}	U_{12}	U_{eq}
Mn(1)	0.8503(2)	0.2060(1)	0.4786(1)	0.741(8)	62(6)	100(6)	127(7)	47(4)	27(4)	17(4)	97(4)
Na(1)	0.8503(2)	0.2060(1)	0.4786(1)	0.259(8)	62(6)	100(6)	127(7)	47(4)	27(4)	17(4)	97(4)
Mn(2)	0.2791(2)	0.06673(8)	0.48762(9)	1.011(5)	87(5)	106(5)	163(6)	59(4)	43(4)	23(3)	118(3)
Mn(3)	0.4229(2)	0.35239(8)	0.48466(9)	0.996(4)	81(5)	115(5)	145(6)	69(4)	46(4)	29(3)	107(3)
Zn(4)	0	0.5	0.5	0.383(4)	77(6)	106(6)	129(7)	43(5)	27(5)	16(4)	107(4)
Mg(4)	0	0.5	0.5	0.117(4)	77(6)	106(6)	129(7)	43(5)	27(5)	16(4)	107(4)
Ti	0.0775(1)	0.08393(7)	0.19176(8)	0.624(6)	47(4)	99(4)	181(5)	73(3)	37(3)	19(3)	104(3)
Nb	0.0775(1)	0.08393(7)	0.19176(8)	0.376(6)	47(4)	99(4)	181(5)	73(3)	37(3)	19(3)	104(3)
Si(1)	0.6796(3)	0.2732(1)	0.2315(2)	1.00	97(8)	82(7)	116(9)	42(6)	21(7)	15(6)	100(4)
Si(2)	0.8142(3)	0.5465(1)	0.2537(2)	1.00	88(8)	80(8)	147(10)	57(7)	30(7)	17(6)	102(4)
Si(3)	0.3799(3)	0.6752(1)	0.2564(2)	1.00	101(8)	88(8)	137(10)	53(7)	22(7)	14(6)	109(4)
Si(4)	0.5077(3)	0.9308(1)	0.2356(2)	1.00	87(8)	123(8)	106(9)	58(7)	36(7)	17(6)	103(4)
K1	0.1351(5)	0.2684(4)	0.9958(3)	0.833(8)							454(8)
K2	0.110(3)	0.216(2)	0.998(1)	0.167(8)							454(8)
Na	0.5	0	0	0.482(7)	364(27)	197(22)	86(22)	47(16)	8(18)	44(17)	229(14)
O(1)	0.7283(8)	0.3209(4)	0.3834(4)	1.00	114(21)	135(21)	156(26)	49(19)	38(18)	55(17)	135(9)
O(2)	0.1480(7)	0.1591(4)	0.3672(4)	1.00	98(20)	100(20)	153(25)	35(18)	21(18)	29(16)	123(9)
O(3)	0.1302(7)	0.3947(4)	0.5951(4)	1.00	69(20)	114(20)	134(24)	59(17)	46(17)	22(16)	103(9)
OH(4)	0.2935(8)	0.4625(4)	0.3988(4)	1.00	152(22)	106(20)	230(27)	99(19)	51(19)	49(17)	150(10)
OH(5)	0.9922(7)	0.1184(4)	0.5961(4)	1.00	106(21)	142(21)	167(26)	47(19)	20(18)	19(17)	148(10)
O(6)	0.5564(8)	0.2581(3)	0.5916(4)	1.00	134(21)	61(19)	174(26)	60(18)	36(18)	17(16)	121(9)
O(7)	0.5727(7)	0.0128(4)	0.3867(4)	1.00	124(21)	116(21)	125(23)	40(18)	61(18)	60(16)	118(9)
O(8)	0.0744(8)	0.5913(4)	0.2021(4)	1.00	113(21)	218(23)	158(26)	101(20)	30(19)	-8(17)	165(10)
O(9)	0.2444(9)	0.0417(4)	0.8270(5)	1.00	227(26)	304(27)	183(29)	-3(21)	132(22)	-183(21)	312(13)
O(10)	0.4293(8)	0.4150(4)	0.8002(4)	1.00	180(23)	218(23)	153(26)	78(20)	57(19)	110(19)	173(10)
O(11)	0.1264(10)	0.8074(5)	0.8299(5)	1.00	489(33)	460(32)	191(30)	163(25)	151(25)	418(28)	315(13)
O(12)	0.2627(10)	0.9565(5)	0.1715(5)	1.00	467(32)	286(28)	195(30)	-47(22)	-107(25)	310(25)	339(14)
O(13)	0.2643(9)	0.6070(4)	0.8085(4)	1.00	395(30)	132(23)	152(27)	21(20)	42(22)	34(21)	247(11)
O(14)	0.5724(9)	0.2225(4)	0.8029(4)	1.00	405(29)	130(22)	166(27)	82(20)	67(22)	44(20)	232(11)
O(15)	0.3834(9)	0.1933(5)	0.1691(5)	1.00	195(26)	478(32)	193(30)	193(25)	-68(22)	-233(22)	337(14)
F(16)	0	0	0	0.50	134(26)	281(29)	223(33)	137(25)	70(23)	82(22)	197(12)

$^{*}U$ij x 10^{4} Å

POSITIONAL AND DISPLACEMENT PARAMETERS AND SITE OCCUPANCIES FOR MSH8

Atom	x	y	z	sof	*U_{11}	U_{22}	U_{33}	U_{23}	U_{13}	U_{12}	U_{eq}
Mn(1)	0.85061(9)	0.20591(4)	0.47956(5)	0.863(5)	102(3)	107(3)	156(3)	63(2)	26(2)	27(2)	120(2)
Na(1)	0.85061(9)	0.20591(4)	0.47956(5)	0.137(5)	102(3)	107(3)	156(3)	63(2)	26(2)	27(2)	120(2)
Mn(2)	0.27913(8)	0.06742(4)	0.48742(5)	0.985(3)	114(2)	124(2)	176(3)	77(2)	45(2)	37(2)	132(2)
Mn(3)	0.42190(9)	0.35173(4)	0.48472(5)	0.974(2)	119(2)	125(2)	184(3)	84(2)	50(2)	47(2)	133(2)
Mn(4)	0	0.5	0.5	0.482(2)	94(3)	93(3)	150(3)	47(2)	15(2)	24(2)	115(2)
Ti	0.07634(7)	0.08332(3)	0.19010(4)	0.553(3)	86(2)	131(2)	196(2)	81(1)	32(1)	37(1)	133(1)
Nb	0.07634(7)	0.08332(3)	0.19010(4)	0.447(3)	86(2)	131(2)	196(2)	81(1)	32(1)	37(1)	133(1)
Si(1)	0.6789(2)	0.27321(7)	0.23102(8)	1.00	124(4)	90(4)	125(4)	41(3)	16(3)	22(3)	116(2)
Si(2)	0.8129(2)	0.54654(8)	0.25206(8)	1.00	177(4)	99(4)	145(4)	57(3)	19(3)	26(3)	142(2)
Si(3)	0.3775(2)	0.67402(8)	0.25469(8)	1.00	175(4)	115(4)	147(4)	71(3)	26(3)	32(3)	143(2)
Si(4)	0.5066(2)	0.93042(8)	0.23529(8)	1.00	134(4)	107(4)	112(4)	57(3)	21(3)	29(3)	116(2)
K	0.1376(2)	0.2716(1)	0.9956(1)	1.003(4)	744(9)	565(8)	368(6)	158(5)	69(6)	139(6)	582(5)
Na	0.5	0	0	0.449(6)	404(12)	209(10)	130(9)	52(7)	31(8)	60(8)	260(7)
Ca	0.5	0	0	0.051(6)	404(12)	209(10)	130(9)	52(7)	31(8)	60(8)	260(7)
O(1)	0.7277(4)	0.3191(2)	0.3833(2)	1.00	140(10)	148(10)	120(10)	50(8)	17(8)	27(8)	141(4)
O(2)	0.1467(4)	0.1597(2)	0.3680(2)	1.00	140(10)	174(11)	144(11)	58(9)	23(8)	33(8)	158(4)
O(3)	0.1300(4)	0.3930(2)	0.5952(2)	1.00	146(10)	117(10)	149(10)	55(8)	5(8)	26(8)	142(4)
OH(4)	0.2956(4)	0.4624(2)	0.3992(2)	1.00	161(11)	175(11)	180(11)	68(9)	39(9)	53(8)	173(5)
OH(5)	0.9932(4)	0.1177(2)	0.5937(2)	1.00	170(11)	194(11)	188(11)	89(9)	37(9)	63(9)	179(5)
O(6)	0.5586(4)	0.2580(2)	0.5914(2)	1.00	154(10)	141(10)	129(10)	58(8)	11(8)	24(8)	145(4)
O(7)	0.5727(4)	0.0131(2)	0.3874(2)	1.00	152(10)	137(10)	124(10)	52(8)	18(8)	40(8)	139(4)
O(8)	0.0715(5)	0.5912(2)	0.1997(2)	1.00	271(13)	320(14)	193(13)	80(11)	27(10)	-74(11)	300(6)
O(9)	0.2479(5)	0.0417(3)	0.8277(2)	1.00	263(13)	377(15)	202(13)	16(11)	96(11)	-169(11)	359(7)
O(10)	0.4299(5)	0.4155(2)	0.8006(2)	1.00	429(16)	310(14)	195(13)	83(11)	12(11)	216(12)	302(6)
O(11)	0.1274(6)	0.8063(3)	0.8316(2)	1.00	578(18)	508(17)	195(13)	167(12)	153(13)	453(15)	362(7)
O(12)	0.2634(5)	0.9559(3)	0.1718(2)	1.00	481(17)	356(15)	192(13)	15(11)	-77(12)	317(13)	349(7)
O(13)	0.2666(5)	0.6068(2)	0.8075(2)	1.00	489(16)	96(10)	192(12)	68(9)	39(11)	28(10)	268(6)
O(14)	0.5716(5)	0.2216(2)	0.8034(2)	1.00	504(17)	133(11)	213(13)	100(10)	39(12)	40(11)	285(6)
O(15)	0.3843(5)	0.1924(3)	0.1681(2)	1.00	216(13)	489(17)	230(13)	181(12)	-43(10)	-168(11)	356(7)
F(16)	0	0	0	0.50	230(14)	266(15)	188(14)	86(12)	37(11)	63(11)	233(6)

*Uij x 10^4 Å

POSITIONAL AND DISPLACEMENT PARAMETERS AND SITE OCCUPANCIES FOR MSH9

Atom	*x*	*y*	*z*	*sof*	$^{*}U_{11}$	U_{22}	U_{33}	U_{23}	U_{13}	U_{12}	U_{eq}
Mn(1)	0.8496(1)	0.20560(7)	0.47845(7)	0.860(5)	76(4)	91(4)	114(4)	51(3)	25(3)	27(3)	90(2)
Na(1)	0.8496(1)	0.20560(7)	0.47845(7)	0.140(5)	76(4)	91(4)	114(4)	51(3)	25(3)	27(3)	90(2)
Mn(2)	0.2797(1)	0.0666(7)	0.48678(7)	0.980(3)	92(4)	114(4)	127(4)	66(3)	42(3)	39(3)	103(2)
Mn(3)	0.4221(1)	0.35134(7)	0.48352(7)	0.973(3)	93(4)	115(4)	139(4)	71(3)	41(3)	41(3)	106(2)
Mn(4)	0	0.5	0.5	0.474(2)	71(5)	90(5)	105(5)	37(4)	14(4)	17(4)	92(3)
Ti	0.0791(1)	0.08608(7)	0.19615(7)	0.929(4)	49(4)	98(4)	101(4)	48(3)	16(3)	20(3)	81(2)
Nb	0.0791(1)	0.08608(7)	0.19615(7)	0.071(4)	49(4)	98(4)	101(4)	48(3)	16(3)	20(3)	81(2)
Si(1)	0.6784(2)	0.2716(1)	0.2299(1)	1.00	79(6)	76(6)	97(6)	38(5)	19(5)	25(5)	83(3)
Si(2)	0.8118(2)	0.5464(1)	0.2528(1)	1.00	105(6)	98(6)	107(6)	48(5)	18(5)	30(5)	101(3)
Si(3)	0.3771(2)	0.6752(1)	0.2555(1)	1.00	95(6)	97(6)	117(6)	63(5)	22(5)	29(5)	97(3)
Si(4)	0.5077(2)	0.9312(1)	0.2343(1)	1.00	85(6)	82(6)	91(6)	48(5)	21(5)	21(5)	82(3)
K	0.1311(3)	0.2630(2)	0.9953(1)	0.90(1)	508(11)	623(12)	265(9)	113(8)	48(8)	151(9)	493(6)
Na	0.1311(3)	0.2630(2)	0.9953(1)	0.10(1)	508(11)	623(12)	265(9)	113(8)	48(8)	151(9)	493(6)
Na	0.5	0	0	0.205(6)	153(10)	121(9)	77(8)	38(6)	13(6)	34(7)	120(6)
Ca	0.5	0	0	0.295(6)	153(10)	121(9)	77(8)	38(6)	13(6)	34(7)	120(6)
O(1)	0.7279(6)	0.3175(3)	0.3817(3)	1.00	106(16)	130(16)	94(15)	48(13)	27(13)	39(13)	108(7)
O(2)	0.1461(6)	0.1585(3)	0.3667(3)	1.00	137(16)	126(16)	92(15)	43(13)	38(13)	42(13)	117(7)
O(3)	0.1282(5)	0.3922(3)	0.5945(3)	1.00	89(15)	139(16)	94(15)	50(12)	15(12)	31(13)	107(6)
OH(4)	0.2976(6)	0.4626(3)	0.3967(3)	1.00	118(16)	137(16)	149(16)	64(13)	16(13)	23(13)	136(7)
OH(5)	0.9913(6)	0.1190(3)	0.5947(3)	1.00	113(16)	138(17)	141(16)	63(13)	34(13)	35(13)	129(7)
O(6)	0.5585(5)	0.2579(3)	0.5917(3)	1.00	87(15)	92(15)	113(15)	46(12)	3(12)	20(12)	98(6)
O(7)	0.5757(6)	0.0136(3)	0.3865(3)	1.00	112(16)	134(16)	94(15)	31(13)	30(13)	59(13)	114(7)
O(8)	0.0694(6)	0.5924(3)	0.2004(3)	1.00	162(17)	199(18)	168(17)	81(14)	51(14)	-9(14)	184(7)
O(9)	0.2456(6)	0.0410(3)	0.8291(3)	1.00	146(17)	238(19)	146(17)	49(14)	67(14)	-44(14)	202(8)
O(10)	0.4342(6)	0.4164(3)	0.7995(3)	1.00	203(18)	217(18)	143(17)	82(14)	32(14)	126(15)	174(7)
O(11)	0.1290(6)	0.8094(3)	0.8337(3)	1.00	258(19)	274(19)	145(17)	98(15)	81(15)	199(16)	198(8)
O(12)	0.2621(6)	0.9567(3)	0.1704(3)	1.00	240(19)	210(18)	116(16)	27(14)	-29(14)	142(15)	193(8)
O(13)	0.2650(6)	0.6068(3)	0.8062(3)	1.00	268(20)	128(17)	142(17)	55(14)	44(15)	41(15)	182(8)
O(14)	0.5699(6)	0.2210(3)	0.8025(3)	1.00	248(19)	132(17)	170(17)	91(14)	41(15)	37(15)	177(7)
O(15)	0.3812(6)	0.1908(3)	0.1669(3)	1.00	107(17)	295(20)	173(18)	138(15)	-10(14)	-62(15)	203(8)
F(16)	0	0	0	0.50	152(19)	138(19)	128(19)	51(15)	11(16)	51(16)	141(8)

$^{*}U$ij x 10^{4} Å

POSITIONAL AND DISPLACEMENT PARAMETERS AND SITE OCCUPANCIES FOR MSH15

Atom	*x*	*y*	*z*	*sof*	$^{*}U_{11}$	U_{22}	U_{33}	U_{23}	U_{13}	U_{12}	U_{eq}
Mn(1)	0.8504(2)	0.20567(9)	0.4786(1)	0.87(1)	104(7)	103(6)	165(6)	71(4)	40(4)	34(4)	118(4)
Na(1)	0.8504(2)	0.20567(9)	0.4786(1)	0.13(1)	104(7)	103(6)	165(6)	71(4)	40(4)	34(4)	118(4)
Mn(2)	0.2790(2)	0.06700(8)	0.48714(9)	1.014(6)	121(6)	132(6)	182(6)	84(4)	55(4)	47(4)	135(4)
Mn(3)	0.4220(2)	0.35166(9)	0.4839(1)	0.972(6)	104(6)	110(5)	176(6)	79(4)	52(4)	41(4)	120(4)
Mn(4)	0	0.5	0.5	0.415(7)	79(9)	62(7)	130(8)	41(6)	10(6)	10(6)	92(5)
Mg(4)	0	0.5	0.5	0.085(7)	79(9)	62(7)	130(8)	41(6)	10(6)	10(6)	92(5)
Ti	0.0773(1)	0.08376(7)	0.19167(8)	0.624(8)	75(5)	101(4)	203(5)	88(3)	44(3)	37(3)	115(3)
Nb	0.0773(1)	0.08376(7)	0.19167(8)	0.376(8)	75(5)	101(4)	203(5)	88(3)	44(3)	37(3)	115(3)
Si(1)	0.6794(3)	0.2729(1)	0.2312(2)	1.00	112(9)	81(7)	121(8)	57(6)	39(7)	33(6)	98(4)
Si(2)	0.8144(3)	0.5467(1)	0.2535(2)	1.00	132(9)	78(8)	152(9)	56(7)	21(7)	24(7)	119(4)
Si(3)	0.3792(3)	0.6750(2)	0.2563(2)	1.00	138(9)	98(8)	155(9)	83(7)	39(7)	40(7)	119(4)
Si(4)	0.5073(3)	0.9308(1)	0.2354(2)	1.00	106(9)	91(7)	105(8)	60(6)	21(6)	27(6)	95(4)
K	0.1337(5)	0.2667(2)	0.9957(2)	0.86(3)	737(21)	456(15)	283(13)	122(10)	60(11)	114(13)	515(10)
Na	0.1337(5)	0.2667(2)	0.9957(2)	0.14(3)	737(21)	456(15)	283(13)	122(10)	60(11)	114(13)	515(10)
Na	0.5	0	0	0.44(1)	434(29)	220(22)	146(21)	88(15)	26(17)	82(18)	267(16)
Ca	0.5	0	0	0.06(1)	434(29)	220(22)	146(21)	88(15)	26(17)	82(18)	267(16)
O(1)	0.7279(8)	0.3192(4)	0.3833(4)	1.00	110(23)	75(20)	167(23)	52(17)	9(18)	26(17)	118(9)
O(2)	0.1479(9)	0.1598(4)	0.3675(4)	1.00	133(24)	119(20)	126(22)	54(17)	9(18)	40(18)	125(9)
O(3)	0.1280(8)	0.3933(4)	0.5947(4)	1.00	117(24)	101(20)	142(21)	53(17)	4(18)	49(18)	118(9)
OH(4)	0.2958(9)	0.4637(4)	0.3999(4)	1.00	156(25)	118(21)	139(22)	50(18)	35(18)	60(18)	135(9)
OH(5)	0.9952(9)	0.1191(4)	0.5950(4)	1.00	218(27)	190(23)	147(23)	97(19)	42(19)	116(21)	165(10)
O(6)	0.5587(8)	0.2577(4)	0.5919(4)	1.00	109(23)	126(21)	145(22)	96(18)	44(18)	57(18)	109(9)
O(7)	0.5711(9)	0.0126(4)	0.3874(4)	1.00	148(24)	134(21)	145(22)	77(18)	57(18)	84(18)	127(9)
O(8)	0.0725(10)	0.5918(5)	0.2018(4)	1.00	240(29)	276(26)	130(23)	82(20)	30(20)	14(22)	228(11)
O(9)	0.2468(11)	0.0423(5)	0.8269(5)	1.00	264(31)	271(27)	148(24)	6(21)	124(22)	-160(23)	291(13)
O(10)	0.4281(9)	0.4139(5)	0.7999(4)	1.00	223(28)	247(25)	181(24)	70(20)	29(21)	133(22)	212(11)
O(11)	0.1276(12)	0.8071(5)	0.8312(5)	1.00	523(37)	387(31)	216(27)	154(24)	184(26)	394(30)	312(14)
O(12)	0.2615(12)	0.9554(6)	0.1723(5)	1.00	488(37)	393(32)	224(28)	29(24)	-54(26)	377(30)	364(15)
O(13)	0.2650(10)	0.6060(4)	0.8071(5)	1.00	407(33)	82(21)	200(25)	77(19)	17(22)	39(21)	231(11)
O(14)	0.5719(10)	0.2222(4)	0.8032(4)	1.00	369(32)	78(20)	165(24)	65(18)	29(22)	-24(20)	217(11)
O(15)	0.3834(10)	0.1930(6)	0.1693(5)	1.00	206(30)	461(34)	235(28)	199(26)	48(23)	-141(25)	326(14)
F(16)	0	0	0	0.50	221(31)	146(25)	165(27)	48(22)	-1(23)	40(23)	188(12)

$^{*}U$ij x 10^{4} Å

POSITIONAL AND DISPLACEMENT PARAMETERS AND SITE OCCUPANCIES FOR MSH15A

Atom	x	y	z	sof	$^{*}U_{11}$	U_{22}	U_{33}	U_{23}	U_{13}	U_{12}	U_{eq}
Mn(1)	0.85042(9)	0.20571(4)	0.47890(5)	0.856(5)	100(3)	97(3)	131(3)	54(2)	30(2)	27(2)	107(2)
Na(1)	0.85042(9)	0.20571(4)	0.47890(5)	0.144(5)	100(3)	97(3)	131(3)	54(2)	30(2)	27(2)	107(2)
Mn(2)	0.27929(8)	0.06722(4)	0.48745(4)	0.996(3)	104(2)	110(2)	147(3)	64(2)	44(2)	34(2)	115(2)
Mn(3)	0.42199(8)	0.35176(4)	0.48450(5)	0.970(3)	106(2)	112(2)	151(3)	72(2)	45(2)	41(2)	115(2)
Mn(4)	0	0.5	0.5	0.434(3)	90(3)	87(3)	121(4)	42(3)	21(2)	23(2)	100(2)
Mg(4)	0	0.5	0.5	0.066(3)	90(3)	87(3)	121(4)	42(3)	21(2)	23(2)	100(2)
Ti	0.07738(7)	0.08381(3)	0.19158(4)	0.594(4)	75(2)	102(2)	172(2)	74(1)	37(1)	29(1)	109(1)
Nb	0.07738(7)	0.08381(3)	0.19158(4)	0.406(4)	75(2)	102(2)	172(2)	74(1)	37(1)	29(1)	109(1)
Si(1)	0.6792(1)	0.27308(7)	0.23175(8)	1.00	118(4)	74(3)	96(4)	31(3)	20(3)	172(3)	100(2)
Si(2)	0.8137(2)	0.54643(7)	0.25341(8)	1.00	129(4)	82(3)	118(4)	47(3)	23(3)	23(3)	110(2)
Si(3)	0.3792(2)	0.67483(7)	0.25600(8)	1.00	128(4)	92(3)	120(4)	58(4)	26(3)	26(3)	110(2)
Si(4)	0.5071(2)	0.93097(7)	0.23585(8)	1.00	117(4)	85(3)	90(4)	46(3)	22(3)	26(3)	95(2)
K	0.1350(3)	0.2679(1)	0.9958(1)	0.976(4)	821(10)	491(7)	287(6)	123(5)	61(5)	117(6)	562(5)
Na	0.5	0	0	0.493(4)	370(13)	159(9)	110(10)	44(7)	18(8)	45(8)	224(6)
O(1)	0.7287(4)	0.3198(2)	0.3833(2)	1.00	140(10)	109(9)	90(10)	32(8)	21(8)	29(8)	117(4)
O(2)	0.1477(4)	0.1600(2)	0.3683(2)	1.00	134(10)	127(10)	116(10)	48(8)	29(8)	29(7)	128(4)
O(3)	0.1290(4)	0.3932(2)	0.5944(2)	1.00	121(10)	117(9)	111(10)	50(8)	30(8)	22(7)	117(4)
OH(4)	0.2957(4)	0.4628(2)	0.3996(2)	1.00	159(10)	148(10)	129(11)	57(9)	35(8)	36(8)	147(4)
OH(5)	0.9927(4)	0.1182(2)	0.5942(2)	1.00	167(11)	152(10)	135(11)	57(9)	36(8)	49(8)	151(4)
O(6)	0.5574(4)	0.2578(2)	0.5916(2)	1.00	134(10)	111(9)	113(10)	56(8)	24(8)	31(8)	117(4)
O(7)	0.5739(4)	0.0133(2)	0.3878(2)	1.00	152(10)	116(9)	86(10)	34(8)	20(8)	32(8)	122(4)
O(8)	0.0743(4)	0.5916(2)	0.2012(2)	1.00	175(11)	240(12)	163(12)	90(10)	51(9)	-8(9)	202(5)
O(9)	0.2460(5)	0.0415(3)	0.8268(2)	1.00	305(14)	361(14)	171(13)	-7(11)	127(11)	-178(11	361(7)
O(10)	0.4278(4)	0.4143(2)	0.7993(2)	1.00	242(12)	242(12)	162(12)	62(10)	27(9)	136(10)	211(5)
O(11)	0.1258(6)	0.8060(3)	0.8301(3)	1.00	639(20)	514(17)	162(13)	149(13)	166(13)	500(16)	370(7)
O(12)	0.2648(6)	0.9571(3)	0.1723(3)	1.00	539(18)	370(15)	164(13)	-10(11)	-100(12	367(14)	365(8)
O(13)	0.2665(5)	0.6068(2)	0.8069(2)	1.00	462(16)	88(9)	144(11)	59(9)	35(10)	33(9)	237(5)
O(14)	0.5715(5)	0.2216(2)	0.8029(2)	1.00	479(16)	102(10)	152(12)	64(9)	51(11)	37(10)	250(6)
O(15)	0.3839(5)	0.1926(3)	0.1692(2)	1.00	231(13)	507(17)	169(13)	154(13)	-63(100	-223(12	364(8)
F(16)	0	0	0	0.50	202(13)	188(12)	153(13)	64(11)	33(10)	47(10)	185(5)

$^{*}U_{ij} \times 10^{4}$ Å

POSITIONAL AND DISPLACEMENT PARAMETERS AND SITE OCCUPANCIES FOR MSH19A

Atom	*x*	*y*	*z*	*sof*	$^{*}U_{11}$	U_{22}	U_{33}	U_{23}	U_{13}	U_{12}	U_{eq}
Mn(1)	0.8507(1)	0.20565(5)	0.47928(6)	0.912(5)	124(3)	131(3)	186(3)	78(2)	44(2)	42(2)	142(2)
Na(1)	0.8507(1)	0.20565(5)	0.47928(6)	0.088(5)	124(3)	131(3)	186(3)	78(2)	44(2)	42(2)	142(2)
Mn(2)	0.2791(1)	0.06728(5)	0.48772(5)	0.986(3)	132(3)	150(3)	207(3)	94(2)	61(2)	49(2)	153(2)
Mn(3)	0.4220(1)	0.35164(5)	0.48418(6)	0.974(3)	132(3)	151(3)	208(3)	99(2)	66(2)	58(2)	150(2)
Fe(4)	0	0.5	0.5	0.427(3)	118(4)	114(4)	175(4)	60(3)	26(3)	34(3)	136(3)
Mg(4)	0	0.5	0.5	0.073(3)	118(4)	114(4)	175(4)	60(3)	26(3)	34(3)	136(3)
Ti	0.07749(9)	0.08461(5)	0.19302(5)	0.646(4)	114(2)	173(3)	228(3)	100(2)	48(2)	52(2)	164(2)
Nb	0.07749(9)	0.08461(5)	0.19302(5)	0.354(4)	114(2)	173(3)	228(3)	100(2)	48(2)	52(2)	164(2)
Si(1)	0.6794(2)	0.27273(9)	0.2310(1)	1.00	155(4)	126(4)	143(5)	53(4)	26(3)	39(3)	143(2)
Si(2)	0.8131(2)	0.54714(9)	0.2532(2)	1.00	221(5)	128(5)	172(5)	66(4)	33(4)	36(4)	176(2)
Si(3)	0.3776(2)	0.6745(1)	0.2558(1)	1.00	218(5)	151(5)	184(5)	95(4)	43(4)	48(4)	177(2)
Si(4)	0.5050(2)	0.93074(9)	0.2357(1)	1.00	158(4)	141(5)	156(5)	81(4)	38(3)	47(3)	145(2)
K	0.1389(3)	0.2695(1)	0.9957(1)	0.979(5)	761(11)	589(9)	392(8)	179(7)	76(7)	133(7)	602(6)
Na	0.5	0	0	0.417(7)	501(15)	276(13)	193(12)	88(9)	39(9)	100(10)	331(9)
Ca	0.5	0	0	0.083(7)	501(15)	276(13)	193(12)	88(9)	39(9)	100(10)	331(9)
O(1)	0.7275(5)	0.3184(2)	0.3830(2)	1.00	173(12)	195(12)	142(13)	75(11)	34(10)	48(10)	169(5)
O(2)	0.1483(5)	0.1610(2)	0.3708(2)	1.00	160(12)	218(13)	192(14)	92(11)	40(10)	61(10)	186(5)
O(3)	0.1288(4)	0.3919(2)	0.5941(2)	1.00	172(12)	158(12)	161(12)	72(10)	45(10)	44(9)	162(5)
OH(4)	0.2970(5)	0.4627(2)	0.4003(3)	1.00	197(12)	234(14)	206(14)	94(12)	62(10)	83(10)	207(6)
OH(5)	0.9924(5)	0.1175(3)	0.5930(3)	1.00	204(13)	235(14)	204(14)	91(12)	47(11)	81(11)	211(6)
O(6)	0.5602(5)	0.2577(2)	0.5911(2)	1.00	186(12)	171(12)	162(13)	91(11)	38(10)	48(10)	167(5)
O(7)	0.5724(5)	0.0137(2)	0.3879(2)	1.00	186(12)	180(13)	163(13)	70(11)	39(10)	57(10)	176(5)
O(8)	0.0738(6)	0.5918(3)	0.2008(3)	1.00	348(16)	401(19)	219(16)	99(15)	50(13)	-82(14)	367(8)
O(9)	0.2500(6)	0.0409(3)	0.8277(3)	1.00	316(16)	429(19)	250(17)	39(15)	114(13)	-149(14)	408(9)
O(10)	0.4297(6)	0.4140(3)	0.7992(3)	1.00	544(20)	366(18)	227(16)	79(14)	30(15)	272(16)	371(8)
O(11)	0.1232(7)	0.8043(3)	0.8305(3)	1.00	647(22)	598(23)	232(16)	198(17)	209(16)	516(19)	415(9)
O(12)	0.2614(6)	0.9557(3)	0.1726(3)	1.00	531(20)	432(19)	268(17)	31(15)	-92(15)	352(16)	420(9)
O(13)	0.2680(6)	0.6058(2)	0.8061(3)	1.00	570(20)	119(13)	233(15)	74(12)	41(14)	34(13)	321(7)
O(14)	0.5716(6)	0.2218(3)	0.8024(3)	1.00	588(20)	157(13)	247(16)	124(13)	85(14)	59(13)	326(7)
O(15)	0.3857(6)	0.1908(3)	0.1676(3)	1.00	246(15)	566(22)	277(17)	213(17)	-34(13)	-174(14)	409(9)
F(16)	0	0	0	0.50	279(17)	302(18)	232(18)	103(15)	48(14)	84(14)	274(7)

$^{*}U$ij x 10^{4} Å

POSITIONAL AND DISPLACEMENT PARAMETERS AND SITE OCCUPANCIES FOR MSH20

Atom	*x*	*y*	*z*	*sof*	$^{*}U_{11}$	U_{22}	U_{33}	U_{23}	U_{13}	U_{12}	U_{eq}
Mn(1)	0.84993(9)	0.20629(4)	0.47899(5)	0.873(5)	87(2)	99(2)	129(3)	56(2)	29(2)	26(2)	102(2)
Na(1)	0.84993(9)	0.20629(4)	0.47899(5)	0.127(5)	87(2)	99(2)	129(3)	56(2)	29(2)	26(2)	102(2)
Mn(2)	0.27976(8)	0.06671(4)	0.48719(4)	0.999(3)	90(2)	111(2)	143(2)	65(2)	41(2)	33(2)	109(1)
Mn(3)	0.42275(8)	0.35210(4)	0.48419(5)	0.992(3)	95(2)	109(2)	150(2)	71(2)	45(2)	39(2)	110(1)
Zn(4)	0	0.5	0.5	0.348(2)	88(3)	100(3)	129(3)	50(2)	20(2)	23(2)	106(2)
Mg(4)	0	0.5	0.5	0.152(2)	88(3)	100(3)	129(3)	50(2)	20(2)	23(2)	106(2)
Ti	0.07958(9)	0.08624(4)	0.19722(5)	1.00	57(2)	86(2)	86(2)	41(2)	18(2)	21(2)	74(1)
Si(1)	0.6786(1)	0.27147(7)	0.23011(8)	1.00	87(3)	89(3)	92(4)	40(3)	17(3)	24(3)	89(2)
Si(2)	0.8117(1)	0.54570(7)	0.25240(8)	1.00	100(4)	86(3)	116(4)	49(3)	19(3)	21(3)	100(2)
Si(3)	0.3771(1)	0.67495(7)	0.25508(8)	1.00	104(4)	93(3)	117(4)	57(3)	24(3)	26(3)	100(2)
Si(4)	0.5076(1)	0.93128(7)	0.23425(8)	1.00	90(3)	85(3)	91(3)	44(3)	20(3)	26(3)	86(1)
K	0.1338(2)	0.2648(1)	0.9957(1)	0.91(1)	517(7)	434(6)	247(5)	113(4)	47(4)	102(5)	417(4)
Na	0.1338(2)	0.2648(1)	0.9957(1)	0.09(1)	517(7)	434(6)	247(5)	113(4)	47(4)	102(5)	417(4)
Na	0.5	0	0	0.295(6)	176(7)	119(6)	84(6)	42(5)	17(4)	34(4)	129(4)
Ca	0.5	0	0	0.205(6)	176(7)	119(6)	84(6)	42(5)	17(4)	34(4)	129(4)
O(1)	0.7289(4)	0.3189(2)	0.3822(2)	1.00	115(9)	129(9)	94(10)	38(8)	11(8)	34(8)	117(4)
O(2)	0.1468(4)	0.1592(2)	0.3669(2)	1.00	121(10)	130(9)	110(10)	44(8)	21(8)	29(8)	124(4)
O(3)	0.1294(4)	0.3937(2)	0.5953(2)	1.00	108(9)	114(9)	132(10)	54(8)	30(8)	26(7)	118(4)
OH(4)	0.2943(4)	0.4629(2)	0.3984(2)	1.00	136(10)	134(9)	135(11)	54(8)	19(8)	33(8)	137(4)
OH(5)	0.9913(4)	0.1188(2)	0.5947(2)	1.00	141(10)	142(10)	145(110	56(9)	25(9)	44(8)	144(4)
O(6)	0.5583(4)	0.2580(2)	0.5920(2)	1.00	113(9)	101(9)	109(10)	41(8)	19(8)	23(7)	110(4)
O(7)	0.5752(4)	0.0138(2)	0.3867(2)	1.00	103(9)	116(9)	98(10)	36(8)	31(8)	34(7)	108(4)
O(8)	0.0710(4)	0.5921(2)	0.1999(2)	1.00	127(10)	237(11)	173(12)	86(10)	39(9)	-19(9)	191(5)
O(9)	0.2469(5)	0.0413(2)	0.8300(2)	1.00	174(11)	263(12)	154(11)	38(10)	80(9)	-66(9)	233(5)
O(10)	0.4326(4)	0.4159(2)	0.8004(2)	1.00	213(11)	216(11)	148(11)	56(9)	27(9)	128(9)	188(5)
O(11)	0.1276(5)	0.8089(2)	0.8326(2)	1.00	330(13)	310(13)	162(12)	111(10)	96(10)	252(11)	231(5)
O(12)	0.2624(5)	0.9564(2)	0.1700(2)	1.00	273(13)	236(11)	147(11)	20(9)	-29(10)	179(10)	224(5)
O(13)	0.2659(5)	0.6078(2)	0.8080(2)	1.00	320(13)	104(9)	147(11)	62(9)	36(10)	33(9)	193(5)
O(14)	0.5704(5)	0.2214(2)	0.8034(2)	1.00	335(13)	114(10)	175(12)	80(9)	47(10)	33(9)	207(5)
O(15)	0.3825(4)	0.1906(2)	0.1667(2)	1.00	136(11)	329(13)	149(11)	107(10)	-7(9)	-91(9)	233(5)
F(16)	0	0	0	0.50	167(12)	166(11)	82(11)	48(10)	5(9)	33(9)	143(5)
H(1)	0.25(1)	0.422(5)	0.306(4)	1.00							826(218)
H(2)	1.059(8)	0.154(3)	0.686(7)	1.00							252(110)

$^{*}U$ij x 10^{4} Å

POSITIONAL AND DISPLACEMENT PARAMETERS AND SITE OCCUPANCIES FOR MSH33A

Atom	*x*	*y*	*z*	*sof*	$^{*}U_{11}$	U_{22}	U_{33}	U_{23}	U_{13}	U_{12}	U_{eq}
Mn(1)	0.8500(2)	0.20625(9)	0.48069(9)	1.001(6)	81(5)	127(5)	168(4)	70(4)	34(4)	35(3)	121(3)
Fe(2)	0.2807(2)	0.06813(8)	0.48939(9)	0.960(5)	92(5)	127(5)	168(5)	69(4)	45(4)	35(4)	124(3)
Fe(3)	0.4231(2)	0.35255(9)	0.48621(9)	0.954(5)	101(5)	123(5)	179(5)	73(4)	51(4)	45(4)	127(3)
Fe(4)	0	0.5	0.5	0.438(6)	77(7)	88(7)	142(7)	45(5)	17(5)	19(5)	104(5)
Mg(4)	0	0.5	0.5	0.062(6)	77(7)	88(7)	142(7)	45(5)	17(5)	19(5)	104(5)
Ti	0.0787(1)	0.08663(7)	0.19725(7)	0.462(9)	64(4)	113(4)	168(4)	69(3)	33(3)	29(3)	110(3)
Zr	0.0787(1)	0.08663(7)	0.19725(7)	0.538(9)	64(4)	113(4)	168(4)	69(3)	33(3)	29(3)	110(3)
Si(1)	0.6784(3)	0.2739(1)	0.2325(2)	1.00	119(9)	72(8)	130(8)	40(6)	31(6)	12(6)	111(4)
Si(2)	0.8140(3)	0.5474(2)	0.2543(2)	1.00	118(9)	119(8)	153(8)	68(7)	20(7)	34(6)	127(4)
Si(3)	0.3778(3)	0.6744(2)	0.2564(2)	1.00	115(9)	130(9)	164(8)	74(7)	33(7)	43(6)	130(4)
Si(4)	0.5059(3)	0.9305(2)	0.2363(2)	1.00	109(9)	107(9)	129(8)	51(7)	26(6)	17(6)	117(4)
K	0.1360(5)	0.2704(2)	0.9956(2)	0.87(2)	867(23)	512(17)	301(13)	137(11)	69(12)	130(13)	585(11)
Na	0.1360(5)	0.2704(2)	0.9956(2)	0.13(1)	517(7)	434(6)	247(5)	113(4)	47(4)	102(5)	417(4)
Na	0.5	0	0	0.36(1)	241(19)	128(17)	112(15)	41(12)	31(11)	37(11)	166(11)
Ca	0.5	0	0	0.14(1)	241(19)	128(17)	112(15)	41(12)	31(11)	37(11)	166(11)
O(1)	0.7260(8)	0.3186(4)	0.3842(4)	1.00	104(22)	149(22)	121(20)	38(18)	26(17)	39(17)	130(9)
O(2)	0.1467(8)	0.1626(4)	0.3756(4)	1.00	65(21)	185(23)	199(23)	72(20)	25(17)	44(17)	151(9)
O(3)	0.1275(8)	0.3918(4)	0.5926(4)	1.00	83(22)	145(22)	144(21)	33(19)	37(17)	18(17)	135(9)
OH(4)	0.2995(9)	0.4637(4)	0.4027(4)	1.00	147(23)	104(22)	152(22)	-11(19)	16(18)	13(17)	160(10)
OH(5)	0.9921(9)	0.1170(4)	0.5934(4)	1.00	173(24)	178(23)	178(22)	115(20)	18(18)	72(18)	160(10)
O(6)	0.5611(8)	0.2578(4)	0.5888(4)	1.00	109(22)	115(21)	156(21)	37(18)	35(17)	28(17)	133(9)
O(7)	0.5721(8)	0.0136(4)	0.3879(4)	1.00	112(22)	118(21)	154(21)	48(18)	22(17)	43(16)	129(9)
O(8)	0.0718(9)	0.5908(5)	0.2021(5)	1.00	195(26)	305(28)	203(24)	55(22)	49(20)	-36(21)	269(12)
O(9)	0.2513(11)	0.0419(6)	0.8271(5)	1.00	288(31)	503(38)	199(26)	-53(26)	153(24)	-216(27)	447(18)
O(10)	0.4292(10)	0.4142(5)	0.7977(5)	1.00	310(30)	339(29)	177(24)	67(23)	25(21)	179(23)	274(12)
O(11)	0.1318(14)	0.8058(6)	0.8311(5)	1.00	776(48)	680(44)	235(28)	238(31)	242(30)	644(39)	461(18)
O(12)	0.2672(12)	0.9570(6)	0.1727(5)	1.00	584(41)	450(37)	227(28)	-73(28)	-173(28)	387(32)	463(18)
O(13)	0.2656(11)	0.6056(4)	0.8045(5)	1.00	575(39)	140(25)	203(25)	95(21)	72(25)	13(24)	314(13)
O(14)	0.5728(12)	0.2208(5)	0.8008(5)	1.00	581(40)	213(28)	229(27)	104(24)	70(26)	61(26)	347(14)
O(15)	0.3863(11)	0.1933(6)	0.1680(5)	1.00	329(32)	503(37)	244(28)	166(28)	-62(24)	-264(28)	431(17)
F(16)	0	0	0	0.50	172(28)	219(27)	193(27)	89(24)	30(22)	76(22)	190(12)
H(1)	0.20(1)	0.407(5)	0.318(3)	1.00							150
H(2)	0.868(10)	0.139(6)	0.546(6)	1.00							150

$^{*}U$ij x 10^{4} Å

POSITIONAL AND DISPLACEMENT PARAMETERS AND SITE OCCUPANCIES FOR MSH34

Atom	x	y	z	sof	*U_{11}	U_{22}	U_{33}	U_{23}	U_{13}	U_{12}	U_{eq}
Mn(1)	0.84970(8)	0.20633(4)	0.48079(5)	0.997(3)	105(2)	110(2)	156(2)	62(2)	32(2)	38(2)	120(2)
Fe(2)	0.28090(7)	0.06816(4)	0.48966(4)	0.970(3)	106(2)	115(2)	160(2)	68(2)	40(2)	42(2)	121(1)
Fe(3)	0.42292(7)	0.35267(4)	0.48662(4)	0.962(3)	110(2)	113(2)	164(2)	68(2)	42(2)	46(2)	122(1)
Fe(4)	0	0.5	0.5	0.461(3)	99(3)	95(3)	141(3)	47(2)	20(2)	35(2)	111(2)
Mg(4)	0	0.5	0.5	0.039(3)	99(3)	95(3)	141(3)	47(2)	20(2)	35(2)	111(2)
Ti	0.07884(7)	0.08690(4)	0.19810(4)	0.621(4)	80(2)	103(2)	145(2)	59(1)	27(1)	36(1)	105(1)
Zr	0.07884(7)	0.08690(4)	0.19810(4)	0.379(4)	80(2)	103(2)	145(2)	59(1)	27(1)	36(1)	105(1)
Si(1)	0.6780(1)	0.27320(7)	0.23265(8)	1.00	131(3)	93(3)	116(4)	36(3)	18(3)	30(3)	117(2)
Si(2)	0.8147(1)	0.54699(8)	0.25422(8)	1.00	125(3)	101(4)	137(4)	53(3)	23(3)	36(3)	119(2)
Si(3)	0.3791(1)	0.67501(8)	0.25657(8)	1.00	124(3)	106(4)	142(4)	64(3)	26(3)	38(3)	119(2)
Si(4)	0.5064(1)	0.93177(8)	0.23693(8)	1.00	132(3)	104(4)	113(4)	52(3)	24(3)	37(3)	114(2)
K	0.1355(3)	0.2694(1)	0.9956(1)	0.89(1)	849(10)	480(7)	292(6)	127(5)	56(5)	129(6)	565(5)
Na	0.1355(3)	0.2694(1)	0.9956(1)	0.11(1)	849(10)	480(7)	292(6)	127(5)	56(5)	129(6)	565(5)
Na	0.5	0	0	0.374(6)	265(9)	153(8)	102(8)	46(6)	13(5)	43(5)	180(6)
Ca	0.5	0	0	0.126(6)	265(9)	153(8)	102(8)	46(6)	13(5)	43(5)	180(6)
O(1)	0.7255(4)	0.3183(2)	0.3847(2)	1.00	143(9)	114(10)	114(10)	42(8)	24(7)	40(7)	125(4)
O(2)	0.1469(4)	0.1626(2)	0.3745(2)	1.00	140(9)	137(10)	185(11)	68(9)	17(8)	30(8)	156(4)
O(3)	0.1268(4)	0.3913(2)	0.5927(2)	1.00	140(9)	115(10)	127(10)	52(8)	22(7)	42(7)	126(4)
OH(4)	0.2986(2)	0.4623(2)	0.4016(2)	1.00	167(10)	140(10)	134(11)	48(9)	22(8)	47(8)	150(4)
OH(5)	0.9891(4)	0.1160(2)	0.5910(2)	1.00	165(10)	152(10)	166(11)	70(9)	31(8)	51(8)	159(4)
O(6)	0.5588(4)	0.2570(2)	0.5893(2)	1.00	133(9)	133(10)	142(10)	61(9)	29(7)	39(8)	134(4)
O(7)	0.5729(4)	0.0154(2)	0.3895(2)	1.00	154(9)	119(10)	114(10)	53(8)	21(7)	50(7)	126(4)
O(8)	0.0746(4)	0.5902(2)	0.2014(2)	1.00	201(11)	328(14)	170(12)	80(11)	47(9)	-8(10)	255(5)
O(9)	0.2485(5)	0.0411(3)	0.8267(3)	1.00	352(14)	451(17)	183(13)	-29(12)	129(11)	-212(12)	436(8)
O(10)	0.4258(4)	0.4130(2)	0.7985(2)	1.00	298(12)	340(14)	202(13)	94(11)	34(10)	201(11)	267(5)
O(11)	0.1293(6)	0.8059(3)	0.8305(3)	1.00	762(21)	623(21)	211(14)	195(14)	201(14)	616(18)	444(8)
O(12)	0.2656(6)	0.9573(3)	0.1719(3)	1.00	612(19)	419(17)	188(13)	-48(12)	-125(12)	408(15)	430(8)
O(13)	0.2676(5)	0.6066(2)	0.8049(2)	1.00	613(18)	121(11)	177(12)	73(10)	28(11)	48(11)	313(6)
O(14)	0.5735(6)	0.2199(2)	0.8007(2)	1.00	654(18)	120(11)	179(13)	74(10)	47(12)	48(11)	327(6)
O(15)	0.3850(5)	0.1927(3)	0.1688(3)	1.00	286(13)	593(20)	201(14)	187(14)	-60(10)	-231(13)	424(8)
F(16)	0	0	0	0.50	194(12)	179(13)	165(13)	63(11)	21(9)	55(10)	183(5)
H(1)	0.23(1)	0.413(5)	0.311(1)	1.00							705(182)
H(2)	1.03(1)	0.151(5)	0.6835(4)	1.00							719(188)

*Uij x 10^4 Å

POSITIONAL AND DISPLACEMENT PARAMETERS AND SITE OCCUPANCIES FOR MSH38A

Atom	*x*	*y*	*z*	*sof*	$^{*}U_{11}$	U_{22}	U_{33}	U_{23}	U_{13}	U_{12}	U_{eq}
Mn(1)	0.85031(8)	0.20574(4)	0.47956(4)	0.897(5)	108(2)	111(2)	141(3)	53(2)	30(2)	33(2)	119(2)
Na(1)	0.85031(8)	0.20574(4)	0.47956(4)	0.103(5)	108(2)	111(2)	141(3)	53(2)	30(2)	33(2)	119(2)
Mn(2)	0.27958(7)	0.06735(4)	0.48803(4)	0.995(3)	115(2)	131(2)	162(2)	69(2)	47(2)	43(2)	131
Mn(3)	0.42231(8)	0.35200(4)	0.48492(4)	0.985(3)	123(2)	127(2)	167(2)	72(2)	51(2)	50(2)	132(1)
Mn(4)	0	0.5	0.5	0.489(2)	101(3)	99(3)	137(3)	42(2)	19(2)	28(2)	115(2)
Ti	0.07825(7)	0.08504(4)	0.19447(4)	0.787(3)	90(2)	125(2)	168(2)	63(2)	35(1)	39(1)	125(1)
Nb	0.07825(7)	0.08504(4)	0.19447(4)	0.213(3)	90(2)	125(2)	168(2)	63(2)	35(1)	39(1)	125(1)
Si(1)	0.6785(1)	0.27211(7)	0.23113(7)	1.00	130(4)	101(3)	116(4)	36(3)	23(3)	30(3)	119(2)
Si(2)	0.8132(1)	0.54620(7)	0.25257(8)	1.00	169(4)	105(3)	135(4)	47(3)	23(3)	28(3)	140(2)
Si(3)	0.3783(1)	0.67446(7)	0.25518(8)	1.00	171(4)	118(3)	137(4)	60(3)	28(3)	37(3)	141(2)
Si(4)	0.5058(1)	0.93099(7)	0.23521(7)	1.00	135(4)	115(3)	112(4)	55(3)	27(3)	36(3)	118(2)
K	0.1365(2)	0.2679(1)	0.9958(1)	0.91(1)	710(8)	491(6)	319(6)	136(5)	67(5)	130(5)	527(4)
Na	0.1365(2)	0.2679(1)	0.9958(1)	0.09(1)	710(8)	491(6)	319(6)	136(5)	67(5)	130(5)	527(4)
Na	0.5	0	0	0.386(6)	394(10)	204(8)	138(8)	53(6)	30(6)	70(6)	256(6)
Ca	0.5	0	0	0.114(6)	394(10)	204(8)	138(8)	53(6)	30(6)	70(6)	256(6)
O(1)	0.7265(4)	0.3182(2)	0.3835(2)	1.00	146(9)	147(9)	115(10)	38(8)	18(7)	28(7)	144(4)
O(2)	0.1475(4)	0.1603(2)	0.3699(2)	1.00	159(10)	149(9)	122(10)	29(8)	26(7)	34(7)	154(4)
O(3)	0.1295(4)	0.3924(2)	0.5948(2)	1.00	150(10)	136(9)	117(9)	45(8)	24(7)	34(7)	138(4)
OH(4)	0.2970(4)	0.4624(2)	0.3998(2)	1.00	181(10)	182(10)	165(11)	62(8)	41(8)	60(8)	177(4)
OH(5)	0.9924(4)	0.1178(2)	0.5938(2)	1.00	191(10)	179(10)	165(11)	64(8)	46(8)	71(8)	177(4)
O(6)	0.5592(4)	0.2579(2)	0.5915(2)	1.00	168(10)	142(9)	122(10)	51(8)	26(8)	41(7)	146(4)
O(7)	0.5728(4)	0.0142(2)	0.3883(2)	1.00	160(9)	135(9)	113(9)	39(8)	18(7)	45(7)	140(4)
O(8)	0.0734(4)	0.5909(2)	0.1999(2)	1.00	264(12)	313(12)	178(12)	67(10)	40(9)	-41(10)	286(5)
O(9)	0.2494(5)	0.0408(2)	0.8281(2)	1.00	289(13)	377(14)	190(12)	17(10)	107(10)	-124(10)	354(6)
O(10)	0.4297(5)	0.4146(2)	0.8005(2)	1.00	395(14)	308(12)	180(12)	66(10)	45(10)	218(11)	286(5)
O(11)	0.1259(5)	0.8068(3)	0.8315(2)	1.00	581(17)	479(15)	214(13)	146(12)	163(12)	458(14)	364(6)
O(12)	0.2642(5)	0.9567(2)	0.1711(2)	1.00	475(13)	362(13)	212(13)	0(11)	-87(11)	314(12)	364(6)
O(13)	0.2681(5)	0.6070(2)	0.8071(2)	1.00	478(15)	111(9)	177(11)	60(8)	37(10)	33(9)	266(5)
O(14)	0.5720(5)	0.2217(2)	0.8032(2)	1.00	499(15)	137(9)	189(12)	84(9)	65(10)	53(10)	277(5)
O(15)	0.3843(4)	0.1910(3)	0.1674(2)	1.00	232(12)	487(15)	218(13)	162(12)	-35(10)	-178(11)	364(7)
F(16)	0	0	0	0.50	228(13)	230(12)	153(13)	53(10)	17(10)	48(10)	217(5)

$^{*}U$ij x 10^{4} Å

POSITIONAL AND DISPLACEMENT PARAMETERS AND SITE OCCUPANCIES FOR MSH42

Atom	*x*	*y*	*z*	*sof*	$^{*}U_{11}$	U_{22}	U_{33}	U_{23}	U_{13}	U_{12}	U_{eq}
Mn(1)	0.8511(3)	0.2057(2)	0.4794(2)	0.91(1)	26(9)	138(11)	163(11)	67(8)	27(7)	31(7)	106(6)
Na	0.8511(3)	0.2057(2)	0.4794(2)	0.09(1)	26(9)	138(11)	163(11)	67(8)	27(7)	31(7)	106(6)
Mn(2)	0.2790(3)	0.0680(2)	0.4871(1)	0.90(3)	38(8)	164(11)	174(10)	91(8)	44(6)	39(7)	115(6)
Zn(2)	0.2790(3)	0.0680(2)	0.4871(1)	0.10(3)	38(8)	164(11)	174(10)	91(8)	44(6)	39(7)	115(6)
Mn(3)	0.4211(3)	0.3512(2)	0.4844(1)	0.85(3)	43(8)	154(11)	185(10)	88(8)	43(6)	35(7)	119(6)
Zn(3)	0.4211(3)	0.3512(2)	0.4844(1)	0.15(3)	43(8)	154(11)	185(10)	88(8)	43(6)	35(7)	119(6)
Mn(4)	0	0.5	0.5	0.33(2)	13(10)	131(14)	166(13)	55(10)	20(8)	-4(9)	110(8)
Zn(4)	0	0.5	0.5	0.17(2)	13(10)	131(14)	166(13)	55(10)	20(8)	-4(9)	110(8)
Nb	0.0749(2)	0.0818(1)	0.1865(1)	0.90(1)	4(5)	133(6)	178(6)	77(5)	37(4)	26(4)	100(4)
Ti	0.0749(2)	0.0818(1)	0.1865(1)	0.10(1)	4(5)	133(6)	178(6)	77(5)	37(4)	26(4)	100(4)
Si(1)	0.6786(6)	0.2745(3)	0.2314(3)	1.00	68(14)	186(18)	154(16)	103(14)	45(11)	60(12)	120(7)
Si(2)	0.8133(6)	0.5470(3)	0.2526(3)	1.00	95(14)	136(17)	146(16)	76(14)	23(12)	24(13)	122(7)
Si(3)	0.3765(6)	0.6737(3)	0.2552(3)	1.00	89(15)	167(18)	149(16)	84(14)	9(11)	18(13)	133(7)
Si(4)	0.5070(5)	0.9296(3)	0.2362(3)	1.00	49(14)	108(16)	139(15)	47(14)	21(11)	18(12)	103(7)
K(1a)	0.097(6)	0.278(1)	0.995(1)	0.41(6)							433(17)
K(1b)	0.164(4)	0.2754(8)	0.9956(8)	0.48(6)							433(17)
Rb(1b)	0.164(4)	0.2754(8)	0.9956(8)	0.065							433(17)
Na	0.5	0	0	0.45	148(39)	200(46)	147(39)	46(33)	-11(28)	33(29)	179(24)
O(1)	0.728(1)	0.3194(7)	0.3832(7)	1.00	28(33)	226(45)	165(39)	102(37)	33(29)	73(32)	126(16)
O(2)	0.146(1)	0.1600(8)	0.3682(7)	1.00	134(40)	167(45)	176(41)	74(37)	21(32)	45(35)	158(17)
O(3)	0.130(1)	0.3931(7)	0.5949(6)	1.00							88(15)
OH(4)	0.295(1)	0.4631(8)	0.3991(7)	1.00	102(36)	210(44)	146(38)	84(36)	74(30)	114(34)	134(16)
OH(5)	0.993(1)	0.1179(7)	0.5944(7)	1.00	104(37)	133(42)	142(38)	23(35)	67(30)	13(32)	139(16)
O(6)	0.559(1)	0.2576(7)	0.5915(6)	1.00	24(32)	161(42)	107(36)	60(34)	24(28)	19(30)	96(16)
O(7)	0.573(1)	0.0134(7)	0.3865(7)	1.00	37(33)	74(39)	184(40)	61(34)	0(29)	-11(29)	102(16)
O(8)	0.072(2)	0.5915(8)	0.2004(7)	1.00	184(43)	284(52)	222(47)	91(43)	131(37)	36(39)	235(20)
O(9)	0.250(2)	0.043(1)	0.8260(9)	1.00	268(53)	597(76)	210(49)	30(51)	51(42)	-337(52)	486(33)
O(10)	0.433(2)	0.4144(8)	0.7988(7)	1.00	215(46)	359(57)	186(46)	98(44)	22(37)	116(42)	254(21)
O(11)	0.129(2)	0.803(1)	0.8297(9)	1.00	683(78)	595(75)	238(52)	182(55)	22(51)	534(67)	431(29)
O(12)	0.267(2)	0.954(1)	0.1723(9)	1.00	709(79)	516(72)	185(49)	-78(45)	-189(50)	526(65)	498(35)
O(13)	0.266(2)	0.6062(8)	0.8075(8)	1.00	508(63)	106(45)	140(41)	18(37)	35(39)	77(45)	266(22)
O(14)	0.571(2)	0.2206(8)	0.8024(8)	1.00	568(66)	88(45)	206(46)	58(40)	29(44)	-14(45)	311(24)
O(15)	0.385(2)	0.197(1)	0.1693(8)	1.00	308(55)	559(74)	240(50)	202(53)	-56(43)	-247(52)	431(30)
O(16)	0	0	0	0.50	76(52)	277(72)	213(62)	121(54)	65(42)	96(47)	172(35)

$^{*}U$ij x 10^{4} Å

APPENDIX D.

MÖSSBAUER SPECTROSCOPY DATA: VOIGT-BASED FITS AND RAW DATA

MOSSBAUER SPECTROSCOPY LOG FOR AGM

Ideal Mass: 48-55 mg in a 1.5° TVM
All doppler velocities: +/- 4.00 mm/s

File (detector)	Date Started	Date Finished	Sample	Mass (mg)	Description	Calibration File	Conditions	Total Counts
PCP001	Nov. 24th, 1997	Dec. 5th, 1997	MSH7	53.7	MSH astrophyllite	Pre: cal3cc49	RT: 21 C	1750000
(#3)					coarse-grained flakes up to 1.5 cm	Post: cal3cc50		
					crushed in isopropanol to a granulate			
					of approx. 60 mesh			
					1.5° TVM			
PCP003	Feb. 19th, 1998	Mar. 9th, 1998	MSH11	56.4 mg	MSH 'astrophyllite'	Pre: cal3cc54	RT: 21.7 C	1600000
(#3)					crushed in methanol	Post: cal3cc55		
					1.5 ° TVM (powder)			
PCP004	May 26th, 1998	June 1st, 1998	MSH10A	57.1 mg	MSH kupletskite	Pre: cal2jj14	RT: 22 C	1788418
(#2)					crushed in ethanol in mortar and	Post: cal3jj15		
					pestle			
					1.5° TVM (powder)			
PCP005	June 1st, 1998	June 11th, 1998	MSH10B	55.1 mg	MSH Nb-rich kupletskite	Pre: cal2jj15	RT: 21 C	2975797
(#2)					crushed in ethanol in mortar and	Post: cal2jj16		
					pestle			
					1.5° TVM (powder)			
PCP006	June 11th, 1998	June 24th, 1998	MSH20	54.4 mg	MSH Zn-rich kupletskite	Pre: cal2jj16	RT: 21.5 C	3927430
(#2)					ground slightly in ethanol	Post: cal2jj17		
					granulate in 1.5° TVM			
PCP007	July 17th, 1998	July 22nd, 1998	MSH30	47.9 mg	MSH astrophyllite	Pre: ovnfe58	RT: 22 C	3243165
(#1)					ground slightly in acetone	Post: ovnfe59		
					granulate in 1.5 ° TVM			
PCP008	July 17th, 1998	July 22nd, 1998	MSH32	48.6 mg	MSH astrophyllite	Pre: cal2jj20	RT: 22 C	1474801
(#2)					very needly crystals	Post: cal2jj21		
					ground slightly in acetone			
					coarse granulate in 1.5 ° TVM			
PCP009	Oct. 22nd, 1998	Oct. 30th, 1998	MSH18A	58.2 mg	MSH kupletskite	Pre: cal2jj29	RT: 22 C	1900000
(#2)					dark brown, coarse-grained xtals	Post: cal2jj30		
					ground under acetone			
					granulate in 1.5 ° TVM			
PCP010	Oct. 22nd, 1998	Oct. 30th, 1998	MSH18B	48.2 mg	MSH kupletskite	Pre: cal3cc69	RT: 22 C	1160000
(#3)					outer rim of MSH18A			
					ground slightly in acetone			
					granulate in 1.5° TVM			

File (detector)	Date Started	Date Finished	Sample	Mass (mg)	Description	Calibration File	Conditions	Total Counts
PCP011	Oct. 30th, 1998	Nov. 13, 1998	MSH28	50.5 mg	MSH astrophyllite	Pre: cal3cc69	RT: 20.75 C	1560000
(#3)					prepared on Oct. 9th, 1998	Post: cal3cc70		
					ground slightly in acetone			
					granulate in 1.5" TVM			
PCP012	Nov. 13th, 1998	Nov. 26th, 1998	MSH29	48.0 mg	MSH astrophyllite	Pre: cal3cc70	RT: 22 C	1430000
(#3)					ground slightly in acetone	Post: cal3cc71		
					granulate in 1.5" TVM			
PCP013	Dec. 22, 1998	Dec. 30th, 1998	MSH32	49.7 mg	finer grind of MSH32 (PCP008)	Pre: cal2jj40	RT : 21 C	1360000
(#2)					ground in acetone	Post: cal2jj41		
					coarse powder in 1.5" TVM			
PCP014	Dec. 28th, 1998	Dec. 30th, 1998	RUS5	46.8 mg	astrophyllite from Khibina	Pre: cal1ee33	RT: 21 C	1670000
(#1)					ground in acetone	Post: cal1ee34		
					coarse powder in 1.5" TVM			
PCP015	March 25th, 1999	March 29th, 1999	MSH10A	57.1 mg	MSH kupletskite	Pre: cal1ee54	RT : 22 C	1560000
(#1)					restirred TVM	Post: cal1ee55		
					identical to PCP004			
PCP016	March 29th, 1999	April 1st, 1999	MSH10B	55.1 mg	MSH Mn-niobo	Pre: calee55	RT : 22 C	1200000
(#1)					restirred TVM	Post: cal1ee57		
					identical to PCP005			
PCP017	March 1999	March 1999	MSH20	54.4 mg	kupletskite with *trace* Fe	none	RT : 22 C	none
PCP018					ground in acetone			(failed due to
PCP019								weak signal)
PCP020	April 21st, 1999	April 25th, 1999	MSH11	56.4 mg	restirred TVM	Pre: cal2jj55	RT: 22 C	1220000
(#2)					equivalent to PCP003	Post: cal2jj56		
PCP021	April 21st, 1999	April 25th, 1999	MSH28	50.5 mg	restirred TVM	Pre: cal3cc86	RT: 22 C	230000
(#3)					equivalent to PCP011	Post: cal3cc87		
PCP022	April 25th, 1999	May 2nd, 1999	MSH15	50.2 mg	Nb-rich kupletskite	Pre: cal2jj56	RT: 22 C	2307687
(#2)					ground in acetone	Post: cal2jj57		
					medium grained powder in 1.5" TVM			
PCP023	April 25th, 1999	May 2nd, 1999	RUS4	50.5 mg	astrophyllite from Khibina	Pre: cal3cc87	RT: 22 C	544688
(#3)					ground in acetone	Post: cal3cc88		
					medium grained powder in 1.5" TVM			
PCP024	May 2nd, 1999	May 6th, 1999	MSH18A	58.2 mg	kupletskite, core of MSH18	Pre: cal2jj57	RT: 22.5 C	1320000
(#2)					restirred (equivalent to PCP009)	Post: cal2jj58		
PCP025	May 2nd, 1999	May 13th, 1999	MSH7	53.7 mg	restirred (equivalent to PCP001)	Pre: cal3cc88	RT: 22.5 C	779548
(#3)						Post: cal3cc89		

File (detector)	Date Started	Date Finished	Sample	Mass (mg)	Description	Calibration File	Conditions	Total Counts
PCP026	May 6th, 1999	May 13th, 1999	MSH18B	48.2 mg	fibrous overgrowths of MSH18	Pre: cal2jj58		2777512
(#2)					ground in acetone	Post: cal2jj59		
					1.5° TVM			
PCP027	May 19th, 1999	May 30th, 1999	MSH10A	57.1 mg	restirred (2nd time)			874250
AM01-AM09	May 13th, 1999	June 21st, 1999	MSH10A	107.5 mg	mosaic of plates on (001)		RT: 22 C	
(#1)			Mosaic					
AM01	May 13th, 1999	May 16th, 1999			theta: 0, phi: 0	Pre: cal1ee64		1691312
						Post: cal1ee65		
AM02	May 16th, 1999	May 19th, 1999			theta: 15, phi: 0	Pre: cal1ee65		1566404
						Post: cal1ee66		
AM03	May 19th, 1999	May 22nd, 1999			theta: 30, phi: 0	Pre: cal1ee66		1720000
						Post: cal1ee67		
AM04	May 22nd, 1999	May 26th, 1999			theta: 45, phi: 0	Pre: cal1ee67		2010000
AM05	May 26th, 1999	May 30th, 1999			theta: 55, phi: 0	none		905568
AM06	May 30th, 1999	June 3rd, 1999			theta: 60, phi: 0	none		1570429
AM07	June 3rd, 1999	June 14th, 1999			theta: 75, phi: 0	none		2370286
AM08	June 14th, 1999	June 17th, 1999			theta: 55, phi: 30	none		598153
AM09	June 17th, 1999	June 21st, 1999			theta: 55, phi: 60	Post: cal1ee68		1886110
AMTVM	Nov. 4th, 1999	Nov. 18th, 1999	MSH10A	52.2 mg	1.5° TVM of material from	Pre: cal3cc93	RT: 22 C	751 967
(#3)					mosaic mount	Post: cal3cc94		
PCP028	Nov. 18th, 1999	Dec. 2nd, 1999	US5	51.3 mg	astrophyllite from Pike's Peak	Pre: cal3cc94	RT: 22 C	500000
(#3)					1.5° TVM	Post: cal3cc95		
					ground in acetone, coarse powder			
PCP029	Dec. 2nd, 1999	Dec. 18th, 1999	NOR9	50.5 mg	astrophyllite from Langesundsfjord	Pre: cal3cc95	RT: 22 C	646547
(#3)					1.5° TVM	Post: cal3cc96		
					ground in acetone, coarse powder			
PCP030	Dec. 18th, 1999	Dec. 27th, 1999	US2	50.6 mg	astrophyllite from Pike's Peak	Pre: cal3cc96	RT: 21 C	350000
(#3)					1.5° TVM	Post: cal3cc97		
					ground in acetone, coarse powder			
PCP031	Jan. 7th, 2000	Jan. 14th, 2000	MSH33	50.8 mg	astrophyllite from MSH	Pre: none	RT: 21 C	231905
(#3)					slightly elongate crystals	Post: cal3cc98		
					1.5° TVM			
					ground in acetone, coarse powder			
PCP032	Jan. 10th, 2000	Jan. 14th, 2000	NOR1	51.0 mg	astrophyllite from Langesundsfjord	Pre: cal2jj93	RT: 21 C	784558
(#2)					1.5° TVM	Post: cal2jj94		
					ground in acetone, coarse powder			
PCP033	Jan. 14th, 2000	Jan. 17th, 2000	MSH6	50.8 mg	kupletskite from MSH, 1.5° TVM	Pre: cal2jj94	RT: 21 C	554124
(#2)					ground in acetone, coarse powder	Post: cal2jj95		

File (detector)	Date Started	Date Finished	Sample	Mass (mg)	Description	Calibration File	Conditions	Total Counts
PCP034	Jan. 14th, 2000	Jan. 17th, 2000	MSH34A	50.8 mg	kpt/ust from MSH	Pre: cal3oc98	RT: 21 C	110924
(#3)					1.5° TVM	Post: cal3oc99		
					ground in acetone, coarse powder			
PCP035	Jan. 17th, 2000	Jan. 21st, 2000	MSH20#2	50.7 mg	second sample of MSH20	Pre: cal2jj95	RT: 21 C	733183
(#2)					1.5° TVM	Post: cal2jj96		
					ground in acetone, coarse powder			
PCP036	Jan. 17th, 2000	Jan. 21st, 2000	RUS8	51.5 mg	astrophyllite from Khibina	Pre: cal3oc99	RT: 21 C	151560
(#3)					1.5° TVM	Post: cal3dd00		
					ground in acetone, coarse powder			
PCP037	Jan. 21st, 2000	Jan. 24th, 2000	CC2a	35.2 mg	astrophyllite from Greenland	Pre: cal3dd00	RT: 21 C	140000
(#3)					1.5° TVM	Post: cal3dd01		
					ground in acetone, coarse powder			
PCP038	Jan. 21st, 2000	Jan. 24th, 2000	CC7I	29.5 mg	kpt/ust from Greenland	Pre: cal2jj95	RT: 21 C	670000
(#2)					1.5° TVM	Post: cal2jj96		
					ground in acetone, coarse powder			
PCP039	Jan. 24th, 2000	Feb. 2nd, 2000	MSH26A	48.3 mg	kupletskite from MSH	Pre: cal1oc88	RT: 21 C	340000
(#1)					1.5° TVM	Post: cal1oc89		
					ground in acetone, coarse powder			
PCP040	Feb. 2nd, 2000	Feb. 8th, 2000	MSH26B	49.4 mg	fibrous overgrowths of MSH26	Pre: cal1oc89	RT: 21 C	180000
(#1)					1.5° TVM	Post: cal1oc90		
					ground in acetone, coarse powder			
PCP041	Feb. 8th, 2000	Feb. 14th, 2000	RUS7	48.2 mg	astrophyllite from Khibina	Pre: cal1oc90	RT: 21 C	220000
(#1)					1.5° TVM	Post: cal1oc91		
					ground in acetone, coarse powder			
PCP042	Feb. 14th, 2000	Feb. 28th, 2000	MSH35	49.7 mg	kupletskite from MSH	Pre: cal1oc91	RT: 21 C	480774
(#1)					1.5° TVM	Post: cal1oc92		
					ground in acetone, coarse powder			

VBF Analysis of Pcp001T7

project:
document: 001qsdt707
data document: Pcp001T7

Fit Summary
no. of data points: 512
no. of QSD sites in model: 2
no. of parameters in model: 25
no. of refined parameters: 18
reduced χ^2 = 1.57688
uncertainties calculated using the covariance matrix

Global Parameters
Background = 3513230(230) counts
Lorentzian HWHM = 0.097* mm/s

Site Distribution Parameters

	δ_0 (mm/s)	δ_1	A (counts·mm/s)	A_1/A_2
Fe3+	0.600(19)	0*	14960(900)	1*
Fe2+	1.14222(43)	0*	599100(1500)	1*

		p (%)	$\langle\Delta\rangle$ (mm/s)	σ_Δ (mm/s)
Fe3+	comp 1	49.3587*	0(20)	0(17)
	comp 2	50(840)	0.56(62)	0.15(66)
Fe2+	comp 1	44.1364*	2.509(19)	0.177(14)
	comp 2	22(11)	2.097(80)	0.237(55)
	comp 3	34(14)	2.321(37)	0.419(40)

Compiled Site Properties

	Site Populations
Fe3+	2.44(14)
Fe2+	97.56(14)

	<CS> (mm/s)	<|Δ|> (mm/s)	stdev(|Δ|) (mm/s)	skew(|Δ|)
Fe3+	0.600051	0.392162	0.231852	0.0646397
Fe2+	1.14222	2.35584	0.33373	-0.308745

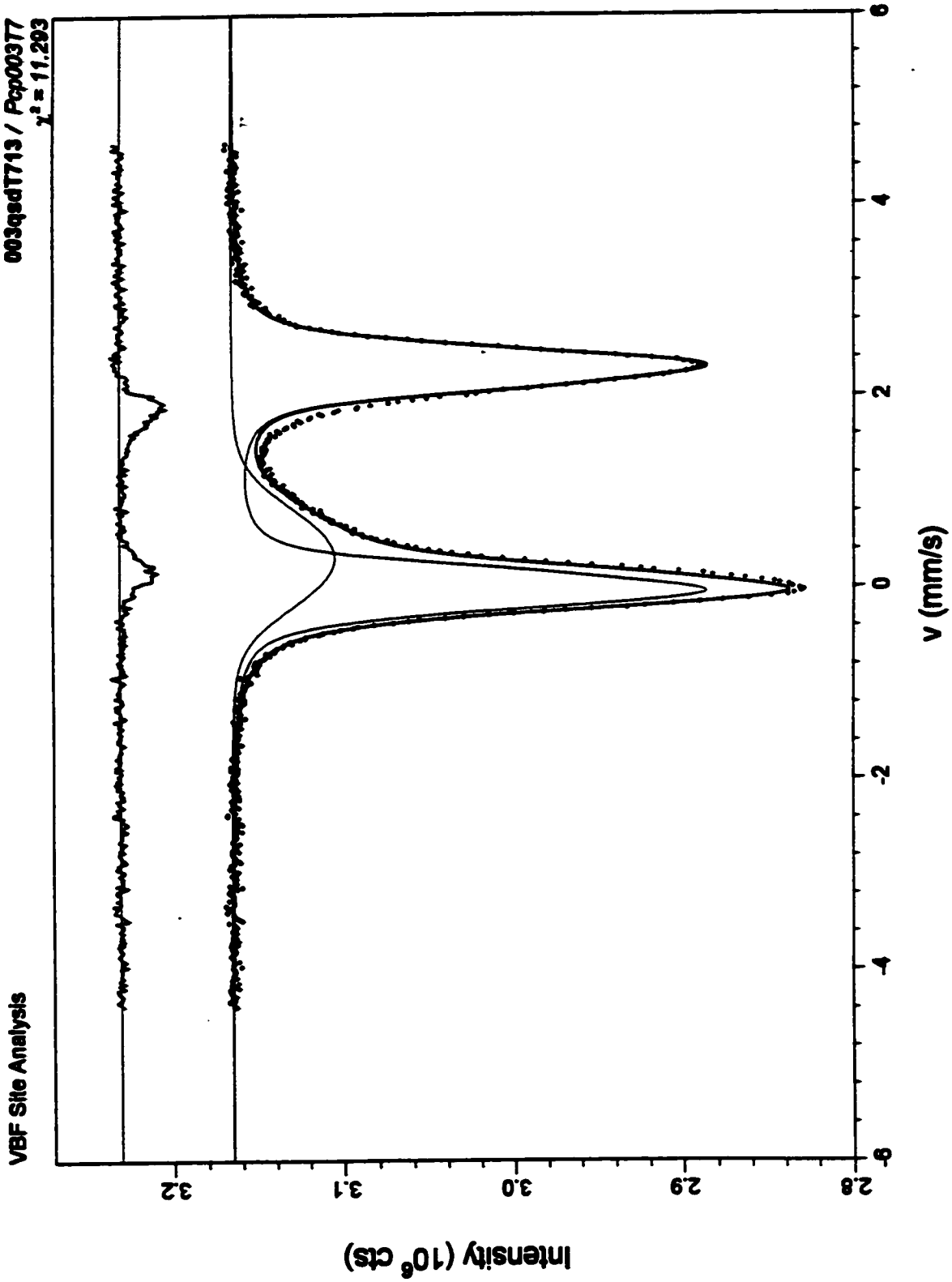
003qsdT713 / Pcp00377
χ² = 11.293
VBF Site Analysis
Intensity (10⁶ cts)
3.2
3.1
3.0
2.9
2.8
-6
-4
-2
0
2
4
6
v (mm/s)

VBF Analysis of Pcp003T7

project:
document: 003qsdT713
data document: Pcp003T7

Fit Summary
no. of data points: 512
no. of QSD sites in model: 3
no. of parameters in model: 32
no. of refined parameters: 8
reduced $\chi^2 = 2.31846$
uncertainties calculated using the covariance matrix

Global Parameters
Background = 3165930(200) counts
Lorentzian HWHM = 0.097* mm/s

Site Distribution Parameters

	δ_0 (mm/s)	δ_1	A (counts·mm/s)	A_1/A_0
[6]Fe3+	0.3000(55)	0*	80300(1200)	1*
[6]Fe2+	1.13022*	0*	336313*	1*
QSD site 3	0.986925*	0*	25812.5*	1*

		p (%)	⟨Δ⟩ (mm/s)	σ_Δ (mm/s)
[6]Fe3+	comp 1	15.8518*	0(70000)	0(20000)
	comp 2	0(2e+08)	0(13000)	0(3800)
[6]Fe2+	comp 1	68.1173*	2.42259*	0.267287*
	comp 2	19.8682*	1.91615*	0.145789*
	comp 3	12.0145*	2.32153*	0.126781*
QSD site 3	comp 1	100*	1.75455*	0.258174*

Compiled Site Properties

	Site Populations
[6]Fe3+	18.16(23)
[6]Fe2+	76.01(21)
QSD site 3	5.834(16)

	<CS> (mm/s)	<|Δ|> (mm/s)	stdev(|Δ|) (mm/s)	skew(|Δ|)
[6]Fe3+	0.299973	0.683886	0.494907	0.843847
[6]Fe2+	1.13022	2.30983	0.307064	0.0137374
QSD site 3	0.986925	1.75455	0.258174	2.06248e-10

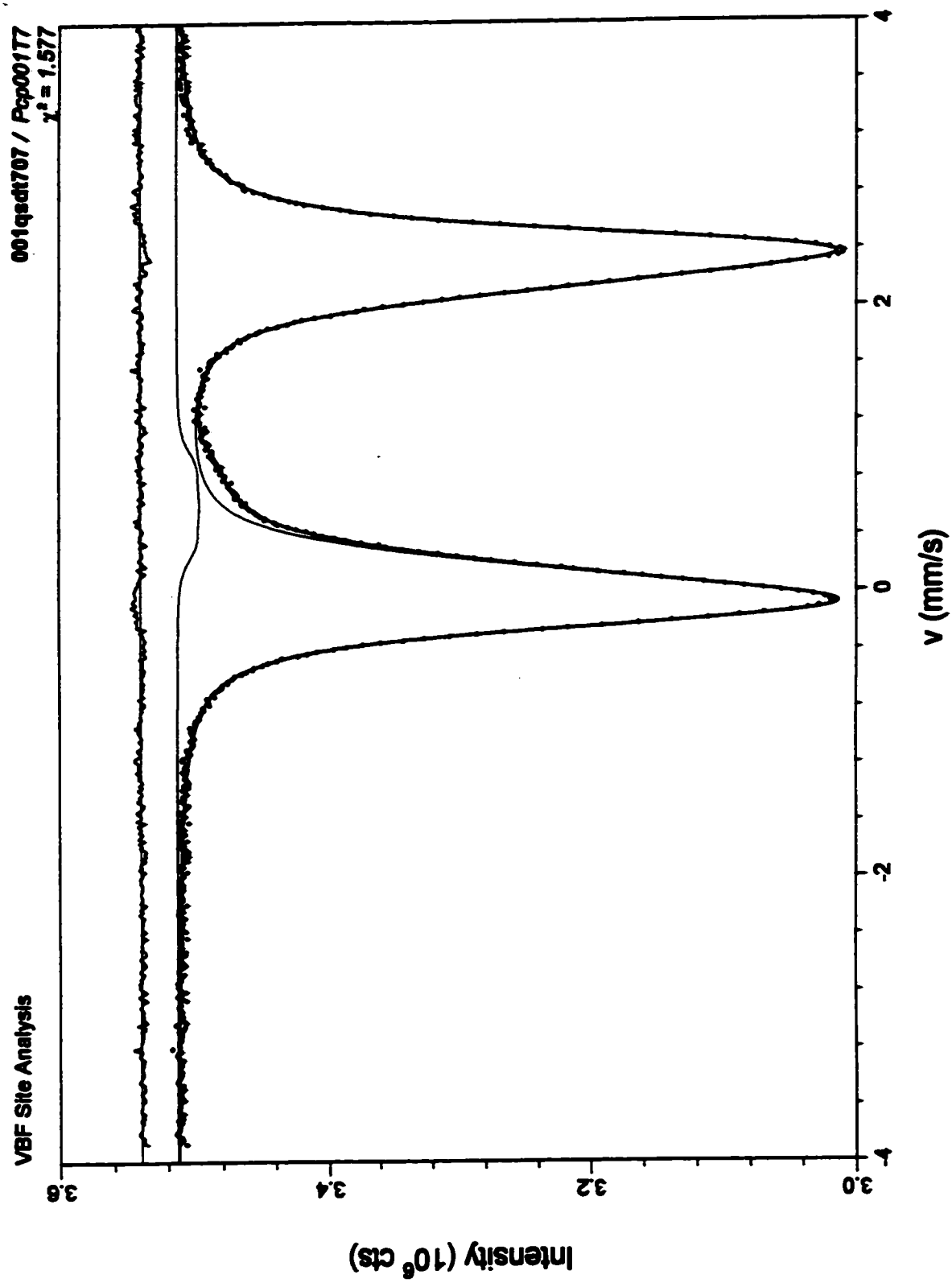
001qsdt707 / Pcp00177
χ² = 1.577
VBF Site Analysis
Intensity (10⁶ cts)
3.0
3.2
3.4
3.6
-4
-2
0
2
4
v (mm/s)

VBF Analysis of Pcp004T7

project:
document: 004qsdT706
data document: Pcp004T7

Fit Summary
no. of data points: 512
no. of QSD sites in model: 3
no. of parameters in model: 32
no. of refined parameters: 20
reduced χ^2 = 1.59758
uncertainties calculated using the covariance matrix

Global Parameters
Background = 3580700(250) counts
Lorentzian HWHM = 0.097* mm/s

Site Distribution Parameters

	δ_0 (mm/s)	δ_1	A (counts·mm/s)	A_-/A_+
Fe2+ [VI]B	1.139(12)	0*	226900(8700)	1*
Fe3+ [VI]B	0.313(11)	0*	98600(1400)	1*
QSD site 3	0.908(63)	0*	27200(9100)	1*

		p (%)	$\langle\Delta\rangle$ (mm/s)	σ_Δ (mm/s)
Fe2+ [VI]B	comp 1	18.5306*	1.979(73)	0.157(56)
	comp 2	2.8(86)	3.1(11)	0.33(52)
	comp 3	79(25)	2.406(53)	0.254(59)
Fe3+ [VI]B	comp 1	47.4419*	0.409858*	0.77(10)
	comp 2	53(14)	0.823083*	0.445(48)
QSD site 3	comp 1	100*	1.91(21)	0.296(81)

Compiled Site Properties

	Site Populations
Fe2+ [VI]B	64.3(19)
Fe3+ [VI]B	28.0(10)
QSD site 3	7.7(24)

	<CS> (mm/s)	<|Δ|> (mm/s)	stdev(|Δ|) (mm/s)	skew(|Δ|)
Fe2+ [VI]B	1.13913	2.34684	0.319696	0.423753
Fe3+ [VI]B	0.31323	0.768893	0.476296	0.579145
QSD site 3	0.908356	1.91135	0.295781	1.87248e-09

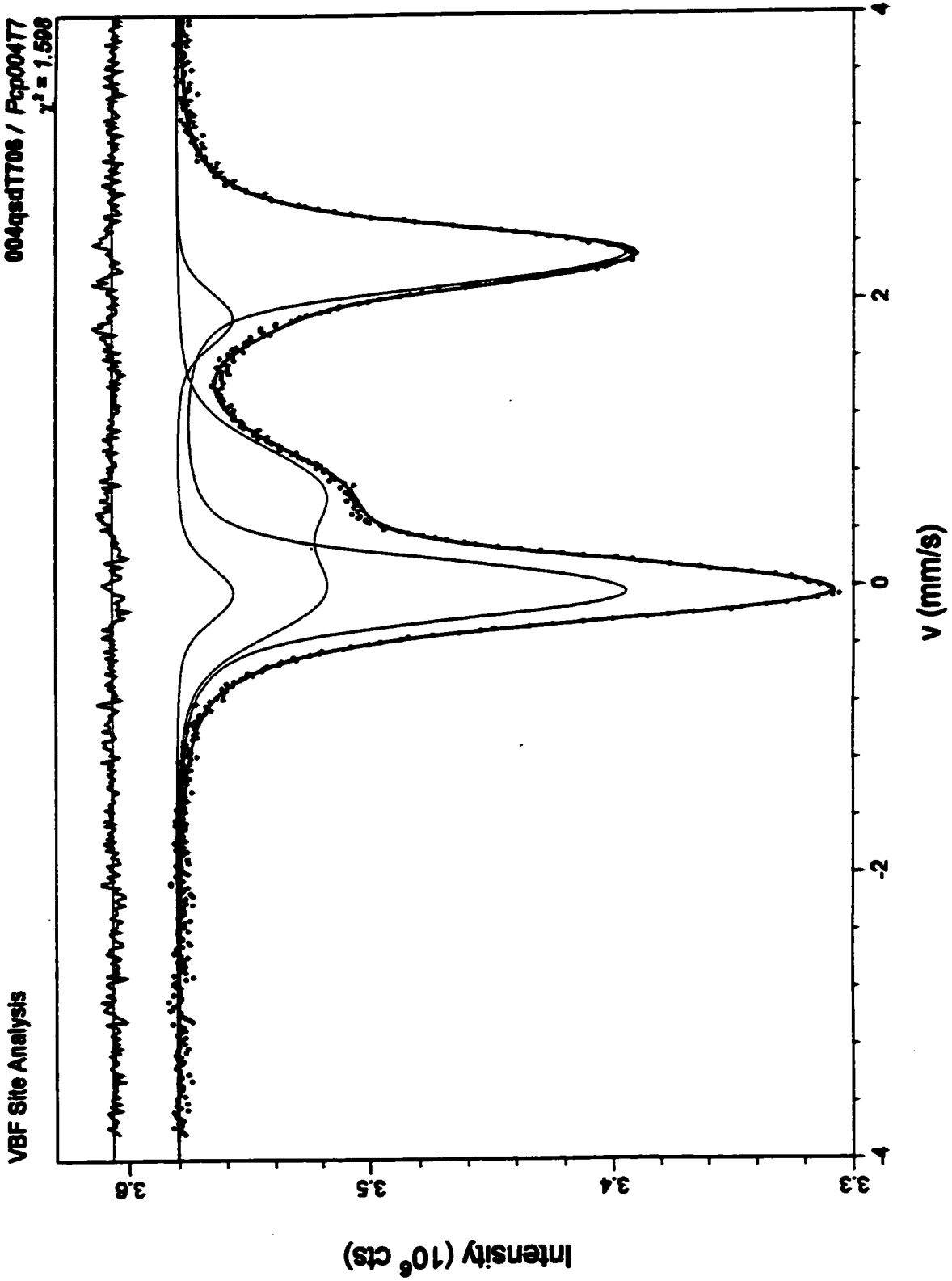
004qsd7706 / Pcp00477
χ² = 1.598
VBF Site Analysis
Intensity (10⁶ cts)
3.3
3.4
3.5
3.6
-4
-2
0
2
4
v (mm/s)

VBF Analysis of Pcp005T7

project:
document: 005qsdt708
data document: Pcp005T7

Fit Summary
no. of data points: 512
no. of QSD sites in model: 2
no. of parameters in model: 22
no. of refined parameters: 17
reduced χ^2 = 1.07681
uncertainties calculated using the covariance matrix

Global Parameters
Background = 5950900(330) counts
Lorentzian HWHM = 0.097* mm/s

Site Distribution Parameters

	δ_0 (mm/s)	δ_1	A (counts·mm/s)	A_-/A_+
Fe2+	1.106(17)	0.0123(69)	303600(5000)	1.214(11)
Fe3+	0.332(25)	0*	69900(4300)	1*

		p (%)	$\langle\Delta\rangle$ (mm/s)	σ_Δ (mm/s)
Fe2+	comp 1	23.8977*	2.145(64)	0.760(88)
	comp 2	13.4(40)	1.971(40)	0.153(35)
	comp 3	62.7(47)	2.470(17)	0.231(14)
Fe3+	comp 1	100*	0.761(35)	0.583(33)

Compiled Site Properties

	Site Populations
Fe2+	81.29(98)
Fe3+	18.71(98)

	<CS> (mm/s)	<|Δ|> (mm/s)	stdev(|Δ|) (mm/s)	skew(|Δ|)
Fe2+	1.13455	2.32553	0.459563	-0.667805
Fe3+	0.331547	0.813847	0.507475	0.513779

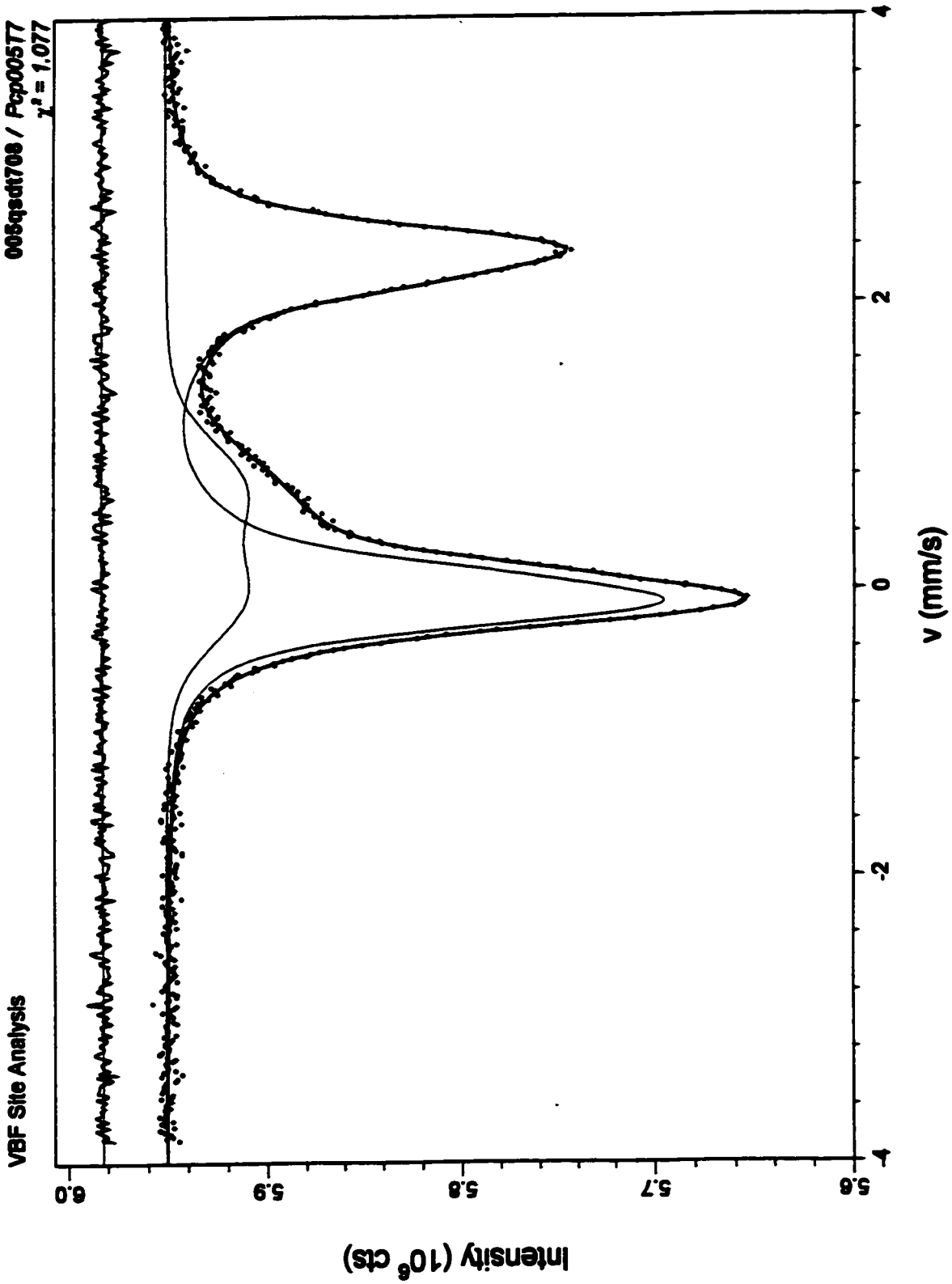
005qsdt708 / Pcp00577
χ² = 1.077
VBF Site Analysis
Intensity (10⁶ cts)
6.0
5.9
5.8
5.7
5.6
-4
-2
0
2
4
v (mm/s)

VBF Analysis of Pcp007T7

project:
document: 007qsdT704
data document: Pcp007T7

Fit Summary
no. of data points: 512
no. of QSD sites in model: 2
no. of parameters in model: 25
no. of refined parameters: 1
reduced χ^2 = 202.769
uncertainties calculated using the covariance matrix

Global Parameters
Background = 6494800(220) counts
Lorentzian HWHM = 0.097* mm/s

Site Distribution Parameters

	δ_0 (mm/s)	δ_1	A (counts-mm/s)	A_-/A_+
Fe2+	1.15366*	-0.00693075*	821000*	1*
Fe3+	0.355069*	0*	21507.6*	1*

		p (%)	$\langle\Delta\rangle$ (mm/s)	σ_Δ (mm/s)
Fe2+	comp 1	5.94386*	2.71329*	0.0562826*
	comp 2	29.7364*	2.47104*	0.113924*
	comp 3	64.3198*	2.30249*	0.314181*
Fe3+	comp 1	3.55552*	0.416123*	0.00223024*
	comp 2	96.4445*	0.624013*	0.392318*

Compiled Site Properties

	Site Populations
Fe2+	97.4472
Fe3+	2.55281

	<CS> (mm/s)	<|Δ|> (mm/s)	stdev(|Δ|) (mm/s)	skew(|Δ|)
Fe2+	1.13719	2.37703	0.283649	-0.46756
Fe3+	0.355069	0.634604	0.356964	0.413932

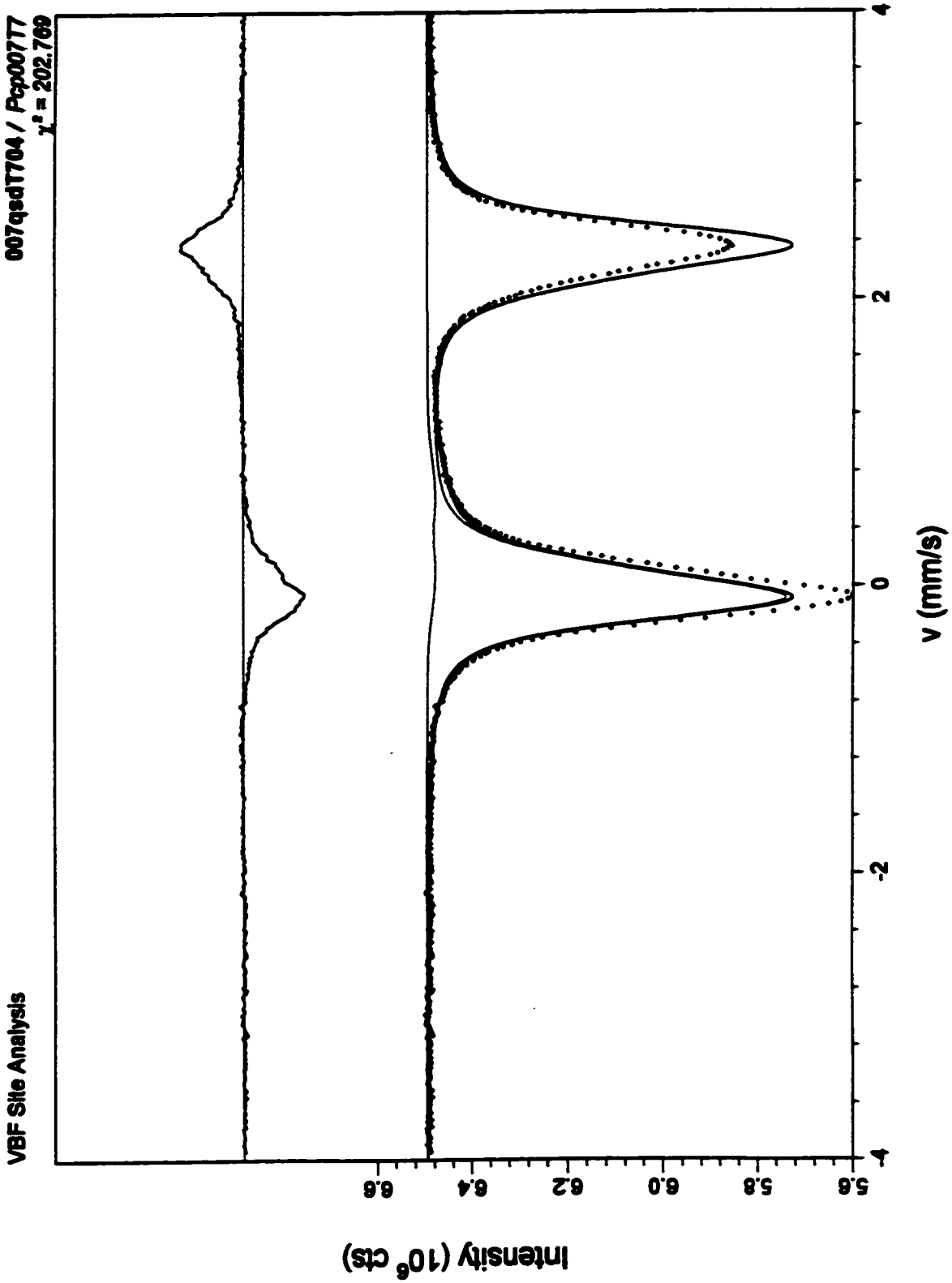
007qsdT704 / Pqp00777
χ² = 202.769
VBF Site Analysis
Intensity (10⁶ cts)
5.6
5.8
6.0
6.2
6.4
6.6
-4
-2
0
2
4
v (mm/s)

VBF Analysis of Pcp008T7

project:
document: 008qsdt701
data document: Pcp008T7

Fit Summary
no. of data points: 512
no. of QSD sites in model: 2
no. of parameters in model: 22
no. of refined parameters: 17
reduced $\chi^2 = 1.42003$
uncertainties calculated using the covariance matrix

Global Parameters
Background = 2954800(220) counts
Lorentzian HWHM = 0.097* mm/s

Site Distribution Parameters

	δ_0 (mm/s)	δ_1	A (counts·mm/s)	A_-/A_+
Fe2+	1.1596(80)	-0.0061(31)	457900(2300)	1.2063(40)
Fe3+	0.297(52)	0*	15200(2200)	1*

		p (%)	$\langle\Delta\rangle$ (mm/s)	σ_Δ (mm/s)
Fe2+	comp 1	40.5641*	2.317(20)	0.392(39)
	comp 2	9.0(75)	2.114(61)	0.153(58)
	comp 3	50.4(86)	2.525(14)	0.177(13)
Fe3+	comp 1	100*	0.824(97)	0.540(93)

Compiled Site Properties

	Site Populations
Fe2+	96.78(45)
Fe3+	3.22(45)

	<CS> (mm/s)	<|Δ|> (mm/s)	stdev(|Δ|) (mm/s)	skew(|Δ|)
Fe2+	1.14488	2.40347	0.313766	-0.448519
Fe3+	0.296988	0.85432	0.491767	0.389481

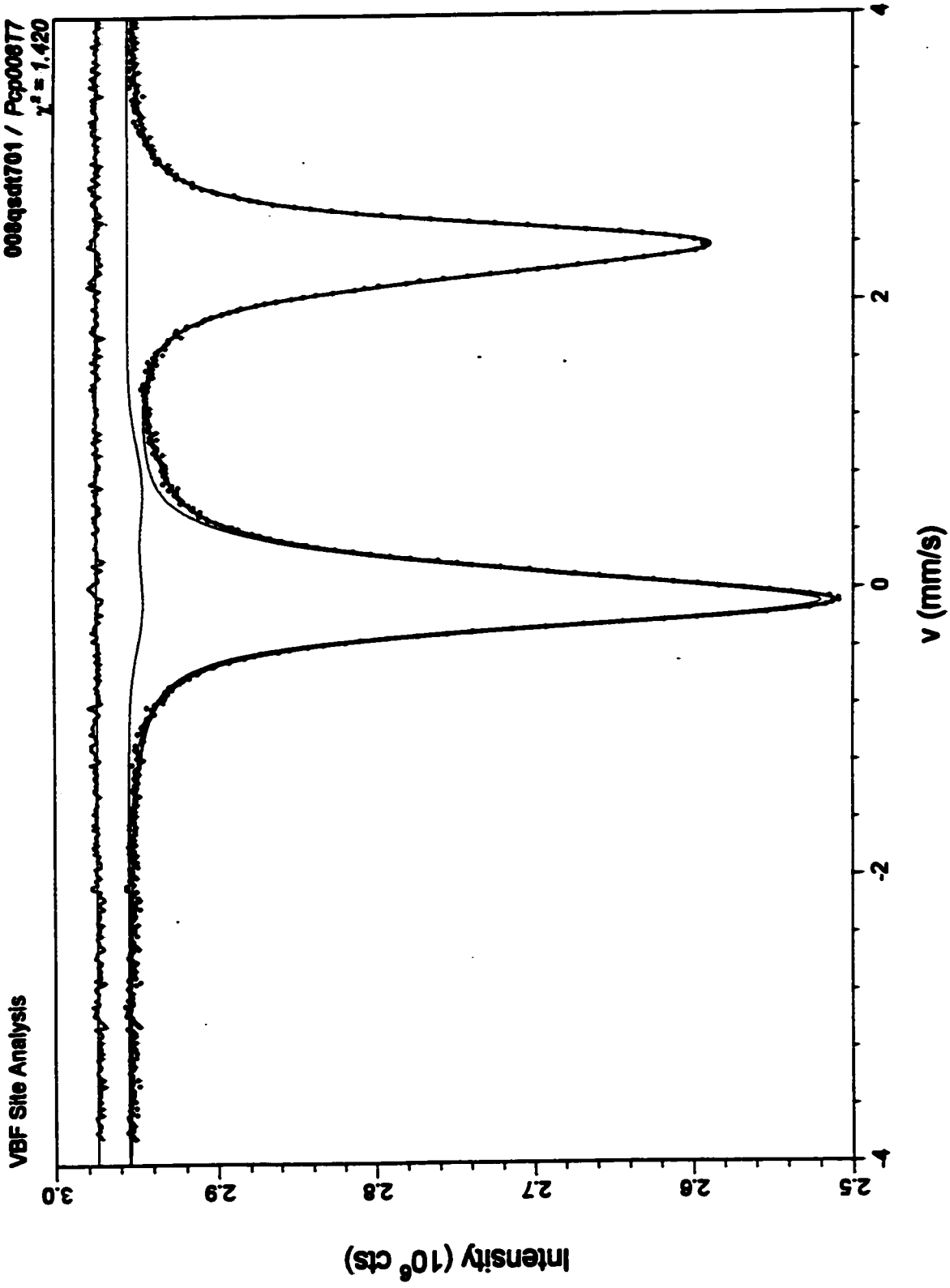
008qsdt701 / Pcp00877
χ² = 1.420
VBF Site Analysis
Intensity (10⁶ cts)
3.0
2.9
2.8
2.7
2.6
2.5
-4
-2
0
2
4
v (mm/s)

VBF Analysis of Pcp009T7

project:
document: 009qsdT707
data document: Pcp009T7

Fit Summary
no. of data points: 512
no. of QSD sites in model: 2
no. of parameters in model: 22
no. of refined parameters: 17
reduced χ^2 = 1.32377
uncertainties calculated using the covariance matrix

Global Parameters
Background = 3227490(230) counts
Lorentzian HWHM = 0.097* mm/s

Site Distribution Parameters

	δ_0 (mm/s)	δ_1	A (counts·mm/s)	A_+/A_-
Fe2+	1.177(10)	-0.0151(46)	354800(3000)	1.2943(70)
Fe3+	0.316(34)	0*	27000(2800)	1*

		p (%)	$\langle\Delta\rangle$ (mm/s)	σ_Δ (mm/s)
Fe2+	comp 1	33.7145*	2.129(38)	0.535(45)
	comp 2	11.4(67)	1.946(61)	0.173(48)
	comp 3	54.9(76)	2.398(27)	0.243(19)
Fe3+	comp 1	100*	0.910(74)	0.385(45)

Compiled Site Properties

	Site Populations
Fe2+	92.94(69)
Fe3+	7.06(69)

	<CS> (mm/s)	<|Δ|> (mm/s)	stdev(|Δ|) (mm/s)	skew(|Δ|)
Fe2+	1.14285	2.25619	0.399613	-0.446541
Fe3+	0.316363	0.912011	0.379063	0.0908551

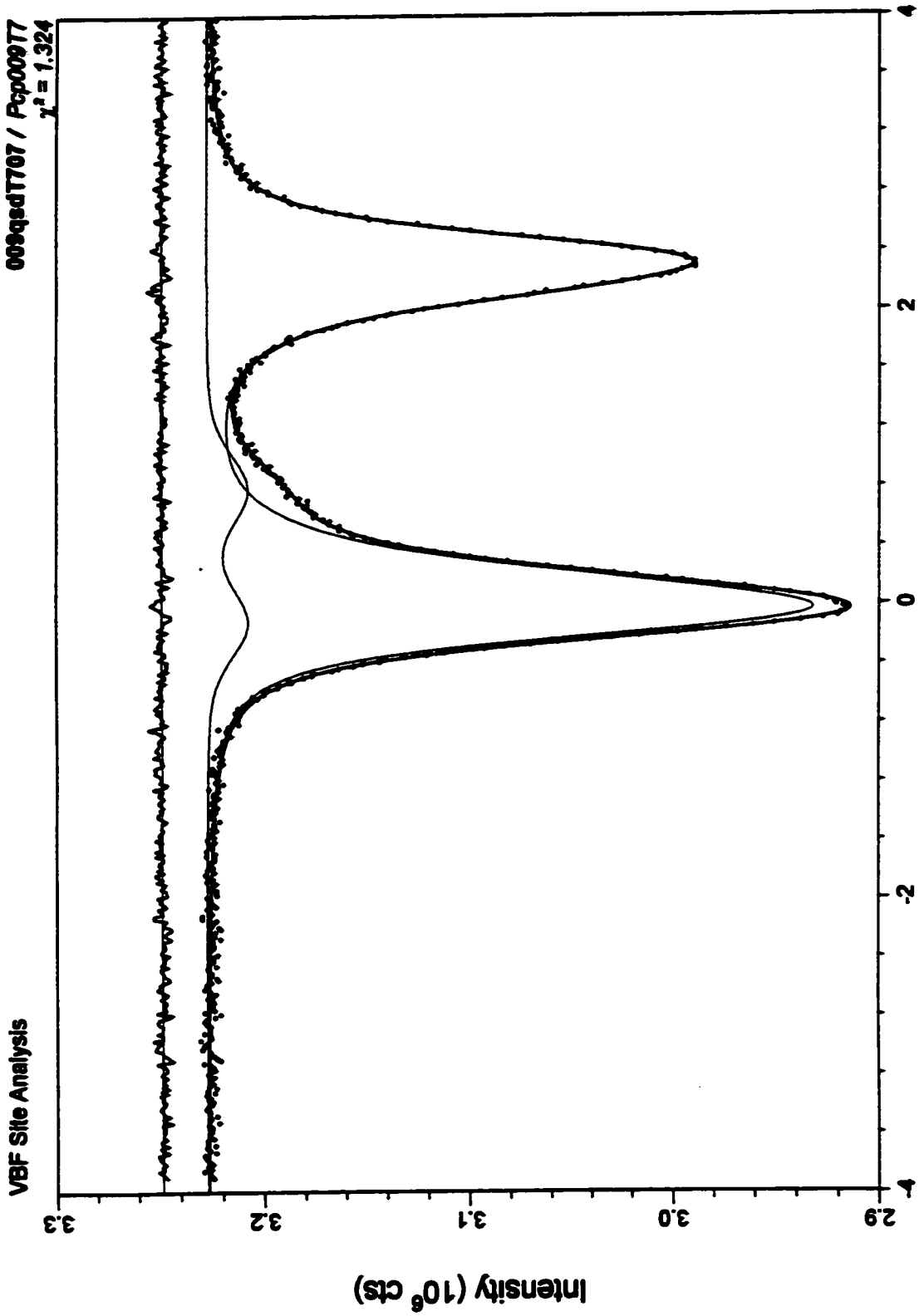
009qsdT707 / Pcp00977
χ² = 1.324
VBF Site Analysis
Intensity (10⁶ cts)
3.3
3.2
3.1
3.0
2.9
-4
-2
0
2
4
v (mm/s)

VBF Analysis of Pcp010T7

project:
document: 010qsdT703
data document: Pcp010T7

Fit Summary
no. of data points: 512
no. of QSD sites in model: 2
no. of parameters in model: 28
no. of refined parameters: 23
reduced χ^2 = 1.03574
uncertainties calculated using the covariance matrix

Global Parameters
Background = 2390200(200) counts
Lorentzian HWHM = 0.097* mm/s

Site Distribution Parameters

		δ_0 (mm/s)	δ_1	A (counts-mm/s)	A_-/A_+
Fe2+		1.133(18)	0.0041(71)	193400(2200)	1.2491(100)
Fe3+		0.3652(79)	0*	84900(2500)	1*
			p (%)	$\langle\Delta\rangle$ (mm/s)	σ_Δ (mm/s)
Fe2+	comp 1		53.4022*	2.406(47)	0.244(98)
	comp 2		0.7(35)	3.1(10)	0.22(71)
	comp 3		50(120)	2.10(78)	0.35(22)
Fe3+	comp 1		59.2072*	0.642(61)	0.246(41)
	comp 2		11(28)	1.7(11)	0.39(49)
	comp 3		29(35)	1.222(80)	0.21(12)

Compiled Site Properties

	Site Populations
Fe2+	69.48(67)
Fe3+	30.52(67)

	<CS> (mm/s)	<|Δ|> (mm/s)	stdev(|Δ|) (mm/s)	skew(|Δ|)
Fe2+	1.14268	2.27225	0.339104	-0.273356
Fe3+	0.365228	0.936557	0.460832	0.719561

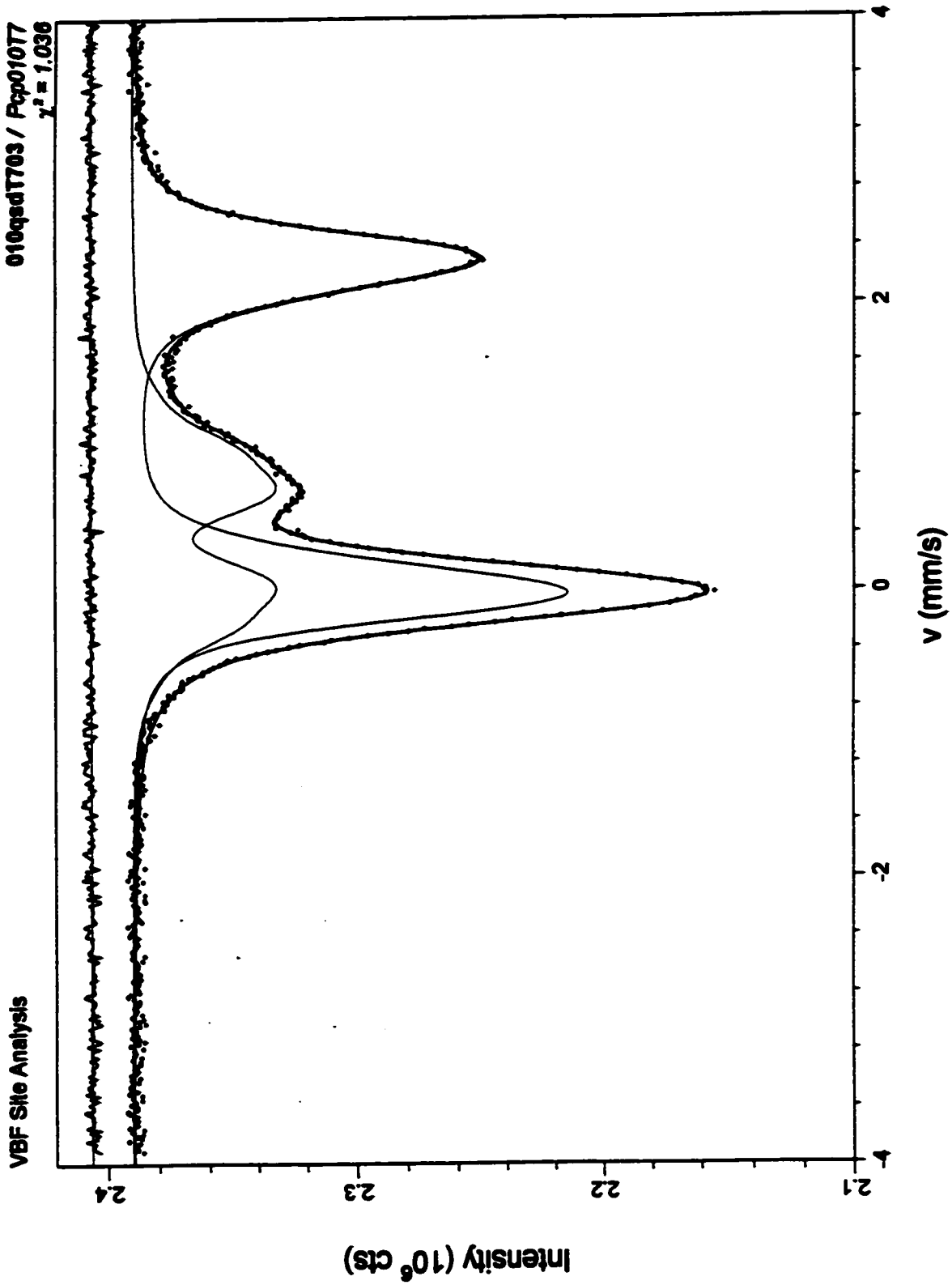
010qsdT703 / Pcp01077
χ² = 1.036
VBF Site Analysis
Intensity (10⁶ cts)
2.4
2.3
2.2
2.1
-4
-2
0
2
4
v (mm/s)

VBF Analysis of Pcp013T7

project:
document: 013qsdt701
data document: Pcp013T7

Fit Summary
no. of data points: 512
no. of QSD sites in model: 2
no. of parameters in model: 22
no. of refined parameters: 17
reduced χ^2 = 6.48486
uncertainties calculated using the covariance matrix

Global Parameters
Background = 2727560(210) counts
Lorentzian HWHM = 0.097* mm/s

Site Distribution Parameters

	δ_0 (mm/s)	δ_1	A (counts·mm/s)	A_1/A_0
Fe2+	1.1792(54)	-0.0062(20)	564700(2400)	1.1678(30)
Fe3+	0.293(18)	0*	33700(2200)	1*

		p (%)	$\langle\Delta\rangle$ (mm/s)	σ_Δ (mm/s)
Fe2+	comp 1	64.3059*	2.400(20)	0.325(12)
	comp 2	9.1(53)	2.16(14)	0.552(82)
	comp 3	26.6(38)	2.6015(63)	0.159(11)
Fe3+	comp 1	100*	0.995(40)	0.479(35)

Compiled Site Properties

	Site Populations
Fe2+	94.36(34)
Fe3+	5.64(34)

	<CS> (mm/s)	<|Δ|> (mm/s)	stdev(|Δ|) (mm/s)	skew(|Δ|)
Fe2+	1.16423	2.43215	0.342236	-0.64748
Fe3+	0.292968	1.00166	0.465231	0.161803

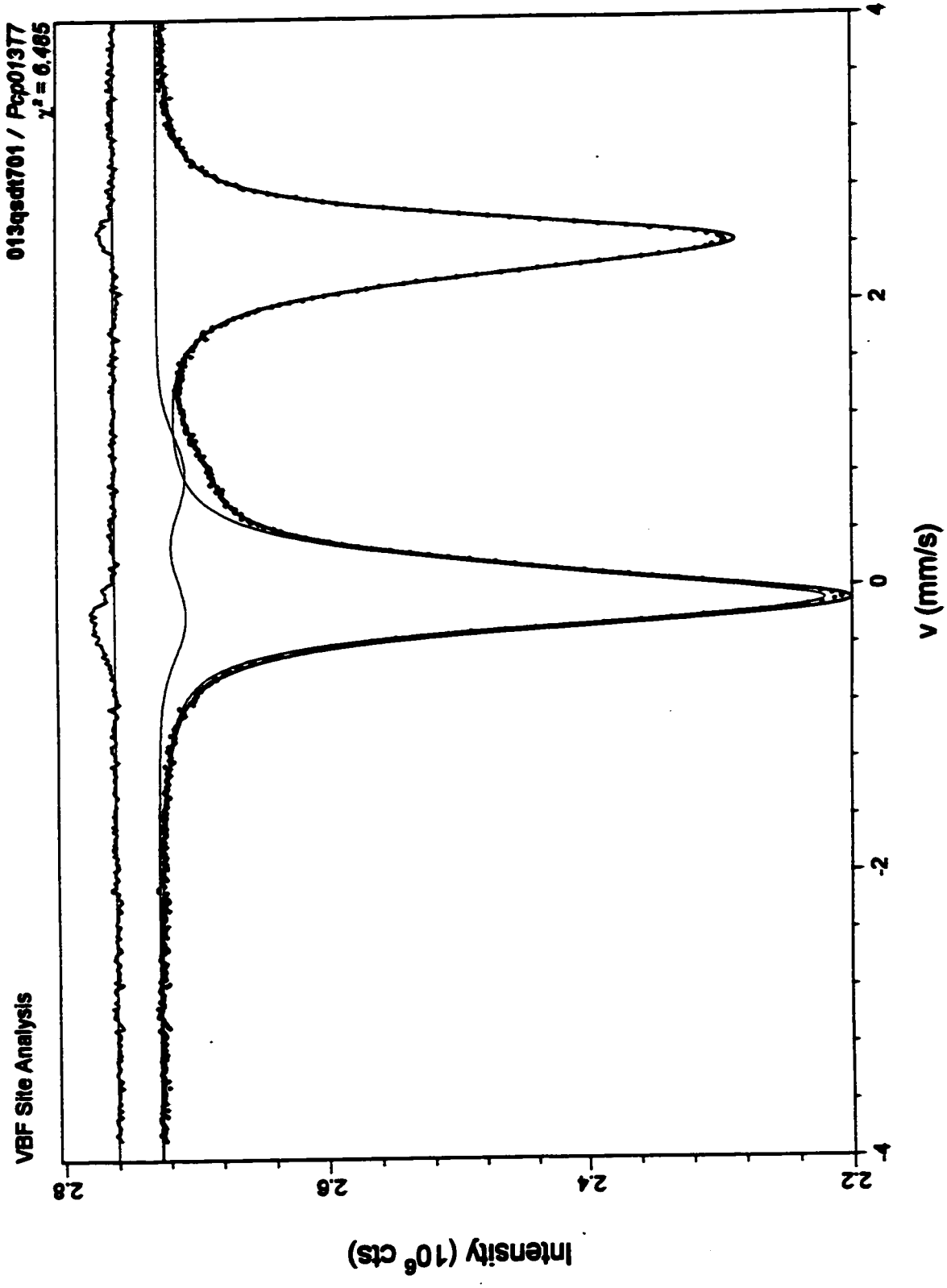
013qsdt701 / Pcp01377
χ^2 = 6.485
VBF Site Analysis
Intensity (10^6 cts)
2.8
2.6
2.4
2.2
-4
-2
0
2
4
v (mm/s)

VBF Analysis of Pcp014t7

project:
document: 014qsdt701
data document: Pcp014t7

Fit Summary
no. of data points: 512
no. of QSD sites in model: 2
no. of parameters in model: 22
no. of refined parameters: 17
reduced χ^2 = 1.40012
uncertainties calculated using the covariance matrix

Global Parameters
Background = 3338070(230) counts
Lorentzian HWHM = 0.097* mm/s

Site Distribution Parameters

	δ_0 (mm/s)	δ_1	A (counts·mm/s)	A_1/A_+
Fe2+	1.1582(67)	-0.0073(28)	472400(2700)	1.1869(46)
Fe3+	0.282(20)	0*	31000(2500)	1*

		p (%)	$\langle\Delta\rangle$ (mm/s)	σ_Δ (mm/s)
Fe2+	comp 1	16.2105*	1.995(37)	0.159(26)
	comp 2	29.5(67)	2.230(22)	0.476(40)
	comp 3	54.3(62)	2.414(16)	0.193(12)
Fe3+	comp 1	100*	0.902(48)	0.427(40)

Compiled Site Properties

	Site Populations
Fe2+	93.84(47)
Fe3+	6.16(47)

	<CS> (mm/s)	<|Δ|> (mm/s)	stdev(|Δ|) (mm/s)	skew(|Δ|)
Fe2+	1.14141	2.29155	0.339002	-0.307261
Fe3+	0.281782	0.907082	0.415164	0.150803

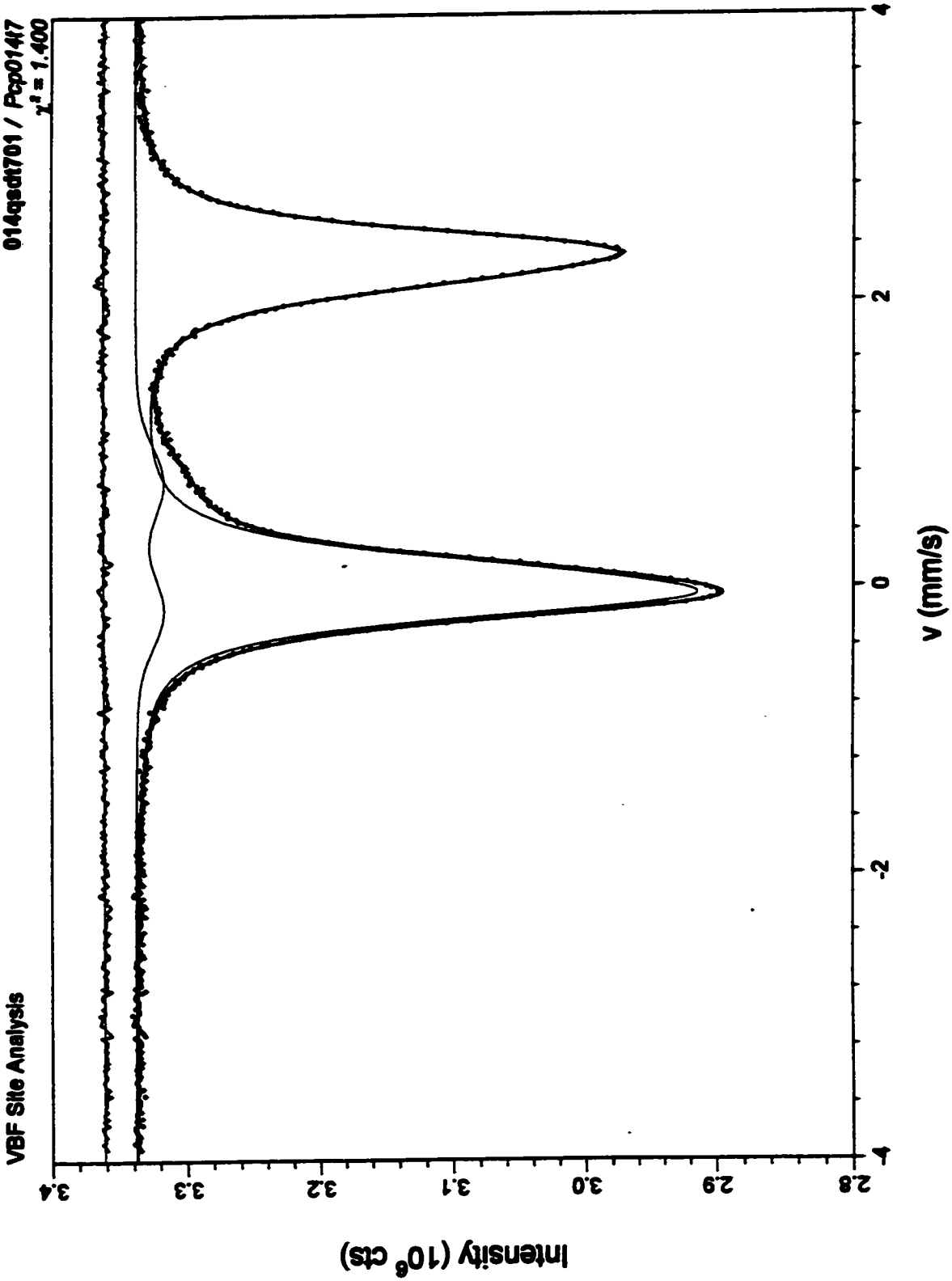
014qsdt701 / Pcp01417
χ² = 1.400
VBF Site Analysis
Intensity (10⁶ cts)
3.4
3.3
3.2
3.1
3.0
2.9
2.8
-4
-2
0
2
4
v (mm/s)

VBF Analysis of Pcp015T7

project:
document: Pcp015T709
data document: Pcp015T7

Fit Summary
no. of data points: 512
no. of QSD sites in model: 2
no. of parameters in model: 22
no. of refined parameters: 17
reduced $\chi^2 = 1.25235$
uncertainties calculated using the covariance matrix

Global Parameters
Background = 3111230(230) counts
Lorentzian HWHM = 0.097* mm/s

Site Distribution Parameters

	δ_0 (mm/s)	δ_1	A (counts-mm/s)	A_1/A_+
Fe2+	1.170(15)	-0.0091(63)	232800(3800)	1.156(12)
Fe3+	0.310(15)	0*	60600(3500)	1*

		p (%)	$\langle\Delta\rangle$ (mm/s)	σ_Δ (mm/s)
Fe2+	comp 1	18.734*	1.91(13)	0.75(14)
	comp 2	32(97)	2.49(16)	0.221(100)
	comp 3	50(100)	2.16(53)	0.30(20)
Fe3+	comp 1	100*	0.898(28)	0.408(26)

Compiled Site Properties

	Site Populations
Fe2+	79.35(97)
Fe3+	20.65(97)

	<CS> (mm/s)	<|Δ|> (mm/s)	stdev(|Δ|) (mm/s)	skew(|Δ|)
Fe2+	1.15008	2.21938	0.452961	-0.916517
Fe3+	0.309708	0.901795	0.399	0.127375

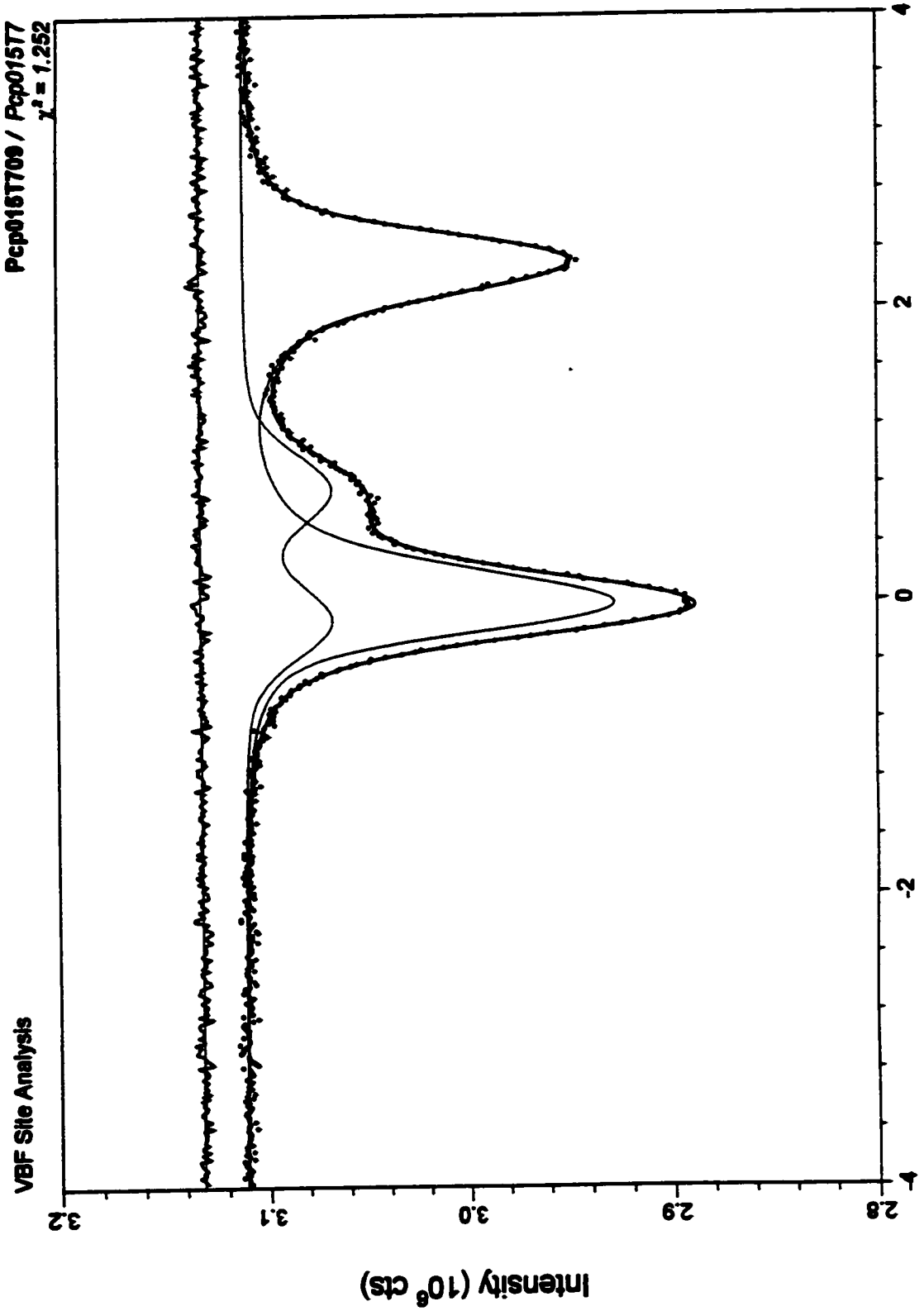
Pcp015T709 / Pcp015T7
χ² = 1.252
VBF Site Analysis
Intensity (10⁶ cts)
3.2
3.1
3.0
2.9
2.8
-4
-2
0
2
4
v (mm/s)

VBF Analysis of Pcp016t7

project:
document: 016qsdt7003
data document: Pcp016t7

Fit Summary
no. of data points: 512
no. of QSD sites in model: 2
no. of parameters in model: 22
no. of refined parameters: 16
reduced $\chi^2 = 0.961285$
uncertainties calculated using the covariance matrix

Global Parameters
Background = 2553720(210) counts
Lorentzian HWHM = 0.097* mm/s

Site Distribution Parameters

	δ_0 (mm/s)	δ_1	A (counts·mm/s)	A_-/A_+
Fe2+	1.076(14)	0.0251(56)	119800(1800)	1*
Fe3+	0.304(27)	0*	31100(1100)	1*

		p (%)	⟨Δ⟩ (mm/s)	σ_Δ (mm/s)
Fe2+	comp 1	19.2439*	2.06(14)	0.71(19)
	comp 2	16.4(100)	1.940(93)	0.186(74)
	comp 3	64.4(95)	2.453(34)	0.228(24)
Fe3+	comp 1	100*	0.794(42)	0.532(34)

Compiled Site Properties

	Site Populations
Fe2+	79.40(65)
Fe3+	20.60(65)

	<CS> (mm/s)	<|Δ|> (mm/s)	stdev(|Δ|) (mm/s)	skew(|Δ|)
Fe2+	1.13329	2.29355	0.426752	-0.797196
Fe3+	0.303535	0.825959	0.481092	0.406232

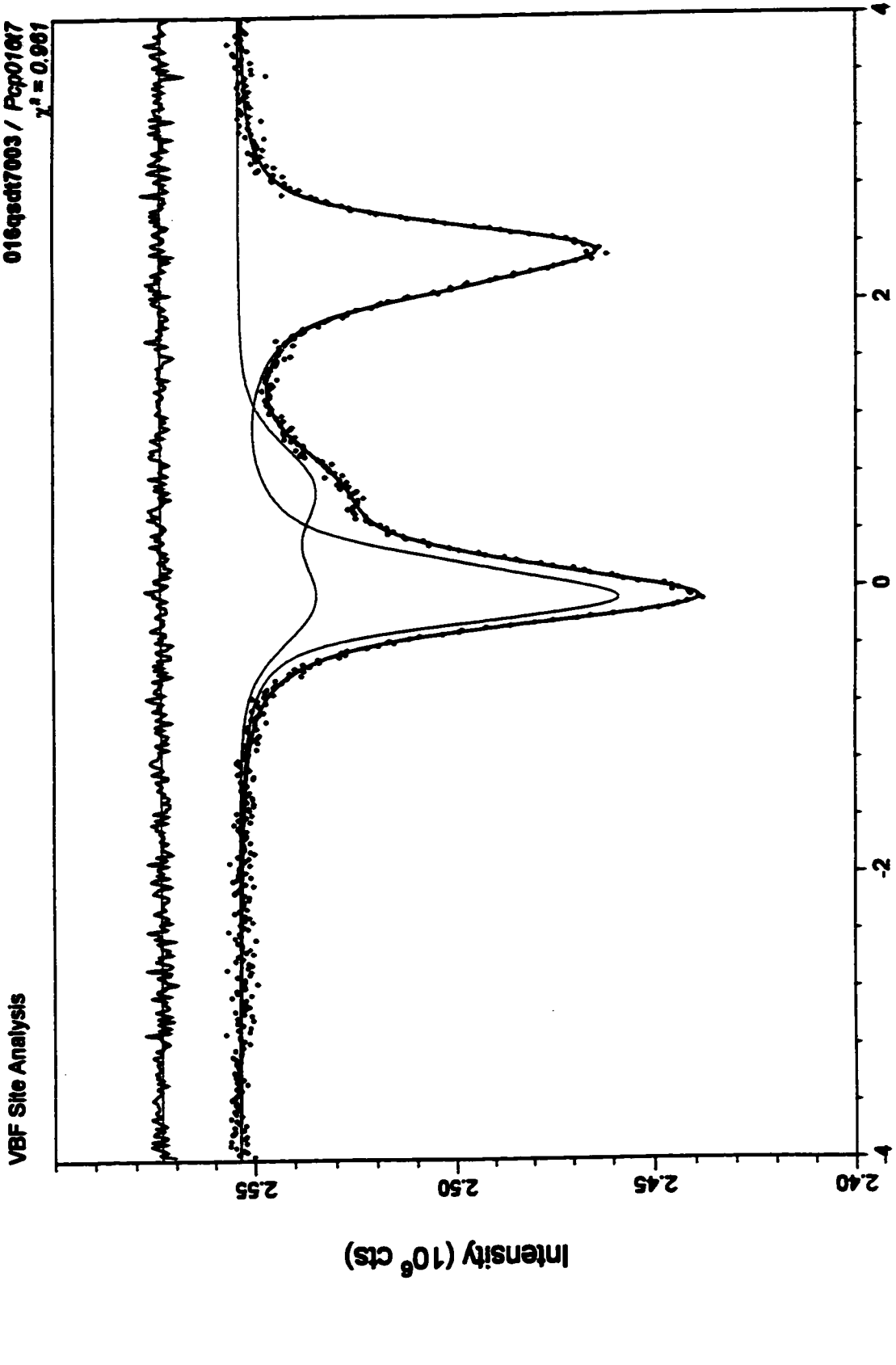
016qsdt7003 / Pcp016t7
χ² = 0.961
VBF Site Analysis
Intensity (10⁶ cts)
2.40
2.45
2.50
2.55
-4
-2
0
2
4
v (mm/s)

VBF Analysis of Pcp020T7

project:
document: 020qsdT703
data document: Pcp020T7

Fit Summary
no. of data points: 512
no. of QSD sites in model: 2
no. of parameters in model: 22
no. of refined parameters: 17
reduced χ^2 = 1.30233
uncertainties calculated using the covariance matrix

Global Parameters
Background = 2441400(200) counts
Lorentzian HWHM = 0.097* mm/s

Site Distribution Parameters

	δ_0 (mm/s)	δ_1	A (counts·mm/s)	A_1/A_0
Fe2+	1.169(14)	-0.0109(58)	267900(3000)	1.1975(95)
Fe3+	0.347(28)	0*	32800(2900)	1*

		p (%)	$\langle\Delta\rangle$ (mm/s)	σ_Δ (mm/s)
Fe2+	comp 1	36.96*	2.128(35)	0.551(43)
	comp 2	8.7(51)	1.918(56)	0.152(53)
	comp 3	54.4(70)	2.375(23)	0.244(18)
Fe3+	comp 1	100*	0.839(55)	0.468(38)

Compiled Site Properties

	Site Populations
Fe2+	89.10(85)
Fe3+	10.90(85)

	<CS> (mm/s)	<|Δ|> (mm/s)	stdev(|Δ|) (mm/s)	skew(|Δ|)
Fe2+	1.14438	2.24401	0.412568	-0.436455
Fe3+	0.347278	0.852708	0.442771	0.263381

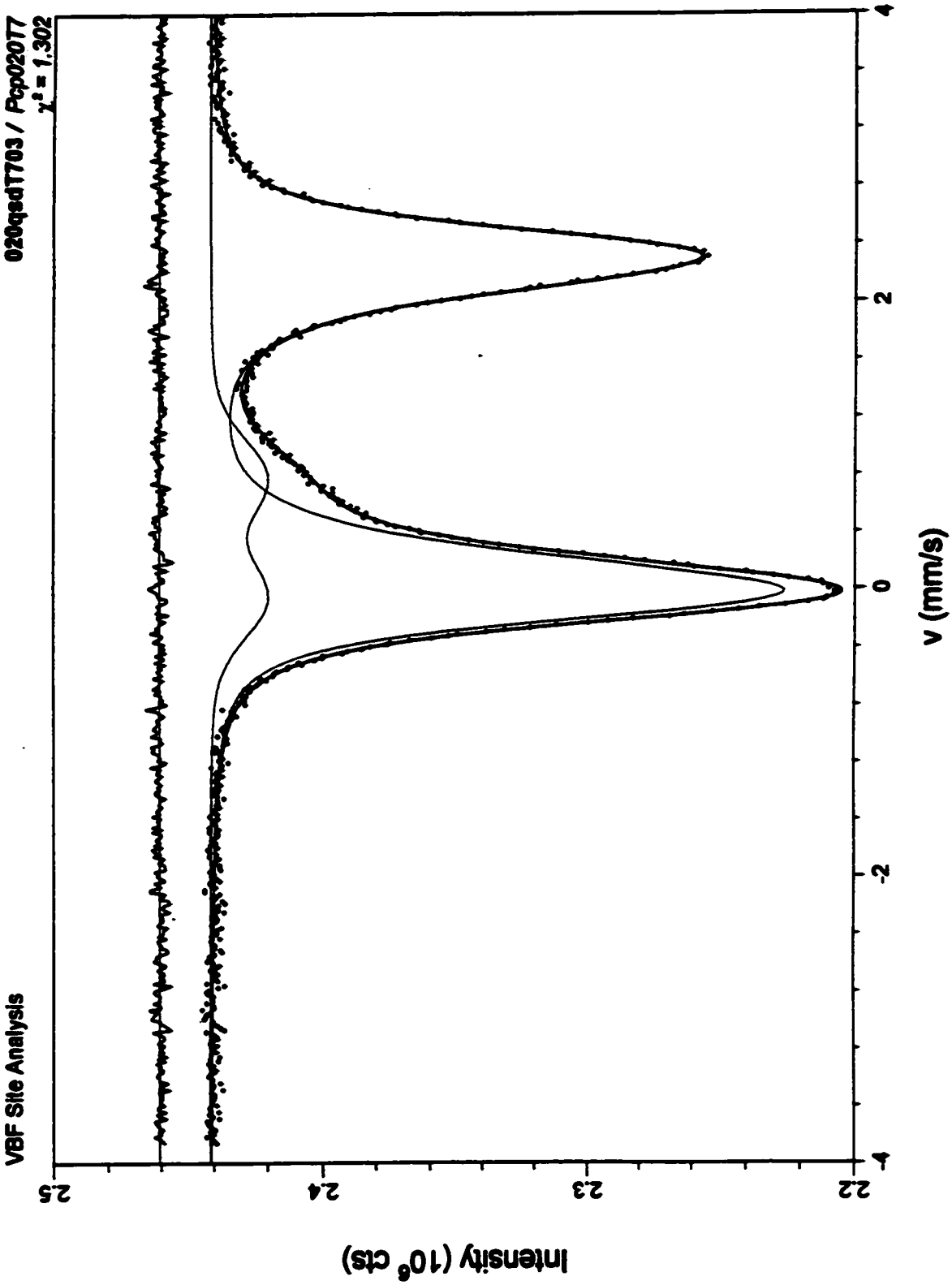
020qsd1703 / Pcp02077
χ² = 1.302
VBF Site Analysis
Intensity (10⁶ cts)
2.5
2.4
2.3
2.2
-4
-2
0
2
4
v (mm/s)

VBF Analysis of Pcp021T7

project:
document: 021qsdt704
data document: Pcp021T7

Fit Summary
no. of data points: 512
no. of QSD sites in model: 2
no. of parameters in model: 22
no. of refined parameters: 14
reduced $\chi^2 = 1.17031$
uncertainties calculated using the covariance matrix

Global Parameters
Background = 474322(85) counts
Lorentzian HWHM = 0.097* mm/s

Site Distribution Parameters

		δ_0 (mm/s)	δ_1	A (counts·mm/s)	A_-/A_+
Fe2+		1.1493(90)	-0.0035(38)	89130(720)	1.1529(54)
Fe3+		0.296*	0*	1240(610)	1*
			p (%)	$\langle\Delta\rangle$ (mm/s)	σ_Δ (mm/s)
Fe2+	comp 1		24.3963*	2.232(44)	0.494(96)
	comp 2		9.2(41)	1.921(37)	0.121(46)
	comp 3		66(10)	2.408(12)	0.222(16)
Fe3+	comp 1		100*	0.904*	0.54*

Compiled Site Properties

	Site Populations
Fe2+	98.62(66)
Fe3+	1.38(66)

	<CS> (mm/s)	<|Δ|> (mm/s)	stdev(|Δ|) (mm/s)	skew(|Δ|)
Fe2+	1.14109	2.32028	0.339408	-0.366636
Fe3+	0.296	0.925033	0.50312	0.315887

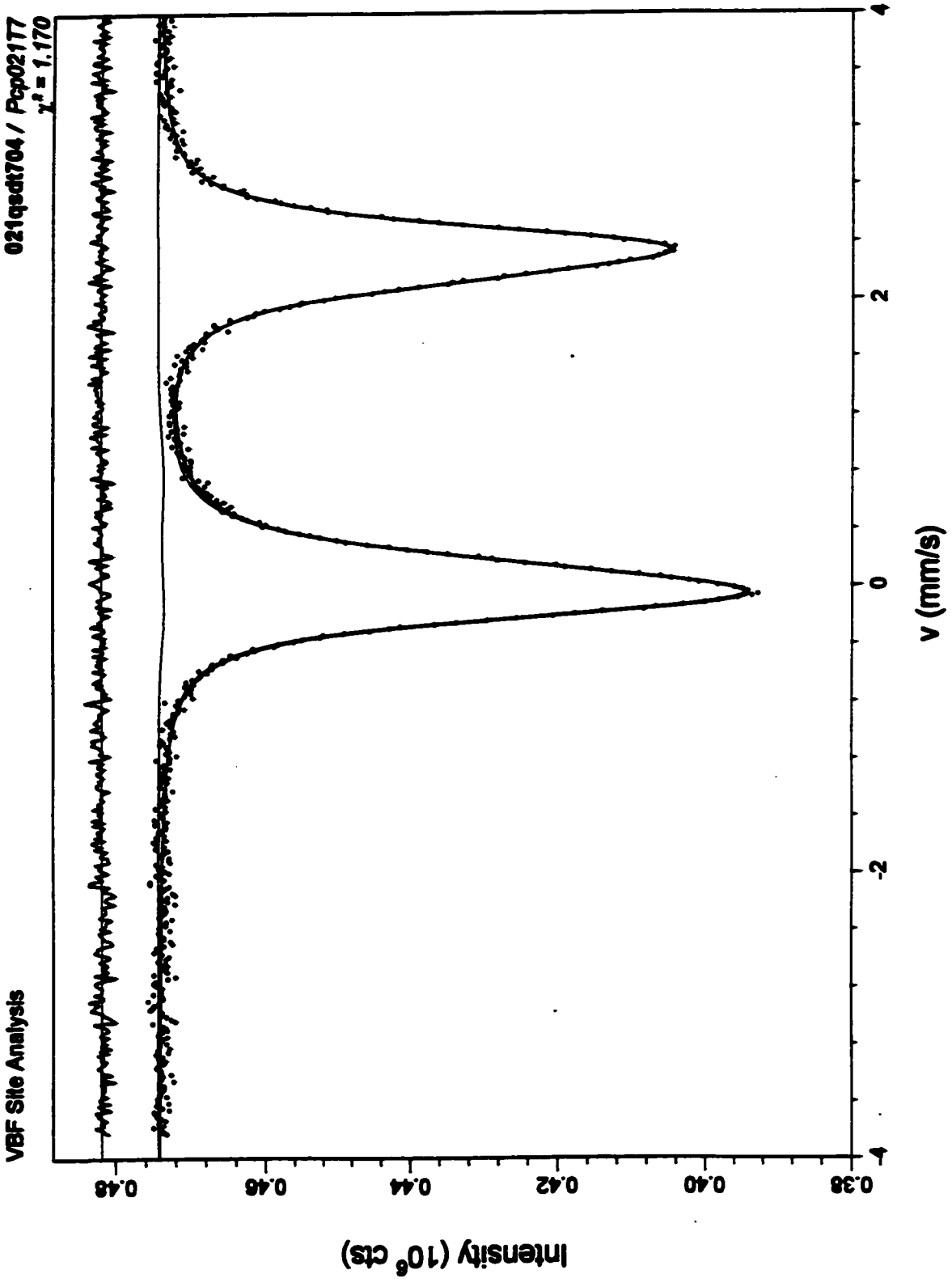
021qsdt704 / Pcp02177
χ^2 = 1.170
VBF Site Analysis
Intensity (10^6 cts)
0.38
0.40
0.42
0.44
0.46
0.48
-4
-2
0
2
4
v (mm/s)

VBF Analysis of Pcp022T7

project:
document: 022qsdt703
data document: Pcp022T7

Fit Summary
no. of data points: 512
no. of QSD sites in model: 2
no. of parameters in model: 22
no. of refined parameters: 17
reduced χ^2 = 1.27339
uncertainties calculated using the covariance matrix

Global Parameters
Background = 4622420(280) counts
Lorentzian HWHM = 0.097* mm/s

Site Distribution Parameters

	δ_0 (mm/s)	δ_1	A (counts·mm/s)	A_1/A_0
Fe2+	1.1753(91)	-0.0122(41)	393900(3200)	1.1705(62)
Fe3+	0.294(26)	0*	25400(2800)	1*

		p (%)	$\langle\Delta\rangle$ (mm/s)	σ_Δ (mm/s)
Fe2+	comp 1	19.0363*	1.90(10)	0.219(54)
	comp 2	46(16)	2.361(60)	0.248(37)
	comp 3	35(15)	2.159(36)	0.542(70)
Fe3+	comp 1	100*	0.979(54)	0.357(48)

Compiled Site Properties

	Site Populations
Fe2+	93.93(63)
Fe3+	6.07(63)

	<CS> (mm/s)	<|Δ|> (mm/s)	stdev(|Δ|) (mm/s)	skew(|Δ|)
Fe2+	1.14851	2.20194	0.41301	-0.164655
Fe3+	0.294044	0.9792	0.355588	0.037984

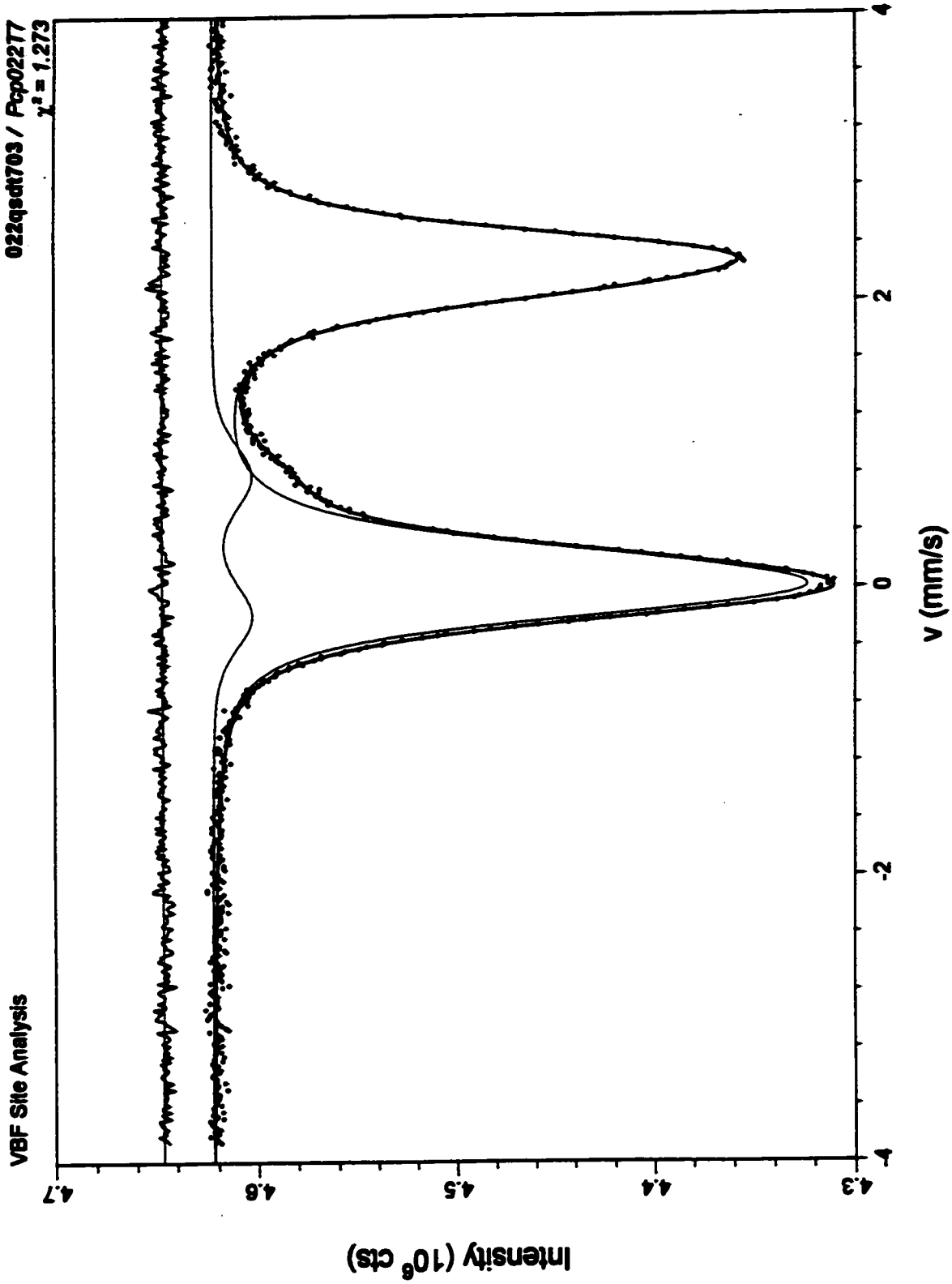
022qsdt703 / Pqp02277
χ^2 = 1.273
VBF Site Analysis
Intensity (10^6 cts)
4.3
4.4
4.5
4.6
4.7
-4
-2
0
2
4
v (mm/s)

VBF Analysis of Pcp023t7

project:
document: 023qsdt703
data document: Pcp023t7

Fit Summary
no. of data points: 512
no. of QSD sites in model: 2
no. of parameters in model: 22
no. of refined parameters: 17
reduced χ^2 = 1.01794
uncertainties calculated using the covariance matrix

Global Parameters
Background = 1089000(130) counts
Lorentzian HWHM = 0.097* mm/s

Site Distribution Parameters

	δ_0 (mm/s)	δ_1	A (counts·mm/s)	A_1/A_2
Fe2+	1.1311(80)	0.0039(32)	237700(1500)	1.0921(52)
Fe3+	0.278(38)	0*	9300(1400)	1*

		p (%)	$\langle\Delta\rangle$ (mm/s)	σ_Δ (mm/s)
Fe2+	comp 1	34.1401*	2.475(41)	0.176(24)
	comp 2	29.9(93)	2.285(34)	0.484(47)
	comp 3	36(22)	2.14(13)	0.243(64)
Fe3+	comp 1	100*	0.871(90)	0.431(79)

Compiled Site Properties

	Site Populations
Fe2+	96.21(56)
Fe3+	3.79(56)

	<CS> (mm/s)	<|Δ|> (mm/s)	stdev(|Δ|) (mm/s)	skew(|Δ|)
Fe2+	1.13998	2.29856	0.348317	-0.160057
Fe3+	0.277816	0.878317	0.416849	0.178939

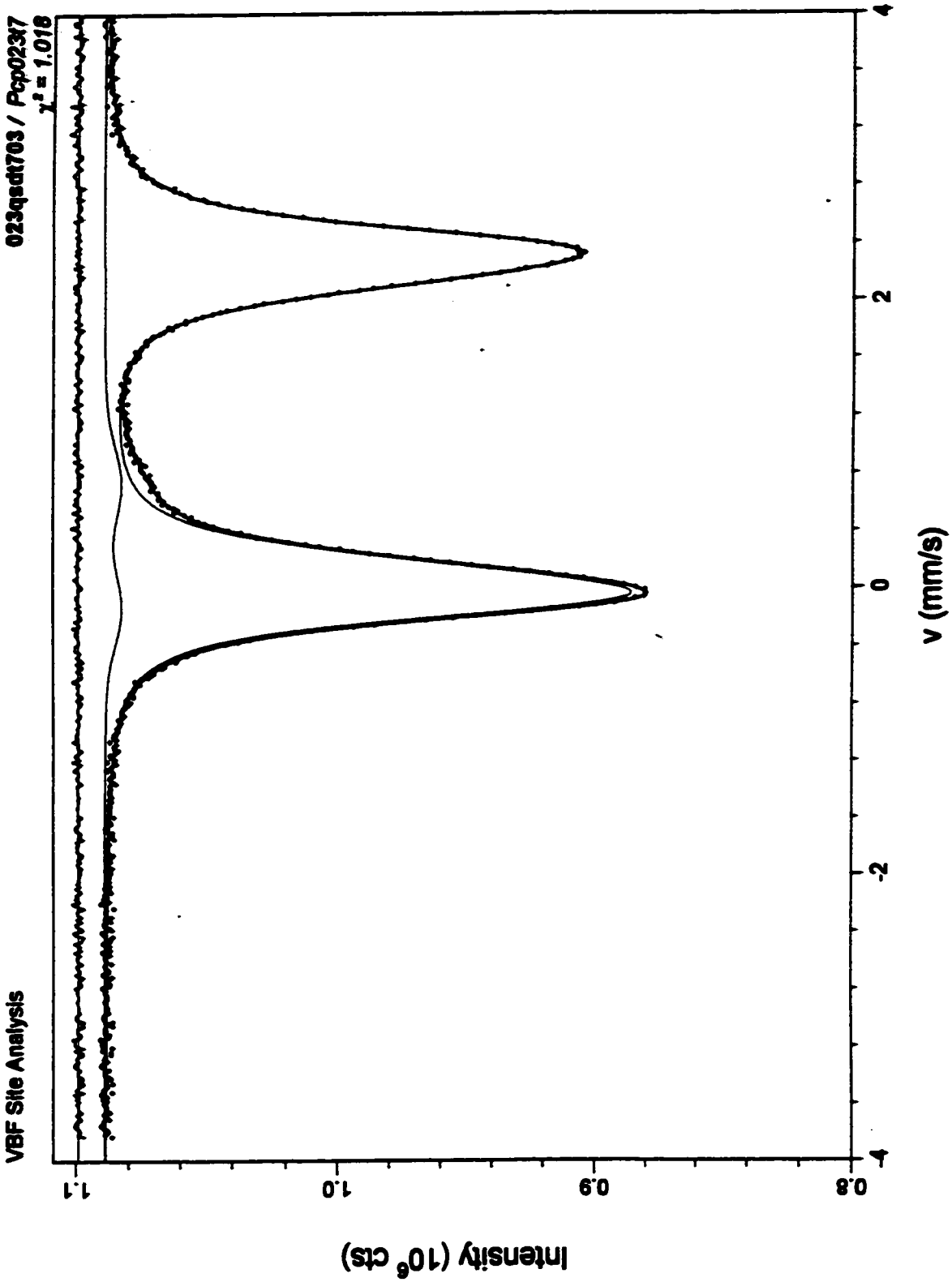
023qsdt703 / Pcp02317
χ² = 1.018
VBF Site Analysis
Intensity (10⁶ cts)
1.1
1.0
0.9
0.8
-4
-2
0
2
4
v (mm/s)

VBF Analysis of Pcp025t7

project:
document: 025qsdt701
data document: Pcp025t7

Fit Summary
no. of data points: 512
no. of QSD sites in model: 2
no. of parameters in model: 22
no. of refined parameters: 17
reduced $\chi^2 = 0.994483$
uncertainties calculated using the covariance matrix

Global Parameters
Background = 1561490(160) counts
Lorentzian HWHM = 0.097* mm/s

Site Distribution Parameters

	δ_0 (mm/s)	δ_1	A (counts-mm/s)	A_-/A_+
Fe2+	1.119(10)	0.0067(41)	261200(2000)	1.0331(57)
Fe3+	0.311(60)	0*	11000(1900)	1*

		p (%)	$\langle\Delta\rangle$ (mm/s)	σ_Δ (mm/s)
Fe2+	comp 1	24.8624*	2.221(34)	0.490(64)
	comp 2	13.3(45)	1.965(31)	0.159(32)
	comp 3	61.8(63)	2.4516(97)	0.204(10)
Fe3+	comp 1	100*	0.76(12)	0.62(13)

Compiled Site Properties

	Site Populations
Fe2+	95.97(65)
Fe3+	4.03(65)

	<CS> (mm/s)	<|Δ|> (mm/s)	stdev(|Δ|) (mm/s)	skew(|Δ|)
Fe2+	1.13421	2.32956	0.344398	-0.472865
Fe3+	0.311181	0.822483	0.526473	0.560739

VBF Analysis of Pcp027T

project:
document: Pcp027qsd
data document: Pcp027T

Fit Summary
no. of data points: 512
no. of QSD sites in model: 2
no. of parameters in model: 25
no. of refined parameters: 20
reduced χ^2 = 1.1237
uncertainties calculated using the covariance matrix

Global Parameters
Background = 1751240(170) counts
Lorentzian HWHM = 0.097* mm/s

Site Distribution Parameters

	δ_0 (mm/s)	δ_1	A (counts·mm/s)	A_-/A_+
Fe2+	1.161(33)	-0.009(11)	146100(5200)	1.109(26)
Fe3+	0.349(36)	0*	40300(5100)	1*

		p (%)	$\langle\Delta\rangle$ (mm/s)	σ_Δ (mm/s)
Fe2+	comp 1	46.019*	2.2(11)	0.31(44)
	comp 2	30(180)	2.50(23)	0.23(18)
	comp 3	22(29)	2.03(27)	0.69(33)
Fe3+	comp 1	47.9797*	0.671(93)	0.28(26)
	comp 2	50(160)	1.1(13)	0.45(43)

Compiled Site Properties

	Site Populations
Fe2+	78.4(22)
Fe3+	21.6(22)

	<CS> (mm/s)	<|Δ|> (mm/s)	stdev(|Δ|) (mm/s)	skew(|Δ|)
Fe2+	1.14044	2.24387	0.445286	-0.67201
Fe3+	0.349474	0.887169	0.424244	0.52149

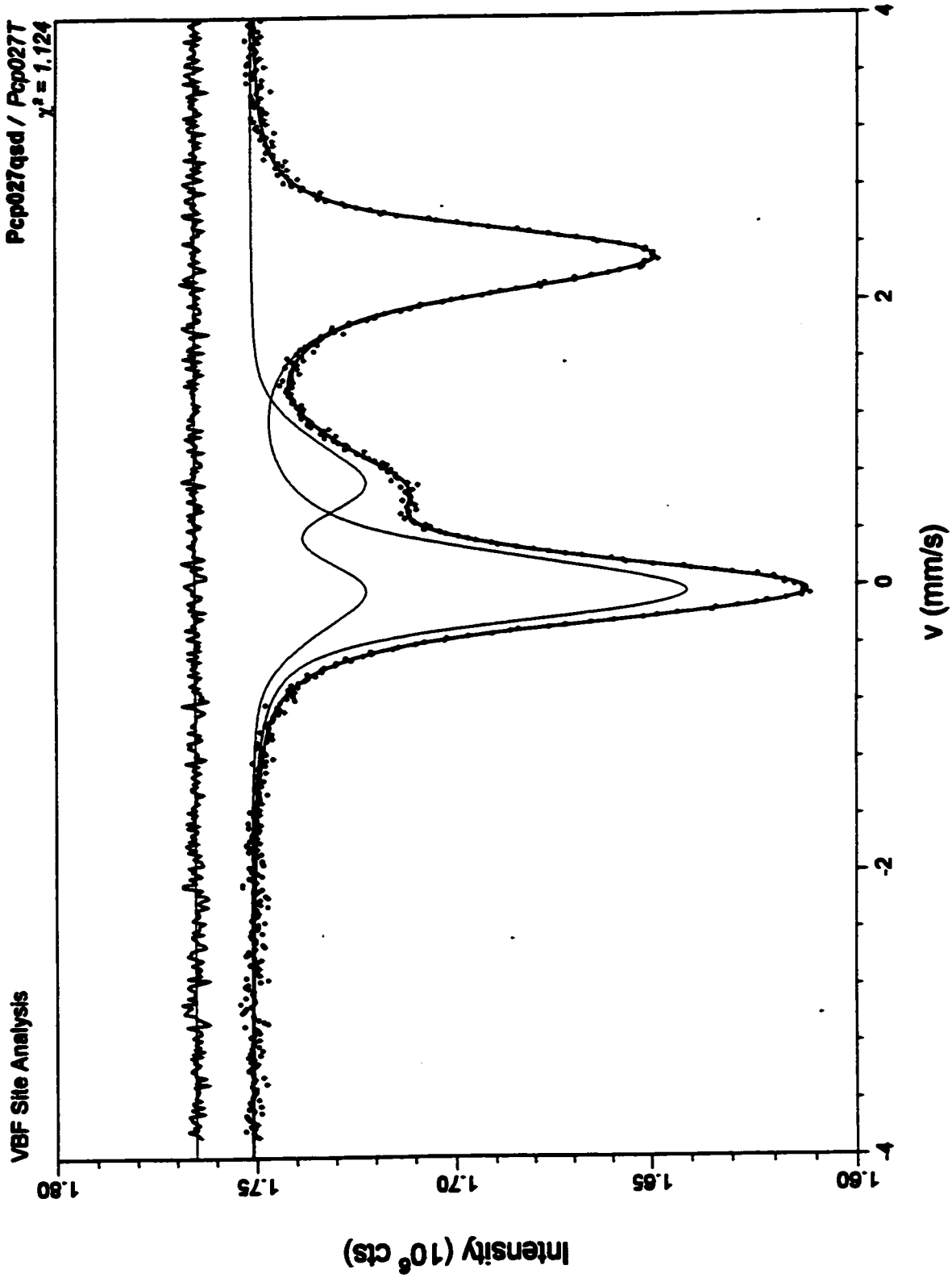
Pcp027qsd / Pcp027T
χ² = 1.124
VBF Site Analysis
Intensity (10⁶ cts)
1.80
1.75
1.70
1.65
1.60
-4
-2
0
2
4
v (mm/s)

VBF Analysis of Pcp028t7

project:
document: 028qsdt701
data document: Pcp028t7

Fit Summary
no. of data points: 509
no. of QSD sites in model: 2
no. of parameters in model: 22
no. of refined parameters: 17
reduced $\chi^2 = 1.15319$
uncertainties calculated using the covariance matrix

Global Parameters
Background = 1160720(140) counts
Lorentzian HWHM = 0.097* mm/s

Site Distribution Parameters

	δ_0 (mm/s)	δ_1	A (counts·mm/s)	A_-/A_+
Fe2+	1.1252(43)	0.0060(18)	326200(1200)	1.1286(26)
Fe3+	0.256(26)	0*	10100(1000)	1*

		p (%)	$\langle\Delta\rangle$ (mm/s)	σ_Δ (mm/s)
Fe2+	comp 1	19.5132*	2.10(12)	0.194(54)
	comp 2	56(16)	2.448(35)	0.182(18)
	comp 3	24.3(92)	2.314(31)	0.429(51)
Fe3+	comp 1	100*	1.036(58)	0.395(56)

Compiled Site Properties

	Site Populations
Fe2+	97.00(30)
Fe3+	3.00(30)

	<CS> (mm/s)	<|Δ|> (mm/s)	stdev(|Δ|) (mm/s)	skew(|Δ|)
Fe2+	1.13919	2.34814	0.296875	-0.256156
Fe3+	0.256039	1.03704	0.392264	0.0506003

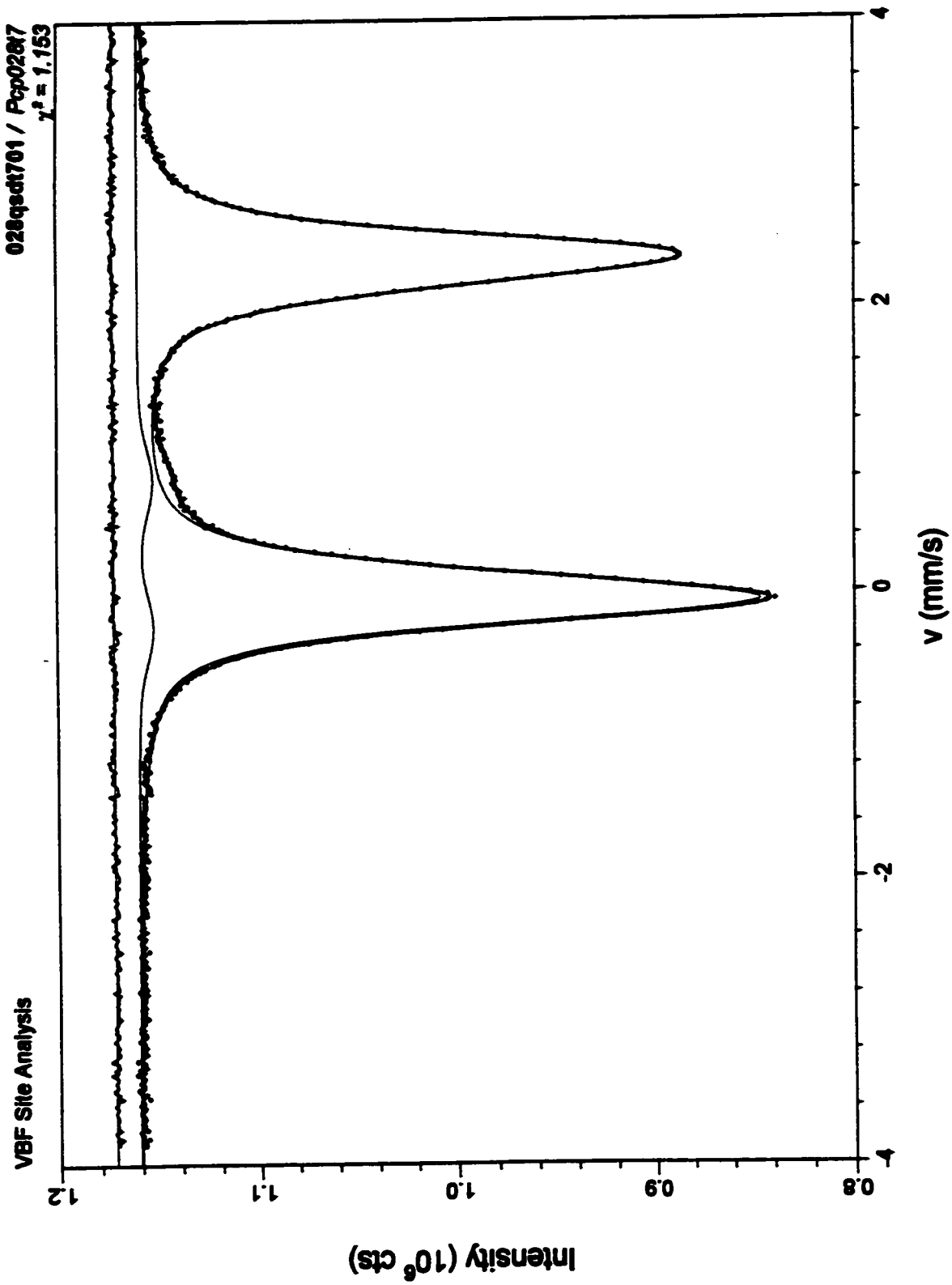
028qsdt701 / Pcp02d7
χ² = 1.153
VBF Site Analysis
Intensity (10⁶ cts)
1.2
1.1
1.0
0.9
0.8
-4
-2
0
2
4
v (mm/s)

VBF Analysis of Pcp029t7

project:
document: 029qsdt701
data document: Pcp029t7

Fit Summary
no. of data points: 512
no. of QSD sites in model: 2
no. of parameters in model: 22
no. of refined parameters: 17
reduced χ^2 = 1.45457
uncertainties calculated using the covariance matrix

Global Parameters
Background = 1299380(150) counts
Lorentzian HWHM = 0.097* mm/s

Site Distribution Parameters

	δ_0 (mm/s)	δ_1	A (counts·mm/s)	A$_1$/A$_0$
FE2+	1.1212(63)	0.0079(24)	340700(1500)	1.1036(31)
Fe3+	0.281(21)	0*	19100(1300)	1*

		p (%)	$\langle\Delta\rangle$ (mm/s)	σ_Δ (mm/s)
FE2+	comp 1	69.1321*	2.5166(76)	0.2031(63)
	comp 2	18.3(44)	2.285(29)	0.532(52)
	comp 3	12.5(30)	2.052(31)	0.168(25)
Fe3+	comp 1	100*	0.929(43)	0.473(38)

Compiled Site Properties

	Site Populations
FE2+	94.68(35)
Fe3+	5.32(35)

	<CS> (mm/s)	<|Δ|> (mm/s)	stdev(|Δ|) (mm/s)	skew(|Δ|)
FE2+	1.14019	2.41584	0.332668	-0.580755
Fe3+	0.281285	0.938231	0.455641	0.198479

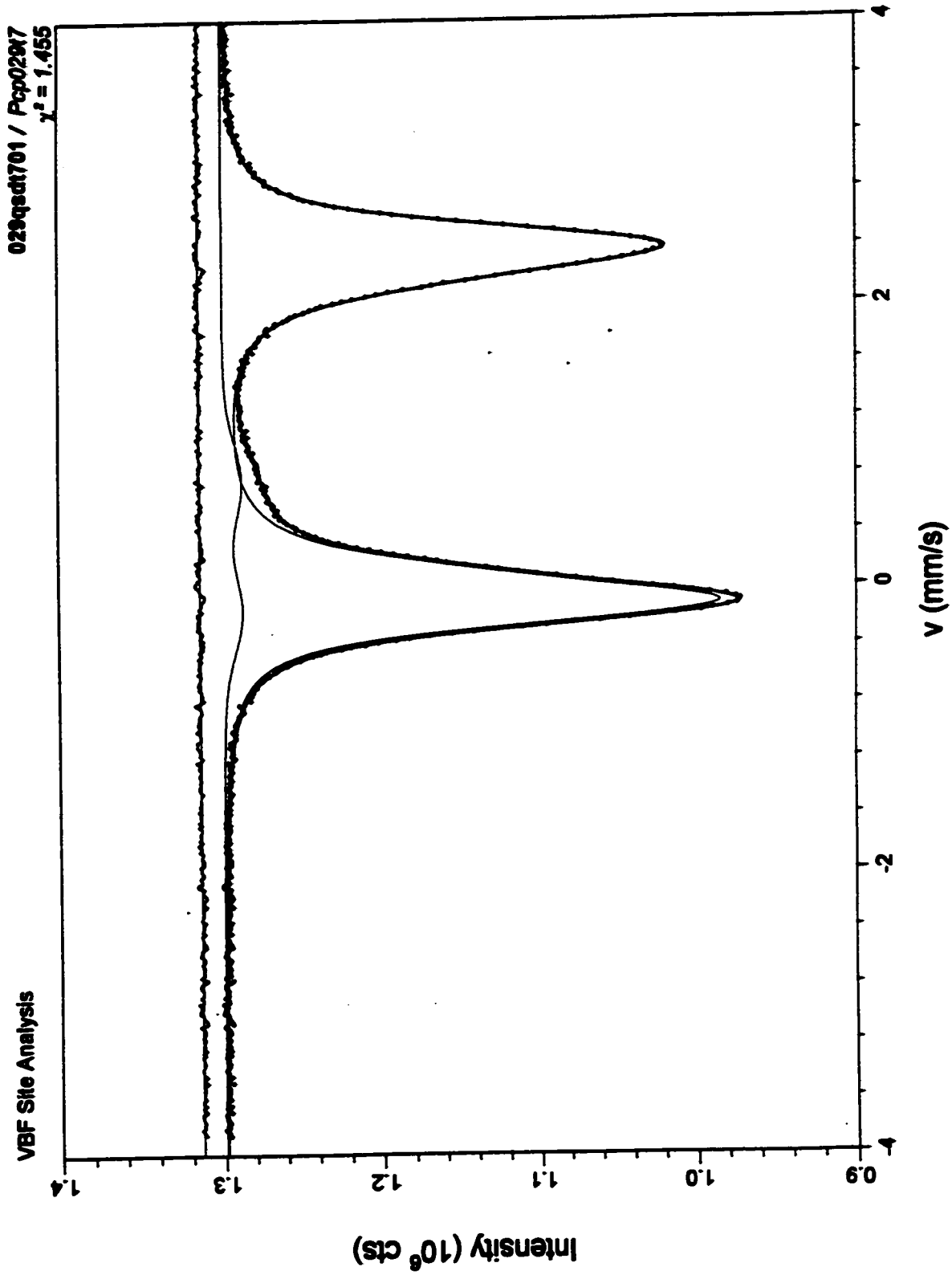
029qsdt701 / Pcp029t7
χ^2 = 1.455
VBF Site Analysis
Intensity (10^6 cts)
v (mm/s)
0.9
1.0
1.1
1.2
1.3
1.4
-4
-2
0
2
4

VBF Analysis of Pcp030T7

project:
document: 030qsdt702
data document: Pcp030T7

Fit Summary
no. of data points: 512
no. of QSD sites in model: 2
no. of parameters in model: 22
no. of refined parameters: 17
reduced $\chi^2 = 1.25026$
uncertainties calculated using the covariance matrix

Global Parameters
Background = 708040(110) counts
Lorentzian HWHM = 0.097* mm/s

Site Distribution Parameters

	δ_0 (mm/s)	δ_1	A (counts·mm/s)	A_1/A_0
Fe2+	1.1090(64)	0.0114(26)	195900(1000)	1.1219(33)
Fe3+	0.282(15)	0*	17080(840)	1*

		p (%)	$\langle\Delta\rangle$ (mm/s)	σ_Δ (mm/s)
Fe2+	comp 1	12.1344*	2.370(63)	0.551(85)
	comp 2	57(26)	2.502(41)	0.187(16)
	comp 3	31(26)	2.19(18)	0.230(68)
Fe3+	comp 1	100*	0.940(31)	0.413(26)

Compiled Site Properties

	Site Populations
Fe2+	91.98(36)
Fe3+	8.02(36)

	<CS> (mm/s)	<|Δ|> (mm/s)	stdev(|Δ|) (mm/s)	skew(|Δ|)
Fe2+	1.13622	2.38946	0.304753	-0.247325
Fe3+	0.282186	0.94288	0.405288	0.109436

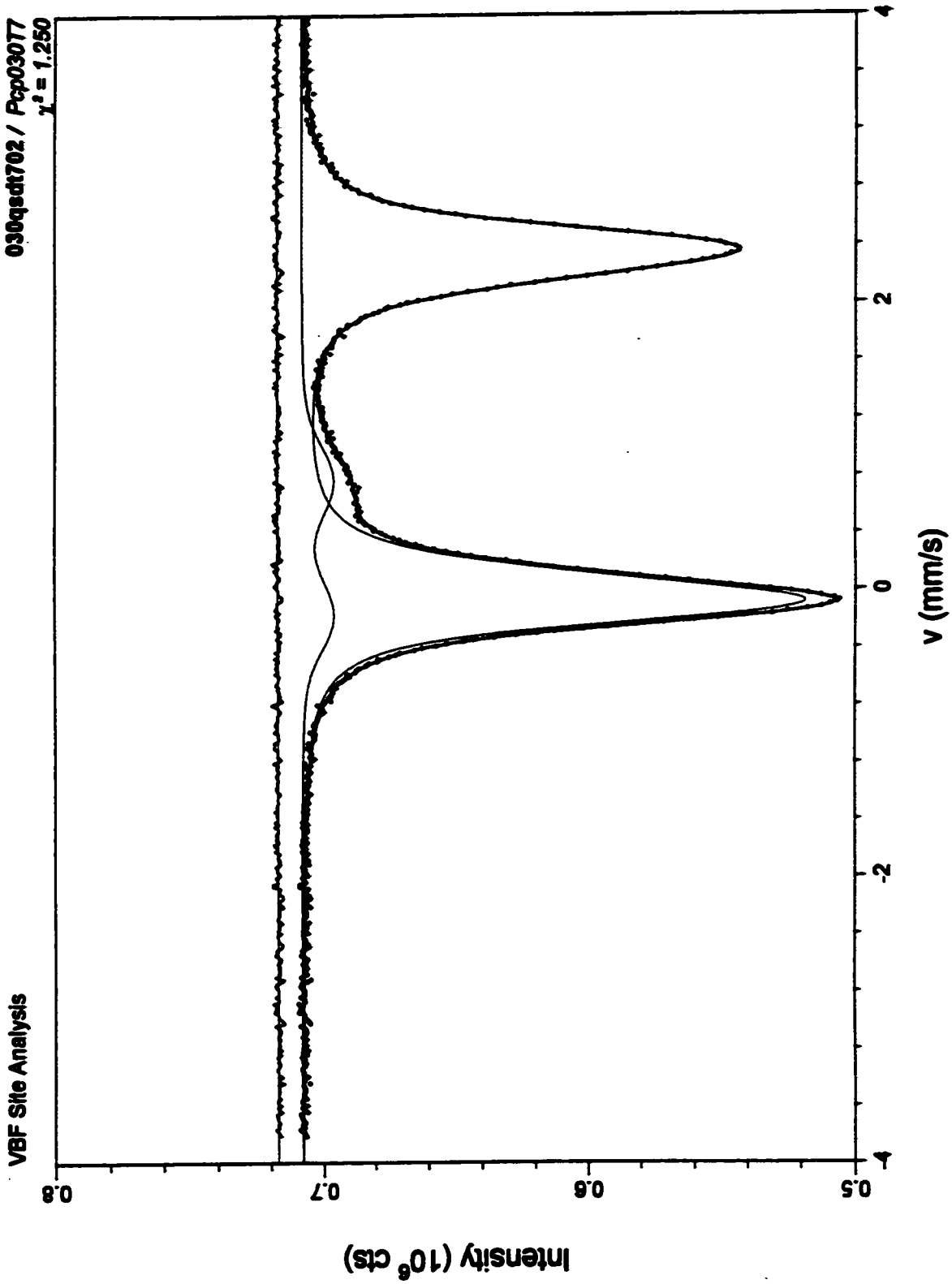
030qsdt702 / Pcp03077
χ² = 1.250
VBF Site Analysis
Intensity (10⁶ cts)
0.8
0.7
0.6
0.5
-4
-2
0
2
4
v (mm/s)

VBF Analysis of Pcp031t7

project:
document: 031qsdt701
data document: Pcp031t7

Fit Summary
no. of data points: 512
no. of QSD sites in model: 2
no. of parameters in model: 22
no. of refined parameters: 17
reduced χ^2 = 1.15278
uncertainties calculated using the covariance matrix

Global Parameters
Background = 465944(91) counts
Lorentzian HWHM = 0.097* mm/s

Site Distribution Parameters

		δ_0 (mm/s)	δ_1	A (counts·mm/s)	A_1/A_0
Fe2+		1.110(15)	0.0099(57)	96010(990)	1.1272(74)
Fe3+		0.289(47)	0*	5870(870)	1*
			p (%)	$\langle\Delta\rangle$ (mm/s)	σ_Δ (mm/s)
Fe2+	comp 1		33.8327*	2.17(19)	0.258(92)
	comp 2		51(24)	2.527(37)	0.183(22)
	comp 3		15.0(96)	2.329(94)	0.56(13)
Fe3+	comp 1		100*	0.836(93)	0.496(86)

Compiled Site Properties

	Site Populations
Fe2+	94.24(81)
Fe3+	5.76(81)

	<CS> (mm/s)	<|Δ|> (mm/s)	stdev(|Δ|) (mm/s)	skew(|Δ|)
Fe2+	1.13366	2.37594	0.336366	-0.370252
Fe3+	0.288716	0.855049	0.462559	0.309452

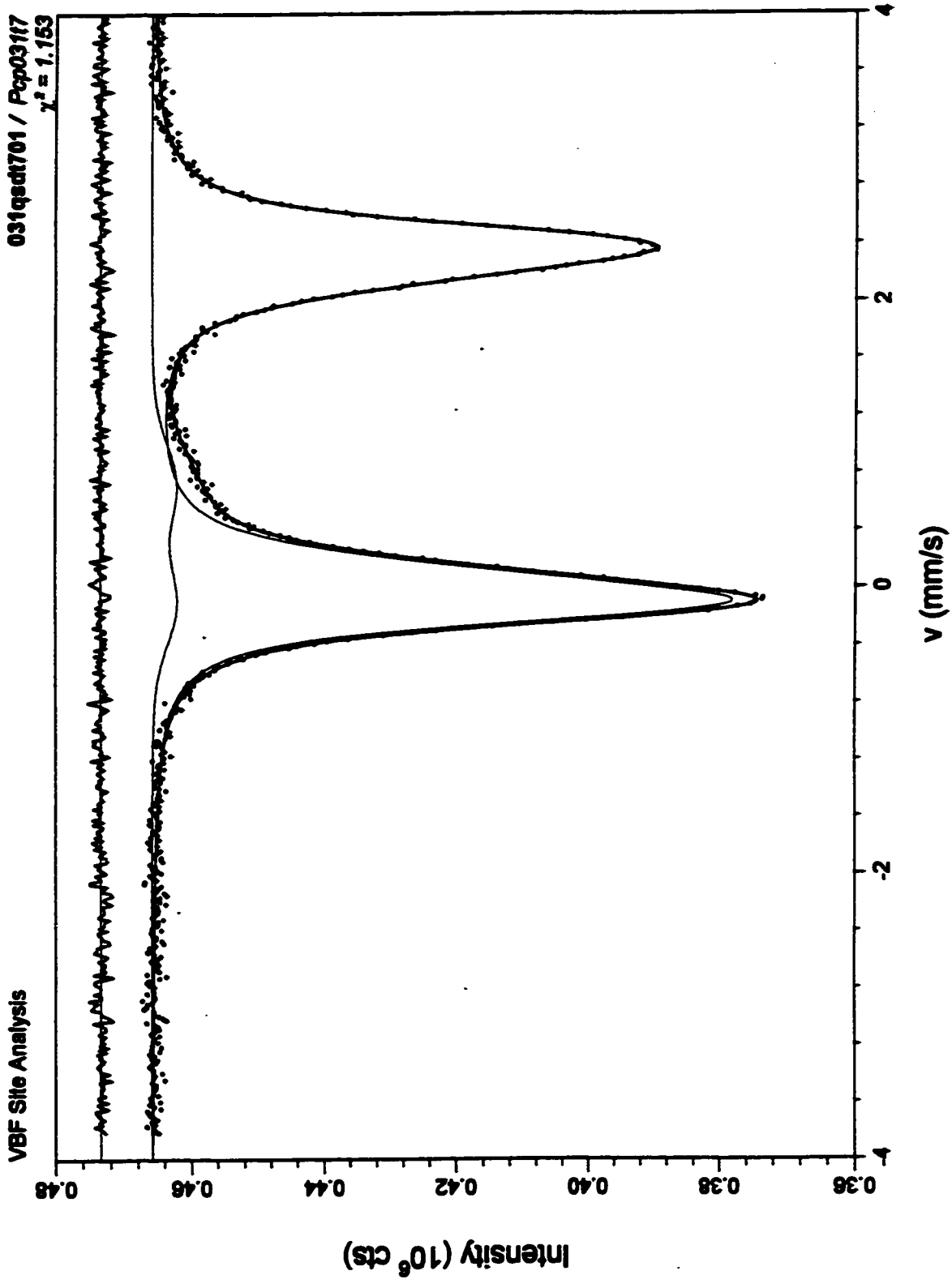
031qsdt1701 / Pcp03117
χ^2 = 1.153
VBF Site Analysis
Intensity (10^6 cts)
0.36
0.38
0.40
0.42
0.44
0.46
0.48
-4
-2
0
2
4
v (mm/s)

VBF Analysis of Pcp032t7

project:
document: 032qsdt701
data document: Pcp032t7

Fit Summary
no. of data points: 512
no. of QSD sites in model: 2
no. of parameters in model: 22
no. of refined parameters: 17
reduced $\chi^2 = 1.18012$
uncertainties calculated using the covariance matrix

Global Parameters
Background = 1570050(170) counts
Lorentzian HWHM = 0.097* mm/s

Site Distribution Parameters

	δ_0 (mm/s)	δ_1	A (counts·mm/s)	A_1/A_+
Fe2+	1.1538(69)	-0.0046(29)	253200(2000)	1.1622(52)
Fe3+	0.319(22)	0*	19600(1700)	1*

		p (%)	$\langle\Delta\rangle$ (mm/s)	σ_Δ (mm/s)
Fe2+	comp 1	14.676*	2.200(55)	0.71(11)
	comp 2	49(28)	2.14(15)	0.284(63)
	comp 3	36(25)	2.493(49)	0.208(26)
Fe3+	comp 1	100*	1.039(46)	0.412(41)

Compiled Site Properties

	Site Populations
Fe2+	92.82(58)
Fe3+	7.18(58)

	<CS> (mm/s)	$\langle\lvert\Delta\rvert\rangle$ (mm/s)	stdev(|Δ|) (mm/s)	skew(|Δ|)
Fe2+	1.1433	2.27602	0.394401	-0.321479
Fe3+	0.318827	1.04006	0.408077	0.0642884

VBF Analysis of Pcp033t7

project:
document: 033qsdt703
data document: Pcp033t7

Fit Summary
no. of data points: 512
no. of QSD sites in model: 2
no. of parameters in model: 22
no. of refined parameters: 16
reduced χ^2 = 1.20388
uncertainties calculated using the covariance matrix

Global Parameters
Background = 1109420(150) counts
Lorentzian HWHM = 0.097* mm/s

Site Distribution Parameters

	δ_0 (mm/s)	δ_1	A (counts·mm/s)	A_-/A_+
Fe2+	1.156(16)	-0.0025(62)	144300(1800)	1.1461(85)
Fe3+	0.3*	0*	11300(1500)	1*

		p (%)	$\langle\Delta\rangle$ (mm/s)	σ_Δ (mm/s)
Fe2+	comp 1	57.3811*	2.290(57)	0.320(33)
	comp 2	35(10)	2.559(11)	0.168(21)
	comp 3	7.9(73)	2.24(16)	0.73(31)
Fe3+	comp 1	100*	0.862(69)	0.464(67)

Compiled Site Properties

	Site Populations
Fe2+	92.76(91)
Fe3+	7.24(91)

	<CS> (mm/s)	<|Δ|> (mm/s)	stdev(|Δ|) (mm/s)	skew(|Δ|)
Fe2+	1.14984	2.37929	0.358137	-0.572448
Fe3+	0.3	0.873232	0.44208	0.237347

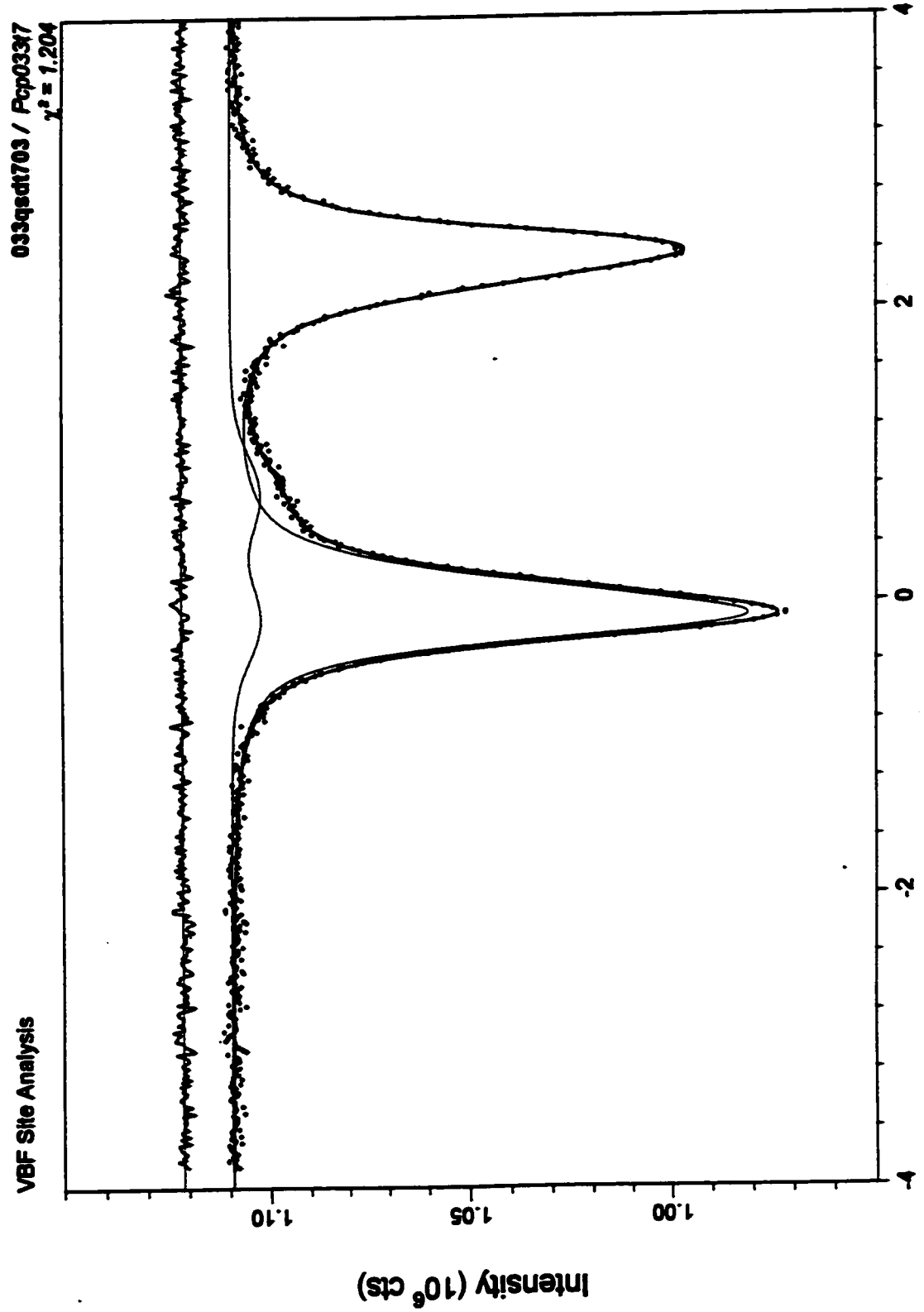
033qsdt703 / Pcp03317
χ^2 = 1.204
VBF Site Analysis
Intensity (10^6 cts)
1.10
1.05
1.00
-4
-2
0
2
4
v (mm/s)

VBF Analysis of Pcp034t7

project:
document: 034qsdt701
data document: Pcp034t7

Fit Summary
no. of data points: 512
no. of QSD sites in model: 2
no. of parameters in model: 22
no. of refined parameters: 17
reduced χ^2 = 0.976404
uncertainties calculated using the covariance matrix

Global Parameters
Background = 223277(59) counts
Lorentzian HWHM = 0.097* mm/s

Site Distribution Parameters

	δ_0 (mm/s)	δ_1	A (counts·mm/s)	A_1/A_0
Fe2+	1.135(11)	0.0039(45)	59160(490)	1.1523(68)
Fe3+	0.263(58)	0*	2250(500)	1*

		p (%)	$\langle\Delta\rangle$ (mm/s)	σ_Δ (mm/s)
Fe2+	comp 1	44.3326*	2.43(23)	0.28(18)
	comp 2	32(95)	2.26(36)	0.38(10)
	comp 3	24(30)	2.547(30)	0.143(62)
Fe3+	comp 1	100*	1.08(14)	0.45(13)

Compiled Site Properties

	Site Populations
Fe2+	96.34(78)
Fe3+	3.66(78)

	<CS> (mm/s)	<|Δ|> (mm/s)	stdev(|Δ|) (mm/s)	skew(|Δ|)
Fe2+	1.14413	2.4055	0.312115	-0.496481
Fe3+	0.262942	1.08187	0.442693	0.0830137

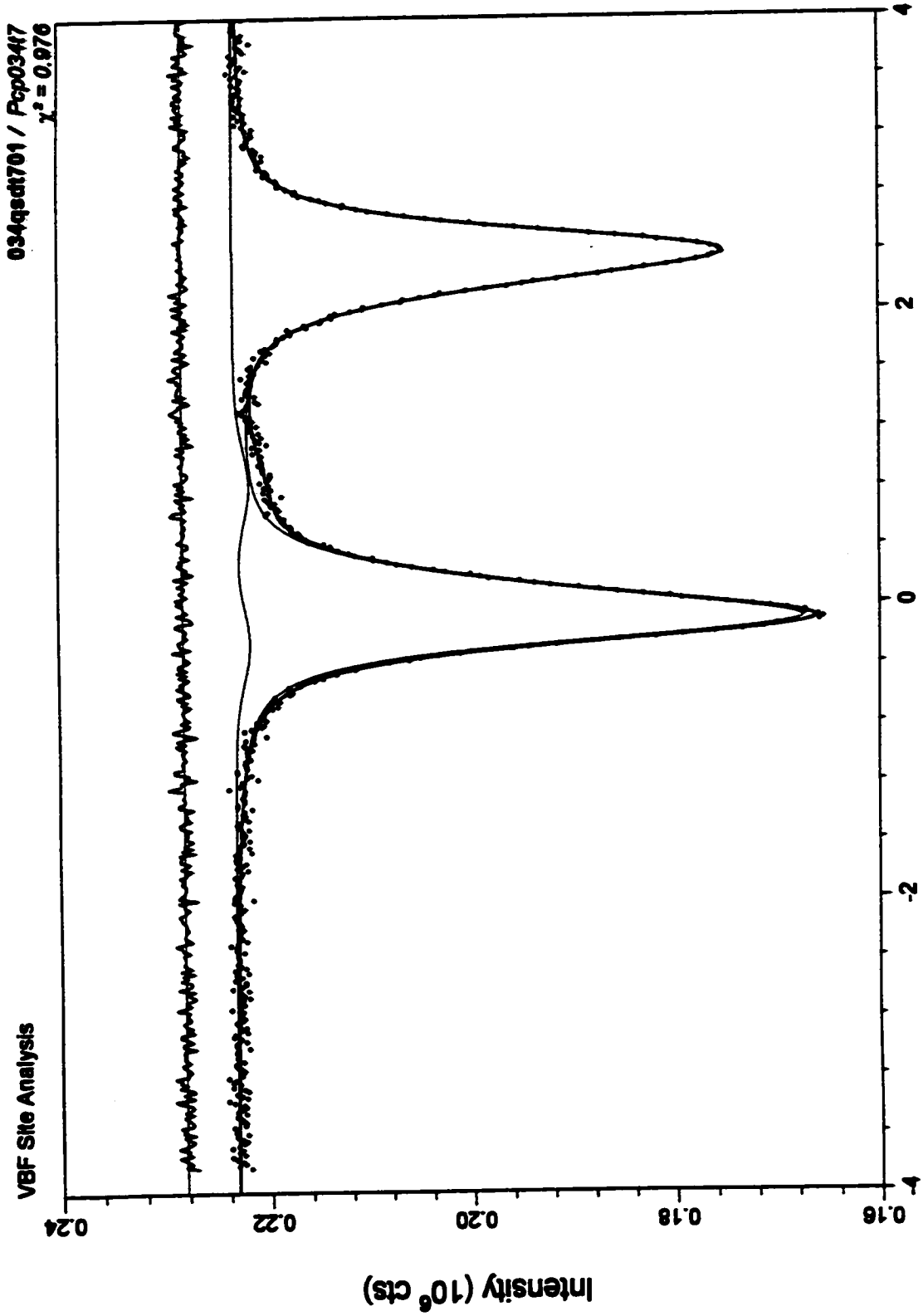
034qsdt701 / Pcp03417
χ^2 = 0.976
VBF Site Analysis
Intensity (10^6 cts)
0.24
0.22
0.20
0.18
0.16
-4
-2
0
2
4
v (mm/s)

VBF Analysis of Pcp036t7

project:
document: 036qsdt701
data document: Pcp036t7

Fit Summary
no. of data points: 512
no. of QSD sites in model: 2
no. of parameters in model: 22
no. of refined parameters: 17
reduced χ^2 = 1.04047
uncertainties calculated using the covariance matrix

Global Parameters
Background = 303189(72) counts
Lorentzian HWHM = 0.097* mm/s

Site Distribution Parameters

	δ_0 (mm/s)	δ_1	A (counts-mm/s)	A_1/A_0
Fe2+	1.111(13)	0.0140(53)	70800(810)	1.0442(86)
Fe3+	0.270(55)	0*	3980(770)	1*

		p (%)	$\langle\Delta\rangle$ (mm/s)	σ_Δ (mm/s)
Fe2+	comp 1	50.5533*	2.458(73)	0.196(36)
	comp 2	19(12)	2.36(11)	0.51(12)
	comp 3	31(28)	2.08(19)	0.229(86)
Fe3+	comp 1	100*	0.92(13)	0.60(14)

Compiled Site Properties

	Site Populations
Fe2+	94.68(98)
Fe3+	5.32(98)

	<CS> (mm/s)	<|Δ|> (mm/s)	stdev(|Δ|) (mm/s)	skew(|Δ|)
Fe2+	1.14311	2.32342	0.33431	-0.0387901
Fe3+	0.26989	0.94985	0.546231	0.388137

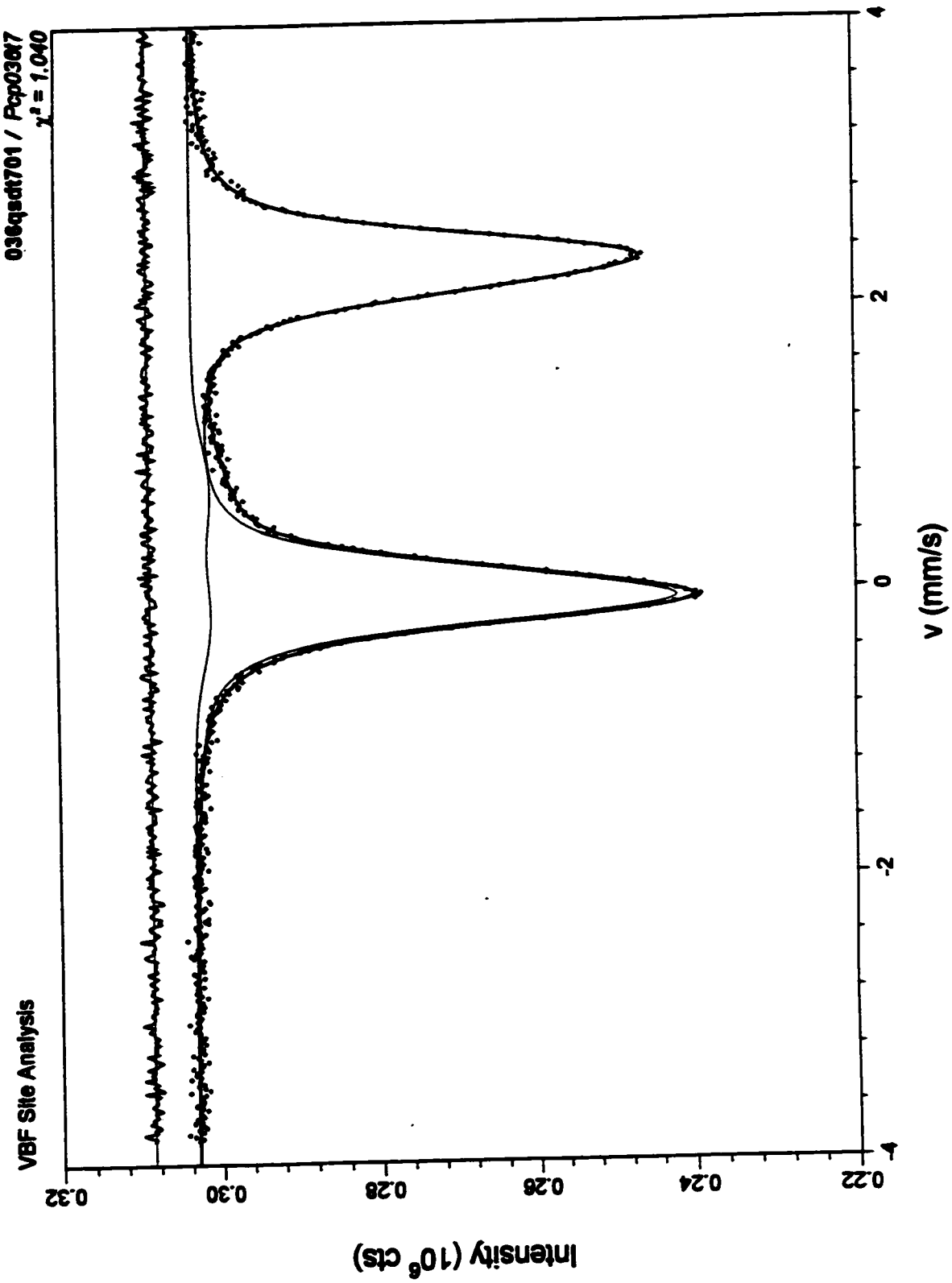
036qsdt701 / Pcp036t7
χ^2 = 1.040
VBF Site Analysis
Intensity (10^6 cts)
0.32
0.30
0.28
0.26
0.24
0.22
-4
-2
0
2
4
v (mm/s)

VBF Analysis of Pcp037t7

project:
document: 037qsdt703
data document: Pcp037t7

Fit Summary

no. of data points: 512
no. of QSD sites in model: 2
no. of parameters in model: 22
no. of refined parameters: 16
reduced χ^2 = 1.14917
uncertainties calculated using the covariance matrix

Global Parameters

Background = 284749(69) counts
Lorentzian HWHM = 0.097* mm/s

Site Distribution Parameters

	δ_0 (mm/s)	δ_1	A (counts·mm/s)	A_-/A_+
Fe2+	1.114(14)	0.0135(55)	63940(560)	1.0701(62)
Fe3+	0.3*	0*	1680(490)	1*

		p (%)	$\langle\Delta\rangle$ (mm/s)	σ_Δ (mm/s)
Fe2+	comp 1	6.95207*	2.70(69)	0.50(24)
	comp 2	68(27)	2.329(81)	0.287(32)
	comp 3	25(19)	2.521(21)	0.153(45)
Fe3+	comp 1	100*	0.81(15)	0.41(17)

Compiled Site Properties

	Site Populations
Fe2+	97.44(73)
Fe3+	2.56(73)

	<CS> (mm/s)	<|Δ|> (mm/s)	stdev(|Δ|) (mm/s)	skew(|Δ|)
Fe2+	1.14613	2.40405	0.304112	0.255881
Fe3+	0.3	0.821661	0.393098	0.185597

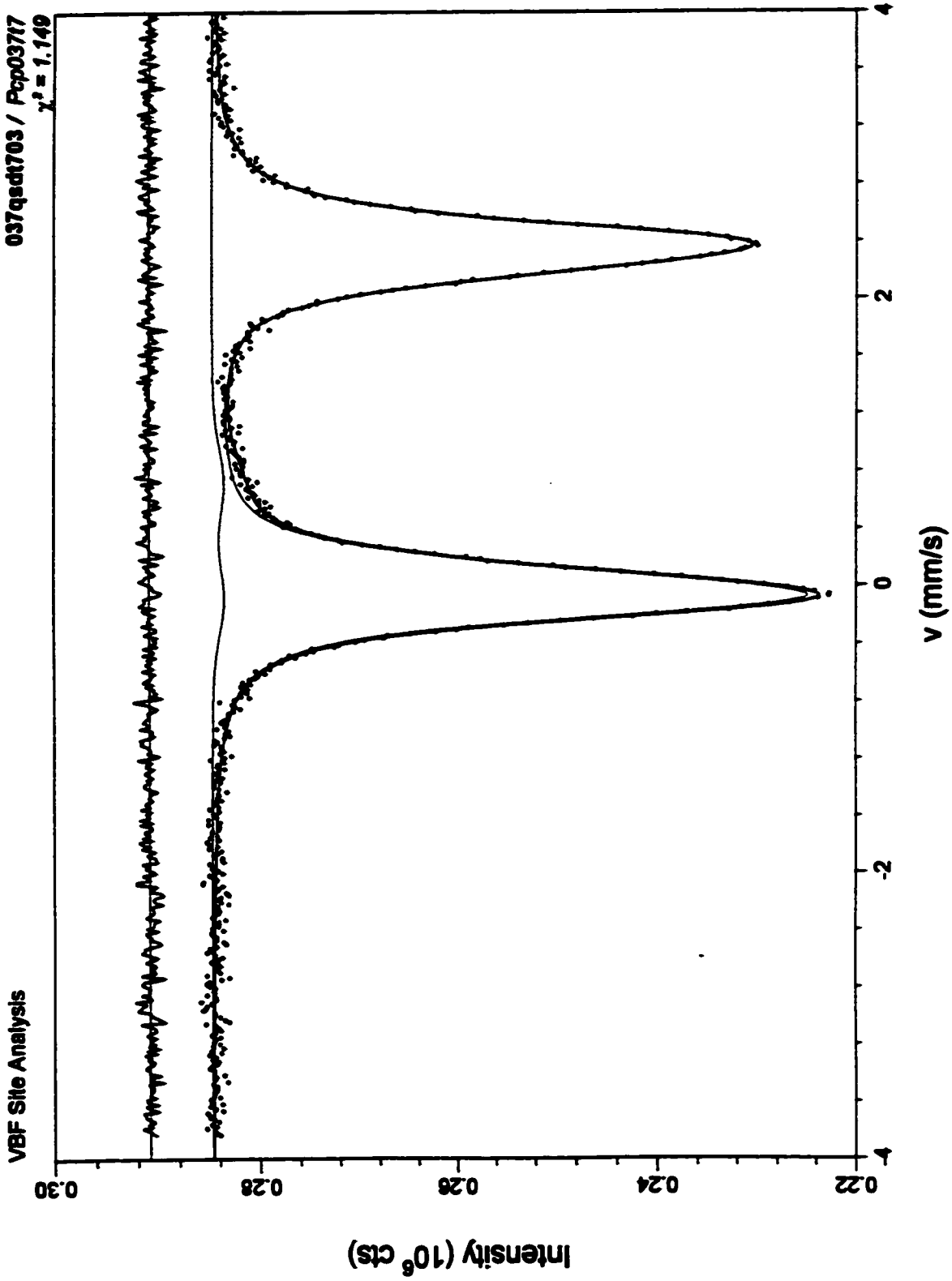
037qsdt703 / Pcp03717
χ² = 1.149
VBF Site Analysis
Intensity (10⁶ cts)
0.30
0.28
0.26
0.24
0.22
-4
-2
0
2
4
v (mm/s)

VBF Analysis of Pcp038t7

project:
document: 038qsdt702
data document: Pcp038t7

Fit Summary
no. of data points: 512
no. of QSD sites in model: 2
no. of parameters in model: 22
no. of refined parameters: 15
reduced χ^2 = 1.13569
uncertainties calculated using the covariance matrix

Global Parameters
Background = 1348120(140) counts
Lorentzian HWHM = 0.097* mm/s

Site Distribution Parameters

	δ_0 (mm/s)	δ_1	A (counts·mm/s)	A_1/A_+
Fe2+	1.1729(97)	-0.0081(38)	183000(1100)	1.1192(45)
Fe3+	0.305*	0*	4000(1100)	1*

		p (%)	$\langle\Delta\rangle$ (mm/s)	σ_Δ (mm/s)
Fe2+	comp 1	30.0086*	2.251(43)	0.439(52)
	comp 2	7.6(45)	2.039(35)	0.113(55)
	comp 3	62.3(79)	2.5093(98)	0.206(12)
Fe3+	comp 1	100*	0.92*	0.44(16)

Compiled Site Properties

	Site Populations
Fe2+	97.88(56)
Fe3+	2.12(56)

	<CS> (mm/s)	$\langle\|\Delta\|\rangle$ (mm/s)	stdev(|Δ|) (mm/s)	skew(|Δ|)
Fe2+	1.1536	2.39582	0.330938	-0.569787
Fe3+	0.305	0.925426	0.423658	0.150972

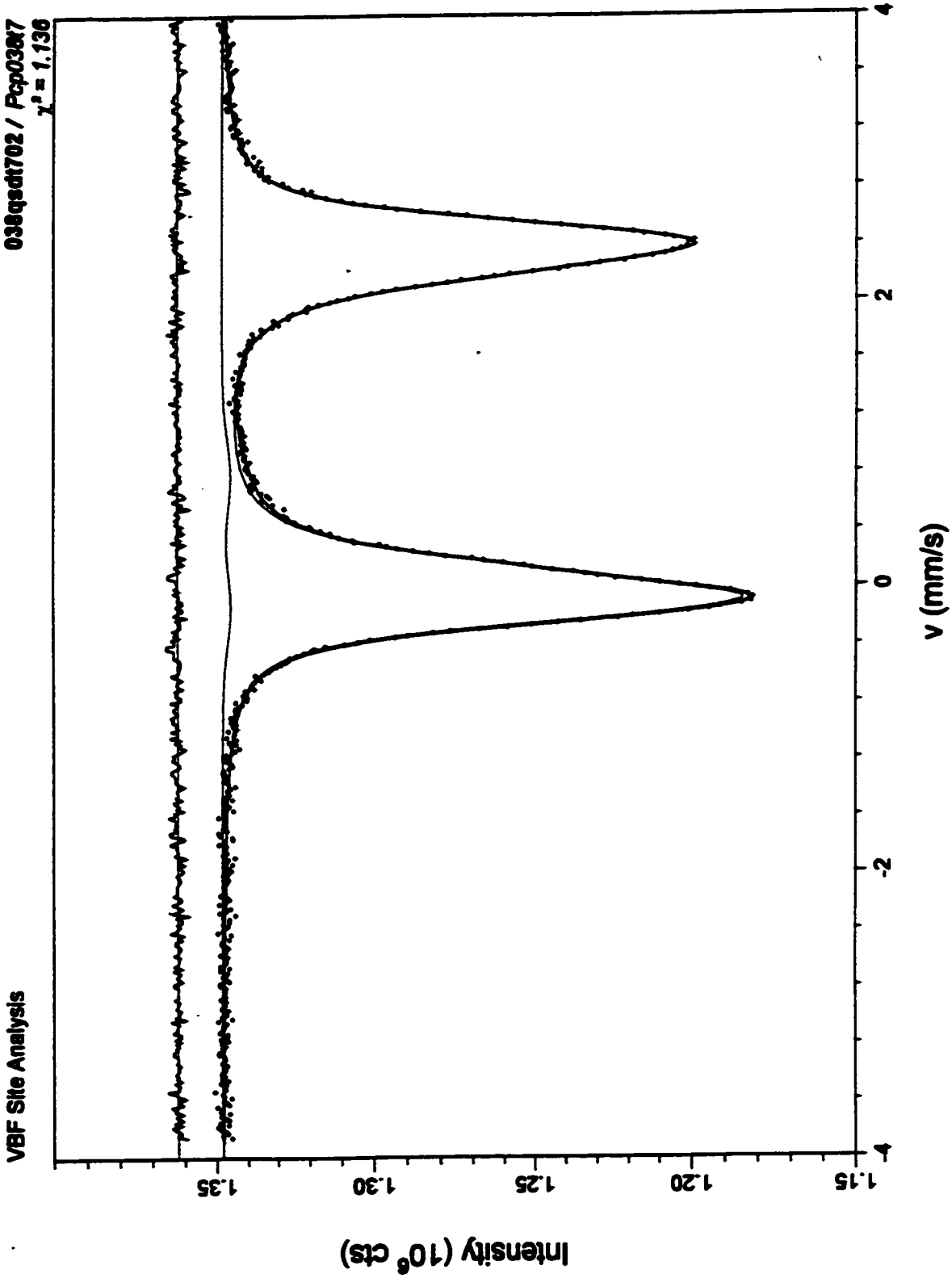
038qsdt702 / Pcp03807
χ^2 = 1.136
VBF Site Analysis
Intensity (10^6 cts)
1.15
1.20
1.25
1.30
1.35
-4
-2
0
2
4
v (mm/s)

VBF Analysis of Pcp039t7

project:
document: 039qsdt702
data document: Pcp039t7

Fit Summary
no. of data points: 512
no. of QSD sites in model: 2
no. of parameters in model: 22
no. of refined parameters: 17
reduced $\chi^2 = 1.1038$
uncertainties calculated using the covariance matrix

Global Parameters
Background = 669620(100) counts
Lorentzian HWHM = 0.097* mm/s

Site Distribution Parameters

	δ_0 (mm/s)	δ_1	A (counts·mm/s)	A_1/A_2
Fe2+	1.142(16)	0.0002(65)	94500(1300)	1.104(11)
Fe3+	0.311(35)	0*	8500(1200)	1*

		p (%)	$\langle\Delta\rangle$ (mm/s)	σ_Δ (mm/s)
Fe2+	comp 1	39.6285*	2.147(50)	0.502(68)
	comp 2	19(26)	2.06(20)	0.20(12)
	comp 3	41(21)	2.462(96)	0.200(44)
Fe3+	comp 1	100*	0.961(85)	0.424(70)

Compiled Site Properties

	Site Populations
Fe2+	91.8(11)
Fe3+	8.2(11)

	<CS> (mm/s)	<|Δ|> (mm/s)	stdev(|Δ|) (mm/s)	skew(|Δ|)
Fe2+	1.142	2.26111	0.391642	-0.458029
Fe3+	0.310777	0.964492	0.416576	0.112292

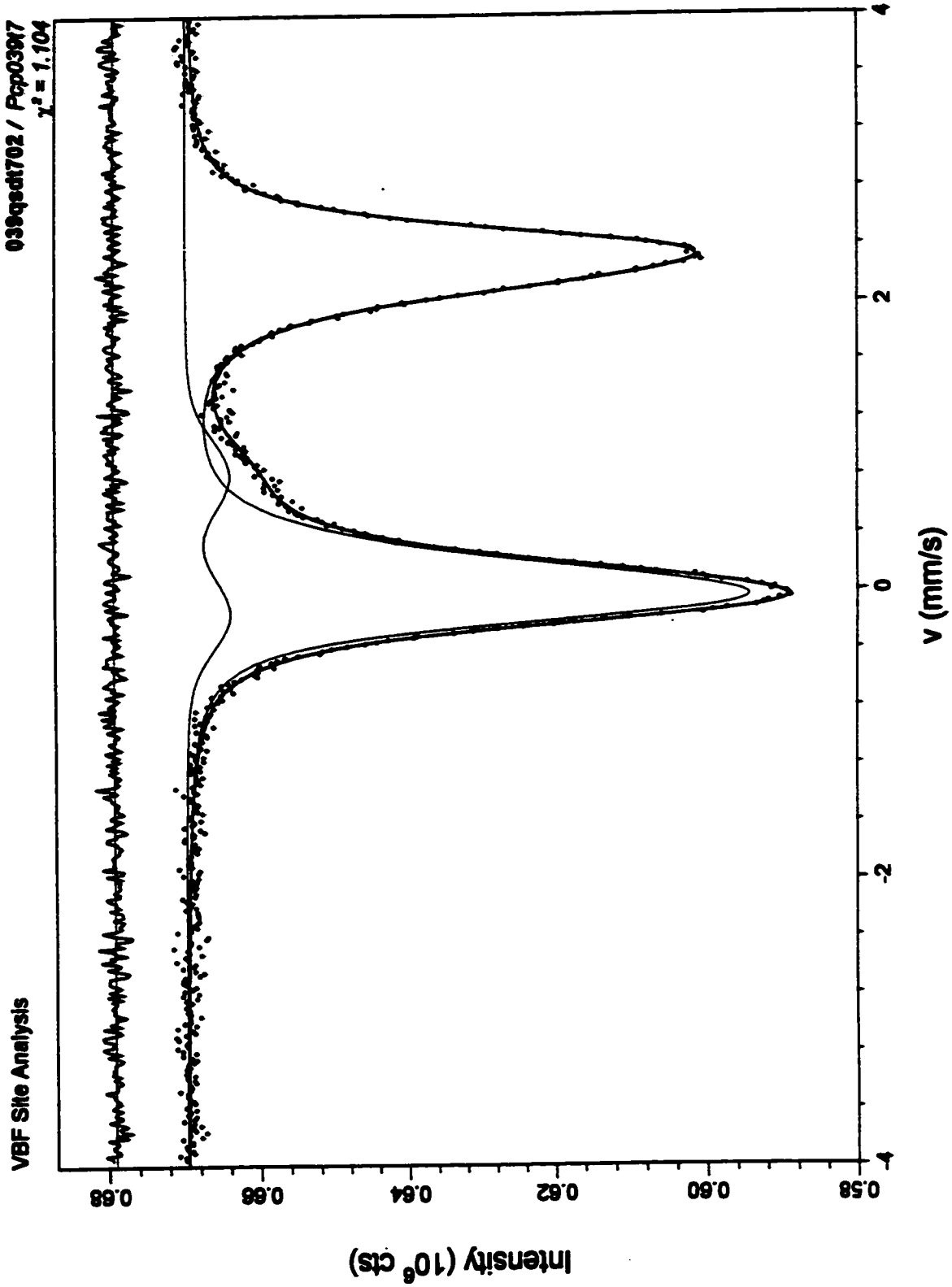
039qsdt702 / Pcp03917
χ^2 = 1.104
VBF Site Analysis
Intensity (10^6 cts)
0.58
0.60
0.62
0.64
0.66
0.68
-4
-2
0
2
4
v (mm/s)

VBF Analysis of Pcp040t7

project:
document: 040qsdt701
data document: Pcp040t7

Fit Summary
no. of data points: 512
no. of QSD sites in model: 2
no. of parameters in model: 22
no. of refined parameters: 17
reduced χ^2 = 1.04241
uncertainties calculated using the covariance matrix

Global Parameters
Background = 380510(79) counts
Lorentzian HWHM = 0.097* mm/s

Site Distribution Parameters

	δ_0 (mm/s)	δ_1	A (counts·mm/s)	A_-/A_+
Fe2+	1.155(15)	-0.0050(60)	76520(880)	1.1851(88)
Fe3+	0.299(57)	0*	4400(790)	1*

		p (%)	$\langle\Delta\rangle$ (mm/s)	σ_Δ (mm/s)
Fe2+	comp 1	47.6078*	2.530(60)	0.187(28)
	comp 2	29(29)	2.16(20)	0.23(10)
	comp 3	23(15)	2.273(64)	0.52(12)
Fe3+	comp 1	100*	0.89(13)	0.390(88)

Compiled Site Properties

	Site Populations
Fe2+	94.56(92)
Fe3+	5.44(92)

	<CS> (mm/s)	$\langle\|\Delta\|\rangle$ (mm/s)	stdev(|Δ|) (mm/s)	skew(|Δ|)
Fe2+	1.14289	2.36119	0.351372	-0.42854
Fe3+	0.299326	0.893513	0.382796	0.107496

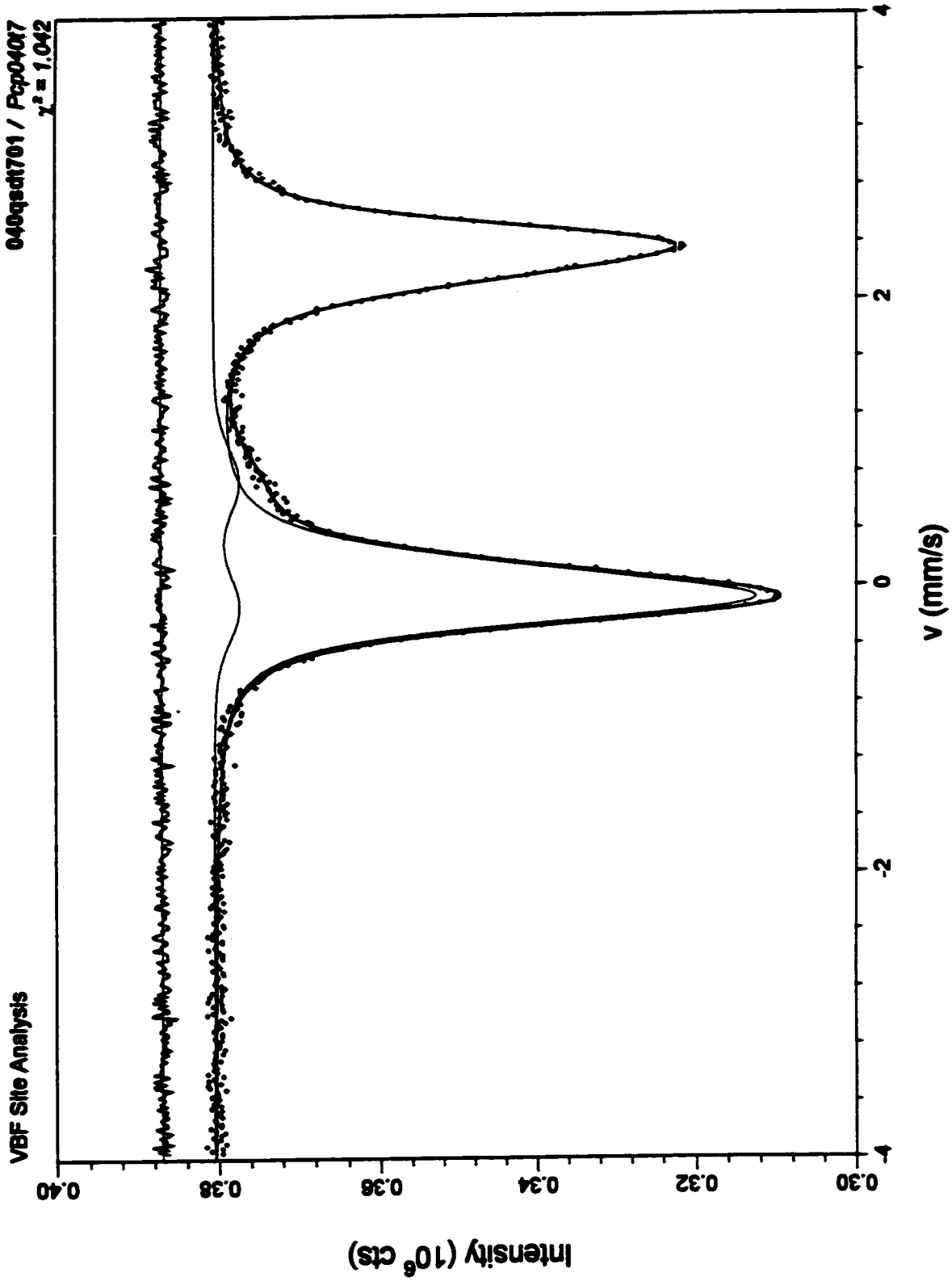
040qsdt701 / Pcp04017
χ^2 = 1.042
VBF Site Analysis
Intensity (10^6 cts)
0.40
0.38
0.36
0.34
0.32
0.30
-4
-2
0
2
4
v (mm/s)

VBF Analysis of Pcp041t7

project:
document: 041qsdt705
data document: Pcp041t7

Fit Summary
no. of data points: 512
no. of QSD sites in model: 2
no. of parameters in model: 22
no. of refined parameters: 16
reduced χ^2 = 1.21332
uncertainties calculated using the covariance matrix

Global Parameters
Background = 447305(83) counts
Lorentzian HWHM = 0.097* mm/s

Site Distribution Parameters

		δ_0 (mm/s)	δ_1	A (counts·mm/s)	A_1/A_0
Fe2+		1.133(13)	-0.0039(51)	106100(1000)	1.2429(81)
Fe3+		0.276225*	0*	1230(960)	1*
			p (%)	$\langle\Delta\rangle$ (mm/s)	σ_Δ (mm/s)
Fe2+	comp 1		29.5561*	2.248(35)	0.482(59)
	comp 2		46(17)	2.415(47)	0.174(26)
	comp 3		24(15)	2.05(12)	0.192(58)
Fe3+	comp 1		100*	0.76(32)	0.35(34)

Compiled Site Properties

	Site Populations
Fe2+	98.85(88)
Fe3+	1.15(88)

	<CS> (mm/s)	<|Δ|> (mm/s)	stdev(|Δ|) (mm/s)	skew(|Δ|)
Fe2+	1.12386	2.27759	0.336313	-0.212364
Fe3+	0.276225	0.761564	0.342167	0.137663

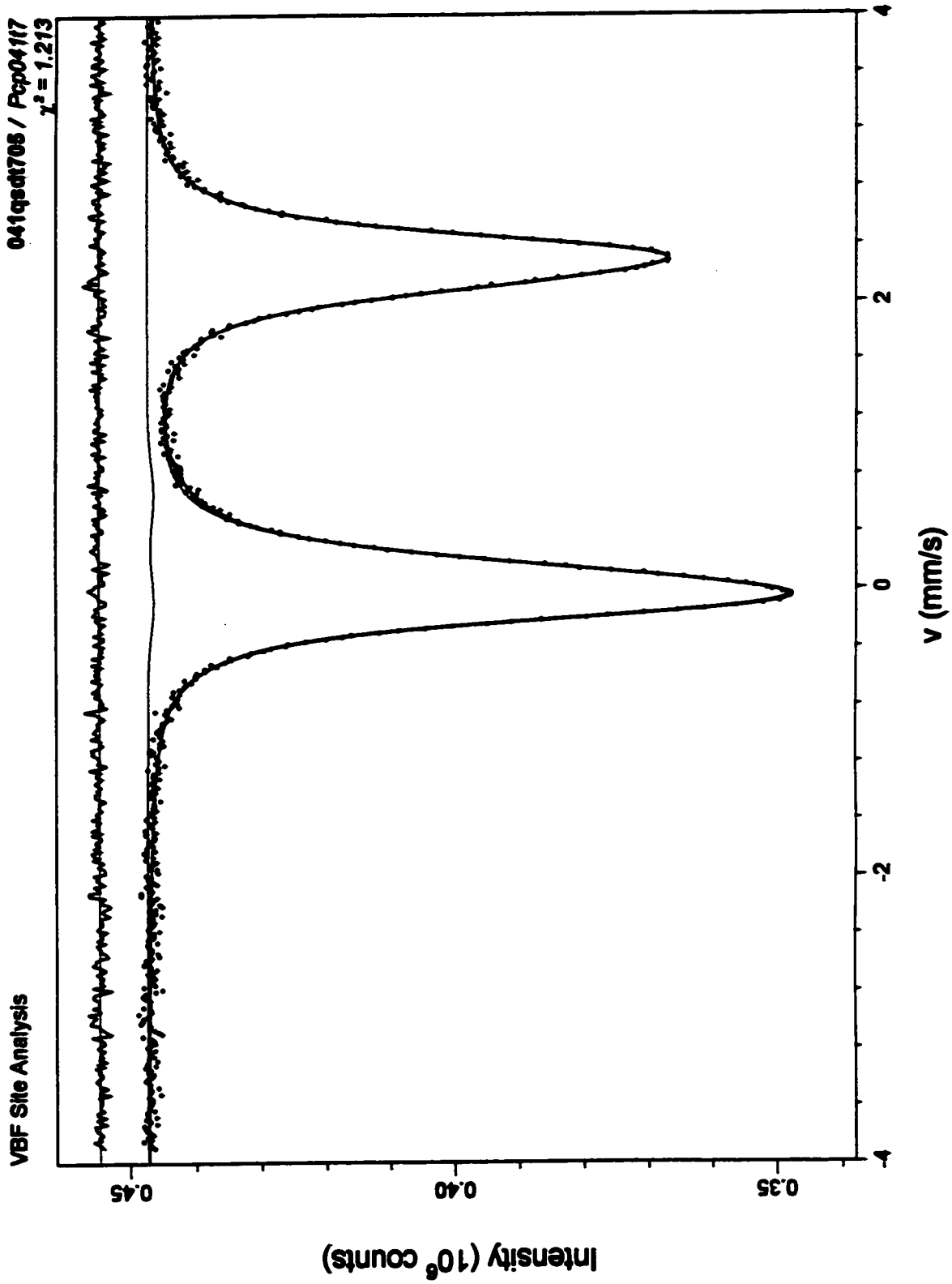
041qsdt706 / Pcp04117
χ^2 = 1.213
VBF Site Analysis
Intensity (10^6 counts)
0.45
0.40
0.35
-4
-2
0
2
4
v (mm/s)

VBF Analysis of Pcp042t7

project:
document: 042qsdt702
data document: Pcp042t7

Fit Summary
no. of data points: 512
no. of QSD sites in model: 2
no. of parameters in model: 22
no. of refined parameters: 17
reduced $\chi^2 = 1.2585$
uncertainties calculated using the covariance matrix

Global Parameters
Background = 960070(140) counts
Lorentzian HWHM = 0.097* mm/s

Site Distribution Parameters

	δ_0 (mm/s)	δ_1	A (counts·mm/s)	A_1/A_0
Fe2+	1.154(15)	-0.0090(60)	149500(2300)	1.177(12)
Fe3+	0.281(59)	0*	8500(2000)	1*

		p (%)	$\langle\Delta\rangle$ (mm/s)	σ_Δ (mm/s)
Fe2+	comp 1	47.489*	2.40(11)	0.249(49)
	comp 2	11.5(59)	2.15(10)	0.85(22)
	comp 3	41(80)	2.06(51)	0.31(17)
Fe3+	comp 1	100*	0.84(13)	0.42(11)

Compiled Site Properties

	Site Populations
Fe2+	94.6(12)
Fe3+	5.4(12)

	<CS> (mm/s)	<|Δ|> (mm/s)	stdev(|Δ|) (mm/s)	skew(|Δ|)
Fe2+	1.13387	2.23359	0.422151	-0.295322
Fe3+	0.281374	0.845688	0.403782	0.183915

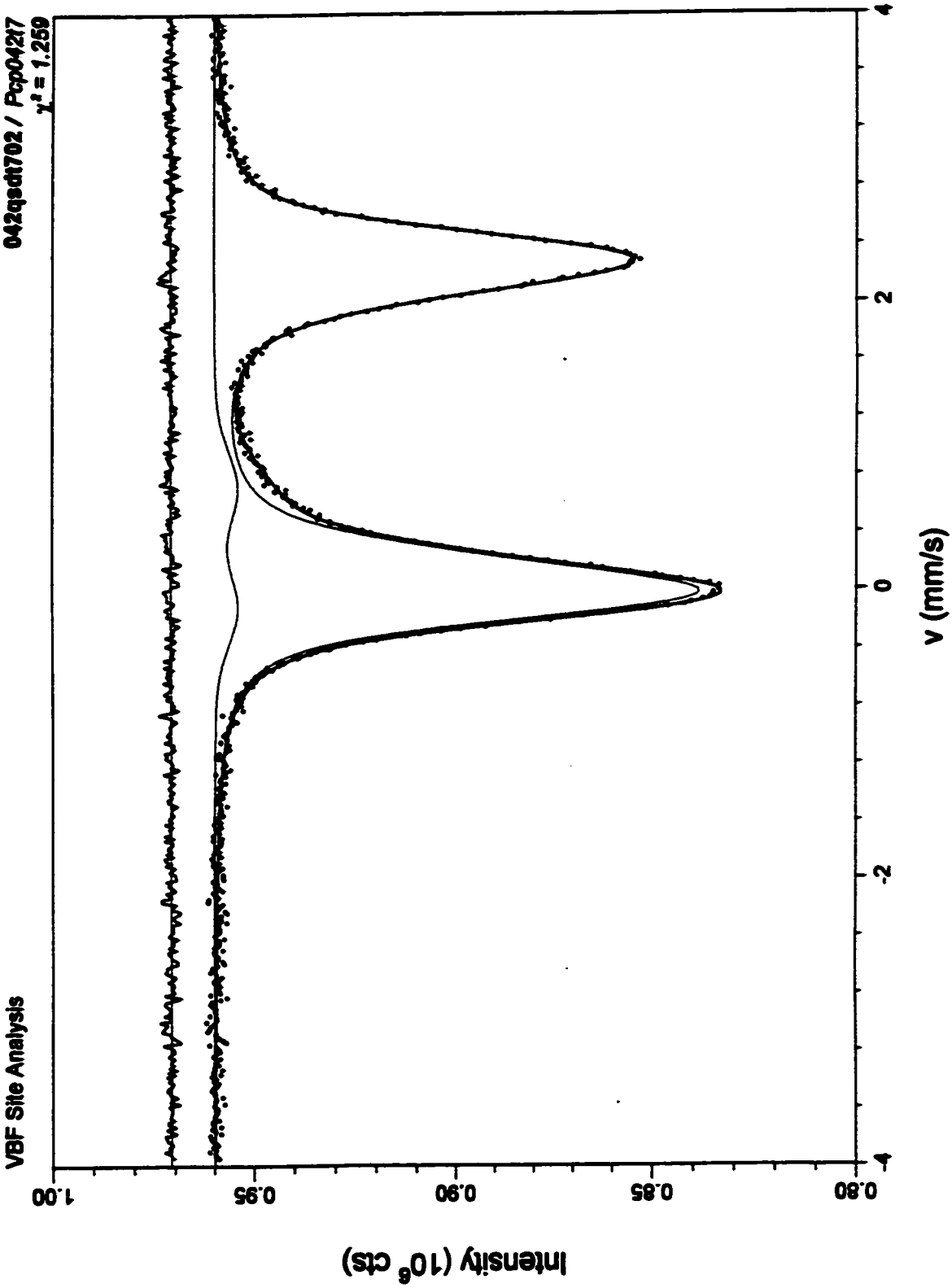
042qsdt702 / Pcp04217
χ^2 = 1.259
VBF Site Analysis
Intensity (10^6 cts)
1.00
0.95
0.90
0.85
0.80
-4
-2
0
2
4
v (mm/s)

VBF Analysis of Amtvmt7

project:
document: Amtvmt7
data document: Amtvmt7

Fit Summary
no. of data points: 512
no. of QSD sites in model: 2
no. of parameters in model: 22
no. of refined parameters: 16
reduced χ^2 = 1.27377
uncertainties calculated using the covariance matrix

Global Parameters
Background = 1503070(160) counts
Lorentzian HWHM = 0.097* mm/s

Site Distribution Parameters

	δ_0 (mm/s)	δ_1	A (counts-mm/s)	A_i/A_+
Fe2+	1.0294(78)	0.0434(31)	145100(1300)	1*
Fe3+	0.288(18)	0*	33750(840)	1*

		p (%)	$\langle\Delta\rangle$ (mm/s)	σ_Δ (mm/s)
Fe2+	comp 1	13.5457*	2.06(17)	0.59(22)
	comp 2	68(16)	2.412(57)	0.252(30)
	comp 3	18(19)	1.94(15)	0.222(91)
Fe3+	comp 1	100*	0.742(32)	0.573(31)

Compiled Site Properties

	Site Populations
Fe2+	81.13(40)
Fe3+	18.87(40)

	<CS> (mm/s)	<|Δ|> (mm/s)	stdev(|Δ|) (mm/s)	skew(|Δ|)
Fe2+	1.12831	2.27691	0.37365	-0.558257
Fe3+	0.287597	0.795047	0.497417	0.519595

VBF Analysis of Am01t71

project:
document: Am01tvmt71
data document: Am01t71

Fit Summary
no. of data points: 512
no. of QSD sites in model: 2
no. of parameters in model: 22
no. of refined parameters: 3
reduced χ^2 = 1.85902
uncertainties calculated using the covariance matrix

Global Parameters
Background = 3385750(160) counts
Lorentzian HWHM = 0.097* mm/s

Site Distribution Parameters

	δ_0 (mm/s)	δ_1	A (counts·mm/s)	A_1/A_2
Fe2+	1.0294*	0.0434*	155344*	2.1827(75)
Fe3+	0.288*	0*	36131.4*	0.733(25)

		p (%)	$\langle\Delta\rangle$ (mm/s)	σ_Δ (mm/s)
Fe2+	comp 1	14*	2.06*	0.59*
	comp 2	68*	2.412*	0.252*
	comp 3	18*	1.94*	0.222*
Fe3+	comp 1	100*	0.742*	0.573*

Compiled Site Properties

	Site Populations
Fe2+	81.13
Fe3+	18.87

	<CS> (mm/s)	<|Δ|> (mm/s)	stdev(|Δ|) (mm/s)	skew(|Δ|)
Fe2+	1.12825	2.27777	0.374392	-0.572032
Fe3+	0.288	0.794739	0.497276	0.519777

VBF Analysis of Am02t71

project:
document: Am02tvmt71
data document: Am02t71

Fit Summary
no. of data points: 512
no. of QSD sites in model: 2
no. of parameters in model: 22
no. of refined parameters: 3
reduced $\chi^2 = 1.77947$
uncertainties calculated using the covariance matrix

Global Parameters
Background = 3094110(150) counts
Lorentzian HWHM = 0.097* mm/s

Site Distribution Parameters

	δ_0 (mm/s)	δ_1	A (counts·mm/s)	A_1/A_+
Fe2+	1.0294*	0.0434*	142092*	2.0074(74)
Fe3+	0.288*	0*	33049.1*	0.782(27)

		p (%)	$\langle\Delta\rangle$ (mm/s)	σ_Δ (mm/s)
Fe2+	comp 1	14*	2.06*	0.59*
	comp 2	68*	2.412*	0.252*
	comp 3	18*	1.94*	0.222*
Fe3+	comp 1	100*	0.742*	0.573*

Compiled Site Properties

	Site Populations
Fe2+	81.13
Fe3+	18.87

	<CS> (mm/s)	$\langle\|\Delta\|\rangle$ (mm/s)	stdev(|Δ|) (mm/s)	skew(|Δ|)
Fe2+	1.12825	2.27777	0.374392	-0.572032
Fe3+	0.288	0.794739	0.497276	0.519777

VBF Analysis of Am03t71

project:
document: Am03tvmt71
data document: Am03t71

Fit Summary
no. of data points: 512
no. of QSD sites in model: 2
no. of parameters in model: 22
no. of refined parameters: 3
reduced χ^2 = 1.80907
uncertainties calculated using the covariance matrix

Global Parameters
Background = 3457140(160) counts
Lorentzian HWHM = 0.097* mm/s

Site Distribution Parameters

	δ_0 (mm/s)	δ_1	A (counts·mm/s)	A_1/A_2
Fe2+	1.0294*	0.0434*	168188*	1.6470(58)
Fe3+	0.288*	0*	39118.9*	0.711(23)

		p (%)	$\langle\Delta\rangle$ (mm/s)	σ_Δ (mm/s)
Fe2+	comp 1	14*	2.06*	0.59*
	comp 2	68*	2.412*	0.252*
	comp 3	18*	1.94*	0.222*
Fe3+	comp 1	100*	0.742*	0.573*

Compiled Site Properties

	Site Populations
Fe2+	81.13
Fe3+	18.87

	<CS> (mm/s)	<|Δ|> (mm/s)	stdev(|Δ|) (mm/s)	skew(|Δ|)
Fe2+	1.12825	2.27777	0.374392	-0.572032
Fe3+	0.288	0.794739	0.497276	0.519777

VBF Analysis of Am04t71

project:
document: Am04tvmt71
data document: Am04t71

Fit Summary
no. of data points: 512
no. of QSD sites in model: 2
no. of parameters in model: 22
no. of refined parameters: 3
reduced $\chi^2 = 1.74675$
uncertainties calculated using the covariance matrix

Global Parameters
Background = 4023720(170) counts
Lorentzian HWHM = 0.097* mm/s

Site Distribution Parameters

	δ_0 (mm/s)	δ_1	A (counts·mm/s)	A_-/A_+
Fe2+	1.0294*	0.0434*	195729*	1.2069(45)
Fe3+	0.288*	0*	45524.5*	0.913(24)

		p (%)	$\langle\Delta\rangle$ (mm/s)	σ_Δ (mm/s)
Fe2+	comp 1	14*	2.06*	0.59*
	comp 2	68*	2.412*	0.252*
	comp 3	18*	1.94*	0.222*
Fe3+	comp 1	100*	0.742*	0.573*

Compiled Site Properties

	Site Populations
Fe2+	81.13
Fe3+	18.87

	<CS> (mm/s)	$\langle\|\Delta\|\rangle$ (mm/s)	stdev(|Δ|) (mm/s)	skew(|Δ|)
Fe2+	1.12825	2.27777	0.374392	-0.572032
Fe3+	0.288	0.794739	0.497276	0.519777

VBF Analysis of Am05t71

project:
document: Am05tvmt71
data document: Am05t71

Fit Summary
no. of data points: 512
no. of QSD sites in model: 2
no. of parameters in model: 22
no. of refined parameters: 3
reduced $\chi^2 = 1.8259$
uncertainties calculated using the covariance matrix

Global Parameters
Background = 4164210(180) counts
Lorentzian HWHM = 0.097* mm/s

Site Distribution Parameters

	δ_0 (mm/s)	δ_1	A (counts-mm/s)	A_1/A_2
Fe2+	1.0294*	0.0434*	180413*	1.0026(45)
Fe3+	0.288*	0*	41962.3*	0.937(27)

		p (%)	$\langle\Delta\rangle$ (mm/s)	σ_Δ (mm/s)
Fe2+	comp 1	14*	2.06*	0.59*
	comp 2	68*	2.412*	0.252*
	comp 3	18*	1.94*	0.222*
Fe3+	comp 1	100*	0.742*	0.573*

Compiled Site Properties

	Site Populations
Fe2+	81.13
Fe3+	18.87

	<CS> (mm/s)	<|Δ|> (mm/s)	stdev(|Δ|) (mm/s)	skew(|Δ|)
Fe2+	1.12825	2.27777	0.374392	-0.572032
Fe3+	0.288	0.794739	0.497276	0.519777

VBF Analysis of Am06t71

project:
document: Am06tvmt71
data document: Am06t71

Fit Summary
no. of data points: 512
no. of QSD sites in model: 2
no. of parameters in model: 22
no. of refined parameters: 3
reduced χ^2 = 1.50303
uncertainties calculated using the covariance matrix

Global Parameters
Background = 3145490(150) counts
Lorentzian HWHM = 0.097* mm/s

Site Distribution Parameters

	δ_0 (mm/s)	δ_1	A (counts·mm/s)	A_1/A_2
Fe2+	1.0294*	0.0434*	92857.8*	0.9320(73)
Fe3+	0.288*	0*	21597.8*	0.774(41)

		p (%)	$\langle\Delta\rangle$ (mm/s)	σ_Δ (mm/s)
Fe2+	comp 1	14*	2.06*	0.59*
	comp 2	68*	2.412*	0.252*
	comp 3	18*	1.94*	0.222*
Fe3+	comp 1	100*	0.742*	0.573*

Compiled Site Properties

	Site Populations
Fe2+	81.13
Fe3+	18.87

	<CS> (mm/s)	<|Δ|> (mm/s)	stdev(|Δ|) (mm/s)	skew(|Δ|)
Fe2+	1.12825	2.27777	0.374392	-0.572032
Fe3+	0.288	0.794739	0.497276	0.519777